INFORMATION TO USERS

This manuscript has been reproduced from the microfilm master. UMI films the text directly from the original or copy submitted. Thus, some thesis and dissertation copies are in typewriter face, while others may be from any type of computer printer.

The quality of this reproduction is dependent upon the quality of the copy submitted. Broken or indistinct print, colored or poor quality illustrations and photographs, print bleedthrough, substandard margins, and improper alignment can adversely affect reproduction.

In the unlikely event that the author did not send UMI a complete manuscript and there are missing pages, these will be noted. Also, if unauthorized copyright material had to be removed, a note will indicate the deletion.

Oversize materials (e.g., maps, drawings, charts) are reproduced by sectioning the original, beginning at the upper left-hand corner and continuing from left to right in equal sections with small overlaps.

Photographs included in the original manuscript have been reproduced xerographically in this copy. Higher quality 6" x 9" black and white photographic prints are available for any photographs or illustrations appearing in this copy for an additional charge. Contact UMI directly to order.

ProQuest Information and Learning
300 North Zeeb Road, Ann Arbor, MI 48106-1346 USA
800-521-0600

INTERMOLECULAR INTERACTIONS IN A SERIES OF ORGANOAMMONIUM TETRAPHENYLBORATES

by

Katherine N. Robertson

Submitted in partial fulfilment
of the requirements
for the degree of Doctor of Philosophy

at

Dalhousie University
Halifax, Nova Scotia
February, 2001

DALHOUSIE UNIVERSITY

FACULTY OF GRADUATE STUDIES

The undersigned hereby certify that they have read and recommend to the Faculty of Graduate Studies for acceptance a thesis entitled "Intermolecular Interactions in a Series of Organoammonium Tetraphenylborates"

by Katherine N. Robertson

in partial fulfillment of the requirements for the degree of Doctor of Philosophy.

Dated: February 22, 2001

External Examiner

Research Supervisor

Research Supervisor

Examining Committee

DALHOUSIE UNIVERSITY

DATE : February 22, 2001

AUTHOR : Katherine N. Robertson

TITLE : Intermolecular Interactions in a Series of Organoammonium Tetraphenylborates

DEPARTMENT OR SCHOOL : Chemistry

DEGREE : Ph.D. CONVOCATION : May YEAR : 2001

Permission is herewith granted to Dalhousie University to circulate and to have copied for non-commercial purposes, at its discretion, the above title upon the request of individuals or institutions.

Signature of Author

In memory of Douglas Grant Robertson

Table of Contents

List of Figures

List of Tables

Appendix 4 Collected Tables

Abstract

High quality, low temperature, x-ray crystallographic data sets were collected for four organoammonium tetraphenylborates. On close scrutiny, two types of N-H...X interactions were identified, the more "traditional" N-H...N hydrogen bonds, and N-H...π(Ph) hydrogen bonds [centroid, edge or single atom type], in which the phenyl ring of the anion serves as the hydrogen bond acceptor. In addition, the four salts were found to form a large number of close C-H...X type contacts. Some of these adopted hydrogen bond type geometries while others were classified as "H...H" type contacts, using criteria developed in this work.

Charge density calculations were carried out on the four salts. From the results, static and dynamic electron density maps were plotted in a variety of planes to see if evidence of the intermolecular interactions would be visible. The conventional N-H...N hydrogen bonds were used as the internal standard with which the other, weaker, interactions could be compared. Certain features were identified in the maps that could consistently be attributed to the formation of N-H...π(Ph) hydrogen bonds.

The electron density distributions calculated using the aspherical models generated in the XD refinements were used as input for topological analyses of the four salts. This allowed a more quantitative investigation of the weak intermolecular interactions. The location of a rational bond path and a (3,-1) bond critical point was characteristic of almost every contact studied. The values, at the bond critical points, of the electron density, $\rho_b(\mathbf{r})$, and the Laplacian of the electron density, $\nabla^2\rho_b(\mathbf{r})$, were calculated. They were always positive, typical of closed shell interactions, and were shown to be correlated with the distance over which the interaction occurred, specified in this work as the H...acceptor distance. In both cases [$\rho_b(\mathbf{r})/\nabla^2\rho_b(\mathbf{r})$ versus d(H...A)], a simple exponential curve was found to model the collected experimental data reasonably well. The experimentally derived topological data from this work were consistent with literature values reported for more traditional hydrogen bonds, which shows the N-H...π(Ph) hydrogen bonds behave topologically like all others. Finally, the majority of the C-H...phenyl interactions were identified as "H...H" type contacts, while the remainder were found to be hydrogen bonds, behaving topologically like other X-H...π(Ph) hydrogen bonds.

Abbreviations and Symbols

MW	Formula weight
Z	Number of molecules in the unit cell
a,b,c	Unit cell dimensions
α,β,γ	Angles between crystal axes
V	Volume of unit cell
μ	Linear absorption coefficient
d_c	Calculated density
θ	Bragg angle
h,k,l	Miller indices of the reflecting plane
MoKα	Molybdenum Kα radiation
λ	Wavelength of X-radiation
x/a,y/b,z/c	Fractional coordinates
B_{eq}	Isotropic temperature factor
U_{ij}'s	Anisotropic temperature factors
F(000)	Number of electrons in the unit cell
F_o, F_{obs}	Observed structure amplitude
F_c, F_{calc}	Calculated structure factor
N_{obs}, d	Number of observed reflections
N_v, p	Number of parameters refined
r	Number of restraints applied
R	R-factor
Rw, wR2	Weighted R-value
R_{merge}	Merging R-value for equivalent reflections
GOF	Goodness of fit parameter

w	Weight in minimized function
TLS	Translation/Libration/Screw
rms	Root mean square
esd	Estimated standard deviation
R, r	Correlation coefficient
R^2, r^2	Coefficient of determination
σ	Standard deviation
$\rho(\mathbf{r})$	Electron density in molecule
$\Delta\rho(\mathbf{r})$	Difference electron density
$\mathbf{r}$	Vector to a point in real space
k	Scale factor
$\mathbf{H}(h_1,h_2,h_3)$	Vector to a point in reciprocal space
$\lvert F_o(\mathbf{H})\rvert$	Observed structure factor amplitude
$\lvert F_c(\mathbf{H})\rvert$	Calculated structure factor amplitude
ρ_c	Core atomic density
ρ_v	Valence density
$Y_{lm}(\theta,\phi)$	Multipolar spherical harmonic functions in real form
κ', κ''	Expansion-contraction parameters
P_c	Core population parameters
P_v	Valence population parameters
P_{lm}	Multipole population parameters
R_l	Radial functions
N_l	Normalization factor
$\delta\rho(\mathbf{r})$	Deformation electron density
$\rho_b(\mathbf{r})$	Electron density at the bond critical point

$\nabla^2\rho_b(\mathbf{r})$	Laplacian of the electron density at the bond critical point
$\lambda_1, \lambda_2, \lambda_3$	Eigenvalues of the Hessian matrix, principal curvatures of the electron density at the bond critical point
ϵ	Ellipticity of the electron density at the bond critical point
R, R_e, R_b r, r_e, r_b	Internuclear separation, its equilibrium value, bond path length
E	Energy
HB	Hydrogen bond
X-H...π(Ph)	Hydrogen bond accepted by a phenyl ring
X-H...phenyl	Any type of interaction involving a phenyl ring, generally not HBs but as a group can include HBs
d(X...A)	Distance characterizing the X-H...A HB
π_c	Phenyl ring centroid
100Δ	[100(maximum - minimum X/H...C_{ring} distance)] a parameter characterizing the X-H...π(Ph) HB
HO	High order
N	Neutron
X	X-ray
CP	Critical point
BP	Bond path
Ph	Phenyl= $-C_6H_5$
TB	Tetraphenylborate anion
CSD	Cambridge Structural Database

Acknowledgements

I would like to thank my supervisors, Dr. T.S. Cameron and Dr. O. Knop, for their encouragement, support and guidance over the lengthy period of time that it took me to complete this work. Their patience was greatly appreciated.

I would also like to thank all of my colleagues at the Dalhousie University X-ray Crystallographic Centre. In particular, I am indebted to Dr. Pradip K. Bakshi who taught me the fundamentals of crystal structure determination and to Dr. Witold Kwiatkowski who introduced me to the theory and practise of charge density calculations. They were valued companions with whom I spent many enjoyable hours. I would also like to thank Ruth Cordes for her contributions in keeping the lab running smoothly and for her willing ear, used as a vent for my many frustrations.

Over the years I have made many friends in the Department of Chemistry and throughout the entire Dalhousie community. Collaboration within the department, particularly with other graduate students, was invaluable to my education. I would like to thank everyone who supported me during this time, especially over the long writing process. In this regard I am most indebted to Sai Chua and to the hockey friends who kept me sane.

I have often neglected those closest to me while trying to complete this work. My parents, sister and extended family have never complained and have forgiven my many transgressions. I thank them for this. Finally, I am grateful for the constant and unwavering support provided by Richard W.P. Nelson. He encouraged me to pursue this dream.

1. Chapter One

1. Introduction

1.1. X-ray Crystallography[1,2]

In x-ray crystallography, the main interaction of interest occurring between the incident radiation and the crystal is coherent scattering. As an x-ray beam passes through a crystal it can cause electrons of the atoms in the material to vibrate. The vibrating electron radiates x-rays of the same frequency as the incident beam but in a variety of directions. Such vibrating electrons act as secondary sources of x-rays of fixed wavelength and give rise to interference effects. The interference phenomena arising from coherent scattering are the basis of x-ray crystallography.

In the x-ray diffraction experiment, coherent and incoherent scattering occur simultaneously. In the latter, a portion of the energy of the incident x-ray photon is converted into kinetic energy by the scattering electron and the re-emitted photon has a lower frequency and longer wavelength. This process is not quantized and the x-rays so scattered appear as background radiation in the experimental measurements. Fortunately, the contribution of the incoherent scattering to the total scattering is normally much smaller than that of the coherent scattering.

The most important quantities derived from the measured coherent diffraction intensities, I(hkl), of a crystal are the structure factor amplitudes, $|F(hkl)|$. The relationship between $|F(hkl)|_{obs}$ and I(hkl) depends on a number of factors, primarily geometric, that are related to the individual reflection and to the apparatus used to measure its intensity.

$$|F(hkl)|_{obs} \quad \alpha \quad (I(hkl)/Lp)^{1/2}$$

Here, p is a correction for polarization of the x-ray beam and L is the Lorentz correction which accounts for the variable time each reciprocal lattice point spends in the reflecting position. I(hkl) can also be corrected for absorption and extinction effects if required; this is more commonly done during the refinement stage than during data reduction.

When a crystal is subjected to the electromagnetic field of an x-ray beam, each electron in the structure scatters a small fraction of the incident energy. The periodic arrangement of atoms in a crystal restricts diffracted intensity maxima to certain directions, those in which reflections from lattice planes satisfy the Bragg condition:

$$2d(\sin \theta) = n\lambda$$

where d is the interplanar spacing, λ is the wavelength and θ is the angle the incident and scattered beams make with the reflecting plane. The Bragg equation thus treats the diffraction/interference process as if it were, formally, reflection.

From the Bragg equation it is evident that sin θ is inversely proportional to d, the interplanar spacing in the crystal lattice. However, interpretation of x-ray diffraction patterns is facilitated if this inverse relationship is replaced by a direct one, by constructing a reciprocal lattice based on 1/d, which varies directly with sin θ. If a, b and c are the elementary translations defining a direct or real space lattice, then a second lattice, reciprocal to the first is defined by the translations a^*, b^* and c^* which must satisfy the following conditions:

$$a^* \cdot b = a^* \cdot c = b^* \cdot a = b^* \cdot c = c^* \cdot a = c^* \cdot b = 0 \quad \text{and}$$

$$a^* \cdot a = b^* \cdot b = c^* \cdot c = 1$$

It follows that a^* will be normal to the (b,c) plane, b^* to the (a,c) plane and c^* to the (a,b) plane, and vice versa [a will be normal to the (b^*,c^*) plane, etc.].

Consider two scattering centers O and O′ from the same family of reflecting planes, that is d(hkl) is equal for both. The amplitude that each scatters with will be A_O and $A_{O'}$, respectively. If both scatter at an angle of 2θ from the incident radiation then the difference in the observed phase will be given by: $\exp(2\pi i\mathbf{H}\cdot\mathbf{r})$

where $\mathbf{H}$ is a vector representing a point in reciprocal space corresponding to the reflecting plane (hkl) and $\mathbf{r}$ is a vector representing a point in real space corresponding to the position of the scatterer. O is taken to be the origin and the phase of O is taken to be zero.

$$\mathbf{H} = a^*h + b^*k + c^*l$$

$$\mathbf{r} = ax + by + cz$$

$$\mathbf{H}\cdot\mathbf{r} = hx + ky + lz \qquad \begin{matrix} h,k,l \text{ of the nth plane} \\ x,y,z \text{ of the jth atom} \end{matrix}$$

If there are N point scatterers to be considered, then

$$F(hkl) = F(\mathbf{H}) = \sum_j A_j \exp(2\pi i\mathbf{H}\cdot\mathbf{r}_j)$$

where A is the amplitude of the jth scatterer.

The intensity scattered by a given center or atom, I, can be expressed in terms of the intensity scattered by a free electron, I_e, in the same direction. The square root of the ratio I/I_e is defined as the scattering factor, f, of that object. If the object is an atom, then f is the atomic scattering factor and the structure factor in vector form is given by: $F(\mathbf{H}) = \sum_j f_j \exp(2\pi i\mathbf{H}\cdot\mathbf{r}_j)$

In exponential form the structure factor is

$$F(hkl) = \sum_j f_j \exp[2\pi i(hx_j + ky_j + lz_j)]$$

The structure factor can be divided into its real and imaginary components

$$F(hkl) = A(hkl) + iB(hkl)$$

where $$A(hkl) = \sum_j f_j \cos[2\pi(hx_j + ky_j + lz_j)]$$

$$B(hkl) = \sum_j f_j \sin[2\pi(hx_j + ky_j + lz_j)]$$

If the scattering centers constitute an infinite, continuous source, an element, dr, of the total volume, V, will contain a number of electrons equal to $\rho(\mathbf{r})d\mathbf{r}$, where $\rho(\mathbf{r})$ is the electron density. The wave scattered on the element dr is given, in amplitude and phase, by

$$\rho(\mathbf{r})d\mathbf{r} \exp(2\pi i\mathbf{H}\cdot\mathbf{r})$$

and therefore,

$$F(\mathbf{H}) = \int_V \rho(\mathbf{r}) \exp(2\pi i\mathbf{H}\cdot\mathbf{r})d\mathbf{r}$$

Mathematically, from the theory of Fourier transforms it is also true that

$$\rho(\mathbf{r}) = \int_{V^*} F(\mathbf{H}) \exp(-2\pi i\mathbf{H}\cdot\mathbf{r})d\mathbf{H}$$

The electron density distribution in a crystal can be represented as a periodic function rather than a continuous function. That is, the structure factors, $F(\mathbf{H})$, are only different from zero at discrete points in reciprocal space. The integral can then be replaced by a Fourier series.

$$\rho(\mathbf{r}) = 1/V \sum_{\mathbf{H}} F(\mathbf{H}) \exp(-2\pi i\mathbf{H}\cdot\mathbf{r})$$

Whatever the representation chosen, the electron density is the Fourier transformation of the structure factors, while in turn, the

structure factors are the Fourier transforms of electron density. Fourier transformation relates a function defined in one space (for example real space) to a second function defined in another space (for example reciprocal space). In x-ray crystallography the structure factors are defined in reciprocal space (**H**) while the electron density is defined in real space (**r**) and Fourier transformations are used to interconvert the two.

The structure factor expression can also be written:

$$F(\mathbf{H}) = |F(\mathbf{H})| \exp 2\pi i \alpha_{\mathbf{H}}$$

And similarly, the electron density can be expressed:

$$\rho(x,y,z) = 1/V \sum_h \sum_k \sum_l |F(hkl)| \exp[-2\pi i(hx_j + ky_j + lz_j - \alpha_{hkl})]$$

where $|F(hkl)|$ or $|F(\mathbf{H})|$ is the structure factor amplitude, obtained from the x-ray diffraction experiment or calculated during refinement and where α_{hkl} or $\alpha_{\mathbf{H}}$ is the phase angle.

Written in this way the central problem of x-ray crystallography is emphasized - the phase problem. Only $|F(\mathbf{H})|$, the structure factor amplitude, can be obtained from the diffraction intensities; the corresponding phase (α) information is lost. For acentric structures, those lacking inversion symmetry, the phase angle may have any value between 0 and 2π while in centrosymmetric structures the phase angle is restricted to values of 0 and π. A general solution to the phase problem has not been found but methods can be applied to obtain models for the phase angles. Those most commonly used are Patterson (based on F^2) and direct methods, as described in any crystallography text.[1,2]

Once both the structure factor amplitudes (derived from the measured intensities) and phase angles (modelled) have been obtained, the electron

density at each point in the unit cell can be calculated.

$$\rho(\mathbf{r}) = 1/V \sum_{\mathbf{H}} |F(\mathbf{H})|_{obs} \exp[-2\pi i(\mathbf{H}\cdot\mathbf{r} - \alpha_{\mathbf{H}})]$$

This resulting distribution is the F_{obs} map of electron density. The atomic positions are located at the highest electron density peaks in the map, meaning that the atomic arrangement can be found directly from $\rho(x,y,z)$. The accuracy of the map will depend on the model chosen to calculate the phases.

Unfortunately, the electron density calculated by this method will suffer from "termination of series error". The perfect representation of a point atom by a Fourier series requires an infinite amount of data. If only a limited number of terms are included in the series, as is always the case with experimentally measured intensities, the electron density maxima will be surrounded by secondary ripples. Fortunately, the ΔF synthesis, $F_{observed} - F_{calculated}$, to a large extent takes care of series termination error.

Let $$\rho(\mathbf{r})_{obs} = 1/V \sum_{\mathbf{H}} |F(\mathbf{H})|_{obs} \exp[-2\pi i(\mathbf{H}\cdot\mathbf{r} - \alpha_{\mathbf{H},calc})] + R$$

and $$\rho(\mathbf{r})_{calc} = 1/V \sum_{\mathbf{H}} |F(\mathbf{H})|_{calc} \exp[-2\pi i(\mathbf{H}\cdot\mathbf{r} - \alpha_{\mathbf{H},calc})] + R'$$

where R and R′ are remainders representing the omitted portion of each series. R and R′ should be nearly equal in each case. Therefore, the difference between the two series, $\Delta\rho(\mathbf{r})$, should be nearly free of termination error.

$$\Delta\rho(\mathbf{r}) = 1/V \sum_{\mathbf{H}} (1/k)|F(\mathbf{H})|_{obs} - |F(\mathbf{H})|_{calc} \exp[-2\pi i(\mathbf{H}\cdot\mathbf{r} - \alpha_{\mathbf{H},calc})]$$

where k is a scale factor used to bring $|F(\mathbf{H})|_{obs}$ and $|F(\mathbf{H})|_{calc}$ to the same scale. It is optimized during the refinement. The difference map

corresponds to a point by point subtraction of an F_{calc} map from an F_{obs} map, each calculated with the same, modelled, phases. Such a map will show peaks everywhere the F_{calc} model fails to provide the electron density implied by the F_{obs} data and holes wherever it supplies too much.

Let $\psi_1(\mathbf{r}) \ldots . \psi_Z(\mathbf{r})$ be the wavefunctions of Z atomic electrons described in Hartree-Fock, self consistent field formalism. Then,

$$\rho_{e,j}\, dV = |\psi_j(\mathbf{r})|^2\, dV$$

is the probability of finding the jth electron in the volume element, dV. If every function can be considered independent of the other, then

$$\rho_{atom}(\mathbf{r})\, dV = \sum_j \rho_{e,j}$$

is the probability of finding an electron in the volume, dV. The Fourier transform of $\rho_a(\mathbf{r})$ is called the atomic scattering factor, f. The scattering factor of the jth atom is defined as

$$f_j = \int \rho_a(\mathbf{r})\, \exp[2\pi i(\mathbf{H}\cdot\mathbf{r})]d\mathbf{r}$$

In the spherical free atom approximation it is the scattering power of the Z atomic electrons, each placed at the atomic origin.

Generally, the function $\rho_a(\mathbf{r})$ does not have spherical symmetry. However, in crystallography deviations from spherical symmetry are neglected in a first approximation suitable for most conventional applications. If spherical atoms are assumed, the scattering power is a function of only atom type and $(\sin\theta)/\lambda$ not of the crystal environment. The $\rho_a(\mathbf{r})$ spherical function, and thus f_j, is known with considerable accuracy for practically all neutral atoms, for lighter atoms from the Hartree-Fock method and for heavier atoms from an approximation from it.

Plots of f_j versus $(\sin\theta)/\lambda$ for any atom have a number of features in common (Figure 1). Each curve reaches its maximum value, equal to the

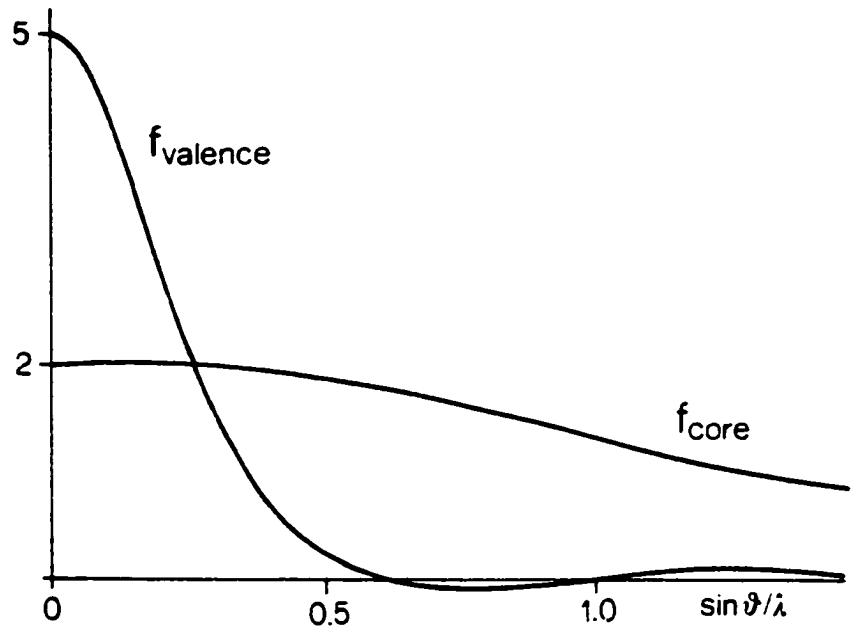

core and valence scattering for nitrogen atom

Figure 1. Variation of the core and valence scattering factors of the nitrogen atom with $\sin\theta/\lambda$.[1]

number of electrons in the atom (Z), at (sin θ)/λ equal to zero. As (sin θ)/λ increases the scattering factor always decreases because the x-rays scattered from an electron in one part of the atom will increasingly be out of phase with those scattered elsewhere in the atom. It can be shown that radiation scattered at high values of (sin θ)/λ is due primarily to electrons of inner shells of the electron cloud, the core electrons. Conversely, scattering by valence electrons is most efficient only at low (sin θ)/λ values.

In the Hartree-Fock description of the atom, core and valence contributions to the electron density can be separated. The atomic scattering factor, f_j, can therefore be considered the sum of core and valence electron scattering.

$$f_j = f_{core} + f_{valence}$$

In the isolated free atom approximation used in conventional x-ray diffraction experiments, the unit cell density is described as a superposition of isolated, spherical atomic densities. These are calculated from Hartree-Fock formalism and atomic wavefunctions composed of linear combinations of atomic orbitals. They are placed at the nuclear positions with the observed thermal motions. The structure factors are calculated using total atomic scattering factors that are a combination of valence and core contributions. This results, as described above, in spherical electron density distributions around each atomic position.

$$F(\mathbf{H}) = \sum_j f_j \exp(2\pi i \mathbf{H}\cdot\mathbf{r}_j)$$

If required, the atomic scattering factors can be corrected for anomalous dispersion. Atomic scattering factors, f_j, are normally represented by real numbers. This is true as long as the frequency of the

incident radiation differs widely from the natural absorption frequencies of the atoms in the crystal. Although this is normally true for lighter atoms at the radiations commonly used in x-ray diffraction, it is often not true for heavier atoms, particularly if their atomic numbers are near to that of the element used to generate the x-rays.

Electrons are bound to the nucleus of the atom by forces which depend on the atomic field strength and on the quantum state of the electron. They can be considered as oscillators with characteristic natural frequencies. If the frequency of the incident beam is near to these natural frequencies, resonance will take place, and an anomalous phase change will occur on scattering. Correction terms can be applied to the real atomic scattering factors to account for this process.

$$f_{j,anomalous} = f_j + \Delta f' + i \Delta f''$$

where $\Delta f'$ is a real correction term and $\Delta f''$ is an imaginary component. The net result is a change in both phase and magnitude for f_j. The correction terms are almost independent of sin θ, indicating that anomalous dispersion involves mainly the core electrons of the atom. For a given atom, the effects of dispersion are relatively greater at high sin θ than at low. Dispersion effects are also usually greater for longer wavelength radiations.

Thermal motion also has an effect on the measured x-ray intensities. The normal scattering factor curves are calculated for an ideal situation, stationary atoms. In fact, the atoms in a crystal are always vibrating, with the extent of vibration depending on temperature, the mass of the atom and the atomic environment (i.e. bonding and other forces). The effect of such thermal motion is to spread the electron cloud over a

larger volume than theoretically predicted, in a process known as thermal smearing. This causes the scattering power of the real atom to decrease more rapidly with $(\sin \theta)/\lambda$ than accounted for in f_j, the atomic scattering factor. The change in the scattering power is given by the expression

$$\exp(-B(\sin^2 \theta)/\lambda^2)$$

where $B = 8\pi^2u^2$ is the isotropic thermal parameter and u^2 is the mean square amplitude of atomic vibration. Thus the proper scattering factor of a real atom is

$$f_{j,real} = f_{j,theoretical} \exp[-B(\sin^2 \theta)/\lambda^2]$$

In general, the atom will not be free to vibrate equally in all directions because of bonding and other constraints. The isotropic description of thermal motion is replaced by an anisotropic model, where an ellipsoidal distribution is used to describe the electron density. The general form of the anisotropic temperature factor expression contains six parameters, U_{ij}, that determine the magnitudes and orientations of the principal axes of the ellipsoidal density distribution relative to the crystallographic axes. Normally these parameters are refined for each heavy atom, along with the atomic positions, using the method of least squares. It is important to mention, however, that the thermal vibrations of atoms can be greatly reduced by lowering the temperature of the crystal during data collection. This will increase the quality of the data collected and lead to improved results.

1.2. Electron Density Calculations

1.2.1. $X - X_{HO}$ Refinement

$X - X_{HO}$ refinement is an empirical method of separating the

diffraction effects of core and valence electrons.[3] Each atom is still assumed to have a spherical distribution of electron density and a single, total atomic scattering factor, f_j, is used to obtain $F(\mathbf{H})_{calculated}$. The scattering factor used is a combination of valence and core electron contributions.

However, in bonded atoms the assumption of a spherical electron density cannot be considered correct. Valence electrons are shared between atoms (bonds) or isolated as lone pairs on certain atoms. The deviation from spherical density is thus due predominantly to valence electrons; the core orbitals retain their spherical distribution to a much greater extent.

As shown in Figure 1, at small θ, scattering by valence electrons is more important while at high θ, scattering is almost entirely by the core electrons, with the valence electrons making little contribution. A given data set can be divided into "high order" and "low order" sets based on a selected value of $(\sin \theta)/\lambda$, generally between 0.6 and 0.8.

First the atomic positions must be found as accurately as possible. Unbiased parameters can be obtained from a refinement including only the "high order" data, where scattering is due largely to the core electrons. To obtain the best possible results, a high quality data set must be available (see the following discussion on error). The "high order" data set must contain sufficient reflections to adequately refine all the desired parameters.

Alternatively, these parameters can be obtained in a separate neutron diffraction experiment, which will give the positions and thermal parameters of the atomic nuclei. Electron density maps obtained using

atomic parameters derived from neutron diffraction experiments are termed X - N maps.[4] However, it is known that electrons do not rigidly follow nuclei during thermal motion and applying neutron thermal parameters to x-ray data can create problems. Care must also be taken to scale the neutron data and the x-ray data correctly.

The "low angle" data contain the majority of the contribution of the valence electrons. It is in the "low angle" data that the deviation from the assumed spherical density is hidden. An F_{obs} - F_{calc} difference map will give the deformation from the spherical model. The calculated structure factors, obtained using the overall atomic scattering factors, will thus be based on the spherical model of electron density while the observed structure factors will contain the total contribution of the valence electrons including nonspherical contributions from bonding and lone pair electrons.

$$\Delta \rho(\mathbf{r}) = 1/V \sum_{\mathbf{H}} [(1/k)F(\mathbf{H})_{obs} - F(\mathbf{H})_{calc}] \exp[-2\pi i(\mathbf{H}\cdot\mathbf{r})]$$

$$\Delta \rho(\mathbf{r}) = \rho(\mathbf{r})_{obs} - \sum_{j} \rho_{j,\text{spherical atom}}(\mathbf{r})$$

The resulting difference is termed the "deformation density" because it displays the deformations that occur in the atomic electron distributions as a result of bonding. Subtle changes in the electron distribution are more clearly visible in the deformation density than in the total electron density distribution which is dominated by large, spherical contributions centered at the atomic positions. Features of the deformation density may be interpreted easily with a qualitative valence bond model of chemical bonding, showing peaks due to both covalent bonding and lone pair, nonbonding electron distributions.

Since $\Delta \rho(\mathbf{r})$ is only a small fraction (approximately 3-6%) of $\rho(\mathbf{r})$

in the region of the atoms, it is very susceptible to experimental error in x-ray measurements.[3,4] The experimental errors can be divided into three broad groups:

(i) Errors in the scale factor - An error in the scale factor acts mainly in the vicinity of the atomic positions but it also has a small effect in the bond region. It has been shown that a change in the radial behaviour of atomic densities in a conventional refinement may change the scale factor by as much as 8 to 10%. The refined scale factor can also be correlated with the thermal parameters introducing further error. Fortunately, the correlation between the scale factor and thermal parameters will be reduced if more high angle data are collected for the refinement. Collecting the x-ray data at low temperature increases the amount of high angle data that can be collected and also decreases the amount of thermal diffuse scattering.

(ii) Errors in the calculated electron densities - These result from errors in the atomic parameters obtained from either neutron or "high order" x-ray data. With a full set of diffraction data and proper corrections for absorption, extinction and thermal diffuse scattering, it is possible to obtain positional parameters accurate to 10^{-3} Å. Improper correction of these problems has a small effect on the positional parameters but introduces a large bias in the scale and thermal parameters, ultimately having a large effect on the deformation density.

(iii) Errors in the observed electron densities - These errors are dominated by errors in the observed structure factors, F_{obs}, and thus depend on experimental conditions and the measurement of intensities. The standard deviation of the measured intensity, I_o, is given by:

$$\sigma^2(I_o) = \sigma^2_c(I_o) + C^2(I_o)^2$$

where $\sigma^2_c(I_o)$ accounts for errors in the counting statistics and the constant, C, is estimated from the agreement between symmetry equivalent reflections. The second term is more important only for strong reflections.

If the crystal is not spherical, the optical paths for equivalent reflections are different. They will suffer from extinction and absorption to different extents. An averaging before corrections are applied will bias the estimate of I_o and C. Symmetry equivalent reflections should be kept as independent data in the first stages of refinement.

During refinement, a rejection test for reflections that are smaller than $n\sigma(I_o)$ is often used to limit the F_{obs} data to be considered. Such a test results in a bias against small structure factors that are systematically underestimated. Some of these small reflections can be very meaningful in terms of bonding features and should be considered.

When a structure is not centrosymmetric, the difficult problem of assigning phases to the structure factors introduces error to both F_{obs} and F_{calc}. Phases can only be obtained for the calculated structure factors and they change with the model chosen to represent F_{calc}. These same modelled phases are also assigned to the corresponding observed structure factor amplitudes. Even a small error for the phase of a structure factor can result in a large error for the phase in the difference Fourier synthesis, $F_{obs} - F_{calc}$. For this reason, most work on experimental charge densities has been carried out on centrosymmetric structures. In the centrosymmetric case, the phase must be 0 or π, and correct assignment of the phases is much more likely. The phase assignments become stable rapidly as improved

models are introduced.

1.2.2. Multipole Refinement

As an alternative to obtaining the deformation density by Fourier series summation, x-ray data may be analyzed using an expanded least squares refinement model. Rather than using the scattering factors of neutral, spherical atoms, the model used in conventional refinement of x-ray data, the refinement model can be expanded to include parameters that describe the distortions of the atomic electron distributions as a result of chemical bonding and the crystalline environment.[5,6]

spherical, free atom approximation $\rho(\text{atom}) = \rho(\text{core}) + \rho(\text{valence})$

multipole $\rho(\text{atom}) = \rho(\text{core}) + \rho(\text{valence}) + \rho(\text{deformation})$

$\rho(\text{deformation}) = \rho(\text{multipole atom}) - \rho(\text{spherical atom})$

where $\rho(\text{deformation})$ is the deformation density, the bonding electron density or the density that is deformed from the spherically averaged free atom model.

As before, $\rho(\text{core})$ and $\rho(\text{valence})$ are described by spherical Slater-type orbitals in Hartree-Fock formalism as linear combinations of atomic orbitals normalized to one electron. However, $\rho(\text{valence})$ is modified slightly to allow for electronegativity differences between atoms, which lead to the transfer of electrons between the valence shells of different atoms. The electron transfer introduces a change in the screening of the nuclear charge by the electrons and therefore affects the radial dependence of the atomic electron distribution. A variable, κ, is introduced to control the diffuseness of the valence orbitals.

$$\rho'_{\text{valence}}(\mathbf{r}) = \kappa^3 \rho_{\text{valence}}(\kappa\mathbf{r})$$

where ρ' is the modified density and κ is an expansion/contraction parameter, which is less than 1 for valence shell contraction (positive charge) and greater than 1 for valence shell expansion (negative charge).

The valence density is normally defined as the outer electron shell from which charge transfer occurs. The inner or core electrons are much less affected by the change in occupancy of the outer shell and to a reasonable approximation retain their radial dependence. The core electron density is not corrected for expansion/contraction. However, the functions describing the deformation density, discussed below, are also corrected for expansion/contraction of the radial function with a Kappa variable.

The deformation density can be written in terms of polar coordinates (r,θ,ϕ) and it is assumed that the radial and angular functions can be separated.

$$\Psi(r,\theta,\phi) = R(r)\Theta(\theta)\Phi(\phi)$$

The radial function, R(r), is spherical. It can be chosen in a number of different forms, although commonly Slater-type radial functions are used. These would be similar to the Slater functions used to describe the valence and core orbitals.

$$R_l(r) = \zeta^{(n+3)}/(n+2)!\ (r)^n \exp(-\zeta r)$$

The angular functions, Θ and Φ, which introduce the deformation from a spherical distribution are based on the spherical harmonic functions, $Y_{l,m}(\theta,\phi)$, defined by:

$$Y_{l,m}(\theta,\phi) = [(2l+1)/4\pi \times (l-|m|)!/(l+|m|)!]^{1/2}\ P_{l,m}(\cos\theta)\ \exp(im\phi)$$

The spherical harmonics are complex, but real functions may be obtained by taking the appropriate linear combinations:

$$Y_{l,m}\text{even}(\theta,\phi) = \cos(m\phi)\ P_{l,m}(\cos\theta)$$

$$Y_{l,m}odd(\theta,\phi) = \sin(m\phi)\ P_{l,m}(\cos\ \theta)$$

The spherical harmonic functions are mutually orthogonal and form a complete set, which if taken to sufficiently high order, can be used to describe any arbitrary angular function. The spherical harmonic functions are often referred to as multipoles and they depend on the quantum numbers of the atom n,l and m. Terms with increasing l in $Y_{l,m}$ are referred to as monopolar (l=0), dipolar (l=1), quadrupolar (l=2), octapolar (l=3) and hexadecapolar (l=4).

$P_{l,m}$, the multipole parameters, are population coefficients and are refined in a multipole analysis. They are frequently defined in terms of local coordinate systems on each atom, making it possible to impose molecular (noncrystallographic) symmetry constraints on the refinement.[7]

Overall $$\rho(\text{deformation}) = \sum_{l} (\kappa'')^3\ R_l(\kappa''r) \sum_{m=-l}^{+l} P_{l,m}\ Y_{l,m}(\theta,\phi)$$

And the atomic density is described by:

$$\rho_{atomic}(\mathbf{r}) = P_c\rho_{core}(\mathbf{r}) + Pv(\kappa')^3\rho_{valence}(\kappa',\mathbf{r}) + \sum_{l}(\kappa'')^3 R_l(\kappa''\mathbf{r}) \sum_{m=-l}^{+l} P_{l,m}Y_{l,m}(\theta,\phi)$$

Fourier transformation of ρ(deformation) gives:

$$f_{j,deformation}(\mathbf{r}^*) = 4\pi \sum_{n,l,m} (i)^l\ f_{n,l}(\mathbf{r}^*)\ Y_{l,m}(\theta^*,\phi^*)$$

where θ^* and ϕ^* are angular components of the Bragg vector

and $$f_{n,l}(\mathbf{r}^*) = \int R_{n,l}(r)\ j_l(\mathbf{r}\cdot\mathbf{r}^*)r^2\ dr$$

($j_l(x)$ is a spherical Bessel function of order l)

The structure factor expression becomes:

$$F(\mathbf{H}) = \sum_{j} [\ P_c\ f_{core}(\mathbf{H}) + P_v\ f_{valence}(\mathbf{H}/\kappa') + \sum_{l} \Phi_{n,l}\ (\mathbf{H}/\kappa'') \sum_{m=-l}^{+l} P_{n,l,m}Y_{n,l,m}(\mathbf{H})]$$
$$\exp(2\pi i\mathbf{H}\cdot\mathbf{r}_{np})\ T_n(\mathbf{H})$$

where f_{core} and $f_{valence}$ are the Fourier transforms of ρ(core) and ρ(valence), respectively, and T is an appropriate temperature factor for

the atom in question. $\Phi_{n,l}$ is the Fourier-Bessel transform of $R_{n,l}$ as described previously.

$$\Phi_{n,l} = 4\pi\ (i)^l\ f_{n,l}(r^*)$$

This structure factor expression is used in the least squares, multipole refinement programs, MOLLY[8] and XD.[9] The programs allow refinement of positional, anisotropic-vibration and extinction parameters, the population coefficients, P_v and $P_{l,m}$ and the radial expansion/ contraction parameters, κ' and κ'', for each atom. In a multipole refinement there may be three times as many parameters to be refined as in a normal spherical refinement. The highest quality data are required, with low temperature collection essential for obtaining sufficient reflections for an acceptable observation-to-parameter ratio.

In the spherical approximation of the multipole refinement ρ(deformation), and therefore $f_{j,deformation}$, are left at zero. $P_{l,m}$ and κ'' are not refined. If P_v is set to be equal to the number of valence electrons on each atom and κ' is set to one, then

$$\rho(atom) = \rho(core) + \rho(valence)$$

This is very similar to the X - X_{HO} spherical approach, with atomic positions again usually obtained from "high angle" x-ray data or neutron diffraction data. Difference maps obtained from F_{obs} - $F_{spherical,calc}$ should be nearly identical to X - X_{HO} maps for the same system.

Dynamic deformation maps are one goal of multipole refinement.

$$\rho(dynamic) = 1/V \sum_{H} [F_{multipole,calc} - F_{spherical,calc}]\ \exp[-2\pi i(H\cdot r)]$$

where $F_{spherical,calc}$ is obtained as just described and $F_{multipole,calc}$ is the result of the multipole refinement. Both $F_{multipole}$ and $F_{spherical}$ must be calculated under identical conditions, with the same scale factor and

atomic positions. As shown on the preceding page, calculation of the structure factor, $F(\mathbf{H})$, includes a term, $T_n(\mathbf{H})$, for inclusion of the appropriate temperature factor. Electron densities calculated from structure factors, and thus dynamic maps, are subject to the effects of thermal motion arising during the data collection process. To remove the effects of thermal motion, static maps are also normally calculated during multipole refinement.

$$\delta\rho(\mathbf{r}) = \rho_{\text{multipole}} - \rho_{\text{spherical}}$$

In static maps, the electron densities are calculated directly in real space using the results from the multipole refinement.

$$\rho_{\text{atomic}}(\mathbf{r}) = P_c\rho_{\text{core}}(\mathbf{r}) + Pv(\kappa')^3\rho_{\text{valence}}(\kappa',\mathbf{r}) + \sum_l(\kappa'')^3R_l(\kappa''\mathbf{r})\sum_{m=-l}^{+l}P_{l,m}Y_{l,m}(\theta,\phi)$$

One final map should also be calculated during multipole refinement, the residual density map. It is a final difference map, $F_{\text{observed}} - F_{\text{multipole,calc}}$, and it should be as flat and featureless as possible by the end of the refinement. Table 1 lists a short summary of the electron density maps discussed in this section.

The procedure for the use of multipole refinement is now well established.[10] The flow scheme shown in Figure 2 summarizes the steps used in multipole refinement. There are certain essential conditions that must be met if meaningful and reliable results are to be obtained from an electron density analysis.[1,11,12] They are outlined below:

(1) The data must be properly corrected for absorption if such a correction is required.

(2) The effect of extinction on the data must be analyzed and corrected for, if required, since extinction forms one of the major obstacles in the

quantitative evaluation of charge densities. Its effect can be described as the weakening of the strong reflections due to the reduction of intensity of the incident beam along its path through the crystal. A distinction should be made between primary and secondary extinction, representing successive scattering processes in the same and different mosaic blocks of the crystal, respectively.

(3) The data must be redundant, collection of many equivalent reflections, to allow assessment of experimental accuracy.

(4) The x-ray data set must be as complete as possible to limit termination of series errors.

(5) The effect of multiple reflections must be considered through analysis of discrepancies between symmetry related reflections. Multiple reflection occurs if more than one reciprocal lattice points are simultaneously in the reflecting position. Under this condition, exchange of energy takes place between three beams (the incident and two diffracted rays) with the result that the weak reflections can be falsely strengthened and the strong ones weakened.

(6) Intensity measurements must be made as carefully and accurately as possible. Optimal scanning modes should be found and peak profiles analyzed to prevent multiple scattering and to allow for proper corrections for absorption and extinction.

(7) Measurement of the data should be carried out at low temperature. Low temperature measurement leads to an increase in resolution by making more high order data accessible. It reduces the temperature factors of the atoms and thus the amount of thermal smearing in the density maps. Finally it reduces the relative importance of thermal diffuse scattering.

Table 1. Electron Density Maps

Direct Fourier Maps

$$\rho(\mathbf{r}) = 1/V \sum_{\mathbf{H}} F(\mathbf{H}) \exp(-2\pi i \mathbf{H}\cdot\mathbf{r})$$

Difference Fourier Maps

$$\Delta\rho(\mathbf{r}) = 1/V \sum_{\mathbf{H}} [F_1(\mathbf{H}) - F_2(\mathbf{H})] \exp(-2\pi i \mathbf{H}\cdot\mathbf{r})$$

where (a) Difference Map

$F_1 = F_{observed}$
$F_2 = F_{calculated}$ (conventional refinement)

(b) $X\text{-}X_{HO}$ Deformation Map

$F_1 = F_{observed}$
$F_2 = F_{calculated}$ (parameters from high order refinement)

Multipole Refinement

(c) Experimental Deformation Map

$F_1 = F_{observed}$
$F_2 = F_{calculated,spherical}$

(d) Dynamic Deformation Map

$F_1 = F_{calculated,multipole}$
$F_2 = F_{calculated,spherical}$

(e) Static Deformation Map

$$\delta\rho(\mathbf{r}) = \rho_{multipole} - \rho_{spherical}$$

(f) Residual Map

$F_1 = F_{observed}$
$F_2 = F_{calculated,multipole}$

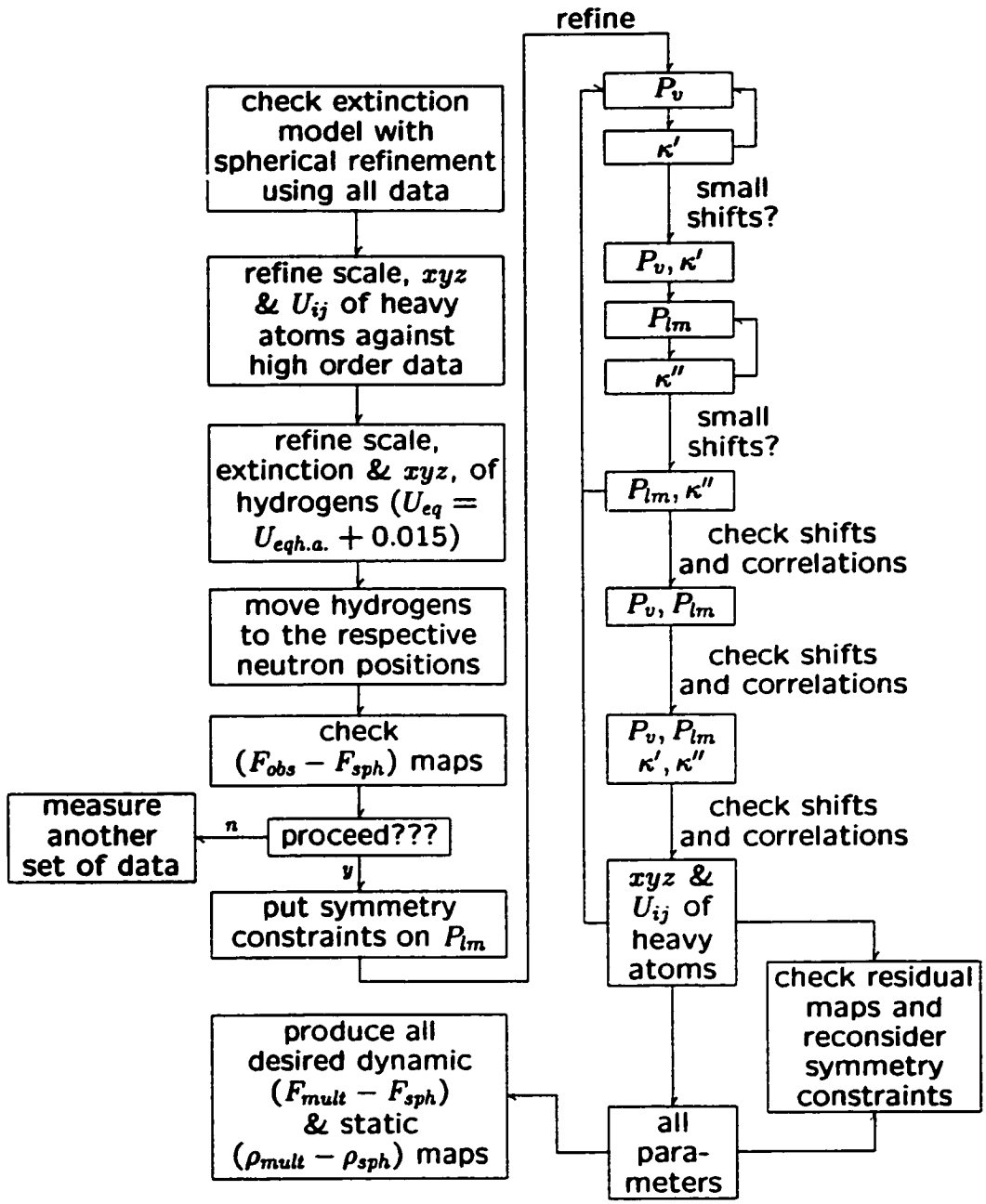

The strategy of multipole refinement to the model given by

$$\rho(r') = \sum_k^{atoms} P_{kc}\rho_{kc}(r) + P_{kv}\kappa'^3\rho_{kv}(\kappa' r) +$$
$$\sum_{l=0}^{L}\sum_{m=-l}^{l}(P_{klm}\kappa''^3\frac{\zeta_{kl}^{n_{kl}+3}}{(n_{kl}+3)!}(r\kappa'')^{n_{kl}}\exp(-\zeta_{kl}r\kappa'')Y_{klm}(\theta_k,\varphi_k))$$

Figure 2. Flow scheme summarizing the strategy utilized in the multipole refinements.

Only certain systems are suitable for collection of the high quality data necessary for electron density analysis. The crystal should be stable, both in the x-ray beam and at the low temperature required for data collection; it should not undergo any destructive phase transitions on cooling. It is better if it does not suffer appreciably from absorption or extinction, as can be the case if there are heavy atoms in the structure. A wide variety of compounds have been the subject of electron density studies. These include small organic molecules, biologically active molecules, carcinogens, drugs, neurotransmitters and transition metal complexes.[13] Multipole refinement gives parameters from which properties such as d-orbital populations, electrostatic potentials, dipole moments and net atomic charges can be obtained.

1.3. Topological Analysis of the Electron Density

The concept of atoms and bonds in molecules is of great importance to chemistry, yet it defies precise numerical definition. In an attempt to quantify the concept of chemical bonding, R.F.W. Bader has proposed a topological theory of "Atoms in Molecules".[14,15] In this approach a rigorous quantum mechanical definition of atoms and bonds is developed based on the properties of the electron density. Bader has pointed out that the topology of the charge density function, $\rho(\mathbf{r})$, as determined by its gradient field, $\nabla\rho(\mathbf{r})$, allows the structure of a molecule to be uniquely defined. From the electron density, interactions occurring between the constituent atoms, structural stability and reactivity, and the properties of the atoms in the molecule can be determined.

The dominant concept of chemistry is that of an atom in a molecule

with a determinable and characteristic set of properties. The physics of an atom in a molecule is that of an open system, one which is free to exchange charge and momentum with neighbouring atoms. To extend the predictions of physics to chemistry, it is necessary to generalize quantum mechanics to a subsystem (atom) of the total system (molecule). Such a generalization is possible only if the open system satisfies a particular boundary condition.

The aforementioned boundary condition demands that the flux in the gradient vector field of the charge density vanish at every point on the surface, $S(\Omega,\mathbf{r})$, that bounds the open system, Ω. The surface is one of zero flux in $\nabla\rho(\mathbf{r})$.

$$\nabla\rho(\mathbf{r})\cdot\mathbf{n}(\mathbf{r}) = 0$$

where $\mathbf{n}(\mathbf{r})$ is a unit vector normal to the surface S.

Because the boundary is defined in terms of the electronic charge density, the quantum subsystems are defined in terms of real space. The dominant topological feature of a molecular charge distribution is that it exhibits maxima at the positions of the atomic nuclei. Combining this feature with the zero flux boundary condition leads to the partitioning of a molecular system into a set of disjointed spatial regions, with each region normally containing only a single nucleus. These regions are identified with the chemical atoms. An atom is thus defined as a region of real space bounded by a set of interatomic surfaces, there being one such surface for each neighbouring atom. Each surface is unique as it exhibits a local zero flux in the gradient field for all points on the surface. The zero flux surfaces are the interatomic surfaces or quantum mechanical boundaries of the atoms.

Once the boundary condition has been met, one obtains the definition of an atom in a molecule and prediction of its properties becomes possible. Inseparable from the quantum definition of an atom in a molecule is the definition of the bonds which link the atoms to yield the molecular structure. In the Bader theory, bonds are defined by their critical points, as described below.

The topological analysis of the properties of a scalar field such as the electron density, $\rho(\mathbf{r})$, are summarized in terms of their critical points, r_c, the points where the first derivatives of the density are equal to zero. The gradient vector of the density in a Cartesian coordinate system $(\mathbf{i},\mathbf{j},\mathbf{k})$ is defined as

$$\nabla\rho(\mathbf{r}) = \mathbf{i}\cdot\delta\rho(\mathbf{r})/\delta x + \mathbf{j}\cdot\delta\rho(\mathbf{r})/\delta y + \mathbf{k}\cdot\delta\rho(\mathbf{r})/\delta z$$

At every critical point, $\nabla\rho(\mathbf{r})$ equals zero because each of the three contributions to the above equation are zero. The gradient will be zero for maxima, minima or saddle points in the electron density. For this reason, critical points are classified by the behaviour of the second derivatives of the density at the critical point, $\nabla^2\rho(\mathbf{r})$.

The Hessian matrix, $H(\mathbf{r})$, is defined as the symmetric matrix composed of the nine second derivatives of the density, $\delta^2\rho/\delta x_i\delta x_j$. Since it is real and symmetrical, the Hessian matrix can be diagonalized. The eigenvectors which result are the principal axes of curvature of the electron density at the critical point. The eigenvalues, λ_1, λ_2 and λ_3 $(\lambda_1\leq\lambda_2\leq\lambda_3)$, characterize the curvature of the electron density at the critical point being considered and are used to determine the rank and signature of the critical point. The rank of the curvature at a critical point is equal to the number of non-zero eigenvalues. The signature at a

critical point is the sum of the signs of the eigenvalues. The critical point is classified as being of type (rank,signature).

The critical points for a stable molecule in a three dimensional scalar field are normally always of rank +3. There are four possible signature values, ±1 or ±3, for a total of four different types of critical points.

(3,-3) Peaks, where all curvatures/eigenvalues are negative and the electron density is a local maximum at the critical point. Nuclear positions, which always exhibit maxima in the electron density, behave topologically as (3,-3) critical points in the charge distribution.

(3,-1) Passes or Saddle Points, where two curvatures are negative at the critical point. The electron density is a maximum in the plane defined by these atoms. The electron density is a minimum at the critical point on the third axis which is perpendicular to the first two. (3,-1) critical points are found between every pair of nuclei considered to be linked by a chemical bond. Being the most important type of critical point for this work, they are discussed more thoroughly below.

(3,+1) Pales, where two curvatures are positive at the critical point and the electron density is a minimum in a plane defined by these axes of curvature. The electron density is a maximum at the critical point along the third axis which is perpendicular to the plane. (3,+1) critical points are found at the centers of rings of bonded atoms.

(3,+3) Pits, where all the curvatures are positive and the electron density is a local minimum at the critical point. (3,+3) critical points are associated with cage structures, being found in the interior of a cage of bonded atoms.

The function $\nabla\rho(\mathbf{r})$ defines a field of vectors directed at each point along the gradient of the charge density. The gradient vectors originate at infinity and at critical points of positive curvature and terminate at points of negative curvature, usually atomic nuclei. The nuclei are the attractors of the gradient vector field of the charge density and the result is a partitioning of the total space of a system into a set of disjointed mononuclear regions or basins. A basin is the open region of space traversed by all the trajectories of $\nabla\rho(\mathbf{r})$ terminating at a given attractor. The union of a basin and its attractor is an alternate quantum mechanical definition of the atom.

The eigenvectors associated with the two negative eigenvalues of a (3,-1) critical point generate a set of gradient paths all of which terminate at the critical point and which define a zero flux interatomic surface. The positive eigenvalue of a (3,-1) critical point defines a unique pair of eigenvectors each of which originates at the critical point and terminates at a neighbouring nucleus. They define a line linking the two nuclei whose basins share an interatomic surface and along which the charge density is a maximum with respect to any neighbouring line. The presence of such an interaction line linking the two nuclei implies that the two atoms are bonded to one another and the line joining them is then termed a bond path.

At the bond critical point, the principal curvature (λ_3) is positive because the electron density is a minimum and increases along the bond path in both directions towards the bonded atoms. The remaining curvatures are both negative (λ_1 and λ_2) because the electron density is decreasing in all other directions. At the bond critical point the electron density

is a minimum along the bond path but it is a maximum in the plane defined by λ_1 and λ_2.

The existence of a (3,-1) critical point and an interaction line/ bond path indicates that electronic charge density is accumulated between the nuclei that are so linked, a necessary condition if two atoms are to be bonded. However, a bond path is not to be understood as necessarily representing a traditional "bond". A bond path can be associated with all types of interatomic interactions including hydrogen bonds and van der Waals interactions. Chemical structure can thus be recovered as a property of the charge distribution. The strength and nature of the chemical bond can be characterized by the value of various properties evaluated at the bond critical points.

For bonds between a given pair of atoms it is possible to define a bond order, whose value is determined by $\rho_b(\mathbf{r})$, the value of the charge density at the bond critical point. The extent of charge accumulation in the interatomic surface and along the bond path increases with the number of bonding electron pairs and this increase is mirrored by the value of $\rho_b(\mathbf{r})$. The value of the electron density at the critical point of a bonding interaction is thus a measure of its strength.

In a bond of cylindrical symmetry, the negative curvatures of the electron density at the (3,-1) critical point are of equal magnitude (λ_1 and λ_2). However, if electronic charge is preferentially accumulated in a given plane along the bond path, as it is in a bond with π character for example, then the rate of fall off in the electron density is less along the axis lying in this plane than in the one perpendicular to it. As a result the magnitude of the corresponding curvature is smaller (λ_2 - note

that λ_1 and λ_2 are negative values and $\lambda_1 \leq \lambda_2 \leq \lambda_3$). If λ_2 is the curvature of smallest magnitude, then the ellipticity of the bond, ϵ, is defined as

$$\epsilon = [(\lambda_1 / \lambda_2) - 1]$$

The ellipticity of a bond provides a measure of the extent to which charge is preferentially accumulated in a given plane. The axis of the curvature λ_2, the less negative minor axis, determines the relative orientation of this plane within the molecule. For σ type bonds, $\epsilon = 0$ and for bonds with increasing π character ϵ also increases.

Another important function used in the classification of (3,-1) bond critical points is the value of the Laplacian of the electron density at that point, which is defined as

$$\nabla^2\rho(\mathbf{r}) = \delta^2\rho(\mathbf{r})/\delta x^2 + \delta^2\rho(\mathbf{r})/\delta y^2 + \delta^2\rho(\mathbf{r})/\delta z^2$$

The Laplacian is scalar, invariant under rotation of the coordinate system and, as already mentioned, is equal to the trace of the Hessian matrix.

$$\nabla^2\rho(\mathbf{r}) = \lambda_1 + \lambda_2 + \lambda_3$$

The sum of the three principal curvatures is equal to the Laplacian of the electron density at the critical point. The sign of the Laplacian may be positive or negative depending on the relationship of the three eigenvalues. The Laplacian can be related to the character of the atomic interaction and results in a natural division of such interactions into two types.

$\nabla^2\rho_b(\mathbf{r}) < 0$	Shared Interactions
	Covalent or Polar Bonds
$\nabla^2\rho_b(\mathbf{r}) > 0$	Closed Shell Interactions
	Ionic or Hydrogen Bonds, van der Waals contacts

The Laplacian of the electron density has physical meaning as

representing local concentrations of charge where $\nabla^2\rho_b(\mathbf{r}) < 0$ and local depletions of charge where $\nabla^2\rho_b(\mathbf{r}) > 0$. Electronic charge is compressed above its average charge distribution in regions where the Laplacian is negative and expanded relative to its average distribution where the Laplacian is positive.

The formation of an interatomic surface and chemical bond is a result of competition between the perpendicular contractions of the electron density, which lead to a concentration of electronic charge along the bond path, and the parallel expansion of ρ which leads to its depletion in the surface and to its separate concentration in the basins of the neighbouring atoms. In (3,-1) critical points, negative values of λ_1 and λ_2 measure the degree of contraction of the electron density toward the critical point perpendicular to the bond path. The positive λ_3 value measures the degree of electron density contraction toward each of the nuclei along the bond path. The sign of the Laplacian indicates which of these two effects is dominant.

When $\nabla^2\rho_b(\mathbf{r}) < 0$ the perpendicular contractions of the electron density dominate the interaction, tending to decrease the magnitude of λ_3 and increase the magnitudes of λ_1 and λ_2. The charge is accumulated and concentrated in the region of space between the nuclei along the bond path. The result is a sharing of the charge by both atoms (the shared interaction) and a relatively large value of $\rho_b(\mathbf{r})$. Covalent and polar bonds are examples of shared interactions.

The opposite extreme to a shared interaction occurs when two closed shell systems interact, as found in ionic, hydrogen bonded or van der Waals contacts. In such closed shell interactions, the requirement of the

Pauli exclusion principle leads to the removal of electron density from the region of contact. The positive curvature of ρ along the bond path is dominant (λ_3), $\nabla^2\rho_b(\mathbf{r}) > 0$, and the interaction is characterized by the contraction of the electron density away from the interatomic surface and by its concentration in the regions of the nuclei. In closed shell interactions electron density is not accumulated in the bond and they are thus characterized by relatively low values of $\rho_b(\mathbf{r})$.

In general, intermolecular interactions, which tend to be closed shell type interactions, give rise to critical points with much smaller magnitudes for $\rho_b(\mathbf{r})$ and $\nabla^2\rho_b(\mathbf{r})$. However, small values for the electron density for the bond critical point in closed shell interactions do not necessarily imply weak interactions. While the values of $\rho_b(\mathbf{r})$ for highly ionic interactions are small in value, the transfer of charge from one atom to another results in a strong interaction. Although the values of $\rho_b(\mathbf{r})$ are smaller for ionic interactions, they still reflect bond strength/order if ranked. Closed shell interactions between neutral atoms, van der Waals type interactions, are in general truly weak, with small values of the electron density and the Laplacian at the bond critical point.

Although not particularly considered in this work, the Laplacian of the electron density has one other important feature of use to chemists. The topology of the electron density gives a faithful mapping of the chemical concepts of atoms, bonds and structure. However, there is no evidence of maxima in ρ corresponding to the localized electron pairs described in the Lewis/VSEPR models of electronic structure, of great importance in the interpretation of chemical reactivity and geometry. The Laplacian distribution recovers the electronic shell model of an atom by

exhibiting a corresponding number of pairs of shells of charge concentration and charge depletion. For a spherical free atom, the outer or valence shell of charge concentration contains a sphere of uniform electronic charge. Upon entering into chemical combination this shell is distorted and maxima, minima and saddle points appear. The maxima correspond in number, location and size to the localized pairs of electrons assumed in the Lewis and VSEPR models. A local charge concentration is a Lewis base site or nucleophile, while a local charge depletion is an area of Lewis acidity or electrophilicity. A chemical reaction corresponds to the combination of complementary features of the valence shell of charge concentration of the acid and base. The Laplacian distribution can thus be used to locate possible sites of chemical reactivity within molecules.

While the Bader theory of "Atoms in Molecules" was initially developed for the analysis of theoretical densities, it is equally applicable to model densities derived from experimental data. Once the absolute values of structure amplitudes have been obtained from the intensities of reflections measured in an x-ray diffraction experiment and their phases have been calculated using an appropriate structural model, the problem of electron density reconstruction is reduced to a choice of method. The electron density can be calculated from a Fourier series with complex structure factor amplitudes as coefficients or it can be calculated directly in real space by fitting some model (multipole) of the structure to those amplitudes.

The experimental electron density calculated from a Fourier series is a dynamic function because it includes the effects of thermal motion. Also, it is subject to truncation effects because of the finite amount of

data collected. These are especially significant in those regions of space where the electron density varies most rapidly, for instance near nuclei. These distortions are magnified even more in the functions $\nabla\rho(\mathbf{r})$ and $\nabla^2\rho(\mathbf{r})$. The density obtained from the Fourier transform of the structure factors is, therefore, generally not suited for the purpose of generating an electron density distribution suitable for topological analysis because of thermal smearing, truncation effects and experimental noise. Models of the electron density reconstructed by fitting to the experimental structure amplitudes are, to a large extent, free from the effects of a limited resolution Fourier series. Such static electron densities, generated using an aspherical, multipole model are preferred for topological analyses. However, highest quality data are still required for an accurate model to be developed if topological analysis is to be meaningful.

One other handicap of the "Atoms in Molecules" quantum theory developed by Bader should be mentioned. It does not support the notion of free molecules. When two molecules are treated as one system, they are always linked by at least one atomic interaction line even if their interaction is negligibly small. The topological approach does not provide a fundamental distinction between the "normal" strong bonds found within molecules and the "bonds" resulting from weak interactions, usually intermolecular, such as van der Waals contacts.

Having said this, the quantum theory of "Atoms in Molecules" has been widely used and has received general acceptance. Its application to experimental x-ray crystallographic results has been greatly enhanced by the aspherical, multipole model of atomic density. Topological analysis

permits the investigation of chemical systems on a common basis, as the theory uses only information contained in the electron density. The electron distribution is of fundamental importance as it is a physical observable and from its topological analysis all static and reactive properties of a system can be characterized. The "Atoms in Molecules" theory has proven to be a feasible approach in describing both chemical bonds and nonbonding interactions in crystal structures.

1.4. Hydrogen Bonding[16,17]

The concept of hydrogen bonding was first introduced to a wide audience by Linus Pauling in the first edition of his book, "The Nature of the Chemical Bond", published in 1939.[18] In a hydrogen bond, a proton donor, X-H, interacts with an acceptor atom or group, A, resulting in the formation of X-H...A. The geometry of the hydrogen bond is described by an X...A distance, which is a function of the X-H covalent bond length, the hydrogen bond length, H...A, and the angle X-H...A.

At first, hydrogen bonding was only recognized between molecules containing hydroxyl (-OH) or amino ($-NH_2$) donor groups, with carbonyl or hydroxyl groups as acceptors. Since that time, many other hydrogen bond donor and acceptors have been identified, leading to an explosion in the literature on hydrogen bonding. It is now recognized that X of the X-H donor need not be particularly electronegative, and that in certain situations even C-H can act as a hydrogen bond donor. Hydrogen bond acceptors are even more varied, with the lone pair of an electronegative atom/group or the π electrons of an unsaturated system being capable of acting in such a capacity.

A hydrogen bond is an attractive force that arises between a donor pair, X-H, in which the hydrogen is covalently bound to a more electronegative atom, X, and to its nearest neighbour, another electronegative atom or group, A, the acceptor.

$$\overset{\delta-}{X} \text{ ---- } \overset{\delta+}{H} \text{ ..... } \overset{\delta-}{A} \text{ ---- } \overset{\delta+}{Y}$$

The electron of the hydrogen atom is involved in the X-H covalent bond, resulting in its electron density being displaced relative to the nucleus, in the direction of X along the X-H bond. The proton is descreened, giving rise to a positive dipole at H, irrespective of whether X itself is electronegative or carries a net charge. It is the Coulombic interaction of the positive dipole at hydrogen with excess electron density at the acceptor atom(s) that results in the formation of the hydrogen bond. Because of the hydrogen bonding interaction between hydrogen of the donor and the acceptor, the covalent bond X-H is lengthened relative to its "free" value. The lengthening of X-H increases with increasing strength of the hydrogen bond, that is with decreasing H...A separation. There is some directional character to the hydrogen bonding interaction but it is much less pronounced than in a covalent bond and for "normal" hydrogen bonds the interaction is primarily electrostatic.

On proceeding from left to right across the periodic table, the elements become more electronegative as the additional charge on the nucleus is increasingly less well screened by the additional electron, even though the overall charge always remains neutral. The proton in the X-H bond is increasingly descreened as X becomes more electronegative on proceeding from carbon to fluorine; the dipole at hydrogen becomes increasingly larger and more positive. For this reason, the strongest

hydrogen bonds tend to involve hydrogen bonded fluorine and the weakest to involve C-H donors. The strength of the hydrogen bond interaction will also be affected by charge resident on the donor or acceptor atoms, if they are cationic or anionic. With very electronegative donor and acceptor atoms, the hydrogen bond becomes more covalent in nature, while with weakly electronegative atoms as donor and acceptor the interaction is primarily Coulombic in nature.

The stabilization accompanying the formation of a covalent bond comes from the overlap either between partially occupied orbitals or between the HOMO of an electron donor and the LUMO of an electron acceptor. When a van der Waals contact is formed, the bonding orbitals are completely occupied. Interaction between completely occupied orbitals leads to destabilization via repulsion, particularly at close distances. The stabilization of intermolecular contacts, including van der Waals contacts and hydrogen bonds, originates from the interactions between (1) permanent multipoles, (2) a permanent multipole and an induced multipole and (3) an induced multipole and an instantaneous (time variable) multipole. The respective energy terms are (1) Coulombic, (2) induction and (3) dispersion type. The second and third terms are attractive, while the Coulombic term can be either attractive or repulsive depending on the mutual orientation of the multipoles; in the hydrogen bonding situation, it is attractive. In most "normal" hydrogen bonds, the Coulombic energy term is dominant while the induction and dispersion terms are less important, contributing only a small fraction to the stabilization. Only in the strongest hydrogen bonds is a covalent interaction an important component of the stabilization.

The above considerations indicate that a completely electrostatic description of the hydrogen bond is often too simplistic and insufficient for many purposes. In very general terms, the contributions of the different components to the total hydrogen bond energy can be broken into four parts. (1) The repulsion or exchange energy which arises from interactions between filled orbitals. This repulsive term is operative at only very short separations and falls off rapidly with increasing distance. (2) The electrostatic energy which can, in turn, be decomposed into a number of different terms arising from the interactions of (a) two permanent multipoles (Coulombic forces), either monopole/monopole (or ion/ion), monopole/dipole (or ion/dipole) or dipole/dipole and (b) a permanent dipole with an induced multipole (Induction forces), either monopole/induced dipole (or ion/induced dipole) or dipole/induced dipole. (3) The polarization or dispersion energy results from the formation of an instantaneous multipole (dipole) in a molecule because of polarization of its electron density. The momentary dipole induces a complementary, momentary dipole in neighbouring atom(s), resulting in a small attractive force. [This is the only attractive interaction formed between neutral molecules containing no permanent multipoles.] (4) The charge transfer or covalent energy is an important contributor to the total energy in strong hydrogen bonds. Intermolecular charge transfer (when present) establishes an at least partially covalent bond between the interacting H(X) atom and the acceptor group of the hydrogen bond. It is often described as the formation of a molecular orbital by donation of electron density from the HOMO of the hydrogen bond acceptor (a lone pair of electrons or π electron density) to the LUMO of the hydrogen bond donor (normally the X-H

antibonding orbital). For this work, particularly in the discussion of the electron density maps generated, a simple partitioning of the hydrogen bond into electrostatic and covalent components is adequate, still an idea of the different contributors to the total hydrogen bond energy is useful.

The Coulombic component of the energy is reduced with increasing distance and with lesser dipole moments or charges involved. For very weak hydrogen bonds, such as C-H...acceptor, the electrostatic component is of similar magnitude to the van der Waals forces. The energies of the weakest hydrogen bonds are very small and difficult to measure accurately by experimental means. C-H...O interaction energies are typically 6 kJ/mol or less and gradually fade away with increasing H...O separations.

Strong and weak hydrogen bonds have very different properties. In strong hydrogen bonds, most of the structural distinction between the covalent X-H bond and the H...A hydrogen bond disappears and the hydrogen atom lies near the midpoint of X...A. Both X-H and H...A have covalent character and the overall geometry of a strong hydrogen bond tends to be quite symmetrical. Examples of strongly hydrogen bonding groups include F-H...F, $^{+}$O-H...O and O-H...O^{-}. Strong hydrogen bonds are short, nearly linear, always unbranched and are highly directional. They are at the high energy end of the hydrogen bond range, 40 kJ/mol or more, compared to less than 20 kJ/mol for normal hydrogen bonds.

The distinction between strong and moderate hydrogen bonds is difficult to define precisely. There is a continuum with respect to most properties from the strongest to the weakest hydrogen bonds. However, there are certain features characteristic of normal or moderate hydrogen bonds. In normal hydrogen bonds, the hydrogen is always unsymmetrically

located, so that one bond is clearly covalent, X-H, while the other interaction(s) can be identified as the electrostatic hydrogen bond(s), H...A. A wide range of H...A distances and X-H...A angles are possible depending on the strength of the interaction and other environmental factors.

Normal hydrogen bonds are "soft" interactions, meaning that they are easily deformed by other intermolecular interactions in the crystal, including other hydrogen bonds and van der Waals contacts. The environmental forces acting within a crystal structure tend to have an overall compression effect, so that a mean hydrogen bond length determined experimentally is generally shorter than that found in the gas phase or calculated for an isolated hydrogen bond. The hydrogen bond lengths and angles found in a given structure depend very much on the environment in which they are observed; the observed values for a given type of bond can vary greatly from one structure to another and even within the same structure.

Hydrogen bond geometry, for a particular class of hydrogen bond, is best described by a statistical analysis of a large group of similar bonds, from which the effective equilibrium bond length and angle can be calculated. If sufficient data are available, the means obtained should be accurate and the distribution of values should be Gaussian. Calculation of the effective equilibrium bond lengths and angles minimizes the effects of other crystal packing forces on the values; individual results can vary by up to ±20% from the group mean.

The normal hydrogen bonds observed in crystal structures are rarely linear. Because of the "softness" of the hydrogen bond bending force constants, the X-H...A angle averages 160±20°. This is not to say,

however, that the linear configuration is not inherently the most stable for an isolated, unbranched hydrogen bond.

The weaker the hydrogen bond, the less are the associated directional characteristics of the bond and the more likely it is to be branched. Currently, the terms "bifurcated" and "three-centered" are used interchangeably in the literature to describe branched hydrogen bonds where a single hydrogen atom is shared between two acceptors.

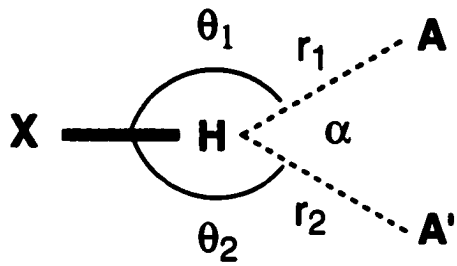

However, the term bifurcated has also been used to describe the rare situation where two protons on the same donor share a single acceptor. To avoid confusion, the term three-centered was introduced to describe the former situation, although bifurcated is still also commonly used.

In the three-centered hydrogen bond, the hydrogen atom is bonded to three other atoms, one by the covalent bond, X-H, and two by hydrogen bonds, H...A,A'. The hydrogen atom should lie close to the plane defined by X, A and A' and the sum of the three angles around hydrogen ($\theta_1 + \theta_2 + \alpha$) should be close to 360°.

Three-centered hydrogen bonds are commonly moderate to weak and found in structures that are proton deficient, where there are more

possible acceptors than there are protons available for bond formation. Three-centered bonds can be symmetrical (A = A', $r_1 \approx r_2$ and $\theta_1 \approx \theta_2$) or, more frequently, unsymmetrical. An asymmetric bond can be described as one normal hydrogen bond perturbed by an additional longer range hydrogen bonding interaction. In the unsymmetrical bond, the acceptors may be the same or different types of atoms and r_1 and r_2 can vary considerably in length (up to 1Å) even if A and A' are the same atom type. The two angles (θ_1 and θ_2) will also be quite different, with one closer to 180° and the other closer to 90°. Both the stronger (major) and weaker (minor) components of the three-centered hydrogen bond will be primarily electrostatic in nature.

While three-centered or bifurcated hydrogen bonds are common, four-centered or trifurcated hydrogen bonds are known but occur much less frequently. The geometric definition is less rigorous than that for three-centered bonds, since it requires only that the X...A,A',A" angles all be greater than 90°. A number of other unusual hydrogen bond geometries have been described in the literature, particularly in the past few years as hydrogen bonding has been more thoroughly investigated.

The hydrogen bonds within a structure can be isolated from one another. They can occur in clusters, resulting in the formation of dimers, trimers, etc. Or, they can occur in a regular, connected arrangement throughout a structure, resulting in the formation of long range networks, extended two or three dimensional arrays. Hydrogen bonds display the property of cooperativity, meaning that the influence of hydrogen bonding on a given structure is greater than would be expected based on the contribution of the individual bonds. The hydrogen bond energy of a

network of linked hydrogen bonds is greater than the sum of the energy of the individual hydrogen bonds. Two types of hydrogen bond cooperativity have been recognized: σ cooperativity where the hydrogen bonds are linked by covalent bonds and polarization occurs through the σ bonds and π cooperativity which requires that adjacent hydrogen bonds be linked by bonds with π electron character. Polarization in the latter occurs through the multiple bonds and for this reason it is sometimes referred to as resonance assisted hydrogen bonding.

Hydrogen bond formation modifies the electronic structure of the molecules/ions involved, to an extent dependent on the strength of the interaction. The perturbation of the electronic structure at the donor and acceptor can extend to their adjacent bonds, depending on the polarizability of the bonding in the molecules/ions. It is greatest in conjugated systems where π cooperativity can arise. Changes in the nonhydrogen bonded, covalent bond lengths in the molecule/ion can occur in the vicinity of the hydrogen bond, X-R or A-Y. For weak hydrogen bonds there are negligible changes in the lengths of the bonds surrounding X and A.

In the earlier days of crystallography, it was often impossible to locate the hydrogen atoms in a crystal structure determination (see below). For this reason, hydrogen bonds were often described by the length of the separation of the nonhydrogen atoms, X...A. For hydrogen bonding to arise, it was considered necessary that the X...A distance be less than the sum of the van der Waals radii of X and A. Unfortunately, this van der Waals radii cutoff criterion was ill-conceived for a number of reasons. However, the sum of the van der Waals radii can still serve as a useful limit at which to first look for hydrogen bonding interactions.

Hydrogen bonds and van der Waals contacts are fundamentally different in their directional characteristics. Hydrogen bonds are directional with linear or nearly linear geometries favoured energetically over bent ones. In contrast, van der Waals contacts are isotropic, with interaction energies normally independent of the contact angle. Weak hydrogen bonds are long range, electrostatic interactions that attenuate with r^{-1}, where r is the separation distance. In comparison, exchange and dispersion forces fall off with r^{-6}, meaning they will become negligible more quickly, at shorter distances, than hydrogen bonds. Hydrogen bonding interactions will still be significant at distances where van der Waals forces no longer have an effect. The concept of looking for hydrogen bonding only at distances of less than the sum of the van der Waals radii of the X and A atoms was incorrect. It also led to the incorrect assumption by some authors that hydrogen bonds become van der Waals interactions at longer distances; it is the electrostatic component of the hydrogen bond that prevails at longer distances. Finally, it delayed recognition of the importance of the three-centered hydrogen bond which tends to have one component at a longer distance, often beyond the arbitrarily chosen cutoff distance.

A further difficulty can arise because in many situations involving hydrogen bond formation the van der Waals radii of the interacting species can be hard to define. For an atom in a bonding situation the van der Waals surface can be far from spherical, with the electron density polarized in specific directions. This is true for the easily polarized hydrogen atom and is equally possible for the lone pairs on many acceptor atoms. The correct choice of van der Waals radii becomes difficult, and

the wrong choice could lead to an even lower cutoff being used to limit the search for hydrogen bonds.

The use of the X...A distance to characterize hydrogen bonds has another problem associated with it. The X...A separation is a function of the covalent bond length, X-H, and the angle X-H...A. As a consequence of repulsive forces, the X...A distances tend to remain relatively constant, while permitting large variations in H...A lengths and X-H...A angles. The hydrogen bond lengths, H...A, and angles, X-H...A, are clearly more sensitive criteria than X...A distances with which to characterize hydrogen bonds, despite any problems of accuracy in locating hydrogen atoms using x-ray crystallography.

It is an unfortunate limitation of crystallography that the position of a hydrogen atom can be difficult to locate accurately; even in the recent past, it was often impossible to determine hydrogen positions using x-ray diffraction. The ability of an atom to scatter x-rays is proportional to the square of its atomic number (the number of electrons). The hydrogen atom, with its one electron, consequently diffracts very little. Its position can be difficult to determine even in compounds where the remaining atoms are relatively light (C,N,O,etc.). Recently, the quality of data, available from CCD and area detectors collected at low temperatures, has improved. This has allowed hydrogen positions to be more frequently located from the Fourier difference map and it is becoming more common for hydrogen coordinates with isotropic temperature factors to be refined during the least squares process. Still, the precision of location of hydrogen atoms is usually only about one tenth that of the heavy atoms.

Sometimes, it is possible to overcome the limitations of locating

hydrogen atoms by x-ray crystallography using simple geometric arguments. For example, in molecules/ions which contain R_3NH^+, R_2NH or conjugated NH_2 donor groups, hydrogen atoms can be placed in reasonable positions based on the location of nitrogen and assuming standard N-H covalent bond lengths and angles. However, for groups where there is rotational freedom, such as $-NH_3^+$, $-NH_2$ or -OH (particularly in water) the hydrogen positions can only be established by accurate x-ray analysis or, better, by neutron diffraction.

The position of a hydrogen atom can be determined with confidence using neutron diffraction, in which neutrons are diffracted by the nuclei of atoms in a single crystal. The absolute neutron scattering amplitude of the proton is only about one half that of the heavier atoms C, N and O, so neutron diffraction is more effective for determining the positions of light atoms in the presence of heavier ones. Moreover, the nucleus is small compared with the neutron wavelengths (~1.0 to 1.5Å) so the scattering power does not fall off with the scattering angle as it does in x-ray diffraction. All this makes neutron diffraction useful for highly accurate studies of hydrogen bonds, since hydrogen atoms can be located with precisions equal to those of the other atoms.

There are, however, several problems associated with neutron diffraction studies in general, and with those of tetraphenylborate salts in particular. It is difficult to grow the large single crystals (~4mm^3 and ~5mg) required for successful neutron diffraction. In these compounds, the number of hydrogen atoms can be comparable to, or even exceed, the number of nonhydrogen atoms. The large incoherent neutron scattering cross section for hydrogen can create difficulties in such cases by adversely

affecting the signal to noise ratio. This problem can often be overcome by deuterium substitution since deuterium has a much lower incoherent scattering cross section than hydrogen. However, complete deuterium substitution, although effective, is often costly and difficult to achieve. If the replacement is not total, individual H/D occupation factors must be determined during the refinement making it more complicated.

Absorption is usually not a problem in neutron diffraction experiments. However, boron has a high thermal neutron absorption coefficient and absorption could become a problem in the neutron analysis of tetraphenylborate salts. Extinction, which is usually only a minor irritation in x-ray diffraction experiments, can be serious and pervasive in neutron diffraction. Extinction tends to have little effect on atomic positional parameters but a much larger effect on thermal parameters. Thorough corrections for extinction must be applied during neutron analysis, particularly if the results are to be scaled with x-ray data or if charge density studies are to be carried out.

Covalent X-H bond lengths determined by x-ray diffraction methods are generally different from those obtained by neutron diffraction. This difference arises because x-ray analysis determines the thermally averaged maxima of the atomic electron density while neutron diffraction determines the "true" nuclear atomic coordinates. For heavy atoms, these two are virtually indistinguishable but for hydrogen the difference is appreciable (~0.25Å). Polarization of the electron density at hydrogen towards X along the X-H bond leads to a significant difference in the position of the nucleus and the position of the electron maximum peak of the hydrogen

atom; the shift is greater the more electronegative X is.

The X-H distances obtained by x-ray analysis are always shorter (~0.1 to 0.3Å) than the X-H distances determined by neutron diffraction. The related H...A distances are correspondingly long. Normalization of covalent X-H bond lengths (x-ray values) to the appropriate neutron values is essential if the two types of results are to be compared. It is also important for statistical analysis of hydrogen bond data if both neutron and x-ray derived data are to be included. The corrections required are larger as X becomes more electronegative. Typical neutron diffraction values for X-H covalent bond lengths are 1.08Å (C-H), 1.02Å (N-H) and 1.00Å (O-H).

1.5. Charge Density Studies of Hydrogen Bonds

Description of the theoretical topology of bonds in general, and hydrogen bonds in particular, leads to an expectation of features to be found in deformation density maps. As discussed previously, hydrogen bonds possess a wide range of properties, from very short, very strong hydrogen bonds that are predominantly covalent in bonding character through a continuous range of intermediate strength bonds to finally long, weak hydrogen bonds that are primarily electrostatic in nature. Covalent contributions are not limited to the shortest bonds but decrease gradually as the hydrogen bond length increases.

By definition, the covalent bond is one where the two bonded atoms share electron density in the region of space between them. In this situation, the deformation density map would be expected to show accumulation of electron density between the bonded atoms with a maximum

of electron density between the nuclei. The weaker hydrogen bonds are classified topologically as closed shell interactions, primarily electrostatic in nature. In pure closed shell interactions, electron density is accumulated in the atomic wells and not in the region of space between the atoms; there is no sharing of electron density between the atoms. Such interactions should also generate characteristic features in deformation density maps. The dipole induced by hydrogen bond formation between the donor hydrogen and the acceptor lone pair should result in depletion of charge in the region of space between the two; a definite minimum should be observed somewhere between the two.

Since hydrogen bonds cover the entire range from covalent (strong) to electrostatic (weak), map features would also be expected to vary over a wide range. Maps of weak hydrogen bonds might show only very subtle features, difficult to identify and interpret, particularly in the face of experimental noise.

Do deformation density maps generated experimentally actually display the features expected for hydrogen bonds of different strengths? Consider first the strongest hydrogen bonds, those that can be proven topologically to have covalent type bonding. Maps of this strongest hydrogen bond type are difficult to locate in the literature.

In 1977, E.D. Stevens et al.[19] published a communication on the experimental electron density distribution of sodium hydrogen diacetate from a low temperature combined x-ray and neutron study. The authors report that large peaks were located on each side of the hydrogen near the midpoints of the O...H bonds in the deformation density map of the O...H...O' hydrogen bond. These peaks were found to merge into the ring

of electron density around each oxygen atom but they were farther from the nuclear positions than typical lone pair peaks. The peaks are evidence for a covalent/shared interaction for both O...H components in the short, symmetric hydrogen bond. The authors also note that no significant charge depletion was observed near the hydrogen atom as would have been expected if the hydrogen bond was primarily electrostatic.

Subsequently, B. Hsu and E.O. Schlemper[20] published "X-N Deformation Density Studies of the Hydrogen Maleate Ion and the Imidazolium Ion" in 1980. Deformation densities for the strongly hydrogen bonding, hydrogen maleate anion in two salts (imidazolium and calcium) were calculated from combined, room temperature x-ray and neutron data. The strong O-H..O hydrogen bond of the anion in the two structures is quite different, being nearly symmetric (although not restricted by crystallographic symmetry) in the former and markedly asymmetric in the latter. Deformation density maps of the two anions show common features for the hydrogen bonds. The density of one of the lone pairs on each oxygen center has been perturbed by formation of the hydrogen bond and moved into the region of space between H and O. The result is covalent type bonds visible between both O...H components of the O...H...O hydrogen bonds in both anions, supporting the results of Stevens et al.

A recent paper on the experimental crystal charge density of methylammonium hydrogen maleate by D. Madsen et al.[21] includes static deformation density maps in the planes of the two independent anions illustrating the very strong O...H/D...O intramolecular hydrogen bonds. These hydrogen bonds were also characterized topologically and their negative Laplacian values confirm the covalency of the interactions. The

static maps shown, $\rho_{multipole} - \rho_{spherical}$, are similar to those reported by Hsu and Schlemper[20] for the same type of anion, hydrogen maleate, but contain significantly more detail than the earlier room temperature study. The maps of Madsen et al. show depletion of the electron density at the proton in the center of the short, symmetric O...H/D...O hydrogen bond. Each oxygen atom in the O...H/D...O interaction clearly shows contours of electron density centered in the space between O and H, directly on the O...H/D...O interaction line. Each oxygen also has only one identifiable set of lone pair contours, as expected if the second lone pair is now involved in the covalent type hydrogen bond. This could be described as complete polarization of the oxygen lone pair density into the hydrogen bond, the extreme case of the weaker polarization seen in a normal hydrogen bond.

No such strong N-H...acceptor hydrogen bonds have ever been reported in the literature. The strongest N-H...A hydrogen bond that has been studied by multipole refinement and subsequent topological analysis of the electron density is the $[N\text{-}H...N]^+$ hydrogen bond characterized by P.R. Mallinson et al.[22] in the 1,2-dichlorohydrogen maleate salt of the proton sponge, 1,8-bis(dimethylammonium)naphthalene. Although the authors do not show deformation electron density maps of the hydrogen bond, they do report that the lone pair of the hydrogen bonded nitrogen is strongly polarized in the direction of N-H. It is unfortunate that the authors do not include maps of the hydrogen bonds in their publication, since the anion also contains a very strong O...H...O hydrogen bond, another example of the hydrogen maleate anion that behaves like a covalent interaction in terms of the topology at the hydrogen bond critical point. It would have

been expected that the maps of this hydrogen bond would have been similar to those described above.

Much of the early knowledge of charge density distributions in "normal" hydrogen bonds was generated as a result of the International Union of Crystallography's sponsorship of the Oxalic Acid Project. In the solid state α-oxalic acid dihydrate contains one short, relatively strong hydrogen bond from the acid to oxygen of a water molecule, O-H...O, and two weaker hydrogen bonds that go from hydrogens of water to oxygen of the acid (C=O). The deformation density of α-oxalic acid dihydrate was studied by a number of groups worldwide to see if a consistent picture would emerge, particularly in the hydrogen bonding regions.

E.D. Stevens and P. Coppens[23] published the results of their 100K multipole refinement in 1980. They found striking features in the map of the strong hydrogen bond, particularly the polarization of the water (acceptor) lone pair electron density towards the side of the molecule that accepts the hydrogen bond. This distortion of the nonbonding density from mirror plane symmetry at oxygen was one of the first clear examples of perturbation of an experimental density distribution by "normal" hydrogen bonding.

J. Dam et al.[24] published their results for the experimental determination of the charge density in α-oxalic acid dihydrate in 1983. Their results substantiate those of Stevens and Coppens, with the polarization of the water oxygen lone pair density even more clearly observed. More recently, D. Zobel et al.[25] have studied the experimental charge distribution of α-oxalic acid dihydrate at 15K. The thermal displacement parameters for the oxalic acid study at 15K were only about

one half the values found in the 100K study of Stevens and Coppens. The resulting maps showed much improved resolution but in the case of the strong O...H...O hydrogen bond the map had the same basic features, with electron density of the water oxygen lone pair polarized towards O-H of the hydrogen bond. Perturbation of the lone pair electron density of the acceptor towards the donor is now considered to be characteristic of strong to normal hydrogen bonds, with the degree of polarization proportional to the strength of the interaction.

It is interesting to note that little or no polarization of acceptor lone pair electron density was observed by any of the groups for the two weaker hydrogen bonds in oxalic acid dihydrate. This result emphasizes that these weak hydrogen bonds are again different in nature, having less of a covalent component and being more purely electrostatic. Electron density is not visibly polarized into the H...A internuclear region but remains isolated, and largely unchanged in distribution, at the atomic centers in the weakest hydrogen bonds.

Stevens and Coppens also observed a second important feature in the maps of <u>all</u> of the hydrogen bonds in α-oxalic acid dihydrate, a slight charge deficiency in the deformation density between the donor and the acceptor. Theoretical calculations of the electron density distribution by the authors showed that the charge deficiency was primarily due to the electrostatic contribution in the hydrogen bond. Zobel et al. also observed such charge deficient areas (minima) in their multipole maps of the hydrogen bonds in α-oxalic acid dihydrate, which they attributed to the electrostatic nature of the interaction.

Because of the experimental interest in the electron density

distribution of α-oxalic acid, a number of parallel theoretical studies have also been published, most notably by Stevens[26] in 1980 and by Krijn et al.[27,28] in 1988. The theoretical results support the experimental results in the hydrogen bonding regions for the most part. The density functional studies by Krijn et al. clearly indicated the polarization of the acceptor density towards the hydrogen atom of the donor in the static density maps that they generated.

Since the original work on α-oxalic acid dihydrate, many multipole refinements of crystallographic data to produce deformation density maps have been published. Hydrates containing several water molecules in different environments have proven to be a fruitful subject for the analysis of hydrogen bonding. Recently published examples are the multipole refinements of the crystal structures of $BeSO_4 \cdot 4H_2O$ and $NH_4[Ti(C_2O_4)_2] \cdot 2H_2O$ by T. Kellersohn et al.[29] (1994) and H.S. Sheu et al.[30] (1996), respectively. Both compounds contain relatively strong hydrogen bonds and in both papers the authors report that the lone pairs of the oxygen acceptor atoms are clearly polarized toward the hydrogen atom of the donor. Kellersohn et al. also describe an area of electron deficiency close to the hydrogen atoms involved in the hydrogen bonds.

The combination of charge depletion near hydrogen of the donor group and polarization of the electron density at the acceptor is seen, to a greater or lesser degree, in most charge density studies of hydrogen bonds. F. Hamzaoui et al.[31] in their multipole refinement of m-nitrophenol report a significant minimum (depletion) occurring close to the hydrogen atom, between it and oxygen, the acceptor in the O-H...O hydrogen bond. This they report as being consistent with an electrostatic description of

the hydrogen bond. They do not report any noticeable polarization of the electron density at the oxygen which accepts the rather long hydrogen bond; the O...O distance is roughly 2.9Å.

A 1991 publication by T. Koritsànszky et al.[32] discusses the hydrogen bonding in (18-crown-6)$_2$cyanamide in terms of the charge densities derived from a combined x-ray and neutron study at 100K. Deformations calculated by the authors in the planes formed by the N-H...O bridges between cyanamide and the crown ether ring showed no evidence of density accumulation midway between the proton and acceptor. This supports the hypothesis that the main contribution to the interaction is electrostatic, as is often observed for "weaker" hydrogen bonds. In addition, electron deficient areas around the central hydrogen atoms were recognized, which were interpreted as the result of increased polarization of the X-H bond in the field of lone pair electrons of the acceptor. Hydrogen bonding was found to lead to extra charge concentration in the lone pair region of the participating oxygen atoms in the direction of N-H (polarization). However, as no further charge accumulation was observed between the donor and acceptor, the authors characterize the hydrogen bond as primarily an electrostatic type interaction.

In another interesting publication from 1991, M. Souhassou et al.[33] describe the experimental charge density of *N*-acetyl-*L*-tryptophan methyl-amide, derived from x-ray data collected at 103K. The experimental results from a multipole refinement were also compared to the results from theoretical calculations. The authors found a significant density minimum in the experimentally derived map, in the region of space between hydrogen and oxygen in the N-H...O hydrogen bond. Although consistent with the

electrostatic description of the hydrogen bond, the authors urge caution in the interpretation of this result. They note that similar minima also occur on the experimental maps for other hydrogen atoms not involved in hydrogen bonding, and that they did not find corresponding minima in the theoretically calculated maps. These differences could arise, they feel, from artifacts of the hydrogen modelling in the experimental analysis. Any error in the hydrogen positions would produce strongly correlated errors in the hydrogen dipole populations. These correlations could be responsible for experimental minima near the hydrogen atoms being too large, indicating that the chosen C-H and N-H bond lengths were slightly too long. It appears from considering all the literature results that charge depletion in the region of the proton is an observable "true" feature in the deformation density maps of hydrogen bonds. However, this work cautions that it is a feature that can be over emphasized by poor modelling of the hydrogen atoms during multipole refinement.

One last publication, the multipole refinement of *L*-alanine from x-ray data collected at 23K by R. Destro et al.[34] (1988), focuses on features of the charge density arising from hydrogen bonding. Once again, the authors report that the most interesting feature of the deformation density maps is the clear polarization of the lone pair peaks of atom O(2) toward hydrogen atoms H(2) and H(3) from whom it accepts two hydrogen bonds. They observe a possible similar, but much weaker, distortion occurring for atom O(1), which is involved in only one, weaker hydrogen bond. Destro et al. also found electropositive regions separating the N-H donors from the acceptor oxygen atoms. Interestingly, they observed the electropositive potential between oxygen and hydrogen atoms to decrease

systematically as the N...O distance became smaller (most likely with the concurrent increase of covalency in the hydrogen bond).

P. Coppens in his book "X-ray Charge Densities and Chemical Bonding"[6a] includes an interesting section on the polarization of the electron density expected on hydrogen bond formation. He writes that ab initio SCF calculations on the water molecule show a depletion of the density of the lone pair in the internuclear region for long bonds, while for short bonds the effect is reversed. The induced polarization of the acceptor density towards the hydrogen atom is apparently still present for the longer distances, but very diffuse and below the lowest contour on most maps.

In summary, during hydrogen bond formation the hydrogen atom donates electron density into the X-H covalent bond, often polarized toward X, the heavy atom. There is a resulting depletion of charge at hydrogen. This depletion of charge near hydrogen results in attraction to the lone pair of the acceptor. The attraction between X-H and A may be purely an electrostatic, charge-based interaction (weaker). It may be covalent, with electron density shared between X-H and A (stronger), or it may be some intermediate combination of the two.

The electron density distribution which results from hydrogen bond formation should be identifiable in charge density maps. The concentration of electron density in the covalent X-H bond is accompanied by an electron deficiency near the proton. This deficiency/minimum is often isolated in the area between hydrogen and the acceptor. In the weakest hydrogen bonds this may be the only visible feature attributable to hydrogen bond formation but the charge depletion may still be considerable.

As the hydrogen bond becomes stronger, the electron density at the hydrogen bond acceptor shows evidence of polarization/perturbation in the direction of the X-H donor. The degree of polarization appears to increase with hydrogen bond strength, and may be accompanied by some degree of charge depletion at the acceptor. In the very strongest hydrogen bonds, peaks characteristic of covalent bonding, sharing of electron density, are found between X-H and H..A. This can be considered the ultimate polarization of the lone pair electron density of the acceptor.

When it occurs, hydrogen bonding must have an effect on the electron density distribution in a crystal structure. These effects should be visible in the deformation density maps calculated from crystallographic data. However, the changes can range from substantial in strong hydrogen bonds, to very small and subtle in maps of weak hydrogen bonds. The highest quality data and level of calculation are required if meaningful features are to be observed, especially if the hydrogen bonds are weak. Over interpretation of small map features must also be avoided.

1.6. Topological Analysis of Hydrogen Bonds

Since only minor features may be found in the deformation density maps of weakly hydrogen bonding species, investigators searched for a more quantitative approach with which to study the properties of the electron density distribution generated from high quality x-ray and neutron diffraction data. The topological approach of Bader[14,15] has proven to be such a method and is now widely used to calculate the electrostatic properties of molecules from experimental charge densities. In fact, topological analysis is now considered to be more informative and useful

than the deformation density maps themselves. Many authors no longer bother to include any plots in their publications on charge density studies.

Experimentally derived topological analyses of compounds containing N-H...acceptor hydrogen bonds are found in publications by R. Destro et al.[35] (*L*-alanine, 1988), W.T. Klooster et al.[36] (1-methyluracil,1992), S.T. Howard et al.[37] (*L*-dopa, 1995), C. Flensburg et al.[38] (methylammonium hydrogen succinate monohydrate, 1995), V.G. Tsirelson[39] (urea, 1996 and 1999), E. Espinosa et al.[40] (*L*-arginine phosphate monohydrate, 1996), K.L. MacCormack et al.[41] (*E*-tetraethyl-1,4-diammoniumbut-2-ene·2PF_6, 1997), P.R. Mallinson et al.[22] (1,8-bis(dimethyl-ammonium)naphthalene 1,2-dichlorohydrogen maleate, 1997), R. Bianchi et al.[42] (4-cyanoimidazolium-5-olate, 1998), D. Madsen et al.[21] (methylammonium hydrogen maleate, 1998) and recently, R. Flaig et al.[43] (D,L-aspartic acid, 1998). In all cases except the hexafluorophosphate salt and the proton sponge of Mallinson, the hydrogen bond acceptor is oxygen; in the exceptions the former acceptor is fluorine and the latter acceptor is nitrogen.

The exact numerical results for the hydrogen bond geometries, d(H...acceptor), electron density at the H...A bond critical points, $\rho_b(\mathbf{r})$, and the Laplacian of the electron density at the bond critical points, $\nabla^2\rho_b(\mathbf{r})$, for each of the experimentally determined hydrogen bonds, N-H...acceptor, are listed in Table 15(a) and will be discussed more thoroughly later on. However, some general features appear consistently through the series of N-H...acceptor hydrogen bonds.

For X-H...A hydrogen bonds, the X-H interaction is always covalent ($\rho_b(\mathbf{r})$ is relatively large and positive; $\nabla^2\rho_b(\mathbf{r})$ is negative). However, the

topological analysis of the electron density in normal strength hydrogen bonds, H...A, always shows features typical of closed shell interactions. As anticipated for such closed shell, primarily electrostatic interactions, and in accordance with the Pauli Principle, charge is removed from the interatomic surface resulting in low values for $\rho_b(\mathbf{r})$, an order of magnitude less than for normal covalent bonds between first row atoms.

The Laplacian of the experimental charge density at the bond critical point of H...A is invariably positive, a characteristic of closed shell interactions that are governed by the contraction of the electron density towards each of the interacting nuclei. The perpendicular curvatures, λ_1 and λ_2, are small and nearly equal while λ_3, the curvature parallel to the bond path, is comparatively large and dominant, resulting in a positive value of the Laplacian. The values obtained experimentally for the topological parameters of normal hydrogen bonds differ very little from those calculated for an isolated assembly of non-interacting molecules. The charge density evidence points to a largely electrostatic interaction for all normal hydrogen bonds.

In addition, R. Flaig et al.[43] report, in their topological study of D,L-aspartic acid, that for the stronger "normal" hydrogen bonds the calculated bond path length is only slightly longer than the geometrical distance connecting the donor and the acceptor. However, for the weaker hydrogen bonds the interaction path length can be considerably longer than the geometrical length of the line joining the donor and the acceptor.

Both $\rho_b(\mathbf{r})$ and $\nabla^2\rho_b(\mathbf{r})$ appear to be correlated in some way with the H...acceptor separation, with shorter distances associated with relatively larger $\rho_b(\mathbf{r})$ and $\nabla^2\rho_b(\mathbf{r})$ values, although the relationship does not appear

to be linear, judging from the combined literature results. The weakest N-H...acceptor hydrogen bond described so far occurs in *L*-arginine phosphate monohydrate, as reported by Espinosa et al.[40] in 1996. The H...O hydrogen bond distance is long, 2.183Å, while both the electron density at the bond critical point ($\rho_b(\mathbf{r})$ = 0.08eÅ^{-3}) and the Laplacian ($\nabla^2\rho_b(\mathbf{r})$ = 1.32eÅ^{-5}) are small but positive.

The strongest N-H...acceptor hydrogen bond yet described in the literature appeared in the 1997 publication by P.R. Mallinson et al.[22] The structure described, the 1,2-dichlorohydrogen maleate salt of the proton sponge cation, 1,8-bis(dimethylamino)naphthalenium(1+), contains a strong [Me_2N-H...NMe_2]$^+$ intracationic hydrogen bond. The geometry of the interaction N(2)-H(1nn)...N(1) is characterized by the distances, N(1)...N(2) = 2.644(2)Å, N(2)-H(1nn) = 1.106(5)Å, and H(1nn)...N(1) = 1.608Å and by the angle N(2)-H(1nn)...N(1) = 153.3(5)°. The covalent bond, N(2)-H(1nn), was found to be described topologically by an electron density at the bond critical point of +1.91(3)eÅ^{-3} and a Laplacian value of -29.7(1)eÅ^{-5}, a negative value as expected for a covalent interaction. For the H(1nn)...N(1) hydrogen bond the corresponding values calculated were $\rho_b(\mathbf{r})$ equal to +0.53(2)eÅ^{-3} and $\nabla^2\rho_b(\mathbf{r})$ equal to +4.27(5)eÅ^{-5}. Although the largest value yet reported for the electron density in an N-H...A hydrogen bond, the Laplacian value is still positive, indicating that this interaction is still of the closed shell type, still predominantly electrostatic in nature.

Several recent studies show that certain very short hydrogen bonds may behave differently in topological terms. These are the short hydrogen bonds that in maps of the deformation density show covalent, bonding

electron density shared between both X-H and H...acceptor. The first such short hydrogen bond was described topologically in 1995 by C. Flensburg et al.,[38] who showed it, by a combined neutron and x-ray study at 110K, to occur in the structure of methylammonium hydrogen succinate monohydrate. The structure is engaged in a number of normal N-H and O-H hydrogen bonds, but it also contains one very short, symmetric O...H...O' intermolecular hydrogen bond between carboxylate groups of the anions. [d(O...H) = 1.2209Å, d(O...O) = 2.4419(11)Å and O...H...O' = 180°]. Topological analysis of the electron density at the two equivalent O...H critical points gave values of 1.06(3)eÅ^{-3} and -6.8(10)eÅ^{-5} for $\rho_b(\mathbf{r})$ and $\nabla^2\rho_b(\mathbf{r})$, respectively. A considerable contraction of the electron density was observed in the plane perpendicular to the bond path (λ_1 = -12.0(5), λ_2 = -11.8(5) and λ_3 = +17.0(2)eÅ^{-5}). These features, particularly a negative value for the Laplacian, reveal significant covalent character in the strong O...H...O hydrogen bond. However, traditional covalent bonds have much more negative values of the Laplacian, by an order of magnitude, than do these strong hydrogen bonds.

The same conclusion is also supported by the charge density/ topological investigation of the 1,2-dichlorohydrogen maleate salt of 1,8-bis(dimethylamino)naphthalene reported by Mallinson et al.[22] The strong intramolecular hydrogen bond within the anion, O(1a)-H(1oo)...O(4a) has a geometry described by the distances O(1a)-H(1oo) = 1.149(7)Å, H(1oo)...O(4a) = 1.235(7)Å, and O(1a)...O(4a) = 2.383(4)Å and the angle O(1a)-H(1oo)...O(4a) = 178.5(6)°. The calculated values of the electron density and the Laplacian at the bond critical points for the O(1a)-H(1oo) and H(1oo)...O(4a) interactions, respectively, were calculated to be

+1.34(3) and +1.02(2)eÅ^{-3} [$\rho_b(\mathbf{r})$] and -11.1(1) and -1.2(1)eÅ^{-5} [$\nabla^2\rho_b(\mathbf{r})$]. Again, the negative value of the Laplacian at the bond critical point indicates predominant covalent character in the H...acceptor region of the strong hydrogen bond.

A similar anion, hydrogen maleate, has recently been shown to contain a symmetric, short, very strong O...H/D...O hydrogen bond in a charge density study of the methylammonium salt published by Madsen et al.[21] in 1998. The structure contains two crystallographically distinct anions, each with similar, almost planar geometries, characterized by bond lengths of O(2)...D(2) = 1.2134(6)Å and O(4)...D(4) = 1.2101(5)Å. The distances and geometries are accurately known because of a parallel neutron diffraction experiment carried out by the authors on a partially deuterated sample of the title compound, $[CH_3ND_3]^+[C_4H_2O_4D]^-$. The topological parameters for the O...H/D...O interactions in the two unique anions are also very similar with $\rho_b(\mathbf{r})$ values of +1.13(2) and +1.09(2)eÅ^{-3} and $\nabla^2\rho_b(\mathbf{r})$ values of -5.9(9) and -7.1(9)eÅ^{-5}, respectively. Taken together, all the experimental data[21,22,38] offer considerable proof that there are strong hydrogen bonds that are predominantly covalent in nature.

Intermolecular interactions even weaker than the hydrogen bonds so far discussed have been investigated using topological analysis by a number of research groups. Whether these are true hydrogen bonds of the type C-H...acceptor or whether these are van der Waals contacts, the interactions can be characterized using Bader's method.[14] The C-H contacts examined so far include those found in the compounds 1-methyluracil (W.T. Klooster et al.,1992)[36], *syn*-1,6:8,13-biscarbonyl[14]annulene (R. Destro et al., 1995)[44], lithium bis(tetramethylammonium) hexanitrocobaltate(III)

(R. Bianchi et al., 1996)[45], citrinin ($C_{13}H_{14}O_5$ - P. Roversi et al., 1996)[46], 1,8-bis(dimethylammonium)naphthalene 1,2-dichlorohydrogen maleate (P.R. Mallinson et al., 1997)[22], 4-cyano-imidazolium-5-olate (R. Bianchi et al., 1998)[42] and D,L-aspartic acid (R. Flaig et al., 1998).[43] The literature results are summarized in the discussion [Table 15(b)]. All of the C-H interactions so far characterized are to the "acceptor" oxygen with the exception of the C-H...N contact found in 4-cyanoimidazolium-5-olate.[42]

All of the literature C-H...O/N interactions are very weak, as weak as the weakest N-H...acceptor hydrogen bonds ever reported, as might be expected. In every case, the C-H bond is covalent with positive electron density and Laplacian values at the bond critical point. The H...O/N interaction always has a very small positive value for $\rho_b(\mathbf{r})$ and a small positive value for the Laplacian, $\nabla^2\rho_b(\mathbf{r})$. These contacts are electrostatic, closed shell interactions.

The strongest interaction between C-H and oxygen reported in the literature is found in 1,8-bis(dimethylammonium)naphthalene 1,2-dichlorohydrogen maleate as described in topological terms by Mallinson et al.[22] A relatively short contact, with an H...O distance of 2.107(2)Å, was located between H(7) of the cation's naphthalene ring and O(3a) of the anion. The bond critical point was characterized by a value for $\rho_b(\mathbf{r})$ of +0.109(6)eÅ^{-3} and a value for $\nabla^2\rho_b(\mathbf{r})$ of +1.951(3)eÅ^{-5}. A contact of almost equal strength was described in the structure of 4-cyanoimidazolium-5-olate by Bianchi et al.[42] The C-H...N interaction was described topologically by values of +0.11(1)eÅ^{-3} and +1.6(1)eÅ^{-5} for the electron density and the Laplacian at the H...N bond critical point, respectively [d(H...N) = 2.20(2)Å].

The weakest C-H...O contact yet investigated was also found in the structure of 1,8-bis(dimethylammonium)naphthalene 1,2-dichlorohydrogen maleate by Mallinson et al.[22] The much longer contact, d(H...O) = 2.718(6)Å, was calculated to have an electron density at the bond critical point of +0.020(1)eÅ^{-3} and a Laplacian value of +0.402(1)eÅ^{-5}. The smallest value reported for the Laplacian at the O...H bond critical point for a C-H...O interaction was found in the compound $Li[N(CH_3)_4][Co(NO_2)_6]$ by R. Bianchi et al.[45] The contact of 2.583(12)Å, d(H...O), was reported to have $\nabla^2\rho_b(\mathbf{r})$ equal to +0.36(1)eÅ^{-5} and $\rho_b(\mathbf{r})$ equal to +0.022(1)eÅ^{-3}.

From these results it appears that for C-H...O contacts the values of the electron density and the Laplacian at the H...O bond critical point are related to the H...O distance. Both sets of values appear to increase steadily as the H...O separation decreases. However, neither relationship [$\rho_b(\mathbf{r})$ vs. d(H...O) and $\nabla^2\rho_b(\mathbf{r})$ vs. d(H...O)] appears to be linear, just as was observed for the case of N-H...acceptor hydrogen bonds.

Since the advent of charge density studies and the topological analysis of experimentally derived electron density distributions, many authors have published the results of parallel theoretical calculations. These results have tended to support the experimental results if the calculations were undertaken at a reasonable level of theory with an extended basis set including polarization functions. There is now substantial evidence that the static electron density extracted from x-ray diffraction data can be reliable enough to provide topological characterization of covalent bonds and nonbonded interactions. The extent to which these topological properties are reproducible depends not only on experimental conditions but also on the interpretation of the data.

The proper treatment of the diffraction data requires guidance from theory. However, there is also need for experimental verification of theoretical results. This poses an interesting dilemma, particularly when trying to compare experimental to theoretical results. There is an additional problem, the applicability of the usual statistical figures of the fit (error) in judging the correctness of the experimental model and the derived topological parameters is very limited. This makes comparison with theory even more difficult.

The experimental results of R. Destro et al.[34,35] for *L*-alanine were compared with the results of theoretical calculations in 1992 by C. Gatti et al.[47] The authors found that ab initio calculations, using an extended basis set including polarization functions and the experimental geometry, gave promising results. Both the experimental and theoretical electron densities when analyzed gave the same number and types of critical points in the gradient field. Close agreement was found for bond critical point locations and density values for both covalent intramolecular interactions and intermolecular hydrogen bonds. Discrepancies in the Laplacian of the electron density were slightly greater; this the authors attributed to the greater sensitivity of this parameter relative to the electron density. Only qualitative agreement was observed (±20%) for some of the more polar covalent bonds, however, the agreement was better for the hydrogen bonding interactions. In fact, the authors conclude that theoretical and experimental densities not only predict the same hydrogen bonding interactions, but also agree on the hydrogen bond critical point locations, as well as the $\rho_b(\mathbf{r})$ and $\nabla^2\rho_b(\mathbf{r})$ values. The reliability of the approach in describing hydrogen bond interactions was supported by the

excellent agreement found when comparing the experimental topological data of *L*-alanine with the corresponding Hartree-Fock data.

V. Tsirelson,[39a] in his discussion of hydrogen bonding in urea, also found quantitative agreement of the topological characteristics when results from the experimental charge density were compared to theoretical results calculated with a 6-31G** basis set using ab initio restricted Hartree-Fock formalism. The experimental electron density values at the bond critical points were found to be larger than the theoretical values, by approximately 10%, for the hydrogen bonds while the theoretical Laplacian values were smaller than the experimental values by roughly the same amount.

In their experimental charge density and topological analysis of *L*-dopa [(2S)-3-(3',4'-dihydroxyphenyl)alanine] S.T. Howard et al.[37] also included a theoretical ab initio calculation carried out using a Dunning double zeta basis set. The authors generated a set of theoretical structure factors from the ab initio charge distribution and then beginning from the final experimental geometry refined the multipole model, to allow a more detailed comparison with experiment. They found that the topological properties for the experimental and ab initio charge distributions were in good agreement, when the latter were projected onto the experimental multipolar model. However, both multipole data sets gave electron density values of up to 20% larger than those calculated using the exact wavefunction. This, the authors felt, demonstrated shortcomings of the multipole model that had been applied experimentally. Greater differences between experiment and theory were expected by the authors in the hydrogen bonding regions since the theoretical calculations were based

on an isolated molecule. However, the differences between experiment and theory were within the estimated experimental error limits. As Tsirelson had found, Howard et al. also found that the refined hydrogen bond critical point densities to be systematically larger than those calculated.

Most recent publications on experimental charge density/topological analysis, including those from the Mallinson[22,41] and Bianchi[42,45] groups, have included ab initio calculations carried out on the crystal geometry using a restricted Hartree-Fock model and an extended 6-31G** or higher level basis set. These single point calculations of the theoretical charge density generally have been found to give good agreement with the experimentally derived values.

R. Flaig et al.[43] in their publication on the topological analysis of D,L-aspartic acid from the charge density, include a detailed discussion on the differences they found in the theoretical and experimental results. Their basic conclusions match well with those of previous groups and they note that the theoretical electron density of the molecule is topologically equivalent to that extracted from the crystal through multipole modelling of the x-ray data. The number and types of critical points of the electron density were found to be the same for both theory and experiment. Even the Laplacian values derived by the two methods were found to exhibit qualitatively equivalent features for both bonded and nonbonded interactions.

However, a detailed comparison of the theoretical and experimental density showed that the locations of the minima of the electron density along the bond paths could differ markedly in the two, especially in polar

bonds. Since the electron density usually has a rather flat minimum between interacting atoms, $\rho_b(\mathbf{r})$, the electron density at the bond critical point, is quite insensitive to the location of the minimum. This is why $\rho_b(\mathbf{r})$ values are usually in good agreement, within the estimated experimental error, when compared to theory. This can also be true for the Laplacian values for bonds formed between like or similar atoms. However, for polar bonds, the critical point may be closer to one of the atoms, in a region where the curvatures change more rapidly. If the bond critical point is located even slightly differently by theory and experiment, it will be reflected particularly in the λ_3 curvature and it can result in very different values for the Laplacian. Hydrogen bonds, although polar interactions, are helped by the fact that they are normally relatively weak.

In comparing their own experimental results with theory, the authors found that for polar bonds the experiment gave somewhat higher $\rho_b(\mathbf{r})$ values and considerably lower $\nabla^2\rho_b(\mathbf{r})$ values than theory. For the nonpolar C-C bonds the opposite trend was observed. Madsen et al.,[21] in their charge density study of methylammonium hydrogen maleate, also compared their experimental results for the C-C bonds in the structure to theoretical values calculated previously. They report excellent agreement between theoretical and experimental values for $\rho_b(\mathbf{r})$ and the negative eigenvalues of the Hessian matrix (λ_1 and λ_2), but the values found for the positive λ_3 curvature were significantly larger than those calculated. Larger experimental values for the Laplacian of the electron density in the C-C bonds are consistent with the observations of Flaig et al.,[43] as just discussed.

Flaig et al. do not explicitly compare their experimental results for the topological properties of the hydrogen bonds with theoretically calculated values. However, they do report that the analysis of the nonbonded interactions in terms of the topology of the experimental electron density deliver chemically significant results. Overall, the authors conclude that theoretical and experimental densities, because of their different natures, may not be directly comparable in all regions. On the other hand, the determination of topological parameters from charge densities derived from x-ray diffraction data is a valid and important exercise.

1.7. The Relationship Between Topological Parameters and Geometry

In 1982, Bader et al.[48] (the father of the "Atoms in Molecules" theory) wrote: " To attain the situation of zero force necessary for the formation of a bond requires that electronic charge be accumulated in the internuclear region in an amount greater than that obtained by the overlap of the undistorted atomic densities. This accumulation of charge is necessary to balance both the large values of the nuclear repulsive force found for the values of the internuclear separation, R, in the neighbourhood of its equilibrium value, R_e, and the force resulting from any polarization of the charge density into antibonding regions. Thus it is to be anticipated that for a pair of atoms which can exhibit a number of characteristic bond lengths, a situation rationalized in terms of the Lewis model by the possibility of "multiple bonds", the value of the charge density at the bond critical point, $\rho_b(\mathbf{r})$, will increase as the bond length decreases."

The authors investigated the variation of $\rho_b(\mathbf{r})$ with R_e for a wide range of C-C bonds (n = 32, R_e 2.2 to 2.9Å and $\rho_b(\mathbf{r})$ 0.23 to 0.37 au) and observed a linear relationship. For a much smaller subset of the data, containing the C-C bonds from ethane, benzene, ethylene and acetylene, the variation of $\rho_b(\mathbf{r})$ with R_e was best represented by the linear equation (in atomic units): $\rho_b(\mathbf{r}) = -0.184R_e + 0.777$ with a root mean square deviation of 0.003 when calculated at the STO-3G level. If the same parameters of the same bonds in the same molecules in the same geometries were recalculated using the 6-31G** basis set an even stronger linear correlation was observed:

$$\rho_b(\mathbf{r}) = -0.283R_e + 1.043 \qquad \sigma = 0.0016$$

The authors also found that when plotted the C-C data fell into four distinct groups corresponding to the Lewis concept of single, aromatic, double and triple bonds, each with a narrow range of $\rho_b(\mathbf{r})$ and R_e values. These characteristic values of $\rho_b(\mathbf{r})$ and R_e were found for C-C bonds in a wide range of differing equilibrium structures, neutral and charged, strained and unstrained. This the authors named the 'bond order - bond length' relationship and it has been subsequently mentioned in many sources. The proposed relationship between R_e and $\rho_b(\mathbf{r})$ shows that a knowledge of the bond lengths of a hydrocarbon molecule infers a knowledge of the values of the charge density at each of its bond critical points.

Recently, P. Roversi et al.[46] have compared their results from experimental charge density studies of C-C (and CO) bonds with the theoretical results of Bader et al.[48] In the molecule citrinin, whose electron density at 19K was generated from crystallographic data by multipole refinement, the topological parameters of 13 C-C and 6 CO bonds

were calculated. When plotting their data, the authors used R_b, the bond path length, rather than R_e, the conventional equilibrium bond length, however, they do note that the difference between these values is always very small in this molecule, less than 0.07% of the value of R_e.

The variation of $\rho_b(\mathbf{r})$ with R_b for the 13 C-C bonds in citrinin was best represented by a straight line, given by the equation (in atomic units):

$$\rho_b(\mathbf{r}) = -0.297(8)R_b + 1.099(23)$$

with a correlation coefficient of -0.996 and a root mean square residual of 0.031. The range of C-C values in the experimental case, R_b from 2.50 to 2.90 au and $\rho_b(\mathbf{r})$ from 0.23 to 0.33 au, was narrower than the set studied theoretically by Bader et al.[48] The experimental fit, however, was very close to that calculated by Bader et al. at the 6-31G** level.

Roversi et al.[46] also attempted to fit six CO bond critical point electron density values and their respective bond path lengths with a linear relationship (in atomic units):

$$\rho_b(\mathbf{r}) = -0.417(29)R_b + 1.385(7) \qquad R = -0.990 \quad \sigma = 0.08$$

A simple power curve was also fitted to the same data with a considerably improved result:

$$\rho_b(\mathbf{r}) = 8.433R_b^{-3.521} \qquad R = -0.998 \quad \sigma = 0.011$$

It appears that for the experimental CO bonds, the relationship between $\rho_b(\mathbf{r})$ and R_b is not linear but rather follows a power function.

This result is supported by later work by Madsen et al.[21] on the experimental charge density of methylammonium hydrogen maleate. These authors used the relationship developed by Roversi et al.[46] and their own experimentally determined CO bond lengths to calculate $\rho_b(\mathbf{r})$ values. These they compared to the experimentally calculated topological values, finding

excellent agreement, and adding further support to the nonlinear relationship between the two values in CO bonds.

The relationship between topological parameters and geometry has also been investigated in the case of hydrogen bonding, beginning with two important contributions by Boyd and Choi.[49,50] Ab initio SCF molecular orbital calculations at the 6-31G** level, including complete geometrical optimizations, were reported for two series of substituted nitrile - hydrogen halide complexes, RCN...HX (R = H, Li, F, Cl, OH, LiO, NC and CH_3 for X = F[49] and Cl[50] and R = HCC and CH_3O for X = F[49]).

In the first paper,[49] which explored the RCN...HF series, the weakest complex formed was NCCN..HF which was calculated to have a hydrogen bond energy, E_{HB}, of 16.35 kJ/mol, a hydrogen bond length, r(H...N), of 2.107Å, a $\rho_b(\mathbf{r})$ value of 0.01490 au and a $\nabla^2\rho_b(\mathbf{r})$ value of 0.05369 au. This is in contrast to the strongest complex, LiOCN...HF, which was calculated to have E_{HB} = 55.24 kJ/mol, r(H...N) = 1.824Å, $\rho_b(\mathbf{r})$ = 0.02984 au and $\nabla^2\rho_b(\mathbf{r})$ = 0.11273 au.

In the second paper,[50] the same calculations were carried out on a series of related nitrile...HX complexes, with the HF replaced by HCl. The hydrogen bond energy calculated for each of the hydrogen bonded complexes formed with HCl as the donor was substantially weaker (~35%) than that of the corresponding complex of HF, as expected based on the higher electronegativity of fluorine relative to chlorine. The hydrogen bond length, r(H...N), was also consistently increased in the HCl series, mainly because of the greater size of chlorine relative to fluorine, however, the amount of the increase varied with the nature of the R group. Again, the weakest complex calculated was NCCN...HCl, with E_{HB} = 10.05 kJ/mol,

r(H...N) = 2.350Å, $\rho_b(\mathbf{r})$ = 0.01103 au and $\nabla^2\rho_b(\mathbf{r})$ = 0.03302 au. The strongest complex, LiCN...HCl, had values of 37.88 kJ/mol, 1.991Å, 0.02391 au and 0.06949 au calculated for the same parameters, respectively.

The hydrogen bond energy calculated by the authors is the total energy calculated for the RCN...HX complex subtract the energy calculated for the two individual components, RCN and HX. This energy could include van der Waals contact energies for the complex as well. The authors also found the calculated hydrogen bond energies for the complexes to be overestimated by roughly 10% relative to the few experimental values available at the time. The bond lengths in the interatomic hydrogen bonds were overestimated, relative to the experimental values, by about the same amounts (~2 to 5%). However, these overestimations were not problematic since the results were discussed on a relative rather than an absolute scale.

Boyd and Choi[49,50] observed a number interesting trends in their data. In particular, they found a strong linear correlation between the charge density at the bond critical point and the theoretically estimated hydrogen bond energy:

HF $\quad \rho_b(\mathbf{r}) = 0.0003904E_{HB} + 0.008539 \qquad R = 0.999$

HCl $\quad \rho_b(\mathbf{r}) = 0.0004665E_{HB} + 0.006144 \qquad R = 0.998$

where $\rho_b(\mathbf{r})$ is in atomic units and E_{HB} is in kJ/mol.

M.T. Carroll and R.F.W. Bader[51] also found a roughly linear relationship between $\rho_b(\mathbf{r})$ and D_e, the theoretically calculated dissociation energy, for a wide range of Base...HF hydrogen bonded complexes (Base = OC, SC, N_2, HCN, O_3, SCO, CO_2, N_2O, SO_2, H_2CO, H_2O, HF, H_3P, H_2S and HCl). The authors attributed the greater scatter they

observed, relative to the results of Boyd and Choi, to the greater diversity of hydrogen bond acceptors studied.

Boyd and Choi also found a strong linear correlation between the value of the Laplacian at the hydrogen bond critical point and the hydrogen bond energy, for both HF (R = 0.999) and HCl (R = 0.993) complexes. In these, and all other relationships studied by the authors, the HCl series showed weaker correlations than the HF series for some reason. There was also a general tendency for the H...X and N...X distances to decrease linearly with increasing bond energy.

The possibility of extending the bond order - bond length approach of Bader et al.[48] to intermolecular interactions was considered by Boyd and Choi.[49,50] Working at the 6-31G** level, the hydrogen bond length (Å) versus the charge density at the bond critical point (au) data were fitted to the following linear equations:

HF $\rho_b(\mathbf{r}) = -0.02944r(N...H) + 0.1309$ R = 0.991 σ = 0.002

HCl $\rho_b(\mathbf{r}) = -0.03634r(N...H) + 0.0955$ R = 0.988 σ = 0.006

The linear relationship between r(N...H) and $\rho_b(\mathbf{r})$ for the intermolecular hydrogen bonds was established with an even stronger correlation than Bader et al. had observed for the intramolecular C-C bonds, even though the former were an order of magnitude weaker than the latter.

In a much more recent publication, Koch and Popelier[52] (1995) carry the work of Bader et al.[48] and Boyd and Choi[49,50] one step further, investigating a number of weak C-H...O hydrogen bonds in van der Waals type complexes (formaldehyde-chloroform, acetone-chloroform, benzene-formaldehyde and 1,1-dichloroethane-acetone). The complexes were optimized using ab initio calculations with RHF formalism and a 6-31G** basis set.

The interaction energies of the complexes were calculated using the Hayes-Stone intermolecular perturbation theory (IMPT) which is valid for regions of moderate and large overlap. It allows the intermolecular interaction energy, E_{IMPT}, to be separated into terms that can be correlated with distinct physical effects, including repulsion, electrostatic, induction, dispersion and charge transfer terms. The energy computed by the IMPT method is the total intermolecular interaction energy for the van der Waals complex; thus, the fit of the correlation for E_{IMPT} must be made to the sum of $\rho_b(\mathbf{r})$ values for the complex. This resulted in an excellent linear fit with an equation (in atomic units):

$$E_{IMPT} = -995.62\rho_b(\mathbf{r})_{TOTAL} + 1.5919 \qquad R = -0.998$$

A linear relationship (R = -0.967) was also found between E_{IMPT} and $\nabla^2\rho_b(\mathbf{r})_{TOTAL}$ of the complexes. The behaviour of the correlation coefficients led the authors to conclude that a linear relationship between interaction energy and the charge density/Laplacian at the bond critical point is also valid for multiple bond critical points being summed in one complex.

The C-H...O hydrogen bonds in the van der Waals complexes studied by Koch and Popelier[52] were calculated to have $\rho_b(\mathbf{r})$ values ranging from 0.004 to 0.021 au and $\nabla^2\rho_b(\mathbf{r})$ values from 0.016 to 0.090 au. Tang et al.[53] also calculated the topological parameters, at a similar level of theory, for a series of FH...π acceptor type complexes (acceptors = acetylene, ethylene, cyclopropane and benzene) held together by weak hydrogen bonds. Both $\rho_b(\mathbf{r})$ [0.005 to 0.013 au] and $\nabla^2\rho_b(\mathbf{r})$ [0.024 to 0.049 au] were found to cover similar ranges in the weakly hydrogen bonding complexes. Recently, Rozas et al.[54] repeated the work of Tang et al., but studying a wider range of FH...π acceptor type complexes at a higher level of theory.

This series of data could also contribute to the study of the relationships between topological parameters and geometrical parameters although the original authors did not specifically investigate such details.

A number of C-H...O interactions have been studied experimentally in the charge density analysis of the 1,2-dichlorohydrogen maleate salt of monoprotonated 1,8-bis(dimethylamino)naphthalene from crystallographic data by P.R. Mallinson et al.[22] The properties of the charge density in these weak interionic hydrogen bonds were found to be systematically related to the structural parameters defining the interaction. In particular, the value of the electron density at the bond critical point was found to correlate very well with the neutron H...acceptor internuclear distances, with a linear correlation coefficient of -0.97 for the seven C-H...O contacts:

$$\rho_b(\mathbf{r}) = -0.13(2)\text{H...A} + 0.37(4)$$

where H...A is in Å and $\rho_b(\mathbf{r})$ is in units of $e\text{Å}^{-3}$. However, the authors also write that the relationships between $\rho_b(\mathbf{r})$ and structural parameters characterizing a weak interaction are probably not linear ones. This they found to be the case when all the hydrogen bonds in the title compound, from very strong [O-H..O]$^-$ to very weak (C-H...O) were considered on the same scale. In such a case, a power fit may be more appropriate, as found, for example, by Roversi et al.[46] for experimentally derived topological parameters of CO bonds when plotted against bond length.

Mallinson et al. also found a good linear correlation between $\rho_b(\mathbf{r})$ ($e\text{Å}^{-3}$) and the values of the Laplacian ($e\text{Å}^{-5}$) at the bond critical points

$$\rho_b(\mathbf{r}) = 0.056(4)\nabla^2\rho_b(\mathbf{r}) + 0.003(4) \qquad R = 0.99$$

and between the Laplacian and the H...A (Å) internuclear distances for the

weak C-H...O contacts:

$$\nabla^2\rho_b(\mathbf{r}) = -2.2(2)H...A + 6.5(6) \qquad R = -0.97$$

These results show that somehow $\rho_b(\mathbf{r})$ and $\nabla^2\rho_b(\mathbf{r})$ carry similar information about the nature of the interaction for weak C-H...O contacts.

Considering all the results published so far, it is clear that there is a definite relationship between topological parameters, whether derived from theory or experimental crystallographic data, and the geometry of the interaction in question. It is not yet clear which relationships are truly linear and which would be better fit by some type of higher function, possibly exponential. Any work that furnished a series of data on the topological properties of related bonds at their critical points could be used to expand the knowledge of the nature of the relationships.

1.8. X-H...π(Ph) Hydrogen Bonding

Hydrogen bonds often provide the strongest intermolecular forces between molecules in molecular crystals and thus often influence the preferred packing arrangement. They tend to form in a pattern which will maximize their contribution to the stabilization of the crystal structure. In classical views,[55] the organization of the hydrogen bonding arrangement in a structure follows laws of hierarchy and of competition. The strongest donor tends to hydrogen bond to the strongest acceptor, the second strongest donor bonds to the second strongest acceptor and so on, until all the traditional strong hydrogen bonding functionalities have been suitably matched. This will be true in most situations, unless other constraints, most notably steric factors, disrupt the preferred pattern of hydrogen bonding.

What happens when the hydrogen bonding of a particular molecule cannot be satisfied because it contains an excess of the conventional donors (OH, NH, etc.) or acceptors (lone pairs on O, N, Cl, etc.)? A variety of strategies are available to accommodate the mismatch.

The case of an excess of hydrogen bond acceptors has been well studied. If there are no alternative donors available in the structure, a new structural motif may arise to relieve the deficiency. Bifurcated or even trifurcated hydrogen bonds may be formed, in which the available donors are shared between two or more acceptors.

It is also possible that the superfluous hydrogen bond acceptors will simply find the next most acidic hydrogens in the structure and form weak C-H...X hydrogen bonds. The most studied acceptor has definitely been oxygen, while acidic C-H groups such as alkynes, aromatics, alkenes or even substituted alkyls have been shown to form C-H...O hydrogen bonds. Recent publications by T. Steiner et al. summarize the available literature on C-H...O interactions.[56,57] They write that C-H...O interactions occur frequently in both small molecule and protein crystal structures. Experimental studies indicate that most kinds of C-H groups can donate weak hydrogen bonds. While the bonds formed by acidic C-H groups (alkynes, haloforms) are moderately strong (on the scale of weak hydrogen bonds), those that involve weakly polarized C-H groups are much weaker, having been estimated at only 0.5 to 1 kcal/mol. Although they obviously still contribute a small amount of stabilization to a crystal structure, they are unlikely to be structure determining except under extraordinary circumstances.

In a molecular assembly with a deficiency of "traditional" hydrogen

bond acceptors, there are again different strategies available to alleviate the problem. Hanton et al.[58] have reported that a potential acceptor can change hybridization to accommodate hydrogen bond formation. More likely, the unpaired donors will look to π electrons in the molecule as the next best hydrogen bond acceptors available. The π electrons can come from alkyne triple bonds, aromatic ring bonds or even isolated alkene double bonds, in the usual order of increasing acceptor ability. Such hydrogen bonds are often designated by X-H...π, and in the case where the hydrogen bond acceptor is a phenyl ring they are sometimes called aromatic hydrogen bonds and designated by X-H...π(Ph). Examples of the formation of X-H...π bonds have been observed where there is a deficiency, or a steric inaccessibility, of traditional strong acceptor sites. A sufficiently rich carbon atom(s) (alkyne, aromatic or alkene) has a propensity to form a hydrogen bond with X-H groups (O, N, or even C) thus contributing to crystal stability.

In summary, acidic C-H groups can function as weak hydrogen bond donors, and hydrogen bonds from C-H to strong acceptors such as O, N and Cl are abundant in organic and biological chemistry. Weak hydrogen bond acceptors, π electron containing functional groups such as aromatic rings, alkenes and alkynes, can interact with the strong donors (O-H, N-H and the hydrogen halides). The hydrogen bonds thus formed, X-H...π, occur in a variety of configurations and are of particular importance in biological systems. There is no fundamental reason, however, that weak donors and acceptors should not interact. Non-traditional donors and acceptors should combine under favourable conditions to form C-H...π hydrogen bonds, which contribute, albeit weakly, to the stability of the crystal structure.

Historically, the first demonstrated existence of an X-H...π hydrogen bond in a crystal structure appears to come from a combined calorimetric and crystallographic study of ammonium tetraphenylborate, $NH_4B(C_6H_5)_4$, by Davies and Staveley in 1957.[59] This would also be the first reported example of an aromatic hydrogen bond, N-H...π(Ph), although one formed between ions rather than neutral species. It is interesting to note that ammonium tetraphenylborate (and its hydrogen bonding) is still a focus of investigation, being one of the compounds studied for this work.

Since then, numerous spectroscopic and theoretical investigations have furnished evidence of such X-H...π interactions. In contrast, crystallographic studies, which would provide direct evidence of such contacts in solids, have been few. For a long time, these weak hydrogen bonds were regarded as exotic and of little general importance in crystallography. As a result, even in structures where X-H...π hydrogen bonding does exist, it often went unnoticed or unreported. Only recently have the structural properties of X-H...π bonds attracted more interest.

The phenomenon of X-H...π hydrogen bonding is not yet well studied even for the most common configurations with O-H and N-H donors. There is evidence that X-H...π hydrogen bonds, though weak, can be structurally significant when they do occur. There has been considerable interest in such weak bonds in the context of crystal engineering, protein conformation and molecular recognition and supramolecular chemistry.[16,17]

1.8.1. The Geometry of the X-H...π(Ph) Hydrogen Bond

In a normal X-H...A hydrogen bond where the acceptor is a single atom, or more properly, an electron pair localized on that atom,

description of the bond geometry presents no problems. The X...A and H...A distances and the X-H...A angle are well defined quantities between atomic nuclei that can readily be measured experimentally. The accuracy with which H...A and X-H...A are known can be problematic in x-ray determinations, depending primarily on the confidence with which the hydrogen atom position has been located. However, in principle there is no fundamental difficulty in characterizing the properties of the bond.

This is not the case for X-H...π(Ph) hydrogen bonds where the acceptor is the delocalized π electrons of an aromatic ring, extending over a group of atomic nuclei. Here, the nature and the position of the acceptor is not well defined. In fact, conventional structure determinations have suggested that in different situations an atom, a bond or the entire π cloud of the ring can serve as the hydrogen bond acceptor. In general, it is impossible to predict where the X-H vector will point and what exact point should be considered the terminus of the X-H...π(Ph) hydrogen bond.

The situation in the crystalline state is further complicated by the fact that the hydrogen bond donor and acceptor pair are not isolated. Constraints arise from packing forces and from multiple hydrogen bond choices within the structure. The environment and relative orientations in a crystal are largely determined by packing efficiency and in ionic crystals by Coulombic interactions. The formation of hydrogen bonds within the structure will generally follow hierarchal rules, previously discussed, within the bounds of stereochemical constraints. To maximize the total hydrogen bond stabilization in a structure, the strength of some individual hydrogen bonds may be sacrificed, resulting in less than ideal

geometries for some interactions. In the case of X-H...π(Ph) hydrogen bonds this makes them even more difficult to define accurately since no prior knowledge of the expected geometry can be assumed.

In the X-H...π(Ph) hydrogen bond, the X-H vector is normally directed at some point in the general area of the associated ring. The parameter ϕ, defined as the angle which the X-H vector makes with the ring plane, varies considerably from situation to situation and is undoubtedly strongly affected by packing ($\phi \leq 90°$). Since the X-H vector can approach the ring from a variety of angles, the angle ψ, formed by the projection of the X-H vector onto the ring plane is sometimes also used to characterize the interaction.[83]

Since the length of the X-H...π(Ph) hydrogen bond cannot be uniquely defined in a normal crystallographic investigation, alternate measurable distances must be investigated. Examination of the six individual X...C and H...C ring distances can be instructive as far as the closest contact and the best (most linear) X-H...C angle are concerned. Standard quantities that can be consistently defined and compared between X-H...π(Ph) hydrogen bonded structures are $\bar{d}$(X...C) and $\bar{d}$[H(X)...C], the mean X or H(X) to carbon separation in the ring, and d(X...π_c) and d[H(X)...π_c], the distance of X or H(X), respectively, from the ring centroid. For either the X...C_{ring} or the H(X)...C_{ring} range of distances, a parameter 100Δ can also be calculated [100(maximum distance - minimum distance)]. An angle X-H...π_c equal to ω can also be defined. The distances and angles involving hydrogen are, in standard x-ray determinations, usually less reliably known but their lower accuracy does not necessarily render them uninformative.

Basing a discussion of the X-H...π(Ph) hydrogen bonding on distances from the ring centroid when the X-H vector in reality points elsewhere is completely arbitrary. However, the distances and angles described above provide a simple, generally applicable scheme that can be used to classify and compare X-H...π(Ph) hydrogen bonds of any type. Some combination of these distances and angles have traditionally been used to characterize X-H...π(Ph) hydrogen bonds in conventional structure determinations.

1.8.2. The O-H...π(Ph) Hydrogen Bond

In the crystalline state, examples of O-H...π(Ph) hydrogen bonds in small molecules have been the best documented. They will be discussed here first, primarily to document the nature of the acceptor in such interactions.

On the whole, studies have indicated that X-H...π(Ph) hydrogen bonds have an extremely soft geometry. For O-H...π(Ph) interactions, crystal structures have been reported where the O-H vector points more or less to the centroid of the phenyl ring acceptor. The first published examples of this interaction geometry were reported by Hardy and MacNicol[60] in 1976 and by Aubry et al.[61] in 1977. There are also off-center arrangements where the O-H vector apparently points to a particular aromatic C-C bond of the phenyl ring acceptor. Examples of this geometry have been published by Nakatsu et al.[62] (1978) and by Ueji et al.[63] (1982). More recently, an example where the O-H vector is aimed directly towards a single carbon atom in a phenyl ring has been reported in a crystal structure by Steiner et al.[64,65]

Originally, views expressed in the literature as to the requirements

for formation of an X-H...π(Ph) hydrogen bond dictated that the X atoms be placed directly above the phenyl ring face and that the X-H vector be oriented more or less towards the center of the aromatic ring. If this was not the case, the arrangement was not considered to fulfil the criteria required for the formation of an aromatic hydrogen bond. In the more recent, alternative view aromatic hydrogen bonds are attributed pronounced conformational variability, as just described. Off-center geometries are regarded as nothing more than less favourable cases, brought about by steric constraints, the need to maximize the entire set of hydrogen bonding interactions or other crystal packing pressures.

In 1976 Hardy and MacNicol[60] reported the first intramolecular O-H...π(Ph) hydrogen bond, located in the structure of 2,2-bis(2-hydroxy-5-methyl-3-*t*-butylphenyl)propane. Although an older investigation, the hydrogen atoms were refined isotropically and the final R factor was only 3.8%, both indicative of reasonable results. The title compound was found to be highly sterically hindered, with two O-H...π(Ph) hydrogen bonds per molecule. The authors write that the hydroxyl hydrogen atoms are situated such that they appear to interact with the π electron density associated with all the ring bonds, C(1) to C(6) and C(15) to C(65), of the molecule. The average perpendicular distance from the hydroxyl hydrogen atom to the aromatic ring plane was found to be 2.09Å, shorter than the closest H...C_{ring} separations reported, C(1)...H(145) = 2.13Å for one ring and C(15)...H(14) = 2.19Å for the other.

Soon after (1977), A. Aubry et al.[61] published the crystal structure determination of tri-*n*-butylammonium tetraphenylborate monohydrate, a compound closely related to those being studied in this investigation.

However, in this tetraphenylborate salt N-H...π(Ph) hydrogen bonding was not observed, rather all hydrogen bonding was found to involve the oxygen atom, from the water of solvation, acting as either the donor or acceptor. The water molecule accepts the hydrogen bond from the cation, N-H...O, and also forms two O-H...π(Ph) hydrogen bonds with two separate aromatic rings of the same tetraphenylborate anion. Each water hydrogen atom is described as being located almost immediately above the center of one of the rings. The distance of the water oxygen to the mean plane of these rings is 3.12Å and 3.17Å, respectively. Again, the hydrogen bonding is described as being to all carbons of the interacting ring; H(w) to C(1) - C(6) has distances ranging from 2.55(3)Å to 2.91(3)Å while H(w)' to C(13) - C(18) ranges from 2.49(3) to 2.87(2)Å. The range of hydrogen to ring carbon distances is narrow, supporting the proposed centroid type hydrogen bond geometry.

Since these first two crystallographic studies of O-H...π(Ph) hydrogen bonds, both of which were found to be accepted by the π electrons of the entire aromatic ring, other similar examples have been reported. One of the most interesting was published by J.L. Atwood et al.[66] in 1991. A low temperature x-ray study of Na_4[calix[4]arene sulphonate]·13.5H_2O showed a water molecule to be embedded within the cavity of the calixarene. The water molecule forms two hydrogen bonds to aromatic rings on opposite sides of the cavity; the water hydrogen to ring centroid separations are 2.38Å and 2.50Å, with O-H...centroid angles of 133° and 127°, respectively. The oxygen atom of the embedded water molecule completes its tetrahedral coordination by accepting hydrogen bonds from two more water molecules lying outside the cavity (O...O separations of 2.86Å and 2.87Å). The authors found that although the hydrogen atoms of

the central water molecule were clearly visible in a final Fourier map, they could not be refined. The evidence of O-H...π(Ph) hydrogen bonding was compelling, however, as the geometry of the water molecule could be accurately determined based only on the refined heavy atom positions around it.

This is in contrast to the problems encountered when trying to study O-H...π(Ph) hydrogen bonds in biological systems. It is likely that O-H...π(Ph) bonds between water and phenyl rings in amino acids containing aromatic groups are common in the natural environment of proteins. However they have been less well studied than their N-H...π(Ph) counterparts. O-H...π interactions may be difficult to study because of the general problems of refining structures containing water crystallographically and the specific problem of locating the water hydrogens accurately, making the hydrogen bonds difficult to identify much less quantify.

Hydrogen bonds in which the O-H vector points to one specific bond of the aromatic ring serving as the acceptor have also been reported beginning with the first example published by Nakatsu et al.[62] in 1978. 2,6-Diphenylphenol was shown to contain an intramolecular hydrogen bond in which the hydroxyl hydrogen, H(1), was found to be located in close proximity to only two carbon atoms of one of the phenyl substituent rings. The O-H bond is almost parallel to that phenyl ring and the perpendicular distances from O(1) and H(1) to the ring plane are 1.924Å and 1.90Å, respectively. The distances H(1)...C(7) = 2.43(4)Å and H(1)...C(12) = 2.40(4)Å are almost equal and much shorter than any of the other H(1)...C_{ring} separations. The distance between H(1) and the midpoint of the C(7)-C(12) bond is 2.31Å and the angle O(1)-H(1)...midpoint is 122°.

Thus, the hydroxyl group is favourably located to bond with one edge of the phenyl ring only, interacting with π electron density in the C(7)-C(12) bond.

The same type of O-H...π(Ph) hydrogen bond, with the O-H vector pointing to only one bond of an aromatic ring, was also reported by S. Ueji et al.[63] in the crystal structure of the related compound, 4-nitro-2,6-diphenylphenol. Again, an intramolecular O-H...π(Ph) hydrogen bond was observed to form between the phenol hydroxyl group and one edge of the substituent phenyl ring. The formation of this type of hydrogen bond most likely arises from steric considerations, since in this case stronger acceptors than the π electrons of the ring are available.

T. Steiner et al.[64] were the first to report a detailed crystallographic study of an O-H...π(Ph) hydrogen bond in which the O-H vector points to a single carbon atom of the aromatic ring acceptor. To define the proposed hydrogen bond geometry unequivocally, the same group published a neutron diffraction study of the same compound a year later.[65] In the crystal structure of 5-ethynyl-5H-dibenzo[*a*,*d*]cyclohepten-5-ol one of the phenyl rings accepts intermolecular hydrogen bonds from a hydroxyl and an ethynyl group, one to each face of the ring. The O-H functional group involved in the O-H...π(Ph) hydrogen bond does not reside above the ring centroid, rather it is very far off-center. The O-H vector points almost linearly to the C(1) atom of the aromatic ring, with H...C(1) = 2.339(6)Å and O-H...C(1) = 174.4(5)°. The other H...C_{ring} distances, and also the hydrogen to ring centroid distance, are all considerably longer. Furthermore, the O-H...π(Ph) interaction is associated with a short H(O)...H(1) contact (2.371Å) which is presumably repulsive.

The title compound is of interest in that it does not follow the hierarchal rules of hydrogen bond formation described earlier. By far the strongest donor available for hydrogen bond formation is the hydroxyl group, the second strongest is the ethynyl group and the remaining C-H donors are all much weaker. The strongest acceptor is also the oxygen atom of the hydroxyl group, followed by the weaker π alkyne and aromatic acceptors. One would predict that a cooperative system of O-H...O-H... hydrogen bonds should form, to satisfy the dual strong donor/acceptor requirements of the hydroxyl group. The ethynyl donor would then form hydrogen bonds with itself or with the phenyl ring. The other possible C-H donors would be expected to play only a marginal role. However, this was not the arrangement observed by the authors. In this case, the normal rules were not followed, presumably due to the complicated shape of the molecule and the consequent steric shielding of the hydroxyl group which prevents effective formation of O-H...O hydrogen bonds. Instead, the O-H donor must resort to the second strongest acceptor available, the phenyl π electrons, which also act as the acceptor for the ethynyl proton. As a result, only weaker hydrogen bonds are formed but these still contribute to the stabilization of the structure.

In the first paper on 5-ethynyl-5H-dibenzo[*a*,*d*]cyclohepten-5-ol, the authors included a number of ab initio molecular orbital calculations carried out on model systems to roughly estimate the interaction energies of the hydrogen bonds. The calculations suggested energies of binding of -1.3 kcal/mol for both the O-H...π(Ph), modelled by methanol/benzene, and the C≡C-H...π(Ph), modelled by propyne/benzene, hydrogen bonds. The calculations were carried out for model pairs with the same contact

geometry as observed in the x-ray crystal structure.

The authors also used the structural results of Rzepa et al.[67] for the compound (*S*)-2,2,2-trifluoro-1-(9-anthryl)ethanol, which had been shown to contain two independent O-H...π(Ph) hydrogen bonds in which the O-H vectors pointed at least roughly toward the phenyl ring centroids of the anthracene. Using the geometry described by Rzepa et al. the authors calculated binding energies of -2.0 and -2.4 kcal/mol for the interactions. As expected, the O-H...π(Ph) centroid type interactions were calculated to be stronger than the off-center O-H...C hydrogen bonds. The O-H...π(Ph) hydrogen bonds were, in general, calculated to be about one third to one quarter the energy of conventional O-H...O hydrogen bonds.

Several more detailed theoretical calculations on model O-H...π(Ph) systems have been reported in the literature. In 1992, S. Suzuki et al.[68] published a combined gas phase spectroscopic and theoretical study on the benzene/water dimer. The ground state microwave spectra of 1:1 clusters of benzene with water (H_2O, HOD or D_2O) were fitted to yield moments of inertia that showed the water molecule to be situated directly above the ring face, in close contact with benzene, a clear indication of hydrogen bond formation. Ab initio calculations (MP2/6-31G** with basis set superposition error correction) gave a binding energy of 1.78 kcal/mol.

The water molecule was found to be situated above the C_6 ring skeleton, with both of the O-H vectors pointing simultaneously toward the π cloud of the benzene ring. The interaction of the H(O) hydrogen atoms with the ring is probably asymmetric, with one being weaker and one being stronger in the minimum energy structure. The two could be interconverted by a rocking motion of the water molecule. The potential surface of the

benzene molecule is very flat, permitting the water molecule to rotate nearly freely with respect to the C_6 axis of benzene. On a vibrationally averaged basis the two water hydrogens are equivalent.

The experimental and ab initio structures of the 1:1 benzene/water dimer were found to be similar, $R_{0,expt}$ = 3.347(5)Å and $\theta_{0,expt}$ = 20±15° versus $R_{0,calc}$ = 3.195Å and $\theta_{0,calc}$ = 24°. R_0 is the distance between the center of mass of the benzene molecule and the center of mass of the water molecule at the zero point vibrational level. The calculated R_0 was somewhat shorter than the experimental value. Both the experimental and theoretical results gave an optimal angle (θ) of roughly 20° between the C_6 axis of benzene and the C_2 axis of water, thus the asymmetric description of the interaction. The water center of mass was allowed to move away from the C_6 axis of benzene during calculations to see if an off-center geometry would be favoured. However, the preferred mode of binding was found to have the water molecule centered on the benzene C_6 axis.

The theoretical study of the benzene/water dimer by Suzuki et al.[68] did not contain a complete geometry optimization. S.Y. Fredricks et al.[69] carried out such an optimization at the MP2 (6-31+G[2d,p]) level of theory and found a minimum energy structure of somewhat different geometry than that reported by Suzuki et al. In the isolated dimer, the water molecule was found to interact more strongly with the benzene ring through one of the H(O) hydrogen atoms than the other. This structure would more closely resemble a situation where one O-H vector points toward the center of the benzene ring. The angle giving the tilt of the water molecule relative to the C_6 axis of the benzene ring was calculated to be 49.3°. The distance from the center of the benzene ring to the interacting hydrogen atom was

calculated to be 2.302Å. The interaction of the water molecule with the benzene ring causes the two O-H bond lengths to become unequal in the theoretically calculated minimum energy structure. The O-H bond associated with the π interaction to the ring was 0.003Å longer and the other O-H bond was 0.001Å shorter than calculated for the equivalent bonds in the free water molecule (0.964Å).

The binding energy of the dimer was calculated by taking its total minimum energy and subtracting the energies of the two individual components. MP2 calculations with basis set superposition error correction gave an energy of 2.49 kcal/mol, somewhat larger than that calculated by Suzuki et al.[68] (1.78 kcal/mol).

Although Fredricks et al.[69] calculated an unsymmetrical arrangement of the water molecule to give the lowest energy dimer, they also found that the symmetrical C_{2v} structure, in which both hydrogen atoms interact with the ring simultaneously, also proposed by Suzuki et al.,[68] had only a slightly higher energy. This symmetric transition structure would allow for interchange of the hydrogen atoms under real conditions, via a rocking motion. Both hydrogen atoms would then interact equally with the benzene ring, on average, restoring the equivalency of the O-H bonds. The water molecule would also undergo large amplitude internal rotation and in plane torsion, resulting in six-fold symmetry being maintained on a vibrationally averaged basis in the gas phase.

1.8.3. The C-H...π(Ph) Hydrogen Bond

C-H...π(Ph) hydrogen bonds are, under normal circumstances, even weaker than O-H...π(Ph) and N-H...π(Ph) interactions because of the

relatively lower electronegativity of carbon as a donor. However, activated donors involving alkyne, aromatic, alkene or even substituted alkyl groups have been shown to form significant C-H...π(Ph) hydrogen bonds. In the past, C-H...π(Ph) interactions were often considered insignificant or unimportant, and in consequence they have not been as well studied as other X-H...π(Ph) bonds. Recently, however, these weak interactions have become the subject of considerable interest. Much of the work is summarized in a 1995 review by M. Nishio et al.[70]

The group of T. Steiner et al. has published a number of crystallographic studies of compounds containing distinct C-H...π(Ph) interactions over the past few years. In these compounds, the interaction studied always involves an acidic C-H donor, typically an alkyne. The 1997 paper by Steiner, Mason and Tamm[65] is most interesting since it involves a neutron crystallographic study of 5-ethynyl-5H-dibenzo[*a*,*d*]cyclohepten-5-ol, in which all the protons are accurately located. In the structure, the intermolecular hydrogen bond donated by the ethynyl group, C≡C-H...π, points to the centroid of one of the aromatic rings, with an H...π_c ring centroid separation of 2.587(5)Å. The ethynyl group itself is placed roughly above the same ring centroid and all the hydrogen to ring carbon distances fall in a narrow range (2.848 to 3.097Å). The distance from hydrogen to the ring centroid is thus shorter than to any of the ring carbons. This is close to the "ideal" geometry, often referred to as a T-shaped or centroid type interaction, which allows the ethynyl donor to bond with the entire π electron cloud.

In a preceding paper on this compound,[64] describing its x-ray crystal structure the authors included ab initio molecular orbital calculations,

using a 6-31G** basis set, on model systems placed in the experimentally determined geometry. In the crystal structure, one of the phenyl groups accepts two hydrogen bonds, from the ethynyl group and from the hydroxyl group, one to each face of the ring. The interaction energies of both hydrogen bonds were calculated to be equal, -1.3 kcal/mol, with the off-center O-H...π(Ph) bond modelled by methanol/benzene and the C-H...π(Ph) bond modelled by propyne/benzene. Owing to the gross simplification used, the results can be taken only as a rough estimate. However, they do show that under certain conditions C-H...π(Ph) hydrogen bonds can have strengths similar to other X-H...π(Ph) bonds (X = O or N) and can have significant influence in a crystal structure.

Steiner et al.[71] have also investigated the C-H...π(Ph) hydrogen bonding in a number of other structures, using conventional x-ray crystallography with isotropic refinement of hydrogen atom positions. (±3)-Phenylbut-1-yn-3-ol was found to have two independent molecules in the unit cell. The alkynyl group of one of the molecules (A) points almost linearly to the centroid of the phenyl ring of the other molecule (B), with a C-H...π_c ring centroid angle of 171°. The H...π_c separation of 2.51Å is reported to be in the range typical for X-H...π(Ph) hydrogen bonds with strong OH and NH donors, immediately suggestive of a significant bonding interaction.

9-Ethynylfluoren-9-ol, closely related to the first compound discussed but with a saturated five-membered central ring rather than a seven-membered ring, was also studied. Again, there are two independent molecules in the unit cell but only one of the ethynyl groups forms a C-H...π(Ph) hydrogen bond, this time to the phenyl ring of a symmetry

related molecule. The H...π_c ring centroid separation, 2.77Å, is longer than in the previous examples.

Model ab initio molecular orbital calculations were also carried out to estimate the interaction energies for these two C-H...π(Ph) hydrogen bonds. These were approximated by contacts of identical geometry between appropriate smaller molecules, propyne and methylbenzene in the former and propyne and benzene in the latter. In the isolated dimers, interaction energies of -1.6 kcal/mol and -1.4 kcal/mol were calculated, respectively. Calculations were also carried out to see if the interconnected hydrogen bonds in (±3)-phenylbut-1-yn-3-ol would exhibit the property of cooperativity. In this structure, the ethynyl group (molecule A) which donates a C-H...π(Ph) hydrogen bond to the phenyl ring (molecule B) also accepts a perpendicular C-H...π contact from the ethynyl group of molecule B'. The ethynyl group of molecule B does not accept a similar interaction, so the arrangement as a whole is finite, C≡C-H...C≡C-H...π(Ph). In the extended system, the C-H...π(Ph) hydrogen bond was calculated to have an interaction energy of -2.2 kcal/mol, a decrease of -0.6 kcal/mol, clearly showing a pronounced cooperativity effect, as would be expected for any true hydrogen bond. The theoretical calculations of Steiner et al. suggest an energy of approximately 2 kcal/mol or less for C-H...π(Ph) hydrogen bonds, similar to the energies calculated for C-H...O interactions and for less than ideal O-H...π(Ph) hydrogen bonds. Of course, the C-H...π(Ph) bonds examined by Steiner et al. are likely stronger than average examples of the type.

In the same paper, Steiner et al. discuss the results of a search of the Cambridge Structural Database in which the closest C-H...X contacts

formed by terminal alkynes were investigated. Of 141 C≡C-H residues in 113 crystal structures, 82 (or 58%) were found to form hydrogen bonds, defined by having an H...X distance of 2.8Å or less, with the conventional acceptors O, N, Cl, Br, F or S. The number of C-H...π type interactions located (31 or 22% of the total) was surprisingly high. Of these, 18 were to an alkyne acceptor, 5 were to an alkene acceptor and 8 were to an arene ring. For the novel C≡C-H...π(Ph) interactions, most were found to have a geometry in which the C-H vector pointed toward the centroid of the phenyl ring. The distance from hydrogen to the ring centroid could be as short as 2.5Å, shorter than any individual H...C_{ring} distance. However, exceptions to the centroid type geometry were also found, geometries in which one or two of the hydrogen to ring carbon distances were shorter than the others and shorter than the H...π_c ring centroid distance. Such interactions could be described as being to an atom or to a bond (edge type), respectively, rather than to the entire π cloud. The above results show that short contacts of sufficiently acidic C-H groups with π bonded aromatic acceptors possess the essential properties of weak hydrogen bonds. A variety of geometries appear possible, just as was observed for O-H...π(Ph) interactions.

Recently, P. Hobza et al.[72] have published a theoretical study on the anti-hydrogen bonding interaction of the C-H...π(Ph) contact in the benzene/benzene dimer. The T-shaped geometry of the dimer was optimized (MP2/6-31G* and 6-31G** basis sets) and found to have C_{2v} symmetry. To the authors' surprise, the C-H bond of the donor was found to become shorter by 0.0033Å relative to the calculated C-H bond length in free benzene (1.0874Å). This C-H bond is also shortened relative to all the other C-H

bonds in the dimer. The C-H bond involved in the T-shaped equilibrium structure of the benzene dimer exhibits features opposite to those observed in normal hydrogen bonds, where the X-H bond is lengthened on hydrogen bond formation (X-H...A). For this reason, the authors termed the interaction the anti-hydrogen bond. They report that the observed shortening of the C-H bond can be seen as evidence for the primarily dispersive nature of this type of hydrogen bond, with an important repulsive component. This is in contrast to "normal" hydrogen bonds which are more electrostatic in nature and which show a lengthening of the X-H bond.

Hobza et al. also calculated a stabilization energy of 1.1 kcal/mol for the benzene dimer in its optimized C_{2v} geometry (MP2/6-31G* with basis set superposition error correction). The stabilization energy is likely underestimated owing to the lack of diffuse polarization functions in the basis set used. The results of Hobza et al. agree well with the less rigourous calculations of Steiner et al. regarding the strength of the C-H...π(Ph) interaction.

1.8.4. The N-H...π(Ph) Hydrogen Bond

The first well documented examples of N-H...π hydrogen bonds were observed in protein crystal structures. In 1986, M.F. Perutz et al.[73] published an investigation on the stereochemistry of drug binding by human haemoglobin. Haemoglobin was found to have a high affinity for the drug bezafibrate. X-ray analysis showed the bezafibrate bound to the walls of the water-filled cavity that runs through the center of the haemoglobin molecule. Among the nine amino acid residues in contact with the drug was

an asparginine whose amino side group pointed at the plane of one of the drug's two benzene rings. Although suggestive of an N-H...π(Ph) hydrogen bond, the resolution was not sufficient to measure the N/H...C_{ring} distances accurately.

Later, E. Tüchsen and C. Woodward[74] reported a similar interaction in pancreatic trypsin inhibitor after studying the high resolution protein structure. The benzene ring of tyrosine-35 was found to be sandwiched between the NH of glycine-37 and the NH_2 side group of asparginine-44, each of them closer to the ring than the sum of the van der Waals radii, providing evidence in favour of hydrogen bond formation.

A further suggestion of the importance of amino-aromatic interactions in the structure of proteins was made by Armstrong et al.[75] The authors synthesized three peptides, the first containing a phenylalanine(i) and a histidine (i+4) four residues apart, optimally spaced for N-H...π interaction in an α-helix structure. In the second peptide the two were separated by five residues, too far apart for interaction to occur, and in the third peptide the phenylalanine was omitted entirely. Circular dichroism measurements showed the first peptide to form the expected α-helical structure while peptides two and three did not. The results proved that the histidine stabilizes the α-helix structure of the peptide by acting as an N-H...π hydrogen bond donor to the phenylalanine acceptor.

Perhaps the most notable example of amino-aromatic hydrogen bonding was described by Waksman et al.[76] in 1992. Tyrosine kinases are vital in cellular signal transduction. Cellular forms of the Rous sarcoma (rsc) tyrosine kinase are transmembrane growth hormone receptors. Activation of the growth hormone receptor causes autophosphorylation of tyrosines on the

cytoplasmic side. This is recognized as a signal by protein domains known as SH2 domains, which then transmit the signal to other proteins in the signal transduction pathway. The complex of the SH2 domain of the viral Rous sarcoma (v-rsc) protein kinase with a peptide from a platelet-derived growth factor was crystallized by the authors. The peptide had a phosphotyrosine at its amino terminus, which was found to bind to the protein via an N-H...π interaction. The guanidinium group of arginine residue 155 was located above the plane of the phenol ring at the short distance of 3.1Å, clearly indicative of hydrogen bond formation.

The chemical literature contains many more examples of interactions between NH proton donors and aromatic acceptors, but the ones quoted here are sufficient to show that such interactions can be biologically important. They can play a significant role in cellular recognition and binding and also contribute to the stability of certain protein structures. A 1993 review by M.F. Perutz[77] details many of the early examples of N-H...π hydrogen bonding studied in proteins, including the ones described and others not mentioned.

Following the report that N-H...π(Ph) hydrogen bonds might be important in the interaction of human haemoglobin with certain drugs, Burley and Petsko[78] were led to search for similar interactions between amino and aromatic groups in 33 highly refined protein crystal structures. The packing geometries in the chosen proteins were analyzed and the position of each amino group was calculated for amino-aromatic contact distances of 10Å or less. These data were compared with the results of an identical calculation for all atoms in the protein less than 10Å from the centroid of an aromatic ring in an amino acid side chain. Amino-aromatic

interactions considered were those between the amino side groups of lysine, arginine, asparginine, glutamine and histidine and the aromatic side chains of phenylalanine, tyrosine and tryptophan.

From the normalized frequency distribution found for the 1556 amino-aromatic contact distances of less than 10Å, which reached a maximum at about 4.75Å, the authors defined the characteristic amino-aromatic interaction distance as being from 3.4 to 6.0Å. (Values below 3.4Å were rarely observed because of the concurrent formation of unfavourable van der Waals contacts.) Of the 401 aromatic residues located in the 33 proteins approximately 50% were found to make close contacts (less than 6Å) with the amino side groups of the amino acids mentioned above. On average, one amino group was found to participate in one amino-aromatic interaction. The observed frequency distributions were significantly different from those that would have been expected if random orientations alone determined interaction geometry.

In fact, the positively charged or $(\delta)+$ amino groups of lysine, arginine, asparginine, glutamine and histidine were found to be preferentially located above the ring centroids (from 3.4 to 6.0Å) of the aromatic side chains of tyrosine, phenylalanine and tryptophan, where they would be in position to hydrogen bond with the $(\delta)-$ π electrons of the ring. This geometric pattern is different from the distribution expected due to random close packing of side chains in a protein, and would be expected to make a significant contribution to the protein stability.

In a later paper, J.B.O. Mitchell et al.[79] dispute, not Burley and Petsko's results, but their interpretation of those results. Mitchell et al. investigated the suggestion that aromatic rings can act as hydrogen

bond acceptors in proteins, by analyzing the geometries of 55 high resolution protein chain structures. Roughly 10% of interactions between sp^2 hybridized nitrogen atoms, from either side chains or main chains, and phenylalanine or tyrosine rings were found to have the nitrogen positioned above the ring plane. Burley and Petsko's results were essentially reproduced. However, Mitchell et al. found that the distribution of interplanar angles was not consistent with a prevalence of amino-aromatic interactions. Rather, the nitrogen containing groups tended to be approximately coplanar with the rings, instead of having the larger interplanar angles expected for N-H...π(Ph) hydrogen bonding. The nitrogen-bearing groups tended to form stacked or parallel interactions with the rings, outnumbering amino-aromatic or perpendicular interactions by a ratio of approximately 2.5 to 1. In the stacked geometries, the NH groups can fulfil their hydrogen bonding potential by forming conventional, energetically stronger, hydrogen bonds with other acceptors in the protein or with the outside environment (solvent water).

The authors used model, ab initio calculations to show that in the gas phase, interaction energies do favour the N-H...π hydrogen bonded structure over the parallel geometry but only by a small amount. However, stacked structures will become favoured when the amino group is able to optimize its conventional hydrogen bonding; in perpendicular interactions the number of conventional hydrogen bonds that can also be formed is limited. The gain in conventional hydrogen bonding presumably more than compensates for the difference between the amino-aromatic and stacked gas phase interaction energies in protein crystal structures.

In the amino-aromatic interactions the authors did study, one H(N)

proton was usually found to point roughly toward a single ring carbon atom. However, since any other hydrogen atoms sharing the same nitrogen tended also to form conventional hydrogen bonds if at all possible, the geometries observed for the N-H...π(Ph) hydrogen bonds were likely to be compromises between the different contacts formed. The N-H...π hydrogen bonds, though observed, were rare and tended to be overshadowed by parallel interactions in the proteins. This is not to say, however, that in certain situations N-H...π(Ph) interactions are not important, the individual cases cited previously show that they can be.

Inspired by the work of Burley and Petsko, Page and Rzepa[80] conducted an analysis of a small molecule search of the Cambridge Structural Database (April 1995 Version) for N-H...π facial distances shorter than the sum of the van der Waals contact distances. The authors searched only for very short N-H...C_{ring} contacts, 1.4 to 2.4Å from the amine hydrogen to either carbon in a C=C system. The structures that fulfilled the contact distance criteria were carefully examined to assess their suitability for more detailed analysis. A number of examples were rejected outright because the close contact was brought about by factors other than the π facial interaction. Other examples were excluded from further analysis because it was not possible to model very large systems or those containing metal centers. The original search located 52 structures, of which 38 were discarded for the reasons mentioned. The remaining 14 structures were accepted for further study; as a group they had acceptably small R-factors, 8% or less, and all had refined hydrogen atom positions. In each of the original reports, the close N-H...π contact was either attributed only to crystal packing effects or else was overlooked

entirely. Of the 14 structures in the final group, remarkably 10 had the close N-H contact to C(3) of an indole ring system.

Semiempirical theoretical calculations were carried out on the 14 structures to estimate the strength of the N-H...π interaction. The methods chosen proved to have shortcomings when used to analyze the hydrogen bonding interactions. Although the results provide only a rough estimate of the true values, they do suggest a small but significant effect from hydrogen bond formation (~1 kcal/mol).

The authors went on to study a group of 12 indole-3-acetic acid (auxin) analogues, those found in the original search plus others located in a search specific for the indole-3-acetamide fragment. The auxin compounds had originally been synthesized to investigate the effects of conformation on plant growth promoting activity. The earlier work had suggested that there was some correlation between the flexibility and orientation of the side chain with respect to the indole ring (influenced by intermolecular hydrogen bonding) and biological activity. However, this new investigation showed that these compounds consistently formed a remarkably short intramolecular N-H...C(3) contact (<2.4Å) between N(22)-H of the acetamide fragment and C(3) of the indole ring. The N-H vector was found to point almost directly toward the center of the indole ring in most cases. The authors contend that the close N(22)-H...C(3) contact is due to the formation of an intramolecular hydrogen bond with the π system of the indole moiety. Semiempirical molecular orbital calculations showed this interaction to vary in strength from about 0.5 to 2 kcal/mol. Considering the short contact distance in these compounds, the strength of the hydrogen bond is probably underestimated slightly. However, there

is no doubt that the N-H...π interaction has an effect on the conformation adopted by the auxin.

A 1993 publication by M.A. Viswamitra et al.[81] included a search of the Cambridge Structural Database (1990 Version) specific for O-H...π(Ph) and N-H...π(Ph) interactions. Again, the search conditions were relatively narrowly defined so some weaker bonds could have been needlessly eliminated; still, the results are informative.

The Cambridge Structural Database search was limited to error-free, nondisordered structures with R less than 10% and refined hydrogen atom positions. The X...C (X = N or O) distance was specified to lie between 2.9 and 3.4Å, and the X-H...C_{ring} angle was constrained to be between 100° and 180°. Intramolecular hydrogen bonds were also excluded. The structures located were always scrutinized manually and in several cases, after reference to the original literature, obviously inappropriate compounds were also eliminated.

The database search located 2823 structures containing both O-H and phenyl groups, of which 5 were found to form O-H...π(Ph) hydrogen bonds. In the analogous N-H...π(Ph) case, 12 bonds were located in the 3057 structures found to contain both N-H and phenyl groups. For the X-H...π(Ph) bonds, overall mean values were calculated using the shorter of the distance between X/H to the ring centroid or X/H to the closest carbon atom in the ring, in each individual case. The O-H...π(Ph) hydrogen bonds were characterized by mean O...C_{ring} and H...C_{ring} separations of 3.29Å and 2.43Å, respectively, and by a mean O-H...C_{ring} angle of 150°. The corresponding mean distances in the N-H...π(Ph) interactions, N...C_{ring} = 3.31Å and H...C_{ring} = 2.47Å, were similar but slightly longer than the

oxygen values, while the mean N-H...C_{ring} angle of 148° was practically identical to the mean O-H...C_{ring} angle.

The authors use their results to suggest that X-H...π(Ph) hydrogen bonds, though rare, can be structurally significant when they do occur. The database analysis also revealed that for the X-H...π(Ph) contacts, the hydrogen atom was usually directed into the middle of the aromatic ring system (centroid type), although examples where the X-H group makes a close approach to only two adjacent carbons of a particular phenyl group (edge type) were also located.

In a 1997 publication by some of the same authors, F.H. Allen et al.[82] briefly report the results of a more recent Cambridge Structural Database search of N-H...π(Ph) interactions. Based on geometrical criteria, the authors suggest that N-H...π(Ph) hydrogen bonds may be structurally significant when the H...π_c ring centroid distance is less than 2.6Å and the N-H...π_c ring centroid angle is between 130° and 180°.

Very few individual structures, in which N-H...π(Ph) hydrogen bonding is discussed as an important feature of the overall structure, have appeared in the literature. The first example of an N-H...π(Ph) hydrogen bond featured in a small molecule crystal structure was reported by L.R. Hanton et al.[58] in 1992. Subsequently, F.H. Allen et al.[82] reported the results of the neutron analyses of 2- and 3-aminophenol, which were both shown to contain structurally important N-H...π(Ph) hydrogen bonds. More recently, T. Steiner et al.[90] have detailed the N-H...π(Ph) hydrogen bonding in the structure of propylargylammonium tetraphenylborate. Finally, Bakshi et al.[83] have published a detailed report, specifically on N-H...π(Ph) hydrogen bonding in an extensive series of organoammonium

tetraphenylborate salts.

L.R. Hanton et al.[58] published the x-ray crystal structure determination of a cyclohexane derivative substituted at one carbon with two 2,4-dimethyl-3-aminobenzene groups in 1992. They report it as the first known example of a compound containing an N-H...π(Ph) hydrogen bond. The compound contains four N-H hydrogen bond donors but no obvious traditional hydrogen bond acceptors. Its crystal structure illustrates two ways in which this situation can be accommodated: (1) through formation of N-H...π(Ph) hydrogen bonds and (2) through a change in hybridization at the nitrogen center in one of the two amino groups.

Location of the hydrogen atoms in the difference Fourier map and subsequent refinement of their positions (final R = 0.050) revealed that the two nitrogen atoms, which had been expected to be chemically equivalent, were in fact different. N(1) was found to be sp^2 hybridized, while N(2), the other nitrogen atom in the same molecule, was found to be tetrahedral with sp^3 hybridization. The hydrogen bonding requirements of the system are so strong that they induce a change in hybridization at one of the nitrogen centers, facilitating formation of $N(sp^2)$-H...$N(sp^3)$ hydrogen bonds. Such a switch in hybridization, resulting from intermolecular hydrogen bonding, could play an important role in the catalytic properties of certain enzymes.

In addition to the N-H...N hydrogen bonds found between the sp^2 $N(1)H_2$ hydrogens (donor) and the sp^3 N(2) lone pairs (acceptor), N-H...π(Ph) hydrogen bonds were also located. The acidic hydrogen H(2A) was found to lie over the geometric center of one aromatic ring (to within 0.15Å) and the N(2)-H(2A) bond was inclined at 49° to the plane of that

ring. The distance between the hydrogen and the plane was 2.42(2)Å and the H...C_{ring} distances ranged from 2.72(2) to 2.87(2)Å [100Δ = 15], indicative of a centroid type interaction.

The hierarchal rules of hydrogen bond formation, discussed previously, are followed in this structure. The best hydrogen bond donors, the sp^2 $N(1)H_2$ hydrogens, are paired with the best acceptors, the lone pairs on the sp^3 hybridized N(2). The other hydrogen bond donors, the sp^3 $N(2)H_2$ hydrogens, are paired with the next best hydrogen bond acceptor, the π electrons of the aromatic ring. In addition, the N-H...π(Ph) hydrogen bond is formed with the best π facial acceptor. In the aromatic ring that has the sp^2 $N(1)H_2$ group bonded to it, the nitrogen lone pair is delocalized into the ring system, giving an electron-rich π cloud. This aromatic ring is, therefore, a better hydrogen bond acceptor than the other one, where delocalization does not occur. It, in fact, serves as the acceptor in the N-H...π(Ph) hydrogen bond.

Low temperature neutron diffraction analyses of 2- and 3-aminophenol were performed by F.H. Allen et al.[82] to explore the existence of N-H...π(Ph) hydrogen bonds in these structures. In addition to O-H...N and N-H...O hydrogen bonds, both the compounds were found to contain weaker N-H...π(Ph), C-H...O and C-H...π(Ph) interactions. The unusual pattern of hydrogen bonding observed in these structures was not observed in 4-aminophenol or other related systems and led the authors to speculate that the formation of weak hydrogen bonds might be important in these instances.

4-Aminophenol forms the hydrogen bonds expected based on the hierarchal rules discussed earlier and only "strong" hydrogen bonds are observed in the structure, two of N-H...O type and one O-H...N. However,

the patterns observed in 2- and 3-aminophenol are quite different and do not follow the predicted hierarchy exactly. In both compounds, one O-H...N, one N-H...O and one N-H...π(Ph) hydrogen bond are formed. The second lone pair on oxygen accepts a C-H...O hydrogen bond to complete the hydrogen bonding arrangement at the tetrahedral oxygen and nitrogen centers. Unlike the situation in 4-aminophenol, a combination of strong and weak hydrogen bonds are formed. In all three compounds an extended network of hydrogen bonding exists and cooperativity would be expected.

Neutron diffraction confirmed the presence of N-H...π(Ph) hydrogen bonds in both 2- and 3-aminophenol. However, it was not possible for the authors to conclude definitively if a C-C bond of the phenyl ring (edge type) or the ring as a whole (centroid type) was the acceptor of the N-H...π(Ph) hydrogen bond. In 2-aminophenol, for example, the shorter approach (N...π_c = 3.199Å and H...π_c = 2.309Å), that to the ring centroid (π_c) is the more bent one (145.0°). A longer approach, to the midpoint of the C(5)-C(6) bond of the ring (N...bond midpoint = 3.438Å and H...bond midpoint = 2.421Å) is more linear (173.9°). A similar geometry was observed in 3-aminophenol where the closest contact is again to the ring centroid (N...π_c = 3.328Å, H...π_c 2.409Å and N-H...π_c = 148.7°) but the best angle is made to a C-C bond in the ring (N...bond midpoint = 3.522Å, H...bond midpoint = 2.504Å and N-H...midpoint = 171.8°). The nitrogen atoms are tetrahedral in both structures, which allows formation of more favourable N-H...π(Ph) hydrogen bonds, relative to a planar geometry at nitrogen.

Interestingly, both 2- and 3-aminophenol pack in an arrangement that the authors describe as the "herringbone fashion", almost identical to

that observed for the aromatic rings in crystalline benzene. The authors note that herringbone interactions are identified by their characteristic T-shaped geometries and that their importance in the crystal structures of aromatic compounds has been discussed repeatedly in the past. An alternative view of the packing arrangement is that C-H...π(Ph) hydrogen bonds form between the aromatic rings in the T-shaped geometry and that the formation of these additional hydrogen bonds serve to stabilize the structure. The structures observed for 2- and 3-aminophenol would be influenced by the optimization of a combination of the strong and weak hydrogen bonds, including C-H...O, N-H...π(Ph) and C-H...π(Ph) interactions, rather than just the strong hydrogen bonds as observed in 4-aminophenol.

The first theoretical calculations, carried out to estimate the strength of the N-H...π(Ph) hydrogen bond, were published by M. Levitt and M.F. Perutz[84] in 1988. The authors used simple energy calculations to determine the strength of an idealized N-H...π(Ph) interaction in which the N-H bond was constrained to lie on the C_6 axis of a benzene ring. The interactions between hydrogen bonded atoms (N-H to all 12 ring atoms) were treated as a simple sum of two terms, the van der Waals and electrostatic contributions to the energy. In this model, the aromatic N-H...π(Ph) hydrogen bond would be described as arising from the small partial charges centered on each atom; there is no need to specifically consider the delocalized π electrons of the aromatic ring.

Levitt and Perutz calculated the optimum interaction, in which the nitrogen atom was separated from the ring centroid by 3.40Å, to have an interaction energy of -3.35 kcal/mol. In this optimum interaction, charges

of +0.119e, -0.119e, -0.333e and +0.333e were placed on the ring hydrogen atoms, the ring carbon atoms, the nitrogen and the interacting hydrogen atom, respectively. Approximately 75% of the calculated interaction energy was found to arise from the electrostatic term. More complete calculations, which did not assume 6-fold symmetry and treated all 14 atoms of the system explicitly, confirmed these results.

The possibility of hydrogen bond formation between two aromatic benzene rings, C-H...π(Ph), was also considered by the authors. The partial charges located on ring carbon and hydrogen atoms were approximately one third those on nitrogen and hydrogen, leading to the expectation that the C-H...π(Ph) interaction would be one third as strong, or about 1 kcal/mol.

In 1993, D.A. Rodham et al.[85] published the results of a combined experimental and theoretical investigation of the benzene/ammonia dimer. High resolution optical and microwave spectra of the dimer in the gas phase demonstrated that symmetry was maintained about the C_6 axis of benzene on a vibrationally averaged basis. The results were consistent with ammonia residing above the benzene plane and undergoing free, or nearly free, internal rotation. This is the same general geometry as had been observed previously in the C_6H_6/H_2O dimer.[68] Experimentally, the distance from the ammonia center of mass to the benzene center of mass, R_{expt}, was found to be 3.590(5)Å, while the tilt angle, θ_{expt}, the angle between the C_6 axis of benzene and the C_3 axis of ammonia, was found to be 59±5°. This geometry would allow the ammonia protons to interact with the π electrons of the benzene ring. An experimental estimate for the zero point dissociation energy of the complex was found to be 1.4 kcal/mol.

In contrast, ab initio molecular orbital calculations (MP2/6-31G**, not corrected for basis set superposition error) gave a binding energy of 2.4 kcal/mol for the benzene/ammonia dimer. Full geometry optimization produced an equilibrium structure (R_{calc} = 3.43Å, θ_{calc} = 52°) which was very similar to that observed experimentally. The calculations indicated that in its minimum energy geometry the dimer has one proton pointing directly to the center of the benzene ring. However, this "monodentate" structure was found to be only slightly more stable than a "bidentate" structure, in which two protons on ammonia point simultaneously toward the benzene ring, the difference in energy being only 0.1 kcal/mol. In both geometries the ammonia center of mass was found to lie above the plane of benzene along its C_6 axis. In the gas phase dimer, the relatively free rotation of ammonia would allow each hydrogen in turn to interact with the π electron cloud, via the "bidentate" intermediate, rendering them equivalent.

The ammonia/benzene dimer was found to have a larger separation and a lower calculated interaction energy than had been found previously for the water/benzene dimer,[68] reflecting the weaker hydrogen bond donor ability of nitrogen relative to oxygen. The calculated minimum energy geometry for the dimer, with one N-H vector of ammonia pointing toward the center of the benzene ring, is similar to the N-H...π(Ph) hydrogen bond geometry observed in both small molecule and protein crystal structures. The calculated interaction energy of 2.4 kcal/mol is somewhat smaller than the 3.35 kcal/mol estimated by Levitt and Perutz.[84]

Very recently, Inoue et al.[86] have used density functional theory to recalculate the interaction energy for the ammonia/benzene dimer. Beginning from the "monodentate" C_6H_6/NH_3 geometry described by Rodham et

al.,[85] an interaction energy of 0.9 kcal/mol was calculated, closer to the experimental value (1.4 kcal/mol) than to the MP2/6-31G** value (2.4 kcal/mol). The distance along the normal line from nitrogen to the benzene ring was calculated to be 3.685Å, which was also in better agreement with the experimentally determined value (3.59Å) than with the MP2 result (3.43Å). The benzene ring in the "monodentate" geometry was found to be slightly concavely deformed, with the hydrogen atoms of the benzene ring displaced very slightly towards ammonia. The authors feel that these results strongly support the applicability of density functional theory to the calculation of subtle intermolecular interactions. However, it is also interesting to note that the calculated interaction energy for the "bidentate" dimer geometry was only 0.1 kcal/mol using density functional theory, not the 2.3 kcal/mol found by Rodham et al.[85] using MP2/6-31G** theory; the reason for this difference is not clear.

The main purpose of the Inoue et al.[86] publication was to compare the strength of amino-aromatic interactions with ammonium-aromatic interactions of similar type. Under physiological conditions most amino acid residues in proteins exist in their protonated ammonium forms (with appropriate counterions) and act as stronger acids than free amines. Ammonium salt-aromatic interactions would thus be expected to contribute more dominantly than amine-aromatic interactions in stabilizing protein structures.

For a model ammonium salt-aromatic interaction the authors began with the "monodentate" geometry of the C_6H_6/NH_3 dimer calculated by Rodham et al.[85] and added an extra proton to ammonia (away from the ring plane in the former lone pair position) and a formate ion to form a salt bridge

with the ammonium ion. The interaction energy calculated for the ammonium formate-benzene complex using density functional theory was 4.06 kcal/mol, for an N...ring plane separation of 3.642Å and an H...ring plane separation of 2.597Å. The results of Inoue et al.[86] show that ammonium salt-aromatic ring interactions could rival or surpass amine-aromatic hydrogen bonds in the stabilization of protein structures.

In a somewhat related paper, E.M. Duffy et al.[87] reported on the possible interactions between protein denaturants and aromatic hydrocarbons in water. Small molecules like urea and guanidinium chloride are routinely used to unfold proteins, but the mechanism of denaturation using these chaotropes has not been well established. It is possible that they act via a direct mechanism, in which specific interactions [N-H...π(Ph)] occur between the denaturant and the protein. To explore this possibility, the authors used Monte Carlo statistical mechanics simulations to see if urea or the guanidinium ion would form complexes with protein constituents both in the presence and absence of water.

In gas phase calculations, the optimal interactions were found to feature Coulombically sensible T-shaped structures. In particular, the guanidinium ion/benzene complex was found to have C_{2v} symmetry with the cation's central carbon atom above the ring plane on the benzene C_6 axis and two hydrogen atoms (on two different nitrogen atoms) pointing directly down into the ring. Although not explicitly stated by the authors, from a diagram they include it appears that the two N-H vectors are centered above and point down to opposing C-C bonds of the benzene ring. The guanidinium carbon to ring centroid distance was calculated to be 3.831Å for the gas phase dimer, while the interaction energy was found to be

-9.63 kcal/mol. In the guanidinium ion/benzene pair the calculated interaction energy was dominated by the electrostatic (as opposed to the van der Waals) contribution, not unexpected for the charged species. The results support the existence of direct chaotrope/arene interactions, through formation of N-H...π(Ph) hydrogen bonds between the denaturant and aromatic side chains on amino acid residues in the protein.

Free energy profiles for the separation of the model complexes in aqueous solution were also calculated. The guanidinium ion/benzene contact minimum in water was found to occur at 3.50Å with a 3.20 kcal/mol well depth. This separation is considerably shorter than that calculated for the gas phase dimer and reflects a shift from a perpendicular interaction in the gas phase to a stacked or parallel interaction in water. In the stacked interaction, the guanidinium ion remains centered over the benzene ring but is oriented in a plane parallel to the ring, similar to the geometry found by Mitchell et al.[79] in their investigation of protein structures. It would be favoured by the formation of strong conventional hydrogen bonds between the guanidinium ion and the solvent water (N-H...O). The parallel geometry allows maximal formation of these strong hydrogen bonds, at the expense of the weaker N-H...π(Ph) interactions. Subsequent gas phase optimizations, constrained to have the guanidinium ion parallel to the benzene ring plane, produced a geometry with a separation distance of 3.59Å and an interaction energy of -4.72 kcal/mol. The large difference in the gas phase interaction energies (4.70 kcal/mol) between the perpendicular and parallel geometries is compensated by the formation of strong hydrogen bonds with water in the latter case.

It is interesting that these results support the findings of

Mitchell et al.[79] who used a database search and analysis to study the interactions between amino and aromatic groups in proteins. Both sets of data indicate that in the presence of conventional hydrogen bond acceptors, the formation of strong N-H...X hydrogen bonds will be maximized. However, in the absence of such acceptors, N-H...π(Ph) hydrogen bonds will be formed if aromatic rings are accessible.

In summary, a new communication by Starikov and Steiner (1998)[88] highlights all the important features of N-H...π(Ph) hydrogen bonds discussed so far. The authors reexamined the neutron diffraction crystal structure of vitamin B12 coenzyme (~18H_2O) at 15K, originally reported by J.P. Bouquiere et al.[89] in 1993, and found it to contain a previously undetected intramolecular N-H...π(Ph) hydrogen bond between the N-H of a propionamide side chain and a benzimidazole group serving as the π acceptor. The original authors had reported these N-H amide hydrogens as being free from hydrogen bonding, illustrating how N-H...π(Ph) interactions have been overlooked, even in the recent past.

The core of the vitamin B12 coenzyme is formed by a corrin ring which complexes a central Co(1+) ion. The corrin ring has eight peripheral methyl groups and seven longer flexible side chains each with an amide functional group. A nucleotide with a 5,6-dimethylbenzimidazole group is bonded to side chain "*f*" via its phosphate group and is also bonded to cobalt via a nitrogen of the imidazole ring. Side chain "*d*" is oriented such that a terminal amide N-H points directly at the center of this benzimidazole group's benzene ring forming the N-H...π(Ph) hydrogen bond.

Owing to its relatively small size (for a biological macromolecule) the vitamin B12 coenzyme could be studied with high resolution and neutron

diffraction allowed the geometry of the N-H...π(Ph) hydrogen bond to be accurately determined. In fact, this is one of the best examples reported to date, not only because it is more reliably determined than previous x-ray diffraction based structures but also because it is one of the shortest and most well-centered interactions ever observed, comparable only to the neutron structures of 2- and 3-aminophenol reported by Allen et al.[82]

The N-H...π(Ph) hydrogen bond in the coenzyme of vitamin B12 was characterized by an N-H covalent bond length of 0.99Å and by a hydrogen to benzene ring centroid distance of 2.58Å, with distances from the hydrogen atom to individual ring carbon atoms ranging from 2.75 to 3.14Å [100Δ = 39]. The corresponding nitrogen to ring centroid distance was 3.42Å [N...C_{ring} distances ranged from 3.36 to 4.02Å] and the N-H...π_c ring centroid angle was 143.3° [N-H...C_{ring} angles ranged from 115.0° to 170.7°].

To estimate the strength of the N-H...π(Ph) hydrogen bond formed in the vitamin B12 coenzyme, ab initio molecular orbital calculations were performed on a model system, the acetamide/1,5,6-trimethylbenzimidazole dimer, placed in the experimental geometry. Using a 6-31G* basis set at the MP2 level of theory and including a basis set superposition error correction, an energy of 16.7 kJ/mol was calculated for the hydrogen bond in the dimer. The authors were surprised by the strength of the interaction, it being similar in energy to many conventional N-H...acceptor hydrogen bonds. It is also similar in magnitude to the energy estimated by Levitt and Perutz[84] for N-H...π(Ph) interactions in proteins. An energy of almost 20 kJ/mol would be expected to be at the high end of the scale

for N-H...π(Ph) hydrogen bonds which rarely exhibit such ideal geometries.

The authors searched the Cambridge Structural Database to see if vitamin B12 coenzyme analogs could be located and shown to contain similar N-H...π(Ph) hydrogen bonds. They found that N-H...π(Ph) hydrogen bonds did not occur in any of the six analogs located, rather these structures were all found to adopt stacked or parallel arrangements of amide and aromatic side groups, allowing formation of the maximum number of conventional N-H...N and N-H...O hydrogen bonds. These results support the earlier conclusions of Mitchell et al.[79] who showed that stacked amino/aromatic arrangements are generally preferred in protein structures because conventional hydrogen bonding is maximized. However, the N-H...π(Ph) hydrogen bond in the vitamin B12 coenzyme also emphasizes that such bonds do naturally occur under some conditions and that when they do occur they can offer significant stabilization to a structure.

1.8.5. The N-H...π(Ph) Hydrogen Bond in Tetraphenylborate Salts

Organoammonium tetraphenylborate salts represent a system in which conventional hydrogen bond donors, H(N) of the cation, usually face a complete lack of conventional hydrogen bond acceptors. To fulfil the hydrogen bonding requirements of the donor(s), in many cases (unless solvent has been incorporated in the crystal) the only available acceptor is an arene ring of the tetraphenylborate anion. Such compounds have thus been shown to form N-H...π(Ph) hydrogen bonds in a wide variety of situations and configurations, making the system an ideal one in which to study the interaction.

The group of Cameron and Knop has been involved in the investigation

of N-H...π(Ph) hydrogen bonds for a number of years. A 1994 publication by P.K. Bakshi et al.[83] describes a systematic, experimental investigation of hydrogen bonding to aromatic π electrons in tetraphenylborate crystals. A total of 15 crystal structure determinations, on a series of organoammonium tetraphenylborate salts, were used to classify N-H...π(Ph) bond types and geometries. In the structures studied, the cation nitrogen atom(s) was found to form, simultaneously, up to four hydrogen bonds (in ammonium tetraphenylborate) equal to the number of protons bonded to it. Hydrogen bonds were formed to any strong acceptors available first, usually solvent lone pairs (N-H...X), and then to aromatic π acceptors [N-H...π(Ph)], such that each N-H available formed some type of interaction unless prevented by severe steric restraints. Examples of normal N-H...π bonds, as well as bifurcated N-H...2π and even trifurcated N-H...3π interactions were observed. In addition to these homodesmic geometries, heterodesmic bifurcation N-H...π,X was also found. Finally, examples were observed in which the H(N) of the cation was bonded to a phenyl ring indirectly, through a solvent molecule, a geometry previously reported by Aubry et al.[61] in the structure of tri-*n*-butylammonium tetraphenylborate monohydrate.

The geometry of each individual N-H...π(Ph) hydrogen bond was studied in detail and the parameters were then used to provide statistical values for the different interaction types (normal, bifurcated, etc.). The mean of the 26 N...π_c and H(N)...π_c (where π_c is the ring centroid) distances in the normal bond sample were 3.25(18)Å and 2.34(19)Å, respectively, with an average N-H(N)...π_c angle equal 156(16)°. For the same set of data, the means of $\bar{d}$(N...C) and $\bar{d}$[H(N)...C], the average

distance to each carbon in the ring, were calculated to be 3.54(16)Å and 2.72(16)Å, respectively.

The set of all bifurcated hydrogen bonds was found to have a mean N...π_c separation of 3.51(29)Å, a mean H(N)...π_c distance of 2.92(40)Å and a mean N-H(N)...π_c angle of 119(22)°. As expected the bifurcated N-H...2π hydrogen bonds occur at longer distances than the normal interactions, in keeping with their "compromise" geometries. The mean angle was also found to be significantly smaller, with a broader distribution, than the normal interaction, again as expected on bifurcation.

The bifurcated N-H...2π hydrogen bonds tended to be asymmetric, with one stronger (larger angle, shorter distance) and one weaker component (smaller angle, longer distance). If the original bifurcated sample was divided into these two groups, based on the value of the N-H(N)...π_c angle, values for $\bar{d}$(N...C), $\bar{d}$[H(N)...C] and N-H(N)...π_c were 3.47(21)Å, 2.70(22)Å and 136(16)° for the stronger component and 3.61(33)Å, 3.21(37)Å and 103(11)° for the weaker component, respectively.

A 1997 publication by T. Steiner et al.[90] also includes a similar geometrical analysis of the N-H...π(Ph) hydrogen bonds formed by propylargylammonium, $[H_3NCH_2C{\equiv}CH]^+$, tetraphenylborate. The conventional, low temperature x-ray refinement showed that C≡C-H...π(Ph) hydrogen bonds were also present in the structure, which contains two cations and two anions per asymmetric unit. The ammonium group of each cation forms three N-H...π(Ph) hydrogen bonds to phenyl rings of neighbouring tetraphenylborate anions. However, the geometries of the hydrogen bonds formed by cations A and B were found to be quite different. Cation B was also found to be disordered at the nitrogen atom, leading to some uncertainty in the

geometrical data.

For cation A, the H(N)...π_c (ring centroid) distances were found to range from 2.08 to 2.37Å, the N...π_c distances from 3.02 to 3.32Å and the N-H(N)...π_c angles from 146 to 164°. In all of these hydrogen bonds, the N-H group was found to sit almost exactly above the ring centroid, pointing directly at the phenyl ring face. The distance from the H(N) atom to the ring centroid was shorter than to any of the six ring carbon atoms, close to the "ideal" centroid type geometry and indicative of relatively strong N-H...π(Ph) interactions. [(i) N(A)-H(1)...Ph3(B), H(1)...π_c = 2.08Å (164°), H(1)...C_{ring} = 2.47-2.53Å, 100Δ = 6; (ii) N(A)-H(2)...Ph1(B), H(2)...π_c = 2.11Å (146°), H(2)...C_{ring} = 2.37-2.68Å, 100Δ = 31; (iii) N(A)-H(3)...Ph4(B), H(3)...π_c = 2.37Å (153°), H(3)...C_{ring} = 2.47-3.00Å, 100Δ = 53]. The geometries of the three N-H...π(Ph) hydrogen bonds of cation B were found to be quite different, with two having closest approaches to individual C-C aromatic bonds (edge type) rather than being centered. [(i) N(B)-H(1)...Ph2(B), edge type, H(1)...π_c = 2.83Å (125°), H(1)...C_{ring} = 2.38-3.78Å, 100Δ = 140; (ii) N(B)-H(2)...Ph4(A), centroid type, H(2)...π_c = 2.39Å (142°), H(2)...C_{ring} = 2.52-2.99Å, 100Δ = 47; (iii) N(B)-H(3)...Ph1(B), edge type, H(3)...π_c = 2.92Å (121°), H(3)...C_{ring} = 2.46-3.85Å, 100Δ = 139]. However, because of the disorder at the nitrogen center in cation B it is not possible to know with certainty the accuracy of these results. Overall, the results of Steiner et al. are consistent with those reported by Bakshi et al.[83], illustrating again the flexible nature of the N-H...π(Ph) interaction.

The results of Bakshi et al.[83] and of Steiner et al.[90] allowed classification of N-H...π(Ph) hydrogen bonds in tetraphenylborate salts

based on geometrical parameters from conventional x-ray determinations. In the present work, the idea was to extend the investigation further. Multipole refinement of high quality, low temperature data collected for selected organoammonium tetraphenylborate salts would be used to generate deformation density maps to visualize the N-H...π(Ph) hydrogen bonds.

1.8.6. The Topology of N-H...π(Ph) Hydrogen Bonds

Few examples of topological analyses of X-H...π(Ph) hydrogen bonds have ever appeared in the literature and, in fact, no experimental examples were located. However, in 1990 Tang et al.[53] published a theoretical study on π-type hydrogen bonded systems in which hydrogen fluoride served as the proton donor and one of the acceptors chosen was benzene. Full geometry optimizations of the constituent molecules and of the C_6H_6/HF dimer were carried out using a 6-31G* basis set. The dimer was found to have C_{6v} symmetry with HF lying on the C_6 axis of benzene and hydrogen pointing directly and most closely at the ring centroid. The HF bond length was calculated to be 0.913Å and the H...π_c ring centroid separation 2.418Å. Within the benzene ring, the C-C bond length was 1.387Å and the C-H bond length was 1.075Å, the former slightly lengthened relative to the value calculated in free benzene, 1.386Å. A single point MP2/6-31G** calculation was performed on the 6-31G* optimized geometry to give an estimation of the hydrogen bond energy, the total calculated energy of the complex subtract the sum of the individual energies of the constituent molecules. The calculated hydrogen bond stabilization energy was 4.81 kcal/mol.

Based on topological analysis of the theoretically determined charge

distribution (6-31G*) hydrogen bonding was found to exist in the C_6H_6/HF dimer. In this system, six bond paths were located, each equivalent by the C_6 symmetry, connecting the hydrogen atom of HF to each of the six carbon atoms in the benzene ring, with the critical points located closer to hydrogen than to the ring. The properties calculated at the bond critical point were $\rho_b(\mathbf{r})$ equal to 0.00502 au or 0.0339 eÅ^{-3} and $\nabla^2\rho_b(\mathbf{r})$ equal to 0.02381 au or 0.5738 eÅ^{-5}.

In a 1997 publication, I. Rozas et al.[54] reoptimized the geometry of the C_6H_6/HF dimer using a larger basis set, 6-311++G**, at both the MP2 level of theory and using density functional theory. The MP2/6-311++G** results matched the quoted experimental values most closely and are the ones discussed here.

In the minimum energy structure of the C_6H_6/HF complex, the hydrogen atom of the HF molecule was found to point towards the middle of one of the C-C ring bonds, quite different from the results of Tang et al.[53] The distances from F and H to the midpoint of that bond in the ring were calculated to be 3.298Å and 2.408Å, respectively, and the F-H...ring plane angle was found to be 89.3°. These are in good agreement with the experimentally determined distances of 3.18Å and 2.25Å, respectively. Formation of the C_6H_6/HF dimer was found to increase the C-C bond lengths within the ring [1.402, 1.402 and 1.401Å - the first being the length of the interacting bond] relative to the same bond length in free benzene [1.400Å]. A loss of symmetry in the aromatic ring was observed on complex formation (mirror symmetry maintained), as reflected in the number of unique C-C bond lengths. The hydrogen bond energy of the MP2/6-311++G** optimized geometry, with basis set superposition error correction applied,

was calculated to be -3.22 kcal/mol, slightly less than that Tang et al.[53] had found.

Considering the results from previous spectroscopic studies of the C_6H_6/HF complex, Rozas et al. interpret their results as being consistent with two equilibrium HF orientations. In one possible equilibrium structure, the fluorine atom is placed over the benzene ring, close to or on the C_6 axis and the HF then oscillates about its center of mass to produce a symmetric cone of all possible HF orientations. In the other possible orientation, the HF axis is placed at some angle to the C_6 axis so that the hydrogen donor points at a single carbon atom in the ring.

A bond critical point was located between the hydrogen atom of HF and one C-C π bond in benzene, a necessary criterion for hydrogen bond formation. The critical point was characterized by a value of 0.0093 au (0.063 $e\text{Å}^{-3}$) for $\rho_b(\mathbf{r})$ and of 0.031 au (0.75 $e\text{Å}^{-5}$) for $\nabla^2\rho_b(\mathbf{r})$. While analyzing the bond path corresponding to the F-H...π(Ph) hydrogen bond, the authors found an unusual situation. The interaction line from the hydrogen of HF was found to proceed to the bond critical point at the midpoint of the C-C bond in the interacting portion of the benzene ring. In the T-shaped interaction, the (3,-1) bond critical point in the interacting ring C-C bond is the attractor for the bond path linking the hydrogen of HF to benzene. This is termed a "conflict catastrophe structure". From the point of view of the electron density this F-H...π configuration is unstable because even a small displacement of the HF molecule from the conflict catastrophe configuration causes the bond path to change drastically. A break in the symmetry of the system seems to be the generator of the major change observed. Such a conflict catastrophe

situation would be unlikely to arise in the crystalline environment of organoammonium tetraphenylborate salts, however, it is interesting that the bond path in the C_6H_6/HF dimer was found to go to the midpoint of a C-C bond rather than to a single carbon atom, as Tang et al.[53] had observed previously.

Recently, P. Tarakeshwar et al.[91] have published the results of ab initio calculations, carried out at the MP2 level using large basis sets, on the benzene-HF system. Although the authors did not include a topological analysis of the theoretically generated electron density, their calculations help to tie together the previously reported results. Tarakeshwar et al. located three different F-H...π(Ph) minima. The "on atom" conformer, with F-H directed towards a single carbon atom of the benzene ring, and the "on bond" conformer, with F-H pointing towards one C-C bond of the benzene ring, were found to be almost isoenergetic and the lowest energy conformers at all levels of theory. However, they were only slightly lower in energy than the symmetrical C_{6v} (centroid type) conformer, again implying that the potential energy surface of the benzene ring is very flat. Although the energies of the "on bond" and "on atom" structures were calculated to be essentially equivalent (4.15 kcal/mol when a basis set superposition error correction was included in the highest level calculation), vibrational frequency analysis showed the "on bond" conformer to be the equilibrium structure, substantiating the results of Rozas et al.[54] Finally, Tarakeshwar et al. calculated that in the C_6H_6...HF dimer the interaction energy is dominated by the electrostatic contribution.

1.9. Summary

This work was begun with the collection of high quality, low temperature sets of x-ray diffraction data for four organoammonium tetraphenylborate salts at Molecular Structure Corporation in the Woodlands, Texas. The compounds studied were ammonium tetraphenylborate ($[NH_4]^+[B(C_6H_5)_4]^-$), [DabcoH]$^+$[$B(C_6H_5)_4$]$^-$ where Dabco is 1,4-diazobicyclo[2.2.2]octane, guanidinium tetraphenylborate acetonitrile solvate ($[C(NH_2)_3]^+[B(C_6H_5)_4]^- \cdot CH_3CN$) and biguanidinium tetraphenylborate ($[N(C[NH_2]_2)_2]^+[B(C_6H_5)_4]^-$). The intention was to use multipole refinement to generate deformation density maps (both static and dynamic) for the compounds under investigation. Maps would be generated in planes suitable for studying the N-H...π(Ph) interactions known to occur in these salts. Would evidence of hydrogen bond formation be visible in features of the maps, as either perturbation or polarization of the electron density in the bonding regions? If features were visible, would they be consistent for each N-H...π(Ph) type interaction?

As the investigation progressed, it became apparent that topological analysis could also be used to characterize the N-H...π(Ph) hydrogen bonds in these compounds. In each case, the experimental multipole model from the crystallographic refinement could be used to generate an experimental electron density distribution for the compound. Bader's theory of "Atoms in Molecules" could then be used to search the experimental charge density for (3,-1) type bond critical points and bond paths in the N-H...π(Ph) interactions.

If the N-H...π(Ph) hydrogen bonds were found to be defined by such (3,-1) critical points and rational bond paths it would be possible to

characterize them using the values of $\rho_b(\mathbf{r})$, the electron density at the bond critical point, and $\nabla^2\rho_b(\mathbf{r})$, the Laplacian of the electron density at the bond critical point. N-H...π(Ph) hydrogen bonds have never previously been subject to such a topological analysis. If this analysis was successful, the results could be compared with the literature available, for topological analysis of the experimental charge density for other types of N-H...X hydrogen bonds, to see if there was any correlation of the data. The weaker C-H...π(Ph) type interactions in these compounds could also be studied in the same way, if the N-H...π(Ph) analysis proved to be informative. In addition, for both types of X-H...π(Ph) [X = N or C] interactions, the bond paths themselves might also provide useful information about the nature of the phenyl acceptor in the hydrogen bonds.

2. Chapter 2

2. Experimental

2.1. Preparation

Ammonium chloride, Dabco (1,4-diazobicyclo[2.2.2]octane), guanidine hydrochloride and sodium tetraphenylborate are all commercially available products and were used as received.

Biguanidinium(2+) sulfate dihydrate ($[C_2N_5H_9]SO_4$) was prepared by Dr. T.S. Cameron, using the method described in Inorganic Syntheses, Volume VII (1963).[92] Solid dicyanodiamide ($H_2NC(=NH)NHCN$) and ammonium chloride were combined in a 1:2.5 molar ratio with heating and the resulting product was then reacted with an ammoniacal copper(II) sulfate solution to give the rose-red coloured copper biguanide sulfate complex, $[Cu(C_2N_5H_7)_2]SO_4$. The reaction of this complex with a 10% solution of sulfuric acid and subsequent recrystallization from water generated biguanidinium(2+) sulfate dihydrate as colourless, water soluble crystals.

Ammonium chloride, Dabco, guanidinium chloride, and biguanidinium sulfate dihydrate were each dissolved in water or aqueous ethanol at room temperature. The Dabco solution was first acidified by the dropwise addition of aqueous HCl. To each solution was then added an aqueous solution of $NaB(C_6H_5)_4$ in a slight molar excess, resulting in the immediate precipitation of the products as white microcrystalline solids. Single crystals were obtained by slow evaporation at room temperature of acetonitrile, or in the case of $NH_4B(C_6H_5)_4$ acetone/water, solutions of the crude solids. The recrystallized salts were all monoprotonated and were unsolvated except for guanidinium tetraphenylborate where an acetonitrile

solvate was recovered. The crystals selected for data collection were mounted on glass fibers.

2.2. Data Collection

High resolution data were collected at Molecular Structure Corporation, the Woodlands, Texas. Data collection was carried out at -120°C (153K) with the low temperature achieved using the standard Rigaku system of effluent gas (liquid nitrogen) cooling. Graphite monochromated, Mo Kα radiation was used for each analysis. The Rigaku x-ray generator was set to nominal values of 90kV and 200mA. A Rigaku RAXIS II image plate detector, with an area of 200mm by 200mm, a crystal to detector distance of 55mm and a detector off-axis angle of 35°, was used for data collection.

For ammonium tetraphenylborate 18 frames of data were collected, while for the other three compounds 36 frames were collected. Each frame covered 10° for a total of 180° [$NH_4B(C_6H_5)_4$] or 360°, the entire sphere of data, in the other three cases. Each frame was exposed for 20 minutes, for total exposure times of 6 or 12 hours, respectively. There were few, if any, reflections where the intensity exceeded the saturation limit of the detector. For each crystal, the data could be collected to the observable limit, $(\sin\theta)/\lambda_{max} \approx 1\text{Å}^{-1}$, on a single setting of the detector off-axis angle.

2.3. Data Processing and Spherical Refinement

The data were first integrated using an integration box of fixed size, then the box was optimized and the frames were reintegrated.

Overlapping reflections and partials, which appear on two or more frames, were rejected. The worst outliers were removed and the data merged, using the statistical approach described and implemented by R. Blessing in the SORTAV group of programs.[93]

Unit cell parameters were derived from the complete data sets. The structures were solved by direct methods using SHELXS-86.[94] In each case, a preliminary least squares refinement with the conventional spherical atom model (SHELXL-93[95]) led to the determination of a scale factor and starting positions and thermal parameters for the multipole refinement. All nonhydrogen atoms were refined anisotropically and hydrogen atoms isotropically. Hydrogen atom positions were refined following their initial location from a Fourier difference map.

2.4. Multipole Refinement

The multipole refinements were performed using the rigid pseudo atom model of R.F. Stewart[96] implemented in the XD software package.[9] The refinement strategy used has previously been summarized in the flow chart of Figure 2.[10] Scattering factors for N, C, B and H were derived from wavefunctions, based on Slater-type basis functions, as tabulated by Clementi and Roetti.[97]

The program XDLSM from the XD package was used for multipole refinement. The function minimized was $\Sigma\, w(|Fo| - |Fc|)^2$, where $w^{-1} = \sigma^2(|Fo|)$. In the multipole refinement, the expansion was truncated at the octapole level ($l_{max} = 3$) for the heavy atoms (N, C and B) and at the quadrupole level ($l_{max} = 2$) for all hydrogen atoms. However, in the ammonium and guanidinium structures it was found that dipolar refinement

(l_{max} = 1) was sufficient for the hydrogen atoms. All bonds involving hydrogen were given cylindrical symmetry about the X-H bonds. Only those multipole parameters symmetrical about (lying along) the bond were refined.

In ammonium tetraphenylborate the multipole parameters on all hydrogen atoms [both H(N) and H(C)] were refined independently. In [DabcoH][$B(C_6H_5)_4$] multipole parameters were only refined for three hydrogen atoms, H(1) [H(N)], H(1A) [$H(C)_{cation}$] and H(22) [$H(C)_{anion}$]. All $H(C)_{aliphatic}$ hydrogen atoms of the cation were assigned equivalent multipole parameters; likewise, all $H(C)_{aromatic}$ hydrogen atoms of the anion were assigned a second set of equivalent multipole parameters. In addition, in the [DabcoH]$^+$ cation, C(1) and C(2) were made equivalent as were C(3) and C(4); only one set of multipole parameters was refined for each pair of atoms.

In guanidinium tetraphenylborate acetonitrile solvate the multipole parameters of the cation hydrogen atoms, H(N), were refined independently. However, the aromatic H(C) atoms of the anion were all assigned equivalent multipole parameters [H(45) refined] as were the three hydrogen atoms of the solvent molecule [H(60) refined]. In biguanidinium tetraphenylborate the H(N) hydrogen atoms of the cation were refined with a single set of multipole parameters [H(2A)] and the $H(C)_{aromatic}$ atoms of the anion were refined with a second set [H(12)].

The space group symmetry restricts the multipoles allowed to be refined, $P_{l,m}$, for atoms lying on symmetry elements (special positions). In this work, both $NH_4B(C_6H_5)_4$ and [DabcoH][$B(C_6H_5)_4$] had heavy atoms with symmetry restricted multipoles, while in the other two compounds all heavy

atoms were found to lie in general positions and all multipoles were refined. In ammonium tetraphenylborate, N(1) and B(1) were assigned $\bar{4}2m$ symmetry, while C(11) and C(14) were given *m* symmetry and all other heavy atoms, C(12) and C(13), were in general positions. In [DabcoH][$B(C_6H_5)_4$], N(1) and N(2) were assigned 3*m* symmetry while *m* symmetry limited the multipoles refined on C(1) = C(2), C(11), C(14), C(21) and C(24). The correct multipoles to refine were determined according to the method of K. Kurki-Suonio[7] and are listed in the Tables of Appendix 4. The local coordinate systems, used to define the multipole orientation on each atom, are also included in the Tables of Appendix 4.

Separate κ' and κ'' parameters (expansion/contraction coefficients) were employed for each chemically different type of atom in each structure (B, N_{cation}, $N_{solvent}$, C_{cation}, $C_{solvent}$, C_{anion}, $H(N)_{cation}$, $H(C)_{cation}$, $H(C)_{anion}$, $H(C)_{solvent}$, etc.). All kappa values were refined and the results are listed in the Tables of Appendix 4, along with the assignment of each atom to the proper kappa set.

In all the structures, except that of $NH_4B(C_6H_5)_4$ where it was found to be unnecessary, an isotropic extinction parameter was refined. The best model in each case was found to be Type I with a Gaussian distribution of the mosaic spread.[98] The final refined values are listed in the Tables in Appendix 4. Also, in all four structures a charge constraint was applied such that the cation, anion (and the solvent where applicable) charges remained fixed at +1, -1 (and 0), respectively, during the refinement.

Each nonhydrogen atom had positional and anisotropic displacement parameters refined, while for hydrogen atoms isotropic displacement parameters were refined. Hydrogen atom positions were constrained such

that all X-H bond lengths corresponded to appropriate neutron values. After each cycle involving positional refinement, the X-H bond lengths were renormalized to the neutron values by adjusting the hydrogen atom coordinates. N-H single bond values (1.032Å), C-H aliphatic values (1.085Å) and C-H aromatic values (1.076Å) were taken from a review article by F.H. Allen.[99] Allen had searched the Cambridge Structural Database to locate structures studied by neutron diffraction containing the different bond types; these were then statistically analyzed to determine mean bond lengths for the different classes of bonds.

The correct N-H neutron bond length to use in the multipole refinement of the guanidinium and biguanidinium cations was more problematic. A search of the Cambridge Structural Database[100] for structures studied by neutron diffraction and containing either cation located only one compound, $(CN_3H_6)_2[(CH_3)_2AsMo_4O_{15}H]\cdot H_2O$.[101] Averaging the 12 independent N-H bond lengths in the two unique guanidinium cations gave a mean N-H bond length of 0.986Å. This value was then used in the present work for the N-H bond length in the guanidinium and biguanidinium cations.

Details of the refinements are given in the tables at the end of the experimental section: Table 2 ($NH_4B(C_6H_5)_4$), Table 3 ([DabcoH][$B(C_6H_5)_4$]), Table 4 ([$C(NH_2)_3$][$B(C_6H_5)_4$]$\cdot CH_3CN$) and Table 5 ([$N(C[NH_2]_2)_2$][$B(C_6H_5)_4$]). Final scale, extinction, kappa and multipole parameters are listed for each compound in the Tables in Appendix 4. Also listed in Appendix 4 are the final atomic positions, temperature factors and the derived bond lengths and angles for each structure. The atom labelling is as shown in the diagrams accompanying the text. Structure factors have not been included in the Appendices but are available upon request.

2.5. Electron Density Maps

The program XDFOUR of the XD package was used to generate dynamic deformation density and residual electron density maps in the required planes for each compound. Residual electron density maps for all four compounds were drawn with a $(\sin\theta)/\lambda$ maximum cutoff of 0.8Å^{-1}, however no such restriction was imposed when drawing the dynamic deformation electron density maps. The XDPROP program from the same package was used to generate static deformation density maps, in a variety of planes and cuts, using the final results of the multipole refinements. In all maps, positive contours were represented with solid lines, negative contours with dashed lines and the zero level contour with a {dash dot dot dot} pattern. The contour interval used was normally 0.05eÅ^{-3}, although static maps in the phenyl ring planes were drawn with a contour interval of 0.10eÅ^{-3}, as noted in the figure captions. Most maps were drawn with a regular contour spacing, beginning from the zero level contour and ascending/descending by the contour interval, ±0.05 or $\pm0.10\text{eÅ}^{-3}$ depending on the map. However, static deformation electron density maps drawn as cuts through the phenyl rings (perpendicular to the plane of the ring) had the first positive contour located at $+0.015\text{eÅ}^{-3}$ for a contour spacing of {...-0.10, -0.05, 0.00, +0.015, +0.065, +0.115,...etc.}, to better examine the weak interactions to the rings [X-H...phenyl].

2.6. Geometry and Topological Analysis of Intermolecular Contacts

The program XDGEOM of the XD package was used to search for all X-H...A intermolecular (interion) contacts of 3.00Å or less [d(H...A)], in each of the four structures. Intramolecular (intra-ion) contacts were

not investigated. The contacts located fell into four broad categories and were grouped accordingly: (i) N-H...N, (ii) N-H...phenyl, (iii) C-H...N and (iv) C-H...phenyl. The geometry of each interaction was investigated, as listed in the tables of the main text (N-H contacts) or the appendix (C-H contacts).

The XDPROP program of the XD package was then used to search for critical points in the electron density distribution, generated from the final multipole model of each compound, for each of the located short contacts, X-H...A. Searches were carried out between complete species (cation,anion or solvent), generated by symmetry if necessary, where possible. However, for C-H...phenyl anion...anion type contacts size limitations of the program prevented generation of a second complete tetraphenylborate anion in the $C(NH_2)_3^+$ and $N(C[NH_2]_2)_2^+$ cases. It was necessary to leave hydrogen atoms off one ring of the new, symmetry generated anion. The hydrogens chosen appeared to have no effect on the results, as long as they were not on the ring involved in the interaction. The missing hydrogen atoms would be expected to have little effect on the results obtained.

Where one species or the other of a given X-H...A interaction had to be generated by symmetry, slightly different results were often obtained depending on how the search was carried out. For consistency, contacts X-H...A were searched keeping the original acceptor, usually the phenyl ring of the anion, and generating a new X-H donor (and the rest of the required cation or solvent molecule) by symmetry if needed. All N-H...N, N-H...phenyl, $C\text{-}H_{solvent}$...phenyl and $C\text{-}H_{cation}$...phenyl contacts were searched in this manner. The only exceptions were contacts in which

the donor was a C-H group of a ring on the tetraphenylborate anion, C-$H_{aromatic}$...acceptor. In those cases the original anion donor was kept and a new acceptor (or as much of it as possible) was generated by symmetry. This method was used for all C-$H_{aromatic}$...phenyl and C-$H_{aromatic}$...N contacts.

In the X-H...phenyl type contacts, the space between X and H to each carbon in the interacting ring was searched. In general, a single (3,-1) bond critical point was located for each interaction.

Bond paths were then generated for each contact, which was found to be characterized by a (3,-1) bond critical point, using the XDPROP program. Bond path diagrams for each interaction studied have been included in the text. The topological parameters characterizing the bond critical points, including $\rho_b(\mathbf{r})$ and $\nabla^2\rho_b(\mathbf{r})$ [the electron density and the Laplacian of the electron density at the bond critical point, respectively] are summarized in the tables of Chapter One (N-H contacts) and Appendix 4 (C-H contacts). Estimates of the errors on $\rho_b(\mathbf{r})$ and $\nabla^2\rho_b(\mathbf{r})$ have been included in the tables. It should however be noted that the error calculations implemented in the version of XDPROP used were subject to severe limitations; only contributions to the error from the multipole populations (not κ values or coordinates) are currently taken into account in the calculation and contributions to the error from symmetry generated atoms are also neglected. The result is a severe underestimation in the uncertainties reported for $\rho_b(\mathbf{r})$ and $\nabla^2\rho_b(\mathbf{r})$.

2.7. Thermal Motion Analysis

A rigid body motion analysis of the atomic vibration tensors was carried out using the method of Schomaker and Trueblood[102] as implemented

in the EKRT computer program by He and Craven.[103] The thermal parameters obtained from the final multipole refinement for each compound were used as input for the calculations. A unit weighting scheme was employed in all cases. The tetraphenylborate anion in each of the four structures was analyzed separately, as were the biguanidinium(1+) and DabcoH$^+$ cations. The ammonium and guanidinium cations contained too few heavy atoms for effective analysis. In every case, hydrogen atoms were not included in the calculations. The results are summarized in the tables of Appendix 4.

Table 2. Crystal data and structure refinement of ammonium tetraphenylborate.

Empirical Formula	$C_{24}H_{24}B_1N_1$
Formula Weight	337.25
Crystal Size, mm^3	0.15 x 0.21 x 0.55
Temperature, K	128(2)
Theta Range, deg	3.64 - 47.30
Crystal System	Tetragonal
a, Å	11.184(2)
b, Å	11.184(2)
c, Å	8.035(2)
α, °	90
β, °	90
γ, °	90
V, $Å^3$	1005.1(3)
Space Group	$I\bar{4}2m$
Z value	2
D_{calc}, g/cm^3	1.114
F(000), e	360
$\mu_{(MoK\alpha)}$, cm^{-1}	0.63
h, *k*, *l* ranges	1\23, 0\16, 0\11
Reflections:	
total measured	4983
unique total	1056
observed	891
$100R_{merge}$	2.90
d/r/p[a]	891 / 0 / 123
$100R$ / $100R_w$ [$F>2\sigma(F)$]	2.94; 2.50
$100R_{all\ data}$	3.90
G.O.F. on F	1.51

[a] Data / restraints / parameters

Table 3. Crystal data and structure refinement of [DabcoH] [$B(C_6H_5)_4$].

Empirical Formula	$C_{30}H_{33}B_1N_2$
Formula Weight	432.39
Crystal Size, mm^3	0.17 x 0.30 x 0.5[b]
Temperature, K	153
Theta Range, deg[a]	2.25° - 44.32°
Crystal System	Orthorombic
a, Å	18.1170(8)
b, Å	13.2230(9)
c, Å	9.9516(4)
α, °	90
β, °	90
γ, °	90
V, $Å^3$	2384.0(2)
Space Group	*Pnma*
Z value	4
D_{calc}, g/cm^3	1.205
F(000), e	928
$\mu_{(MoK\alpha)}$, cm^{-1}	0.69
h, *k*, *l* ranges	0/35, -26/0, 0/18
Reflections:	
total measured	30392
unique total	9434
observed	3204
$100R_{merge}$	5.50
d/r/p[a]	3204 / 0 / 422
$100R$ / $100R_w$ [$F>3\sigma(F)$]	4.68, 3.79
$100R_{all\ data}$	14.73
G.O.F. on F	1.189
Extinction Coefficient	0.29(2)

[a] Data / restraints / parameters

[b] Diamond shaped with major and minor axes 0.3 and 0.45 mm.

Table 4. Crystal data and structure refinement of guanidinium tetraphenylborate acetonitrile solvate.

Empirical Formula	$C_{27}H_{29}B_1N_4$
Formula Weight	420.35
Crystal Size, mm^3	0.18 x 0.28 x 0.43
Temperature, K	153
Theta Range, °	2.15 - 45.29
Crystal System	triclinic
a, Å	9.679(2)
b, Å	13.643(3)
c, Å	9.160(2)
α, °	90.70(3)
β, °	101.23(3)
γ, °	91.08(3)
V, $Å^3$	1186.1(4)
Space Group	$P\bar{1}$
Z value	2
D_{calc}, g/cm^3	1.177
F(000), e	448
$\mu_{(MoK\alpha)}$, cm^{-1}	0.70
h, *k*, *l* ranges	-19/18, -27/27, 0/12
Reflections:	
total measured	29477
unique total	8733
observed	6726
$100R_{merge}$	3.80
d/r/p[a]	6726 / 0 / 838
$100R$ / $100R_w$ [$F>3\sigma(F)$]	5.07, 4.94
$100R_{all\ data}$	7.06
G.O.F. on F	1.4682
Extinction Coefficient	0.237(10)

[a] Data / restraints / parameters

Table 5. Crystal data and structure refinement of biguanidinium tetraphenylborate.

Empirical Formula	$C_{26}H_{28}B_1N_5$
Formula Weight	421.34
Crystal Size, mm^3	0.16 x 0.23 x 0.41
Temperature, K	128(2)
Theta Range, °	2.58 - 44.33
Crystal System	monoclinic
a, Å	10.181(2)
b, Å	14.232(2)
c, Å	16.250(2)
α, °	90
β, °	104.340(10)
γ, °	90
V, $Å^3$	2281.2(6)
Space Group	$P2_1/c$
Z value	4
D_{calc}, g/cm^3	1.227
F(000), e	896
$\mu_{(MoK\alpha)}$, cm^{-1}	0.74
h, *k*, *l* ranges	-12/13, 0/27, 0/31
Reflections:	
total measured	21493
unique total	12658
observed	7376
$100R_{merge}$	4.44
d/r/p[a]	7376 / 0 / 822
$100R$ / $100R_w$ [F>3sigma(F)]	5.25, 4.13
$100R_{all\ data}$	9.50
G.O.F. on F	1.8017
Extinction Coefficient	0.88(2)

[a] Data / restraints / parameters

3. Chapter 3

3. Results and Discussion

3.1. Thermal Motion Analysis

Because of space considerations and the length of this thesis the detailed discussion of the thermal motion analysis has been moved to Appendix 1. Only a short summary, which follows, has been retained in the main text. Appendix 1 is available in the second volume of this thesis for those who require more information.

Least squares analyses of the rigid body motion of the tetraphenylborate anions in all four structures, and the two cations containing sufficient heavy atoms for analysis, were carried out according to the model of Schomaker and Trueblood.[102] The mean square atomic displacements (U_{calc}) were modelled by fitting T, L and S tensors to the experimental U_{ij}'s (U_{obs}) obtained from the multipole refinement of the low temperature x-ray data. T, L and S (torsion, libration and screw) axes model the external lattice vibrations of the ion as a whole. Hydrogen atoms were not included in the calculations.

3.1.1. Summary

The TLS analysis showed that the tetraphenylborate anions in all four structures did not conform well to the rigid body model of motion. The large, flexible anions have significant internal modes of motion, which could not be successfully approximated by the simple model used. Only two of the four cations could be studied by TLS analysis and of these two only the DabcoH$^+$ cation fit the rigid body model well. The bond length

corrections due to libration were significant in the cations, often larger than three times the esd on the bond length, and are given in the appropriate tables of Appendix 4. However, the corrected bond lengths were not used in subsequent work since not all cation bond lengths could be corrected.

3.2. Individual Structures and Their N-H...π(Ph) Hydrogen Bonds

3.2.1. Ammonium tetraphenylborate, $NH_4B(C_6H_5)_4$

Ammonium tetraphenylborate (Figure 3) is an unusual solid being one of the few known water insoluble simple salt of the ammonium ion. The structure of ammonium tetraphenylborate was first discussed in a 1957 publication by Davies and Staveley.[59] These authors reported the results of a calorimetric study of ammonium tetraphenylborate but also included preliminary results from an x-ray crystallographic investigation carried out by M.S. Webster. The structure was redetermined at both room temperature and at 120K by Westerhaus et al.[105] in 1980, when the positions of the hydrogen atoms were first established. Our multipole refinement of low temperature x-ray data for ammonium tetraphenylborate is the first reported investigation since that time and seeks to improve on the previously published results. In particular, more accurate location of the hydrogen atom positions would allow N-H...π(Ph) hydrogen bonding between the cation and anion in ammonium tetraphenylborate to be studied in detail.

The hypothesized hydrogen bonding in $NH_4B(C_6H_5)_4$ led to a number of non-crystallographic investigations beginning with the thermodynamic study of Davies and Staveley[59] in 1957. The structure determination reported by

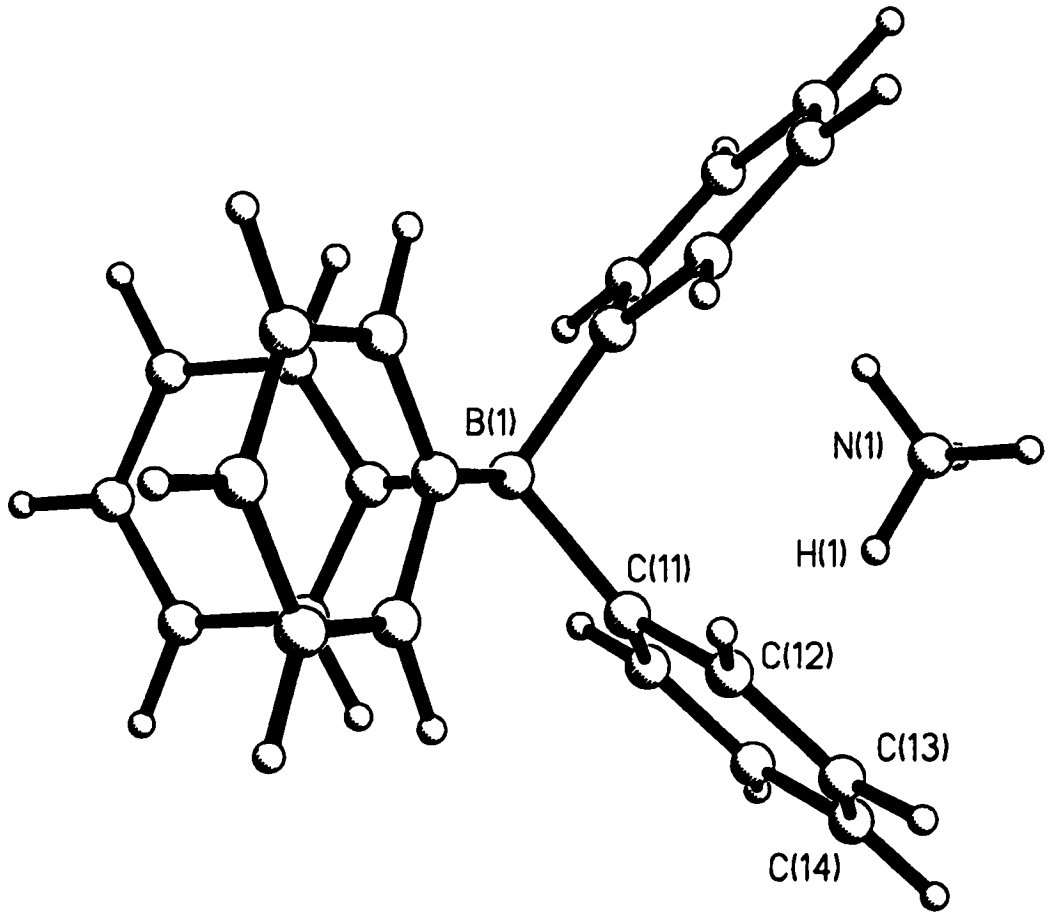

Figure 3. The structure of ammonium tetraphenylborate.

Westerhaus et al.[105] (1980) also included an infrared spectroscopic investigation of the title compound between 10K and room temperature. In addition, a detailed infrared analysis was published by M.P. Roberts et al.[106] in 1987. The same group also reported the results of Raman and neutron scattering experiments on ammonium tetraphenylborate over the next several years.[107-110] Finally, in 1990 Gruwel and Wasylishen[111] published a deuterium nmr study of $ND_4B(C_6H_5)_4$. All of these investigations focused, at least in part, on N-H...π(Ph) hydrogen bonding and its effect on the free rotation of the NH_4^+ ion in ammonium tetraphenylborate.

3.2.1.1. Non-crystallographic Investigations of Hydrogen Bonding and Reorientation of the Cation in $NH_4B(C_6H_5)_4$

Prior to accurate x-ray crystallographic investigation of hydrogen positions and N-H...π(Ph) hydrogen bonding in ammonium tetraphenylborate, a number of non-crystallographic studies were carried out. Davies and Staveley[59] (1957) relied on the structural details provided by M.S. Webster (included in reference 59), particularly the isomorphism of $NH_4B(C_6H_5)_4$ and $RbB(C_6H_5)_4$, in their calorimetric investigation of the ammonium salt. These authors measured the molar heat capacity of ammonium tetraphenylborate from 20K to room temperature; they found that $NH_4B(C_6H_5)_4$ underwent no phase transitions over the temperature range studied. However, they did note that between 20K and 100K the heat capacity of $NH_4B(C_6H_5)_4$ showed a region of extra energy intake attributed to some unexplained type of non-cooperative change.

Davies and Staveley then compared the molar heat capacity curves of ammonium and rubidium tetraphenylborate, isostructural salts. The authors assumed that the contributions of the tetraphenylborate anion (torsional

oscillations and internal vibrations) to the heat capacity were equal in both salts at any given temperature. From this, they calculated the quantity $\Delta Cp(NH_4 - Rb)$ which is equal to $Cp(NH_4) + Cp_{internal}(NH_4) - Cp(Rb)$. At a given temperature the value of ΔCp is equal to the contribution made by the torsional oscillations/rotations of the NH_4^+ ion plus the difference in the contributions made by the lattice vibrations of the different cations. At sufficiently high temperatures, in this case well below room temperature, the lattice vibrations of the cation in each salt will reach a limiting value. Thus, at room temperature the observed finite value of ΔCp is determined primarily by the internal vibrations of the ammonium ion. From their comparison of the molar heat capacity curves of $NH_4B(C_6H_5)_4$ and $RbB(C_6H_5)_4$, Davies and Staveley concluded that even at higher temperatures (up to R.T.) the ammonium ion could not be freely rotating in the crystal lattice. In fact, from their calculation of $Cp_{internal}(NH_4)$ they felt that the barrier to rotation in $NH_4B(C_6H_5)_4$ was considerable.

To support their experimental results, Davies and Staveley also carried out simple potential energy calculations on the NH_4^+ ion and the two $B(C_6H_5)_4^-$ anions nearest to it, considering electrostatic forces only. The calculations showed the most stable arrangement to have each of the four H(N) ammonium hydrogen atoms lying as close as possible to the benzene ring nearest to it. Although not reported as such, this was the first investigation of the N-H...π(Ph) hydrogen bond and its role in preventing free rotation of the ammonium ion in solid $NH_4B(C_6H_5)_4$.

Davies and Staveley calculated the low energy configuration, just described above, to be more stable by 8.11 kcal/mol than the geometry obtained by rotating the cation through 90° about the *c* axis. The change

in energy of the ammonium ion with reorientation in other directions was found to be complex with multiple and unequal maxima and minima. Looking back today at the results of Davies and Staveley, the calculated barrier to rotation of the ammonium ion in $NH_4B(C_6H_5)_4$ seems rather high, however, the simplicity of the model used must be taken into account.

The 1980 publication by W.J. Westerhaus et al.[105] of the room and low temperature conventional structure determinations of $NH_4B(C_6H_5)_4$, also included an analysis of the infrared spectrum and limited point charge calculations of the cation/anion interactions in ammonium tetraphenylborate. The calculations of Westerhaus et al. confirmed the findings of Davies and Staveley, showing the lowest energy configuration to have the hydrogen atoms of the ammonium ion pointing towards the centers of the four nearest, tetrahedrally oriented phenyl rings.

Westerhaus et al.[106] measured the infrared spectra of $NH_4B(C_6H_5)_4$, and isotopically substituted $NH_3DB(C_6H_5)_4$ and $ND_4B(C_6H_5)_4$, between 10K and room temperature. No evidence of a phase transition was found in the infrared spectra at the temperatures measured, in accordance with the heat capacity measurements of Davies and Staveley.[59] The N-H/D stretching and bending vibrations were carefully analyzed in an attempt to determine the effect of N-H...π(Ph) hydrogen bonding on the infrared spectra and perhaps to infer the strength of the interaction.

Crystallography had shown the ammonium ion in $NH_4B(C_6H_5)_4$ to reside at a site of D_{2d} symmetry. However, the infrared analysis showed that the distortion of the ammonium ion from the ideal tetrahedral geometry was only very slight. The authors found that the N-H...π(Ph) interaction between the cation and the anion was strong enough to prevent the ammonium

ion from rotating freely. However, the effect of the anion on the strength of the N-H bond was small, comparable to that in other weakly (but conventionally) hydrogen bonded ammonium salts, which show similar infrared stretching frequencies. Westerhaus et al. felt that the barrier to rotation was likely small and that displacements of the N-H bonds from the optimal tetrahedral geometry were likely appreciable even at low temperatures. In summary, the authors conclude that hydrogen bonding is present in $NH_4B(C_6H_5)_4$ and that its effect is evident in the infrared spectrum, which however also suggests a relatively weak N-H...π(Ph) interaction.

In their subsequent analysis of the infrared spectrum of ammonium tetraphenylborate, M.P. Roberts et al.[106] reach many similar conclusions to those of Westerhaus et al.[105]; there are, however, some notable differences in their analyses. Roberts et al. felt that Westerhaus et al. had failed to correctly interpret the infrared spectrum of $NH_4B(C_6H_5)_4$ because the analysis had been carried out with the expectation that the rotational barrier would agree with that anticipated on the basis of the extent of the hydrogen bonding. This, in turn, had been inferred from the vibrational frequencies and calculated interatomic distances. Roberts et al. feel that in highly symmetric salts, such as $NH_4B(C_6H_5)_4$, the crystal structure cannot be determined by the requirements of hydrogen bonding alone. In $NH_4B(C_6H_5)_4$, the ammonium ion sits in a position of high symmetry (D_{2d}) determined by both long and short range forces; the barrier to its rotation has no simple relationship to the hydrogen bond strength. Rather, to assign the infrared spectrum Roberts et al. consider the selection rules of the combined group formed by the molecular (NH_4^+ - T_d) and site

(D_{2d}) symmetries in the free rotation limit and its correlation to the high barrier (libration) limit.

The previously unexplained multiplicity of bands observed in the infrared N-H stretching fundamental region at low temperatures (T < 30K) prompted Roberts et al. to re-examine the spectrum of $NH_4B(C_6H_5)_4$. Careful analysis of the N-H stretching and bending bands suggested nearly free rotation of the ammonium ion, with only a small barrier to free rotation, in keeping with the earlier results of Westerhaus et al.[105]

In a later paper, Roberts et al.[109] examined the N-H stretching and low frequency regions of the Raman spectra of $NH_4B(C_6H_5)_4$ and $NH_4B(C_6D_5)_4$ at low temperatures (100K and below). The low frequency Raman spectra confirmed that the effective site symmetry of the ammonium ion in both is D_{2d}. The Raman N-H spectrum showed features similar to those in the infrared spectra, many bands of which were assigned as arising from the nearly free rotational motion of the ammonium ion. Many of the features of both the low frequency and N-H stretching regions arise from the effect of the D_{2d} site symmetry on the otherwise tetrahedral (T_d) NH_4^+ ion. Roberts et al. conclude that the ammonium ions in this crystal are perturbed but very nearly free to rotate based on their combined Raman and infrared investigations.

M.P. Roberts et al.[107, 108] also performed incoherent quasielastic and inelastic neutron scattering experiments on polycrystalline samples of $NH_4B(C_6H_5)_4$ and $NH_4B(C_6D_5)_4$ in the 1.5K to 350K temperature range. The authors modelled five different possible rotational reorientations for the ammonium ion. From the variations of the quasielastic incoherent neutron scattering, it was shown that a $2\pi/2$ reorientational jump process about

a two-fold (C_2) axis best fit the ammonium ion rotational motion in the 30K to 350K temperature range. This finding is in agreement with the D_{2d} site symmetry determined by x-ray crystallography and Raman spectroscopy.

An Arrhenius log plot of the reorientational correlation time, calculated from the half width at half maximal peak height in the quasi-elastic neutron spectrum, versus reciprocal temperature for $NH_4B(C_6D_5)_4$ showed three distinct regions. From room temperature (350K) down to 120K the Arrhenius log plot was smooth, corresponding to an exceptionally low barrier for the C_2 reorientation of the ammonium ions, with an activation energy of only 2.9 kJ/mol. From 80K to 40K the Arrhenius log plot suggested an activation energy of only 1.44 kJ/mol, a decrease of about one half from its high temperature value. A sharp discontinuity in the Arrhenius log plot between 80K and 120K was interpreted as indicating a change in the dynamics of the reorientation process at these temperatures, a result in keeping with the subsequently published inelastic neutron study by the same authors.

The inelastic neutron scattering spectra recorded by Roberts et al.[108] strongly suggested the presence of two distinct ammonium ions, present in about equal amounts, each with its own dynamic reorientation process, at very low temperatures. At higher temperatures, above approximately 100K, the combined spectral results were interpreted as indicating that all ammonium ions become equivalent and are nearly free to rotate. The authors attribute the very low temperature inelastic neutron scattering spectrum as arising from one half of the ammonium ions nearly freely rotating, with an estimated barrier to rotation of only 14 cm^{-1} and the other half of the cations librating with a relatively high

barrier of 280 cm^{-1}. These ions undergo rotational tunnelling between potential minima.

At the temperature of the published (and this) x-ray structural determinations (~120K) the combined results of Roberts et al.[106 - 110] suggest that all the ammonium ions in $NH_4B(C_6H_5)_4$ are equivalent, librating with an activation energy to reorientation of only 2.9 kJ/mol. This low barrier allows nearly free rotation of the ammonium ions in the crystal lattice. The infrared and Raman spectra are best assigned as arising from the tetrahedral ammonium ion being slightly perturbed by its site symmetry (D_{2d}) constraint. The quasielastic neutron spectrum suggests a reorientation model of $2\pi/2$ rotational jumps about a C_2 axis of the ammonium ion. The results of M.P. Roberts et al. are consistent with those deduced by Westerhaus et al.[105] in the same temperature range using infrared spectroscopy and x-ray crystallography.

Gruwel and Wasylishen[111] used deuterium ^2H nmr to study the rotational dynamics of the ammonium ion in $NH_4B(C_6H_5)_4$, as reported in a 1990 publication. The variable temperature ^2H relaxation measurements on $ND_4B(C_6C_5)_4$ suggested a relatively large amount of rotational freedom for the ammonium ion, in keeping with the previous Raman and infrared studies. The authors concluded that over the temperature interval 148K to 298K the spectral density of the motion could be described by a single correlation time, allowing the use of an isotropic reorientation model. The model, consisting of rapid C_2 and C_3 rotations/flips of the cation, was found to correspond to an activation energy of 5.0±0.5 kJ/mol.

The authors go on to compare the calculated activation energy for the NH_4^+ reorientation in $ND_4B(C_6H_5)_4$ with values for several other ammonium

salts, also with anions of unit charge. ND_4Cl, ND_4Br, ND_4I (tetragonal form), ND_4NCS and ND_4NO_3 had all previously been calculated to have activation energies two to four times larger than $ND_4B(C_6H_5)_4$. However, ND_4ClO_4 and ND_4I (cubic form) had been shown to have activation energies similar to, but slightly smaller, than that found for $ND_4B(C_6H_5)_4$. The results also agree with the infrared observations, at least in terms of the weakness of the ammonium ion (cation)/phenyl ring (anion) interactions. The barrier to the reorientation is, however, larger than suggested by the infrared investigations. The ^2H nmr results (5.0(5) kJ/mol) are in reasonably good agreement with those derived by Roberts et al. using quasielastic neutron scattering techniques. Roberts et al. calculated an activation energy of 2.9 kJ/mol for the $2\pi/2$ reorientation of the ammonium ion about a C_2 axis in $NH_4B(C_6D_5)_4$ at room temperature.

All of the spectral investigations reported in this section agree on the relatively free rotation of the ammonium ion in crystalline $NH_4B(C_6H_5)_4$. It is probable that the barrier to free rotation arises, at least in part, from the N-H...π(Ph) hydrogen bonding between the cation and the anion in the structure. There is some discrepancy as to the height of the barrier preventing free rotation but by all accounts it is weak, perhaps on the order of 3-5 kJ/mol at the temperature of interest here.

3.2.1.2. Crystallographic Investigations of $NH_4B(C_6H_5)_4$

The crystallographic investigations of ammonium tetraphenylborate are consistent on important details, including the unit cell dimensions outlined below. As expected, *a* and *c* and the resulting cell volume all decrease with decreasing data collection temperature. The 120K data of

Westerhaus et al.[105] show good agreement with the results of this investigation carried out at 128K. The estimated standard deviations on the unit cell dimensions also decrease with decreasing temperature. As well, the more sophisticated multipole refinement has smaller deviations on the cell parameters than the conventional spherical refinements, which in turn have lower esds than Webster's photographic determination.[59]

Unit Cell Dimensions of Ammonium Tetraphenylborate

Parameter	Webster[59]	Westerhaus[105]		this work
	R.T.	R.T.	120K	128K
a, Å	11.24(2)	11.229(5)	11.176(4)	11.184(2)
b, Å	8.08(2)	8.060(8)	8.032(4)	8.035(2)
Volume, Å^3	1021(7)	1016.3(2)	1003.2(2)	1005.1(3)

where R.T. is room temperature

In each study, the space group of ammonium tetraphenylborate was determined to be body-centered, $I\bar{4}2m$, with both boron and nitrogen located on the $\bar{4}$ axis at a site symmetry of $\bar{4}2m$ (D_{2d}). As a result, the cation contains four symmetry equivalent hydrogen atoms about the central nitrogen atom, while the anion contains only boron, four carbons and three hydrogen atoms in uniquely defined positions; the rest of the anion is generated by symmetry.

Packing diagrams of ammonium tetraphenylborate are shown in Figure 4 (a) and (b). The structure is composed of linear columns running parallel to the *c* axis. Each column is, in turn, composed of alternating cations and anions. The columns are staggered relative to one another so that the

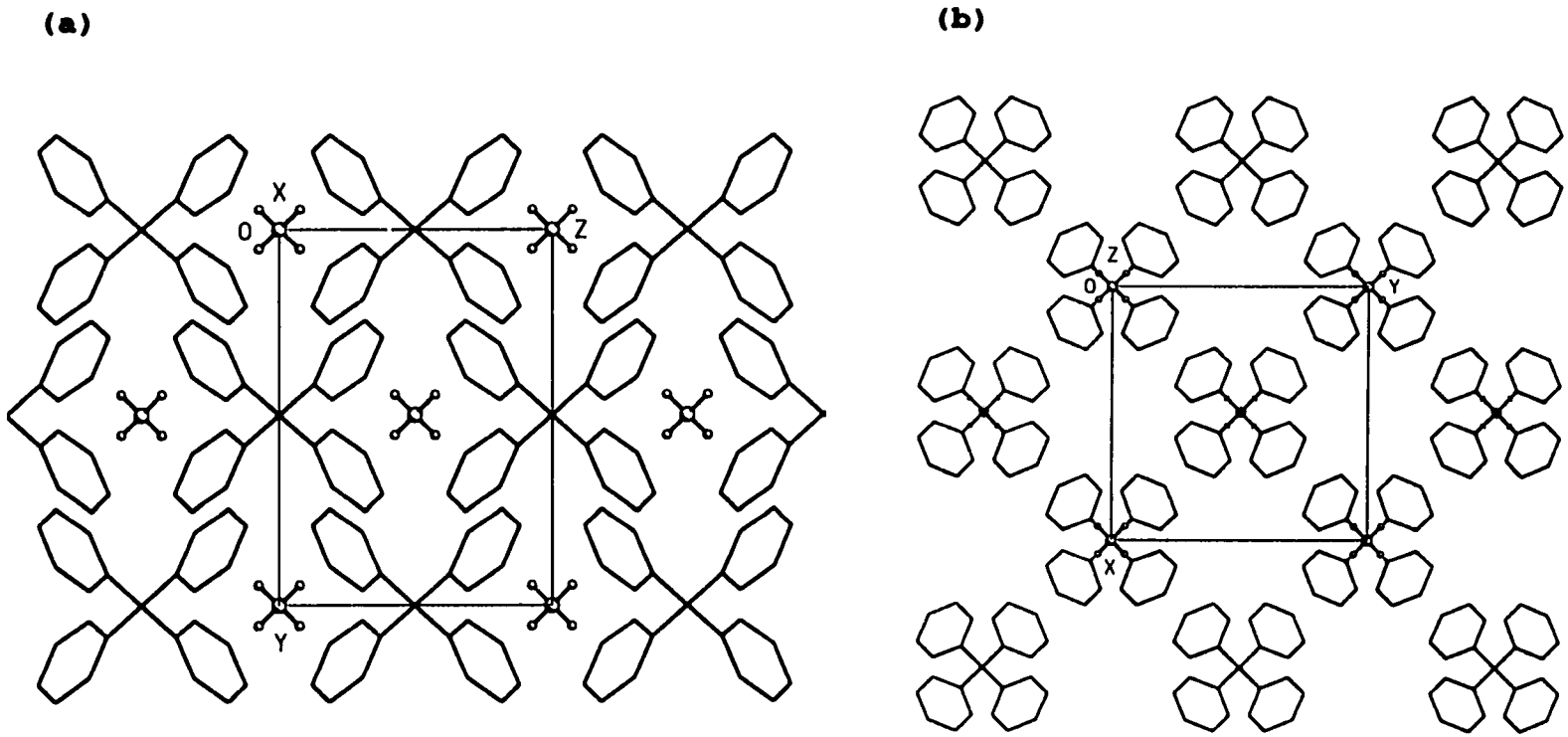

Figure 4. Ammonium tetraphenylborate: (a) projection on (100) and (b) projection on (001). Hydrogen atoms have been removed from the anion for clarity.

nearest neighbour between adjacent columns are ions of opposite charge. Within a column, the ammonium ion is nestled in a "cage" formed by four phenyl rings (two pairs), each pair belonging to a different anion, one above and one below the cation along the *c* axis (Figure 5). The two anion pairs are rotated by 90° relative to each other in a tetrahedral arrangement.

Overall, the ion packing of ammonium tetraphenylborate can be described as tetragonally distorted NaCl-type, with each ion having six nearest neighbours of opposite charge (octahedral coordination). In the *ab* plane each cation or anion has four equidistant, neighbouring ions of opposite charge at the same height, one each from the four nearest columns running parallel to *c*. There is also an ion of opposite charge directly above and below the chosen ion at ±½ along *z*. Since the *c* dimension of the unit cell is somewhat different from *a*,*b* the packing is distorted from the ideal NaCl-type.

Direct investigation of the N-H...π(Ph) hydrogen bonding interaction in ammonium tetraphenylborate, or any structure, is only possible if the x-ray crystallographic determination is of sufficient quality to allow accurate location of the hydrogen atom. The photograph-based refinement of Webster, reported by Davies and Staveley,[59] did not include hydrogen atom positions, however, even here some speculation on the strength of the N-H...π(Ph) interaction proved possible (although not described in such terms). Webster found rubidium tetraphenylborate to be isostructural with the ammonium salt, with both having nearly identical unit cell dimensions at room temperature. Since N-H...π(Ph) hydrogen bonding is not possible in $RbB(C_6H_5)_4$, the authors concluded that such hydrogen bonding does not

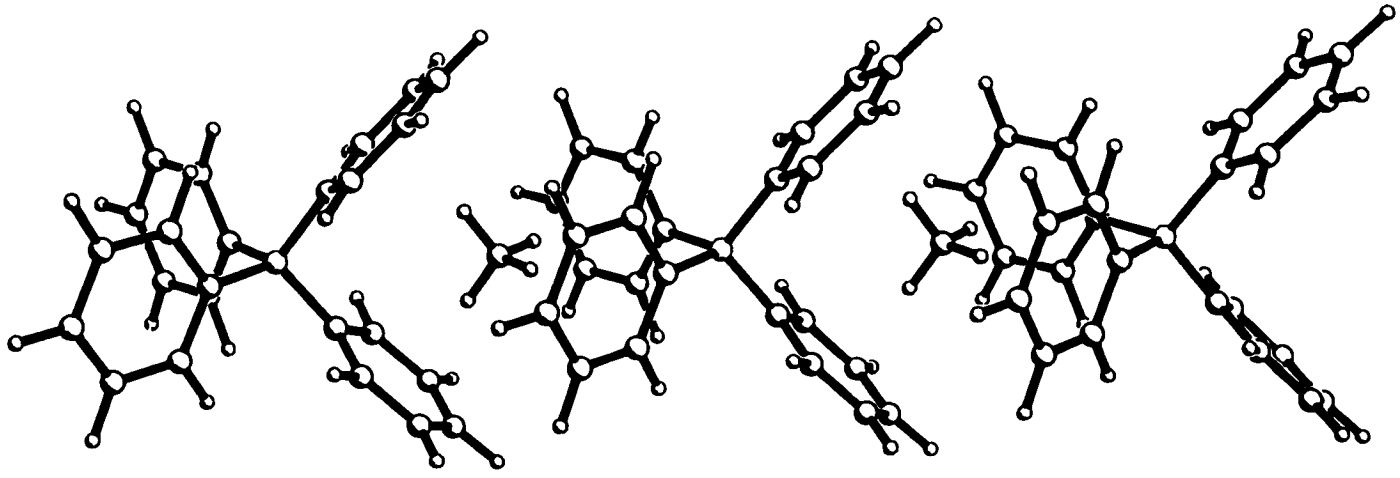

Figure 5. Orientation of the ammonium ion within a cavity formed by two tetraphenylborate anions in the structure of ammonium tetraphenylborate.

play a structure determining role in $NH_4B(C_6H_5)_4$, which implies that it must be weak at best.

Before examining the N-H...π(Ph) hydrogen bond in ammonium tetraphenylborate, it is instructive to compare the details of the low temperature (120K), spherical refinement of Westerhaus et al.[105] with the low temperature (128K), multipole refinement carried out for this investigation. The spherical refinement of Westerhaus et al. was based on 293 independent reflections ($I>2\sigma(I)$) and 70 parameters, and gave final R and R_w values of 4.4% and 4.1%, respectively. The multipole refinement, carried out at a nearly identical temperature, was based on 891 reflections with $I>2\sigma(I)$ and 123 parameters and gave a final value for R of 2.94% and for R_w of 2.50%.

To compare the positional parameters and their estimated standard deviations, the results of Westerhaus et al.[105] were transformed to match the atomic parameters as they had been chosen in the multipole refinement, $(x, y, z)_{spherical} \rightarrow (y, x, z+\frac{1}{2})_{multipole}$. The estimated standard deviations on the positional coordinates were compared and found to be, on average, 3.6 times larger in the conventional spherical refinement than in the multipole refinement. This is not surprising considering the more detailed model and the larger data set used in the multipole refinement. However, the positions of the heavy atoms were found to be very consistent in the two determinations. The average difference in the (x, y, z) components of the position was less then 0.001 (in fractional coordinates) for the two refinements.

It was also possible to compare the anisotropic displacement parameters, and their associated estimated standard deviations, for the

heavy atoms in the two refinements. The anisotropic thermal parameters were found to be virtually identical, on average, in the two determinations; the U_{ij} values of the spherical refinement were only 1.1 times larger than the corresponding values of the multipole refinement, consistent with their nearly identical data collection temperatures. The size of the anisotropic displacements of the ring carbon atoms increase steadily in both refinements, with those of C(1)/C(11) smallest and those of C(4)/C(14) largest. This is also not surprising, a larger degree of thermal motion would be expected at the untethered, far end of the ring, opposite the B-C bond. The ratio of the estimated standard deviations of the spherical refinement to the multipole refinement for the U_{ij} values was 2.3, again being larger for the spherical parameters.

Derived bond lengths and angles, involving the heavy atoms of the anion, were reported for both the spherical and multipole determinations. The estimated standard deviations for both the bond lengths and angles were, on average, 8 times larger in the spherical refinement than those in the multipole refinement. The large difference is a magnification of the difference in the uncertainty of the atomic positions in the two refinements. The average difference in the bond lengths between the two determinations was slightly less than 0.01Å. There was no consistent trend seen in the bond length differences; the B(1)-C(11) and the C(12)-C(13) bonds were shorter, while the C(11)-C(12) and the C(13)-C(14) were longer in the multipole refinement. The C-C ring bonds were more equal in length, covering a narrower range of values, in the multipole refinement. The bond angles involving the heavy atoms of the anion also agreed very closely in both determinations. The average difference in the angles was only 0.6Å,

with the largest difference being observed for the C(13)-C(14)-C(13)' angle, 1.6°.

In both the multipole and spherical crystal structure determinations, the boron atom was found to lie at a position of $\bar{4}2m$ symmetry, giving an overall anion symmetry of D_{2d}. The bond angles surrounding the boron atom fall into two distinct groups, two of the angles are smaller [103.7(1)° - multipole, 103.2(8)° - spherical] while four angles are larger [112.4(1)° - multipole, 112.7(9)° - spherical] consistent with D_{2d} symmetry. Also by symmetry, all B-C bonds in the anion are of equal length [1.6443(10)Å - multipole, 1.645(7)Å - spherical]. The C(12)-C(11)-C(12)' angle is also equivalent in all four phenyl rings by symmetry [115.6(1)° - multipole, 115.7(9)° - spherical]. The geometry of the anion is close to identical in the two refinements.

The room temperature crystal structure determination of ammonium tetraphenylborate carried out by Webster[59] using photographic methods did not provide any indication of where the ammonium ion hydrogens might be located. Westerhaus et al.[105] began their redetermination of the room temperature structure, and an accompanying low temperature spherical refinement, with the hope of accurately locating the H(N atom to resolve the problem. The authors write, "in $NH_4B(C_6H_5)_4$ there is no reason why the reorientation of the ammonium ion should not approximate to a very weakly hindered free rotation, unless interaction between the ammonium hydrogen and the charge in the π-system of the benzene ring is significant. If it is, there ought to be a reasonable chance of finding the ammonium hydrogens located in regions of space corresponding to the hydrogen bonding geometry between reorientations."[105] Although the calculated

barrier to rotation is small, as discussed previously, the crystallographic results (including those reported here) show that it is possible to accurately locate the ammonium hydrogen atom position.

The room temperature, spherical refinement of Westerhaus et al. showed diffuse maxima attributable to the four, symmetry related ammonium hydrogens, at about 1Å from the nitrogen atom, in the Fourier difference map after location of the heavy atoms. However, if the ammonium hydrogens were fixed in these positions and included in the refinement, they tended to move closer to the nitrogen center (0.63Å) and acquire very large estimated standard deviations. The authors conclude that no meaningful statement can be made about the most probable positions of the ammonium hydrogen atoms, based on the room temperature refinement.

The low temperature refinement of Westerhaus et al.,[105] based on data collected at 120(10)K, began from the room temperature, heavy atom parameters. A Fourier difference map, after refinement of the heavy atoms, clearly showed regions of excess electron density associated tetrahedrally with the nitrogen atom, at a distance of 0.98Å. Including hydrogen with these positional parameters and isotropic thermal parameters in the least squares refinement gave stable results.

The treatment of the ammonium hydrogen atom was handled somewhat differently in the multipole refinement. Again, maxima attributable to the ammonium hydrogen atoms were visible in the difference Fourier map after refinement of the heavy atoms. Initially, one unique H(N) atom was placed in this position. If it was included in the overall refinement with an isotropic temperature factor, the parameters obtained were reasonable but the N-H bond length tended to shorten slightly and the HNH′ angles tended

to move slightly away from the initial tetrahedral values. The best results were obtained by keeping the tetrahedral geometry for the cation and renormalizing the N-H bond length to its neutron value of 1.032Å after each cycle of least squares refinement.

The final position of the ammonium hydrogen atom, H(N), in the two determinations turned out to be quite different. If the low temperature, spherical refinement position is transformed to match the multipole coordinates, its position in fractional coordinates is (0.0604, 0.0604, 0.9705), in contrast to the multipole position of (0.0533, 0.0533, 0.9259). The difference occurs in spite of the fact that the position of the nitrogen atom is identical and uniquely determined in both structures (0, 0, 1) since it lies on a special position. The difference in the atomic coordinates for H(N) is substantial, particularly in the *z* direction. The different location of H(N) in the two determinations results in quite substantially different cation geometries in the two. The spherical refinement gives an ammonium cation with N-H bond lengths of 0.98Å and HNH' angles of 152° (2x) and 93° (4x). In contrast, the multipole determination resulted in a cation with N-H bond lengths of 1.032Å and all HNH' angles equal to 109°. Based solely on the cation geometry, the location of H(N) in the multipole refinement seems more reasonable than that in the spherical refinement of Westerhaus et al. (as would also be expected on the basis of the improved data collection and refinement method used in the former determination).

Westerhaus et al. describe the N-H vectors of the ammonium cation in their structure as pointing into the phenyl rings of the nearest, neighbouring tetraphenylborate anions. The radius vector, N-H(N), forms

an angle of roughly 60° with an imaginary line joining C(1) and C(4) of the phenyl ring. This is in contrast to the angle expected for an undistorted NH_4^+ tetrahedron in the same orientation, where the angle between the N-H(N) vector and the C(1)...C(4) line would be approximately 80°. In the multipole refinement, the idealized, tetrahedral cation geometry results in an angle of 81° being formed.

The results of the low temperature, spherical refinement of Westerhaus et al.[105] were used by Bakshi et al.[83] to characterize the N-H...π(Ph) hydrogen bond in ammonium tetraphenylborate based on its geometry. Bakshi et al. report a mean N...C_{ring} distance of 3.34(6)Å and an N...π_c (ring centroid) distance of 3.04Å. The corresponding mean H(N)...C_{ring} distance is 2.60(12)Å and the H(N)...π_c distance is 2.20Å. In the spherical determination both N and H(N) are closest to C(1) of the phenyl ring [N...C(1) = 3.26Å; H(N)...C(1) = 2.44Å] while they are farthest from C(4) [N...C(4) = 3.42Å; H(N)...C(4) = 2.78Å]. Bakshi et al. define a value which characterizes the range of X (X = N or H(N)) to ring carbon distances, 100Δ = 100(maximum distance - minimum distance). In ammonium tetraphenylborate they calculate 100Δ values of 16 for N...C_{ring} and of 34 for H(N)...C_{ring}.

The tables including the data derived from the multipole refinement to characterize the N-H...π(Ph) hydrogen bond in ammonium tetraphenylborate are found at the end of the current section, as is a diagram illustrating the interaction (Figure 6). The results of the multipole refinement are virtually identical as far as the N...C_{ring} distances are concerned, with individual N...C_{ring} distances, the mean N...C_{ring} distance (3.345Å) and the N...π_c distance (3.038Å) corresponding closely with the

spherical refinement values. This is not surprising since the heavy atom positions were relatively constant in the two refinements. Both the multipole and the spherical determinations show the nitrogen center of the cation to be closest to C(1)/C(11) and farthest from C(4)/C(14) at the far end of the phenyl ring.

The ammonium hydrogen to phenyl ring carbon distances vary considerably between the two refinements. The range of $H(N)\ldots C_{ring}$ distances is much narrower in the multipole determination; 100Δ equals 6 versus 34 in the spherical case. All of the individual $H(N)\ldots C_{ring}$ distances are shorter in the multipole refinement as well. In consequence, the mean $H(N)\ldots C_{ring}$ distance (2.452Å) and the distance from H(N) to the ring centroid (2.013Å) are both approximately 0.2Å shorter than the corresponding values from the spherical refinement. This is largely a result of placing H(N) at the neutron N-H bond length of 1.032Å in the multipole refinement as opposed to refining the H(N) position to an N-H bond length of 0.98Å, the treatment adopted by Westerhaus et al. Changing the geometry of the ammonium cation also changes the angle of the N-H(N) vector relative to the ring plane, which results in the narrower range of $H(N)\ldots C_{ring}$ distances observed in the multipole determination.

Based on the results from the multipole refinement of the structure of ammonium tetraphenylborate the geometry of the N-H...π(Ph) interaction would be described as being of the centroid type or T-shaped (Figure 6). The distances of both N and H(N) from the phenyl ring centroid are substantially shorter than any of the corresponding individual $N\ldots C_{ring}$ or $H(N)\ldots C_{ring}$ distances. The range of both $N\ldots C_{ring}$ (100Δ = 17) and $H(N)\ldots C_{ring}$ (100Δ = 6) individual distances is very narrow. Finally, the

angle to the ring centroid, N-H(N)...π_c, is very nearly linear (172°), much closer to 180° than the angle to any individual ring carbon. The N-H vector makes an angle of 81° with the phenyl ring plane, close to perpendicular.

The results from the multipole refinement do contain a minor discrepancy, perhaps arising from a small error in the placement of the ammonium hydrogen atom. In their determination, Westerhaus et al. found both N and H(N) of the cation to be closest to C(1), the carbon bonded to boron, and farthest from C(4) at the opposite end of the phenyl ring. The multipole refinement also showed N(1) to be closest to C(11) = $C(1)_{spherical}$ and farthest from C(14) = $C(4)_{spherical}$. However, H(N) was found to be closest to C(12), 2.426Å, and not to C(11), 2.448Å, while it was still farthest from C(14), 2.484Å. The N-H vector makes the best angle to a ring carbon to C(14), N(1)-H(1)...C(14) = 153°. This shows that the N-H vector is not quite centered over the phenyl ring, nor is it exactly perpendicular to the ring plane. The range of H(N)...C_{ring} distances is very narrow, so which distance is actually the shortest is probably not particularly important.

It is also possible to compare the results from the multipole refinement of $NH_4B(C_6H_5)_4$ with the averages calculated by Bakshi et al.[83] based on the geometric investigation of a large number of N-H...π(Ph) hydrogen bonds using conventional, spherical refinements. For single, unbifurcated N-H...π(Ph) interactions, Bakshi et al. report average N...π_c and H(N)...π_c values of 3.31(23)Å and 2.35(23)Å, respectively. In comparison, the multipole refinement of $NH_4B(C_6H_5)_4$ led to corresponding values of 3.038Å and 2.013Å. Similarly, Bakshi et al. report average mean

N...C_{ring} and mean H(N)...C_{ring} distances of 3.59(20)Å and 2.73(18)Å, respectively, for N-H...π(Ph) hydrogen bonds, while the ammonium tetraphenylborate values calculated from the multipole refinement were 3.345[2]Å and 2.452Å. In every case, the $NH_4B(C_6H_5)_4$ values are shorter, often considerably, than the calculated averages. While this is, to some extent, dependent on the N-H bond length used in the refinements, it also shows the relative strength of the N-H...π(Ph) interaction in ammonium tetraphenylborate.

From the final results of the multipole refinement, the geometry of the N-H...π(Ph) hydrogen bond in $NH_4B(C_6H_5)_4$ would be described as close to ideal (centroid type), based on criteria discussed in the introduction (Figure 6). The single, unique N-H...π(Ph) interaction in the structure allows its geometry to be optimized. The multipole results are quite different from those reported by Westerhaus et al. for the same structure, but determined from a conventional spherical refinement at roughly the same temperature. Based on geometrical considerations, the multipole results seem the more reasonable. This is not unexpected considering the larger data set and expanded refinement used in the higher quality multipole determination.

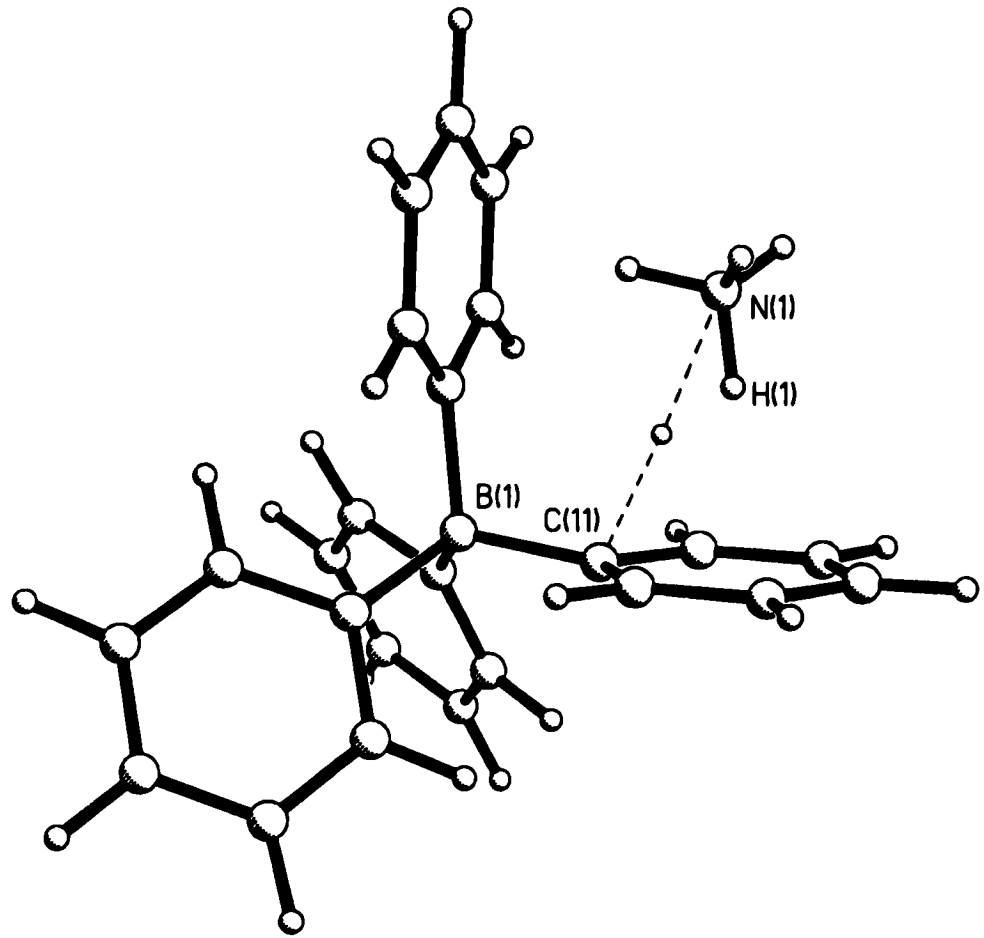

Figure 6. The N-H...π(Ph) hydrogen bond formed in the structure of ammonium tetraphenylborate, drawn to emphasize the role of the phenyl ring as the acceptor of the interaction. The small open circle represents the location of the bond critical point of the interaction.

Table 6. Intermolecular contacts for ammonium tetraphenylborate.

Hydrogen bonded contacts N-H...π (cation/anion)			
contact	N...C (Å)	H...C (Å)	N-H...C (°)
N(1)-H(1)...ring 1	symmetry (x, y, z) and (y, x, z)		
C(11)	3.268(1)	2.448	135.8
C(12)	3.2908(8)	2.426	140.8
C(13)	3.3904(9)	2.464	149.0
C(14)	3.437(1)	2.484	153.3
mean	**3.345[2]**	**2.452**	**144.8**
centroid[a]	3.038	2.013	172.0
plane[b]	3.031	2.012	80.6

[a] The position of the centroid of ring 1 is (0.1459, 0.1459, 0.7541). The values listed are *d*(N...centroid), *d*(H...centroid) and the angle N-H...centroid.

[b] The mean deviation of the carbon atoms from the ring 1 plane is 0.0028Å. The values listed are *d*(N...plane), *d*(H...plane) and the angle the N-H vector makes with the plane of the ring.

Table 7. Bond critical points for the intermolecular contacts in ammonium tetraphenylborate.

Hydrogen bonded contacts N-H...π (cation/anion)									
Contact	Hessian Eigenvalues			Charge Density	Laplacian	Ellipticity	Position		
Bond Path	λ_1	λ_2	λ_3	$\rho_b(\mathbf{r})$ ($e\text{Å}^{-3}$)	$\nabla^2\rho_b(\mathbf{r})$ ($e\text{Å}^{-5}$)	ε	x	y (fractional)	z
ring 1...H(1)-N(1)*	symmetry (x, y, z)			centroid type hydrogen bond					
C(11)...N(1)	-0.25,	-0.05,	1.17	0.099(7)	0.872(1)	4.03	0.0450,	0.0450,	0.8097

Bond Lengths and Angles at the Critical Point			
Atoms	Distance (Å)	Atoms	Angle (°)
Cp...N(1)	1.687	N(1)...Cp...C(11)	176.6
Cp...H(1)	0.943	H(1)...Cp...C(11)	150.4
Cp...C(11)	1.583	N(1)-H(1)...Cp	117.2
Cp...plane	1.450		
Cp...centroid	1.658		

* The bond path is unusual beginning from N(1) not H(1); from N(1) it follows the N(1)-H(1) bond for only approximately one third of its length before proceeding to C(11) of the ring.

3.2.2. Crystallographic Investigations of Hydrogen Bonding in [DabcoH][$B(C_6H_5)_4$]

The room temperature, conventional spherical refinement based structure determination of [DabcoH][$B(C_6H_5)_4$] was reported in the 1994 publication by P.K. Bakshi et al.[83] In the same paper, the authors also characterize the geometry of the single N-H...π(Ph) hydrogen bond in the structure. These results can be compared with the results of the low temperature, multipole refinement of the [DabcoH][$B(C_6H_5)_4$] structure (Figure 7) carried out in this investigation.

It is interesting to note that Bakshi et al.[83] were trying to prepare the diprotonated Dabco salt, [$DabcoH_2$][$B(C_6H_5)_4]_2$. An aqueous solution of Dabco was neutralized with HCl to $DabcoH_2^{2+}$ and an aqueous solution of $NaB(C_6H_5)_4$ was added to give a $DabcoH_2^{2+}$:$B(C_6H_5)_4^-$ ratio of 1:2. However, in spite of this solution stoichiometry, the precipitate recovered was always the 1:1 salt, [DabcoH][$B(C_6H_5)_4$] and never the 1:2 salt.

A Dabco tetraphenylborate salt of stoichiometry of 2:1 has also recently been reported in the literature. H. Bock et al.[112] discuss the 200K crystal structure determination of [$(Dabco)_2H$][$B(C_6H_5)_4$] in a 1997 publication. The 2:1 salt was crystallized from an acetone solution of [DabcoH][$B(C_6H_5)_4$] and Dabco by diffusion with hexane to give colourless, polyhedral crystals. The structure was found to crystallize in the monoclinic space group, $P2_1/n$, with Z = 4 and unit cell dimensions of a = 9.595(1)Å, b = 19.034(2)Å, c = 16.875(1)Å and β = 96.13(1)°. The unusual, N-H...N hydrogen bond bridged cations, [DabcoH...Dabco]$^+$, were found to be completely separated from one another in the crystal by the tetraphenylborate anions. Unlike the structure of [DabcoH][$B(C_6H_5)_4$] which contains an N-H...π(Ph) hydrogen bond between the cation and the anion,

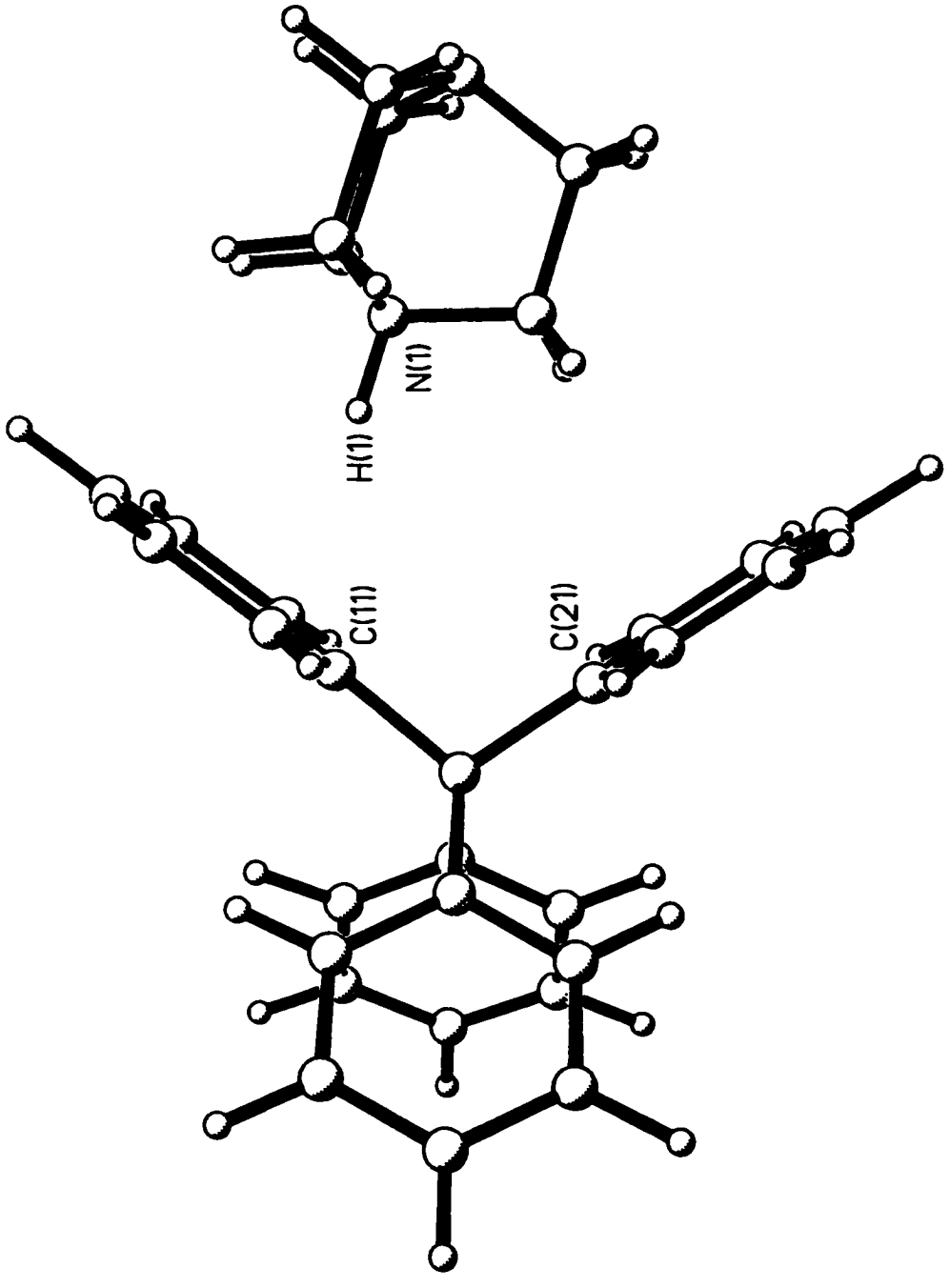

Figure 7. The structure of [DabcoH][B(C$_6$H$_5$)$_4$].

$[(Dabco)_2H][B(C_6H_5)_4]$ forms a conventional N-H...N hydrogen bond, although in an unusual bridge between the two Dabco moieties of the cation. The hydrogen bridge bond distance N...N was found to be 2.70Å (no esd was given), while a rough determination of the H(N) hydrogen position resulted in an N-H(N) distance of 1.08Å and an N-H(N)...N angle of 175°. From this information, an H(N)...N distance of 1.62Å could also be calculated, completing the bridge geometry.

Most interestingly, the unprotonated of the two independent Dabco molecules in the cation was found to be rotationally disordered about its N...N axis. Surprisingly, 85% of the cations were found to be in an eclipsed orientation while only 15% were found to be in a staggered conformation (rotated by 60° about the N...N axis relative to the eclipsed orientation). The eclipsed conformation has relatively short C...C contacts between Dabco moieties in the cation of 3.60Å, while in the staggered conformation the minimum C...C contact increases to 4.10Å. For some reason, the short C...C contacts must stabilize the [DabcoH...Dabco]$^+$ cation in the crystal structure.

The authors also include semi-empirical charge calculations for the atoms in the $[(Dabco)_2H]^+$ cation, based on the experimental geometry.

cation :	N -	(CH_2 - CH_2)$_3$	- N -	H	N -	(CH_2 - CH_2)$_3$	- N		
charge :	+0.01	C -0.12	-0.23	+0.47	+0.15	-0.02	-0.14	-0.12	+0.01
		H +0.10	+0.11				+0.08	+0.08	

The charges show that stabilizing attractions could occur between C-H groups on opposing Dabco molecules of the cation, perhaps explaining the observed preference for the eclipsed conformation. The authors also calculate a formation enthalpy for the cation, $\Delta\Delta H_f$, defined as:

$\Delta\Delta H_f$ = [ΔH_f (DabcoH)$^+$ + ΔH_f (Dabco)] - [ΔH_f (DabcoH...Dabco)$^+$] = 54 kJ/mol.

Of more direct interest in relation to the multipole investigation of [DabcoH][$B(C_6H_5)_4$] is the room temperature, conventional spherical refinement of the same structure reported by Bakshi et al.[83] in 1994. Before examining the N-H...π(Ph) hydrogen bond in detail, it is possible to compare other general features of the two structural determinations. Both refinements resulted in a space group assignment of orthorhombic, *Pnma*. As outlined below, the low temperature unit cell dimensions are consistently shorter than the room temperature values, as expected because of lattice contraction at lower temperatures. The estimated standard deviations on the room temperature (spherical refinement) unit cell dimensions were, on average, three times larger than those on the low temperature (multipole) values. This also is not surprising considering the higher quality of the low temperature data collection.

Unit Cell Dimensions of [DabcoH][$B(C_6H_5)_4$]

Parameter	Bakshi[83]	this work
	R.T.	153K
a, Å	18.208(3)	18.1170(8)
b, Å	13.303(3)	13.2230(9)
c, Å	9.987(2)	9.9516(4)
Volume, Å^3	2419(1)	2384.0(2)

where R.T. is room temperature

The room temperature (18°C) spherical refinement was based on 1061 unique reflections with I > 3σ(I) and 162 refined parameters for a d/p

ratio of roughly 6.5. Hydrogen atoms were not refined but were placed geometrically with U_{iso} equal to $1.2U_{eq}$ of the heavy atom to which the hydrogen atom was bonded. The final R factors of the spherical refinement were calculated to be 3.9% and 3.6% for R and R_w, respectively. The low temperature (153K) multipole refinement was based on 3204 observed reflections and 422 refined parameters for a d/p ratio of approximately 7.6. In the multipole refinement, hydrogen atom positions were refined, then normalized to the appropriate X-H neutron bond length values. An extinction parameter (0.29(2)) was also refined in the multipole determination. Final residual values for R and R_w of 4.68% and 3.79% were calculated for the multipole refinement.

Using the numbering chosen for the multipole refinement (Figure 7), one can easily see that both the cation and the anion in [DabcoH]-$[B(C_6H_5)_4]$ have C_s symmetry. In the cation, N(1) and N(2), and C(1) and C(2) lie directly on the mirror plane, as does H(N) = H(1). The atoms C(3) and C(4) are in general positions and are replicated across the mirror plane, as are each of the H(C) cation hydrogens [H(1A), H(2A), H(3A), H(3B), H(4A) and H(4B)]. Similarly, the anion includes a mirror plane on which lie B(1), C(11), C(14), H(14), C(21), C(24) and H(24). Only one half of anion phenyl rings 1 and 2 are unique, with the other halves generated by symmetry. All of the atoms of phenyl ring 3 occupy general positions; the fourth phenyl ring is generated by symmetry across the mirror plane.

The packing diagrams for [DabcoH]$[B(C_6H_5)_4]$ are shown in Figure 8 (a), (b), (c). Overall, the ion packing is best described as being of a distorted NaCl-type. Each cation is found in a cavity formed by four tetraphenylborate anions (Figure 9), with all of the B and N atoms

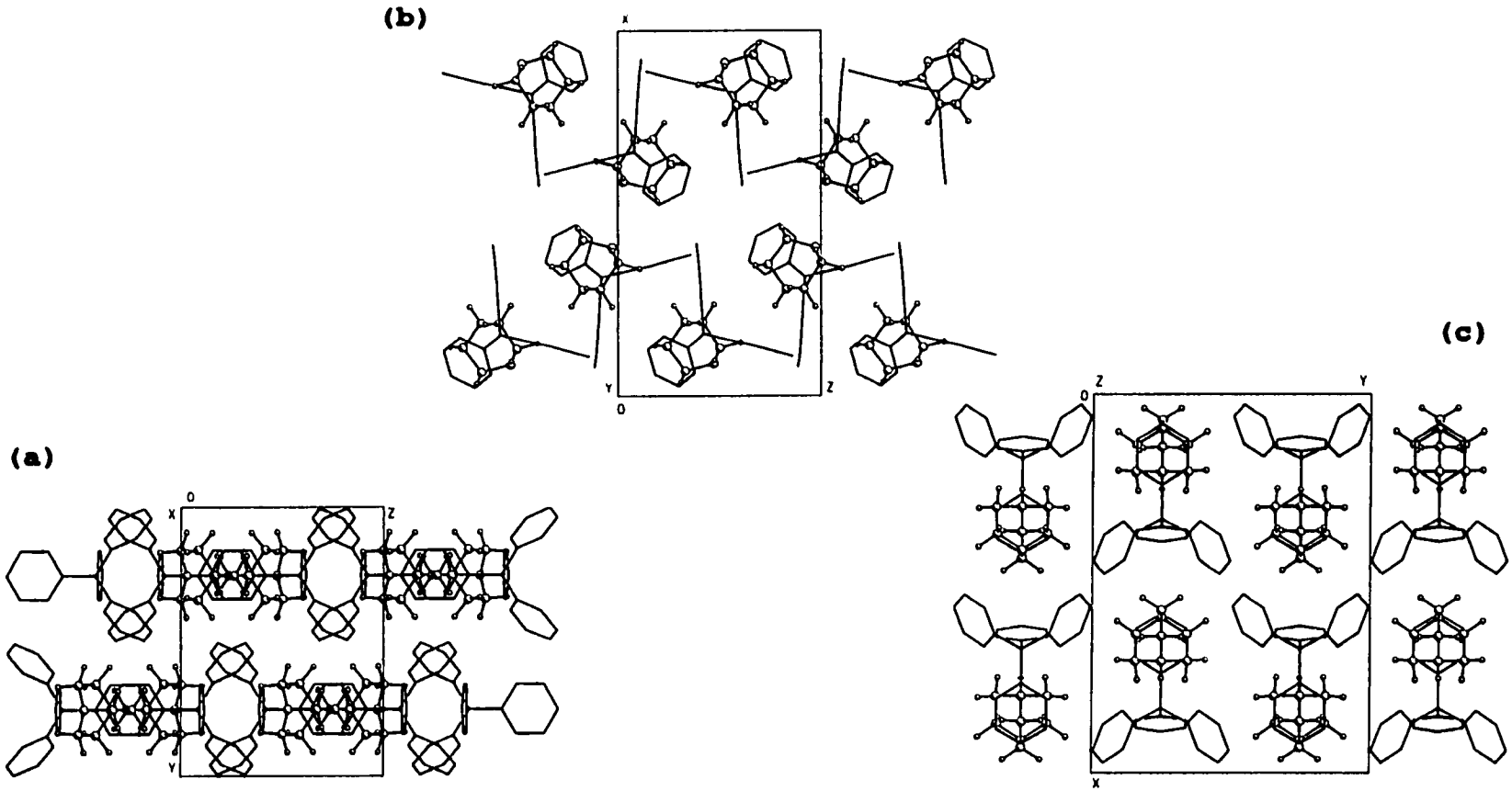

Figure 8. [DabcoH][$B(C_6H_5)_4$]: (a) projection on (100), (b) projection on (010) and (c) projection on (001). Hydrogen atoms have been removed from the anion for clarity.

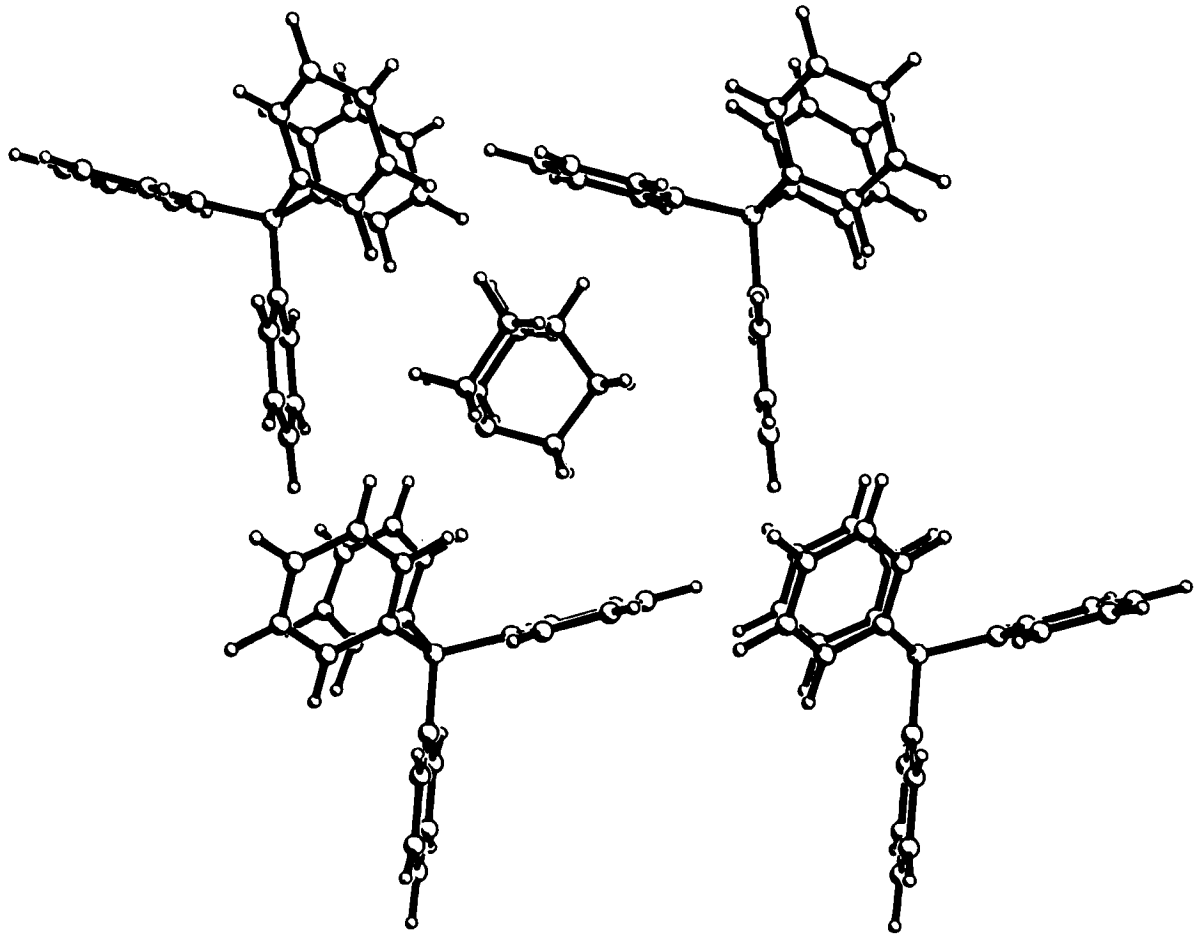

Figure 9. Orientation of the DabcoH$^+$ cation within a cavity formed by six anions in the structure of [DabcoH][$B(C_6H_5)_4$]. Two of those anions, in front and in back of the cation, have been omitted for clarity.

involved having the same *y* coordinate. Directly above and below the cation, along the *y* axis, two more tetraphenylborate anions completely enclose the cation, for an overall octahedral coordination. Similarly, each anion has six nearest cation neighbours in an octahedral arrangement. The packing is distorted from NaCl-type because the unit cell is orthorhombic rather than cubic.

The atom numbering and the unique atom positions chosen are somewhat different in the two refinements. In the cation, the numbering of the heavy atoms is identical in the two determinations. For comparison, the spherical coordinates can be transformed to the chosen multipole coordinate system using the relationship, $(x,\ y,\ z)_{spherical,cation} \rightarrow (\frac{1}{2}+x,\ \frac{1}{2}-y,\ \frac{1}{2}-z)_{multipole}$. In the anion, rings 1, 2, 3 of the multipole refinement are respectively numbered 3, 2, 1 in the spherical refinement. Once renumbered, the anionic, spherical refinement positional parameters can be moved to the multipole coordinate system using the transformation, $(x,\ y,\ z)_{spherical,anion} \rightarrow (x,\ y-1,\ z+1)_{multipole}$.

Once both determinations had been placed on an equal footing, direct comparison of the atomic positional parameters, and their estimated standard deviations, proved possible. Overall, the average difference in the *x*, *y* or *z* fractional coordinate of a given atom was slightly less than 0.001, relatively small. No consistent trend was seen in the differences between the two refinements; both the anion and the cation occupy the same relative positions in the two determinations. The estimated standard deviations on the positional parameters averaged 1.7 times larger in the spherical refinement compared to the corresponding multipole values.

The first section of the discussion, on TLS analysis, included a

comparison of the DabcoH$^+$ cation in the room temperature, spherical and low temperature, multipole refinement. The anisotropic temperature factors of the heavy atoms were found to be, on average, 1.5 times larger in the room temperature, spherical refinement than in the low temperature, multipole refinement. The estimated standard deviations on the U_{ij} values were, on average, larger by a factor of 3 in the spherical refinement than in the multipole refinement.

Selected bond lengths and angles in the tetraphenylborate anion in [DabcoH] [$B(C_6H_5)_4$] were reported by Bakshi et al.[83] and so can be compared with the corresponding values from the multipole refinement. The mean B-C bond length in the anion was found to be 1.646Å in the spherical refinement and a very similar 1.644Å in the multipole refinement. The estimated standard deviations on these few reported bond lengths were approximately two times larger in the spherical refinement larger than they were in the multipole refinement. Similarly, the estimated standard deviations on the reported anion bond angles were approximately twice as large in the spherical determination as those in the multipole determination. The angles centered on the boron atom fall into two distinct groups. Using the multipole nomenclature, the C(11)-B(1)-C(21) and C(31)-B(1)-C(31)' angles average 104.6° [107.5(2)° in the former and 101.7(2)° in the latter]. This is exactly the same mean value reported by Bakshi et al. for the corresponding angles in the spherical refinement. The remaining four boron-centered angles, two unique angles replicated twice by symmetry [C(21)-B(1)-C(31) = 112.1(1)° and C(11)-B(1)-C(31) = 118.1(1)°], have a mean of 112.0°, very similar to the average reported by Bakshi et al., 111.9°, for the corresponding set of angles. The angles at the α carbon

of the phenyl rings, C(x1), were also reported by Bakshi et al. and calculated to have a mean of 114.8°. The same angles in the multipole refinement were calculated to have the slightly different mean of 115.6°.

The mean bond lengths and angles determined from the multipole refinement for the C_s symmetry anion in [DabcoH][$B(C_6H_5)_4$] agree closely with the corresponding values from the multipole refinement of $NH_4B(C_6H_5)_4$ in which the anion is of higher symmetry (D_{2d}). In the multipole refinement of the anion in ammonium tetraphenylborate, the angles at boron were found to be 103.7(1)° (2x) and 112.4(1)° (4x), while the B-C bond length was determined to be 1.644(1)Å and the interior angle at the α carbon of the phenyl ring was 115.6(1)°.

The 1994 publication of Bakshi et al.[83] does not include bond lengths or angles from the DabcoH$^+$ cation, other than those directly pertaining to the N-H...π(Ph) hydrogen bond. However, the PhD. thesis of P.K. Bakshi (1995)[113] does contain selected bond lengths and angles, about the nitrogen atoms in the cation, from the same room temperature, spherical refinement reported in 1994. Bakshi reports mean bond lengths of 1.496Å and 1.456Å for N(1)-C(x) and N(2)-C(y) bonds in the cation, respectively. Similar mean values of 1.500Å and 1.458Å were calculated for the corresponding bond lengths in the multipole refinement. The estimated standard deviations on these bond lengths were more than twice as large in the spherical refinement as in the multipole refinement, as had previously been observed in the comparison of the anion bond lengths. The bonds about the tetrahedrally coordinated ammonium N(1) center [multipole mean 1.500Å] were found to be significantly longer than those about the amine N(2) center [multipole mean 1.458Å] in both refinements. The bonds at N(1)

would be expected to lengthen upon its protonation. The C-N(1)-C bond angles in the cation were calculated to have a mean value of 109.7°, almost equal to the average C-N(2)-C angle of 109.4°, in the multipole refinement. Bakshi reports mean values of 110.0° [C-N(1)-C] and 108.9° [C-N(2)-C] for the corresponding angles in the spherical refinement of [DabcoH][$B(C_6H_5)_4$]. The angles calculated in the multipole refinement are consistently closer to the ideal tetrahedral value than those from the room temperature, spherical refinement.

To compare the N-H...π(Ph) hydrogen bond geometries calculated in the two structure determinations of [DabcoH][$B(C_6H_5)_4$], the treatment of the H(N) hydrogen atom during the refinement must be considered. In the room temperature spherical refinement of Bakshi et al.[83] the H(N) atom was placed geometrically and kept fixed during the refinement at a bond length (N-H) of 1.02Å. It was assigned an isotropic temperature factor equal to 1.2 times that of N(1). In contrast, in the multipole refinement the ammonium hydrogen was refined, although its position was renormalized to the neutron bond length (N-H = 1.032Å) after each cycle of least squares.

In the multipole refinement, the final positions of N(1) and H(1) were calculated to be (0.7952(2), -¼, 0.6707(2)) and (0.7481, -¼, 0.7290), respectively. The spherical refinement, after transformation to the multipole system, gave coordinates for N(1) and H(N) of (0.7947(2), -¼, 0.6686(4)) and (0.745, -¼, 0.718). The position of H(1)/H(N) is quite different in the two determinations, particularly relative to the small shift seen for N(1). The largest difference in the position is observed along the *z* axis. This difference can only be partially accounted for by the difference in the chosen N-H bond length, 1.02Å in the spherical

refinement versus 1.032Å in the multipole refinement.

[DabcoH][$B(C_6H_5)_4$] forms only a single, interionic N-H...π(Ph) hydrogen bond (Figure 10). The geometry of this interaction is summarized in Table 8, based on the results of the multipole determination. As in the $NH_4B(C_6H_5)_4$ structure, it appears that since only a single N-H...π(Ph) hydrogen bond is present, its geometry can be optimal. The geometry of the interaction in [DabcoH][$B(C_6H_5)_4$] would be described in traditional terminology as being of the centroid type. First, only a narrow range of $N(1)...C_{ring}$ and $H(1)...C_{ring}$ values are observed. In the case of N(1), the closest phenyl ring carbon is C(14) at 3.353(4)Å, while the farthest is C(11) at 3.593(4)Å, a difference of 024Å [100Δ = 24] for the multipole refinement. In contrast, H(1) was found to be closest to C(12) [2.537Å] and farthest from C(14) [2.640Å], a difference of only 0.10Å [100Δ = 10]. The mean distances from N(1) and H(1) to ring 1 of the tetraphenylborate anion were calculated to be 3.447[8]Å and 2.580Å, respectively.

The second reason to describe the geometry of the N-H...π(Ph) interaction as being of the centroid type is that the distances from N(1) and H(1) to the centroid (π_c) of phenyl ring 1 are shorter than any of the corresponding distances from N(1) or H(1) to individual ring 1 carbon atoms. The $N(1)...\pi_c$ distance was calculated to be 3.152Å, while the $H(1)...\pi_c$ distance was calculated to be 2.169Å. Finally, the $N(1)-H(1)...\pi_c$ angle was found to be close to linear (158.6°), another characteristic of a centroid type interaction. The angle between the N-H vector and the ring plane is reasonably close to perpendicular, 70.7°. The N-H vector points into the ring just off the centroid toward the C(11) end of the anion ring, similar to the arrangement in ammonium tetraphenylborate.

As in the ammonium tetraphenylborate case, the geometry of the N-H...π(Ph) hydrogen bond in [DabcoH][$B(C_6H_5)_4$], determined from the multipole refinement, is somewhat difficult to describe. The closest N(1)...C_{ring} contact is to C(14), while the closest H(1)...C_{ring} contact is to C(12) and the most linear N(1)-H(1)...C_{ring} angle is made with C(11), 167.4°. The importance of each of these features in determining the nature of the interaction is difficult to ascertain. However, overall the geometry of the N-H...π(Ph) hydrogen bond in [DabcoH][$B(C_6H_5)_4$] is close to the "ideal" centroid type, indicative of a relatively strong interaction. The N-H...π(Ph) hydrogen bond can be optimized because it is the only such interaction occurring in the structure.

The geometry of the N-H...π(Ph) hydrogen bond in [DabcoH][$B(C_6H_5)_4$] can be contrasted in the two structure determinations, multipole/low temperature versus spherical/room temperature. Somewhat surprisingly, the individual N(1)...C_{ring} distances in the multipole refinement are all consistently shorter in the multipole refinement than in the spherical refinement, the average difference being 0.013Å, and the greatest difference being found at the C(11),C(12) end of the ring. [Multipole numbering is used throughout this discussion; ring 1 multipole = ring 3 spherical.] Even more surprisingly, Bakshi et al.[83] report the N(1) to ring centroid distance as being 3.12Å which is shorter than the value of 3.152Å found in the multipole determination, opposite to what would be expected from the N(1)...C_{ring} comparison. The range of N(1)...C_{ring} distances is about the same in the two determinations, with 100Δ being slightly less in the multipole refinement (24) than in the spherical refinement (27).

The range of H(N)...C_{ring} distances was found to be the same in both

refinements, with 100Δ equal to 10. However, the different positioning of H(N) in the two determinations results in a different position and inclination of the N-H vector relative to the phenyl ring. This in turn results in a slightly different geometry for the N-H...π(Ph) bond, which is particularly reflected in the H(N)...C_{ring} distances. For example, in the multipole refinement H(N) is 2.579Å from the α carbon, C(x1), of the phenyl ring while it is 2.640Å from C(x4) at the opposite end of the ring. In contrast, in the spherical refinement H(N) is closer to the C(x4) end of the ring (2.56Å) and farther from the α carbon at the C(x1) end of the ring (2.65Å). Overall, the mean distance to the phenyl ring, H(N)...C_{ring}, is about the same, 2.580Å in the multipole refinement and 2.57Å in the spherical refinement. However, even this is somewhat surprising considering that a longer N-H bond length was used in the multipole refinement (1.032Å versus 1.02Å) which should have resulted in H(N) being closer to the ring in the multipole refinement. A similar reversal was also observed in the H(N) to ring centroid distance, which was found to be 2.169Å in the multipole refinement but only 2.11Å in the spherical refinement. The minimum H(N)...C_{ring} distance reported by Bakshi et al. is to C(33) = $C(13)_{multipole}$, 2.55Å, in contrast to the minimum distance in the multipole refinement (H(1)...C(12) = 2.537Å) which is actually slightly shorter as would reasonably be expected.

The centroid geometry N-H...π(Ph) hydrogen bond in [DabcoH] [$B(C_6H_5)_4$] is characterized by an H(N)...π_c distance of 2.169Å, a short distance indicative of a relatively strong interaction. It is, however, slightly longer than the corresponding H(N)...π_c distance of 2.013Å observed for the N(1)-H(1)...ring 1 hydrogen bond in $NH_4B(C_6H_5)_4$. In ammonium tetraphenyl-

borate the cation forms four equivalent N-H...π(Ph) hydrogen bonds, with each H(N) atom of the cation bearing an equal portion of the total (+1) charge. In [DabcoH][$B(C_6H_5)_4$] the situation is somewhat different. The $DabcoH^+$ cation also carries a single positive charge but in [DabcoH][$B(C_6H_5)_4$] only a single N-H...π(Ph) hydrogen bond is formed, since only a single nitrogen center of the cation is monoprotonated. On the basis of charge and the competition for best geometry, the single N-H...π(Ph) hydrogen bond formed in [DabcoH][$B(C_6H_5)_4$] might be expected to be stronger than the four equivalent bonds formed in $NH_4B(C_6H_5)_4$. However, as observed from the from the H(N)...π_c distances, it is actually found to be slightly weaker.

The discrepancy can be attributed to the different sizes of the cations (the number of atoms in each) and the ability to distribute the positive charge over other atoms in the cation. The $DabcoH^+$ cation has, besides the single N-H group, seven other heavy atoms and twelve other hydrogen atoms. As well as the single, centroid type N-H...π(Ph) hydrogen bond, the cation has been found to participate in a large number of C-H...phenyl interactions; these will be discussed in detail later. The positive charge must be distributed, at least to a certain extent, over the entire cation rather than isolated at the N-H group. The N-H...π(Ph) hydrogen bond must also compete with the weaker, C-H...phenyl interactions so that all will be formed with the best possible geometries. For both of these reasons, it is not surprising that the N-H...π(Ph) hydrogen bond in [DabcoH][$B(C_6H_5)_4$] is slightly weaker, based on the H(N)...π_c distance, than that in $NH_4B(C_6H_5)_4$.

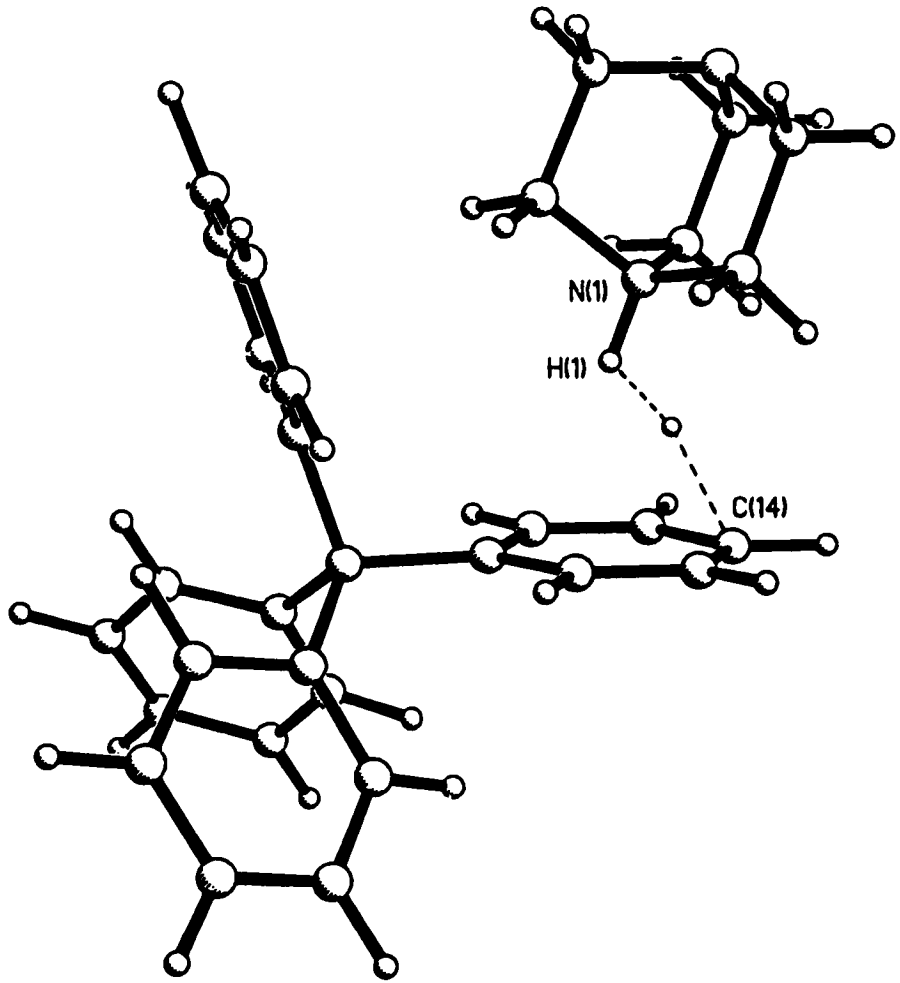

Figure 10. The N-H...π(Ph) hydrogen bond formed in the structure of [DabcoH][$B(C_6H_5)_4$], drawn to emphasize the role of phenyl ring #1 as the acceptor of the interaction. The small open circle represents the location of the bond critical point of the interaction.

Table 8. Intermolecular contacts for [DabcoH][$B(C_6H_5)_4$].

Hydrogen bonded contacts N-H...π (cation/anion)			
contact	N...C (Å)	H...C (Å)	N-H...C (°)
N(1)-H(1)...ring 1 symmetry (x, y, z) and (x, -1/2-y, z)			
C(11)	3.593(4)	2.579	167.4
C(12)	3.480(3)	2.537	151.7
C(13)	3.389(3)	2.595	133.5
C(14)	3.353(4)	2.640	126.1
mean	**3.447[8]**	**2.580**	**144.0**
centroid[a]	3.152	2.169	158.6
plane[b]	3.141	2.206	70.7

[a] The position of the centroid of ring 1 is (0.6314, -0.2500, 0.7772). The values listed are *d*(N/C...centroid), *d*(H...centroid) and the angle N/C-H...centroid.

[b] The mean deviation of the carbon atoms from the ring 1 plane is 0.0100Å. The values listed are *d*(N/C...plane), *d*(H...plane) and the angle the N/C-H vector makes with the plane of the ring.

Table 9. Bond critical point for the intermolecular contact in [DabcoH][$B(C_6H_5)_4$].

Hydrogen bonded contacts N-H...π (cation/anion)									
Contact	Hessian Eigenvalues			Charge Density	Laplacian	Ellipticity	Position		
Bond Path	λ_1	λ_2	λ_3	$\rho_b(\mathbf{r})$ ($eÅ^{-3}$)	$\nabla^2\rho_b(\mathbf{r})$ ($eÅ^{-5}$)	ε	x	y (fractional)	z
ring 1...H(1)-N(1)*	symmetry (x, y, z)			centroid type hydrogen bond					
C(14)...H(1)	-0.20,	-0.06,	1.08	0.086(5)	0.823(3)	2.66	0.6980,	-0.2500,	0.6758

Bond Lengths and Angles at the Critical Point			
Atoms	Distance (Å)	Atoms	Angle (°)
Cp...N(1)	1.762	N(1)...Cp...C(14)	165.5
Cp...H(1)	1.051	H(1)...Cp...C(14)	162.6
Cp...C(14)	1.618	N(1)-H(1)...Cp	115.5
Cp...plane	1.426		
Cp...centroid	1.573		

* Single atom type bond path from H(1) to C(14).

3.2.3. Crystallographic Investigations of Hydrogen Bonding in Guanidinium Tetraphenylborate Acetonitrile Solvate

Unlike the first two compounds studied, where the results of conventional spherical refinements were available for comparison with the multipole results, the structure of guanidinium tetraphenylborate acetonitrile solvate (Figure 11) had never previously been reported. However, the conventional structure determinations of two closely related compounds have been published, one quite recently. The 1994 paper by P.K. Bakshi et al.[83] included the structure of guanidinium tetraphenylborate monohydrate and an analysis of its hydrogen bonding, while the structure of *N, N, N', N', N'', N''*-hexamethylguanidinium tetraphenylborate was described by W. Frey et al. in 1998.[114]

Both conventional refinements were carried out using data collected at room temperature with Mo Kα radiation. The guanidinium tetraphenylborate monohydrate structure determination was based on 1268 observed reflections [$I > 1.5\sigma(I)$] with a reflection to parameter ratio of only 4.7 and final residual values of R = 3.5% and R_w = 3.5%. Perhaps because of a shortage of data, all hydrogen atoms were placed in their geometrical positions and not refined. The refinement of hexamethylguanidinium tetraphenylborate was based on 1763 observed reflections [$I > 2\sigma(I)$] and included 176 parameters. The cation was found to be disordered at the two unique nitrogen atom positions, with occupation factors of 0.8:0.2. The final R factor calculated was 5.6%.

In contrast, the data collection for the multipole refinement of guanidinium tetraphenylborate acetonitrile solvate was carried out at 153K, using Mo Kα radiation. A total of 29477 reflections were collected, of which 8733 were unique and 6726 were observed [$I > 3\sigma(I)$]. The

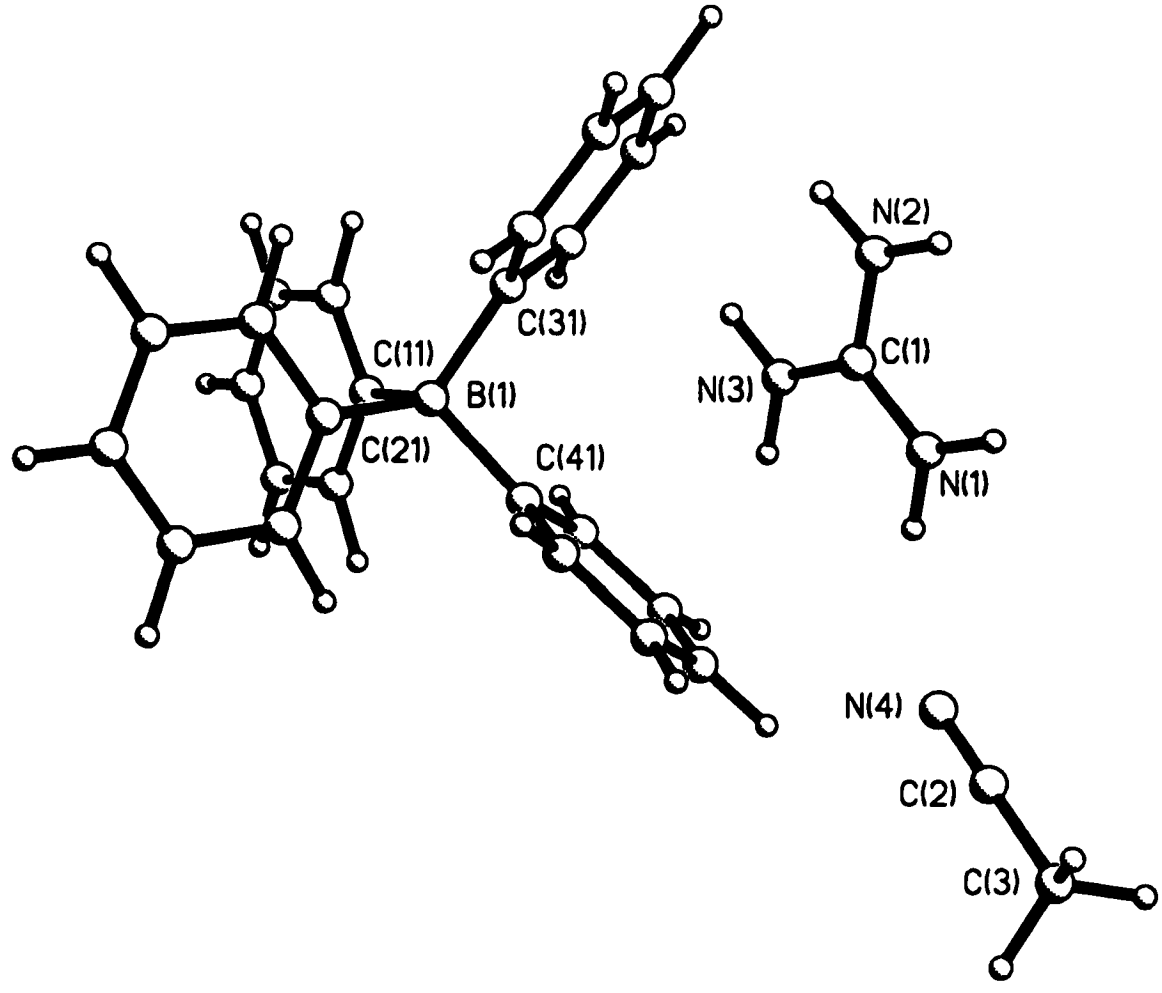

Figure 11. The structure of guanidinium tetraphenylborate acetonitrile solvate.

multipole refinement was based on 838 parameters, for a reflection to parameter ratio of 8.0, and gave final R and R_w values of 5.07% and 4.94%, respectively.

The three compounds were found to crystallize in quite different space groups ($[C(NH_2)_3][B(C_6H_5)_4]\cdot CH_3CN$ triclinic, $P\bar{1}$; $[C(NH_2)_3][B(C_6H_5)_4]\cdot H_2O$ monoclinic, $P2_1/c$; $[C(N[CH_3]_2)_3][B(C_6H_5)_4]$ trigonal, $P3_121$). However, guanidinium tetraphenylborate monohydrate [a = 10.411(4)Å, b = 9.524(3)Å, c = 23.102(7)Å, β = 103.50(3)°] and hexamethylguanidinium tetraphenylborate [$a = b$ = 9.821(1)Å, c = 25.170(6)Å, $\alpha = \beta$ = 90°, γ = 120°] have similar unit cell dimensions and cell volumes, 2227(3)Å^3 in the former versus 2102Å^3 in the latter. In guanidinium tetraphenylborate acetonitrile solvate a = 9.679(2)Å, b = 13.643(3)Å, c = 9.160(2)Å, α = 90.70(3)°, β = 101.23(3)°, γ = 91.08(3)° and the unit cell volume is 1186.1(4)Å^3.

The guanidinium cation, $[C(NH_2)_3]^+$, is a simple extension of the ammonium ion case in the first tetraphenylborate salt studied. Although in the crystal structure of guanidinium tetraphenylborate acetonitrile solvate the cation is in a general position, its geometry is essentially planar and close to D_{3h} symmetry. In the multipole refinement a best plane calculation involving all atoms gave a mean deviation of 0.017Å; with only the heavy atoms included, the mean deviation from the best plane was only 0.0091Å. The average bond angle about the central carbon atom of the cation, N(x)-C(1)-N(y), was calculated to be 120.0°, the ideal value. The mean C(1)-N bond length in the cation, 1.332Å, falls between the usual C-N single bond length (1.47Å) and the C=N double bond length (1.27Å).[1]

The geometry of the anion in guanidinium tetraphenylborate acetonitrile solvate (multipole refinement) was found to be very similar

to that in $NH_4B(C_6H_5)_4$ (D_{2d}) and [DabcoH][$B(C_6H_5)_4$] (C_s) although it has no internal symmetry. The mean B-C bond length of 1.646Å, is close to the mean values reported previously for the anions in the $DabcoH^+$ and NH_4^+ structures. The C(x1)-B-C(y1) angles again fell into two distinct groups, with mean values of 104.0° (2 angles) and 112.3° (4 angles), respectively. The internal angle at the α carbon of the phenyl ring was found to average 115.5°, again similar to the values found for the corresponding angles in the previous structures.

The packing diagrams for guanidinium tetraphenylborate acetonitrile solvate are shown in Figure 12 (a),(b),(c). The packing, which cannot be assigned to any simple type, is dominated by the large, bulky anions with the gaps between anions filled by either cation or solvent molecules. It is obviously difficult to efficiently pack the small, planar cations with the large, non-planar anions. Because of this difficulty, guanidinium tetraphenylborate shows a tendency to crystallize with solvent molecules included in the lattice, whether acetonitrile or water.

The packing in *N*, *N*, *N'*, *N'*, *N''*, *N''*-hexamethylguanidinium tetraphenylborate [Figure 13(c) viewed down the *y* axis] is somewhat different from that in either the acetonitrile or water solvate of guanidinium tetraphenylborate. In the hexamethylguanidinium salt, substitution results in a less planar cation skeleton and its planarity is further reduced by the observed disorder at the N(1) and N(2) positions. The more spherical cation appears to allow more efficient packing in the hexamethylguanidinium structure and solvent molecules are not required to fill voids in the structure.

The monohydrate of guanidinium tetraphenylborate packs more like its

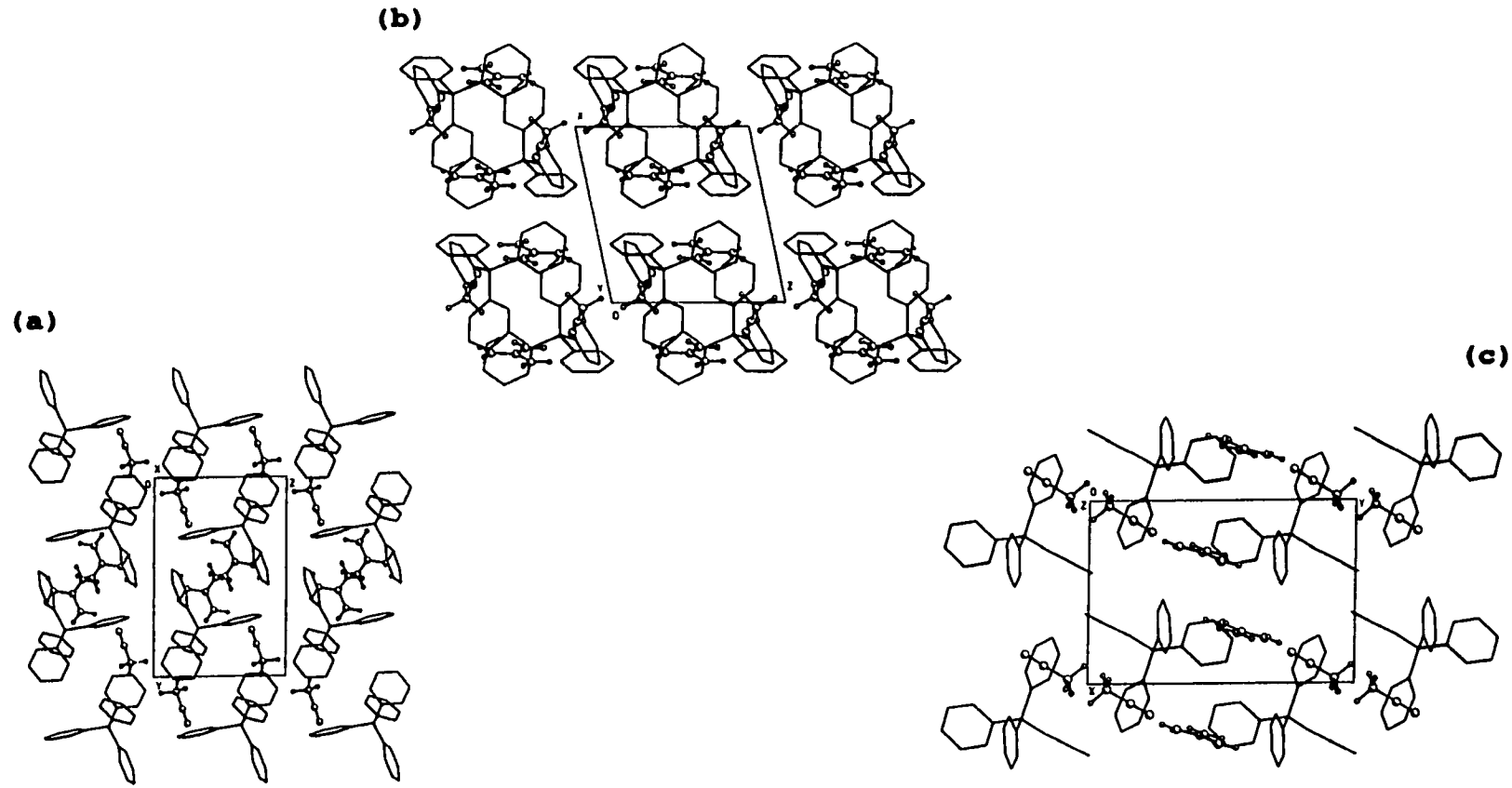

Figure 12. Guanidinium tetraphenylborate acetonitrile solvate: (a) projection on (100), (b) projection on (010) and (c) projection on (001). Hydrogen atoms have been removed from the anion for clarity.

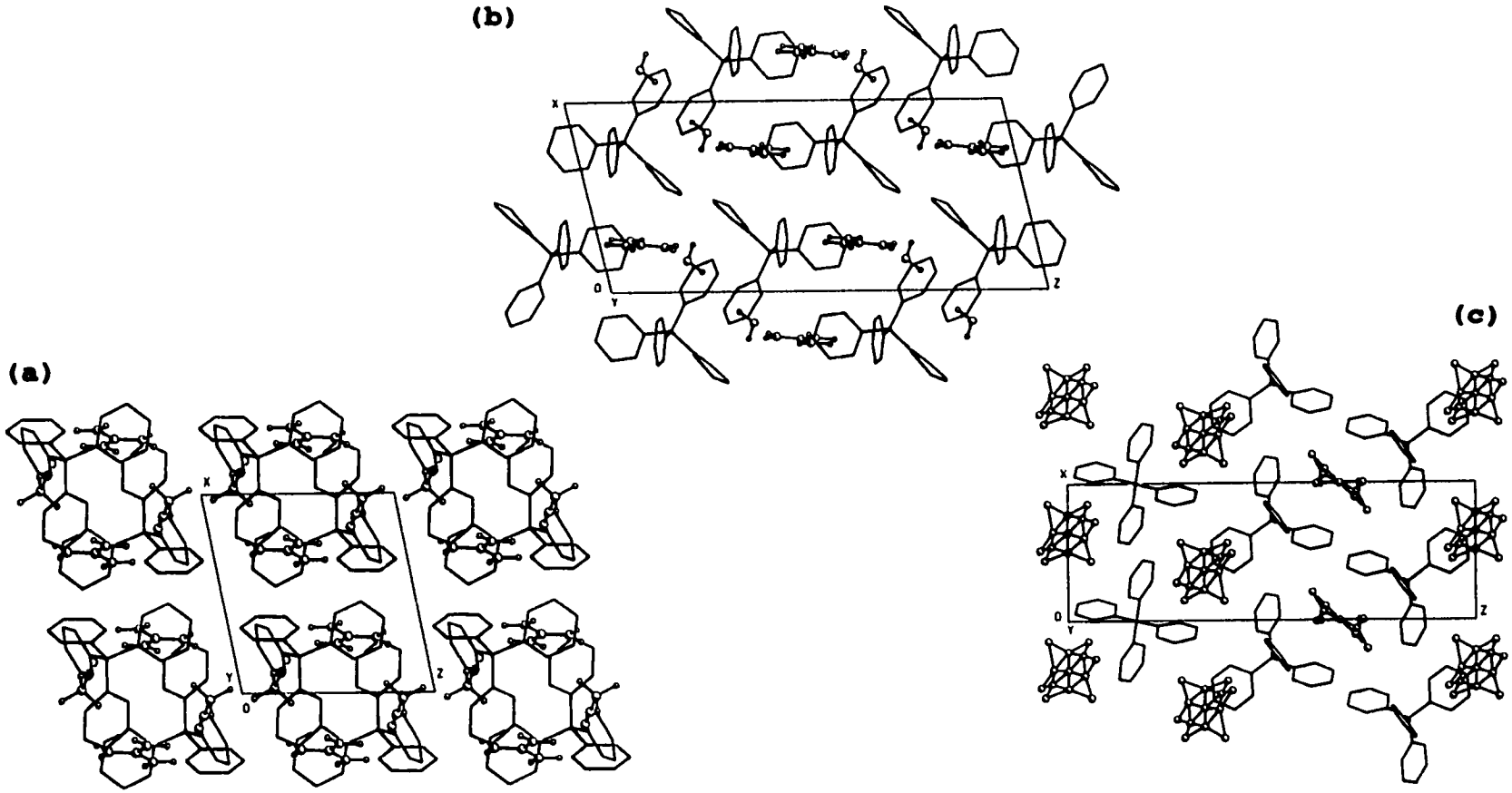

Figure 13. Projection on (010) for (a) guanidinium tetraphenylborate acetonitrile solvate, (b) guanidinium tetraphenylborate monohydrate and (c) *N,N,N',N',N",N"*-hexamethylguanidinium tetraphenylborate. Hydrogen atoms have been removed from the anions for clarity.

acetonitrile solvate counterpart. A packing diagram of the monohydrate salt, viewed down the *y* axis, is shown in Figure 13(b). Comparison to the view down the *y* axis in the acetonitrile solvate [Figure 13(a)] shows discrete units consisting of two anions, two cations and two solvent molecules in both structures. In both structures, the cations are oriented in positions parallel to each other and to the *x* axis, in a head to tail arrangement. The two parallel cations in one of the discrete units occupy spaces between the rings in a pair of opposing tetraphenylborate anions, giving a centrosymmetric grouping.

Differences in the packing of the two structures likely arise from the different sizes of the included solvent molecules, water versus acetonitrile. In the monohydrate, the relatively small water molecule is included in the same cavity between anions as the guanidinium cation. In the acetonitrile solvate, the solvent molecule is larger and bulkier. As a result, the structure forms essentially two different cavities, as shown in Figure 14, with one cavity type containing a pair of guanidinium cations sandwiched between a pair of tetraphenylborate anions and the second type of cavity enclosing two acetonitrile solvent molecules, arranged $NCCH_3$ to CH_3CN, between a pair of anions.

The cation containing cavity in guanidinium tetraphenylborate acetonitrile solvate has one cation oriented such that two of its NH_2 groups point toward one ring of the first anion (ring 2) and the third NH_2 group pointing between two rings of the second anion (rings 3 and 4). The second cation is parallel to the first but oriented in the opposite direction, such that both of the cations and both of the anions are related by the same center of symmetry. The second cation also has two NH_2

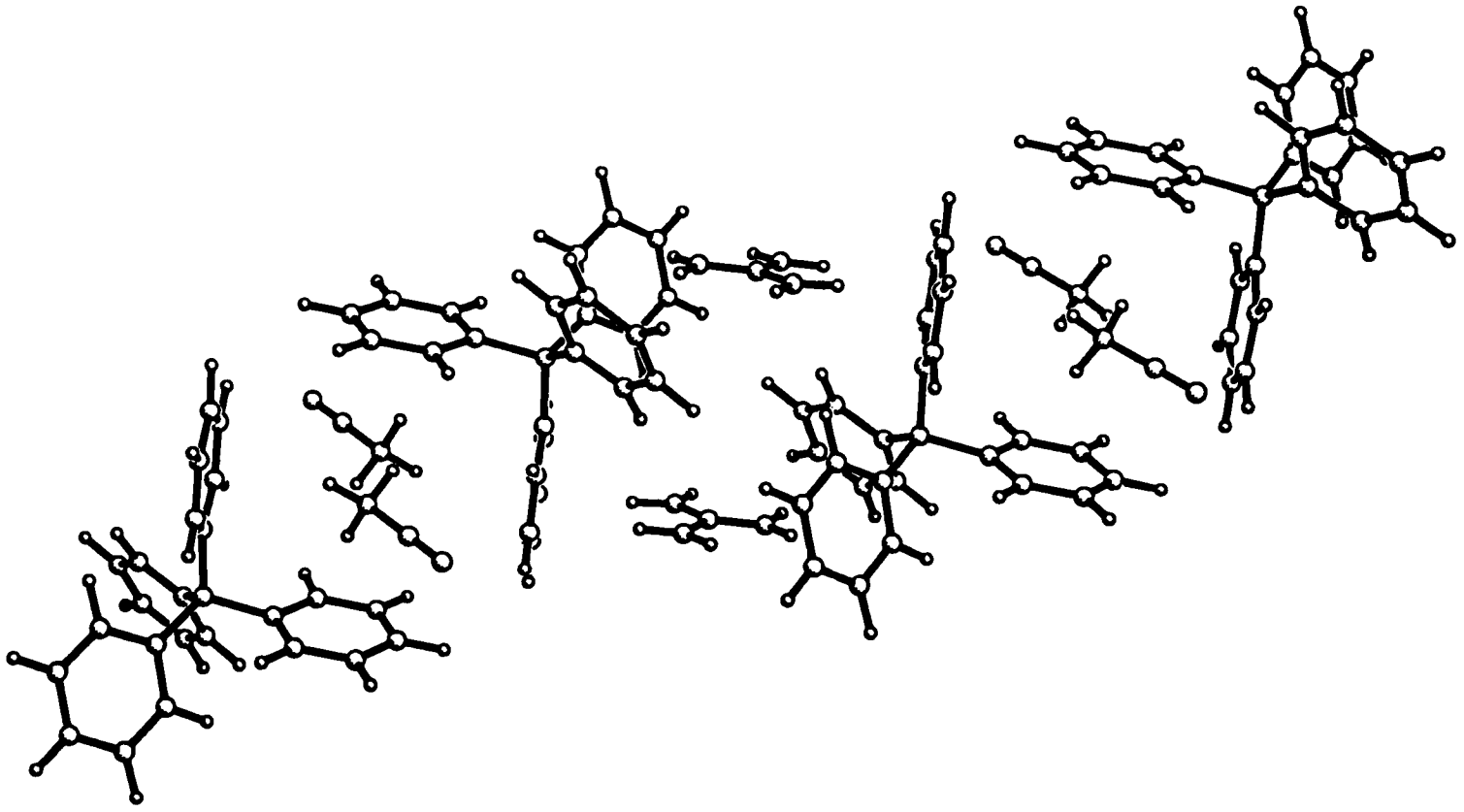

Figure 14. Cavities formed by the arrangement of the anions in the structure of guanidinium tetraphenylborate acetonitrile solvate. Note that the cation and the solvent occupy separate cavities.

groups pointing toward one ring of the second anion (ring 2) and the third NH_2 group pointing between two rings of the first anion (rings 3 and 4). The cation in guanidinium tetraphenylborate acetonitrile solvate interacts only with three of the four phenyl rings on the anion (rings 2, 3 and 4) while the acetonitrile solvate solvent forms close contacts with only two rings of the anion (rings 1 and 2).

In the multipole refinement of guanidinium tetraphenylborate acetonitrile solvate, the H(N) hydrogen atom parameters were freely refined. However, after each cycle of least squares the H(N) positions were altered to give N-H bond lengths equal to reported neutron values. The appropriate N-H neutron bond length was determined after a search of the Cambridge Structural Database[100] for compounds containing guanidinium or biguanidinium cations, as previously described in the experimental section. Only a single structure was located, $(CN_3H_6)_2[(CH_3)_2AsMo_4O_{15}H]\cdot H_2O$, where neutron diffraction had been used to determine the N-H bond length in a guanidinium cation.[101] The mean N-H bond length was calculated to be 0.986Å and this value was used to renormalize the N-H bond lengths in the multipole refinement.

The cation in guanidinium tetraphenylborate acetonitrile solvate contains six independent N-H groups capable of forming hydrogen bonds (donors). The results of the low temperature, multipole refinement of the structure show that, in fact, five N-H...π(Ph) hydrogen bonds are formed between the cation and phenyl rings of the anion, while the sixth N-H group forms a traditional N-H...N hydrogen bond with nitrogen of the acetonitrile solvate. All available N-H donor groups of the cation thus form hydrogen bonds of some type (Figure 15).

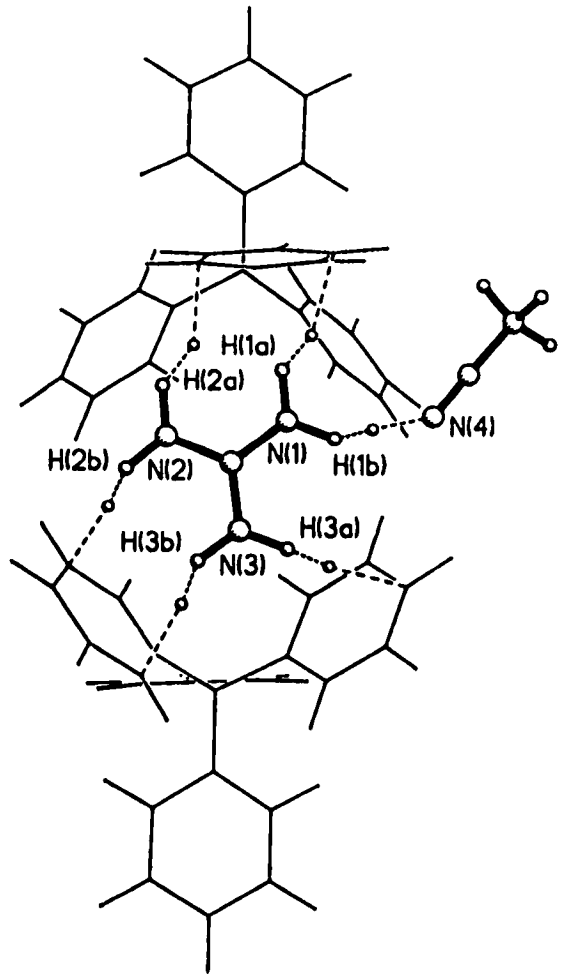

Figure 15. The N-H...X [X = N or π(Ph)] hydrogen bonds formed in the structure of guanidinium tetraphenylborate acetonitrile solvate, drawn to emphasize the role of the cation as the donor of all the interactions. The small open circles represent the locations of the bond critical points of the interactions.

Of these hydrogen bonds, the N(1)-H(1B)...N(4) interaction would be expected to be the strongest and this is reflected in its geometry (Figure 16). Although the N(1)-H(1B)...N(4) angle (143.4°) is not as linear as might be expected for a relatively strong hydrogen bond, both the N(1)...N(4) and H(1B)...N(4) distances, 2.933(4)Å and 2.082Å, are far shorter than the corresponding distances (N/H(N)...C_{ring}) in the N-H...π(Ph) hydrogen bonds of the same cation. If it is assumed that the acetonitrile nitrogen atom is the best hydrogen bond acceptor available in the system, better than the phenyl rings of the anion, then N(1)-H(1B) must be the best donor available in the cation.

The N-H...π(Ph) hydrogen bonds in guanidinium tetraphenylborate acetonitrile solvate can be divided into three groups. Ring 2 of the anion accepts two hydrogen bonds, from N(1)-H(1A) and N(2)-H(2A), as does ring 3 of the anion, from N(2)-H(2B) and N(3)-H(3B). The final interaction, N(3)-H(3A), is accepted by ring 4 of the anion. Perhaps surprisingly, phenyl ring 1 of the anion is not involved in any N-H...π(Ph) hydrogen bonds with the cation. These interactions are illustrated in Figures 17 (ring 2), 18 (ring 3) and 19 (ring 4), at the end of this section.

The geometry of the N(1)-H(1A)...ring 2 [symmetry (*x*, *y*, *z*)] hydrogen bond is best described as being of the centroid type. Only a narrow range of N(1)...C_{ring} [minimum C(23) 3.354(3)Å; maximum C(26) 3.649(3)Å; 100Δ = 29.5] and H(1A)...C_{ring} [minimum C(23) 2.458Å; maximum C(26) 2.806Å; 100Δ = 35] distances are observed. The distances of N(1) and H(1A) to the centroid of ring 2 (π_c) are substantially shorter than the corresponding distances to any individual ring carbon [N(1)...π_c = 3.214Å; H(1A)...π_c = 2.238Å]. The N(1)-H(1A)...π_c angle, 170.1°, is more linear

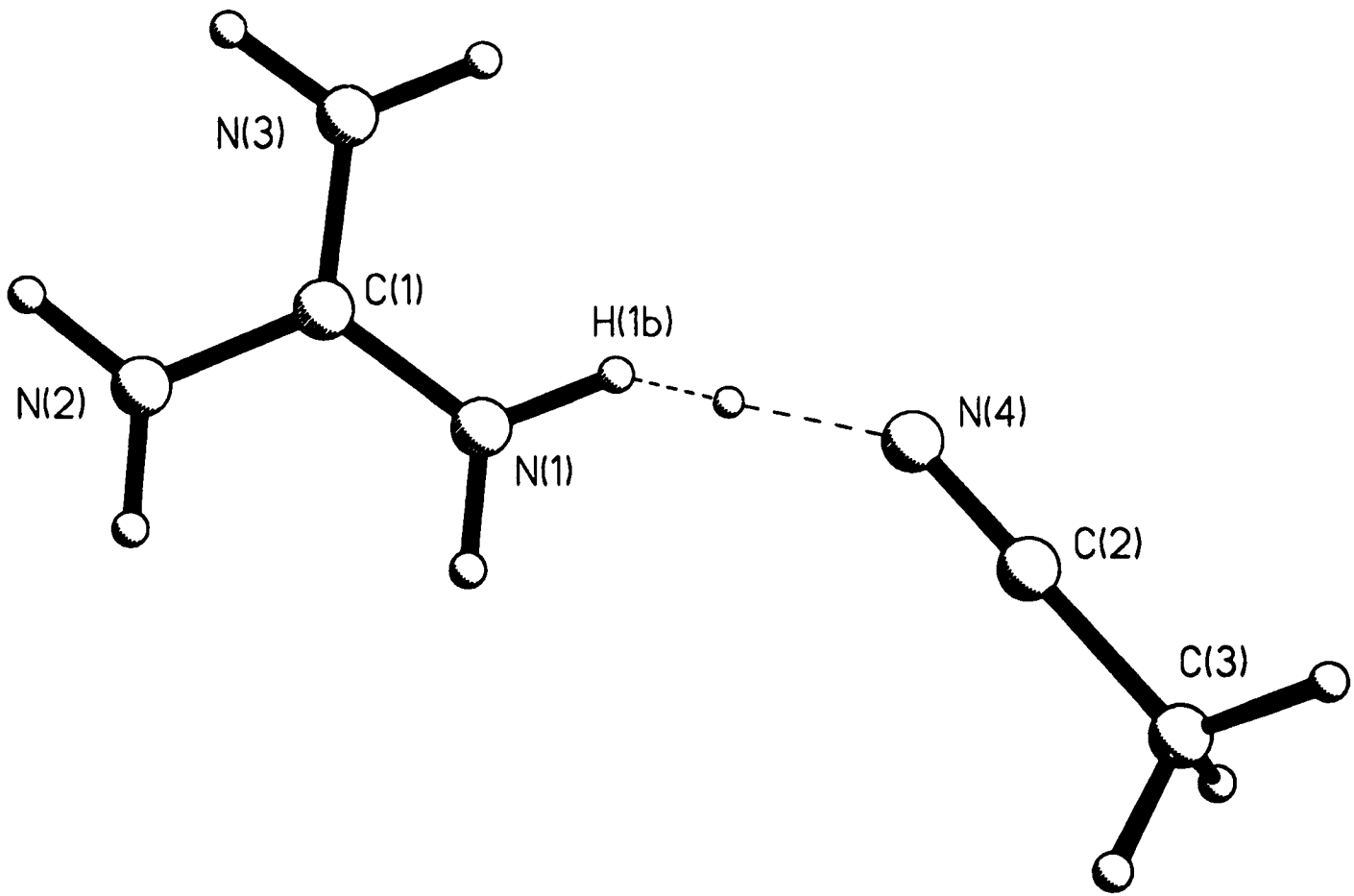

Figure 16. The N-H...N (cation/solvent) hydrogen bond in the structure of guanidinium tetraphenylborate acetonitrile solvate. The small open circle represents the location of the bond critical point of the interaction.

than the angle to any individual ring carbon [N(1)-H(1A)...C(24) = 155.4°]. The N(1)-H(1A) vector makes an angle of 84.6° with the plane of ring 2, close to perpendicular. It points almost directly towards the ring centroid, just off center, slightly toward the C(23)-C(24) bond.

N(2)-H(2A) of the original cation also interacts with ring 2 of the original anion [symmetry (*x*, *y*, *z*)] at the same time that N(1)-H(1A) does, resulting in a "fork" or "pincer" type interaction, illustrated in Figure 17. However, while the N(1)-H(1A) vector projects almost directly onto the centroid of phenyl ring 2, the N(2)-H(2A) vector projects outside the ring, below the C(25)-C(26) bond. As a result, the geometry of this interaction is not of the centroid type but rather could be described as an edge type or bond type interaction. There are two relatively short N(2)...C_{ring} distances [C(25) 3.597(3)Å; C(26) 3.585(3)Å]; all others are much longer with the maximum distance N(2)...C(23) being 4.736(4)Å and 100Δ being equal to 115. The distance from N(2) to the centroid of ring 2, 3.959Å, is also longer. Similarly, two short H(2A)..C_{ring} distances are observed to C(25), 2.689Å, and to C(26), 2.672Å, with all other H(2A)... C_{ring} distances being much longer to a maximum of 4.122Å to C(23) [100Δ = 145]. The distance from H(2A) to the centroid of ring 2, 3.178Å, is also longer than the minimum values. The largest angles are made to C(25), 153.1°, and to C(26), 154.1°, not to the ring centroid, N(2)-H(2A)...π_c = 137.2°. The N(2)-H(2A) vector is almost perpendicular to the plane of ring 2, 86.9°. This is not unexpected since N(1)-H(1A) and N(2)-H(2A) are roughly parallel in the original cation with both facing toward ring 2 of the anion.

The N(2)-H(2A)...ring 2 edge type hydrogen bond might be expected

to be weaker than the N(1)-H(1A)...ring 2 centroid type hydrogen bond based on geometrical considerations. The mean N...C_{ring} and H(N)...C_{ring} distances are considerably shorter for the N(1)-H(1A)..ring 2 interaction [3.507[8]Å; 2.640Å] than for the N(2)-H(2A)...ring 2 interaction [4.175[8]Å; 3.425Å].

There are also two hydrogen bonds accepted by phenyl ring 3 of the anion, from N(2)-H(2B) and N(3)-H(3B) of the same cation, arranged in a second "fork" or "pincer" type interaction with a single ring. They are shown in Figure 18. Beginning from the original cation, the interacting anion is generated by symmetry (2-*x*, 1-*y*, 1-*z*) from the original cation.

Of the two N-H...π(Ph) hydrogen bonds formed to anion ring 3, the second [N(3)-H(3B)...ring 3] would be described as being of the centroid type. The N(3)...C_{ring} [minimum C(32) 3.398(3)Å; maximum C(34) 3.702(3)Å; 100Δ = 30] and H(3B)...C_{ring} [minimum C(32) 2.498Å; maximum C(35) 2.868Å; 100Δ = 37] distances cover a relatively narrow range of values. The N(3)...π_c (3.248Å) and H(3B)...π_c (2.308Å) distances to ring 3 are both shorter than any of the corresponding individual ring N(3)...C_{ring} or H(3B)...C_{ring} values. The angle N(3)-H(3B)...π_c is relatively linear, 159.1°, although in this case the best angle formed is N(3)-H(3B)...C(33) at 168.4°. The N(3)-H(3B) vector is not quite perpendicular to the plane of anion ring 3, forming an angle of 72.5° with the ring. The N(3)-H(3B) vector projects inside the phenyl ring but points more directly toward C(33) rather than toward the ring centroid.

The second component of the "pincer" type interaction to phenyl ring 3, N(2)-H(2B)...π(Ph), is best described as an edge type interaction, involving the C(34)-C(35) bond of the anion. The N(2)...C_{ring} distances to

C(34), 3.613(3)Å, and C(35), 3.460(4)Å, are considerably shorter than the distances to any other ring carbons [maximum C(32) 4.679(3)Å; 100Δ = 122] and to the ring centroid [N(2)...π_c = 3.883Å]. Similarly, the H(2B)...C_{ring} distances to C(34), 2.668Å, and C(35), 2.622Å, are shorter than those to any other carbons in the ring [maximum C(31) 4.079Å; 100Δ = 146] and to the ring centroid [H(2B)...π_c = 3.119Å]. The most linear angle formed is N(2)-H(2B)...C(34) at 160.7°. The N(2)-H(2B) bond is roughly parallel to the N(3)-H(3B) bond in the cation and thus makes essentially the same angle with the plane of ring 3, 72.3°. However, the N(2)-H(2B) vector does not project within the confines of ring 3, as the N(3)-H(3B) vector had. Rather, N(2)-H(2B) projects outside the ring, pointing most directly toward H(34) [N(2)-H(2B)...H(34) = 169.2°].

As with the contacts to ring 2, the centroid type interaction to ring 3, N(3)-H(3B)...π(Ph), would be expected to be stronger than the edge type interaction, N(2)-H(2B)...π(Ph), based on the geometry of the two hydrogen bonds. The mean N...C_{ring} and H(N)...C_{ring} distances for the centroid type interaction [3.536[7]Å; 2.698Å] are considerably shorter than the corresponding mean values for the edge type interaction [4.102[8]Å; 3.370Å].

Both ring 2 and ring 3 of the tetraphenylborate anion in guanidinium tetraphenylborate acetonitrile solvate accept a pair of N-H...π(Ph) hydrogen bonds, one of the centroid type geometry and the second of the edge type. In ring 2 the centroid type interaction [N(1)-H(1A)] has slightly shorter mean bond lengths and the edge type interaction [N(2)-H(2A)] has slightly longer mean bond lengths than the corresponding interactions accepted by ring 3 [N(3)-H(3B) centroid type; N(2)-H(2B) edge

type]. Overall, it would appear that both rings accept N-H...π(Ph) hydrogen bonds that are relatively equal in magnitude. It seems that for both rings, the geometry of one hydrogen bond is optimized as much as possible, the centroid type interaction, while the second hydrogen bond takes what is left over, forming the edge type interaction.

The final N-H...π(Ph) hydrogen bond in guanidinium tetraphenylborate acetonitrile solvate is formed between N(3)-H(3A) of the cation and phenyl ring 4 of the anion (Figure 19). It has an off-center, centroid type geometry, with distances all considerably longer than the other two centroid type arrangements to rings 2 and 3. The interaction occurs between N(3)-H(3A) of the original cation and ring 4 of an anion generated by the symmetry (2-*x*, 1-*y*, 1-*z*), the same anion whose ring 3 was found to interact with N(3)-H(3B) and N(2)-H(2B).

In the N(3)-H(3A)...ring 4 hydrogen bond, the N(3)...C_{ring} distances cover a relatively narrow range [minimum C(46) 3.312(3)Å; maximum C(43) 3.649(3)Å; 100Δ = 34] and all of the N(3)...C_{ring} distances are longer than the N(3)...π_c distance of 3.202Å. Also following the same pattern are the H(3A)...C_{ring} distances [minimum C(44) 2.668Å; maximum C(41) 2.940Å; 100Δ = 27] which fall in a narrow range, all longer than the H(3A)...π_c separation of 2.405Å. However, the angle N(3)-H(3A)...π_c of 137.5° is relatively far from linearity. The largest angle formed with a ring carbon atom is N(3)-H(3A)...C(44) which is equal to 161.9°. The N(3)-H(3A) vector actually projects to the outside of ring 4, pointing most directly toward C(44), as shown by the preceding angle. The N(3)-H(3A) vector makes an angle of only 52.5° with the plane of ring 4. It is the least perpendicular interaction of all the N-H...π(Ph) hydrogen bonds in

guanidinium tetraphenylborate acetonitrile solvate.

All of the H(N) hydrogen atoms available for hydrogen bonding in guanidinium tetraphenylborate acetonitrile solvate do form such interactions, five forming N-H...π(Ph) hydrogen bonds with the phenyl rings of the anion and one forming an N-H...N hydrogen bond with the nitrogen atom of the solvent molecule (Figure 15). The hydrogen bonds formed are a compromise of the individual bond strengths to maximize the entire network. Despite this, guanidinium tetraphenylborate acetonitrile solvate still forms N-H...π(Ph) hydrogen bonds with centroid type geometries to all three of the phenyl rings which act as hydrogen bond acceptors in the structure, and three of the five N-H...π(Ph) hydrogen bonds formed are of the centroid type. There are other, longer N-H...π(Ph) contacts possible to many rings but none appear to be of importance relative to the stronger interactions. The hydrogen bonding can be summarized as follows:

	Acceptor	Donor	Description
solvent	N(4)	N(1)-H(1B)	conventional N-H...N
anion	ring 1	none	
	ring 2	N(1)-H(1A)	centroid type "pincer"
		N(2)-H(2A)	edge type
	ring 3	N(3)-H(3B)	centroid type "pincer"
		N(2)-H(2B)	edge type
	ring 4	N(3)-H(3A)	centroid type

Experimentally, the "pincer" or "fork" type interaction of two N-H groups on a single cation to a single phenyl ring is new; it was not included in the classification of N-H...π(Ph) hydrogen bond types

published by Bakshi et al.[83] in 1994. However, this exact geometry was predicted by Duffy et al.[87] (1993) after Monte Carlo statistical mechanics simulations were used to model the interactions between the guanidinium ion and benzene, both in the presence and absence of water. As discussed previously in the introduction, these authors were investigating the mechanism of protein denaturation by small organic molecules (chaotropes).

In gas phase calculations, the isolated $C(NH_2)_3^+/C_6H_6$ dimer was found to have C_{2v} symmetry and a perpendicular interaction geometry. The central carbon atom of the cation was found to lie directly above the benzene ring centroid, with the principal C_2 axis of the dimer passing through both the ring centroid and the cation carbon atom. Two hydrogen atoms, on two different nitrogen atoms, thus point directly down toward the ring plane. Although not explicitly stated by the authors, from a diagram included in the publication it appears that the two N-H vectors are centered above and point down to opposing C-C ring bonds. The guanidinium carbon to ring centroid distance in the isolated gas phase dimer was calculated to be 3.831Å. An interaction energy (for the two hydrogen bonds in the dimer) of -9.63 kcal/mol was also calculated. It was found to be dominated by the electrostatic (as opposed to the van der Waals) contribution, as expected for a charged species.

The geometries of the theoretical and experimental "pincer" type N-H...π(Ph) hydrogen bond pairs are remarkably similar. In the crystal structure of $[C(NH_2)_3][B(C_6H_5)_4]\cdot CH_3CN$ two pairs of such "pincer" type hydrogen bonds were located, N(1)-H(1A) and N(2)-H(2A) to ring 2 and N(2)-H(2B) and N(3)-H(3B) to ring 3. Each set of contacts arises from a pair of adjacent N-H donor groups on a single cation interacting with one

ring of a tetraphenylborate anion. The formation of such "pincer" type interactions, in which two N-H groups interact with a single phenyl ring, is an advantage when trying to fit the larger acceptor around the smaller guanidinium cation, with its six N-H groups all available for hydrogen bond formation.

In $[C(NH_2)_3][B(C_6H_5)_4]\cdot CH_3CN$ the pair of interactions made to ring 2 come from a guanidinium cation whose central carbon atom lies 4.050Å from the ring 2 centroid. The angle made between the plane of ring 2 of the anion and the plane of the cation (both planes defined by their heavy atoms only) is 89.6°, close to perpendicular. In the "pincer" type arrangement made to ring 3 in the same structure, the carbon atom of the guanidinium cation lies 3.998Å from the phenyl ring centroid and the angle made between the cation and the ring 3 planes is 69.8°, much further from perpendicular. Both of the $C_{cation}\cdots\pi_c$ ring centroid distances are slightly longer than the corresponding distance calculated for the isolated gas phase dimer (3.831Å). The experimental "pincer" type interactions are also less perpendicular, by a very small amount in the ring 2 case and by a much larger amount in the ring 3 case.

It is not surprising that the distance and angle calculated for the theoretical, isolated dimer in the gas phase are more "ideal" than those found in the experimental examples. In the theoretical calculations, only one pair of "pincer" type N-H...π(Ph) hydrogen bonds to a single benzene ring were investigated. In reality, a total of three pairs of such interactions could be formed between a single guanidinium cation and three benzene rings, and this would affect the geometry of each individual interaction even in the theoretical calculations. In the experimentally

determined structure, all six N-H groups of the cation are involved in and competing for hydrogen bond formation and, in fact, two pairs of "pincer" type interactions do occur, all of which likely contributes to the less than ideal geometries found for some interactions.

The experimental "pincer" type interactions located are all of general (C_1) symmetry as compared to the C_{2v} symmetry of the theoretical dimer. C_{2v} symmetry, with the two interacting N-H vectors of the cation pointing down towards opposing C-C ring bonds, is no longer possible in the experimental structures where benzene has been replaced by a phenyl ring of the $B(C_6H_5)_4^-$ anion. In the theoretical dimer two equivalent and symmetric N-H...π(Ph) hydrogen bonds are formed in the "pincer" type arrangement. This is not possible in the experimental examples, rather they were always found to involve one centroid type and one edge type N-H...π(Ph) hydrogen bond. It appears that the geometry of one hydrogen bond in each pair is optimized to the favoured centroid type while the second forms an edge type contact, as dictated by the disposition of the two N-H groups involved in the "pincer" type interaction. In the crystal, the formation of these two hydrogen bond types must be favoured over the other possible arrangements for the "pincer" type interactions.

The hydrogen bonding in guanidinium tetraphenylborate acetonitrile solvate can also be considered from the perspective of the cation (Figure 15). Each NH_2 group of the cation forms a pair of hydrogen bonds with the following geometries:

N(1)	H(1A)	centroid	H(1B)	N-H...N
N(2)	H(2A)	edge type	H(2B)	edge type
N(3)	H(3A)	centroid	H(3B)	centroid

It is interesting to note that N(2) forms two hydrogen bonds with less than optimal edge type geometries, while both N(1) and N(3) form stronger pairs of interactions, either involving a pair of centroid type hydrogen bonds, N(3), or one centroid type and one traditional N-H...N hydrogen bond, N(1). It is not clear what factors contribute to this arrangement of hydrogen bond distributions.

It is also interesting to contrast the pattern of hydrogen bonding observed for the H(N) hydrogen atoms of the cation in guanidinium tetraphenylborate acetonitrile solvate with that observed in the monohydrate solvate of the same salt. The conventional spherical refinement of guanidinium tetraphenylborate monohydrate, reported by Bakshi et al.[83] in 1994, was used to investigate the hydrogen bond geometry in the structure. Beginning from the atomic coordinates, available as supplemental material to the original publication, a rather different pattern of hydrogen bonds was found, compared to that described by Bakshi et al. in the original publication.

As in the acetonitrile solvate, the monohydrate structure contains an extensive system of hydrogen bonds, with all available H(N) and H(O) donors participating in the interactions. The network formed is again a compromise of the individual hydrogen bonds to give the maximal overall strength for the total system. In the monohydrate, one H(N) atom of the guanidinium cation forms a "traditional" N(1)-H(N11)...O(1) hydrogen bond with the water solvate, similar to the N-H...N hydrogen bond found between the cation and the solvate in the acetonitrile compound. A phenyl ring (#3) of the tetraphenylborate anion also accepts a pair of N-H...π(Ph) interactions in a "pincer" type arrangement, as had been observed in the

acetonitrile solvate. N(3)-H(N31) was found to form a centroid type interaction with ring 3, while N(2)-H(N21) was also found to interact with ring 3, most likely through a single ring carbon, C(34).

Here, the similarities in hydrogen bonding patterns in the two structures end. While the acetonitrile solvate has two rings that accept double or "pincer" type interactions, only one ring in the monohydrate does so. While three N-H...π(Ph) hydrogen bonds in the acetonitrile solvate would be described as having a centroid type geometry, only one interaction in the monohydrate does [N(3)-H(N31)...ring 3]. The monohydrate has three N-H...π(Ph) hydrogen bonds that closely contact only a single atom of the interacting phenyl ring, N(1)-H(N12)...C(24), N(2)-H(N21)...C(34) and N(3)-H(N32)...C(45), and the last of these is weakly bifurcated, N(3)-H(N32)...O(1). The remaining proton of the cation in the monohydrate, N(2)-H(N22), appears to form a very weak, trifurcated hydrogen bond with three phenyl rings on different anions.

Overall, the N-H...π(Ph) hydrogen bonds formed in the acetonitrile solvate appear, based on the observed geometries, to be stronger than those in the monohydrate. However, in the monohydrate, the solvent water molecule also has two H(O) protons available for hydrogen bonding. The two O-H...π(Ph) hydrogen bonds formed by the water molecule to a single tetraphenylborate anion, O(1)-H(O1)...ring 1 [edge type interaction with C(15)-C(16)] and O(1)-H(O2)...ring 2 [edge type interaction with C(25)-C(26)], strengthen the total hydrogen bonded network. This extra O-H...π(Ph) hydrogen bonding in the monohydrate, not available in the acetonitrile solvate, must compensate for the poorer observed N-H...π(Ph) geometries in the former.

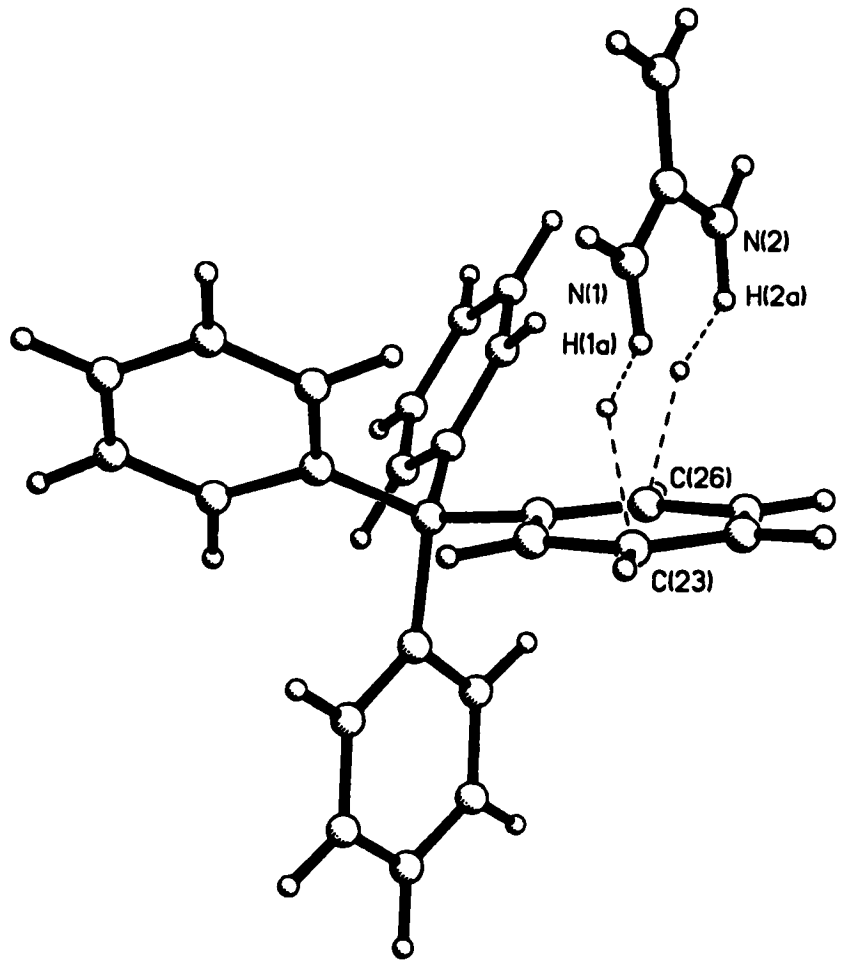

Figure 17. The N-H...π(Ph) hydrogen bonds accepted by phenyl ring #2 in the structure of guanidinium tetraphenylborate acetonitrile solvate. The small open circles represent the locations of the bond critical points of the interactions. The diagram highlights the fork or "pincer" type arrangement of two N-H...π(Ph) hydrogen bonds made to one face of the phenyl ring.

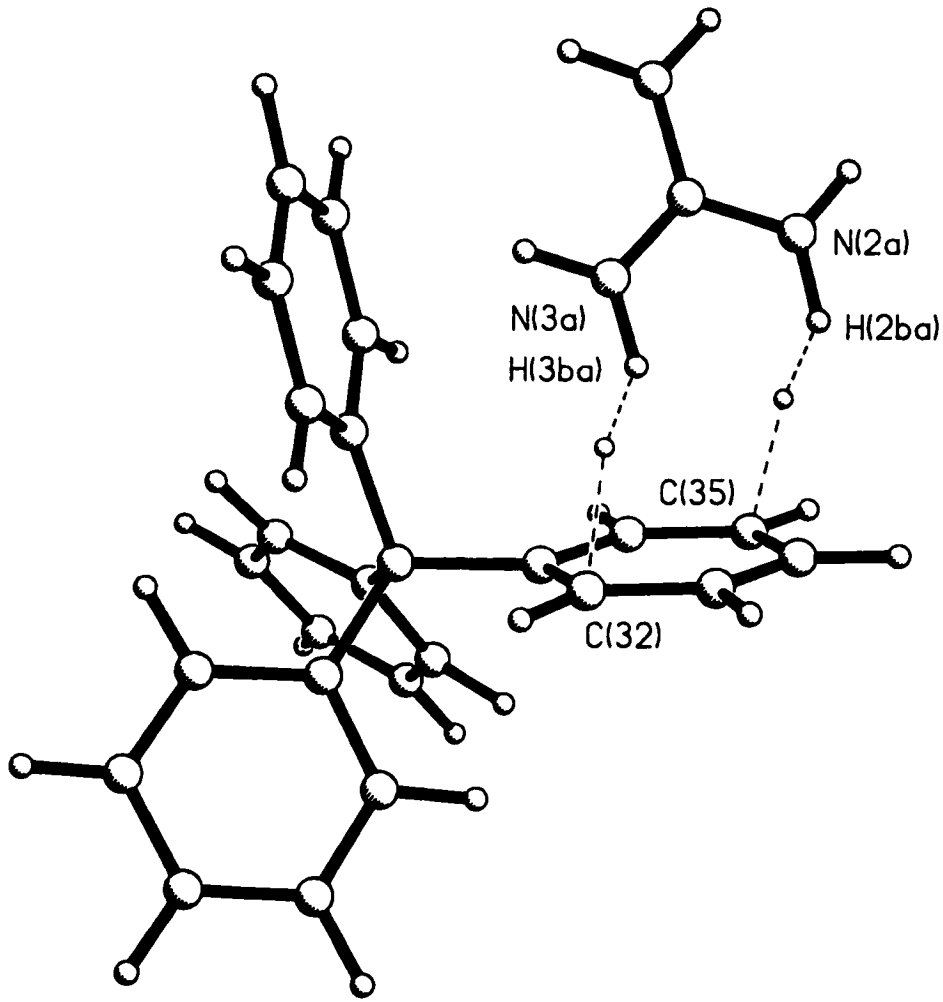

Figure 18. The N-H...π(Ph) hydrogen bonds accepted by phenyl ring #3 in the structure of guanidinium tetraphenylborate acetonitrile solvate. The small open circles represent the locations of the bond critical points of the interactions.

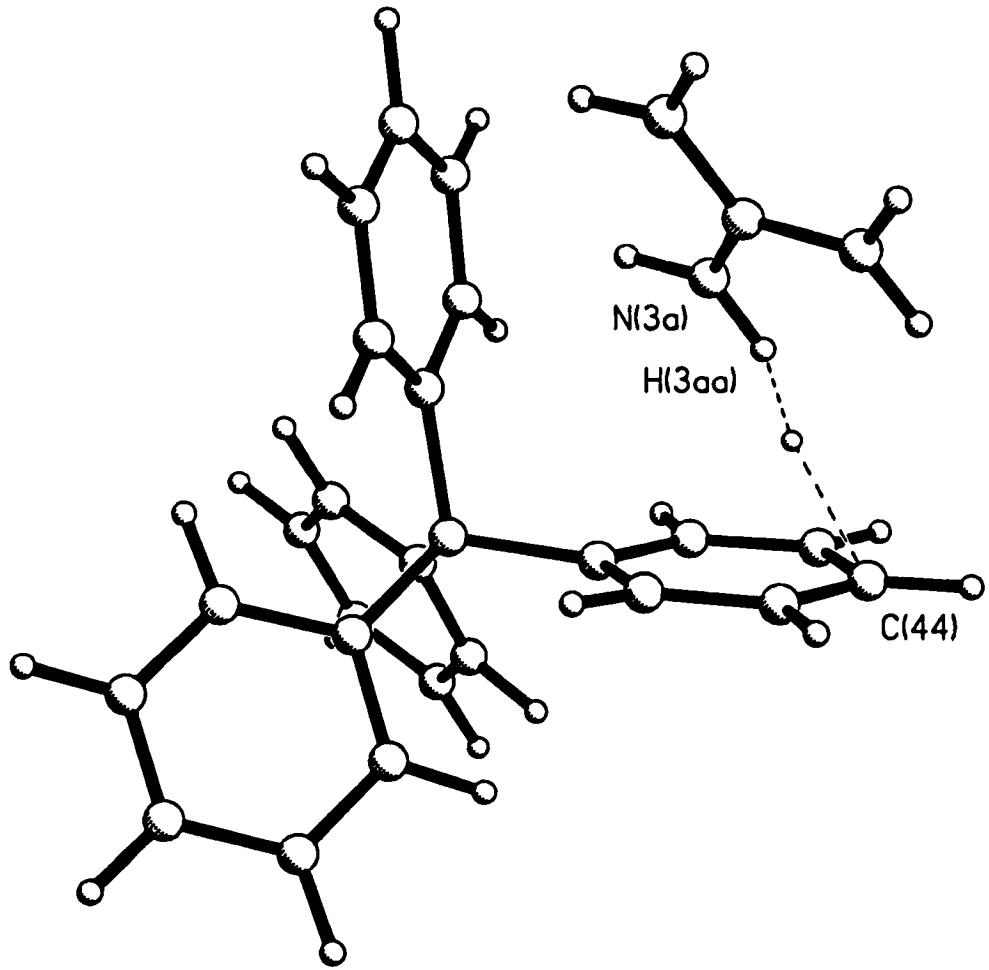

Figure 19. The N-H...π(Ph) hydrogen bond accepted by phenyl ring #4 in the structure of guanidinium tetraphenylborate acetonitrile solvate. The small open circle represents the location of the bond critical point of the interaction.

Table 10. Intermolecular contacts for guanidinium tetraphenylborate acetonitrile solvate.

Part 1 Hydrogen bonded contacts N-H...N (cation/solvent)			
contact	N...N (Å)	H...N (Å)	N-H...N (°)
N(1)-H(1B)...N(4) acetonitrile symmetry (x, y, z)			
N(4)	2.933(4)	2.082	143.4

Part 2 Hydrogen bonded contacts N-H...π (cation/anion)			
contact	N...C (Å)	H...C (Å)	N-H...C (°)
N(1)-H(1A)...ring 2 symmetry (x, y, z)			
C(21)	3.605(3)	2.801	139.1
C(22)	3.443(3)	2.603	143.1
C(23)	3.354(3)	2.458	151.0
C(24)	3.418(4)	2.497	155.4
C(25)	3.572(4)	2.677	151.1
C(26)	3.649(3)	2.806	143.9
mean	**3.507[8]**	**2.640**	**147.3**
centroid[a]	3.214	2.238	170.1
plane[b]	3.192	2.211	84.6
N(2)-H(2A)...ring 2 symmetry (x, y, z)			
C(21)	4.200(3)	3.475	132.1
C(22)	4.726(3)	4.107	123.7
C(23)	4.736(4)	4.122	123.3
C(24)	4.207(4)	3.487	131.6
C(25)	3.597(3)	2.689	153.1
C(26)	3.585(3)	2.672	154.1
mean	**4.175[8]**	**3.425**	**136.3**
centroid[a]	3.959	3.178	137.2
plane[b]	3.429	2.444	86.9

Table 10. Intermolecular contacts for guanidinium tetraphenylborate acetonitrile solvate (continued).

Part 2 Hydrogen bonded contacts N-H...π (cation/anion)			
contact	N...C (Å)	H...C (Å)	N-H...C (°)
N(2)-H(2B)...ring 3	symmetry (2-x, 1-y, 1-z)		
C(31)	4.628(3)	4.079	118.3
C(32)	4.679(3)	4.038	125.4
C(33)	4.239(3)	3.436	140.0
C(34)	3.613(3)	2.668	160.7
C(35)	3.460(4)	2.622	143.0
C(36)	3.993(3)	3.380	122.1
mean	**4.102[8]**	**3.370**	**134.9**
centroid[c]	3.883	3.119	135.3
plane[d]	3.380	2.441	72.3
N(3)-H(3B)...ring 3	symmetry (2-x, 1-y, 1-z)		
C(31)	3.406(3)	2.655	133.2
C(32)	3.398(3)	2.498	151.6
C(33)	3.563(3)	2.592	168.4
C(34)	3.702(3)	2.791	153.9
C(35)	3.655(3)	2.868	137.4
C(36)	3.492(3)	2.783	129.3
mean	**3.536[7]**	**2.698**	**145.6**
centroid[c]	3.248	2.308	159.1
plane[d]	3.222	2.282	72.5

Table 10. Intermolecular contacts for guanidinium tetraphenylborate acetonitrile solvate (continued).

Part 2 Hydrogen bonded contacts N-H...π (cation/anion)			
contact	N...C (Å)	H...C (Å)	N-H...C (°)
N(3)-H(3A)...ring 4	symmetry (2-x, 1-y, 1-z)		
C(41)	3.405(3)	2.940	110.0
C(42)	3.538(3)	2.845	128.0
C(43)	3.649(3)	2.723	156.7
C(44)	3.618(3)	2.668	161.9
C(45)	3.440(3)	2.705	131.7
C(46)	3.312(3)	2.816	111.9
mean	**3.494[7]**	**2.783**	**133.4**
centroid[e]	3.202	2.405	137.5
plane[f]	3.175	2.392	52.5

[a] The position of the centroid of ring 2 is (0.8786, 0.8300, 0.2694). The values listed are *d*(N/C...centroid), *d*(H...centroid) and the angle N/C-H...centroid.

[b] The mean deviation of the carbon atoms from the ring 2 plane is 0.0066Å. The values listed are *d*(N/C...plane), *d*(H...plane) and the angle the N/C-H vector makes with the plane of the ring.

[c] The position of the centroid of ring 3 is (1.3136, 0.7167, 0.6643). The values listed are *d*(N...centroid), *d*(H...centroid) and the angle N-H...centroid.

[d] The mean deviation of the carbon atoms from the ring 3 plane is 0.0065Å. The values listed are *d*(N...plane), *d*(H...plane) and the angle the N-H vector makes with the plane of the ring.

[e] The position of the centroid of ring 4 is (1.2244, 0.5533, 0.1933). The values listed are *d*(N...centroid), *d*(H...centroid) and the angle N-H...centroid.

[f] The mean deviation of the carbon atoms from the ring 4 plane is 0.0041Å. The values listed are *d*(N...plane), *d*(H...plane) and the angle the N-H vector makes with the plane of the ring.

Table 11. Bond critical points for the intermolecular contacts in guanidinium tetraphenylborate acetonitrile solvate.

Hydrogen bonded contacts N-H...N (cation/solvent)									
Contact	Hessian Eigenvalues			Charge Density	Laplacian	Ellipticity	Position		
Bond Path	λ_1	λ_2	λ_3	$\rho_b(\mathbf{r})$ (eÅ^{-3})	$\nabla^2\rho_b(\mathbf{r})$ (eÅ^{-5})	ε	x	y (fractional)	z
N(4)...H(1B)-N(1) symmetry (x, y, z)									
N(4)...H(1B)	-0.77,	-0.72,	3.13	0.200(54)	1.637(4)	0.07	0.7820,	0.7108,	0.6268

Bond Lengths and Angles at the Critical Point			
Atoms	Distance (Å)	Atoms	Angle (°)
Cp...N(1)	1.697	N(1)...Cp...N(4)	161.2
Cp...H(1B)	0.807	H(1B)...Cp...N(4)	177.5
Cp...N(4)	1.275	N(1)-H(1)...Cp	142.0

Table 11. Bond critical points for the intermolecular contacts in guanidinium tetraphenylborate acetonitrile solvate (continued).

Contact	Hessian Eigenvalues			Charge Density	Laplacian	Ellipticity	Position		
Bond Path	λ_1	λ_2	λ_3	$\rho_b(\mathbf{r})$ ($eÅ^{-3}$)	$\nabla^2\rho_b(\mathbf{r})$ ($eÅ^{-5}$)	ε	x	y (fractional)	z
Hydrogen bonded contacts N-H...π (cation/anion)									
ring 2...H(1A)-N(1)*	symmetry (x, y, z)			centroid type hydrogen bond					
C(22)-C(23)...H(1A)	-0.31,	-0.02,	1.04	0.073(34)	0.706(11)	16.61	0.8224,	0.7766,	0.4217

Bond Lengths and Angles at the Critical Point

Atoms	Distance (Å)	Atoms	Angle (°)
Cp...N(1)	1.738	N(1)...Cp...C(23)	159.7
Cp...H(1A)	0.908	H(1A)...Cp...C(23)	143.3
Cp...C(23)	1.669	N(1)...Cp...C(22)	152.1
Cp...C(22)	1.809	H(1A)...Cp...C(22)	144.5
		N(1)-H(1A)...Cp	133.1
Cp...plane	1.535		
Cp...centroid	1.754		

* The bond path from H(1A) follows the C(22)-C(23) bond of the ring for approximately one third of its length before terminating at C(23).

Table 11. Bond critical points for the intermolecular contacts in guanidinium tetraphenylborate acetonitrile solvate (continued).

Contact	Hessian Eigenvalues			Charge Density	Laplacian	Ellipticity	Position		
Bond Path	λ_1	λ_2	λ_3	$\rho_b(\mathbf{r})$ (eÅ^{-3})	$\nabla^2\rho_b(\mathbf{r})$ (eÅ^{-5})	ε	x	y (fractional)	z
Hydrogen bonded contacts N-H...π (cation/anion)									
ring 2...H(2A)-N(2)*	symmetry (x, y, z)			edge type hydrogen bond					
C(25)-C(26)...H(2A)	-0.14,-0.01, 0.63			0.055(20)	0.474(12)	11.01	0.8208,	0.6768,	0.2220

Bond Lengths and Angles at the Critical Point

Atoms	Distance (Å)	Atoms	Angle (°)
Cp...N(2)	1.895	N(2)...Cp...C(26)	166.5
Cp...H(2A)	1.056	H(2A)...Cp...C(26)	148.4
Cp...C(26)	1.715	N(2)...Cp...C(25)	139.9
Cp...C(25)	1.934	H(2A)...Cp...C(25)	125.6
		N(2)-H(2A)...Cp	136.2
Cp...plane	1.648		
Cp...centroid	2.169		

* The bond path from H(2A) follows the C(25)-C(26) bond of the ring for approximately one quarter of its length before terminating at C(26).

Table 11. Bond critical points for the intermolecular contacts in guanidinium tetraphenylborate acetonitrile solvate (continued).

Hydrogen bonded contacts N-H...π (cation/anion)									
Contact	Hessian Eigenvalues			Charge Density	Laplacian	Ellipticity	Position		
Bond Path	λ_1	λ_2	λ_3	$\rho_b(\mathbf{r})$ ($e\text{Å}^{-3}$)	$\nabla^2\rho_b(\mathbf{r})$ ($e\text{Å}^{-5}$)	ε	x	y (fractional)	z
ring 3...H(2B)-N(2)* symmetry (2-x, 1-y, 1-z) edge type hydrogen bond									
C(35)...H(2B)	-0.22,	-0.14,	1.04	0.087(23)	0.677(12)	0.57	1.2693,	0.5757,	0.7736

Bond Lengths and Angles at the Critical Point			
Atoms	Distance (Å)	Atoms	Angle (°)
Cp...N(2)	1.850	N(2)...Cp...C(35)	167.6
Cp...H(2B)	0.999	H(2B)...Cp...C(35)	170.6
Cp...C(35)	1.631	N(2)-H(2B)...Cp	137.4
Cp...C(34)	1.929		
Cp...plane	1.552		
Cp...centroid	2.251		

* Surprisingly, a single atom type bond path is observed, from H(2B) to C(35).

Table 11. Bond critical points for the intermolecular contacts in guanidinium tetraphenylborate acetonitrile solvate (continued).

Hydrogen bonded contacts N-H...π (cation/anion)									
Contact	Hessian Eigenvalues			Charge Density	Laplacian	Ellipticity	Position		
Bond Path	λ_1	λ_2	λ_3	$\rho_b(\mathbf{r})$ ($e\text{Å}^{-3}$)	$\nabla^2\rho_b(\mathbf{r})$ ($e\text{Å}^{-5}$)	ε	x	y (fractional)	z
ring 3...H(3B)-N(3)* symmetry (2-x, 1-y, 1-z) centroid type hydrogen bond									
C(32)...H(3B)	-0.22,	-0.08,	1.19	0.102(29)	0.885(11)	1.75	1.3498,	0.6293,	0.5593

Bond Lengths and Angles at the Critical Point			
Atoms	Distance (Å)	Atoms	Angle (°)
Cp...N(3)	1.834	N(3)...Cp...C(32)	166.5
Cp...H(3B)	0.949	H(3B)...Cp...C(32)	159.1
Cp...C(32)	1.588	N(3)-H(3B)...Cp	142.7
Cp...plane	1.433		
Cp...centroid	1.609		

* Single atom type bond path from H(3B) to C(32).

Table 11. Bond critical points for the intermolecular contacts in guanidinium tetraphenylborate acetonitrile solvate (continued).

Contact	Hydrogen bonded contacts N-H...π (cation/anion)								
	Hessian Eigenvalues			Charge Density	Laplacian	Ellipticity	Position		
Bond Path	λ_1	λ_2	λ_3	$\rho_b(\mathbf{r})$ ($eÅ^{-3}$)	$\nabla^2\rho_b(\mathbf{r})$ ($eÅ^{-5}$)	ε	x	y (fractional)	z
ring 4...H(3A)-N(3)*	symmetry (2-x, 1-y, 1-z)				centroid type hydrogen bond				
C(43)-C(44)...H(3A)	-0.17,	-0.06,	0.87	0.081(28)	0.638(14)	1.80	1.2934,	0.4823,	0.3182

Bond Lengths and Angles at the Critical Point

Atoms	Distance (Å)	Atoms	Angle (°)
Cp...N(3)	1.944	N(3)...Cp...C(44)	172.2
Cp...H(3A)	0.997	H(3A)...Cp...C(44)	169.2
Cp...C(44)	1.683	N(3)...Cp...C(43)	142.7
Cp...C(43)	1.907	H(3A)...Cp...C(43)	137.1
		N(3)-H(3A)...Cp	157.4
Cp...plane	1.452		
Cp...centroid	1.564		

* The bond path from H(3A) follows the C(43)-C(44) bond of the ring for approximately one quarter of its length before terminating at C(44).

3.2.4. Crystallographic Investigations of Hydrogen Bonding in Monoprotonated Biguanidinium Tetraphenylborate

The multipole refinement of the structure of monoprotonated biguanidinium tetraphenylborate (Figure 20) was carried out at 128K using Mo Kα radiation. A total of 21493 reflections were collected of which 12658 were unique and 7376 were observed [$I>3\sigma(I)$]. A total of 822 parameters were refined for a reflection to parameter ratio of 9 to 1. Upon completion of the multipole refinement, the final residuals R and R_w were 5.25% and 4.13%, respectively.

The conventional, spherical refinement of biguanidinium tetraphenylborate has not previously been reported in the literature. Therefore, direct comparison of the multipole results is not possible. However, A. Martin et al.[115-117] have published a series of papers on the crystal structure determinations of energetic materials containing the monoprotonated biguanidinium cation. The geometry of the biguanidinium cation can be compared between the structures.

The results of the multipole refinement showed biguanidinium tetraphenylborate to crystallize in the monoclinic space group $P2_1/c$, cell choice 2, unique axis *b*, with the origin at $\bar{1}$, or more simply $P2_1/n$. The unit cell dimensions, a = 10.181(2)Å, b = 14.232(2)Å, c = 16.250(2)Å and β = 104.34(1)°, result in a cell of volume 2281.2(6)Å^3. As all atoms in the structure occupy general positions, neither the cation nor the anion possess internal symmetry.

The tetraphenylborate anion in the biguanidinium salt (C_1) was found to have a geometry very similar to those observed in the previous three structures, NH_4^+ (D_{2d}), DabcoH$^+$ (C_s), and $C(NH_2)_3^+$ (C_1), despite their disparate site symmetries. The mean B-C bond length in the anion was

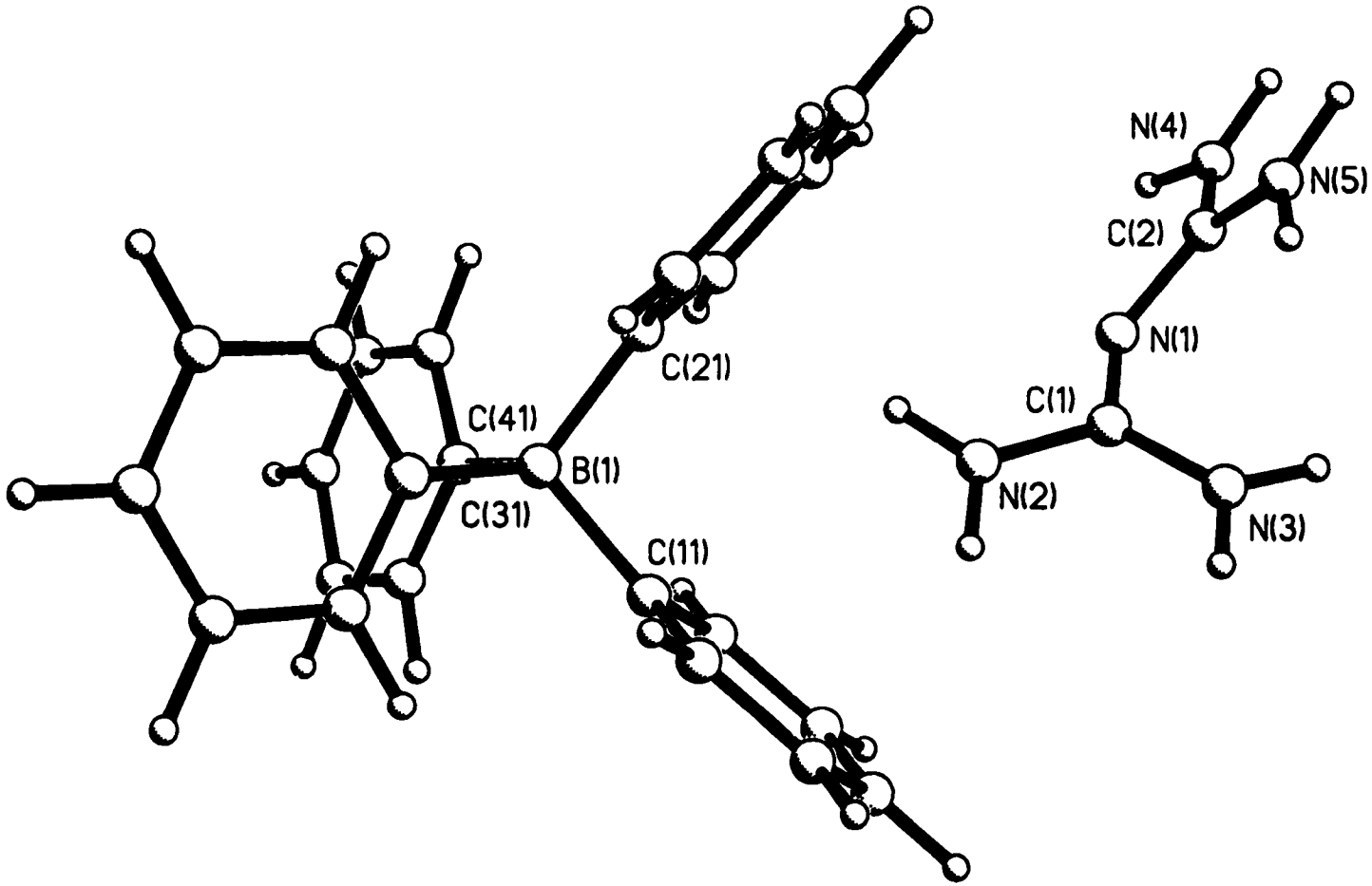

Figure 20. The structure of biguanidinium tetraphenylborate.

calculated to be 1.641Å, close to the mean values in the first three structures. The two smaller bond angles at boron, C(11)-B(1)-C(21) = 102.5(1)° and C(31)-B(1)-B(41) = 103.9(1)°, gave a mean value of 103.2°, while the four larger angles ranged from 111.2(1)° [C(11)-B(1)-C(41)] to 114.6(1)° [C(21)-B(1)-C(41)] with a mean of 112.7°. Again, these values are very similar to the means calculated for the anions of the previous structures. The internal angles at the α carbons of the four phenyl rings in the tetraphenylborate anion, C(x6)-C(x1)-C(x2), were calculated to have a mean of 115.6°, virtually identical to the means in all three of the other structures. Although the anion in biguanidinium tetraphenylborate has no internal symmetry, its geometry approximates the higher symmetries observed in the NH_4^+ and DabcoH$^+$ salts, just as the anion in guanidinium tetraphenylborate acetonitrile solvate had been found to.

As already mentioned, the geometry of the cation in biguanidinium tetraphenylborate can be compared with the results from conventional, spherical structure determinations reported by Martin et al. for a series of monoprotonated biguanidinium salts, including the perchlorate[115], the nitrate[116] and the dinitramide, $[N(NO_2)_2]^-$.[117] These compounds were being studied as potential energetic materials for use as explosives and/or propellants, their utility deriving from their rapid thermal decomposition into all gaseous products.

All of the structures were found to share several important features, centered about the biguanidinium cations and their common geometries. In all of the aforementioned biguanidinium salts, the cation consists of two planar halves, with the central nitrogen atom common to the two halves. In the tetraphenylborate salt, the two essentially planar

halves of the cation have mean deviations from their best planes (non-hydrogen atoms only) of 0.0057Å [N(1)-C(1)-N(2),N(3)] and 0.0106Å [N(1)-C(2)-N(4),N(5)], respectively.

The two halves of the biguanidinium cation are twisted relative to each other because of H...H intranuclear repulsion between terminal NH_2 groups on the two different carbon centers. The twist angle, or the angle between the two planes in the cation, was calculated to be 36.3° in the tetraphenylborate salt. This is intermediate between the values reported by Martin et al. for the dinitramide (34.2°)[117] and the nitrate (37.8°)[116] compounds. Martin et al.[117] quote a range of 34.2° to 49.1° for the twist angle in biguanidinium cations reported in the literature, so the tetraphenylborate result falls at the low end of the range. Torsion angles of 133.9° [C(2)-N(1)-C(1)-N(2)], -48.4° [C(2)-N(1)-C(1)-N(3)], 172.6° [C(1)-N(1)-C(2)-N(4)] and -11.7° [C(1)-N(1)-C(2)-N(5)] were calculated for the biguanidinium cation in the tetraphenylborate salt.

All of the bond lengths in the biguanidinium cations are short, owing to extensive π delocalization which produces bond orders greater than one. In the paper on the structure determination of monoprotonated biguanidinium perchlorate, Martin et al.[115] note that the C-N bridging bonds (mean 1.338Å) in the cation are slightly longer than the C-N terminal bonds (mean 1.333Å) and this same trend was observed in the nitrate (1.337Å vs. 1.327Å)[116] and dinitramide (1.333Å vs. 1.329Å)[117] salts. However, in the multipole refinement of biguanidinium tetraphenylborate the mean C-N bridging bond length (1.337Å) is not longer than the mean C-N terminal bond length (1.338Å) in the cation. Rather, there is an alternation of bond lengths observed in the cation [N-C(1) terminal bonds

are short, the C(1)-N(1) bridging bond is longer, the N(1)-C(2) bridging bond is shorter and the C(2)-N terminal bonds are long], which results in an interesting disparity in the bond lengths in the two halves of the cation. While the C-N bridging bond C(1)-N(1), 1.350(2)Å, is longer than C(2)-N(1), 1.325(2)Å, the two terminal C(1)-N bonds are shorter [C(1)-N(2) = 1.321(2)Å and C(1)-N(3) = 1.336(2)Å] than the terminal C(2)-N bonds [C(2)-N(4) = 1.349(2)Å and C(2)-N(5) = 1.347(2)Å]. A possible explanation for this disparity in bond lengths might be found in the hydrogen bonds formed by the cation (to be discussed later). Stronger hydrogen bonds are formed involving the N(1)-C(2)-N(4),N(5) half of the cation, relative to the N(1)-C(1)-N(2),N(3) half. In addition, the N(1)-C(2)-N(4),N(5) half of the cation is directly involved in the formation of a hydrogen bonded dimer (also to be discussed subsequently) while the other half is not. Perhaps this has an effect on the bond lengths in the two halves of the cation.

The C(1)-N(1)-C(2) bond angle in the cation of biguanidinium tetraphenylborate is 121.5(2)°. This is slightly smaller than the angles reported by Martin et al. in the dinitramide (122.9°)[117] and nitrate (123.4°)[116] salts but very similar to the angles found in the two unique cations of the perchlorate salt (121.2° and 121.3°)[115]. The angles about the central carbon atoms, C(1) and C(2), in the cation of the tetraphenylborate salt show similar distributions. There are two smaller angles of approximately equal size, mean 117.8°, and one larger angle of mean 124.2°. In the Martin papers, these angles have similar mean values of 117° (2 angles) and 125° (1 angle) overall in the three structures. The large angle always involves the bridging nitrogen atom, C(x) and the

terminal nitrogen atom that is located *cis* to the other half of the cation. In the tetraphenylborate salt, the two large angles are N(1)-C(1)-N(3) = 123.1(2)° and N(1)-C(2)-N(5) = 125.3°. This presumably maximizes the separation between the two halves of the cation.

The biguanidinium cations in the three structures reported by Martin et al.[115-117] were all characterized by their participation in extensive hydrogen bonded networks. In all of the structures, each of the H(N) protons of the cation was found to form at least one hydrogen bond, usually of less than 2.5Å [d(H...A)]. The hydrogen bonds in these structures were always to "traditional" acceptors, lone pairs on nitrogen or oxygen, usually in the anion. In contrast, all the H(N) atoms of biguanidinium tetraphenylborate were also found to form hydrogen bonds, but these tended to be longer since in the majority of cases the only available acceptors were the π electrons of the phenyl rings in the anion.

The most striking feature of the cation in biguanidinium tetraphenylborate, and in the salts studied by Martin et al., is that it forms a hydrogen bonded dimer to its symmetry related partner across an inversion center (Figure 21). This dimer is held together by a pair of symmetry related hydrogen bonds between a terminal H(N) donor of one cation and the bridging nitrogen atom acceptor on the other cation, and vice versa. These traditional hydrogen bonds tend always to be among the shortest (strongest) and most linear in the entire structure. The results from the multipole refinement of biguanidinium tetraphenylborate are contrasted below with the very similar results of Martin et al. for the dimer forming hydrogen bonds in the salts they examined.

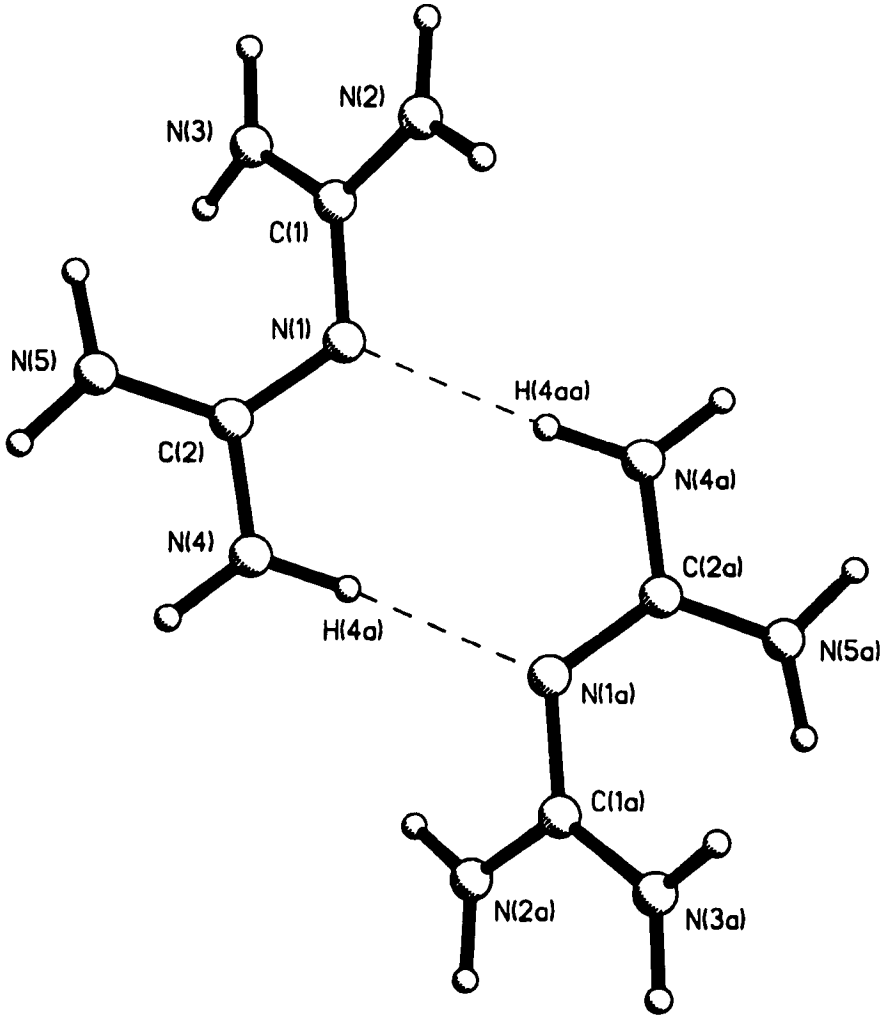

Figure 21. The cation dimer formed in the structure of biguanidinium tetraphenylborate. It is held together by a pair of equivalent N-H...N (cation/cation) hydrogen bonds.

Anion	Hydrogen Bond	N-H(Å)	H...N(Å)	N-H...N(°)
$[B(C_6H_5)_4]^-$	N(4)-H(4A)...N(1)	0.986	2.127	175.1
dinitramide[117]	N(8)-H(8)...N(6)	0.92(3)	2.10(3)	176(2)
nitrate[116]	N(1)-H(1B)...N(3)	0.86(2)	2.14(2)	173(2)
perchlorate[115, *]	N(4)-H(6)...N(3)	0.95	1.98	177

* The structure of monoprotonated biguanidinium perchlorate was found to contain two unique cations and two unique anions in its asymmetric unit. Only one of the cations forms the characteristic hydrogen bonded dimer. One of the anions is disordered and this, in turn, caused problems for the location and refinement of the hydrogen atoms in the structure. They were placed geometrically rather than refined, which could account for the slight differences in the hydrogen bond geometry noted for the cation dimer in the perchlorate salt relative to the other three compounds.

Monoprotonated biguanidinium tetraphenylborate is one further step up the sequence begun with the multipole refinements of the ammonium, NH_4^+, and guanidinium, $C(NH_2)_3^+$, salts. The biguanidinium cation, $[N(C[NH_2]_2)_2]^+$, with its two planar halves twisted relative to one another, is larger and less planar than the guanidinium cation. This allows it to pack more efficiently with the bulky tetraphenylborate anion and no solvent is included in the structure, as had been observed in guanidinium tetraphenylborate ($\cdot CH_3CN$ or $\cdot H_2O$). The packing diagrams of biguanidinium tetraphenylborate are shown in Figure 22 (a),(b),(c). The packing cannot be described by any simple aristotype.

In the monoprotonated biguanidinium tetraphenylborate salt, the

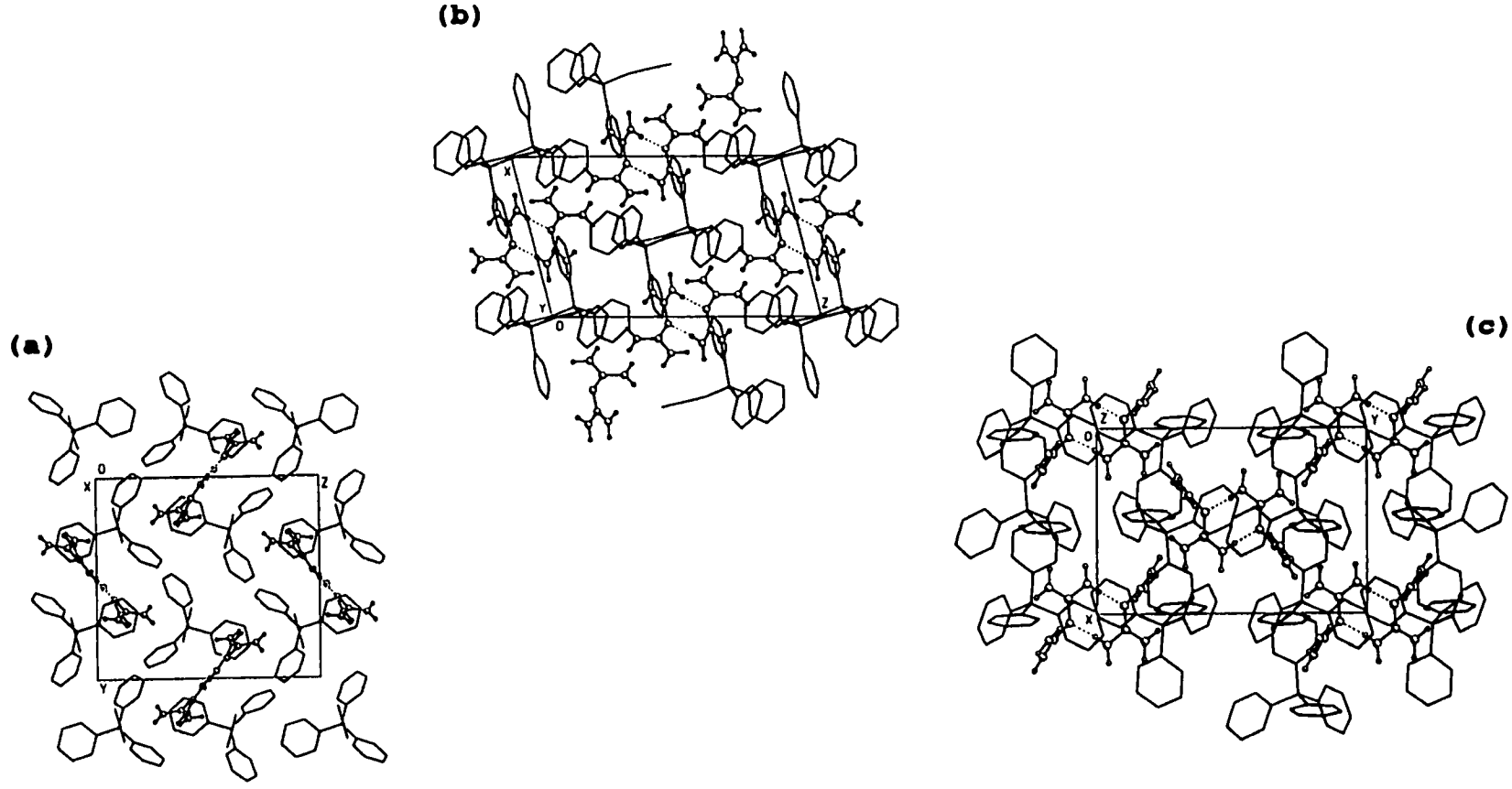

Figure 22. Biguanidinium tetraphenylborate: (a) projection on (100), (b) projection on (010) and (c) projection on (001). Hydrogen atoms have been removed from the anion for clarity.

hydrogen bonded cation dimer lies in a cavity formed by eight anions, with four anions surrounding each cation. (Only six of the eight anions hydrogen bond directly with the two cations of the dimer.) The anions form a parallelogram around the cation dimer in the cavity if the boron atoms of the anion are joined, with the parallelogram oriented along the *x* axis. Four anions in one layer (boron atoms at general *x* positions [*x*, *y*, *z*]) are repeated identically in a layer above it [*x*+1, *y*, *z*]; *y* and *z* coordinates are common in both layers for each pair of boron atoms marking the corners of the parallelogram. The entire arrangement is centrosymmetric about the inversion center at the midpoint of the cation dimer, as illustrated in Figure 23.

The cation dimers in the monoclinic unit cell of biguanidinium tetraphenylborate, symmetry $P2_1/n$, are found about the pair of related inversion centers located at (½, ½, 0) and (0, 0, ½). Thus, the cation dimers are centered at the midpoints of the *ab* faces of the cell and at the midpoints of the *c* axes/edges of the cell, respectively. This means that the cations are distributed only about the exterior regions of the cell, along the cell edges and faces; there are no cations in the central, interior region of the cell. At the very center of the cell, a pair of anions are centrosymmetrically related by the (½, ½, ½) inversion center and form relatively close contacts. In fact, a number of close anion/anion contacts were identified in biguanidinium tetraphenylborate, more than had been observed in the previous three structures.

In the multipole refinement of biguanidinium tetraphenylborate the H(N) hydrogen atoms were refined as described in the experimental section; the N-H bond lengths were then normalized to the neutron derived value of

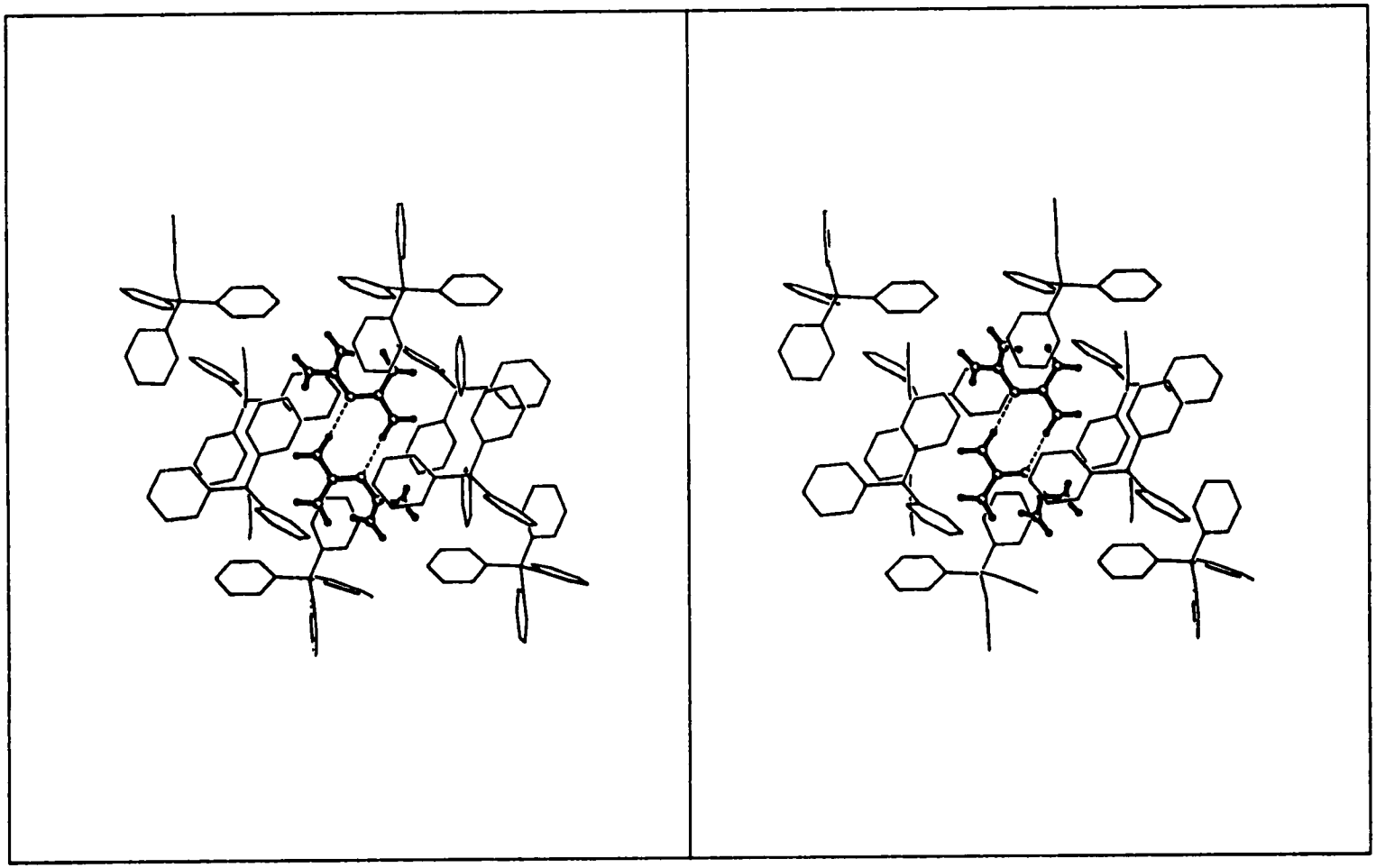

Figure 23. Orientation of the biguanidinium cation dimer within a cavity formed by the arrangement of the anions in the structure of biguanidinium tetraphenylborate. A stereo view is shown in the diagram.

0.986Å. The most appropriate N-H bond length to use was determined from a search of the Cambridge Structural Database[100] for neutron structures containing similar N-H bonds, as described previously. The cation of biguanidinium tetraphenylborate contains eight H(N) atoms all of which were found to form hydrogen bonds in the crystal structure. One hydrogen bond, the "traditional" N(4)-H(4A)...N(1) interaction which holds the cation dimer together has already been discussed (Figure 21). As expected, it is a short, strong and essentially linear hydrogen bond. Because there are no other traditional hydrogen bond acceptors available in the structure, the remaining seven H(N) atoms of the cation form N-H...π(Ph) hydrogen bonds of varying geometries (Figure 24).

In the case of biguanidinium tetraphenylborate, it is instructive to consider the hydrogen bonds formed to each individual anion phenyl ring in turn. Anion ring 1 (C(11) to C(16)) serves as the acceptor to a total of three N-H...π(Ph) hydrogen bonds donated by H(N) atoms of the cation (Figure 25 - at the end of this section). Interestingly, N(4)-H(4B)...ring 1 and N(5)-H(5B)...ring 1 form the now familiar "pincer" or "fork" type pair of interactions, previously observed in guanidinium tetraphenylborate acetonitrile solvate, to one face of ring 1. N(4) and N(5) are terminal nitrogen atoms in the same half of the biguanidinium cation, similar to a guanidinium group, and the nearly parallel N(4)-H(4B) and N(5)-H(5B) bonds are oriented such that the interactions are possible. There is a third hydrogen bond to the second face of ring 1, involving N(2)-H(2B) from a second biguanidinium cation.

The N(5)-H(5B)...ring 1 hydrogen bond occurs between the original cation and anion and has a geometry best described as being of the

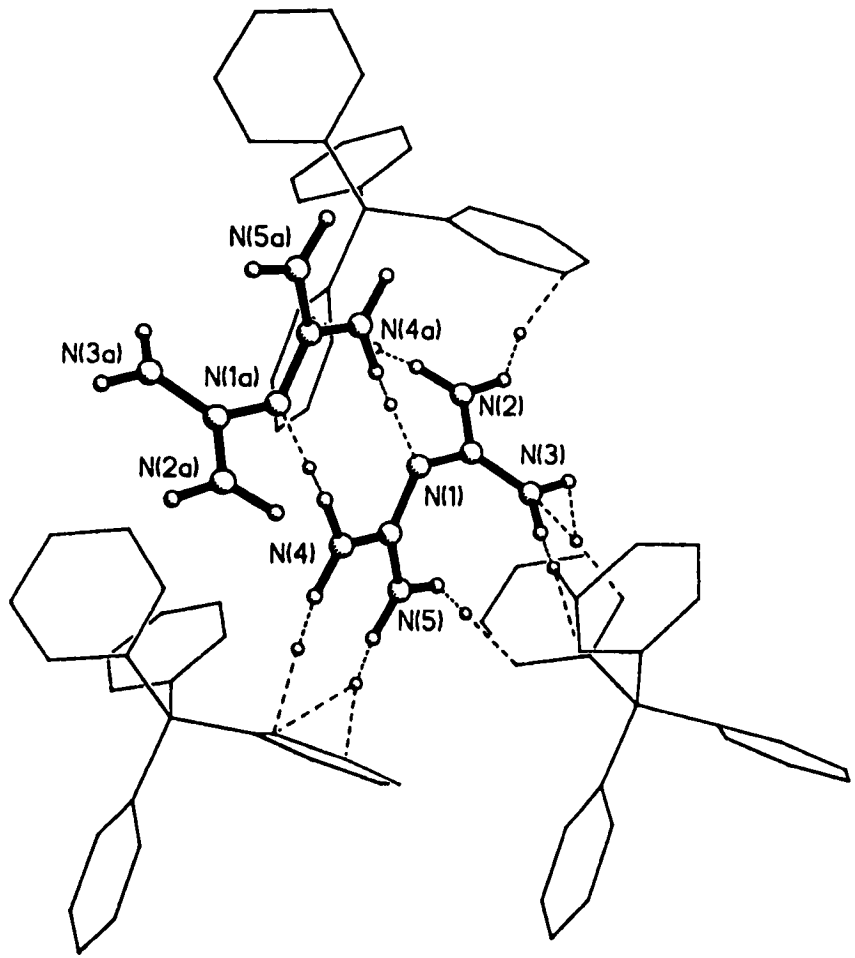

Figure 24. The N-H...X [X = N or π(Ph)] hydrogen bonds formed in the structure of biguanidinium tetraphenylborate, drawn to emphasize the role of the cation as the donor of all the interactions. The small open circles represent the locations of the bond critical points of the interactions.

centroid type. The N(5)...C_{ring} distances cover a relatively narrow range of values, from a minimum of 3.460(2)Å [C(15)] to a maximum of 3.646(2)Å [C(11); 100Δ = 19]. The distance from N(5) to the centroid of ring 1, π_c, is shorter than any of the individual N(5)...C_{ring} distances, 3.268Å. The H(5B)...C_{ring} distances also cover a narrow range, with the minimum value to C(15), 2.560Å, and the maximum value to C(12), 2.806Å [100Δ = 25]. The H(5B)...π_c distance of 2.299Å is again shorter than any of the individual H(5B)...C_{ring} distances. The N(5)-H(5B)...π_c angle of 167.3° is closer to linearity than any of the individual N(5)-H(5B)...C_{ring} angles. The N(5)-H(5B) vector projects inside the ring, very close to the ring centroid, as expected from the N(5)-H(5B)...π_c angle. The N(5)-H(5B) vector makes an angle of 81.2° with the plane of ring 1, relatively close to perpendicular. Clearly, the N(5)-H(5B)...ring 1 hydrogen bond has a close to "ideal" centroid type geometry.

N(4)-H(4B) of the same biguanidinium cation as N(5)-H(5B) also interacts with the same face of ring 1, in the "pincer" type arrangement. N(4) makes close contact with two carbon atoms from ring 1, C(15) [3.714(2)Å] and C(16) [3.583(2)Å]; all other N(4)...C_{ring} distances are greater than 4Å with a maximum of 5.041(2)Å to C(13) [100Δ = 146]. The N(4)...π_c distance, 4.145Å, is also longer than the minimum values to the closest carbon atoms of ring 1. The corresponding H(4B)...C(15), 2.901Å, and H(4B)...C(16), 2.661Å, distances are considerably shorter than any other of the H(4B)...C_{ring} values, which are all longer than 3.5Å [maximum C(13) 4.454Å; 100Δ = 179]. The H(4B)...π_c distance of 3.394Å is longer than either the H(4B)...C(15) or the H(4B)...C(16) distance. The N(4)-H(4B)...π_c angle of 134.5° is far from linearity; the best angle is made with C(16),

155.7°, while the N(4)-H(4B)...C(15) angle is 140.4°. The N(4)-H(4B) vector projects well outside the confines of ring 1, below the C(15)-C(16) bond, slightly toward C(16). In fact, the closest contact with the ring is to H(16), with the distance H(4B)...H(16) equal to 2.510Å and the N(4)-H(4B)...H(16) angle equal to 169.4°. The N(4)-H(4B) vector makes an angle of 81.8° with the ring plane, nearly identical to the angle between N(5)-H(5B) and the plane of ring 1 (81.2°). This is not surprising since the two bonds are nearly parallel in the same half of one biguanidinium cation. The interaction of N(4)-H(4B) with ring 1, C(15)-C(16), is best described as having an edge type geometry. Thus the "pincer" type arrangement found in biguanidinium tetraphenylborate, having one centroid and one edge type interaction, is identical to those observed in guanidinium tetraphenylborate acetonitrile solvate.

The second face of phenyl ring 1 in biguanidinium tetraphenylborate also accepts an N-H...π(Ph) hydrogen bond, from N(2)-H(2B) of a second cation (symmetry [1+*x*, *y*, *z*]). Looking at this hydrogen bond from the opposite perspective, N(2)-H(2B) from the original cation forms a hydrogen bond with ring 1 of a tetraphenylborate anion generated by the symmetry (-1+*x*, *y*, *z*). The geometry of the N-H...π(Ph) hydrogen bond is different from any of those examined so far.

If N(2) is projected onto the plane of ring 1, it is found to lie very close to the ring centroid. It therefore exhibits the narrow range of N(2)...C_{ring} distances [minimum C(13) 3.316(2)Å; maximum C(15) 3.421(2)Å; 100Δ = 11] and the short N(2)...π_c distance, 3.070Å, expected for a centroid type interaction. However, H(2B) projects onto the ring 1 plane close to C(13). The distance H(2B)...C(13), 2.490Å, is considerably

less than that to any other ring 1 phenyl carbon atom [maximum C(16) 3.329Å; 100Δ = 84] and is less than the H(2B)...π_c distance of 2.595Å. Based on the H(2B)...C_{ring} distance distribution this interaction could be described as being to a single carbon atom, N(2)-H(2B)...C(13).

The N(2)-H(2B) vector makes an angle of only 39.6° with the plane of ring 1, far from perpendicular. The angle N(2)-H(2B)...π_c is only 109.6°, not surprising since the N(2)-H(2B) vector points across the ring toward C(13) [N(2)-H(2B)...C(13) = 141.1°] not toward the ring centroid. In fact, the N(2)-H(2B) vector projects onto the plane outside of ring 1 and makes an even better angle with H(13) [N(2)-H(2B)...H(13) = 162.1° and H(2B)...H(13) = 2.891Å]. However, H(2B) is still closer to C(13) than to H(13).

The second hydrogen atom on N(2) of the same cation, H(2A), also makes a relatively close contact to phenyl ring 1 of the same anion [H(2A)...C(11) = 2.962Å]. However, as will be discussed next, the main interaction of N(2)-H(2A) is actually with ring 2 of this same anion. The geometry of the N(2)-H(2A)...ring 1 contact is far from ideal, with very poor N-H...C_{ring} angles, the mean value being only 84.3°. The contact of N(2)-H(2A) with ring 1 appears to be incidental, brought about by the need to form two N-H...π(Ph) hydrogen bonds between a single NH_2 group and two adjacent rings on the same anion [N(2)-H(2B)...ring 1 and N(2)-H(2A)...ring 2]. Already, looking only at the N-H...π(Ph) contacts to ring 1 of the anion in biguanidinium tetraphenylborate, one can see an even greater compromise in the individual hydrogen bond geometries because of the need to form so many interactions to one cation.

Based on the geometries of the interactions, the N(5)-H(5B)...ring 1

centroid type hydrogen bond, with mean N...C_{ring} and mean H(N)...C_{ring} distances of 3.555[5]Å and 2.691Å, respectively, would be expected to be stronger than the N(4)-H(4B)...ring 1 edge type hydrogen bond (4.341[5]Å, 3.611Å). The same relationship had been observed previously between the centroid and edge type hydrogen bonds in the "pincer" type interactions of guanidinium tetraphenylborate acetonitrile solvate. In fact, the mean N...C_{ring} and H(N)...C_{ring} distances for both the centroid and edge type contacts to ring 1 in biguanidinium tetraphenylborate are very similar to those found for the corresponding bond types in the guanidinium salt.

It is difficult to know where to place the N(2)-H(2B)...ring 1 hydrogen bond (atom type) in the hierarchy of the individual hydrogen bonds. The mean N...C_{ring} distance is the shortest of the three interactions to ring 1, 3.375[5]Å, but the mean N-H(N)...C_{ring} angle is the farthest from linearity, 110.4° [N(5)-H(5B) 147.5° and N(4)-H(4B) 134.3°]. Based on the mean H(N)...C_{ring} distance of 2.934Å, the N(2)-H(2B) hydrogen bond would seem to be intermediate between the other two contacts to ring 1.

As previously mentioned, the major interaction of N(2)-H(2A) is to ring 2 of the same anion which also forms the N(2)-H(2B)..ring 1 hydrogen bond (Figure 26 - at the end of this section). If N(2)-H(2A) and N(2)-H(2B) are from the original cation, then the interacting anion must be generated by applying the symmetry (-1+*x*, *y*, *z*).

Both N(2) and H(2A) project onto the plane inside phenyl ring 2, N(2) almost at the ring centroid but slightly toward C(21) and H(2A) between the ring centroid and C(26). The N(2)-H(2A) vector points almost directly at C(26) [N(2)-H(2A)...C(26) = 174.3°], rather than towards the

ring centroid [N(2)-H(2A)...π_c = 141.3°]. Thus, the N(2)-H(2A)...ring 2 interaction is best described as an off-center, centroid type hydrogen bond. The N(2)...C_{ring} values cover a narrow range of distances [maximum C(24) 3.585(2)Å; minimum C(26) 3.375Å; 100Δ = 21] and the N(2)...π_c distance, 3.198Å, is shorter than the minimum N(2)...C_{ring} length. The H(2A)...C_{ring} distances also cover a relatively narrow (but larger) range of values [maximum C(23) 3.048Å; minimum C(26) 2.392Å; 100Δ = 66]. The distance from H(2A) to the centroid of ring 2, 2.368Å, is in this case only very slightly shorter than the minimum H(2A)...C_{ring} distance, confirming the description of the N(2)-H(2A)...ring 2 hydrogen bond as having an off-center, centroid type geometry.

The N(2)-H(2A) vector makes an angle of only 67.0° with the plane of ring 2. The fact that this hydrogen bond is not as linear as might be expected must arise because N(2)-H(2B) from the same cation also interacts with ring 1 of the same anion. It is not possible to form these two hydrogen bonds without compromising the angles, and in fact the N(2)-H(2B) vector makes an angle of only 39.6° with the plane of ring 1.

The off-center, centroid type geometry of the N(2)-H(2A)...ring 2 hydrogen bond is characterized by mean N...C_{ring} and mean H(N)...C_{ring} distances of 3.490[5]Å and 2.742Å, respectively, and a mean N-H(N)...C_{ring} angle of 137.6°. The H(N)...C_{ring} mean is slightly longer and the mean angle is slightly smaller than the corresponding values in the N(5)-H(5B)...ring 1 centroid type hydrogen bond, perhaps indicating that the former is a slightly weaker interaction.

Like ring 2, ring 3 accepts only a single N-H...π(Ph) hydrogen bond in biguanidinium tetraphenylborate (Figure 27 - at the end of this

section). N(3)-H(3A) of the original cation forms the hydrogen bond with ring 3 of an anion generated by the symmetry (-½+*x*, ½-*y*, -½+*z*). This is the third, and final, different anion to be involved with the formation of N-H hydrogen bonds from the cation.

The geometry of the N(3)-H(3A)...ring 3 hydrogen bond is very similar to that just described for the N(2)-H(2A)...ring 2 interaction, both having off-center, centroid type geometries. The range of N(3)...C_{ring} distances [minimum C(36) 3.366(2)Å; maximum C(33) 3.662(2)Å; 100Δ = 30] and H(3A)...C_{ring} distances [minimum C(36) 2.408Å; maximum C(33) 3.059Å; 100Δ = 65] are relatively narrow. However, in this case, the N(3)...C(35) [3.376(2)Å] and H(3A)...C(35) [2.430Å] distances are also very close to the minimum values. The distances from N(3) and H(3A) to the centroid of ring 3, 3.233Å and 2.378Å respectively, are shorter than any of the minimum individual distances. The largest angle is made not to the ring centroid [N(3)-H(3A)...π_c = 144.6°] but rather to C(36) of the ring [N(3)-H(3A)...C(36) = 163.8° and N(3)-H(3A)...C(35) = 160.6°]. The N(3)-H(3A) vector makes an angle of 72.3° with the plane of ring 3, again relatively far from perpendicular. It appears that the perpendicular orientation of the N-H...π(Ph) hydrogen bond is most easily compromised when a number of interactions must be formed simultaneously involving the same cations and tetraphenylborate anions.

Both N(3) and H(3A) fall inside the ring when projected on the plane of phenyl ring 3. N(3) projects close to the ring centroid but shifted slightly toward the C(35)-C(36) bond. H(3A) projects just inside the ring near the midpoint of the C(35)-C(36) bond. As shown by the angles above, the N(3)-H(3A) vector projects outside of the confines of ring 3, between

C(35) and C(36), slightly closer to C(36). The off-center, centroid geometry of the N(3)-H(3A)...ring 3 hydrogen bond is directed to the midpoint of a bond rather than to an individual atom.

The mean N...C_{ring} distance (3.521[5]Å) and the mean H(N)...C_{ring} distance (2.747Å) for the N(3)-H(3A)...ring 3 interaction are very similar to those found for the N(2)-H(2A)...ring 2 contact, as is the mean N-H(N)...C_{ring} angle of 139.2°. This would suggest that the two interactions are of approximately equal strengths.

There are two interactions from a single cation to one face of phenyl ring 4 in biguanidinium tetraphenylborate (Figure 28 - at the end of this section). However, the two donors, N(3)-H(3B) and N(5)-H(5A), come from the two different halves of the cation and thus a "pincer" type arrangement of the two bonds is not formed.

The N(3)-H(3B)...ring 4 hydrogen bond is best described as being of the edge type. Although the N(3)...C_{ring} distances cover a relatively narrow range of values [minimum C(42) 3.498(2)Å; maximum C(45) 3.861(2)Å; 100Δ = 36], all longer than the N(3)...π_c distance of 3.419Å, indicative of a centroid type arrangement, there are two H(3B)...C_{ring} distances considerably shorter than the rest [H(3B)...C(42) = 2.934Å and H(3B)...C(43) = 2.982Å]. The remaining H(3B)...C_{ring} distances are considerably longer, with a maximum of 3.809Å to C(45) [100Δ = 88], and the H(3B)...π_c distance, 3.108Å, is longer than the minimum H(3B)...C_{ring} lengths. The angles, N(3)-H(3B)...C(42) = 117.3° and N(3)-H(3B)...C(43) = 124.6°, are more linear than the N(3)-H(3B)...π_c angle of 99.9°, although all are far from linear. Overall, the results suggest an edge type geometry for the N(3)-H(3B)...ring 4 hydrogen bond.

When projected onto the plane of ring 4, both N(3) and H(3B) fall inside the ring, N(3) roughly midway between the centroid and C(42) and H(3B) very close to the midpoint of the C(42)-C(43) bond. As a result, the N(3)-H(3B) vector projects outside and well away from ring 4. This in turn gives the very poor observed values for the N(3)-H(3B)...C_{ring} angles. This is also reflected in the angle the N(3)-H(3B) vector makes with the plane of ring 4, only 31.0°, far from perpendicular.

The second contact to the same face of ring 4, N(5)-H(5A)...ring 4, involves the same biguanidinium cation as the previous interaction but comes from its opposite half. It is also best described as an edge type interaction. The overall geometry of the contacts is thus different from the "pincer" or "fork" type arrangements observed previously for two interactions to the same ring, one centroid type and one edge type from two parallel N-H donor bonds in a guanidinium fragment. Here, the interactions to ring 4 are both of the edge type and come from two different halves of the biguanidinium cation.

There are two N(5)...C_{ring} distances that are considerably shorter than any of the other individual values [N(5)...C(45) = 3.668(3)Å and N(5)...C(46) = 3.487(2)Å], all others being greater than 4.2Å and the maximum being 5.099(2)Å to C(43) [100Δ = 161]. The distance from N(5) to the centroid of ring 4, 4.141Å, is also longer than the minimum values. Similarly, the H(5A)...C(45), 2.788Å, and H(5A)...C(46), 2.664Å, distances are shorter than any other H(5A)...C_{ring} values [maximum C(43) 4.114Å; 100Δ = 145]. These minimum values are also shorter than the H(5A)...π_c distance of 3.175Å.

The N(5)-H(5A)...π_c angle is not far from linear, 166.5°, and the

angle N(5)-H(5A)...C(43) is even better at 176.5°. In contrast, the N(5)-H(5A)...C(45) and N(5)-H(5A)...C(46) angles are less linear, being 148.9° and 141.2°, respectively. As shown by these angles, the geometry of the N(5)-H(5A)...ring 4 hydrogen bond is far from ideal. Both N(5) and H(5A) project onto the ring plane well outside the ring itself, H(5A) below the midpoint of the C(45)-C(46) bond and N(5) even farther away. The N(5)-H(5A) vector points back toward the ring and across its face, making an almost linear angle with C(43), the carbon atom in the ring farthest from N(5) and H(5A). The N(5)-H(5A) vector makes an angle of only 41.5° with the plane of ring 4.

The two edge type N-H...π(Ph) hydrogen bonds made to phenyl ring 4, N(3)-H(3B)..ring 4 and N(5)-H(5A)...ring 4, have somewhat different mean N...C_{ring} and mean H(N)...C_{ring} distances and mean N-H(N)...C_{ring} angles. In the former interaction these are 3.692[6]Å, 3.392Å and 101°, respectively, while in the latter they are 4.329[6]Å, 3.426Å and 156°. In the N(3)-H(3B) contact, the mean N...C_{ring} distance is longer than that in the N(5)-H(5A) contact. However, this is offset by a less linear mean N-H(N)...C_{ring} angle in the former. The net result is that the two edge type interactions to ring 4 have similar mean H(N)...C_{ring} distances, perhaps indicating that they would be expected to be of similar strengths.

Compared to the centroid type interactions of biguanidinium tetraphenylborate, N(5)-H(5B)...ring 1 [2.691Å], N(2)-H(2A)...ring 2 [2.742Å] and N(3)-H(3A)...ring 3 [2.747Å], which have the mean H(N)...C_{ring} distances shown in brackets, the edge type geometries of the two interactions to ring 4 have longer mean H(N)...C_{ring} values. As observed previously, the edge type interactions appear to be weaker than those of

the centroid type. The edge type hydrogen bonds to ring 4 are more similar to the N(4)-H(4B)...ring 1 edge type component of the "fork" arrangement, where the mean H(N)...C_{ring} distance was calculated to be 3.611Å.

Several other contacts of the type N-H(N)...phenyl ring [H(N)...C_{ring} > 3.0Å] were observed in biguanidinium tetraphenylborate. However, these contacts were judged to be relatively minor when compared to the N-H...π(Ph) hydrogen bonds examined in detail and reported here. The N-H...X [X = N or π(Ph)] hydrogen bonding in biguanidinium tetraphenylborate can be summarized as follows:

	Acceptor	Donor	Description
cation	N(4)	N(1)-H(1B)	conventional N-H...N
anion	ring 1 (face a)	N(5)-H(5B)	centroid type "pincer"
		N(4)-H(4B)	edge type
	(face b)	N(2)-H(2B)	atom type
	ring 2	N(2)-H(2A)	off-center, centroid type
	ring 3	N(3)-H(3A)	off-center, centroid type
	ring 4	N(3)-H(3B)	edge type non"pincer"
		N(5)-H(5A)	edge type

It is interesting to note that the hydrogen bonds formed by the N(1)-C(2)-N(4),N(5) half of the cation appear to be stronger overall than those formed by the other half. This was already invoked as a possible explanation for the unequal bond lengths observed in the two halves of the cation. There are other possible consequences arising from this disparity, such as differences in charge distribution and reactivity in the two halves of the cation, but these have not been investigated further.

The distribution of the N-H...X [X = N or π(Ph)] hydrogen bond geometries in biguanidinium tetraphenylborate is also of interest. As shown in Figure 24, each terminal NH_2 group of the cation forms two hydrogen bonds as follows:

N(2)	H(2A)	centroid	H(2B)	atom type
N(3)	H(3A)	centroid	H(3B)	edge type
N(4)	H(4A)	N-H...N	H(4B)	edge type
N(5)	H(5A)	edge type	H(5B)	centroid

Every terminal nitrogen center is involved in one relatively strong traditional N-H...N or centroid geometry N-H...π(Ph) hydrogen bond. The second interaction in each pair has a less ideal geometry, being either an edge type or single atom type N-H...π(Ph) hydrogen bond. The distribution of hydrogen bond types is balanced over the entire cation. At each nitrogen center, one stronger interaction, with better geometry, is balanced by a second interaction which takes what is left over to form its best possible geometry.

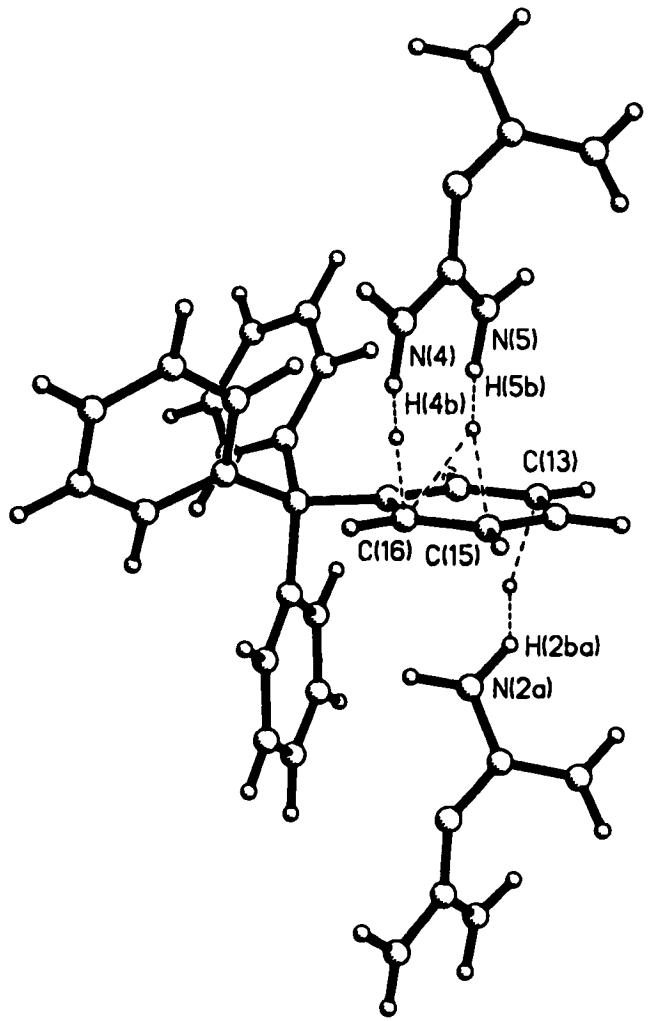

Figure 25. The N-H...π(Ph) hydrogen bonds accepted by phenyl ring #1 in the structure of biguanidinium tetraphenylborate. The small open circles represent the locations of the bond critical points of the interactions.

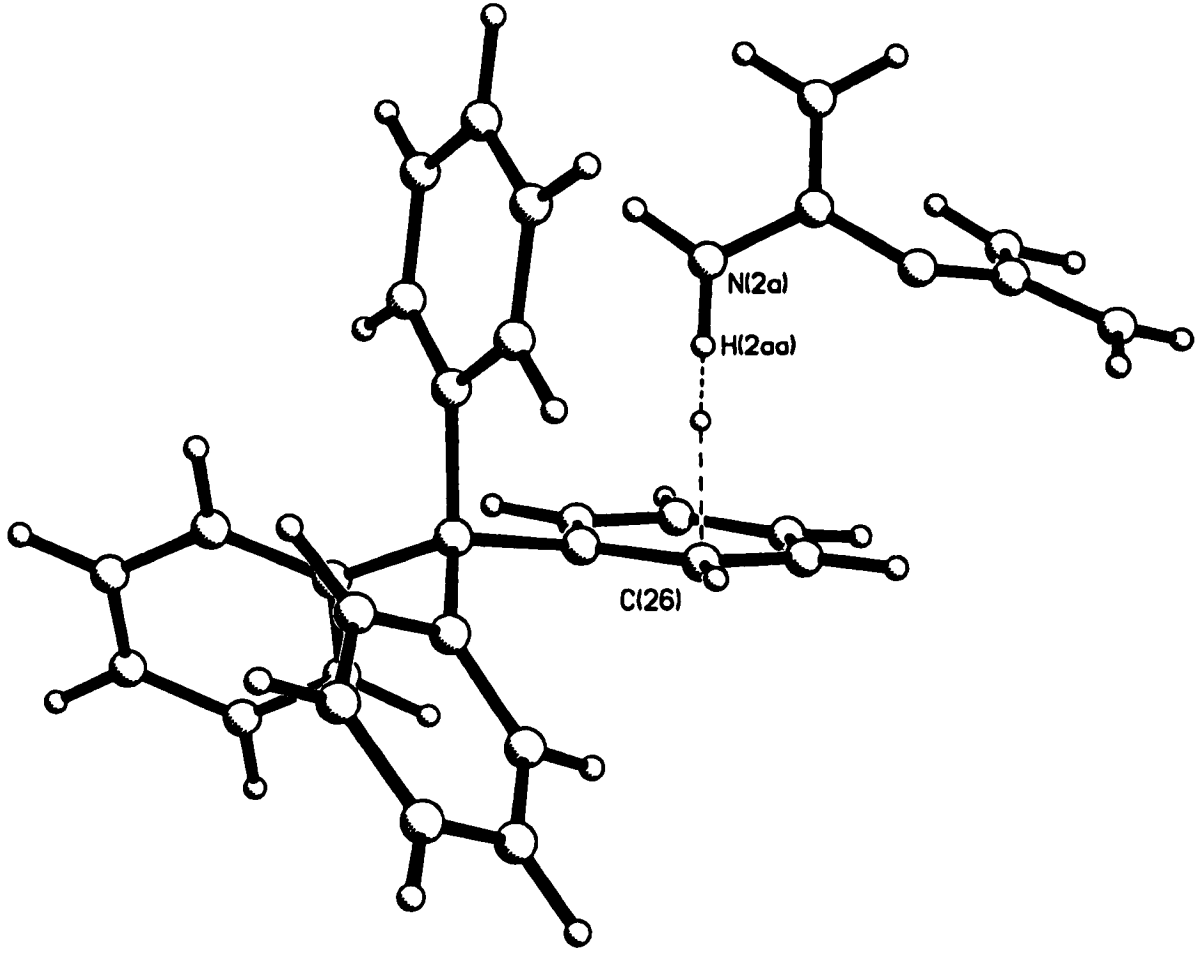

Figure 26. The N-H...π(Ph) hydrogen bond accepted by phenyl ring #2 in the structure of biguanidinium tetraphenylborate. The small open circle represents the location of the bond critical point of the interaction.

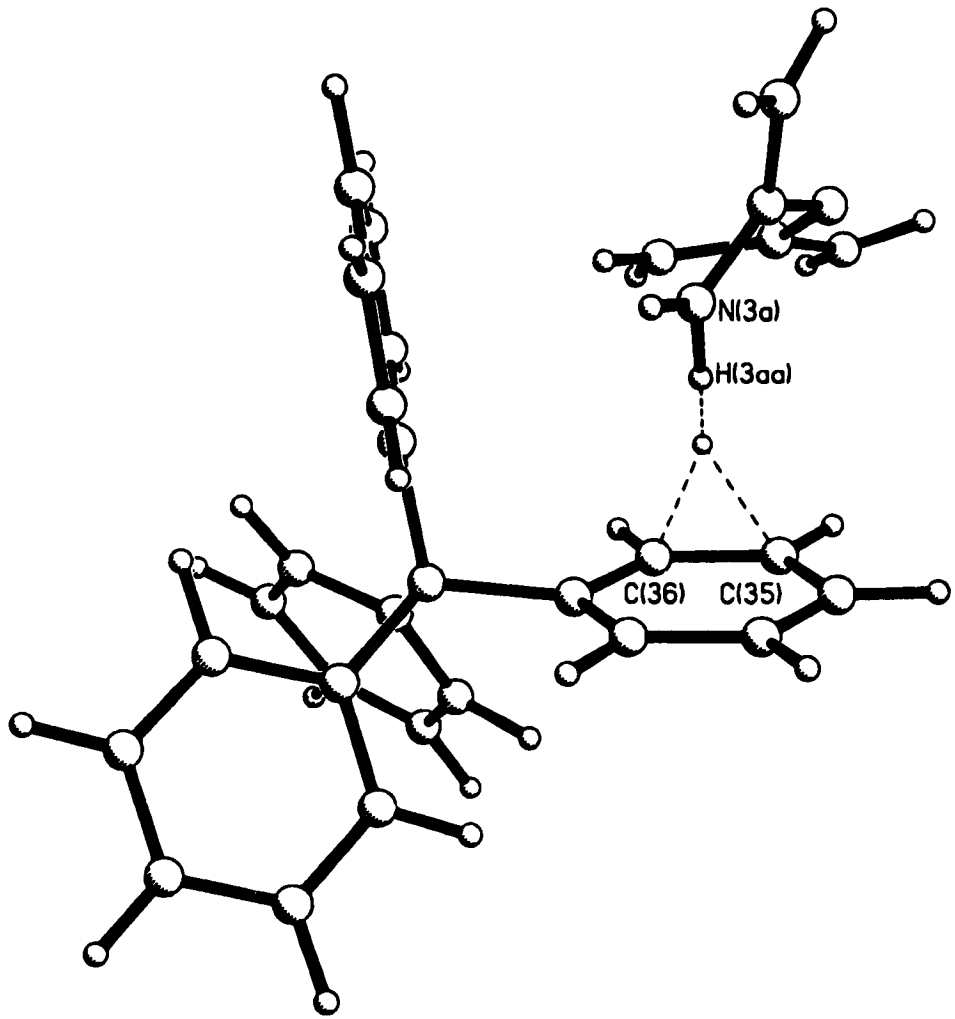

Figure 27. The N-H...π(Ph) hydrogen bond accepted by phenyl ring #3 in the structure of biguanidinium tetraphenylborate. The small open circle represents the location of the bond critical point of the interaction.

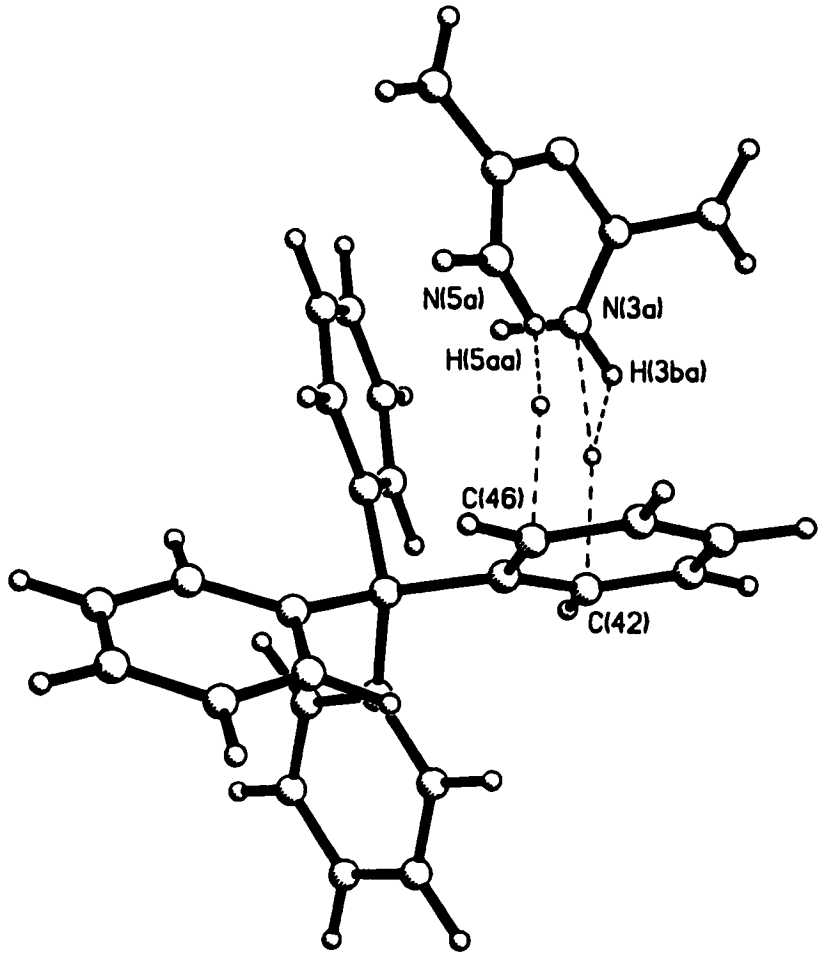

Figure 28. The N-H...π(Ph) hydrogen bonds accepted by phenyl ring #4 in the structure of biguanidinium tetraphenylborate. The small open circles represent the locations of the bond critical points of the interactions.

Table 12. Intermolecular contacts for biguanidinium tetraphenylborate.

Part 1 Hydrogen bonded contacts N-H...N (cation/cation)			
contact	N...N (Å)	H...N (Å)	N-H...N (°)
N(4)-H(4A)...N(1)	symmetry (-1-x, 1-y, -z)		
N(1)	3.111(2)	2.127	175.1

Part 2 Hydrogen bonded contacts N-H...π (cation/anion)			
contact	N...C (Å)	H...C (Å)	N-H...C (°)
N(2)-H(2A)...ring 1	symmetry (-1+x, y, z)		
C(11)	3.398(2)	2.962	107.9
C(12)	3.324(2)	3.244	86.0
C(13)	3.316(2)	3.602	65.4
C(14)	3.373(2)	3.704	63.0
C(15)	3.421(2)	3.444	80.4
C(16)	3.420(2)	3.059	103.1
mean	**3.375[5]**	**3.336**	**84.3**
centroid[a]	3.070	3.039	82.5
plane[b]	3.067	2.900	9.7
N(2)-H(2B)...ring 1	symmetry (-1+x, y, z)		
C(11)	3.398(2)	3.186	93.9
C(12)	3.324(2)	2.740	118.4
C(13)	3.316(2)	2.490	141.1
C(14)	3.373(2)	2.723	123.8
C(15)	3.421(2)	3.138	98.2
C(16)	3.420(2)	3.329	86.8
mean	**3.375[5]**	**2.934**	**110.4**
centroid[a]	3.070	2.595	109.6
plane[b]	3.067	2.439	39.6

Table 12. Intermolecular contacts for biguanidinium tetraphenylborate (continued).

Part 2 Hydrogen bonded contacts N-H...π (cation/anion)			
contact	N...C (Å)	H...C (Å)	N-H...C (°)
N(4)-H(4B)...ring 1	symmetry (x, y, z)		
C(11)	4.280(2)	3.501	137.5
C(12)	4.939(2)	4.296	125.9
C(13)	5.041(2)	4.454	121.6
C(14)	4.489(2)	3.856	124.6
C(15)	3.714(2)	2.901	140.4
C(16)	3.583(2)	2.661	155.7
mean	**4.341[5]**	**3.611**	**134.3**
centroid[a]	4.145	3.394	134.5
plane[b]	3.348	2.373	81.8
N(5)-H(5B)...ring 1	symmetry (x, y, z)		
C(11)	3.646(2)	2.745	152.2
C(12)	3.639(2)	2.806	142.5
C(13)	3.576(2)	2.787	137.4
C(14)	3.491(2)	2.673	140.5
C(15)	3.460(2)	2.560	151.7
C(16)	3.521(2)	2.576	160.5
mean	**3.555[5]**	**2.691**	**147.5**
centroid[a]	3.268	2.299	167.3
plane[b]	3.258	2.284	81.2

Table 12. Intermolecular contacts for biguanidinium tetraphenylborate (continued).

Part 2 Hydrogen bonded contacts N-H...π (cation/anion)			
contact	N...C (Å)	H...C (Å)	N-H...C (°)
N(2)-H(2A)...ring 2	symmetry (-1+x, y, z)		
C(21)	3.435(2)	2.565	147.2
C(22)	3.498(2)	2.851	123.9
C(23)	3.581(2)	3.048	115.2
C(24)	3.585(2)	2.965	121.9
C(25)	3.469(2)	2.630	143.0
C(26)	3.375(2)	2.392	174.3
mean	**3.490[5]**	**2.742**	**137.6**
centroid[c]	3.198	2.368	141.3
plane[d]	3.187	2.279	67.0
N(3)-H(3A)...ring 3	symmetry (-1/2+x, 1/2-y, -1/2+z)		
C(31)	3.536(2)	2.768	135.1
C(32)	3.650(2)	3.037	121.5
C(33)	3.662(2)	3.059	120.7
C(34)	3.535(2)	2.782	133.7
C(35)	3.376(2)	2.430	160.6
C(36)	3.366(2)	2.408	163.8
mean	**3.521[5]**	**2.747**	**139.2**
centroid[e]	3.233	2.378	144.6
plane[f]	3.206	2.266	72.3

Table 12. Intermolecular contacts for biguanidinium tetraphenylborate (continued).

Part 2 Hydrogen bonded contacts N-H...π (cation/anion)			
contact	N...C (Å)	H...C (Å)	N-H...C (°)
N(3)-H(3B)...ring 4	symmetry (-1/2+x, 1/2-y, -1/2+z)		
C(41)	3.598(2)	3.403	93.4
C(42)	3.498(2)	2.934	117.3
C(43)	3.634(2)	2.982	124.6
C(44)	3.826(3)	3.456	104.6
C(45)	3.861(3)	3.809	85.6
C(46)	3.736(2)	3.768	80.6
mean	**3.692[6]**	**3.392**	**101.0**
centroid[g]	3.419	3.108	99.9
plane[h]	3.385	2.878	31.0
N(5)-H(5A)...ring 4	symmetry (-1/2+x, 1/2-y, -1/2+z)		
C(41)	4.241(2)	3.398	144.6
C(42)	4.954(2)	4.016	160.1
C(43)	5.099(2)	4.114	176.5
C(44)	4.528(3)	3.577	162.7
C(45)	3.668(3)	2.788	148.9
C(46)	3.487(2)	2.664	141.2
mean	**4.329[6]**	**3.426**	**155.7**
centroid[g]	4.141	3.175	166.5
plane[h]	3.186	2.533	41.5

[a] The position of the centroid of ring 1 is (-0.0292, 0.3086, -0.0952). The values listed are *d*(N...centroid), *d*(H...centroid) and the angle N-H...centroid.

[b] The mean deviation of the carbon atoms from the ring 1 plane is 0.0014Å. The values listed are *d*(N...plane), *d*(H...plane) and the angle the N-H vector makes with the plane of the ring.

[c] The position of the centroid of ring 2 is (0.3670, 0.2301, 0.0968). The values listed are *d*(N...centroid), *d*(H...centroid) and the angle N-H...centroid.

[d] The mean deviation of the carbon atoms from the ring 2 plane is 0.0065Å. The values listed are *d*(N...plane), *d*(H...plane) and the angle the N-H vector makes with the plane of the ring.

[e] The position of the centroid of ring 3 is (-0.0586, 0.0596, 0.1388). The values listed are *d*(N...centroid), *d*(H...centroid) and the angle N-H...centroid.

[f] The mean deviation of the carbon atoms from the ring 3 plane is 0.0015Å. The values listed are *d*(N...plane), *d*(H...plane) and the angle the N-H vector makes with the plane of the ring.

[g] The position of the centroid of ring 4 is (-0.0243, 0.3786, 0.2159). The values listed are *d*(N...centroid), *d*(H...centroid) and the angle N-H...centroid.

[h] The mean deviation of the carbon atoms from the ring 4 plane is 0.0075Å. The values listed are *d*(N...plane), *d*(H...plane) and the angle the N-H vector makes with the plane of the ring.

Table 13. Bond critical points for the intermolecular contacts in biguanidinium tetraphenylborate.

Hydrogen bonded contacts N-H...N (cation/cation)									
Contact	Hessian Eigenvalues			Charge Density	Laplacian	Ellipticity	Position		
Bond Path	λ_1	λ_2	λ_3	$\rho_b(\mathbf{r})$ ($eÅ^{-3}$)	$\nabla^2\rho_b(\mathbf{r})$ ($eÅ^{-5}$)	ε	x	y (fractional)	z
N(1)...H(4A)-N(4) symmetry (-1-x, 1-y, -z)									
N(1)...H(4A)	-0.60,	-0.56,	2.68	0.141(2)	1.519(3)	0.07	-0.5959,	0.4611,	-0.0276

Bond Lengths and Angles at the Critical Point			
Atoms	Distance (Å)	Atoms	Angle (°)
Cp...N(4)	1.712	N(4)...Cp...N(1)	176.9
Cp...H(4A)	0.728	H(4A)...Cp...N(1)	179.3
Cp...N(1)	1.399	N(4)-H(4A)...Cp	175.3

Table 13. Bond critical points for the intermolecular contacts in biguanidinium tetraphenylborate (continued).

Hydrogen bonded contacts N-H...π (cation/anion)									
Contact	Hessian Eigenvalues			Charge Density	Laplacian	Ellipticity	Position		
Bond Path	λ_1	λ_2	λ_3	$\rho_b(\mathbf{r})$ ($e\text{Å}^{-3}$)	$\nabla^2\rho_b(\mathbf{r})$ ($e\text{Å}^{-5}$)	ε	x	y (fractional)	z
ring 1...H(2A)-N(2) symmetry (1+x, y, z)									
no critical point located									
ring 1...H(2B)-N(2) symmetry (1+x, y, z)							single atom type hydrogen bond		
C(13)...H(2B)	-0.16,	-0.10,	1.14	0.081(2)	0.883(1)	0.71	0.1006,	0.2639,	-0.1340

Bond Lengths and Angles at the Critical Point			
Atoms	Distance (Å)	Atoms	Angle (°)
Cp...N(2)	1.778	N(2)...Cp...C(13)	172.6
Cp...H(2B)	0.977	H(2B)...Cp...C(13)	161.3
Cp...C(13)	1.544	N(2)-H(2B)...Cp	129.9
Cp...plane	1.464		
Cp...centroid	1.720		

Table 13. Bond critical points for the intermolecular contacts in biguanidinium tetraphenylborate (continued).

Contact	Hydrogen bonded contacts N-H...π (cation/anion)								
	Hessian Eigenvalues			Charge Density	Laplacian	Ellipticity	Position		
Bond Path	λ_1	λ_2	λ_3	$\rho_b(\mathbf{r})$ ($eÅ^{-3}$)	$\nabla^2\rho_b(\mathbf{r})$ ($eÅ^{-5}$)	ε	x	y (fractional)	z
ring 1...H(4B)-N(4)*	symmetry (x, y, z)			intermediate type contact					
C(16)-H(16)...H(4B)	-0.15,	-0.10,	0.73	0.055(1)	0.477(1)	0.55	-0.1481,	0.4298,	-0.0248

Bond Lengths and Angles at the Critical Point

Atoms	Distance (Å)	Atoms	Angle (°)
Cp...N(4)	1.940	N(4)...Cp...C(16)	164.1
Cp...H(4B)	0.987	H(4B)...Cp...C(16)	174.5
Cp...C(16)	1.677	N(4)...Cp...H(16)	155.0
Cp...H(16)	1.628	H(4B)...Cp...H(16)	146.5
		N(4)-H(4B)...Cp	159.1
Cp...plane	1.468		
Cp...centroid	2.538		

* The bond path from H(4B) follows the C(16)-H(16) bond of the ring for approximately one third of its length before terminating at C(16).

Table 13. Bond critical points for the intermolecular contacts in biguanidinium tetraphenylborate (continued).

Contact	Hessian Eigenvalues			Charge Density	Laplacian	Ellipticity	Position		
Bond Path	λ_1	λ_2	λ_3	$\rho_b(\mathbf{r})$ (eÅ^{-3})	$\nabla^2\rho_b(\mathbf{r})$ (eÅ^{-5})	ε	x	y (fractional)	z
Hydrogen bonded contacts N-H...π (cation/anion)									
ring 1...H(5B)-N(5)*	symmetry (x, y, z)			centroid type hydrogen bond					
C(15)-C(16)...H(5B)	-0.14,	-0.04,	0.83	0.071(1)	0.654(1)	2.63	-0.1661,	0.3436,	-0.0962

Bond Lengths and Angles at the Critical Point

Atoms	Distance (Å)	Atoms	Angle (°)
Cp...N(5)	1.896	N(5)...Cp...C(15)	152.5
Cp...H(5B)	0.928	H(5B)...Cp...C(15)	160.7
Cp...C(15)	1.665	N(5)...Cp...C(16)	147.9
Cp...C(16)	1.768	H(5B)...Cp...C(16)	143.8
		N(5)-H(5B)...Cp	164.0
Cp...plane	1.388		
Cp...centroid	1.477		

* The bond path from H(5B) follows the C(15)-C(16) bond of the ring for approximately one third of its length before terminating at C(15).

Table 13. Bond critical points for the intermolecular contacts in biguanidinium tetraphenylborate (continued).

Hydrogen bonded contacts N-H...π (cation/anion)									
Contact	Hessian Eigenvalues			Charge Density	Laplacian	Ellipticity	Position		
Bond Path	λ_1	λ_2	λ_3	$\rho_b(\mathbf{r})$ (eÅ^{-3})	$\nabla^2\rho_b(\mathbf{r})$ (eÅ^{-5})	ε	x	y (fractional)	z
ring 2...H(2A)-N(2)* symmetry (1+x, y, z) centroid type hydrogen bond									
C(26)...H(2A)	-0.30,	-0.20,	1.42	0.104(14)	0.918(19)	0.50	0.2915,	0.3054,	0.0185

Bond Lengths and Angles at the Critical Point			
Atoms	Distance (Å)	Atoms	Angle (°)
Cp...N(2)	1.818	N(2)...Cp...C(26)	177.1
Cp...H(2A)	0.837	H(2A)...Cp...C(26)	174.1
Cp...C(26)	1.558	N(2)-H(2A)...Cp	171.3
Cp...plane	1.469		
Cp...centroid	1.696		

* Single atom type bond path from H(2A) to C(26).

Table 13. Bond critical points for the intermolecular contacts in biguanidinium tetraphenylborate (continued).

Contact	Hessian Eigenvalues			Charge Density	Laplacian	Ellipticity	Position		
Bond Path	λ_1	λ_2	λ_3	$\rho_b(\mathbf{r})$ ($eÅ^{-3}$)	$\nabla^2\rho_b(\mathbf{r})$ ($eÅ^{-5}$)	ε	x	y (fractional)	z
Hydrogen bonded contacts N-H...π (cation/anion)									
ring 3...H(3A)-N(3)*	symmetry (1/2+x, 1/2-y, 1/2+z)					centroid type hydrogen bond			
C(35)-C(36)...H(3A)	-0.28,	-0.15,	1.29	0.097(2)	0.857(1)	0.87	-0.0306,	0.1073,	0.2376

Bond Lengths and Angles at the Critical Point

Atoms	Distance (Å)	Atoms	Angle (°)
Cp...N(3)	1.834	N(3)...Cp...C(35)	150.7
Cp...H(3A)	0.850	H(3A)...Cp...C(35)	150.2
Cp...C(35)	1.655	N(3)...Cp...C(36)	157.8
Cp...C(36)	1.596	H(3A)...Cp...C(36)	158.7
		N(3)-H(3A)...Cp	174.8
Cp...plane	1.438		
Cp...centroid	1.700		

* The bond path is from H(3A) to the approximate midpoint of the C(35)-C(36) bond in the ring and terminates at C(35).

Table 13. Bond critical points for the intermolecular contacts in biguanidinium tetraphenylborate (continued).

Contact	Hessian Eigenvalues			Charge Density	Laplacian	Ellipticity	Position		
Bond Path	λ_1	λ_2	λ_3	$\rho_b(\mathbf{r})$ ($e\text{Å}^{-3}$)	$\nabla^2\rho_b(\mathbf{r})$ ($e\text{Å}^{-5}$)	ε	x	y (fractional)	z
Hydrogen bonded contacts N-H...π (cation/anion)									
ring 4...H(3B)-N(3)* symmetry (1/2+x, 1/2-y, 1/2+z)									
C(42)-C(43)...N(3)	-0.11,	-0.04,	0.69	0.049(1)	0.544(1)	1.39	-0.1347,	0.2714,	0.2185

Bond Lengths and Angles at the Critical Point

Atoms	Distance (Å)	Atoms	Angle (°)
Cp...N(3)	1.777	N(3)...Cp...C(42)	170.1
Cp...H(3B)	1.284	H(3B)...Cp...C(42)	152.5
Cp...C(42)	1.734	N(3)...Cp...C(43)	146.3
Cp...C(43)	2.019	H(3B)...Cp...C(43)	127.7
		N(3)-H(3B)...Cp	102.2
Cp...plane	1.673		
Cp...centroid	1.902		

* The unusual bond path begins from N(3) and not H(3B). It follows the C(42)-C(43) bond of the ring for a short distance before terminating at C(42).

Table 13. Bond critical points for the intermolecular contacts in biguanidinium tetraphenylborate (continued).

Contact	Hessian Eigenvalues			Charge Density	Laplacian	Ellipticity	Position		
Bond Path	λ_1	λ_2	λ_3	$\rho_c(\mathbf{r})$ ($eÅ^{-3}$)	$\nabla^2\rho_c(\mathbf{r})$ ($eÅ^{-5}$)	ε	x	y (fractional)	z
Hydrogen bonded contacts N-H...π (cation/anion)									
ring 4...H(5A)-N(5)*	symmetry (1/2+x, 1/2-y, 1/2+z)					edge type hydrogen bond			
C(45)-C(46)...H(5A)	-0.14	-0.08	0.83	0.059(1)	0.614(1)	0.80	0.0950	0.2741	0.3138

Bond Lengths and Angles at the Critical Point

Atoms	Distance (Å)	Atoms	Angle (°)
Cp...N(5)	1.883	N(5)...Cp...C(46)	156.9
Cp...H(5A)	0.994	H(5A)...Cp...C(46)	171.9
Cp...C(46)	1.675	N(5)...Cp...C(45)	148.4
Cp...C(45)	1.929	H(5A)...Cp...C(45)	143.0
		N(5)-H(5A)...Cp	143.9
Cp...plane	1.579		
Cp...centroid	2.294		

* The bond path from H(5A) follows the C(45)-C(46) bond of the ring for approximately one quarter of its length before terminating at C(46).

3.3. N-H...X [X = N or Ph] Hydrogen Bonds in the Four Structures - A Summary

3.3.1. N-H...N Hydrogen Bonds

Two N-H...N hydrogen bonds were identified in the four structures studied by multipole refinement, one in guanidinium tetraphenylborate acetonitrile solvate and the other in biguanidinium tetraphenylborate. In the first instance, the hydrogen bond is formed between one N-H donor of the cation and the acceptor, the lone pair electrons on the nitrogen of the acetonitrile solvate molecule. The second N-H...N interaction was located in the structure of biguanidinium tetraphenylborate, holding together the centrosymmetric, hydrogen bonded cation dimer. In this case, both the donor N-H group and the acceptor nitrogen atom are found within the cation itself. Both of these hydrogen bonds are the shortest (and therefore the strongest) interactions in their respective structures. The geometrical parameters of the two N-H...N hydrogen bonds are resummarized as follows:

	N-H(N) (Å)	N...N (Å)	H(N)...N (Å)	N-H(N)...N (°)
N(1)-H(1B)...N(4) $[C(NH_2)_3]^+$	0.986	2.933(4)	2.082	143.4
N(4)-H(4A)...N(1) $[N(C(NH_2)_2)_2]^+$	0.986	3.111(2)	2.127	175.1

3.3.2. N-H...π(Ph) Hydrogen Bonds

Every N-H group in the four multipole refined structures studied was found to participate in some form of N-H...X [X = N or π(Ph)] hydrogen bond. Of the 16 possible interactions, 14 N-H...π(Ph) type hydrogen bonds were identified, one in $NH_4B(C_6H_5)_4$, one in [DabcoH][$B(C_6H_5)_4$], five in

$[C(NH_2)_3][B(C_6H_5)_4]\cdot CH_3CN$ and seven in $[N(C[NH_2]_2)_2][B(C_6H_5)_4]$. All of the N-H...π(Ph) hydrogen bonds were found to be unbranched/unbifurcated, single interactions, from the N-H donor in a cation to one phenyl ring of the anion acting as the acceptor. The geometries of these hydrogen bonds were found to vary widely but they could be divided into three broad groups based on the observed $H(N)...C_{ring}$ distances, centroid type (8), edge type (5) and those to a single atom (1). The $N...C_{ring}$ distance distributions were sometimes not so characteristic. Centroid type N-H...π(Ph) hydrogen bonds were empirically identified as having the $H(N)...\pi_c$ (ring centroid) distance shorter than any of the six individual $H(N)...C_{ring}$ distances. Similarly, single atom type and edge type hydrogen bonds were identified as having the $H(N)...\pi_c$ distance shorter than five or four of the $H(N)...C_{ring}$ distances, respectively. The edge type interaction thus has two shorter $H(N)...C_{ring}$ distances while the single atom type interaction has only one.

The N-H...π(Ph) hydrogen bonds studied experimentally illustrate the extremely soft geometry of such interactions, i.e. those made to aromatic acceptors. Examples of hydrogen bonds with centroid, edge and single atom type geometries were located in the four experimental structures. The literature of N-H...π(Ph) hydrogen bonds explicitly investigated in small molecule x-ray crystal structures is rather sparse making comparison to the current results difficult. Only a few, well characterized examples have been reported in publications[58,82,90] and only very recently has a single atom type geometry even been described.[118] (The numerous N-H...π(Ph) hydrogen bonds examined in the 1994 publication of Bakshi et al.[83] were not characterized by their individual interaction geometries in this way.)

Comparison to the more developed literature on O-H...π(Ph) hydrogen bonds, where a number of crystal structures have been reported for each possible geometry, is however possible. Well documented examples of centroid type hydrogen bonds (Hardy and MacNicol (1976)[60] and Aubry et al. (1977)[61]) and edge type hydrogen bonds (Nakatsu et al. (1978)[62] and Ueji et al. (1982)[63]) have been known for a number of years, while the investigation of a single atom type O-H...π(Ph) hydrogen bond is more recent (Steiner et al. (1996)[64,65]). The conformational variability of X-H...π(Ph) hydrogen bonds, observed experimentally for the X = N bonds studied, is substantiated by the literature data accumulated for X = O type bonds.

Of the fourteen N-H...π(Ph) hydrogen bonds studied experimentally, eight were found to be centroid type, five edge type and only one a single atom type based on the interaction geometries. The overall results support the idea that centroid geometry N-H...π(Ph) hydrogen bonds are favoured experimentally, being formed in every situation if at all possible. However, a number of other forces, including competition within a structure because of the need to form multiple hydrogen bonds, precludes the formation of centroid type interactions in all cases.

It is instructive to consider the distribution of the N-H...π(Ph) hydrogen bond types in each of the experimental structures studied. The N-H...X [X = N or π(Ph)], and all other, hydrogen bonds in a structure are a compromise of the individual geometries, to maximize the strength of the total network. Because, in most cases, a number of hydrogen bonds must be formed from a single cation, to a limited number of acceptors, it is not possible for each individual interaction to have a centroid type geometry. In both $NH_4B(C_6H_5)_4$ and [DabcoH] $[B(C_6H_5)_4]$ only a single unique N-H...π(Ph)

hydrogen bond is formed (although in NH_4^+ it is formed four times) and in both cases close to the "ideal" centroid geometry is observed. In $[C(NH_2)_3][B(C_6H_5)_4]\cdot CH_3CN$ the number of N-H...π(Ph) hydrogen bonds formed increases to five, of which three are found to maintain a centroid type geometry (60%) while the other two form edge type interactions (two "pincer" or "fork" type arrangements). Finally, in biguanidinium tetraphenylborate seven N-H...π(Ph) hydrogen bonds are formed, three of which are of the centroid type (43%), although two of these have off-center geometries. The remaining four N-H...π(Ph) hydrogen bonds are either of the edge type (three) or to a single atom (one) and only one double "pincer" type arrangement is observed. As the number of hydrogen bonds per cation increases, their geometries become less than ideal because of the competition between donors for the available acceptors.

This effect is magnified when the charge distribution on each cation is also considered. The ammonium, guanidinium and biguanidinium cations have four, six and eight H(N) atoms, respectively, over which to share the single positive charge. This would be expected to have an effect on the strength of the N-H...X [X = N or π(Ph)] hydrogen bonds formed in each case, with progressively weaker hydrogen bonds being formed overall as the number of N-H groups per cation increases, and the corresponding charge on each individual hydrogen atom decreases.

A rough comparison can be made by considering the average H(N)...π_c distances for the centroid type N-H...π(Ph) hydrogen bonds in the different structures. These are usually the strongest hydrogen bonds formed in each structure and give an indication of the overall strength of interaction. Ammonium tetraphenylborate forms four equivalent centroid

type N-H...π(Ph) hydrogen bonds from each cation, with an H(N)...π_c distance of 2.013Å. Guanidinium tetraphenylborate acetonitrile solvate forms a total of six N-H...X [X = N or π(Ph)] hydrogen bonds from each cation; half are N-H...π(Ph) hydrogen bonds with centroid geometries having an average H(N)...π_c distance of 2.317Å. Similarly, in biguanidinium tetraphenylborate the cation forms eight N-H...X hydrogen bonds of which three are centroid type N-H...π(Ph) interactions having an average H(N)...π_c distance of 2.348Å. A progressive lengthening of the centroid type N-H...π(Ph) hydrogen bonds is observed, on average, as the number of N-H groups per cation increases. This likely results from a combination of charge dilution and competition for optimal hydrogen bond formation as the number of N-H groups per cation increases.

The experimental conclusion, that centroid type N-H...π(Ph) hydrogen bonds are formed preferentially in the four structures studied, can be compared to the rather limited data available in the literature. The first evidence for the existence of N-H...π(Ph) hydrogen bonds came from the investigation of protein structures (as detailed in the introduction). However, few examples of well characterized individual N-H...π(Ph) hydrogen bonds, in which the contact is discussed as an important feature of the structure, have appeared in the literature. These have also been described in detail in the introduction but are briefly resummarized here.

The first example of an N-H...π(Ph) hydrogen bond located in a small molecule crystal structure was published in 1992. L.R. Hanton et al.[58] examined the crystal structure of a derivative of cyclohexane substituted at one carbon atom by two 2,4-dimethyl-3-aminobenzene groups and found it to contain an N-H...π(Ph) hydrogen bond with a centroid type geometry.

The H(N)...π_c ring centroid distance was not given by the authors but the H(N) to ring plane distance is quoted, 2.42(2)Å [100Δ = 15].

In 1997, F.H. Allen et al.[82] published the results of single crystal neutron diffraction analyses of 2- and 3-aminophenol. Both structures were found to contain a single, unique N-H...π(Ph) hydrogen bond. However, the authors could not determine if a C-C bond of the phenyl ring (edge type) or if the ring as a whole (centroid type) served as the acceptor in these two interactions. From the rather limited data presented, it appears that by using the geometric criteria developed in this investigation these would both be classified as centroid type hydrogen bonds; the distance from H(N) to the midpoint of the interacting C-C ring bond is longer than the H(N)...π_c ring centroid distance in both cases. In the N-H...π(Ph) hydrogen bond of 2-aminophenol the H(N)...π_c ring centroid distance is 2.309Å (neutron data) while in 3-aminophenol it is 2.409Å.

The N-H...π(Ph) hydrogen bonds in the crystal structure of propylargylammonium tetraphenylborate were investigated by T. Steiner et al.[90] as reported in a 1997 publication. In spite of some disorder in the structure, a total of six N-H...π(Ph) hydrogen bonds were characterized. Of these, four were determined to have centroid type geometries, while two were found to be edge type interactions (using criteria similar to those used in this investigation). Overall, the H(N)...π_c ring centroid distance in the four centroid type hydrogen bonds averages 2.24Å, while the two edge type interactions have an average H(N)...π_c distance of 2.88Å, 0.64Å longer than the centroid average. The range of H(N)...C_{ring} distances is also larger in the edge type interactions, as expected [centroid type - average 100Δ = 34 and edge type - average 100Δ = 140].

The intramolecular N-H...π(Ph) hydrogen bond in crystalline vitamin B12 coenzyme has been characterized using neutron diffraction by Starikov and Steiner (1998).[88] The high quality data generated to characterize the hydrogen bond allow it to be included with the small molecule results. The authors describe the single, unique N-H...π(Ph) centroid geometry hydrogen bond as being one of the shortest and best centered examples ever reported [$H(N)\ldots\pi_c$ = 2.58Å, 100Δ = 39].

Very recently, T. Steiner[118] has published the x-ray crystal structure determination of 1-(2-fluorophenyl)thiourea, a compound containing an N-H...π(Ph) hydrogen bond. This hydrogen bond is described as having a very off-center arrangement, being made to a single carbon atom of the phenyl ring acceptor [N(2)-H(21)...C(5)]. However, the exact geometric criteria used to reach this conclusion are not given. The $H(N)\ldots\pi_c$ ring centroid distance (3.23Å) is longer than the H(N)...C(5) distance of 2.61Å as expected [100Δ = 165]. This is the only known example of a single atom type N-H...π(Ph) hydrogen bond reported in the literature.

The literature data collected for N-H...π(Ph) hydrogen bonds show that centroid type interactions appear to be the most favoured geometry. Almost all of the examples located are centroid type hydrogen bonds (8 of 11). In this investigation, centroid type N-H...π(Ph) hydrogen bonds were also found to predominate, presumably because this conformation allows the strongest interaction between the H(N) donor and the entire phenyl ring acceptor, conferring the maximum possible stabilization to the structure. Centroid type interactions are formed if at all possible, more off-center arrangements arising only when other factors dictate that they must be.

Of course, the fact that centroid type hydrogen bonds predominate

in the rather sparse literature accounts may be purely fortuitous. If centroid type interactions are the only ones that have been looked for, they may be the only ones that have been found. Centroid type hydrogen bonds may be more readily identified than other conformations during a structural investigation because they normally occur at the shortest donor/acceptor distances. This could be a partial explanation as to why so many, of the albeit few, examples of N-H...π(Ph) hydrogen bonds in the literature have been found to have centroid type geometries.

A similar situation also arises when the results of a Cambridge Structural Database search for N-H...π(Ph) hydrogen bonds, carried out by Viswamitra et al.[81] in 1993, are considered. The authors found centroid geometries to predominate in the N-H...π(Ph) hydrogen bonds located, although single atom and edge type examples were also found. However, rather narrow criteria were used in the search; only interactions with $N...C_{ring}$ distances of from 2.9 to 3.4Å were accepted into the data set. Arbitrarily cutting off the interaction distance in this way would be more likely to eliminate edge or single atom type bonds since they are normally longer, while centroid type bonds would be more likely to be retained since they generally occur with shorter donor/acceptor distances. In this way, the results of the search may be artificially skewed. Still, overall it appears, based on the complete evidence amassed to date, that centroid geometry hydrogen bonds are favoured over the other possible conformations because of the extra stability they normally confer.

This conclusion is also supported by the results from theoretical calculations that have been reported in the literature, most importantly those of Rodham et al.[85] published in 1993. Using somewhat simpler calcul-

ations, both Steiner et al.[64] and Levitt and Perutz[84] have also determined that (other factors being equal) centroid type interactions are more stable than other possible geometries for X-H...π(Ph) hydrogen bonds.

Rodham et al.[85] used ab initio molecular orbital calculations, carried out at the MP2 level of theory with 6-31G** basis sets, to optimize the geometry of the benzene/ammonia dimer. The minimum energy conformation was found to have one proton of ammonia pointing directly toward the center of the benzene ring. This "monodentate" structure is equivalent to the formation of an N-H...π(Ph) hydrogen bond in the C_6H_6/NH_3 dimer, again substantiating the fact that this is the most favourable geometry. However, at least in the theoretical calculations the "monodentate" structure was found to be only slightly more stable than a "bidentate" structure in which two protons of ammonia point simultaneously toward the benzene ring (an off-center arrangement of some type). In both geometries, the center of mass of the ammonia molecule lies on the C_6 axis of benzene, with a calculated separation of 3.43Å in the minimum energy structure. The angle made between the C_6 axis of benzene and the C_3 axis of ammonia was calculated to be 52°.

Rodham et al.[85] also compared their calculated theoretical results to experimental values generated from microwave and optical spectral investigations of the gas phase C_6H_6/NH_3 dimer. Experimentally, the dimer was found to maintain its symmetry about the C_6 axis of benzene on a vibrationally averaged basis, indicating that all three ammonia protons are equivalent. Relatively free rotation about of NH_3 allows each proton in turn to interact with the ring, with the interchange between the "monodentate" minima occurring via the slightly higher energy "bidentate"

intermediate. The gas phase dimer was found to have a separation between the centers of mass of 3.590(5)Å and a difference between the axes of 59±5°.

The experimentally and theoretically derived parameters characterizing N-H...π(Ph) hydrogen bonds found in the literature can be compared to the results obtained in this investigation:

	mean N...π_c (Å)	mean H(N)...π_c (Å)	mean N-H(N)...π_c (°)
All (n = 14)	3.44	2.63	145
σ	0.39	0.44	21
Centroid (n = 8)	3.19	2.28	156
σ	0.07	0.12	13
Edge (n = 5)	3.91	3.19	135
σ	0.27	0.10	21

	mean N...C_{ring} (Å)	mean H(N)...C_{ring} (Å)	mean N-H(N)...C_{ring} (°)
All (n = 14)	3.71	2.96	137
σ	0.35	0.38	14
Centroid (n = 8)	3.49	2.67	142
σ	0.06	0.10	5
Edge (n = 5)	4.13	3.44	132
σ	0.24	0.09	18

where the standard deviation of the population, $\sigma = [(\Sigma x_i^2 - n(\Sigma x_i)^2) / n]^{1/2}$

Of the 14 N-H...π(Ph) hydrogen bonds studied, eight were found to have centroid type geometries, five edge type geometries and only one a single atom type geometry. The single atom category, containing only one example, was not included as a separate entry in the following statistical breakdown. However, the first two types of N-H...π(Ph) hydrogen bond

geometries could be separated, studied and compared to the overall hydrogen bond statistics.

All of the mean distances in the centroid type hydrogen bonds are shorter, often considerably, than those of the edge type hydrogen bonds (and those of the overall group). The mean angles are always larger (closer to linear) in the centroid type group than in the edge type group or in the overall group. The calculated deviations are smallest on the mean $H(N)\ldots\pi_c$ and the mean $H(N)\ldots C_{ring}$ distances, where the centroid type values (2.277Å and 2.667Å, respectively) were found to be significantly shorter than the edge type values (3.195Å and 3.445Å). The calculated deviations on the mean $N\ldots\pi_c$ and on the mean $N\ldots C_{ring}$ distances, and on the mean $N\text{-}H(N)\ldots\pi_c$ and the mean $N\text{-}H(N)\ldots C_{ring}$ angles are larger for the edge type geometry group than for the centroid type geometry group. This is in keeping with a greater variation in the geometry of the edge type hydrogen bonds. All of the results support the idea that the centroid type hydrogen bond is the more "ideal" geometry, allowing closer approach of the donor and acceptor groups. However, this is not to say that individual $N/H(N)\ldots C_{ring}$ distances to one or two atoms in the ring may not be equally short or shorter in edge type hydrogen bonds as those found in the centroid type bonds, where all carbon atoms in the ring are normally reasonably close.

The experimental results generated in this investigation can be compared with the many and varied data located in the literature to characterize $N\text{-}H\ldots\pi(Ph)$ hydrogen bonds. Theoretical calculations carried out by Rodham et al.[85] suggested a separation of 3.43Å between the centers of mass of the two components of the benzene/ammonia dimer in its minimum

energy "monodentate" (centroid type) conformation. The same authors used spectroscopic data to calculate a corresponding separation distance of 3.59Å in the isolated gas phase dimer. Levitt and Perutz[84] also used theoretical calculations to find a similar optimum separation distance ($N...\pi_c$ = 3.40Å) in an N-H...π(Ph) hydrogen bond with an ideal centroid geometry, in which the N-H vector lies on the C_6 axis of the benzene ring and is directed towards the ring centroid. The two sets of theoretical results are consistent. They are best compared to the mean $N...\pi_c$ ring centroid distance found for the centroid group of experimental N-H...π(Ph) hydrogen bonds, $N...\pi_c$ = 3.19Å (overall in the experimental bonds $N...\pi_c$ = 3.44Å). The experimental average $N...\pi_c$ distance for the centroid type hydrogen bonds is shorter than the theoretically calculated distances and considerably shorter than the separation found in the gas phase dimer. The experimental results indicate that stronger N-H...π(Ph) hydrogen bonds are formed, on average, in the low temperature solid state structures than in the isolated C_6H_6/NH_3 dimer in the gas phase. The hydrogen bonds in the solid state are not isolated but are influenced by other forces and interactions within the crystal perhaps explaining the observed differences between the experimental and theoretical values.

The experimental results can also be compared to the geometric data gathered separately by Viswamitra et al.,[81] Allen et al.[82] and Umezawa et al.[120] after searching the Cambridge Structural Database for examples of N-H...π(Ph) hydrogen bonds. Care must be taken when making these comparisons because the results of the database searches depend directly on the search parameters chosen and on how the mean distances reported have been defined. As already mentioned, Viswamitra et al.[81] used a rather narrow

range of distance criteria in their search, perhaps limiting the number of bonds located and favouring identification of centroid type hydrogen bonds over other possible conformations. Having said this, Viswamitra et al. found the mean N...C_{ring} distance to be 3.31Å, the mean H(N)...C_{ring} distance to be 2.47Å and the mean N-H...C_{ring} angle to be 148° in the N-H...π(Ph) hydrogen bonds they located. The mean values reported were calculated using the shorter of the two distances, N/H...π_c (ring centroid) or N/H...C_{ring} minimum, for each individual interaction. In the present work, the mean N/H...C_{ring} distance was calculated for each interaction by averaging all six N/H...C_{ring} distances. For each group, the 14 mean values were then averaged to give the overall mean value which has been reported. Thus, it is actually more reasonable to compare the literature results (in all cases) to the mean N/H...π_c ring centroid distances calculated for the experimental data, since these are based on a single (and often the minimum) N/H...ring distance from each individual interaction. For the experimental data set, the mean N...C_{ring} distance was calculated to be 3.44Å, the mean H(N)...C_{ring} distance 2.63Å and the mean N-H...C_{ring} angle 145°. The experimental distances are consistently somewhat longer than the corresponding values obtained from the database search of Viswamitra et al. This result is directly attributable to the narrower range of search criteria used to identify the presence of N-H...π(Ph) interactions in the paper compared to this work. However, it also arises from the fact that the individual experimental N/H...π_c distances used in the mean calculations are not always the minimum contact distance; five of the fourteen interactions studied do not have centroid type geometries. Because they have been defined in different ways, the experimental mean N/H...π_c values

are naturally longer than the corresponding mean N/H...C_{ring} distances reported by Viswamitra et al.

Allen et al.[82] carried out a similar, although less well documented, search of the Cambridge Structural Database in 1997. The authors report that N-H...π(Ph) hydrogen bonds may be structurally significant when the H(N)...π_c ring centroid distance is less than 2.6Å and the N-H...π_c angle is between 130° and 180°. The criteria used in this search are not given in the publication, making a comparison to these results even more tenuous. The experimental average for all data, H(N)...π_c = 2.63Å, is almost equal to the suggested maximum from the database search, leading to the conclusion that Allen et al. used a narrow range of distance criteria to limit their search.

In a very recent publication (1999), Y. Umezawa et al.[120] report the results of yet another search of the Cambridge Structural Database for X-H...π(Ph) [X = N, O or C] type interactions. The authors first isolated subsets of the data, containing all organic compounds having one (or more) X-H groups and at least one six membered aromatic ring. They then chose a relatively long H(X)...C_{ring} cutoff distance of 3.05Å as the maximum for which an interaction would be considered to form in each search. Based on these criteria, 9.3% of the eligible compounds were found to participate in intermolecular N-H...π(Ph) type interactions. The mean H(N)...C_{ring} atomic distance for this group (again based on the H(N)...π_c or the H(N)...C_{ring} minimum distance, which ever was less, for each interaction) was calculated to be 2.78±0.19Å. This is slightly longer than the most comparable experimental parameter, the mean H(N)...π_c distance (2.63Å). Again, the observed difference is directly related to the longer distance

limit chosen by Umezawa et al., 3.05Å, compared to the experimental limit of 3.0Å. Also, the experimental group was found to be quite homogeneous with a majority of the interactions having the favoured centroid type geometry. This would decrease the mean distance relative to a less biased group, such as would presumably have been located in the CSD search of Umezawa et al. And, of course, the two mean values must be compared with caution since they have not been defined in quite the same way. Taking all of these factors into account, the two means, 2.63Å for the experimental $H(N)\ldots\pi_c$ distances and 2.78Å for the $H(N)\ldots C_{ring}$ minimum distances in the literature group, are reasonably close. In fact, the experimental value of 2.63Å falls exactly halfway between the mean $H(N)\ldots C_{ring}$ distances reported by Viswamitra et al. (2.47Å) and by Umezawa et al. (2.78Å), from two different searches of the Cambridge Structural Database.

It is also difficult to compare the experimental results to the literature data reported for N-H...π(Ph) hydrogen bonds in individual, small molecule crystal structures. Differences in the methods of data generation, collection, quality and treatment, as well as differences in the structures themselves, all suggest that the results may not be directly comparable on a one to one basis. However, if all the literature data are considered as a single group, comparison becomes perhaps more reasonable. And, on the whole the literature group is composed of high quality, low temperature x-ray and neutron based structure determinations.

The characterizations of a total of 11 N-H...π(Ph) hydrogen bonds were located in the literature, excluding the results of Bakshi et al.[83] that will be discussed subsequently [Hanton et al.[58] (1), Allen et al.[82] (2), Steiner et al.[90] (6), Starikov and Steiner[88] (1) and Steiner[118] (1)].

The parameter most commonly used to characterize these interactions appears to be the H(N)...π_c ring centroid distance, only Hanton et al. do not directly include it in their publication. If the N-H...π(Ph) hydrogen bonds in the structures of 2- and 3-aminophenol (Allen et al.[82]) are assigned centroid type geometries (using the criteria developed in this investigation) then the literature group consists of eight centroid type bonds, two edge type bonds and one single atom type bond. Overall, as a group the literature data have an average H(N)...π_c distance of 2.52Å. This is shorter than the corresponding experimental mean H(N)...π_c distance of 2.63Å, not surprising since the literature group is comprised almost entirely of centroid type bonds (8 of 11) while the experimental data set has a lower percentage of such bonds (8 of 14).

It is more instructive to compare the group of centroid type N-H...π(Ph) hydrogen bonds located in the literature with the subgroup of centroid type bonds in the experimental data set. In the former group, the average H(N)...π_c distance is 2.32Å, while in the latter group it is almost equal, 2.28Å. The experimental and literature data are in complete agreement, a very satisfactory result. Averaging the literature data compensates for any minor discrepancies in the individual structures. The experimental group of N-H...π(Ph) centroid type hydrogen bonds doubles the number of such bonds that have been well characterized (again, excluding the results of Bakshi et al.[83]), yet the mean H(N)...π_c distance remains unchanged despite the fact that the data come from a wide variety of sources. The mean H(N)...π_c ring centroid distance of 2.3Å appears to be a truly representative value for centroid type N-H...π(Ph) hydrogen bonds in crystal structures.

The literature group of edge type N-H...π(Ph) hydrogen bonds, containing only two examples (from a slightly disordered structure), has a mean H(N)...π_c distance of 2.88Å. The experimental subgroup of edge type hydrogen bonds has a mean H(N)...π_c distance of 3.19Å, somewhat longer than the literature average. This is not an important distinction since so few examples were located in the literature group. Similarly, there are too few examples of single atom type N-H...π(Ph) hydrogen bonds, only one in each group, for a meaningful comparison to be made.

Perhaps most importantly, the average geometries of the N-H...π(Ph) hydrogen bonds studied by multipole refinement in this work can be compared with the results reported by P.K. Bakshi et al.[83] in a 1994 publication. The authors investigated a series of related organoammonium tetraphenylborate salts and include a complete geometric characterization of the many N-H...π(Ph) hydrogen bonds in the structures studied. Again, caution must be exercised when comparing the results from the low temperature, multipole refinements (this work) to the results from the mostly room temperature, conventional spherical refinements (Bakshi et al.). For a total of 26 normal, single N-H...π(Ph) hydrogen bonds the authors report mean N...π_c and mean H(N)...π_c distances of 3.25(18)Å and 2.34(19)Å, respectively, while mean N...C_{ring} and mean H(N)...C_{ring} distances of 3.54(16)Å and 2.72(16)Å were found. All of the mean distances calculated by Bakshi et al. are shorter than the corresponding, overall mean distances from the multipole refined structures, by from 0.2 to 0.3Å. In fact, the mean distances reported by Bakshi et al. are always closer to the multipole, centroid type only data set than to the overall multipole results, the difference being only 0.05 to 0.06Å in the former. The mean

angle N-H(N)...π_c calculated by Bakshi et al., 156°, is also larger than the overall mean angle for the 14 N-H...π(Ph) hydrogen bonds studied in this work, 145°. However, it is equal to the mean calculated for the eight centroid type bonds in the multipole refinements, 156°.

Part of the difference observed in the average distances for the H(N)...π_c and H(N)...C_{ring} contacts comes from the difference in the lengths used for the N-H(N) bond itself, 1.032Å (NH_4^+ and DabcoH$^+$; 2 bonds) or 0.986Å ($[C(NH_2)_3]^+$ and $[N(C[NH_2]_2)_2]^+$; 12 bonds) in the multipole refinements depending on the structure versus 1.02Å in the conventional spherical refinements. However, this is not sufficient to explain the differences also observed in the mean N...π_c and the mean N...C_{ring} distances, nor does it explain why the multipole, centroid type group of hydrogen bonds compares most closely with the overall results of Bakshi et al. (particularly considering how well the experimental centroid data fit with centroid data collected from the literature). The hydrogen bonds in the multipole refined structures (as a group) must have less ideal geometries than the group studied by Bakshi et al. They have longer distances and less linear angles, if any differences inherent to the refinement methods are ignored. This could be because the compounds studied by multipole refinement, particularly guanidinium tetraphenylborate acetonitrile solvate and biguanidinium tetraphenylborate, form multiple N-H...π(Ph) hydrogen bonds from the same cation (5 and 7, respectively), compromising the geometries of the individual bonds. The bonds in the group studied by Bakshi et al. were less likely to do so.

Bakshi et al. report the statistics on a subgroup of the normal bonds, which they term competing bonds, those to a single acceptor ring

under constraint in cations with multiple hydrogen bonding arrangements. These bonds would be expected to be more similar to the multipole refined, overall group of this work. However, the distances reported by Bakshi et al. for the competing group, mean N...π_c = 3.22(12)Å and mean H(N)...π_c = 2.36(19)Å, are essentially unchanged from their overall values and still agree more closely with the multipole, centroid type group of bonds than with the overall multipole results. The mean N-H(N)...π_c angle calculated by Bakshi et al. for the competing bond subgroup, equal to 144(12)°, matches the overall multipole result of 145°. [The change in the angle on going from the overall group of bonds (156°) to the competing group (144°) while the distances remain largely unchanged again illustrates how the angle in the N-H...π(Ph) hydrogen bond is the first parameter sacrificed in a competitive situation.]

The geometries of the hydrogen bonds in the multipole refined structures have considerably longer mean distances than even the competing group of bonds in the Bakshi study, indicative of weaker interactions. It is not completely clear why this should be so, although the large number of competing bonds formed in several of the multipole structures likely contributes to their less than ideal geometries, even relative to the competing group studied by Bakshi et al. It is also possible that the multipole derived distance parameters are subject to a slight vibrational lengthening because of the low temperatures at which the present data were collected. It must also be remembered, however, that the quality of the low temperature data collection and the multipole refinement used in this work make the present results superior to those previously reported by Bakshi et al.

3.4. C-H...Acceptor Interactions

Again, because of the final length of this thesis the complete discussion of the geometries of the C-H...acceptor interactions has been moved to Appendix 2. Only a brief introduction and a summary of the final conclusions reached are included here in the main text. For those interested in a more detailed description of the geometries, Appendix 2 is available in the second volume of the thesis.

During the course of the investigation of the N-H...X [X = N or Ph] hydrogen bonds in the four multipole refined structures, two most interesting features were observed. The first was found in the structure of [DabcoH] [$B(C_6H_5)_4$] where the cation was found to be completely enclosed in a cavity formed by the phenyl rings of six anions (Figure 9). As well as the N-H...π(Ph) hydrogen bond formed between the cation and one of the phenyl rings, all of the C-H groups of the cation were also found to form relatively short (less than 3Å) contacts with anion phenyl rings, often with favourable geometries.

Similar interactions were also noted in the structure of guanidinium tetraphenylborate acetonitrile solvate. In this structure, two different types of cavities were found, one enclosing a pair of cations and the other enclosing a pair of acetonitrile solvent molecules (Figure 14). Somewhat surprisingly, ring 1 of the tetraphenylborate anion was not found to act as the acceptor for any of the N-H...π(Ph) hydrogen bonds formed by the guanidinium cation, although all other of the three rings did. Instead, ring 1 was found to engage in short contacts, of less than 3Å, with the alkyl C-H groups of the acetonitrile solvent molecule.

This pair of observations led to the systematic investigation of all

C-H...acceptor interactions in the four structures, using the geometric criterion that the H(C)...acceptor distance be less than 3Å. A total of 43 such interactions were located, with acceptors being either nitrogen atoms (of the cation or solvent molecule - 9 in total) or the phenyl rings of the tetraphenylborate anions (34), and the donor C-H groups coming from the cation (DabcoH$^+$, 9), the solvent molecule (CH_3CN, 3) or the anion (all four structures, 22). The C-H donor groups can thus be either aliphatic (DabcoH$^+$ or CH_3CN) or aromatic (the $B(C_6H_5)_4^-$ anion). As expected from their diverse natures, these interactions were found to exhibit a wide variety of geometries. The most important question which arises is, what is the contribution of such C-H contacts? Can any be considered equivalent to the N-H...π(Ph) and N-H...N hydrogen bonds located in the four structures? Even if they are weaker, can they still be considered hydrogen bonds?

3.4.5. C-H...Acceptor Contacts in the Four Structures - A Summary

The majority of the C-H...phenyl interactions were found to fall into one of two distinct categories, after studying the geometries of all such contacts of less than 3Å located experimentally. The first category contains those interactions with **hydrogen bond type** geometries. Of the 34 C-H...phenyl contacts studied, 14 were classified as hydrogen bonds. A variety of configurations are possible and were observed experimentally, including centroid type (4), edge type (8) and single atom type (2) contacts. The second category contains **H...H type** interactions; with configurations exactly as described, these are likely related to van der Waals type contacts. Fifteen of the experimental C-H...phenyl interactions were identified as H...H type contacts.

The C-H...phenyl interactions tend to fall clearly into one category or the other based on their geometries. The hydrogen bond type contacts have minimum H(C)...C_{ring} distance(s) shorter than the related minimum H(C)...H_{ring} distance(s). Generally, H(C)...C_{ring} is significantly shorter than H(C)...H_{ring}, however, in some cases they can be close to equal. Even in those cases where H(C)...C_{ring} is close to H(C)...H_{ring} the interaction has been classified as a hydrogen bond as long as the H(C)...C_{ring} minimum distance is the shorter. The different possible hydrogen bond types (centroid, edge or single atom) have been described previously and are analogous to those found in the N-H...π(Ph) hydrogen bonds.

In the H...H type contacts, the H(C)...H_{ring} minimum distance is considerably shorter than any H(C)...C_{ring} distance or any other distance in the interaction. The H(C)...H_{ring} distance is usually less than 2.5Å, while the H(C)...C_{ring} distance is greater than 2.5Å and normally closer to 3.0Å. The minimum H(C)...H_{ring} distance is, on average, 0.5Å shorter than the corresponding H(C)...C_{ring} distance. In the 14 H(C)...H_{ring} anion/anion type contacts in the four compounds studied for this work, the average difference in the two distances was calculated to be 0.52Å, H(C)...H_{ring} < H(C)...C_{ring}. The very short H(C)...H_{ring} distance, sometimes only slightly greater than 2.0Å, dominates the interaction. In general, all H...H type contacts appear to be very similar, involving directly only the two hydrogen atoms that make close contact. The C-H...H_{ring} angles cover a wide range, often far from 180°, suggesting a nondirectional type contact. H...H type contacts often appear to arise as secondary effects, a consequence of the formation of other stronger interactions in the structure.

A few of the C-H...phenyl interactions studied did not fall clearly into either group. These five contacts were placed, rather arbitrarily, into an **"intermediate" type** category. In the intermediate group of contacts, the $H(C)...H_{ring}$ minimum distance is shorter than the corresponding $H(C)...C_{ring}$ distance but the two are relatively equal. Both distances tend to fall in the range 2.6±0.2Å. This type of interaction is difficult to interpret based solely on geometry. It is hard to know which distance will dominate the interaction or to tell how the contact should best be described. However, of the 22 $(C-H)_{anion}...(phenyl)_{anion}$ interactions investigated, 14 were found to be H...H type contacts and six were found to have hydrogen bond type geometries, while only two fell into the intermediate category, indicating that they are relatively rare.

C-H...π(Ph) hydrogen bonds of all three possible geometric types, centroid, edge and single atom, were identified and characterized in this investigation. The pronounced conformational variability exhibited by the C-H...π(Ph) type hydrogen bonds is not unexpected, having been observed previously for other X-H...π(Ph) [X = N or O] hydrogen bonds, including X = N in this work. Also, Steiner et al.[71] (1995) have published the results from a search of the Cambridge Structural Database in which the closest C-H...X contacts formed by terminal alkynes (donor group) were investigated. A total of 31 C-H...π type interactions were located, 18 to an alkyne acceptor, 5 to an alkene acceptor and 8 to an arene ring acceptor. Most of the C-H...π(Ph) interactions were found to have a geometry in which the C-H vector pointed toward the centroid of the arene ring. However, exceptions to the centroid geometry were also located, geometries in which one or two of the $H...C_{ring}$ distances were shorter than

the H...π_c ring centroid distance. Such interactions correspond to single atom and edge type hydrogen bonds, respectively. The authors interpret their results as showing that short contacts of sufficiently acidic C-H groups with π type aromatic acceptors possess all the essential properties of weak hydrogen bonds. A variety of geometries are possible, just as observed for other types of X-H...π(Ph) hydrogen bonds and experimentally for C-H...π(Ph) hydrogen bonds in this work. In a related paper, Steiner et al.[64] also report the results from a series of ab initio molecular orbital calculations on simple model systems that suggest, that under certain conditions, C-H...π(Ph) hydrogen bonds can have strengths similar to other X-H...π(Ph) hydrogen bonds and can have significant influence in a crystal structure.

In this work, a considerable number of C-H...X [X = N or π(Ph)] interactions have been investigated. As described above, not all of these were found to have hydrogen bond type geometries; in fact, the majority turned out to be better defined as H...H type contacts. It is even more difficult to compare the results because of the different origins of the contacts studied. In the C-H...X interactions, cation/anion, solvent/anion and anion/anion combinations were all observed. It is not certain that all these interaction types are directly comparable, particularly considering differences in charges and sizes amongst the various components of the different combinations. Because of the fragmentation of the results into so many small groups, a statistical comparison of the C-H...X interaction geometries, most notably the different hydrogen bond types, is not really possible. However, in all the C-H...X hydrogen bond type contacts studied, the characteristic distances appear longer than those in comparable

N-H...X hydrogen bonds.

The group of Y. Umezawa et al.[120] has recently published the results of a Cambridge Structural Database search for C-H...π(Ph) interactions in organic compounds. For the entire subset of structures containing at least one C-H group and at least one six membered aromatic ring an astonishing 75.1% were found to form C-H...π(Ph) interactions with a minimum contact distance of 3.05Å or less. For this subset of the data, the mean $H(C)\ldots C_{ring}$ atomic distance was calculated to be 2.91±0.12Å. The minimum $H(C)\ldots C_{ring}$ contact distance for each interaction (whether the $H(C)\ldots\pi_c$ or the minimum $H(C)\ldots C_{ring}$ distance) were averaged to generate this mean value. The C-H...π(Ph) average can be compared with corresponding mean values calculated for O-H and N-H subsets of the CSD data by Umezawa et al., as reported in the same publication. The O-H...π(Ph) interactions (5.1% of the O-H set) were characterized by a mean $H(O)\ldots C_{ring}$ distance of 2.80±0.21Å, while the N-H...π(Ph) interactions (9.3%) were found to have a similar mean $H(N)\ldots C_{ring}$ distance of 2.78±0.19Å. The authors make the observation that the C-H...π(Ph) interactions as a group occur at longer distances and are thus weaker, on average, than the O-H...π(Ph) or N-H...π(Ph) type interactions. This result is entirely consistent with the findings of the present experimental investigation.

Although overall mean values were not calculated for the distances and angles characterizing the C-H...phenyl interactions studied in this work, it is possible to compare the mean $H(C)\ldots C_{ring}$ distance reported by Umezawa et al. (2.91±0.12Å) to certain of the experimental results. In the set of all experimental C-H...phenyl interactions, a total of 14 were found to have hydrogen bond type geometries. In connection with later work

on the topological analysis of the experimental electron densities, the minimum contact distance for each of these hydrogen bonds (the minimum H(C)...C_{ring} distance) was determined. The overall mean H(C)...C_{ring} distance for this group, calculated from the individual values, was found to be 2.89Å with a standard deviation of 0.07Å. Similarly, for the smaller group of intermediate contacts (n = 4) a mean distance of 2.85Å with a standard deviation of 0.05Å was calculated. [The relevant mean distance in the appropriately named H...H group of contacts (H(C)...H_{ring}) is not comparable to the mean H(C)...C_{ring} distance calculated for the literature and other experimental groups (hence the absence of an overall mean calculation for the experimental data).] Both of the experimental mean H(C)...C_{ring} values (hydrogen bond and intermediate contact) are virtually identical to that reported by Umezawa et al., even though the search criteria employed were slightly different in each case. Umezawa et al. limited their search to interactions with minimum H(C)...C_{ring} distances of 3.05Å or less, while in this work a cutoff of 3.0Å was used. In this comparison, all mean values, both literature and experimental, have been defined in almost the same way, so are truly equal. The experimental results are in excellent agreement with the limited literature data available.

Perhaps more fruitful than a statistical analysis of the C-H...X hydrogen bonds located, is a simple comparison of the hydrogen bond distributions in the four compounds studied. In all four compounds, N-H...X [X = N or π(Ph)] hydrogen bonds were found to be present and were well characterized. Such hydrogen bonds were formed by every N-H group in all four structures and in each structure the geometries of the hydrogen

bonds were optimized to centroid type as much as possible. As the cations grew larger, with more N-H groups to satisfy, optimization of all the N-H...π(Ph) hydrogen bonds to centroid type geometries was no longer possible and a wider variety of hydrogen bond geometries were observed. In $NH_4B(C_6H_5)_4$ and [DabcoH] $[B(C_6H_5)_4]$ the cation contains only a single N-H group and a single N-H...π(Ph) hydrogen bond with a centroid type geometry is formed in each case. In guanidinium tetraphenylborate acetonitrile solvate five N-H...π(Ph) hydrogen bonds are formed, three with centroid type geometries and two with edge type geometries. Finally, in the structure of biguanidinium tetraphenylborate the seven N-H...π(Ph) hydrogen bonds are distributed amongst centroid type (3), edge type (3) and single atom type (1) geometries. In the two structures with multiple N-H...π(Ph) hydrogen bonds, the different types of geometries tend to be distributed throughout the structure, generally with one of the preferred centroid type interactions made to each ring of the anion, if at all possible. Would the C-H...X interactions, particularly the C-H...phenyl contacts with hydrogen bond type geometries, show the same patterns of optimization and distribution as observed for the N-H...X interactions?

[DabcoH] $[B(C_6H_5)_4]$ is the only one of the four structures studied, in which the cation contains C-H groups capable of interaction with the anion. In this structure a total of ten C-H...X [X = N or π(Ph)] cation/anion interactions were located, with every C-H group of the cation involved in at least one interaction. Nine $(C\text{-}H)_{cation}\cdots(phenyl)_{anion}$ contacts and one $(C\text{-}H)_{anion}\cdots N_{cation}$ contact were studied in detail, each characterized by a minimum H...X [X = N or C] distance of less than 3Å. The majority were found to have hydrogen bond type geometries; only one

was a definite H...H type contact. Of the six interactions classified as $(C\text{-}H)_{cation}\cdots(phenyl)_{anion}$ hydrogen bonds, five were found to have edge type geometries and one had a single atom geometry; none were found to have centroid type geometries.

It is clear that the $(C\text{-}H)_{cation}\cdots(phenyl)_{anion}$ interactions formed are important in the $[DabcoH][B(C_6H_5)_4]$ structure. They help to tether and orient the $DabcoH^+$ cation in the anion-formed cavity in which it resides. In fact, the single N-H...π(Ph) hydrogen bond between the cation and anion occurs with an N-H...π_c angle, 158.6°, that is less linear than might normally be expected and this has been attributed to the combined effects of the other cation/anion C-H...X contacts in the structure.

It appears that the $(C\text{-}H)_{cation}\cdots(phenyl)_{anion}$ contacts are optimized to the best possible hydrogen bond geometries; only a single H...H type contact is observed. This is another indication that such contacts are important and purposely formed. None have centroid type geometries but five of the six are edge type interactions. This is likely because of the large number of interactions arising from a single cation (11); there are six unique C-H groups. The competition to make all of these interactions as effective as possible precludes the formation of any with centroid type geometries. In any event, $(C\text{-}H)_{cation}\cdots(phenyl)_{anion}$ contacts are important in determining the structure of $[DabcoH][B(C_6H_5)_4]$. Along with the stronger N-H...π(Ph) centroid geometry hydrogen bond formed, these C-H...phenyl hydrogen bonds help to orient the cation and anion relative to one another in the crystal structure.

While the structure of $[DabcoH][B(C_6H_5)_4]$ contains the only studied examples of $(C\text{-}H)_{cation}\cdots(phenyl)_{anion}$ contacts, $[C(NH_2)_3][B(C_6H_5)_4]\cdot CH_3CN$

contains the only $(C\text{-}H)_{solvent}\cdots(phenyl)_{anion}$ contacts. Three such interactions were found to occur at reasonable distances between the solvent and the anion, one for each C-H group of acetonitrile. Again, the majority were found to have hydrogen bond type geometries, with one forming a very short centroid type hydrogen bond, one forming an edge type hydrogen bond and the third forming a difficult to characterize intermediate type interaction. None were clear H...H type contacts.

The three, related $(C\text{-}H)_{solvent}\cdots(phenyl)_{anion}$ interactions have been optimized to the best possible geometries, with the centroid type contact, C(3)-H(61)...ring 1, being particularly important. In the structure, N-H...π(Ph) hydrogen bonds are formed between the cation and only phenyl rings 2, 3 and 4 of the anion. The C(3)-H(61)...ring 1 hydrogen bond is the only short/strong contact made to ring 1 of the anion and helps to orient a pair of solvent molecules in the centrosymmetric cavity formed by the rings 1 and 2 of the anions. The $(C\text{-}H)_{solvent}\cdots(phenyl)_{anion}$ contacts are clearly important in the structure of $[C(NH_2)_3][B(C_6H_5)_4]\cdot CH_3CN$, playing a role similar to the C-H...phenyl cation/anion contacts in the structure of $[DabcoH][B(C_6H_5)_4]$.

The last category of C-H...phenyl contacts studied contains the anion/anion type interactions, which were found to occur in all four structures. However, the anion/anion contacts fall into two distinct groups. The first group contains the $(C\text{-}H)_{anion}\cdots(phenyl)_{anion}$ interactions of $[DabcoH][B(C_6H_5)_4]$ and $[C(NH_2)_3][B(C_6H_5)_4]\cdot CH_3CN$, not surprisingly the two structures discussed above. $[DabcoH][B(C_6H_5)_4]$ was found to have only two short anion/anion contacts and neither of these had hydrogen bond type geometries. In $[C(NH_2)_3][B(C_6H_5)_4]\cdot CH_3CN$ six such contacts were investigated

and only one was found to have a hydrogen bond geometry (of the single atom type). In both of these structures, the majority (5 of 8 total) of the contacts were clearly H...H type interactions and not hydrogen bonds.

It is suggested that in these two compounds, the anion/anion type C-H...phenyl interactions are of minor importance and make little contribution to the packing of the structures. They appear to be predominantly incidental contacts arising from the optimization of other, stronger interactions in the structures, $(C\text{-}H)_{cation}\cdots(phenyl)_{anion}$ in $[DabcoH][B(C_6H_5)_4]$, $(C\text{-}H)_{solvent}\cdots(phenyl)_{anion}$ in $[C(NH_2)_3][B(C_6H_5)_4]\cdot CH_3CN$ and N-H...π(Ph) hydrogen bonds in both. This is perhaps not surprising. Cation(+1)/anion(-1) contacts would be expected to have more favourable charge distributions than solvent(0)/anion(-1) contacts and both would be expected to be preferred relative to the anion(-1)/anion(-1) contacts, other factors being equal. Also, the large and bulky tetraphenylborate anions would be expected to be more difficult to pack in close proximity to one another, discouraging the formation of multiple, short anion/anion contacts in a structure. It should be easier to form cation/anion or solvent/anion type interactions based on the smaller size of the second component (cation or solvent) and the resulting increased ease of packing.

In ammonium tetraphenylborate and biguanidinium tetraphenylborate, on the other hand, the only source of C-H groups is the anion and only anion/anion type C-H...phenyl contacts can be formed in the structures. Besides the N-H...π(Ph) hydrogen bond(s) formed, these are the only other X-H...phenyl contacts that could possibly have hydrogen bond type geometries.

In $NH_4B(C_6H_5)_4$, two short $(C\text{-}H)_{anion}\cdots(phenyl)_{anion}$ contacts were

located and investigated. One contact was found to be an H...H type interaction, based on its geometry, but the second was found to be a hydrogen bond with a centroid type configuration. Similarly, 12 anion/anion type C-H...phenyl contacts were studied in biguanidinium tetraphenylborate. Eight were found to be H...H type contacts, while four were found to be hydrogen bonds based on their geometries. More specifically, two were found to have centroid type configurations and two were found to be edge type interactions.

It is interesting to note that both compounds form centroid type $(C\text{-}H)_{anion}\cdots(phenyl)_{anion}$ hydrogen bonds while neither $[DabcoH][B(C_6H_5)_4]$ nor $[C(NH_2)_3][B(C_6H_5)_4]\cdot CH_3CN$ were found to. It seems that in these two compounds, which contain only anion/anion type C-H...phenyl contacts, these interactions form hydrogen bonds where possible. Since the anion/anion contacts involve very large and bulky groups, it appears that only a small number can have centroid type hydrogen bond geometries in a given structure. H...H type contacts also often seem to arise as a secondary consequence of the formation of close hydrogen bond type anion/anion interactions. The presence of $(C\text{-}H)_{anion}\cdots(phenyl)_{anion}$ hydrogen bonds with centroid type geometries must be an important feature of both structures. In biguanidinium and ammonium tetraphenylborates, the $(C\text{-}H)_{anion}\cdots(phenyl)_{anion}$ interactions do not have to compete with other types of C-H...phenyl interactions, be they cation/anion or solvent/anion. They can form hydrogen bonds with reasonable geometries whereas in the preceding structures other types of C-H..phenyl interactions were found to be more dominant.

Finally, it is suggested that the $(C\text{-}H)_{anion}\cdots(phenyl)_{anion}$ hydrogen

bond type interactions in biguanidinium tetraphenylborate and ammonium tetraphenylborate play a role in determining the packing of their respective crystal structures. Such interactions were found to be relatively unimportant in [DabcoH][$B(C_6H_5)_4$] and [$C(NH_2)_3$][$B(C_6H_5)_4$]·CH_3CN. The most compelling evidence comes from the structure and packing of biguanidinium tetraphenylborate where the interaction of three different adjacent anions with ring 1 of the original anion has already been described. Each of these anions is oriented such that one ring will interact with ring 1 of the original anion via the formation of at least one $(C\text{-}H)_{anion}\cdots(phenyl)_{anion}$ hydrogen bond. The different anions are arranged so that the $(C\text{-}H)_{anion}\cdots(phenyl)_{anion}$ hydrogen bonds between the rings have the best possible geometries, two are centroid type and two are edge type. Only ring 1 of the anion is involved in all four of the $(C\text{-}H)_{anion}\cdots(phenyl)_{anion}$ hydrogen bonds, serving as the "donor" in all of the interactions. It would definitely appear that formation of such $(C\text{-}H)_{anion}\cdots(phenyl)_{anion}$ hydrogen bonds influences the packing geometry adopted by biguanidinium tetraphenylborate.

A similar situation appears to exist in the structure of ammonium tetraphenylborate. Besides the single, unique N-H...π(Ph) hydrogen bond, formed four times between the cation and two anions, the anion rings are oriented such that the C(14)-H(14) group of each ring (all four rings are equivalent) forms a $(C\text{-}H)_{anion}\cdots(phenyl)_{anion}$ hydrogen bond to the face of a perpendicular ring. The hydrogen bond has a favourable centroid type geometry suggesting that it has been fully optimized in the structure. The packing in ammonium tetraphenylborate appears to have been influenced by the chance of forming and optimizing the geometry of this anion/anion type

C-H...phenyl hydrogen bond.

In conclusion, in structures capable of forming other types of C-H...phenyl interactions, specifically those having hydrogen bond geometries whether cation/anion or solvent/anion type, these other types of interactions appear to be favoured at the expense of anion/anion type contacts. This could arise because of simple charge considerations [cation +1, solvent 0, anion -1], because of size considerations [the tetraphenylborate anion is larger and bulkier than any of the cations or the solvent studied] or some combination of the two. However, in structures where the only possible type of C-H...phenyl interaction is of the anion/anion variety these contacts will form with hydrogen bond geometries where possible. It also appears that in cases where $(C\text{-}H)_{anion}\cdots(phenyl)_{anion}$ hydrogen bonds are formed, they will have an impact on the packing arrangement adopted in the crystal structure. In all four structures C-H...phenyl hydrogen bond type interactions appear to play an important role in determining the crystal packing.

F.H. Allen et al.[82] reached a similar conclusion after studying the low temperature, neutron diffraction based crystal structures of 2- and 3-aminophenol. These structures had previously been investigated using x-ray diffraction and the probable existence of N-H...π(Ph) hydrogen bonds noted, prompting the reinvestigation by Allen et al. Neutron diffraction confirmed the presence of N-H...π(Ph) hydrogen bonds in both compounds (as discussed in detail previously). Interestingly, both structures were also found to contain weak C-H...O and C-H...π(Ph) type contacts, in addition to N-H...π(Ph) and strong N-H...O and O-H...N hydrogen bonds.

Both 2- and 3-aminophenol were found to pack in an arrangement that

the authors describe as the "herringbone" fashion. The herringbone pattern is a well known structural motif, with multiple phenyl/phenyl contacts identified by their T-shaped geometries. An alternative view of this packing arrangement is that centroid type C-H...π(Ph) hydrogen bonds are formed between the phenyl rings involved in the T-shaped interactions and the formation of these additional hydrogen bonds serve to stabilize the structures. The structures of both 2- and 3-aminophenol appear to be influenced by the optimization of a combination of the strong and weak hydrogen bonds, including the C-H...O, C-H...π(Ph) and N-H...π(Ph) interactions. In fact, the authors write "the formation of weaker [N-H...π(Ph), C-H...π(Ph) and C-H...O] bonds would hint that the optimization of the weak interactions rather than formation of N-H...O hydrogen bonds is the primary structural effect in these compounds." Their conclusion is very similar to that reached in this work, on the importance of C-H...π(Ph) hydrogen bonds in the crystal structures of organoammonium tetraphenylborate salts.

Two recent papers by Y. Umezawa et al.[119,120] also discuss the importance of C-H...π(Ph) type interactions in organic compounds. The authors base their conclusions on the results of a Cambridge Structural Database search for X-H...π(Ph) [X = N, O or C] interactions, particularly C-H...π(Ph) contacts. Both intra- and intermolecular interactions were identified and studied, to determine their possible contributions to molecular conformation and crystal packing, respectively. The C-H...π(Ph) interactions were found to play an important role in both instances, the latter being of more interest in relation to this investigation.

The basic results of the CSD search have been described previously.

Most importantly, 75.1% of the structures containing at least one C-H group of any type and at least one six membered aromatic ring were found to form intermolecular C-H...π(Ph) interactions with a minimum contact distance of 3.05Å or less. The mean H(C)...C_{ring} distance for this group was determined to be 2.91±0.12Å. Similar searches revealed that only 5.1% of the OH/π group (mean 2.80±0.21Å) and 9.3% of the NH/π group (mean 2.78±0.19Å) participated in comparable X-H...π(Ph) type interactions. It is reasonable that a much larger proportion of C-H...π(Ph) interactions might be formed, since C-H groups are much more prevalent than N-H or O-H groups in organic compounds. Also, N-H and O-H groups are more likely to participate in hydrogen bonds with "traditional" lone pair acceptors, lessening the probability of their forming X-H...π(Ph) type interactions in many structures. Still, the great abundance of potential intermolecular C-H...π(Ph) interactions in organic compounds led the authors to speculate on the role such interactions might play in determining crystal packing. They wanted to see if the weak C-H...π(Ph) interactions would influence the crystal packing adopted in the structure or if this was determined by other, stronger intermolecular forces. To obtain insight into the nature of the interaction, data were collected for a wide range of possible C-H...π(Ph) interaction geometries.

The H(C) atoms were found to be concentrated at positions above the plane of the aromatic ring with the hydrogen atoms tending to point towards the center of the ring. For many of the C-H...π(Ph) interactions the characteristic distances were observed to be shorter than the sum of the van der Waals radii. However, C-H...π(Ph) interactions were also found to occur at longer distances and their distribution was observed to fall

off only slowly with increasing distance. The C-H...π(Ph) interactions were thus found to be both directionally sensitive and effective over a wide range of distances. This led the authors to suggest that the C-H...π(Ph) interactions do not arise simply a result of dispersion type forces. They describe the interactions as originating largely from a charge transfer (covalent) process, involving donation from the π system of the aromatic ring to the antibonding orbital of the C-H bond. Superimposed on this effect are the weak dispersion forces. The electrostatic forces they describe as not as important but still contributing to the total bond. This is in direct contrast to the results obtained in this work, particularly the conclusions reached after careful examination of the electron density maps, which suggest that C-H...π(Ph) interactions are primarily electrostatic in nature, with perhaps a small covalent component.

The authors also identified a smaller subset of the original CH/π group, containing only structures solved from neutron diffraction data, with accurately located hydrogen atoms. They found that the C-H...π(Ph) interaction geometries in the neutron structures were not significantly different from those in the original group. Every structure in the neutron subset was carefully inspected by the authors to see if the C-H...π(Ph) interaction(s) played a role in the observed crystal packing motif. [A number of these individual structures are discussed in some detail in the publication.[119]] Based on the observations made, the authors conclude that the formation of C-H...π(Ph) type interactions constitute one of the important factors controlling the crystal packing of organic molecules. This conclusion is similar to that reached in this investigation but was

arrived at from a rather different direction. The results of the present experimental study are even more specific, identifying a population of "true" C-H...π(Ph) hydrogen bonds (as opposed to H...H type contacts) that have the greater impact on crystal packing.

3.5. Electron Density Maps

The complete discussion of the analysis of the electron density maps is found in Appendix 3 in the second volume of this thesis. Only brief summaries of the different sections are included in the main text. It seemed reasonable to move this entire section to the Appendix, when length became an issue, for the reason described below.

The multipole refinements carried out in this investigation were begun as a means to generate high quality electron density maps that could be used to study the N-H...π(Ph) hydrogen bonds present in all four structures. The idea was to generate new information about such bonds by carefully examining the maps. The two N-H...N type, conventional hydrogen bonds also present in the structures would be used as a benchmark with which to compare the N-H...π(Ph) hydrogen bonds. Subsequently it was learned that much more quantitative information could be generated from a topological analysis of the experimental electron densities using Bader's theory of "Atoms in Molecules".[14] Analysis of the generated bond paths and the properties of the electron density at the bond critical points provides detailed information about the nature of all the interactions studied. However, observation of the electron density maps generated still provides useful information about the four structures. A general introduction to the features of electron density maps has been

presented previously.

A variety of maps were drawn for each of the four experimental structures. First, maps were plotted in the plane(s) of the cations and the anion phenyl rings. For each compound a complete set of maps covering the entire structure (cation, anion and/or solvent) was generated. Three types of inplane maps were prepared in each case; dynamic deformation density maps, static deformation density maps and residual electron density maps were plotted in each required plane. The nature of each type of map has been discussed in the introduction (Table 1). Maps are included as figures in the discussion where they are specifically referenced. A complete set of all maps for all the structures is available upon request.

The contour interval chosen for the inplane maps was 0.05 e/Å^3, increasing (solid contours) and decreasing (dashed contours) at this constant interval from the zero level contour (..._...._). The only exception made was in the static maps of the phenyl ring planes where a contour interval of 0.10 e/Å^3 proved more appropriate.

The static and dynamic deformation density maps convey essentially the same information. However, the former are often preferred for discussion purposes, the effects of thermal motion having been removed. After a general comparison of the two types of maps in the four structures, only the static maps will be discussed in detail. In fact, in the second set of maps, generated to study the hydrogen bonding interactions, only the static maps were plotted.

The second group of maps prepared were cuts through all the phenyl rings of the tetraphenylborate anions in the four experimental structures. These cuts were made perpendicular to the phenyl ring planes, through

either opposing ring C-C bonds or through opposing C_{ring} atoms. A phenyl ring occupying entirely general positions requires three cuts of each type to be totally defined. The static deformation density perpendicular cuts were all drawn with a contour interval of 0.05 e/Å^3, like the majority of the inplane maps. However, the first positive contour was drawn at the +0.015 e/Å^3 level, to better illustrate regions of low density such as might be observed in weak interactions. The perpendicular cuts through the anion phenyl rings were generated in an attempt to observe any changes in the distribution of the electron density in the rings brought about by their participation in X-H...π(Ph) [X = N or C] type interactions as either donor or acceptor groups.

The perpendicular cuts were defined by specifying the plane required using only carbon atoms from the ring. However, any possible interacting N-H and/or C-H groups were also always included (generated by symmetry where necessary) in the original map. Once the original map had been examined, any of these groups not in a position to interact with the ring in the plane drawn and the remaining rings of the tetraphenylborate anion were removed for simplification. The results from the examination of the perpendicular cuts will be discussed in terms of the X-H...π(Ph) type interactions, after the inplane results have been presented.

3.5.1. Tetraphenylborate Anions - Inplane Maps of the Phenyl Rings

3.5.1.5. Summary

Overall, the maps drawn in the planes of the anion phenyl rings in the four structures studied, whether static, dynamic or residual, are excellent. The maps of $NH_4B(C_6H_5)_4$ and $[N(C[NH_2]_2)_2][B(C_6H_5)_4]$ are, in

general, slightly better than those of the other two structures, although the static map of $NH_4B(C_6H_5)_4$ does show low electron density on the C-H bonds of the ring for some reason. The dynamic and static maps of $[C(NH_2)_3][B(C_6H_5)_4]\cdot CH_3CN$ exhibit a lack of electron density on all the bonds, and a more uneven distribution of the density that is present, detracting from their appearance. In contrast, the dynamic and static maps of [DabcoH][$B(C_6H_5)_4$] suffer from poor alignment of the contours on the bonds and the displacement of the bond maxima from their expected positions. This led to the suspicion that the multipole parameters might not have been assigned completely correctly on some of the atoms in this structure. The residual maps of the [DabcoH][$B(C_6H_5)_4$] anion were also poorer than those of any other structure, another sign of problems in the refinement, likely arising from a lower quality data set. However, the real value of this investigation comes not from the fact that four individual structures have been studied, but from the cumulative knowledge gained by combining the results from four related compounds. The total information generated by comparing and contrasting the individual results from the four structures is greater than the sum of the independent parts.

3.5.2. Cation - Inplane Maps

3.5.2.5. Summary

The results obtained after analysis of the inplane maps for the cations of the four compounds investigated experimentally are not as consistent as the results obtained for the corresponding anions. This is not surprising considering that four different cations are involved, while each structure contains the same anion. Also, the cations studied are

considerably smaller than the tetraphenylborate anion, sometimes making them more difficult to model accurately. This could account for many of the inconsistencies observed.

Overall, the cation of the $[N(C[NH_2]_2)_2][B(C_6H_5)_4]$ structure was judged to have the best maps, being both self-consistent and consistent with the anion results from the same structure. Some unevenness was observed in the density distribution on the bonds of the cation but otherwise the maps were of reasonable quality with well defined features. The question remains as to whether the density differences observed on the bonds of all the cations are artifacts of the refinements or whether they arise as a consequence of the hydrogen bonds in which the cations participate. The likelihood that the latter is true appears to be minimal, except perhaps for the N-H bonds, based on the lack of evidence observed in the inplane static maps of the cations.

Considering the maps of the rings in the tetraphenylborate anions, those of the ammonium and biguanidinium structures were found to be of higher overall quality than those of the DabcoH$^+$ and guanidinium structures. The biguanidinium cation was also judged to have the best maps of the four cations studied. The inplane maps of the cation in $NH_4B(C_6H_5)_4$ suffer from smearing of the electron density around the cation, thought to arise from rotation of the cation in the crystal structure. The guanidinium and DabcoH$^+$ cation maps show problems on the contours of several of the bonds, with double maxima attributed to multipole populations being incorrectly assigned on some atoms. The $C(NH_2)_3^+$ and DabcoH$^+$ maps also did not show the consistent trends expected on going from the dynamic to the static maps. The results suggest that, like the anion

maps, the cation maps of [DabcoH] $[B(C_6H_5)_4]$ and $[C(NH_2)_3][B(C_6H_5)_4]\cdot CH_3CN$ are of slightly lower overall quality than those of $[N(C[NH_2]_2)_2][B(C_6H_5)_4]$, with the maps of the $NH_4B(C_6H_5)_4$ cation left out of the ranking because of the motion problems they exhibit.

3.5.3. Hydrogen Bonds in the Electron Density Maps

3.5.3.1. N-H...N Hydrogen Bonds

The investigation of the N-H...X [X = N or π(Ph)] hydrogen bonds in the four structures studied experimentally located two N-H...N type hydrogen bonds and 14 N-H...π(Ph) type hydrogen bonds. Of these, the N-H...N type interactions would be expected to be the stronger, since the lone pair at nitrogen is a better acceptor than the π electrons of the phenyl ring. The geometric investigation of the N-H...X hydrogen bonds also showed the N-H...N type contacts to have short H(N)...N distances, indicative of stronger interactions compared to the N-H...π(Ph) contacts. In the N-H...π(Ph) interactions the H(N)...π_c ring centroid distance was sometimes found to be shorter than the H(N)...N distances. However, the minimum H(N)...C_{ring} distance was always longer than the H(N)...N distances characterizing the N-H...N hydrogen bonds. Thus, by all criteria the N-H...N type interactions are the strongest studied and their static maps were the first investigated.

3.5.3.1.1. Summary

Of the two N-H...N hydrogen bonds studied in this work, that in the structure of $[C(NH_2)_3][B(C_6H_5)_4]\cdot CH_3CN$ was predicted to be the stronger based on its geometry. The N(1)-H(1B)...N(4) hydrogen bond is formed

between the guanidinium cation and the acetonitrile solvent molecule, with the lone pair of electrons on N(4) acting as the hydrogen bond acceptor. Importantly, this hydrogen bond is not linear but is significantly bent.

To investigate the N(1)-H(1B)...N(4) hydrogen bond a static map was drawn in the plane defined by N(1) of the cation and N(4) and C(2) of the acetonitrile molecule, a plane not far different from that of the guanidinium cation itself. The static map clearly shows that the contours of the N(1)-H(1B) bond of the cation are shared with the contours arising from the lone pair on N(4) of the solvent molecule. The outermost contour is common, spanning the area between the two groups. Electron density has been moved into the area between N(1)-H(1B), the hydrogen bond donor, and N(4), the hydrogen bond acceptor. This concentration of electron density in the area between the interacting groups shows that the hydrogen bond must have a significant covalent component. However, significant charge depletion is also observed at H(1B) in the static map, where a hole of four negative contours is visible. The hydrogen bond, therefore, likely has a sizable electrostatic component as well.

The static map drawn in the plane of the N(1)-H(1B)...N(4) interaction from the $[C(NH_2)_3][B(C_6H_5)_4]\cdot CH_3CN$ structure is an excellent example of a relatively strong hydrogen bond which visibly exhibits both covalent and electrostatic features. The fact that the hydrogen bond is not linear does not appear to significantly diminish its strength. The nonlinearity actually aids in showing the concentration of electron density in the region between the interacting groups, a feature often not clear in the maps of linear hydrogen bonds. The perturbation of the bonding electron density into the region between the interacting groups

is seen only in the maps of strong hydrogen bonds. Maps of N-H...X type hydrogen bonds strong enough to contain a visible covalent component contribution are not common in the literature. The best literature examples tend to have been described for strong O-H...O hydrogen bonds, but these are undoubtedly stronger than the present example, even though the maps share many common features. The static map drawn in the plane of the N(1)-H(1B)...N(4) interaction from the $[C(NH_2)_3][B(C_6H_5)_4]\cdot CH_3CN$ structure is an important contribution to the current volume of static maps detailing hydrogen bonding interactions of different types.

The second N-H...N type hydrogen bond studied in this investigation was located in the structure of biguanidinium tetraphenylborate where it was found to hold the cation dimer together. The N(4)-H(4A) group of one cation serves as the hydrogen bond donor while the lone pair at N(1) of a symmetry related cation (inversion) serves as the hydrogen bond acceptor and vice versa. The geometry of this hydrogen bond suggests that it is the weaker of the two N-H...N contacts studied, however, it is a much more linear interaction.

The static map drawn to emphasize the N(4)-H(4A)...N(1) hydrogen bond was plotted in a plane defined by N(1) and N(4) of the original cation and C(2) of a symmetry related cation. The map drawn clearly shows that the density on the N(4)-H(4A) bond is not visibly involved in the hydrogen bonding interaction, in contrast to the guanidinium case. The contours on the N(4)-H(4A) bond are somewhat unsymmetrical, being elongated perpendicular to the bond more in one direction than the other but they remain discrete. They do not curve down toward, or join with, the lone pair density on N(1) of the second cation in any way. There is no

significant indication in the N(4)-H(4A) bond contours of their having been affected by participation in the N-H...N hydrogen bond.

A large diffuse hole, four contours in depth, is visible beyond H(4A) in the region between N(4)-H(4A) and the lone pair density on N(1) in the hydrogen bond static map. This indicates a significant electrostatic component in the N(4)-H(4A)...N(1) hydrogen bond of biguanidinium tetraphenylborate, which is typical of a normal to weaker strength hydrogen bond. It is more difficult, however, to discern whether there is a covalent component to this hydrogen bond which makes itself evident in the static map drawn. Because the hydrogen bond is essentially linear, the lone pair density at N(1) naturally lies on the interaction line. There is no need for it to be perturbed into a new area for it to lie between the two interacting groups (unlike the guanidinium case), if a covalent contribution is involved in this hydrogen bond. It does appear that the contours arising from the lone pair at N(1), although regularly shaped, are somewhat diffuse, being expanded toward H(4A) of the second cation. This likely indicates that there is some covalent character in the N(4)-H(4A)...N(1) hydrogen bond, however, it also appears that it must be relatively slight. The biguanidinium tetraphenylborate maps were judged to be the best of the four compounds studied experimentally so the small effects visible in this map are likely to be true features and not artifacts of the refinement.

The N(4)-H(4A)...N(1) hydrogen bond static map in the structure of $[N(C[NH_2]_2)_2][B(C_6H_5)_4]$ is more like the maps expected for "normal" strength hydrogen bonds from the literature survey. Effects observed in the map and attributed to the covalency of the interaction are minor at best. The

N(4)-H(4A)...N(1) hydrogen bond is likely predominantly electrostatic in nature with a small covalent component. This is in contrast to the N(1)-H(1B)...N(4) hydrogen bond in the $[C(NH_2)_3][B(C_6H_5)_4]\cdot CH_3CN$ structure which was found to have a more significant covalent component, with clearly visible features in the static map drawn.

3.5.3.2. X-H...π(Ph) Hydrogen Bonds [X = N or C]

Although significant features attributable to the N(1)-H(1B)...N(4) hydrogen bond were observed in the $[C(NH_2)_3][B(C_6H_5)_4]\cdot CH_3CN$ static maps, only small effects were observed in the static maps drawn to study the N(4)-H(4B)...N(1) hydrogen bond in the $[N(C[NH_2]_2)_2][B(C_6H_5)_4]$ structure. If the stronger N-H...N hydrogen bonds can have such minimal visible effects on the static maps, what influence would the normally weaker X-H...π(Ph) [X = N or C] hydrogen bonds be expected to show? If minor changes were to occur in the maps because of the formation of such interactions, would they be consistent and identifiable? Or, would they remain mixed with background noise and artifacts of the refinement process, such that they could not be singled out as characteristic features of the X-H...π(Ph) type interactions? In an attempt to answer these questions, it seemed most reasonable to begin with the structure found to have the best inplane maps for both the cation and the anion, biguanidinium tetraphenylborate. If characteristic features were identified in these maps, the maps of the other structures could then be compared to see if they showed the same effects. Overall, the same changes should be consistently observed in all the static maps where such contacts occur, if they are truly characteristic of X-H...π(Ph) interactions.

Two types of maps were plotted to investigate the effect of the X-H...π(Ph) [X = N or C] interactions on the electron density distributions of the phenyl rings of the $B(C_6H_5)_4^-$ anions in the four experimental structures. In the first set of static maps, perpendicular cuts were made through opposing C-C bonds of the phenyl ring planes. Three cuts were made through each ring (if it occupied general positions) so that the contours of every C-C ring bond would be (approximately) bisected. In the second set of maps drawn, the cuts were made vertically through a pair of opposing ring carbon atoms. Again, three different cuts were required to completely define each phenyl ring occupying totally general positions. Every unique phenyl ring and its X-H...π(Ph) interactions, in every anion, in the four structures studied were analyzed from the complete set of static maps of both types plotted.

3.5.3.2.1. Summary

Interpretation of the static maps plotted to investigate the X-H...π(Ph) [X = N or C] interactions formed in the four experimental structures proved difficult for a variety of reasons. The maps were found to contain many features, not all of which could be assigned to the hydrogen bonds formed, "true" features being intermingled with peaks arising for a variety of other reasons. In addition, different interactions were found to give rise to effects differing in origin, position and magnitude in the maps, depending on the nature and the strength of the hydrogen bond formed. All of this made analysis of the maps difficult. However, a variety of characteristic features were identified and these were shown to be consistently observed when similar

strength X-H...π(Ph) hydrogen bonds are present in the static maps of the anion phenyl rings.

In the first maps studied, the inplane static maps of the cations and the anions, no correlation was found between the observed bond densities and the formation of X-H...π(Ph) hydrogen bonds. The density on the C-C bonds of the anion phenyl rings was often observed to be somewhat uneven around a given ring in a given structure, however, the variation could not be shown to be related to the X-H...π(Ph) hydrogen bond(s) formed to that ring. Similarly, the variation in the average C-C bond density, between rings in the anion of a given structure and the variation observed between the four experimental structures, could not be correlated with the various combinations of X-H...π(Ph) hydrogen bonds formed. The density observed on the N-H bonds of the cations and that on the C-H bonds of groups participating as donors in C-H...π(Ph) type hydrogen bonds, were again not obviously correlated with the X-H...π(Ph) hydrogen bonds nor with their strengths.

Two different types of static maps were plotted in planes perpendicular to the anion phenyl rings, to illustrate and study the X-H...π(Ph) hydrogen bonds formed in the four structures. In the first group of maps, the plane bisects a pair of opposing C-C ring bonds, while in the second it passes through a pair of opposing ring carbon atoms. Analysis of the combination of the two complete sets of maps allowed the following conclusions to be reached.

The features arising from C-H...π(Ph) interactions in the static maps will be discussed first since they form a relatively consistent group. Generally only C-H...π(Ph) interactions with hydrogen bond type

geometries are ever clearly visible in the maps drawn. Overall, the formation of C-H...π(Ph) interactions of any type appears to have little effect on the electron density of the interacting groups in all of the static maps plotted. The contours on the C-H bonds of the donor groups are not visibly perturbed in the static maps; they remain regular, symmetrical and well centered on the bonds. Charge depletion is observed, in the area towards the anion ring, at every H(C) atom that participates in a C-H...π(Ph) hydrogen bond, a feature characteristic of an electrostatic interaction.

It was possible to study the maps of several anion phenyl rings involved as the acceptor in only C-H...π(Ph) interactions from the four structures investigated (rings 2 and 3 in [DabcoH][$B(C_6H_5)_4$] and ring 1 in [$C(NH_2)_3$][$B(C_6H_5)_4$]·CH_3CN). These maps also showed only minimal effects (at best) that were consistently observed and could be attributed to the C-H...π(Ph) interactions made to the ring. The only regularly observed feature was a slight diffuseness/expansion of the outermost contour on all of the C-C bonds of the interacting ring. No characteristic features were identified in the maps drawn through opposing ring carbon atoms. All of the maps suggest that the C-H...π(Ph) interactions are almost completely electrostatic in nature, with possibly a very small covalent component.

The N-H...π(Ph) interactions were found to give rise to quite different effects in the static maps drawn, illustrating the fact that they do differ in a substantial way from the C-H...π(Ph) interactions. The differences observed in the map features for the two type of interactions suggest that the effects observed are real and characteristic of each group. The maps drawn to study the N-H...π(Ph) hydrogen bonds also show

varying effects depending on the strength of the interaction formed. The features observed range from very minor to large and extensive, involving the entire phenyl ring of the anion acceptor.

The N-H bond density, in both types of phenyl ring maps, is consistently perturbed when involved in an N-H...π(Ph) interaction. In the maps, the N-H contours tend to be elongated more on one side of the bond than the other, such that they no longer remain well centered on the bond. The contours are drawn down off the bond towards the ring plane, to an extent that appears to be related to the strength of the interaction formed. In the stronger interactions, the density on the cation N-H bond is usually more obviously perturbed. The outer N-H bond contour is often more distorted, pulled further off the bond towards the anion ring plane. In the most extreme case, ring 3 in the anion of $[C(NH_2)_3][B(C_6H_5)_4]\cdot CH_3CN$, the electron density of the cation N-H bond actually meets and is shared with density arising from the anion ring. Accumulation of electron density between the interacting groups, visible in the static maps, is indicative of a covalent contribution to the hydrogen bond being formed. The fact that the N-H...π(Ph) hydrogen bonds have an even larger electrostatic component is evident in the large areas of significantly depleted charge observed in the static maps at every interacting cation H(N) atom and oriented toward the phenyl ring plane of the anion.

In the maps drawn, in planes cut perpendicular to the anion phenyl rings through opposing C-C bonds, a certain diffuseness/expansion was observed on the outer C-C bond contours when the ring was found to participate in N-H...π(Ph) hydrogen bond(s). This diffuseness is visible and relatively equal on all the C-C bonds around the interacting ring. It

is also observed to be relatively equal both above and below the ring plane, regardless of the face to which the interaction(s) is made. A very similar effect was observed for all the X-H...π(Ph) interactions studied [X = N or C], making it difficult to correlate the magnitude of this feature with the strength of the interaction(s) made to the ring. This was further complicated by the fact that the diffuseness observed on the outer C-C bond contours appears also to be related to the original bond density. Still, diffuseness of the outer C-C bond contours around the phenyl ring is a feature consistently observed in the static maps plotted through pairs of opposing C-C bonds, in rings accepting X-H...π(Ph) hydrogen bonds.

It is the cuts made through pairs of opposing anion phenyl ring carbon atoms that most clearly show the effects of the N-H...π(Ph) interactions on the electron density distribution of the ring. The features observed in these maps vary quite consistently and characteristically with the strength of the interaction formed. The strength of an N-H...π(Ph) hydrogen bond was first estimated from its geometry, particularly the minimum H(N)...C_{ring} distance(s), and later was determined from the bond path and the properties of the electron density at the bond critical point.

The weakest N-H...π(Ph) hydrogen bonds investigated, normally do not give rise to any visible features in the static maps drawn through pairs of opposing ring carbon atoms. This was found to be especially true of isolated interactions, single weak interactions made to one face of an anion ring. No peaks are observed in the maps, in the middle region between the ring plane and the interacting N-H group of the cation. No

specific deformations of the density on any of the ring bonds (C-C, C-H or C-B) are observed either.

Other peaks are often observed in these maps but not in areas considered characteristic of the N-H...π(Ph) interactions. These peaks tend to lie right on, or very close to, the ring plane. There is never any obvious pattern in their number and distribution around the ring. They tend to complicate the maps and make the analysis more difficult but they can usually be differentiated from the "true" peaks arising from the N-H...π(Ph) interactions. The spurious peaks arise for a number of different reasons, from poor assignment of the multipoles on the ring carbon atoms to their being artifacts of the refinement process.

As the N-H...π(Ph) hydrogen bonds become somewhat stronger, new features, attributed to the interaction, become visible in the static maps. The first characteristic feature usually observed is a single small peak (1 contour) lying somewhat off of the ring plane at one of the ring carbon atoms. This peak is normally observed at that ring carbon atom making the closest contact with the H(N) atom of the interacting cation and will lie directly between those two groups. Only one peak arising from the weak interaction is usually observed for each ring, so a peak is observed in only one of the three map planes drawn, that cut where the appropriate ring carbon atom is bisected.

There is some overlap between these first two groups of N-H...π(Ph) hydrogen bonds, those weak interactions which do not show features (peaks) in the static maps and those slightly stronger interactions that do (sometimes slightly stronger interactions show no features while other times slightly weaker interactions do). This most likely has to do with the way

the map planes are defined and with the fact that the peaks involved are of only very low density, normally only one contour or +0.015 e/Å^3. The maps are not plotted exactly in the planes of the N-H...π(Ph) hydrogen bonds; this would be impossible since the nature of the acceptor is ill-defined. Rather, the maps are defined using the phenyl ring carbon atoms themselves. There will often be a slight discrepancy between the map plane and the plane of the N-H...π(Ph) hydrogen bond, that plane in which electron density is actually shared between the cation and the anion. Because of the very low levels of electron density involved, peaks lying even slightly out of the map plane have a good chance of not being observed. If a peak is observed, it represents a visible accumulation of electron density between the interacting anion phenyl ring and the N-H group of the cation, characteristic of a covalent component in the hydrogen bond. Again, only a very low level of electron density is actually shared between the two groups, usually a peak of one contour or +0.015 e/Å^3 is observed, meaning that the hydrogen bond remains predominantly electrostatic. However, N-H...π(Ph) hydrogen bonds do contain a covalent contribution which appears to increase somewhat with the strength of the interaction.

As the N-H...π(Ph) hydrogen bonds become even stronger, or if two weak interactions act in a concerted fashion to a single ring face (the "pincer" type arrangement of bonds in particular), even more prominent features are observed in the static maps drawn through opposing ring carbon atoms. In addition to peaks at the appropriate ring carbon atoms (which may or may not be observed depending on the geometry of the interaction), perturbation of the σ electron density on certain of the

ring bonds becomes evident in the maps. For example, the C(11)-B(1) bond density is visibly distorted towards the cation in the static maps of $NH_4B(C_6H_5)_4$ because of the N(1)-H(1)...ring 1 hydrogen bond formed in the structure, the third strongest studied overall. A similar perturbation of the C(21)-B(1) bond density, and also of the adjacent C(26)-H(26) bond density, is observed in the static maps of ring 2 from the structure of $[C(NH_2)_3][B(C_6H_5)_4]\cdot CH_3CN$. In this case, two weaker N-H...π(Ph) interactions are formed to one face of the anion ring but they appear to act in a concerted fashion to give rise to the significant features observed in the maps. Electron density, at least partially from σ bonds of the anion phenyl ring, is visibly perturbed into the region between the two interacting groups, suggesting an even larger covalent contribution to these hydrogen bonds. In this group, only one or two specific atom(s) and/or bond(s), in one distinct region of the anion ring, are visibly involved in the interaction made with the cation, not the entire ring. These are normally the atom(s)/bond(s) lying closest to the cation, as predicted from the geometry of the interaction.

In the very strongest N-H...π(Ph) hydrogen bonds studied in this work, the electron density of the entire phenyl ring is visibly perturbed because of the interaction(s) it accepts. The strongest individual N-H...π(Ph) hydrogen bond is formed to ring 2 in the $[N(C[NH_2]_2)_2][B(C_6H_5)_4]$ structure and it gives rise to such significant features in the static maps plotted. The second strongest N-H...π(Ph) hydrogen bond investigated is made to ring 3 in the structure of $[C(NH_2)_3][B(C_6H_5)_4]\cdot CH_3CN$. However, the maps of ring 3 have the most prominent features observed in any of the static maps drawn for the anion phenyl rings in the four experimental

structures. This presumably occurs because there are actually two hydrogen bonds formed to one face of ring 3 in a "pincer" type arrangement and these act in a concerted fashion on the electron density of the phenyl ring acceptor, causing the large effects observed in the maps. In fact, in the ring 3 maps of $[C(NH_2)_3][B(C_6H_5)_4]\cdot CH_3CN$, the electron density on the cation and anion is so greatly perturbed that it actually meets and is shared in the area between the two interacting ions.

In the strongest N-H...π(Ph) hydrogen bonds, the entire anion ring is visibly involved in the interaction. Peaks at ring carbon atoms and/or perturbation of the σ bond density (C-H or C-B) is observed all around the phenyl ring. Where C-H bonds are involved, the outer bond contour curves over/under the ring plane to form a lobe of electron density lying between the anion and the N-H group of the cation. The peaks observed also lie well off of the ring plane, between the ring carbon atom involved and the cation. Normally one feature or the other (not both) is observed at every carbon atom of the ring.

Participation of the σ electron density of the anion phenyl ring C-H and C-B bonds in the N-H...π(Ph) type hydrogen bonds has never before been demonstrated or even postulated. The features observed in the maps from this investigation, for two different rings in two different structures, suggest that in the strongest such interactions the σ electron density of the ring does become involved. In addition to the π electron density of the aromatic ring, the "traditional" acceptor of the N-H...π(Ph) hydrogen bond, the σ electron density is perturbed all around the ring in the strongest interactions. The magnitude of the features observed also suggest that the covalent contribution to the N-H...π(Ph) hydrogen bond

is larger in the stronger interactions.

There are no electron density maps illustrating X-H...π(Ph) hydrogen bonds [X = O, N or C] available in the literature with which the experimental results might be compared. However, the present results do fit reasonably well with the maps and features described for hydrogen bonds with traditional acceptors (summarized in the introduction) being only somewhat weaker in most instances. The fact that such consistent and similar results were observed for the 14 N-H...π(Ph) hydrogen bonds and 12 unique anion phenyl rings in the four different structures investigated in this work, supports the idea that the conclusions reached are valid.

A 1997 book by P. Coppens, "X-ray Charge Density and Chemical Bonding",[6a] includes a chapter on electron density structures of molecular crystals, in which electron density maps and the effect of hydrogen bonding on those maps are discussed. In it the author writes "the induced polarization of the [hydrogen bond] acceptor density towards the H atom is apparently still present for the longer distances, but very diffuse and below the lowest contour level on most maps." It is being suggested that a covalent contribution is still made in weak hydrogen bonds but that it may be too small to be observed in the maps plotted under normal circumstances. The present results support this observation. The static electron density maps drawn to investigate the weak X-H...π(Ph) hydrogen bonds were plotted with an extra, low level positive contour (+0.015 e/Å^3) included. In many cases, this allowed perturbation of the electron density on the groups involved in the hydrogen bonding interaction to be observed in the maps, perturbation that might otherwise not have been visible. Even though the X-H...π(Ph) hydrogen bonds investigated were weak, they often

gave rise to visible effects in the static maps (as had been predicted by Coppens) when an extra, low level contour was drawn. This substantiates the idea that a covalent contribution, though it may be small, is still present in even very weak hydrogen bonds. The results from this study also suggest that for some X-H...π(Ph) hydrogen bonds the covalent contribution may be significant.

In most cases, the features observed in the static maps plotted can be directly correlated with the geometry of the N-H...π(Ph) interaction(s) made to the ring. Only the very strongest N-H...π(Ph) hydrogen bonds studied affect the electron density of the entire anion phenyl ring. The weaker hydrogen bonds tend to visibly affect only the geometrically closest ring carbon atoms. In the static maps, features are observed only at specific ring carbon atoms and/or bonds, rather than distributed around the entire ring. The "principal" acceptor of the hydrogen bond may be an isolated fragment of the ring, an atom or a bond, rather than the complete ring. As already has been shown, this can be predicted reasonably well from the geometry of the interaction. It will be shown subsequently that the map features observed (and the geometry of the interaction) are also directly related to the bond path of the hydrogen bond and its properties at the bond critical point.

3.6. Topological Analysis of the Electron Density

3.6.1. Introduction

According to Bader's theory of "Atoms in Molecules" if two atoms are to be considered bonded, a necessary condition is the existence of a (3,-1) critical point and a bond path between the two interacting centers,

indicating that electronic charge density is accumulated between the nuclei that are so linked. However, a bond path does not necessarily represent a bond in the traditional sense. A bond path will be associated with all types of interatomic interactions including hydrogen bonds and van der Waals contacts (H...H type contacts). The strength and nature of the interaction can then be characterized by the value of various properties ($\rho_b(\mathbf{r})$ - the electron density, and $\nabla^2\rho_b(\mathbf{r})$ - the Laplacian of the electron density) at the bond critical point.

If the interactions predicted by geometry, whether N-H...X or C-H...X [X = N or π(Ph)] hydrogen bonds or H...H type contacts, are true interactions they must be defined by a rational bond path, joining the "donor" and "acceptor" groups of the contact and a (3,-1) bond critical point. The electron density calculated from the final multipole parameters in all four structures was searched for critical points in the regions of all the geometrically predicted interactions. The XDPROP program of the XD package[9] was employed for the search using the method described in the experimental section. Once a (3,-1) bond critical point had been located, XDPROP was again used to calculate the associated bond path.

A total of 17 potential N-H...X type interactions and 43 potential C-H...X type interactions were identified in the geometry search, carried out to locate H...X contacts of 3Å or less, for a total of 60 possible interactions in the four experimental structures. Of the 17 proposed N-H...X interactions, 2 N-H...N type and 15 N-H...π(Ph) type contacts were predicted from the geometries. There are only 16 unique N-H groups in the cations of the four structures (1 in $NH_4B(C_6H_5)_4$, 1 in [DabcoH][$B(C_6H_5)_4$], 6 in $[C(NH_2)_3][B(C_6H_5)_4]\cdot CH_3CN$ and 8 in $[N(C[NH_2]_2)_2][B(C_6H_5)_4]$). The results

of the geometry search suggest that one N-H group must be involved in a bifurcated hydrogen bond. This was determined to be the N(2)-H(2A) group of the cation in the structure of $[N(C[NH_2]_2)_2][B(C_6H_5)_4]$. The N(2)-H(2A) group was found to make close physical contact with all of the ring 2 carbon atoms of a $B(C_6H_5)_4^-$ anion, typical of a centroid type hydrogen bond. In addition, N(2)-H(2A) was also found to make one contact of less than 3Å with C(11) of ring 1 from the same anion [H(2A)...C(11) = 2.962Å]. When the bond path and critical point search was carried out, the N(2)-H(2A)...ring 2 interaction was readily characterized (and found to be the strongest of the experimental N-H...π(Ph) hydrogen bonds). However, no bond path could be located for the second proposed component of the bifurcated hydrogen bond [N(2)-H(2A)...ring 1]. The results indicate that the N(2)-H(2A) group does not, in fact, participate in a bifurcated hydrogen bond. Instead, it serves as the donor group in only a single, relatively strong hydrogen bond, N(2)-H(2A)...ring 2. This fits with the rest of the data collected; all other N-H groups were found to participate in one single, unbranched N-H...X type hydrogen bond [X = N or π(Ph)]. There is no reason to expect that the strongest N-H...π(Ph) hydrogen bond formed in this work should be bifurcated. Rather, it is likely that the relatively close contact made between H(2A) and C(11) of ring 1 in the anion is incidental, arising as a secondary consequence of the very strong N(2)-H(2A)...ring 2 hydrogen bond in $[N(C[NH_2]_2)_2][B(C_6H_5)_4]$. It is not surprising that a bond path could not be located for the second component of the proposed bifurcated hydrogen bond.

Bond paths were located for all of the remaining 16 N-H...X interactions (1 per unique N-H group), as were (3,-1) type bond critical

points. Only two of these interactions were determined to have bond paths that were unusual in any major respect. The N(1)-H(1)..ring 1 hydrogen bond in $NH_4B(C_6H_5)_4$ and the N(3)-H(3B)...ring 4 hydrogen bond in the structure of $[N(C[NH_2]_2)_2][B(C_6H_5)_4]\cdot CH_3CN$ were both found to have bond paths originating from the nitrogen atom rather than the hydrogen atom of the cation N-H group. This is in contrast to all of the other N-H...X bond paths which clearly originate from the hydrogen atom of the donor group. The behaviour of the bond paths in the region of the "acceptor" groups was found to vary widely, but quite consistently and predictably, as will be discussed in the following section.

Of the 43 potential C-H...X interactions [X = N or phenyl] identified in the geometry search, 9 were predicted to be C-H...N type and 34 were predicted to be C-H...phenyl type contacts. Rational bond paths and (3,-1) type bond critical points were located for all but one of these possible interactions, confirming their formation in the four structures studied. The one exception noted, the only physically close C-H...phenyl contact for which no bond path could be located, was identified in $[DabcoH][B(C_6H_5)_4]$. Based on its geometry, an edge type hydrogen bond was predicted for the $[C(3)\text{-}H(3A)]_{cation}\cdots[ring\ 1]_{anion}$ interaction [H(3A)...C(13) = 2.894Å, H(3A)...C(14) = 2.918Å], with possible involvement of the H(13) and H(14) ring atoms as well. However, no bond path could be found for this proposed interaction. As will be described in more detail later, an unfavourable configuration likely precludes formation of an interaction in this case. The remaining 42 C-H...phenyl type interactions located in the geometry search were all confirmed and characterized using their bond paths and properties at the

bond critical points.

Of the 60 possible interactions originally identified in the geometry search, a total of 58 were substantiated by location of their bond paths and (3,-1) type bond critical points. However, during the bond path search involving the C-H groups of the methyl functionality in the acetonitrile solvent molecule of $[C(NH_2)_3][B(C_6H_5)_4]\cdot CH_3CN$ an interesting observation was made. Although the geometry search had suggested the formation of three $(C\text{-}H)_{solvent}\cdots(phenyl)_{anion}$ type contacts (as expected), a total of five bond paths (and bond critical points) were actually located. This unusual situation, possibly arising because of rotation of the CH_3CN methyl group in the solid state, will be discussed in more detail later. Three of these five bond paths were found to be rather uncommon as well, beginning from C(3) of the CH_3CN methyl group rather than from a hydrogen atom; all other C-H...phenyl interactions were found to have bond paths originating at the H atom of the C-H donor group. Thus, overall, a total of 60 interactions were characterized in the four experimental structures (16 N-H...X and 44 C-H...X [X = N or phenyl]). These proved to be slightly different from the 60 potential interactions first identified in the geometry search. Of the 60 confirmed interactions, 5 were found to have unusual bond paths in the region of the X-H donor group (2 N-H type and 3 C-H type), beginning from the X atom rather than the expected H atom. The bond paths were observed to exhibit a wide variety of behaviours in the region of the "acceptor" groups, as will be described in the next section.

The properties of the electron density, $\rho_b(\mathbf{r})$, and the Laplacian of the electron density, $\nabla^2\rho_b(\mathbf{r})$, at the bond critical points have been used

to characterize the different interactions investigated. The results will be discussed in detail later. However, the observed bond paths themselves have also been analyzed to extract any useful information about the nature of the interactions studied, particularly in comparison to their individual geometries. Tables have been prepared summarizing the results obtained for each of the 60 bond critical point [(3,-1) type] and bond path searches carried out in the four experimental structures. These tables include not only the properties of the electron density at the bond critical points but also the position of the bond critical point in relation to the groups participating in the interaction. The interactions studied in ammonium tetraphenylborate are summarized in Table 7 of the main text [N-H...π(Ph)] and Table 23 of Appendix 4 [C-H...phenyl]. The N-H...π(Ph) interaction located in the structure of [DabcoH][$B(C_6H_5)_4$] is summarized in Table 9, while the C-H...N and C-H...phenyl (cation/anion type), and the C-H...phenyl (anion/anion type) interactions are found in Appendix 4, Tables 31 and 33 respectively. For guanidinium tetraphenylborate acetonitrile solvate Table 11 lists the N-H...X [X = N or π(Ph)] interactions and Appendix 4 Tables 41 and 43 the C-H...N and C-H...phenyl (solvent/anion type), and the C-H...phenyl (anion/anion type) interactions, respectively. Finally, the biguanidinium tetraphenylborate interactions are summarized in Table 13, N-H...X type, and Tables 51 and 53 of Appendix 4, C-H...N and C-H...phenyl (anion/anion type). Having completely defined the geometry of each interaction, including its bond critical point, a detailed comparison with the observed bond path becomes possible.

3.6.2. Bond Paths

3.6.2.1. Introduction

To briefly summarize the results that will be detailed in the following section, H...H type contacts, intermediate type contacts and hydrogen bonds have all been found to have different, distinct bond paths, each characteristic of the specific type of interaction. Analysis of the bond paths allowed the interaction type to be readily and consistently identified. The results obtained from the bond path analyses are in close agreement with the identifications made on the basis of the interaction geometries (from atomic positions). In fact, the geometric criteria previously developed have been refined and narrowed further after comparison to the results of the bond path investigation. In general, from any bond path the type of interaction (H...H, intermediate or hydrogen bond) and its basic geometry can be predicted and conversely, given the geometry of an interaction its expected bond path can be deduced. The nature of the interaction, whether from an N-H or a C-H "donor" group, does not appear to visibly affect the characteristic bond path for any given type of interaction. Similarly, the origin of interaction, whether cation/anion, solvent/anion or anion/anion, does not appear to influence the characteristic bond path observed. Hydrogen bonds of different conformations (single atom, edge or centroid types) were also found to have completely characteristic bond paths, normally predictable from the geometry of the interaction, particularly the $H(X)...C_{ring}$ distances. Only in the close to ideal, centroid type hydrogen bonds could the bond path not always be predicted accurately from the geometric data.

In every interaction studied, the bond path was found to travel from

the (3,-1) bond critical point, smoothly back in one direction to the N-H or C-H "donor" group and on in the other direction to some "acceptor", either a nitrogen atom or some component of a phenyl ring (a C atom or an H atom or a C-H or C-C ring bond, depending on the nature of the interaction). As the bond path approaches the C-H or N-H group of the "donor" or the "acceptor" of the interaction, it can be influenced by the high electron density built up in those regions, along covalent bonds or near the atomic centers. The bond path often changes direction quite sharply when it reaches such an area. The bond path to this point, usually very linear, will give the first indication as to the nature of the interaction. The bond path, after it changes direction (if it does), will always terminate at a single, specific atom of the "acceptor" (whether C, H or N) also characteristic of the interaction. Using the information supplied by the bond path, coupled with that determined from the geometry, much can be learned about the C-H...X and N-H...X [X = N or π(Ph)] interactions in organoammonium tetraphenylborate salts. Information that can potentially be transferred to the study of such interactions in other structures.

3.6.2.2. C-H...N Interactions

The bond paths observed in the C-H...X [X = N or π(Ph)] interactions will be discussed first because of the greater number of such contacts studied, 44 C-H...X versus 16 N-H...X. Of the 44 C-H...X interactions investigated, 9 are C-H...N type interactions and 35 are C-H...phenyl type interactions. They will be discussed in two groups, C-H...N first and then C-H...phenyl, with all of the diagrams found between the two sections.

Nine potential C-H...N type interactions were identified in the original geometry search, all with H(C)...N distances of 3Å or less, and all nine were later confirmed by location of their bond paths. Of these nine C-H...N interactions, four were found to be anion/solvent C-H...N type contacts and five were found to be $(C\text{-}H)_{anion}\cdots N_{cation}$ type contacts. All of the former type were located in the structure of guanidinium tetraphenylborate acetonitrile solvate while the latter type were located in the structures of [DabcoH] $[B(C_6H_5)_4]$ (1), guanidinium tetraphenylborate acetonitrile solvate (2) and biguanidinium tetraphenylborate (2), a wider distribution. They have each previously been discussed in detail in the geometry section. The necessary bond path diagrams are illustrated in Figure 90, [DabcoH] $[B(C_6H_5)_4]$, Figure 91, guanidinium tetraphenylborate acetonitrile solvate, and Figure 92, biguanidinium tetraphenylborate.

In every single one of the C-H...N interactions studied a (3,-1) bond critical point and a reasonable bond path were located. Even more importantly, every bond path was found to share a number of characteristic features. In every one of the contacts, the bond path was found to travel from H(C) of the "donor" group directly to N, the nitrogen atom of the "acceptor". The bond paths observed were consistent regardless of whether they arose from anion/solvent or cation/solvent type contacts.

In the interactions studied, the H(C)...N distances were found to range from a minimum of 2.561Å ($[C(33)\text{-}H(33)]_{anion}\cdots[N(4)]_{solvent}$ in guanidinium tetraphenylborate acetonitrile solvate) to 2.963Å ($[C(36)\text{-}H(36)]_{anion}\cdots [N(4)]_{solvent}$ in the same structure). The C-H...N angles range from 161.8° (in the first contact mentioned) to 109.9° ($[C(45)\text{-}H(45)]_{anion}\cdots [N(4)]_{solvent}$ also in the structure of guanidinium

tetraphenylborate acetonitrile solvate). Changes in either of these two geometric parameters characteristic of C-H...N type interactions, distance or angle, has no visible effect on the observed bond paths, they all begin from H(C) and terminate at a nitrogen atom.

The majority of the $(C\text{-}H)_{anion}\cdots N_{cation}$ interactions studied were also found to have short H...H anion/cation distances involved in the contact. This was not the case in the $[C(32)\text{-}H(32)]_{anion}\cdots[N(2)]_{cation}$ interaction of [DabcoH] $[B(C_6H_5)_4]$ where N(2) of the cation was not protonated and no short $H(32)\cdots H_{cation}$ distances were found. However in the other four anion/cation C-H...N contacts studied, $H_{anion}\cdots H_{cation}$ distances shorter than the $H_{anion}\cdots N_{cation}$ distances were located. The four relevant contacts are $[C(46)\text{-}H(46)]_{anion}\cdots[N(2)]_{cation}$ and $[C(43)\text{-}H(43)]_{anion}\cdots[N(2)]_{cation}$ in the structure of guanidinium tetraphenylborate acetonitrile solvate and $[C(26)\text{-}H(26)]_{anion}\cdots[N(4)]_{cation}$ and $[C(42)\text{-}H(42)]_{anion}\cdots[N(4)]_{cation}$ from the structure of biguanidinium tetraphenylborate. In the final contact mentioned, the H(42)...N(4) distance of 2.867Å (119.6°) is actually 0.350Å longer than the H(42)...H(4B) distance of 2.517Å (110.5°). This is, in fact, the largest difference observed between the longer H...N and the shorter H...H distances in the four interactions investigated. The average difference in the two distances in the four contacts is 0.25Å, H...H always being shorter than H...N. However, all of the contacts were found to have clear H(C) to N bond paths. The short H...H distances have no visible effect on the observed bond paths. All interactions found by geometry to be of the C-H...N type, regardless of their origin or short H...H distances, will always have bond paths that travel from H(C) of the "donor" to N, the nitrogen atom of the "acceptor".

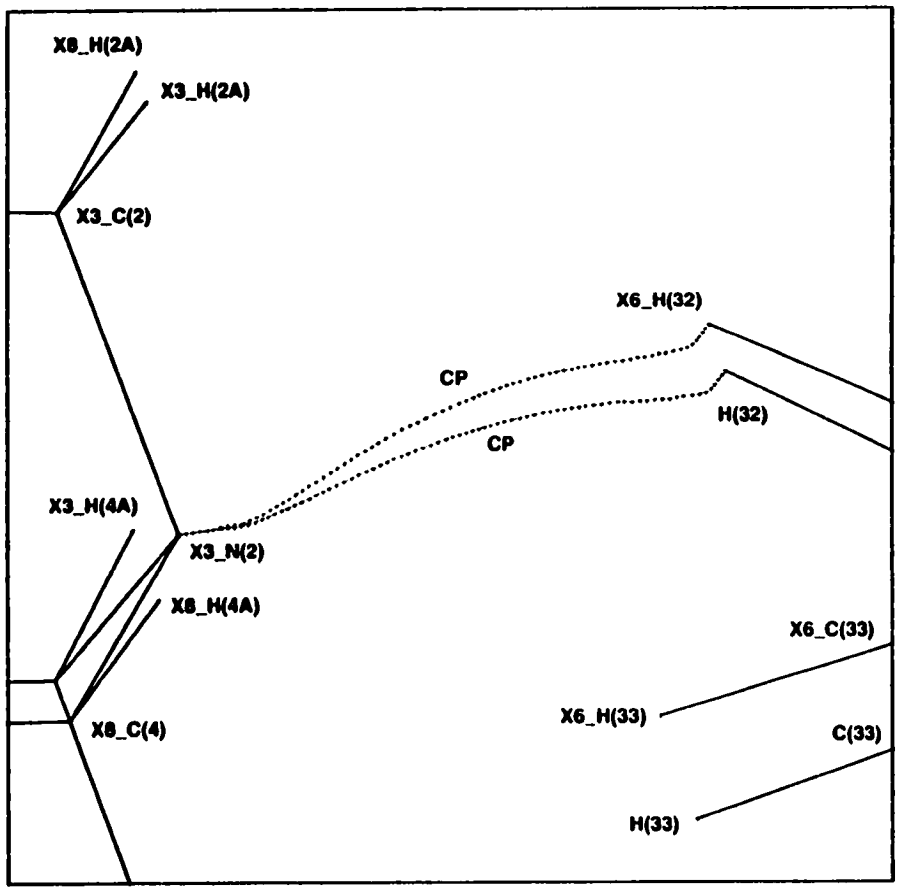

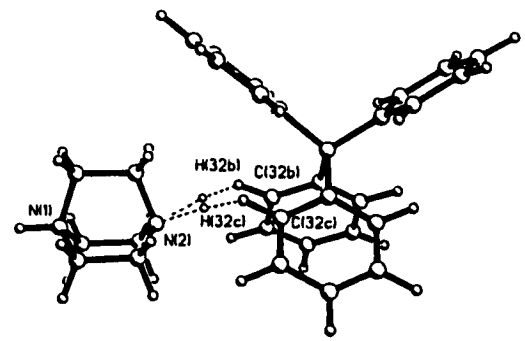

Figure 90. Bond path located for the one unique C-H...N contact of less than 3Å in the structure of [DabcoH][$B(C_6H_5)_4$]. CP marks the location of the bond critical point.

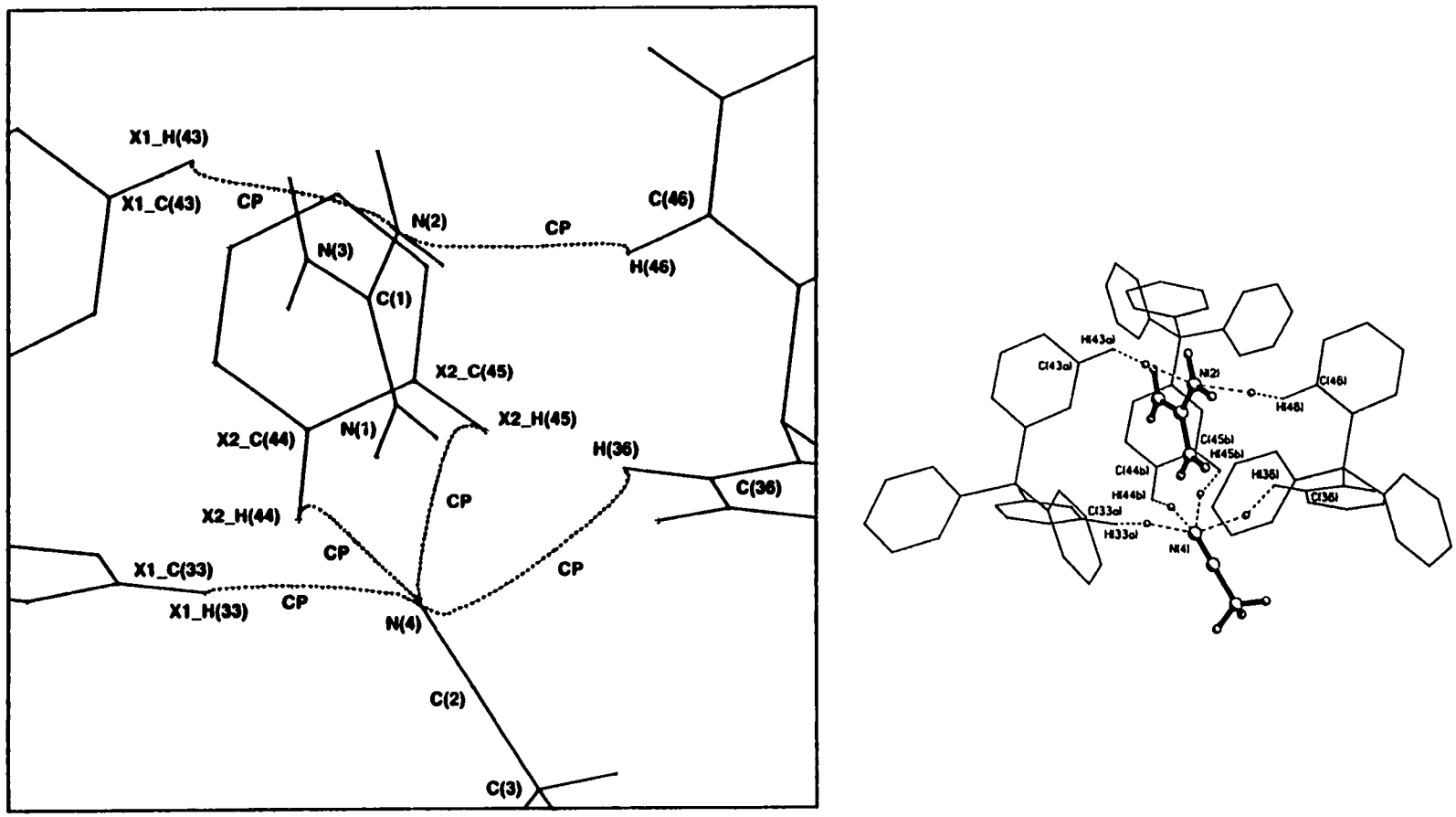

Figure 91. Bond paths located for the C-H...N contacts of less than 3Å in the structure of guanidinium tetraphenylborate acetonitrile solvate. CP marks the locations of the bond critical points. The uninvolved rings on the interacting tetraphenylborate anions have been omitted for clarity.

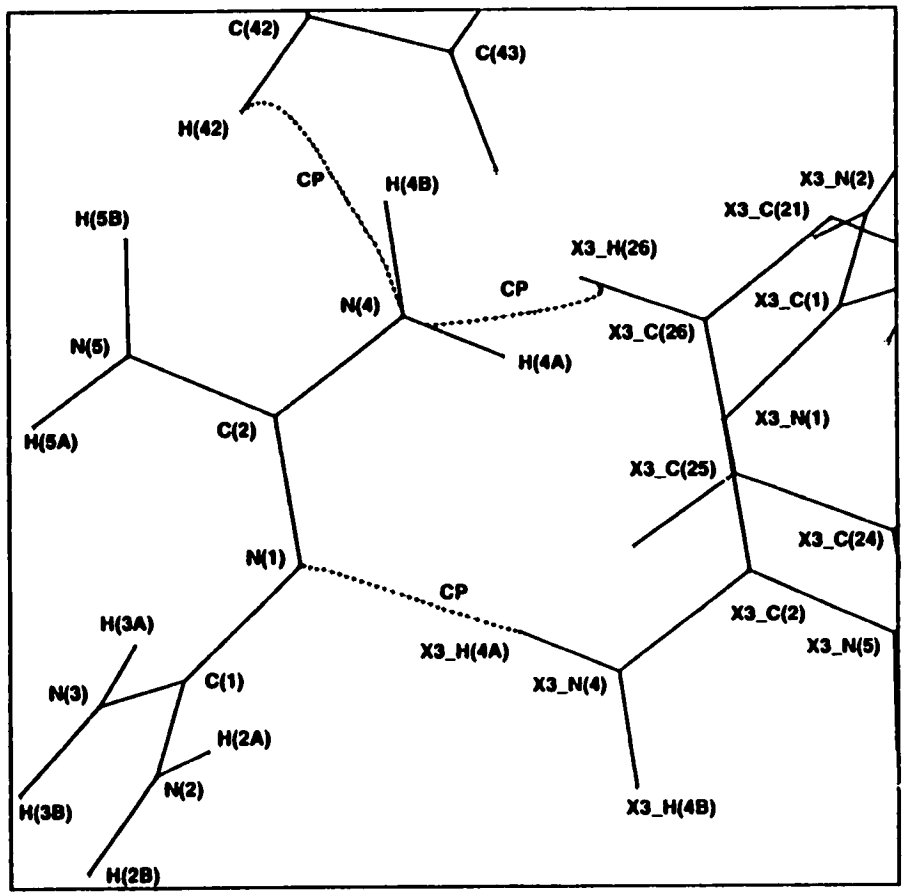

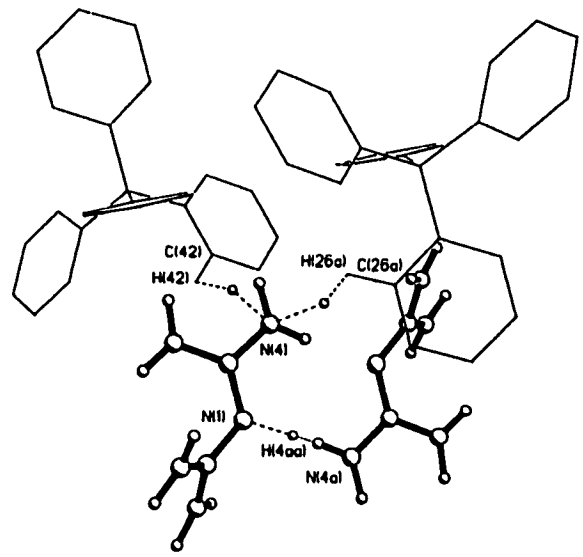

Figure 92. Bond paths located for the C-H...N contacts of less than 3Å in the structure of biguanidinium tetraphenylborate. CP marks the locations of the bond critical points.

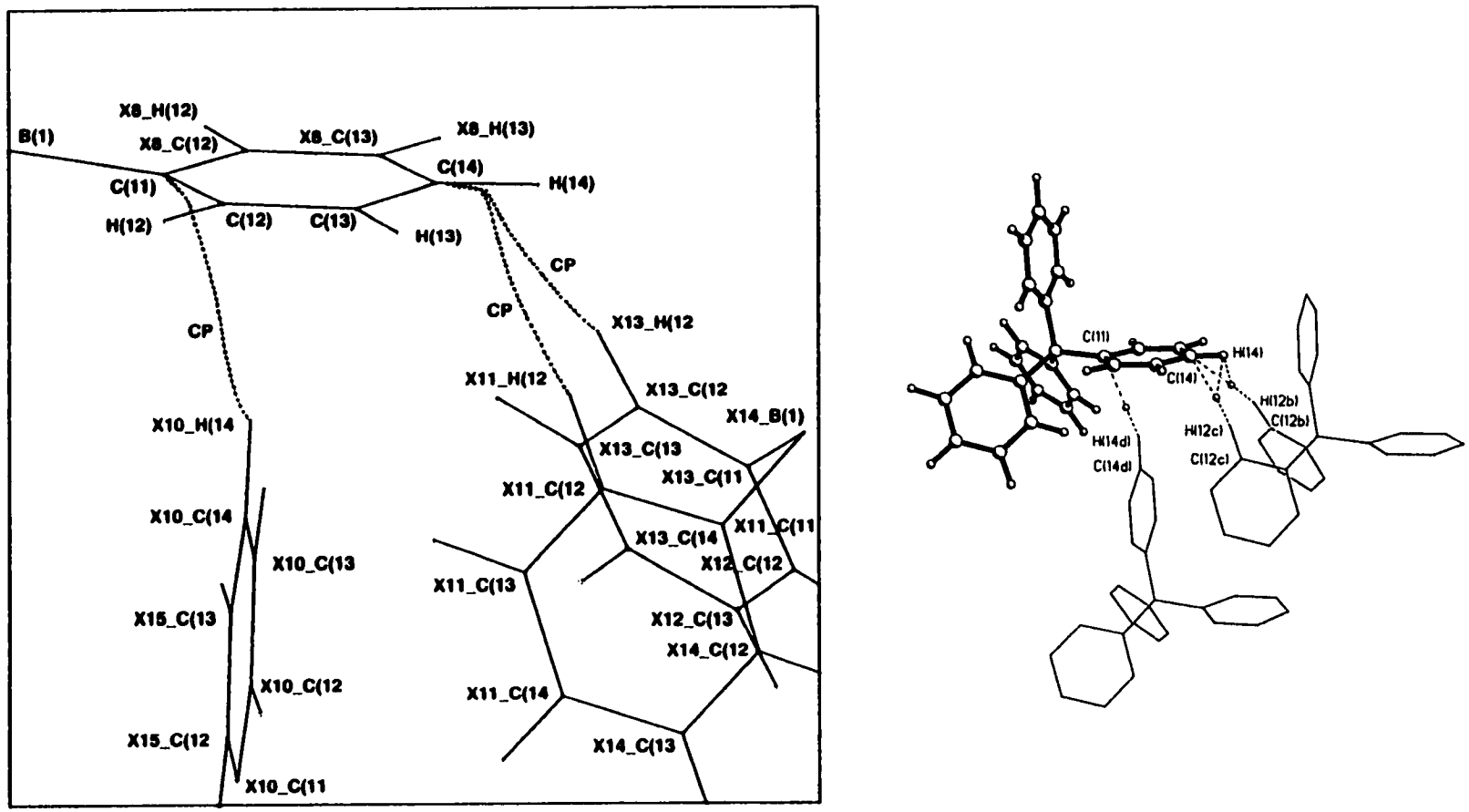

Figure 93. Bond paths located for the C-H...phenyl interactions of less than 3Å in the structure of ammonium tetraphenylborate, drawn to emphasize the role of the phenyl ring as the acceptor of the interactions. CP marks the locations of the bond critical points. The outlines of the uninvolved rings on the tetraphenylborate anions have been omitted for clarity.

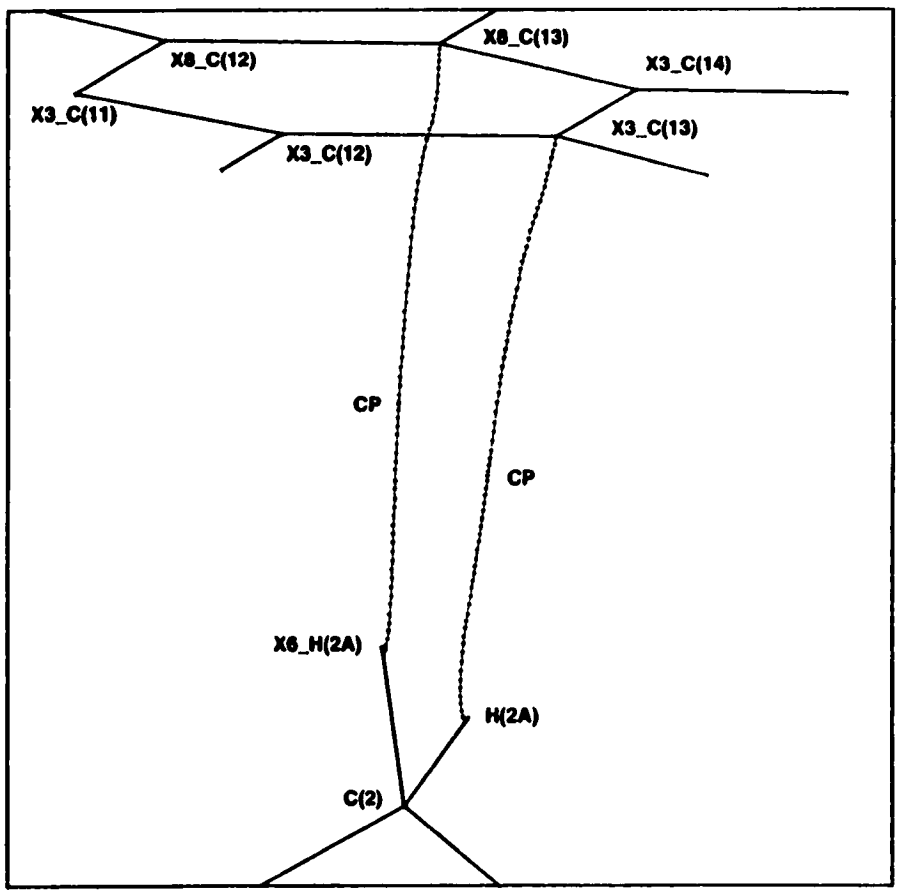

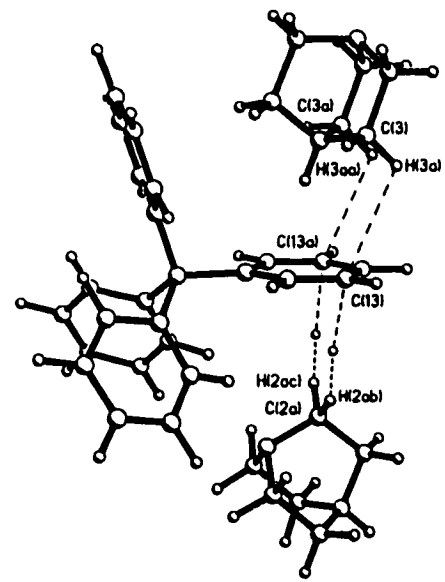

Figure 94. Bond path located for only one of the C-H...phenyl interactions of less than 3Å accepted by ring #1 in the structure of [DabcoH][$B(C_6H_5)_4$]. CP marks the location of the bond critical point. The outlines of the uninvolved rings on the tetraphenylborate anion have been omitted for clarity.

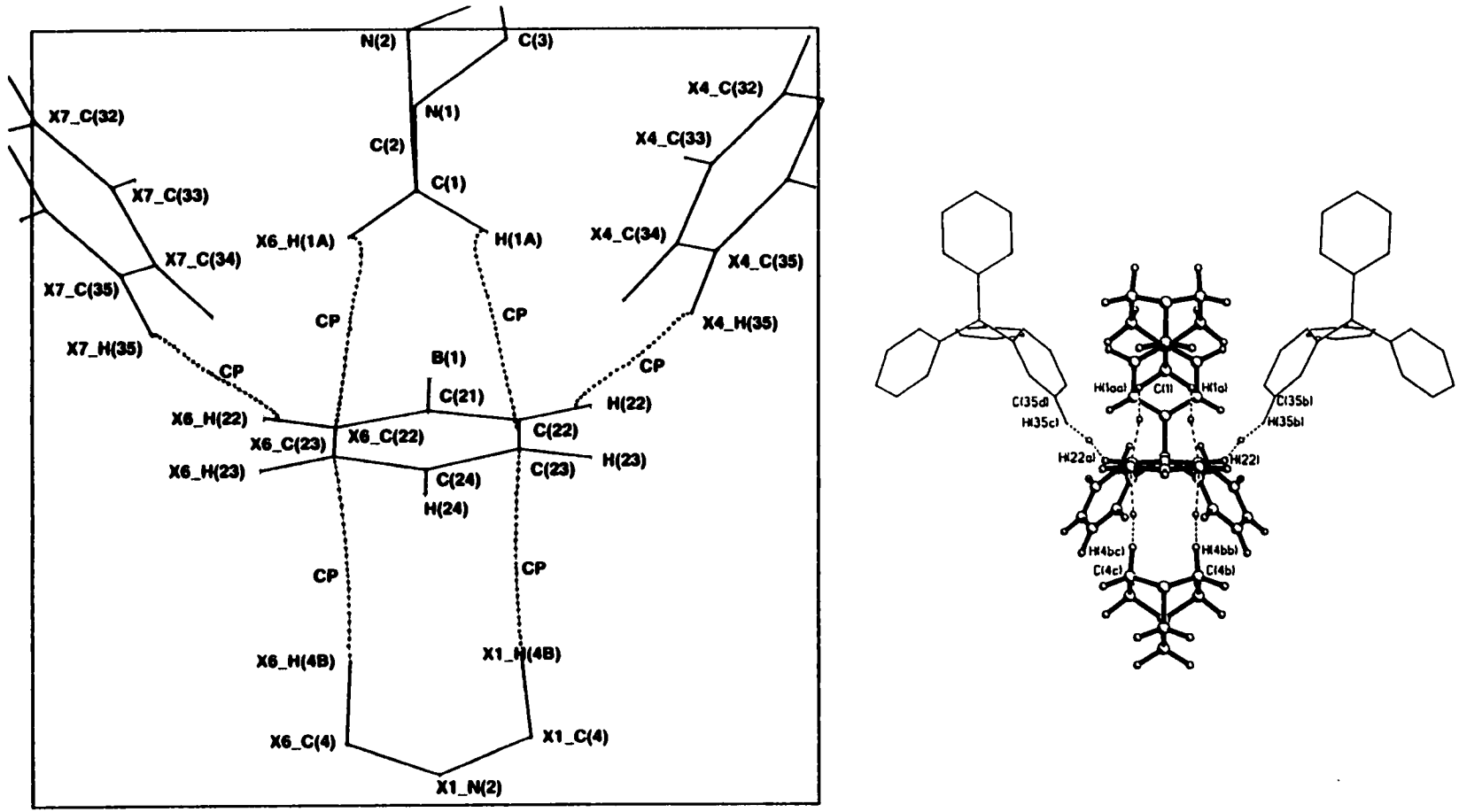

Figure 95. Bond paths located for the C-H...phenyl interactions of less than 3Å accepted by ring #2 in the structure of [DabcoH][$B(C_6H_5)_4$]. CP marks the locations of the bond critical points. The outlines of the uninvolved rings on the tetraphenylborate anions have been omitted for clarity.

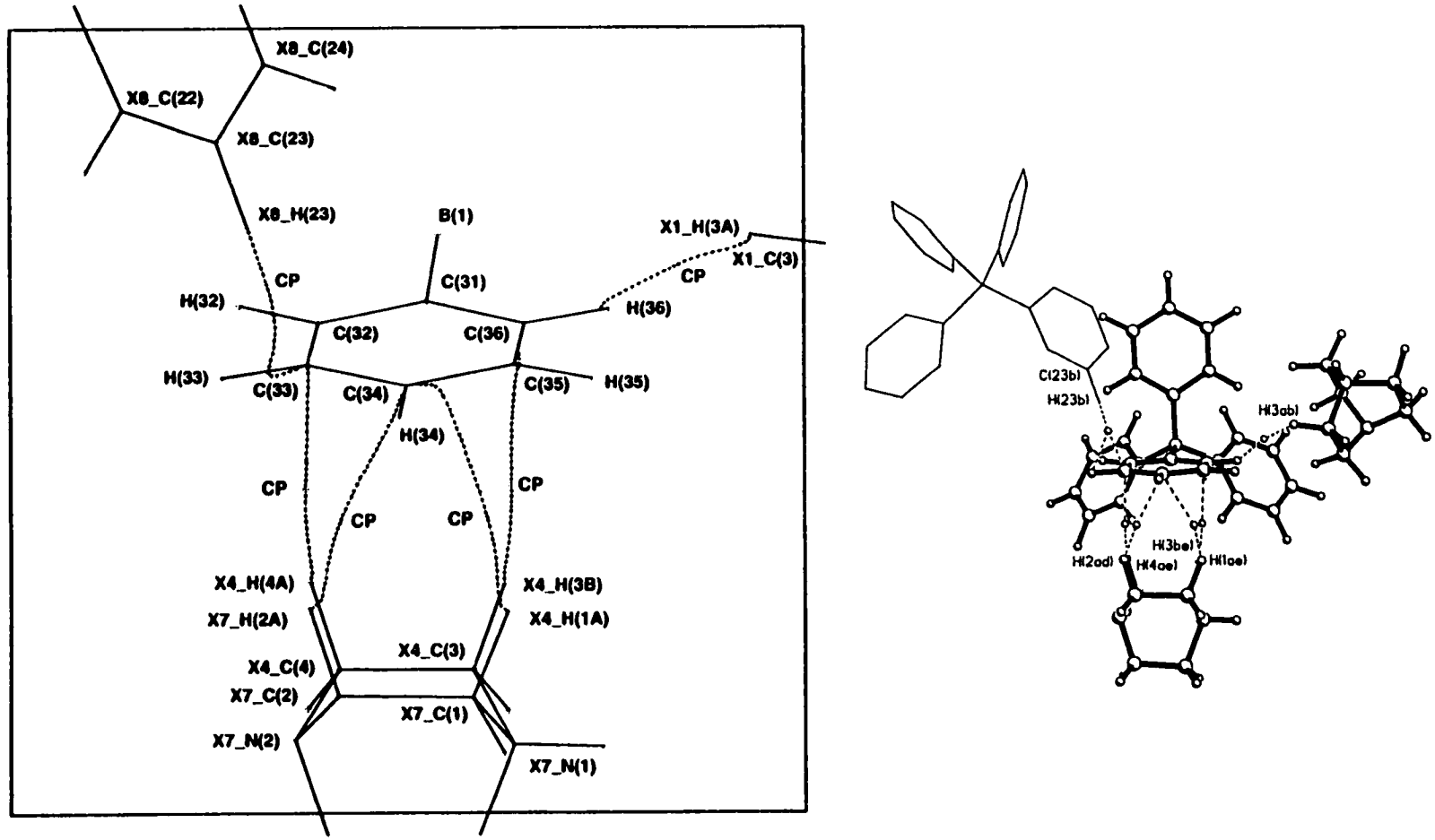

Figure 96. Bond paths located for the C-H...phenyl interactions of less than 3Å accepted by ring #3 in the structure of [DabcoH][$B(C_6H_5)_4$]. CP marks the locations of the bond critical points. The outlines of the uninvolved rings on the tetraphenylborate anions have been omitted for clarity.

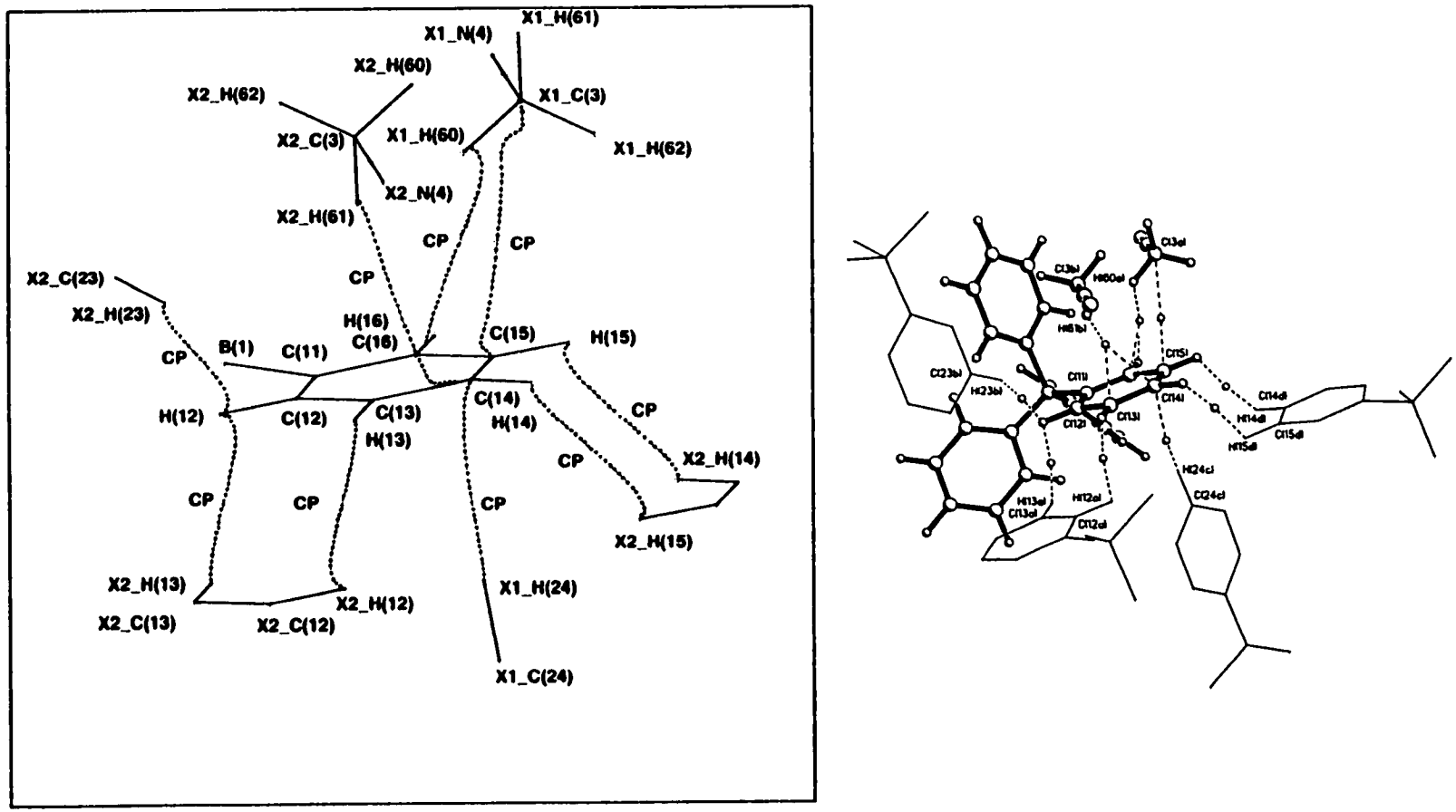

Figure 97. Bond paths located for the C-H...phenyl interactions of less than 3Å accepted by ring #1 in guanidinium tetraphenylborate acetonitrile solvate. CP marks the locations of the bond critical points. The outlines of all except the interacting bonds of the tetraphenylborate anions have been omitted for clarity.

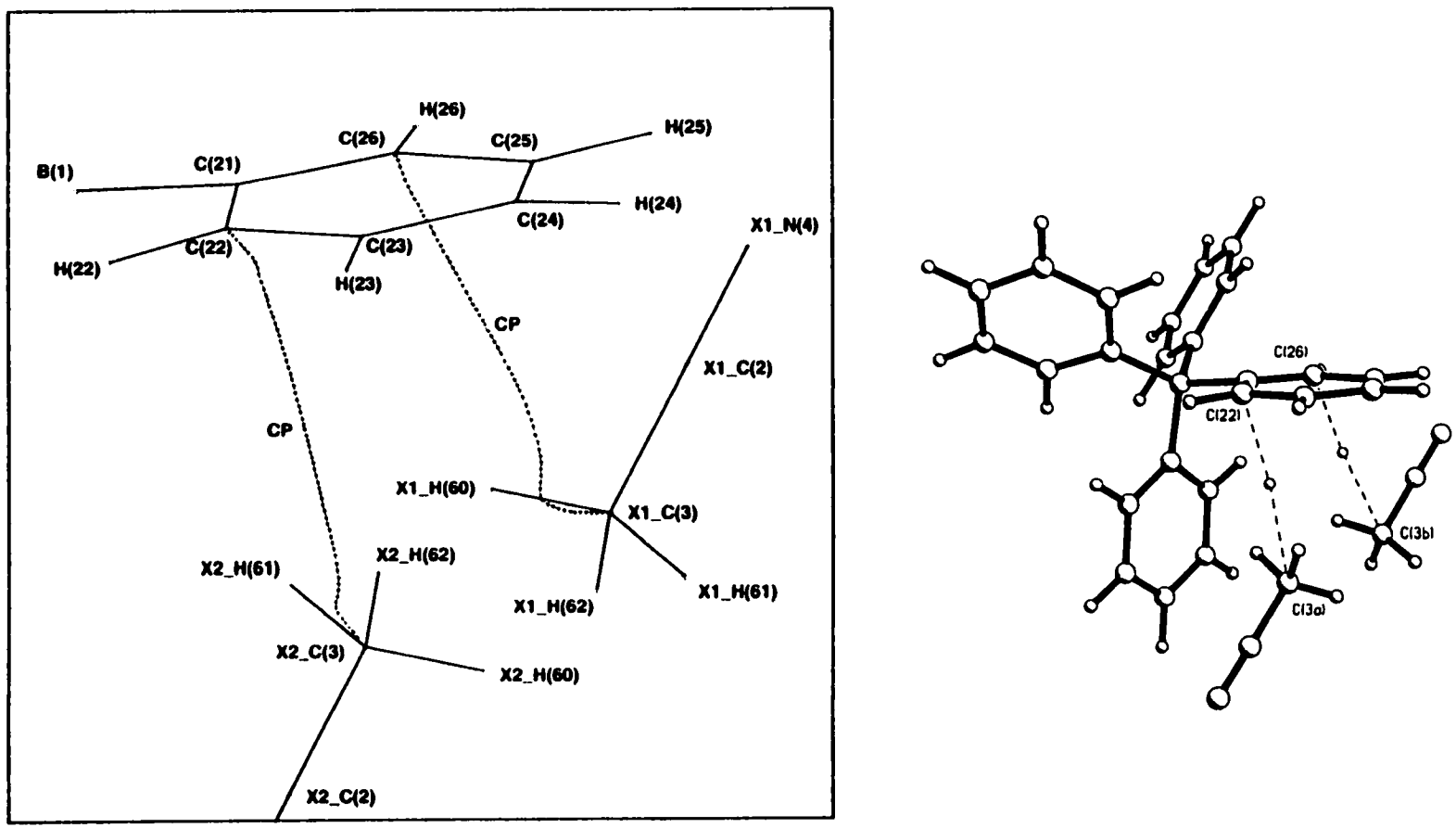

Figure 98. Bond paths located for the C-H...phenyl interactions of less than 3Å accepted by ring #2 in guanidinium tetraphenylborate acetonitrile solvate. CP marks the locations of the bond critical points. The outlines of the uninvolved rings on the tetraphenylborate anion have been omitted for clarity.

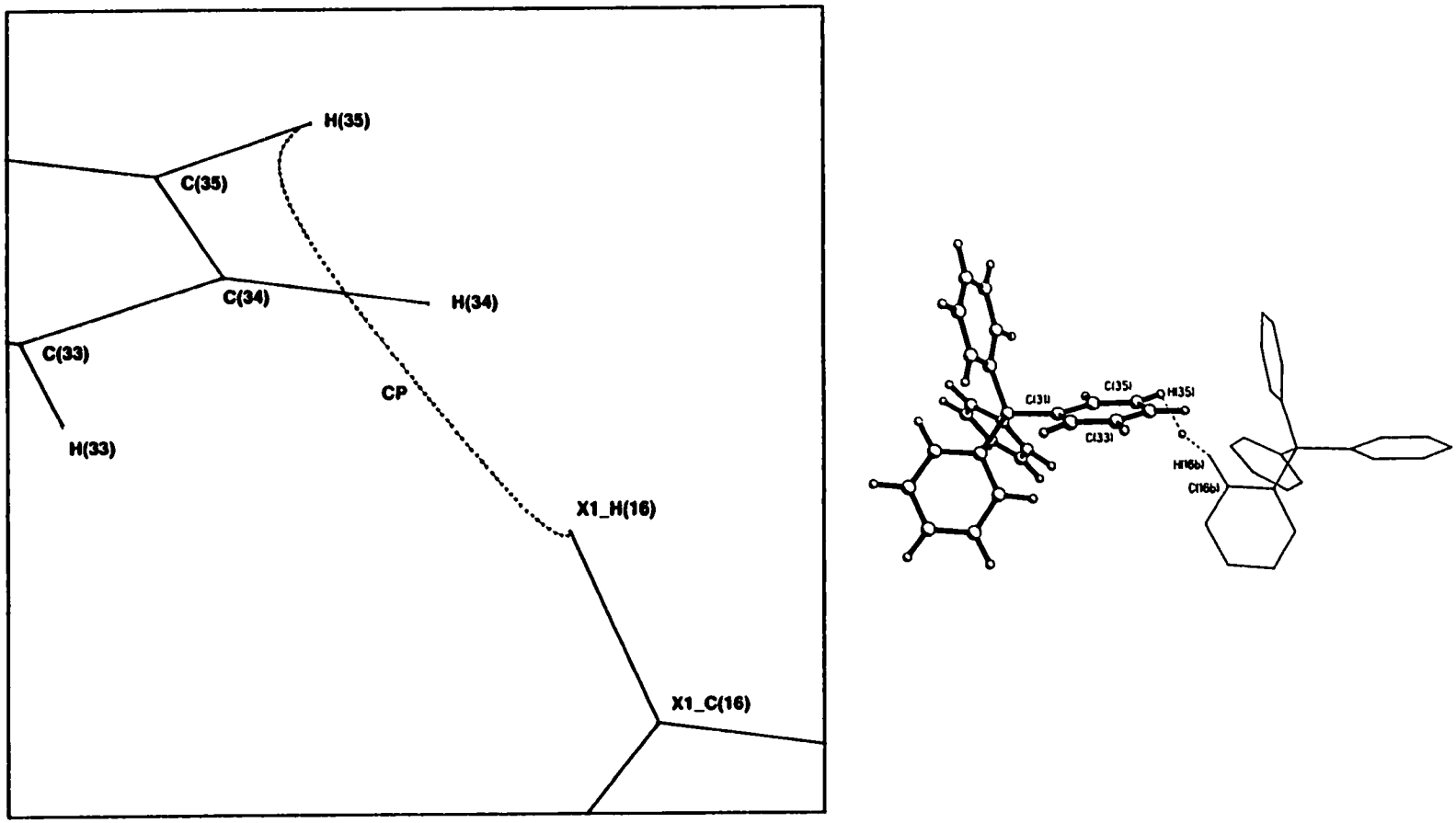

Figure 99. Bond path located for the C-H...phenyl interaction of less than 3Å accepted by ring #3 in guanidinium tetraphenylborate acetonitrile solvate. CP marks the location of the bond critical point. The outlines of the uninvolved rings on the tetraphenylborate anion have been omitted for clarity.

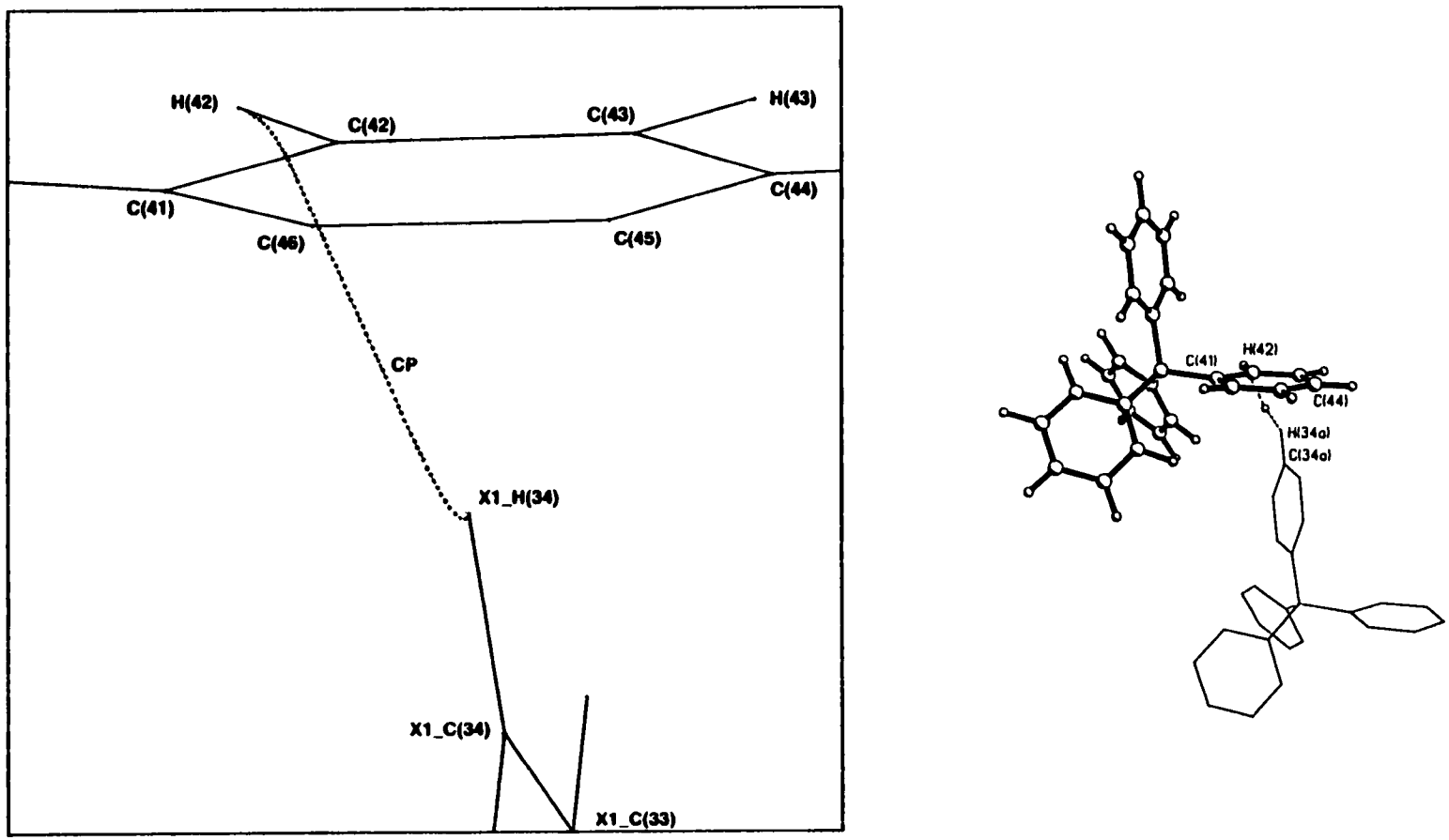

Figure 100. Bond path located for the C-H...phenyl interaction of less than 3Å accepted by ring #4 in guanidinium tetraphenylborate acetonitrile solvate. CP marks the location of the bond critical point. The outlines of the uninvolved rings on the tetraphenylborate anion have been omitted for clarity.

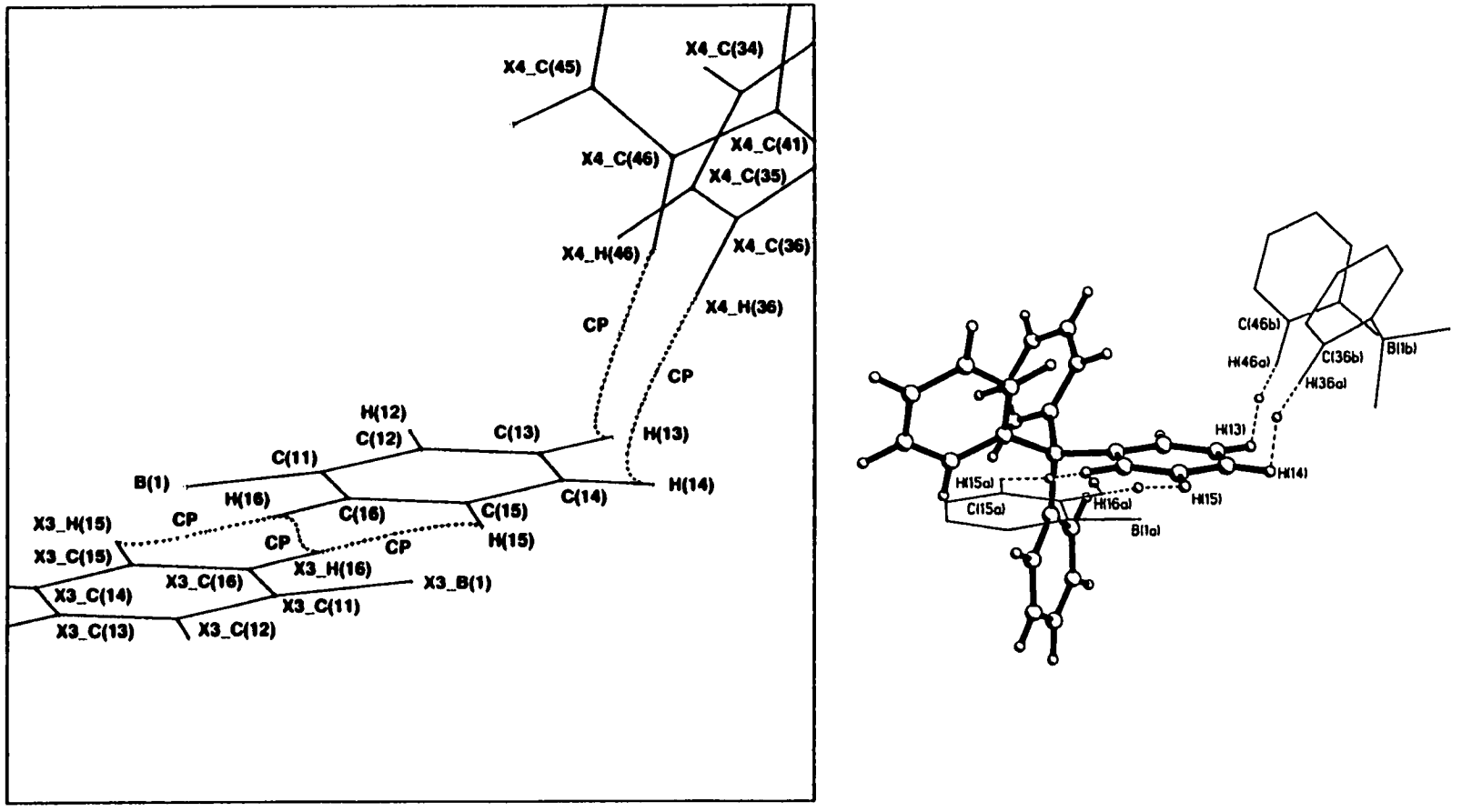

Figure 101. Bond paths located for the C-H...phenyl interactions of less than 3Å accepted by ring #1 in biguanidinium tetraphenylborate. CP marks the locations of the bond critical points. The outlines of the uninvolved rings on the tetraphenylborate anions have been omitted for clarity.

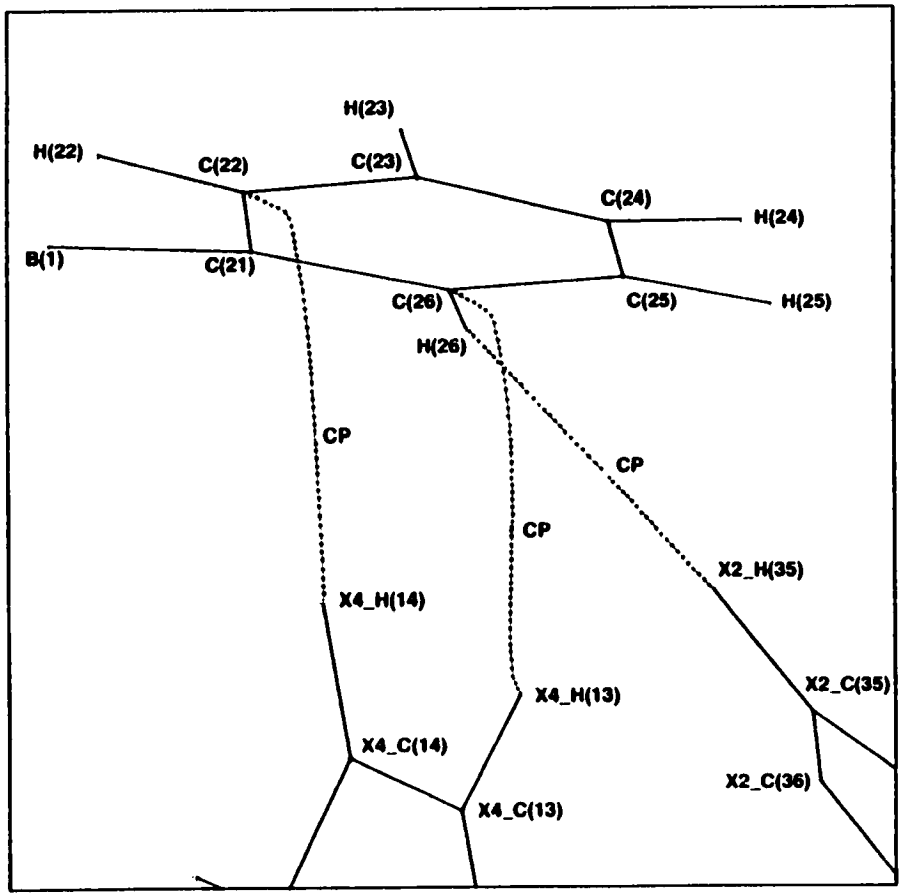

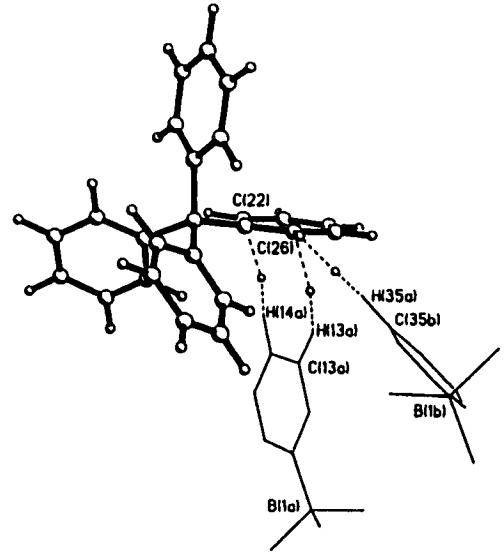

Figure 102. Bond paths located for the C-H...phenyl interactions of less than 3Å accepted by ring #2 in biguanidinium tetraphenylborate. CP marks the locations of the bond critical points. The outlines of the uninvolved rings on the tetraphenylborate anions have been omitted for clarity.

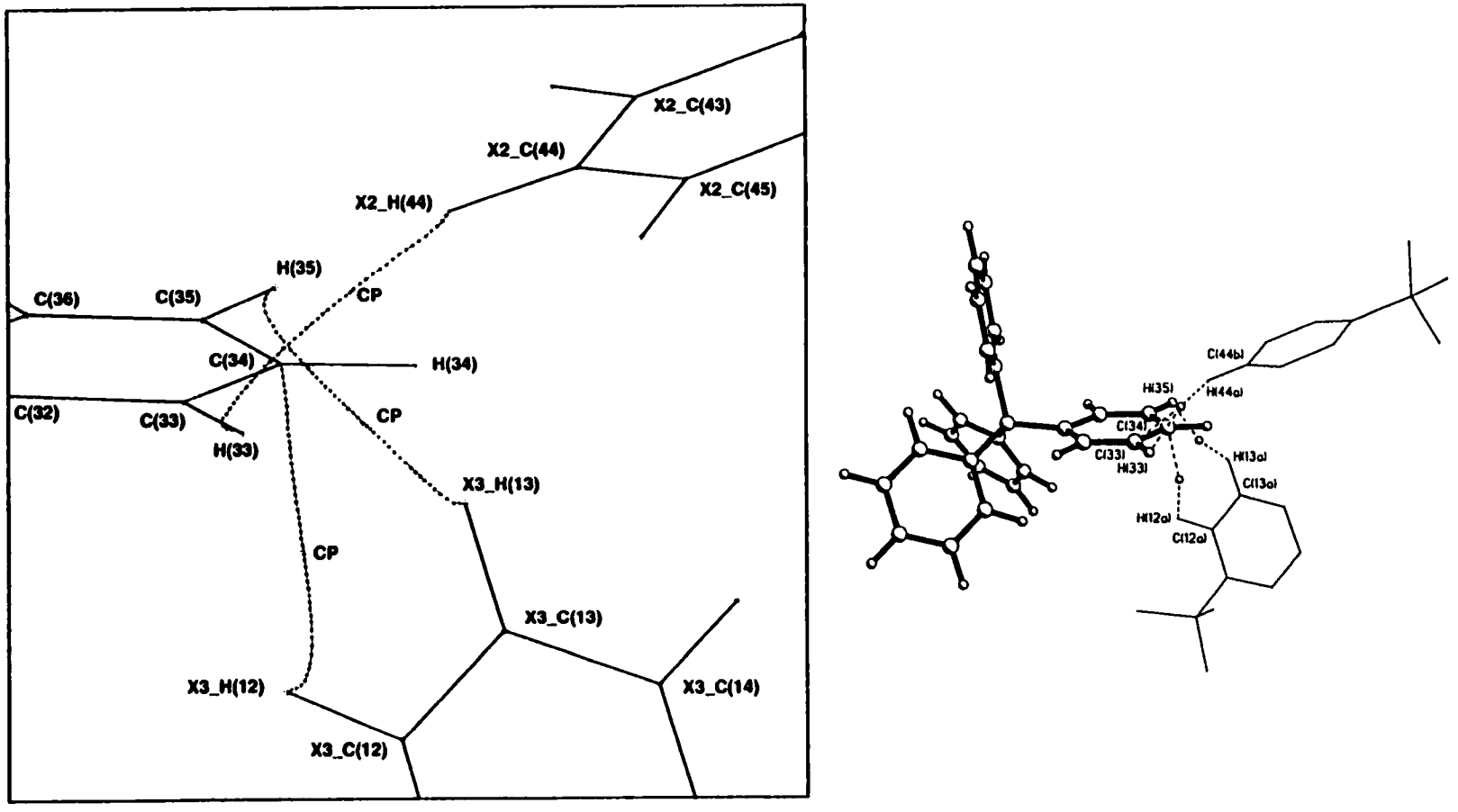

Figure 103. Bond paths located for the C-H...phenyl interactions of less than 3Å accepted by ring #3 in biguanidinium tetraphenylborate. CP marks the locations of the bond critical points. The outlines of the uninvolved rings on the tetraphenylborate anions have been omitted for clarity.

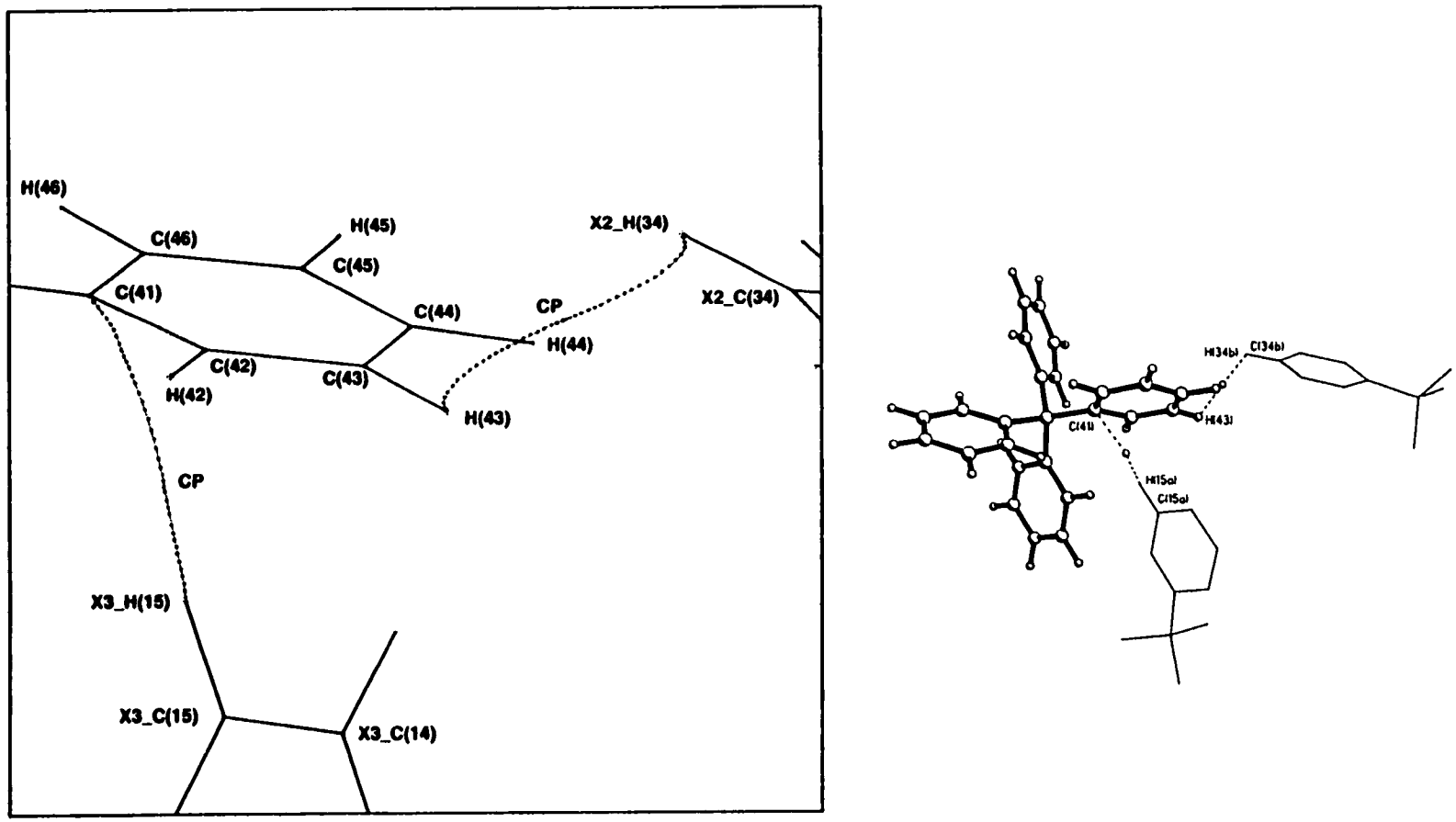

Figure 104. Bond paths located for the C-H...phenyl interactions of less than 3Å accepted by ring #4 in biguanidinium tetraphenylborate. CP marks the locations of the bond critical points. The outlines of the uninvolved rings on the tetraphenylborate anions have been omitted for clarity.

3.6.2.3. C-H...Phenyl Interactions

A total of 34 potential C-H..phenyl interactions were located in the original geometry search [H(C)...X less than 3Å] carried out for the four structures studied. Bond paths were later located for 33 of these 34 interactions, plus two extra located in the $[C(NH_2)_3][B(C_6H_5)_4]\cdot CH_3CN$ structure, for a total of 35 fully characterized C-H...phenyl type contacts. The 34 geometrically proposed C-H...phenyl interactions can be categorized in a number of different ways. Of the original 34 interactions, the geometries showed that 22 would be $(C\text{-}H)_{anion}\cdots(phenyl)_{anion}$ type, 9 would be $(C\text{-}H)_{cation}\cdots(phenyl)_{anion}$ type (all in $[DabcoH][B(C_6H_5)_4]$) and 3 would be $(C\text{-}H)_{solvent}\cdots(phenyl)_{anion}$ type contacts (all in guanidinium tetraphenylborate acetonitrile solvate). From another perspective, 2 of the potential contacts were found in the structure of $NH_4B(C_6H_5)_4$ (both anion/anion type), 11 were found in the structure of $[DabcoH][B(C_6H_5)_4]$ (9 cation/anion and 2 anion/anion type), 9 were found in the structure of $[C(NH_2)_3][B(C_6H_5)_4]\cdot CH_3CN$ (3 solvent/anion and 6 anion/anion type), and finally 12 were found in the structure of $[N(C[NH_2]_2)_2][B(C_6H_5)_4]$ (all of the anion/anion type). The bond path diagrams illustrating these interactions are divided according to the structure of origin and broken down further according to the phenyl ring accepting the interactions. Thus Figure 93 includes all the C-H...phenyl interactions (anion/anion type) of ammonium tetraphenylborate and Figures 94 to 96 illustrate the C-H...phenyl interactions (both cation/anion and anion/anion type) of $[DabcoH][B(C_6H_5)_4]$ phenyl rings 1, 2 and 3, respectively. Similarly, Figures 97 to 100 and Figures 101 to 104 show the bond paths of the C-H...phenyl interactions of all types in the structures of guanidinium

tetraphenylborate acetonitrile solvate and biguanidinium tetraphenylborate, respectively, in the order phenyl ring 1, 2, 3 and 4, in both cases. For simplicity, all of these Figures are presented at the beginning of the C-H...phenyl bond path section.

Each of the interactions was located in a geometry search for H...C_{ring} distances of 3Å or less. Their geometries were then carefully studied and the interactions were classified further, as being H...H type contacts, intermediate type contacts or hydrogen bonds with centroid, edge or single atom configurations. Of the 34 potential C-H...phenyl interactions, 15 were classified by their geometries as being H...H type contacts, 5 were found to fall into the intermediate category and 14 had geometries consistent with hydrogen bonds (4 centroid, 8 edge and 2 single atom configurations). The assignment of each individual interaction to a particular type has been clearly described in the previous geometry section.

Fifteen C-H...phenyl interactions (out of a total of 34 proposed) were predicted, after careful analysis of their geometries, to be **H...H type contacts**. Of the 15 H...H type contacts identified, 14 interactions are $(C\text{-}H)_{anion}\cdots(phenyl)_{anion}$ type (1 in $NH_4B(C_6H_5)_4$, 1 in [DabcoH][$B(C_6H_5)_4$], 4 in $[C(NH_2)_3][B(C_6H_5)_4]\cdot CH_3CN$ and 8 in $[N(C[NH_2]_2)_2][B(C_6H_5)_4]$), while only one is of the $(C\text{-}H)_{cation}\cdots(phenyl)_{anion}$ type ([DabcoH][$B(C_6H_5)_4$]). The bond path of this last interaction is shown in Figure 105 as an example of a typical H...H contact.

The $[C(3)\text{-}H(3A)]_{cation}\cdots[ring\ 3]_{anion}$ interaction of [DabcoH][$B(C_6H_5)_4$] is characterized as an H...H type contact based on the H(3A)...H(36) distance of 2.262Å (132.8°), 0.70Å shorter than the H(3A)...C(36) distance

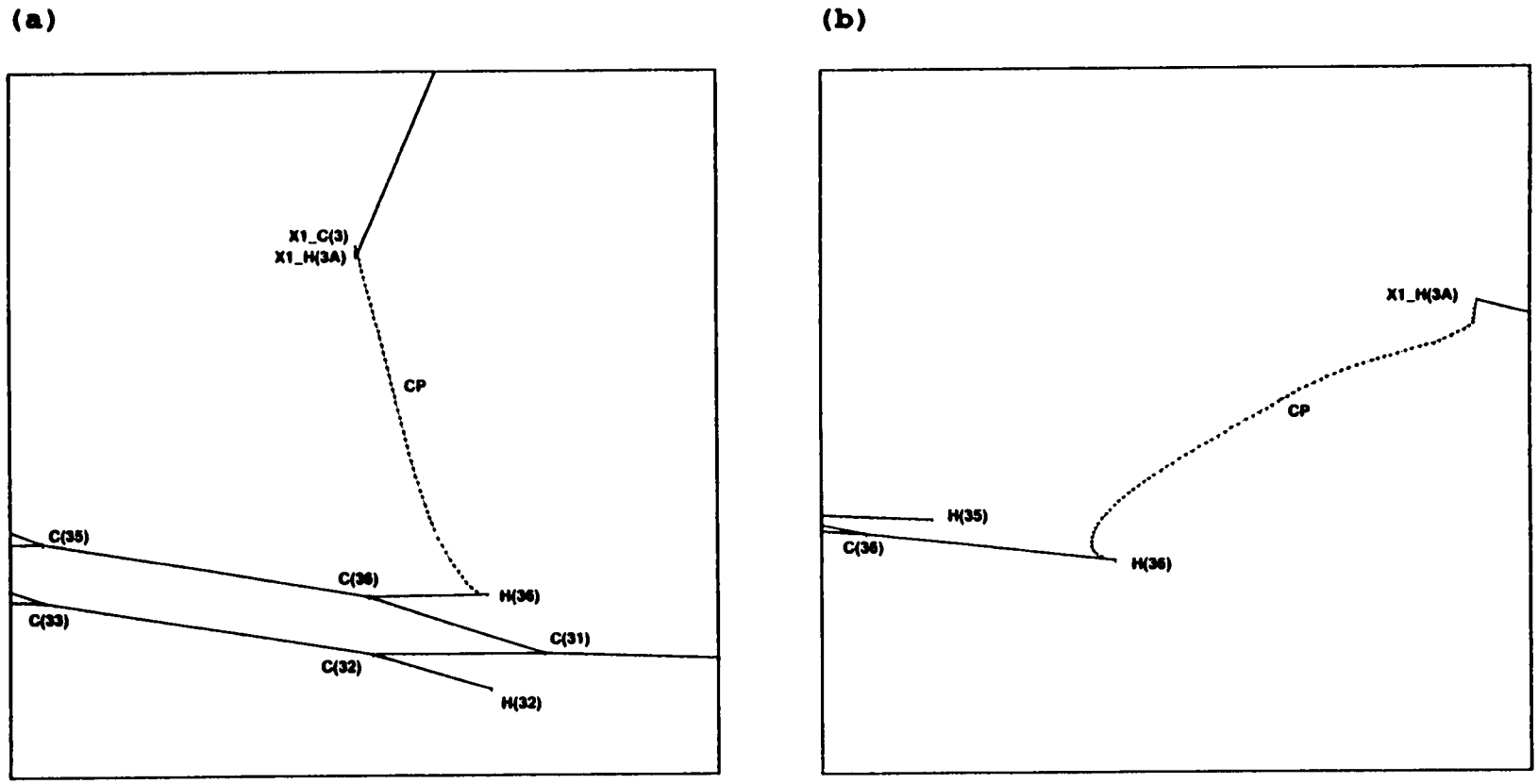

Figure 105. Typical bond path of a C-H...phenyl, H...H type contact. The C(3)-H(3A)...ring 3 interaction of [DabcoH][$B(C_6H_5)_4$] viewed (a) down the C-H bond and (b) approximately perpendicular to the plane of the phenyl ring. CP marks the location of the bond critical point.

of 2.961Å (147.0°). This illustrates the geometric criteria developed to characterize all H...H type contacts. The minimum H...H_{ring} distance is considerably shorter than the minimum H...C_{ring} distance, with the difference between the two approximately 0.5Å or greater. The H...H_{ring} distance is less than 2.5Å, while the H...C_{ring} distance is greater than 2.5Å and closer to 3.0Å.

Of the 15 H...H type contacts, assigned as such by meeting these geometric criteria, 14 were found to have bond paths consistent with this classification. There were no differences observed in the bond path of the single cation/anion contact studied relative to those of the anion/anion type contacts. In the group of 14 well behaved H...H type contacts, the bond paths were all found to proceed from H(C) of the "donor" group to a single hydrogen atom of the "acceptor", H_{anion}, as illustrated in Figure 105. The bond paths tend to be direct and quite linear for the most part, particularly in their central regions. In some instances, one or other of the ends of the bond path was found to curve slightly (less than 10% of the bond length) along the C-H bond before progressing toward the other hydrogen atom. This describes the majority of the bond paths very well; only a few minor exceptions were noted. The bond paths were always found to travel between the two hydrogen atoms making the closest contact, the shortest H...H_{ring} distance in the interaction. Thus, contacts predicted from their atomic positions to be of the H...H type have bond paths that travel between the two closest hydrogen atoms in the interaction, H(C) of the "donor" to H_{ring} of the "acceptor". The geometric criteria, developed to identify H...H type contacts, must be correct.

The one major exception noted, was a single interaction found not

to have a characteristic H...H type bond path even though it had been placed in that category by geometry. The $[C(12)\text{-}H(12)]_{anion}\cdots[ring\ 1]_{anion}$ interaction was located in the structure of ammonium tetraphenylborate. It was classified as an H...H type contact, to H(14) of ring 1, from its geometry. It was found to have an H(12)...H(14) separation of 2.468Å, less than 2.5Å, and a minimum $H(14)\cdots C_{ring}$ distance, to C(14) of 2.873Å. The H(12)...C(14) separation is more than 2.5Å and closer to 3.0Å, as expected for H...H type contacts. Thus, by geometry it was classified as an H...H type contact. However, the bond path for this interaction was found to proceed from H(12) to the approximate midpoint of the C(14)-H(14) phenyl ring bond (Figure 93). It then changes direction sharply and follows the C(14)-H(14) bond along to its termination at C(14). Clearly, this is not an H...H type contact. In fact, as will be described subsequently, this bond path is of the type characteristic of an intermediate contact.

Examining the geometry of the interaction more closely, the fact that it behaves as an intermediate type contact is perhaps not so surprising. The difference in the H(12)...H(14) distance and the H(12)...C(14) distance is only 0.40Å ($H\cdots H_{ring} < H\cdots C_{ring}$), below the criterion suggested from studying the geometries of many of these type of H...H interactions, 0.50Å. This difference is the smallest found in any of the 15 contacts studied; the next shortest distance difference being 0.44Å. In the 14 true H...H type contacts the distance difference was found to range from 0.44Å to 0.70Å, the latter in the [DabcoH][$B(C_6H_5)_4$] contact, $[C(3)\text{-}H(3A)]_{cation}\cdots[H(36)]_{anion}$.

This information provides new boundary conditions that can be used to modify the criteria, derived from the geometry analysis, allowing the

identification of H...H type contacts. The fact that it was suggested that the H...H distance be less than 2.5Å does not appear to be of primary importance. The H(12)...H(14) separation in the C(12)-H(12)...ring 1 [to C(14) not H(14)] intermediate type contact, 2.468Å, was the second longest in the 15 contacts studied but was still less than 2.5Å. The H(12)...H(14) distance is similar to the corresponding distances in contacts found to be true H...H type contacts.

More important appears to be the difference between the minimum $H...H_{ring}$ and $H...C_{ring}$ distances characterizing the interaction. The C(12)-H(12)...ring 1 contact of ammonium tetraphenylborate has the smallest difference observed in all the contacts studied in this group, 0.40Å. This difference must be too small for the H...H contact to dominate the interaction, it is still controlled in large part by the $H...C_{ring}$ contact even though it is longer. The second shortest difference observed, 0.44Å, was located in the structure of guanidinium tetraphenylborate acetonitrile solvate. The bond path showed this clearly to be an H...H type interaction, to H(35) of anion ring 3. H...H type interactions were found to occur whenever the $H...H_{ring}/H...C_{ring}$ distance difference is roughly 0.40Å or greater. If the difference is approximately 0.40Å or less, up to a certain minimum value to be discussed subsequently, an intermediate type contact is formed. This difference, 0.40Å, is less than the 0.50Å limit predicted by geometry alone to be the cutoff for H...H type contacts, a modification of the original criteria.

In a few of the H...H type contacts, where the difference between the $H...H_{ring}$ and $H...C_{ring}$ distances was relatively small (but still greater than 0.40Å) the bond path would begin from the H(C) atom of the "donor"

and pass to somewhere along the C-H bond of a phenyl ring of the anion before proceeding along the bond to finally end at the second hydrogen atom, H_{ring}. Two examples are the $[C(44)-H(44)]_{anion}\cdots[ring\ 3]_{anion}$ contact of biguanidinium tetraphenylborate and the $[C(35)-H(35)]_{anion}\cdots[ring\ 2]_{anion}$ contact in $[DabcoH][B(C_6H_5)_4]$. These are shown in Figures 103 and 95, respectively. In the former, the bond path proceeds from H(44) to the approximate midpoint of the C(33)-H(33) bond before travelling along the bond to end at H(33), making it clearly an H...H type contact. By geometry it was also characterized as an H...H type contact, based on an H(44)...C(33) distance of 2.899Å, an H(44)...H(33) distance of 2.454Å and a difference between the two of only 0.44Å. In the second contact mentioned, the bond path proceeds from H(35) to a point roughly three quarters of the way along the C(22)-H(22) bond, closer to H(22), before changing direction and following the bond to its end at H(22). The H(35)...H(22) distance in this interaction is 2.354Å and the H(35)...C(22) distance is 2.841Å, resulting in a difference of 0.49Å between the two. Most of the contacts with smaller $H\cdots H_{ring}/H\cdots C_{ring}$ distance differences (less than 0.50Å) tended to show some involvement of the $(C-H)_{anion}$ "acceptor" bond in the bond path. However, the distance the bond path was found to follow the bond was not entirely consistent with, or predictable from, the difference in the $H\cdots H_{ring}/H\cdots C_{ring}$ distances.

Overall, H...H type contacts are remarkably consistent and predictable, both by geometry and from their bond paths. H...H contacts are characterized by $H\cdots H_{ring}$ distances of less than 2.5Å and $H\cdots C_{ring}$ distances of greater than 2.5Å, usually closer to 3.0Å ($H\cdots H_{ring} < H\cdots C_{ring}$). The difference in the $H\cdots H_{ring}$ and $H\cdots C_{ring}$ distances must be

roughly 0.40Å or greater; values of up to 0.70Å have been observed. Contacts predicted by geometry to be of the H...H type will have bond paths that travel ultimately always from one hydrogen atom to another. Conversely, if such a bond path is observed it must arise from an H...H type contact with a predictable basic geometry.

Besides the **intermediate type contact** located in the structure of ammonium tetraphenylborate, first thought to be an H...H type contact, five other intermediate type interactions were predicted on the basis of their geometries. Three of these contacts were located in the structure of [DabcoH][$B(C_6H_5)_4$] [2 $(C\text{-}H)_{cation}\cdots(phenyl)_{anion}$ and 1 $(C\text{-}H)_{anion}\cdots(phenyl)_{anion}$ type] and two in the structure of [$C(NH_2)_3$][$B(C_6H_5)_4$]·CH_3CN [1 $(C\text{-}H)_{solvent}\cdots(phenyl)_{anion}$ and 1 $(C\text{-}H)_{anion}\cdots(phenyl)_{anion}$ type].

Intermediate type interactions were identified by the following criteria, developed on the basis of their observed geometries. The minimum $H\cdots H_{ring}$ distance is smaller than the corresponding $H\cdots C_{ring}$ distance, as in the H...H type contacts, but in the intermediate type contacts the two distances are relatively equal. The $H\cdots H_{ring}$ distance is normally greater than 2.5Å, as is $H\cdots C_{ring}$, with both usually falling in the range 2.6±0.2Å. The difference in the two distances is relatively small, usually considerably less than the separation observed in the H...H type contacts (0.4Å to 0.7Å).

Of the six interactions placed in this group, four were found to have similar bond paths, taken to be the standard bond path characteristic of intermediate type contacts. It did not appear to matter the origin of the contact studied, whether cation/anion, solvent/anion or anion/anion type, the bond paths were remarkably similar. Two of the four interactions

were found in [DabcoH][$B(C_6H_5)_4$], $[C(23)-H(23)]_{anion}\cdots[C(33)-H(33)]_{anion}$ and $[C(2)-H(2A)]_{cation}\cdots[C(34)-H(34)]_{anion}$, one was located in the structure of $[C(NH_2)_3][B(C_6H_5)_4]\cdot CH_3CN$, $[C(3)-H(60)]_{solvent}\cdots[C(16)-H(16)]_{anion}$, and the fourth was the previously discussed $[C(12)-H(12)]_{anion}\cdots[C(14)-H(14)]_{anion}$ interaction in the structure of $NH_4B(C_6H_5)_4$. This last interaction was chosen as an example of a typical intermediate contact and its bond path is illustrated in Figure 106.

In each of these interactions, the bond paths share many common features. Beginning from H(C) of the "donor" group it proceeds linearly and quite directly to a point slightly above the C-H phenyl bond of a ring in the anion "acceptor". It then changes direction to curve down and along the bond to its termination at a single ring carbon atom, C_{ring}. The bond path always travels to the C-H bond that makes the closest contact with the "donor" H(C) atom, agreeing exactly with the predicted geometry. It appears to be most common for the bond path to approach the midpoint of the C-H bond, which it does in three of the four interactions studied. In one case, the $[C(2)-H(2A)]_{cation}\cdots[C(34)-H(34)]_{anion}$ contact of [DabcoH][$B(C_6H_5)_4$], the bond path meets the C(34)-H(34) bond at about one third of its length, closer to C(34), before proceeding to C(34).

Contacts predicted by geometry to be intermediate interactions will have bond paths of this type. Conversely, bond paths that begin from H(C) and travel to near the midpoint of the $(C-H)_{anion}$ bond, before following the bond along to end at the closest ring carbon atom are characteristic of intermediate type contacts. Since the bond paths terminate at carbon rather than at hydrogen of the $(C-H)_{anion}$ bond, they are clearly not H...H type contacts and must share many common features with hydrogen bonds.

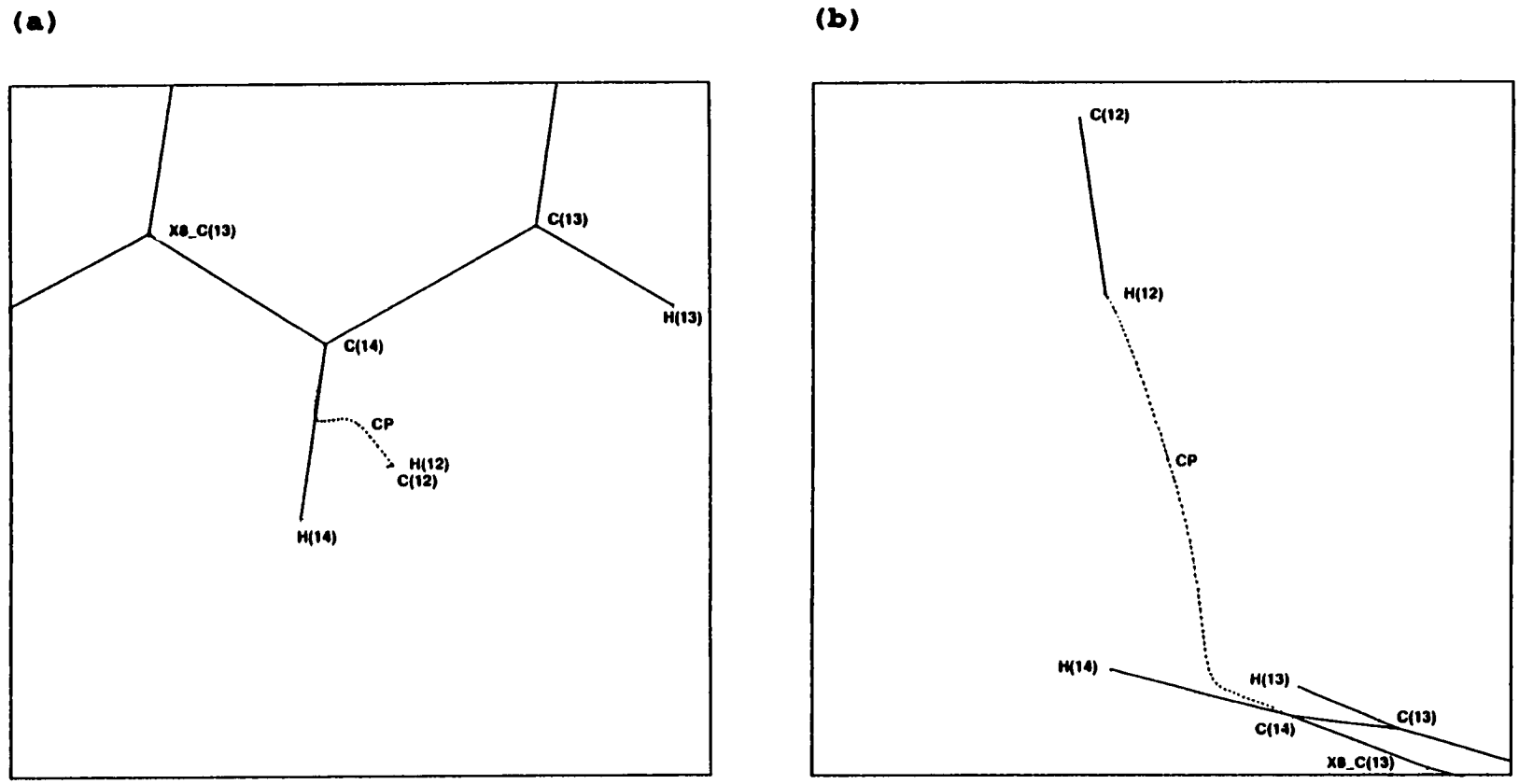

Figure 106. Typical bond path of a C-H...phenyl, intermediate type contact. The C(12)-H(12)...ring 1 interaction of ammonium tetraphenylborate viewed (a) down the C-H bond and (b) approximately perpendicular to the plane of the phenyl ring. CP marks the location of the bond critical point.

In the four intermediate type interactions studied, the H(C)...C_{ring} minimum distances range from 2.468Å (in the anion/anion type contact of $NH_4B(C_6H_5)_4$) to 2.657Å (in the solvent/anion type contact of $[C(NH_2)_3]$-$[B(C_6H_5)_4]\cdot CH_3CN$), while the corresponding H(C)...C_{ring} distances range from 2.799Å (in the solvent/anion type contact of $[C(NH_2)_3][B(C_6H_5)_4]\cdot CH_3CN$) to 2.901Å (in the anion/anion type contact of [DabcoH][$B(C_6H_5)_4$]). The most important characteristic feature, the difference between the minimum H(C)...H_{ring} distance (shorter) and the corresponding H(C)...C_{ring} distance (longer), was calculated for each interaction. In increasing order, the differences are 0.14Å (solvent/anion contact in $[C(NH_2)_3][B(C_6H_5)_4]\cdot CH_3CN$), 0.24Å (cation/anion contact in [DabcoH][$B(C_6H_5)_4$]), 0.29Å (anion/anion contact in [DabcoH][$B(C_6H_5)_4$]) and 0.40Å (anion/anion contact in $NH_4B(C_6H_5)_4$). From this, it appears that intermediate type contacts will arise if the geometry of the interaction is defined by an H(C)...H_{ring} minimum distance that is less than the corresponding H(C)...C_{ring} distance by from 0.14Å to 0.40Å. In the previous section, it was observed that H...H type contacts would arise if the distance difference was greater than 0.44Å. It would appear that at a difference of approximately 0.40Å either type of interaction may arise, probably determined by other circumstances in the contact, while above 0.40Å H...H type contacts are formed and below 0.40Å, to a minimum difference of roughly 0.15Å, intermediate type interactions will be found.

Two of the five intermediate type contacts, so determined on the basis of their geometries, were found to have "non-intermediate" type bond paths moving them into different categories than those originally assigned. The first, the $[C(1)\text{-}H(1A)]_{cation}$...$[ring\ 3]_{anion}$ interaction of

[DabcoH] $[B(C_6H_5)_4]$ was characterized as an intermediate type contact based on an H(1A)...C(34) distance of 2.874Å (133.2°) and an H(1A)...H(34) distance of 2.709Å. The difference in the two distances is only 0.16Å, the second smallest difference found when analyzing the intermediate group of contacts. Only the $[C(3)\text{-}H(60)]_{solvent}\cdots[C(16)\text{-}H(16)]_{anion}$ contact of $[C(NH_2)_3][B(C_6H_5)_4]\cdot CH_3CN$ has a smaller distance difference, 0.14Å.

The bond path of the $[C(1)\text{-}H(1A)]_{cation}\cdots[ring\ 3]_{anion}$ interaction (Figure 96) was found to proceed from H(1A) of the cation to a point above the C(34)-C(35) bond of the anion phenyl ring 3, about one quarter of the way along the bond, closer to C(34). It then curves down and along the bond to terminate at C(34). As will be discussed subsequently, this interaction clearly has a bond path characteristic of an edge type hydrogen bond.

The geometry of the interaction supports the idea that such a bond path might be reasonable. The H(1A)...C(35) distance, 2.975Å (151.9°), is slightly longer than the H(1A)...C(34) distance but is the second shortest of the $H(1A)\ldots C_{ring}$ distances and is shorter than the $H(1A)\ldots\pi_c$ distance. Thus, the bond path is as would be expected for an edge type hydrogen bond, going to the C-C ring bond with the two shortest $H(C)\ldots C_{ring}$ distances and terminating at the C_{ring} atom with the shortest $H(C)\ldots C_{ring}$ distance. Only the fact that the shorter $H(C)\ldots H_{ring}$ contacts have no obvious effect on the interaction must be explained.

This is possible by slightly modifying the geometric criteria used to distinguish between hydrogen bonds and intermediate type contacts. There is some overlap of the distance criteria used for the separation of these bond types but the trends are clear. Intermediate type contacts were

found to have H(C)...H_{ring}/H(C)...C_{ring} distance differences [H(C)...H_{ring} < H(C)...C_{ring}] of from 0.14Å to 0.40Å. This contact, with an edge type bond path, has a distance difference of 0.16Å. Thus, it appears that if the minimum H(C)...H_{ring} distance is shorter than the related H(C)...C_{ring} distance by approximately 0.15Å or more (up to a maximum of approximately 0.40Å) an intermediate type contact results. If the minimum H(C)...H_{ring} distance is any amount longer than the H(C)...C_{ring} distance or if H(C)...H_{ring} is shorter than H(C)...C_{ring} by roughly 0.15Å or less, a hydrogen bond type interaction is formed. The configuration of the hydrogen bond, centroid, edge or single atom type, will depend on other features of the interaction geometry. If the difference in the two distances is close to 0.15Å either type of interaction, hydrogen bond or intermediate type contact, may possibly form, swung in favour of one or the other by other factors.

The second interaction found not to have a bond path characteristic of an intermediate type contact, although it had been placed in that category based on its geometry, was the $[C(34)\text{-}H(34)]_{anion}\cdots[ring\ 4]_{anion}$ interaction of $[C(NH_2)_3][B(C_6H_5)_4]\cdot CH_3CN$. It was characterized as having an intermediate type geometry from its H(34)...H(42) distance of 2.574Å [greater than 2.5Å] and its H(34)...C(42) distance of 2.930Å [greater than 2.5Å and closer to 3.0Å]. The difference in the distances was calculated to be 0.36Å, the second largest difference observed in the intermediate group, the largest being the anion/anion type contact in $NH_4B(C_6H_5)_4$.

The bond path of the $[C(34)\text{-}H(34)]_{anion}\cdots[ring\ 4]_{anion}$ interaction (Figure 100) begins from H(34) of one anion and proceeds to the C(42)-H(42) bond of the second anion, about two thirds of the way along

the bond, closer to H(42). The bond path then changes direction sharply and follows the bond along to its termination at H(42). Thus, although it begins like the bond paths of other intermediate type interactions, it terminates at the hydrogen atom, H(42), rather than the carbon atom, C(42), placing it in the category comprised of H...H type contacts. In fact, this interaction has a bond path very similar to those of several other of the H...H type contacts studied; see for example Figure 103, the $[C(44)-H(44)]_{anion}\cdots[ring\ 3]_{anion}$ interaction of biguanidinium tetraphenylborate. There, the bond path was found to pass from H(44) to the midpoint of the C(33)-H(33) ring bond before ending at H(33).

The fact that the $[C(34)-H(34)]_{anion}\cdots[H(42)]_{anion}$ interaction behaves as an H...H type contact is a bit surprising. The difference in the minimum $H(C)\cdots H_{ring}/H(C)\cdots C_{ring}$ distances in this interaction is only 0.36Å. In the previous section of the discussion, on H...H type contacts, interactions with differences of 0.44Å or greater (up to an observed maximum of 0.70Å) were found to behave as H...H type contacts, while the $[C(12)-H(12)]_{anion}\cdots[C(14)-H(14)]_{anion}$ interaction in $NH_4B(C_6H_5)_4$ was found to behave as an intermediate type contact by bond path with a distance difference of 0.40Å. Here, a contact found to be of the intermediate type by geometry moves into the H...H type contact category based on its bond path, even though the difference in the contact distances is only 0.36Å. Again, some overlap of the distance differences between categories is observed but the general trends are consistent. The cutoff appears to occur at roughly 0.40Å, with a larger difference resulting in an H...H type contact and a smaller difference resulting in an intermediate type contact. If the difference is approximately equal to 0.40Å, either type

of interaction may be formed, depending on other factors influencing the interaction.

In summary then, the original geometric criteria, used to identify the different interaction types, have been modified slightly based on the bond path analysis carried out. In a given C-H...phenyl interaction, it appears that if the minimum H(C)...H_{ring} distance is shorter than the corresponding H(C)...C_{ring} distance by 0.40Å or more an H...H type interaction should be formed. If the distance difference is from 0.15Å to 0.40Å an intermediate type contact should result. If the difference is approximately equal to 0.40Å, either type of interaction may be formed, H...H or intermediate. If the distance difference is less than 0.15Å or if the minimum H(C)...C_{ring} distance(s) are any amount shorter than H(C)...H_{ring} then hydrogen bonds will be formed. Their type, whether centroid, edge or single atom, will be determined by other features of the geometry. If the H(C)...H_{ring} distance is less than H(C)...C_{ring} by approximately 0.15Å, again either type of interaction, hydrogen bond or intermediate type contact, may result. Each class of interaction has a completely characteristic bond path.

H...H type contacts have bond paths that begin from the H(C) atom of the "donor" group and travel to the closest hydrogen atom of the "acceptor", possibly following a C-H bond of the anion "acceptor" for part of its length. Intermediate type contacts have bond paths that also begin from H(C) of the "donor" group. They then proceed to the approximate midpoint of a C-H bond in the anion "acceptor" before changing directions and following the bond to their termination at a ring carbon atom. The atom(s) involved at the "acceptor" in the bond paths of both types of

interactions are always those that make the closest contact(s).

Originally, 34 C-H...phenyl interactions were analyzed according to their geometries and divided into three distinct categories, H...H type contacts (15), intermediate type contacts (5) and hydrogen bonds of different configurations (14). After careful consideration of each bond path only a slight redistribution of the interactions was noted. There were now 35 C-H...phenyl type contacts to consider in total after two new bond paths were located in the structure of $[C(NH_2)_3][B(C_6H_5)_4]\cdot CH_3CN$. There were still 15 H...H type contacts (15 original - 1 to intermediate + 1 from intermediate), while 4 interactions remained in the intermediate category (5 original - 1 to H...H - 1 to hydrogen bond + 1 from H...H) and 13 were found to be hydrogen bonds (14 original + 1 from intermediate - 1 no bond path located - 1 unusual bond path). The 32 contacts whose bond paths are classified here (15 H...H + 4 intermediate + 13 hydrogen bonds) plus the three contacts found to have unusual bond paths in the structure of $[C(NH_2)_3][B(C_6H_5)_4]\cdot CH_3CN$, give the expected total of 35 C-H...phenyl interactions. The results confirm that the original classifications, based solely on geometry, were very accurate; only a few interactions changed categories after consideration of their bond paths. The bond path analysis allowed the geometric criteria to be tightened even further and more accurate predictions of interaction types and their bond paths should be possible in the future. The different classes of bond paths did not appear to be affected by the origin of the interaction, whether cation/anion, solvent/anion or anion/anion. Different classes of interactions were found to have completely characteristic geometries and bond paths, allowing prediction of one from the other and vice versa.

Before proceeding to the hydrogen bond type interactions, one other group of C-H...phenyl contacts should be mentioned. These were not located in the original geometry search for contacts of less than 3Å but were only found during the search for bond paths of other suspected interactions. They were all located in the structure of guanidinium tetraphenylborate acetonitrile solvate, occurring always between the solvent molecule and a phenyl ring of the anion. They are in addition to the interactions predicted by geometry, which were found to have more traditional bond paths travelling from H(C) of the "donor" to the phenyl ring "acceptor" in each case. Those interactions have been discussed in the previous section.

Three interactions with unusual bond paths were located while the geometric contacts were being investigated. The bond paths of these interactions are included in Figures 97 (ring 1) and 98 (ring 2), diagrams from the structure of guanidinium tetraphenylborate acetonitrile solvate. In each of the three interactions, the bond path was found to begin from C(3) of the acetonitrile molecule rather than from one of its hydrogen atoms, making them different from all the other C-H...phenyl interactions studied. In each interaction the bond path does not appear to be clearly associated with any C(3)-H bond of the "donor" solvent molecule. Considering a single acetonitrile molecule, the bond paths travel to two different anions, forming interactions with rings 1 and 2 of one anion, generated by the symmetry (x, y, $1+z$), and with only ring 2 of the second anion, generated by the symmetry ($2-x$, $2-y$, $1-z$).

The lone interaction to the second anion has a bond path (Figure 98) that travels from C(3) of the solvent to a point above the C(22)-C(23)

bond of phenyl ring 2, about one quarter of the way along the bond, closer to C(22). It then changes direction, following the bond to its termination at C(22). The C(3)...C(22) distance, 3.752Å, is the shortest C(3)...C_{ring} distance in the interaction while the C(3)...C(23) distance, 3.775Å, is the second shortest. Thus, the termination of the bond path at C(22) after following the C(22)-C(23) bond for part of its length is reasonable based on the C(3)...C_{ring} distances. The C(3)...C_{ring} distances must be studied because there are no H...C_{ring} distances clearly associated with this type of interaction.

The interaction involving ring 1 of the first anion (Figure 97) was found to have a bond path joining C(3) of the solvent and a C-C bond of the phenyl ring. The bond path begins from C(3) then makes a sharp change in direction in the region of space between H(60) and H(62) before proceeding to the anion. It reaches a point above the C(15)-C(16) bond of ring 1, about one quarter of the way along the bond, closer to C(15), before again changing direction, curving down and along the bond to end at C(15). The two shortest C(3)...C_{ring} distances are made to C(15), 3.721Å, and to C(16), 3.715Å, respectively, so it is not surprising that the bond path proceeds to the C(15)-C(16) bond. However, it would have been expected that the bond path would terminate at C(16) based on these distances; the fact that it instead ends at C(15) is somewhat surprising. The two C(3)...C_{ring} distances in this interaction are very nearly equal, the difference is only 0.01Å, and perhaps it is not unreasonable that the bond path should terminate at C(15), driven there by some other minor factor.

The last interaction, involving ring 2 of the same anion that also

participates in the previous interaction, has the most unusual bond path of all (Figure 98). From C(3), it curves down and around the C(3)-H(60) bond of the solvent, cutting across the bond at its approximate midpoint, before proceeding directly to C(26) of the anion. The C(3)...C(26) distance of 3.918Å is considerably shorter than the next closest C(3)...C_{ring} contact, 3.986Å, made to C(25). The fact that the bond path ends at the single closest ring carbon atom, C(26), based on the C(3)...C_{ring} distances, is reasonable considering the large difference, 0.07Å, between the two minimum values.

In all three interactions, the bond paths behave consistently and rationally in their approaches to the phenyl rings of the $B(C_6H_5)_4^-$ anion "acceptors", if the appropriate C(3)...C_{ring} distances are considered. The only truly unique feature of these bond paths, and interactions, is that they begin from C(3), a carbon atom, rather than from a hydrogen atom of the "donor" group. They are the only C-H...phenyl interactions found to do so and they occur only between the solvent molecule and the anion in the structure of $[C(NH_2)_3][B(C_6H_5)_4]\cdot CH_3CN$. The nature of these interactions must be different from all the others studied, neither hydrogen bonds nor H...H type contacts. It is not completely clear why these interactions arise but it likely has something to do with the charge at C(3) of the solvent molecule or rotation of its methyl group even in the solid state.

Fourteen C-H...phenyl interactions were identified as **hydrogen bonds** using geometric criteria and one more interaction was found to be a hydrogen bond after observation of its bond path (it was originally classified as an intermediate type contact), for a total of 15 potential contacts in this group. Of those fifteen, four were classified as centroid

type hydrogen bonds, nine as edge type hydrogen bonds and two as single atom type hydrogen bonds, again based on their geometries. In all of the interactions but one, the minimum H(C)...C_{ring} distance(s) were found to be shorter than the corresponding H(C)...H_{ring} distance(s) and H(C)...H_{ring} contacts were found to have no effect on the observed bond paths.

In C-H...phenyl hydrogen bonds having **single atom type** geometries, only one H(C)...C_{ring} distance is shorter than the H(C)...π_c ring centroid distance. Of all the C-H...phenyl interactions investigated, only two were found to adopt this configuration. The first interaction is found in the structure of $[C(NH_2)_3][B(C_6H_5)_4]\cdot CH_3CN$, $[C(24)-H(24)]_{anion}\cdots[ring\ 1]_{anion}$, the only one of six anion/anion contacts in that structure with a hydrogen bond type geometry. The interaction is characterized by an H(24)...C(14) distance of 2.863Å (164.8°) and thus the bond path would be expected to travel between these two atoms. The second contact is found in the structure of [DabcoH][$B(C_6H_5)_4$], $[C(2)-H(2A)]_{cation}\cdots[ring\ 1]_{anion}$, and is characterized by a slightly longer principal distance, H(2A)...C(13) equal to 3.044Å (131.4°).

Both interactions were found to have similar bond paths. Figure 107 illustrates the bond path of a typical single atom type hydrogen bond, using the $[C(24)-H(24)]_{anion}\cdots[ring\ 1]_{anion}$ interaction of guanidinium tetraphenylborate acetonitrile solvate as an example. This interaction is one of those shown in Figure 97, while the $[C(2)-H(2A)]_{cation}\cdots[ring1]_{anion}$ interaction of [DabcoH][$B(C_6H_5)_4$] may be seen in Figure 94. In each case, the bond path begins from H(C) of the "donor" and travels linearly and quite directly to a single C_{ring} atom of the anion "acceptor". The carbon atom at which the bond path terminates is always the one that makes the

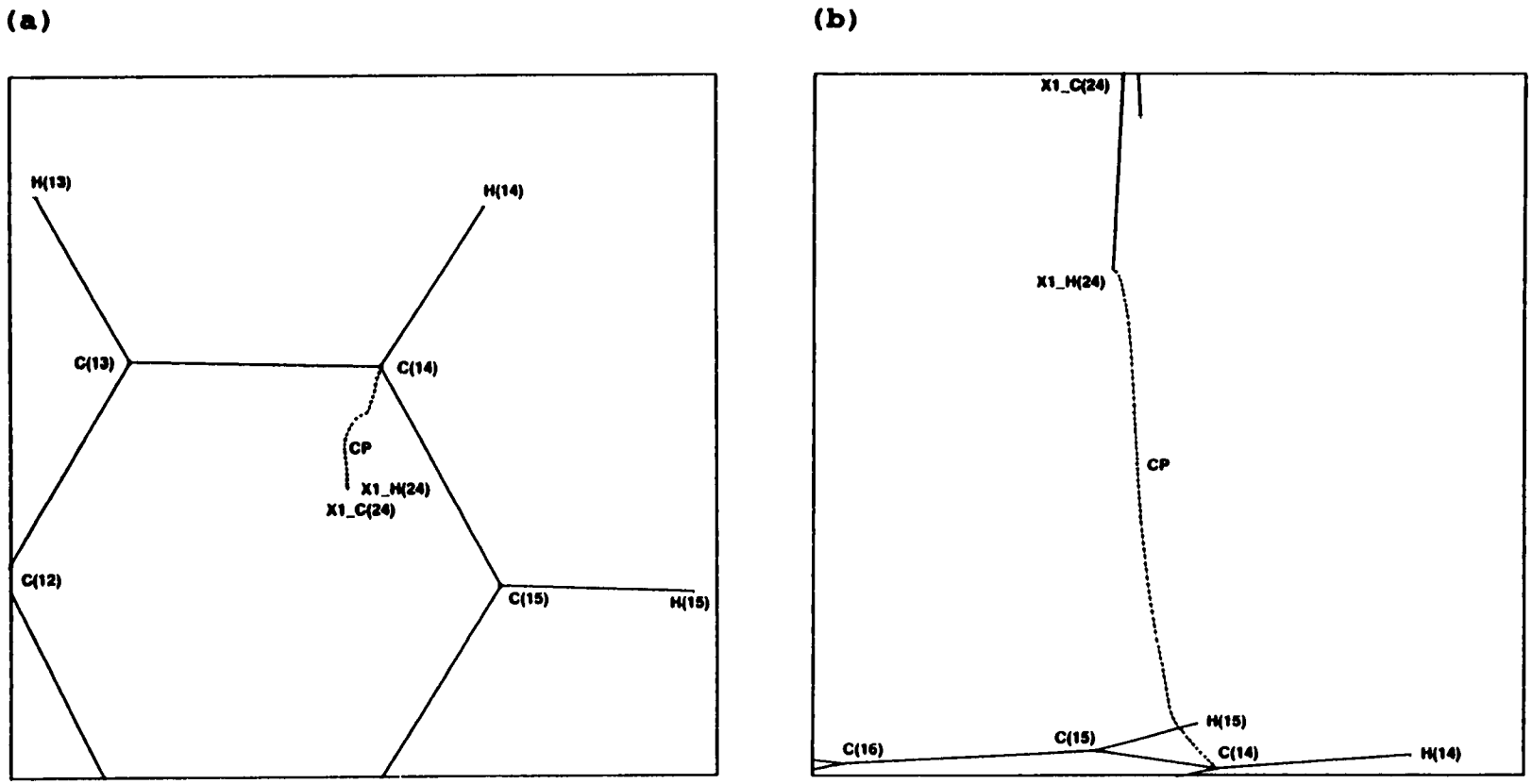

Figure 107. Typical bond path of a C-H...phenyl, single atom type hydrogen bond. The C(24)-H(24)...ring1 [C(14)] interaction of guanidinium tetraphenylborate acetonitrile solvate viewed (a) down the C-H bond and (b) approximately perpendicular to the plane of the phenyl ring. CP marks the location of the bond critical point.

shortest H(C)...C_{ring} contact. Thus the geometry of this type of interaction agrees completely with the characteristic bond path adopted. All single atom type hydrogen bonds would be expected to exhibit such a bond path. The origin of the interaction does not appear to matter, cation/anion and anion/anion types both show consistent bond paths. Nor does the minimum H(C)...C_{ring} distance characterizing the interaction appear to have an effect on the bond path adopted. The [DabcoH][$B(C_6H_5)_4$] interaction occurs over a distance longer than 3.0Å but still shows the same characteristic bond path.

Of the nine interactions in the **edge type** hydrogen bond category, two were excluded immediately, for rather different reasons. The first excluded interaction was the [C(3)-H(3A)]$_{cation}$...[ring 1]$_{anion}$ contact of [DabcoH][$B(C_6H_5)_4$]. This was expected, from its geometry, to be an edge type hydrogen bond involving the anion C(13)-C(14) bond, H(3A)...C(13) = 2.894Å and H(3A)...C(14) = 2.918Å. The corresponding H(3A)...H_{ring} distances are very slightly longer, 2.905Å and 2.963Å, respectively.

However, this was the only interaction of all those studied where a (3,-1) bond critical point and a bond path could not be located, even after extensive searching. The reason that this might be so is suggested by the geometry of the interaction. The C(3)-H(3A) vector of the cation does project toward the ring 1 plane of the anion but it points directly away from the ring itself. This is evident in the very nonlinear angles, C(3)-H(3A)...C_{ring}, formed in the interaction, 108.6° to C(13) and 122.3° to C(14). These angles are considerably smaller than any of those characterizing the other [DabcoH][$B(C_6H_5)_4$] cation/anion type interactions. This geometry suggests that it may be impossible for an interaction of any

consequence to occur.

It is also interesting to note that the C(3)-H(3A) group of the DabcoH$^+$ cation was predicted by geometry to form a pair of bifurcated interactions to ring 1 and ring 3 of two different anions. The former interaction, or lack of it, was just discussed and the latter interaction was found, by both geometry and bond path, to be an H...H type contact, $[C(3)-H(3A)]_{cation}\cdots[H(36)]_{anion}$. Thus, C(3)-H(3A) of the DabcoH$^+$ cation is not involved in any hydrogen bond type interactions. It is the only C-H group of the cation that does not participate in at least one hydrogen bond.

The second interaction found to be excluded from the study of edge type hydrogen bonds was the $[C(3)-H(62)]_{solvent}\cdots[ring\ 2]_{anion}$ contact in the structure of $[C(NH_2)_3][B(C_6H_5)_4]\cdot CH_3CN$. From its geometry, this was predicted to be an edge type hydrogen bond involving the C(22)-C(23) bond of the anion. The H(62)...C(22) distance of 3.130Å (117.2°) and the H(62)...C(23) distance of 2.886Å (139.2°) were both shorter than the corresponding $H(62)\cdots H_{ring}$ distances, 3.414Å and 3.070Å, respectively. The reason that this interaction was excluded from the study of edge type C-H...phenyl hydrogen bonds was that its bond path was found to begin from C(3) rather than from H(62) of the "donor" group (Figure 98). Several of the solvent/anion type interactions in $[C(NH_2)_3][B(C_6H_5)_4]\cdot CH_3CN$ were found to have such unusual bond paths, beginning from C(3) rather than a hydrogen atom of the acetonitrile solvent molecule. They have been discussed as a separate group, being rather different from any other of the C-H...phenyl interactions studied. All other C-H interactions showed the expected bond path origin, H(C) of the "donor" group.

The seven remaining interactions in the edge type hydrogen bond group were compared by both geometry and bond path. Two of the interactions were found in the structure of biguanidinium tetraphenylborate, while five were from the [DabcoH][$B(C_6H_5)_4$] structure. All have been described in detail in the geometry section but the pertinent details are summarized here. The first interaction, $[C(13)\text{-}H(13)]_{anion}\cdots[ring\ 2]_{anion}$ (bond path Figure 95), in biguanidinium tetraphenylborate is predicted to involve the C(25)-C(26) bond of the second anion based on the distances H(13)...C(25) = 2.873Å and H(13)...C(26) = 2.762Å, a difference of 0.11Å between the two closest H(13)...C_{ring} contacts. The second interaction in biguanidinium tetraphenylborate, $[C(12)\text{-}H(12)]_{anion}\cdots[ring\ 3]_{anion}$ (bond path Figure 103), is characterized by H(12)...C(34) and H(12)...C(35) distances of 2.865Å and 3.073Å, respectively, for a difference between the two of 0.21Å. The C(1)-H(1A) group of the $DabcoH^+$ cation was found to be involved in two edge type hydrogen bonds, $[C(1)\text{-}H(1A)]_{cation}\cdots[ring\ 2]_{anion}$ (bond path Figure 95), with H(1A)...C(22) = 2.911Å and H(1A)...C(23) = 2.847Å for a difference of 0.06Å, and $[C(1)\text{-}H(1A)]_{cation}\cdots[ring\ 3]_{anion}$ (bond path Figure 96), with H(1A)...C(34) = 2.874Å and H(1A)...C(35) = 2.975Å (difference = 0.10Å). The third interaction in the structure, $[C(3)\text{-}H(3B)]_{cation}\cdots[ring\ 3]_{anion}$ (bond path Figure 96), was predicted, based on the H(3B)...C(35), 2.975Å, and H(3B)...C(36), 3.055Å, distances (difference = 0.08Å), to involve the C(35)-C(36) bond of the anion. The $[C(4)\text{-}H(4A)]_{cation}\cdots[ring\ 3]_{anion}$ interaction in the same structure (bond path Figure 96) is accepted by the C(32)-C(33) bond of the anion, with defining distances of 3.026Å [H(4A)...C(32)] and 2.854Å [H(4A)...C(33)] respectively (difference = 0.17Å). The last contact, is also from the

structure of [DabcoH][$B(C_6H_5)_4$]; $[C(4)\text{-}H(4B)]_{cation}\cdots[ring\ 2]_{anion}$ (bond path Figure 95) has an edge type hydrogen bond geometry with an H(4B)...C(22) distance of 3.105Å and an H(4B)...C(23) distance of 2.921Å, for a difference between the two of 0.18Å.

The bond paths of these seven interactions were carefully examined and compared. Again, they did not appear to be affected by the origin of the interaction, whether anion/anion or cation/anion type only a single characteristic bond path pattern was observed. Six of the seven interactions were found to have bond paths consistent with their proposed edge type hydrogen bond geometries. The bond path of the [DabcoH][$B(C_6H_5)_4$] $[C(1)\text{-}H(1A)]_{cation}\cdots[ring\ 2]_{anion}$ is illustrated in Figure 108 as an example of a typical edge type hydrogen bond. In all of these interactions the bond path begins at H(C) of the "donor" group and proceeds linearly and quite directly to a point just above the C-C anion ring bond of the "acceptor" that makes the closest $H(C)\cdots C_{ring}$ contacts. It then changes direction, curving down to and along the bond before terminating at the single, closest ring carbon atom. The interacting bond was always that predicted from the geometry, that with the two shortest $H(C)\cdots C_{ring}$ distances, and the bond path always terminated at the carbon atom with the shortest $H(C)\cdots C_{ring}$ separation. The bond path would either approach the midpoint of the C-C bond (2 examples) or it would approach the closer C_{ring} atom in the bond (4 examples), following the C-C bond for approximately one quarter of its length before ending at the carbon atom with the shorter $H(C)\cdots C_{ring}$ distance.

It is interesting to note that in the two examples with bond paths that approach the midpoint of the C-C bond, the differences in the two

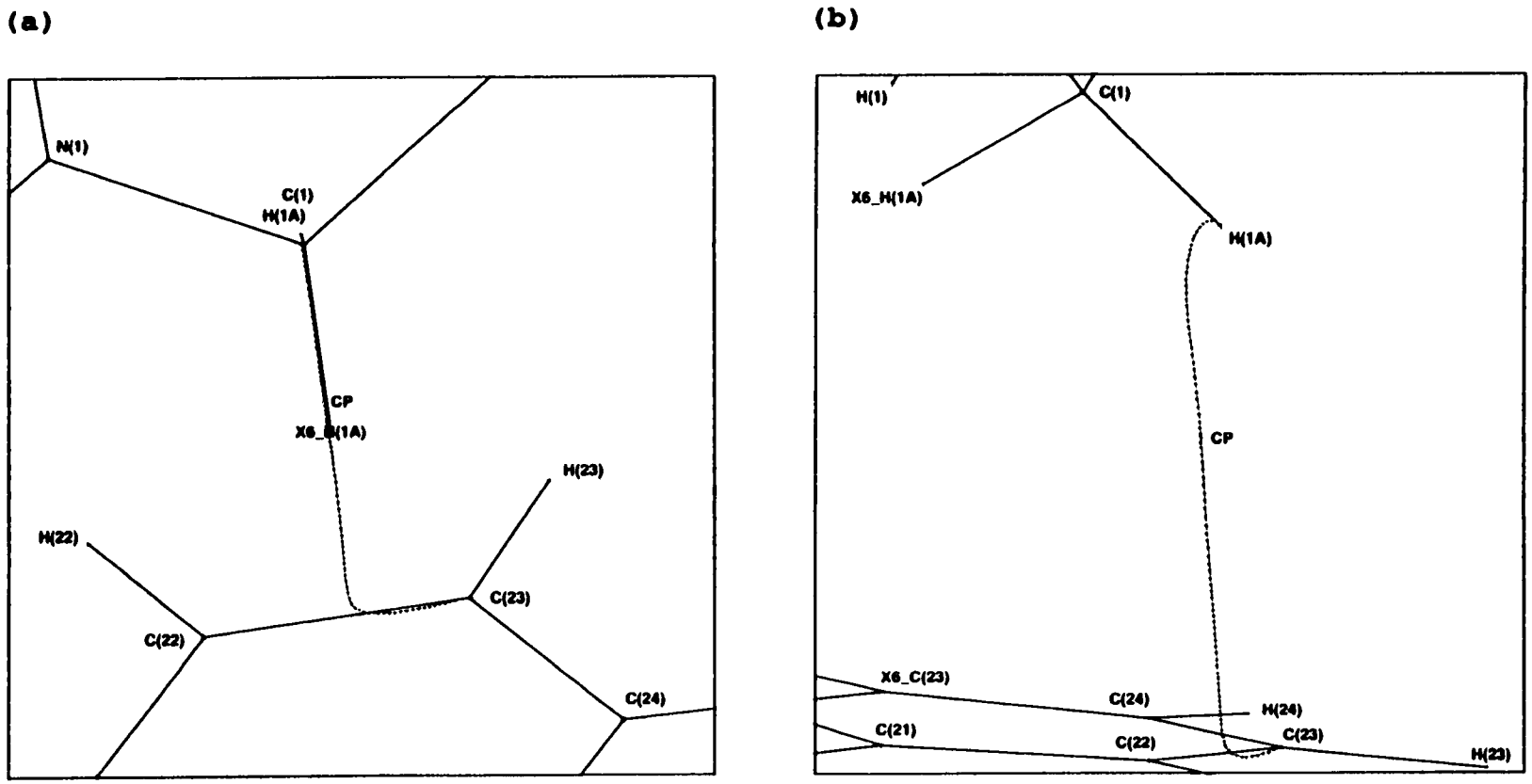

Figure 108. Typical bond path of a C-H...phenyl, edge type hydrogen bond. The C(1)-H(1A)...ring 2 [C(22)-C(23)] interaction of [DabcoH][$B(C_6H_5)_4$] viewed (a) down the C-H bond and (b) approximately perpendicular to the plane of the phenyl ring. CP marks the location of the bond critical point.

minimum H(C)...C_{ring} distances are 0.06Å (C(1)-H(1A)...C(22)-C(23)* in [DabcoH][$B(C_6H_5)_4$]) and 0.08Å (C(3)-H(3B)...C(35)*-C(36) also in [DabcoH][$B(C_6H_5)_4$]). These are the two smallest differences observed in the seven contacts studied. The four interactions that follow the C-C bond for only one quarter of its length were found to have distance differences ranging from 0.10Å (C(1)-H(1A)...C(34)*-C(35) in [DabcoH][$B(C_6H_5)_4$]) to 0.18Å (C(4)-H(4B)...C(22)-C(23)* in [DabcoH][$B(C_6H_5)_4$]). In the cases where the two minimum H(C)...C_{ring} distances are more unequal, 0.10Å or more, the bond path approaches the C-C bond nearer to the closer ring carbon atom. In cases where the two minimum H(C)...C_{ring} are more nearly equal, with a difference of 0.10Å or less, the bond path approaches the midpoint of the interacting C-C bond.

Examination of differences in the two minimum H(C)...C_{ring} distances can be taken one step further, in connection with the last interaction in this category, that found not to have a bond path characteristic of an edge type hydrogen bond. It is the $[C(12)-H(12)]_{anion}$...$[ring\ 3]_{anion}$ interaction in the structure of biguanidinium tetraphenylborate (Figure 103) which by geometry was also predicted to have an edge type hydrogen bond configuration, to the C(34)-C(35) bond of the second anion [H(12)...C(34) = 2.865Å and H(12)...C(35) = 3.073Å, difference = 0.21Å]. However, the bond path was found to proceed from H(12) directly to C(34) of anion ring 3. Rather than behaving as an edge type interaction, the bond path shows this to be a single atom type hydrogen bond. This is readily explained by considering the difference in the two minimum H(C)...C_{ring} distances in this interaction, 0.21Å. This difference is greater than that in any other edge type hydrogen bond studied, the next

closest difference being only 0.18Å. The results suggest that if the difference in the two shortest H(C)...C_{ring} distances becomes too great, roughly 0.20Å or larger, the interaction will behave like a single atom type hydrogen bond rather than as an edge type hydrogen bond.

To summarize this section, edge type hydrogen bonds have geometries in which two, and only two, H(C)...C_{ring} distances are shorter than the H(C)...π_c ring centroid distance. The two H(C)...C_{ring} distances must be close to equal, differing by less than roughly 0.20Å. If the two distances are different by 0.20Å or more, or if there is only one H(C)...C_{ring} distance shorter than the H(C)...π_c distance, then a single atom type hydrogen bond will be formed. In either of these types of hydrogen bonds, the pertinent H(C)...C_{ring} distance(s) must be less than the related H(C)..H_{ring} distance(s) or the H(C)...H_{ring} distance(s) may be very slightly shorter than the H(C)...C_{ring} distance(s), approximately 0.15Å or less.

Single atom type hydrogen bonds have a characteristic bond path that travels from H(C) directly to the C_{ring} atom with which it makes the closest contact. The characteristic bond path of an edge type hydrogen bond travels from H(C) to a C-C ring bond of the anion, to that bond with the two shortest H(C)...C_{ring} distances. The bond path then travels along the C-C bond to the closer C_{ring} atom, that with the shortest H(C)...C_{ring} separation. If the difference in the two minimum H(C)...C_{ring} distances is small, roughly 0.10Å or less, the bond path will proceed from H(C) to near the midpoint of the interacting C-C bond. If the difference in the two distances is longer, 0.10Å to 0.20Å, then the bond path will make an off-center approach to the C-C ring bond, coming nearer to the closer C_{ring} atom. Using these criteria, the bond paths of edge type or single atom

type hydrogen bonds can be predicted from their geometries.

A total of four **centroid type** C-H...phenyl hydrogen bonds were identified by their geometries, one in the structure of $NH_4B(C_6H_5)_4$, one in the structure of $[C(NH_2)_3][B(C_6H_5)_4]\cdot CH_3CN$ and two in the structure of $[N(C[NH_2]_2)_2][B(C_6H_5)_4]$. Three were found to be $(C\text{-}H)_{anion}\cdots(phenyl)_{anion}$ type interactions while one, that in the structure of $[C(NH_2)_3][B(C_6H_5)_4]\cdot CH_3CN$, was found to be of the $(C\text{-}H)_{solvent}\cdots(phenyl)_{anion}$ type. In all of the centroid type hydrogen bonds, $H(C)\cdots H_{ring}$ contact distances are longer and do not have a visible influence on the interaction.

The $[C(14)\text{-}H(14)]_{anion}\cdots[ring\ 1]_{anion}$ interaction in ammonium tetraphenylborate is characterized by an $H(14)\cdots\pi_c$ distance of 2.717Å (171.6°). The range of $H(14)\cdots C_{ring}$ distances is narrow, with 100Δ equal to 45, and all are longer than the $H(14)\cdots\pi_c$ distance [100Δ = (maximum $H\cdots C_{ring}$ - minimum $H\cdots C_{ring}$) X 100]. The shortest $H(14)\cdots C_{ring}$ distance is made to C(11), 2.841Å (158.4°), and the next shortest is made to C(12), 2.935Å (155.3°), a difference between the two of 0.09Å. The bond path for this interaction (Figure 93) proceeds from H(14) to a point above the plane of ring 1, just inside the ring closest to C(11). It then curves gently down and out, ending at C(11). The bond path is not unreasonable, passing to the ring carbon atom with the shortest $H(C)\cdots C_{ring}$ distance.

The second centroid type hydrogen bond was located in the structure of $[C(NH_2)_3][B(C_6H_5)_4]\cdot CH_3CN$, $[C(3)\text{-}H(61)]_{solvent}\cdots[ring\ 1]_{anion}$. The bond path of this interaction is included in Figure 97 but is also shown in Figure 109 in an expanded view, to show in more detail the bond path of a centroid type hydrogen bond. The bond path travels from H(61) to the approximate midpoint of the C(13)-C(14) bond of the anion, where it

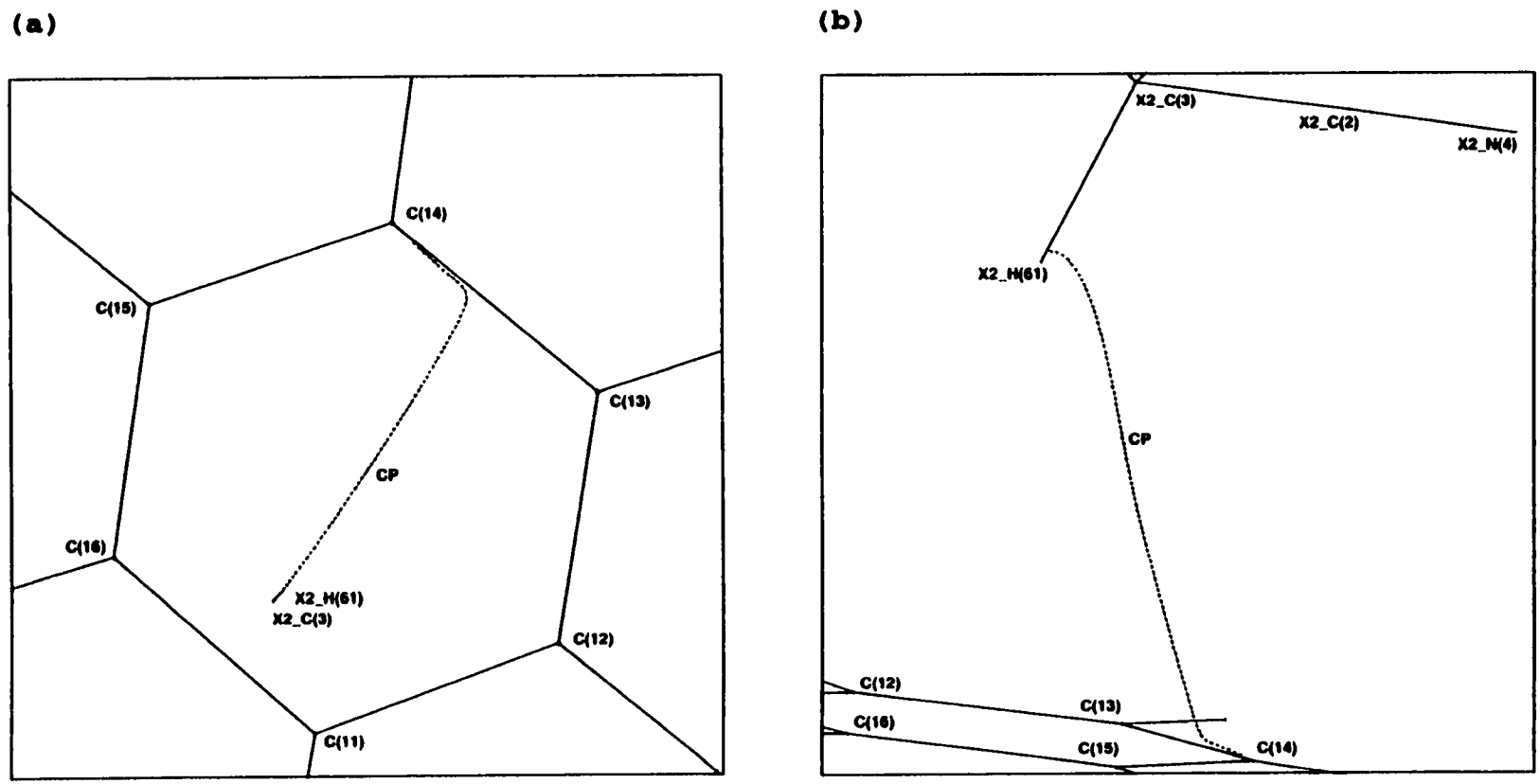

Figure 109. Typical bond path of a C-H...phenyl, centroid type hydrogen bond. The C(3)-H(61)...ring 1 interaction of guanidinium tetraphenylborate acetonitrile solvate viewed (a) down the C-H bond and (b) approximately perpendicular to the plane of the phenyl ring. CP marks the location of the bond critical point.

changes direction and proceeds along the bond to its termination at C(14). In this case, the bond path does not go to the carbon atom with the shortest H(61)...C_{ring} distance [C(12) 2.765Å (145.1°)], nor does it go the bond with the closest pair of H(61)...C_{ring} contacts [C(12) and C(13) 2.781Å (130.2°)]. Rather, the bond path travels to the bond with the second and third shortest H(61)...C_{ring} distances [C(13) and C(14) 2.847Å (129.6°)] and terminates at the atom with only the third shortest H(61)...C_{ring} distance, C(14). The difference in the H(61)...C(13) and H(61)...C(14) distances is small, only 0.07Å, as is the entire range of H(61)...C_{ring} distances; 100Δ equals only 14.

The first centroid type hydrogen bond in $[N(C[NH_2]_2)_2][B(C_6H_5)_4]$, is the $[C(14)\text{-}H(14)]_{anion}$...$[ring\ 2]_{anion}$ contact, which has an H(14)...π_c distance of 2.797Å (135.0°) and a value of 100Δ equal to 53, indicative of a more off-center arrangement. The two minimum H(14)...C_{ring} distances are 2.849Å (154.5°) and 2.904Å (156.4°) to C(22) and C(23), respectively, for a difference of 0.06Å between the two. The bond path (Figure 102) travels from H(14) to a point just above the C(22)-C(23) bond of the anion, roughly one quarter of the way along the bond, closer to C(22). It then changes direction, curving down and along the bond before ending at C(22). In this case, the bond path is as expected, at least in so far as it travels to the anion ring 2 bond with the two shortest H(14)...C_{ring} distances and it terminates at the carbon ring atom making the closest contact with H(14), C(22).

The last centroid type hydrogen bond investigated is also from the structure of $[N(C[NH_2]_2)_2][B(C_6H_5)_4]$, $[C(15)\text{-}H(15)]_{anion}$...$[ring\ 4]_{anion}$. It is characterized by an H(15)...π_c distance of 2.650Å (149.7°) and a narrow

range of H(15)...C_{ring} distances; 100Δ = 14. The two shortest H(15)...C_{ring} distances are H(15)...C(42) equal to 2.927Å (147.0°) and H(15)...C(41) equal to 2.952Å (174.3°), a difference of 0.02Å. The bond path of this interaction (Figure 104) proceeds from H(15) to a point above the C(41)-C(42) bond of the second anion, approximately one quarter of the distance along the bond, closer to C(41). The bond path then curves down and along the bond until it reaches C(41) where it ends. It does travel to the bond with the two shortest H(15)...C_{ring} distances, however, it terminates at C(41) which is not the closest ring carbon atom involved in the interaction. It would have been expected to end at C(42) based on all the previous interactions studied. In this case, the two minimum H(15)...C_{ring} distances are close to equal, the difference is only 0.02Å, and a more linear C(15)-H(15)...C_{ring} angle is made to C(41), 174.3°, than to the closer C(42), 147.0°. It is perhaps not unreasonable that the bond path should end at C(41) instead of C(42).

Centroid type hydrogen bonds are readily characterized by their geometries, with all H(C)...C_{ring} distances shorter than the H(C)...π_c ring centroid distances. However, it is very difficult to predict the bond path that will be adopted in such interactions. Large variations in bond paths are observed with very small differences in geometry. The bond path does not conform to that expected by geometry in some cases. Why might this be so? The six H(C)...C_{ring} distances in a centroid geometry hydrogen bond normally cover only a small range of values; the distances are often nearly equal. This is reflected in the 100Δ parameter which is often very small for centroid type geometries. In the four centroid type interactions studied, 100Δ ranges from only 14 to 53. Because many of the H(C)...C_{ring}

distances are so similar, unlike those in other types of hydrogen bonding interactions where one or two distances are significantly shorter than the rest, other factors, normally minor, may influence where the bond path actually travels. Rather than the distance over which the interaction occurs dominating, perhaps the angle of the interaction, more linear approaches being favoured, and/or the atomic charge distribution determine the bond path.

It does appear that the narrower the range of $H(C)\ldots C_{ring}$ distances, and thus the smaller 100Δ is, the harder it becomes to predict where the bond path will travel. As the range of distances narrows, the greater the effect of the other, normally minor, factors, tipping the balance in favour of one ring atom or another, not necessarily the closest contact. In those cases where the range of $H(C)\ldots C_{ring}$ distances is larger, 100Δ equals approximately 45 or greater based on the experimental results, the bond path is more easily predicted. Distance again becomes the factor determining where the bond path will go, resulting in it approaching the closest $H(C)\ldots C_{ring}$ contact(s).

In the centroid type hydrogen bonds that do behave predictably, those with larger values for 100Δ, it appears that if the two minimum $H(C)\ldots C_{ring}$ distances are close to equal (experimental differences of 0.02Å and 0.06Å) the bond path will proceed to the C-C ring bond with the two shortest $H(C)\ldots C_{ring}$ distances. In the one example where the two minimum $H(C)\ldots C_{ring}$ distances are more unequal (a difference of 0.09Å) the bond path travels directly to the closer ring carbon atom rather than to the bond. This is exactly the same pattern as observed in the bond paths of edge type hydrogen bonds but on a more compressed distance scale,

likely because of the smaller differences in distances found in centroid type hydrogen bonds.

Centroid type hydrogen bonds have bond paths that are equivalent to those observed for single atom and edge type hydrogen bonds. Therefore, geometry must first be used to determine the nature of the C-H...phenyl hydrogen bond configuration, whether single atom, edge or centroid type. Once the configuration of the hydrogen has been decided the bond path can usually be predicted reasonably well.

In all cases, H...H type contacts, intermediate type contacts, or hydrogen bonds, the general bond path can always be predicted from the observed geometry. Each type of interaction has a completely characteristic bond path and from any bond path the nature of the interaction can be discerned. The origin of the interaction, whether anion/anion, cation/anion or solvent/anion, appears to have no visible effect on the bond path adopted; the bond path remains characteristic of its type. Narrower ranges of distance criteria have been developed, based on the observed bond paths, to predict interaction types from the observed geometries.

Analysis of the bond paths supports all the conclusions made previously, on the basis of geometry, of the importance of C-H...phenyl interactions, particularly those of hydrogen bond type, in the four structures studied. The N-H...π(Ph) hydrogen bonds play an even more important role in these structures. However, there are far fewer of such interactions, 16 N-H...X versus 44 C-H...X [X = N or π(Ph)], making them more difficult to characterize. Would the bond paths of N-H...X hydrogen bonds follow similar patterns and the same rules as the C-H...X interactions studied?

3.6.2.4. N-H...N Interactions

Sixteen N-H...X [X = N or π(Ph)] interactions were studied in the course of this investigation, of which fourteen were of the N-H...π(Ph) type while only two were conventional N-H...N hydrogen bonds. As discussed previously, the first interaction, $[N(1)\text{-}H(1B)]_{cation}\cdots[N(4)]_{solvent}$, was located in the structure of $[C(NH_2)_3][B(C_6H_5)_4]\cdot CH_3CN$ and the second interaction, $[N(4)\text{-}H(4A)]_{cation}\cdots[N(1)]_{cation}$, was located in the structure of $[N(C[NH_2]_2)_2][B(C_6H_5)_4]$. In the latter, a pair of equivalent N-H...N hydrogen bonds hold a cation dimer together, while in the former the interaction occurs between the cation and the acetonitrile solvent molecule.

Geometrically, the two interactions are similar, having close to equal H(N)...N distances. The $[N(1)\text{-}H(1B)]_{cation}\cdots[N(4)]_{solvent}$ interaction of $[C(NH_2)_3][B(C_6H_5)_4]\cdot CH_3CN$ is characterized by a short H(1B)...N(4) distance of 2.082Å and an N(1)-H(1B)...N(4) angle of 143.4°. Similarly, the $[N(4)\text{-}H(4A)]_{cation}\cdots[N(1)]_{cation}$ interaction of $[N(C[NH_2]_2)_2][B(C_6H_5)_4]$ has an H(4A)...N(1) distance of 2.127Å, but also a more linear angle, N(4)-H(4A)...N(1) = 175.1°. Experimentally, both N-H...N hydrogen bonds were found to have similar bond paths as well, proceeding from the H(N) atom of the donor directly to the nitrogen atom acceptor, whether in the cation or in the solvent molecule. The origin of the interaction, cation/solvent or cation/cation type, has no visible effect on the bond path adopted. The bond paths of these two interactions are illustrated in Figures 110 and 111 (at the end of this section) for the N-H...N hydrogen bonds in guanidinium tetraphenylborate acetonitrile solvate and biguanidinium tetraphenylborate respectively.

It is interesting to note that the 1997 publication by Mallinson et al.[22] includes a diagram showing the bond path of the internal N-H...N hydrogen bond in the monoprotonated cation of 1,8-bis(dimethylamino)-naphthalene. The bond path is shown to proceed from H(1nn) directly to N(1) in the N(2)-H(1nn)...N(1) hydrogen bond. This appears to be the only known example of a topological analysis of an N-H...N type hydrogen bond reported in the literature. The bond path matches exactly with those determined in this work. Even with so few examples available, it appears that the characteristic bond path of an N-H...N type hydrogen bond is as observed, travelling directly between H(N) of the donor and N, the nitrogen atom acceptor.

The bond paths of the N-H...N hydrogen bonds also conform to those of the C-H...N interactions studied. A total of nine such contacts were investigated and in every case the bond path was found to proceed from H(C) of the "donor" group to a nitrogen atom of the "acceptor" either a cation or a solvent molecule. This helps to substantiate the proposal that the bond paths observed in the N-H...N hydrogen bonds are indeed characteristic of such interactions. It is also the first evidence that perhaps C-H...X and N-H...X interactions of the same type, in this case X = N, have the same characteristic bond paths.

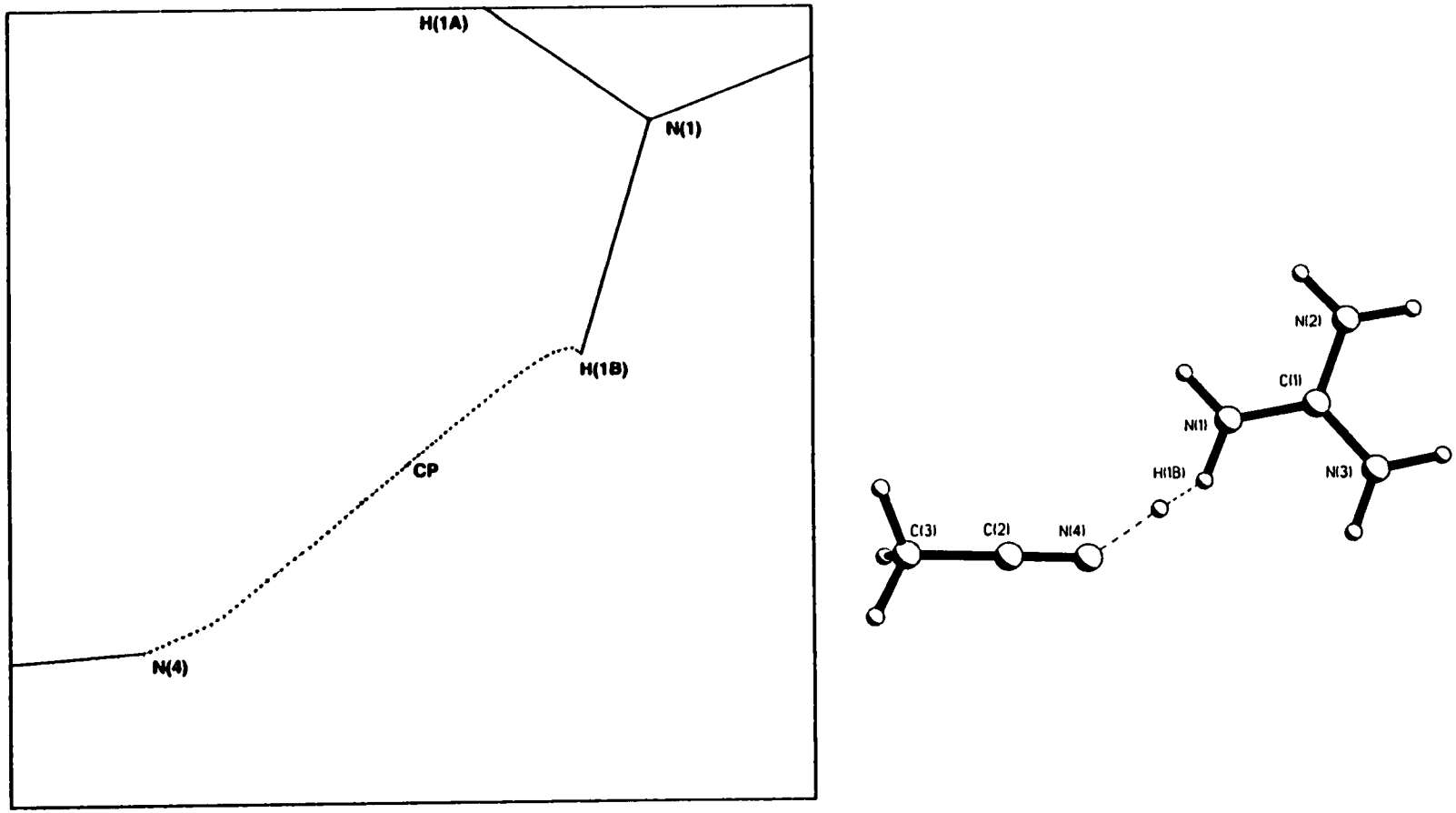

Figure 110. Bond path of the N-H...N (cation/solvent) hydrogen bond in the structure of guanidinium tetraphenylborate acetonitrile solvate. CP marks the location of the bond critical point.

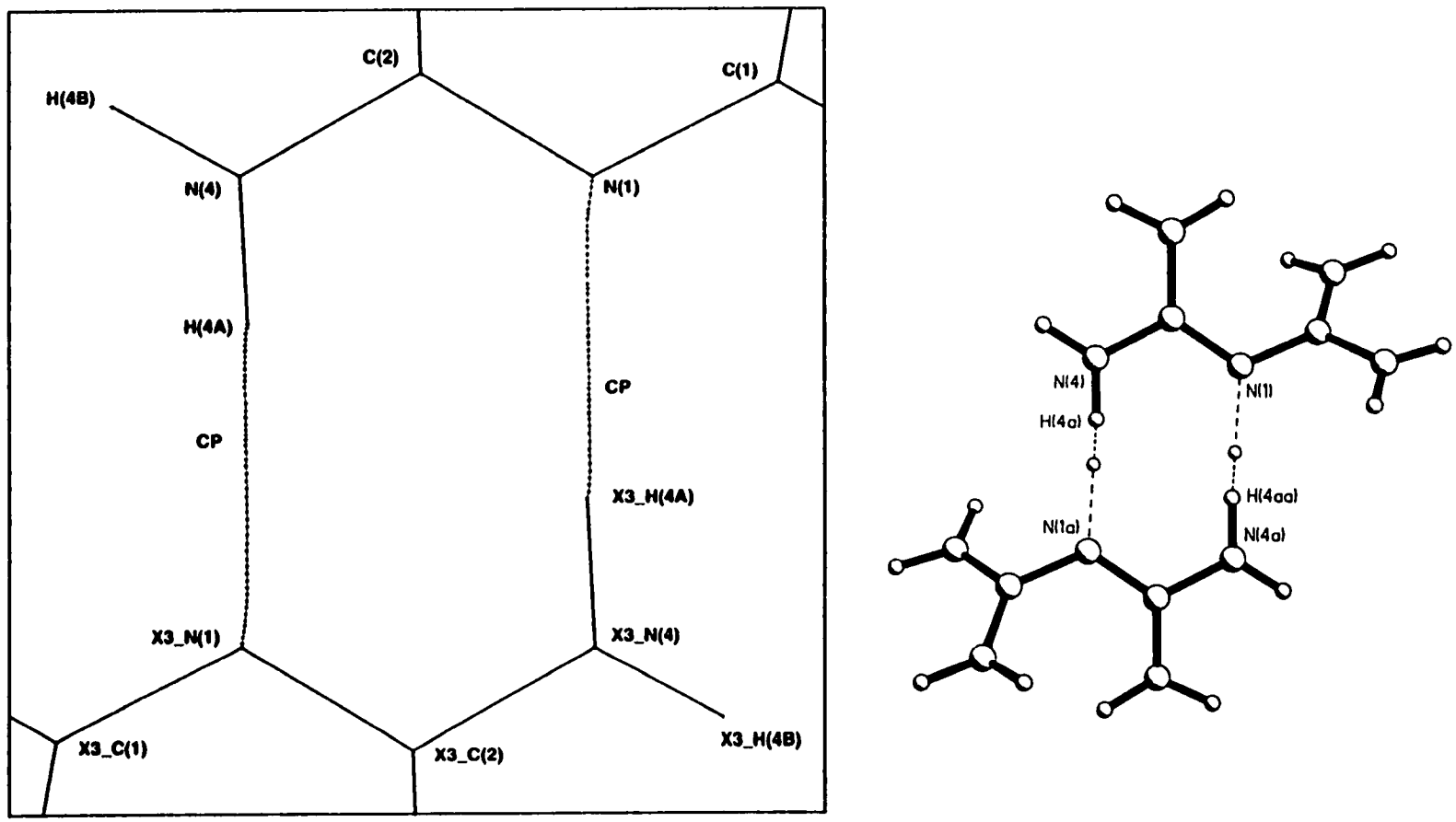

Figure 111. Bond path of the N-H...N hydrogen bond in the cation dimer of biguanidinium tetraphenylborate (two equivalent hydrogen bonds hold the dimer together). CP marks the location of the bond critical point.

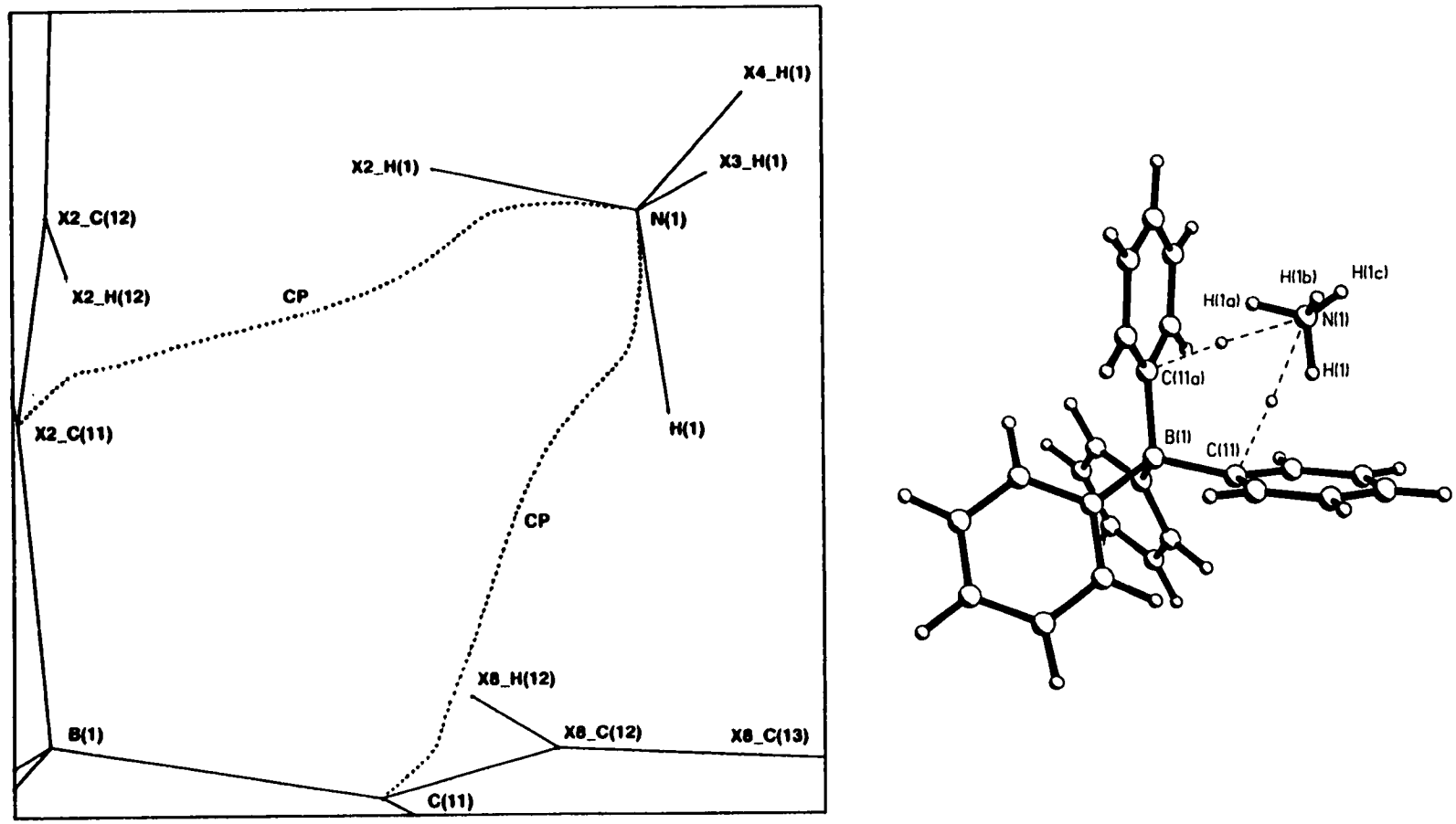

Figure 112. Bond path located for the N-H...π(Ph) hydrogen bond in the structure of ammonium tetraphenylborate, drawn to emphasize the role of the phenyl ring as the acceptor of the interaction. CP marks the location of the bond critical point.

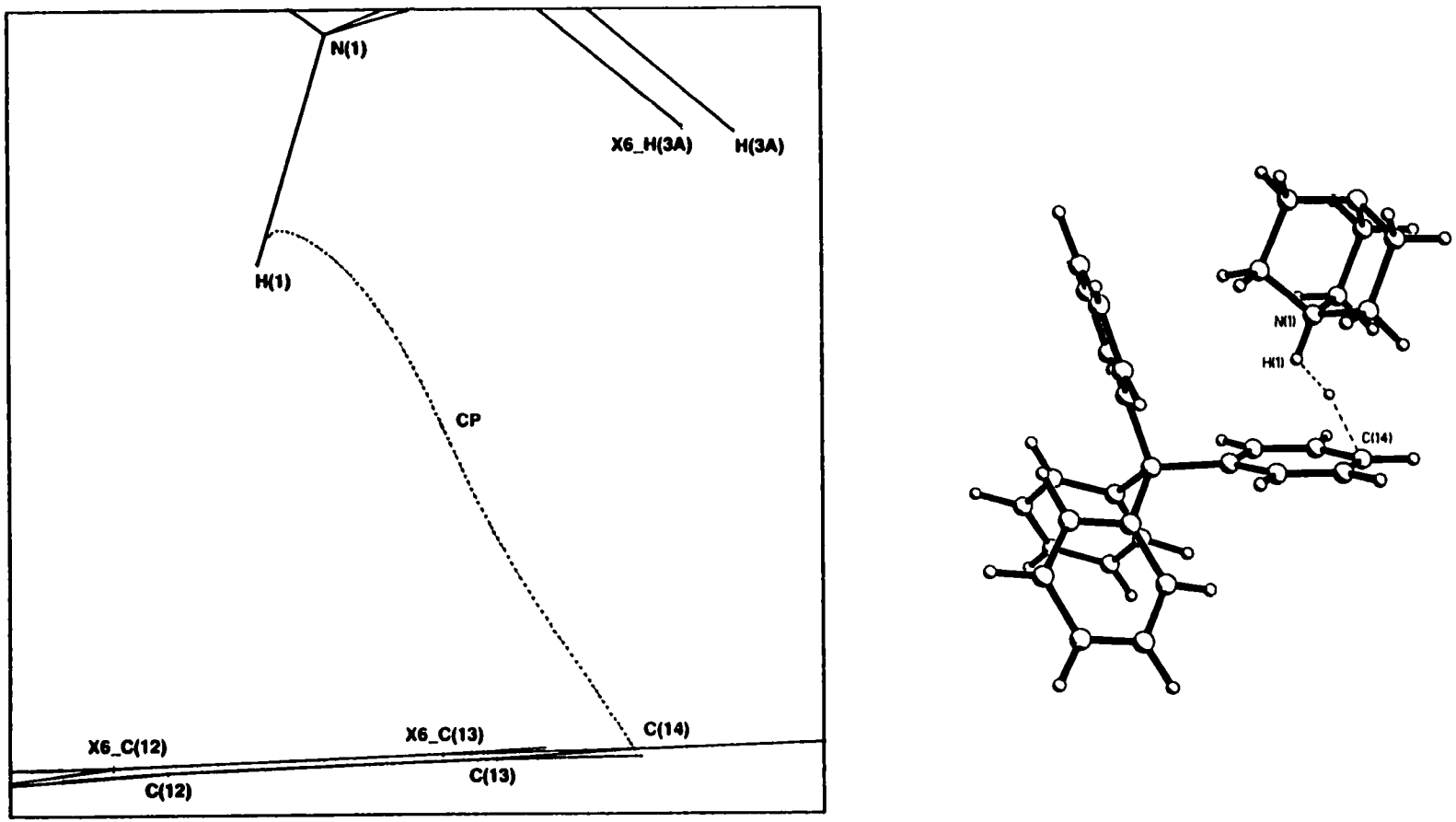

Figure 113. Bond path located for the N-H...π(Ph) hydrogen bond in the structure of [DabcoH][$B(C_6H_5)_4$], drawn to emphasize the role of phenyl ring #1 as the acceptor of the interaction. CP marks the location of the bond critical point.

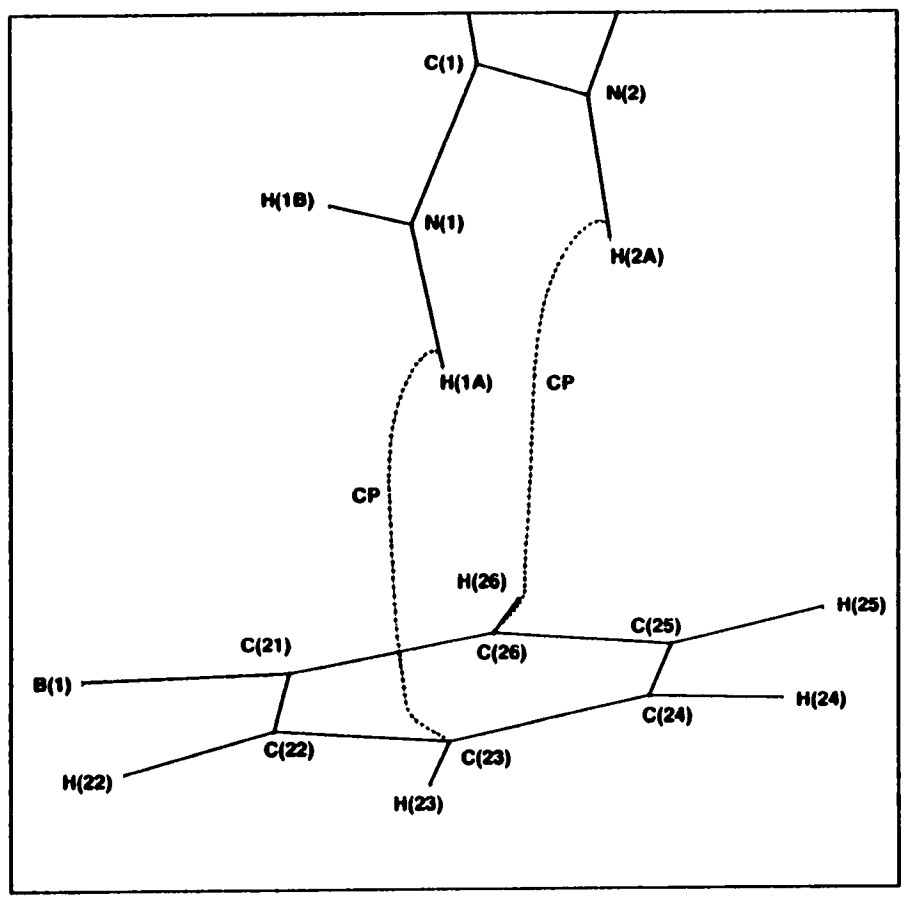

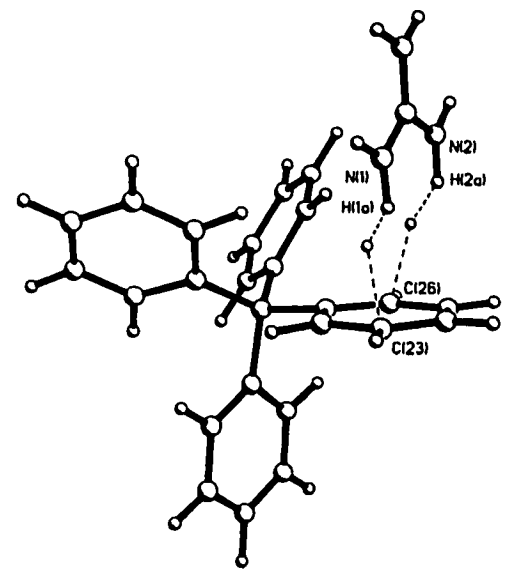

Figure 114. Bond paths located for the N-H...π(Ph) hydrogen bonds accepted by ring #2 in the structure of guanidinium tetraphenylborate acetonitrile solvate. CP marks the locations of the bond critical points. The outlines of the uninvolved rings on the tetraphenylborate anion have been omitted for clarity.

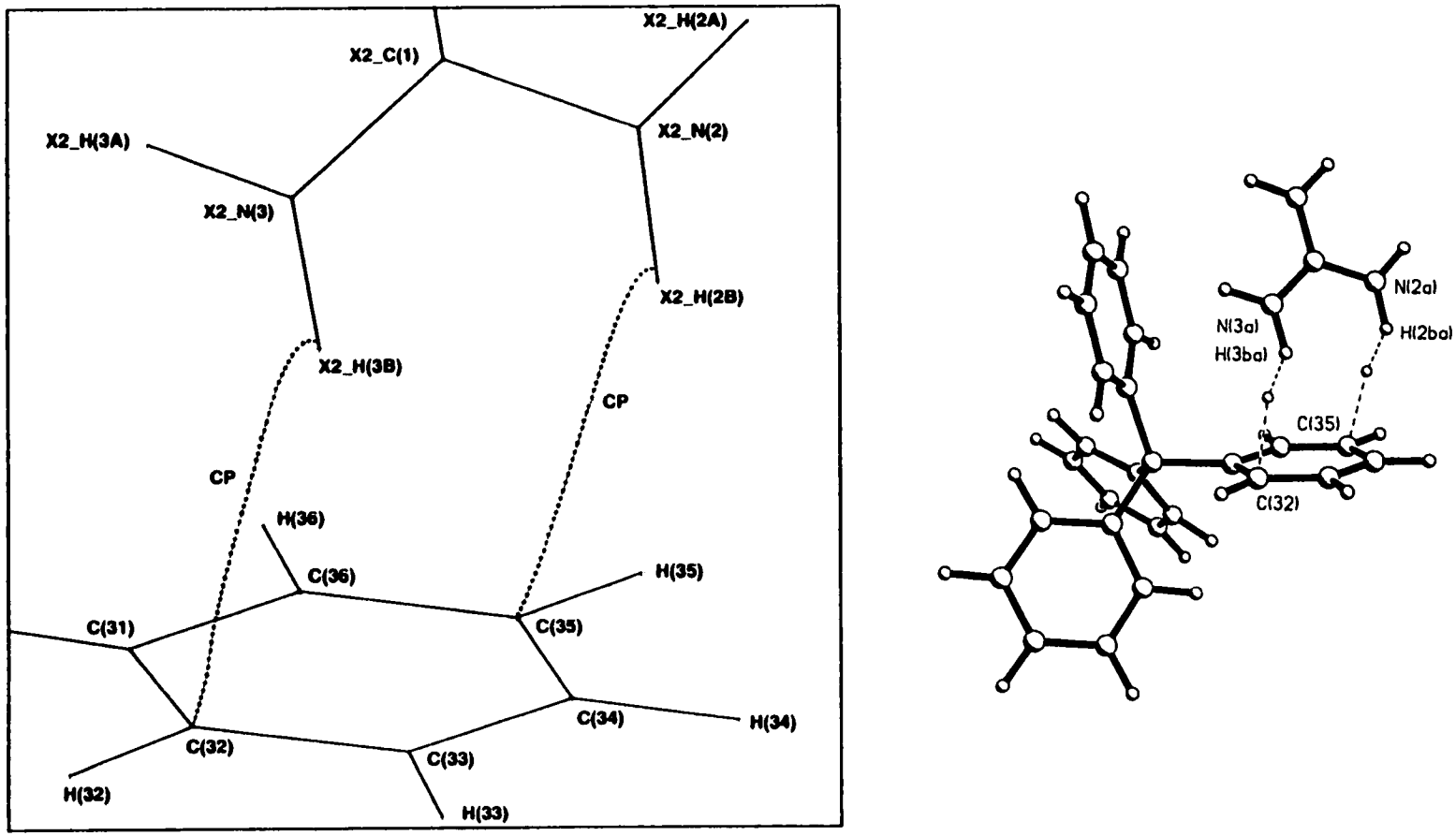

Figure 115. Bond paths located for the N-H...π(Ph) hydrogen bonds accepted by ring #3 in the structure of guanidinium tetraphenylborate acetonitrile solvate. CP marks the locations of the bond critical points.

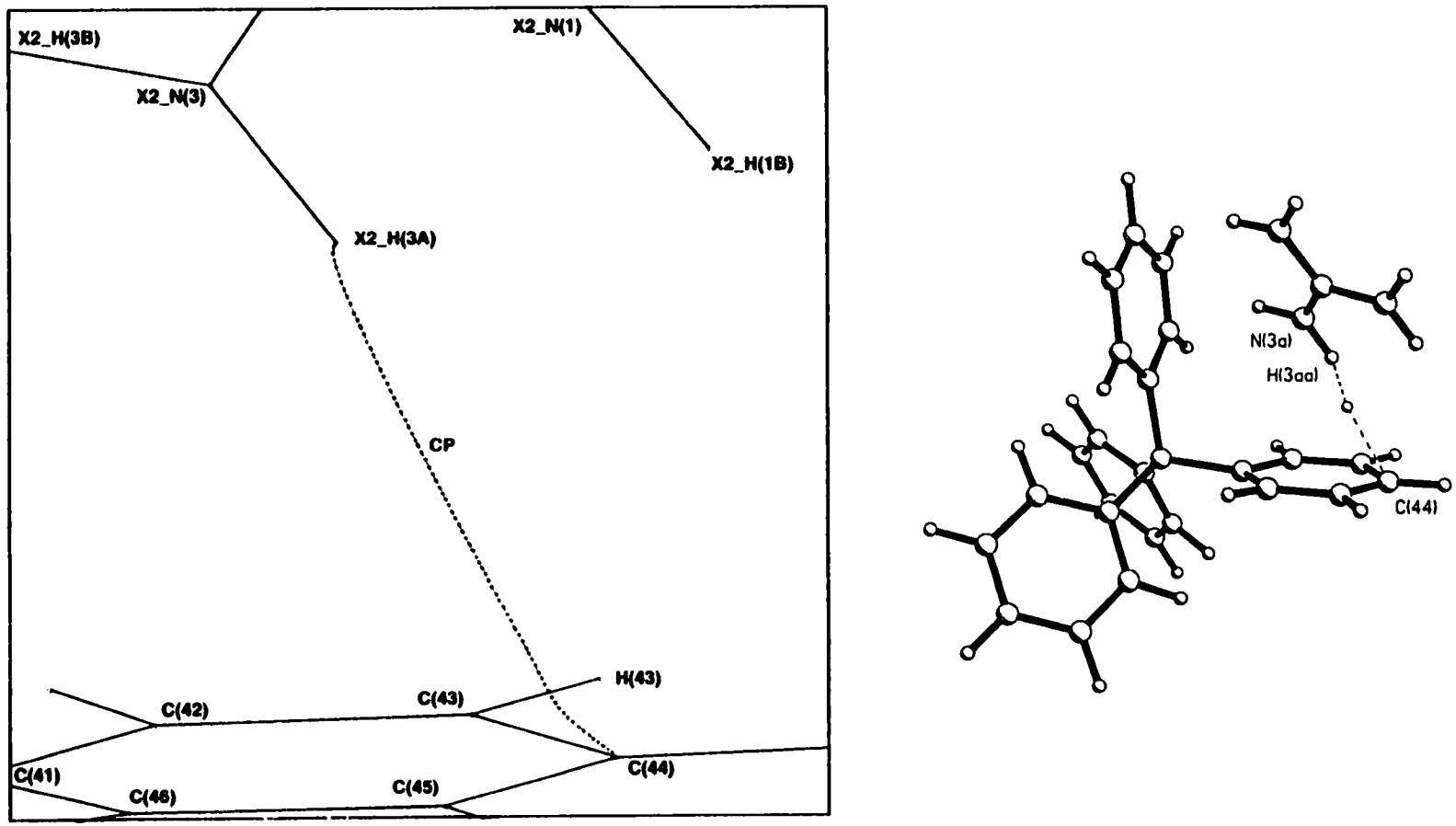

Figure 116. Bond path located for the N-H...π(Ph) hydrogen bond accepted by ring #4 in the structure of guanidinium tetraphenylborate acetonitrile solvate. CP marks the location of the bond critical point.

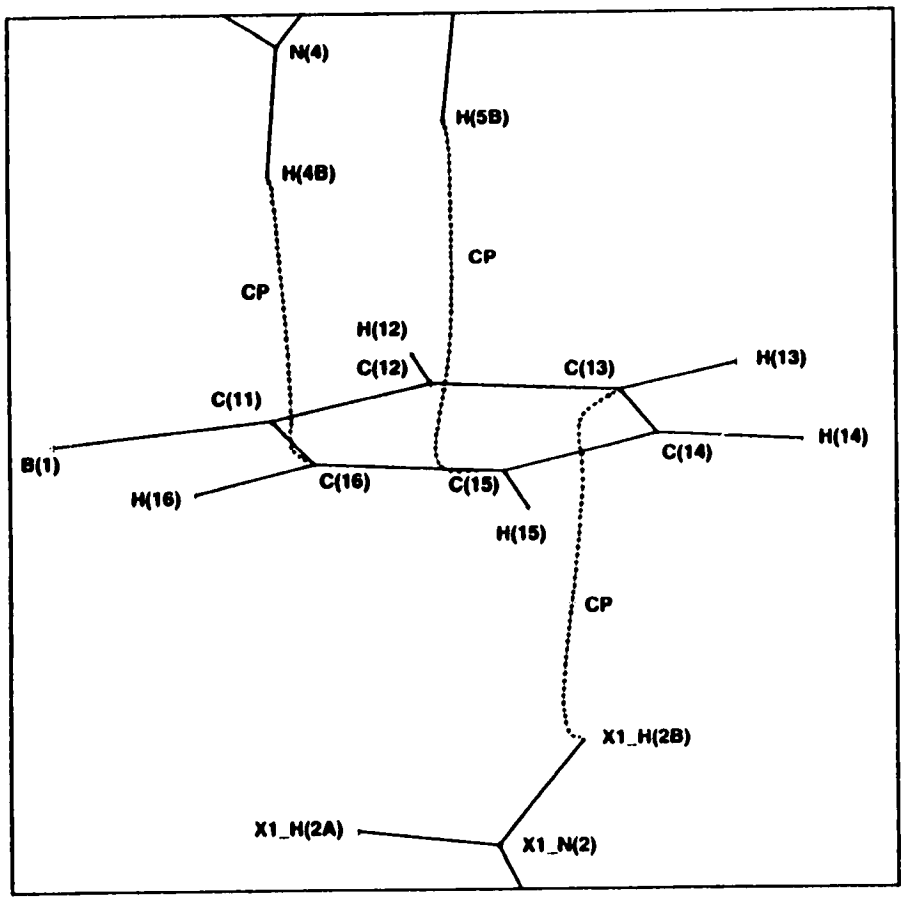

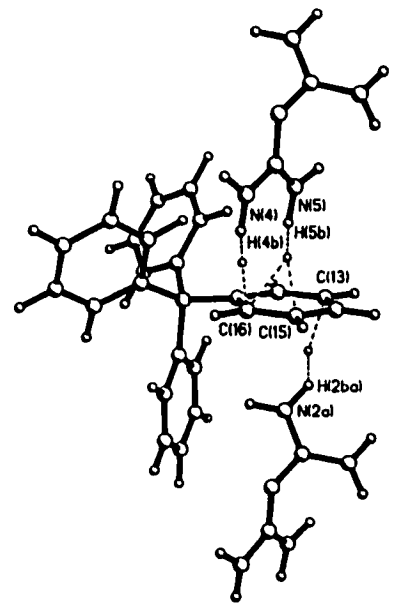

Figure 117. Bond paths located for the N-H...π(Ph) hydrogen bonds accepted by ring #1 in the structure of biguanidinium tetraphenylborate. CP marks the locations of the bond critical points. The outlines of the uninvolved rings on the tetraphenylborate anion have been omitted for clarity.

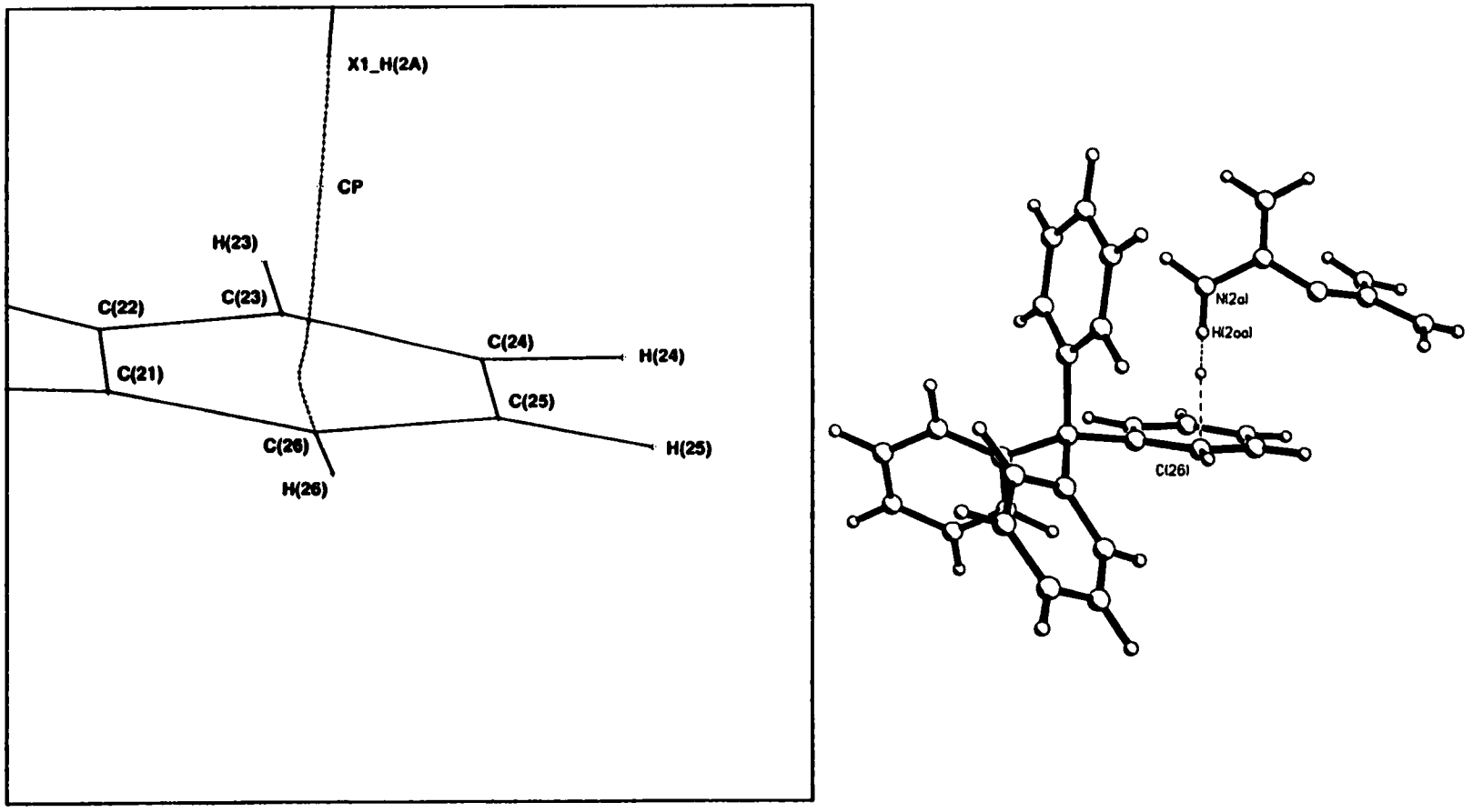

Figure 118. Bond path located for the N-H...π(Ph) hydrogen bond accepted by ring #2 in the structure of biguanidinium tetraphenylborate. CP marks the location of the bond critical point. The outlines of the uninvolved rings on the tetraphenylborate anion have been omitted for clarity.

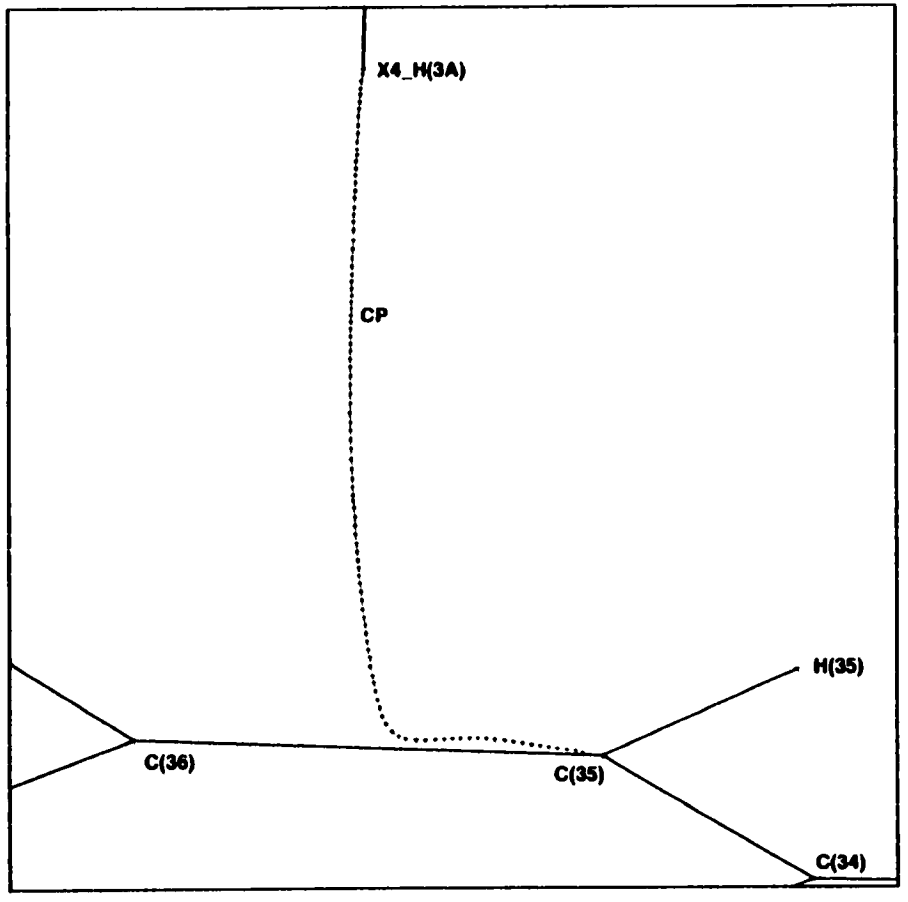

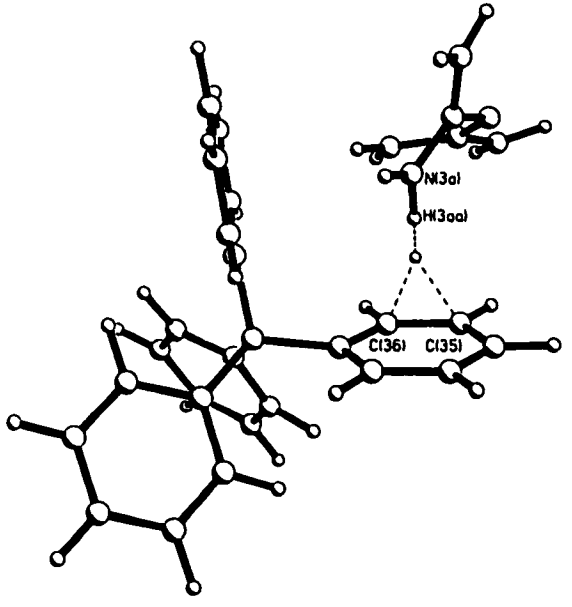

Figure 119. Bond path located for the N-H...π(Ph) hydrogen bond accepted by ring #3 in the structure of biguanidinium tetraphenylborate. CP marks the location of the bond critical point. The outlines of the uninvolved rings on the tetraphenylborate anion have been omitted for clarity.

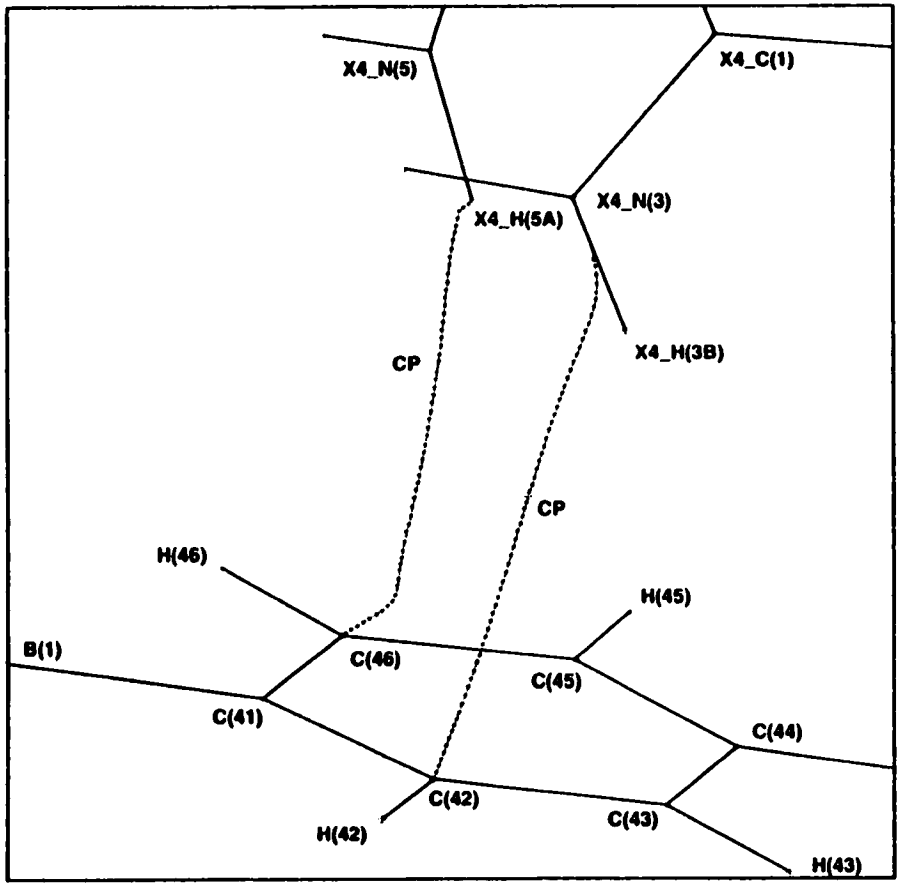

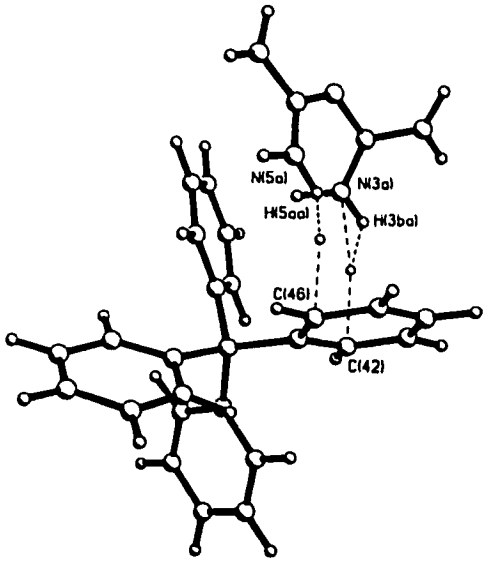

Figure 120. Bond paths located for the N-H...π(Ph) hydrogen bonds accepted by ring #4 in the structure of biguanidinium tetraphenylborate. CP marks the locations of the bond critical points. The outlines of the uninvolved rings on the tetraphenylborate anion have been omitted for clarity.

3.6.2.5. N-H...Phenyl Interactions

When first investigating the geometries of the N-H...π(Ph) contacts, it was assumed that they would all be hydrogen bond type interactions. H(N)...H_{ring} distances were not considered, H(N)...H_{ring} contacts were identified as nothing more than interesting, if minor, contributors to the interaction and the possibility of H...H type contacts arising was not even thought of. However, after characterization of all the varied, and more numerous, C-H...phenyl interactions on the basis of their geometries, different classes of contacts (H...H type, intermediate type and hydrogen bonds of varying configurations), with different distance criteria, were identified. Reviewing the N-H...π(Ph) interactions, using the geometry criteria developed for the C-H...phenyl interactions, resulted in the reassignment of only a single contact, out of a total of 14. The other 13 interactions maintained their classifications as hydrogen bonds of varying configurations, after reassessment of their geometries including possible short H(N)...H_{ring} contacts. The bond path diagrams for the N-H...π(Ph) hydrogen bonds have been included before the beginning of this section, Figure 112 for $NH_4B(C_6H_5)_4$, Figure 113 for $[DabcoH][B(C_6H_5)_4]$, Figures 114 to 116 for $[C(NH_2)_3][B(C_6H_5)_4]\cdot CH_3CN$ (rings 2 to 4 respectively) and Figures 117 to 120 for $[N(C[NH_2]_2)_2][B(C_6H_5)_4]$ (rings 1 to 4 respectively).

The interaction whose classification was changed after consideration of the H(N)...H_{ring} distances was the $[N(4)\text{-}H(4B)]_{cation}$...$[ring\ 1]_{anion}$ contact of $[N(C[NH_2]_2)_2][B(C_6H_5)_4]$. This had been classified as an edge type hydrogen bond, to the C(15)-C(16) bond of the anion, based on H(4B)...C_{ring} distances of 2.901Å (140.4°) to C(15) and 2.661Å (155.7°) to C(16), respectively, both shorter than the H(4B)...π_c ring centroid distance.

However, on consideration of the corresponding H(4B)...H_{ring} distances, H(4B)...H(15) = 2.955Å (136.6°) and H(4B)...H(16) = 2.510Å (169.4°), it becomes apparent that this interaction is better characterized as an intermediate type contact. The H(4B)...H(16) distance is shorter than the H(4B)...C(16) distance, but only slightly. The two distances are close to equal and both are longer than 2.5Å. The difference in the two distances is 0.15Å. All are characteristic properties of the geometries of intermediate type contacts.

Using the results determined from the analysis of the C-H...phenyl interactions, it is possible to predict even more about the expected bond path of the N(4)-H(4B)...ring 1 intermediate type contact. In the C-H...phenyl interactions, if the H(C)...H_{ring}/H(C)...C_{ring} distance difference [H(C)...H_{ring} < H(C)...C_{ring}] was between 0.15Å to 0.40Å an intermediate type contact was predicted. So this N-H...phenyl interaction still falls in the intermediate category. The bond path characteristic of an intermediate type C-H...phenyl interaction begins from H(C) and proceeds to the $(C-H)_{anion}$ bond making the closest contact, before changing direction and following the bond along to its termination at the closest ring carbon atom. If N-H...phenyl intermediate type interactions show comparable bond paths, the N(4)-H(4B)...ring 1 [C(16)-H(16)] contact would be expected to have a bond path that travels from H(4B) of the cation to a point slightly above the C(16)-H(16) bond of the anion, close to the midpoint of the bond. It would then curve down and along the bond before ending at C(16) of the ring.

In fact, this is exactly the bond path observed for the interaction, as shown in Figure 117. The bond path from H(4B) meets the C(16)-H(16)

bond about one third of the distance along the bond, closer to C(16), before proceeding along the bond to C(16). This result is very interesting for several reasons. It appears to support the idea that C-H...phenyl interactions and similar type N-H...phenyl interactions have the same characteristic bond paths. It is also powerful evidence that basic properties of the geometry of an interaction can be used to predict its bond path and to discern the nature of the interaction.

The interaction just described was the only N-H...π(Ph) contact found not to have a true hydrogen bond geometry. Of the remaining 13 interactions, eight were predicted to be centroid type, four were predicted to be edge type and only one was predicted to be a single atom type hydrogen bond based on their geometries. The only example of a **single atom type** hydrogen bond, $[N(2)\text{-}H(2B)]_{cation}\cdots[ring\ 1]_{anion}$ was identified in the structure of $[N(C[NH_2]_2)_2][B(C_6H_5)_4]$. It is characterized by a single $H(2B)\cdots C_{ring}$ distance, 2.490Å (141.1°) to C(13), less than the $H(2B)\cdots\pi_c$ ring centroid distance. The H(2B)...H(13) distance is longer, 2.891Å (162.1°), confirming that this is a hydrogen bond type interaction, in this case of the single atom variety.

The bond path observed for this interaction (Figure 117) agrees well with that predicted on the basis of geometry. It proceeds from H(2B) to C(13) of ring 1 of the anion, although it does follow the C(12)-C(13) bond for a short distance before terminating at C(13). The bond path travels to C(13), the single closest $H(2B)\cdots C_{ring}$ contact, as expected. The N-H...π(Ph) single atom type hydrogen bond follows a bond path exactly as predicted from its geometry. The bond path also corresponds with those of the single atom type C-H...phenyl hydrogen bonds studied previously. This

again demonstrates the transferability of the characteristic bond paths for different interaction types between C-H...X and N-H...X contacts.

Originally, five interactions were classified as N-H...π(Ph) **edge type** hydrogen bonds based on their geometries. However, one was reclassified as an intermediate type interaction when $H(N)...H_{ring}$ distances were considered, leaving only four possible edge type hydrogen bonds, two in the structure of $[C(NH_2)_3][B(C_6H_5)_4]\cdot CH_3CN$ and two in the structure of $[N(C[NH_2]_2)_2][B(C_6H_5)_4]$. Upon analysis of the bond paths of this group of interactions, one other contact was also removed from consideration because of its unusual bond path. Thus, only three interactions were left from which to draw conclusions about N-H...π(Ph) edge type hydrogen bonds and their characteristic bond path.

First, the excluded interaction with the unusual bond path will be discussed. This interaction, $[N(3)-H(3B)]_{cation}...[ring\ 4]_{anion}$, located in the structure of biguanidinium tetraphenylborate, was predicted from its geometry to involve the C(42)-C(43) bond of the anion. Two $H(3B)...C_{ring}$ distances, 2.934Å to C(42) and 2.982Å to C(43), are shorter than the $H(3B)...\pi_c$ distance, while the corresponding $H(3B)...H_{ring}$ distances are both slightly longer, consistent with the prediction of an edge type hydrogen bond.

Surprisingly, in the N(3)-H(3B)...ring 4 interaction the bond path (Figure 120) begins from N(3) of the cation and not directly from H(3B) as expected. However, it generally follows the N(3)-H(3B) bond direction for most of its length before proceeding towards the anion. The bond path reaches a point above the C(42)-C(43) bond, very close to C(42), where it changes direction and curves down to end at C(42). The anion "acceptor"

end of the bond path is not unreasonable for an edge type hydrogen bond. The bond path agrees with the predicted geometry in so far as it travels to the ring bond with the two shortest H(N)...C_{ring} distances and it terminates at C(42), the atom with the shortest H(N)...C_{ring} distance.

However, it is rather unusual for the bond path to begin from N(3) of the cation and not directly from H(3B). Although several C-H...phenyl interactions of this type (from C(3) of the solvent to an anion ring) were located in the structure of $[C(NH_2)_3][B(C_6H_5)_4]\cdot CH_3CN$, only one other N-H...$\pi$(Ph) hydrogen bond, the $[N(1)\text{-}H(1)]_{cation}$...$[ring\ 1]_{anion}$ interaction of $NH_4B(C_6H_5)_4$, was found to adopt a similar bond path. In both of the N-H...π(Ph) interactions, there appear to be reasonable explanations as to why the bond path might begin from the nitrogen atom rather than the hydrogen atom of the donor N-H group.

There are two interactions from a single cation to one face of ring 4 of the anion in the structure of $[N(C[NH_2]_2)_2][B(C_6H_5)_4]$. However, the two donors, N(3)-H(3B) and N(5)-H(5A) come from the two different halves of the cation and a "pincer" type arrangement of the two hydrogen bonds is not formed. Instead, both interactions are predicted to form edge type hydrogen bond configurations to the same face of the same ring, on the basis of geometry.

The N(3)-H(3B) vector projects outside and well away from the ring 4 plane. This, in turn, gives rise to the very nonlinear values obtained for the N(3)-H(3B)...C_{ring} angles, 117.3° to C(42) and 124.6° to C(43). This is also reflected in the angle the N(3)-H(3B) vector makes to the plane of ring 4, only 31.0°. The vector points away from ring 4 and makes a very shallow angle with the ring plane so that it projects down to the ring

plane far away from the ring itself.

The angle the N(3)-H(3B) vector makes with the plane of ring 4, 31.0°, is by far the smallest and least perpendicular angle in any of the seven N-H...π(Ph) interactions in the structure of $[N(C[NH_2]_2)_2][B(C_6H_5)_4]$; the next smallest angle is almost 10° larger. It is also the smallest angle made between a N-H vector and an anion phenyl ring plane in any of the N-H...π(Ph) interactions located in all four compounds. In those 14 interactions, the average angle made between the N-H vector and the plane of the interacting phenyl ring is 66.8°, more than 35° larger than the angle made in the N(3)-H(3B)...ring 4 interaction of biguanidinium tetraphenylborate. This unfavourable geometry may explain why the bond path of this interaction begins from N(3) of the cation rather than from the expected H(3B) atom. The more direct interaction with N(3) is favoured since H(3B) points outside and away from ring 4.

With only three edge type N-H...π(Ph) hydrogen bonds to work from, it may be difficult to reach detailed conclusions about the characteristic bond path of this type of interaction. Seven such C-H...phenyl contacts were investigated, allowing definite criteria to be developed for the identification of edge type C-H...phenyl hydrogen bonds and a completely characteristic bond path was recognized for this type of interaction. It will be instructive to see if the geometric criteria and characteristic bond path of the C-H...phenyl interactions are also transferred to the N-H...π(Ph) edge type hydrogen bonds.

In the C-H...phenyl edge type hydrogen bond investigation it was shown that the characteristic bond path for this type of interaction begins from H(C) of the "donor" group and travels to the anion phenyl ring

bond with the two closest H(C)...C_{ring} distances (Figure 108). The bond path then changes direction and follows the bond along to the ring carbon with the shortest H(C)...C_{ring} distance where it terminates. More specific information was also obtained. If the difference in the two minimum H(C)...C_{ring} distances is 0.10Å or less, the bond path will proceed to the midpoint of the phenyl ring bond, then to the closer C_{ring} atom. If the difference in the two minimum H(C)...C_{ring} distances is between roughly 0.10Å and 0.20Å, the bond path will make an off-center approach to the interacting ring bond, nearer to the closest C_{ring} atom, where it will also terminate. Finally, if the difference in the minimum H(C)...C_{ring} distances is greater than approximately 0.20Å, the bond path will resemble that of a single atom type hydrogen bond, travelling to the atom with the shortest H(C)...C_{ring} distance. Such detailed conclusions will likely not be possible for the fewer N-H...π(Ph) edge type hydrogen bonds but it will be interesting to see how well they meet the criteria developed using the C-H...phenyl data.

Two related edge type hydrogen bonds were identified from their geometries in the structure of $[N(C[NH_2]_2)_2][B(C_6H_5)_4]$. The first was found to have an unusual bond path, as just described, and was removed from the analysis of the N-H...π(Ph) edge type hydrogen bonds. The remaining interaction, $[N(5)\text{-}H(5A)]_{cation}$...$[ring\ 4]_{anion}$, has two H(5A)...$C_{ring}$ distances shorter than the H(5A)...π_c distance, 2.788Å (148.9°) to C(45) and 2.664Å (141.2°) to C(46). The corresponding H(5A)...H_{ring} distances are slightly longer, 2.933Å to H(45) and 2.695Å to H(46), respectively, limiting their contribution to the edge type interaction. The difference in the two minimum H(5A)...C_{ring} distances is 0.12Å.

The bond path (Figure 120) travels from H(5A) of the cation to a point just above the C(45)-C(46) bond of ring 4 of the anion, roughly three quarters of the way along the bond closer to C(46). It then changes direction and follows the bond, curving down to end at C(46). The bond path agrees with that predicted on the basis of the interaction geometry. It proceeds to the anion phenyl ring 4 bond that makes the two shortest H(5A)...C_{ring} contacts and terminates at C(46) which makes the closest contact to H(5A). The bond path approaches the C(45)-C(46) bond in an off-center fashion. Using the criteria developed from the C-H...phenyl edge type hydrogen bond analysis, such an approach would be expected when the difference in the two minimum H(C)...C_{ring} distances is between 0.10Å and 0.20Å. The corresponding distance difference is 0.12Å in the interaction between N(5)-H(5A) and ring 4, in the range proposed on the basis of the C-H...phenyl study. All of the features of the bond path in the N(5)-H(5A)...ring 4 interaction match those predicted using the criteria developed by investigating the C-H...phenyl edge type hydrogen bonds.

The other two N-H...π(Ph) edge type hydrogen bonds were located in the structure of $[C(NH_2)_3][B(C_6H_5)_4]\cdot CH_3CN$. The first interaction, $[N(2)-H(2A)]_{cation}$...$[ring\ 2]_{anion}$, is characterized by two H(2A)...C_{ring} distances, 2.689Å (153.1°) to C(25) and 2.672Å (154.1°) to C(26), shorter than the H(2A)...π_c ring centroid distance. The corresponding H(2A)...H_{ring} distances are slightly longer, H(2A)...H(25) = 2.738Å and H(2A)...H(26) = 2.761Å. The difference in the two minimum H(2A)...C_{ring} distances is only 0.02Å.

The bond path of the N(2)-H(2A)...ring 2 interaction (Figure 114) begins from H(2A) and travels to a point just above the C(25)-C(26) bond

of the anion, roughly three quarters of the way along the bond, closer to C(26). It then changes direction and follows the bond along until it terminates upon reaching C(26). The bond path is in general agreement with that predicted from the geometry. It proceeds to the edge of the ring with the two shortest H(2A)...C_{ring} distances and it terminates at the carbon atom, C(26), with the shortest H(2A)...C_{ring} distance. However, it does deviate slightly from the bond path that would have been predicted on the basis of the C-H...phenyl results. In the C-H...phenyl group, edge type hydrogen bonds were found to have bond paths that travelled directly from H(C) to the midpoint of the interacting C-C ring bond if the difference in the two minimum H(C)...C_{ring} distances was approximately 0.10Å or less. In the N(2)-H(2A)...ring 2 interaction, the difference in the two H(2A)...C_{ring} distances is small, only 0.02Å, and the bond path would have been expected to travel to the midpoint of the C(25)-C(26) bond on this basis. The N(2)-H(2A)...ring 2 interaction does not meet quite all of the criteria developed by studying the C-H...phenyl contacts of the same type. Still, despite this one minor discrepancy the N(2)-H(2A)...ring 2 interaction does have the basic characteristic bond path expected for an edge type hydrogen bond, whether from a C-H or N-H donor.

The last N-H...π(Ph) edge type hydrogen bond and the second in the structure of guanidinium tetraphenylborate acetonitrile solvate is the contact $[N(2)\text{-}H(2B)]_{cation}$...$[ring\ 3]_{anion}$. The H(2B)...$\pi_c$ ring centroid distance is shorter than all but two of the H(2B)...C_{ring} distances, H(2B)...C(34) = 2.668Å (160.7°) and H(2B)...C(35) = 2.622Å (143.0°). The difference between the two minimum H(2B)...C_{ring} distances is also relatively small, 0.05Å. The corresponding H(2B)...H_{ring} distances are

again slightly longer, 2.802Å to H(34) and 2.700Å to H(35), and are likely not important contributors to the interaction.

The bond path of the N(2)-H(2B)...ring 3 interaction (Figure 115) proceeds linearly and directly between H(2B) of the cation and C(35) of ring 3 in the anion. This bond path is somewhat surprising considering the geometry of the interaction. On the plus side, it does travel to the ring carbon atom, C(35), that has the shortest H(2B)...C_{ring} distance. However, by all expectations the bond path should travel to the C(34)-C(35) bond rather than directly to a single atom. The difference in the two minimum H(2B)...C_{ring} distances is small, 0.05Å, characteristic of a bond path that will travel to a bond and not a single atom. In the C-H...phenyl interactions, only if the difference in the two minimum H(C)...C_{ring} distances was 0.20Å or greater was a single atom type hydrogen bond adopted. In this N-H...π(Ph) edge type hydrogen bond the difference is much smaller. In fact, it is also smaller than the difference in the N(5)-H(5A)...ring 4 edge type hydrogen bond of $[N(C[NH_2]_2)_2][B(C_6H_5)_4]$ (0.124Å) where the bond path travels to the C(42)-C(43) bond exactly as predicted from the geometry. There is no clear reason why the edge type N(2)-H(2B)...ring 3 hydrogen bond of $[C(NH_2)_3][B(C_6H_5)_4]\cdot CH_3CN$ adopts a single atom bond path.

The edge type N-H...π(Ph) hydrogen bonds studied do not conform to as clear or as detailed a set of criteria as the edge type C-H...phenyl interactions. However, they still form a relatively consistent group, that also matches the C-H...phenyl interactions, at least to a certain extent. Two of the three edge type N-H...π(Ph) hydrogen bonds have bond paths that travel to the predicted C-C bond of the anion. The third interaction has a bond path characteristic of a single atom type hydrogen bond. All three

interactions do have bond paths that end at the C_{ring} atom that makes the closest H(N)...C_{ring} contact. Two of the three bond paths do go to the bond with the two shortest H(N)...C_{ring} distances, as expected for edge type hydrogen bonds. It is not clear why the N(2)-H(2B)...ring 3 interaction of $[C(NH_2)_3][B(C_6H_5)_4]\cdot CH_3CN$ goes to the single atom, C(35), rather than to the C(34)-C(35) bond. This is the only major discrepancy observed and there is no obvious reason for it, since the difference in the two minimum H(2B)...C_{ring} distances, to C(34) and C(35), is only small.

The N-H...π(Ph) edge type hydrogen bonds are not as consistent in their relationship between the bond path and geometry as the edge type C-H...phenyl interactions had been found to be. In the C-H...phenyl edge type interactions it was possible to predict where along the C-C bond the bond path would proceed, based only on the difference in the two pertinent H(C)...C_{ring} distances. This is not the case in the edge type N-H...π(Ph) hydrogen bonds where there is no obvious correlation between the difference in the two minimum H(N)...C_{ring} distances and where along the C-C bond the bond path goes (or even if it will go to the bond rather than to a single atom). This is not to say, however, that all is lost. In general, the N-H...π(Ph) hydrogen bonds do follow the characteristic bond path expected for edge type interactions. With so few examples available it is difficult to reach detailed conclusions. The majority of the observations made for the N-H...π(Ph) interactions do agree with the more general results found by studying C-H...phenyl interactions having edge type geometries. The characteristic bond path is expected to proceed from the hydrogen atom of the "donor", either H(N) or H(C), to a point along the C-C ring bond of the anion "acceptor" having the two shortest H...C_{ring}

distances. It then curves along the bond, following the bond to the C_{ring} atom that makes the closest H...C_{ring} contact. Only in the C-H...phenyl interactions can more detailed predictions about the bond path be made.

In the four compounds studied, a total of eight N-H...π(Ph) hydrogen bonds of the **centroid type** were identified from their geometries. Of these eight examples, one was from the structure of $NH_4B(C_6H_5)_4$, one from the structure of [DabcoH][$B(C_6H_5)_4$] and three each from the structures of [$C(NH_2)_3$][$B(C_6H_5)_4$]·CH_3CN and [$N(C[NH_2]_2)_2$][$B(C_6H_5)_4$]. When the bond paths of the eight interactions were examined, one was found to have an unusual bond path and was removed from the group analysis. It will be discussed first, then the bond paths of the seven remaining interactions will be compared to see what can be learned of a characteristic N-H...π(Ph) centroid type hydrogen bond.

Surprisingly, the unusual bond path was found to occur in the salt with the simplest cation studied, ammonium tetraphenylborate, when the $[N(1)\text{-}H(1)]_{cation}$...$[ring\ 1]_{anion}$ centroid type hydrogen bond was investigated. The bond path, which is shown in Figure 112, begins from N(1) of the cation not from H(1), the expected origin. It follows the general direction of the of the N(1)-H(1) bond for about one third of its length before turning and heading to ring 1 of the anion acceptor. The bond path proceeds to a point just above the plane of ring 1, just inside the confines of the ring, close to C(11). It then curves down to end at C(11). Only one other bond path similar to this, beginning from nitrogen rather than hydrogen of the donor group, was observed in the N-H...π(Ph) interactions studied for this work, the $[N(3)\text{-}H(3B)]_{cation}$...$[ring\ 4]_{anion}$ contact in the structure of [$N(C[NH_2]_2)_2$][$B(C_6H_5)_4$].

The geometry of the $[N(1)-H(1)]_{cation}\cdots[ring\ 1]_{anion}$ interaction in $NH_4B(C_6H_5)_4$ is characterized by an $H(1)\cdots\pi_c$ distance of 2.013Å (172.0°) and a 100Δ value of only 6, indicative of a narrow range of $H(1)\cdots C_{ring}$ distances. The acceptor end of the bond path terminates at C(11) of the anion phenyl ring, which is not the closest $H(1)\cdots C_{ring}$ contact. The distance from H(1) to C(11), 2.448Å (135.8°), is slightly longer than the minimum distance, H(1)...C(12) = 2.426Å (140.8°). The difference in these, the two minimum $H(1)\cdots C_{ring}$ distances, is only small, 0.02Å.

The study of C-H...phenyl interactions with centroid type geometries had shown that, in general, if 100Δ was 15 or less then the bond path would be unpredictable. It could travel to any C_{ring} atom or to any C-C bond in the interacting phenyl ring. It was concluded that if all the $H(C)\cdots C_{ring}$ distances are relatively equal, then distance will no longer be the factor determining where the bond path will travel. Instead, other, normally minor, factors will influence the bond path and decide where it will terminate. In the N(1)-H(1)...ring 1 interaction of $NH_4B(C_6H_5)_4$, 100Δ is equal to only 6. Thus, it is perhaps not surprising that the bond path is unpredictable, as far as its termination at C(11) rather than C(12) is concerned. Although C(12) is closer to H(1) than is C(11), the difference in the two distances is only 0.02Å, and this is likely compensated by a more favourable atomic charge at C(11) compared to C(12).

It is, however, quite unusual for the bond path to begin from N(1) of the cation rather than from the hydrogen atom, H(1). As mentioned, only one other of the N-H...π(Ph) interactions investigated was also found to do so. In the N(1)-H(1)...ring 1 hydrogen bond of $NH_4B(C_6H_5)_4$ a reasonable explanation for the unusual bond path origin could involve the observed

rotation of the ammonium cation within its anion cavity. As discussed previously, a number of literature investigations[106-111] have shown that the NH_4^+ cation undergoes relatively free rotation in crystalline $NH_4B(C_6H_5)_4$. It is probable that the N-H...π(Ph) hydrogen bond between the cation and the anion contributes to the observed barrier to completely free rotation but this barrier is low, likely only 3 to 5 kJ/mol. The cation is constantly reorienting within the anion cavity, likely by rotation/flips around its C_2 and C_3 axes.

The rapid motion of NH_4^+, the ammonium ion, could cause the bond path to truly begin from N(1), the most fixed point in the cation. Or, perhaps more likely, it could cause problems in locating a "true" position for the hydrogen atom, H(1), in the multipole analysis. The rapid motion could result in some smearing of the electron density in the region of the cation. These factors could, in turn, then cause problems in locating an accurate bond path for the interaction, resulting in it missing H(1) and travelling directly to N(1) of the cation. Whatever its origin, the unusual bond path of the N(1)-H(1)...ring 1 interaction in ammonium tetraphenylborate caused it to be removed from the study of N-H...π(Ph) hydrogen bonds.

Before beginning an investigation of the individual N-H...π(Ph) centroid geometry hydrogen bonds, it is instructive to summarize the results obtained, and conclusions reached, after studying the centroid type C-H...phenyl interactions. In the C-H...phenyl contacts it was found that 100Δ was an important parameter in determining the nature of the interaction. If 100Δ was small, and the range of H...C_{ring} distances narrow (100Δ < 14 in the experimental examples), it was not possible to predict

where the bond path might terminate. From H(C) it could travel to any one C_{ring} atom or to any C-C ring bond, not necessarily the closest H...C_{ring} contact(s). It was thought that other factors, usually too minor to affect the bond path when it is dominated by distance differences, become important when all the H...C_{ring} distances are nearly equal. These other factors determine the bond path's approach to the acceptor in close, centroid type interactions.

If the interaction has a more off-center centroid type geometry, the range of H...C_{ring} distances will increase and consequently so will 100Δ. In those cases (100Δ > 45 in the experimental examples) one or two of the H...C_{ring} distances become significantly shorter than the others and the bond path becomes much more predictable in the region of the acceptor. If there is a single short H...C_{ring} distance, determined by a difference in the two minimum H...C_{ring} distances of 0.09Å or larger (experimentally determined value), the bond path will terminate at that single C_{ring} atom. If there are a pair of short, relatively equal H...C_{ring} distances (0.06Å or less, as determined experimentally) the bond path will travel first to that C-C ring bond and then terminate at the closer C_{ring} atom.

The first N-H...π(Ph) centroid type hydrogen bond studied was the $[N(1)\text{-}H(1)]_{cation}\cdots[ring\ 1]_{anion}$ interaction from the $[DabcoH][B(C_6H_5)_4]$ structure. It is characterized by an H(1)...π_c ring centroid distance of 2.169Å (158.6°) and a narrow range of H(1)...C_{ring} distances, 100Δ = 6. The bond path of this interaction (Figure 113) travels directly from H(1) of the cation to C(14) of the anion. The H(1)...C(14) distance, 2.640Å, is actually the longest H(1)...C_{ring} distance, and the N(1)-H(1)...C(14) angle, 126.1°, is the least linear angle made to the ring. However, the

H(1)...C(14) distance is only 0.06Å longer than the minimum H(1)...C_{ring} distance of 2.579Å (167.4°) made to C(11).

This contact can be interpreted according to the rules developed for C-H...phenyl centroid type interactions. In such C-H...phenyl interactions if 100Δ was small, less than 14, the bond path could not be predicted based on geometric criteria. In the N(1)-H(1)...ring 1 interaction of [DabcoH] $[B(C_6H_5)_4]$ 100Δ is very small and the bond path does not proceed to the expected closest H...C_{ring} contact(s). Instead, it travels to the ring carbon atom, C(14), making the longest contact. The results are consistent with the criteria developed after studying the C-H...phenyl interactions. In the cases where all H...C_{ring} distances are nearly equal, such as this one, it is likely that other, normally minor, factors determine where the bond path will travel. In this interaction, it is suggested that the many $(C\text{-}H)_{cation}\cdots(phenyl)_{anion}$ contacts that the $DabcoH^+$ cation engages in may influence the N(1)-H(1)...ring 1 centroid type hydrogen bond and the bond path it adopts.

Three N-H...π(Ph) hydrogen bonds with centroid type geometries are formed in the structure of $[C(NH_2)_3][B(C_6H_5)_4]\cdot CH_3CN$, the first being $[N(1)\text{-}H(1A)]_{cation}\cdots[ring\ 2]_{anion}$. The bond path of this interaction (Figure 114) proceeds from H(1A) to a point just above the C(22)-C(23) bond in the anion, approximately two thirds of the distance along the bond, closer to C(23). It then changes direction and follows the bond to its termination at C(23).

The geometry of this interaction falls in an intermediate category, not really covered in the C-H...phenyl interactions studied. In the C-H...phenyl investigation, interactions with 100Δ values of 14 or less

had unpredictable bond paths, while those with 100Δ values of 45 or more always followed a recognizable set of rules and had completely predictable bond paths. In the N(1)-H(1A)...ring 2 interaction, 100Δ = 35, and the behaviour it will show is unclear.

The minimum H(1A)...C_{ring} distance in the N(1)-H(1A)...ring 2 interaction occurs to C(23), 2.458Å (151.0°), followed by contacts to C(24), 2.497Å (155.4°), and then to C(22), 2.603Å (143.1°). The bond path does terminate at C(23), the atom with the shortest H(1A)...C_{ring} distance, as normally expected. However, it does travel first to the C(22)-C(23) bond, where C(22) is only the third shortest H(1A)...C_{ring} contact, rather than to the C(23)-C(24) bond, as would have been predicted by geometry. This interaction is not well behaved, in the sense that its bond path could not be correctly predicted on the basis of its geometry. It falls into the group of centroid type interactions where the bond path is not controlled simply by the distance at which the contact occurs. In the study of C-H...phenyl interactions this group included those contacts with 100Δ values of 14 or less. If the two groups, N-H and C-H, are comparable it now appears that if 100Δ is 35 or less, an interaction for which the bond path cannot be predicted will occur. This does not contravene the rules developed on the basis of the C-H...phenyl study, rather it just narrows the criteria for their application slightly.

The second interaction with a centroid type geometry in the structure of $[C(NH_2)_3][B(C_6H_5)_4]\cdot CH_3CN$, $[N(3)-H(3A)]_{cation}\cdots[ring\ 4]_{anion}$, also has an intermediate value of 100Δ equal to 27. The minimum H(3A)...C_{ring} distance, to C(44), is 2.668Å (161.9°), while that to C(45), 2.705Å (131.7°), is the second shortest and that to C(43), 2.723Å

(156.7°), is the third shortest. The bond path in the N(3)-H(3A)...ring 4 interaction begins from H(3A) of the cation, as shown in Figure 116. It travels to a point just above the plane of ring 4, approximately three quarters of the way along the C(43)-C(44) bond, closer to C(44). The bond path then changes direction and follows the bond until it reaches C(44) where it ends.

The bond path does terminate at C(44), the atom with the shortest H(3A)...C_{ring} distance. It travels first to a bond rather than to a single atom which is also not unreasonable. However, the bond path goes to the bond, C(43)-C(44), involving the third shortest H(3A)...C_{ring} contact, rather than to the expected C(44)-C(45) bond which has the two shortest H(3A)...C_{ring} distances. In this case, there is not much difference between the two distances, H(3A)...C(43) and H(3A)...C(45), only 0.02Å, and the angle N(3)-H(3A)..C(43) is the more linear (156.7° versus 131.7°) so the observed result is not too surprising. Still, this is another example where the bond path cannot be correctly predicted from the geometry of the interaction.

The N(3)-H(3A)...ring 4 interaction is very similar to the previous interaction described, N(1)-H(1A)...ring 2, also located in the structure of $[C(NH_2)_3][B(C_6H_5)_4]\cdot CH_3CN$. Both have similar values of 100Δ, 27 in the former and 35 in the latter, and similar bond paths, both travelling to the C-C ring bond with the first and third shortest H(N)...C_{ring} distances before terminating at the closest C_{ring} atom. In neither case could the bond path be correctly predicted from the geometry of the interaction. It appears, based on these results and the results of the C-H...phenyl study, that if 100Δ is 35 or less in an interaction with a centroid type

configuration, whether C-H or N-H, the bond path cannot be anticipated from the distances involved in the contact.

The last interaction in the structure of $[C(NH_2)_3][B(C_6H_5)_4]\cdot CH_3CN$ found to have an N-H...π(Ph) hydrogen bond centroid type configuration, $[N(3)\text{-}H(3B)]_{cation}\cdots[ring\ 3]_{anion}$, has a bond path that begins from H(3B) as expected (Figure 115). From H(3B) it travels directly to C(32) of the anion. In this interaction, again 100Δ falls in the intermediate range of values; it is equal to 37, similar to the previous two interactions. However, in this case the bond path does match that predicted by geometry, following the C-H...phenyl criteria. The bond path terminates at C(32), the atom with the shortest $H(3B)\cdots C_{ring}$ distance, 2.498Å (151.6°). In this interaction the second closest $H(3B)\cdots C_{ring}$ distance is made to C(33), 2.592Å (168.4°), and the difference between the two minimum distances is 0.09Å. According to the C-H...phenyl results, the bond path could be predicted if 100Δ was greater than 45. In those cases, if the difference in the two minimum $H(C)\cdots C_{ring}$ distances was 0.09Å or greater, then the bond path would proceed to the closer C_{ring} atom and not to the bond. In this N-H...π(Ph) centroid type interaction 100Δ equals 37 and the difference in the two minimum $H(3B)\cdots C_{ring}$ distances is 0.09Å. A bond travelling to the single closest C_{ring} atom, C(32), is exactly as expected. It appears that the criteria are transferable between C-H and N-H interactions of the same type. It also seems likely that the 100Δ limit for interactions with predictable bond paths can be lowered from 45 to 35 based on this result. The previous interaction had a bond path that could not be predicted, with a 100Δ value of 35. There is likely some overlap between the two regions, predictable versus unpredictable bond paths, when

100Δ is approximately equal to 35.

Three centroid geometry N-H...π(Ph) hydrogen bonds were also located in the structure of biguanidinium tetraphenylborate. The first of these, $[N(2)-H(2A)]_{cation}\cdots[ring\ 2]_{anion}$, is characterized by a large 100Δ value of 66, indicative of an off-center type centroid arrangement. On this basis, a value of 100Δ greater than 35, the bond path should match that predicted from geometry. The two minimum $H(2A)\cdots C_{ring}$ distances are 2.392Å (174.3°) to C(26) and 2.565Å (147.2°) to C(25) and the difference between the two distances is large, 0.17Å. The C-H...phenyl criteria are such that when the two minimum $H(C)\cdots C_{ring}$ distances are relatively unequal, greater than 0.09Å, the bond path is predicted to travel to the single closest C_{ring} atom and not to the C-C bond. As shown in Figure 118, the bond path of the N(2)-H(2A)...ring 2 interaction in $[N(C[NH_2]_2)_2][B(C_6H_5)_4]$, travels from H(2A) to C(26), exactly as predicted. Again, this interaction supports the criteria being developed to characterize centroid geometry hydrogen bonds, whether C-H or N-H type.

The sixth hydrogen bond with a centroid configuration studied and the second from the structure of biguanidinium tetraphenylborate was the $[N(3)-H(3A)]_{cation}\cdots[ring\ 3]_{anion}$ interaction. The bond path (Figure 119) travels from H(3A) to a point just above the middle of the C(35)-C(36) anion ring 3 bond. There it changes direction and follows the bond to its termination at C(35). The value of 100Δ for this interaction is 65, again indicative of a slightly off-center geometry and what should be a predictable bond path. The two minimum $H(3A)\cdots C_{ring}$ distances, H(3A)...C(35) = 2.430Å (160.6°) and H(3A)...C(36) = 2.408Å (163.8°), are considerably shorter than any of the others. The difference between the

two minimum distances is small, only 0.02Å. The C-H...phenyl criteria suggest that under these conditions the bond path should travel to a bond, C(35)-C(36), not just to a single atom and this is what, in fact, is observed. There is, however, one minor surprise observed in the bond path of this interaction. The bond path terminates at C(35), the second closest H(3A)...C_{ring} contact, rather than at C(36), the closest contact. This is very unusual; all other centroid type interactions with 100Δ greater than 25, whether C-H or N-H, have been found to have bond paths that terminate ultimately at the closest C_{ring} atom, regardless of what they did beforehand. It is not clear why in this instance the bond path turns toward C(35). The two distances, H(3A)...C(35) and H(3A)...C(36), are close to equal and it is likely only a minor effect that leads to C(35) being favoured over the expected C(36).

The last N-H...π(Ph) hydrogen bond with a centroid type geometry studied was the $[N(5)\text{-}H(5B)]_{cation}\cdots[ring\ 1]_{anion}$ interaction in the structure of $[N(C[NH_2]_2)_2][B(C_6H_5)_4]$. It has a bond path (Figure 117) that proceeds from H(5B) to the C(15)-C(16) anion ring 1 bond, about one third of the distance along the bond, closer to C(15). The bond path then curves and follows the bond along to C(15) where it ends.

This interaction is characterized by a 100Δ value of 25, which leads to the conclusion that the bond path likely cannot be accurately predicted from its geometry. However, in this case even though 100Δ is relatively small, the bond path conforms exactly to that predicted from the geometry using the criteria that have been developed. According to these criteria, the bond path will travel to a C-C bond if the two minimum H...C_{ring} distances are close to equal, their difference being 0.06Å or less

(experimentally determined value). In this interaction, the difference between the two minimum H(5B)...C_{ring} distances, 2.560Å (151.7°) to C(15) and 2.576Å (160.5°), is only 0.02Å. The bond path would be expected to travel to the C(15)-C(16) bond and it does. The bond path also terminates at the C_{ring} atom with the shortest H(5B)...C_{ring} distance, C(15), as expected. This interaction, like all the other centroid type N-H...π(Ph) hydrogen bonds studied, follow the rules developed by investigating C-H...phenyl hydrogen bonds with the same centroid configurations.

In fact, the criteria developed by considering the C-H...phenyl centroid type interactions can be narrowed even further if the results of the N-H...π(Ph) study are included. It appears that if 100Δ is 35 or less the bond path adopted may not be easily predictable (from the C-H...phenyl interactions this was only known for 100Δ values of 15 or less). If 100Δ is very small, 15 or less, the bond path may go anywhere, any C_{ring} atom or C-C bond of the interacting ring, in a seemingly random fashion. However, this is likely determined by small differences in parameters usually overshadowed by the dominant distance effect. If 100Δ has a more intermediate value, the bond path will usually terminate at the ring carbon atom with the shortest H(N)...C_{ring} distance, but how it will reach that point will still be unpredictable. If 100Δ is 35 or greater, the bond path becomes well behaved, conforming to a specific set of rules determined by the geometry of the interaction. In the C-H...phenyl group of interactions studied, it was only shown that this would occur if 100Δ was greater than 45. Under these conditions, if the difference in the two H(N)...C_{ring} minimum distances is small, less than 0.06Å was determined experimentally, an edge type bond path to a C-C anion bond will be adopted. If the

difference in the two minimum distances is large, greater than 0.09Å was determined experimentally, the bond path will travel to the single closest carbon atom in the anion phenyl ring. The bond paths of the interactions with centroid type configurations are characteristic and predictable once 100Δ becomes larger than roughly 35. The N-H and C-H results are entirely complementary; centroid configuration hydrogen bonds from either group conform to the same set of geometry based criteria from which their bond path may be determined.

3.6.2.6. Summary and Comparison to the Literature

To summarize the results, in this investigation there were far fewer N-H...X [X = N or π(Ph)] interactions available for analysis than there were C-H...X interactions, 16 versus 44. The bond paths of all of the N-H...X hydrogen bonds studied are summarized in the four cation based diagrams included at the beginning of this section, Figure 121 for the cation in $NH_4B(C_6H_5)_4$, Figure 122 for [DabcoH][$B(C_6H_5)_4$], Figure 123 for $[C(NH_2)_3][B(C_6H_5)_4]\cdot CH_3CN$ and Figure 124 for $[N(C[NH_2]_2)_2][B(C_6H_5)_4]$. In the N-H...X group there were no H...H type contacts found and only one intermediate type contact was located. Even in the hydrogen bonds there were fewer N-H...X type than C-H...X type for all groups except that of the centroid configuration. However, the N-H...X interactions studied, consistently and almost universally met the criteria developed after investigation of the analogous C-H...X groups of contacts, criteria developed by comparing characteristic bond paths to common features of the geometries. In fact, in some cases, centroid type hydrogen bonds for example, the criteria arising from the study of the C-H...phenyl

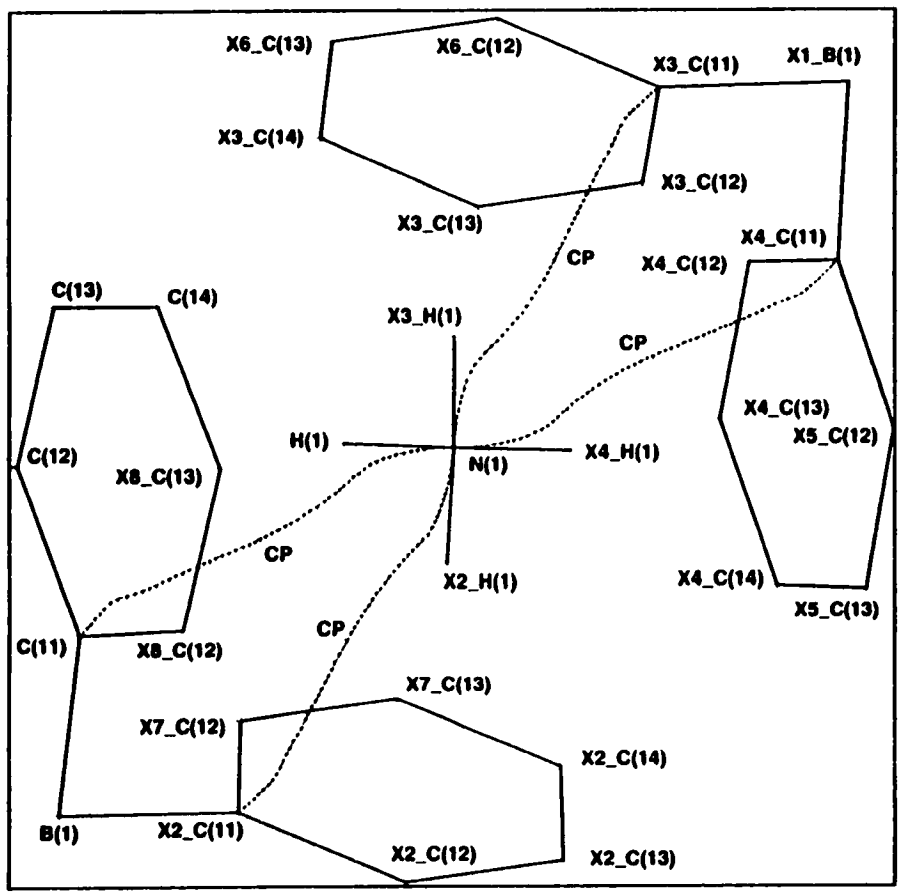

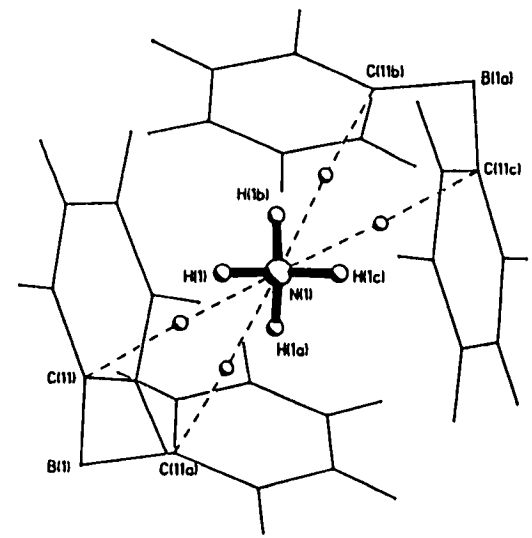

Figure 121. Bond paths located for all the interactions involving the cation in ammonium tetraphenylborate. There are four equivalent N-H...π(Ph) hydrogen bonds from one cation to two different anions in the structure. CP marks the locations of the bond critical point. The outlines of the uninvolved rings on the tetraphenylborate anions have been omitted for clarity.

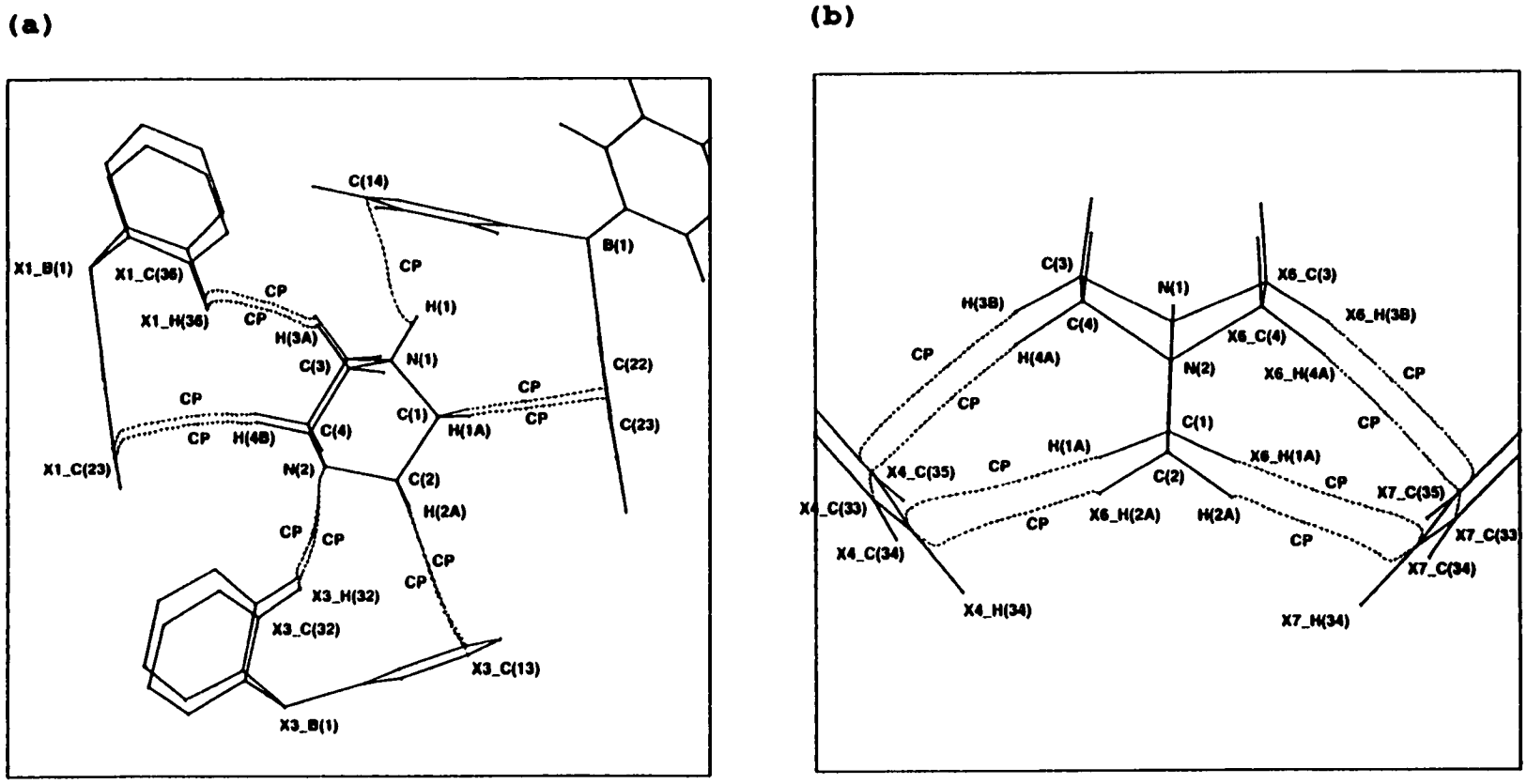

Figure 122. Bond paths located for interactions involving the cation in the structure of [DabcoH][$B(C_6H_5)_4$]. There are eight unique C-H...phenyl interactions of different types, one unique C-H...N interaction and one N-H...π(Ph) hydrogen bond from the cation in the cavity to the anions that surround it included in the diagrams. The views in (a) and (b) are rotated by roughly 90° relative to one another. CP marks the locations of the bond critical points. The outlines of the uninvolved rings on the tetraphenylborate anions have been omitted for clarity.

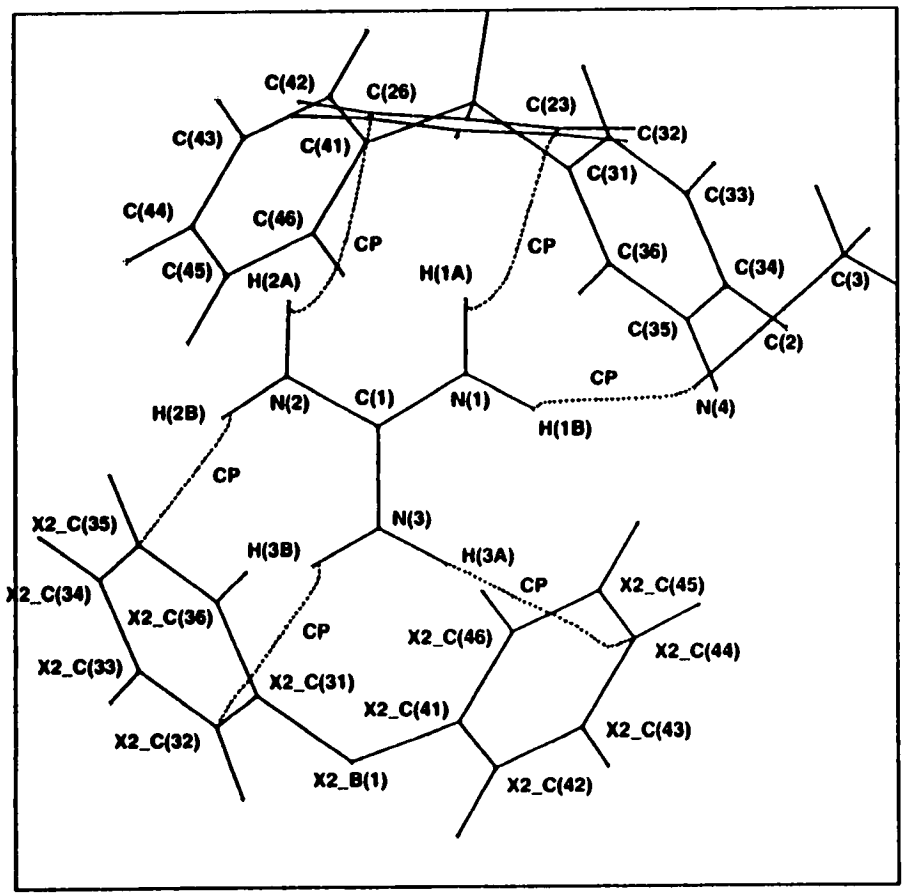

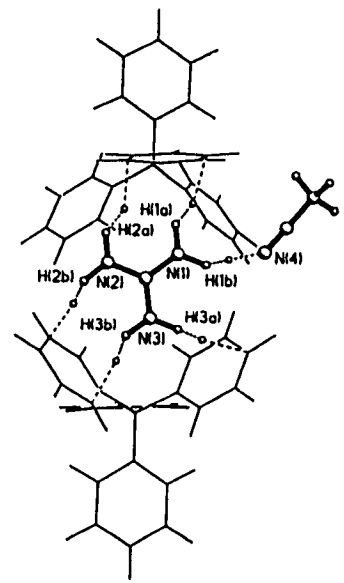

Figure 123. Bond paths located for interactions involving the cation in guanidinium tetraphenylborate acetonitrile solvate. There are five N-H...π(Ph) hydrogen bonds (cation/anion) and one N-H...N hydrogen bond (cation/solvent) shown in the diagram [C-H...N interactions were not included]. CP marks the locations of the bond critical points. The outlines of the uninvolved rings on the tetraphenylborate anions have been omitted for clarity.

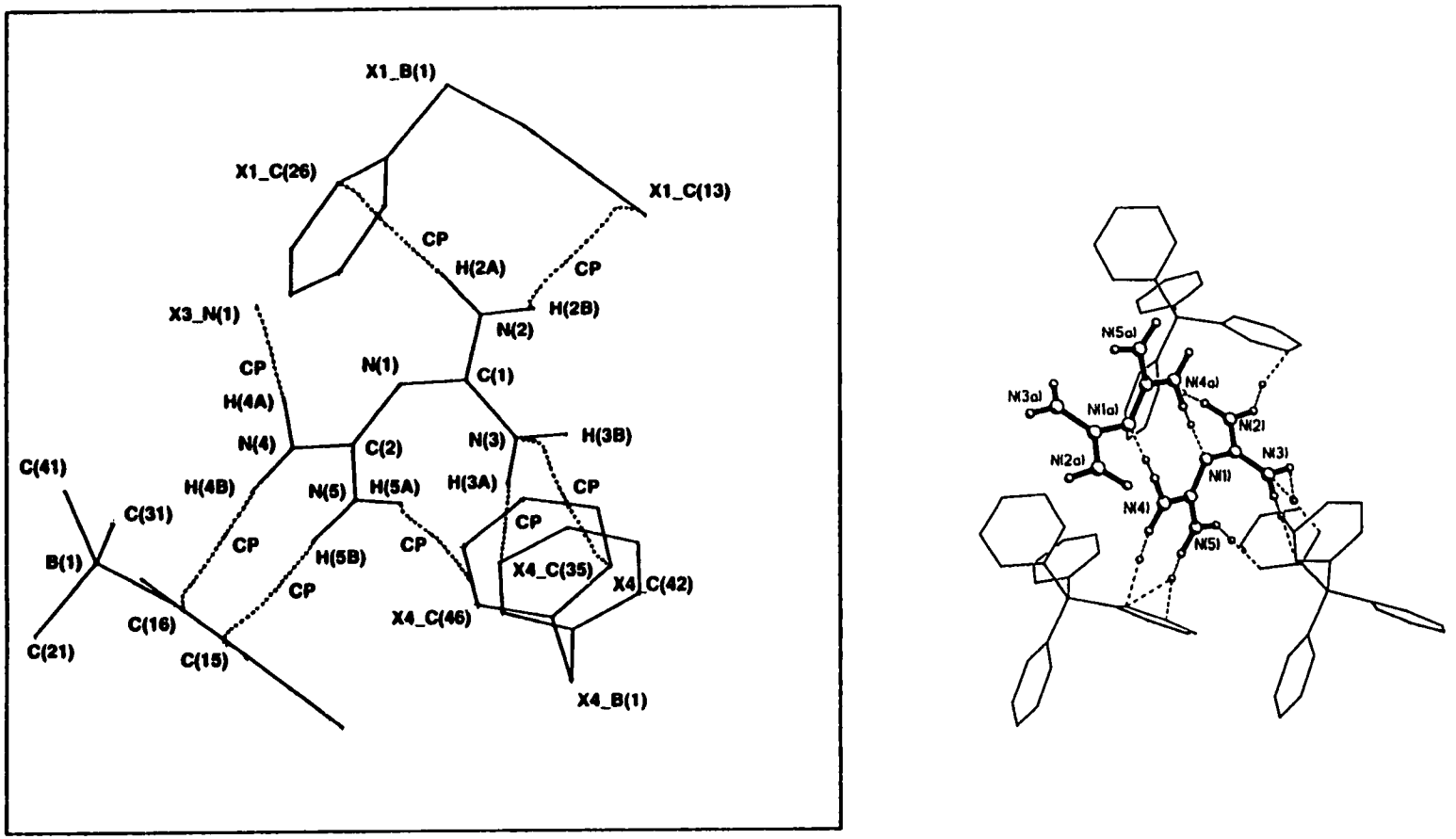

Figure 124. Bond paths located for interactions involving the cation in biguanidinium tetraphenylborate. There are six N-H...π(Ph) hydrogen bonds (cation/anion), one N-H...phenyl interaction (cation/anion) and one N-H...N hydrogen bond (cation/cation) shown in the diagram [C-H...N interactions were not included]. CP marks the locations of the bond critical points. The outlines of the uninvolved rings on the tetraphenylborate anions have been omitted for clarity, as has all but N(1)' of the second cation.

interactions could be narrowed further after consideration of the comparable N-H...π(Ph) interactions. C-H...X and N-H...X interactions of the same type, including hydrogen bonds of all configurations, follow the same set of rules and share the same characteristic bond paths. From the geometry of an interaction, its type (H...H contact, intermediate contact or hydrogen bond) and its general bond path can always be decided. If it is a hydrogen bond type interaction the geometry can also be used to decide the configuration of the contact and in most cases, except "true" centroid type bonds, the correct, characteristic bond path can also be predicted. In all interactions, except the "true" centroid type hydrogen bonds, the bond path is determined by the distance(s) at which the interaction occurs.

There are few other examples of experimentally determined bond paths for X-H...π(Ph) hydrogen bonds with which the present work might be compared. Yang and Craven have recently reported the topological analysis of three C-H...phenyl type interactions occurring in the structure of 2-pyridone,[121] after generation of an experimental charge density from crystallographic data. However, little description of the actual bond paths of these interactions is included in the paper. Its discussion will be saved until the following section on the analysis of the bond critical points.

A 1999 publication by P.R. Mallinson et al.[122] on the charge density distribution in the neutral "proton sponge" compound, 1,8-bis(dimethylamino)naphthalene also includes a brief discussion of intermolecular C-H...π type interactions occurring in the structure. [This work is directly related to an earlier paper on the protonated "proton sponge"

salt,[22] with the charge density distributions of both generated from experimental crystallographic data.] Despite finding a number of geometrically close contacts between the methyl hydrogen atoms and the aromatic carbon atoms in neighbouring 1,8-bis(dimethylamino)naphthalene molecules, the authors located only two (3,-1) type bond critical points, which they attributed to C-H...π type interactions. This is in direct contrast to the present work where a total of 34 close C-H...phenyl contacts were identified in a geometry search for H(C)...C_{ring} distances of 3.0Å or less in the four compounds. Of these 34 potential interactions, (3,-1) type bond critical points and bond paths were located in 33 cases; only in one instance were a bond path and bond critical point not found.

The Mallinson paper includes a bond path diagram illustrating the two interactions, which occur between the same pair of adjacent molecules. The two C-H groups, one from each *N*-methyl group on the same molecule, interact with one six membered ring from naphthalene of the second molecule. The bond paths, although not completely clear in the diagram provided, seem to be analogous to those found for the C-H...π(Ph) hydrogen bonds in this work. They each appear to travel from H(C) smoothly and directly to a carbon atom of the aromatic ring. In the terminology developed in this investigation, the bond paths would correspond to single atom type interactions. The authors describe the H(C)...$C_{aromatic}$ bond paths as being curved close to the hydrogen atoms and almost perpendicular to the aromatic rings. This they conclude is consistent with the interactions being of the C-H...π type. It is also entirely consistent with the observations made in this work.

There are a number of theoretical investigations of the benzene/HF

dimer that report bond paths calculated for the F-H...π(Ph) hydrogen bond, as discussed previously in the introduction. In addition, Cubero et al.[123] have recently reported a theoretical investigation of the C-H...π(Ph) interaction in the benzene/benzene dimer. The experimental results can be compared with these theoretical calculations.

In hydrogen bonds with traditional acceptors, X-H...A [A = N, O, S, Cl, etc.], the bond path normally behaves in a completely predictable fashion, travelling directly between hydrogen of the donor group and the acceptor atom, whatever it is. For example, in all of the X-H...N [X = N or C] interactions studied in this work, the bond path always proceeds from H(X) to the nitrogen atom of the acceptor, regardless of the nature of the interaction or its geometry. Before this investigation was carried out, the behaviour of the bond path in an X-H...π(Ph) hydrogen bond was difficult to predict because of the ill-defined nature of the phenyl ring acceptor. In this work, a number of C-H...π(Ph) [35] and N-H...π(Ph) [14] interactions were studied and of these 26 were found to be "true" hydrogen bonds, 13 of each type. From these, a better understanding of the bond paths expected for X-H...π(Ph) [X = N or C] hydrogen bonds was achieved. Specific rules were developed to allow prediction of the bond path from the geometry of the interaction.

In the hydrogen bond type interactions studied (as opposed to H...H type or intermediate type contacts), the bond path was normally found to travel from H(X) of the donor group to either a single ring carbon atom or to a C-C bond of the acceptor phenyl ring. In most cases, where the bond path approaches the acceptor appears to depend on the minimum $H(X)\ldots C_{ring}$ distances characterizing the interaction. The bond path will

travel to a single atom when the difference in the two minimum $H(X)...C_{ring}$ distances is large and to a bond when the same difference is small. In those hydrogen bonds with close to ideal centroid type geometries [100Δ is small], the behaviour of the bond path in the region of the acceptor can no longer be so accurately predicted. The termination of the bond path is not always determined by the minimum $H(X)...C_{ring}$ distance(s). The bond path still proceeds to a single ring carbon atom or to a C-C ring bond but these are no longer always the closest atoms. In the more ideal centroid geometry hydrogen bonds all of the $H(X)...C_{ring}$ distances are close to equal and other factors appear to determine where the bond path will ultimately travel.

The present experimental results can be compared with theoretical data available in the literature. For example, in the continuing investigation of the "anti-hydrogen bond",[72] an X-H...π(Ph) type interaction in which the covalent X-H bond length actually decreases upon formation of the contact, E. Cubero et al.[123] have carried out ab initio molecular orbital calculations on a series of $R_nC-H...C_6H_6$ complexes, including the benzene/benzene dimer. In a paper published in 1999, the geometry optimizations of the selected complexes and their component monomers, carried out at the MP2 level using 6-31G(d,p) basis sets, are described. No symmetry constraints were imposed on the optimizations and the starting geometry chosen always had the C-H donor group oriented along a line normal to the plane of the benzene ring and passing through the center of the ring. The optimized geometry of the benzene dimer was found to maintain the same symmetrical orientation, with the donor C-H group pointing directly toward the center of the second benzene ring. The

covalent C-H bond length of the donor was calculated to have decreased by 0.0034Å upon complexation, as expected for the so-called anti-hydrogen bond. The geometry adopted by the benzene dimer is that of an ideal, centroid type C-H...π(Ph) hydrogen bond. However, the remaining geometric parameters defining the complex are not included in the publication, making comparison to the current experimental results more difficult.

The bond path for the C-H...π(Ph) interaction in the benzene dimer was found to link the hydrogen donor atom to each equivalent carbon atom of the benzene ring, via the corresponding (3,-1) type bond critical points. Because of the symmetry of the complex, there is only one unique bond path and one unique (3,-1) bond critical point in the dimer. In addition to the six (3,-1) type bond critical points distributed around the ring, six (3,+1) type ring critical points were identified, located above the ring plane between each pair of bond critical points; again only one is unique. Finally, one (3,+3) type cage critical point was also found within the dimer.

The C-H...π(Ph) hydrogen bond described by Cubero et al. within the benzene dimer is very similar in nature to the C-H...phenyl interactions studied experimentally in the tetraphenylborate complexes. However, its centroid type geometry is more symmetrical than any of the experimental examples. The bond path located for the C-H...π(Ph) interaction in the theoretically optimized benzene dimer is clearly of the single atom type according to the experimental criteria developed. Based on the experimental observations, in such an idealized contact, where all the $H(C)...C_{ring}$ distances are equal [100Δ = 0], the bond path can be determined by factors other than distance. In the benzene dimer, symmetry

obviously has an important influence on the bond path adopted. The results of Cubero et al. are in good general agreement with the conclusions reached after studying the experimentally determined bond paths.

These experimental results can also be compared to the theoretical studies of the C_6H_6/HF dimer that have been published. In 1990, Tang et al.[53] reported a full geometry optimization of the dimer using a 6-31G* basis set. The minimum energy conformation was found to have the maximum possible symmetry, C_{6v}, with HF lying on the C_6 axis of C_6H_6 and hydrogen pointing directly at the ring centroid. The H(F)...π_c ring centroid distance was calculated to be 2.418Å, similar to many of the experimental values. This conformation corresponds to an ideal centroid geometry hydrogen bond. In this system, six symmetry equivalent bond paths were located, each connecting H(F) to one of the six symmetry equivalent ring carbon atoms. The one unique bond path, H(F) to C_{ring}, is of the single atom type. The (3,-1) bond critical point was found to lie closer to H(F) than to the ring. Unfortunately, since all the H(F)...C_{ring} distances are equal in the dimer [100Δ = 0], the bond path cannot be predicted using the experimentally determined criteria. However the HF/C_6H_6 results of Tang et al. agree well with those calculated by Cubero et al. for $(C_6H_6)_2$.

A 1997 study by Rozas et al.,[54] carried out with a larger basis set at a higher level of theory, reached a rather different conclusion about the bond path of the F-H...π(Ph) hydrogen bond in the C_6H_6/HF dimer. The geometry of the dimer was reoptimized using a 6-311++G** basis set at the MP2 level of theory. In the one minimum energy structure located, the hydrogen atom of the HF molecule was found to point the middle of one of the C-C ring bonds, quite different from the results of Tang et al.[53] A

loss of symmetry in the aromatic ring was observed on complex formation, although vertical mirror symmetry was maintained (bisecting opposing ring bonds) as reflected in the three unique C-C ring bond lengths calculated.

A (3,-1) bond critical point was located between H(F) of the donor and that C-C ring bond of the acceptor at which the F-H vector pointed. When analyzing the bond path corresponding to this F-H...π(Ph) hydrogen bond, the authors found an unusual situation. The bond path was found to travel from H(F) to the exact midpoint of the C-C ring bond, terminating in fact at the (3,-1) critical point of that bond. The bond path lies in the vertical mirror plane that bisects this C-C bond. In the interaction, the bond critical point of the C-C bond serves as the attractor for the bond path linking the hydrogen of HF to the C_6H_6 ring.

The minimum energy conformation adopted by the dimer is termed a "conflict catastrophe structure" because it is by nature an unstable arrangement. Even a small displacement of the HF molecule from the calculated geometry would cause the bond path to change dramatically. Movement of HF from its equilibrium position would destroy the symmetry of the interaction and result in a radical breakdown in the observed bond path. It would not necessarily be expected that such a conflict catastrophe situation could ever arise experimentally, where there are many external pressures on each individual interaction acting to reduce the symmetry. However, it is interesting to note that in the calculations of Rozas et al.[54] the bond path of the F-H...π(Ph) hydrogen bond travels to a C-C bond of the benzene ring acceptor and not to a single ring carbon atom (as Tang et al.[53] had previously calculated). In both the theoretically and experimentally generated bond paths for X-H...π(Ph)

hydrogen bonds, the interaction line always travels from H(X) of the donor group to a well-defined region of the acceptor, either to a single ring carbon atom or to a C-C bond of the ring. It has not been found to travel to a more ill-defined region of the diffuse π electron cloud surrounding the phenyl ring acceptor, even in centroid type hydrogen bonds.

The experimental X-H...π(Ph) hydrogen bonds investigated can never achieve the same high symmetry possible for the C_6H_6/HF dimer modelled in the reported theoretical calculations. In the experimental structures the maximum symmetry is lower at both the donor and the acceptor of the hydrogen bond. At the donor, rather than the simple HF molecule ($C_{\infty v}$), the X-H group is always a part of a larger cation, anion or solvent molecule. Although it has been shown that the individual N/C-H group can sometimes be aligned directly above the centroid of the interacting ring, the symmetry of the complete "donor" must be lower than that of HF, which can lie entirely on the C_6 axis of benzene in the dimer. Similarly, in the experimental structures benzene is replaced by a phenyl ring of the tetraphenylborate anion as the hydrogen bond acceptor. The C_{6v} symmetry of the ring is lost in the anion. In this experimental investigation only two of the structures were found to have anions containing phenyl rings with higher than C_1 symmetry. Both $NH_4B(C_6H_5)_4$ and [DabcoH] $[B(C_6H_5)_4]$ have phenyl rings that are bisected by vertical mirror planes, but these pass through the C(x1) and C(x4) ring atoms rather than through opposing ring bonds. Only two of the N-H...π(Ph) hydrogen bonds studied in this work are made to such rings, one in each structure; all other N-H...π(Ph) hydrogen bonds are made to phenyl rings occupying completely general positions.

This lower symmetry must be remembered when comparing the present

experimental results to the results of the theoretical calculations. It must also be remembered that the theoretical calculations are made on an isolated C_6H_6/HF dimer. In the experimental situation, the X-H...π(Ph) hydrogen bonds are not isolated; they are influenced by the many other internal forces acting within the crystal and by the competition which arises from the need to form multiple interactions in the same structure. This will also cause differences to arise between the theoretical and experimental results and must be considered when comparing the two. The geometry of an experimental interaction will never be exactly equivalent to the theoretical model.

The first of the two "higher symmetry" interactions investigated experimentally is the only N-H...π(Ph) hydrogen bond in the structure of [DabcoH][$B(C_6H_5)_4$]. The $[N(1)\text{-}H(1)]_{cation}\cdots[\text{ring } 1]_{anion}$ hydrogen bond has a centroid type geometry and a bond path that travels from H(1) to a single ring carbon atom of the acceptor, C(14). The bond path lies on the vertical mirror plane that bisects the ring, as does the terminal C(14) atom. The bond path does not travel to the atom with the shortest H...C_{ring} distance but rather to that with the longest. Such unpredictable behaviour is often observed for centroid type hydrogen bonds with small values of 100Δ such as this one.

Similarly, there is only a single unique N-H...π(Ph) hydrogen bond in the structure of $NH_4B(C_6H_5)_4$, $[N(1)\text{-}H(1)]_{cation}\cdots[\text{ring } 1]_{anion}$. It also has a centroid type geometry and a bond path that travels to a single acceptor atom, in this case from N(1) of the cation to C(11) of the anion phenyl ring. Again, the bond path lies on the vertical mirror plane that bisects the phenyl ring and that also contains the C(11) atom. The bond path does

not travel to the closest C_{ring} atom in this interaction either.

It is also interesting to note that there is a single C-H...π(Ph) centroid type hydrogen bond in the ammonium tetraphenylborate structure, $[C(14)-H(14)]_{anion}...[ring\ 1]_{anion}$. In this interaction, the bond path is again guided by symmetry, lying on the same vertical mirror plane that bisects the ring 1 plane. It ends on one of the ring carbon atoms that lies on this plane. In fact, it also ends at C(11) but the approach is made from the opposite side of the ring plane relative to the N-H...π(Ph) interaction. The experimental results suggest that in centroid type hydrogen bonds **symmetry** can be one of the factors that determines where the bond path will travel and where it will meet the acceptor. Such interactions, with small values of 100Δ, have bond paths that are not determined solely by distance considerations.

In all of these experimental interactions, and these were the only ones located with such symmetric bond paths, there is only one unique bond path joining H(X) to the acceptor ring. That bond path lies on the vertical mirror plane that bisects the phenyl ring and ends at a single ring carbon atom that also lies on the same mirror plane, either C(x1) or C(x4). In this respect the results are more in keeping with the theoretical calculations of Tang et al.[53] than those of Rozas et al.[54] The bond paths travel to a single ring carbon atom rather than to a C-C ring bond, or more specifically to the (3,-1) critical point of that bond. The "catastrophe conflict situation" described by Rozas et al. appears to be avoided experimentally.

In the many lower symmetry (C_1) X-H...π(Ph) [X = N or C] hydrogen bonds studied, bond paths to single ring carbon atoms and to C-C ring

bonds were both observed in appreciable numbers. Because of the general symmetry of these interactions, "conflict catastrophe situations" cannot arise, and in fact the experimental bond paths do not necessarily travel to the midpoint of the C-C acceptor bond. Although the (3,-1) critical points of the covalent C-C ring bonds were not investigated, they do not appear to serve as the attractor in any of the experimental hydrogen bonds studied. This is contrary to the results of Rozas et al.[54] However, the fact that experimental bond paths can approach either a single ring carbon atom or a C-C ring bond of the acceptor, is supported by the calculations of both groups, the former by Tang et al. and the latter by Rozas et al.

The same experimental observations are also supported by theoretical calculations reported by Tarakeshwar et al.[91] in a 1998 publication. The authors again optimized the geometry of the C_6H_6/HF dimer using large basis sets at the MP2 level of theory. Although a topological analysis of the electron densities were not carried out, and thus no bond paths were calculated, it is still instructive to compare these results to the experimental data.

The authors located three different minimum energy conformations for the F-H...π(Ph) complex. In the first, the "on atom" conformation, the F-H vector is directed perpendicularly toward a single carbon atom of the C_6H_6 ring. In the second "on bond" conformation, the F-H vector is directed perpendicularly toward a C-C bond of the benzene ring. The third minimum energy structure located was the C_{6v} conformation, in which HF lies on the C_6 axis of the benzene molecule and the hydrogen atom points directly towards the ring centroid, the same conformation identified in the calculations of Tang et al.[53] The three minima identified by Tarakeshwar

et al.[91] correspond in a general way to the single atom type, edge type and centroid type hydrogen bonds observed experimentally. All three conformations were calculated to be of similar energies. The authors found the "on atom" and "on bond" geometries to be essentially isoenergetic and the lowest energy conformers at all levels of theory. The totally symmetric conformation was found to be slightly less stable and higher in energy than the other two conformations. Still, this illustrates the flat potential energy surface of the benzene ring, which is also presumably reasonably true for the phenyl rings of the tetraphenylborate anion.

Although Tarakeshwar et al. did not calculate bond paths for the minimum energy conformations located, it seems reasonable to assume that they would behave as described, travelling from H(F) to either a single ring carbon atom in the "on atom" conformation or to a C-C ring bond in the "on bond" conformation. The fact that both conformations were calculated to be equal in energy, and thus both bond path types are equally possible (at least theoretically) in the absence of other interfering factors, supports the experimental results. In the experimental interactions studied, bond paths of both edge and single atom types were located. Where the bond path travelled was found to depend, in most cases, on the distance(s) at which the interaction occurred. This could only be true if both types of interactions ("on atom" and "on bond") were in general equally stable and probable, as indicated by the calculations of Tarakeshwar et al.

The conclusions reached by Tarakeshwar et al.[91] are substantiated by two publications that have appeared in the past year. Cubero et al.[123,124] have reinvestigated the F-H...π(Ph) interaction in the HF/C_6H_6 dimer at two

different levels of theory. In the earlier publication [124] the geometry of the HF/benzene complex was fully optimized at the RHF level using a 6-31G(d,p) basis set. The minimum energy conformation located by Cubero et al. was found to be analogous to that determined previously by Tang et al.,[53] not surprising considering the similarity of the computations carried out. In this orientation the F-H bond lies along the line normal to the plane of the benzene ring that passes through the ring centroid. Cubero et al. identified six (3,-1) bond critical points symmetrically distributed around the ring. The bond paths link the donor hydrogen atom of HF to each of the ring carbon atoms, proceeding via the (3,-1) bond critical points. In keeping with the C_{6v} symmetry of the complex only one bond critical point and one bond path is unique. The bond path is quite linear; it follows the geometric line joining the hydrogen atom and any ring carbon atom very closely. Cubero et al. also located six (3,+1) ring critical points, each lying on a line connecting the donor hydrogen atom with the midpoint of one of the ring C-C bonds. Again, only one of the six (3,+1) ring critical points is unique because of symmetry. The (3,+1) ring critical points separate every pair of (3,-1) bond critical points above the C_6H_6 ring. Finally, a (3,+3) cage critical point was located along a line joining the hydrogen atom to the ring centroid. Although this is a reasonable result for theoretical calculations carried out of this level of theory, the optimized complex is more symmetrical than any of the experimental contacts studied. Still, experimental examples of single atom type X-H...π(Ph) interactions, with characteristic bond paths from H(X) to one C_{ring} atom, were observed.

In a paper that appeared later in the same year, Cubero et al.[123]

describe the optimization of the same HF/C_6H_6 dimer but at a higher level of theory. The geometry of the complex and the isolated monomers were optimized at the MP2 level using the same 6-31G(d,p) basis set and the frozen core approximation. In the starting geometry the F-H group was placed on the line normal to the ring plane above the ring centroid. No symmetry constraints were applied to the optimization. The optimized dimer was found, however, to possess C_s symmetry, with the F-H bond pointing directly toward one carbon atom of the benzene ring. The F-H vector forms an angle of approximately 15° with the normal to the benzene ring plane. A single bond path was located, linking the donor hydrogen atom with the carbon atom to which the F-H bond points. One (3,-1) type bond critical point was found to lie between the two interacting groups, on the calculated bond path. This also corresponds to a single atom type interaction/bond path according to the experimental observations made but is a less symmetrical example than previously observed theoretically. It actually matches the experimental examples more closely than the other single atom type conformations calculated for the F-H...π(Ph) interaction.

The authors reach several valid conclusions based on the results presented in the two publications. The energy of the optimized dimers in the two conformations [C_{6v} versus C_s] is very close, indicating that the calculated interaction energy surface is very flat with a shallow minimum. This supports the results reported earlier by Tarakeshwar et al.[91] Although the energy difference between the C_{6v} and the C_s geometries is small, there are marked changes in the topology of the electron density, particularly in the number of critical points and their distribution. Finally, it is apparent that the computational methods chosen in theoretical calculations

can greatly influence the topological results obtained, higher levels of theory seeming to favour less symmetrical configurations in the case of the F-H...π(Ph) interaction of the HF/C_6H_6 dimer.

3.6.3. Bond Critical Points

3.6.3.1. Introduction

As already discussed, a total of 60 interactions [16 N-H...X and 44 C-H...X, X = N or π(Ph)] were characterized in this work, by location of the (3,-1) type bond critical points and associated bond paths for the H...X portion of the contact. The topological analysis was carried out after generation of an experimental charge density, from x-ray crystallographic data, for each of the four tetraphenylborate salts studied. The (3,-1) type critical points or bond critical points were the only ones specifically investigated, although other types [(3,-3) nucleus; (3,+1) ring; (3,+3) cage] were sometimes also located in the searches carried out. If the contacts in question are defined, in very general terms, as X-H...acceptor, the bond critical point was normally located between H(X) and the acceptor. No corresponding bond critical point or bond path would be found between X and the acceptor although that area was also searched. In the few experimental cases where the bond path was actually found to proceed from X to the acceptor, the converse was usually true and no bond critical point would be located between H(X) and the acceptor. Except for a few rare instances, all of them involving the acetonitrile solvent molecule in the structure of $[C(NH_2)_3][B(C_6H_5)_4]\cdot CH_3CN$, only a single (3,-1) type bond critical point was located for each potential interaction identified in the geometry search for contacts of 3Å or less. The

$[C(NH_2)_3][B(C_6H_5)_4]\cdot CH_3CN$ results are likely an anomaly, arising from poor modelling of the acetonitrile molecule, specifically its methyl region.

At the bond critical point [(3,-1) type] the electron density, $\rho_b(\mathbf{r})$, is a minimum in relation to the bond path and a maximum in relation to all other directions. From the bond critical point, the density increases in both directions along the bond path towards the two interacting centers. The principal curvature λ_3, that parallel to the bond path, is dominant and positive. The two perpendicular curvatures, λ_1 and λ_2, are negative since the electron density decreases in all other directions away from the bond path and the critical point. The sum of the three principal curvatures defines the Laplacian of the electron density at the bond critical point, $\nabla^2\rho(\mathbf{r}) = \lambda_1 + \lambda_2 + \lambda_3$. The value of $\nabla^2\rho(\mathbf{r})$ can be either positive or negative, depending on the relationship of the three eigenvalues, while in contrast, the value of $\rho_b(\mathbf{r})$ is invariably positive. A positive Laplacian value ($\nabla^2\rho_b(\mathbf{r}) > 0$) has physical meaning as representing a local depletion of charge while a negative value ($\nabla^2\rho_b(\mathbf{r}) < 0$) corresponds to a local accumulation of charge.

Topologically, interactions are usually characterized by the values of the electron density, $\rho_b(\mathbf{r})$, and the Laplacian of the electron density, $\nabla^2\rho_b(\mathbf{r})$, at the bond critical point. The ellipticity of an interaction or bond ($\epsilon = [(\lambda_1 / \lambda_2) - 1]$) is another parameter that is also often quoted but it tends not to be well behaved in weak intermolecular interactions, where λ_1 and λ_2 are both very small and nearly equal. For this reason it will not be discussed any further in this work. Recently, Espinosa et al.[125] have suggested that λ_3 is the best topological parameter with which to compare data from different structures and investigations as far as

hydrogen bonds are concerned.

The experimental interactions studied in this investigation [H...X] were all found to have positive $\rho_b(\mathbf{r})$ values as expected. The electron density at the bond critical point was observed to increase from 0.031 to 0.200 $e\text{Å}^{-3}$ in the experimental set, all relatively small values. All of the experimental Laplacian values were also found to be positive ($\nabla^2\rho_b(\mathbf{r}) > 0$), ranging from 0.240 to 1.637 $e\text{Å}^{-5}$. Thus topologically (at least) all of the experimental, (3,-1) type, bond critical points belong to a single group (defined by $\rho_b(\mathbf{r}) > 0$ and $\nabla^2\rho_b(\mathbf{r}) > 0$), differing only in the magnitudes of the values observed.

Is this a reasonable experimental result? In discussions of the topological properties of the electron density (see the introduction) all possible types of interactions are normally divided into two broad groups, covalent or shared interactions and ionic (electrostatic) or closed shell interactions. In the former group of interactions, electron density is accumulated and concentrated in the area between the "bonded" nuclei along the bond path; relatively large values of $\rho_b(\mathbf{r})$ are normally observed. The magnitude of λ_3 is decreased, while λ_1 and λ_2 increase in magnitude when a shared interaction is formed. Since λ_1 and λ_2 are negative curvatures, the Laplacian of the electron density at the bond critical point is always less than zero in covalent or shared interactions ($\nabla^2\rho_b(\mathbf{r}) < 0$). In contrast, in closed shell interactions electron density is removed from the region between the "bonded" nuclei and concentrated at the atomic centers. The positive curvature of the electron density along the bond path, λ_3, is increased and dominant while λ_1 and λ_2 remain small and negative. In closed shell interactions electron density is not accumulated

along the bond and so they are characterized by relatively low values of $\rho_b(\mathbf{r})$, often an order of magnitude less than those of comparable covalent bonds. The Laplacian of the electron density at the bond critical point is invariably positive for closed shell interactions ($\nabla^2\rho_b(\mathbf{r}) > 0$). Many types of interactions are included in the closed shell category; it encompasses all those based on ionic, electrostatic or dispersion forces. Thus, almost all intermolecular contacts would be expected to fall into this group, including most hydrogen bonds and all van der Waals contacts.

It is completely reasonable that all the experimental interactions studied here should behave topologically as closed shell interactions, with low positive values of $\rho_b(\mathbf{r})$ and positive values of $\nabla^2\rho_b(\mathbf{r})$ in all cases. For certain of the experimental C-H...phenyl contacts the exact nature of the interaction is still somewhat unclear (the H...H contacts) but they too consistently behave topologically as closed shell interactions. All other N-H...X (X = N, C or O) and C-H...X (X = N or O) hydrogen bonds reported so far in the literature also have topological values (for the H...X region) characteristic of closed shell interactions, substantiating the present results. In fact, as previously discussed in the introduction, only a few, strong $[O\text{-}H...O]^-$ hydrogen bonds have ever been shown to behave differently in topological terms. Both OH components in such strong, often symmetrical, hydrogen bonds are characterized by negative Laplacian values ($\nabla^2\rho_b(\mathbf{r}) < 0$), showing that they are covalent or shared interactions. However, such covalent hydrogen bonds are very rare and none involving N-H donors are known. Although in this work a covalent component has been postulated for the N-H...π(Ph) hydrogen bonds, they remain primarily electrostatic in nature. This conclusion, which was

reached after careful examination of the static electron density maps, is confirmed by the experimental topological data collected. It fits with all the data previously reported in the literature that the experimental interactions (whether N-H...X or C-H...X type, whether hydrogen bonds or other types of intermolecular contacts) should behave as closed shell interactions in topological terms.

Certain other questions logically arise once a topological analysis of the electron density has been carried out. For example, can the topological parameters generated be combined with geometric data to learn something more about the interactions being studied? Do the topological data vary in any consistent and reproducible way with any of the geometric parameters defining the interaction? From previous work available in the literature (and summarized in the introduction) it seemed reasonable to try and correlate the variation of $\rho_b(\mathbf{r})$ and $\nabla^2\rho_b(\mathbf{r})$ with a distance characteristic of the X-H...acceptor interactions. The distance chosen was that between the two terminal atoms of the bond path, normally the distance from the H(X) atom of the donor group to an N atom (X-H...N type) or to a ring H or C atom (X-H...phenyl type) of the acceptor group. This removes the uncertainty in the definition of the π(Ph) type hydrogen bond acceptor. Plots of the experimental $\rho_b(\mathbf{r})$ and $\nabla^2\rho_b(\mathbf{r})$ data versus the H...acceptor distance were fitted to simple model functions in order to establish the relationship that might exist between the topological and geometric parameters. The ultimate goal was to try and prove that (at least topologically) X-H...π(Ph) hydrogen bonds behave consistently and reproducibly, comparable to hydrogen bonds formed with "traditional" lone pair acceptors.

Table 14 contains a summary of the pertinent topological and geometric data for all 60 interactions studied in this investigation. The table includes $\rho_b(\mathbf{r})$ and $\nabla^2\rho_b(\mathbf{r})$ values as well as the distance characterizing the contact and a classification of its type based on the geometry of the interaction. The interactions are ranked in order of decreasing electron density at the bond critical point [$\rho_b(\mathbf{r})$] and certain general trends are immediately apparent. For example, the N-H...X type interactions [X = N or π(Ph)] are found at the top of the table and the C-H...X interactions at the bottom. There is some overlap between the two groups in the intermediate region of the table but the division is still obvious. For the N-H...X type interactions, the N-H...N hydrogen bonds are clearly stronger than the N-H...π(Ph) hydrogen bonds, the former appearing at the very top of the table. The separation of the C-H...X interactions into different types having different characteristic strengths is not so clear cut and will be discussed in more detail later.

The strongest interactions, those found at the top of the table, are characterized by the largest $\rho_b(\mathbf{r})$ and $\nabla^2\rho_b(\mathbf{r})$ values and the shortest H...acceptor distances (if the anomalously short H...H contacts are ignored for the moment). As the distance increases, the $\rho_b(\mathbf{r})$ and $\nabla^2\rho_b(\mathbf{r})$ values generally decrease, the $\rho_b(\mathbf{r})$ values somewhat more smoothly and consistently than the $\nabla^2\rho_b(\mathbf{r})$ values. Even at first glance, it appears likely that there is a definite relationship between the topological parameters characterizing an interaction and the distance over which that interaction occurs. This relationship will be explored further in the following section.

Table 14. Summary of the bond critical points located in the four tetraphenylborate compounds studied.

	Compound and Contact[a]	Type of Interaction[b]	Bond Path[c,d]	Contact Distance (Å)	Charge Density[e] $\rho_b(\mathbf{r})$ ($eÅ^{-3}$)	Laplacian $\nabla^2\rho_b(\mathbf{r})$ ($eÅ^{-5}$)
G	N(1)-H(1B)...N(4) N-H...N hydrogen bond	c/s	H(1B)...N(4)	2.082	0.200(54)	1.637(4)
B	N(4)-H(4A)...N(1) N-H...N hydrogen bond	c/c	H(4A)...N(1)	2.127	0.141(2)	1.519(3)
B	N(2)-H(2A)...ring 2 N-H...π(Ph) centroid type hydrogen bond	c/a	H(2A)...C(26)	2.392	0.104(14)	0.918(19)
G	N(3)-H(3B)...ring 3 N-H...π(Ph) centroid type hydrogen bond	c/a	H(3B)...C(32)	2.498	0.102(29)	0.885(11)
N	N(1)-H(1)...ring 1 N-H...π(Ph) centroid type hydrogen bond - unusual bond path	c/a	N(1)...C(11)	3.268	0.099(7)	0.872(1)
B	N(3)-H(3A)...ring 3 N-H...π(Ph) centroid type hydrogen bond	c/a	H(3A)...C(35)-C(36)	2.430	0.097(2)	0.857(1)
G	N(2)-H(2B)...ring 3 N-H...π(Ph) hydrogen bond - edge type by geometry and single atom type by bond path	c/a	H(2B)...C(35)	2.622	0.087(23)	0.677(12)
D	N(1)-H(1)...ring 1 N-H...π(Ph) centroid type hydrogen bond	c/a	H(1)...C(14)	2.640	0.086(5)	0.823(3)

Table 14. Summary of the bond critical points located in the four tetraphenylborate compounds studied (continued).

	Compound and Contact[a]	Type of Interaction[b]	Bond Path[c,d]	Contact Distance (Å)	Charge Density[e] $\rho_b(\mathbf{r})$ ($eÅ^{-3}$)	Laplacian $\nabla^2\rho_b(\mathbf{r})$ ($eÅ^{-5}$)
G	N(3)-H(3A)...ring 4 N-H...π(Ph) centroid type hydrogen bond	c/a	H(3A)...C(43)-C(44)	2.668	0.081(28)	0.638(14)
B	N(2)-H(2B)...ring 1 N-H...π(Ph) single atom type hydrogen bond	c/a	H(2B)...C(13)	2.490	0.081(2)	0.883(1)
B	C(46)-H(46)...ring 1 C-H...phenyl interaction - H...H type contact	a/a	H(46)...H(13)	2.179	0.078(1)	0.703(1)
G	N(1)-H(1A)...ring 2 N-H...π(Ph) centroid type hydrogen bond	c/a	H(1A)...C(22)-C(23)	2.458	0.073(34)	0.706(11)
B	N(5)-H(5B)...ring 1 N-H...π(Ph) centroid type hydrogen bond	c/a	H(5B)...C(15)-C(16)	2.560	0.071(1)	0.654(1)
G	C(44)-H(44)...N(4) C-H...N interaction	a/s	H(44)...N(4)	2.805	0.066(3)	0.633(2)
D	C(35)-H(35)...ring 2 C-H...phenyl interaction - H...H type contact	a/a	H(35)...C(22)-H(22)	2.354	0.065(0)	0.441(0)
G	C(46)-H(46)...N(2) C-H...N interaction	a/c	H(46)...N(2)	2.775	0.062(1)	0.527(1)

Table 14. Summary of the bond critical points located in the four tetraphenylborate compounds studied (continued).

	Compound and Contact[a]	Type of Interaction[b]	Bond Path[c,d]	Contact Distance (Å)	Charge Density[e] $\rho_b(\mathbf{r})$ ($eÅ^{-3}$)	Laplacian $\nabla^2\rho_b(\mathbf{r})$ ($eÅ^{-5}$)
G	C(3)-H(61)...ring 1 C-H...π(Ph) centroid type hydrogen bond	s/a	H(61)...C(13)-C(14)	2.847	0.062(2)	0.498(1)
G	C(43)-H(43)...N(2) C-H...N interaction	a/c	H(43)...N(2)	2.797	0.061(1)	0.522(1)
G	C(14)-H(14)...ring 1 C-H...phenyl interaction - H...H type contact	a/a	H(14)...H(15)	2.357	0.061(2)	0.504(1)
B	N(5)-H(5A)...ring 4 N-H...π(Ph) edge type hydrogen bond	c/a	H(5A)...C(45)-C(46)	2.664	0.059(1)	0.614(1)
G	C(13)-H(13)...ring 1 C-H...phenyl interaction - H...H type contact	a/a	H(13)...H(12)	2.454	0.058(1)	0.467(1)
B	C(16)-H(16)...ring 1 C-H...phenyl interaction - H...H type contact	a/a	H(16)...H(16)	2.261	0.057(1)	0.782(1)
B	C(13)-H(13)...ring 2 C-H...π(Ph) edge type hydrogen bond	a/a	H(13)...C(25)-C(26)	2.762	0.057(1)	0.608(1)
B	C(16)-H(16)...ring 1 C-H...phenyl interaction - H...H type contact	a/a	H(16)...H(15)	2.205	0.056(1)	0.583(1)

Table 14. Summary of the bond critical points located in the four tetraphenylborate compounds studied (continued).

	Compound and Contact[a]	Type of Interaction[b]	Bond Path[c,d]	Contact Distance (Å)	Charge Density[e] $\rho_b(\mathbf{r})$ ($eÅ^{-3}$)	Laplacian $\nabla^2\rho_b(\mathbf{r})$ ($eÅ^{-5}$)
D	C(3)-H(3A)...ring 3 C-H...phenyl interaction - H...H type contact	c/a	H(3A)...H(36)	2.262	0.056(0)	0.413(1)
B	C(42)-H(42)...N(4) C-H...N interaction	a/c	H(42)...N(4)	2.867	0.055(1)	0.679(1)
B	N(4)-H(4B)...ring 1 N-H...phenyl interaction - intermediate type contact	c/a	H(4B)...C(16)-H(16)	2.661	0.055(1)	0.477(1)
G	N(2)-H(2A)...ring 2 N-H...π(Ph) edge type hydrogen bond	c/a	H(2A)...C(25)-C(26)	2.672	0.055(20)	0.474(12)
B	C(13)-H(13)...ring 3 C-H...phenyl interaction - H...H type contact	a/a	H(13)...H(35)	2.347	0.053(1)	0.626(1)
D	C(2)-H(2A)...ring 3 C-H...phenyl interaction - intermediate type contact	c/a	H(2A)...C(34)-H(34)	2.819	0.053(1)	0.379(1)
G	C(33)-H(33)...N(4) C-H...N interaction	a/s	H(33)...N(4)	2.561	0.052(2)	0.588(1)
D	C(23)-H(23)...ring 3 C-H...phenyl interaction - intermediate type contact	a/a	H(23)...C(33)-H(33)	2.901	0.052(0)	0.472(0)

Table 14. Summary of the bond critical points located in the four tetraphenylborate compounds studied (continued).

	Compound and Contact[a]	Type of Interaction[b]	Bond Path[c,d]	Contact Distance (Å)	Charge Density[e] $\rho_b(\mathbf{r})$ ($eÅ^{-3}$)	Laplacian $\nabla^2\rho_b(\mathbf{r})$ ($eÅ^{-5}$)
G	C(23)-H(23)...ring 1 C-H...phenyl interaction - H...H type contact	a/a	H(23)...H(12)	2.337	0.051(1)	0.442(1)
D	C(4)-H(4A)...ring 3 C-H...π(Ph) edge type hydrogen bond	c/a	H(4A)...C(32)-C(33)	2.854	0.051(1)	0.253(1)
D	C(32)-H(32)...N(2) C-H...N interaction	a/c	H(32)...N(2)	2.743	0.051(0)	0.456(1)
G	C(45)-H(45)...N(4) C-H...N interaction	a/s	H(45)...N(4)	2.947	0.050(2)	0.544(1)
B	C(15)-H(15)...ring 4 C-H...π(Ph) centroid type hydrogen bond	a/a	H(15)...C(41)-C(42)	2.952	0.050(1)	0.412(1)
D	C(1)-H(1A)...ring 3 C-H...π(Ph) edge type hydrogen bond	c/a	H(1A)...C(34)-C(35)	2.874	0.050(7)	0.346(2)
B	N(3)-H(3B)...ring 4 N-H...π(Ph) edge type hydrogen bond - unusual bond path	c/a	N(3)...C(42)	3.498	0.049(1)	0.544(1)
D	C(1)-H(1A)...ring 2 C-H...π(Ph) edge type hydrogen bond	c/a	H(1A)...C(22)-C(23)	2.874	0.049(4)	0.467(2)

Table 14. Summary of the bond critical points located in the four tetraphenylborate compounds studied (continued).

	Compound and Contact[a]	Type of Interaction[b]	Bond Path[c,d]	Contact Distance (Å)	Charge Density[e] $\rho_b(\mathbf{r})$ (eÅ^{-3})	Laplacian $\nabla^2\rho_b(\mathbf{r})$ (eÅ^{-5})
B	C(14)-H(14)...ring 2	a/a	H(14)...C(22)-C(23)	2.849	0.049(1)	0.451(1)
	C-H...π(Ph) centroid type hydrogen bond					
G	C(16)-H(16)...ring 3	a/a	H(16)...H(35)	2.464	0.049(1)	0.439(1)
	C-H...phenyl interaction - H...H type contact					
B	C(12)-H(12)...ring 3	a/a	H(12)...C(34)	2.865	0.048(4)	0.553(1)
	C-H...π(Ph) single atom type hydrogen bond					
G	C(3)...ring 2	s/a	C(3)...C(22)-C(23)	3.752	0.047(1)	0.402(1)
D	C(4)-H(4B)...ring 2	c/a	H(4B)...C(22)-C(23)	2.921	0.047(1)	0.248(1)
	C-H...π(Ph) edge type hydrogen bond					
G	C(34)-H(34)...ring 4	a/a	H(34)...C(42)-H(42)	2.574	0.046(1)	0.405(1)
	C-H...phenyl interaction - H...H type contact					
N	C(12)-H(12)...ring 1	a/a	H(12)...C(14)-H(14)	2.873	0.046(9)	0.495(6)
	C-H...phenyl interaction - intermediate type contact					
B	C(44)-H(44)...ring 3	a/a	H(44)...C(33)-H(33)	2.454	0.045(1)	0.479(1)
	C-H...phenyl interaction - H...H type contact					

Table 14. Summary of the bond critical points located in the four tetraphenylborate compounds studied (continued).

	Compound and Contact[a]	Type of Interaction[b]	Bond Path[c,d]	Contact Distance (Å)	Charge Density[e] $\rho_b(\mathbf{r})$ ($eÅ^{-3}$)	Laplacian $\nabla^2\rho_b(\mathbf{r})$ ($eÅ^{-5}$)
B	C(36)-H(36)...ring 1	a/a	H(36)...H(14)	2.446	0.045(1)	0.406(1)
	C-H...phenyl interaction - H...H type contact					
D	C(3)-H(3B)...ring 3	c/a	H(3B)...C(35)-C(36)	2.975	0.045(1)	0.240(1)
	C-H...π(Ph) edge type hydrogen bond					
N	C(14)-H(14)...ring 1	a/a	H(14)...C(11)	2.841	0.044(8)	0.514(4)
	C-H...π(Ph) centroid type hydrogen bond					
G	C(3)...ring 1	s/a	C(3)...C(15)-C(16)	3.721	0.044(4)	0.449(3)
G	C(3)-H(60)...ring 1	s/a	H(60)...C(16)-H(16)	2.799	0.043(7)	0.441(6)
	C-H...phenyl interaction - intermediate type contact					
B	C(35)-H(35)...ring 2	a/a	H(35)...H(26)	2.391	0.043(1)	0.423(1)
	C-H...phenyl interaction - H...H type contact					
B	C(26)-H(26)...N(4)	a/c	H(26)...N(4)	2.912	0.042(1)	0.520(1)
	C-H...N interaction					
G	C(24)-H(24)...ring 1	a/a	H(24)...C(14)	2.863	0.042(1)	0.371(1)
	C-H...π(Ph) single atom type hydrogen bond					

Table 14. Summary of the bond critical points located in the four tetraphenylborate compounds studied (continued).

	Compound and Contact[a]	Type of Interaction[b]	Bond Path[c,d]	Contact Distance (Å)	Charge Density[e] $\rho_b(\mathbf{r})$ ($eÅ^{-3}$)	Laplacian $\nabla^2\rho_b(\mathbf{r})$ ($eÅ^{-5}$)
B	C(34)-H(34)...ring 4	a/a	H(34)...H(43)	2.508	0.040(1)	0.533(1)
	C-H...phenyl interaction - H...H type contact					
G	C(36)-H(36)...N(4)	a/s	H(36)...N(4)	2.963	0.035(1)	0.384(1)
	C-H...N type interaction					
D	C(2)-H(2A)...ring 1	c/a	H(2A)...C(13)	3.044	0.035(1)	0.322(1)
	C-H...π(Ph) single atom type hydrogen bond					
G	C(3)...ring 2	s/a	C(3)...C(26)	3.918	0.031(2)	0.284(2)

[a] N - ammonium tetraphenylborate B - biguanidinium tetraphenylborate
D - [DabcoH][$B(C_6H_5)_4$] G - guanidinium tetraphenylborate acetonitrile solvate

[b] a - anion c - cation s - solvent

[c] If the bond path is directed towards a bond it is shown; the underlined atom is where the bond path terminates.

[d] The distance quoted is the calculated direct separation between the two atoms joined by the bond path.

[e] The data are sorted in order of decreasing charge density at the bond critical point.

Table 15a. Summary of the bond critical points reported for N-H...acceptor hydrogen bonds in the literature.

Compound Interaction	Contact Distance H...O/N/F (Å)	Charge Density $\rho_b(\mathbf{r})$ ($eÅ^{-3}$)	Laplacian $\nabla^2\rho_b(\mathbf{r})$ ($eÅ^{-5}$)
L-alanine[35] (23K)			
N-H(1)...O(1)	1.827	0.19	3.5
N-H(2)...O(2)	1.832	0.20	3.6
N-H(3)...O(2)	1.722	0.27	4.7
Urea[39] (148K)			
N-H(1)...O	2.014	0.159	1.58
N-H(2)...O	2.071	0.142	1.53
1-Methyluracil[36] (123K)			
N(3)-H(3)...O(4)	1.77	0.23(3)	2.1(8)
L-Arginine Phosphate Monohydrate[40,a] (130K)			
N(4)-H(15)...O(3) anion	1.824	0.14	3.32
N(4)-H(14)...O(w) water	1.867	0.11	2.70
N(3)-H(12)...O(6) carboxyl	1.982	0.11	1.98
N(2)-H(11)...O(6) carboxyl	2.183	0.08	1.32
N(3)-H(13)...O(1) anion	2.506	no cp located	
Methylammonium Hydrogen Succinate Monohydrate[38] (110K)			
N(1)-H(4)...O(2)	1.858(3)	0.221(5)	1.86(10)
N(1)-H(5)...O(3)	1.725(5)	0.285(9)	2.46(20)
L-Dopa (2*S*)-3-(3',4'-Dihydroxyphenyl)alanine[37] (173K)			
N(1)-H(2N)...O(1)	1.96	0.145	2.65
N(1)-H(3N)...O(1)	1.94	0.192	2.91
N(1)-H(1N)...O(2)	1.83	0.243	3.64

Table 15a. Summary of the bond critical points reported for N-H...acceptor hydrogen bonds in the literature (continued).

Compound Interaction	Contact Distance H...O/N/F (Å)	Charge Density $\rho_b(\mathbf{r})$ ($e Å^{-3}$)	Laplacian $\nabla^2\rho_b(\mathbf{r})$ ($e Å^{-5}$)
4-Cyanoimidazolium-5-olate[42] (120K)			
N(1)-H(1)...O(8)	1.77(2)	0.23(2)	4.0(1)
N(3)-H(3)...O(8)	1.68(2)	0.33(2)	4.2(2)
D,L-aspartic Acid[43] (20K)			
N(1)-H(1)...O(2)	1.8075(2)	0.25(1)	3.6(2)
N(1)-H(2)...O(2)	1.8480(2)	0.26(1)	3.2(2)
N(1)-H(3)...O(3)	1.9794(2)	0.10(1)	2.2(2)
Methylammonium Hydrogen Maleate[21] (122K)			
N(1)-D(5)...O(1)	1.834(3)	0.24(1)	2.1(2)
N(1)-D(6)...O(1)	1.910(3)	0.19(1)	2.0(1)
N(1)-D(7)...O(3)	1.792(3)	0.29(1)	1.7(2)
1,8-Bis(dimethylammonium)naphthalene 1,2-dichlorohydrogenmaleate[22] (100K)			
N(2)-H(1nn)...N(1)	1.608(6)	0.53(2)	4.27(5)
E-Tetraethyl-1,4-diammoniumbut-2-ene·$2PF_6$[41] (100K)			
N(1)-H(1N)...F(3)	1.994(2)	0.09(2)	2.1(1)
N(1)-H(1N)...F(4)	2.050(2)	0.08(1)	1.7(1)

[a] X-ray results used. There are other N-H...O hydrogen bonds in the structure but they were not analyzed topologically.

Table 15b. Summary of the bond critical points reported for C-H...acceptor hydrogen bonds in the literature.

Compound Interaction	Contact Distance H...O/N (Å)	Charge Density $\rho_b(\mathbf{r})$ ($eÅ^{-3}$)	Laplacian $\nabla^2\rho_b(\mathbf{r})$ ($eÅ^{-5}$)
1-Methyluracil[36] (123K)			
C(6)-H(6)...O(2)	2.37	0.07(2)	1.1(1)
C(1)-H(11)...O(4)	2.34	0.06(8)	0.6(25)
syn-1,6:8,13-Biscarbonyl[14]annulene[44] (19K)			
C(2)-H(2)...O(1)	2.596(7)	0.043(2)	0.67(2)
C(7)-H(7)...O(1)	2.601(7)	0.041(2)	0.58(1)
C(9)-H(9)...O(1)	2.451(7)	0.060(3)	0.74(2)
C(10)-H(10)...O(1)	2.686(7)	0.040(2)	0.54(2)
C(11)-H(11)...O(1)	2.589(7)	0.050(2)	0.67(2)
C(3)-H(3)...O(2)	2.599(7)	0.043(2)	0.56(1)
C(9)-H(9)...O(2)	2.428(7)	0.062(3)	0.91(2)
Lithium bis(tetramethylammonium) hexanitrocobaltate(III)[45] (113K)			
C(1)-H(11)...O(1)	2.583(12)	0.022(1)	0.36(1)
C(1)-H(12)...O(2)	2.519(9)	0.050(4)	0.77(2)
C(2)-H(21)...O(1)	2.498(13)	0.035(2)	0.66(2)
C(2)-H(21)...O(2)	2.591(13)	0.034(2)	0.59(2)
Citrinin[46] ($C_{13}H_{14}O_5$, 19K)			
C(5)-H(5)...O(13)	2.329(8)	0.070(4)	0.97(3)
C(16)-H(6A)...O(18)	2.399(10)	0.070(5)	0.86(3)
C(16)-H(6C)...O(11)	2.421(9)	0.060(4)	0.86(2)
C(8)-H(8)...O(17)	2.423(9)	0.060(3)	0.90(2)
1,8-Bis(dimethylammonium)naphthalene 1,2-dichloromaleate[22] (100K)			
C(11)-H(111)...O(2a)	2.410(6)	0.073(2)	1.121(2)
C(14)-H(141)...O(2a)	2.535(6)	0.053(2)	0.815(1)
C(7)-H(7)...O(3a)	2.107(7)	0.109(6)	1.951(3)
C(14)-H(142)...O(4a)	2.353(5)	0.065(2)	1.095(1)
C(14)-H(143)...O(3a)	2.570(6)	0.038(1)	0.662(1)
C(11)-H(113)...O(4a)	2.718(6)	0.020(1)	0.402(1)

Table 15b. Summary of the bond critical points reported for C-H...acceptor hydrogen bonds in the literature (continued).

Compound Interaction	Contact Distance H...O/N (Å)	Charge Density $\rho_b(\mathbf{r})$ ($e\text{Å}^{-3}$)	Laplacian $\nabla^2\rho_b(\mathbf{r})$ ($e\text{Å}^{-5}$)
1,8-Bis(dimethylammonium)naphthalene 1,2-dichloromaleate[22] (100K) (continued)			
C(11)-H(113)...O(1a)	2.797(6)	0.028(1)	0.435(1)
D,L-aspartic Acid[43] (20K)			
C(1)-H(4)...O(3)	2.5033(2)	0.04(1)	0.8(2)
C(3)-H(6)...O(4)	2.5621(2)	0.04(1)	0.7(2)
4-Cyanoimidazolium-5-olate[42] (120K)			
C(2)-H(2)...N(7)	2.20(2)	0.11(1)	1.6(1)

3.6.3.2. N-H...N Hydrogen Bonds

As expected, and as just mentioned, the two N-H...N type hydrogen bonds were found to be the two strongest interactions of the experimental study. They were characterized by the shortest H(N)...X distances, the largest $\rho_b(\mathbf{r})$ values and the largest $\nabla^2\rho_b(\mathbf{r})$ values of any of the N-H...X interactions investigated. They thus appear as the first two entries in the interactions table. The $[N(1)\text{-}H(1B)]_{cation}\cdots[N(4)]_{solvent}$ hydrogen bond from the structure of $[C(NH_2)_3][B(C_6H_5)_4]\cdot CH_3CN$ would be expected to be stronger than the $[N(4)\text{-}H(4A)]_{cation}\cdots[N(1)]_{cation}$ hydrogen bond in $[N(C[NH_2]_2)_2][B(C_6H_5)_4]$ on the basis of charge and interaction distance, H(N)...N, it being 2.082Å in the former and 2.127Å in the latter. This is also reflected in the topological parameters calculated. The value of $\rho_b(\mathbf{r})$ is considerably larger in the first named interaction (0.200 eÅ^{-3}) than it is in the second (0.141 eÅ^{-3}). The value of $\nabla^2\rho_b(\mathbf{r})$ is also larger in the first interaction (1.637 eÅ^{-5}) than in the second (1.519 eÅ^{-5}), although in the case of the Laplacian of the electron density the relative difference between the two is less. Calculation of the mean values for the N-H...N hydrogen bonds is rather meaningless with only two interactions available. [Note, esd's will not be quoted on the topological parameters in the discussion section since, as mentioned in the experimental section, these values are not correctly calculated by the XD program when one of the interacting groups must be generated by symmetry.]

Only one N-H...N hydrogen bond has been reported in the literature with which the experimental data can be compared. Mallinson et al.[22] have carried out a topological analysis on the monoprotonated "proton sponge", 1,8-bis(dimethylamino)naphthalene, after determination of the charge

density of the 1,2-dichlorohydrogenmaleate salt using crystallographic data and multipole refinement. The asymmetric [N(2)-H(1nn)...N(1)]$^+$ bond was characterized by distances of 1.608(6)Å, N(1)...H(1nn), and 1.106(5)Å, H(1nn)-N(2), and an N(1)...H(1nn)-N(2) angle of 153.3(5)°. The covalent portion of the hydrogen bond, N(2)-H(1nn), was determined to have an electron density at the bond critical point, $\rho_b(\mathbf{r})$, of 1.91(3) eÅ^{-3} and a Laplacian value of -29.7(1) eÅ^{-5}. The hydrogen bond itself, H(1nn)...N(1), was found to have $\rho_b(\mathbf{r})$ equal to 0.53(2) eÅ^{-3} and $\nabla^2\rho_b(\mathbf{r})$ equal to +4.3(1) eÅ^{-5}. The N-H...N hydrogen bond in the protonated "proton sponge" cation is much shorter and stronger than either of the experimental examples, judging from the topological parameters. This is not unexpected. "Proton sponges" are a class of organic diamines with unusually high basicity. With acids, "proton sponges" form very stable ionic complexes containing strong, charge supported intramolecular [R_2N-H...NR_2]$^+$ hydrogen bonds. This is reflected in the very short H(N)...N distance [1.608(6)Å] and the large $\rho_b(\mathbf{r})$ and $\nabla^2\rho_b(\mathbf{r})$ values determined by Mallinson et al. for the N-H...N hydrogen bond in the protonated cation of 1,8-bis(dimethylamino)naphthalene. Compared to the longer H(N)...N distances in the experimental examples it is not surprising that it shows considerably larger values for $\rho_b(\mathbf{r})$ and $\nabla^2\rho_b(\mathbf{r})$. In fact, it is interesting that this very strong [N(2)-H(1nn)...N(1)]$^+$ hydrogen bond still behaves topologically as a closed shell interaction ($\rho_b(\mathbf{r}) > 0$ and $\nabla^2\rho_b(\mathbf{r}) > 0$). Several strong [O-H...O]$^-$ type hydrogen bonds have been described in the literature in which both OH components behave topologically like covalent or shared interactions ($\rho_b(\mathbf{r}) > 0$ and $\nabla^2\rho_b(\mathbf{r}) < 0$). The 1,2-dichlorohydrogenmaleate anion in Mallinson's protonated "proton sponge" salt contains such an

$[O\text{-}H...O]^-$ hydrogen bond. It is characterized by two very short O-H distances, 1.149(7)Å and 1.235(7)Å, likely explaining its observed topological difference from the $[N\text{-}H...N]^+$ hydrogen bond in the same structure. All of the known N-H...N hydrogen bonds, including those studied in this work and the much stronger example described by Mallinson et al., occur with longer distances [H...acceptor] and topological parameters characteristic of closed shell interactions.

A number of other N-H...X hydrogen bonds, where X is a "traditional" lone pair acceptor (either O or F), have been studied topologically from charge densities derived from crystallographic data. The pertinent data for the literature interactions are summarized in Table 15a. The 26 examples located, 1 N-H...N, 2 N-H...F and 23 N-H...O, are a reasonably complete survey of the literature to the end of 1998. Comparison of the experimental N-H...N hydrogen bonds with the literature N-H...X hydrogen bonds [X = N, F or O] must be made with some caution, as the values calculated for $\rho_b(\mathbf{r})$ and $\nabla^2\rho_b(\mathbf{r})$ depend on the nature of X. Still, in this set of data the differences arising from the change of acceptor do not appear to be that large. The literature data can be summarized as follows:

Interaction	d(H(N)...X) (in Å)	$\rho_b(\mathbf{r})$ (in eÅ^{-3})	$\nabla^2\rho_b(\mathbf{r})$ (in eÅ^{-5})
N-H...N (n = 1)	1.608	0.53	4.27
N-H...O (n = 23)	1.87 (0.12)	0.200 (0.066)	2.73 (0.93)
N-H...F (n = 2)	2.02 (0.03)	0.085 (0.005)	1.9 (0.2)
overall N-H...X (n = 26)	1.87 (0.13)	0.204 (0.095)	2.73 (0.96)

the σ values (in brackets) are the standard deviations of the population, $[(\Sigma x_i^2 - n(\Sigma x_i)^2) / n]^{\frac{1}{2}}$

In comparison, the mean values for the two experimental N-H...N bonds are, d(H(N)...N) = 2.105Å (σ = 0.023), $\rho_b(\mathbf{r})$ = 0.171 eÅ^{-3} (σ = 0.030) and $\nabla^2\rho_b(\mathbf{r})$ = 1.58 eÅ^{-5} (σ = 0.06). On average, the experimental N-H...N hydrogen bonds are longer than the literature bonds, with correspondingly smaller $\rho_b(\mathbf{r})$ and $\nabla^2\rho_b(\mathbf{r})$ values. The experimental examples are most similar to the two N-H...F hydrogen bonds reported and characterized by Mallinson et al.[41] in the structure of E-tetraethyl-1,4-diammoniumbut-2-ene·2PF_6. Somewhat surprisingly, the shortest and strongest N-H...X hydrogen bond in the literature group is the N-H...N hydrogen bond reported by Mallinson et al.[22] in the "proton sponge" complex; none of the N-H...O examples studied are any stronger.

The experimental N-H...N examples do fall within the limits of the literature N-H...X group, however. The literature H(N)...X distances were found to range from 1.608Å [H(N)...N] in the Mallinson "proton sponge" salt[22] to a maximum of 2.183Å [H(N)...O] in the structure of L-arginine phosphate monohydrate published by Espinosa et al.[40] The experimental H(N)...N distances fall within this range, although rather closer to the upper limit than the lower. The maximum literature $\rho_b(\mathbf{r})$ value of 0.53 eÅ^{-3} was also reported for the [N-H...N]$^+$ hydrogen bond in the protonated "proton sponge" cation[22] while the minimum $\rho_b(\mathbf{r})$ value of 0.08 eÅ^{-3} comes again from the investigation of N-H...O type hydrogen bonds in L-arginine phosphate monohydrate.[40] Both of the experimental N-H...N hydrogen bonds have $\rho_b(\mathbf{r})$ values that fall within the literature range, close to the middle of the group. Perhaps somewhat surprisingly, the maximum $\nabla^2\rho_b(\mathbf{r})$ literature value is reported for an N-H...O hydrogen bond in the structure of L-alanine (4.7 eÅ^{-5}) and not for the "proton sponge" cation. The minimum

$\nabla^2\rho_b(\mathbf{r})$ value of 1.32 eÅ^{-5} again comes from an N-H...O hydrogen bond in the structure of L-arginine phosphate monohydrate. The experimental $\nabla^2\rho_b(\mathbf{r})$ values also fall within the literature range but close to the lower limit of the data. Overall, the two experimental N-H...N hydrogen bonds do appear to behave topologically in a fashion comparable to the other N-H...X examples reported in the literature. The topological parameters calculated for the experimental N-H...N hydrogen bonds, $\rho_b(\mathbf{r})$ and $\nabla^2\rho_b(\mathbf{r})$, appear reasonable and consistent with the literature data available for other N-H...X type hydrogen bonds. Although the nature of the acceptor does appear to influence the topological parameters to a certain extent, the effect appears to be relatively small over the range of distances being considered. The fact that so few examples of N-H...N and N-H...F hydrogen bonds have been studied topologically probably influences the results more than any other factor.

3.6.3.3. N-H...π(Ph) Hydrogen Bonds

Of the 14 N-H...π(Ph) hydrogen bonds studied in this investigation, two were found to have unusual bond paths, beginning from the N atom rather than the H(N) atom of the donor group. These two interactions were characterized by abnormally long distances between the two terminal atoms of the bond path, being defined by N...C distances rather than the usual H(N)...C distances. For this reason they were omitted from further calculations and are not included in the discussion.

As a group, the experimental N-H...π(Ph) hydrogen bonds were found to behave quite consistently. They tend to fall together in the interaction table, below the stronger N-H...N hydrogen bonds and above

the weaker C-H...X interactions [X = N or π(Ph)], although there is some overlap with the latter group. Overall, the average N(H)...C distance characterizing the 12 pertinent hydrogen bonds was calculated to be 2.56Å (σ = 0.10), while the average $\rho_b(\mathbf{r})$ value was found to be 0.079 eÅ^{-3} (σ = 0.016) and the mean $\nabla^2\rho_b(\mathbf{r})$ value was 0.72 eÅ^{-5} (σ = 0.15). These results can be compared with the corresponding parameters determined for the two N-H...N hydrogen bonds from the same experimental structures. As expected, the N-H...π(Ph) bonds occur at substantially longer distances; the mean distance is 0.46Å longer in the N-H...π(Ph) hydrogen bonds compared to the N-H...N hydrogen bonds. In consequence, the N-H...π(Ph) hydrogen bonds are also characterized by topological parameters, $\rho_b(\mathbf{r})$ and $\nabla^2\rho_b(\mathbf{r})$, that are often an order of magnitude smaller than the N-H...N values. The mean $\rho_b(\mathbf{r})$ values actually differ by 0.09 eÅ^{-3} and the mean $\nabla^2\rho_b(\mathbf{r})$ values by 0.86 eÅ^{-5} both always being larger for the N-H...N hydrogen bonds.

Of the 12 N-H...π(Ph) interactions with reasonable bond paths found in the experimental group, seven are best described as centroid geometry bonds, two as edge type hydrogen bonds and two as single atom hydrogen bonds. The last interaction is actually defined as an intermediate type contact but it was included in the overall group discussed above. With such an uneven distribution of the interactions, the group statistics are not that meaningful but a few general observations are possible.

Interaction	d(H(N)...C) (in Å)	$\rho_b(\mathbf{r})$ (in eÅ^{-3})	$\nabla^2\rho_b(\mathbf{r})$ (in eÅ^{-5})
centroid (n = 7)	2.521 (0.098)	0.088 (0.013)	0.78 (0.11)
edge (n = 2)	2.668 (0.004)	0.057 (0.002)	0.54 (0.07)
single atom (n = 2)	2.556 (0.066)	0.084 (0.003)	0.78 (0.15)

overall (n = 12)	2.56 (0.10)	0.079 (0.016)	0.72 (0.15)

the σ values (in brackets) are the standard deviations of the population, $[(\Sigma x_i^2 - n(\Sigma x_i)^2) / n]^{1/2}$

The statistics of the centroid type and the single atom type hydrogen bonds are very similar, occurring at similar interaction distances with almost equal mean $\rho_b(\mathbf{r})$ and $\nabla^2\rho_b(\mathbf{r})$ values. For this set of experimental N-H...π(Ph) hydrogen bonds at least, the edge type hydrogen bonds are somewhat weaker, occurring at longer average distances and with correspondingly smaller mean $\rho_b(\mathbf{r})$ and $\nabla^2\rho_b(\mathbf{r})$ values. However, this may only have resulted because the edge and single atom groups are so small in this sample; it may not be generally true.

No experimentally derived charge density analyses of N-H...π(Ph) hydrogen bonds are available in the literature. For that matter, there are no examples of X-H...π(Ph) hydrogen bonds of any type (of experimental origin), that have been characterized by topological analysis, described in the literature. This leaves only theoretical studies of X-H...π(Ph) hydrogen bonds with which the current results might be compared. There is not an overwhelming amount of theoretical data available in the literature either. However, a number of groups have studied the F-H...π(Ph) hydrogen bond in the HF/C_6H_6 dimer, at varying levels of theory, over the past several years.[53,54,123,124] The theoretically optimized geometries of the HF/C_6H_6 dimer have been discussed previously. Comparison of the N-H...π(Ph) experimental topological data to the theoretical F-H...π(Ph) data seems reasonable, for although the X group in the X-H...π(Ph) hydrogen bond is expected to influence the interaction, the contact itself (H...π) is the same in both bonds. Thus, the overall effect on the topological parameters

might not be that great.

In 1990, Tang et al.[53] reported the results of a full geometry optimization of the HF/C_6H_6 dimer carried out at the Hartree-Fock level using a 6-31G* basis set. The dimer was found to have a symmetrical C_{6v} geometry with the HF molecule lying along the C_6 axis of benzene and the F-H vector pointing directly at the centroid of the benzene ring. The distance from H(F) to the plane of the benzene ring was calculated to be 2.418Å. A topological analysis of the calculated electron density located only a single unique bond path travelling from H(F) to one of the ring carbon atoms; six equivalent bond paths are, however, generated by symmetry, from H(F) to each of the six equivalent ring carbon atoms. The values of $\rho_b(\mathbf{r})$ and $\nabla^2\rho_b(\mathbf{r})$ at the bond critical point were calculated to be 0.00502 au and 0.02381 au, respectively. On conversion from atomic units these values become 0.0339 eÅ^{-3} [$\rho_b(\mathbf{r})$] and 0.574 eÅ^{-5} [$\nabla^2\rho_b(\mathbf{r})$].

More recently, Cubero et al.[124] have reported on the full geometry optimization of the HF/C_6H_6 dimer using a 6-31G(d,p) basis set at the Hartree-Fock level of theory. These authors obtained the same symmetric C_{6v} geometry for the dimer as had been determined by Tang et al.[53] The calculated values for the topological parameters were found to be 0.00481 au (0.0325 eÅ^{-3}) for $\rho_b(\mathbf{r})$ and 0.01981 au (0.477 eÅ^{-5}) for $\nabla^2\rho_b(\mathbf{r})$. The Cubero[124] results are very nearly the same as those reported by Tang et al.,[53] as would be expected since the calculations carried out were very similar.

In an even more recent publication, Cubero et al.[123] describe an optimization of the HF/C_6H_6 dimer carried out at a higher level of theory (HF/MP2) but with the same 6-31G(d,p) basis set. The minimum energy

structure obtained did not have the C_{6v} symmetry described in the previous papers. Instead, the F-H bond was found to point towards a single carbon atom of the ring, giving a dimer with overall C_s symmetry. To compare the topological properties of the electron density of the HF/C_6H_6 dimer with those of other structures they had optimized, the authors then constrained the geometry of the dimer to C_{6v} symmetry. This kept the geometry of the actual hydrogen bond consistent with those in the other structures in the paper and kept the geometry of the dimer equivalent to that obtained in the previous calculations. The values reported by Cubero et al.[123] are those calculated for the dimer with C_{6v} symmetry. At the bond critical point, the value of $\rho_b(\mathbf{r})$ was determined to be 0.0083 au (or 0.056 $e\text{Å}^{-3}$) and the value of $\nabla^2\rho_b(\mathbf{r})$ to be 0.0319 au (or 0.769 $e\text{Å}^{-5}$). Increasing the level of theory at which the calculation was carried out without changing the basis set or the basic geometry of the dimer increases the magnitudes of $\rho_b(\mathbf{r})$ and $\nabla^2\rho_b(\mathbf{r})$ at the bond critical point.

I. Rozas et al.[54] (1997) have also published the results of a theoretical calculation on the optimization of the HF/C_6H_6 dimer, using a 6-311++G** basis set at the HF/MP2 level of theory. Additional calculations, using density functional theory (DFT) at the B3LYP level, were also carried out using the large basis set. Both calculations located a minimum energy structure for the dimer in which the F-H bond was found to point towards the middle of a benzene C-C ring bond, quite different from the optimized geometries located in the previously described calculations. The bond path was shown to travel from H(F) to the (3,-1) bond critical point at the midpoint of the interacting C-C ring bond. Topological analyses were also carried at both of the described levels of theory for this

minimum energy geometry of the dimer. The HF/MP2 calculations gave an H(F) to C-C bond critical point (centroid) distance of 2.408Å, a $\rho_b(\mathbf{r})$ value of 0.0093 au (0.0628 eÅ^{-3}) and a $\nabla^2\rho_b(\mathbf{r})$ value of 0.031 au (0.747 eÅ^{-5}). In the DFT/B3LYP calculation the corresponding values determined were 2.627Å (d), 0.0123 au (0.0830 eÅ^{-3},ρ) and 0.036 au (0.868 eÅ^{-5}, ∇^2), respectively. The density functional theory calculation has increased the distance characterizing the interaction but also increased the electron density and the Laplacian of the electron density at the bond critical point. The topological parameters [$\rho_b(\mathbf{r})$ and $\nabla^2\rho_b(\mathbf{r})$] characterizing the hydrogen bond in the HF/C_6H_6 dimer are larger in the calculations of Rozas et al. than in those described by the other authors, but what part of the increase arises from the larger basis set / higher level of theory and what part comes from the different hydrogen bond geometry is not certain. The difference more likely comes from the former than the latter, if it is assumed that all of the minimized geometries are of similar energies.

Overall, increasing the level of theory and the complexity of the basis set used in the optimization of the HF/C_6H_6 dimer and the subsequent topological analysis of the electron density was observed to increase the magnitudes of the topological parameters calculated at the hydrogen bond critical point, regardless of the geometry of the dimer. The theoretically calculated $\rho_b(\mathbf{r})$ values were found to range from 0.0325 eÅ^{-3} [Cubero et al.,[124] HF/6-31G(d,p)] to 0.0830 eÅ^{-3} [Rozas et al.,[54] DFT/B3LYP/6-311++G**] a rather large spread of values. Similarly, the Laplacian values, $\nabla^2\rho_b(\mathbf{r})$, were shown to range from 0.477 eÅ^{-5} to 0.868 eÅ^{-5} in the same calculations. The mean experimental N-H...π(Ph) parameters, $\rho_b(\mathbf{r})$ = 0.0793 eÅ^{-3} and $\nabla^2\rho_b(\mathbf{r})$ = 0.717 eÅ^{-5}, can be compared with these theoretically calculated

F-H...π(Ph) values. Both mean experimental values fall within the calculated theoretical limits, at the high end of either range. Since the effect of X (X = N or F) on the X-H...π(Ph) hydrogen bonds is not known, it is impossible to determine which level of theory or basis set is optimal for these calculations. Still, a comparison of the N-H...π(Ph) and F-H...π(Ph) hydrogen bonds does appear to have been reasonable, with both having been shown to possess relatively similar topological properties. The theoretical calculations help to substantiate the experimental results obtained in this work.

Interestingly, Cubero et al.[124] have also reported theoretically calculated topological parameters for an N-H...π(Ph) interaction occurring in an NH_4^+/C_6H_6 dimer. The geometry of the complex was not optimized but rather was constrained to have one N-H bond lying on the C_6 axis of benzene and that N-H bond pointing directly towards the ring centroid. After calculation of the electron density at the Hartree-Fock level using a 6-31G(d,p) basis set, a topological analysis gave $\rho_b(\mathbf{r})$ equal to 0.00973 au (0.0657 eÅ^{-3}) and $\nabla^2\rho_b(\mathbf{r})$ equal to 0.03374 au (0.813 eÅ^{-5}) at the bond critical point. These calculated theoretical values are in good agreement with the respective, mean experimental parameters determined in this work for the N-H...π(Ph) hydrogen bonds. Since the experimental mean $\rho_b(\mathbf{r})$ value is larger than the theoretical value, while the experimental mean $\nabla^2\rho_b(\mathbf{r})$ value is smaller than the corresponding theoretical value, it is not clear if the level of theory / basis set should be increased in complexity to improve the calculated results. The results do show that under certain circumstances, such as those described here, theoretically and experimentally determined topological parameters may be directly comparable.

As a group, the experimental N-H...π(Ph) hydrogen bonds were found to have relatively consistent $\rho_b(\mathbf{r})$ and $\nabla^2\rho_b(\mathbf{r})$ topological parameters. These values appear to increase quite regularly with increasing $H(N)\ldots C_{ring}$ distance, the distance characterizing the bond path and thus the interaction. However, the question as to whether the N-H...π(Ph) hydrogen bonds as a group behave topologically like N-H...X, and other, hydrogen bonds formed with "traditional" lone pair acceptors remains to be answered. Can the N-H...π(Ph) hydrogen bond topological versus distance data be fit to a simple mathematical function that will also model the behaviour of other N-H..X hydrogen bonds with reasonable accuracy? Before these questions can be answered, a consideration of the hydrogen bonds involved must be undertaken to show that the chosen approach is logical.

It is well known that the nature of the atoms involved in any interaction (AB) affects the topological parameters at the (3,-1) bond critical point, whether that interaction is a covalent bond (A-B) or a hydrogen bond (A...B). The electron density in the region of the interaction is directly affected by the electronic configurations of the atoms involved. In the case of the hydrogen bond, D-H...X, the nature of the donor atom, D, also influences the electron density at the bond critical point, via its effect on the hydrogen atom. However, for the D-H...π(Ph) family of hydrogen bonds there are no other known examples of experimentally derived topological values for D = N or any other atom. The influence of the donor D-H group on the interaction cannot be determined from the limited data available. The only possible comparison for the experimental N-H...π(Ph) hydrogen bonds is with other N-H...X type hydrogen bonds, where X is a "traditional" lone pair acceptor.

Changing the acceptor in the N-H...X hydrogen bond directly changes the interaction being studied, H(N)...X, and would also be expected to directly affect the topological parameters [$\rho_b(\mathbf{r})$ and $\nabla^2\rho_b(\mathbf{r})$] at the bond critical point. Thus, comparing topological data generated for N-H...π(Ph) hydrogen bonds [H(N)...C] and other N-H...X hydrogen bonds [H(N)...X] is not on the surface the most reasonable thing to do. However, if it could be shown that a group of varied N-H...X type hydrogen bonds did behave similarly and predictably, as far as the relationships between $\rho_b(\mathbf{r})$ / $\nabla^2\rho_b(\mathbf{r})$ and the H...X (acceptor) distance were concerned, then making the comparison becomes more reasonable.

If the data can be fit to a single function for all N-H...X type hydrogen bonds, it also suggests that the nature of the acceptor is not of overwhelming importance in determining the topological parameters characterizing the interaction. Because hydrogen bonds are relatively weak (compared to covalent bonds for example) it may be that if the acceptors chosen are not too disparate they will show relatively uniform behaviour of the electron density at the bond critical point, particularly if the donor group is unaltered. The exact atom serving as the acceptor (H...X) in a closed shell or primarily electrostatic interaction would be expected to be less important than it would be for a covalent bond (H-X). In an electrostatic interaction the strength of the contact will be determined solely by the atomic charges and the distance over which it occurs. If the N-H...π(Ph) interactions truly are predominantly electrostatic, involving in most cases only a specific acceptor atom(s) of the phenyl ring at a specific distance, then they might reasonably be expected to behave similarly to other N-H...X hydrogen bonds. And, if the charges involved

in the N-H...π(Ph) interactions are similar to those developed in other N-H...X hydrogen bonds that occur at equivalent distances, then the entire group of interactions might show relatively uniform behaviour that could be fit to one simple mathematical function with reasonable accuracy. Uncertainty would be introduced into the fit by using a data set involving different hydrogen bond acceptors but if the uncertainty was not too large a good fit still might be obtained. This, in turn, would substantiate the initial proposition, that N-H...π(Ph) hydrogen bonds behave topologically like other N-H...X type hydrogen bonds formed with "traditional" lone pair acceptors.

In an attempt to show that all N-H...X hydrogen bonds behave similarly in topological terms, the N-H...π(Ph) experimental data were first plotted with the data from the two experimental N-H...N hydrogen bonds. Plots including only the combined experimental data are shown in Figure 125 (a) $\rho_b(\mathbf{r})$ versus d(H(N)...X) [X = N or C] and (b) $\nabla^2\rho_b(\mathbf{r})$ versus d(H(N)...X). Both graphs suggest that the data do belong to a single, relatively homogeneous set. Although the N-H...N interactions are characterized by shorter distances and larger topological parameters [$\rho_b(\mathbf{r})$ and $\nabla^2\rho_b(\mathbf{r})$], so that they are physically separated on the graph from the N-H...π(Ph) data points, it appears that all of the data should fit reasonably well to a single continuous function. There is enough scatter in the experimental data points that it is somewhat difficult to discern visually what the appropriate function might be. However, the relationships between the topological parameters [particularly $\rho_b(\mathbf{r})$] and the H...acceptor distance do appear to be nonlinear. The value of $\rho_b(\mathbf{r})$ must be positive at all the (3,-1) bond critical points, regardless of the

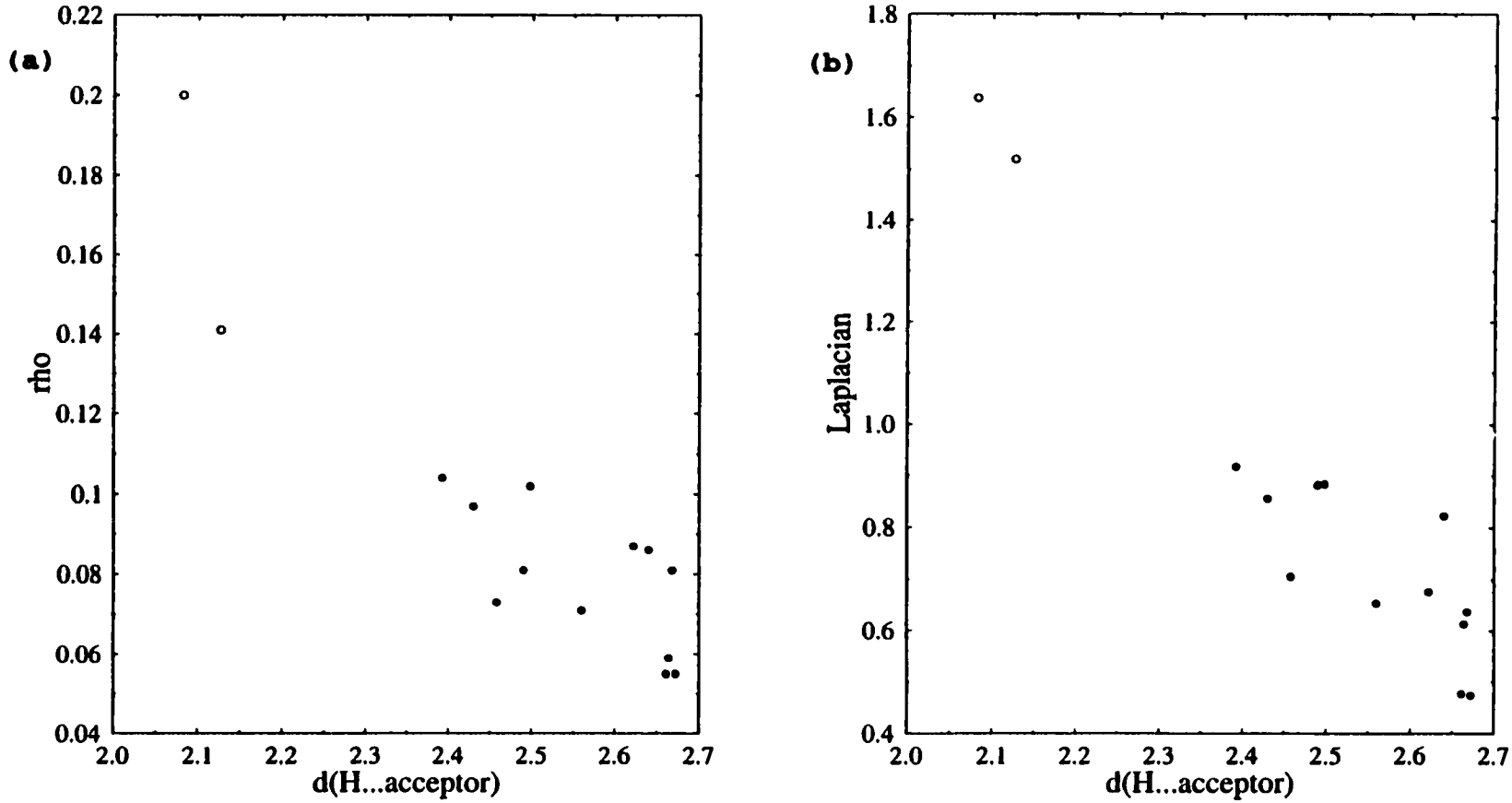

Figure 125. Topological data for the experimental N-H...X [X = N or π(Ph)] hydrogen bonds. Plots of (a) $\rho_b(\mathbf{r})$ and (b) $\nabla^2\rho_b(\mathbf{r})$ versus d(H...A) are shown for the data only, with no fit applied. The N-H...N hydrogen bonds are represented by open circles and the N-H...π(Ph) hydrogen bonds by filled circles.

interaction distance. It is also readily apparent that as the distance at which the interaction occurs increases, the value of $\rho_b(\mathbf{r})$ decreases asymptotically towards zero but always remains positive. Thus it seemed most reasonable to try and fit the experimental $\rho_b(\mathbf{r})$ versus d(H(N)...X) data to simple functions that would satisfy such asymptotic behaviour at longer distances. Three different functions were chosen to model the combined N-H...X experimental data. First, a simple linear function [y = a*x + b, $\rho_b(\mathbf{r})$ = a*d + b] was used to demonstrate that the data do not conform well to a linear model. Then the data were fitted to simple power [y = a*(x)^b, $\rho_b(\mathbf{r})$ = a*d^(b)] and exponential [y = a*exp(b*x), $\rho_b(\mathbf{r})$ = a*exp(b*d)] functions to see which would give better results. For the $\rho_b(\mathbf{r})$ [in eÅ^{-3}] versus d(H(N)...X) [in Å] plots the optimized equations and their fit statistics are summarized below.

linear	$\rho_b(\mathbf{r})$ = 0.541 - 0.180*d	r^2 = 0.807	σ = 0.0176
power	$\rho_b(\mathbf{r})$ = 3.411*d^(-4.019)	r^2 = 0.857	σ = 0.0152
exponential	$\rho_b(\mathbf{r})$ = 6.230*exp(-1.710*d)	r^2 = 0.850	σ = 0.0155

where $\sigma = [\Sigma(\text{residual})^2 / (n-2)]^{\frac{1}{2}}$

The nonlinear models obviously fit the data slightly better than the linear model. A graph of the experimental $\rho_b(\mathbf{r})$ versus d(H(N)...X) data, with the exponential curve included, is shown in Figure 126(a). Both the exponential and power fits model the data reasonably and equally well. The relatively low value for the coefficient of determination (r^2) in the power and exponential cases likely arises primarily because the experimental data set contains both N-H...N and N-H...π(Ph) hydrogen bonds. This extends the range of H...acceptor distances far enough for the

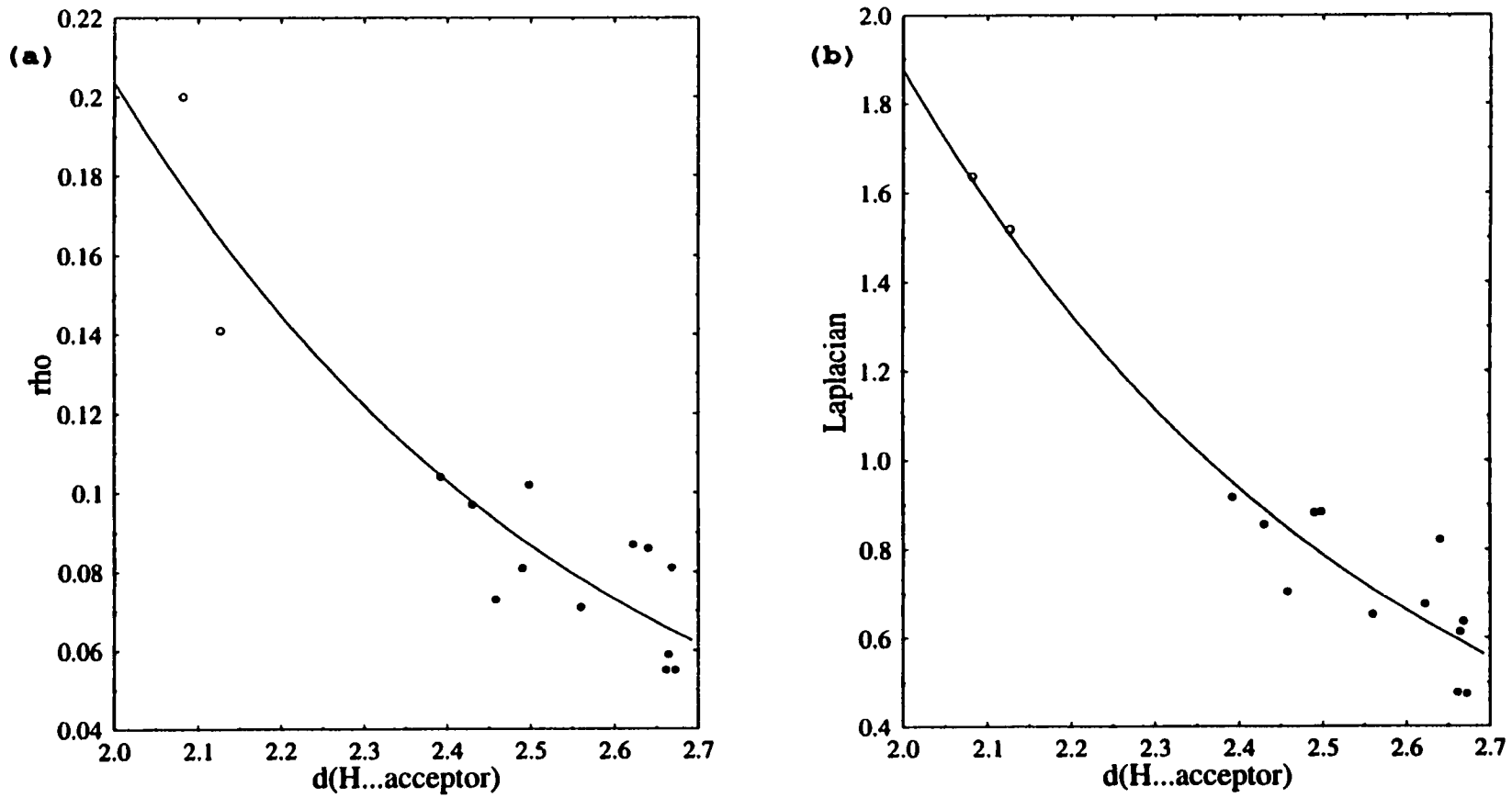

Figure 126. Topological data for the experimental N-H...X [X = N or π(Ph)] hydrogen bonds. Plots of (a) $\rho_b(\mathbf{r})$ and (b) $\nabla^2\rho_b(\mathbf{r})$ versus d(H...A) are shown with a fitted exponential curve included. The N-H...N hydrogen bonds are represented by open circles and the N-H...π(Ph) hydrogen bonds by filled circles.

nonlinear distribution of the $\rho_b(\mathbf{r})$ values to become apparent but changing the hydrogen bond acceptor also undoubtedly has an effect on an interaction's topological parameters, including $\rho_b(\mathbf{r})$. This introduces some uncertainty into the fit when a single simple model function is applied to all the data. The fact that the simple power and exponential functions applied to the experimental data fit as well as they do, suggests that the exact nature of the acceptor is of limited influence in these N-H...X hydrogen bonds. The value of $\rho_b(\mathbf{r})$ is determined more by the charges developed and the distance at which the interaction occurs than by the acceptor itself. All of the data appear to belong to a single broad group. The N-H...π(Ph) hydrogen bonds behave in a fashion consistent with the more traditional N-H...N hydrogen bonds, as far as the topological parameters at the bond critical point defining the interaction are concerned (at least in this limited experimental sample).

Similar simple model functions were also fitted to the experimental $\nabla^2\rho_b(\mathbf{r})$ [in $e\text{Å}^{-5}$] versus d(H(N)...X) [in Å] data. The results are summarized below.

linear	$\nabla^2\rho_b(\mathbf{r}) = 5.082 - 1.698*d$	$r^2 = 0.899$	$\sigma = 0.114$
power	$\nabla^2\rho_b(\mathbf{r}) = 32.236*d\text{^}(-4.060)$	$r^2 = 0.927$	$\sigma = 0.0967$
exponential	$\nabla^2\rho_b(\mathbf{r}) = 60.189*\exp(-1.734*d)$	$r^2 = 0.926$	$\sigma = 0.0974$

As observed for the $\rho_b(\mathbf{r})$ versus d(H(N)...X) data, the $\nabla^2\rho_b(\mathbf{r})$ versus d(H(N)...X) data fit both the power and exponential functions equally well. In the case of the experimental Laplacian versus distance plots, the fits are actually somewhat better than had been found for the corresponding $\rho_b(\mathbf{r})$ versus distance models. In fact, the $\nabla^2\rho_b(\mathbf{r})$ versus d(H(N)...X)

data fit even the linear model reasonably well; the linear model is almost as good as the nonlinear functions, to which it is an approximation over the narrow range of H(N)...X distances covered by the experimental data set. A more complete set of data, covering a larger range of distances, would be expected to be nonlinear. A plot of the experimental $\nabla^2\rho_b(\mathbf{r})$ versus d(H(N)...X) data, with the model exponential equation included, is shown in Figure 126(b).

There is data available in the literature with which the present results (the observed nonlinear relationship between topological parameters and interaction distance) can be compared. A summary of the previously published literature has been included in the introduction. The relationship between the topological parameters $\rho_b(\mathbf{r})$ and/or $\nabla^2\rho_b(\mathbf{r})$ and interaction distance has been explored by both Boyd and Choi[49,50] (ab initio calculations) and by Mallinson et al.[22] (experimental, crystallographically derived data).

In two publications from the mid 1980's, Boyd and Choi[49,50] report the results of ab initio calculations for a series of hydrogen bonded complexes of the type RCN...H-X (X = F[49] or Cl[50]). The geometry of each dimer was optimized at the Hartree-Fock level using a 6-31G** basis set, before calculation of the electron density and the topological parameters at the bond critical point. The calculated $\rho_b(\mathbf{r})$ values (in atomic units, au) versus the hydrogen bond lengths (d = $r_{(NH)}$, in Å) were fitted to linear equations with excellent results:

HF	$\rho_b(\mathbf{r}) = 0.1309 - 0.02944*d$	$r^2 = 0.991$	$\sigma = 0.02$
HCl	$\rho_b(\mathbf{r}) = 0.0955 - 0.03634*d$	$r^2 = 0.988$	$\sigma = 0.0006$

These appear to be the first published attempts to correlate the hydrogen bond length with a topological parameter [$\rho_b(\mathbf{r})$] and the results are somewhat different from those obtained in this work. Not surprisingly, the theoretical data show much less scatter than the experimental results because they are calculated values, free from instrumental and other associated experimental errors. Also, the sets of hydrogen bonds studied theoretically are much more internally consistent being calculated for isolated molecules at 0 K. In the theoretical calculations all of the hydrogen bonds in a set are of the N...H-X type (X = F or Cl). Still, this difference on its own is not enough to explain why the results of Boyd and Choi suggest a linear relationship between $\rho_b(\mathbf{r})$ and distance, while the current results suggest a nonlinear relationship. A possible reason will be discussed subsequently as shown by the work of Alkorta et al.[126,127]

More recently (1997), Mallinson et al.[22] have discussed the relationship between $\rho_b(\mathbf{r})$ and the H(C)...O distance for a series of seven, weak C-H...O type interactions. The experimental topological data were generated after calculation of the charge density for the 1,2-dichloro-hydrogenmaleate salt of the protonated "proton sponge", 1,8-bis(dimethyl-amino)naphthalene, from crystallographic measurements. The very weak interactions again fit a linear function best, for both $\rho_b(\mathbf{r})$ [in $e\text{Å}^{-3}$] versus the H(C)...O distance [d, in Å] and for $\nabla^2\rho_b(\mathbf{r})$ [in $e\text{Å}^{-5}$] versus the H(C)...O distance [d, in Å].

$$\rho_b(\mathbf{r}) = 0.37(4) - 0.13(2)*d \quad r = -0.97$$

$$\nabla^2\rho_b(\mathbf{r}) = 6.5(6) - 2.2(2)*d \quad r = -0.97$$

However, the authors do write, "In general such relationships

between $\rho_b(\mathbf{r})$ and structural parameters characterizing a weak interaction are probably not linear ones. This seems to be the case, for example, when all types of hydrogen bonds (the strongest [N-H...N]$^+$ and [O-H...O]$^-$ through the weakest C-H...O type) in the structure are considered on the same scale." This observation appears to be borne out by the present results.

In the past few years new topological data characterizing hydrogen bonds have been generated from both theoretical calculations[126,127] and from experimentally derived[125] charge densities, expanding knowledge in the field considerably. In a series of papers based on theoretical calculations, Alkorta et al.[126,127] have demonstrated that if a large set of related bonds/interactions, covering a wide range of distances, is examined, then a logarithmic relationship will be found to exist between $\rho_b(\mathbf{r})$ and the bond length (whether A-B or A...B for the AB pair). For any pair of atoms (AB), the logarithmic relationship (equivalent to the simple exponential function used in this work) is capable of simultaneously modelling covalent bonds (A-B), hydrogen bonds (A...B) and intermediate situations. The theoretical results discussed by Alkorta et al. cover a wide range of bond lengths/interaction distances, and so are much more universal for any particular AB pair, than any of the previous studies carried out.

For example, Alkorta et al.[126] have examined a variety of covalent C-H bonds in simple hydrocarbon molecules and combined the theoretically calculated topological data with the corresponding data from a set of hydrogen bonded complexes of the type X-H...CR_n. Because there was a gap between the covalent C-H data (shorter distances) and the hydrogen bond

C...H data (longer distances), the authors included topological data calculated for different conformations along the HF/:CH_2 (carbene) reaction coordinate. The dimer's H...C distance was varied from 1.0 to 3.0Å (11 points) and the remaining geometrical parameters were optimized before calculation of the charge density and the topological parameters. All of this theoretical data was collected and plotted as a logarithmic function of $r_{(CH)}$ [in Å] versus $\rho_b(\mathbf{r})$ [in au] with very good results over the entire range.

$$r_{(CH)} = 0.52(2) - 0.425(3)*\ln\rho_b(\mathbf{r}) \quad n = 33 \quad r^2 = 0.996$$

If this equation is transformed into an exponential function with units of Å [$r_{(CH)}$] and eÅ^{-3} [$\rho_b(\mathbf{r})$] it becomes comparable (in form at least) to the equation derived in this investigation for the N-H...X [X = N or π(Ph)] experimental data.

$$\rho_b(\mathbf{r}) = 22.9*\exp(-2.353*r_{(CH)})$$

Alkorta et al.[126] conclude from their calculations that for a wide range of CH distances (1.0 to 3.0Å) covering a wide range of bond/interaction types, the relationship of distance to the electron density at the bond critical point is not linear but logarithmic. This helps to substantiate the present experimental results although the "universal" CH equation has quite different coefficients from the experimental exponential fit (a = 6.23 and b = -1.71). This is not unexpected. The experimental data for the N-H...π(Ph) hydrogen bonds all involve N-H...C type contacts and therefore describe H...C distances that could fall onto the Alkorta "universal" curve. However, the true nature of the acceptor in the experimental N-H...π(Ph) interactions may not always be so straightforward. And, more importantly, the experimental data set also includes two N-H...N hydrogen

bonds, which are essential in determining the overall fit of the data to the exponential function, since they occur at the shortest distances and with the largest $\rho_b(\mathbf{r})$ values. These NH points likely move the experimental exponential fit away from the theoretical CH curve calculated by Alkorta et al. for a uniform set of CH bonds. Finally, it is also true that the experimental N-H...X [X = N or π(Ph)] hydrogen bonds cover only a relatively narrow range of distances (since no covalent bonds are involved) and therefore only a small portion of the Alkorta "universal" curve. This would also influence the coefficients obtained when fitting the experimental exponential curve, giving values different to those of the "universal" curve.

Alkorta et al.[126] have addressed this last issue in their 1998 publication. After examination of the "universal" CH curve [$\rho_b(\mathbf{r})$ versus distance] the authors observed that a linear relationship might be obtained if only a narrow range of distances was considered. This narrow range would have to fall entirely within either the covalent bond region (short distances) or the hydrogen bond region (longer distances) of the "universal" curve, regions where the exponential function exhibits quasilinear behaviour; in the intermediate region the curve is visibly nonlinear. The slopes of the two linear regions are quite different, being much larger for the covalent region than for the intermolecular/hydrogen bonding region. The authors even relate their observations to the work of Boyd and Choi,[49,50] who (as previously described) had found a linear relationship between $\rho_b(\mathbf{r})$ and distance [$r_{(NH)}$] for a series of RCN...H-X (X = F[49] or Cl[50]) type hydrogen bonded complexes. Alkorta et al.[126] show that the results of Boyd and Choi belong to a quasilinear portion of the

much larger NH exponential curve, obtained because only a specific small portion (narrow range of distances) of the overall curve was examined. If Boyd and Choi had included related covalent N-H bonds (or even a wider range of N...H hydrogen bonds) in their calculations, they would have obtained a set of NH data covering the wider range of distances needed to define a more universal curve. In such a case they would have recognized the nonlinear relationship between $\rho_b(\mathbf{r})$ and distance which exists over the entire range of NH interactions (at least theoretically).

It is interesting to note that the inclusion of the two N-H...N hydrogen bonds in the experimental N-H...X [X = N or π(Ph)] set probably was the factor that allowed the nonlinear relationship between $\rho_b(\mathbf{r})$ and distance to be recognized. Although the H...N components of these two bonds were included in the experimental data set for a rather different reason, and although they do not fit exactly on the same exponential curve as the N-H...π(Ph) data (H...C), their presence extended the range of distances enough to allow the nonlinear relationship of $\rho_b(\mathbf{r})$ and distance to be identified. If only the N-H...π(Ph) topological data had been plotted, a linear fit might have best described the data over the limited range of H...C distances covered. This is likely also the same problem encountered by Mallinson et al.[22] who found a linear relationship between $\rho_b(\mathbf{r})$ and distance for a set of weak (experimental) C-H...O hydrogen bonds. The authors observed that they might have obtained a nonlinear distribution if a wider range of interactions had been included in the data set and this is likely true. Again, Mallinson et al. have probably isolated a small "quasilinear" region of a larger exponential curve by studying only a narrow range of H...O distances, limited by the C-H...O contacts

they selected. In fact, their data should fit reasonably well onto the intermolecular/hydrogen bond region of the Alkorta and Elguero[127] O-H/O...H curve described below.

In a second, related paper, Alkorta and Elguero[127] have performed a similar series of calculations on an extended set of O-H covalent bonds and O...H(X) type hydrogen bonds. The results are of particular interest because, in addition to the theoretically calculated data, the authors have included experimental data derived from crystallographic measurements. The combined data set, involving 18 experimental points and 25 theoretical points, gives the following logarithmic fit for the $\rho_b(\mathbf{r})$ [in $e\text{Å}^{-3}$] versus distance [d,in Å] plot:

$$\ln \rho_b(\mathbf{r}) = 1.18(9) - 2.457(50)*d \qquad r^2 = 0.98$$

Transformed into an exponential function the equation becomes

$$\rho_b(\mathbf{r}) = 3.25*\exp(-2.457*d)$$

The "universal" OH curve does not match the experimental fit for the N-H...X [X = N or π(Ph)] hydrogen bonds that well (a = 6.23, b = -1.71), when the two are compared in the same exponential form. This is not unexpected since the bonds being considered involve different groups and the range of distances covered are quite different. The "universal" exponential OH curve derived by Alkorta and Elguero[127] from a combination of theoretical and experimental data is important because it predicts the expected behaviour of $\rho_b(\mathbf{r})$ at intermediate distances (between covalent bonds and hydrogen bonds). Unlike other types of hydrogen bonds, in the OH group a number of strong experimental $[O\text{-}H...O]^-$ examples have been characterized in the literature. Topological analyses have shown that both OH components in such strong hydrogen bonds are covalent interactions

($\rho_b(\mathbf{r}) > 0$, $\nabla^2\rho_b(\mathbf{r}) < 0$). Alkorta et al.[127] showed that the data from these unusual, experimental examples of hydrogen bonds still fit on their overall, exponential OH curve, helping to substantiate its universality.

Alkorta and Elguero[127] have successfully shown that theoretically calculated and experimentally derived topological data can be combined to generate a homogeneous data set. From this data an overall "universal" curve can be derived for the relationship between $\rho_b(\mathbf{r})$ and distance for any particular set of atoms AB. Because of this, experimental data can now be used to verify related theoretical results or vice versa. Suitably calculated data can be used to fill holes/gaps if for some reason experimental data is not available. The work of Alkorta et al.[126,127] is also important because it connects covalent bonds (large $\rho_b(\mathbf{r})$ and short distances) and intermolecular interactions/hydrogen bonds (small $\rho_b(\mathbf{r})$ and long distances) of a given type by a single, simple function. It allows predictions to be made as to what will occur at intermediate distances, at the interface between shared and closed shell interactions. It also models the behaviour of $\rho_b(\mathbf{r})$ at very short and very long distances, conditions for which experimental data may not be attainable. However, a cautionary note must be added. Recent theoretical calculations carried out by Knop et al.[128] on a series of N-H...N interactions have suggested that their covalent (N-H) and hydrogen bond (H...N) components may be better modelled by two different [nonlinear] functions (rather than one uniform function) for the relationship between $\rho_b(\mathbf{r})$ and distance.

A recent publication (1999) by Espinosa et al.[125] also examines the relationship between topological and geometrical parameters in hydrogen bonds of the type X-H...O [X = N, C or O] in some detail. This study is

based on experimental data, generated from crystallographic measurements, from a wide range of complexes on which charge density studies had been performed. The results will be discussed more thoroughly in the following section, however, the authors did obtain exponential relationships between the topological parameters [$\rho_b(\mathbf{r})$ and $\nabla^2\rho_b(\mathbf{r})$] and the hydrogen bond O...H distance for the data they examined. In conjunction with the work of Alkorta et al.[126,127] it appears that the $\rho_b(\mathbf{r})$ versus distance relationship is best fit by an exponential function [y = a*exp(b*x)], as was also found to be reasonable for the experimental data set.

For completely homogeneous sets of data, closely related bonds and interactions such as the CH and OH groups of Alkorta et al.[126,127] for example, the fit should be very good. On this basis the experimental results are quite acceptable. The experimental N-H...X [X = N or π(Ph)] data set does fit reasonably well to a single, exponential function. The majority of the uncertainty in the fit likely arises from experimental error and because the data really do involve two different groups [N-H...N and N-H...π(Ph)] with different hydrogen bond acceptors. However, one function does model the experimental data quite well, showing that the exact nature of the acceptor is not that important in these weak, primarily electrostatic interactions (where charge and distance are more likely to determine the strength of the contact). And, the inclusion of the N-H...N data with the experimental N-H...π(Ph) data allowed the exponential relationships between $\rho_b(\mathbf{r})/\nabla^2\rho_b(\mathbf{r})$ and distance to be recognized and explored.

As already mentioned, there are no other examples of X-H...π(Ph) hydrogen bonds that have been subject to topological analysis (charge

densities derived from crystallographic data) available in the literature. There are, however, a wide variety of N-H...X [X = N, F or O] hydrogen bonds that have been described and characterized. Since the experimental data, involving both N-H...N and N-H...π(Ph) hydrogen bonds, had been shown to behave as a reasonably consistent set, modelled by a single exponential function, it was decided to compare the experimental results to the available literature data [$\rho_b(\mathbf{r})/\nabla^2\rho_b(\mathbf{r})$ versus d(H(N)...X)]. This would serve two purposes. First, it would shed more light on the role of the acceptor in determining the topological parameters of an interaction at its bond critical point. In the literature data set, N-H...X hydrogen bonds with the acceptors X = N, F and O are included. If the (literature and experimental) data can be fit to a single exponential function with reasonable results it demonstrates that the exact nature of the acceptor is not that important in determining the topological parameters of these relatively weak, primarily electrostatic interactions. Secondly, it would show even more conclusively that N-H...π(Ph) hydrogen bonds behave, at least topologically, like other N-H...X hydrogen bonds formed with more "traditional" lone pair acceptors. Note that in the previous section of the discussion the term "experimental" was used to refer to the results of the present investigation while the term "theoretical" was used to refer to parameters calculated using ab initio molecular orbital methods. In this section, the term "experimental" still refers to the current results, which have been derived from x-ray crystallographic data. However, the "literature" data also come from charge density studies that have been carried out on a variety of compounds using crystallographic methods. In this sense, the literature data are also experimental (rather

than theoretical) values.

The topological and geometric parameters for the 26 N-H...X [X = N(1), F(2) and O(23)] hydrogen bonds located in the literature survey are summarized in Table 15(a). The literature data set was plotted and studied alone first, to determine its individual properties. Graphs of the literature data, with the optimized exponential curve included, are shown in Figure 127 (a) $\rho_b(\mathbf{r})$ versus d(H(N)...X) and (b) $\nabla^2\rho_b(\mathbf{r})$ versus d(H(N)...X), where d(H(N)...X) or d represents the H...acceptor distance. Fitting a simple exponential function to the $\rho_b(\mathbf{r})$ versus d(H(N)...X) data from the literature group gave the following results.

$$\rho_b(\mathbf{r}) = 133.1*\exp(-3.517*d) \quad r^2 = 0.824 \quad \sigma = 0.0416$$

The coefficient of determination ($r^2 = 0.824$) indicates that the literature data fit an exponential function almost equally well as the experimental data had ($r^2 = 0.850$). However, the parameters a and b of the exponential fit equations [$\rho = a*\exp(b*d)$] are quite different in the two cases; in the experimental fit a = 6.23 and b = -1.71. The profile of the fit equation is quite different for the two sets of data. This is not surprising since the range of distances covered by the two sets of data is also quite different. The experimental data come mainly from the generally weaker N-H...π(Ph) hydrogen bonds and thus occur at longer distances (roughly 2.0 to 2.7Å) than the literature N-H...X [X = N, F or O] hydrogen bonds (roughly 1.6 to 2.2Å). The corresponding topological parameters [$\rho_b(\mathbf{r})$ and $\nabla^2\rho_b(\mathbf{r})$] are consistently larger in the literature data set as well, as expected. Different coefficients are obtained for the exponential fit equation when different (relatively narrow) regions of the overall $\rho_b(\mathbf{r})$ versus distance curve are explored.

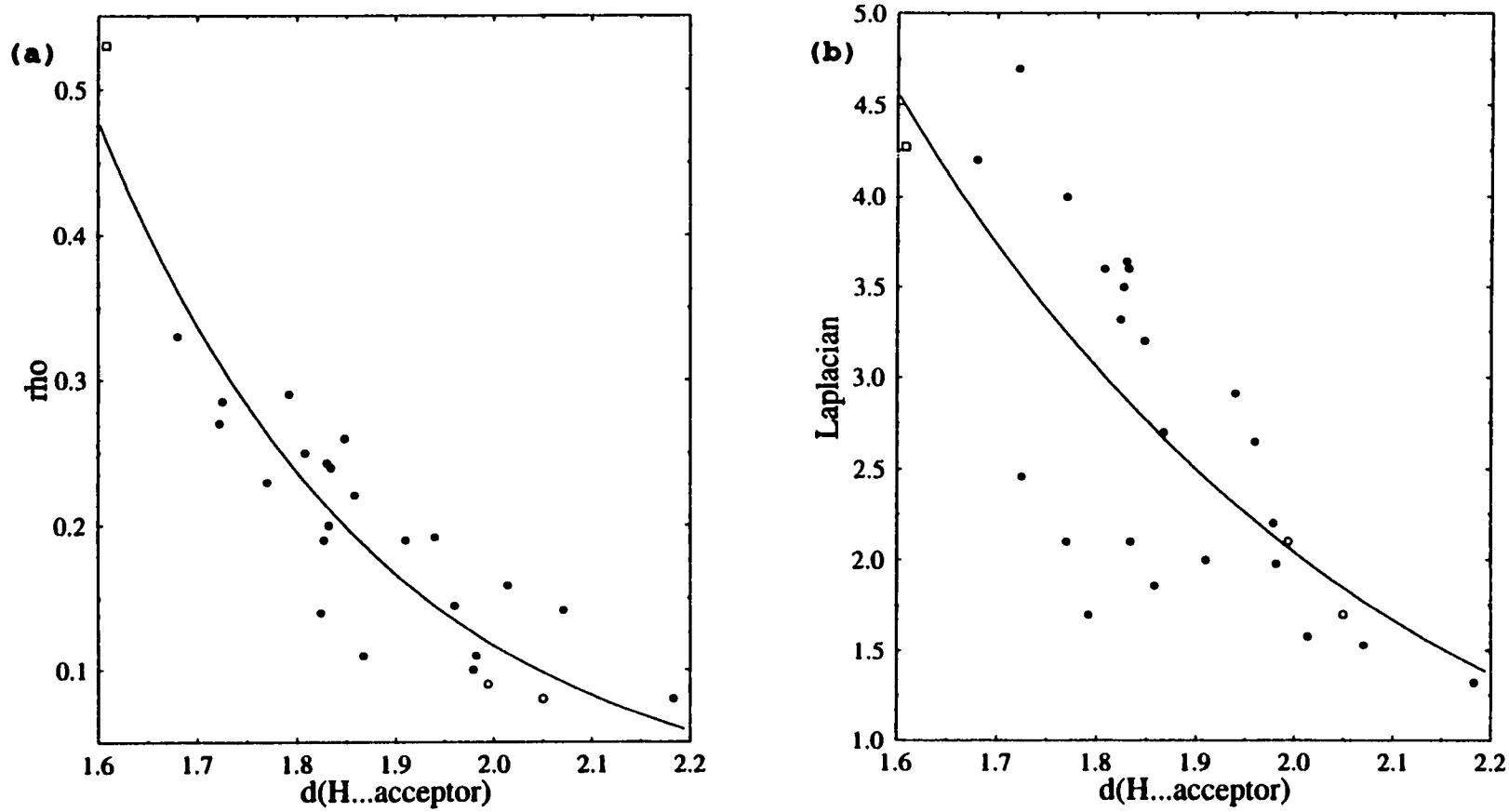

Figure 127. Topological data for a set of literature N-H...X [X = N, O or F] hydrogen bonds. Plots of (a) $\rho_b(\mathbf{r})$ and (b) $\nabla^2\rho_b(\mathbf{r})$ versus d(H...A) are shown with a fitted exponential curve included. The N-H...N hydrogen bond is represented by an open square, the N-H...O hydrogen bonds by filled circles and the N-H...F hydrogen bonds by open circles.

The literature data fit a single exponential function, modelling $\rho_b(\mathbf{r})$ versus distance, reasonably well, almost equally well as the experimental data. The literature data set would be expected to incorporate more "experimental" error since it comes from a number of different sources, with data collected and treated in a variety of different ways, while in this work all the topological data were generated in a consistent fashion. Some of the uncertainty in the literature fit also undoubtedly arises because the set of N-H...X [X = N, F or O] hydrogen bonds, with a number of different acceptors, has been modelled with a single function. However, the literature data do conform to one function well enough to suggest that the exact nature of the acceptor is of relatively minor importance in these interactions. It seems reasonable to consider all the N-H...X [X = N, F or O] hydrogen bonds of the literature as a single group, which will behave in a consistent and predictable (exponential) fashion in regards to the relationship between $\rho_b(\mathbf{r})$ and the distance characterizing the interaction. The literature results are completely analogous to those obtained for the experimental N-H...X [X = N or π(Ph)] hydrogen bonds.

The fit of the literature N-H...X [X = N, F or O] hydrogen bond data to an exponential function for the $\nabla^2\rho_b(\mathbf{r})$ versus distance [d(H(N)...X)] plot is somewhat less satisfactory.

$$\nabla^2\rho_b(\mathbf{r}) = 114.1*\exp(-2.011*d) \quad r^2 = 0.539 \quad \sigma = 0.458$$

In fact, the data do not conform well to linear (r^2 = 0.539), power (r^2 = 0.534) or exponential (r^2 = 0.539) models. The plot of $\nabla^2\rho_b(\mathbf{r})$ versus d(H(N)...X), with the optimized exponential equation included, is shown in Figure 127(b). It is clear from the graph shown that there is

substantial scatter in the literature data but it does not appear to arise (in any important way) from the fact that more than one type of acceptor atom has been included in the bonds that make up the literature set; it is the N-H...O data alone that appears to show the majority of the scatter.

Other authors have commented on the fact that experimental (crystallographically derived) $\nabla^2\rho_b(\mathbf{r})$ values are particularly sensitive to the conditions under which the data sets are collected and refined to generate the charge density, much more so than $\rho_b(\mathbf{r})$.[46,125] The results obtained here substantiate this observation. The $\nabla^2\rho_b(\mathbf{r})$ values in the experimental data set, from the present investigation, were all calculated from charge densities derived using a uniform method, from x-ray data collected under very similar conditions. The experimental data for the $\nabla^2\rho_b(\mathbf{r})$ versus distance plot behave as a homogeneous set (for all N-H...X) and conform well to a single exponential function (r^2 = 0.926). In contrast, the literature data come from a group of 11 different structures, in which the charge densities have been calculated using a variety of different strategies and software programs, from crystallographic measurements (x-ray and/or neutron) made under a wide variety of different conditions. The values of the Laplacian of the electron density [$\nabla^2\rho_b(\mathbf{r})$] are very sensitive to these differences (while $\rho_b(\mathbf{r})$ is not) and this is reflected in the poor fit of the literature data to the exponential function (r^2 = 0.539) and to other simple functions.

The plots of $\rho_b(\mathbf{r})$ versus the H...acceptor distance [d(H(N)...X)] for both the experimental [X = N or π(Ph)] and literature [X = N, F or O] data sets of N-H...X hydrogen bonds conform quite well to simple exponential models, even though more than one type of acceptor is involved in each

group. It thus seemed reasonable to try and combine the two sets of data, to see if all the available N-H...X hydrogen bonds could be shown to belong to a single broader and more comprehensive group. And, to see if the complete set of interactions would still show a consistent and predictable, exponential relationship between $\rho_b(\mathbf{r})$ and distance.

A plot of the combined $\rho_b(\mathbf{r})$ versus distance data, with the optimized exponential equation curve included, is shown in Figure 128(a). By combining the experimental and literature data, the range of distances covered (roughly 1.6 to 2.7Å) is expanded quite considerably compared to either individual set. As expected, the N-H...π(Ph) experimental values are found at the longer distances, and with lower $\rho_b(\mathbf{r})$ values, since they are the weakest N-H...X type interactions in the combined group. The two experimental N-H...N data points overlap with the tail end of the stronger interactions in the literature group. A single exponential function was found to model the combined $\rho_b(\mathbf{r})$ versus distance data acceptably, as suggested by the plot shown and by the fit statistics.

$$\rho_b(\mathbf{r}) = 17.66*\exp(-2.377*d) \quad r^2 = 0.762 \quad \sigma = 0.048$$

Some of the uncertainty in the fit of the combined data, which is slightly larger than in either of the individual experimental (r^2 = 0.850) or literature (r^2 = 0.824) plots, must again arise because N-H...X hydrogen bonds with different acceptors have been included in a single group [X = 2 in the experimental set, X = 3 in the literature set and X = 4 in the combined data set]. Increasing the number of different N-H...X hydrogen bond acceptors considered in a given $\rho_b(\mathbf{r})$ versus distance plot would be expected to introduce more scatter to the data, helping to explain why the exponential fit is slightly worse for the combined data set compared

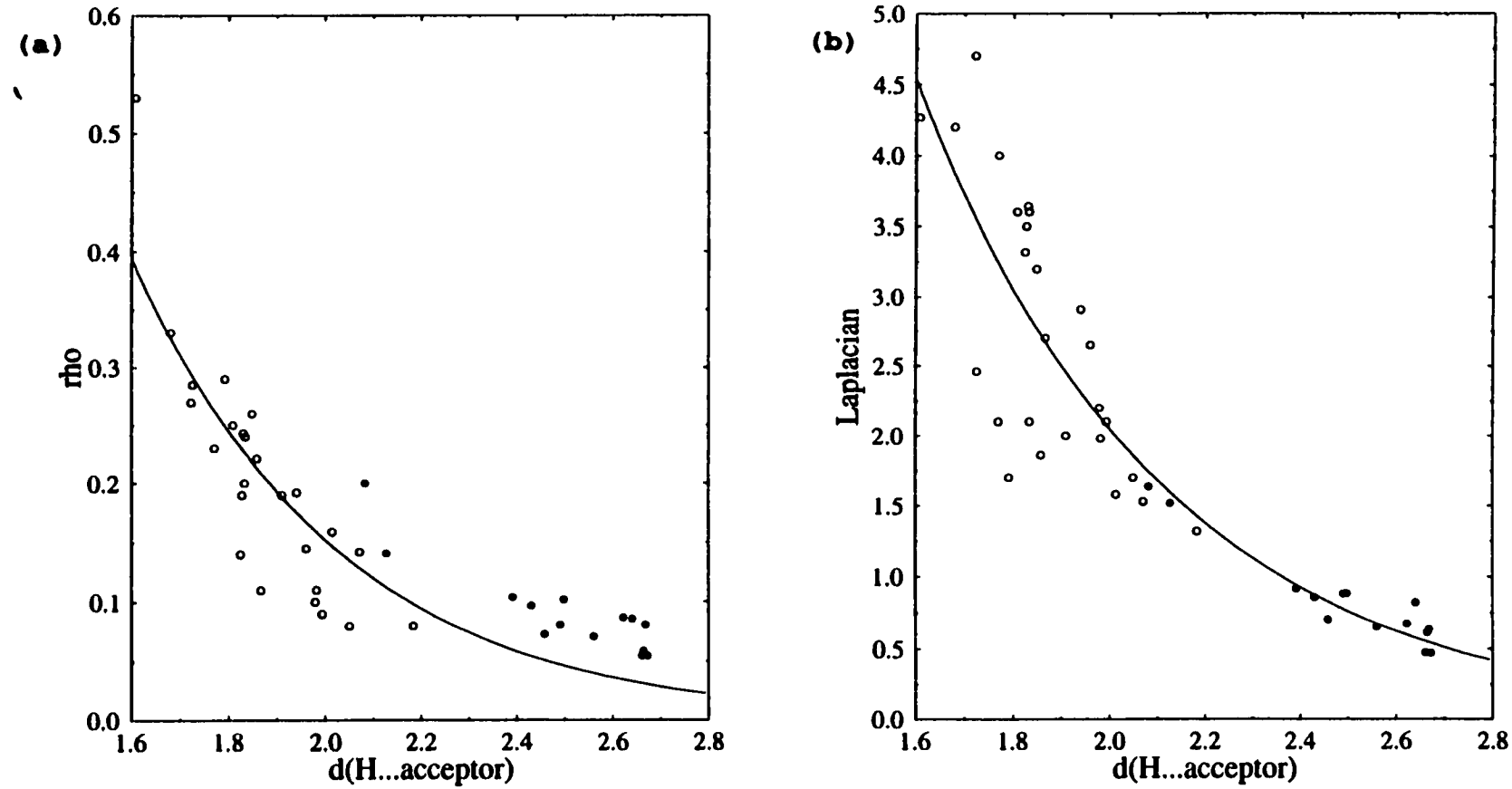

Figure 128. Topological data for a combined set of the experimental N-H...X [X = N or π(Ph)] and literature N-H...X [X = N, O or F] hydrogen bonds. Plots of (a) $\rho_b(\mathbf{r})$ and (b) $\nabla^2\rho_b(\mathbf{r})$ versus d(H...A) are shown with a fitted exponential curve included. The literature hydrogen bonds are represented by open circles and the experimental hydrogen bonds by filled circles.

to the literature or experimental groups. Combining the experimental data with the literature data would also increase the uncertainty arising from "experimental" error, that caused by the different conditions and methods used, in the overall group.

However, there is an even more obvious feature that becomes apparent when the graph of the combined data for the $\rho_b(\mathbf{r})$ versus distance relationship is examined. The experimental points all fall above the best exponential curve fit to the set of combined data. The experimental data are consistently underestimated by the exponential function optimized using the complete (experimental and literature) range of data available. There is no obvious reason that this should have occurred. At first, it was postulated that the N-H...π(Ph) hydrogen bonds (the majority of the experimental data set) might be fundamentally different from the N-H...X hydrogen bonds formed with "traditional" lone pair acceptors [X = N, F or O]. For example, their covalent component might result in larger than expected $\rho_b(\mathbf{r})$ values relative to the "traditional" group. However, from the graph it is obvious that the $\rho_b(\mathbf{r})$ values of the experimental N-H...N hydrogen bonds have also been underestimated and by a similar amount. It seems more likely that some systematic difference has been introduced into the experimental results, either during data collection or during the refinement process.

In spite of this, the plot of $\rho_b(\mathbf{r})$ versus the H...acceptor distance for the combined literature and experimental data set suggests that a single exponential function does model all the data reasonably well. The effect of the acceptor (X) on the topological parameters of the N-H...X hydrogen bonds appears to be limited. All of the N-H...X interactions

appear to belong to a single, broadly homogeneous group, including those of the N-H...π(Ph) type. The N-H...π(Ph) interactions behave topologically like all other N-H...X hydrogen bonds that have been described to date. This observation suggests that all the N-H...X hydrogen bonds are predominantly electrostatic, closed shell interactions, whether the acceptor (X) is a phenyl ring or the lone pair of electrons on a more "traditional" acceptor atom (N, F or O). It also suggests that the N-H...π(Ph) interactions are true hydrogen bonds and not merely some form of incidental contact. Their topological parameters fit the same exponential curves (versus distance) as do other N-H...X hydrogen bonds.

A corresponding plot of the $\nabla^2\rho_b(\mathbf{r})$ versus H...acceptor distance [d(H(N)...X)] for the combined literature and experimental N-H...X hydrogen bond data set was also prepared. It is shown in Figure 128(b) with the optimized exponential curve included. The exponential model fits the combined data set surprisingly well.

$$\nabla^2\rho_b(\mathbf{r}) = 108.5*\exp(-1.984*d) \quad r^2 = 0.807 \quad \sigma = 0.542$$

The results were somewhat unexpected because the literature data, when considered alone, had not fit an exponential model at all well (r^2 = 0.539). In fact, in the combined plot shown it is apparent that most of the scatter still comes from the literature data; the experimental data points fall exactly on the fitted curve. The experimental $\nabla^2\rho_b(\mathbf{r})$ values are not consistently over- or underestimated as the experimental $\rho_b(\mathbf{r})$ values had been. Combining the literature and experimental data into a single set extends the range of distances covered considerably and allows a better fit to be made over the entire range of $\nabla^2\rho_b(\mathbf{r})$ values. The results obtained by modelling the combined $\nabla^2\rho_b(\mathbf{r})$ versus distance data set

to a single exponential function substantiate the observations made after considering the $\rho_b(\mathbf{r})$ versus distance relationship. In both cases, all N-H...X hydrogen bonds have been shown to be of a single, broad type, N-H...π(Ph) hydrogen bonds being no different from the other members of the group in topological terms.

In a recent paper (1999) Espinosa et al.[125] have described a similar investigation of the relationship between the topological and geometric parameters of hydrogen bonds, in their case X-H...O type [X = N, C or O]. This investigation was carried out for rather different reasons; the authors studied the topological properties of hydrogen bond charge densities derived from crystallographic data to try and determine the effect of the initial method of data collection (x-ray, neutron or joint methods) on the final parameters obtained. They also investigated which topological parameter [$\nabla^2\rho_b(\mathbf{r})$, $\rho_b(\mathbf{r})$ or λ_3] would show the best correlation with a variety of characteristic geometric parameters defining the hydrogen bond, including the H...acceptor distance.

Espinosa et al. assembled a group of 83 X-H...O [X = N, C or O] hydrogen bonds that had been subject to topological analysis of the experimental (crystallographically derived) charge density. Their data set is rather different from the literature group compiled for this work since it involves C-H...O and O-H...O hydrogen bonds in addition to those of the N-H...O type. Their set of values would be expected to behave relatively consistently, since although the nature of X will influence the hydrogen bond to a certain extent, the actual H...O interaction is the same in every case. It is different from the data considered so far in that they have kept the acceptor constant and varied the donor (X) atom; in the

present investigation the donor N-H group has been kept constant and the acceptor varied. Experimental error, one of the factors the authors chose to investigate, would also be expected to be significant in their set of hydrogen bond parameters because of the many varied sources of the data they have included. There is some overlap between the set of literature data assembled for this study (N-H...O type) and the Espinosa data set, however it is only slight. Much of the information Espinosa et al. utilized was generated from their own personal work, data that had not previously been published and so were unavailable for inclusion in our literature data set. They did not include in their study all the hydrogen bond topological data that actually were available in the literature of the time. Thus the overlap between our literature data set and the Espinosa data set is actually relatively small.

In any event, Espinosa et al. have compiled a fairly comprehensive and wide-ranging set of topologically characterized X-H...O hydrogen bonds, with H...O distances of between 1.56 and 2.63Å in the group. They then divided this data into two groups. In the first category they placed those hydrogen bonds whose charge densities and topological parameters had been generated from x-ray measurements only (X-X), roughly three quarters of the original data set (n = 60). In the multipole refinements of these x-ray only data sets, the hydrogen atom positions were usually corrected to match average X-H neutron bond lengths from the literature but no other adjustments were made to accommodate the x-ray data. In the second category of X-H...O hydrogen bonds (n = 23), the experimental charge densities were calculated after first determining all the atomic positions (X-N) or the hydrogen positions only (X-(X+N)) from neutron data and then

completing the multipole refinement using the x-ray data.

Ultimately, Espinosa et al. were able to conclude that the two data sets were equivalent (at the level of accuracy studied). Topological parameters ($\nabla^2\rho_b(\mathbf{r})$, $\rho_b(\mathbf{r})$ or λ_3) plotted versus distances characteristic of the X-H...O hydrogen bonds [including the H...acceptor distance, d(H...O)] were fitted to simple exponential functions of the form y = a*exp(b*x). Comparison of the statistics of the fits showed that all of the topological data, regardless of its experimental origin, behaved as if it came from a single population of X-H...O hydrogen bonds. This, the authors felt, occurred because the implicit neutron information introduced into the x-ray investigations, by correcting hydrogen atom positions to neutron values, allowed accurate determination of the charge densities and subsequently of the topological parameters. The results obtained from x-ray only experiments (such as those carried out in the present work) are comparable to those obtained from the more complex and difficult to perform joint x-ray and neutron investigations, if the hydrogen atom positions are adjusted to reflect average X-H neutron bond lengths. Topological parameters characterizing hydrogen bonds can be accurately determined from charge densities derived entirely from x-ray crystallographic data, an important result.

Along the way, Espinosa et al. fit their x-ray data set and their joint x-ray and neutron data set to simple exponential functions [y = a*exp(b*x)] for, among other things, $\rho_b(\mathbf{r})$ versus d(H...O) and $\nabla^2\rho_b(\mathbf{r})$ versus d(H...O). These fits, which can be directly compared to the results of the current investigation, are summarized below:

$\rho_b(\mathbf{r})$ [in eÅ^{-3}] versus d(H...O) [d, in Å]

x-ray	$\rho_b(\mathbf{r})$ = 65(27)*exp(-3.2(2)*d)	χ^2 = 0.0016	n = 60
joint	$\rho_b(\mathbf{r})$ = 8(4)*exp(-2.1(3)*d)	χ^2 = 0.0015	n = 23

$\nabla^2\rho_b(\mathbf{r})$ [in eÅ^{-5}] versus d(H...O) [d, in Å]

x-ray	$\nabla^2\rho_b(\mathbf{r})$ = 130(30)*exp(-2.0(1)*d)	χ^2 = 0.16	n = 60
joint	$\nabla^2\rho_b(\mathbf{r})$ = 330(180)*exp(-2.6(3)*d)	χ^2 = 0.44	n = 23

Some observations on the Espinosa results are useful. For the $\rho_b(\mathbf{r})$ versus d(H...O) fits the χ^2 values are almost equal; the scatter of the data about each exponential curve is roughly the same. However, the coefficients of the exponential fit equations for the two data sets (x-ray and joint) are quite different. For the $\nabla^2\rho_b(\mathbf{r})$ versus d(H...O) data the difference between the joint and x-ray fits is even more apparent, since the χ^2 values are very different. The fit of the x-ray data to its equation is much better than that of the joint data to its exponential model. Again, the coefficients of the exponential equations for the two data sets are also somewhat different.

The fits for the x-ray data set are actually somewhat better than those of the joint data set, which is surprising considering the higher quality expected for the joint x-ray/neutron investigations. In the x-ray only experiments hydrogen atoms are positioned to match known X-H bond lengths from previous neutron investigations. This will introduce uncertainty into the x-ray only data set, however, the method employed and the distances chosen are normally very consistent from one experiment to the next. The joint data set (from combined x-ray and neutron experiments) potentially contains more variability because of the difficulty in, and the many possible ways of, scaling and combining the x-ray and neutron

results. This is particularly reflected in the scatter of the $\nabla^2\rho_b(\mathbf{r})$ data, a parameter more sensitive to experimental conditions and methods than $\rho_b(\mathbf{r})$. The x-ray data set also contains more points which could help when fitting to the exponential model functions, especially if a wider range of values were represented.

Despite the observed differences between the x-ray and joint data sets, Espinosa et al. were able to demonstrate that both groups came from the same general population of X-H...O type hydrogen bonds. In topological terms both groups were shown to behave in a consistent function that could be modelled by a simple exponential function [y = a*exp(b*x)] for both $\rho_b(\mathbf{r})$ and $\nabla^2\rho_b(\mathbf{r})$ versus d(H...A).

Using these literature results a final attempt was made to prove that the present set of experimental N-H...X hydrogen bonds [X = N or π(Ph)] belongs to the same larger population as the X'-H...O hydrogen bonds [X' = N, C or O] assembled by Espinosa et al. Plots were made of the experimental N-H...X data including the original exponential fit and the two individual exponential curves (x-ray and joint) calculated by Espinosa et al., for both (a) $\rho_b(\mathbf{r})$ versus the H...acceptor distance and for (b) $\nabla^2\rho_b(\mathbf{r})$ versus d(H...A). These are shown in Figure 129 (a) and (b) respectively.

The original exponential fits to the experimental N-H...X data can be compared to the Espinosa results in a number of different ways.

[Experimental $\rho_b(\mathbf{r}) = 6.23*\exp(-1.71*d)$; $r^2 = 0.850$, $\sigma = 0.0155$

$\nabla^2\rho_b(\mathbf{r}) = 60.2*\exp(-1.73*d)$; $r^2 = 0.926$, $\sigma = 0.0974$]

A simple visual comparison of the equations and their coefficients suggests that for $\rho_b(\mathbf{r})$ versus d(H...A) the experimental model lies closer

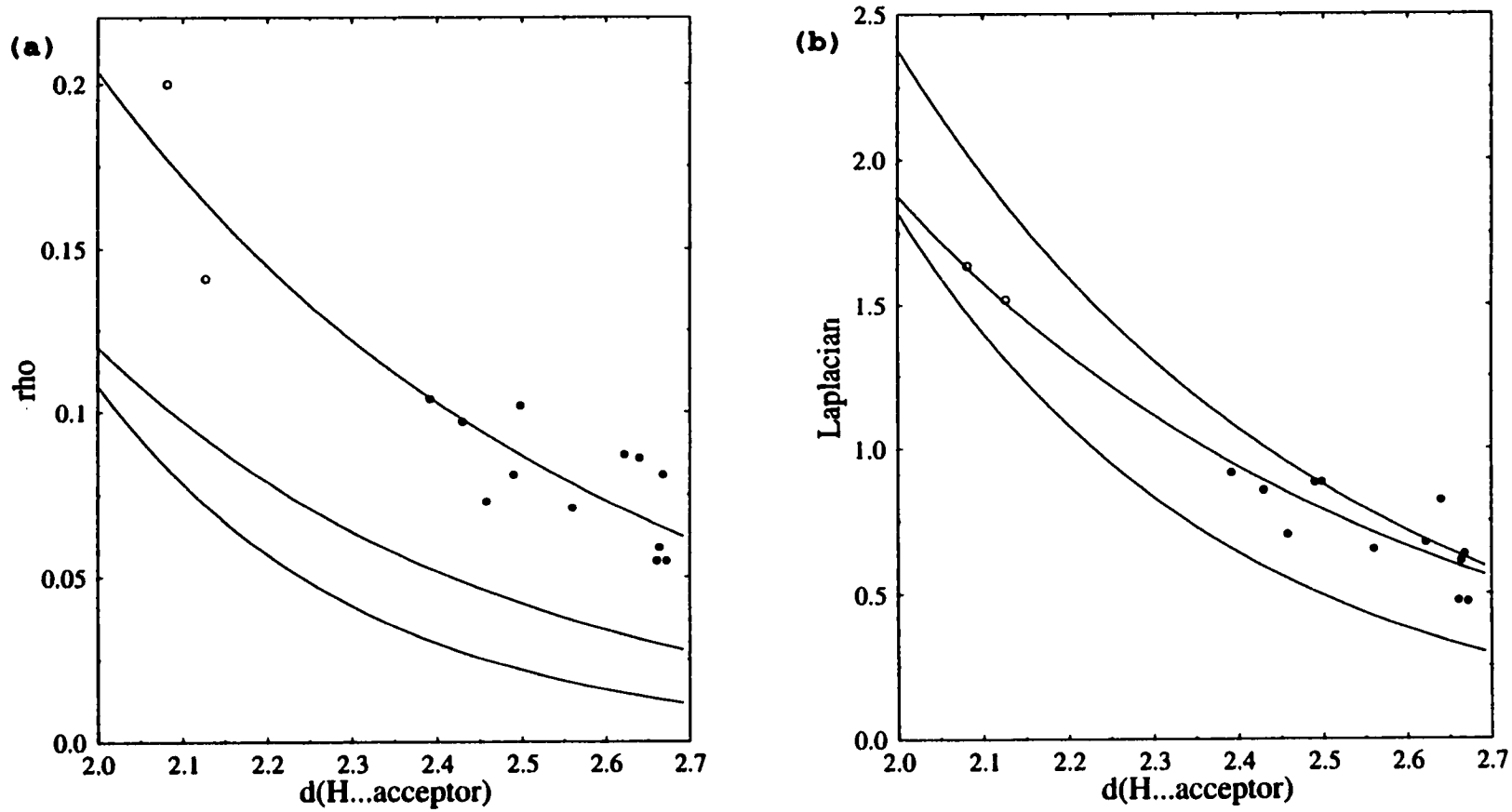

Figure 129. Topological data for the experimental N-H...X [X = N (open circles) or π(Ph) (closed circles)] hydrogen bonds. Plots of (a) $\rho_b(\mathbf{r})$ and (b) $\nabla^2\rho_b(\mathbf{r})$ versus d(H...A) are shown with (i) a fitted exponential curve, (ii) Espinosa's joint data exponential model and (iii) Espinosa's x-ray only data exponential model included. In (a) the experimental exponential fit lies above the Espinosa joint data model which in turn lies above the Espinosa x-ray only data model. In (b) the Espinosa x-ray only data model lies above the experimental exponential curve, while the Espinosa joint data model lies below it.

to the joint data equation of Espinosa than to the x-ray data only equation. For $\nabla^2\rho_b(\mathbf{r})$ the opposite appears to be true; the x-ray only equation has parameters closer to the experimental model.

This same information is conveyed by a visual examination of the two plots in Figure 129, each showing the experimental N-H...X data [X = N or π(Ph)] and the three related exponential curves. In the plot of $\rho_b(\mathbf{r})$ vs. d(H...A) it is evident that the experimental data are well distributed about the experimental exponential curve, as expected. However, all of the experimental points lie well above both of the Espinosa curves (x-ray and joint data) showing that neither literature model fits the present results well. All three curves are of similar shape but are offset relative to one another, displaced along the y-axis. The joint data equation of Espinosa et al. lies closer to the experimental curve than does the x-ray only equation. This suggests that the experimental data set is more closely related to the joint data set of Espinosa et al. than to the x-ray derived data set. This observation is somewhat surprising considering that the present results were derived from x-ray crystallographic measurements only (no neutron data were collected).

The experimental $\rho_b(\mathbf{r})$ value for a given H...acceptor distance is always larger than would be predicted using either of the Espinosa equations. One possibility is that the Espinosa functions do not model the weak N-H...π(Ph) hydrogen bonds of the present work well for the relationship between $\rho_b(\mathbf{r})$ and d(H...A). A second possibility is that the experimental results contain a small systematic deviation that results in their being slightly, but consistently, underestimated by the Espinosa models. This second possibility seems the more reasonable when it is

considered that points arising from the two experimental N-H...N hydrogen bonds also lie above the Espinosa curves. The N-H...N type hydrogen bonds would be expected to be closely related to the X'-H...O [X' = N, C or O] hydrogen bonds used in the Espinosa work since all involve hydrogen bonds formed with "traditional" acceptors. Their location above both the Espinosa fitted curves suggests that a slight systematic error may in fact be present in the experimental data. A similar observation was made when the $\rho_b(\mathbf{r})$ versus d(H...A) data for the N-H...X [X = N or π(Ph)] hydrogen bonds of this work were combined with literature data generated for N-H...X [X = N, O or F] type hydrogen bonds from crystallographic sources. Again, the experimental N-H...X data were slightly underestimated by the exponential model function fit to the combined literature and experimental data, leading to the conclusion that a minor systematic error might have been introduced in our calculations of $\rho_b(\mathbf{r})$. Such a systematic error could have been generated when the experimental hydrogen atom positions were moved to match neutron X-H bond lengths from the literature.

The situation for the $\nabla^2\rho_b(\mathbf{r})$ versus d(H...A) plot is quite different from that for $\rho_b(\mathbf{r})$ versus d(H...A). As shown in Figure 129(b), the experimental exponential curve fit to the N-H...X data actually falls between the two Espinosa curves; the x-ray model lies above and the joint data function falls below the experimental curve. The function modelling the joint data set of Espinosa lies close to the experimental curve at shorter H...acceptor distances and further away at longer distances. The opposite is true of the Espinosa x-ray data function, which lies close to the experimental curve at longer distances and further away at shorter distances. The experimental N-H...N hydrogen bonds have values that lie

close to the joint data fit of Espinosa while the N-H...π(Ph) hydrogen bonds are modelled quite well by the Espinosa x-ray fit. All of the experimental N-H...X data lie above the Espinosa joint data curve meaning that the experimental $\nabla^2\rho_b(\mathbf{r})$ value for a given H...acceptor distance would be underestimated using the joint data model. The experimental N-H...N hydrogen bonds and the majority of the N-H...π(Ph) data fall below the curve defined by the Espinosa x-ray data set. However, some of the N-H...π(Ph) values are actually distributed above the Espinosa x-ray data curve. In this case, the Espinosa equation derived from x-ray data only would generally overestimate the experimental $\nabla^2\rho_b(\mathbf{r})$ values at a given H...A distance. It is impossible to say which of the Espinosa curves actually models the total experimental data set more closely using a simple visual examination but both obviously show better agreement than was the case for the $\rho_b(\mathbf{r})$ versus d(H...A) data.

A somewhat more quantitative comparison of the three curves shown on each plot in Figure 129 is possible. The complete experimental N-H...X data set [X = N or π(Ph), n = 14] was fitted to each of the Espinosa equations (for the x-ray and joint data sets) and the standard deviation of the fit (σ) compared to that of the original exponential model.

For the plot of $\rho_b(\mathbf{r})$ versus d(H...A), the original exponential curve fit the experimental N-H...X data set with σ equal to 0.0155. When the same set of data was fitted to the curve generated by modelling Espinosa's x-ray data a σ value of 0.0732 was obtained, 4.7 times larger than the experimental value. Fitting the experimental data to the joint data derived curve of Espinosa generated a somewhat smaller σ value, 0.0539, but it is still almost four times larger than the experimental σ value

($3.8\sigma_{exp}$). Using these values to discriminate between the two Espinosa models leads to the same conclusion as was reached after a simple visual examination, the joint data model of Espinosa fits the experimental data better than the x-ray only data model. However, neither of the Espinosa curves offers a close match to the experimental data set, at least based on a comparison of the standard deviations.

In the case of $\nabla^2\rho_b(\mathbf{r})$ versus d(H...A), the experimental N-H...X data set was fitted to a simple exponential function with σ = 0.0974. Fitting the same data set to the Espinosa curve modelled on the x-ray derived data resulted in σ = 0.195, exactly twice the experimental value. The fit to Espinosa's joint data derived exponential curve was somewhat worse, with σ equal to 0.307, 3.2 times the experimental value. In contrast to the $\rho_b(\mathbf{r})$ versus d(H...A) case, the $\nabla^2\rho_b(\mathbf{r})$ versus d(H...A) relationship for the experimental N-H...X data is better modelled by the x-ray derived function of Espinosa than by the joint data function. The σ values also suggest that both Espinosa equations (x-ray and joint) fit the experimental N-H...X data when $\nabla^2\rho_b(\mathbf{r})$ is plotted versus d(H...A) better than when $\rho_b(\mathbf{r})$ is plotted versus d(H...A). This could result because the greater spread inherent in the $\nabla^2\rho_b(\mathbf{r})$ data sets increases the latitude when fitting one set of data to another.

Espinosa et al. report χ^2 values to describe the fit of the exponential curves [$\rho_b(\mathbf{r})$ and $\nabla^2\rho_b(\mathbf{r})$ versus d(H...A)] to their assembled data sets [x-ray and joint]. These values cannot be directly compared with the r^2 and σ values characterizing the experimental models. How then could the data sets be compared to determine if all the hydrogen bonds come from a single general population? The method that was chosen makes use of the

quoted errors on the a and b regression coefficients calculated by Espinosa et al. for each of their exponential fit equations (for the x-ray and joint data sets). Using these errors it is possible to estimate limits for the Espinosa exponential models over the range of applicable distances for both $\rho_b(\mathbf{r})$ and $\nabla^2\rho_b(\mathbf{r})$ versus d(H...A).

The results for $\rho_b(\mathbf{r})$ versus d(H...A) are shown graphically in Figure 130, which compares the present experimental results to both Espinosa's joint data model (a) and to the x-ray model (b). Each plot includes the entire experimental N-H...X [X = N or π(Ph)] data set and the experimental exponential model curve (the thicker solid line in each graph). Then to each plot is added one of the Espinosa curves (the thinner solid line in each case, (a) joint or (b) x-ray). The limits calculated on the Espinosa curves are shown as dotted lines bracketing the Espinosa model function on each graph.

The first $\rho_b(\mathbf{r})$ versus d(H..A) plot [Figure 130(a)] combines the experimental results with the exponential function calculated by Espinosa et al. from their joint data set of X'-H...O type hydrogen bonds. Using this function, and the errors reported for the a and b parameters, limits were calculated for the model over the entire range of H...acceptor distances studied. From the plot, it is readily apparent that the entire experimental data set is well within the range of values covered by the Espinosa joint data exponential model. The experimental data set of N-H...X hydrogen bonds is included in the same population described and analyzed by Espinosa et al. in their joint data set of hydrogen bonds.

The plot of the experimental data with the Espinosa x-ray derived exponential function and its calculated limits [Figure 130(b)] shows a

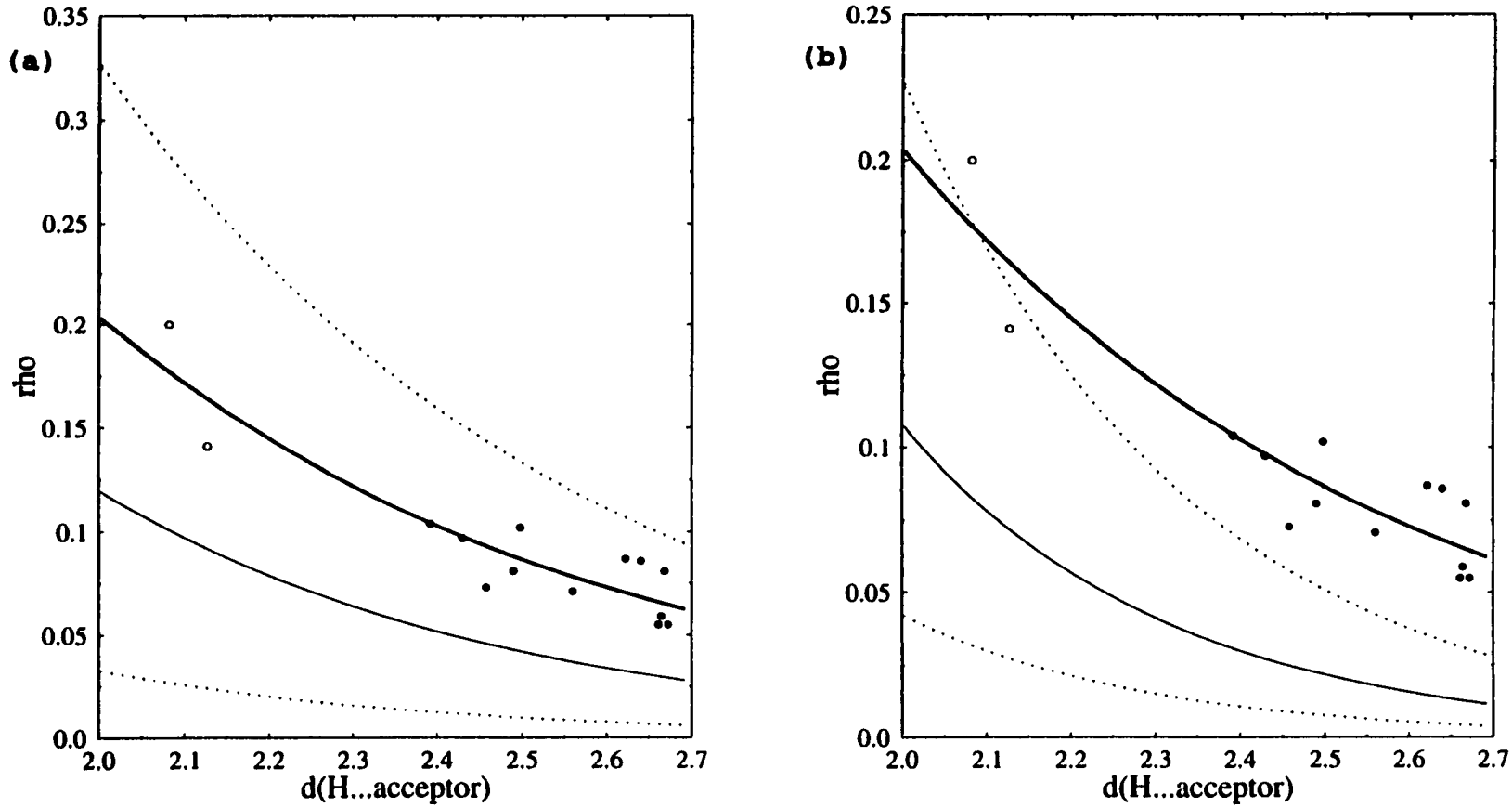

Figure 130. Topological data, $\rho_b(\mathbf{r})$ versus d(H...A), for the experimental N-H...X [X = N (open circles) or π(Ph) (closed circles)] hydrogen bonds. The plots include the fitted experimental exponential curve (heavy solid line) and either (a) Espinosa's joint data exponential model or (b) Espinosa's x-ray only data exponential model (solid line) and the ranges calculated for the Espinosa models (dotted lines).

somewhat surprising result. All of the experimental data points, except that for one of the two N-H...N hydrogen bonds, lie outside the range covered by the Espinosa x-ray data model (i.e. the experimental data set does not fall within the boundary limits of the Espinosa x-ray data set). Thus, the two sets of data, x-ray and experimental, do not appear to come from the same population. This is particularly surprising in light of the results observed in part (a) and because the experimental data were generated using only x-ray crystallographic data. The experimental data set would be expected to conform to Espinosa's x-ray model function more closely than to the joint model function. However, the converse is in fact observed.

The results of fitting the experimental data graphically to the Espinosa joint and x-ray data sets, if somewhat unexpected, are at least consistent with the σ values calculated by fitting the experimental data to the Espinosa equations. Both literature models are considerably worse than the exponential function fit to the experimental $\rho_b(\mathbf{r})$ versus d(H...A) data and the Espinosa x-ray model is worse than the joint data model by a significant amount. This is also observed in the plots shown, where the experimental data fit entirely within the limits of Espinosa's joint data model but not into the range covered by the x-ray model. It is not immediately clear why this should be so, especially considering the fact that all the experimental data were generated from only x-ray crystallographic measurements, equivalent to Espinosa's x-ray data set (which it does not match).

One possible explanation does come to mind. It may be that the joint data set of Espinosa et al. really is a better model for the "true"

relationship between $\rho_b(\mathbf{r})$ and d(H...A), the values being more accurately determined using the neutron positions for the hydrogen atoms. Perhaps the x-ray only data sets do include some (reasonably small) amount of error introduced when the hydrogen atom positions are approximated. In the set of experimental data from the present investigation, a slight systematic error was suspected in the $\rho_b(\mathbf{r})$ values. This may have been introduced during the positioning of the hydrogen atoms, which were corrected to N-H bond lengths, chosen based on the limited amount of neutron data available in the literature for similar compounds. A slight misplacement of the hydrogen atoms could have translated the experimental x-ray data away from the "true" $\rho_b(\mathbf{r})$ versus d(H...A) relationship in a systematic fashion. If errors in the Espinosa x-ray data set moved that curve away from the "true" function but in the opposite direction, then the joint data model would end up a closer fit to the experimental data set.

However, it must be remembered that all of these differences are relatively slight. Espinosa et al. were able to demonstrate that both of their samples (derived from x-ray and joint data sets) came from the same general population of X'-H...O type hydrogen bonds. The present results, obtained by comparing the experimental data set to the exponential model functions of Espinosa et al., suggest that the experimental hydrogen bonds (both N-H...N and N-H...π(Ph) type) also come from the same general population of hydrogen bonds. The data suggest that there is a common relationship, modelled reasonably well by a simple exponential function, between $\rho_b(\mathbf{r})$ and d(H...A) for all [non-covalent] hydrogen bonds, whether formed with traditional acceptors or with π(Ph) electron density serving as the acceptor of the interaction.

The experimental results for N-H...X type hydrogen bonds [X = N or π(Ph)] were also fitted to the Espinosa equations, derived from their x-ray and joint data sets, for the exponential relationship between $\nabla^2\rho_b(\mathbf{r})$ and d(H...A). The resulting plots are shown in Figure 131 for the joint data set (a) and for the x-ray data set (b). As before, limits were calculated (dashed lines) to show the range covered by the Espinosa model function, using the reported exponential equation, the coefficients (a and b) of that equation and the errors quoted on those parameters. In both plots, the x-ray and joint data functions of Espinosa cover a wide range of $\nabla^2\rho_b(\mathbf{r})$ values over the H...acceptor distances shown, much larger relatively compared to the $\rho_b(\mathbf{r})$ versus d(H...A) plots. This results from the relatively larger errors determined on the a and b coefficients in the $\nabla^2\rho_b(\mathbf{r})$ versus d(H...A) equations, and again likely arises because of the greater sensitivity of $\nabla^2\rho_b(\mathbf{r})$ to experimental conditions. This larger spread in the $\nabla^2\rho_b(\mathbf{r})$ values compared to $\rho_b(\mathbf{r})$ could actually ease the fitting of one data set to another.

All of the experimental N-H...X data points easily fall within the range calculated for the Espinosa joint model function (a). In fact, although all the experimental $\nabla^2\rho_b(\mathbf{r})$ values fall above the Espinosa exponential joint data curve, they are all close to that line relative to the area included between the upper and lower limits. The situation when the experimental data is compared to the Espinosa x-ray data set for $\nabla^2\rho_b(\mathbf{r})$ versus d(H...A), Figure 131(b), is similar but even more favourable. The range calculated for the Espinosa x-ray function is actually narrower than that for the joint data model. However, the experimental points still fall closer to the x-ray exponential curve,

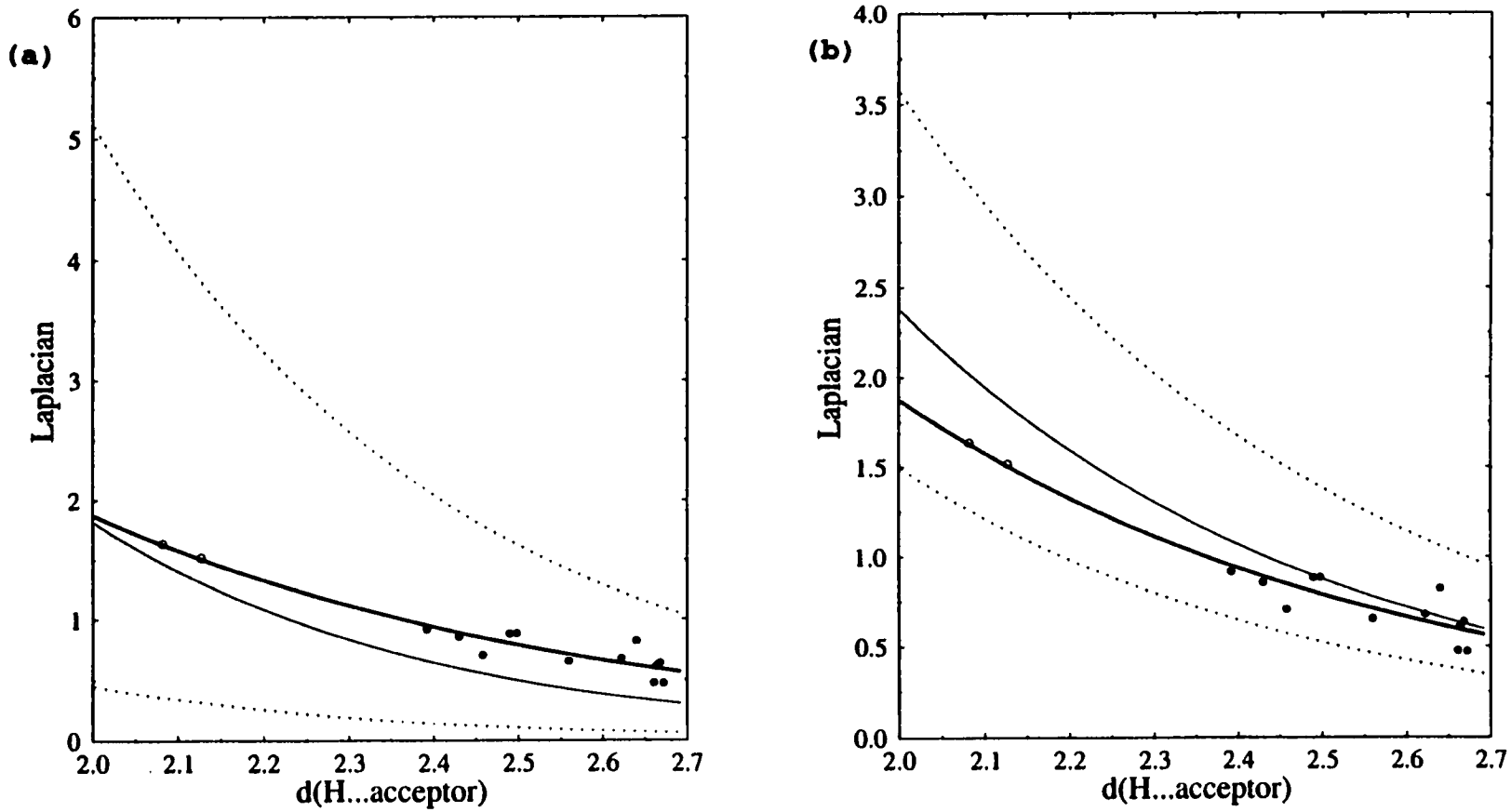

Figure 131. Topological data, $\nabla^2\rho_b(\mathbf{r})$ versus d(H...A), for the experimental N-H...X [X = N (open circles) or π(Ph) (closed circles)] hydrogen bonds. The plots include the fitted experimental exponential curve (heavy solid line) and either (a) Espinosa's joint data exponential model or (b) Espinosa's x-ray only data exponential model (solid line) and the ranges calculated for the Espinosa models (dotted lines).

lying both above and below the line. The better fit of the experimental data to the x-ray model of Espinosa than to the joint data model was also observed when the σ values of the fits were compared. Why the experimental data fit the joint data model of Espinosa better for $\rho_b(\mathbf{r})$ versus d(H...A) and the x-ray model better for $\nabla^2\rho_b(\mathbf{r})$ versus d(H...A) is not completely clear. However, this is a minor point since Espinosa et al. have already proven that both data sets (x-ray and joint) came from one population.

In any event, in both cases the [$\nabla^2\rho_b(\mathbf{r})$, d(H...A)] values for the experimental hydrogen bonds [X = N or π(Ph)] fall within the range calculated for the Espinosa model function, whether derived from x-ray or joint crystallographic data. The literature data sets had already been shown by Espinosa et al. to come from one general population of hydrogen bonds and it is now apparent that the N-H...X hydrogen bonds studied in this work also belong to that same general population. Even though the experimental data set contains many hydrogen bonds formed to a non-traditional acceptor, N-H...π(Ph) type, they still behave topologically like other hydrogen bonds when $\nabla^2\rho_b(\mathbf{r})$ is compared to the H...acceptor distance. All of the collected data suggest that the $\nabla^2\rho_b(\mathbf{r})$ versus d(H...A) relationship is reasonably modelled by an exponential function, as was also the case for the $\rho_b(\mathbf{r})$ versus d(H...A) relationship.

None of the data discussed in this section, experimental from the present work or the Espinosa literature sets, fits the calculated exponential curves exceptionally well. There are several obvious reasons for the observed discrepancies. Each of the data sets consists of crystallographically derived topological and geometric parameters which were collected under a variety of experimental conditions and subject to

a variety of experimental methods and errors. Not all of the data were generated nor treated in exactly the same way; in the x-ray only data sets, hydrogen atom positions were approximated to neutron X-H bond lengths, while in the joint data set fitting of the x-ray and neutron data can be difficult and can be handled by somewhat different methods. Both of these factors introduce scatter into the data sets. Finally, each of the data sets contains a less than uniform collection of hydrogen bonds, with a variety of different donors and/or acceptors for the interactions. This also increases the spread of the observed data in a given set and makes fitting the data to a single model more difficult.

Overall, comparison of the topological parameters [$\rho_b(\mathbf{r})$ and $\nabla^2\rho_b(\mathbf{r})$] to the geometric parameter [d(H...A)] for the hydrogen bonds studied, both in this work and in the literature data sets of Espinosa et al., suggests that they all belong to a single population. The relationship between these parameters takes the same form for all of these hydrogen bonds and can be modelled reasonably well by a simple exponential function of the form y = a*exp(b*x). Of particular note is the fact that N-H...π(Ph) hydrogen bonds behave topologically like other hydrogen bonds formed to more traditional acceptors. One of the ultimate goals of this investigation has been proven to be true.

3.6.3.4. C-H...X [X = N or Phenyl] Interactions

In this study of four tetraphenylborate salts a total of 43 C-H...X [X = N or phenyl] contacts were located in a geometry search for H...X interionic distances of 3.0Å or less. A topological investigation of these potential C-H...X interactions led to the location of 44 bond paths and

(3,-1) type bond critical points. Three of the bond paths were found to be different from the others, in that they begin from carbon of the donor C-H group rather than from the hydrogen atom. These were removed from the subsequent analysis of the topological results, discussed here, leaving a total of 41 C-H...X interactions in the experimental group.

The 41 C-H...X interactions can be divided into two subsets, the C-H...N contacts (n = 9) and the C-H...phenyl contacts (n = 32). The mean topological parameters (with their standard deviations) characterizing the two groups are summarized below for comparison purposes.

Interaction	d(H(X)...C) (in Å)	$\rho_b(\mathbf{r})$ (in eÅ^{-3})	$\nabla^2\rho_b(\mathbf{r})$ (in eÅ^{-5})
C-H...N (n = 9)	2.82 (0.12)	0.053 (0.009)	0.54 (0.08)
C-H...phenyl (n = 32)	2.64 (0.27)	0.051 (0.008)	0.46 (0.12)

The most readily apparent difference on examining the two groups is that the average H(C)...X distance is actually shorter for the C-H...phenyl contacts than it is for the C-H...N contacts. However, this result is somewhat misleading since the C-H...phenyl group contains the H...H type interactions that are characterized by short H...acceptor distances. This skews the entire C-H...phenyl subset to a shorter than expected mean H(C)...X distance.

The topological parameters characterizing each group are quite similar. The C-H...N group does have slightly larger mean $\rho_b(\mathbf{r})$ and $\nabla^2\rho_b(\mathbf{r})$ values compared to the C-H...phenyl group as might be predicted. Nitrogen, a "traditional" hydrogen bond acceptor, would be expected to form stronger interactions than comparable contacts formed with π electron density as the acceptor. However, the difference between the two C-H...X groups

[X = N or π(Ph)] is not nearly so pronounced as was observed for the N-H...N [mean values d = 2.105Å, $\rho_b(\mathbf{r})$ = 0.171 eÅ^{-3}, $\nabla^2\rho_b(\mathbf{r})$ = 1.58 eÅ^{-5}] and N-H...π(Ph) [mean values d = 2.563Å, $\rho_b(\mathbf{r})$ = 0.079 eÅ^{-3}, $\nabla^2\rho_b(\mathbf{r})$ = 0.72 eÅ^{-5}] groups already discussed. In the C-H...X case both classes of interactions occur at similar distances, particularly if the H...H type contacts are excluded. In contrast, N-H...N hydrogen bonds are significantly shorter and stronger than those of the N-H...π(Ph) type. All C-H...X contacts are weaker than their N-H...X counterparts under normal circumstances, meaning that on a relative scale they [C-H...N and C-H...phenyl] will be more similar.

All X-H...π(Ph) hydrogen bonds (or other types of X-H...phenyl contacts) are normally weak. The large difference observed between the experimental N-H...N and C-H...N groups is not observed when the N-H...π(Ph) and C-H...phenyl groups are compared. Again, relatively weaker interactions show less difference between the mean topological values. However, the C-H...phenyl contacts are on average longer and weaker than the N-H...π(Ph) hydrogen bonds studied experimentally, as expected.

The experimental C-H...N interactions occur at much longer distances and are much weaker (according to the observed topological parameters) than the N-H...N hydrogen bonds. As a donor group, C-H is less satisfactory than N-H in most situations, explaining the origin of the observed difference. Yet, the group of C-H...N interactions identified in this work are so weak that their real nature is difficult to discern. It is not clear if they are true hydrogen bonds or merely contacts arising as a consequence of other forces acting on the structure in the solid state.

The topological parameters (derived from the crystallographically determined electron density) of one C-H...N hydrogen bond have previously been reported in the literature. These can be compared to the experimental C-H...N values. Bianchi et al.[42] characterized such an interaction in the structure of 4-cyanoimidazolium-5-olate from x-ray data collected at 120K. The C(2)-H(2)...N(7) interaction was determined to have a geometry with an H(2)...N(7) distance of 2.20(2)Å, a C(2)...N(7) distance of 3.150(2)Å and a C(2)-H(2)...N(7) angle of 145(1)°. At the (3,-1) bond critical point located for this contact an electron density [$\rho_b(\mathbf{r})$] of 0.11(1) eÅ^{-3} and a Laplacian [$\nabla^2\rho_b(\mathbf{r})$] value of 1.6(1) eÅ^{-5} were calculated. The literature interaction is much stronger than any of the experimental examples, its H(C)...N distance being 0.62Å shorter than the experimental average. The topological parameters reported are correspondingly larger, about twice as large for $\rho_b(\mathbf{r})$ and three times as large for $\nabla^2\rho_b(\mathbf{r})$, when compared to the present experimental values. The C(2)-H(2)...N(7) contact described by Bianchi et al. is more typical of what would be expected for a true C-H...N hydrogen bond, judging from the many C-H...O interactions already well characterized in the literature. Its geometry and topological parameters have more in common with those C-H...O interactions than with the experimental C-H...N group. This is additional evidence that the C-H...N interactions located in this investigation are somewhat unusual. They may be weak hydrogen bonds or they may just be incidental contacts formed as a result of other stronger interactions being formed in their vicinity. It is not possible to discover any more about the true nature of the experimental C-H...N contacts from the information available.

In contrast, the C-H...phenyl interactions located in this

investigation are more numerous and can be subdivided in various ways to gain more insight from the topological parameters calculated. Our first instinct was to examine the C-H...phenyl contacts on the basis of the origin of the interacting groups by dividing them into the following subsets, anion(-1)/anion(-1), cation(+1)/anion(-1) and solvent(0)/ anion(-1). It was thought that charge differences might give rise to differences in the interaction geometries and their strengths and thus ultimately in the topology of the interaction. Distinct differences were observed between the three groups; for example, anion/anion contacts were found to be much shorter on average than the other two groups and also tended to have correspondingly larger topological parameters. However, after further investigation it became apparent that the true cause of the observed differences between the groups was not their origin (a/a, c/a or s/a) but rather the geometries adopted by the interactions included in each group (hydrogen bond, intermediate contact or H...H type contact). The geometry of an interaction does not appear to be directly, or simply, related to the charges of the groups involved; all three charge based subgroups were found to contain examples of all possible geometries. It became clear that a comparison based on geometry was more reasonable and would be more profitable than one based on the origin of the interacting groups.

The C-H...phenyl interactions were divided into three groups using a classification based on the geometry/bond path of the contacts and the criteria developed experimentally. Average values for the geometric and topological parameters characteristic of the interactions are given below for each group, hydrogen bond, intermediate contact or H...H type contact,

as well as for the overall C-H...phenyl group which is included for comparison.

Interaction	d(H(C)...C) (in Å)	$\rho_b(\mathbf{r})$ (in eÅ^{-3})	$\nabla^2\rho_b(\mathbf{r})$ (in eÅ^{-5})
C-H...phenyl (n = 32)	2.64 (0.27)	0.051 (0.008)	0.46 (0.12)
H...H contacts (n = 15)	2.37 (0.11)	0.054 (0.009)	0.51 (0.11)
Intermediate contacts (n = 4)	2.85 (0.04)	0.048 (0.004)	0.45 (0.04)
Hydrogen bonds (n = 13)	2.89 (0.07)	0.048 (0.006)	0.41 (0.12)

Classification of the experimental C-H...phenyl contacts into these three groups, based on the geometry/bond path of the interactions, clearly shows the natural division between the groups. The H...H type contacts are characterized by much shorter donor...acceptor distances than the other two groups, which are H...C type contacts. Consequently, the H...H group is also characterized by larger average $\rho_b(\mathbf{r})$ and $\nabla^2\rho_b(\mathbf{r})$ topological parameters. The question which remains to be answered, "are the differences between the groups proportional, such that they can all be modelled by one simple function" will be covered in the following section. However, even the simple statistics included here illustrate the obvious differences between the H...H type contacts and the other C-H...phenyl interactions studied, both in terms of geometry and in terms of the topological description of the electron density.

It is possible to subdivide the C-H...phenyl hydrogen bond group further, again based on the geometries/bond paths of the individual interactions. The hydrogen bonds have already been classified as centroid type, edge type or single atom type and now the mean topological

parameters of the different groups can now be compared. However, as was also the case for the N-H...π(Ph) interactions, there is not enough data available for a detailed statistical analysis of the different hydrogen bond geometries. The discussion is limited to a few general observations.

Interaction	d(H(C)...C) (in Å)	$\rho_b(\mathbf{r})$ (in eÅ^{-3})	$\nabla^2\rho_b(\mathbf{r})$ (in eÅ^{-5})
centroid (n = 4)	2.872 (0.046)	0.051 (0.006)	0.47 (0.04)
edge (n = 6)	2.877 (0.065)	0.050 (0.004)	0.36 (0.14)
single atom (n = 3)	2.924 (0.085)	0.042 (0.005)	0.42 (0.10)
overall (n = 13)	2.886 (0.069)	0.048 (0.006)	0.41 (0.12)

The centroid and edge type hydrogen bonds are characterized by relatively equal average H...acceptor distances and $\rho_b(\mathbf{r})$ values; the mean Laplacian value is slightly larger for the centroid geometry hydrogen bonds than for the edge group suggesting that the former are the somewhat stronger interactions overall. Both the centroid and edge type hydrogen bonds appear to be stronger (judging from the $\rho_b(\mathbf{r})$ values), on average, than the single atom type interactions. This seems to be a reasonable observation since geometry suggests that these should be the stronger contacts.

A similar comparison of the experimental N-H...π(Ph) hydrogen bonds showed that for those interactions the centroid and single atom type contacts were stronger (shorter distances and larger topological values) than the edge type contacts. The differences between the N-H and C-H groups likely arise from the limited data available for analysis rather than from true differences in the preference for different hydrogen bond geometries. Obviously all of these interactions are relatively weak and

therefore quite similar in strength when considered over the entire spectrum of hydrogen bonds. It is perhaps reasonable to assume, and the combined results suggest, that in general the centroid geometry forms stronger interactions than either the edge or single atom type geometries. However, even this remains to be proven unequivocally.

The experimental results can be compared with the rather limited literature data available on C-H...π(Ph) hydrogen bonds. Yang and Craven[121] and Mallinson et al.[122] have published crystallographically derived electron density studies that include topological analyses of C-H...phenyl type interactions. In addition, Cubero et al.[123] have investigated the gas phase benzene/benzene dimer using ab initio molecular orbital calculations in their study of the "anti-hydrogen bond." This paper includes a theoretically derived, topological analysis of the C-H...π(Ph) hydrogen bond in the dimer.

The "anti-hydrogen bond" has received considerable attention in the recent literature.[72] Cubero et al.[123] have reported a geometry optimization and topological characterization of the C-H...π(Ph) hydrogen bond in the benzene dimer in connection with this phenomenon, in which the covalent C-H bond length actually decreases on complex formation. The authors carried out molecular orbital calculations, at the MP2 level using the 6-31G(d,p) basis set, on a series of R_nC-H...acceptor complexes including the benzene dimer. The minimum energy conformation of $(C_6H_6)_2$ was found to be symmetric with the C-H donor group of one benzene ring oriented along a line normal to the plane of the second ring and passing through its centroid. Unfortunately, a complete geometric description of the dimer is not included in the paper, limiting possible comparisons with the

experimental results. The authors located a number of critical points of different types in the complex, including six equivalent [one unique] (3,-1) type bond critical points linking the donor hydrogen atom to each of the ring carbon atoms. Topological analysis of the electron density at this bond critical point gave values of 0.0077 au (0.052 eÅ^{-3}) and 0.0271 au (0.65 eÅ^{-5}) for $\rho_b(\mathbf{r})$ and $\nabla^2\rho_b(\mathbf{r})$, respectively. These values, the authors report, fall within the range expected for theoretically calculated hydrogen bonds. For $\rho_b(\mathbf{r})$ they report a typical range of 0.002 to 0.034 au (0.013 to 0.23 eÅ^{-3}) while the value of $\nabla^2\rho_b(\mathbf{r})$ they report as varying between 0.014 and 0.139 au (0.34 - 3.3 eÅ^{-5}) for typical hydrogen bonds. Obviously, the weak C-H...π(Ph) interaction described by Cubero et al. fall at the low end of each topological range.

The theoretical parameters calculated by Cubero et al. for the C-H...π(Ph) hydrogen bond in the gas phase benzene dimer are in good agreement with the current experimental results. The calculated $\rho_b(\mathbf{r})$ value of Cubero et al. (0.052 eÅ^{-3}) is almost identical to the mean $\rho_b(\mathbf{r})$ value for the experimental centroid type C-H...π(Ph) hydrogen bonds (0.051 eÅ^{-3}), while the mean $\rho_b(\mathbf{r})$ values are smaller for the other experimental geometries studied. This is in keeping with the optimized geometry of the benzene dimer which was also found to adopt a centroid type arrangement. The mean Laplacian value for the experimental group of centroid type hydrogen bonds (0.47 eÅ^{-5}) is somewhat smaller than that calculated by Cubero et al. (0.65 eÅ^{-5}). Again, this illustrates the relatively greater sensitivity of the Laplacian, compared to $\rho_b(\mathbf{r})$, in this case to its method of generation. Still, the experimental and theoretical results are reasonably close and the $\nabla^2\rho_b(\mathbf{r})$ value calculated by Cubero et al. is

closer to the centroid geometry average than it is to that of either the single atom or edge type groups.

In a recent crystallographic investigation Yang and Craven[121] collected high resolution x-ray data at 123K for a topological analysis of 2-pyridone. C-H and N-H bond lengths were adjusted to match those obtained by neutron diffraction for the chemically related benzamide molecule. In the structure, the 2-pyridone units are linked by N-H...O hydrogen bonds forming puckered chains. Weaker C-H...O and C-H...π interactions are formed on both sides of the pyridone ring. A comprehensive geometric and topological examination of all close intermolecular contacts was carried out. The authors located three C-H...π type interactions which are summarized below.

Interaction	d(H(C)...C) (in Å)	$\rho_b(\mathbf{r})$ (in eÅ^{-3})	$\nabla^2\rho_b(\mathbf{r})$ (in eÅ^{-5})
C5c-H5c...C3	2.83	0.040(3)	0.49(4)
C4c-H4c...C4	2.89	0.036(2)	0.47(3)
C6d-H6d...C6	2.70	0.045(3)	0.62(4)

The three interactions were all found to have small but significantly non-zero electron densities at the (3,-1) bond critical points and positive Laplacian values. The electron density at the bond critical points was observed to be very flat, as expected. The three interactions also show the expected general correlation between distance and the topological parameters, with the longer contacts being the weaker.

The authors chose the strongest interaction, C6d-H6d...C6, for a more detailed analysis. In this contact the C6d-H6d group points more linearly towards the ring atom C5 (162°) than towards C6 (139°), and the

two H6d...C_{ring} distances are almost equal (2.71Å to C5 and 2.70Å to C6). However, no critical point was located between H6d and C5. This, the authors felt, occurs because the position of the critical point is more strongly influenced by C6d and less by H6d owing to the greater electron density centered on the carbon atom (C6d...C6 = 3.59Å; C6d...C5 = 3.75Å). Comparison to the present experimental results is difficult since Yang and Craven have not included a bond path diagram nor a list of the H6d...H_{ring} contact distances.

Based on their observations, Yang and Craven ultimately conclude that the C6d-H6d...C6 interaction, and the other two similar contacts in the structure, are best described as van der Waals contacts rather than C-H...π type interactions. Their calculations show that only the spherical components of the individual atomic valence shell densities are involved in the interactions. Higher multipole terms would have to be significantly populated if a delocalized π type interaction were to occur and they are not. This is not inconsistent with the results presented in this work, where similar interactions were determined to be primarily electrostatic although directional in their effect. Yang and Craven suggest that much more work will have to be carried out before the exact nature of such contacts is defined. They conclude by making an important point. "The study of weak interactions...involves the region between molecules where the electron density is very small and subject to the dynamic effects of thermal vibrations which are likely to be considerable. Thus the static picture of weak interactions...gives only a snapshot of what is occurring. Nevertheless, estimates of electrostatic properties obtained should be typical and of use for comparison with future results."

The lack of H(C)...C/H_{ring} data and bond paths in the paper by Yang and Craven makes comparison of their C-H...π contacts to the present experimental results somewhat difficult. The H(C)...C_{ring} distances that they do report, particularly for the C6d-H6d...C6 interaction (2.70Å), suggest that one or more of these may be what we have termed H...H contacts rather than hydrogen bonds. Unfortunately, there is not enough information available to determine the true situation. The $\rho_b(\mathbf{r})$ values reported by Yang and Craven for their C-H...π interactions are all smaller than any of the experimental averages (hydrogen bond, intermediate contact or H...H type contact), for some reason likely related to the different computational methods used. In contrast, the Laplacian values of Yang and Craven appear to be slightly larger than the values calculated in this work for interactions occurring at similar distances. Still, the experimental and literature values for all the measured parameters are relatively consistent, if considered over the range of all possible hydrogen bonds.

If it assumed that the three C-H...π interactions characterized by Yang and Craven are hydrogen bonds, all with single atom type geometries as suggested by the data presented, then their mean values (2.81Å, 0.040 eÅ^{-3}, 0.53 eÅ^{-5}) can be compared with those of the experimental single atom group (2.92Å, 0.042 eÅ^{-3}, 0.42 eÅ^{-5}). The experimental single atom hydrogen bonds occur at a considerably longer average distance than those described by Yang and Craven, again evidence that theirs may not all be true hydrogen bonds as have been defined in this work (H...H contacts are characterized by shorter distances). The average $\rho_b(\mathbf{r})$ values are very similar for the two groups, while the mean $\nabla^2\rho_b(\mathbf{r})$ value is somewhat larger

for the Yang and Craven set of interactions than for the experimental single atom group. While all the reported values are reasonably close, the lack of complete geometric information for the published interactions makes comparison difficult and less informative than might be hoped.

A more fruitful comparison can be made between the current experimental results and a pair of C-H...π(Ph) interactions described and characterized by Mallinson et al.[122] from a combined x-ray and neutron crystallographic investigation of the 'proton sponge', 1,8-bis(dimethyl-amino)naphthalene. Although a number of close geometric contacts were located in the structure, only two were found to have (3,-1) bond critical points and rational bond paths. For each interaction a curved bond path was located, linking a donor methyl hydrogen atom in one molecule to an aromatic carbon atom of the naphthalene ring in an adjacent molecule, the same two molecules being involved in both contacts. The authors include a diagram of the bond paths in their publication and both appear to be single atom type hydrogen bonds using the terminology developed in this work. In the first interaction, C(11)-H(113)...C(9), a (3,-1) type bond critical point was located 1.279Å from the hydrogen atom. The bond critical point was characterized by an electron density of 0.033(2) eÅ^{-3} and a Laplacian value of 0.423(1) eÅ^{-5}. The H(C)...C_{ring} distance in both interactions was determined to be 2.91Å. However, the topological parameters of the second interaction were found to be slightly smaller, $\rho_b(\mathbf{r})$ = 0.022(6) eÅ^{-3} and $\nabla^2\rho_b(\mathbf{r})$ = 0.375(3) eÅ^{-5}, indicative of a somewhat weaker interaction.

The geometric and topological parameters calculated for the C-H...π(Ph) interactions in the proton sponge are remarkably similar to

those calculated for the single atom type hydrogen bonds in the present investigation. The mean distance in the former (2.91Å) is almost identical to the average H(C)...C_{ring} distance in the experimental single atom group (2.92Å). The average Laplacian values are almost identical as well, 0.40 eÅ^{-5} in the literature group compared to 0.42 eÅ^{-5} in the experimental group. Only the electron density at the bond critical point varies somewhat between the two groups, averaging only 0.028 eÅ^{-3} for the two Mallinson interactions but 0.042 eÅ^{-3} for the three experimental examples. [Obviously, having more data in both sets would be helpful.] The difference is considerably lessened, for $\nabla^2\rho_b(\mathbf{r})$ as well as for $\rho_b(\mathbf{r})$, if only the stronger of the two Mallinson interactions is considered. The second literature interaction seems particularly weak for the stated distance (for some undetermined reason) even in comparison to the other interaction described in the same paper. Overall, the data collected by Mallinson et al. for the two C-H...π(Ph) interactions match the statistics of the single atom group of the experimental interactions much better than those of either the centroid or edge groups. The excellent agreement observed helps to substantiate the validity of dividing the C-H...phenyl contacts into groups of different geometries.

The consistency of the present experimental C-H...phenyl results, both internally and when compared to data available in the literature, is very encouraging. The geometric and topological parameters calculated in this work show good agreement with both crystallographically[121,122] and theoretically[123] derived values for similar interactions reported previously in the literature. In fact, the comparisons are detailed enough to show that the various hydrogen bond geometries (centroid type[123] and

single atom type[122] in particular) have similar and predictable topological and geometric parameters even when determined under different conditions. These results should allow the topological parameters of C-H...phenyl interactions to be estimated based on the geometry of the observed contact.

One final comparison to the experimental C-H...phenyl data is of interest here. Those contacts characterized as hydrogen bonds in the N-H...π(Ph) experimental group, a total of 11 interactions, can be compared with the contacts best described as C-H...π(Ph) hydrogen bonds from the C-H...phenyl experimental group.

Interaction	d(H(X)...C) (in Å)	$\rho_b(\mathbf{r})$ (in eÅ^{-3})	$\nabla^2\rho_b(\mathbf{r})$ (in eÅ^{-5})
N-H...π(Ph) [n = 11]	2.55 (0.10)	0.081 (0.015)	0.74 (0.14)
C-H...π(Ph) [n = 13]	2.89 (0.07)	0.048 (0.006)	0.41 (0.12)

The most obvious difference between the two groups is the larger mean value calculated for $\rho_b(\mathbf{r})$ in the case of the N-H...π(Ph) hydrogen bonds compared to the C-H...π(Ph) group. The C-H...π(Ph) hydrogen bonds are also characterized by a mean H...acceptor distance that is 0.34Å longer than the comparable mean distance of the N-H...π(Ph) group. This translates into topological parameters that are almost twice as large, on average, for the N-H group compared to the C-H group. The general relationship observed, that the C-H...π(Ph) hydrogen bonds are longer and weaker than their N-H...π(Ph) counterparts, is as expected. One question remains however, can more information be extracted from a comparison of the two groups? Most importantly, can it be shown that the C-H...π(Ph) hydrogen bonds behave topologically in a manner consistent with the N-H...π(Ph)

interactions? Since the experimental N-H...π(Ph) hydrogen bonds have already been proven to belong to the larger general population of all hydrogen bonds, including those formed to traditional acceptors, this would place the C-H...π(Ph) hydrogen bonds in the same group. For this to be true, the experimental C-H...π(Ph) and N-H...π(Ph) hydrogen bonds would have to have topological parameters that could be fit to a common function for the relationship between $\rho_b(\mathbf{r})$ and/or $\nabla^2\rho_b(\mathbf{r})$ versus the H...acceptor distance. The results of the graphical fittings are shown and discussed in the following section.

The first graphs plotted, Figure 132 (a) $\rho_b(\mathbf{r})$ versus d(H...A) and (b) $\nabla^2\rho_b(\mathbf{r})$ versus d(H...A), show the relationship between the topological parameters and the H...acceptor distance for all 41 experimental C-H...X interactions [X = N, open circles, n = 9 and X = phenyl, filled circles, n = 32]. The H...acceptor distance in both plots ranges from approximately 2.1Å to 3.1Å, while in each case the range of topological values covered is very narrow. Each set of data, (a) $\rho_b(\mathbf{r})$ versus d(H...A) and (b) $\nabla^2\rho_b(\mathbf{r})$ versus d(H...A), was fitted using three simple functions.

A linear model [y = a + b*x], a power model [y = a*(x)^b] and an exponential model [y = a*exp(b*x)] were applied to the C-H...X set of 41 experimental points. For the $\rho_b(\mathbf{r})$ versus d(H...A) data the linear (r^2 = 0.176, σ = 0.0079), the power (r^2 = 0.180, σ = 0.0079) and the exponential (r^2 = 0.177, σ = 0.0079) fits were all equally poor. Slightly worse statistics were obtained for the linear (r^2 = 0.156, σ = 0.109), power (r^2 = 0.157, σ = 0.109) and exponential (r^2 = 0.156, σ = 0.109) mcdels when fitted to the C-H...X $\nabla^2\rho_b(\mathbf{r})$ versus d(H...A) data. The plots are shown with none of the calculated fits applied since none of the functions model

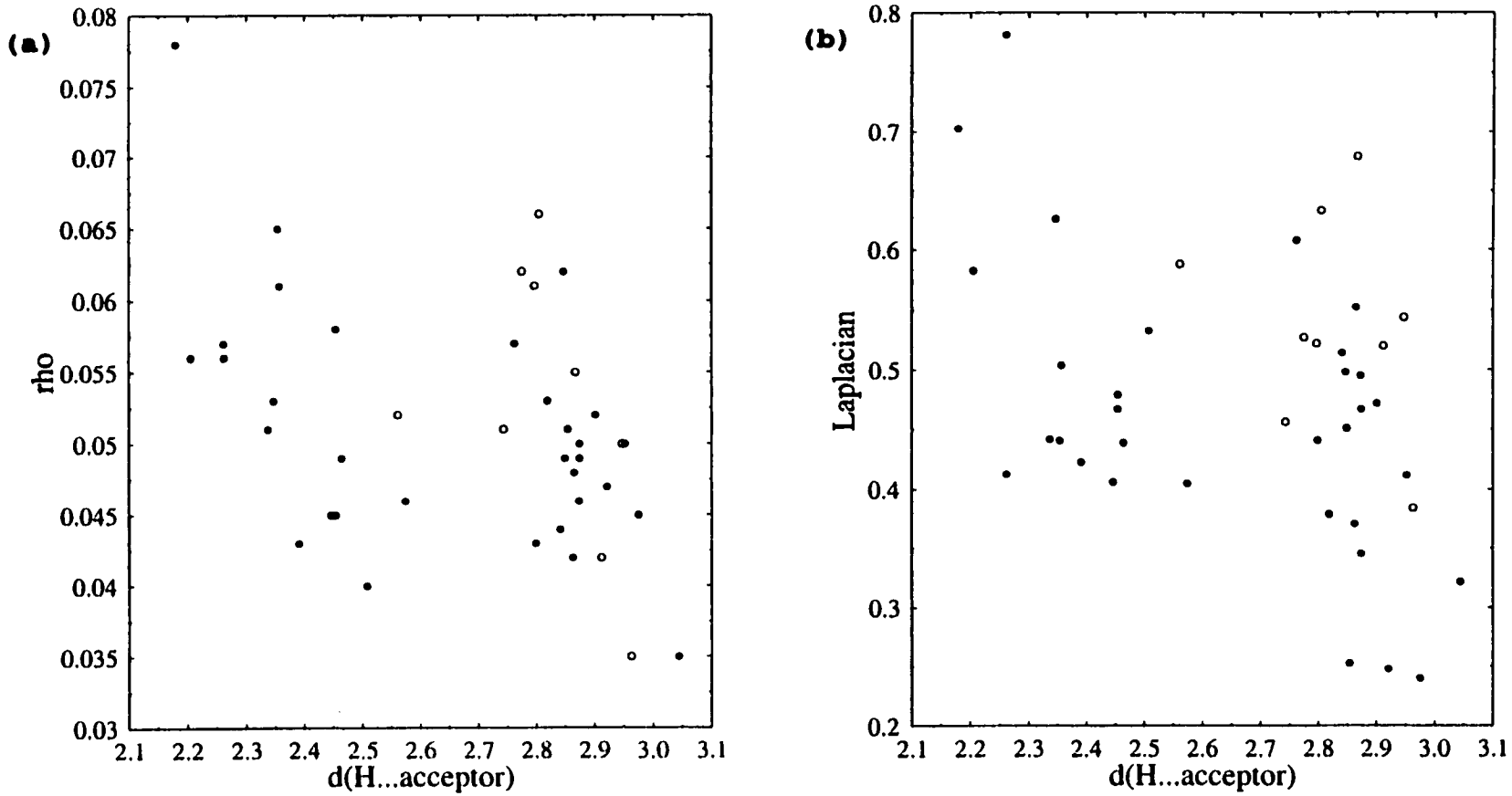

Figure 132. Topological data for the experimental C-H...X [X = N or phenyl] interactions studied. Plots of (a) $\rho_b(\mathbf{r})$ and (b) $\nabla^2\rho_b(\mathbf{r})$ versus d(H...A) are shown for the data only, with no fit applied. The C-H...N interactions are represented by open circles and the C-H...phenyl interactions by filled circles.

the data sets well. In fact, both plots are sufficiently bad that it is impossible to even determine if the distributions are generally linear or nonlinear in nature.

There are several possible explanations as to why the experimental C-H...X interactions cannot be well modelled by one simple function for the relationship between the topological parameters [$\rho_b(\mathbf{r})$ or $\nabla^2\rho_b(\mathbf{r})$] and d(H..A). In these interactions the H...acceptor distance is generally long, often close to 3Å, and they are characterized by correspondingly weak topological parameters. The experimental errors are relatively greater in proportion to these smaller topological parameters. In addition, the C-H...X interactions cover only a relatively narrow range of donor...acceptor distances, all long, and have very similar topological values. Most importantly, the C-H...X data sets contain no defining values; that is, at neither end of the distance range are there values that help to fit the model functions.

This is in contrast to the experimental N-H...X data set of this investigation, for example. The N-H...X group of interactions contains two N-H...N type hydrogen bonds that are considerably shorter and stronger (in topological terms) than the remaining N-H...π(Ph) hydrogen bonds. These two N-H...N hydrogen bonds, at short d(H...A) and large $\rho_b(\mathbf{r})/\nabla^2\rho_b(\mathbf{r})$, define one end of the experimental data distribution and make fitting a model function to the data much easier. Compared to the C-H...X data, the N-H...X data set fits both the power function (r^2 = 0.856, σ = 0.0152) and the exponential function (r^2 = 0.850, σ = 0.0155) equally well and better than the simple linear model (r^2 = 0.807, σ = 0.0176).

The C-H...X set contains no such defining values, which makes

fitting the relatively uniform data set more difficult and ultimately less successful. Of course, it must be remembered that what appears as appreciable scatter in these data sets and plots would be considered minor over the range covered by all hydrogen bonds. It is only because the data cover a narrow range with similar and weak topological parameters that the scatter appears to be magnified and the proper fit becomes more difficult to discern.

Visual examination of the plots in Figure 132 shows that there is no clear separation of the C-H...N (open circles) and C-H...phenyl (filled circles) derived data points in either graph. Both the C-H...N and the C-H...phenyl data are distributed over the range of H...acceptor distances although the C-H...N contacts are observed primarily at longer distances. The C-H...phenyl data points show a somewhat larger d(H...A) spread because of the inclusion of H...H type interactions in the group, the H...H contacts being characterized by short H...acceptor distances. The separation of the C-H...phenyl contacts into two broad groups, those with short H...acceptor [H...H] distances (H...H type contacts) and those with longer H...acceptor [H...C] distances (hydrogen bonds and intermediate contacts), visible in these graphs will become even more apparent in subsequent plots.

Attempts were made to fit the experimental C-H...N (n = 9) and C-H...phenyl (n = 32) data separately to the simple model functions chosen, for both $\rho_b(\mathbf{r})$ versus d(H...A) and $\nabla^2\rho_b(\mathbf{r})$ versus d(H...A). The individual C-H...N and C-H...phenyl plots with the fitted curves included are not shown here since none of the model functions accommodated the experimental data well. For the C-H...N (n = 9) subset of the original

C-H...X data, the $\rho_b(\mathbf{r})$ versus d(H...A) relationship [Figure 133(a)] was not successfully modelled using a linear fit (r^2 = 0.189, σ = 0.0095), a power fit (r^2 = 0.152, σ = 0.0097) or an exponential fit (r^2 = 0.166, σ = 0.0096). For the $\nabla^2\rho_b(\mathbf{r})$ versus d(H..A) data [Figure 133(b)] the models chosen were even less adequate and were all equally poor (linear fit, r^2 = 0.0716, σ = 0.0911; power fit, r^2 = 0.0662, σ = 0.0914; exponential fit, r^2 = 0.0690, σ = 0.0912). Again, the distances cover a very narrow range of values, with d(H...N) falling between roughly 2.5Å and 3.0Å. This is a partial explanation for the poor fits obtained in the plots of both $\rho_b(\mathbf{r})$ and $\nabla^2\rho_b(\mathbf{r})$ versus d(H...N). However, the nature of the experimental C-H...N interactions remains ambiguous at best. As discussed previously, these interactions do not behave as expected for hydrogen bonds and they may, in fact, just be incidental contacts formed in consequence of other stronger interactions occurring in the structures.

The C-H...phenyl subset of the original C-H...X data covers H...acceptor distances ranging from roughly 2.1Å to 3.1Å, considerably wider than the C-H...N data spread. The fits applied to the C-H...phenyl data are correspondingly better but overall they are still very poor. Although the C-H...phenyl data set covers a wider range of distances it still suffers from a lack of defining values at either end of the distribution. The 32 C-H...phenyl data points do not fit a linear model (r^2 = 0.250, σ = 0.0073), a power model (r^2 = 0.266, σ = 0.0073) or an exponential model (r^2 = 0.256, σ = 0.0073) for the relationship between $\rho_b(\mathbf{r})$ and d(H...A) [Figure 134(a)]. The $\nabla^2\rho_b(\mathbf{r})$ versus d(H...A) data [Figure 134(b)] fit the same simple model functions almost as poorly (linear, r^2 = 0.299, σ = 0.102; power, r^2 = 0.307, σ = 0.101; exponential,

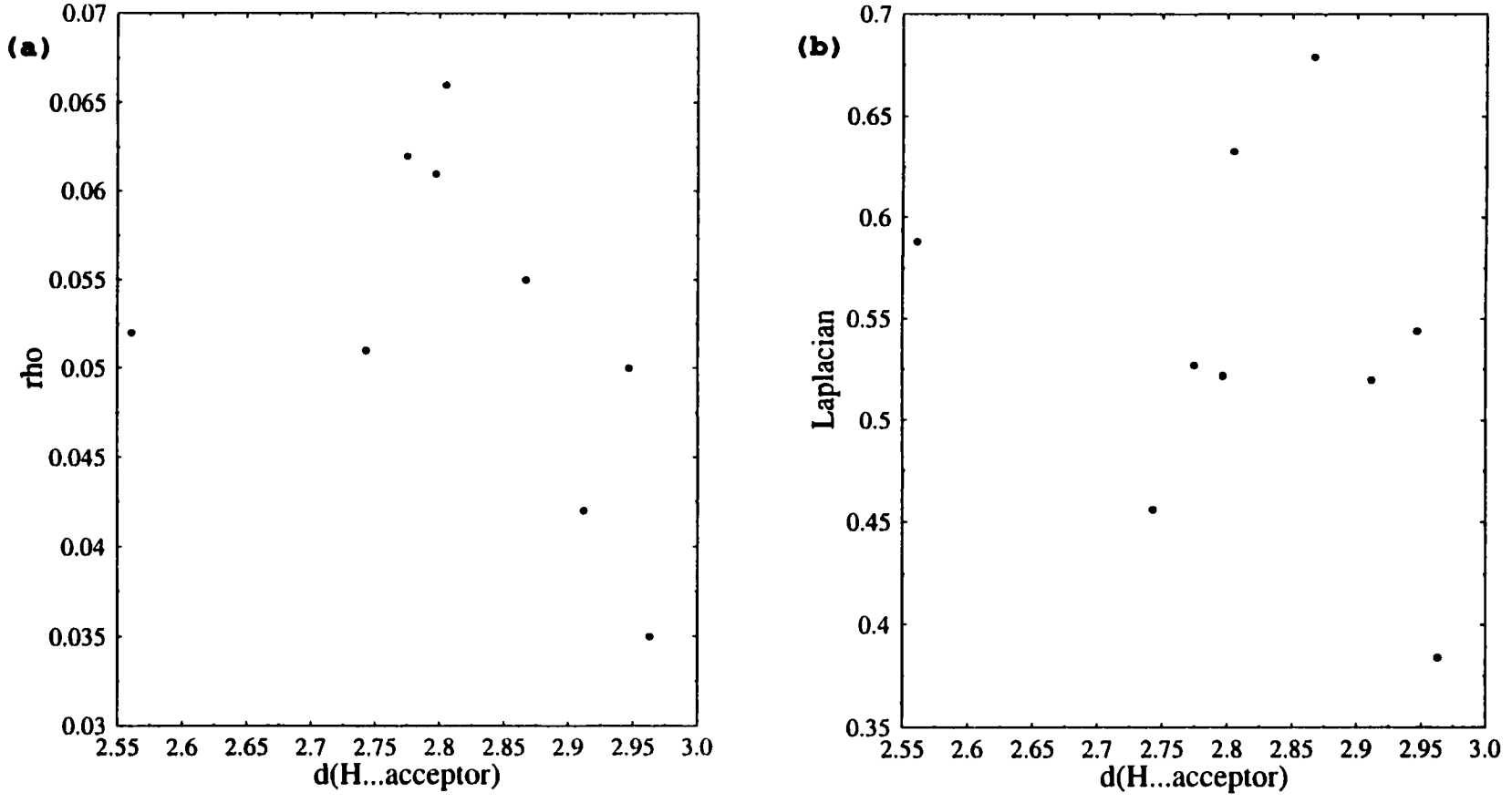

Figure 133. Topological data for the experimental C-H...N interactions. Plots of (a) $\rho_b(\mathbf{r})$ and (b) $\nabla^2\rho_b(\mathbf{r})$ versus d(H...A) are shown for the data only, with no fit applied.

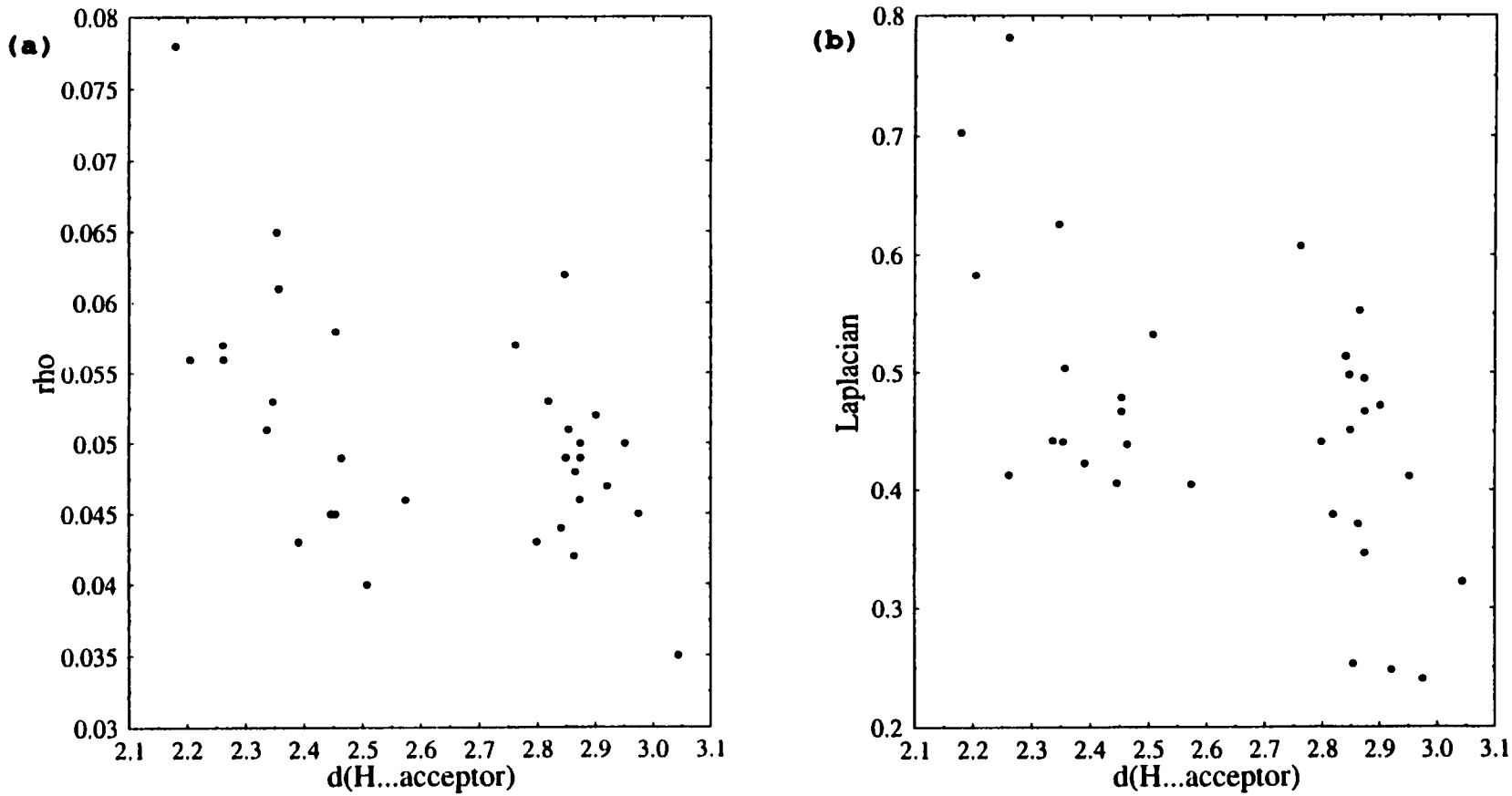

Figure 134. Topological data for the experimental C-H...phenyl interactions. Plots of (a) $\rho_b(\mathbf{r})$ and (b) $\nabla^2\rho_b(\mathbf{r})$ versus d(H...A) are shown for the data only, with no fit applied.

$r^2 = 0.303$, $\sigma = 0.102$).

The C-H...phenyl data set is slightly better fit by all the model functions, for both $\rho_b(\mathbf{r})$ versus d(H...A) and $\nabla^2\rho_b(\mathbf{r})$ versus d(H...A), than the C-H...N data or the overall C-H...X data set. However, none of the data [C-H...phenyl, C-H...N or C-H...X] are modelled well by any of the simple model functions chosen. As already discussed, the relatively narrow range of distances, the weakness of the interactions and the lack of defining values magnifies the experimental scatter and makes fitting difficult.

There has been one other investigation of crystallographically derived topological parameters for a series of C-H...X type interactions published in the recent literature. Mallinson et al.[22] studied seven weak C-H...O hydrogen bonds occurring in the protonated "proton sponge" salt, 1,8-bis(dimethylammonium)naphthalene 1,2-dichlorohydrogenmaleate. The topological parameters, $\rho_b(\mathbf{r})$ and $\nabla^2\rho_b(\mathbf{r})$, derived from combined x-ray and neutron crystallographic data, were fitted to a simple linear model for their relationship with d(H...O).

$$\rho_b(\mathbf{r}) = 0.37(4) - 0.13(2)*d \quad r = -0.97$$

$$\nabla^2\rho_b(\mathbf{r}) = 6.5(6) - 2.2(2)*d \quad r = -0.97$$

In both cases, the data fit the linear model chosen by the authors with good agreement. This is unlike the present experimental C-H...X results which do not fit a linear, power or exponential model for either the $\rho_b(\mathbf{r})$ versus d(H...A) or the $\nabla^2\rho_b(\mathbf{r})$ versus d(H...A) relationship. The Mallinson set of C-H...O contacts is more homogeneous than the current C-H...X [X = N or phenyl] data but other than that it is not certain why the former

shows considerably less scatter than the latter. However, it must be remembered that the linear models chosen by Mallinson et al. likely do not reflect the true relationship for either $\rho_b(\mathbf{r})$ versus d(H...A) or $\nabla^2\rho_b(\mathbf{r})$ versus d(H...A). As already discussed, in both cases the topological parameter is not linearly related to the donor...acceptor distance, although it may appear so over a limited range of distances. Instead, the relationships should conform to nonlinear functions that display asymptotic behaviour as the H...acceptor distance increases to infinity. Either a power or an exponential curve may be the better model.

If the C-H...phenyl plots of Figure 134 (a) $\rho_b(\mathbf{r})$ versus d(H...A) and (b) $\nabla^2\rho_b(\mathbf{r})$ versus d(H...A) are examined, it is obvious that the data fall into two broad groups. The first group encompasses the shorter d(H...A) distances, roughly 2.1Å to 2.6Å, and the other involves the longer d(H...A) distances, roughly 2.7Å to 3.1Å. However, the topological parameters in each plot cover a relatively narrow range of values over all distances. Why does the C-H...phenyl data segregate in this way when the topological parameters are plotted versus the H...acceptor distance? How does this separation in the C-H...phenyl data set arise?

In an attempt to answer these questions, the C-H...phenyl data set (n = 32) was first subdivided according to the origin of each interaction [cation/anion, n = 8, open circles; anion/anion, n = 22, filled circles; solvent/anion, n = 2, open squares]. The entire C-H...phenyl data set was then replotted, as shown in Figure 135 (a) $\rho_b(\mathbf{r})$ versus d(H...A) and (b) $\nabla^2\rho_b(\mathbf{r})$ versus d(H...A), to highlight the distribution of the various contacts based on their origin. The fits made to the entire C-H...phenyl data set for both $\rho_b(\mathbf{r})$ versus d(H...A) and $\nabla^2\rho_b(\mathbf{r})$ versus d(H..A) were all

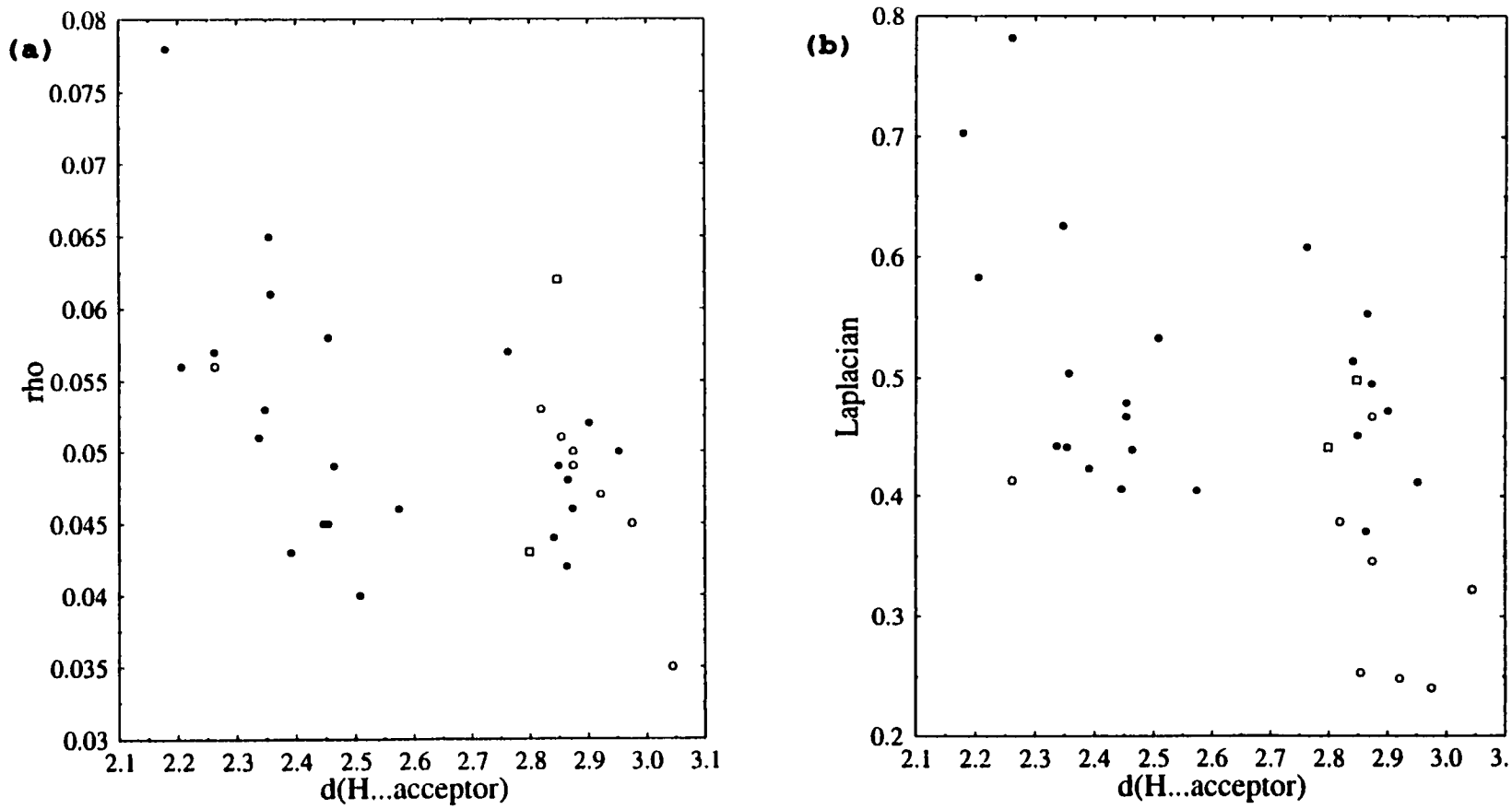

Figure 135. Topological data for the experimental C-H...phenyl interactions subdivided according to the origin of the interaction, cation/anion type open circles, anion/anion type filled circles and solvent/anion type open squares. Plots of (a) $\rho_c(\mathbf{r})$ and (b) $\nabla^2\rho_c(\mathbf{r})$ versus d(H...A) are shown for the data only, with no fit applied.

poor as already discussed, so the plots are shown with no model functions included.

It is clear from the plots of Figure 135 that the origin of the interactions [c/a, a/a or s/a] is not the primary cause of the segregation observed in the C-H...phenyl data. Although there are some differences observed in the distributions of the three types of interactions [c/a, a/a or s/a] they do not exactly coincide with the separation evident in the plots. For example, most cation/anion and all the solvent/anion contacts fall into the broad group having longer d(H...A) distances but there are also cation/anion interactions which occur at shorter distances. Conversely, the shorter contacts are almost all of the anion/anion variety but again there are also longer anion/anion type interactions. In fact, eight anion/anion contacts fall in the group with longer H...acceptor distances while 14 anion/anion contacts are included in the group with shorter d(H...A) values. A division based on the origin (or the overall charge) of the interacting groups does not explain the observed segregation of the experimental C-H...phenyl data.

In consequence, the complete C-H...phenyl data set was then subdivided according to the geometries/bond paths of the individual interactions. Again, a total of three new subgroups were obtained [hydrogen bonds, n = 13, open circles; intermediate contacts, n = 4, open squares; H...H contacts, n = 15, filled circles]. Plots of the C-H...phenyl data subdivided in this way are shown in Figure 136 for (a) $\rho_b(\mathbf{r})$ versus d(H...A) and (b) $\nabla^2\rho_b(\mathbf{r})$ versus d(H...A). No model functions are included since none fit the data well.

The plots of Figure 136 clearly illustrate why and how the

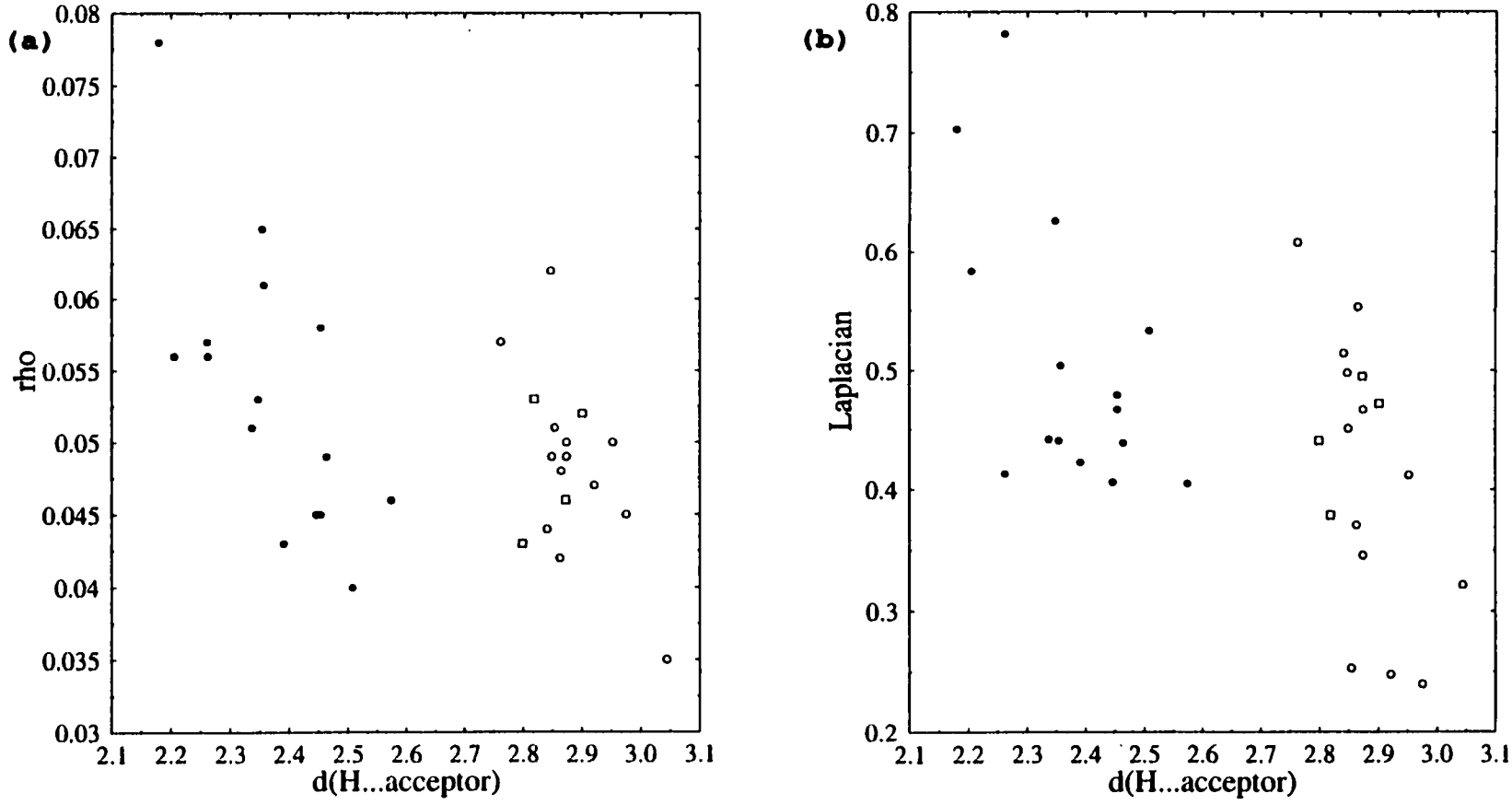

Figure 136. Topological data for the experimental C-H...phenyl interactions subdivided according to the bond path/geometry of the interaction, hydrogen bonds open circles, H...H type contacts filled circles and intermediate type contacts open squares. Plots of (a) $\rho_b(\mathbf{r})$ and (b) $\nabla^2\rho_b(\mathbf{r})$ versus d(H...A) are shown for the data only, with no fit applied.

segregation of the C-H...phenyl data arises. It can be explained by considering the geometries/bond paths of the individual interactions included in the overall C-H...phenyl group. Those contacts falling into the group with shorter H...acceptor distances, from roughly 2.1Å to 2.6Å, are all H...H type contacts. The group of contacts with longer H...acceptor distances, roughly 2.7Å to 3.1Å, are all hydrogen bonds or intermediate contacts. Both groups [long and short d(H...A)], however, cover approximately the same range of topological values for both $\rho_b(\mathbf{r})$ and $\nabla^2\rho_b(\mathbf{r})$. This gives a broad band of data spread across each of the plots shown, segregated into two rough groups based on distance. The mean $\rho_b(\mathbf{r})$ and $\nabla^2\rho_b(\mathbf{r})$ values appear to be similar for the group of H...H contacts (small d) and for the hydrogen bonds/intermediate contacts (large d).

The segregation of the C-H...phenyl data into these two groups of course occurs because of the way the contacts have been defined. In the H...H type contacts, the shortest distance (and the bond path) between the interacting groups is always between two close hydrogen atoms and is necessarily short, explaining the short H...acceptor distances observed. In those interactions classified as hydrogen bonds or intermediate contacts the bond path characterizing the interaction is from the hydrogen donor atom to a carbon atom of the adjacent phenyl ring and there are usually no shorter H...H distances formed in the interaction (intermediate contacts are sometimes the exception). The $H...C_{ring}$ distances characteristic of the hydrogen bonds and intermediate contacts are necessarily longer for reasons of geometry and these comprise the longer d(H...A) group seen in the plots.

The division observed in the C-H...phenyl data is perhaps

artificial, arising from the way the interactions have been defined, based on geometries/bond paths. However, the relationship between topological parameters and the geometry of interactions (particularly the H...acceptor distance for hydrogen bonds) has been investigated extensively in both theoretically and crystallographically based studies by various groups, as has previously been discussed. It appears to be a legitimate way to classify the experimental C-H...phenyl data and the results truly do reflect a fundamental difference between the two basic groups of interactions studied, H...H contacts versus hydrogen bonds. The plots of the C-H..phenyl data illustrate a difference that really does exist between the two groups. A different distance could have been used to define the H...H type contacts, for example the minimum H...C_{ring} distance could have been used to be consistent with the other types of interactions studied. But the H...H type interactions would still behave differently from the others. In the given example they would be defined by longer H...C_{ring} distances than the other interactions and the plots would still segregate into two broad groups based on distance.

The H...H contacts, as they have been defined for this investigation, are characterized by shorter H...acceptor distances than the hydrogen bonds but have topological parameters [$\rho_b(\mathbf{r})$ and $\nabla^2\rho_b(\mathbf{r})$] that are similar to the longer contacts. This suggests that the strength of the H...H contacts falls off more quickly with increasing distance than does the strength of hydrogen bonds. The H...H contacts likely are (or are closely related to) van der Waals contacts and are quite different from hydrogen bonds in both their geometries and topological parameters.

In the plots shown in Figure 136 it is clear that the intermediate

contacts fall with the hydrogen bonds rather than with the H...H contacts. This observation is consistent with the results of the statistical analysis which also suggested that intermediate contacts are more similar geometrically and topologically to hydrogen bonds than to H...H contacts. Both hydrogen bonds and intermediate contacts are characterized by H...C_{ring} distances rather than by minimum H...H_{ring} distances, explaining why they are grouped together in the plots and why they have similar topological properties.

The simple model functions chosen for this investigation were fitted to the geometric subgroups of the experimental C-H...phenyl data for both $\rho_b(\mathbf{r})$ versus d(H...A) and $\nabla^2\rho_b(\mathbf{r})$ versus d(H...A). The hydrogen bond data (n = 13) and that for the H...H contacts (n = 22) were fitted to linear, power and exponential functions but the intermediate group of contacts (n = 4) did not contain enough values for such an analysis.

For those interactions having hydrogen bond type geometries, the $\rho_b(\mathbf{r})$ versus d(H...A) relationship was modelled equally poorly by a linear (r^2 = 0.436, σ = 0.0052), power (r^2 = 0.425, σ = 0.0052) or exponential (r^2 = 0.427, σ = 0.0052) function. The H...H type contacts fit the same functions somewhat better [linear, r^2 = 0.495, σ = 0.0072; power, r^2 = 0.511, σ = 0.0071; exponential, r^2 = 0.507; σ = 0.0072] but still they are all equally poor overall. The fits are actually slightly better for the individual geometry types than they are for the entire set of C-H...phenyl data. However, neither the H...H contacts nor the hydrogen bonds are well modelled by any of the functions chosen. Again, a narrow range of H...acceptor distances and a correspondingly small range of topological parameters makes fitting the data difficult.

The $\nabla^2\rho_b(\mathbf{r})$ versus d(H...A) data are also modelled poorly by the functions chosen. The hydrogen bond subgroup of the original C-H...phenyl data fit the linear [r^2 = 0.402, σ = 0.0979], power [r^2 = 0.438, σ = 0.0949] and exponential [r^2 = 0.438, σ = 0.0948] functions slightly better than the H...H group of contacts [linear, r^2 = 0.350, σ = 0.0966; power, r^2 = 0.373, σ = 0.0949; exponential, r^2 = 0.368, σ = 0.0953]. This is opposite to what was observed for the $\rho_b(\mathbf{r})$ versus d(H...A) data but is likely unimportant considering all the fits are so poor. Overall, the $\nabla^2\rho_b(\mathbf{r})$ fits are slightly worse than the $\rho_b(\mathbf{r})$ fits for both the hydrogen bonds and the H...H contacts. Like the $\rho_b(\mathbf{r})$ versus d(H...A) fits, the individual geometry types are modelled better than the entire set of C-H...phenyl data, likely because they are more homogeneous. However, the fits are not good to any of the simple functions chosen; all are equally poor models of the true relationship.

Part of the problem in fitting the experimental C-H...phenyl data to any of the chosen model functions arose because of the narrow range of distances covered and the lack of defining values in the data set. In an attempt to minimize these problems the complete C-H...X [X = N or phenyl] data set (n = 41) was combined with the experimental N-H...X data (n = 14). The N-H...X set of interactions contains two short and strong N-H...N hydrogen bonds that extend the range of distances and topological parameters covered. It has already been shown that the experimental N-H...X data can be successfully modelled using simple nonlinear models for both $\rho_b(\mathbf{r})$ and $\nabla^2\rho_b(\mathbf{r})$ versus d(H...A). It was hoped that the C-H...X data might be better modelled when combined with the N-H...X data, and more specifically that the combined data set of interactions could be fit

to one single model function for $\rho_b(\mathbf{r})/\nabla^2\rho_b(\mathbf{r})$ versus d(H...A).

Plots of the combined N-H...X (n = 14, filled circles) and C-H...X (n = 41, open circles) data set are shown in Figure 137 for (a) $\rho_b(\mathbf{r})$ versus d(H...A) and (b) $\nabla^2\rho_b(\mathbf{r})$ versus d(H...A). Again, both are shown with no model curves included since none of the applied functions fit the data well. For the $\rho_b(\mathbf{r})$ versus d(H...A) plot of the combined N-H...X and C-H...X data, the linear fit [r^2 = 0.296, σ = 0.0230] was slightly worse than either the power fit [r^2 = 0.353, σ = 0.0220] or the exponential fit [r^2 = 0.332, σ = 0.0224]. The $\nabla^2\rho_b(\mathbf{r})$ versus d(H...A) data also fit the nonlinear functions slightly better [linear, r^2 = 0.328, σ = 0.210; power, r^2 = 0.385, σ = 0.201; exponential, r^2 = 0.365, σ = 0.204]. Overall, the $\nabla^2\rho_b(\mathbf{r})$ versus d(H...A) data fit the chosen models slightly better than the $\rho_b(\mathbf{r})$ versus d(H...A) data. When the N-H...X and C-H...X data are combined, both topological parameters appear to vary in a non-linear fashion, which has yet to be clearly defined, with the H...acceptor distance. Still, the complete set of combined data does not fit any of the model functions well for the relationship between $\rho_b(\mathbf{r})$ or $\nabla^2\rho_b(\mathbf{r})$ and d(H...A).

If the plots of the combined N-H...X and C-H...X data set (Figure 137) are scrutinized, several features are immediately apparent. In general, the N-H...X interactions have larger topological parameters than the C-H...X interactions. Surprisingly, the C-H...X interactions cover a wider range of distances but all have relatively weak and quite constant topological parameters. There are no defining values in the C-H...X group, unlike the N-H...X group in which the two N-H...N hydrogen bonds are considerably shorter and stronger than any other members of the group. The C-H...X interactions of all types form a relatively diffuse

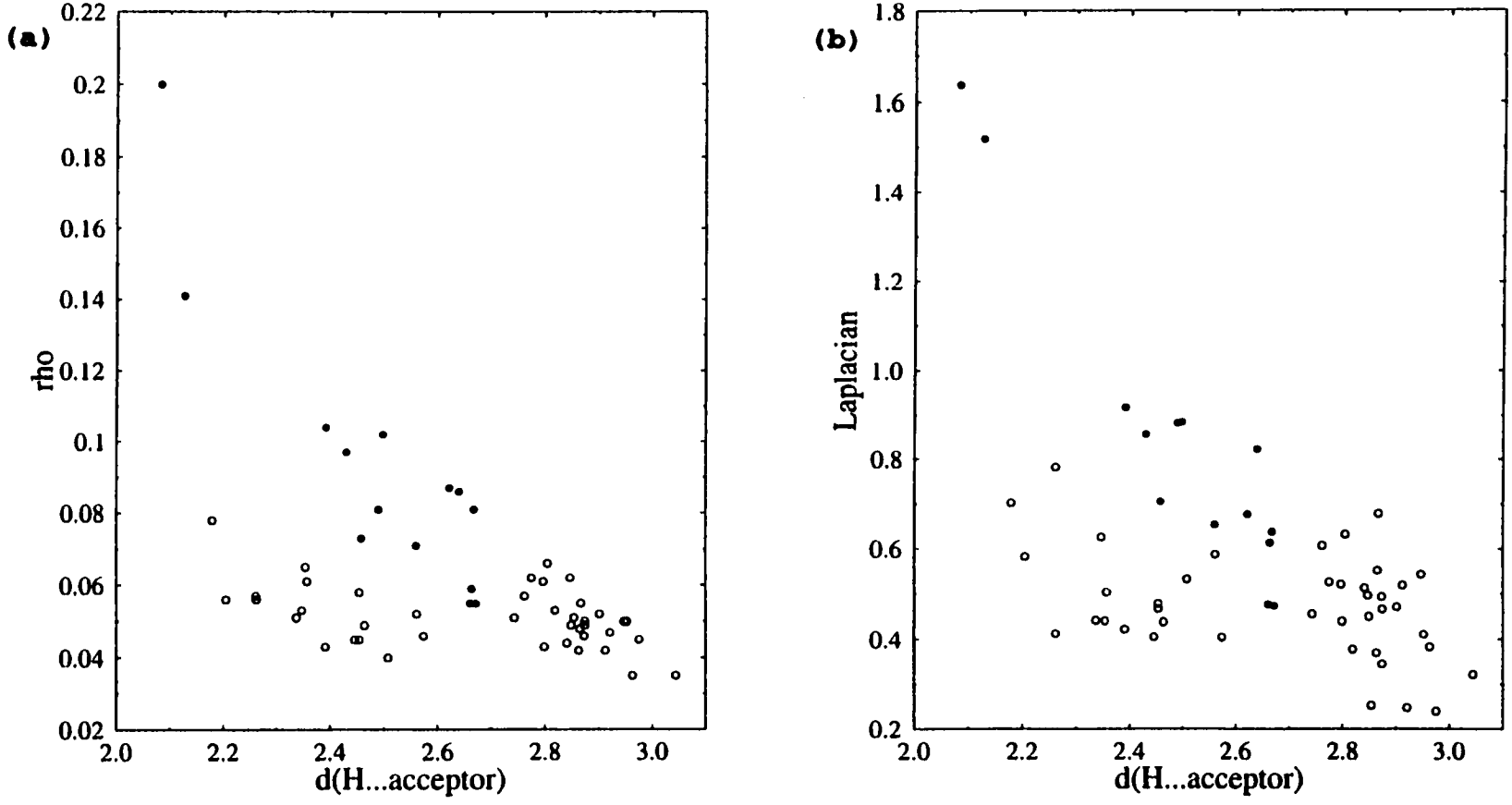

Figure 137. Topological data for the combined experimental N-H...X [X = N or π(Ph)] hydrogen bonds (filled circles) and C-H...phenyl interactions (open circles). Plots of (a) $\rho_b(\mathbf{r})$ and (b) $\nabla^2\rho_b(\mathbf{r})$ versus d(H...A) are shown for the data only, with no fit applied, for the set of all experimental data points.

band across the lower region of each plot. As noted earlier, they fall into two broad groups, the H...H contacts which occur at relatively short distances, and the hydrogen bonds and intermediate contacts that occur at longer distances.

In Figure 137 (a), $\rho_b(\mathbf{r})$ versus d(H...A) for the combined data set, the short C-H...X interactions [the H...H contacts] fall as a group directly below the N-H...X interactions of similar distance. In other words, for the $\rho_b(\mathbf{r})$ versus d(H...A) data the C-H...X interactions, specifically the H...H contacts, are weaker than the N-H...X contacts occurring with the same H...acceptor separation. The distribution of the combined data in the $\nabla^2\rho_b(\mathbf{r})$ versus d(H...A) plot [Figure 137(b)] is slightly different. The N-H...N data lie at shorter distances and considerably larger $\nabla^2\rho_b(\mathbf{r})$ values than any other of the experimental points, just as was observed in the $\rho_b(\mathbf{r})$ case. However, the remaining N-H...X data lie at only slightly higher average $\nabla^2\rho_b(\mathbf{r})$ values than the C-H...X data. In fact, the N-H...π(Ph) data lie generally interspersed with the C-H...X data. The N-H...π(Ph) interactions occur at the intermediate distances covered by the plot, longer than the majority of the H...H contacts but generally shorter than the remainder of the C-H...phenyl data. In both plots, the C-H...X interactions, specifically the H...H type contacts, do not appear to share a discernable common relationship with the N-H...X group.

Observation of the graphs plotted with the combined N-H...X and C-H...X data set (Figure 137) did however suggest a logical next step for this phase of the investigation. The N-H...X type contacts had been determined overwhelmingly to be hydrogen bonds when classified according

to bond path/geometry (13 hydrogen bonds and 1 intermediate contact). And, as just mentioned, their topological parameters could be reasonably well fit to simple, nonlinear model functions for the relationship with the H...acceptor distance. The C-H...X interactions as a group are far less homogeneous, comprising nine C-H...N interactions of somewhat uncertain nature and 32 C-H...phenyl interactions, only 13 of which were actually classified as hydrogen bonds. When the C-H...phenyl data set was plotted [for either $\rho_b(\mathbf{r})$ or $\nabla^2\rho_b(\mathbf{r})$], it clearly fell into two broad groups based on the H...acceptor distance, short d(H...A) involving only H...H type contacts and longer d(H...A) involving both the hydrogen bonds and the intermediate contacts. The short C-H...X interactions (H...H contacts) clearly hindered fitting the combined N-H...X and C-H...X data set to a single model function. The plots did suggest that the N-H...X data and the C-H...X interactions occurring with longer H...acceptor distances might share a common relationship for both $\rho_b(\mathbf{r})$ and $\nabla^2\rho_b(\mathbf{r})$ versus d(H...A). It seemed logical to graph the complete set of N-H...X data (n = 14) with the C-H...X interactions identified unambiguously as hydrogen bonds (n = 13), 27 points in total. The C-H...N contacts were excluded from the plots because their exact nature was not well defined. If this new combined data set of N-H...X and C-H...π(Ph) hydrogen bonds could be successfully modelled by a single function for $\rho_b(\mathbf{r})/\nabla^2\rho_b(\mathbf{r})$ versus d(H....A), it would demonstrate that all the interactions belong to the same population, with common relationships between geometry and topological parameters. It would also validate the classification of all interactions based on geometry using criteria such as those developed in this investigation.

Figure 138 (a) and (b) shows the combined hydrogen bond data set

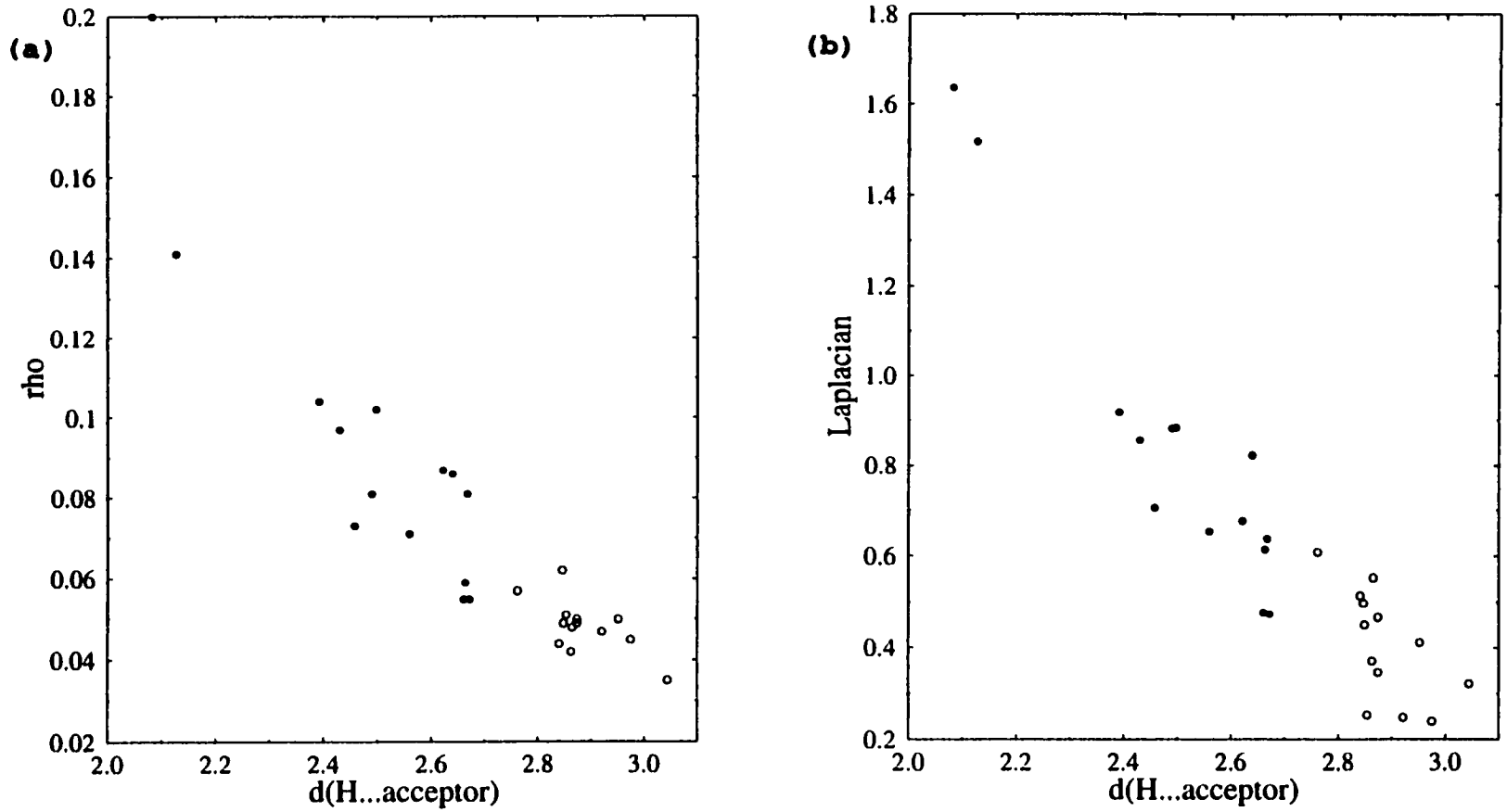

Figure 138. Topological data for the combined experimental N-H...X [X = N or π(Ph)] hydrogen bonds (filled circles) and C-H...π(Ph) hydrogen bonds (open circles). Plots of (a) $\rho_b(\mathbf{r})$ and (b) $\nabla^2\rho_b(\mathbf{r})$ versus d(H...A) are shown for the data only, with no fit applied, for the set containing only those interactions determined to be hydrogen bonds.

for $\rho_b(\mathbf{r})$ versus d(H...A) and $\nabla^2\rho_b(\mathbf{r})$ versus d(H...A), respectively. In both plots, the N-H...X data points (n = 14) are represented by the filled circles while the C-H...π(Ph) data points (n = 13) are represented by the open circles. The plots shown in Figure 138 include only data, with no fit applied, to emphasize the distribution. The graphs do suggest a common relationship for the combined hydrogen bond data set for both $\rho_b(\mathbf{r})$ versus d(H...A) and $\nabla^2\rho_b(\mathbf{r})$ versus d(H...A). Visual observation suggests that in each case the entire data set can be fit by one, simple, nonlinear model function. The plots suggest that the longer, weaker C-H...π(Ph) hydrogen bonds and the shorter, stronger N-H...X hydrogen bonds do come from the same population.

To prove the same point more quantitatively, the $\rho_b(\mathbf{r})$ versus d(H...A) values for the combined hydrogen bond data set were fitted to the same three model functions used previously. The results obtained are summarized below.

linear	$\rho_b(\mathbf{r})$ = 0.424 - 0.131*d	r^2 = 0.823	σ = 0.0152
power	$\rho_b(\mathbf{r})$ = 3.418*d^(-4.021)	r^2 = 0.906	σ = 0.0111
exponential	$\rho_b(\mathbf{r})$ = 5.306*exp(-1.639*d)	r^2 = 0.901	σ = 0.0114

The power and exponential functions model the distribution of the combined experimental hydrogen bond data for $\rho_b(\mathbf{r})$ versus d(H...A) better than the linear function. The former two fits are reasonably good and relatively equal in their ability to model the data. In fact, the combined set of N-H...X and C-H...π(Ph) hydrogen bonds have $\rho_b(\mathbf{r})$ values that vary more consistently with the H...acceptor distance than either of the individual groups alone. The combined data set fits the simple nonlinear

model functions better than the N-H...X data alone. The improvement is reasonable considering that the number of values being considered has doubled and that the range of H...acceptor distances has been considerably extended.

To be consistent with the previous N-H...X hydrogen bond analysis, the calculated exponential curve is shown with the $\rho_b(\mathbf{r})$ versus d(H...A) data in Figure 139 (a); the power fit would be an equally good choice. Both the distribution of the data and the fit statistics to the three model functions suggest that there is a definite relationship between $\rho_b(\mathbf{r})$ and d(H...A) for all the experimental hydrogen bonds and that this relationship is not a linear one. Whether the relationship is better represented by a power or exponential function is, however, impossible to discern.

Similar results were obtained when the $\nabla^2\rho_b(\mathbf{r})$ versus d(H...A) data for the combined C-H...π(Ph) and N-H...X hydrogen bonds were fitted to the model functions.

linear	$\nabla^2\rho_b(\mathbf{r}) = 4.104 - 1.294*d$	$r^2 = 0.874$	$\sigma = 0.123$
power	$\nabla^2\rho_b(\mathbf{r}) = 36.89*d\hat{}(-4.226)$	$r^2 = 0.921$	$\sigma = 0.0970$
exponential	$\nabla^2\rho_b(\mathbf{r}) = 60.18*\exp(-1.733*d)$	$r^2 = 0.924$	$\sigma = 0.0950$

Like the $\rho_b(\mathbf{r})$ versus d(H...A) data, all models fit reasonably well but the power and exponential functions are better than the linear function. Again, this suggests a nonlinear relationship exists between $\nabla^2\rho_b(\mathbf{r})$ and d(H...A) even though the correct model function is not yet known. The combined N-H and C-H hydrogen bond data set, with the calculated exponential curve included, is shown in Figure 139 (b) for the $\nabla^2\rho_b(\mathbf{r})$

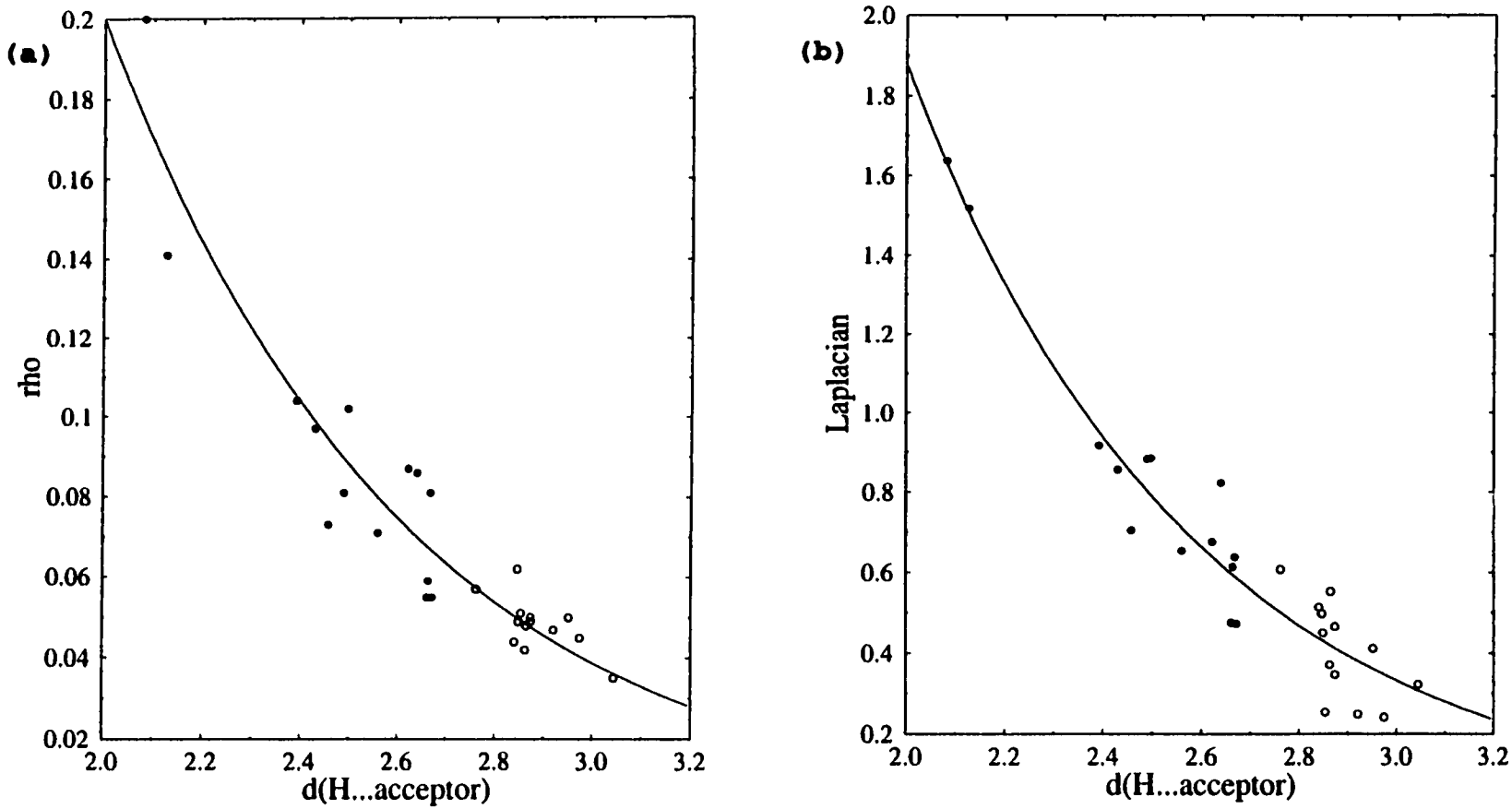

Figure 139. Topological data for the combined experimental N-H...X [X = N or π(Ph)] hydrogen bonds (filled circles) and C-H...π(Ph) hydrogen bonds (open circles). Plots of (a) $\rho_b(\mathbf{r})$ and (b) $\nabla^2\rho_b(\mathbf{r})$ versus d(H...A) are shown with a fitted exponential curve included, for the set containing only those interactions determined to be hydrogen bonds.

versus d(H...A) data.

All of the model fits are somewhat better for the $\nabla^2\rho_b(\mathbf{r})$ versus d(H...A) data than they are for the $\rho_b(\mathbf{r})$ versus d(H...A) data but the difference is slight and may in fact be statistically insignificant. In the case of the $\nabla^2\rho_b(\mathbf{r})$ versus d(H...A) data, the combined group of C-H...π(Ph) and N-H...X hydrogen bonds fit the model functions with statistics similar to the N-H...X interactions alone; the exponential equations in particular are almost identical. Of course, the combined data set fits the model functions significantly better than the C-H...π(Ph) interactions alone. Overall, the $\nabla^2\rho_b(\mathbf{r})$ versus d(H...A) data for the combined experimental N-H...X and C-H...π(Ph) hydrogen bonds can be successfully modelled using one simple, nonlinear model function.

What can be concluded from the results obtained by combining the N-H...X and C-H...X interactions characterized in this investigation? From the graphs plotted for both $\rho_b(\mathbf{r})$ versus d(H...A) and $\nabla^2\rho_b(\mathbf{r})$ versus d(H...A) it appears that the C-H...π(Ph) hydrogen bonds (but not all of the C-H...phenyl contacts) belong to the same population as the N-H...X hydrogen bonds. In both cases [$\rho_b(\mathbf{r})$ versus d(H...A) and $\nabla^2\rho_b(\mathbf{r})$ versus d(H...A)] the combined C-H...π(Ph) and N-H...X experimental hydrogen bond data can be modelled very well by one simple, nonlinear model function. In both cases, power and exponential functions fit the combined data set equally well; the exponential curves are shown only for consistency with the previous results discussed, in particular for comparison to the literature.

The C-H...π(Ph) hydrogen bonds behave topologically like the other N-H...X type hydrogen bonds studied in this work. For a given donor

H...acceptor distance consistent and predictable topological parameters [$\rho_b(\mathbf{r})$ and $\nabla^2\rho_b(\mathbf{r})$] are observed. In the previous section, the experimental N-H...π(Ph) hydrogen bonds were shown to belong to a more general population of hydrogen bonds from the literature; assembled by Espinosa et al.[125] the comparison group contained a large number of X'-H...O type hydrogen bonds [X' = N, C or O] all formed to the "traditional" acceptor oxygen. Taken together, it appears that both N-H...π(Ph) hydrogen bonds and the even weaker (generally) C-H...π(Ph) hydrogen bonds behave topologically like all other hydrogen bonds. They are legitimate hydrogen bonds with predictable geometries and topological parameters, consistent with all others.

Not all of the C-H...phenyl interactions studied, however, behaved topologically in a fashion consistent with hydrogen bonds. In fact, a large number of the contacts investigated (the so-called H...H contacts) were found to behave predictably but differently from the other C-H...phenyl interactions (the hydrogen bonds and the intermediate contacts). All of the experimental C-H...phenyl contacts were found to have topological parameters of similar strengths but the H...H contacts were characterized by considerably shorter donor...acceptor distances than the C-H...π(Ph) hydrogen bonds. The strength of the H...H contacts falls off more quickly with increasing distance, suggesting that they are, in fact, more similar to van der Waals contacts than to hydrogen bonds, as was suggested by other of their features as well.

The ability to identify and differentiate C-H...π(Ph) hydrogen bonds from other C-H...phenyl contacts helps to strengthen the argument that C-H...π(Ph) hydrogen bonds really do behave topologically like other

hydrogen bonds. The fact that C-H...π(Ph) hydrogen bonds can be differentiated from the other C-H...phenyl contacts on the basis of their geometries and topological parameters also shows the value of the criteria that have been developed to characterize such interactions in this investigation. The geometry of an interaction can be used to predict its bond path and topological properties as well as to classify it according to type. Interactions identified as hydrogen bonds will have geometries and topological parameters quite different from other types of contacts. Topologically those interactions identified as hydrogen bonds will have $\rho_b(\mathbf{r})$ and $\nabla^2\rho_b(\mathbf{r})$ values that obey the same relationship versus the H...acceptor distance as all other hydrogen bonds.

3.6.3.5. Summary

In this work a total of 60 interactions, 16 N-H...X and 44 C-H...X [X = N or phenyl], were investigated and characterized topologically by location of a unique (3,-1) type bond critical point and an associated, rational bond path. In every interaction studied, the electron density at the bond critical point [$\rho_b(\mathbf{r})$] was found to have a small but definitely nonzero value, while the Laplacian of the electron density at the bond critical point [$\nabla^2\rho_b(\mathbf{r})$] was in every case positive. Positive $\nabla^2\rho_b(\mathbf{r})$ values are characteristic of closed shell interactions, including almost all hydrogen bonds, while negative $\nabla^2\rho_b(\mathbf{r})$ values are characteristic of covalent bonds. Only a very small number of very strong hydrogen bonds (all of the O-H...O type) have ever been shown to have negative values for the Laplacian. None of the hydrogen bonds investigated in the experimental structures behaved topologically in this manner.

The experimental N-H...X hydrogen bonds [n = 14 after two with unusual bond paths were removed from consideration; 2 N-H...N and 12 N-H...π(Ph)] were fitted to simple nonlinear models (power and exponential) for the relationships between $\rho_b(\mathbf{r})$ and H...acceptor distance [$r^2 \approx 0.85$, $\sigma \approx 0.015$] and $\nabla^2\rho_b(\mathbf{r})$ and d(H...A) [$r^2 \approx 0.93$, $\sigma \approx 0.097$] with good success. The fits of the experimental N-H...X data were compared to results available in the literature for both crystallographically and theoretically derived topological parameters of hydrogen bonds. Both Alkorta et al.[126,127] (theoretical) and Espinosa et al.[125] (crystallographic) found an exponential relationship between $\rho_b(\mathbf{r})/\nabla^2\rho_b(\mathbf{r})$ versus d(H...A) for hydrogen bonds of a variety of donor/acceptor combinations. The literature models are consistent with the experimental results, although in the present investigation the power and exponential fits could not be differentiated on the basis of their ability to model the data.

Next, a set of N-H...X (X = F, N or O) hydrogen bonds that had been subject to topological analysis (based on crystallographic measurements) was assembled from the literature (n = 26). This literature data set was fitted successfully to an exponential model function for the relationship between $\rho_b(\mathbf{r})$ and d(H...A) [$r^2 = 0.82$, $\sigma = 0.042$] but rather unsuccessfully for $\nabla^2\rho_b(\mathbf{r})$ versus d(H...A) [$r^2 = 0.54$]. The literature and experimental N-H...X data sets were then combined and fitted to a common exponential model for both $\rho_b(\mathbf{r})$ versus d(H...A) [$r^2 = 0.76$, $\sigma = 0.048$] and for $\nabla^2\rho_b(\mathbf{r})$ versus d(H...A) [$r^2 = 0.81$, $\sigma = 0.54$]. The combined $\rho_b(\mathbf{r})$ data when plotted suggested that a small systematic error might have been introduced into the experimental set of values at some point during the investigation. Still, in both cases the combined data sets were reasonably well modelled

by one simple exponential function.

The experimental N-H...X hydrogen bonds were also compared to a set of X'-H...O [X' = N, O or C] type hydrogen bonds from the literature (crystallographic studies) that had been assembled by Espinosa et al.[125] for their own topological investigation. It was shown that the experimental N-H...X hydrogen bonds were included in the Espinosa population for both $\rho_b(\mathbf{r})$ versus d(H...A) and $\nabla^2\rho_b(\mathbf{r})$ versus d(H...A). The boundaries for the Espinosa exponential models were calculated and graphed, along with the experimental data sets [$\rho_b(\mathbf{r})$ and $\nabla^2\rho_b(\mathbf{r})$], and in both cases the experimental data set was entirely included within the limits of the Espinosa model. This proved that the experimental N-H...X hydrogen bonds, and in particular the N-H...π(Ph) hydrogen bonds, belong to the larger general population of hydrogen bonds formed to traditional lone pair acceptors. The N-H...π(Ph) hydrogen bonds behave topologically like other hydrogen bonds, with predictable and consistent nonlinear relationships between topological parameters [$\rho_b(\mathbf{r})/\nabla^2\rho_b(\mathbf{r})$] and geometry [d(H...A)]. Examples of the rare, covalent hydrogen bonds were not included in any of these analyses and may be exceptions to these general observations.

Forty-one C-H...X interactions with reasonable bond paths and geometries, 9 C-H...N and 32 C-H...phenyl, were located and characterized topologically in this investigation. However, as a group the C-H...X data (unlike the N-H...X data) could not be fit to any simple model function for either $\rho_b(\mathbf{r})$ or $\nabla^2\rho_b(\mathbf{r})$ versus the H...acceptor distance. When divided into the logical C-H...N and C-H...phenyl subgroups fitting of the data to the same model functions was only marginally better. The long, weak C-H...N interactions did not behave as a group in a predictable fashion.

It seems likely that these are not true hydrogen bonds but rather some form of incidental contact.

The C-H...phenyl data when plotted fell into two broad groups, divided into those contacts with short and long H...acceptor distances, respectively. It was shown that this division could be attributed to the geometries of the C-H...phenyl interactions, short d(H...A) corresponding to H...H type contacts and long d(H...A) to hydrogen bonds (or intermediate contacts). Neither, the C-H...phenyl data nor either of its two geometry based subgroups (H...H contacts and hydrogen bonds) could be successfully modelled using any of the simple functions chosen.

To obtain a better understanding of the C-H...X interactions (n = 41), they were combined with the experimental N-H...X interactions (n = 14) for further topological comparisons. Plots of the total combined data set still did not fit any of the simple models (linear or nonlinear) for either $\rho_b(\mathbf{r})$ or $\nabla^2\rho_b(\mathbf{r})$ versus d(H...A). It was apparent that the short C-H...X interactions (the H...H contacts) were hindering fitting of the combined data set.

In consequence, the experimental N-H...X data set (13 hydrogen bonds and one intermediate contact) was then combined with the C-H...π(Ph) hydrogen bonds (n = 13) identified in the experimental C-H...phenyl data set. This new combined hydrogen bond data set was found to fit simple nonlinear models (power or exponential) very well for both $\rho_b(\mathbf{r})$ versus d(H...A) [$r^2 \approx 0.90$, $\sigma \approx 0.11$] and $\nabla^2\rho_b(\mathbf{r})$ versus d(H...A) [$r^2 \approx 0.92$, $\sigma \approx 0.096$]. The C-H...π(Ph) hydrogen bonds behave topologically just like the N-H...π(Ph) hydrogen bonds, sharing common, nonlinear relationships for both $\rho_b(\mathbf{r})$ versus d(H...A) and $\nabla^2\rho_b(\mathbf{r})$ versus d(H...A). They must belong

to the same population, comprised of all X-H...π(Ph) hydrogen bonds. Comparison to data available in the literature had previously shown the N-H...π(Ph) hydrogen bonds to come from a larger general population of hydrogen bonds, including those formed with "traditional" lone pair acceptors. By extension, the C-H...π(Ph) hydrogen bonds must also come from that same larger general population.

In addition, the results show the importance of the criteria developed in this work to identify and classify intermolecular X-H...π(Ph) interactions on the basis of geometry. Once geometry has been used to identify an interaction and determine its type, topological properties including the bond path can be predicted using the rules developed herein. Different classes of interactions (H...H contacts, intermediate contacts or hydrogen bonds of different types) will have different geometries and predictable but different topological parameters and bond paths. Those contacts identified as X-H...π(Ph) hydrogen bonds will, however, have topological parameters consistent with all other hydrogen bonds when compared on the basis of the H...acceptor distance. The same nonlinear models will fit all hydrogen bonds (except perhaps the rare covalent examples) for the relationships between topology [$\rho_b(\mathbf{r})$ or $\nabla^2\rho_b(\mathbf{r})$] and geometry [d(H...A)]. N-H...π(Ph) hydrogen bonds and the generally even weaker C-H...π(Ph) hydrogen bonds are included in that group.

4. Chapter Four

4. Conclusions

The final overall conclusions were assembled by combining the summaries found at the end of each discussion section. Some repetition proved unavoidable.

This investigation was begun with the intention of studying N-H...π(Ph) hydrogen bonds. In particular, the ill-defined nature of the phenyl ring as the hydrogen bond acceptor was of interest. It was hoped that a detailed crystallographic investigation of the N-H...π(Ph) hydrogen bonds in a series of ammonium and related organoammonium tetraphenylborate salts would allow the character of such interactions to be further elucidated. For this to be possible, it was first necessary to collect high quality x-ray crystallographic data sets for each of the four chosen compounds. The low temperature, massively redundant data sets were then subjected to multipole refinement using the new XD program. After the data were refined, there were two initial facets of the investigation. First, the individual structures were studied in detail. The geometries of the ionic compounds and in particular the N-H...π(Ph) hydrogen bonds were thoroughly characterized and compared. The influence of the hydrogen bonds on the crystal structure and packing adopted in each case was considered. Second, after the multipole refinements, difference electron density maps were plotted in a wide variety of planes to see if characteristic features and/or patterns could be identified as arising from the formation of the N-H...π(Ph) hydrogen bonds in the different structures. It was anticipated that electron density might consistently be observed to accumulate in some

region of space defining the N-H...π(Ph) hydrogen bonds. In that way the nature of the phenyl ring acceptor and its role in the interactions might be better understood.

Subsequently, this investigation of N-H...π(Ph) hydrogen bonds was considerably expanded. It became possible to implement Bader's[14] theory of "Atoms in Molecules" to carry out a quantitative topological analysis of the crystallographically derived electron density distributions. The N-H...π(Ph) hydrogen bonds (and all other contacts in the structures) were characterized by determination of their unique bond paths and (3,-1) bond critical points. Numerical values were calculated for both the electron density and the Laplacian of the electron density at each of the located bond critical points. The topological parameters provided a new means of comparing the interactions being studied, both within the experimental group and with interactions previously subject to such topological analysis and reported in the literature. The topological analysis also allowed the experimental results to be compared with theoretically calculated values, another source of valuable information available in the literature.

The four tetraphenylborate salts chosen for this study were subjected to detailed structural analyses after completion of the multipole refinements. These have been discussed in detail, and where possible, the experimental results have been compared to data available in the literature. In this respect there is one further comparison that can and should now be made. Steiner and Mason have very recently reported the results of a low temperature neutron crystallographic investigation of the structure of ammonium tetraphenylborate.[129] Their results, including

the geometry characterizing the one unique N-H...π(Ph) hydrogen bond present in the structure, are remarkably consistent with the x-ray derived results reported in this work. Even at 20K they found the ammonium cation to perform large amplitude motions within the cavity it occupies, exactly as determined in this investigation. The authors describe the N-H...π(Ph) hydrogen bond in the structure of ammonium tetraphenylborate as being exceptionally short with the N-H vector tending to point towards the centroid of the aromatic ring. Although the strength of the interaction is described as arising predominantly from the charge attraction between the cation N-H and the π electron cloud of the aromatic ring, the directional nature of the interaction suggested to the authors that it is not purely electrostatic. Again, this is in total agreement with the results from the present investigation.

Two conventional N-H...N hydrogen bonds were identified in the four structures studied in this work, and these proved to be the shortest and the strongest of the experimental interactions. They were used as internal standards with which the N-H...π(Ph) and the other interactions studied could be compared. Every N-H group in the four multipole refined structures was found to participate in some form of N-H...X [X = N or π(Ph)] hydrogen bond. Of the 16 possible interactions, 14 N-H...π(Ph) type hydrogen bonds were identified, one in $NH_4B(C_6H_5)_4$, one in the structure of [DabcoH][$B(C_6H_5)_4$], five in $[C(NH_2)_3][B(C_6H_5)_4]\cdot CH_3CN$ and seven in $[N(C[NH_2]_2)_2][B(C_6H_5)_4]$. All of the N-H...π(Ph) hydrogen bonds were found to be unbranched, single interactions, from the N-H donor in a cation to one phenyl ring of the anion acting as the acceptor. The geometries of these hydrogen bonds were found to vary widely but they could be divided

into three broad groups based on the observed H(N)...C_{ring} distances: centroid type (8), edge type (5) and single atom type (1) interactions. Centroid type N-H...π(Ph) hydrogen bonds were empirically identified as having the H(N)...π_c (ring centroid) distance shorter than any of the six individual H(N)...C_{ring} distances. Similarly, single atom type and edge type hydrogen bonds were identified as having the H(N)...π_c distance shorter than five or four of the H(N)...C_{ring} distances, respectively. The edge type interaction thus has two shorter H(N)...C_{ring} distances while the single atom type interaction has only one.

The N-H...π(Ph) hydrogen bonds studied experimentally illustrate the extremely soft geometry of such interactions, those made to aromatic phenyl ring acceptors. Examples of hydrogen bonds with centroid, edge and single atom type geometries were all located in the four experimental structures. The conformational variability of the experimental N-H...π(Ph) hydrogen bonds, is substantiated by data accumulated in the literature for similar X-H...π(Ph) type hydrogen bonds.

The overall results also support the idea that centroid geometry N-H...π(Ph) hydrogen bonds are favoured experimentally, being formed whenever possible. However, a number of other forces, including competition within a crystal structure when there is the possibility of forming a number of different hydrogen bonds, precludes the formation of centroid type interactions in all cases. The hydrogen bonds in a crystal structure are a compromise of the geometries of the individual bonds balanced against the need to maximize the strength of the total network. Because, in most cases, a number of hydrogen bonds must be formed from a single cation, to a limited number of acceptors, it is not possible for

each individual interaction to have the ideal centroid geometry. As the number of hydrogen bonds per cation increases, their geometries become less than ideal because of the competition between donors for the available acceptors. This effect is magnified when the charge distribution on each cation is also considered. The ammonium, guanidinium and biguanidinium cations have four, six and eight H(N) atoms, respectively, over which to share the single positive charge. This has an effect on the strength of N-H...X [X = N or π(Ph)] interactions formed in each case, with progressively weaker hydrogens bond being formed overall as the number of N-H groups per cation increases, and the corresponding charge on each individual hydrogen atom decreases.

The conclusion from experiment, that centroid type N-H...π(Ph) hydrogen bonds are formed preferentially in the four structures studied, was compared with the rather limited data available in the literature. The literature data (both crystallographic and theoretical) collected for N-H...π(Ph) hydrogen bonds showed that centroid type interactions do appear to be the most favoured geometry. In this investigation, centroid type N-H...π(Ph) hydrogen bonds were also found to predominate, presumably because this conformation allows the strongest interaction between the H(N) donor and the entire phenyl ring acceptor, conferring the maximum possible stabilization to the structure. Centroid type interactions are formed if at all possible, more off-center arrangements arising only when other factors, outlined above, dictate a compromise be reached.

Of the 14 N-H...π(Ph) hydrogen bonds studied experimentally, the majority were found to have centroid type geometries (8) or edge type geometries (5); only one was found to have a single atom type geometry.

The centroid and edge type N-H...π(Ph) hydrogen bonds were compared on the basis of their average geometrical parameters. The mean distances in the centroid type hydrogen bonds were found to be shorter, often considerably, than those of the edge type hydrogen bonds. The mean angles were always larger (closer to linear) in the centroid type group than in the edge type group. All of the results support the idea that the centroid type hydrogen bond is the more "ideal" geometry, allowing closer approach of the donor and acceptor groups. However, this is not to say that individual $N/H(N)\ldots C_{ring}$ distances to one or two atoms in the ring can not be equally short or shorter in single atom or edge type hydrogen bonds as those found in the centroid type bonds, where all carbon atoms in the ring are normally reasonably close.

The fact that every possible N-H donor group in the four structures participates in some form of hydrogen bond shows the importance of their formation. The N-H...X [X = N or π(Ph)] hydrogen bonds play an important role in determining and stabilizing the crystal packing adopted. However, during the course of the investigation of the N-H...X [X = N or Ph] hydrogen bonds two other most interesting and unexpected features were also observed. The first was found in the structure of [DabcoH][$B(C_6H_5)_4$] where the cation was shown to be completely enclosed in a cavity formed by the phenyl rings of six surrounding anions (Figure 9). As well as the N-H...π(Ph) hydrogen bond formed between the cation and one of the phenyl rings, all of the C-H groups of the cation were also found to form relatively short (less than 3Å) contacts with anion phenyl rings, often with favourable geometries.

Similar interactions were also noted in the structure of guanidinium

tetraphenylborate acetonitrile solvate. In this structure, two different types of cavities were found, one enclosing a pair of cations and the other enclosing a pair of acetonitrile solvent molecules (Figure 14). Somewhat surprisingly, ring 1 of the tetraphenylborate anion was not found to act as the acceptor for any of the five N-H...π(Ph) hydrogen bonds formed by the guanidinium cation, although all three other rings of the anion did. Instead, ring 1 was found to engage in short contacts (<3Å) with the alkyl C-H groups of the acetonitrile molecule.

This pair of observations led to the systematic investigation of all intermolecular C-H...acceptor interactions in the four structures, using the geometric criterion that the H(C)...acceptor distance be less than 3Å. A total of 43 such interactions were located, with acceptors being either nitrogen atoms (of the cation or solvent molecule - 9 in total) or the phenyl rings of the tetraphenylborate anions (34), and the donor C-H groups coming from the cation (DabcoH$^+$, 9), the solvent molecule (CH_3CN, 3) or the anion (all four structures, 22). As expected from their diverse natures, these interactions were found to exhibit a wide variety of geometries.

After studying all of the C-H...phenyl type interactions of less than 3Å located experimentally, the majority of the geometries were found to fall into one of two distinct categories. The first category contained those contacts with hydrogen bond type geometries. Of the 34 C-H...phenyl interactions studied, 14 were classified as hydrogen bonds. A variety of configurations were observed experimentally, including centroid type (4), edge type (8) and single atom type (2) contacts. The second category contained H...H type interactions; with configurations exactly as

described, these are likely related to van der Waals type contacts. Fifteen of the experimental C-H...phenyl interactions were identified as H...H type contacts.

The C-H...phenyl interactions tended to fall clearly into one category or the other based on their geometries. The hydrogen bond type contacts were found to have minimum H(C)...C_{ring} distance(s) shorter than the related minimum H(C)...H_{ring} distance(s). Generally, H(C)...C_{ring} was significantly shorter than H(C)...H_{ring}, however, in some cases they were nearly equal. Even in those cases where H(C)...C_{ring} was close to H(C)...H_{ring} the interaction was classified as a hydrogen bond as long as the H(C)...C_{ring} minimum distance was the shorter. The different hydrogen bond types (centroid, edge or single atom) observed for the C-H...phenyl contacts were analogous to those found for the N-H...π(Ph) hydrogen bonds.

In the H...H type contacts, the H(C)...H_{ring} minimum distance was found to be considerably shorter than any H(C)...C_{ring} distance or any other distance in the interaction. The H(C)...H_{ring} distance was usually less than 2.5Å, while the corresponding H(C)...C_{ring} distance was greater than 2.5Å and normally closer to 3.0Å. The minimum H(C)...H_{ring} distance was, on average, 0.5Å shorter than the corresponding H(C)...C_{ring} distance. The very short H(C)...H_{ring} distance, sometimes only slightly greater than 2.0Å, dominates the interaction. In general, all H...H type contacts appear to be very similar, involving directly only the two hydrogen atoms that make close contact. The C-H...H_{ring} angles cover a wide range, often far from 180°, indicative of a nondirectional type contact.

A few of the C-H...phenyl interactions studied did not fall clearly into either group (hydrogen bond or H...H type contact). These five

interactions were placed, rather arbitrarily, into an "intermediate" type category. In the intermediate group of contacts, the H(C)...H_{ring} minimum distance was always shorter than the corresponding H(C)...C_{ring} distance but the two were relatively equal. Both distances tended to fall in the range 2.6±0.2Å. This type of interaction was difficult to interpret based solely on geometry, it being hard to tell which distance would dominate the interaction. However, intermediate type contacts though relatively rare were found to have completely characteristic bond paths.

In this work, a considerable number of C-H...X [X = N or π(Ph)] interactions were investigated. As described above, not all of these were found to have hydrogen bond type geometries; in fact, the majority turned out to be better defined as H...H type contacts. Overall for the C-H...X hydrogen bond type contacts studied, the characteristic distances were generally found to be longer than those in comparable N-H...X hydrogen bonds. C-H...π(Ph) hydrogen bonds of all three possible geometric types, centroid, edge and single atom, were identified and characterized. The pronounced conformational variability exhibited by the C-H...π(Ph) type hydrogen bonds was not unexpected, having also been observed for the experimental N-H...π(Ph) hydrogen bonds.

[DabcoH] [$B(C_6H_5)_4$] was the only one of the four structures studied, in which the cation contains C-H groups capable of interaction with the anion. A total of ten C-H...X [X = N, one; π(Ph) nine] short cation/anion interactions were located, with every C-H group of the cation involved in at least one contact of less than 3Å. The majority were found to have hydrogen bond type geometries. Of the six interactions classified as $(C\text{-}H)_{cation}\cdots(phenyl)_{anion}$ hydrogen bonds, five were found to have edge type

geometries and one had a single atom geometry; none were found to have centroid type geometries.

It is clear that the $(C\text{-}H)_{cation}\cdots(phenyl)_{anion}$ interactions formed are important in the $[DabcoH][B(C_6H_5)_4]$ structure. They help to tether and orient the $DabcoH^+$ cation in the anion-formed cavity in which it resides. In fact, the single N-H...π(Ph) hydrogen bond between the cation and anion occurs with an N-H...π_c angle of only 158.6°. The angle is further from 180° than might normally be expected and this has been attributed to the combined effects of the other cation/anion C-H...X contacts in the structure. It also appears that the $(C\text{-}H)_{cation}\cdots(phenyl)_{anion}$ contacts are optimized to the best possible hydrogen bond geometries, only a single H...H type contact being observed. This is another indication that such contacts are important and purposely formed. None have centroid geometries but five of the six are edge type hydrogen bonds. The competition amongst the large number of interactions arising from the six unique C-H groups of a single cation (9) must preclude the formation of any with centroid geometries. Still, the $(C\text{-}H)_{cation}\cdots(phenyl)_{anion}$ contacts are important in determining the structure of $[DabcoH][B(C_6H_5)_4]$. Along with the stronger N-H...π(Ph) centroid geometry hydrogen bond formed, the C-H...phenyl hydrogen bonds help to orient the cation and anion relative to one another in the crystal structure.

While the structure of $[DabcoH][B(C_6H_5)_4]$ contains the only studied examples of $(C\text{-}H)_{cation}\cdots(phenyl)_{anion}$ contacts, $[C(NH_2)_3][B(C_6H_5)_4]\cdot CH_3CN$ contains the only experimental $(C\text{-}H)_{solvent}\cdots(phenyl)_{anion}$ contacts. Three such interactions were found to occur at reasonable distances between the solvent and the anion, one for each C-H group of acetonitrile. Again, the

majority were found to have hydrogen bond type geometries, with one forming a very short centroid type hydrogen bond, one forming an edge type hydrogen bond and the third forming an intermediate type interaction; none were found to be H...H type contacts.

In the guanidinium tetraphenylborate acetonitrile solvate structure, N-H...π(Ph) hydrogen bonds are formed between the cation and only phenyl rings 2, 3 and 4 of the anion. The C(3)-H(61)...ring 1 hydrogen bond is the only short/strong contact made to ring 1 of the anion and it helps to orient a pair of solvent molecules in the centrosymmetric cavity formed by rings 1 and 2 of a pair of anions. The $(C\text{-}H)_{solvent}\cdots(phenyl)_{anion}$ contacts are clearly important in $[C(NH_2)_3][B(C_6H_5)_4]\cdot CH_3CN$, playing a role similar to the C-H...phenyl cation/anion contacts in the structure of $[DabcoH][B(C_6H_5)_4]$, helping to determine the packing arrangement adopted.

One other category of C-H...phenyl contacts was identified in this investigation. Anion/anion type C-H...phenyl interactions were found to occur in all four structures. However, these contacts were found to fall into two distinct groups. The first group contained the anion/anion type interactions of $[DabcoH][B(C_6H_5)_4]$ and $[C(NH_2)_3][B(C_6H_5)_4]\cdot CH_3CN$, not surprisingly the two structures discussed above. $[DabcoH][B(C_6H_5)_4]$ was found to have only two short anion/anion contacts and neither of these had hydrogen bond type geometries. In $[C(NH_2)_3][B(C_6H_5)_4]\cdot CH_3CN$ six such contacts were investigated and only one was found to have a hydrogen bond geometry (of the single atom type). In both of these structures, the majority of the anion/anion contacts were clearly H...H type interactions and not hydrogen bonds.

It appears that in these two compounds, the anion/anion type

C-H...phenyl interactions are of minor importance and have little effect on the packing of the structures. They appear to be predominantly incidental contacts arising from the optimization of other, stronger interactions in the structures, $(C\text{-}H)_{cation}\cdots(phenyl)_{anion}$ in $[DabcoH][B(C_6H_5)_4]$, $(C\text{-}H)_{solvent}\cdots(phenyl)_{anion}$ in $[C(NH_2)_3][B(C_6H_5)_4]\cdot CH_3CN$ and N-H...π(Ph) hydrogen bonds in both. This is perhaps not surprising. Cation(+1)/anion(-1) contacts would be expected to have more favourable charge distributions than solvent(0)/anion(-1) contacts. Both would be expected to be preferred relative to the anion(-1)/anion(-1) contacts, other factors being equal. Also, the large and bulky tetraphenylborate anions would be expected to be more difficult to pack in close proximity to one another, discouraging the formation of multiple, short anion/anion contacts in a structure. It should be easier to form cation/anion or solvent/anion type interactions based on the smaller size of the second component (cation or solvent) and the resulting increased ease of packing.

In ammonium tetraphenylborate and biguanidinium tetraphenylborate, on the other hand, the only source of C-H groups is the anion and only anion/anion type C-H...phenyl contacts can be formed in the structures. Besides the N-H...X [X = N or π(Ph)] hydrogen bond(s) formed, these are the only other potential hydrogen bonds in the structure. In $NH_4B(C_6H_5)_4$, two short $(C\text{-}H)_{anion}\cdots(phenyl)_{anion}$ contacts were investigated. One contact was found to be an H...H type interaction, but the second was found to be a hydrogen bond with a centroid type geometry. Similarly, of the 12 anion/anion type C-H...phenyl contacts studied in biguanidinium tetraphenylborate, eight were found to be H...H type contacts, while four were determined to be hydrogen bonds, two with favourable centroid type

geometries and two with edge type geometries.

It is interesting to note that both compounds form centroid type $(C\text{-}H)_{anion}\cdots(phenyl)_{anion}$ hydrogen bonds while neither [DabcoH] $[B(C_6H_5)_4]$ nor $[C(NH_2)_3][B(C_6H_5)_4]\cdot CH_3CN$ were found to do so. It seems that in these two compounds, which contain only anion/anion type C-H...phenyl contacts, hydrogen bonds are formed preferentially. Since the anion/anion contacts involve very large and bulky groups, only a small number can have hydrogen bond type geometries (particularly centroid type) in a given structure. H...H type contacts also often arise as a secondary consequence of the formation of close anion/anion type hydrogen bonds. The presence of $(C\text{-}H)_{anion}\cdots(phenyl)_{anion}$ hydrogen bonds with centroid type geometries is an important feature of both structures. In biguanidinium and ammonium tetraphenylborates, the $(C\text{-}H)_{anion}\cdots(phenyl)_{anion}$ interactions do not have to compete with other types of C-H...phenyl interactions, be they cation/anion or solvent/anion. They can form hydrogen bonds with reasonable geometries whereas in the preceding structures other types of C-H..phenyl interactions were found to be more favourable and therefore more dominant. The $(C\text{-}H)_{anion}\cdots(phenyl)_{anion}$ hydrogen bond type interactions in biguanidinium tetraphenylborate and ammonium tetraphenylborate have been shown to play a significant role in determining the packing of their respective crystal structures.

In conclusion, the results of this investigation show that all structures capable of forming C-H...phenyl interactions will do so. The most favourable of the C-H...phenyl interactions in a given structure, whether cation/anion, solvent/anion or anion/anion type, will form true hydrogen bonds where possible. Cation/anion and solvent/anion interactions

appear to be favoured at the expense of anion/anion type contacts. This could arise because of simple charge considerations [cation +1, solvent 0, anion -1], because of size considerations [the tetraphenylborate anion is larger and bulkier than any of the cations or the solvent studied] or more likely some combination of the two. In structures where the only possible C-H...phenyl interactions are of the anion/anion variety these contacts will still form, and some will have favourable hydrogen bond geometries. It also appears that in cases where $(C\text{-}H)_{anion}\cdots(phenyl)_{anion}$ hydrogen bonds are formed, they will have an impact on the packing arrangement adopted in the crystal structure. In all four of the structures studied, C-H...phenyl hydrogen bond interactions of different types play a definite role in determining the crystal packing.

The multipole refinements carried out in this investigation were begun as a means of generating high quality electron density maps that could be used to study the N-H...π(Ph) hydrogen bonds present in all four structures. The idea was to generate new information about such bonds by carefully examining the maps. The two N-H...N hydrogen bonds also present in the structures would be used as internal standards with which to compare the N-H...π(Ph) hydrogen bonds. Subsequently it was learned that much more quantitative information could be generated from a topological analysis of the experimental electron densities using Bader's theory of "Atoms in Molecules".[14] Analysis of the generated bond paths and the properties of the electron density at the bond critical points provided detailed information about the nature of all the interactions studied. However, observation of the electron density maps generated still provided useful information about the nature of the X-H...π(Ph) [X = N or C]

hydrogen bonds in the four experimental structures.

Interpretation of the static maps plotted to investigate the X-H...π(Ph) [X = N or C] interactions formed in the four experimental structures proved difficult for a variety of reasons. The maps were found to contain many features, not all of which could be assigned to the hydrogen bonds formed, "true" features being intermingled with peaks arising for a variety of other reasons. In addition, different contacts were found to give rise to effects differing in origin, position and magnitude in the maps, depending on the nature and the strength of the hydrogen bond formed. All of this made analysis of the maps difficult. However, a variety of characteristic features were identified and these were shown to be consistently observed when similar strength X-H...π(Ph) hydrogen bonds were present in the static maps of the anion phenyl rings.

In the first maps studied, the inplane static maps of the cations and the anions, no correlation was found between the observed bond densities and the formation of X-H...π(Ph) hydrogen bonds. The density on the C-C bonds of the anion phenyl rings was often observed to be somewhat uneven around a given ring in a given structure. However, the variation could not be shown to be related to the X-H...π(Ph) hydrogen bond(s) formed to that ring. Similarly, the variation in the average C-C bond density between rings in the anion of a given structure and the variation observed between the four experimental structures could not be correlated with the various combinations of X-H...π(Ph) hydrogen bonds formed. The density observed on the N-H bonds of the cations and that on the C-H bonds of groups participating as donors in C-H...π(Ph) type hydrogen bonds in the inplane maps, were again not obviously correlated with the X-H...π(Ph)

hydrogen bonds nor with their strengths.

Two types of static maps were plotted in planes perpendicular to the anion phenyl rings to illustrate and study the X-H...π(Ph) hydrogen bonds formed in the four structures. In the first group of maps, the plane was chosen to bisect a pair of opposing C-C ring bonds, while in the second it passed through a pair of opposing ring carbon atoms. Analysis of the combination of the two complete sets of maps led to the following conclusions.

The features arising from C-H...π(Ph) interactions in all of the static maps tended to be minor. Although the C-H...phenyl interactions in general, and the C-H...π(Ph) hydrogen bonds in particular, were found to be structurally important, their effects in the difference electron density maps plotted was observed to be minimal. Generally only those C-H...π(Ph) interactions with hydrogen bond type geometries were ever clearly visible in the maps drawn. Overall, the formation of C-H...π(Ph) interactions of any type appeared to have little effect on the electron density of the interacting groups in all of the static maps plotted. The contours on the C-H bonds of the donor groups were not visibly perturbed in the static maps; they remained regular, symmetrical and well centered on the bonds. Charge depletion was observed, in the area towards the anion ring, at every H(C) atom that participated in a C-H...π(Ph) hydrogen bond, a feature characteristic of electrostatic interactions.

It was possible to study the maps of several anion phenyl rings involved as the acceptor in only C-H...π(Ph) type interactions. These maps again showed only minimal effects (at best) that were consistently observed and could be attributed to the C-H...π(Ph) interactions made to

that ring. The only regularly observed feature was a slight diffuseness of the outermost contour on all of the C-C bonds of the interacting ring. No characteristic features were identified in the maps drawn through opposing ring carbon atoms. All of the maps suggest that the C-H...π(Ph) interactions are almost completely electrostatic in nature, with possibly a very small covalent component.

The N-H...π(Ph) hydrogen bonds, on the other hand, gave rise to more significant features in the static maps plotted. These effects tended to vary depending on the strengths and the number of interactions formed. The features observed ranged from very minor to large and extensive, involving the entire phenyl ring of the anion acceptor.

The N-H bond density, in both types of maps cut through the phenyl rings, was consistently perturbed when involved in an N-H...π(Ph) hydrogen bond. In the maps, the N-H contours tended to be elongated more on one side of the bond than the other, such that they no longer remained well centered on the bond. The contours were drawn down off the bond towards the ring plane, to an extent that appeared to be related to the strength of the interaction formed. In the stronger interactions, the density on the cation N-H bond was usually more obviously and more significantly perturbed. In the most extreme case, the electron density of the cation N-H bond actually met and was shared with density arising from the anion ring. Accumulation of electron density between the interacting groups, visible in these static maps, is indicative of a covalent contribution to the hydrogen bond being formed. The fact that the N-H...π(Ph) hydrogen bonds have an even larger electrostatic component was evident in the large areas of significantly depleted charge observed in the static maps at

every interacting cation H(N) atom and oriented toward the phenyl ring plane of the anion.

In the maps drawn, in planes cut perpendicular to the anion phenyl rings through opposing C-C bonds, a certain diffuseness was observed on the outer C-C bond contours when the ring was found to participate in N-H...π(Ph) hydrogen bond(s). This diffuseness was relatively equal on all the C-C bonds around the interacting ring and also relatively equal both above and below the ring plane, regardless of the face to which the interaction(s) was actually made. A very similar effect was observed for all the X-H...π(Ph) interactions studied [X = N or C]. The extent of this effect was impossible to characterize nor could it normally be correlated with the strength of the interaction(s) being formed.

It was the cuts made through pairs of opposing anion phenyl ring carbon atoms that most clearly showed the effects of the N-H...π(Ph) interactions on the electron density distribution of the ring. The features observed in these maps were found to vary quite consistently and characteristically with the strength of the interaction formed. The weakest N-H...π(Ph) hydrogen bonds investigated, normally did not give rise to any visible features in the static maps drawn through pairs of opposing ring carbon atoms. This was found to be especially true of isolated interactions, single weak interactions made to one face of an anion ring. No peaks were observed in the maps, in the middle region between the ring plane and the interacting N-H group of the cation. No specific deformations of the density on any of the ring bonds (C-C, C-H or C-B) were observed either.

Other peaks were often observed in these maps but not in areas

considered characteristic of the N-H...π(Ph) interactions. These peaks tended to lie right on, or very close to, the ring plane. There was never any obvious pattern in their number and distribution around the ring. They tended to complicate the maps and make the analysis more difficult but they could usually be differentiated from the "true" peaks arising from the N-H...π(Ph) interactions. The spurious peaks could arise for a number of different reasons, from poor assignment of the multipoles on the ring carbon atoms to their being artifacts of the refinement process.

As the N-H...π(Ph) hydrogen bonds became somewhat stronger, new features, attributed to the interaction, became visible in the static maps. The first characteristic feature usually observed was a single small peak (one contour of only +0.015 $e\text{Å}^{-3}$) lying somewhat off of the ring plane at one of the ring carbon atoms. This peak was normally observed at that ring carbon atom making the closest contact with the H(N) atom of the interacting cation, lying directly between those two groups. Only one peak arising from the weak interaction was usually observed for each ring, so a peak was observed in only one of the three map planes drawn, that cut where the appropriate ring carbon atom was bisected. Only a very low level of electron density is actually shared between the two groups meaning that the hydrogen bond remains predominantly electrostatic. However, these N-H...π(Ph) hydrogen bonds do contain a small covalent contribution which appears to increase somewhat with the strength of the interaction.

As the N-H...π(Ph) hydrogen bonds became even stronger, or if two weak interactions acted in a concerted fashion to a single ring face (the "pincer" type arrangement of bonds in particular), even more prominent features were observed in the static maps drawn through opposing ring

carbon atoms. In addition to peaks at the appropriate ring carbon atoms (which might or might not be observed depending on the geometry of the interaction), perturbation of the σ electron density on certain of the ring bonds became evident in the maps. For example, the B-C and\or C-H bond density might be visibly distorted towards the cation in the static maps. Electron density, at least partially from σ bonds of the anion phenyl ring, was sometimes visibly perturbed into the region between the two interacting groups, suggesting an even larger covalent contribution to these hydrogen bonds. In this group, only one or two specific atom(s) and/or bond(s), in one distinct region of the anion ring, were visibly involved in the interaction made with the cation, not the entire ring. These were normally the atom(s)/bond(s) lying closest to the cation, as predicted from the geometry of the interaction.

In the strongest N-H...π(Ph) hydrogen bonds studied in this work, the electron density of the entire phenyl ring was visibly perturbed because of the interaction(s) it accepted. Peaks at ring carbon atoms and/or perturbation of the σ bond density (C-H or C-B) was observed all around the phenyl ring. Where anion C-H bonds were involved, the outer bond contour curved over/under the ring plane to form a lobe of electron density lying between the anion and the N-H group of the cation. The peaks observed also lay well off of the ring plane, between the ring carbon atom involved and the cation. Normally one feature or the other (not both) was observed at every carbon atom of the ring.

Participation of the σ electron density of the anion phenyl ring C-H and C-B bonds in the N-H...π(Ph) type hydrogen bonds has never before been demonstrated. The features observed in the maps from this investigation,

for two different rings in two different structures, suggest that in the strongest such interactions the σ electron density of the ring does become involved. In addition to the π electron density of the aromatic ring, the "traditional" acceptor of the N-H...π(Ph) hydrogen bond, the σ electron density is perturbed all around the ring in the strongest interactions. The magnitude of the features observed also suggest that the covalent contribution to the N-H...π(Ph) hydrogen bond is larger in the stronger interactions.

In most cases, the features observed in the static maps plotted could be directly correlated with the geometry of the N-H...π(Ph) interaction(s) made to that ring. Only the strongest N-H...π(Ph) hydrogen bonds studied affected the electron density of the entire anion phenyl ring. The weaker hydrogen bonds tended to visibly affect only the geometrically closest ring carbon atoms. In the static maps, features were observed only at specific ring carbon atoms and/or bonds, rather than distributed around the entire ring. The "principal" acceptor of the hydrogen bond might be an isolated fragment of the ring, an atom or a bond, rather than the complete ring. As already has been shown, this could be predicted reasonably well from the geometry of the interaction. The map features observed (and the geometry of the interaction) are also directly related to the bond path of the hydrogen bond and its properties at the bond critical point.

The original geometric criteria, used to identify the different interaction types, were modified slightly after the bond path analysis was carried out using Bader's theory of "Atoms in Molecules". Originally, 34 C-H...phenyl interactions were analyzed and divided into three distinct

categories, H...H type contacts (15), intermediate type contacts (5) and hydrogen bonds of different geometries (14). After careful consideration of each bond path only a slight redistribution of the interactions was noted. There were now 35 C-H...phenyl type contacts to consider in total after two new bond paths were located in $[C(NH_2)_3][B(C_6H_5)_4]\cdot CH_3CN$ and one contact from the structure of $[DabcoH][B(C_6H_5)_4]$ was eliminated since it did not have an associated bond path. There were 15 H...H type contacts, 4 intermediate contacts, 13 hydrogen bonds of varying geometries and 3 interactions having unusual bond paths to consider for the C-H...phenyl group. The results confirm that the original classifications, based solely on geometry, were very accurate; only a few interactions changed categories after consideration of their bond paths.

There were far fewer N-H...X [X = N or π(Ph)] interactions available for analysis than there were C-H...X interactions, 16 versus 44. Before investigation of the C-H...phenyl interactions it was assumed that all of the N-H...π(Ph) interactions in the four structures were hydrogen bonds. When the N-H...phenyl contacts were subject to the geometric criteria developed using the C-H...phenyl contacts, one intermediate type contact was identified. Bond path analysis confirmed that this one interaction was indeed an intermediate type contact and not a hydrogen bond. No H...H type contacts were located in the N-H...phenyl group leaving 13 N-H...π(Ph) hydrogen bonds of different geometries to analyze topologically. Two of these hydrogen bonds were later found to have unusual bond paths.

Each class of interaction studied was found to have a completely characteristic bond path. C-H...X and N-H...X interactions of the same type, including hydrogen bonds of all configurations, followed the same

set of rules and shared the same characteristic bond paths. The bond paths of H...H type contacts always begin from the hydrogen atom of the "donor" group and travel to the closest hydrogen atom of the "acceptor", possibly following a C-H bond of the anion "acceptor" for part of its length. Intermediate type contacts have bond paths that also begin from the hydrogen atom of the "donor" group. The bond path then proceeds to the approximate midpoint of a C-H bond in the anion "acceptor" before changing direction and following the bond to its termination, always at a ring carbon atom. The atom(s) involved at the "acceptor" in the bond paths of both types of interactions are always those that make the closest contact(s). Experimentally, both the H...H and intermediate groups of contacts were found to contain predominantly C-H...phenyl interactions; only one N-H...phenyl type intermediate contact was identified.

The original geometric criteria, used to identify the different interaction types, were modified slightly after the bond path analysis was carried out. In a given X-H...phenyl interaction, it appears that if the minimum $H(X)\ldots H_{ring}$ distance is shorter than the corresponding $H(X)\ldots C_{ring}$ distance by 0.40Å or more an H...H type interaction will be formed. If the distance difference is from 0.15Å to 0.40Å, an intermediate type contact will result. If the difference is approximately equal to 0.40Å, either type of interaction may be formed. If the distance difference is less than 0.15Å or if the minimum $H(X)\ldots C_{ring}$ distance(s) is any amount shorter than $H(X)\ldots H_{ring}$, then hydrogen bonds will be formed. Their type, whether centroid, edge or single atom, is determined by other features of the geometry. If the $H(X)\ldots H_{ring}$ distance is less than $H(X)\ldots C_{ring}$ by approximately 0.15Å, again either type of interaction, hydrogen bond or

intermediate type contact, may result. Each class of interaction has a completely characteristic bond path as just described.

Hydrogen bonds, whether N-H...X or C-H...X [X = N or π(Ph)], were also found to have completely characteristic bond paths that could be related to their associated geometries. The X-H...N type hydrogen bonds studied always have bond paths that begin from H(X) and travel directly to the single atom acceptor, a nitrogen center of the solvent or cation. X-H...π(Ph) hydrogen bonds were found to adopt a variety geometries under different conditions (single atom, edge or centroid type) but each of these types was found to have a completely characteristic bond path. Single atom type hydrogen bonds have bond paths that travel from the hydrogen donor atom to the C_{ring} atom with which it makes the closest contact. The characteristic bond path of an edge type hydrogen bond travels from hydrogen to that C-C bond of the anion with the two shortest H...C_{ring} distances. The bond path then travels along the C-C bond to the closer C_{ring} atom, that with the shortest H...C_{ring} separation. If the difference in the two minimum H...C_{ring} distances is small, roughly 0.10Å or less, the bond path will normally proceed from hydrogen to near the midpoint of the interacting C-C bond. If the difference in the two distances is longer, then the bond path will make an off-center approach to the C-C ring bond, nearer to the closer C_{ring} atom. Finally, if the difference in the minimum H...C_{ring} distances is large, the bond path will resemble that of a single atom type hydrogen bond, travelling to the atom with the shortest H...C_{ring} distance. Using these criteria, the bond paths of edge type or single atom type hydrogen bonds, whether C-H or N-H type, can be predicted from their geometries.

The centroid type X-H...π(Ph) hydrogen bonds studied were found to adopt a variety of bond paths that could also be correlated with their individual geometries. The centroid type hydrogen bonds were readily identified from their geometries, having all six H(X)...C_{ring} distances longer than the H(X)...π_c ring centroid distances. However, it sometimes proved difficult to predict the bond path for such contacts. Large variations in bond paths were observed for very small differences in geometry and the bond path did not conform to that expected by geometry in all cases. The six H(X)...C_{ring} distances in a centroid geometry hydrogen bond normally cover only a small range of values; the distances are often nearly equal. This is reflected in the 100Δ parameter [100Δ = 100(maximum H...C_{ring} distance - minimum H...C_{ring} distance)] which is often very small for centroid type geometries. Because many of the H(X)...C_{ring} distances are so similar, unlike those in other types of hydrogen bonding interactions where one or two distances are significantly shorter than the rest, other factors, normally minor, will influence where the bond path actually travels. Rather than the distance over which the interaction occurs dominating, these other factors determine the bond path. The narrower the range of H(X)...C_{ring} distances, and thus the smaller 100Δ, the harder it becomes to predict where the bond path will terminate, since all the ring carbon atoms become essentially equivalent.

It was found that if 100Δ is 35 or less the bond path adopted will not be easily predictable. If 100Δ is very small, 15 or less, the bond path may go anywhere, any C_{ring} atom or C-C bond of the interacting ring, in a seemingly random fashion. However, this is likely determined by small differences in parameters usually overshadowed by the dominant distance

effect. If 100Δ has a more intermediate value, the bond path will usually terminate at the ring carbon atom with the shortest $H(X)...C_{ring}$ distance, but how it will reach that point is still unpredictable. If 100Δ is 35 or greater, the bond path normally becomes well behaved, conforming to a specific set of rules determined by the geometry of the interaction. Distance again becomes the factor determining where the bond path will go, resulting in it approaching the closest $H(X)...C_{ring}$ contact(s). Under these conditions, if the difference in the two $H(X)...C_{ring}$ minimum distances is small (0.06Å or less was determined in this work) an edge type bond path to a C-C anion bond will be adopted. If the difference in the two minimum distances is larger (0.09Å or more was determined in this work) the bond path will travel to the single closest carbon atom in the anion phenyl ring. The bond paths of the interactions with centroid type configurations are characteristic and predictable once 100Δ becomes larger than approximately 35. The N-H and C-H results proved to be entirely complementary; centroid configuration hydrogen bonds from both groups conform to the same set of geometry based criteria from which their bond path may be determined.

Centroid type hydrogen bonds can have bond paths that are equivalent to those observed for single atom and edge type hydrogen bonds, only occurring over a more compressed distance scale. Therefore, geometry must first be used to determine the nature of the X-H...π(Ph) hydrogen bond, whether single atom, edge or centroid type. Once the configuration of the hydrogen has been decided the bond path can usually be predicted reasonably well.

In all cases, H...H type contacts, intermediate type contacts, or

hydrogen bonds, the bond path can always be predicted from the observed geometry. Each type of interaction has a completely characteristic bond path and from the bond path the nature of the interaction can normally be discerned. The origin of the interaction, whether N-H or C-H, whether cation/anion, solvent/anion or anion/anion, appears to have no visible effect on the bond path adopted; the bond path remains characteristic of its type. In all interactions, except the "true" centroid type hydrogen bonds, the bond path is determined by the distance(s) at which the interaction occurs. Narrow ranges of distance criteria have been developed, based on the observed bond paths, to predict interaction types from the observed geometries.

In this work a total of 60 interactions, 16 N-H...X and 44 C-H...X [X = N or phenyl], were investigated and characterized topologically by location of a unique (3,-1) type bond critical point and an associated, rational bond path. In every interaction studied, the electron density at the bond critical point [$\rho_b(\mathbf{r})$] was found to have a small but significantly nonzero value, while the Laplacian of the electron density at the bond critical point [$\nabla^2\rho_b(\mathbf{r})$] was in every case positive. Positive $\nabla^2\rho_b(\mathbf{r})$ values are characteristic of closed shell interactions, including almost all hydrogen bonds, while negative $\nabla^2\rho_b(\mathbf{r})$ values are characteristic of covalent bonds. Only a very small number of very strong hydrogen bonds (all of the O-H...O type) have ever been shown experimentally to have negative values for the Laplacian. None of the hydrogen bonds investigated in the four tetraphenylborate structures behaved topologically in this manner (as expected).

The experimental N-H...X hydrogen bonds [n = 14 after two with

unusual bond paths were removed from consideration; 2 N-H...N and 12 N-H...π(Ph)] were fitted to simple nonlinear (power and exponential) models for the relationships between $\rho_b(\mathbf{r})$ and H...acceptor distance [r^2 = 0.85] and $\nabla^2\rho_b(\mathbf{r})$ and d(H...A) [r^2 = 0.93] with good success. The fits of the experimental N-H...X data were compared with results available in the literature for both crystallographically and theoretically derived topological parameters of hydrogen bonds. Both Alkorta et al.[126,127] (theoretical) and Espinosa et al.[125] (crystallographic) found an exponential relationship between $\rho_b(\mathbf{r})$ and/or $\nabla^2\rho_b(\mathbf{r})$ versus d(H...A) for hydrogen bonds of a variety of donor/acceptor combinations. The literature models are consistent with the experimental results, although in the present investigation the power and exponential fits could not be differentiated on the basis of their ability to model the data.

Next, a set of 26 N-H...X (X = F, N or O) hydrogen bonds that had been subject to topological analysis (following crystallographic data measurements) was assembled from the literature. This literature data set was fitted successfully to an exponential model function for the relationship between $\rho_b(\mathbf{r})$ and d(H...A) [r^2 = 0.82] but rather unsuccessfully for $\nabla^2\rho_b(\mathbf{r})$ versus d(H...A). The literature and experimental N-H...X data sets were then combined and fitted to a common exponential model for both $\rho_b(\mathbf{r})$ versus d(H...A) [r^2 = 0.76] and for $\nabla^2\rho_b(\mathbf{r})$ versus d(H...A) [r^2 = 0.81]. The combined $\rho_b(\mathbf{r})$ data when plotted suggested that a small systematic error might have been introduced into the experimental set of values at some point during the calculations. Still, in both cases the combined data sets were reasonably well fitted by one single, simple exponential model. The results show a common basis exists for the N-H...π(Ph) hydrogen bonds

and those hydrogen bonds formed with "traditional" single atom acceptors.

The experimental N-H...X hydrogen bonds were also compared with a set of X'-H...O [X' = N, O or C] type hydrogen bonds from the literature (crystallographic studies) that had been assembled by Espinosa et al.[125] for their own topological investigation. The experimental N-H...X hydrogen bonds were shown to be included in the Espinosa population for both $\rho_b(\mathbf{r})$ versus d(H...A) and $\nabla^2\rho_b(\mathbf{r})$ versus d(H...A). The boundaries for the Espinosa exponential models (x-ray and joint data sets) were calculated and graphed, along with the experimental data sets [$\rho_b(\mathbf{r})$ and $\nabla^2\rho_b(\mathbf{r})$], and in both cases the experimental data was entirely included within the limits for at least one of the Espinosa models. This proved that the experimental N-H...X hydrogen bonds, and in particular the N-H...π(Ph) hydrogen bonds, belong to the larger general population of hydrogen bonds formed to traditional lone pair acceptors. The N-H...π(Ph) hydrogen bonds behave topologically like other hydrogen bonds, with predictable and consistent nonlinear relationships between topological parameters [$\rho_b(\mathbf{r})/\nabla^2\rho_b(\mathbf{r})$] and geometry [d(H...A)]. Examples of covalent hydrogen bonds were not included in any of these analyses and may be exceptions to these general observations.

Forty-one C-H...X interactions with reasonable bond paths and geometries, 9 C-H...N and 32 C-H...phenyl, were characterized in this topological investigation. However, as a group the C-H...X data (unlike the N-H...X data) could not be fitted to any simple model function (either linear or nonlinear) for either $\rho_b(\mathbf{r})$ or $\nabla^2\rho_b(\mathbf{r})$ versus the H...acceptor distance. The narrow range of topological values covered made fitting the C-H...phenyl data to model functions very difficult. When divided into the

logical C-H...N and C-H...phenyl subgroups fitting of the data to the same model functions was only marginally better. The long, weak C-H...N interactions did not behave as a group in a predictable fashion. It seems likely that these are not true hydrogen bonds but rather some form of incidental contact. The C-H...phenyl data when plotted fell into two broad groups, divided into those contacts with short and long H...acceptor distances, respectively. It was shown that this division could be attributed to the geometries of the C-H...phenyl interactions, short d(H...A) corresponding to H...H type contacts and long d(H...A) to hydrogen bonds (or intermediate contacts). The distribution of the data did not correspond in any visible way with the origin of the interaction (cation/anion, solvent/anion or anion/anion). Neither the C-H...phenyl data nor either of its two geometry based subgroups (H...H contacts and hydrogen bonds) could be successfully modelled using any of the simple functions chosen.

To obtain a better understanding of the C-H...X interactions (n = 41), they were combined with the experimental N-H...X interactions (n = 14) for further comparisons. Plots of the total combined data set still did not fit any of the simple models (linear or nonlinear) for either $\rho_b(\mathbf{r})$ or $\nabla^2\rho_b(\mathbf{r})$ versus d(H...A). It was apparent that the short C-H...X interactions (the H...H contacts) were hindering fitting of the combined data set. As a result, the experimental N-H...X data set (13 hydrogen bonds and one intermediate contact) was then combined with the C-H...π(Ph) hydrogen bonds (n = 13) identified in the experimental C-H...phenyl data set. This new combined hydrogen bond data set was found to fit simple nonlinear models (power or exponential) very well for both $\rho_b(\mathbf{r})$ versus

d(H...A) [r^2 = 0.90] and $\nabla^2\rho_b(\mathbf{r})$ versus d(H...A) [r^2 = 0.92]. The C-H...π(Ph) hydrogen bonds behave topologically just like the N-H...π(Ph) hydrogen bonds, sharing common, nonlinear relationships for both $\rho_b(\mathbf{r})$ versus d(H...A) and $\nabla^2\rho_b(\mathbf{r})$ versus d(H...A). They must belong to the same population, comprised of all X-H...π(Ph) hydrogen bonds. Comparison to data available in the literature had previously shown the N-H...π(Ph) hydrogen bonds to come from a larger general population of hydrogen bonds, including those formed with "traditional" lone pair acceptors. By extension, the C-H...π(Ph) hydrogen bonds must also come from that same larger general population.

In addition, the results show the importance of the criteria developed in this work to identify and classify intermolecular X-H...π(Ph) interactions on the basis of geometry. Once geometry has been used to identify an interaction and determine its type, topological properties including the bond path can be predicted using the rules developed herein. Different classes of interactions (H...H contacts, intermediate contacts or hydrogen bonds of different types) will have different geometries and predictable but different topological parameters and bond paths. Those contacts identified as X-H...π(Ph) hydrogen bonds will, however, have topological parameters consistent with all other hydrogen bonds when compared on the basis of the H...acceptor distance. The same nonlinear models will fit all hydrogen bonds (except perhaps the rare covalent examples) for the relationships between topology [$\rho_b(\mathbf{r})$ or $\nabla^2\rho_b(\mathbf{r})$] and geometry [d(H...A)]. N-H...π(Ph) hydrogen bonds and the generally even weaker C-H...π(Ph) hydrogen bonds are included in that group.

References

(1) "Fundamentals of Crystallography." C. Giacovazzo, H.L. Monaco, D. Viterbo, F. Scordari, G. Gilli, G. Zanotti and M. Catti (C. Giacovazzo editor), International Union of Crystallography, Oxford University Press, England (1992).

(2) "X-ray Structure Determination, A Practical Guide, Second Edition." G.H. Stout and L.H. Jensen, John Wiley and Sons, New York (1989).

(3) P. Becker, Physica Scripta, 15, 119 (1977).

(4) P. Coppens in "Neutron Diffraction." H. Dachs editor, Chapter 3, page 71 (1978).

(5) Israel Journal of Chemistry, Volume 16(2-3), F.L. Hirshfeld guest editor, all included papers.

(6) "X-ray Charge Densities and Chemical Bonding." P. Coppens, International Union of Crystallography, Oxford University Press, England (1997).

N.K. Hansen and P. Coppens, Acta Crystallogr., A34, 909 (1978);

P. Coppens, T.N. Guru Row, P. Leung, E.D. Stevens, P.J. Becker and

Y.W. Yang, Acta Crystallogr., A35, 63 (1979);

P. Coppens, J. Chem. Ed., 61, 761 (1984);

P. Coppens, J. Phys. Chem., 93, 7979 (1989).

(7) K. Kurki-Suonio, Israel J. Chem., 16, 115 (1977).

(8) N.K. Hansen, T. Koritsanszky and P.R. Mallinson, MOLLY: Program for Multipole Refinement (1991).

(9) T. Koritsanszky, S.T. Howard, T. Richter, P.R. Mallinson, Z. Su and N.K. Hansen, XD: A Computer Program Package for Multipole Refinement and Analysis of Charge Densities from X-ray Diffraction Data (1995).

(10) M. Souhassou, E. Espinosa, C. Lecomte and R.H. Blessing, Acta Crystallogr., B51, 661 (1995).

(11) E.D. Stevens and P. Coppens, Acta Crystallogr., A32, 915 (1976).

(12) P. Coppens and E.D. Stevens, Adv. Quantum Chem., 10, 1 (1977).

(13) C.L. Klein and E.D. Stevens in "Structure and Reactivity." J.F. Liebman and A. Greenberg editors, Chapter 2, 25 (1988).

(14) "Atoms in Molecules - A Quantum Theory." R.F.W. Bader, University of Oxford Press, England (1990).

(15) R.F.W. Bader, Chem. Rev., 91, 893 (1991).

(16) "Hydrogen Bonding in Biological Structures." G.A. Jeffrey and W. Saenger, Springer-Verlag, Berlin (1991).

(17) G.A. Jeffrey, Cryst. Rev., 4, 213 (1995).

(18) "The Nature of the Chemical Bond." Linus Pauling, Cornell University Press, Ithaca, New York (1939).

(19) E.D. Stevens, M.S. Lehmann and P. Coppens, J. Amer. Chem. Soc., 99, 2829 (1977).

(20) B. Hsu and E.O. Schlemper, Acta Crystallogr., B36, 3017 (1980).

(21) D. Madsen, C. Flensburg and S. Larsen, J. Phys. Chem., A102, 2177 (1998).

(22) P.R. Mallinson, K. Woźniak, G.T. Smith and K.L. MacCormack, J. Amer. Chem. Soc., 119, 11502 (1997).

(23) E.D. Stevens and P. Coppens, Acta Crystallogr., B36, 1864 (1980).

(24) J. Dam, S. Harkema and D. Feil, Acta Crystallogr., B39, 760 (1983).

(25) D. Zobel, P. Luger, W. Dreisig and T. Koritsànszky, Acta Crystallogr., B48, 837 (1992).

(26) E.D. Stevens, Acta Crystallogr., B36, 1876 (1980).

(27) M.P.C.M. Krijn, H. Graafsma and D. Feil, Acta Crystallogr., B44, 609 (1988).

(28) M.P.C.M. Krijn and D. Feil, J. Chem. Phys., 89, 4199 (1988).

(29) T. Kellersohn, R.G. Delaplane and I. Olovsson, Acta Crystallogr., B50, 316 (1994).

(30) H.S. Sheu, J.C. Wu, Y. Wang and R.B. English, Acta Crystallogr., B52, 458 (1996).

(31) F. Hamzaoui, F. Baert and G. Wojcik, Acta Crystallogr., B52, 159 (1996).

(32) T. Koritsànszky, J. Buschmann, L. Denner, P. Luger, A. Knöchel, M. Haarich and M. Patz, J. Amer. Chem. Soc., 113, 8388 (1991).

(33) M. Souhassou, C. Lecomte, R.H. Blessing, A. Aubry, M.-M. Rohmer, R. Weist, M. Bénard and M. Marraud, Acta Crystallogr., B47, 253 (1991).

(34) R. Destro, R.E. Marsh and R. Bianchi, J. Phys. Chem., 92, 966 (1988).

(35) R. Destro, R. Bianchi, C. Gatti and F. Merati, Chem. Phys. Lett., 186, 47 (1991).

(36) W.T. Klooster, S. Swaminathan, R. Nanni and B. M. Craven, Acta Crystallogr., B48, 217 (1992).

(37) S.T. Howard, M.B. Hursthouse, C.W. Lehmann and E.A. Poyner, Acta Crystallogr., B51, 328 (1995).

(38) C. Flensberg, S. Larsen and R.F. Stewart, J. Phys. Chem., 99, 10130 (1995).

(39) V.G. Tsirelson, Can. J. Chem., 74, 1171 (1996).

V. Zavodnik, A. Stash, V. Tsirelson, R. De Vries and D. Feil, Acta Crystallogr., B55, 45 (1999).

(40) E. Espinosa, C. Lecomte, E. Molins, S. Veintemillas, A. Cousson and W. Paulus, Acta Crystallogr., B52, 519 (1996).

(41) K.L. MacCormack, P.R. Mallinson, B.C. Webster, D.S. Yufit, L.A. Slater and D.J. Robins, Acta Crystallogr., B53, 181 (1997).

(42) R. Bianchi, G. Gervasio and G. Viscardi, Acta Crystallogr., B54, 66 (1998).

(43) R. Flaig, T. Koritsanszky, D. Zobel and P. Luger, J. Amer. Chem. Soc., 120, 2227 (1998).

(44) R. Destro and F. Merati, Acta Crystallogr., B51, 559 (1995).

(45) R. Bianchi, C. Gatti, V. Adovasio and M. Nardelli, Acta Crystallogr., B52, 471 (1996).

(46) P. Roversi, M. Barzaghi, F. Merati and R. Destro, Can. J. Chem., 74, 1145 (1996).

(47) C. Gatti, R. Bianchi, R. Destro and F. Merati, J. Mol. Struct. (Theochem), 255, 409 (1992).

(48) R.F.W. Bader, T.-H. Tang, Y. Tal and F.W. Biegler-König, J. Amer. Chem. Soc., 104, 946 (1982).

(49) R.J. Boyd and S.C. Choi, Chem. Phys. Lett., 120, 80 (1985).

(50) R.J. Boyd and S.C. Choi, Chem. Phys. Lett., 129, 62 (1986).

(51) M.T. Carroll and R.F.W. Bader, Mol. Phys., 65, 695 (1988).

(52) U. Koch and P.L.A. Popelier, J. Phys. Chem., 99, 9747 (1995).

(53) T.-H. Tang, W.-J. Hu, D.-Y. Yan and Y.-P. Cui, J. Mol. Struct. (Theochem), 207, 319 (1990).

(54) I. Rozas, I. Alkorta and J. Elguero, J. Phys. Chem., A101, 9457 (1997).

(55) M.C. Etter, Acc. Chem. Res., 23, 120 (1990).

(56) T. Steiner, Chem. Commun., 727 (1997).

(57) T. Steiner and G.R. Desiraju, Chem. Commun., 891 (1998).

(58) L.R. Hanton, C.A. Hunter and D.H. Purvis, J. Chem. Soc., Chem. Commun., 1134 (1992).

(59) T. Davies and L.A.K. Staveley, Trans. Faraday Soc., 53, 19 (1957).

(60) A.D.U. Hardy and D.D. MacNicol, J. Chem. Soc., Perkin Trans II, 1140 (1976).

(61) A. Aubry, J. Protas, E. Moreno-Gonzalez and M. Marraud, Acta Crystallogr., B33, 2572 (1977).

(62) K. Nakatsu, H. Yoshioka, K. Kunimoto, T. Kinugasa and S. Ueji, Acta Crystallogr., B34, 2357 (1978).

(63) S. Ueji, K. Nakatsu, H. Yoshioka and K. Kinoshita, Tetrahedron Letters, 23, 1173 (1982).

(64) T. Steiner, E.B. Starikov and M. Tamm, J. Chem. Soc., Perkin Trans 2, 67 (1996).

(65) T. Steiner, S.A. Mason and M. Tamm, Acta Crystallogr., B53, 843 (1997).

(66) J.L. Atwood, F. Hamata, K.D. Robinson, G.W. Orr and R.L. Vincent, Nature, 349, 683 (1991).

(67) H.S. Rzepa, M.L. Webb, A.M.Z. Slawin and D.J. Williams, J. Chem. Soc., Chem. Commun., 765 (1991).

(68) S. Suzuki, P.G. Green, R.E. Bumgarner, S. Dasgupta, W.A. Goddard III and G.A. Blake, Science, 257, 942 (1992).

(69) S.Y. Fredricks, K.D. Jordan and T.S. Zwier, J. Phys. Chem., 100, 7810 (1996).

(70) M. Nishio, Y. Umezawa, M. Hirota and T. Takeuchi, Tetrahedron, 51, 8665 (1995).

(71) T. Steiner, E.B. Starikov, A.M. Amado and J.J.C. Teixeira-Dias, J. Chem. Soc., Perkin Trans. 2, 1321 (1995).

(72) P. Hobza, V. Spirko, H.L. Selzle and E.W. Schlag, J. Phys. Chem., A102, 2501 (1998).

(73) M.F. Perutz, G. Fermi, D.J. Abraham, C. Poyart and E. Bursaux, J. Amer. Chem. Soc., 108, 1064 (1986).

(74) E. Tüchsen and C. Woodward, Biochemistry, 26, 1918 (1987).

(75) K.M. Armstrong, R. Fairman and R.L. Baldwin, J. Mol. Biol., 230, 284 (1993).

(76) G. Waksman, D. Kominos, S.C. Robertson, P. Nalin, D. Baltimore, R.B. Birge, D. Cowburn, H. Hanafusa, B.J. Mayer, M. Overduim, M.D. Resh, C.B. Rios, L. Silverman and J. Kuriyan, Nature (London), 358, 646 (1992).

(77) M.F. Perutz, Phil. Trans. R. Soc., A345, 105 (1993).

(78) S.K. Burley and G.A. Petsko, FEBS Letters, 203, 139 (1986).

(79) J.B.O. Mitchell, C.L. Nandi, I.K. McDonald, J.M. Thornton and S.L. Price, J. Mol. Biol., 239, 315 (1994).

(80) C.S.Page and H.S. Rzepa, Electron. Conf. Trends Org. Chem. [CD-ROM], paper 47 (1995).

(81) M.A. Viswamitra, R. Radhakrishnan, J. Bandekar and G.R. Desiraju, J. Amer. Chem. Soc., 115, 4868 (1993).

(82) F.H. Allen, V.J. Hoy, J.A.K. Howard, V.R. Thalladi, G.R. Desiraju, C.C. Wilson and G.J. McIntyre, J. Amer. Chem. Soc., 119, 3477 (1997).

(83) P.K. Bakshi, A. Linden, B.R. Vincent, S.P. Roe, D. Adhikesavalu, T.S. Cameron and O. Knop, Can. J. Chem., 72, 1273 (1994).

(84) M. Levitt and M.F. Perutz, J. Mol. Biol., 201, 751 (1988).

(85) D.A. Rodham, S. Suzuki, R.D. Suenram, F.J. Lovas, S. Dasgupta, W.A. Goddard III and G.A. Blake, Nature, 362, 735 (1993).

(86) Y. Inoue, S. Sugio, J. Andzelm and N. Nakamura, J. Phys. Chem., A102, 646 (1998).

(87) E.M. Duffy, P.J. Kowalczyk and W.L. Jorgensen, J. Amer. Chem. Soc., 115, 9271 (1993).

(88) E.B. Starikov and T. Steiner, Acta Crystallogr., B54, 94 (1998).

(89) J.P. Bouquiere, J.L. Finney, M.S. Lehmann, P.F. Lindley and H.F.J. Savage, Acta Crystallogr., B49, 79 (1993).

(90) T. Steiner, A.M.M. Schreurs, J.A. Kanters, J. Kroon, J. van der Maas and B. Lutz, J. Mol. Struct., 436-437, 181 (1997).

(91) P. Tarakeshwar, S.J. Lee, J.Y. Lee and K.S. Kim, J. Phys. Chem., 108, 7217 (1998).

(92) Inorganic Syntheses, Volume VII, J. Kleinberg (editor in chief), McGraw-Hill Book Company Inc, U.S.A. (1963).

(93) R.H. Blessing, Program SORTAV, Hauptman-Woodward Institute, Buffalo, New York, U.S.A. (1996).

(94) G.M. Sheldrick, SHELXS-86, in "Crystallographic Computing 3" (G.M. Sheldrick, C. Kruger and R. Goddard editors) Oxford University Press, pp. 175-189 (1985).

(95) G.M. Sheldrick, SHELXL-93: Crystal Structure Refinement Program, Institute of Inorganic Chemistry, University of Gottingen, Germany (1993).

(96) R.F. Stewart, Acta Crystallogr., A32, 565 (1976).

(97) E. Clementi and C. Roetti, Atomic Data and Nuclear Data Tables, 14, 177 (1974).

(98) P.J. Becker and P. Coppens, Acta Crystallogr., A30, 129 (1974).

P.J. Becker and P. Coppens, Acta Crystallogr., A30, 148 (1974).

P.J. Becker and P. Coppens, Acta Crystallogr., A31, 417 (1975).

(99) F.H. Allen, Acta Crystallogr., B42, 515 (1986).

(100) F.H. Allen and O. Kennard, " 3D Search and Research Using the Cambridge Structural Database." Chemical Design Automation News, 8(1), 1 and 31 (1993). Cambridge Structural Database Version of April 1997.

(101) K.M. Barkigia, L.M. Rajković-Blazer, M.T. Pope, E. Prince and C. Quicksall, Inorg. Chem., 19, 2531 (1980).

(102) V. Schomaker and K.N. Trueblood, Acta Crystallogr., B24, 63 (1968).

(103) X. He and B.M. Craven, EKRT program, Acta Crystallogr., A49, 10 (1993).

(104) M.A. James, O. Knop and T.S. Cameron, Can. J. Chem., 70, 1795 (1992).

(105) W.J. Westerhaus, O. Knop and M. Falk, Can. J. Chem., 58, 1355 (1980).

(106) M.P. Roberts, D. Clavell-Grunbaum and H.L. Strauss, J. Chem. Phys., 87, 6393 (1987).

(107) G. Lucazeau, A. Chahid, J.F. Bocquet, A.J. Dianoux and M.P. Roberts, Physica B, 164, 313 (1990).

(108) M.P. Roberts, G. Lucazeau, G.J. Kearly and A.J. Dianoux, J. Chem. Phys., 93, 8963 (1990).

(109) M.P. Roberts, R.M. Cavagnat, G. Lucazeau, J.-F. Bocquet and H.L. Strauss, J. Chem. Phys., 93, 7632 (1990).

(110) M.P. Roberts, J. Chem. Phys., 93, 8524 (1990).

(111) M.L.H. Gruwel and R.E. Wasylishen, Z. Naturforsch., 45A, 55 (1990).

(112) H. Bock, T. Vaupel and H. Schödel, J. prakt. Chem., 339, 26 (1997).

(113) P.K. Bakshi, PhD. Thesis, Dalhousie University, Halifax, Nova Scotia, Canada (1995).

(114) W. Frey, M. Vettel, K. Edelmann and W. Kantlehner, Z. Kristallogr. - New Cryst. Struct., 213, 77 (1998).

(115) A. Martin and A.A. Pinkerton, Acta Crystallogr., C52, 1048 (1996).

(116) A. Martin, A.A. Pinkerton and A. Schiemann, Acta Crystallogr., C52, 996 (1996).

(117) A. Martin, A.A. Pinkerton, R.D. Gilardi and J.C. Bottaro, Acta Crystallogr., B53, 504 (1997).

(118) T. Steiner, Acta Crystallogr., C54, 1121 (1998).

(119) Y. Umezawa, S. Tsuboyama, K. Honda, J. Uzawa and M. Nishio, Bull. Chem. Soc. Jpn., 71, 1207 (1998).

(120) Y. Umezawa, S. Tsuboyama, H. Takahashi, J. Uzawa and M. Nishio, Tetrahedron, 55, 10047 (1999).

(121) H.W. Yang and B.M. Craven, Acta Crystallogr., B54, 912 (1998).

(122) P.R. Mallinson, K. Woźniak, C.C. Wilson, K.L. MacCormack and D.S. Yufit, J. Amer. Chem. Soc., 121, 4640 (1999).

(123) E. Cubero, M. Orozco, P. Hobza and F.J. Luque, J. Phys. Chem., A103, 6394 (1999).

(124) E. Cubero, M. Orozco and F.J. Luque, J. Phys. Chem., A103, 315 (1999).

(125) E. Espinosa, M. Souhassou, H. Lachekar and C. Lecomte, Acta Crystallogr., B55, 563 (1999).

(126) I. Alkorta, I. Rozas and J. Elguero, Struct. Chem., 9, 243 (1998).

(127) I. Alkorta and J. Elguero, J. Phys. Chem., A103, 272 (1999).

(128) O. Knop, unpublished results.

(129) T. Steiner and S.A. Mason, Acta Crystallogr., B56, 254 (2000).

INTERMOLECULAR INTERACTIONS IN A SERIES OF ORGANOAMMONIUM TETRAPHENYLBORATES

VOLUME TWO

by

Katherine N. Robertson

Submitted in partial fulfilment
of the requirements
for the degree of Doctor of Philosophy

at

Dalhousie University
Halifax, Nova Scotia
February, 2001

Table of Contents

Page

Volume Two

List of Figures

List of Tables

Appendix 1

3.1. Thermal Motion Analysis

Least squares analyses of the rigid body motion of the tetraphenylborate anions in all four structures, and the two cations containing sufficient heavy atoms for analysis, were carried out according to the model of Schomaker and Trueblood.[102] The mean square atomic displacements (U_{calc}) were modelled by fitting T, L and S tensors to the experimental U_{ij}'s (U_{obs}) obtained from the multipole refinement of the low temperature x-ray data. T, L and S (torsion, libration and screw) axes model the external lattice vibrations of the ion as a whole. Hydrogen atoms were not included in the calculations.

How closely a structure approximates the rigid body model of motion is measured by the magnitude of $R(U_{ij})$ or $rms(U_{ij})$ as obtained from the TLS analysis, and/or by comparing $rms(U_{ij})$ with the $rms[esd(U_{ij})]$ from the crystal structure refinement.

$$R(U_{ij}) = [\ \Sigma(\Delta U_{ij})^2 / \Sigma(U_{ij})^2\ ]^{\frac{1}{2}}$$

$$rms(U_{ij}) = [\ \Sigma(\Delta U_{ij})^2 / n\ ]^{\frac{1}{2}}$$

$$rms[esd(U_{ij})] = [\ \Sigma(U_{ij})^2 / n\ ]^{\frac{1}{2}}$$

where $\Delta U_{ij} = U_{obs} - U_{calc}$ and n = number of U_{ij} parameters.

Both $R(U_{ij})$ and $rms(U_{ij})$ reflect the fit of the calculated U_{ij}'s (rigid body model) to the experimental U_{ij}'s. However, $R(U_{ij})$ is sometimes less suitable for this purpose because the contribution of numerically small U_{ij} values suffering from a large percentage error can be out of all proportion to their importance and may create a misleading impression of how well the thermal motion approximates to the rigid body model. If the

motion does correspond to the rigid body model, the fit to the observed U_{ij}'s, rms(U_{ij}), should be equal to or better than the mean estimated standard deviations on the observed U_{ij} values, rms[esd(U_{ij})].

For the four tetraphenylborate anions, R(U_{ij}) values of 0.0615 (NH_4^+), 0.153 (DabcoH$^+$), 0.0967 (guanidinium) and 0.0933 (biguanidinium) were obtained. The rms(U_{ij}) value for the anion in ammonium tetraphenylborate was also calculated, 1.07×10^{-4}, as was its rms[esd(U_{ij})] value, 3.15×10^{-4}. The ratio rms(U_{ij})/rms[esd(U_{ij})], equal to 3.40, is considerably larger than 1, the ratio expected if the anion were to approximate rigid body motion. By either criterion, the tetraphenylborate anions do not conform well to the rigid body model of motion.

Comparison of the R(U_{ij}) values for the different anions shows that although the fit is poor in all cases, it is relatively better in the ammonium case and worse in the DabcoH$^+$ structure. The ammonium tetraphenylborate anion is held more rigidly in place by its high symmetry and the constraints so imposed. It is not immediately clear why the anion in the DabcoH$^+$ structure has a fit much worse than the others.

It is not surprising that the tetraphenylborate anions do not fit the rigid body model of motion; they are large and bulky, but floppy, anions unlikely to move as a concerted rigid body. Internal modes of motion would be expected to make significant contributions. Attempts to model the internal motion in the anions, using a simple model of four torsions and six bends about the central B-C bonds, were unsatisfactory in all four cases. R(U_{ij}) did not decrease appreciably even though the number of fit parameters was increased by ten. The values obtained for the magnitudes of the internal motions were sometimes unreasonable.

All these results confirm the fact that the tetraphenylborate anions do not conform to any simple model of motion. The rigid body model of the motion is not sufficient; internal modes of motion cannot be neglected. However, the large, flexible anion is a complicated mixture of many internal modes, intractable to model in any simple way.

Despite the poor fit to the rigid body model, the translational amplitudes calculated for the four anions were always relatively small and isotropic, generally on the order of 0.15Å in all three directions. Although $R(U_{ij})$ varied considerably in the four structures, the mean librational amplitudes tended to be relatively constant as well, with average values of 1.7° about L_1, 1.6° about L_2 and 2.6° about L_3. Calculated librational corrections to the bond lengths in the four anions were consistently small, 0.0010 to 0.0030Å, and always of the same order as the estimated standard deviations of the experimental bond lengths. Bond length corrections were not applied.

The results were somewhat different for the two cations that could be studied by TLS analysis. The biguanidinium cation was fitted to the rigid body model of motion with an $R(U_{ij})$ value of 0.0723. The $rms(U_{ij})$ value of 1.98×10^{-3} and the $rms[esd(U_{ij})]$ value of 6.49×10^{-4} led to a ratio of 3.05 for $rms(U_{ij})/rms[esd(U_{ij})]$. Both $R(U_{ij})$ and the ratio show that the fit to the rigid body model is not particularly good in this case. Again, internal modes must make a significant contribution to the motion of the cation and should not be neglected. However, attempts to model the internal motion using a simple model of two torsions and one bend about the central N-C bonds of the cation were completely unsuccessful. It is possible that the analysis failed because the biguanidinium cation

consists of two nearly planar $[(NH_2)_2C]N$ fragments, hinged at the central nitrogen atom. The planarity of the sections could have caused problems to arise in the TLS calculations due to matrix singularities. For this, or some other reason, no sensible results were obtained.

Using the rigid body model, the translational components of the motion were calculated to be 0.16Å on average, relatively small and isotropic. Librational motions were calculated to be 3.2° about L_1, 2.7° about L_2 and 8.0° about L_3, larger and more anisotropic than had been observed in the tetraphenylborate anions. Corrections to the bond lengths due to libration ranged from 0.0059 to 0.0153Å, also considerably longer than had been observed in the anions. The corrections were also significantly larger than the estimated standard deviations on the experimental bond lengths in the cation (0.00020Å), often larger than three times the esds. Corrected bond lengths for the biguanidinium cation are reported in Table 49 of Appendix 4.

The biguanidinium cation exists as a hydrogen bonded dimer in the tetraphenylborate structure. The rigid body model of motion was applied to the N-H...N hydrogen bonded dimer, as well as to the cation monomer. $R(U_{ij})$ was calculated to be 0.183 for the dimer, significantly higher than $R(U_{ij})$ of the monomer, 0.0723, showing a considerably worse fit to the rigid body model. This result is not unexpected. The strength of the interaction holding the dimer together will be reflected in its thermal motion. The rigidity of the dimer should always be less than that of the constituent monomers.[104] For this reason, the monomer would be expected to approximate rigid body motion more closely than the dimer, the very results observed.

The DabcoH$^+$ cation is small and relatively rigidly bonded, thus it is not surprising that it was found to conform best to the rigid body model of motion. The calculated $R(U_{ij})$ value of 0.0465 is lower than that of any other anion or cation studied. The $rms(U_{ij})$ value of $1.51x10^{-3}$ and the $rms[esd(U_{ij})]$ value of $8.82x10^{-4}$ result in a $rms(U_{ij})/rms[esd(U_{ij})]$ ratio equal to 1.71, which is much closer to unity than any other of the ratios previously discussed. In fact, this appears to be the only instance where the rigid body model of motion holds reasonably well. Relative to the previous cases, internal modes must make a smaller contribution to the overall motion in the DabcoH$^+$ cation, resulting in the better observed fit to the rigid body model.

In the DabcoH$^+$ cation approximation to rigid body motion, the translational components are still relatively small and isotropic (0.17Å in each direction on average). The librational components (L_1 - 5.5°, L_2 - 3.9° and L_3 - 6.9°) are larger and more anisotropic, similar in magnitude to those observed for the biguanidinium cation. Also, as in the biguanidinium case, the corrections to the bond lengths due to libration in the DabcoH$^+$ cation are relatively large (0.0114 to 0.0167Å). They are considerably larger than the estimated standard deviations on the experimental bond lengths (0.0030 to 0.0040Å) and are often larger than three times the observed esds. Bond lengths in the DabcoH$^+$ cation, corrected for libration after being fitted to the rigid model of motion, are included in Table 29 of Appendix 4.

It is possible to compare these results for the TLS analysis of the DabcoH$^+$ cation [low temperature, multipole refinement] to the results reported by Bakshi et al.[83] for the same cation [room temperature,

conventional refinement] also in the tetraphenylborate salt. Judging from the U_{ij} values, even at low temperature appreciable thermal motion is present, although the low temperature values are smaller, by an average factor of 1.5, than those obtained in the conventional room temperature refinement. The estimated standard deviations of the U_{ij}'s are on average three times larger in the room temperature structure, likely due not only to the change in temperature but also to the difference in the refinement method (multipole versus spherical) used.

Bakshi et al.[83] report $R(U_{ij})$ as being equal to 5.1%, $rms(U_{ij})$ equal to 0.0025, $rms[esd(U_{ij})]$ equal to 0.0021 and $rms(U_{ij})/rms[esd(U_{ij})]$ equal to 1.19 for their rigid body motion analysis of the DabcoH$^+$ cation. The room temperature results thus show good agreement with the rigid body model of motion. In fact, although $R(U_{ij})$ is slightly larger than the low temperature value (4.65%), the ratio of $rms(U_{ij})/rms[esd(U_{ij})]$, equal to 1.19, shows the fit to the rigid body model to be even better at room temperature than at low temperature (1.71). This result is not unreasonable. At low temperatures, lattice or external modes are damped relative to their values at room temperature. The contributions of internal modes of motion can become relatively more important at low temperature, resulting in a worse overall fit to the rigid body model.

The calculated librational modes of the room temperature cation are consistently 1.2 times larger than the low temperature values. However, the positions of the libration axes and the relative magnitudes of the librations are consistent between the two determinations. The room temperature librations would be expected to be larger because of the thermal motion at higher temperatures, as observed.

3.1.1. Summary

The TLS analysis showed that the tetraphenylborate anions in all four structures did not conform well to the rigid body model of motion. The large, flexible anions have significant internal modes of motion, which could not be successfully approximated by the simple model used. Only two of the four cations could be studied by TLS analysis and of these two only the DabcoH$^+$ cation fit the rigid body model well. The bond length corrections due to libration were significant in the cations, often larger than three times the esd on the bond length, and are given in the appropriate tables of Appendix 4. However, the corrected bond lengths were not used in subsequent work since not all cation bond lengths could be corrected.

Appendix 2

3.4. C-H...Acceptor Interactions

During the course of the investigation of the N-H...X [X = N or Ph] hydrogen bonds in the four multipole refined structures, two most interesting features were observed. The first was found in the structure of [DabcoH] [$B(C_6H_5)_4$] where the cation was found to be completely enclosed in a cavity formed by the phenyl rings of six anions (Figure 9). As well as the N-H...π(Ph) hydrogen bond formed between the cation and one of the phenyl rings, all of the C-H groups of the cation were also found to form relatively short (less than 3Å) contacts with anion phenyl rings, often with favourable geometries.

Similar interactions were also noted in the structure of guanidinium tetraphenylborate acetonitrile solvate. In this structure, two different types of cavities were found, one enclosing a pair of cations and the other enclosing a pair of acetonitrile solvent molecules (Figure 14). Somewhat surprisingly, ring 1 of the tetraphenylborate anion was not found to act as the acceptor for any of the N-H...π(Ph) hydrogen bonds formed by the guanidinium cation, although all other of the three rings did. Instead, ring 1 was found to engage in short contacts, of less than 3Å, with the alkyl C-H groups of the acetonitrile solvent molecule.

This pair of observations led to the systematic investigation of all C-H...acceptor interactions in the four structures, using the geometric criterion that the H(C)...acceptor distance be less than 3Å. A total of 43 such interactions were located, with acceptors being either nitrogen atoms (of the cation or solvent molecule - 9 in total) or the phenyl rings

of the tetraphenylborate anions (34), and the donor C-H groups coming from the cation (DabcoH$^+$, 9), the solvent molecule (CH_3CN, 3) or the anion (all four structures, 22). The C-H donor groups can thus be either aliphatic (DabcoH$^+$ or CH_3CN) or aromatic (the $B(C_6H_5)_4^-$ anion). As expected from their diverse natures, these interactions were found to exhibit a wide variety of geometries. The most important question which arises is, what is the contribution of such C-H contacts? Can any be considered equivalent to the N-H...π(Ph) and N-H...N hydrogen bonds located in the four structures? Even if they are weaker, can they still be considered hydrogen bonds?

3.4.1. C-H...Acceptor Contacts in Ammonium Tetraphenylborate

In the course of the search for C-H...acceptor interactions of 3Å or less, based on H(C)...acceptor distances, two such interactions were located in ammonium tetraphenylborate. They are illustrated in Figure 29, which shows the network of contacts formed between the anions in the strucure. Both interactions were found to be of the anion/anion type, with aromatic donor and acceptor groups, not surprising since the anion is the only source of C-H groups in the structure. Figure 30 shows the same two C-H...phenyl contacts; it is drawn to emphasize the role of the phenyl ring as the acceptor of the interactions in ammonium tetraphenylborate.

The first contact located occurs between C(14)-H(14) of the original anion and ring 1 of a second anion generated by the symmetries (1/2-*x*, 1/2-*y*, 1/2+*z*) and (1/2-*y*, 1/2-*x*, 1/2+*z*). It is best described as having a centroid type geometry. The C(14)-H(14) vector points most directly and nearly linearly at the centroid of the interacting ring [C(14)-H(14)...π_c = 171.6°]. The distances C(14)...π_c (3.785Å) and H(14)...π_c (2.717Å) are

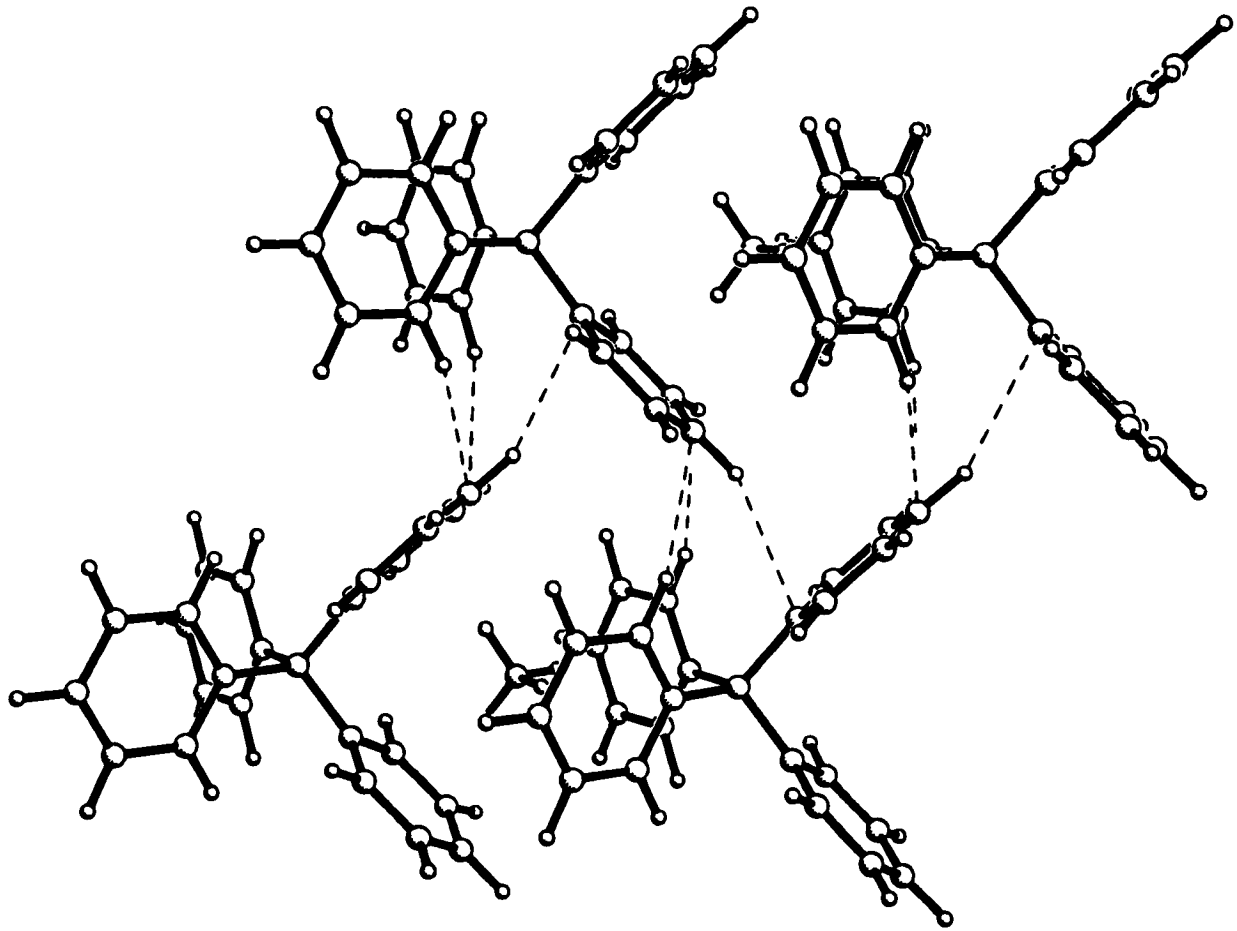

Figure 29. The network of C-H...phenyl interactions formed in the structure of ammonium tetraphenylborate.

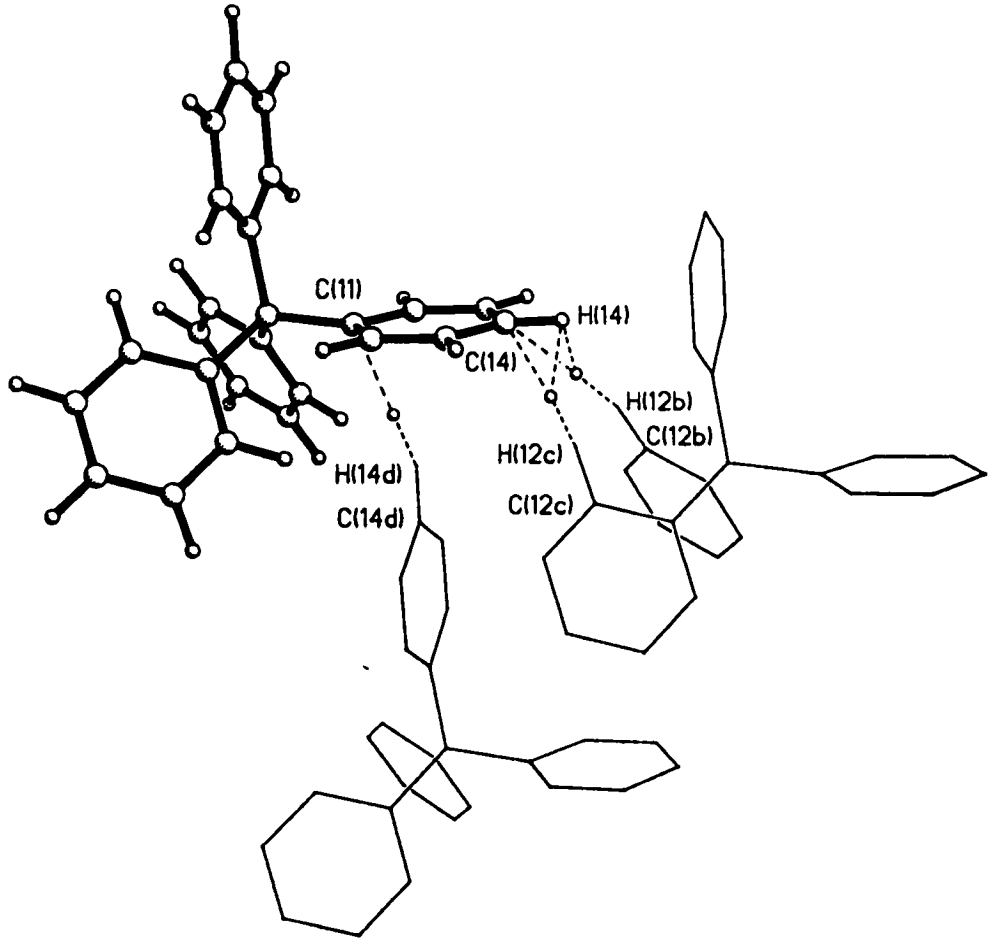

Figure 30. The C-H...phenyl interactions (less than 3Å) in the structure of ammonium tetraphenylborate, drawn to emphasize the role of the phenyl ring as the acceptor of the interactions. The small open circles represent the locations of the bond critical points of the interactions.

also shorter than any of the distances to individual ring carbon atoms. The minimum C(14)...C_{ring} distance is to C(11), 3.862(1)Å, while the maximum is to C(14), 4.225(6)Å [100Δ = 36]. Similarly, the minimum H(14)...C_{ring} distance is to C(11), 2.841Å, while the maximum is to C(14), 3.286Å [100Δ = 44]. The range of C(14)...C_{ring} and H(14)...C_{ring} distances are both relatively narrow.

By geometrical criteria at least, this interaction appears to be a C-H...π(Ph) hydrogen bond. It is equivalent to the so-called T-shaped interactions of phenyl rings described by other authors. However, it should be noted that all the distances are significantly longer than observed in the corresponding N-H...π(Ph) hydrogen bond of $NH_4B(C_6H_5)_4$, as exemplified by an H(N)...π_c distance of 2.013Å in the N-H...π(Ph) bond versus an H(C)...π_c distance of 2.717Å in the C-H...π(Ph) interaction. If N-H...π(Ph) hydrogen bonds are considered to be very weak as an overall group, what possible effects might be ascribed to the even weaker C-H...π(Ph) hydrogen bond? And yet, if the contribution is so weak why do such interactions consistently form?

The description of the second interaction as a C-H...π(Ph) hydrogen bond, based on geometry, is even more tenuous than the previous assignment. It occurs between C(12)-H(12) of the original tetraphenylborate anion and ring 1 of a second anion generated by the symmetries (1/2-*y*, -1/2+*x*, 3/2-*z*) and (1/2-*x*, -1/2+*y*, 3/2-*z*). As shown in the accompanying diagram, Figure 30, there are two such C(12)-H(12) interactions, from two different rings of a single anion, pointing simultaneously at the acceptor ring. The geometry of this interaction is far from ideal, as can easily be seen.

The C(12)-H(12) vector points most directly to C(14) of the acceptor ring, with a C(12)-H(12)...C(14) angle of 163.3°. However, it would be described as having an edge type geometry with H(12) approaching C(14), 2.873Å, and C(13), 2.998Å [C(12)-H(12)...C(13) = 149.1°], of the second phenyl ring most closely. All other H...C_{ring} distances are much longer, as is the H...π_c distance of 3.838Å (148.5°). More importantly, the C(12)-H(12) group makes even closer contacts to H(14) and H(13) of the acceptor ring, interactions expected to be repulsive on the basis of hydrogen atom charges. The H(12)...H(14) distance is 2.468Å and the C(12)-H(12)...H(14) angle is 163.8°, while the corresponding distance and angle to H(13) are 2.748Å and 138.7°, respectively. The C(12)-H(12) vector actually points slightly below the midpoint of the C(14)-H(14) bond, making an angle of 58.7° with the ring plane. The geometry of the C(12)-H(12) contact suggests an interaction with the C(14)-H(14) bond of a second phenyl ring on an adjacent anion. Should this anion/anion C-H...π(Ph) interaction still be described as a hydrogen bond? The geometry in this case, with the H...H_{ring} contact of 2.468Å being significantly shorter than any other distance, suggest that this is not a hydrogen bond in the conventional sense but rather some other type of weak interaction.

3.4.2. C-H...Acceptor Contacts in [DabcoH][$B(C_6H_5)_4$]

Packing of the $DabcoH^+$ cation in the cavity formed by the phenyl rings of six different tetraphenylborate anions showed that all the H(C) hydrogen atoms appeared to form close contacts with anion phenyl rings. For this reason, a search was carried out for all H(C)...X contacts [X =

N or π(Ph)] of less than 3Å. Amongst other things, this geometry search showed that all 12 H(C) protons (of these six are unique) of the cation form close contacts to phenyl rings of the surrounding anions. These are described in detail in Tables 30 and 31 and shown in Figure 31 (a) and (b). The geometry search also disclosed one other cation/anion contact of less than 3Å, however, in this case the C-H donor comes from the anion and the acceptor is the unprotonated nitrogen atom of the DabcoH$^+$ cation (also illustrated in Figure 31). Finally, [DabcoH][$B(C_6H_5)_4$] was found to form a pair of short anion/anion interactions, indicative of close approach between two different pairs of tetraphenylborate anions.

The importance of C-H...acceptor interactions in the structure of [DabcoH][$B(C_6H_5)_4$] is readily apparent from the number of close contacts, H...X [X = C or N], located experimentally. The importance of C-H type interactions was also speculated upon by Bock et al.[112] in their 1997 publication on the structure of [$(Dabco)_2H$][$B(C_6H_5)_4$]. In this closely related compound, the monoprotonated cation contains a pair of Dabco molecules bridged by a conventional N-H$^+$...N hydrogen bond. The authors found the unprotonated of the two independent Dabco molecules in the cation to be rotationally disordered about its N..N axis. The eclipsed orientation of the cation was found to be favoured (85%) over the staggered orientation (15%), which is rotated by 60° about the N...N axis relative to the eclipsed orientation. This was somewhat surprising since the eclipsed orientation has relatively short C...C contacts between Dabco moieties of the cation (3.60Å), compared to C...C distances of 4.10Å in the staggered conformation. These C...C contacts had been expected to destabilize the eclipsed conformation relative to the staggered

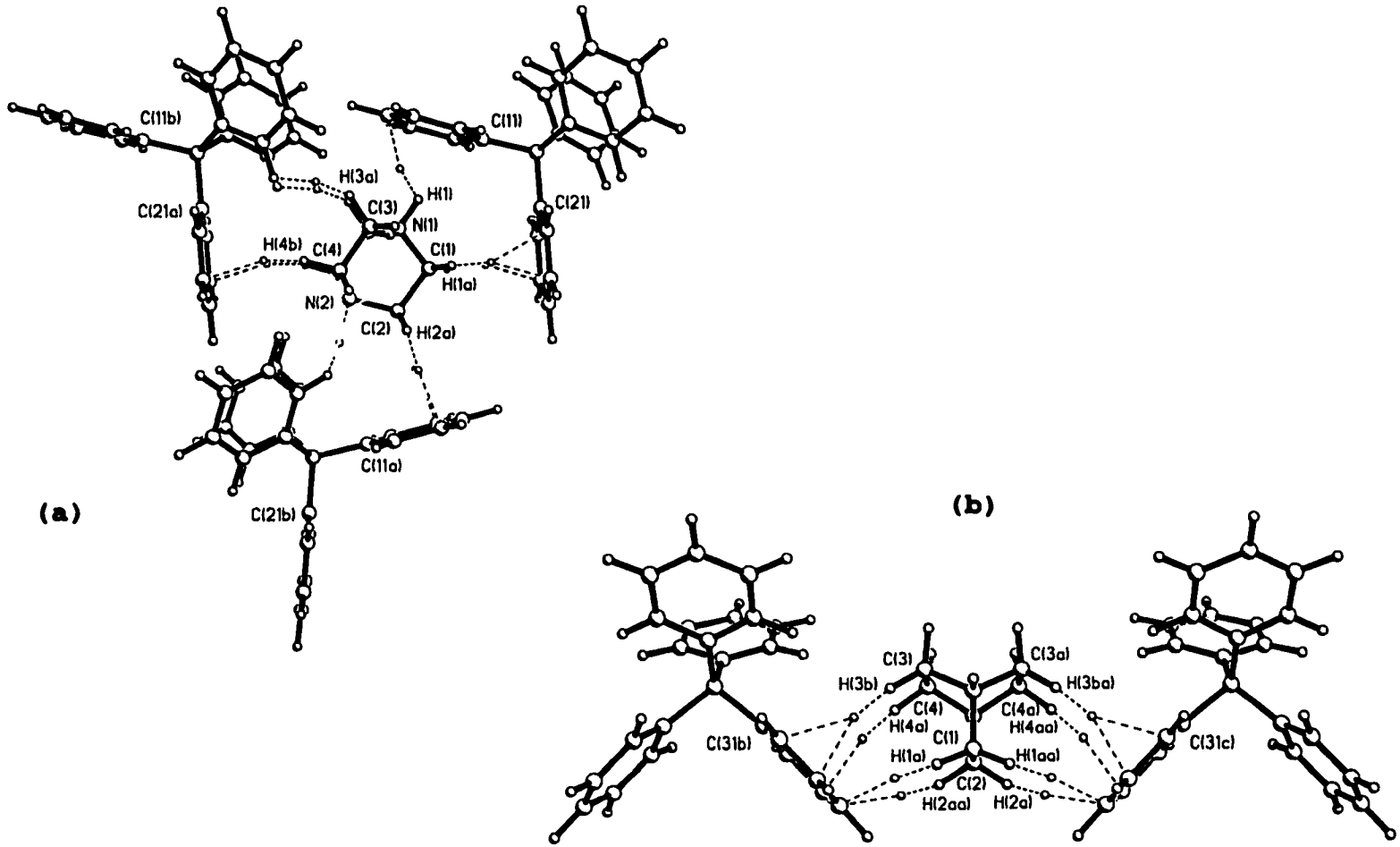

Figure 31. The interactions of all types (less than 3Å) located between the cation and the anion in the structure of [DabcoH][$B(C_6H_5)_4$]. The views in (a) and (b) are rotated by roughly 90° relative to one another. The small open circles represent the locations of the bond critical points of the interactions.

conformation but instead the eclipsed conformation was found to predominate (85% versus 15%). The authors suggest that stabilizing attractions could occur between C-H groups on opposing Dabco moieties of the cation, favouring formation of the eclipsed conformation in which these interactions are stronger. Semi-empirical charge calculations, supporting the proposed formation of C-H type interactions, were also included in the publication. In this structure, the acceptors of the C-H type interactions are not phenyl rings of the anion, as observed experimentally in the [DabcoH][$B(C_6H_5)_4$] structure. Rather the acceptors are other C-H groups of the cation, making them more like the H...H type contacts sometimes located in the experimental structures. However, the results do show the propensity of Dabco cations to become involved in C-H type interactions of all types.

The $DabcoH^+$ cation forms close C-H...acceptor interactions with five of the six anions that form the cavity surrounding it (Figure 31). C(1)-H(1A) and its symmetry equivalent both interact with ring 2 of the original cation. C(2)-H(2A) and its symmetry equivalent both interact with ring 1 of an anion generated by the symmetries (1/2+*x*, -1/2-*y*, 3/2-*z*) and (1/2+*x*, *y*, 3/2-*z*). Both the C(1)-H(1A) and the C(2)-H(2A)' interactions are bifurcated, also forming C-H contacts with ring 3 of an anion of symmetry (3/2-*x*, -1-*y*, -1/2+*z*). C(3)-H(3B) and C(4)-H(4A) also form close interactions with the same face of the same ring for a total of four contacts to a single anion phenyl ring face. On the opposite side of the cation there are four equivalent interactions to ring 3 of another anion of symmetry (3/2-*x*, 1/2+*y*, -1/2+*z*). The final anion with which the cation interacts is generated by the symmetry operations (*x*, *y*, -1+*z*) and

(x, -1/2-y, -1+z). C(4)-H(4B) and its symmetry equivalent both interact with ring 2 of this anion, while C(3)-H(3B) interacts with one ring 3 of this anion and its symmetry equivalent interacts with the second equivalent ring 3 of the same anion. The $(C\text{-}H)_{cation}\cdots(phenyl)_{anion}$ interactions of [DabcoH] [$B(C_6H_5)_4$] are illustrated in Figures 32 to 34 for rings 1 to 3 of the anion, respectively.

The first H(C) proton of the DabcoH$^+$ cation, H(1A), was found to form a bifurcated interaction with the rings of two different anions, ring 2 [symmetries (x, y, z) and (x, -1/2-y, z) - the original anion] and ring 3 [symmetry (3/2-x, -1-y, -1/2+z)]. There are two interactions of the type C(1)-H(1A)...ring 2 between one cation and a single ring 2 of the anion, each C-H group interacting with opposite sides of the ring (Figure 33).

C(1) projects onto the plane of ring 2 close to the ring centroid. The $C(1)\ldots C_{ring}$ distances thus cover a narrow range of values [100Δ = 10], all longer than the $C(1)\ldots\pi_c$ distance of 3.404Å. However, H(1A) projects onto the plane of ring 2 close to the midpoint of the C(22)-C(23) bond. The H(1A)...C(22), 2.911Å, and the H(1A)...C(23), 2.874Å, distances are shorter than all other $H(1A)\ldots C_{ring}$ distances [maximum 3.547Å; 100Δ = 67] including that to the ring centroid, 2.942Å. The corresponding angles in the edge type interaction are, respectively, C(1)-H(1A)...C(22) = 128.0° and C(1)-H(1A)...C(23) = 128.8°, both far from linearity. In fact, the C(1)-H(1A) vector makes an angle of only 33.8° with the plane of ring 2 and the $C(1)\text{-}H(1A)\ldots\pi_c$ angle is only 106.0°. The geometry of the edge type interaction is far from perpendicular, perhaps not surprising for a bifurcated bond. The C(1)-H(1A) vector points well outside of ring 2 closer to ring 3 of a second anion, the other half of the bifurcation.

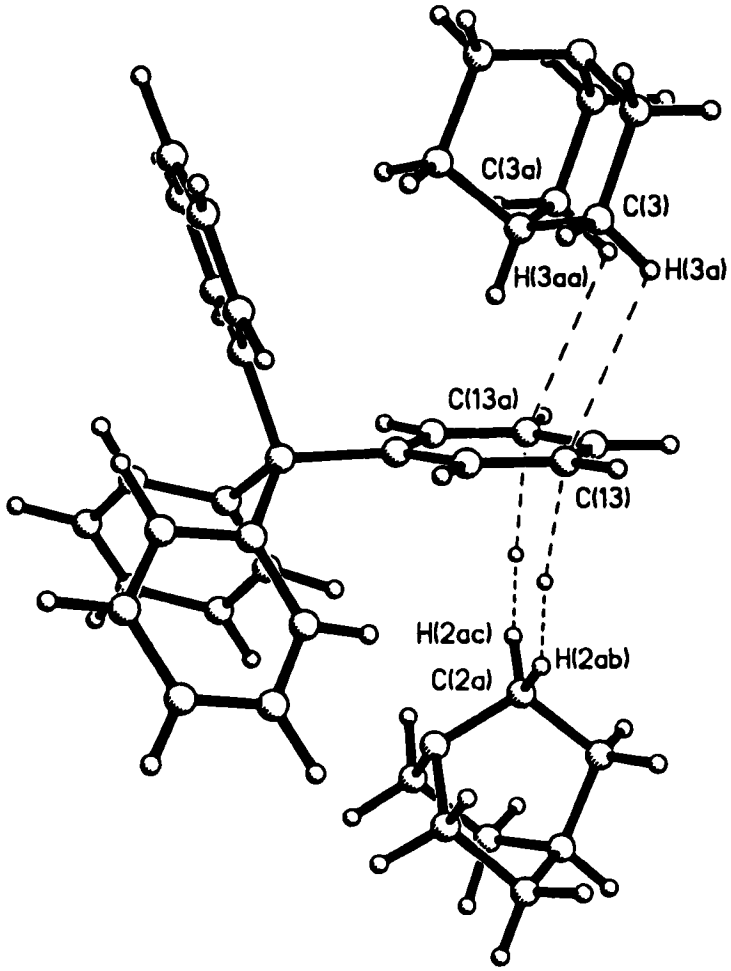

Figure 32. The C-H...phenyl interactions (cation/anion type - less than 3Å) accepted by ring #1 in the structure of [DabcoH][$B(C_6H_5)_4$]. The small open circles represent the locations of the bond critical points of the interactions.

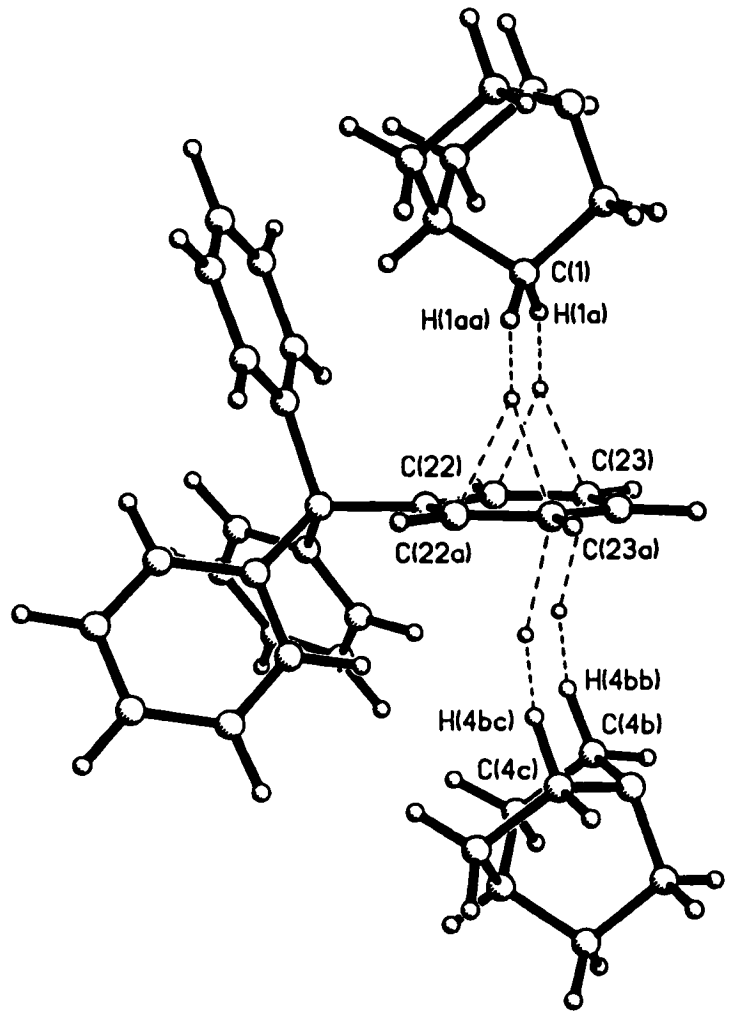

Figure 33. The C-H...phenyl interactions (cation/anion type - less than 3Å) accepted by ring #2 in the structure of [DabcoH][$B(C_6H_5)_4$]. The small open circles represent the locations of the bond critical points of the interactions.

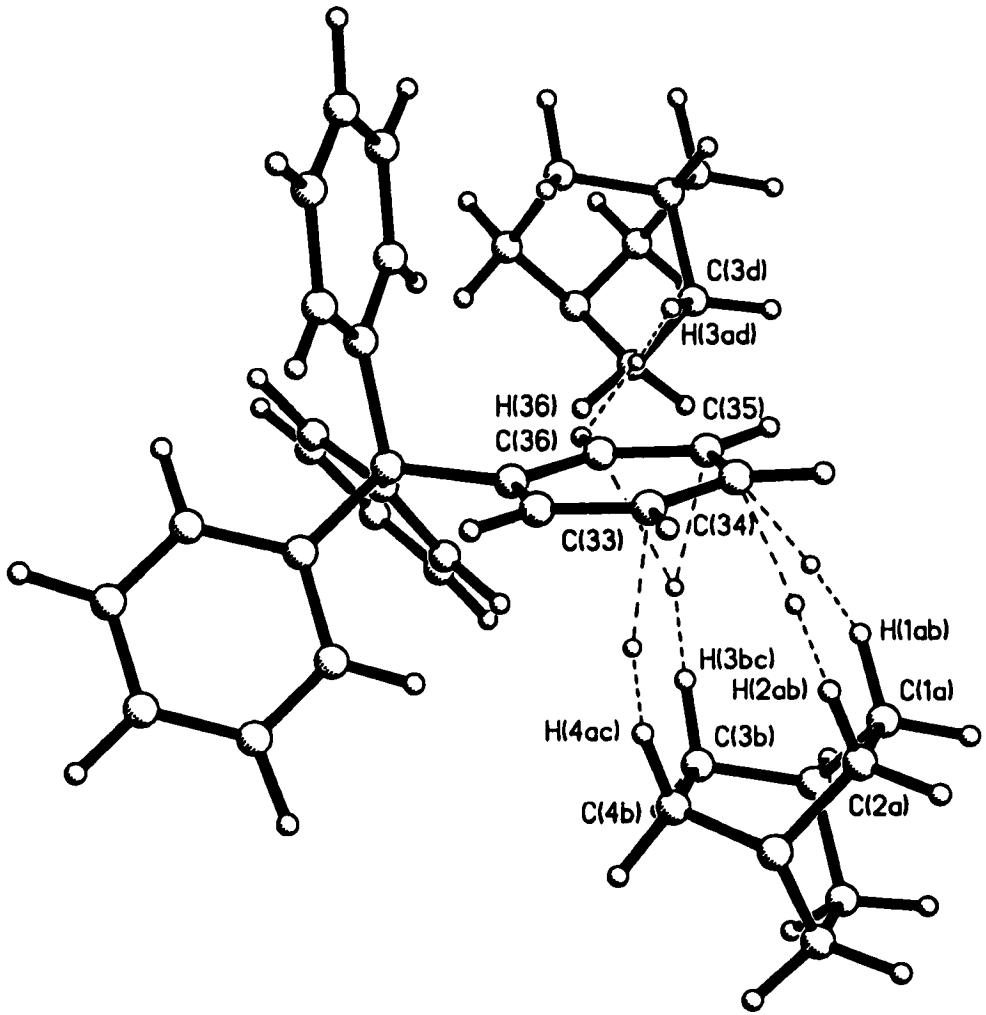

Figure 34. The C-H...phenyl interactions (cation/anion type - less than 3Å) accepted by ring #3 in the structure of [DabcoH][$B(C_6H_5)_4$]. The small open circles represent the locations of the bond critical points of the interactions.

The C(1)-H(1A) vector makes a more perpendicular approach to the plane of ring 3 of the second anion, making an angle of 61.9° with it (Figure 34). Both C(1) and H(1A) show short interactions with C(34) [3.703(2)Å and 2.874Å, respectively] and C(35) [3.965(2)Å and 2.975Å] of phenyl ring 3; all other distances, C(1)...C_{ring} [maximum C(31) 5.433(2)Å; 100Δ = 173] and H(1A)...C_{ring} [maximum C(31) 4.723Å; 100Δ = 185], are much longer, as are the corresponding distances to the centroid of ring 3 [C(1)...π_c = 4.416Å; H(1A)...π_c = 3.631Å]. The most linear angle is made to C(35), 151.9°, while that to C(34) is 133.2°. The C(1)-H(1A) vector projects onto the plane of ring 3 between H(34) and H(35). In fact, H(1A) is actually slightly closer to H(34), 2.709Å, than it is to C(34) [C(1)-H(1A)...H(34) = 128.7°] and the best angle is made to H(35) [C(1)-H(1A)...H(35) = 171.3° and H(1A)...H(35) = 2.882Å]. Although still described as having an edge type geometry, the C(1)-H(1A) interaction likely involves H(34) and H(35) in some way, as well as the C(34)-C(35) bond itself.

C(2)-H(2A) also forms a bifurcated interaction with two phenyl rings of different anions, ring 1 symmetries (1/2+*x*, -1/2-*y*, 3/2-*z*) and (1/2+*x*, *y*, 3/2-*z*), and ring 3 symmetry (3/2-*x*, 1/2+*y*, -1/2+*z*). The first component of the bifurcated interaction, C(2)-H(2A)...ring 1, occurs twice between each cation and opposite sides of ring 1 of a single anion (Figure 32). The second component, C(2)-H(2A)....ring 3, interacts with the same anion as the C(1)-H(1A)'...ring 3 contact (Figure 34).

C(2) projects onto the plane of ring 1 midway between the centroid and C(14), and therefore is closest to C(14) of the ring, 3.778(3)Å, and even closer to π_c, 3.674Å. The maximum C(2)...C_{ring} distance is to C(11),

4.080(3)Å, for a relatively narrow distribution of values [100Δ = 30]. H(2A) projects onto the plane of ring 1 very close to C(13) and just inside the ring itself. The distance H(2A)..C(13), 3.044Å, is the only H(2A)...C_{ring} value closer than that to the ring centroid, 3.187Å, and the angle C(2)-H(2A)...C(13), 131.4°, is the most linear formed to the ring. Although C(12), 3.277Å, and C(14), 3.275Å, are also reasonably close to H(2A), the geometry of the C(2)-H(2A)...ring 1 interaction is best described as being to a single atom, C(13); in this interaction, there are no close H(2A)...H_{ring} contacts. The C(2)-H(2A) vector projects well outside the ring and the interaction is far from perpendicular, with the C(2)-H(2A) vector making an angle of only 35.4° with the plane of ring 1.

The C(2)-H(2A)..ring 3 component of the bifurcated contact, forms the closest C(2)...C_{ring} interaction with C(34), 3.688(2)Å, with only C(2)...C(33) at 3.964(2)Å also being reasonably close; all other distances are longer than that to the ring centroid, 4.429Å [maximum 5.466(2)Å to C(31); 100Δ = 178]. The H(2A)...C(33), 3.002Å, and H(2A)...C(34), 2.819Å, distances are shorter than any other of the H(2A)...C_{ring} distances and are also shorter than that of H(2A)...π_c, 3.660Å [maximum C(31) 4.804Å; 100Δ = 199]. While the distance to C(34) is shorter, the more linear angle is made to C(33), 148.1° versus 137.1°. The geometry of this interaction would thus best be described as being of the edge type.

The C(2)-H(2A) vector makes an angle of 69.9° with the plane of ring 3, a more perpendicular contact than the C(2)-H(2A)...ring 1 component makes. However, both C(2) and H(2A) project onto the plane of ring 3 well outside the confines of the ring, beyond H(34). The C(2)-H(2A) vector points toward the ring plane but away from the ring itself,

approaching most closely to H(33), with the C(2)-H(2A)...C(33) angle equal to 160.6°. The distances from H(2A) to H(33), 2.920Å, and to H(34), 2.580Å, are shorter than the corresponding H(2A)...C_{ring} values, suggesting that H...H interactions should be important in the C(2)-H(2A)...ring 3 contact. In fact, the H(2A)...H(34) distance in this interaction, 2.580Å, is considerably shorter than any other H(2A)...X_{ring} (X = C or H) distance, showing the importance of the H...H contribution to this contact.

C(3)-H(3A) would also be expected to form a bifurcated interaction on the basis of geometry, with contacts of less than 3Å to ring 1 of the original anion, symmetries (*x*, *y*, *z*) and (*x*, -1/2-*y*, *z*) and ring 3, symmetry (*x*, *y*, -1+*z*). Again, there are two interactions of the type C(3)-H(3A)...ring 1 from one cation to opposite sides of the same ring 1 of a single anion (Figure 32). The second component of the bifurcation, C(3)-H(3A)... ring 3, also occurs twice from each cation because of symmetry, the acceptors being the two equivalent ring 3's of a second anion (Figure 34).

C(3) projects onto the plane of ring 1 outside the confines of the ring, close to the midpoint of the C(13)-H(13) bond. H(3A) projects even further outside the ring, approximately midway between H(13) and H(14), The C(3)-H(3A) vector points toward the ring plane but away from the ring itself. The C(3)-H(3A) vector is far from perpendicular to the ring 1 plane, making an angle of only 42.3° with it. Only two C(3)...C_{ring} distances are less than the C(3)...π_c distance of 3.754Å, C(3)...C(13) at 3.399(4)Å and C(3)...C(14) at the somewhat longer 3.616(4)Å [maximum 4.511(3)Å; 100Δ = 111]. Similarly, only H(3A)...C(13), 2.894Å, and H(3A)...C(14), 2.918Å, are shorter than H(3A)...π_c = 3.438Å [maximum

4.408Å; 100Δ = 151]. The best angle is made to C(14), the rather nonlinear 122.3°. The C(3)-H(3A)...ring 1 interaction exhibits an edge type geometry involving the C(13)-C(14) bond of the anion. However, once again H(3A) also makes relatively close contact with H(13), 2.905Å (115.0°), and H(14), 2.963Å (142.7°), of phenyl ring 1. These H...H contacts (although slightly longer than the corresponding H...C_{ring} distances they form more linear angles) could play a part in the C(3)-H(3A)...ring 1 interaction.

In the C(3)-H(3A)...ring 3 component of the bifurcated interaction, the C(3)-H(3A) vector is almost parallel to the plane of ring 3, making an angle of only 8.2° with it. The nearly parallel geometry is not favourable for any type of C-H interaction with the aromatic ring. Both C(3), farther away, and H(3A) project onto the plane of ring 3 well below the approximate midpoint of the C(35)-C(36) ring bond, but slightly closer to C(36). Only the distances C(3)...C(36), 3.916(3)Å, and C(3)...C(35), 4.087(3)Å, are shorter than the C(3)...π_c distance of 5.094Å [100Δ = 245]. The H(3A)...C_{ring} distances to C(36), 2.961Å (147.0°), and C(35), 3.169Å (142.9°), are also much shorter than any other of the values [maximum C(33) 5.358Å; 100Δ = 240] and shorter than the distance to the ring centroid, 4.095Å. The most linear angle is actually made to C(32) of the ring, 158.0°, but the angles mean little since C(3)-H(3A) is almost parallel to the plane of ring 3. As expected from the geometry of the interaction, H(3A) is closer to H(35), 2.700Å (126.7°), and H(36), 2.262Å (132.8°), than it is to the corresponding ring carbon atoms. The C(3)-H(3A) interaction to ring 3 must be influenced by the H...H contact between H(3A) and H(36). Based on the very short H(3A)...H(36) distance of only 2.262Å, this is likely not a hydrogen bond in the conventional

sense but rather some other type of weak contact.

C(3)-H(3B) forms a single, unbranched interaction with ring 3 of an anion having the symmetry (3/2-*x*, -1-*y*, -1/2+*z*), as shown in Figure 34. This is the same ring which also forms contacts with C(1)-H(1A), C(2)-H(2A)' and C(4)-H(4A). C(3) projects onto the plane of ring 3 between the ring centroid and the approximate midpoint of the C(35)-C(36) bond. H(3B) projects just inside the ring, again below the approximate midpoint of the C(35)-C(36) bond. The C(3)-H(3B) vector projects onto the ring plane very near the midpoint of the same bond. The C(3)-H(3B) vector makes an angle of 67.4° with the plane of ring 3.

The C(3)...C_{ring} distances are all longer than the C(3)...π_c distance of 3.975Å [100Δ = 44] and the range of these distances is narrow, indicative of a centroid type distribution. However, there are only two H(3B)...C_{ring} distances, H(3B)...C(35) = 2.975Å and H(3B)...C(36) = 3.055Å, that are shorter than the H(3B)...π_c distance of 3.071Å. The more linear angle is actually made to C(36), 163.0°, rather than to C(35), 155.1°. The geometry of the C(3)-H(3A)...ring 3 interaction is thus best described as being of the edge type, to the C(35)-C(36) bond. There are no similarly short H(3A)...H contacts to phenyl ring 3 of the anion.

As mentioned above, C(4)-H(4A) interacts with ring 3 of an anion generated by the symmetry (3/2-*x*, -1-*y*, -1/2+*z*), the same ring which also accepts interactions from C(1)-H(1A), C(2)-H(2A)' and C(3)-H(3B). The C(4)-(H4A) interaction is best described as an edge type contact based on its geometry. It has two H(4A)...C_{ring} distances, 2.854Å to C(33) and 3.026Å to C(32), that are shorter than the H(4A)...π_c distance of 3.128Å. The corresponding C(4)-H(4A)...C_{ring} distances and angles are 3.870(3)Å,

156.0° to C(33) and 4.054(2)Å, 158.4° to C(32), with the better angle being made to C(32) rather than closer C(33). The H(4A)...C_{ring} distances range from the minimum of 2.854Å to a maximum of 3.902Å to C(36) [100Δ = 105], while the C(4)...C_{ring} distances range from 3.870(3)Å, C(33), to 4.584(2)Å, C(36) [100Δ = 71]. C(4) projects onto the plane of ring 3 near C(33), about one quarter of the way along the C(33)-C(32) bond. H(4A) projects slightly below the bond, outside the ring, again about one quarter of the way between C(33) and C(32). As a result, the C(4)-H(4A) vector projects toward the ring, making an angle of 71.4° with the ring plane and projecting below the C(33)-C(32) bond closer to C(33) than to C(32). In fact, C(4)-H(4A) makes contact to H(33), 3.113Å (155.3°), and to H(32), 3.377Å (160.9°), at slightly longer distances than the corresponding H(4A)..C_{ring} values but with slightly better (more linear) angles.

The last $(C\text{-}H)_{cation}\cdots(phenyl)_{anion}$ interaction located, occurs between C(4)-H(4B) of the original cation and ring 2 of an anion generated by the symmetries (*x*, *y*, -1+*z*) and (*x*, -1/2-*y*, -1+*z*). There are two such contacts, from the two equivalent C(4)-H(4B) groups on each cation, to either side of a single anion ring 2 (Figure 33). As already mentioned, the C(3)-H(3B)...ring 3 interaction also involves the same cation/anion pair. However, this is the only interaction in which C(4)-H(4B) is involved.

C(4) projects onto the plane of ring 2 very close to C(23), while H(4B) projects close to the midpoint of the C(23)-C(22) bond but again slightly closer to C(23). As a result, the C(4)-H(4B) vector also projects close to the midpoint of the C(23)-C(22) bond of the acceptor ring. The

C(4)-H(4B) vector makes an angle of 69.7° with the plane of ring 2.

The geometry of the C(4)-H(4B)...ring 2 interaction is best described as being of the edge type. There are two H(4B)...C_{ring} distances shorter than the H(4B) to ring centroid distance of 3.125Å, H(4B)...C(23) = 2.921Å and H(4B)...C(22) = 3.105Å. The more linear angle is actually made to C(22), 174.1°, rather than to C(23), 153.4°, although the distance to C(22) is longer. The distribution of C(4)...C_{ring} distances range from a minimum of 3.922(2)Å to C(23) to a maximum of 4.815(2)Å to C(22)' [100Δ = 89]. Similarly, the H(4B)...C_{ring} distances range from 2.921Å, C(23), to 3.861Å, C(22)' [100Δ = 89]. The H(4B)...C_{ring} distances are all shorter than the corresponding H(4B)...H_{ring} values.

None of the $(C\text{-}H)_{cation}\cdots(phenyl)_{anion}$ contacts in [DabcoH][$B(C_6H_5)_4$] have the "ideal" geometry, with C-H pointing toward a phenyl ring centroid and all the H...C_{ring} distances (including H...π_c) being short. Rather, all but one interaction are best described as being of the edge type, with two and only two H...C_{ring} distances being less than H...π_c; the C-H donor group of the cation makes close approach to one edge of a phenyl ring in the anion acceptor. The one exception is the C(2)-H(2A)...ring 1 contact where the closest approach is to a single carbon atom, H(2A)...C(13) = 3.044Å. This single atom type interaction was the longest studied and presumably one of the weakest.

The remaining edge type interactions all had similar minimum H...C_{ring} distances, ranging from 2.819Å, C(2)-H(2A)...ring 3, to 2.975Å, C(3)-H(3B)...ring 3. The C-H...C_{ring} angles (for the minimum H...C_{ring} contacts) were also generally similar and somewhat less than linear, ranging from 129°, C(1)-H(1A)...ring 2 in a bifurcated contact, to 156°,

C(4)-H(4A)...ring 3. It would be expected that the shorter, more linear contacts would be stronger than the longer, more bent interactions. However, as a group they are all quite similar and likely very weak in nature. It should also be noted that other contacts, longer than the arbitrarily chosen 3Å cutoff, were located but were not investigated.

Several of the $(C\text{-}H)_{cation}\cdots(phenyl)_{anion}$ contacts in the structure of [DabcoH][$B(C_6H_5)_4$] showed closer approaches and more linear angles to phenyl ring hydrogen atoms than to the corresponding ring carbon atoms [$H\cdots H_{ring}$ distance < $H\cdots C_{ring}$; $C\text{-}H\cdots H_{ring}$ angle > $C\text{-}H\cdots C_{ring}$]. Such H...H contacts would normally be expected to be repulsive in nature based on simple charge considerations. Their contribution to/effect on the overall C-H...phenyl interactions is difficult to ascertain. In one particular instance, that of C(3)-H(3A)...ring 3, where the H(3A)...H(36) distance is only 2.262Å, it becomes fairly certain that this is no longer a hydrogen bond but some other type of weak contact.

The C-H...phenyl ring contacts occurring between the $DabcoH^+$ cation and the tetraphenylborate anion can be compared to the single N-H...π(Ph) hydrogen bond found in the same structure. This interion hydrogen bond, N(1)-H(1)...ring 1, has a centroid type geometry with an H(1)...π_c ring centroid distance of only 2.169Å and an N(1)-H(1)...π_c angle of 158.6°. In this interaction, all of the $H(1)\cdots C_{ring}$ distances are less than 2.640Å. Obviously, the N(1)-H(1)...ring 1 hydrogen bond is much stronger than any of the C-H...phenyl contacts based on the close approach of H(1) to all of the carbon atoms in phenyl ring 1. This is in contrast to even the closest approach of an H(C) atom to a single carbon atom of an interacting ring, 2.819Å, in the C(2)-H(2A)...ring 3 contact. In this contact the

distance from H(2A) to the centroid of ring 3 is 3.660Å, 1.5Å longer than the corresponding distance in the N-H...π(Ph) hydrogen bond, and this is the shortest C-H...phenyl contact located. All of the other C-H contacts involving the DabcoH$^+$ cation have even longer minimum H...C_{ring} distances.

All of the $(C\text{-}H)_{cation}\cdots(phenyl)_{anion}$ contacts in [DabcoH][$B(C_6H_5)_4$] would be expected to be weak based on their less than optimal geometries. Although weaker than the N-H...π(Ph) hydrogen bond, they must by their number have some influence on the structure. It is suggested that these interactions control the orientation of the DabcoH$^+$ cation within the anion cavity, which in turn produces the slightly less than ideal centroid geometry of the single N(1)-H(1)...ring 1 hydrogen bond. (The N(1)-H(1) vector points most directly to C(11) of the ring, N(1)-H(1)...C(11) = 167.4°, rather than towards the ring centroid, N(1)-H(1)...π_c = 158.6°.).

Somewhat surprisingly, the DabcoH$^+$ cation was found to form one other contact of less than 3Å with the tetraphenylborate anion when the geometry search was carried out. Figure 31 clearly shows this interaction which occurs between the unprotonated N(2) of the cation and C(32)-H(32) of an adjacent phenyl ring of symmetry (1/2+*x*, -1/2-*y*, 3/2-*z*). This makes it different from the previous cation/anion interactions since in this case the acceptor is the N(2) atom, or more specifically lone pair electron density at N(2), of the cation.

Two C(32)-H(32) groups from the same anion (ring 3 is present twice by symmetry) form equivalent interactions with the single N(2) atom of each cation (Figure 35). The geometry of the contact is characterized by an H(35)...N(2) distance of 2.743Å, a C(35)...N(2) distance of 3.631(3)Å and a C(35)-H(35)...N(2) angle of 139.7°. Like the other C-H...acceptor

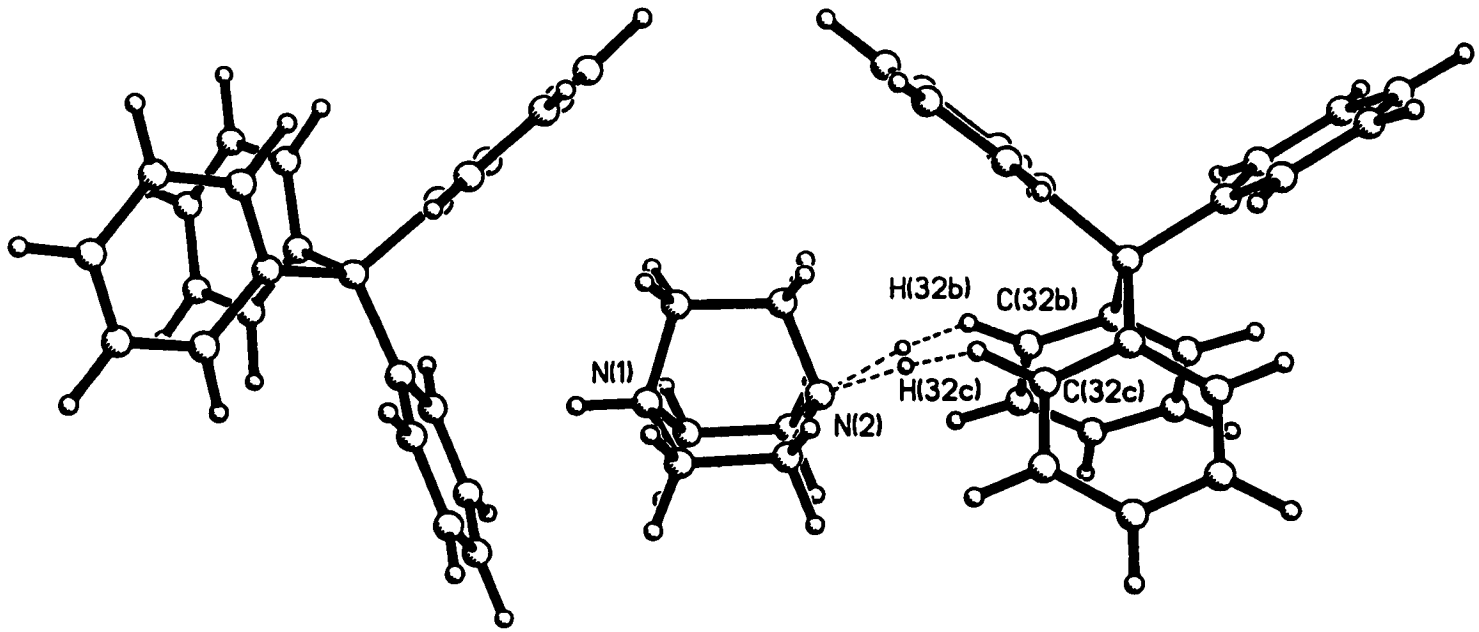

Figure 35. The C-H...N interaction located (less than 3Å) in the structure of [DabcoH][$B(C_6H_5)_4$]. The small open circle represents the location of the bond critical point of the interaction.

interactions, this contact is likely very weak. However, it would be expected to help tether the DabcoH$^+$ cation in the cavity formed by the $B(C_6H_5)_4^-$ anions. It was the first such C-H...N type contact encountered but subsequently others were located in both guanidinium tetraphenylborate acetonitrile solvate and biguanidinium tetraphenylborate.

The geometry search, for contacts of less than 3Å in the structure of [DabcoH] [$B(C_6H_5)_4$], also located three H...C_{ring} distances corresponding to two different anion/anion type C-H...phenyl interactions (Figures 36 and 37). The first such interaction was found to occur between C(35)-H(35) of the original anion and ring 2 of an anion generated by the symmetries (3/2-*x*, -1-*y*, 1/2+*z*) and (3/2-*x*, 1/2+*y*, 1/2+*z*), the former symmetry being used to generate the atoms actually involved in the contact. Considered in the opposite way, ring 2 of one anion accepts two such interactions, from two different C(35)-H(35) groups on two different anions approaching each side of one phenyl ring 2 (Figure 36).

In either case, H(35) of the first anion makes close contact with both C(22), 2.841Å [C(35)-H(35)...C(22) = 145.1°] and C(23), 2.873Å [C(35)-H(35)...C(23) = 128.8°] of the second anion. All other H...C_{ring} distances are much longer. However, the closest approaches are actually made between H(35)...H(22), 2.354Å (159.6°), and H(35)...H(23), 2.431Å (122.5°). The H(35)...H_{ring} contacts are considerably shorter and more linear than the corresponding H(35)...C_{ring} contacts in this interaction. This is also reflected by the C(35)-H(35) vector which points towards the ring but well outside it, forming an angle of 60.0° with the ring 2 plane. The vector passes closest to H(22) but projects even a little further away from the ring than that, giving the most linear angle of 159.6° to H(22).

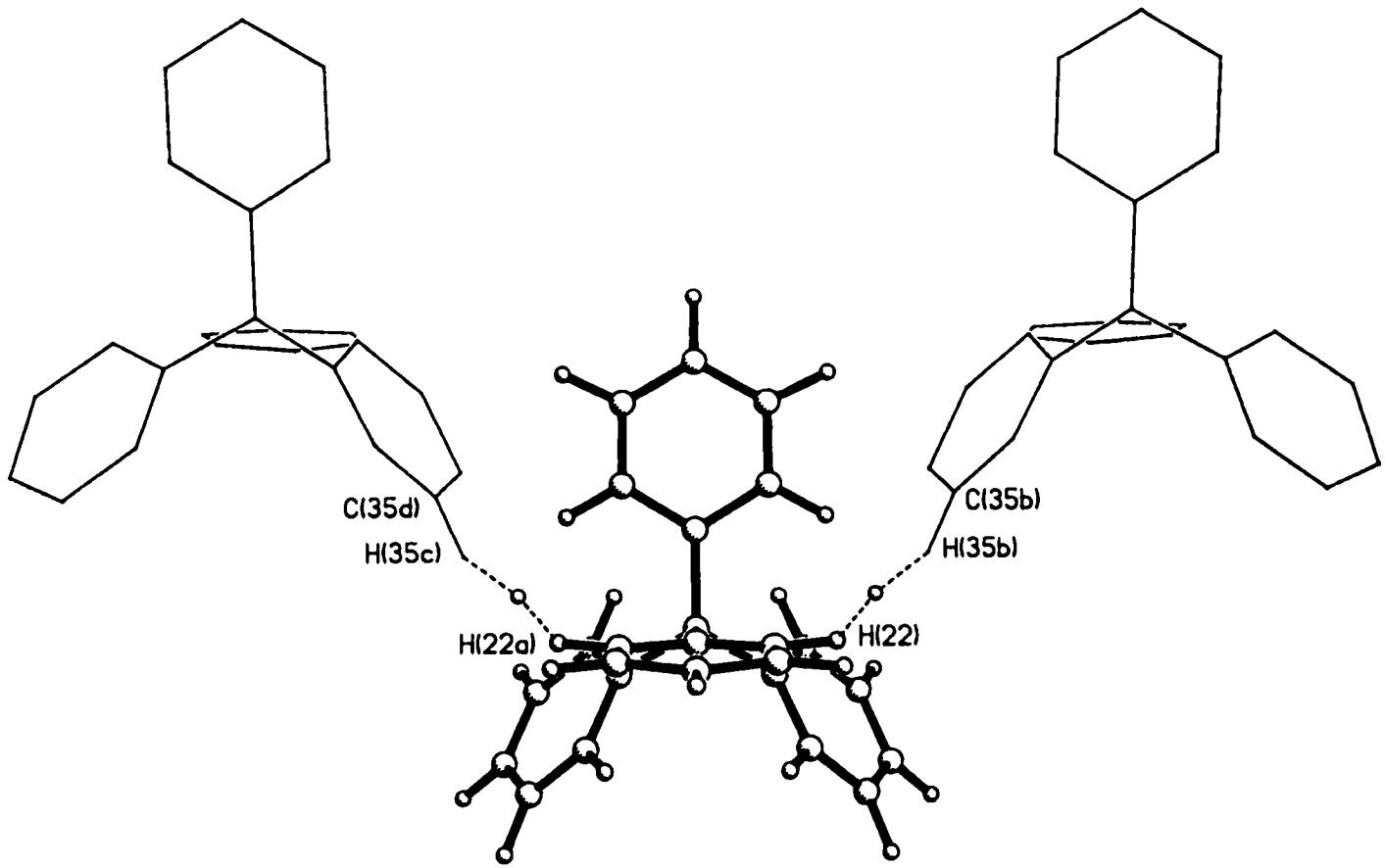

Figure 36. The C-H...phenyl interaction (anion/anion type - less than 3Å) accepted by ring #2 in the structure of [DabcoH][$B(C_6H_5)_4$]. The small open circle represents the location of the bond critical point of the interaction.

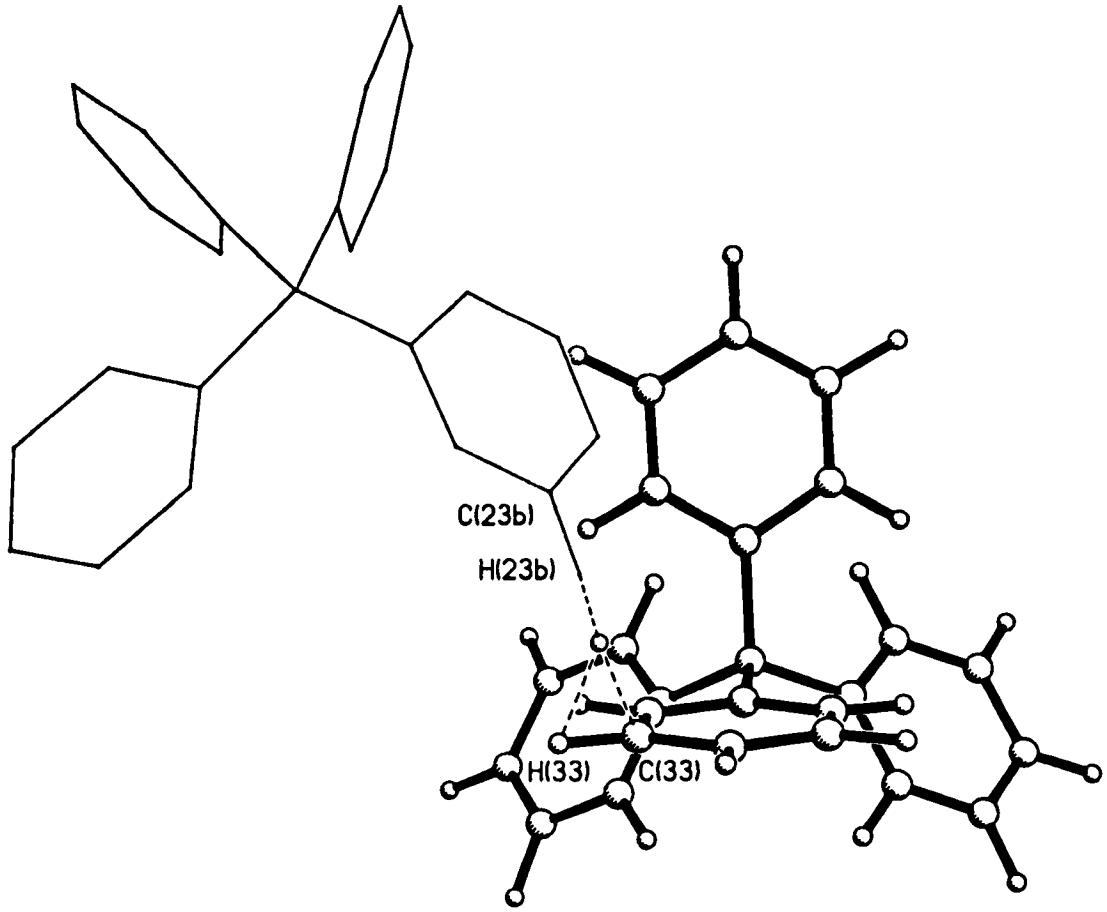

Figure 37. The C-H...phenyl interaction (anion/anion type - less than 3Å) accepted by ring #3 in the structure of [DabcoH][$B(C_6H_5)_4$]. The small open circle represents the location of the bond critical point of the interaction.

Again, such an interaction is likely not a hydrogen bond but some other type of weak contact.

The second anion/anion type C-H...phenyl interaction studied in [DabcoH][$B(C_6H_5)_4$] is donated by the C(23)-H(23) group of the original anion and accepted by ring 3 of an anion generated by the symmetry (1/2+*x*, *y*, 5/2-*z*). Since only one half of each ring 2 is unique, there are two equivalent C(23)-H(23) groups on each anion and they interact with the two symmetry related ring 3's present on a second anion (Figure 37).

The geometry of the interaction is characterized by H(23)...C_{ring} distances of 2.901Å [C(33)] and 3.033Å [C(34)], and C(23)-H(23)...C_{ring} angles of 124.0° [C(33)] and 138.9° [C(34)]. As with the previous anion/anion C-H...phenyl interaction, the C(23)-H(23) group actually forms closer contacts with H(33), 2.613Å (123.9°), and with H(34), 2.874Å (157.1°), from ring 2 of the second anion than with the ring carbon atoms themselves. The C(23)-H(23) vector makes an angle of 60.4° with the ring 2 plane of the second anion. The vector points towards the ring plane but outside and away from the ring itself. It passes closest to H(34), making an angle of 157.1° with that atom, but projects even further away from the ring than that. Both C(23) and H(23) also project onto the plane of ring 2 well outside the confines of the ring itself.

Neither of the anion/anion C-H...phenyl type contacts studied in [DabcoH][$B(C_6H_5)_4$] appear to be likely candidates for hydrogen bonds in the conventional geometrical sense. In both cases, the closest approaches are made between hydrogen atoms on adjacent anions, rather than being directional C-H...π(Ph) interactions. These would better be characterized as incidental close contacts, brought about by packing pressures on the

bulky tetraphenylborate anions.

3.4.3. C-H...Acceptor Contacts in Guanidinium Tetraphenylborate Acetonitrile Solvate

The structure of guanidinium tetraphenylborate acetonitrile solvate contains two very different types of cavities, shown most clearly in Figure 14 and already discussed. The first type of cavity is enclosed by rings 1 and 2 of two different anions, in a nearly square centrosymmetric arrangement. This cavity contains a pair of acetonitrile solvent molecules also centrosymmetrically arranged in a head to head fashion, with the two methyl groups closest to each other. Its position, buried in the first cavity, means that the acetonitrile solvent molecule, or more specifically its C-H groups, could only possibly interact with rings 1 and/or 2 of the anion; no close contacts with rings 3 or 4 are possible.

The second type of cavity in the structure is formed by rings 2, 3 and 4 of two different anions and encloses a pair of cations in an arrangement already described. Because the cation is contained within this second type of cavity, ring 1 can make no close approach to the cation and none of the N-H...π(Ph) hydrogen bonds formed involve ring 1 of the anion. It would be expected that anion ring 1 would form some alternate type of interaction(s) if possible, to satisfy its hydrogen bond "acceptor" potential.

In fact, the geometry search of guanidinium tetraphenylborate acetonitrile solvate located a strong interaction between C(3)-H(61) of an acetonitrile molecule and ring 1 of the anion. All six H(61)...C_{ring} distances were found to be less than 3.00Å, clearly indicative of a strong centroid type hydrogen bond geometry. As well, two weaker interactions

between the acetonitrile solvent molecule and the anion were also located, C(3)-H(60)...ring 1 and C(3)-H(62)...ring 2. The geometries of these interactions are given in Tables 40 and 41 of Appendix 4.

In addition, a number of $(C\text{-}H)_{anion}\cdots N$ contacts of less than 3Å were found, with the "acceptor" nitrogen atom coming from either the solvent, N(4), or the cation, N(2). For some reason, only N(2) of the guanidinium cation was found to engage in C-H...N interactions of less than 3Å, being involved in two such contacts. Four C-H...N interactions terminating at N(4) of the acetonitrile molecule were studied. All of these contacts tended to be rather long, close to the 3Å cutoff, with the exception of one, C(33)-H(33)...N(4) [H(33)...N(4) = 2.561Å], which was considerably shorter than the others.

Guanidinium tetraphenylborate acetonitrile solvate was also found to form six anion/anion C-H..phenyl contacts of less than 3Å. Again, all of these interactions were found to have relatively long $H\cdots C_{ring}$ distances, close to the 3Å cutoff. The shortest contact, C(24)-H(24) to C(14) of ring 1, is 2.863Å. No anion hydrogen atoms were found to make multiple close contacts to the carbon atoms of a single ring on an adjacent anion, meaning that none of the interactions have centroid type geometries. From the distances alone, the $(C\text{-}H)_{anion}\cdots(phenyl)_{anion}$ contacts in guanidinium tetraphenylborate acetonitrile solvate would be expected to be very weak.

Five of the six anion/anion contacts in guanidinium tetraphenylborate acetonitrile solvate were found to involve ring 1 of the anion, as either the "donor" or the "acceptor" for the interaction. The structure and packing of the salt provides a clue as to why this might be so. Ring 1

of the anion participates in no N-H...π(Ph) hydrogen bonds. It is not closely associated with the cation, rather only with the acetonitrile solvent molecule. This allows it to form closer contacts with phenyl rings on adjacent anions since it is not shielded by the cation in any direction. And, the formation of such contacts will be favoured, to fulfil the acceptor potential of ring 1, since it is not involved in any of the N-H...π(Ph) hydrogen bonds.

In guanidinium tetraphenylborate acetonitrile solvate, the solvent molecule serves as a possible source of C-H groups for contacts of the type $(C\text{-}H)_{solvent}\cdots(phenyl)_{anion}$. A geometry search was carried out for close contacts between each of the three alkyl C-H groups of the solvent to phenyl rings of the anion and, in fact, all three hydrogens of the solvent were found to form close contacts with anion phenyl rings. They are illustrated in Figures 38 and 39 on the following pages.

The first and most intriguing interaction was found to occur between C(3)-H(61) of the solvent molecule and phenyl ring 1 of the anion (Figure 38). H(61) of the original solvent molecule was found to make close approach, less than 3Å, to all six carbon atoms of a phenyl ring 1 generated by the symmetry (2-*x*, 2-*y*, 1-*z*). Such close and equal distances are indicative of a centroid type geometry for a hydrogen bonding interaction.

Both C(3) and H(61) were found to project onto the plane of ring 1 very close to the ring centroid. H(61) projects almost on top of the centroid, while C(3) lies a bit off the centroid, approximately midway between the centroid and the midpoint of the C(13)-C(14) bond. The C(3)-H(61) vector points generally toward the ring 1 centroid (157.9°).

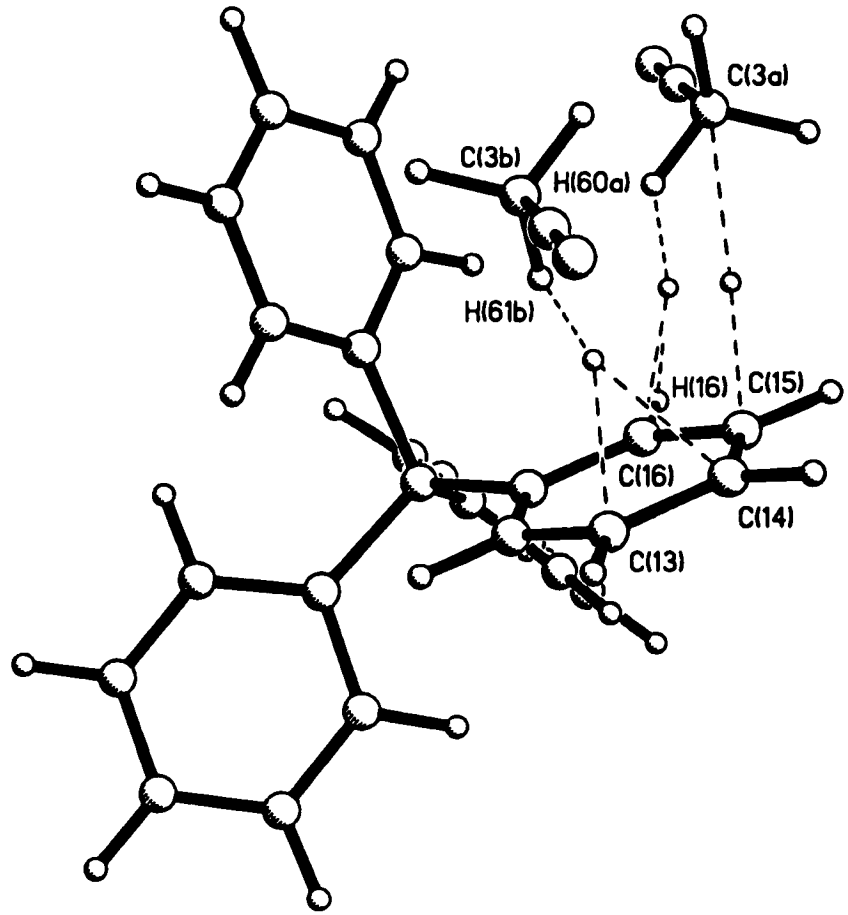

Figure 38. The C-H...phenyl interactions (solvent/anion type - less than 3Å) accepted by ring #1 in the structure of guanidinium tetraphenylborate acetonitrile solvate. The small open circles represent the locations of the bond critical points of the interactions.

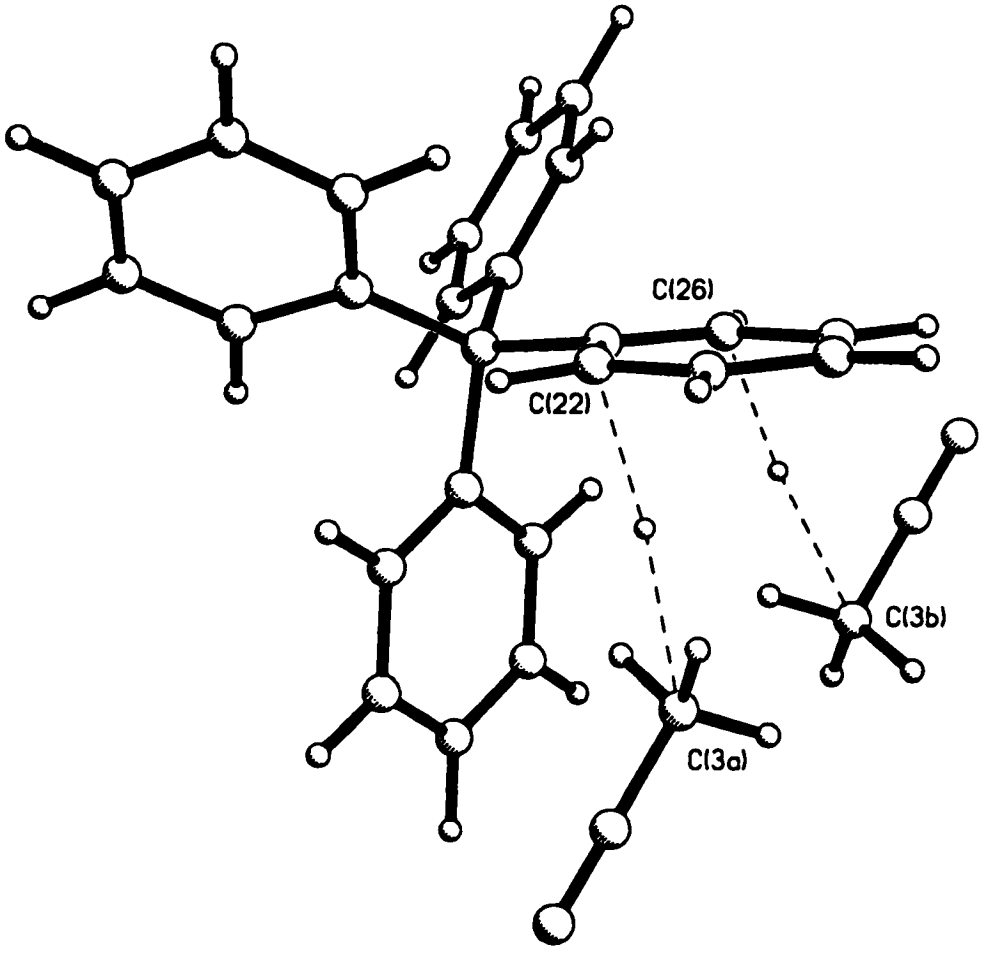

Figure 39. The C-H...phenyl interactions (solvent/anion type - less than 3Å) accepted by ring #2 in the structure of guanidinium tetraphenylborate acetonitrile solvate. The small open circles represent the locations of the bond critical points of the interactions.

However, it is angled slightly toward the midpoint of the C(11)-C(16) bond and thus the most linear C(3)-H(61)...C_{ring} angles are formed to C(11) and C(16), 166.6° and 164.0°, respectively. The C(3)-H(61) vector makes an angle of 66.5° with the plane of ring 1 in the anion.

The C(3)-H(61)...ring 1 interaction has a definite centroid type geometry. The H(61)...C_{ring} distances cover a narrow range of values, from a maximum of 2.901Å to C(15) to a minimum of 2.765Å to C(11) [100Δ = 14], all greater than the H(61)...π_c ring centroid distance of 2.472Å. Similarly, the C(3)...C_{ring} distances range from only 3.579(3)Å, C(13), to 3.941(3)Å, C(16) [100Δ = 36], and all are longer than the C(3)...π_c ring centroid distance of 3.501Å. Because of the centroid type geometry of this interaction, all of the H(61)...H_{ring} distances are longer than the corresponding H(61)...C_{ring} values; H...H contacts are not important in this instance. This interaction has all the characteristics of a C-H...π(Ph) hydrogen bond.

The C(3)-H(61)...π_c (ring 1) interaction in guanidinium tetraphenylborate acetonitrile solvate can be compared to the three N-H...π(Ph) hydrogen bonds with centroid type geometries found in the same structure. These three N-H...π(Ph) hydrogen bonds were characterized by H(N)...π_c distances and N-H...π_c angles of 2.238Å, 170.1° [N(1)-H(1A)...ring 2], 2.308Å, 159.1° [N(3)-H(3B)...ring 3], and 2.405Å, 137.5° [N(3)-H(3A)...ring 4], respectively. The average H...π_c distance is 2.317Å and the average N-H...π_c angle is 156° for the three N-H...π(Ph) hydrogen bonds. These can be compared to the same values for the C(3)-H(61)...ring 1 interaction, H(61)...π_c = 2.472Å and C(3)-H(61)...π_c = 157.9°. Obviously, the C(3)-H(61)...ring 1 interaction has a geometry very similar to the

N-H...π(Ph) hydrogen bonds. However, it does occur at a slightly longer distance than the N-H...π(Ph) contacts, indicating a somewhat weaker interaction. Still, this provides more evidence that the contact, C(3)-H(61)...ring 1, should be considered a hydrogen bond. It is also interesting to note that if this is true, all four rings of the anion serve as the acceptor in one centroid type hydrogen bond in guanidinium tetraphenylborate acetonitrile solvate.

The C(3)-H(61)...ring 1 interaction in guanidinium tetraphenylborate acetonitrile solvate can also be compared to the similar interaction, C(14)-H(14)...ring 1, located in ammonium tetraphenylborate. Both C-H...π(Ph) contacts were found to have centroid type geometries, although the former occurs between the solvent and the anion while the latter involves an anion/anion contact. The C(14)-H(14)...ring 1 interaction is characterized by an H(14)...π_c ring centroid distance of 2.717Å and a C(14)-H(14)...π_c angle of 171.6°. The C(3)-H(61)...ring 1 interaction has a considerably shorter H...π_c distance (2.472Å) but a less linear C-H...π_c angle (157.9°). Still, on the basis of distance it would appear that the C(3)-H(61)...ring 1 interaction in guanidinium tetraphenylborate acetonitrile solvate is the stronger. This is not surprising considering the less favourable overall charge difference in the anion/anion contact (-1,-1) compared to the solvent/anion (0,-1) interaction.

The same acetonitrile solvent molecule that was involved in the first $(C\text{-}H)_{solvent}\cdots(phenyl)_{anion}$ contact was found to form a contact of less than 3Å with ring 2 of the anion also involved in the first interaction, symmetry (2-*x*, 2-*y*, 1-*z*). This C(3)-H(62)...ring 2 interaction is shown in Figure 39. It is not as strong a contact as the C(3)-H(61)...ring 1

interaction, based on a comparison of the geometries. In fact, considering a single acetonitrile molecule, C(3)-H(61)...ring 1 forms a hydrogen bond with a direct centroid type geometry, C(3)-H(62) forms a less ideal interaction with ring 2 of the same anion, and C(3)-H(60) points away from this anion, forming a weak contact with ring 1 of the second anion which participates in formation of the cavity. Both C(3)-H(60) and C(3)-H(62) form weaker interactions, taking what is left over after optimization of the first stronger C(3)-H(61)...ring 1 hydrogen bond.

The C(3)-H(62) vector makes an angle of 47.9° with the plane of ring 2 in the second interaction. C(3) projects onto the plane of ring 2 inside the ring, close to the midpoint of the C(22)-C(23) bond, slightly closer to C(23). H(62) projects almost exactly onto the C(22)-C(23) ring bond, about three quarters of the way along the bond toward C(23). The C(3)-H(62) vector points toward the ring plane but away from the ring itself. The best angle with a ring atom is made to H(23), 157.8°, but the C(3)-H(62) vector points even slightly further outside the ring than that.

The C(3)-H(62)...ring 2 interaction has an edge type geometry. There are two C(3)...C_{ring} distances, C(3)...C(23) = 3.752(3)Å and C(3)...C(22) = 3.775(4)Å, less than the C(3)...π_c ring centroid distance of 3.786Å. The maximum C(3)...C_{ring} distance, to C(25), 4.284(4)Å, results in a value for 100Δ of 53. Similarly, there are two H(62)...C_{ring} distances, H(62)...C(23) = 2.886Å and H(62)...C(22) = 3.130Å, that are shorter than the H(62)...π_c distance of 3.210Å, although it should be noted that H(62)...C(23) is considerably shorter than the H(62)...C(22) distance. The maximum H(62)...C_{ring} distance is made to C(26), 4.012Å, for a 100Δ value of 113. The corresponding C(3)-H(62)...C_{ring} angles are 139.2° to C(23), 117.2° to

C(22) and 114.2° to the ring centroid, π_c. The individual H(62)...H_{ring} distances are all longer than the corresponding H(62)...C_{ring} values. However, the H(62)...H(23) distance (3.070Å) is close to the minimum H(62)...C_{ring} distances and the C(3)-H(62)...H(23) angle (157.8°) is more linear. The C(3)-H(62)...ring 2 interaction is best described as having an edge type geometry, to C(22)-C(23) of ring 2, with a possible contribution by the close H...H contact. By any of the possible geometric criteria the C(3)-H(62)...ring 2 interaction would be expected to be weaker than C(3)-H(61)...ring 1 but the former would still be described in terms of a hydrogen bond.

The last $(C\text{-}H)_{solvent}\cdots(phenyl)_{anion}$ interaction in guanidinium tetraphenylborate acetonitrile solvate, C(3)-H(61)...ring 1, proceeds from the original solvent molecule to an anion ring 1 of symmetry (*x*, *y*, 1+*z*), a different anion than that involved in the first two contacts. It is illustrated in Figure 38. Considered in the opposite direction, both acetonitrile molecules interact with the same face of a single anion ring 1. Again, the C(3)-H(60)...ring 1 contact has a much less favourable geometry than the C(3)-H(61)...ring 1 interaction; it is much more similar to C(3)-H(62)...ring 2. Both of the two weaker interactions have compromise geometries, the first strong interaction being formed at their expense.

In the C(3)-H(60)...ring 1 interaction, both C(3) and H(60) project onto the plane of ring 1 well outside the confines of the ring itself, H(60) closest to H(16) and C(3) even further beyond ring 1. The C(3)-H(60) vector runs almost parallel to the plane of ring 1, making an angle of only 26.7° with the ring. The C(3)-H(60) vector projects toward the ring

plane but passes across the ring face forming an angle of 165.3° with C(12) and 172.2° with H(12) on the opposite side of the ring; the H(60)...C(12) and H(60)...H(12) distances are too long to be important.

The C(3)-H(60)...ring 1 interaction has an edge type geometry based on the C(3)...C_{ring} and H(60)...C_{ring} distances. Both the C(3)...C(15), 3.721(3)Å, and the C(3)...C(16), 3.715(3)Å, distances are shorter than the C(3)...π_c ring centroid distance of 4.440Å [maximum C(13) 5.434(3)Å; 100Δ = 172]. Similarly, H(60)...C(15), 2.965Å, and H(60)...C(16), 2.799Å, are shorter than the H(60)...π_c distance of 3.465Å [maximum C(13) 4.481Å; 100Δ = 168]. The angle to the ring centroid, C(3)-H(60)...π_c, is 150.3°, while that to the closest ring carbon atom, C(3)-H(60)...C(16), is 142.1°.

Based on the geometry described thus far, the C(3)-H(60)...ring 2 interaction would be considered an edge type contact, to the C(15)-C(16) bond of phenyl ring 1. However, in this case the H(60)...H_{ring} contacts are also important, with H(60)...H(16) = 2.657Å (125.6°) and H(60)...H(15) = 3.009Å (106.5°). The H(60)...H(16) distance is actually the shortest contact to ring 1 and must be considered; it should make a significant contribution to the interaction. Still, the distances H(60)...C(16) and H(60)...H(16) are relatively equal so this cannot be considered solely an H...H type interaction. It is, by geometry, some type of intermediate type interaction.

Guanidinium tetraphenylborate acetonitrile solvate was found to form six $(C\text{-}H)_{anion}$...N interactions of less than 3Å (Figure 40), four to N(4) of the acetonitrile solvent molecule and two to N(2) of the cation. They were found to range in H...N distance from 2.561Å [C(33)-H(33)...N(4)] to well above the 3Å cutoff [not studied]. Most of the contacts studied are

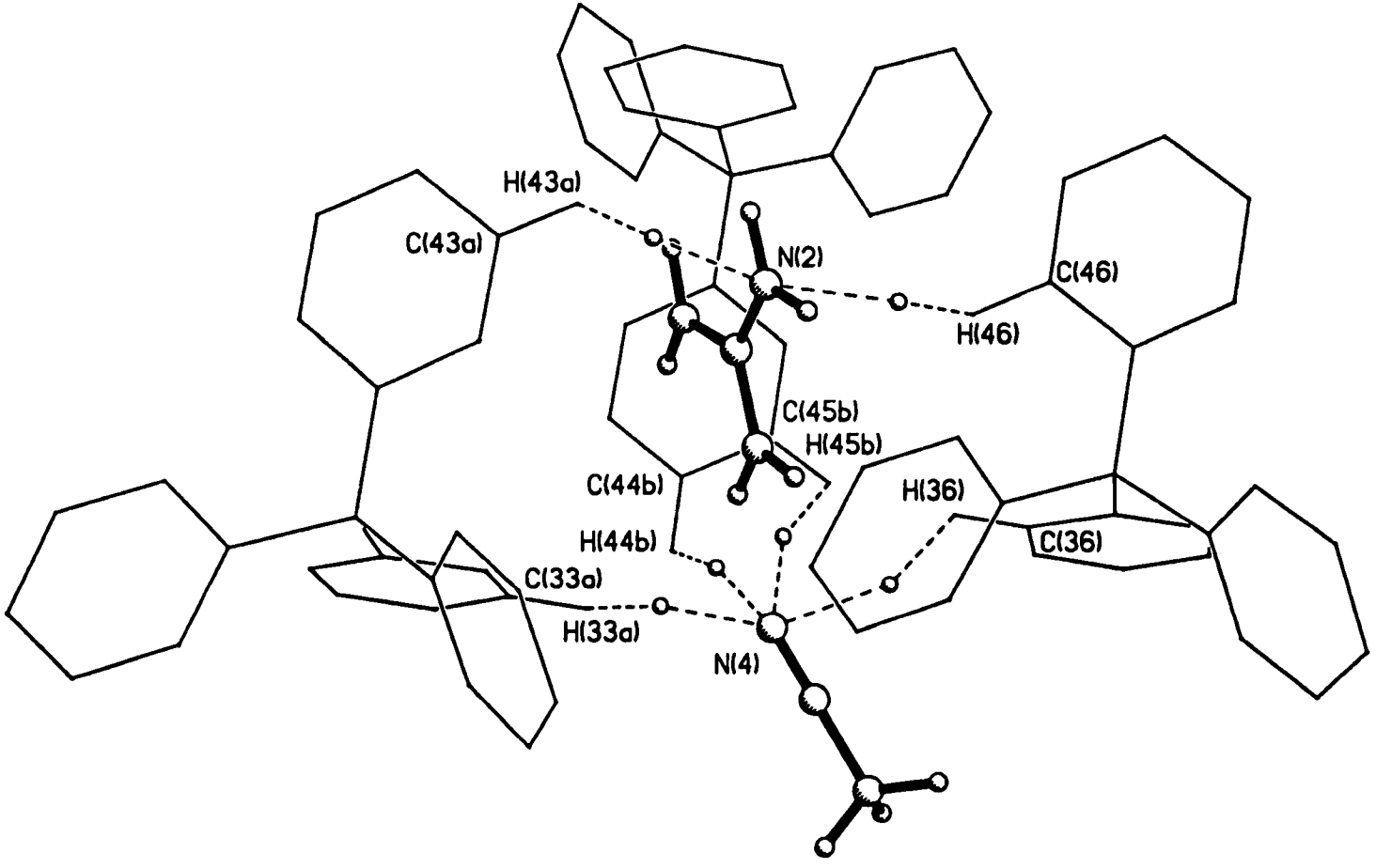

Figure 40. The C-H...N interactions located (less than 3Å) in the structure of guanidinium tetraphenylborate acetonitrile solvate. The small open circles represent the locations of the bond critical points of the interactions.

close to the 3Å cutoff chosen and are likely weak and not particularly important.

It is not surprising that N(4) of acetonitrile, with its lone pair of electrons and triple bond, should participate in a number of C-H...N anion/solvent type interactions. Of the four located at an H...N distance of less than 3Å, only one was short enough to be of significant interest. In the C(33)-H(33)...N(4) contact, the original anion interacts with an acetonitrile molecule of symmetry $(1+x, y, z)$, or conversely, the original solvent molecule interacts with ring 3 of an anion having the symmetry $(-1+x, y, z)$. The angle made between the plane of ring 3 and the line defined by N(4), C(2) and C(3) of the acetonitrile backbone is 124.2°. The acetonitrile molecule, C(3)-C(2)-N(4), projects toward the plane of ring 3 but never actually meets the ring, projecting instead directly below H(33). The C(33)-H(33) vector points quite directly toward N(4). The C(33)-H(33)...N(4) interaction is characterized by a C(33)...N(4) distance of 3.598Å, an H(33)...N(4) distance of 2.561Å and a relatively linear C(33)-H(33)...N(4) angle of 161.8°.

The three remaining $(C\text{-}H)_{anion}\cdots N_{solvent}$ contacts are all expected to be much weaker, with longer H...N(4) distances and smaller C-H...N angles. The second interaction, C(36)-H(36)...N(4), occurs between the original anion and solvent molecule. H(36), as a result of the packing geometry, makes relatively close contact to both N(4) of the solvent and N(1) of the cation [H(36)...N(1) = 3.010Å]. The C(36)-H(36) vector proceeds linearly from the anion towards N(1) of the cation (171.5°) rather than towards N(4) or any other part of the solvent. The C(3)-C(2)-N(4) backbone of acetonitrile projects toward the plane of ring 3 but away from the ring

itself. N(4) projects far to the outside of ring 3, beyond H(36); it is not close to any other of the ring atoms. The contact C(36)-H(36)...N(4) is characterized by a C(36)...N(4) distance of 3.739Å, an H(36)...N(4) distance of 2.963Å and a C(36)-H(36)...N(4) angle of 129.3°. By geometry, it is likely weak and relatively unimportant, especially when compared to the shorter and more linear C(33)-H(33)...N(4) contact.

The final two $(C\text{-}H)_{anion}$...N(4) contacts involve C(44)-H(44) and the adjacent C(45)-H(45) from the same ring 4 of the original anion to an acetonitrile molecule generated by the symmetry (2-*x*, 1-*y*, 1-*z*). The angle between the plane of ring 4 and the line defined by the acetonitrile backbone, N(4)-C(2)-C(3), is only 7.4°, indicating that the two are nearly parallel. A projection of the acetonitrile backbone will not intersect the plane of ring 4 at any reasonable distance and, in fact, acetonitrile is angled slightly away from the ring. Conversely, neither the C(44)-H(44) vector nor the C(45)-H(45) vector are directed toward N(4) of the solvent, which projects onto the plane of ring 4 somewhere between them, slightly closer to H(44) than to H(45). C(44)-H(44)...N(4) has a C(44)...N(4) separation of 3.399Å, an H(44)...N(4) separation of 2.805Å and a C(44)-H(44)...N(4) angle of 114.8°. The corresponding values for the C(45)-H(45)...N(4) contact are 3.452Å, 2.947Å and 109.0°, respectively, slightly longer and less linear. Both contacts appear to be too long and distorted to be of great importance.

Guanidinium tetraphenylborate acetonitrile solvate was found to make two additional $(C\text{-}H)_{anion}$...N contacts of less than 3Å, both to N(2) of the cation (Figure 40). Many other longer $(C\text{-}H)_{anion}$...N_{cation} contacts were located, to all terminal nitrogen centers of the cation, including the

next longest and already mentioned C(36)-H(36)...N(1) contact, but these were not studied further.

Although theoretically the isolated guanidinium cation contains three equivalent terminal NH_2 groups, in the crystal structure N(2) must differ from N(1) and N(3) in some way since only it is involved in the shortest $(C\text{-}H)_{anion}\cdots N_{cation}$ contacts. Based on geometrical observations, a possible explanation emerges. The N(1) center of the cation is involved in two strong hydrogen bonds, one of the N-H...N type, the strongest in the structure, and one N-H...π(Ph) interaction with a centroid type geometry. Similarly, N(3) is involved in two relatively strong N-H...π(Ph) hydrogen bonds both with centroid type geometries. N(2) forms the weakest pair of hydrogen bonds in the cation, both having edge type geometries and longer contact distances. Perhaps, N(2) seeks to fulfil its interaction potential by forming two more, even weaker, contacts with C-H groups of the anion. Of course, it is also possible that the $(C\text{-}H)_{anion}\cdots N(2)_{cation}$ interactions are purely incidental, a result of the formation and optimization of the stronger N-H...π(Ph) hydrogen bonds in the structure. The fact that both close $(C\text{-}H)_{anion}\cdots N_{cation}$ contacts are made to N(2) may be accidental, a consequence of the packing geometry. In fact, after studying the two interactions, the latter explanation may be the more reasonable.

The first contact, C(46)-H(46)...N(2), is formed between atoms of the original cation and anion, and is related to the C(36)-H(36)...N(1) contact mentioned earlier, occurring between the same cation/anion pair. It is likely that hydrogen bonding and other packing forces exert the pressures that result in the formation of these weak contacts. For

example, in the original cation, N(1)-H(1A) [centroid type] and N(2)-H(2A) [edge type] both form hydrogen bonds to ring 2 of the original anion. The formation of these stronger interactions brings the cation and anion into close proximity so that the weaker C-H...N contacts also result.

Because of the orientation of the anion relative to the cation, both C(36)-H(36) and C(46)-H(46) of the anion are directed toward the cation plane, with both vectors aimed nearly linearly toward N(1) of the cation [C(36)-H(36)...N(1) = 171.5° and C(46)-H(46)...N(1) = 171.9°]. The cation plane and the ring 4 plane make an angle of 54.0°, while the C(46)-H(46) vector makes an angle of 49.6° with the ring 4 plane. H(46) projects onto the cation plane close to H(2A), just slightly shifted towards H(1A). The C(46)...N(2) distance is 3.697Å, the H(46)...N(2) distance is 2.775Å and the C(46)-H(46)...N(2) angle is 143.6°, much less linear than the C(46)-H(46)...N(1) angle. The distance between H(46)and H(2A), 2.492Å, is the shortest contact H(46) makes to the cation [C(46)-H(46)...N(2) = 136.4°]. The H(46)...H(2A) separation of 2.492Å is considerably shorter than the H(46)...N(2) separation of 2.775Å, supporting the idea that this contact could be predominantly a weak H...H contact rather than a hydrogen bond.

The geometry of the second contact, C(43)-H(43)...N(2), is similar to that of the first contact. This interaction occurs between the original cation and an anion generated by the symmetry (-1+*x*, *y*, *z*). It occurs to the opposite face of the cation relative to the first C(46)-H(46)...N(2) contact. Ring 4 of the two anions involved in the two contacts are related by a translation of ±1 along the *x* axis and lie parallel to one another.

The C(43)-H(43) vector and the cation plane form an angle of 53.5°,

with the vector projecting toward the cation plane. Both C(43) and H(43) project onto the cation plane closest to, but further beyond, H(2B). The C(43)-H(43) also passes closest to H(2B) of the cation but even that angle is poor [C(43)-H(43)...H(2B) = 139.7°]. In the C(43)-H(43)...N(2) contact, the C(43)...N(2) distance is 3.567Å, the H(43)...N(2) distance is 2.797Å and the C(43)-H(43)...N(2) angle is 128.4°. As in the first contact, the closest cation/anion approach is actually made between H(43) and H(2B), 2.485Å, shorter than the H(43)...N(2) distance. Both of the $(C\text{-}H)_{anion}\cdots N(2)_{cation}$ contacts likely contain significant H...H components to the interactions. They could easily arise as an incidental consequence of the formation of other stronger interactions in the structure.

One final type of C-H...X contact was located in a geometry search of the structure of guanidinium tetraphenylborate acetonitrile solvate, $(C\text{-}H)_{anion}\cdots(phenyl)_{anion}$. Six such anion/anion contacts of less than 3Å were found, the shortest being C(24)-H(24)...ring 1 at 2.863Å to C(14) of the anion ring. All other interactions were longer, approaching the chosen 3Å cutoff, and are likely weak. The contacts studied are shown in Figures 41 to 43, for acceptor phenyl rings 1, 3 and 4, respectively. None of the interactions were found to have centroid type geometries; in each case only a single $H\cdots C_{ring}$ contact of less than 3.00Å was located. In fact, in almost every interaction the $H\cdots H_{ring}$ contacts were found to be shorter than the minimum $H\cdots C_{ring}$ distances, leading to the suspicion that these are not hydrogen bonds but rather some other form of weak interaction.

Of the six $(C\text{-}H)_{anion}\cdots(phenyl)_{anion}$ contacts studied, five were found to involve ring 1 of the anion, as either "acceptor", "donor" or both (Figure 41). This is perhaps not surprising since ring 1 is not involved

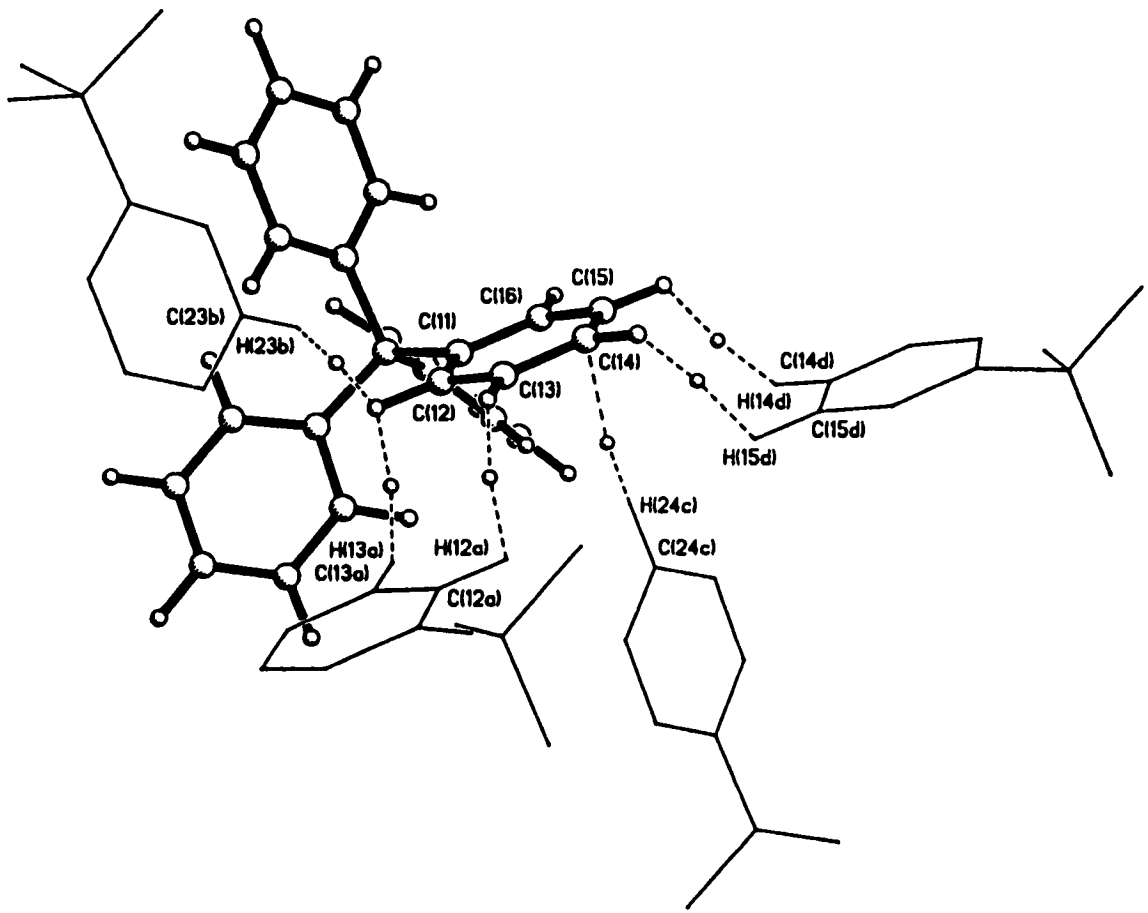

Figure 41. The C-H...phenyl interactions (anion/anion type - less than 3Å) accepted by ring #1 in the structure of guanidinium tetraphenylborate acetonitrile solvate. The small open circles represent the locations of the bond critical points of the interactions. Uninvolved rings on the interacting tetraphenylborate anions have been omitted for clarity.

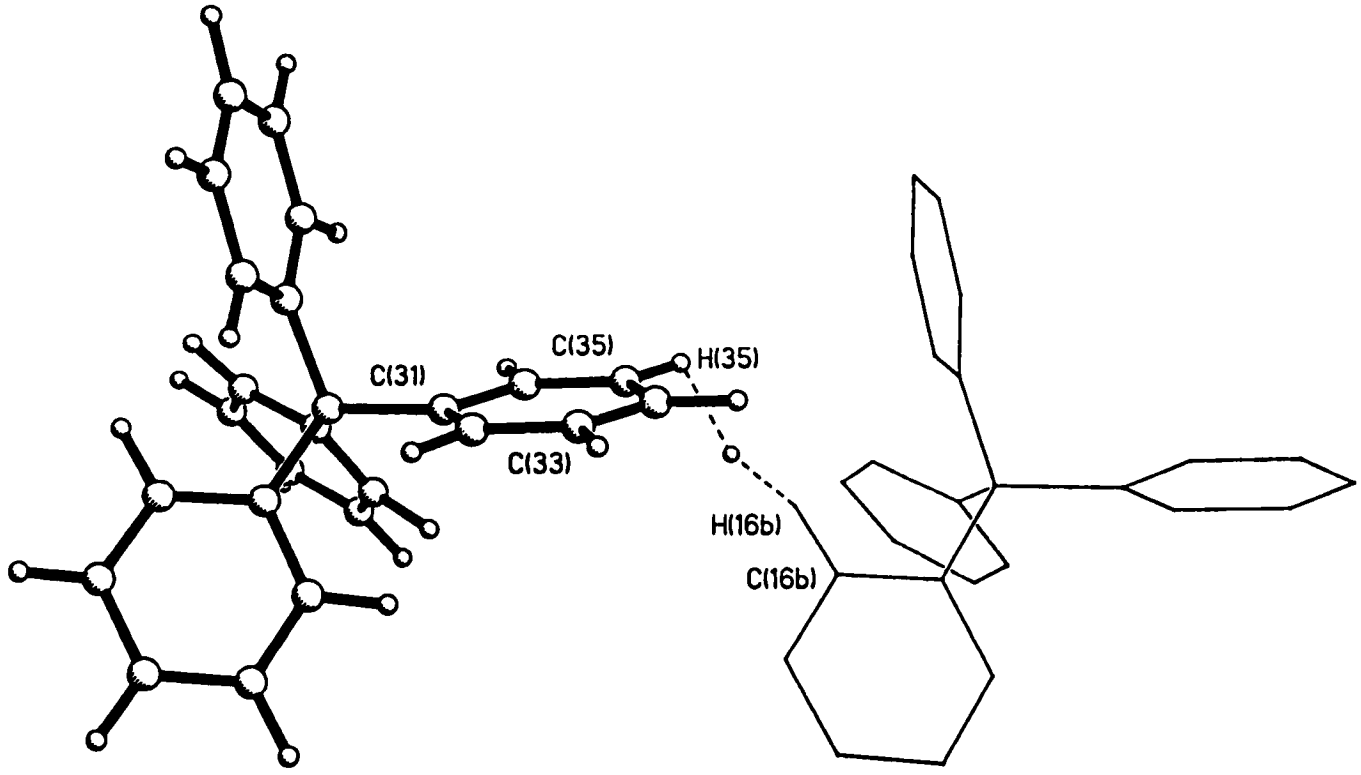

Figure 42. The C-H...phenyl interaction (anion/anion type - less than 3Å) accepted by ring #3 in the structure of guanidinium tetraphenylborate acetonitrile solvate. The small open circle represents the location of the bond critical point of the interaction.

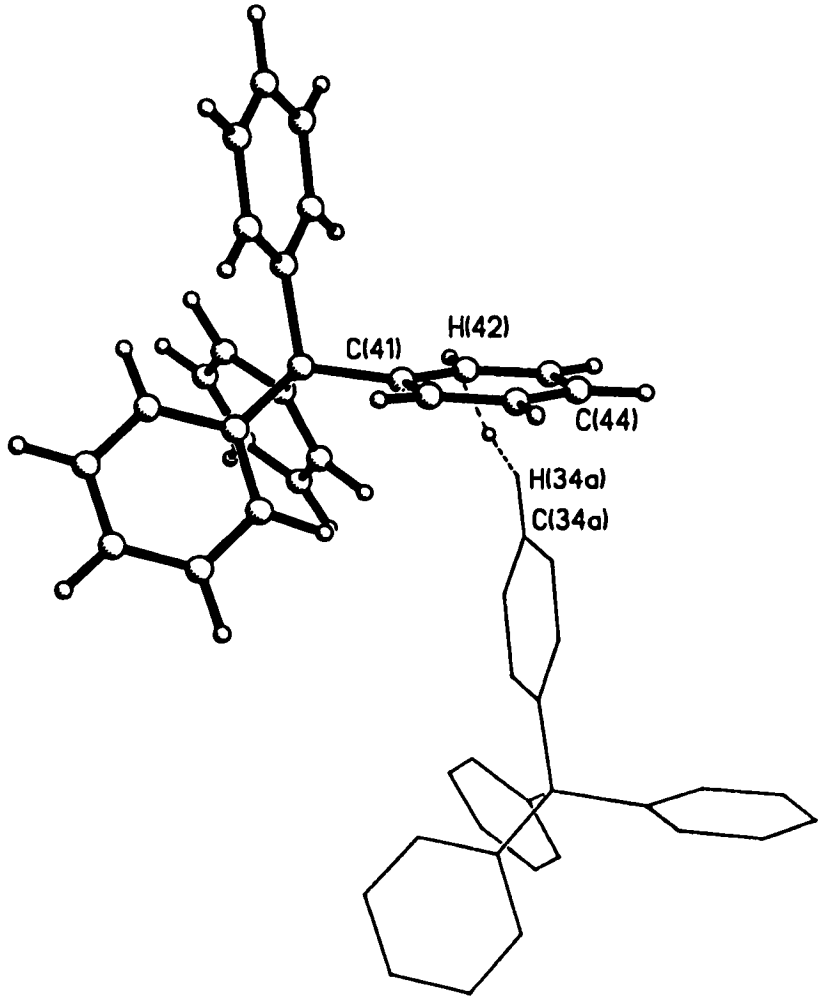

Figure 43. The C-H...phenyl interaction (anion/anion type - less than 3Å) accepted by ring #4 in the structure of guanidinium tetraphenylborate acetonitrile solvate. The small open circle represents the location of the bond critical point of the interaction.

in any of the N-H...π(Ph) hydrogen bonds in the structure. Ring 1 does form a strong C-H...π(Ph) centroid geometry bond with the acetonitrile solvent molecule but is obviously still available to participate in other close C-H type interactions. Since ring 1 forms no close contacts with the cation, it can likely form closer approaches with both the solvent and adjacent anion phenyl rings since it is not blocked in any direction by the cation.

There are two $(C\text{-}H)_{anion}\cdots(phenyl)_{anion}$ interactions in guanidinium tetraphenylborate acetonitrile solvate which occur between ring 1 of two adjacent anions. They both have similar geometries, involving parallel rings related by a center of symmetry between them. This arrangement of anions could also help explain why ring 1 is involved in so many of the anion/anion contacts.

The first interaction, C(13)-H(13)...ring 1 [H(13)...C(12) = 2.981Å], occurs between ring 1 of the original anion and ring 1 of an anion generated by the symmetry (3-*x*, 2-*y*, 1-*z*). There are two equivalent contacts between the interacting rings, C(13)-H(13)...C(12)' and C(13)'-H(13)'...C(12). Because of the arrangement of the interacting rings, C(12)-H(12)...C(13)' and its symmetry equivalent should also make relatively close contacts.

The two interacting ring 1s lie in parallel planes but they are not coplanar and are aligned in opposite directions. They do not overlap at all if projected onto a common plane. H(12) of one ring projects very near H(13)' of the second ring and vice versa; they are just slightly offset. There is a center of symmetry relating the two rings, located at the intersection of H(12)...H(12)' and H(13)...H(13)'. The C(12)-C(13) and

C(13)'-C(12)' ring bonds are parallel to each other and only slightly offset. They are the closest ring bonds between the two interacting rings, while the overall closest approaches are made between H(12)/H(13)' and H(12)'/H(13).

Since the two ring 1s lie in parallel planes, the C(13)-H(13) vector from each ring will never intercept the plane of the other ring 1. The angle between the two ring 1 planes is 0.0°, as expected, while the C(13)-H(13) vector makes an angle of only 0.1° with the plane of the second ring 1. If the two rings could be superimposed, the C(13)-H(13) vector would point almost directly at H(12)' of the second ring, whereas the C(12)-H(12) vector would point outside and away from the second ring.

The C(13)-H(13)...ring 1 contact is characterized by one most important distance, H(13)...H(12)', equal to 2.454Å. The corresponding C(13)-H(13)...H(12)' angle is 124.0° while the C(12)-H(12)...H(13)' angle is 108.9°. The H(13)...H(12)' distance is considerably shorter than either H(13)...C(12)', 2.981Å (130.6°) or H(12)...C(13)', 3.183Å (115.3°). The H(13)...H(13)' distance, 3.026Å (93.1°), is also significantly longer than H(13)...H(12)'. All of the angles are relatively nonlinear, not surprising considering the geometry of the interaction. This contact, occurring twice between the two rings, is best considered an H...H type interaction and not a hydrogen bond. The very short H(13)...H(12)' distance, 2.454Å, and the unfavourable parallel ring geometry both preclude hydrogen bond formation.

There is a second, nearly identical $(C\text{-}H)_{anion}\cdots(phenyl)_{anion}$ contact in guanidinium tetraphenylborate acetonitrile solvate, also involving ring 1 of two adjacent anions, C(14)-H(14)...ring 1 [H(14)...C(15) =

2.966Å]. C(14)-H(14) of the original anion interacts with a second ring 1 of an anion generated by the symmetry (3-*x*, 2-*y*, -*z*), a translation of ±1 along the *z* axis from the anion involved in the first interaction.

In this interaction, the two ring 1s again lie in parallel planes and are oriented in opposite directions such that the C(14)-C(15) bond of one ring is parallel and closest to the C(15)'-C(14)' bond of the second ring. The two interacting rings are related by a center of symmetry which lies at the intersection of H(14)...H(14)' and H(15)...H(15)'. In projection H(14) of the first ring 1 lies close to H(15)' in the plane of the second ring 1 and vice versa; these are definitely the closest contacts between the two rings. There are thus two equivalent interactions, C(14)-H(14)...C(15)' and C(14)'-H(14)'...C(15), between the two ring 1s. Also, from the geometry of the interaction, it would be expected that C(15)-H(15)...C(14)' and C(15)'-H(15)'...C(14) would form reasonably close contacts.

The C(14)-H(14) vector makes an angle of only 1.4° with the plane of the second ring 1. Since the two rings lie in parallel planes, the angle between them is 0.0°, one vector will never project onto the plane of the other ring. However, if the two ring 1s could be projected onto a common plane, C(14)-H(14) of one ring would point directly toward H(15)' of the second ring and vice versa. The C(15)-H(15) vector would, on the other hand, point outside and away from the second ring.

Just as in the first interaction, the important distance defining the contact is the H...H separation, in this case H(14)...H(15)' equal to 2.357Å. This distance is much shorter than either H(14)...C(15)', 2.966Å (126.7°), or H(15)...C(14)', 3.057Å (119.8°), and is also much shorter

than all other H...H_{ring} contacts. The C(14)-H(14)...H(15)' angle is 121.3°, while the C(15)-H(15)...H(14)' angle is 114.3°. All of the C-H...X_{ring} (X = C or H) angles are much less than 180°, as expected from the geometry of the interaction. Based on its parallel ring geometry and very short H(14)...H(15)' distance, this interaction is also best considered as a weak H...H contact, C(14)-H(14)...H(15)', rather than as a hydrogen bond.

There are two other $(C\text{-}H)_{anion}$...$(phenyl)_{anion}$ interactions "accepted" by ring 1 of the anion. The first of these, C(23)-H(23)...ring 1, with a minimum H(23)...C_{ring} distance to C(12), 2.922Å, proceeds from ring 2 of the original anion to ring 1 of an anion generated by the symmetry (2-*x*, 2-*y*, 1-*z*). The second interaction, C(24)-H(24)...ring 1 [H(24)...C(14) = 2.863Å], proceeds also from ring 2 of the original anion to a different anion phenyl ring 1 generated by the symmetry (-1+*x*, *y*, *z*).

In the C(23)-H(23)..ring 1 contact, the angle between the planes of rings 1 and 2 is 93.1°; they are approximately perpendicular. However, the angle between the C(23)-H(23) vector and the plane of ring 1 is only 33.5°. The C(23)-H(23) vector points most directly at C(12) in the ring plane, forming an almost linear angle of 172.5° with it. If projected onto the plane of ring 1, C(23), H(23) and all other ring 2 atoms lie far from ring 1. H(23) projects directly above C(12) but far outside even H(12) of ring 1, at roughly twice the C(12)-H(12) distance, while C(23) projects even further away from the ring.

In the C(23)-H(23)...ring 1 interaction, the only close H(23)...C_{ring} contact (less than 3Å) is to C(12), 2.922Å, forming a C(23)-H(23)...C(12) angle of 172.5°. This distance is eclipsed, however, by the very short

H(23)...H(12) separation of only 2.337Å (154.8°). The only other close contact, made to H(13) of ring 1 [H(23)...H(13) = 2.970Å (133.4°)], is also much longer than the H(23)...H(12) distance. Once again, this interaction, C(23)-H(23)...H(12), appears to be a weak H...H type contact rather than a hydrogen bond.

The C(24)-H(24)...ring 1 contact is different from any other $(C\text{-}H)_{anion}\cdots(phenyl)_{anion}$ interaction in guanidinium tetraphenylborate acetonitrile solvate. Its H(24)...C(24) distance of 2.863Å is the shortest such contact located in the geometry search. And, the angle made by the C(24)-H(24) vector to the plane of ring 1 is 83.5°, an almost T-shaped or perpendicular interaction. This is the only anion/anion contact in the structure that has a geometry suggestive of a hydrogen bonding interaction. Both C(24) and H(24) project onto the plane of ring 1 inside the confines of the ring. Because the interaction is close to perpendicular, both C(24) and H(24) project to almost exactly the same point, close to C(14), just inside the ring. This is also directly where the C(24)-H(24) vector projects.

The $H(24)\cdots C_{ring}$ distances range from a minimum of 2.863Å, to C(14), to a maximum of 3.707Å, to C(11) [100Δ = 84]. The corresponding angle, C(24)-H(24)...C(14), is a relatively linear 164.8° and the C(24)...C(14) distance is 3.912Å. Only the minimum $H(24)\cdots C_{ring}$ distance, to C(14), is shorter than the $H(24)\cdots\pi_c$ ring centroid distance of 2.988Å (166.1°). Unlike the previous interactions, there are no close $H(14)\cdots H_{ring}$ contacts, the shortest being H(24)...H(14) at 3.186Å (145.7°). H...H contacts likely do not determine the nature of this interaction. Rather, it would be described as a $(C\text{-}H)_{anion}\cdots(phenyl)_{anion}$ interaction having a

single atom type hydrogen bond geometry, C(24)-H(24)...C(14).

The last $(C\text{-}H)_{anion}\cdots(phenyl)_{anion}$ contact involving ring 1 of the anion was found to proceed from C(16)-H(16) of the original anion to ring 3 of an anion generated by the symmetry (*x*, *y*, -1+*z*). It is shown in Figure 42, which is drawn to emphasize the fact that ring 3 acts as the acceptor of this interaction. The only short $H(16)\cdots C_{ring}$ distance located in the geometry search was 2.903Å to C(35). The C(16)-H(16) vector makes an angle of 54.4° with the plane of ring 3. The vector is directed towards the ring plane but projects outside the ring. It points most directly toward H(35) of ring 3, C(16)-H(16)...H(35) = 167.9°, but even a little further away from the ring. Both C(16) and H(16) also project onto the plane of ring 3 well outside the confines of the ring, H(16) closest to but beyond H(35) and C(16) even further away from the ring. Actually, H(15) of ring 1 projects almost directly onto C(34) of the ring 3 plane. However, the C(15)-H(15) vector is nearly parallel to the plane of ring 3 and it does not project toward the ring. The shortest contact made, H(15)...C(34) = 3.496Å, is too long to be important.

The C(16)-H(16)...ring 3 interaction forms two $H(16)\cdots C_{ring}$ contacts that are shorter than the $H(16)\cdots\pi_c$ ring centroid distance of 3.870Å (129.8°), H(16)...C(35) = 2.903Å (146.9°) and H(16)...C(34) = 3.068Å (124.5°). Based on the $H(16)\cdots C_{ring}$ distances, this would be described as having an edge type geometry. However, the more important contacts are made between H(16) and the hydrogen atoms of ring 3, H(16)...H(35) = 2.464Å (167.9°) and H(16)...H(34) = 2.798Å (114.7°). The $H(16)\cdots H_{ring}$ contacts, particularly H(16)...H(35), are considerably shorter and more linear than the corresponding $H(16)\cdots C_{ring}$ values. Like three of the four

previous interactions, this would not be considered a hydrogen bond but rather some other type of weak H...H contact, C(16)-H(16)...H(35).

In the last $(C\text{-}H)_{anion}\cdots(phenyl)_{anion}$ contact (Figure 43), the only one not involving ring 1 of the anion, C(34)-H(34) of the original anion interacts with ring 4 [H(34)...C(42) = 2.930Å] of an anion generated by the symmetry (*x*, *y*, 1+*z*). The two interacting rings lie in nearly perpendicular planes (83.6°), while the C(34)-H(34) vector makes an angle of 82.8° with the plane of ring 4. The C(34)-H(34) vector points directly toward the plane of ring 4, as expected for a perpendicular interaction, but it projects away from ring 4 itself. It projects, as do C(34) and H(34), almost directly below C(42) of the ring, at about twice the C(42)-H(42) distance. The closest contact would thus be expected to occur between H(34) and H(42) of the second ring. H(35) also actually projects very close to C(42) on the ring 4 plane. However, the C(35)-H(35) vector points across the face of ring 4 toward H(46), 161.7°, but even further beyond that. The closest contact is H(35)...C(42), 3.430Å, which is too long to be considered important.

The C(34)-H(34)..ring 4 interaction has two $H(34)\cdots C_{ring}$ contacts, to C(42), 2.930Å (137.9°) and to C(43), 3.043Å (131.1°), that are shorter than the $H(34)\cdots\pi_c$ ring centroid distance of 3.803Å (123.1°). As in the previous interaction, this would seem to indicate an edge type geometry for the contact. However, once again the $H(34)\cdots H_{ring}$ distances are considerably shorter and the angles more linear than the corresponding $H(34)\cdots C_{ring}$ values. The contacts H(34)...H(42), 2.574Å (151.6°) and H(34)...H(43), 2.788Å (134.0°) would be expected to dominate the interaction. It would be characterized as a weak H...H contact,

C(34)-H(34)...H(42), and not a hydrogen bond.

All of the anion/anion interactions in guanidinium tetraphenylborate acetonitrile solvate, save one, seem to be best characterized, based on their geometries, as weak H...H contacts rather than as hydrogen bonds. Short $H...H_{ring}$ distances dominate the interactions, with the minimum $H...H_{ring}$ separation usually less than 2.5Å, while the minimum $H...C_{ring}$ separation in the same interaction is generally close to 3.0Å. The angles in such interactions (C-H...X, X = C or H) cover a wide range but tend to be less than linear, as expected for nondirectional contacts.

The one exception in the six anion/anion contacts studied is the C(24)-H(24)..ring 1 interaction, where the two rings involved are close to perpendicular and the C(24)-H(24) vector makes an angle of 83.5° with the plane of ring 1. The C(24)-H(24) vector projects directly toward C(14) in the ring 1 plane and H(24) makes its only close approach to C(14) of the ring, 2.863Å. The most linear $C(24)-H(24)...X_{ring}$ (X = C or H) angle is made to C(14), 164.8°, and there are no close $H(24)...H_{ring}$ contacts. This interaction, although it occurs at a rather long distance, is best described as a $(C-H)_{anion}...(phenyl)_{anion}$ contact with a single atom type geometry, C(24)-H(24)...C(14). It is the only such anion/anion contact present in the structure.

However, a number of similar C-H...phenyl interactions were located in guanidinium tetraphenylborate acetonitrile solvate, occurring between C-H groups of the solvent molecule and phenyl rings of the anion. All three solvent alkyl C-H groups were found to participate in such $(C-H)_{solvent}...(phenyl)_{anion}$ interactions and one, C(3)-H(61)...ring 1, was found to form a strong, centroid type geometry, hydrogen bond.

Finally, a number of C-H...N interactions were located in the structure, terminating at either N(4) of acetonitrile (four) or at N(2) of the cation (two). These interactions are more difficult to interpret. All but one occur at long distances, close to 3.00Å, and those to N(2) also are influenced by short H...H_{cation} contacts. The only reasonably short contact of this type, C(33)-H(33)...N(4), is characterized by a distance H(33)...N(4) = 2.561Å and a relatively linear C(33)-H(33)...N(4) angle of 161.8°. This would be expected to be the strongest C-H...N interaction in the structure.

3.4.4. C-H...Acceptor Contacts in Biguanidinium Tetraphenylborate

The cation in biguanidinium tetraphenylborate contains no C-H groups and there is no solvent included in the crystal during its formation. As a result, all C-H contacts must involve the anion, specifically as the "donor" in any C-H...X type interactions which arise. If hydrogen bonds are to be formed, possible "acceptors", X, in the structure include the nitrogen centers of the cation and the phenyl rings of the anion. A geometry search for C-H...X contacts with H...X distances of less than 3Å was carried out. A total of fourteen such contacts were located, twelve anion/anion type C-H...phenyl interactions and two anion/cation type C-H...N interactions.

The two $(C\text{-}H)_{anion}\cdots N_{cation}$ interactions located were similar to those studied previously in both [DabcoH] $[B(C_6H_5)_4]$ and $[C(NH_2)_3]$ $[B(C_6H_5)_4]\cdot CH_3CN$. They were both characterized by relatively long H...N_{cation} distances, close to 3.00Å, and both were also found to have comparatively short H...H_{cation} distances. They are likely weak contacts, perhaps arising as secondary

interactions incidental to formation of stronger N-H...π(Ph) hydrogen bonds between the cation and anion. Interestingly, both $(C\text{-}H)_{anion}\cdots N_{cation}$ interactions of less than 3.00Å were found to terminate at N(4) of the cation. This is similar to the situation in guanidinium tetraphenylborate acetonitrile solvate where the two shortest $(C\text{-}H)_{anion}\cdots N_{cation}$ contacts were both found to involve N(2) of the cation.

A total of twelve $(C\text{-}H)_{anion}\cdots(phenyl)_{anion}$ contacts of less than 3Å were located in the structure of biguanidinium tetraphenylborate. Of these twelve interactions, nine were found to involve ring 1 of the anion, as "donor" (five), "acceptor" (two) or both (two). This is an interesting observation since ring 1 also serves as the acceptor in three of the seven N-H...π(Ph) hydrogen bonds formed in the structure. It is possible that some type of cooperative effect is in operation. The involvement of ring 1 as the acceptor in three N-H...π(Ph) hydrogen bonds, could dispose it to serve as the "donor" in a significant number of the C-H...phenyl anion/anion type interactions.

The $(C\text{-}H)_{anion}\cdots(phenyl)_{anion}$ contacts were found to range in minimum $H\cdots C_{ring}$ distance from 2.640Å, C(46)-H(46)...ring 1, right up to the 3.00Å limit, with the majority of the interactions studied being longer rather than shorter. Many of the interactions were found to have geometries unsuitable for hydrogen bond formation, as will be discussed, indicating their nature as weak H...H type contacts. The geometries of all the $(C\text{-}H)_{anion}\cdots(phenyl)_{anion}$ interactions studied are summarized in Tables 52 and 53 of Appendix 4.

Two $(C\text{-}H)_{anion}\cdots N_{cation}$ interactions of less than 3Å were located in the structure of biguanidinium tetraphenylborate, C(26)-H(26)...N(4) and

C(42)-H(42)...N(4), as shown in Figure 44. Somewhat surprisingly, both contacts were found to involve N(4) of the cation, one of its four terminal nitrogen centers. This is similar to the situation in guanidinium tetraphenylborate acetonitrile solvate where both $(C\text{-}H)_{anion}\cdots N_{cation}$ contacts were found to involve N(2) of the cation. Theoretically, in the isolated biguanidinium cation all four of the terminal NH_2 groups would be equivalent, with equal probability of forming C-H...N type contacts. The fact that both proceed to N(4) in the crystal structure of biguanidinium tetraphenylborate suggests that N(4) differs from the other three terminal nitrogen centers, N(2), N(3) and N(5), in some way. One obvious difference is that the N-H...π(Ph) hydrogen bonds formed by the cation include one having edge type geometry and one having centroid type geometry to each of N(2), N(3) and N(5). N(4) forms only a single N-H...π(Ph) hydrogen bond, having an edge type geometry, while its second hydrogen bond is the stronger N-H...N contact that holds the cation dimer together. It is possible that the involvement of N(4) as the donor in the contact, N(4)-H(4A)...N(1), the strongest hydrogen bond in the structure, increases its ability to act as an "acceptor" in the C-H...N interactions.

Of course, it is also possible that the relatively long and weak $(C\text{-}H)_{anion}\cdots N_{cation}$ contacts arise as a secondary effect, their components being held in close proximity by the formation of stronger interactions in the structure. For example, consider the C(42)-H(42)...N(4) contact, which occurs between the original cation and anion in biguanidinium tetraphenylborate. The original cation forms two hydrogen bonds [N(4)-H(4B) and N(5)-H(5A)] to phenyl ring 1 of the original anion. The formation of these two relatively strong N-H...π(Ph) hydrogen bonds (and other packing

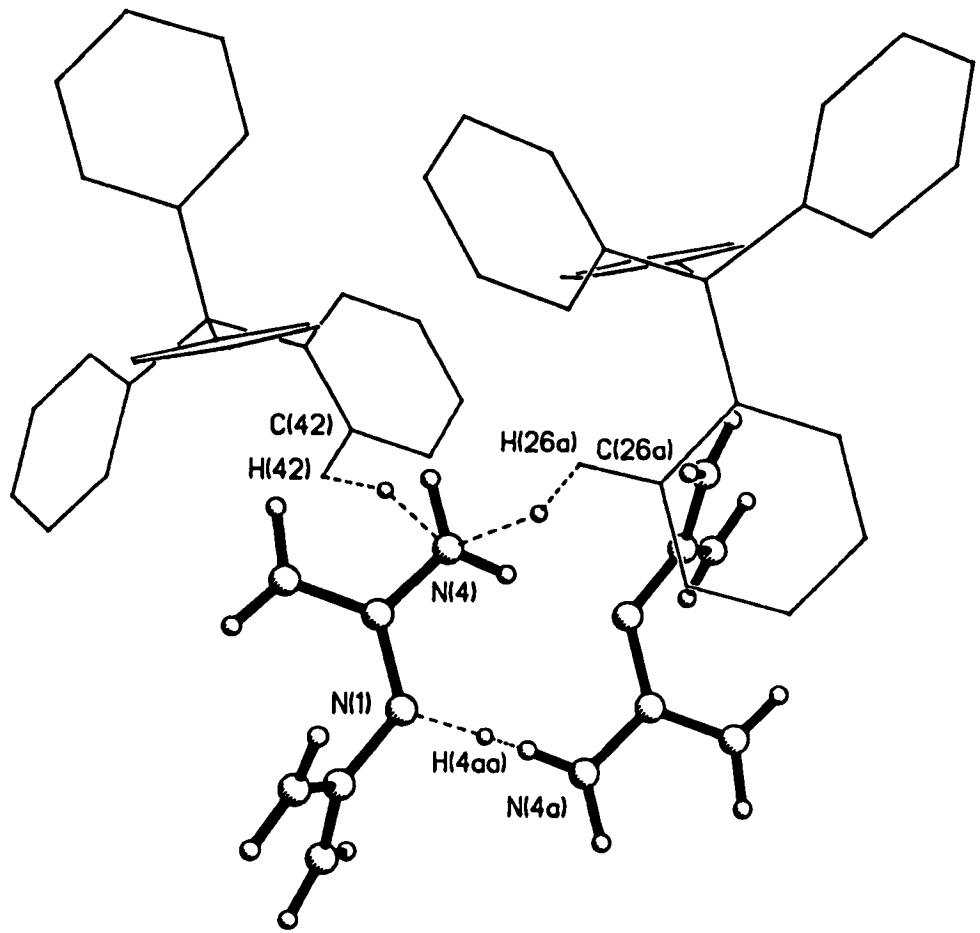

Figure 44. The C-H...N interactions located (less than 3Å) in the structure of biguanidinium tetraphenylborate. The small open circles represent the locations of the bond critical points of the interactions.

forces) bring the cation and anion into close contact. The N-H...π(Ph) interactions of the cation with phenyl ring 1 orient rings 3 and 4 of the anion such that C(32)-H(32) and C(42)-H(42) both point directly toward one plane of the cation, defined by N(1), C(2), N(4) and N(5). Both vectors project most linearly to H(5A) in that plane, C(32)-H(32)...H(5A) = 174.4° and C(42)-H(42)...H(5A) = 169.1°, although these are not necessarily the closest ring/cation contacts. The shortest H(32)...X_{cation} [X = N or H] contacts, H(32)...N(5), 3.330Å (165.0°) and H(32)...H(5A), 3.482Å (174.4°), are made to that region of the cation but are too long to be important.

In the shorter C(42)-H(42)...N(4) contact, the C(42)-H(42) vector makes an angle of 30.6° with the [N(1), C(2), N(4), N(5)] plane of the cation. Both C(42) and H(42) project onto the cation plane closest to H(4B), with H(42) shifted slightly toward N(4), even though the C(42)-H(42) vector projects directly toward H(5A). The contact is characterized by a relatively long H(42)...N(4) separation of 2.867Å and a C(42)-H(42)...N(4) angle of only 119.6°. H(42) actually makes its closest contact to H(4B) of the cation, 2.517Å (110.5°) and another reasonable contact, 2.846Å (146.1°), to H(5B). The shortest distances involve H...H_{cation} contacts and the C(42)-H(42)...N(4) interaction must be influenced by them. This is possible evidence that the $(C\text{-}H)_{anion}\cdots N_{cation}$ interaction is an incidental contact brought about by other stronger influences on the cation and anion. The C(42)-H(42)...N(4) contact could arise as a consequence of the stronger N-H...π(Ph) hydrogen bonds and other packing forces in the structure.

The second $(C\text{-}H)_{anion}\cdots N_{cation}$ interaction in biguanidinium

tetraphenylborate occurs between C(26)-H(26) of the original anion and N(4) of a cation generated by the symmetry (*-x*, 1-*y*, *-z*). If considered to a single cation, the C(26)-H(26)...N(4) interaction is made to the opposite face of that cation compared to the C(42)-H(42)...N(4) interaction. The C(26)-H(26) vector of the anion is not directed toward any region of the original cation, nor is it directed toward either of the other two cations which form N-H...π(Ph) hydrogen bonds to the original anion; H(26) makes no close contacts with any of these cations. In this case, the C(26)-H(26)...N(4) interaction cannot arise as a result of the formation of stronger N-H...π(Ph) hydrogen bonds between the cation and anion in the structure. However, it still could be an incidental contact arising as a result of other packing forces.

The C(26)-H(26) vector makes an angle of only 13.5° with the [N(1), C(2), N(4), N(5)] plane of the half cation. The vector does not project anywhere near the cation in this plane, running almost parallel to it. In fact, it points most directly toward the ring 1 plane of an adjacent anion, although it makes no close contact with that ring [H(26)...H(15) = 3.109Å (153.3°)]. If projected onto the plane of the appropriate half of the cation, H(26), C(26) and all of ring 2 lie well away from the cation; they do not overlap at all. H(26) projects closest to, but still well away from, H(4B) of the cation.

In the C(26)-H(26)...N(4) interaction, the H(26)...N(4) distance is 2.912Å and the C(26)-H(26)...N(4) angle is 114.6°. As in the previous interaction, the shortest H...X_{cation} [X = N or H] contact is actually made to a hydrogen atom, H(26)...H(4B) = 2.864Å (125.6°). The H...H_{cation} contact must again influence the C(26)-H(26)...N(4) interaction, although unlike

the previous case the presence of N-H...π(Ph) hydrogen bonds cannot be used to explain its formation.

C(25)-H(25) of the same ring 2 of the same anion also forms a relatively close physical contact with the [N(1), C(2), N(4), N(5)] plane of the cation. The C(25)-H(25) vector again runs almost parallel to the cation plane and the two do not intersect anywhere near the cation. The H(25)...N(4) distance, 3.149Å (106.7°), is too long to have been located in the geometry search. However, the H(25)...H(4A) distance, 2.811Å (102.4°), is comparable to the minimum H(26)...X_{cation} [X = N or H] distance in the C(26)-H(26)...N(4) interaction. The fact that both C(26)-H(26) and C(25)-H(25) groups from the same ring of the same anion interact with a single nitrogen center of the cation, N(4), support the idea that this is a nondirectional, incidental contact rather than a hydrogen bond.

Both $(C\text{-}H)_{anion}\cdots N_{cation}$ contacts in biguanidinium tetraphenylborate share common characteristics, including relatively long H...N_{cation} separations, shorter but comparable H...H_{cation} separations and relatively nonlinear C-H...N_{cation} angles. Although somewhat difficult to interpret purely on this basis, it is likely that these interactions are influenced by their H...H_{cation} contacts. They are best described as weak, incidental contacts, brought about as a secondary result of the formation of stronger N-H...π(Ph) hydrogen bonds and other packing forces, rather than as directional hydrogen bonds.

As in the three previous structures studied, the majority of the $(C\text{-}H)_{anion}\cdots(phenyl)_{anion}$ contacts in biguanidinium tetraphenylborate tend to have geometries indicative of H...H type interactions rather than true hydrogen bonds. The interactions studied are shown in Figures 45 (ring 1),

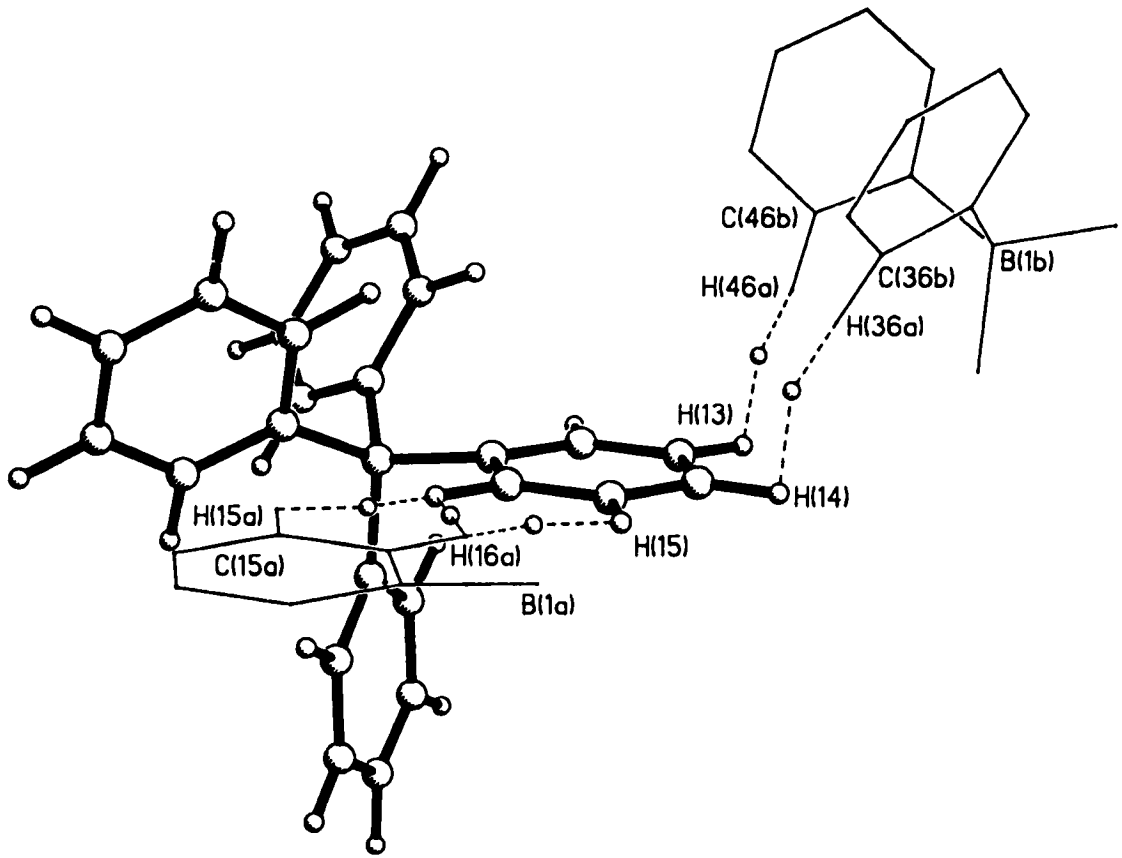

Figure 45. The C-H...phenyl interactions (anion/anion type - less than 3Å) accepted by ring #1 in biguanidinium tetraphenylborate. The small open circles represent the locations of the bond critical points of the interactions. Uninvolved rings on the interacting tetraphenylborate anions have been omitted for clarity.

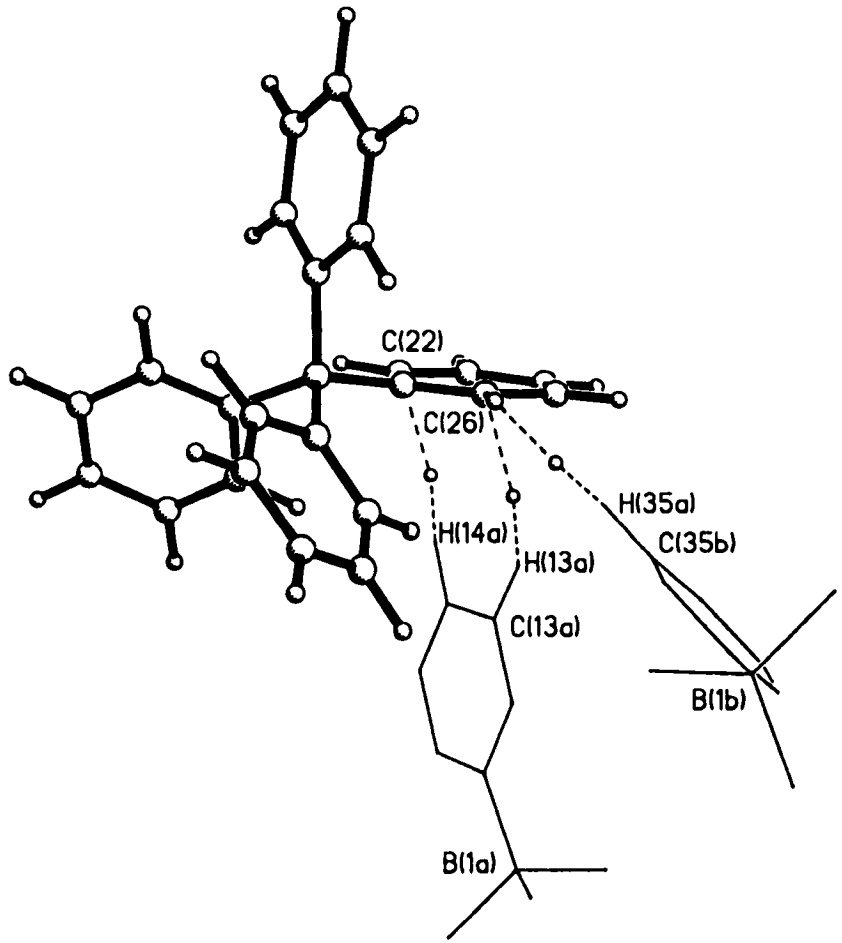

Figure 46. The C-H...phenyl interactions (anion/anion type - less than 3Å) accepted by ring #2 in biguanidinium tetraphenylborate. The small open circles represent the locations of the bond critical points of the interactions. Uninvolved rings on the interacting tetraphenylborate anions have been omitted for clarity.

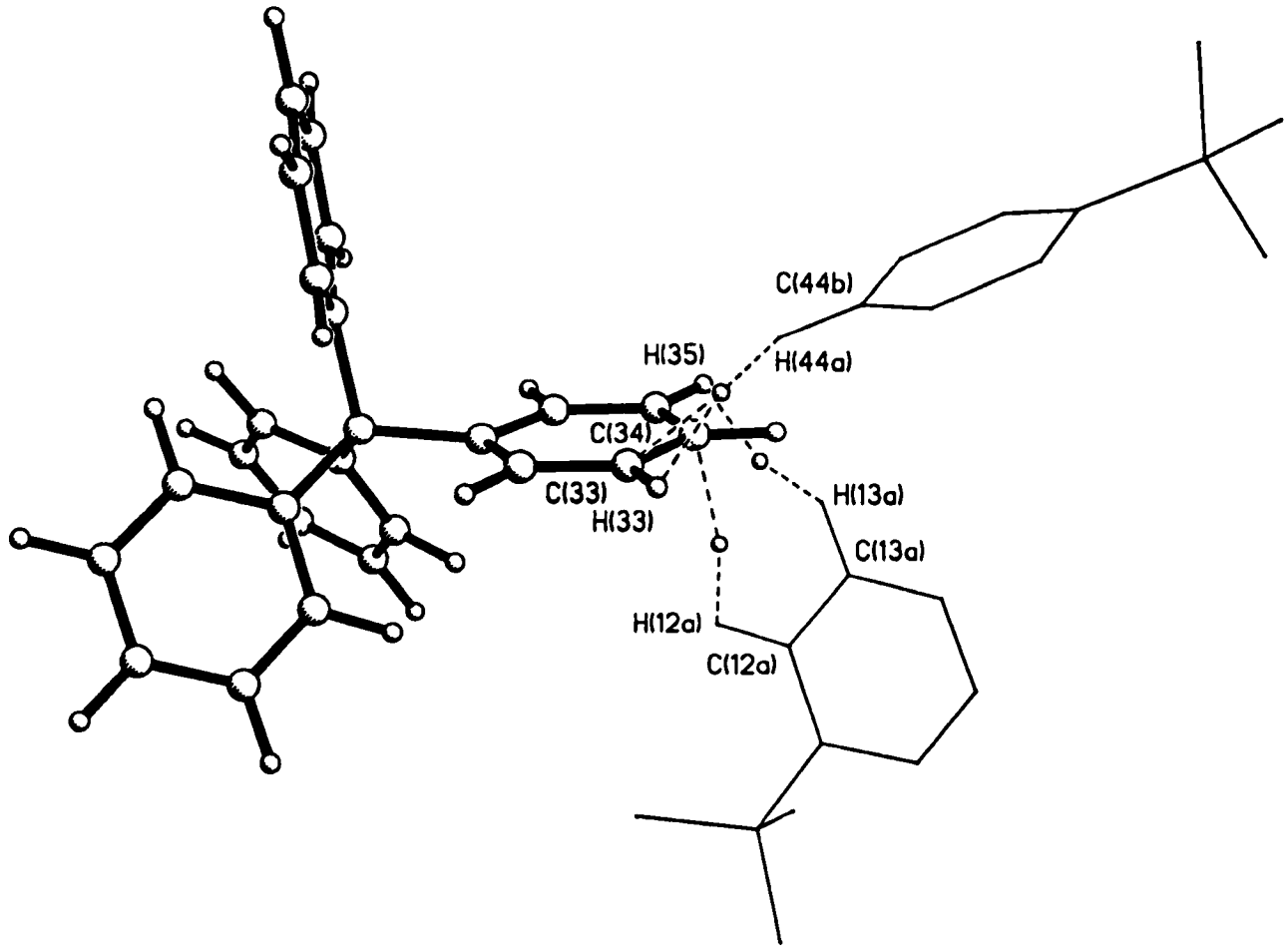

Figure 47. The C-H...phenyl interactions (anion/anion type - less than 3Å) accepted by ring #3 in biguanidinium tetraphenylborate. The small open circles represent the locations of the bond critical points of the interactions. Uninvolved rings on the interacting tetraphenylborate anions have been omitted for clarity.

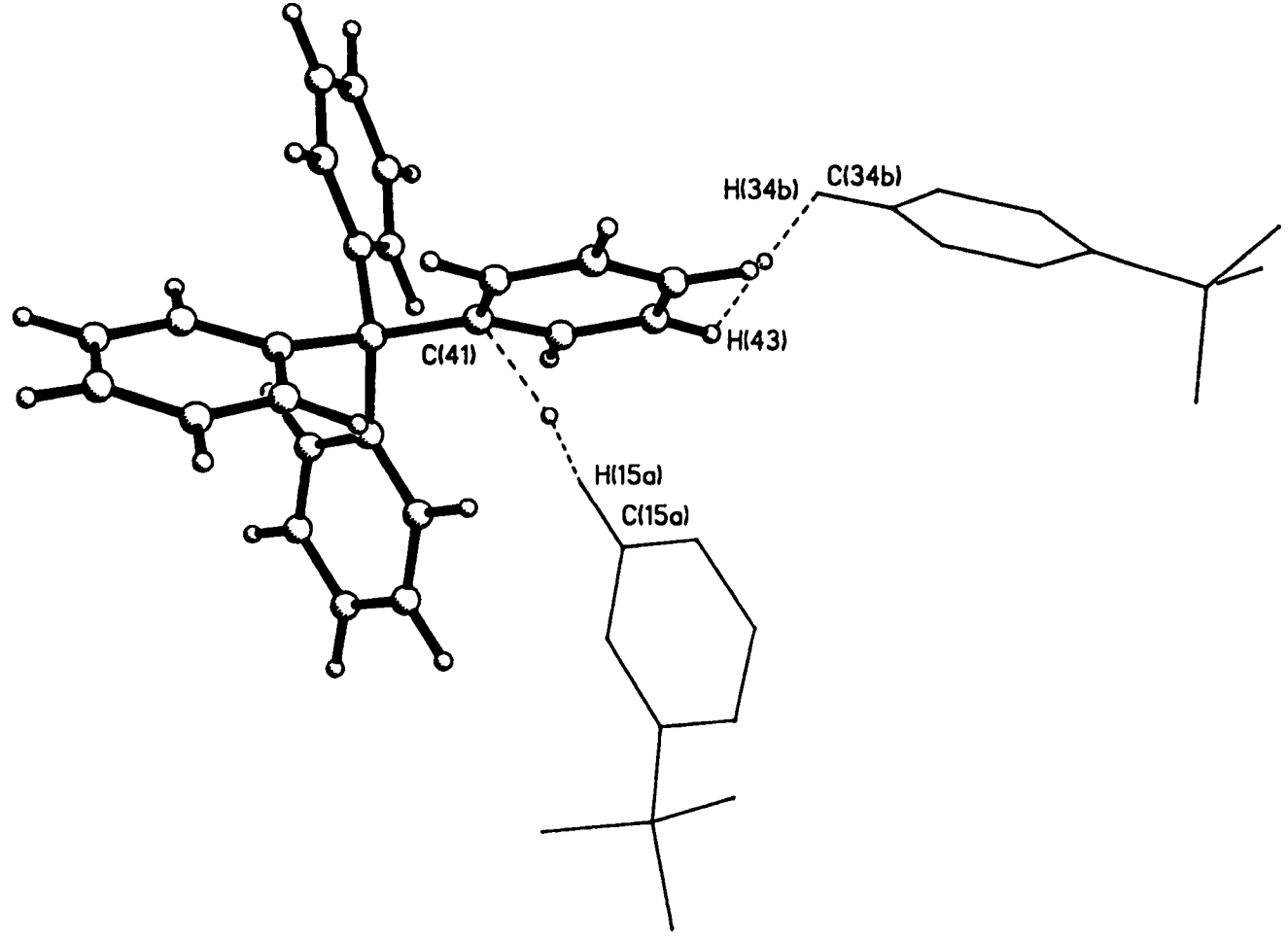

Figure 48. The C-H...phenyl interactions (anion/anion type - less than 3Å) accepted by ring #4 in biguanidinium tetraphenylborate. The small open circles represent the locations of the bond critical points of the interactions. Uninvolved rings on the interacting tetraphenylborate anions have been omitted for clarity.

46 (ring 2), 47 (ring 3) and 48 (ring 4), drawn to emphasize the role of the phenyl ring as the "acceptor" in the contact. An excellent example is the C(16)-H(16)...ring 1 interaction which was found to form a pair of close contacts, H(16)...C(15) = 2.863Å and H(16)...C(16) = 2.887Å. In both instances, ring 1 of the anion serves as both "donor" and "acceptor" for the interaction. Ring 1 of the interacting anion is generated by the symmetry (*-x*, 1-*y*, *-z*) from the original anion, as shown in Figure 45.

In the biguanidinium tetraphenylborate structure, the two interacting ring 1s are oriented in a parallel and coplanar fashion. They are arranged in opposite directions such that the C(15)-C(16) bond of one ring is parallel to the C(16)'-C(15)' bond of the second ring 1. These are the ring bonds that lie closest together between the two anions. However, they are offset such that C(16) of one ring aligns itself almost exactly with C(16)' of the second ring 1, even though the two rings are oriented in opposite directions.

The two rings are related by a center of symmetry, which also lies in their common plane, midway between H(16)...H(16)' and H(15)...H(15)'. Thus there are two equivalent interactions between the two rings, C(16)-H(16)...X(15)' and C(16)'-H(16)'...X(15) [X = C or H]. Because of the offset between the two rings, C(16)-H(16)...X(16)' and its equivalent C(16)'-H(16)'...X(16), also make close contact. Although not located in the geometry search, it is likely that C(15)-H(15)...X(16)' and its counterpart C(15)'-H(15)'...X(16) could make reasonably close contact as well. This arrangement is similar to several of those in guanidinium tetraphenylborate acetonitrile solvate, except here the two interacting, equivalent ring 1s are actually coplanar rather than simply lying in

parallel planes.

Since the interacting rings are coplanar in this case, there is no need to project one onto the plane of the other. The two rings do not overlap at all, with the closest contacts being made between H(15) and H(16) of the two rings. The C(16)-H(16) vector of one ring projects directly toward H(15)' of the second phenyl ring and vice versa, C(16)'-H(16)'...H(15). However, the C(15)-H(15) vector does not point toward ring 1 of the second anion, rather it angles off toward ring 4 of that anion. The C(16)-H(16) vector makes an angle of only 0.3° with the plane of the opposing ring 1, while the C(15)-H(15) vector forms a similarly small angle of only 1.2° with that plane.

As it turns out, the only important distances describing the contacts between the two ring 1s are H...H_{ring} distances. There are only two types of interactions between the rings, H(16)...H(15)' (and its equivalent) and H(16)...H(16)'. Because of the shorter H(16)...C(15)' distance and the more linear C(16)-H(16)...X(15)' [X = C or H] angles, the former contact is described in terms of C(16)-H(16)...X(15)' rather than C(15)-H(15)...X(16)'. The second interaction, C(16)-H(16)...X(16)', occurs only once between the two rings.

In the C(16)-H(16)...ring 1 interaction(s), H(16) makes relatively close approach to both C(15)', 2.863Å (163.0°), and C(16)', 2.887Å (134.8°), of the opposing ring 1. Both of these distances are shorter than the H...π_c ring centroid distance of 3.986Å (148.9°), while all other H(16)...C_{ring} distances are longer. In a hydrogen bonding situation this would be described as a single interaction having an edge type geometry.

However, in this instance the H...H_{ring} distances are significantly

shorter than the corresponding H...C_{ring} values. The H(16)...H(15)' distance is only 2.205Å and the C(16)-H(16)...H(15)' angle is a linear 175.5°. Clearly, the C(16)-H(16)...H(15)' interaction is an H...H type contact. Interestingly, this ring 1/ring 1 interaction differs from those in guanidinium tetraphenylborate acetonitrile solvate in that there is a second very short H...H_{ring} contact between the two rings, H(16)...H(16)' = 2.261Å (115.1°). This is also clearly an important H...H type contact. The question is, do these represent a single interaction, as would be described for a X-H...π(Ph) hydrogen bonds having edge type geometries, or do they represent a pair of separate H...H type interactions between the two rings? Subsequent evidence suggests that these are two distinct interactions, H(16)...H(15)' and H(16)...H(16)', rather than a single interaction to the hydrogen atoms at one edge of the phenyl ring.

The same two anions, as those involved in the first interaction(s), were also found to participate in the C(15)-H(15)...ring 4 contact (Figure 48), which proceeds from the original anion to ring 4 of the second anion generated by the symmetry transformation (-*x*, 1-*y*, -*z*). In the first interaction(s), the two ring 1s are parallel and coplanar. Ring 4 of the second anion thus lies roughly perpendicular to ring 1 of the original anion but is tilted slightly toward that ring. Ring 4 is approximately bisected horizontally by the plane of the original ring 1. The orientation of the two adjacent anion rings is such that hydrogen bond formation appears possible and, in fact, one is observed.

The first hint of this interaction came when the C(15)-H(15) vector was found to project toward ring 4 when the ring 1/ring 1 contacts were being investigated. In fact, H(15) makes reasonably close contact to all

six ring 4 carbon atoms (2.927Å to 3.063Å) indicative of a centroid type geometry for the C(15)-H(15)...ring 4 interaction and possible hydrogen bond formation. The C(15)-H(15) vector and the plane of ring 4 of the second anion make an angle of 61.5°. The vector projects directly and almost linearly to C(14), 174.3°, in the plane of that ring. Both C(15) and H(15) project onto the plane of ring 4 very close to the ring centroid. H(15) is shifted slightly toward C(41) and C(15) is shifted by a slightly greater amount toward the midpoint of the C(43)-C(44) bond.

The C(15)-H(15)...ring 4 interaction definitely exhibits a centroid type geometry. The C(15)...C_{ring} distances cover a narrow range, from a minimum of 3.734Å, to both C(43) and C(44), to a maximum of 4.024Å, to C(41) [100Δ = 29]. All of the C(15)...C_{ring} distances are longer than the C(15)...π_c ring centroid distance of 3.620Å. Similarly, all six of the H(15)...C_{ring} distances are longer than the H(15)...π_c distance of 2.650Å (149.7°). They range from a minimum of 2.927Å, to C(42), to a maximum of 3.063Å, to C(45) [100Δ = 14]. The most linear C(15)-H(15)...C_{ring} angle is made to C(41), 174.3°, and the H(15)...C(41) distance is the second shortest to the ring, 2.952Å. As with all centroid type interactions, the H...H_{ring} distances are all longer than the corresponding H...C_{ring} distances and are not an important consideration.

The C(15)-H(15)...ring 4 interaction has a configuration suitable for hydrogen bond formation. However, the H(15)...π_c distance is longer than the corresponding distances in the two previously studied centroid type C-H...phenyl interactions. The anion/anion type C(14)-H(14)...ring 1 contact in $NH_4B(C_6H_5)_4$ has an H(14)...π_c distance of 2.717Å (171.6°) and the solvent/anion C(3)-H(61)...ring 1 contact in $[C(NH_2)_3][B(C_6H_5)_4]\cdot CH_3CN$

has an H(61)...π_c distance of 2.472Å (157.9°). The C(15)-H(15)...π_c angle of 149.7° is less linear than those of the other interactions as well. Both facts are indications that the interaction C(15)-H(15)... ring 4 is weaker than the previous examples of C-H...phenyl contacts having centroid type geometries.

A second group of four related $(C\text{-}H)_{anion}\ldots(phenyl)_{anion}$ contacts in biguanidinium tetraphenylborate occur between another pair of adjacent, symmetry related anions. Ring 1 of the original anion and ring 2 of an anion generated by the symmetry (-1/2+*x*, 1/2-*y*, -1/2+*z*) are oriented in a perpendicular fashion, the two ring planes making an angle of 89.0°. Ring 1 cuts approximately through the middle of the ring 2 plane when projected onto that plane, roughly bisecting the C(25)-C(26) and the C(22)-C(23) bonds of ring 2 of the second anion. C(13)-H(13) of ring 1 is associated with the C(25),C(26) region of ring 2, forming contacts of less than 3Å with both atoms [H(13)...C(25) = 2.873Å, H(13)...C(26) = 2.762Å]. C(14)-H(14) of ring 1 interacts with the C(22),C(23) region of the second ring, with relatively short H(14)...C_{ring} contacts to both C(22), 2.849Å, and C(23), 2.904Å. This orientation, with both ring 1 vectors projecting directly to opposite edges of the perpendicular ring 2 of the second anion, is suitable for hydrogen bond formation.

Because of the interactions between ring 1 of the original anion and the adjacent ring 2 of an anion generated by symmetry, rings 3 and 4 of that anion are also in position to interact with ring 1 of the original anion (Figure 45). Specifically, C(36)-H(36) from ring 3 and C(46)-H(46) from ring 4 project directly toward ring 1 and form close contacts with that ring [H(36)...C(14) = 2.941Å and H(46)...C(13) = 2.640Å]. The

H(46)...C(13) separation is the shortest $(C\text{-}H)_{anion}\cdots(phenyl)_{anion}$ contact located in the geometry search of the biguanidinium tetraphenylborate structure.

Both the C(36)-H(36) and C(46)-H(46) vectors project toward the same face of ring 1, not surprising given that they originate from the same anion. The C(36)-H(36) vector makes an angle of 57.7° with the plane of ring 1 of the original anion, while the C(46)-H(46) vector makes a similar angle of 66.4° with the same plane. The C(36)-H(36) vector projects toward the plane of ring 1, making the most linear angle to C(14) in that plane [C(36)-H(36)...C(14) = 173.4°]. The vector actually projects close to the midpoint of the C(14)-H(14) bond of ring 1, forming an angle of 177.0° to that point. H(36) projects onto the plane of ring 1 directly along a continuation of the C(14)-H(14) bond just past H(14) and C(36) projects a bit farther away roughly along the same line.

In the C(36)-H(36)...ring 1 interaction, H(36) makes close contact to only one ring carbon atom, C(14), 2.941Å (173.4°). The H(36)...H(14) distance is significantly shorter, 2.446Å, although the corresponding C(36)-H(36)...H(14) angle is less linear, 166.0°. Since these are the only close contacts between the rings and since H(36)...H(14) is considerably shorter than H(36)...C(14), this is best considered an H...H type interaction, C(36)-H(36)...H(14), rather than a hydrogen bond.

The C(46)-H(46) vector also projects toward the plane of ring 1 pointing most directly toward H(13) [C(46)-H(46)...H(13) = 165.8°] but even a bit farther outside the ring than that. H(46), quite close, and C(46), farther away, also project onto the plane of ring 1 closest to H(13). Both C(46) and H(46) form no other close contacts with ring 1 other

than those to X(13) [X = C or H]. The C(46)-H(46)...X(13) contacts are shorter but less linear than the C(36)-H(36)...X(14) contacts.

Just as with the previous interaction, in the C(46)-H(46)...ring 1 interaction, H(46) makes close contact to only a single ring carbon atom, C(13), 2.640Å (162.6°). Even though this is the shortest anion/anion contact in the structure, based on H...C_{ring} distance, the H(46)...H(13) separation is still significantly shorter than H(46)...C(13), the exceedingly short 2.179Å (165.8°). The C(46)-H(46)...ring 1 interaction is also best considered an H...H type contact rather than as a hydrogen bond. The two interactions, C(36)-H(36)...H(14) and C(46)-H(46)...H(13) likely arise as weaker, secondary contacts after the two anions are oriented such that rings 2 and 1 can form the stronger interion contacts to be discussed in the next section.

The interactions between ring 1 of the original anion and ring 2 of the second anion, best illustrated in Figure 46, have geometries more suitable for stronger hydrogen bond formation. The C(13)-H(13) vector from ring 1 of the first anion and the plane of ring 2 in the second anion make an angle of 62.1°. The C(13)-H(13) vector projects toward the ring 2 plane but away from the ring itself. The vector projects approximately midway between H(25) and H(26) but even a bit farther outside the ring. The best angle, C(13)-H(13)...X_{ring} [X = C or H], made to ring 2 involves H(26), 150.7°. C(13) projects onto the plane of ring 2 just outside the confines of the ring, close to the midpoint of the C(25)-C(26) bond. H(13) projects farther outside the ring, also roughly midway between C(25) and C(26) but approximately equidistant to H(25) and H(26) as well.

The C(13)-H(13)...ring 2 interaction has an H(13)...π_c ring centroid

distance of 3.227Å (117.1°). There are two H(13)...C_{ring} distances shorter than this value, H(13)...C(25) = 2.873Å (135.2°) and H(13)...C(26) = 2.762Å (137.3°); all other of the H(13)...C_{ring} distances are longer. The corresponding H...H_{ring} distances are both slightly longer, H(13)...H(25) = 3.068Å (145.0°) and H(13)...H(26) = 2.862Å (150.7°), but the angles C(13)-H(13)...H_{ring} are more linear. Based on these parameters, the C(13)-H(13)...ring 2 interaction would best be described as a hydrogen bond having an edge type geometry, to the C(25)-C(26) bond of ring 2. The fact that the H...H_{ring} distances are longer but comparable to the H...C_{ring} values suggest that the H...H contacts could also contribute to the interaction.

The final contact between these two anions, C(14)-H(14)...ring 2, also visible in Figure 46 involves the same two rings as the previous interaction. The C(14)-H(14) vector projects toward the plane of ring 2 but terminates at the other side of the ring away from the previous interaction. The vector and the plane of ring 2 make an angle of 57.7°. It projects onto the ring 2 plane near the midpoint of the C(22)-C(23) bond but outside the ring, roughly equidistant between these atoms and H(22) and H(23). The most linear angle is actually made with H(23), C(14)-H(14)...H(23) = 160.5°. Somewhat surprisingly, both C(14) and H(14) project onto the plane of ring 2 within the confines of the ring itself. C(14) projects very close to the ring centroid, displaced only slightly toward C(21), while H(14) projects approximately midway between the ring centroid and the midpoint of the C(22)-C(23) bond. This orientation suggests formation of a somewhat off-center, centroid type geometry, hydrogen bond.

The C(14)-H(14)...ring 2 interaction is characterized by the distances and angles made to the ring 2 centroid, C(14)...π_c = 3.637Å, H(14)...π_c = 2.797Å and C(14)-H(14)...π_c = 135.0°. All of the C(14)...C_{ring} distances, which range from a minimum of 3.844Å to C(21) to a maximum of 3.952Å to C(24) [100Δ = 11], are longer than the C(14)...π_c distance. H(14)...C_{ring} also displays a narrow range of distances, 100Δ = 53, all longer than H(14)...π_c. The minimum H(14)...C_{ring} contact of 2.849Å (154.5°) is made to C(22) while the maximum separation is to C(25), 3.379Å (114.1°). The most linear C(14)-H(14)...C_{ring} angle is actually made to C(23), 156.4°, which also exhibits a relatively short H(14)...C(23) distance of 2.904Å. All of the H(14)...H_{ring} distances are too long to be important, another characteristic of a centroid type hydrogen bonding interaction. The H(14)...π_c distance in this interaction is longer than the corresponding distance in any previously studied centroid type contact, including the C(15)-H(15)...ring 4 contact just described in biguanidinium tetraphenylborate. The C(14)-H(14)...ring 2 interaction must be the weakest of the centroid geometry hydrogen bonds yet studied.

Ring 1 of the original anion and ring 2 of the adjacent, symmetry generated anion form a pair of related hydrogen bonding type interactions between the close to perpendicular rings. C(13)-H(13) forms an interaction with an edge type geometry to the C(25)-C(26) bond of ring 2, while the adjacent C(14)-H(14) forms an interaction with an off-center, centroid type geometry to ring 2. This is somewhat analogous to the "fork" type N-H...π(Ph) hydrogen bonds sometimes found between a pair of N-H donors on a single cation to a single anion phenyl ring. In those cases, one hydrogen bond tends to have a centroid type geometry while the other forms

a less optimal edge type interaction with the ring, just as is observed here.

Ring 1 of the original anion forms a close approach to one other anion (the third) in the structure of biguanidinium tetraphenylborate. This anion is generated by the symmetry transformation (*-x, -y, -z*). Its ring 3 is oriented approximately perpendicularly to the plane of ring 1 but tilted slightly toward that ring; the two planes make an angle of 58.6°. Ring 3 is slightly offset from the plane of ring 1, such that the ring 1 plane cuts approximately through C(31) and C(35) of the second anion. In the geometry search, ring 1 of the original anion was found to form two close contacts (less than 3Å) to ring 3 of the second anion, H(12)...C(34) = 2.865Å and H(13)...C(35) = 2.850Å. These interactions are best shown in Figure 47. No other of the phenyl rings in this second anion were found to interact with ring 1 of the original anion in any appreciable way.

In the C(12)-H(12)...ring 3 interaction, the C(12)-H(12) vector makes a relatively small angle of 25.8° with the plane of ring 3. The vector does project toward the ring 3 plane but because of the shallow angle it passes across the face of ring 3 and projects beyond the ring. The most linear C(12)-H(12)...X_{ring} [X = C or H] angle is made with C(31), 159.4°, while the C(12)-H(12)...B(1) angle is 164.8°. H(12) projects onto the plane of ring 3 about one quarter of the way along the C(34)-C(35) bond, closer to C(34), but displaced just outside the ring. C(12) projects at about the same relative position but farther outside the ring, closer to H(34) than to H(35).

There are two H(12)...C_{ring} distances, H(12)...C(34) = 2.865Å

(119.6°) and H(12)...C(35) = 3.073Å (122.6°), that are shorter than the H(12)...π_c distance of 3.234Å (144.0°). The H(12)...C(34) distance is noticeably less than H(12)...C(35), although the C(12)-H(12)...C(35) angle is the more linear. The corresponding H(12)...H_{ring} distances are consistently longer than the H(12)...C_{ring} values, H(12)...H(34) = 3.052Å (99.6°) and H(12)...H(35) = 3.387Å (106.1°). The C(12)-H(12)...ring 3 interaction has an edge type hydrogen bond geometry involving the C(34)-C(35) bond of ring 3.

In the C(13)-H(13)...ring 3 interaction, the C(13)-H(13) vector points more directly toward the plane of ring 3 than does the C(12)-H(12) vector of the previous interaction. The C(13)-H(13) vector makes an angle of 59.3° with the plane of ring 3. However, it also projects outside and away from the ring, approaching H(35) most directly (151.1°) but projecting even farther outside the ring than that. H(13) projects onto the ring 3 plane closest to, but beyond, H(35), while C(35) projects at about the same distance from the ring but displaced towards H(34).

The C(13)-H(13)...ring 3 interaction has only a single H(13)...C_{ring} distance of less than 3Å, H(13)...C(35) = 2.850Å (130.6°). However, the H(13)...C(34) distance of 3.036Å (112.3°) is also less than the H(13)...π_c ring centroid distance of 3.888Å (114.8°). All of these contacts are substantially longer than the H(13)...H(35) separation of 2.347Å (151.1°); the H(13)...H(34) distance, 2.730Å (107.4°), is also relatively short but longer than that of H(13)...H(35). The C(13)-H(13)...ring 3 interaction is thus not a hydrogen bond. It is better described as an H...H type contact, C(13)-H(13)...H(35). It is likely that this is a secondary contact, incidental to the formation of the stronger C(12)-H(12)...ring 3

[C(34)-C(35)] edge type hydrogen bond between the same two rings.

Nine of the twelve $(C\text{-}H)_{anion}\ldots(phenyl)_{anion}$ contacts in biguanidinium tetraphenylborate, with $H\ldots C_{ring}$ distances of less than 3Å, have been described. All of these contacts involve interactions of ring 1 with the phenyl rings of one of three adjacent anions. Of the nine interactions, four were found to have geometries suitable for hydrogen bond formation, while the remaining five were found to be H...H type contacts between the rings. None of the three remaining anion/anion contacts of less than 3Å involve ring 1 on either anion. There are far fewer of this type of interaction and they tend to occur at long $H\ldots C_{ring}$ distances, very close to the 3.00Å cutoff. Two of the three interactions are related, occurring between rings 3 and 4 of two different anions [H(34)...C(43) = 2.977Å; H(44)...C(33) = 2.899Å and H(44)...C(34) = 2.978Å]. The final interaction, C(35)-H(35)...ring 2, involves a relatively short contact to C(25) of the second ring on an adjacent anion [H(35)...C(25) = 2.985Å].

The C(35)-H(35)...ring 2 interaction (Figure 46) proceeds from ring 3 of the original anion to ring 2 of an anion generated by the symmetry $(1/2\text{-}x,\ -1/2+y,\ 1/2+z)$. The two ring planes form an angle of 39.9°, while the C(35)-H(35) vector makes an angle of 36.9° with the plane of ring 2. The C(35)-H(35) vector projects toward the plane of ring 2, making the most linear angle with H(26) of the ring, 173.7°. It is actually directed to a point slightly inside H(26) closer to the ring. H(35) lies directly but far below C(26) when projected onto the ring 2 plane, at more than twice the C(26)-H(26) distance. C(35) projects even farther away from the ring, below the approximate midpoint of the C(25)-C(26) bond. H(34) of ring 3 also projects onto the plane of ring 2

at about the same distance from H(25). However, the two atoms are actually quite far apart [H(34)...H(25) = 3.093Å] and the C(34)-H(34) vector projects away from the plane of ring 2, so this potential contact was not investigated further.

In the C(35)-H(35)...ring 2 interaction there are two H(35)...C_{ring} distances shorter than the H(35)...π_c distance of 4.045Å (151.1°), H(35)...C(26) = 2.985Å (165.3°) and H(35)...C(25) = 3.072Å (142.4°). However, the corresponding H(35)...H_{ring} distances are consistently and substantially shorter than the H(35)...C_{ring} values, H(35)...H(26) = 2.391Å (173.7°) and H(35)...H(25) = 2.606Å (128.0°). The H(35)...H(26) distance is far shorter and the C(35)-H(35)...H(26) angle more linear than any others in the interaction, leading to its description as an H...H type contact, C(35)-H(35)...H(26), rather than a hydrogen bond.

The last two $(C\text{-}H)_{anion}\cdots(phenyl)_{anion}$ contacts in the structure, C(34)-H(34)...ring 4 (Figure 48) and C(44)-H(44)...ring 3 (Figure 47), are related, involving the same two phenyl rings (3 and 4 respectively) on adjacent anions. If ring 3 of the original anion is chosen to begin from, then ring 4 of the second anion is generated by the symmetry (-1/2-*x*, -1/2+*y*, 1/2+*z*). The angle between the planes of rings 3 and 4 is only 19.8°; the rings do not lie in parallel planes but they are relatively close to being parallel. If projected onto a common plane, the two interacting rings do not overlap at all. The closest approaches are made between [H(34) and H(43)] and [H(33) and H(44)] of the two rings respectively. There are various possible ways to describe these two interactions. However, based on the minimum H...C_{ring} distances, the most linear C-H...X_{ring} [X = C or H] angles and the projections of the C-H

vectors, they are best discussed in terms of C(34)-H(34)...ring 4 [to X(43)] and C(44)-H(44)...ring 3 [to X(33)], respectively. Each interaction corresponds to one of the short H...C_{ring} distances located in the geometry search, H(34)...C(43) = 2.977Å and H(44)...C(33) = 2.899Å. The only other reasonably close approach made between the two rings is the cross contact, H(44)...H(34), with a separation of 2.631Å [H(44)...C(34) = 2.978Å]. It can be described as either C(44)-H(44)... X(34) or C(34)-H(34)...X(44) [X = C or H] which shows it can be considered as a component of the two principal interactions, C(44)-H(44)...ring 3 and C(34)-H(34)...ring 4, and will be discussed as such.

If projected onto a common plane, the C(44)-H(44) vector from ring 4 appears to point directly toward H(33) of ring 3, while the C(43)-H(43) vector from the same ring points outside ring 3 beyond H(35). Considered from the opposite direction, the C(34)-H(34) vector from ring 3 points directly toward C(43) of ring 4. The C(33)-H(33) vector points away from ring 4, past H(44) and H(45) without coming close to either. These observations substantiate the decision to treat the first interaction as a C(44)-H(44)...ring 3 contact and the second as C(34)-H(34)...ring 4.

In the C(44)-H(44)...ring 3 interaction, the C(44)-H(44) vector makes a very shallow angle, 18.3°, with the plane of ring 3. It is directed toward the ring 3 plane but passes across the face of the ring past H(33) and H(32). It actually projects beyond the ring but the most linear angle is made to H(32), C(44)-H(44)...H(32) = 170.4°. H(44) projects onto the plane of ring 3 in the area between H(33) and H(34), slightly beyond both and roughly equidistant from each. C(44) lies even farther away from ring 3 on the projected plane; it is, however, closer

to H(34) than H(33).

The C(44)-H(44)...ring 3 interaction has two H(44)...C_{ring} distances of less than 3.00Å, both of which are also the only distances shorter than the H(44)...π_c ring centroid distance of 3.853Å (138.2°). The shorter separation is made between H(44)...C(33), 2.899Å (147.4°), while the H(44)...C(34) separation is slightly longer, 2.978Å (121.6°), and has a less linear C(44)-H(44)...C_{ring} angle. However, as with most of the previous interactions, the H(44)...H_{ring} distances are shorter than the corresponding H(44)...C_{ring} distances. The H(44)...H(33) distance of 2.454Å (149.5°) is also shorter and the angle more linear than the H(44)...H(34) values, 2.631Å (102.1°). The C(44)-H(44)...ring 3 interaction appears to be an H...H type contact best described as C(44)-H(44)...H(33) based on its geometry.

In the C(34)-H(34)...ring 4 interaction, the C(34)-H(34) vector makes an angle of 18.1° with the plane of ring 4. In fact, the vector actually projects away from the ring 4 plane and will not intersect the plane at any reasonable distance. The most linear C(34)-H(34)...X_{ring} [X = C or H] angle is made to C(41), 141.0°, on the opposite side of the ring away from the close contact. H(34) projects onto the plane of ring 4 between H(43) and H(44), slightly closer to H(43) and slightly farther away from the ring than either. C(34) projects even farther away from ring 3, still between H(43) and H(44).

There are two H(34)...C_{ring} distances in the C(34)-H(34)...ring 4 contact, to C(43), 2.977Å (126.5°), and to C(44), 3.044Å (116.9°), that are shorter than the H(34)...π_c ring centroid distance of 3.976Å (132.5°). The H(34)...H_{ring} distances are shorter than the corresponding H(34)...C_{ring}

distances, although in this case the differences are not as large as often observed. The H(34)...H(43) distance is 2.508Å (115.1°), while the H(34)...H(44) distance is slightly longer, 2.631Å (98.0°). Still, this interaction should be considered an H...H type contact based on its geometry, best described as C(34)-H(34)...H(43) rather than as a hydrogen bond.

The question as to whether H(44)...H(34) [2.631Å] represents a separate interaction remains. However, since this distance is longer than the minimum H...H_{ring} distance in either the C(44)-H(44)...H(33) or the C(34)-H(34)...H(43) contact, it is likely that it is not as important a contact between the rings. It appears to be a more incidental contact, secondary to the two H...H type interactions just discussed.

Biguanidinium tetraphenylborate was found to have twelve anion/anion C-H...phenyl interactions of less than 3Å in its structure. Of these, eight were classified as H...H type contacts and four were classified as hydrogen bonding type interactions based on their geometries. All of the H...H contacts were found to have the minimum H...H_{ring} distance shorter than the minimum H...C_{ring} distance, while the opposite was found to be true in the hydrogen bonds (H...C_{ring} < H...H_{ring}).

Of the four hydrogen bonds located, two were found to have centroid type geometries and two were found to have edge type geometries. The two centroid type interactions, C(14)-H(14)...ring 2 and C(15)-H(15)...ring 4, are characterized by H...π_c distances and C-H...π_c angles of 2.797Å, 135.0° and 2.650Å, 149.7°, respectively, the former interaction being slightly off-center. The distances are long and the angles relatively far from linear, indicative of weak contacts despite their favourable geometries.

In the centroid type hydrogen bonds, all H...H_{ring} distances are longer than the corresponding H...C_{ring} distances by a considerable amount, a simple requirement of the centroid type geometry.

Two of the hydrogen bonds were found to have edge type geometries, C(13)-H(13)...C(25)-C(26) [ring 2] and C(12)-H(12)...C(34)-C(35) [ring 3]. In these interactions, the two minimum H...C_{ring} distances, to the ring atoms actually involved in the contact, are considerably shorter than the corresponding H...H_{ring} distances. In fact, in these two hydrogen bonds, the pertinent H...C_{ring} distances are shorter than the related H...H_{ring} distances by an average of 0.2Å.

Eight H...H type contacts were studied in the structure, all of which were found to have H...H_{ring} separations shorter than any other distances between the interacting rings. The minimum H...H_{ring} distances defining the interactions range from the very short 2.179Å (165.8°) in the C(46)-H(46)...H(13) contact to the longer 2.508Å (115.1°) in the contact C(34)-H(34)...H(43). The C-H...H_{ring} angles in these contacts were found to range from 115.1° to 175.5°, from nearly linear to clearly nonlinear. The longer contacts appear often to be less linear as well. In all the H...H type contacts, the minimum H...H_{ring} distance is generally less than 2.5Å, while the corresponding H...C_{ring} distance tends to be greater than 2.5Å and usually closer to 3.0Å. The average difference between the minimum H...H_{ring} distance and the corresponding H...C_{ring} distance in the eight contacts is 0.5Å. On average, in an H...H type contact, the H...H_{ring} minimum distance is 0.5Å shorter than the corresponding H...C_{ring} distance. This observation is substantiated by the results obtained for H...H type contacts in the other three structures studied.

It is interesting that nine of twelve anion/anion C-H...phenyl contacts investigated in biguanidinium tetraphenylborate involve ring 1 of the anion, as either "donor" (five), "acceptor" (two) or both (two). Even more interesting is the fact that in all four of the hydrogen bond type interactions identified, the C-H "donor" group comes from ring 1 of the anion. The importance of ring 1 in the structure is also evident in the N-H...π(Ph) hydrogen bond distribution. Three of the seven N-H...π(Ph) hydrogen bonds in the structure were found to be accepted by ring 1 of the anion, N(2)-H(2B) [atom type], N(4)-H(4B) [edge type] and N(5)-H(5B) [centroid type], more interactions than any other ring participates in. It appears that a cooperative effect exists among the hydrogen bonds involving ring 1 of the anion. Ring 1 accepts three N-H...π(Ph) hydrogen bonds which, in turn, is compensated for by its serving as the "donor" in all four C-H...phenyl hydrogen bonds in the structure. No other ring of the anion exhibits such an effect, all being involved in far fewer contacts and no C-H...phenyl hydrogen bonds.

The packing geometry in biguanidinium tetraphenylborate is interesting to observe, particularly in relation as to how ring 1 of the anion can be involved in so many close contacts with both adjacent cations and anions in the structure (Figure 49). Directly above and below the face of ring 1 lie cations, allowing the formation of the three N-H...π(Ph) hydrogen bonds; N(2)-H(2B) from one cation interacts with one face and N(4)-H(4B) and N(5)-H(5B) from the second cation form interactions to the second face of ring 1. The cations are both oriented approximately perpendicular to the plane of ring 1 and parallel to the plane of ring 2 in the anion. This is important because these cations do not, therefore,

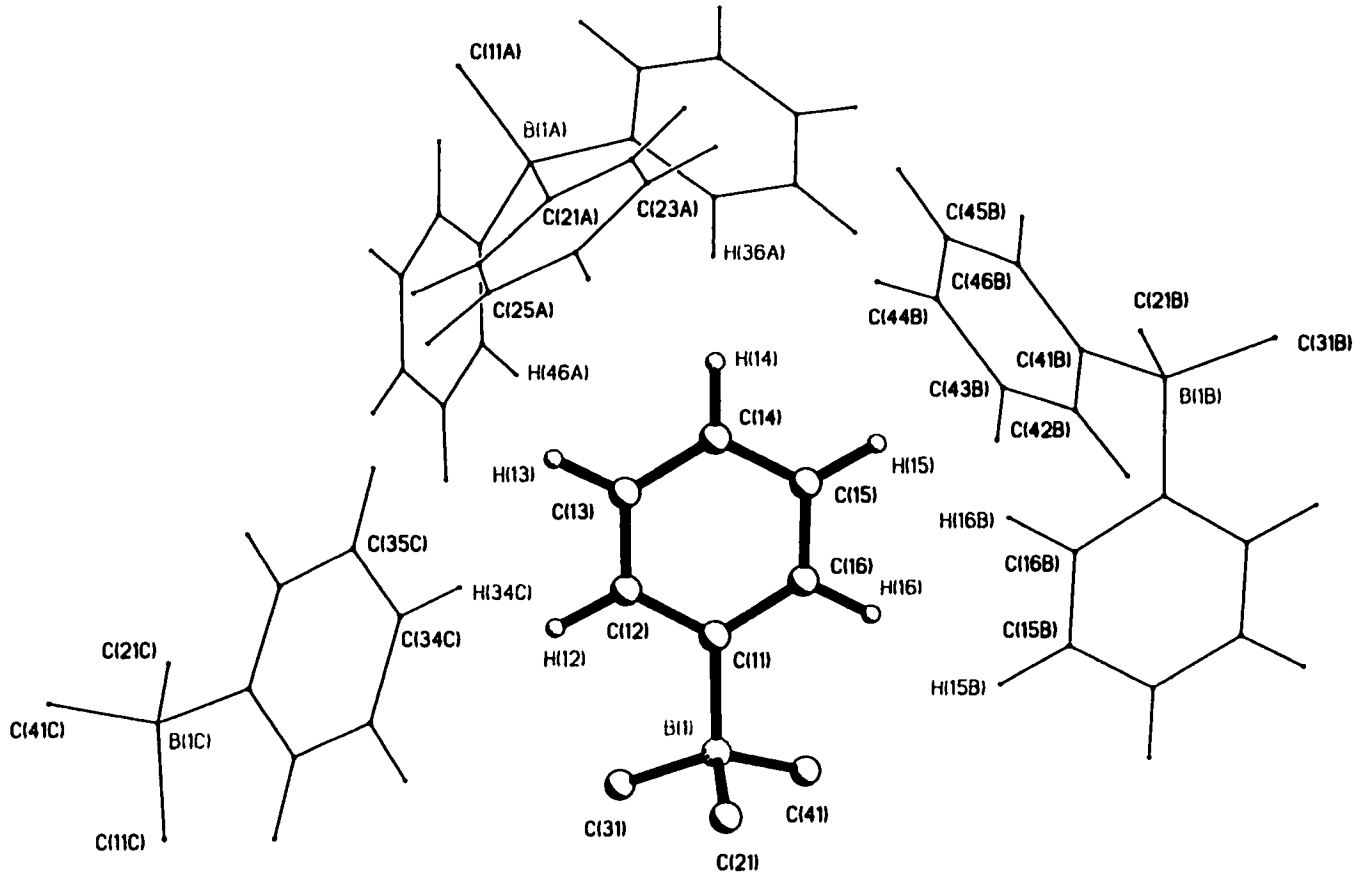

Figure 49. Arrangement of the nearest anions around phenyl ring #1 in the structure of biguanidinium tetraphenylborate. Uninvolved rings on the interacting tetraphenylborate anions have been omitted for clarity.

block access to the edges of ring 1 (in-plane contacts) by other anions (or cations). This is not true for any of the other anion rings, where only one face of each ring interacts with a single cation. In the other rings' interactions, the cation tends to overhang the ring, blocking access to that ring in at least some directions.

In the plane of ring 1 surrounding the original anion are three reasonably close, adjacent anions oriented such that anion/anion type interactions are possible. These interactions have been discussed individually in the previous section but are briefly summarized here. In all three of the interacting anions, one ring is oriented roughly perpendicular to the plane of the original anion's ring 1 and that ring is approximately bisected by the projected plane of ring 1. Thus, each of the surrounding anions is oriented in a way that at least one hydrogen bonding type interaction with ring 1 is possible.

In the first interacting anion, ring 1 is coplanar with the original anion's ring 1 and a number of H...H type contacts are formed between the two equivalent rings, 2x[C(16)-H(16)...H(15)] and C(16)-H(16)...H(16). Ring 4 of the first interacting anion is the one oriented perpendicularly to the plane of the original ring 1 and a centroid geometry hydrogen bond, C(15)-H(15)...ring 4, is formed between the two rings. Thus, this first interacting anion engages primarily C(15)/H(15) of the original ring 1, with C(16)/H(16) also involved via H...H type contacts.

In the second interacting anion, ring 2 lies in a plane nearly perpendicular to ring 1 of the original anion. This allows a pair of close contacts to form between the two rings, C(13)-H(13)...C(25)-C(26), an edge type interaction, and C(14)-H(14)...ring 2 which has a centroid type

geometry. As well as forming these two hydrogen bonds involving ring 2, rings 3 and 4 of this anion are involved in a pair of incidental H...H type contacts to ring 1 of the original anion, C(36)-H(36)...H(14) and C(46)-H(46)...H(13). The more important interactions made to this second anion engage the C(13),C(14) edge of ring 1 of the original anion.

Finally, in the third interacting anion, its ring 3 is approximately perpendicular to ring 1 of the original anion. A single edge type hydrogen bond is formed between this ring 3 and ring 1, C(12)-H(12)...C(34)-C(35). As well, an incidental H...H type contact forms between the same two rings, C(13)-H(13)...H(35). Ring 1 of the original anion interacts with this third anion primarily via C(12).

Ring 1 of the original anion is totally surrounded in its plane by a semi-circle formed by the three adjacent anions: anion 1...C(15) [of the original anion], anion 2...C(14), C(13) and anion 3...C(12). In ring 1 only C(16)-H(16) is not involved as the "donor" in one of the four C-H...phenyl hydrogen bonds formed in the structure. It is, however, a participant in an H...H type contact with a ring in one of the adjacent anions. In fact, all of the ring 1 hydrogen atoms except H(12) are involved in close H...H type contacts between anions and all the C-H groups from ring 1 participate in some form of anion/anion contact.

The orientation of anions around ring 1 of the original anion maximizes its ability to engage in anion/anion interactions, both of the H...H type and more importantly those having hydrogen bond geometries. No other rings in the anion are completely surrounded in this way. In fact, in the remainder of the structure, there are only three more H...H type interactions, having minimum H...C_{ring} distances of less than 3.00Å, that

do not involve ring 1 and there are no C-H...phenyl hydrogen bonds that do not involve ring 1 of the anion. As discussed earlier, this is likely a cooperative effect, arising because ring 1 of the anion serves as the acceptor in three N-H...π(Ph) hydrogen bonds (out of a total of seven in the structure). In turn, ring 1 then serves as the "donor" in all four of the C-H type contacts having hydrogen bond geometries in the structure.

3.4.5. C-H...Acceptor Contacts in the Four Structures - A Summary

The majority of the C-H...phenyl interactions were found to fall into one of two distinct categories, after studying all such contacts of less than 3Å located experimentally. The first category contains those interactions with **hydrogen bond type** geometries. Of the 34 C-H...phenyl contacts studied, 14 were classified as hydrogen bonds. A variety of configurations are possible and were observed experimentally, including centroid type (4), edge type (8) and single atom type (2) contacts. The second category contains **H...H type** interactions; with configurations exactly as described, these are likely related to van der Waals type contacts. Fifteen of the experimental C-H...phenyl interactions were identified as H...H type contacts.

The C-H...phenyl interactions tend to fall clearly into one category or the other based on their geometries. The hydrogen bond type contacts have minimum H(C)...C_{ring} distance(s) shorter than the related minimum H(C)...H_{ring} distance(s). Generally, H(C)...C_{ring} is significantly shorter than H(C)...H_{ring}, however, in some cases they can be close to equal. Even in those cases where H(C)...C_{ring} is close to H(C)...H_{ring} the interaction has been classified as a hydrogen bond as long as the H(C)...C_{ring} minimum

distance is the shorter. The different possible hydrogen bond types (centroid, edge or single atom) have been described previously and are analogous to those found in the N-H...π(Ph) hydrogen bonds.

In the H...H type contacts, the H(C)...H_{ring} minimum distance is considerably shorter than any H(C)...C_{ring} distance or any other distance in the interaction. The H(C)...H_{ring} distance is usually less than 2.5Å, while the H(C)...C_{ring} distance is greater than 2.5Å and normally closer to 3.0Å. The minimum H(C)...H_{ring} distance is, on average, 0.5Å shorter than the corresponding H(C)...C_{ring} distance. In the 14 H(C)...H_{ring} anion/anion type contacts in the four compounds studied for this work, the average difference in the two distances was calculated to be 0.52Å, H(C)...H_{ring} < H(C)...C_{ring}. The very short H(C)...H_{ring} distance, sometimes only slightly greater than 2.0Å, dominates the interaction. In general, all H...H type contacts appear to be very similar, involving directly only the two hydrogen atoms that make close contact. The C-H...H_{ring} angles cover a wide range, often far from 180°, suggesting a nondirectional type interaction. H...H type contacts often appear to arise as secondary effects, a consequence of the formation of other stronger interactions in the structure.

A few of the C-H...phenyl interactions studied did not fall clearly into either group. These five were placed, rather arbitrarily, into an **"intermediate" type** category. In the intermediate group of contacts, the H(C)...H_{ring} minimum distance is shorter than the corresponding H(C)...C_{ring} distance but the two are relatively equal. Both distances tend to fall in the range 2.6±0.2Å. This type of interaction is difficult to interpret based solely on geometry. It is hard to know which distance will dominate

the interaction or to tell how the contact should best be described. However, of the 22 $(C\text{-}H)_{anion}\ldots(phenyl)_{anion}$ interactions investigated, 14 were found to be H...H type contacts and six were found to have hydrogen bond type geometries, while only two fell into the intermediate category, indicating that they are relatively rare.

C-H...π(Ph) hydrogen bonds of all three possible geometric types, centroid, edge and single atom, were identified and characterized in this investigation. The pronounced conformational variability exhibited by the C-H...π(Ph) type hydrogen bonds is not unexpected, having been observed previously for other X-H...π(Ph) [X = N or O] hydrogen bonds, including X = N in this work. Also, Steiner et al.[71] (1995) have published the results from a search of the Cambridge Structural Database in which the closest C-H...X contacts formed by terminal alkynes (donor group) were investigated. A total of 31 C-H...π type interactions were located, 18 to an alkyne acceptor, 5 to an alkene acceptor and 8 to an arene ring acceptor. Most of the C-H...π(Ph) interactions were found to have a geometry in which the C-H vector pointed toward the centroid of the arene ring. However, exceptions to the centroid geometry were also located, geometries in which one or two of the $H\ldots C_{ring}$ distances were shorter than the $H\ldots\pi_c$ ring centroid distance. Such interactions correspond to single atom and edge type hydrogen bonds, respectively. The authors interpret their results as showing that short contacts of sufficiently acidic C-H groups with π type aromatic acceptors possess all the essential properties of weak hydrogen bonds. A variety of geometries are possible, just as observed for other types of X-H...π(Ph) hydrogen bonds and experimentally for C-H...π(Ph) hydrogen bonds in this work. In a related paper, Steiner

et al.[64] also report the results from a series of ab initio molecular orbital calculations on simple model systems that suggest, that under certain conditions, C-H...π(Ph) hydrogen bonds can have strengths similar to other X-H...π(Ph) hydrogen bonds and can have a significant influence in a crystal structure.

In this work, a considerable number of C-H...X [X = N or π(Ph)] interactions have been investigated. As described above, not all of these were found to have hydrogen bond type geometries; in fact, the majority turned out to be better defined as H...H type contacts. It is even more difficult to compare the results because of the different origins of the contacts studied. In the C-H...X interactions, cation/anion, solvent/anion and anion/anion combinations were all observed. It is not certain that all these interaction types are directly comparable, particularly considering differences in charges and sizes amongst the various components of the different combinations. Because of the fragmentation of the results into so many small groups, a statistical comparison of the C-H...X interaction geometries, most notably the different hydrogen bond types, is not really possible. However, in all the C-H...X hydrogen bond type contacts studied, the characteristic distances appear longer than those in comparable N-H...X hydrogen bonds.

The group of Y. Umezawa et al.[120] has recently published the results of a Cambridge Structural Database search for C-H...π(Ph) interactions in organic compounds. For the entire subset of structures containing at least one C-H group and at least one six membered aromatic ring an astonishing 75.1% were found to form C-H...π(Ph) interactions with a minimum contact distance of 3.05Å or less. For this subset of the data, the mean

H(C)...C_{ring} atomic distance was calculated to be 2.91±0.12Å. The minimum H(C)...C_{ring} contact distance for each interaction (whether the H(C)...π_c or the minimum H(C)...C_{ring} distance) were averaged to generate this mean value. The C-H...π(Ph) average can be compared with corresponding mean values calculated for O-H and N-H subsets of the CSD data by Umezawa et al., as reported in the same publication. The O-H...π(Ph) interactions (5.1% of the O-H set) were characterized by a mean H(O)...C_{ring} distance of 2.80±0.21Å, while the N-H...π(Ph) interactions (9.3%) were found to have a similar mean H(N)...C_{ring} distance of 2.78±0.19Å. The authors make the observation that the C-H...π(Ph) interactions as a group occur at longer distances and are thus weaker, on average, than the O-H...π(Ph) or N-H...π(Ph) type interactions. This result is entirely consistent with the findings of the present experimental investigation.

Although overall mean values were not calculated for the distances and angles characterizing the C-H...phenyl interactions studied in this work, it is possible to compare the mean H(C)...C_{ring} distance reported by Umezawa et al.(2.91±0.12Å) to certain of the experimental results. In the set of all experimental C-H...phenyl interactions, a total of 13 were found to have hydrogen bond type geometries. In connection with later work on the topological analysis of the experimental electron densities, the minimum contact distance for each of these hydrogen bonds (the minimum H(C)...C_{ring} distance) was determined. The overall mean H(C)...C_{ring} distance for this group, calculated from the individual values, was found to be 2.89Å with a standard deviation of 0.07Å. Similarly, for the smaller group of intermediate contacts (n = 4) a mean distance of 2.85Å with a standard deviation of 0.05Å was calculated. [The relevant mean distance in the

appropriately named H...H group of contacts ($H(C)...H_{ring}$) is not comparable to the mean $H(C)...C_{ring}$ distance calculated for the literature and other experimental groups (hence the absence of an overall mean calculation for the experimental data).] Both of the experimental mean $H(C)...C_{ring}$ values (hydrogen bond and intermediate contact) are virtually identical to that reported by Umezawa et al., even though the search criteria employed were slightly different in each case. Umezawa et al. limited their search to interactions with minimum $H(C)...C_{ring}$ distances of 3.05Å or less, while in this work a cutoff of 3.0Å was used. In this comparison, all mean values, both literature and experimental, have been defined in almost the same way, so are truly equal. The experimental results are in excellent agreement with the limited literature data available.

Perhaps more fruitful than a statistical analysis of the C-H...X hydrogen bonds located, is a simple comparison of the hydrogen bond distributions in the four compounds studied. In all four compounds, N-H...X [X = N or π(Ph)] hydrogen bonds were found to be present and were well characterized. Such hydrogen bonds were formed by every N-H group in all four structures and in each structure the geometries of the hydrogen bonds were optimized to centroid type as much as possible. As the cations grew larger, with more N-H groups to satisfy, optimization of all the N-H...π(Ph) hydrogen bonds to centroid type geometries was no longer possible and a wider variety of hydrogen bond geometries were observed. In $NH_4B(C_6H_5)_4$ and [DabcoH][$B(C_6H_5)_4$] the cation contains only a single N-H group and a single N-H...π(Ph) hydrogen bond with a centroid type geometry is formed in each case. In guanidinium tetraphenylborate acetonitrile

solvate five N-H...π(Ph) hydrogen bonds are formed, three with centroid type geometries and two with edge type geometries. Finally, in the structure of biguanidinium tetraphenylborate the seven N-H...π(Ph) hydrogen bonds are distributed amongst centroid type (3), edge type (3) and single atom type (1) geometries. In the two structures with multiple N-H...π(Ph) hydrogen bonds, the different types of geometries tend to be distributed throughout the structure, generally with one of the preferred centroid type interactions made to each ring of the anion, if at all possible. Would the C-H...X interactions, particularly the C-H...phenyl contacts with hydrogen bond type geometries, show the same patterns of optimization and distribution as observed for the N-H...X interactions?

[DabcoH] $[B(C_6H_5)_4]$ is the only one of the four structures studied, in which the cation contains C-H groups capable of interaction with the anion. In this structure a total of ten C-H...X [X = N or π(Ph)] cation/anion interactions were located, with every C-H group of the cation involved in at least one interaction. Nine $(C\text{-}H)_{cation}\cdots(phenyl)_{anion}$ contacts and one $(C\text{-}H)_{anion}\cdots N_{cation}$ contact were studied in detail, each characterized by a minimum H...X [X = N or C] distance of less than 3Å. The majority were found to have hydrogen bond type geometries; only one was a definite H...H type contact. Of the six interactions classified as $(C\text{-}H)_{cation}\cdots(phenyl)_{anion}$ hydrogen bonds, five were found to have edge type geometries and one had a single atom geometry; none were found to have centroid type geometries.

It is clear that the $(C\text{-}H)_{cation}\cdots(phenyl)_{anion}$ interactions formed are important in the [DabcoH] $[B(C_6H_5)_4]$ structure. They help to tether and orient the $DabcoH^+$ cation in the anion-formed cavity in which it resides.

In fact, the single N-H...π(Ph) hydrogen bond between the cation and anion occurs with an N-H...π_c angle, 158.6°, that is less linear than might normally be expected and this has been attributed to the combined effects of the other cation/anion C-H...X contacts in the structure.

It appears that the $(C\text{-}H)_{cation}\cdots(phenyl)_{anion}$ contacts are optimized to the best possible hydrogen bond geometries; only a single H...H type contact is observed. This is another indication that such contacts are important and purposely formed. None have centroid type geometries but five of the six are edge type interactions. This is likely because of the large number of interactions arising from a single cation (9); there are six unique C-H groups. The competition to make all of these interactions as effective as possible precludes the formation of any with centroid type geometries. In any event, $(C\text{-}H)_{cation}\cdots(phenyl)_{anion}$ contacts are important in determining the structure of [DabcoH] $[B(C_6H_5)_4]$. Along with the stronger N-H...π(Ph) centroid geometry hydrogen bond formed, these C-H...phenyl hydrogen bonds help to orient the cation and anion relative to one another in the crystal structure.

While the structure of [DabcoH] $[B(C_6H_5)_4]$ contains the only studied examples of $(C\text{-}H)_{cation}\cdots(phenyl)_{anion}$ contacts, $[C(NH_2)_3][B(C_6H_5)_4]\cdot CH_3CN$ contains the only $(C\text{-}H)_{solvent}\cdots(phenyl)_{anion}$ contacts. Three such interactions were found to occur at reasonable distances between the solvent and the anion, one for each C-H group of acetonitrile. Again, the majority were found to have hydrogen bond type geometries, with one forming a very short centroid type hydrogen bond, one forming an edge type hydrogen bond and the third forming a difficult to characterize intermediate type interaction. None were clear H...H type contacts.

The three, related $(C\text{-}H)_{solvent}\cdots(phenyl)_{anion}$ interactions have been optimized to the best possible geometries, with the centroid type contact, C(3)-H(61)...ring 1, being particularly important. In the structure, N-H...π(Ph) hydrogen bonds are formed between the cation and only phenyl rings 2, 3 and 4 of the anion. The C(3)-H(61)...ring 1 hydrogen bond is the only short/strong contact made to ring 1 of the anion and helps to orient a pair of solvent molecules in the centrosymmetric cavity formed by the rings 1 and 2 of the anions. The $(C\text{-}H)_{solvent}\cdots(phenyl)_{anion}$ contacts are clearly important in the structure of $[C(NH_2)_3][B(C_6H_5)_4]\cdot CH_3CN$, playing a role similar to the C-H...phenyl cation/anion contacts in the structure of $[DabcoH][B(C_6H_5)_4]$.

The last category of C-H...phenyl contacts studied contains the anion/anion type interactions, which were found to occur in all four structures. However, the anion/anion contacts fall into two distinct groups. The first group contains the $(C\text{-}H)_{anion}\cdots(phenyl)_{anion}$ interactions of $[DabcoH][B(C_6H_5)_4]$ and $[C(NH_2)_3][B(C_6H_5)_4]\cdot CH_3CN$, not surprisingly the two structures discussed above. $[DabcoH][B(C_6H_5)_4]$ was found to have only two short anion/anion contacts and neither of these had hydrogen bond type geometries. In $[C(NH_2)_3][B(C_6H_5)_4]\cdot CH_3CN$ six such contacts were investigated and only one was found to have a hydrogen bond geometry (of the single atom type). In both of these structures, the majority (5 of 8 total) of the contacts were clearly H...H type interactions and not hydrogen bonds.

It is suggested that in these two compounds, the anion/anion type C-H...phenyl interactions are of minor importance and make little contribution to the packing of the structures. They appear to be predominantly incidental contacts arising from the optimization of other,

stronger interactions in the structures, $(C\text{-}H)_{cation}\cdots(phenyl)_{anion}$ in [DabcoH] $[B(C_6H_5)_4]$, $(C\text{-}H)_{solvent}\cdots(phenyl)_{anion}$ in $[C(NH_2)_3][B(C_6H_5)_4]\cdot CH_3CN$ and N-H...π(Ph) hydrogen bonds in both. This is perhaps not surprising. Cation(+1)/anion(-1) contacts would be expected to have more favourable charge distributions than solvent(0)/anion(-1) contacts and both would be expected to be preferred relative to the anion(-1)/anion(-1) contacts, other factors being equal. Also, the large and bulky tetraphenylborate anions would be expected to be more difficult to pack in close proximity to one another, discouraging the formation of multiple, short anion/anion contacts in a structure. It should be easier to form cation/anion or solvent/anion type interactions based on the smaller size of the second component (cation or solvent) and the resulting increased ease of packing.

In ammonium tetraphenylborate and biguanidinium tetraphenylborate, on the other hand, the only source of C-H groups is the anion and only anion/anion type C-H...phenyl contacts can be formed in the structures. Besides the N-H...π(Ph) hydrogen bond(s) formed, these are the only other X-H...phenyl contacts that could possibly have hydrogen bond type geometries.

In $NH_4B(C_6H_5)_4$, two short $(C\text{-}H)_{anion}\cdots(phenyl)_{anion}$ contacts were located and investigated. One contact was found to be an H...H type interaction, based on its geometry, but the second was found to be a hydrogen bond with a centroid type configuration. Similarly, 12 anion/anion type C-H...phenyl contacts were studied in biguanidinium tetraphenylborate. Eight were found to be H...H type contacts, while four were found to be hydrogen bonds based on their geometries. More specifically, two were found to have centroid type configurations and two were found to be edge

type interactions.

It is interesting to note that both compounds form centroid type $(C\text{-}H)_{anion}\cdots(phenyl)_{anion}$ hydrogen bonds while neither [DabcoH] $[B(C_6H_5)_4]$ nor $[C(NH_2)_3][B(C_6H_5)_4]\cdot CH_3CN$ were found to. It seems that in these two compounds, which contain only anion/anion type C-H...phenyl contacts, these interactions form hydrogen bonds whenever possible. Since the anion/anion contacts involve very large and bulky groups, it appears that only a small number can form centroid type hydrogen bonds in a given structure. H...H type contacts also often seem to arise as a secondary consequence of the formation of close hydrogen bond type anion/anion interactions. The presence of $(C\text{-}H)_{anion}\cdots(phenyl)_{anion}$ hydrogen bonds with centroid type geometries must be an important feature of both structures. In biguanidinium tetraphenylborate and ammonium tetraphenylborate, the $(C\text{-}H)_{anion}\cdots(phenyl)_{anion}$ interactions do not have to compete with other types of C-H...phenyl interactions, be they cation/anion or solvent/anion. They can form hydrogen bonds with reasonable geometries whereas in the preceding structures other types of C-H..phenyl interactions were found to be more dominant.

Finally, it is suggested that the $(C\text{-}H)_{anion}\cdots(phenyl)_{anion}$ hydrogen bond type interactions in ammonium tetraphenylborate and biguanidinium tetraphenylborate play a role in determining the packing of their respective crystal structures. Such interactions were found to be relatively unimportant in [DabcoH] $[B(C_6H_5)_4]$ and $[C(NH_2)_3][B(C_6H_5)_4]\cdot CH_3CN$. The most compelling evidence comes from the structure and packing of biguanidinium tetraphenylborate where the interaction of three different adjacent anions with ring 1 of the original anion has already been

described. Each of these anions is oriented such that one ring will interact with ring 1 of the original anion via the formation of at least one $(C\text{-}H)_{anion}\cdots(phenyl)_{anion}$ hydrogen bond. The different anions are arranged so that the $(C\text{-}H)_{anion}\cdots(phenyl)_{anion}$ hydrogen bonds between the rings have the best possible geometries, two are centroid type and two are edge type. Only ring 1 of the anion is involved in all four of the $(C\text{-}H)_{anion}\cdots(phenyl)_{anion}$ hydrogen bonds, serving as the "donor" in all of the interactions. It would definitely appear that formation of such $(C\text{-}H)_{anion}\cdots(phenyl)_{anion}$ hydrogen bonds influences the packing geometry adopted by biguanidinium tetraphenylborate.

A similar situation appears to exist in the structure of ammonium tetraphenylborate. Besides the single, unique N-H...π(Ph) hydrogen bond, formed four times between the cation and two anions, the anion rings are oriented such that the C(14)-H(14) group of each ring (all four rings are equivalent) forms a $(C\text{-}H)_{anion}\cdots(phenyl)_{anion}$ hydrogen bond to the face of a perpendicular ring. The hydrogen bond has a favourable centroid type geometry suggesting that it has been optimized in the structure. The packing in ammonium tetraphenylborate appears to have been influenced by the chance of forming and optimizing the geometry of this anion/anion type C-H...phenyl hydrogen bond.

In conclusion, in structures capable of forming other types of C-H...phenyl interactions, specifically those having hydrogen bond geometries whether cation/anion or solvent/anion type, these other types of interactions appear to be favoured at the expense of anion/anion type contacts. This could arise because of simple charge considerations [cation +1, solvent 0, anion -1], because of size considerations [the tetraphenyl-

borate anion is larger and bulkier than any of the cations or the solvent studied] or some combination of the two. However, in structures where the only possible type of C-H...phenyl interaction is of the anion/anion variety these contacts will form with hydrogen bond geometries where possible. It also appears that in cases where $(C\text{-}H)_{anion}\cdots(phenyl)_{anion}$ hydrogen bonds are formed, they will have an impact on the packing arrangement adopted in the crystal structure. In all four structures C-H...phenyl hydrogen bond type interactions appear to play an important role in determining the crystal packing.

F.H. Allen et al.[82] reached a similar conclusion after studying the low temperature, neutron diffraction based crystal structures of 2- and 3-aminophenol. These structures had previously been investigated using x-ray diffraction and the probable existence of N-H...π(Ph) hydrogen bonds noted, prompting the reinvestigation by Allen et al. Neutron diffraction confirmed the presence of N-H...π(Ph) hydrogen bonds in both compounds (as discussed in detail previously). Interestingly, both structures were also found to contain weak C-H...O and C-H...π(Ph) type contacts, in addition to N-H...π(Ph) and strong N-H...O and O-H...N hydrogen bonds.

Both 2- and 3-aminophenol were found to pack in an arrangement that the authors describe as the "herringbone" fashion. The herringbone pattern is a well known structural motif, with multiple phenyl/phenyl contacts identified by their T-shaped geometries. An alternative view of this packing arrangement is that centroid type C-H...π(Ph) hydrogen bonds are formed between the phenyl rings involved in the T-shaped interactions and the formation of these additional hydrogen bonds serve to stabilize the structures. The structures of both 2- and 3-aminophenol appear to be

influenced by the optimization of a combination of the strong and weak hydrogen bonds, including the C-H...O, C-H...π(Ph) and N-H...π(Ph) interactions. In fact, the authors write "the formation of weaker [N-H...π(Ph), C-H...π(Ph) and C-H...O] bonds would hint that the optimization of the weak interactions rather than formation of N-H...O hydrogen bonds is the primary structural effect in these compounds." Their conclusion is very similar to that reached in this work, on the importance of C-H...π(Ph) hydrogen bonds in the crystal structures of organoammonium tetraphenylborate salts.

Two recent papers by Y. Umezawa et al.[119,120] also discuss the importance of C-H...π(Ph) type interactions in organic compounds. The authors base their conclusions on the results of a Cambridge Structural Database search for X-H...π(Ph) [X = N, O or C] interactions, particularly C-H...π(Ph) contacts. Both intra- and intermolecular interactions were identified and studied, to determine their possible contributions to molecular conformation and crystal packing, respectively. The C-H...π(Ph) interactions were found to play an important role in both instances, the latter being of more interest in relation to this investigation.

The basic results of the CSD search have been described previously. Most importantly, 75.1% of the structures containing at least one C-H group of any type and at least one six membered aromatic ring were found to form intermolecular C-H...π(Ph) interactions with a minimum contact distance of 3.05Å or less. The mean H(C)...C_{ring} distance for this group was determined to be 2.91±0.12Å. Similar searches revealed that only 5.1% of the OH/π group (mean 2.80±0.21Å) and 9.3% of the NH/π group (mean 2.78±0.19Å) participated in comparable X-H...π(Ph) type interactions. It

is reasonable that a much larger proportion of C-H...π(Ph) interactions might be formed, since C-H groups are much more prevalent than N-H or O-H groups in organic compounds. Also, N-H and O-H groups are more likely to participate in hydrogen bonds with "traditional" lone pair acceptors, lessening the probability of their forming X-H...π(Ph) type interactions in many structures. Still, the great abundance of potential intermolecular C-H...π(Ph) interactions in organic compounds led the authors to speculate on the role such interactions might play in determining crystal packing. They wanted to see if the weak C-H...π(Ph) interactions would influence the crystal packing adopted in the structure or if this was determined by other, stronger intermolecular forces. To obtain insight into the nature of the interaction, data were collected for a wide range of possible C-H...π(Ph) interaction geometries.

The H(C) atoms were found to be concentrated at positions above the plane of the aromatic ring with the hydrogen atoms tending to point towards the center of the ring. For many of the C-H...π(Ph) interactions the characteristic distances were observed to be shorter than the sum of the van der Waals radii. However, C-H...π(Ph) interactions were also found to occur at longer distances and their distribution was observed to fall off only slowly with increasing distance. The C-H...π(Ph) interactions were thus found to be both directionally sensitive and effective over a wide range of distances. This led the authors to suggest that the C-H...π(Ph) interactions do not arise simply a result of dispersion type forces. They describe the interactions as originating mainly from a charge transfer (covalent) process, involving donation from the π system of the aromatic ring to the antibonding orbital of the C-H bond. Superimposed on

this effect are the weak dispersion forces. The electrostatic forces they describe as not as important but still contributing to the total bond. This is in direct contrast to the results obtained in this work, particularly the conclusions reached after careful examination of the electron density maps, which suggest that C-H...π(Ph) interactions are primarily electrostatic, with perhaps a small covalent component.

The authors also identified a smaller subset of the original CH/π group, containing only structures solved from neutron diffraction data, with accurately located hydrogen atoms. They found that the C-H...π(Ph) interaction geometries in the neutron structures were not significantly different from those in the original group. Every structure in the neutron subset was carefully inspected by the authors to see if the C-H...π(Ph) interaction(s) played a role in the observed crystal packing motif. [A number of these individual structures are discussed in some detail in the publication.[119]] Based on the observations made, the authors conclude that the formation of C-H...π(Ph) type interactions constitute one of the important factors controlling the crystal packing of organic molecules. This conclusion is similar to that reached in this investigation but was arrived at from a rather different direction. The results of the present experimental study are even more specific, identifying a population of "true" C-H...π(Ph) hydrogen bonds (as opposed to H...H type contacts) that have the greater impact on crystal packing.

Appendix 3

3.5. Electron Density Maps

The multipole refinements carried out in this investigation were begun as a means to generate high quality electron density maps that could be used to study the N-H...π(Ph) hydrogen bonds present in all four structures. The idea was to generate new information about such bonds by carefully examining the maps. The two N-H...N type, conventional hydrogen bonds also present in the structures would be used as a benchmark with which to compare the N-H...π(Ph) hydrogen bonds. Subsequently it was learned that much more quantitative information could be generated from a topological analysis of the experimental electron densities using Bader's theory of "Atoms in Molecules".[14] Analysis of the generated bond paths and the properties of the electron density at the bond critical points provides detailed information about the nature of all the interactions studied. However, observation of the electron density maps generated still provides useful information about the four structures. A general introduction to the features of electron density maps has been presented previously.

A variety of maps were drawn for each of the four experimental structures. First, maps were plotted in the plane(s) of the cations and the anion phenyl rings. For each compound a complete set of maps covering the entire structure (cation, anion and/or solvent) was generated. Three types of inplane maps were prepared in each case; dynamic deformation density maps, static deformation density maps and residual electron density maps were plotted in each required plane. The nature of each type

of map has been discussed in the introduction (Table 1). Maps are included as figures in the discussion where they are specifically referenced. A complete set of all maps for all the structures is available upon request.

The contour interval chosen for the inplane maps was 0.05 e/Å^3, increasing (solid contours) and decreasing (dashed contours) at this constant interval from the zero level contour (..._...). The only exception made was in the static maps of the phenyl ring planes where a contour interval of 0.10 e/Å^3 proved more appropriate.

The static and dynamic deformation density maps convey essentially the same information. However, the former are often preferred for discussion purposes, the effects of thermal motion having been removed. After a general comparison of the two types of maps in the four related structures, only the static maps will be discussed in detail. In fact, in the second set of maps, generated to study the hydrogen bonding interactions, only the static maps were plotted.

The second group of maps prepared were cuts through all the phenyl rings of the tetraphenylborate anions in the four experimental structures. These cuts were made perpendicular to the phenyl ring planes, through either opposing ring C-C bonds or through opposing C_{ring} atoms. A phenyl ring occupying entirely general positions requires three cuts of each type to be totally defined. The static deformation density perpendicular cuts were all drawn with a contour interval of 0.05 e/Å^3, like the majority of the inplane maps. However, the first positive contour was drawn at the +0.015 e/Å^3 level, to better illustrate regions of low density such as might be observed in weak interactions. The perpendicular cuts through the anion phenyl rings were generated in an attempt to observe any changes in

the distribution of the electron density in the rings brought about by their participation in X-H...π(Ph) [X = N or C] type interactions as either donor or acceptor groups.

The perpendicular cuts were defined by specifying the plane required using only carbon atoms from the ring. However, any possible interacting N-H and/or C-H groups were also always included (generated by symmetry where necessary) in the original map. Once the original map had been examined, any of these groups not in a position to interact with the ring in the plane drawn and the remaining rings of the tetraphenylborate anion were removed for simplification. The results from the examination of the perpendicular cuts will be discussed in terms of the X-H...π(Ph) type interactions, after the inplane results have been presented.

3.5.1. Tetraphenylborate Anions - Inplane Maps of the Phenyl Rings

In the four structures studied, a total of 12 unique phenyl rings exist in the anions and are available for examination and comparison (1 in NH_4^+, 3 in DabcoH$^+$ and 4 each in $C(NH_2)_3^+$ and $N(C[NH_2]_2)_2^+$). Inplane maps (dynamic, static and residual) have been plotted for each of the phenyl rings, making detailed comparisons possible. The quality of these maps is very high overall, however, some variation is evident between the maps of the individual rings and between those of the different structures. To aid the discussion, examples of the best experimental maps (ring 1 in NH_4^+ - with symmetry and ring 1 in $N(C[NH_2]_2)_2^+$ - with no symmetry) and of maps with somewhat less than ideal distributions (ring 1 in DabcoH$^+$ - with symmetry and ring 3 in $C(NH_2)_3^+$ - with no symmetry) have been included with the diagrams in this section.

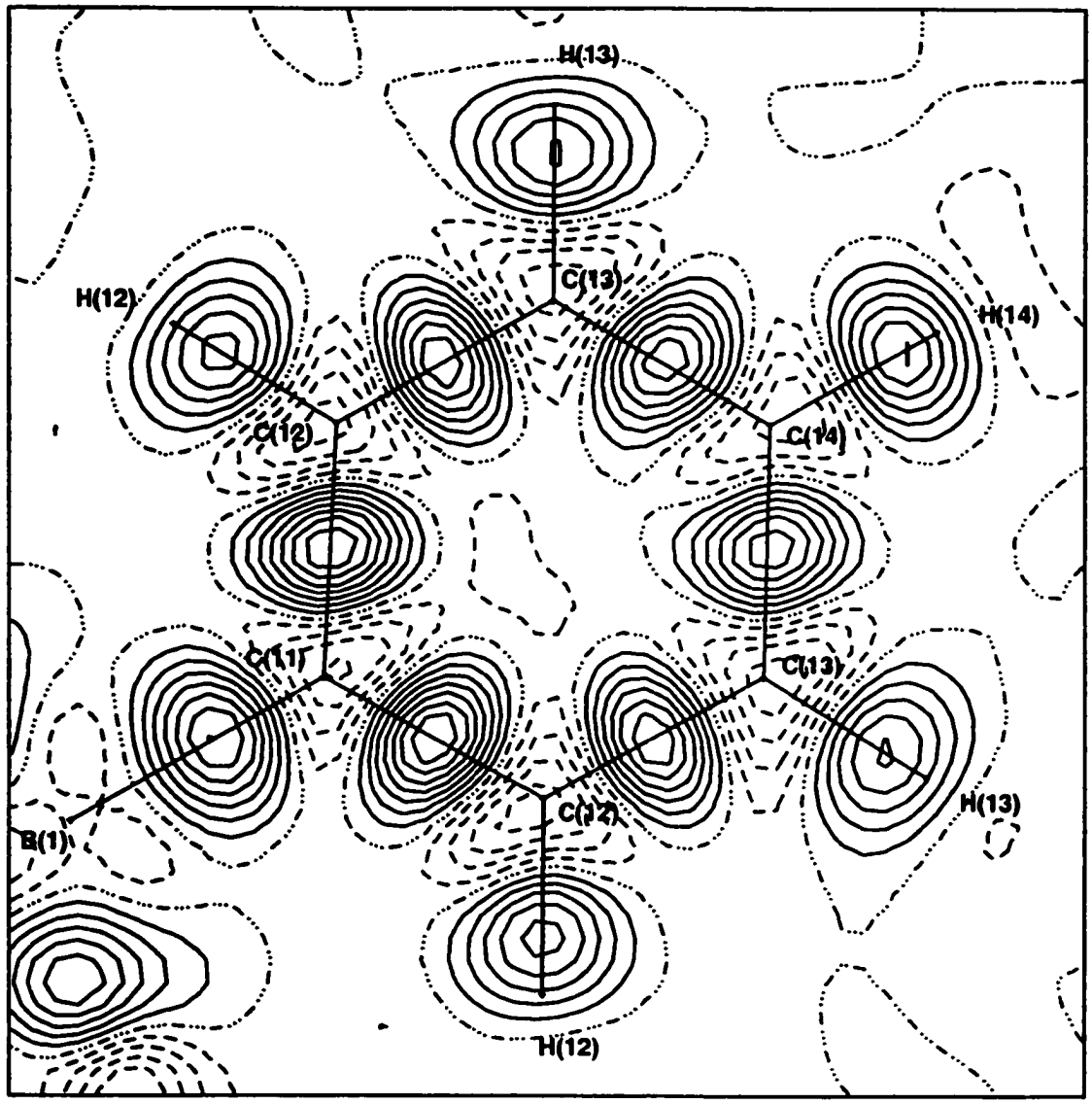

Figure 50. Dynamic deformation density map drawn in the plane of phenyl ring #1 from the structure of ammonium tetraphenylborate. Positive contours are drawn with solid lines, negative contours with dashed lines and the zero level contour with a {dash dot dot dot} pattern. The contour interval is 0.05 $e\text{Å}^{-3}$. This was chosen as one of the best examples of this type of map from the four structures studied.

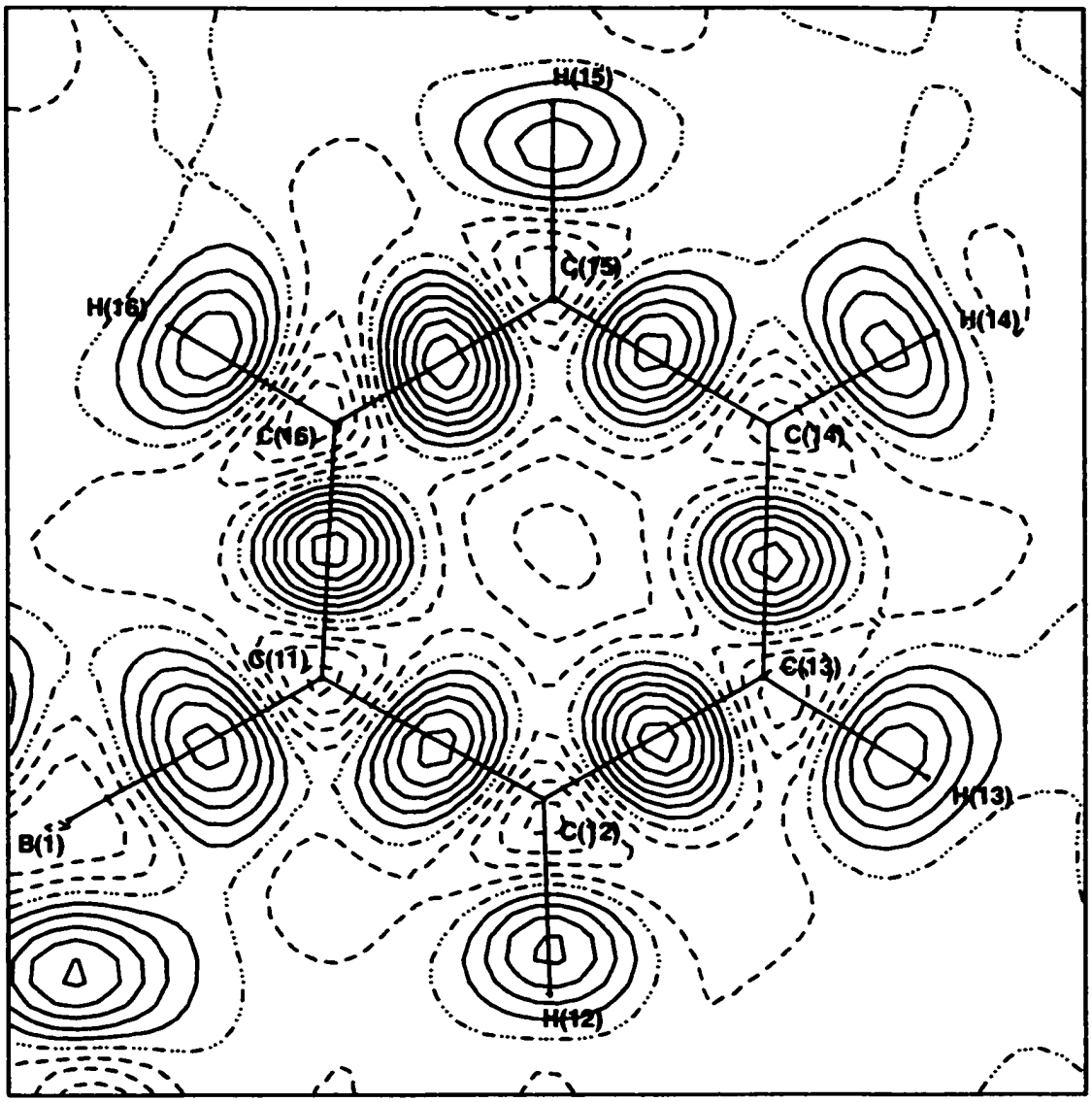

Figure 51. Dynamic deformation density map drawn in the plane of phenyl ring #1 from the structure of biguanidinium tetraphenylborate. Positive contours are drawn with solid lines, negative contours with dashed lines and the zero level contour with a {dash dot dot dot} pattern. The contour interval is 0.05 $e\text{Å}^{-3}$. This was chosen as one of the best examples of this type of map from the four structures studied.

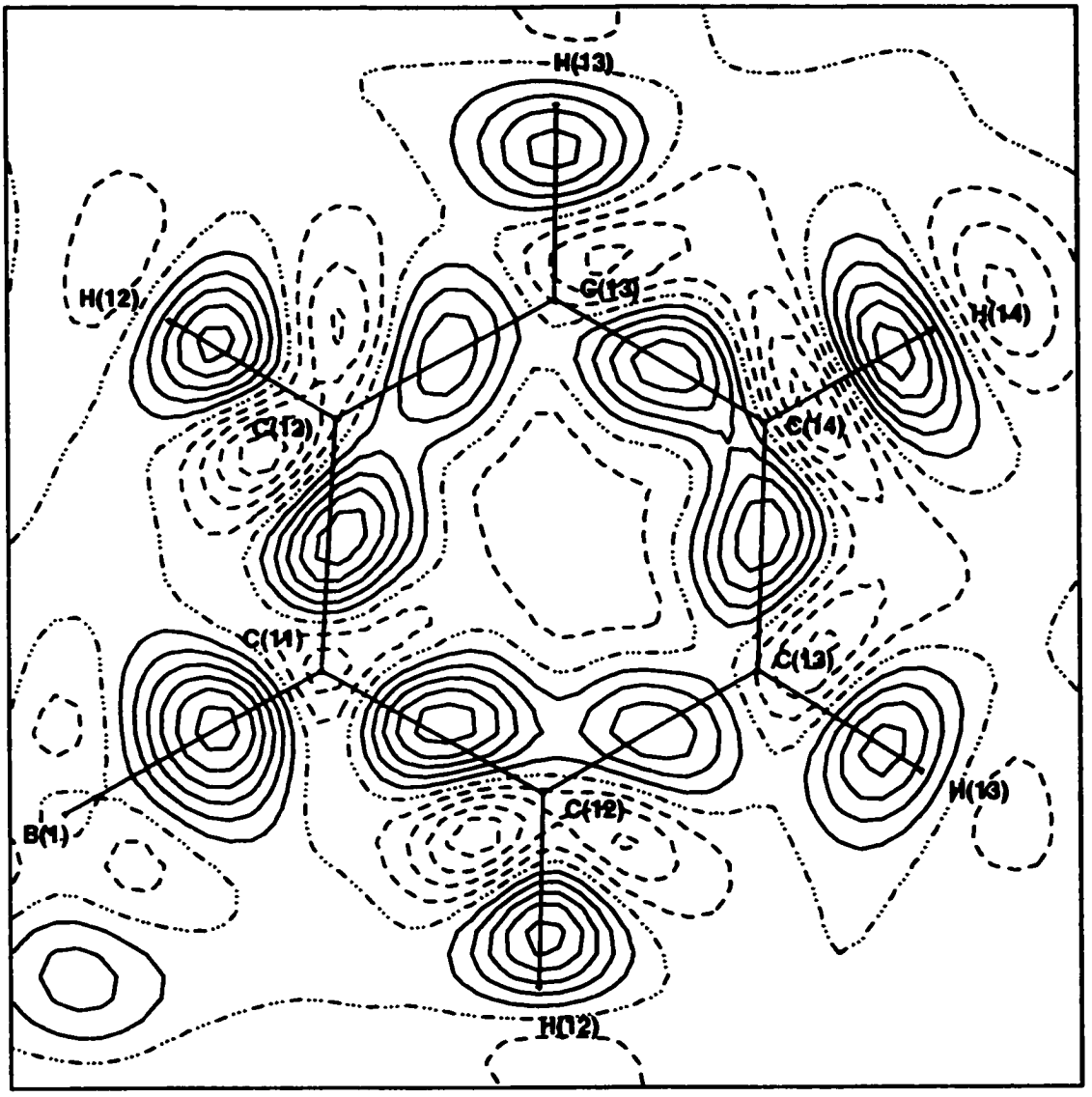

Figure 52. Dynamic deformation density map drawn in the plane of phenyl ring #1 from the structure of [DabcoH][$B(C_6H_5)_4$]. Positive contours are drawn with solid lines, negative contours with dashed lines and the zero level contour with a {dash dot dot dot} pattern. The contour interval is 0.05 $eÅ^{-3}$. This was chosen as one of the worst examples of this type of map from the four structures studied.

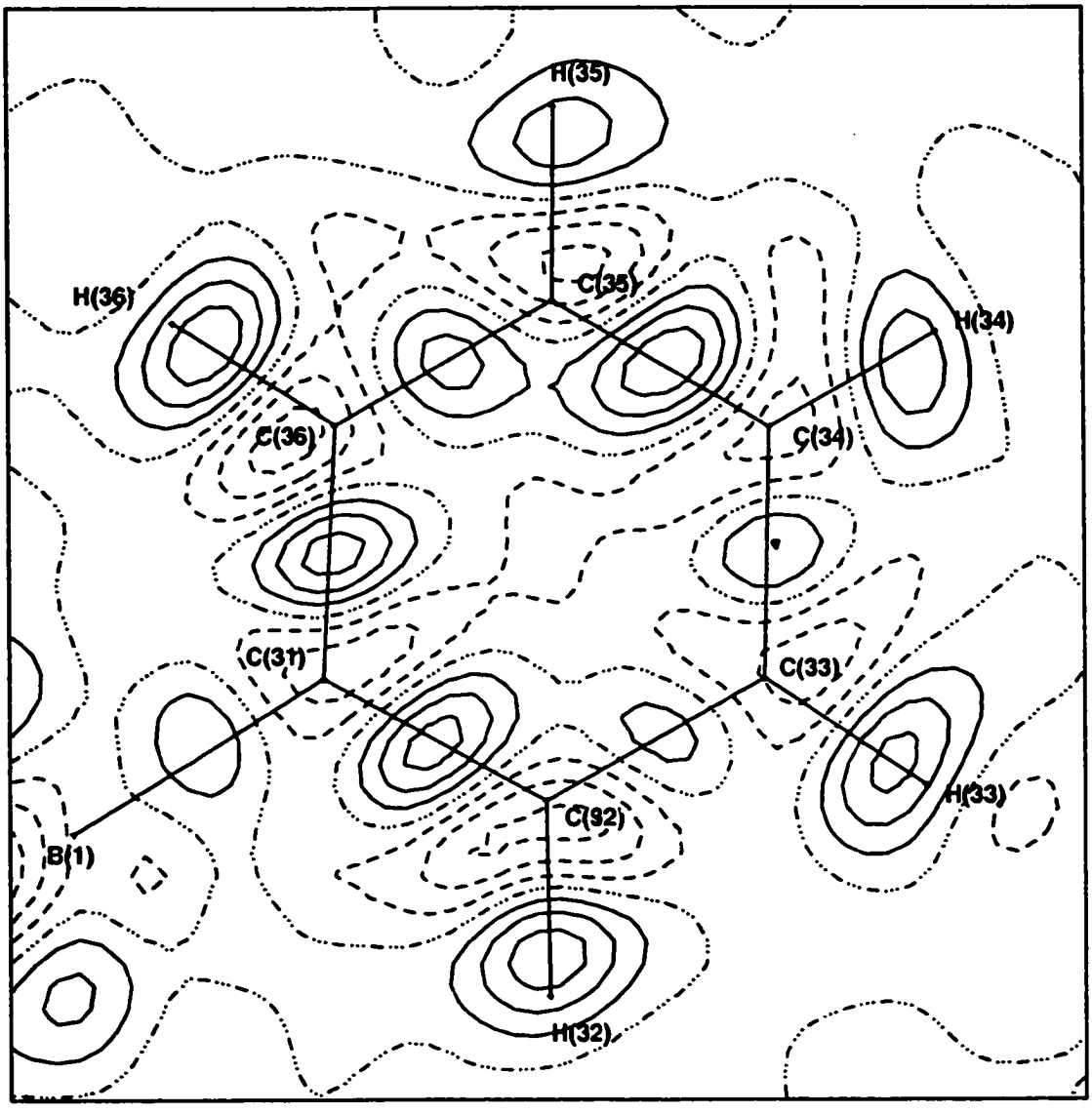

Figure 53. Dynamic deformation density map drawn in the plane of phenyl ring #3 from the structure of guanidinium tetraphenylborate acetonitrile solvate. Positive contours are drawn with solid lines, negative contours with dashed lines and the zero level contour with a {dash dot dot dot} pattern. The contour interval is 0.05 $eÅ^{-3}$. This was chosen as one of the worst examples of this type of map from the four structures studied.

3.5.1.1. Dynamic Deformation Density Maps

The inplane dynamic deformation density maps of the selected phenyl rings are reproduced in Figures 50 to 53, while the complete set of dynamic maps for the anions of the four structures is available upon request. It is possible to study the characteristic features of the best dynamic maps and to compare them with those of the less favourable maps. Overall, the two most important differences observed are that the better maps have a more even distribution of density in the bonds of different types around the ring, relative to the worse looking maps. And, the better maps tend to have more density/contours centered on the bonds. The worse looking maps often have lower levels of density/contours visible on all the bonds by comparison. In fact, in extreme cases, observable density may be entirely missing on some bonds.

In the C-C bonds of the best dynamic maps, the contours are discrete, lying on the bonds well away from any involvement with the atomic centers (C_{ring} atoms) or with the contours on other bonds. In the worse looking maps, the C-C bond contours may no longer be discrete. Rather, the outer contours on one bond may be shared with contours of an adjacent bond or bonds, usually connected via the inside of the ring. This effect is visible in the [DabcoH][$B(C_6H_5)_4$] ring 1 inplane dynamic map (Figure 52) where the contours on the C-C bonds are joined into three pairs, separated by C(11), C(13) and C(13)'. Alternately, in a poorer map, the contours on adjacent C-C bonds may not actually be shared but they may be drawn together in such a way that they show a tendency to join. This effect is visible in the ring 3 map from the [$C(NH_2)_3$][$B(C_6H_5)_4$]·CH_3CN structure (Figure 53) where the contours on the C(34)-C(35) and

C(35)-C(36) bonds curve inward toward each other, such that they appear nearly to touch.

In the better dynamic maps, the C-C bond contours have a regular, nearly uniform shape on all the bonds around the ring. The contours occur as compact sets of neatly shaped ovals, elongated and oriented perpendicular to the bonds themselves. The contours are all well centered on the bonds, with the maxima located close to the bond midpoints. The contours are relatively symmetrical with respect to the bond that bisects them. In contrast, in the worse looking dynamic maps, one or more of these features will always be less than ideal. The C-C bond contours may be ragged or misshapen, no longer nearly symmetrical ovals. They may be more diffuse than normal. They tend no longer to be uniform in appearance around the ring. The contours may no longer be well centered on the bonds or the maxima may be shifted off the midpoints of the bonds. They may be skewed on the bond such that they no longer lie perpendicular to it. The more of these undesirable features a map possesses, and the greater they are in magnitude, the worse it will appear overall.

The C-H bond contours of the inplane phenyl ring dynamic maps share many common features with those of the C-C bonds, but are somewhat different in overall appearance. The better maps have relatively more density on the bonds and an even distribution of that density on the C-H bonds around the ring. The contours are discrete and oval shaped. They are elongated perpendicular to the bond, normally more than the C-C bond contours. In particular, the contours on the C(x4)-H(x4) bonds are often elongated more than those on the other C-H bonds of the ring because of its relatively greater thermal motion. The contours in the best maps are

well centered on the bonds and are symmetrical on both sides of the bond such that they have a relatively uniform appearance around the ring. However, on the C-H bonds the maxima lie much closer to the hydrogen atom than to the carbon atom, approximately three quarters of the distance along the bond. In the worse looking maps, there tends to be an uneven distribution of density on the C-H bonds around the ring and the contours themselves tend to be less uniform in appearance. In some cases, the contours may no longer even be discrete but instead join with the contours of an adjacent C-C bond. The contours may appear ragged or misshapen or they may be more diffuse than normal. The contours may no longer be well centered on the bonds or they may not be symmetrical with respect to the bond. All of these features detract from the appearance of the C-H bonds in a dynamic map.

The contours on the B-C bonds in the dynamic maps are also similar in appearance. In the best maps, the contours are discrete ovals, elongated perpendicular to the bond. The contours are well centered on the bond with the maximum lying slightly closer to the carbon atom than to boron. In the poorer maps, the B-C bond has fewer but more diffuse contours which tend to be not as well centered on the bond.

In the dynamic deformation density maps of the phenyl ring planes, negative contours are visible at each carbon atom. Generally, a triangularly shaped hole is well centered on the carbon atom with its vertices oriented between the bonds. There may be from one to four negative contours at each ring carbon atom, with the better maps having a more even distribution. In the worse maps, the negative contours may not be so well centered on the C_{ring} atoms or they may be unusual in shape or

area. In maps where contours of adjacent C-C bonds are joined, the negative contours at the carbon atoms are often displaced, lying only to the exterior of the ring. Normally peaks of negative contours are not visible beyond any of the hydrogen atoms in the phenyl ring plane dynamic maps. Sometimes, some or all of the hydrogen atoms have one (or very rarely more) negative contour beyond the hydrogen atom but this is unusual. These are often not evenly distributed around the ring and the contours may be oddly shaped or sized.

In the structure of ammonium tetraphenylborate, only one half of one ring is unique, the rest of the anion being generated by symmetry. Only a single dynamic inplane map needs to be drawn, and that map has a vertical mirror plane that bisects the ring at C(11) and C(14). The dynamic map of the phenyl ring plane of the tetraphenylborate anion in $NH_4B(C_6H_5)_4$ is close to ideal in appearance. It was chosen as an example of one of the best experimental dynamic maps obtained in the four structures studied (Figure 50). The bonds of different types have contours that are very regular and uniform in appearance. There is an even distribution of density in the bonds around the ring. In fact, this map shows the greatest average density on the bonds of all types of any of the rings studied.

In the structure of [DabcoH][$B(C_6H_5)_4$] rings 1 and 2 also possess vertical mirror symmetry, with the mirror passing through (and including) the C(x1) and C(x4) atoms. In ring 3 all atoms occupy general positions and the fourth ring is generated, using the same vertical mirror symmetry, from ring 3. The dynamic deformation density map in the plane of ring 1 is the worst looking map of the three in [DabcoH][$B(C_6H_5)_4$] and, in fact, it was chosen to illustrate the less desirable features of such maps

(Figure 52). The ring 1 map shows significantly less density on all its bonds than the other two DabcoH$^+$ dynamic maps for some unknown reason. Rings 2 and 3 have similar bond densities, both compared to each other and to the previous NH_4^+ ring. However, the distribution of the density in the DabcoH$^+$ rings is not as even as had been observed in the NH_4^+ ring and the C-C bond contours in the DabcoH$^+$ maps are not discrete as had been found for the corresponding bonds in the NH_4^+ map. Overall, the $[DabcoH][B(C_6H_5)_4]$ dynamic maps are somewhat less satisfactory than that of $NH_4B(C_6H_5)_4$. The DabcoH$^+$ ring 3 map, although it contains no higher symmetry, has a slightly nicer appearance than that of ring 2. It is the best dynamic map from the $[DabcoH][B(C_6H_5)_4]$ structure even though it is the only one which does not benefit from the additional mirror symmetry.

The tetraphenylborate anions in $[C(NH_2)_3][B(C_6H_5)_4]\cdot CH_3CN$ and $[N(C[NH_2]_2)_2][B(C_6H_5)_4]$ occupy completely general positions, meaning that there are four unique rings in each structure, unlike those of NH_4^+ (one ring) and DabcoH$^+$ (three rings). Both the $[C(NH_2)_3][B(C_6H_5)_4]\cdot CH_3CN$ and $[N(C[NH_2]_2)_2][B(C_6H_5)_4]$ ring plane dynamic maps show less overall density on the bonds (of all types) than those of the previous two structures. This is likely related to the symmetry present in the first two structures and how its application is dealt with by the XD program during refinement.

Overall, $[C(NH_2)_3][B(C_6H_5)_4]\cdot CH_3CN$ has the least density on all its bonds, on average, in the inplane dynamic maps of the four structures studied. This directly contributes to the observation that the dynamic maps of $[C(NH_2)_3][B(C_6H_5)_4]\cdot CH_3CN$ are the least satisfactory of those investigated for this work. In the inplane dynamic map of phenyl ring 1 the C-C bond contours are expanded and very diffuse. The distribution of

the density around the ring is also uneven, combining to give a poor map even though the bond densities are reasonable. The ring 2 map has similar bond densities to ring 1 but it looks better because the bond contours are more compact, even though the distribution of the contours on the C-C bonds is still uneven. The map of ring 3 is the worst in the structure and is, quite possibly, the worst dynamic map of all the phenyl ring planes studied. It was chosen to illustrate the less desirable features sometimes visible in the dynamic maps of the ring planes (Figure 53). The ring 3 map has considerably less density on all the bonds, on average, than the other maps of the anion rings in this structure. The distribution of the density in the C-C bonds remains uneven in both the ring 3 and ring 4 maps. However, the ring 4 map is by far the best in the structure, having the highest density of contours on the bonds of all the rings in the structure of $[C(NH_2)_3][B(C_6H_5)_4]\cdot CH_3CN$.

The inplane dynamic deformation density maps of the anion phenyl bonds in $[N(C[NH_2]_2)_2][B(C_6H_5)_4]$ are better looking overall than those of [DabcoH]$[B(C_6H_5)_4]$, with a more even distribution of density on all the bonds and a cleaner separation of the C-C bond contours, or those of $[C(NH_2)_3][B(C_6H_5)_4]\cdot CH_3CN$, with more density visible on the bonds and a more even distribution of that density around the ring. The best map of a phenyl ring plane in $[N(C[NH_2]_2)_2][B(C_6H_5)_4]$ is that of ring 1; it is shown as a good example in Figure 51. The ring 1 map shows more density on the bonds than the other three rings and an even distribution of that density in all the ring bonds. Rings 2, 3 and 4 all show about equal bond densities, all less than that observed for ring 1. Ring 2 is the worst looking map of the four in biguanidinium tetraphenylborate; the C-C bond

contours are not discrete but are joined into two large sets, each spreading over one half of the ring. The maps of rings 3 and 4 are similar in appearance but that of ring 3 is slightly better than that of ring 4, where the distribution of density on the C-C ring bonds is more uneven. Thus, overall the phenyl ring maps of $[N(C[NH_2]_2)_2][B(C_6H_5)_4]$ fall in the order ring 1, ring 3, ring 4 and ring 2, from best to worst. The dynamic deformation density maps of the phenyl ring planes are best in the NH_4^+ and $N(C[NH_2]_2)_2^+$ structures and of somewhat lesser quality in the DabcoH$^+$ and $C(NH_2)_3^+$ structures.

It is possible to compare the contour density on the C-C bonds of the anion phenyl rings in the inplane dynamic maps of the four compounds studied. Considering all the C-C bonds in all the rings in all the structures, an average of 5.0 contours per bond is observed. However, among the four individual structures there are discrepancies from this overall average. The single map from the structure of $NH_4B(C_6H_5)_4$ shows the highest C-C bond density, 6.3 contours/bond on average. The maps from $[DabcoH][B(C_6H_5)_4]$ show a similar, but slightly lower, average density, of 5.8 contours per C-C bond. In both of these, the average density is considerably higher than it is in the other two structures, 3.4 contours per C-C bond on average in $[C(NH_2)_3][B(C_6H_5)_4]\cdot CH_3CN$ and 4.6 contours per C-C bond on average in $[N(C[NH_2]_2)_2][B(C_6H_5)_4]$. The difference between the highest and the lowest averages, in the NH_4^+ and $C(NH_2)_3^+$ structures respectively, is approximately 3 contours/bond, a significant difference.

Within each individual structure, except that of $NH_4B(C_6H_5)_4$, where there is only one unique ring, differences are also observed in the C-C bond densities between the anion rings. In the dynamic inplane phenyl ring

maps of [DabcoH][$B(C_6H_5)_4$], ring 3 (6.5 contours/bond) and ring 2 (6.3 contours/bond) show similar C-C bond densities, while ring 1 has considerably less density on the C-C bonds (4.0 contours/bond) for some reason. The difference between the best and the worst maps in the DabcoH$^+$ structure is 2.5 contours on each C-C bond on average, the largest difference observed in the structures studied. In the dynamic maps of [$N(C[NH_2]_2)_2$][$B(C_6H_5)_4$] the average number of contours on the C-C bonds is distributed among the rings, from highest to lowest, as follows, ring 1 (5.5 contours/bond), ring 3 (4.6 contours/bond), ring 4 (4.5 contours/bond) and ring 2 (3.7 contours/bond). The difference between the highest and lowest C-C bond densities is an average of 1.8 contours/bond. Similarly, in the structure of [$C(NH_2)_3$][$B(C_6H_5)_4$]·CH_3CN the dynamic maps of the phenyl rings show the average number of contours on the C-C bonds to range from 4.5 contours/bond in ring 4 to 2.3 contours/bond in ring 3 (3.7 contours/bond in ring 1 and 3.0 contours/bond in ring 2 are the intermediate values), for a difference of 2.2 contours/bond. Overall, in the three structures where the comparison is applicable, the average difference in the C-C bond density between the ring with the greatest number of contours and the ring with the least is very constant, roughly 2.2 contours/bond.

Within each individual ring, the distribution of the density on the C-C ring bonds can also vary greatly. However, even when the distribution is very uneven, it cannot be correlated in any meaningful way to the interactions in which the ring is involved. Bonds making the closest geometric contacts in X-H...π(Ph) [X = N or C] hydrogen bonds do not consistently show either an increase or depletion of their densities. This

is not surprising, however, since the inplane maps focus on the σ bond density, while hydrogen bonds in which the phenyl ring acts as the acceptor of the interaction participate through the π electron density which lies out of the ring plane.

A similar comparison can be made between the observed distributions in the C-H bonds of the phenyl rings in the inplane dynamic maps of the four experimental structures. Overall, on all the C-H bonds in all of the rings in all of the structures, an average of 4.0 contours/bond is observed. This is 1.0 fewer contour per bond than the overall C-C bond average (5.0 contours/bond). The C-H bonds have less density than the C-C bonds on average, and in each individual structure this observation also holds true.

As with the C-C bonds, the observed average C-H bond density varies somewhat between the four structures studied. It is higher in the dynamic maps of $NH_4B(C_6H_5)_4$, 5.0 contours per bond, and $[DabcoH][B(C_6H_5)_4]$, 5.1 contours per bond, and much lower in the maps of $[C(NH_2)_3][B(C_6H_5)_4]\cdot CH_3CN$, 3.0 contours per bond, and $[N(C[NH_2]_2)_2][B(C_6H_5)_4]$, 3.2 contours per bond. A similar, but less sharp, division had also been observed in the C-C bond densities in the four structures. However, for the C-H bonds the highest density is observed in the maps of $[DabcoH][B(C_6H_5)_4]$ rather than that of $NH_4B(C_6H_5)_4$. The difference between the minimum ($[C(NH_2)_3][B(C_6H_5)_4]\cdot CH_3CN$) and the maximum ($[DabcoH][B(C_6H_5)_4]$) C-H bond density in the four structures is 2.1 contours/bond on average. This difference is smaller than that observed for the C-C bonds (3.0 contours/bond), which shows that there is more consistency among the average C-H densities in the four structures than was observed for the C-C bonds.

Within the individual structures (except for $NH_4B(C_6H_5)_4$ where there is only one unique ring), the different rings also show some variation in the average C-H bond density observed in the inplane dynamic maps. In the structure of [DabcoH][$B(C_6H_5)_4$] the maximum difference occurs between ring 2 (5.4 contours/bond) and ring 1 (4.6 contours/bond) and is equal to 0.8 contours/bond on average. The C-H contours on the ring 3 bonds are similar in number to those on the ring 2 bonds (5.2 contours/bond). In the maps of [$N(C[NH_2]_2)_2$][$B(C_6H_5)_4$], ring 1 (3.8 contours/bond) shows somewhat more density on the C-H bonds, on average, than ring 4 (3.2 contours/bond), ring 2 (3.0 contours/bond) or ring 3 (2.8 contours/bond). The difference in the C-H bond density between the ring with the most contours per bond and that with the fewest is 1.0 contour/bond. The dynamic maps of [$C(NH_2)_3$][$B(C_6H_5)_4$]·CH_3CN show the least variation in the C-H bond density, from a maximum of 3.2 contours/bond in ring 4, through 3.0 contours/bond in rings 1 and 2, to a minimum of 2.6 contours/bond in ring 3. The difference of only 0.6 contours/bond is the smallest in the structures studied. Overall, the average difference in the number of C-H contours per bond, on the ring with the greatest density compared to that with the least, in the three applicable structures is 0.8 contours/bond. Within a given structure the distribution of the C-H density in the various rings is much more even (an average difference of 0.8 contours per bond) than was observed for the C-C bonds (a corresponding difference of 2.2 contours per bond). Some slight differences are observed in the ring ordering of the average C-C and C-H bond densities in a given structure but none appear to be significant.

Within any individual ring, in any structure, the C-H bond density

may show some variation around that ring. However, this variation is normally small, usually less than observed for the C-C ring bonds. The density on the C-H bonds tends to be more evenly distributed than the density on the C-C bonds in the dynamic maps of the phenyl ring planes.

Finally, in the dynamic maps of the phenyl ring planes the B-C bonds show an average density of 5.2 contours/bond. This is nearly equal to the overall average density on the C-C bonds (5.0 contours per bond) and roughly 1 contour/bond more than the density observed on the C-H bonds (4.0 contours per bond). However, the density on the B-C bonds falls into two distinct groups if the individual structures are considered. The dynamic maps of $NH_4B(C_6H_5)_4$, 7.0 contours/bond, and of [DabcoH][$B(C_6H_5)_4$], 6.5 contours/bond on average, show considerably more density on the B-C bonds than found in the maps of the other two structures. In [$C(NH_2)_3$]-[$B(C_6H_5)_4$]·CH_3CN, 3.0 contours per bond, and in [$N(C[NH_2]_2)_2$][$B(C_6H_5)_4$], 4.2 contours per bond, the average B-C bond density is considerably reduced, a trend that has also been observed for the C-C and C-H bonds and that could be related to the symmetry of the anions.

Overall, the bond densities (whether C-C, C-H or B-C) were found to contribute to the quality of the dynamic maps observed, but they were not the only contributing factors. The best inplane maps were found for the ammonium and biguanidinium structures, even though the average densities on the bonds of the latter are smaller than those of [DabcoH][$B(C_6H_5)_4$]. The dynamic maps of the phenyl rings in the $DabcoH^+$ and guanidinium structures are of slightly lower quality for the variety of reasons just discussed.

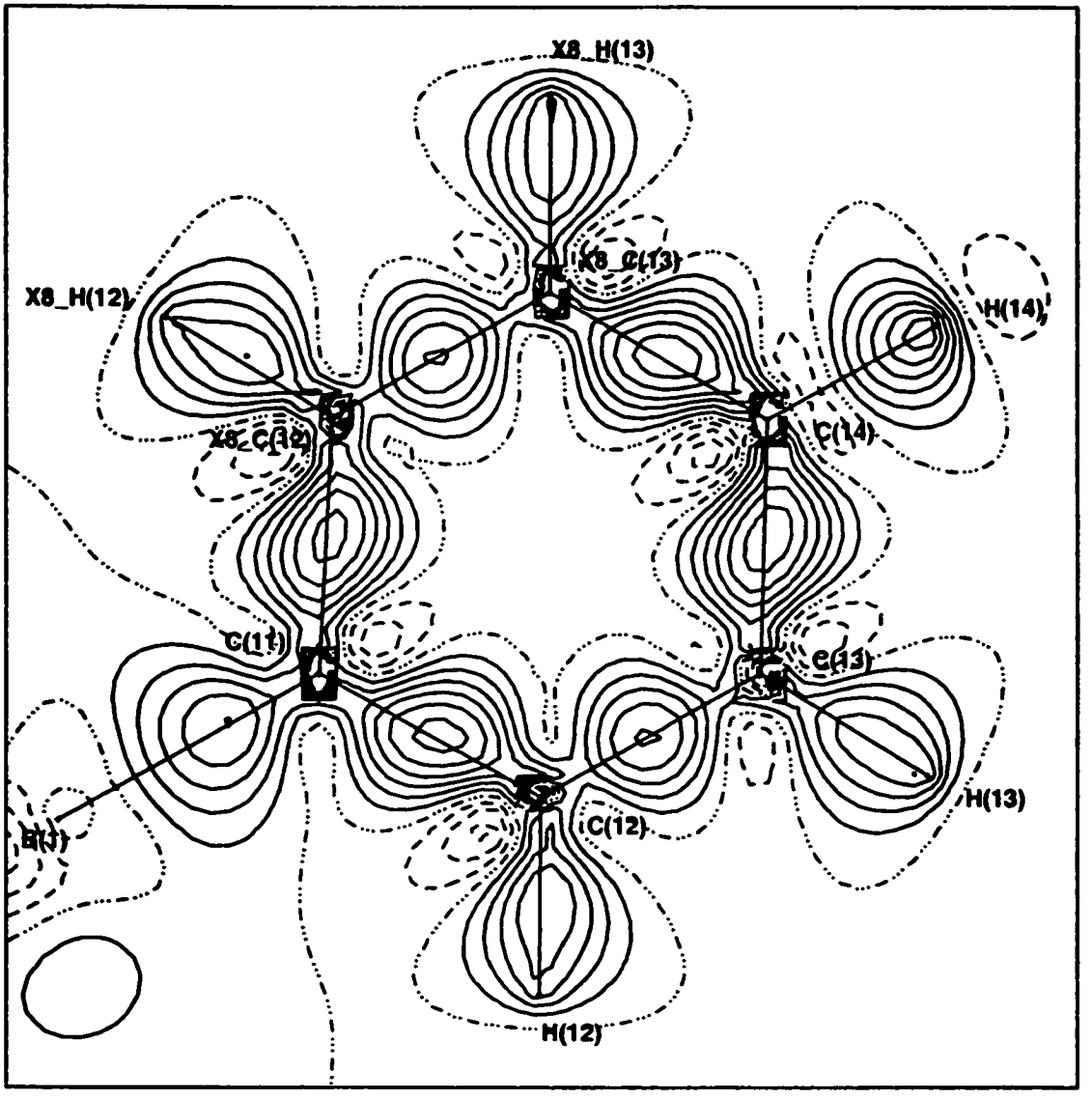

Figure 54. Static deformation density map drawn in the plane of phenyl ring #1 from the structure of ammonium tetraphenylborate. Positive contours are drawn with solid lines, negative contours with dashed lines and the zero level contour with a {dash dot dot dot} pattern. The contour interval is 0.10 $e\text{Å}^{-3}$. This was chosen as one of the best examples of this type of map from the four structures studied.

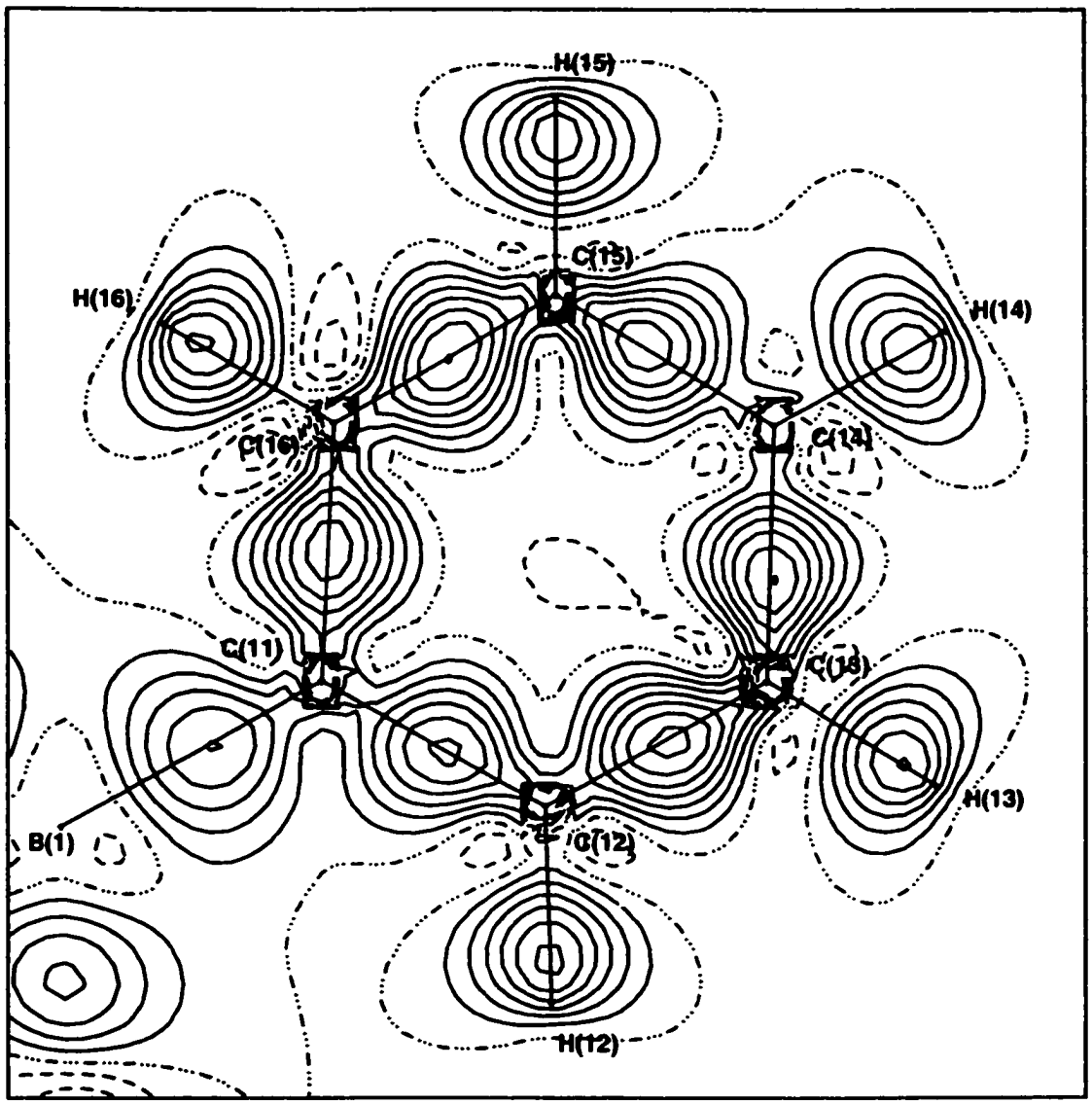

Figure 55. Static deformation density map drawn in the plane of phenyl ring #1 from the structure of biguanidinium tetraphenylborate. Positive contours are drawn with solid lines, negative contours with dashed lines and the zero level contour with a {dash dot dot dot} pattern. The contour interval is 0.10 $e\text{Å}^{-3}$. This was chosen as one of the best examples of this type of map from the four structures studied.

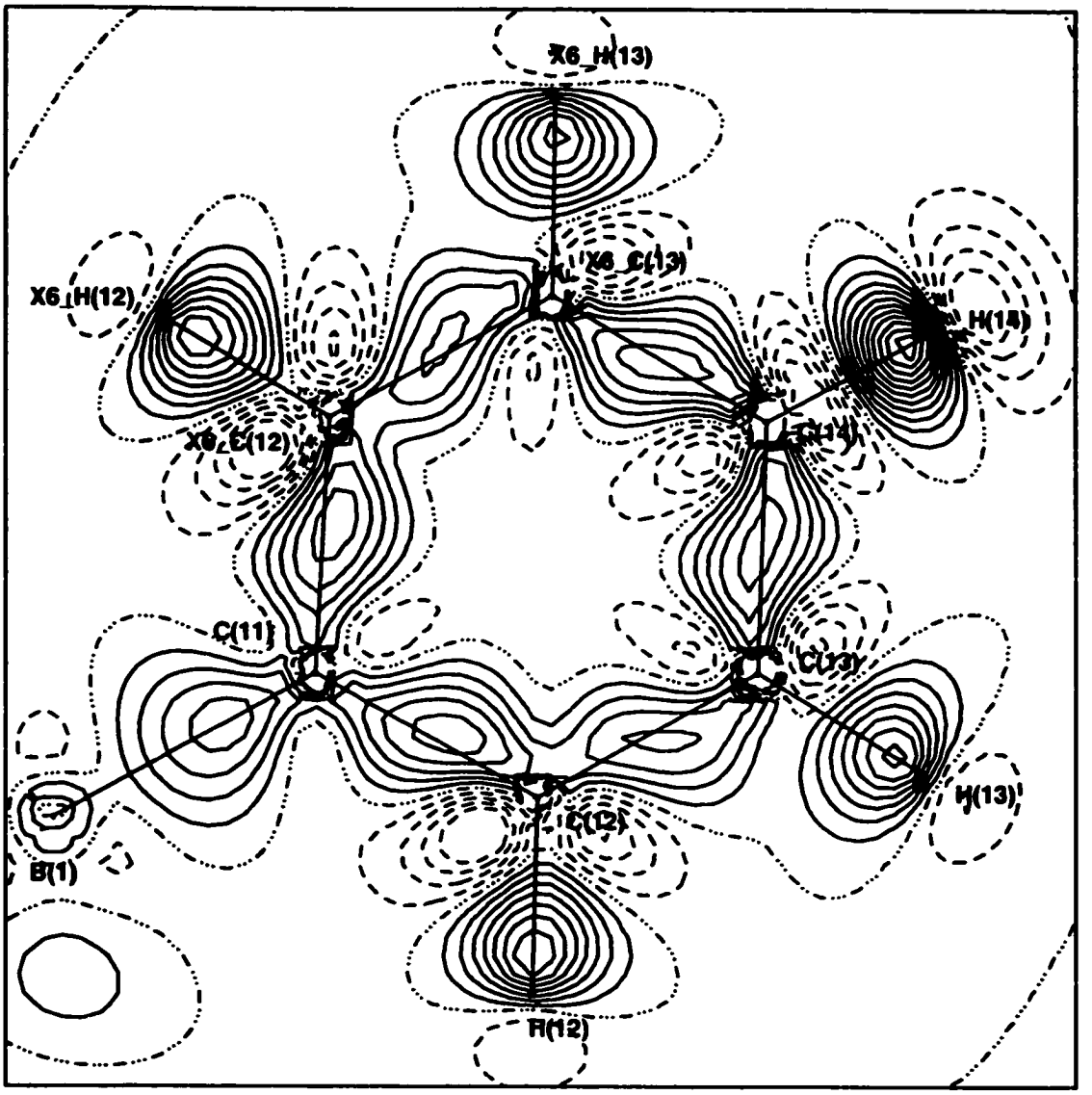

Figure 56. Static deformation density map drawn in the plane of phenyl ring #1 from the structure of [DabcoH][$B(C_6H_5)_4$]. Positive contours are drawn with solid lines, negative contours with dashed lines and the zero level contour with a {dash dot dot dot} pattern. The contour interval is 0.10 $eÅ^{-3}$. This was chosen as one of the worst examples of this type of map from the four structures studied.

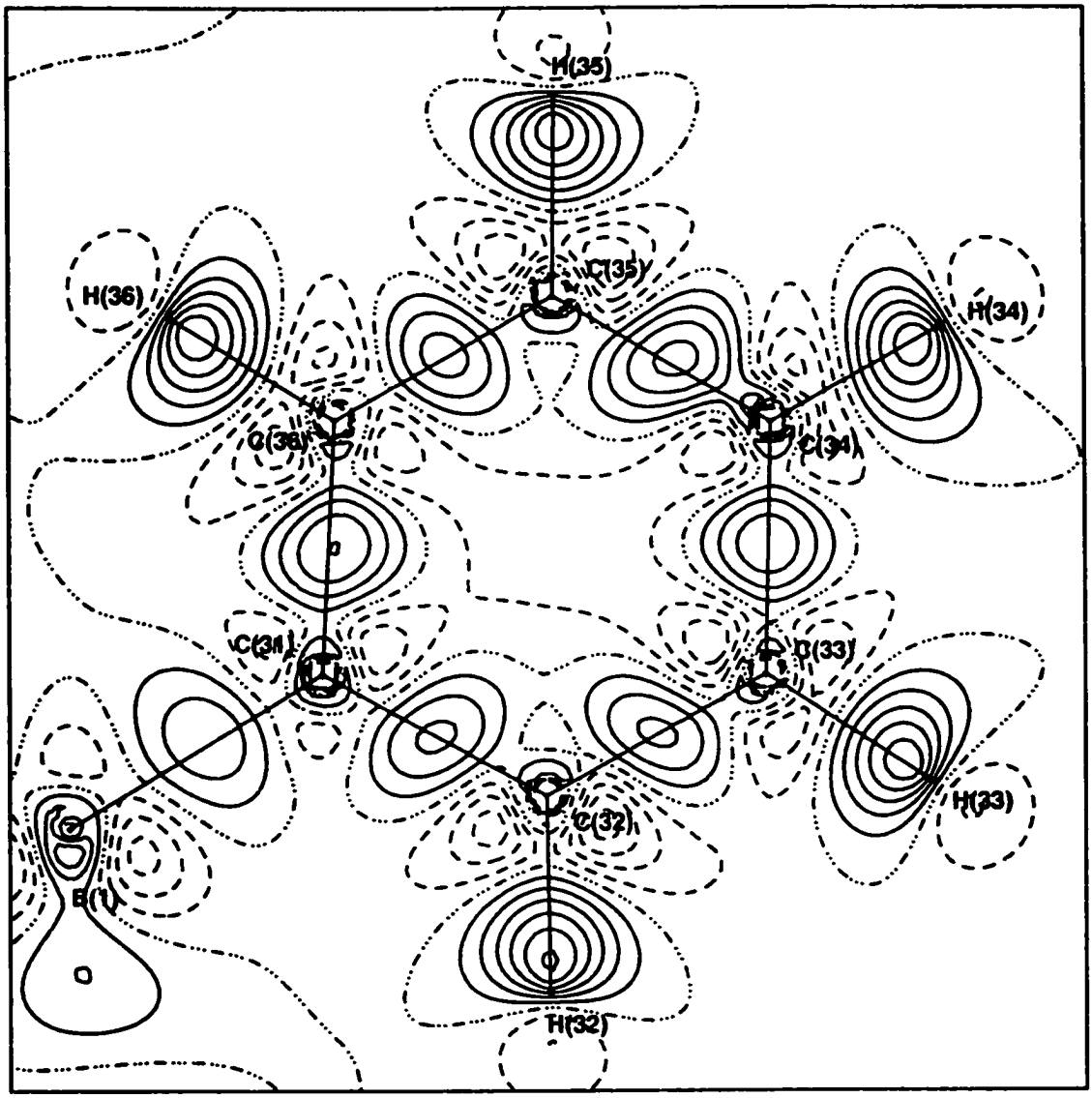

Figure 57. Static deformation density map drawn in the plane of phenyl ring #3 from the structure of guanidinium tetraphenylborate acetonitrile solvate. Positive contours are drawn with solid lines, negative contours with dashed lines and the zero level contour with a {dash dot dot dot} pattern. The contour interval is 0.10 $e\text{Å}^{-3}$. This was chosen as one of the worst examples of this type of map from the four structures studied.

3.5.1.2. Static Deformation Density Maps

It is also possible to identify desirable (and less desirable) features in the static deformation density maps plotted in the planes of the anion phenyl rings for the four experimental structures. These maps differ from the dynamic maps in that the effects of thermal motion have been removed. This should have easily recognizable effects on the static maps, such as cleaner features and increased bond densities, but it could also have more subtle effects on the maps. These might be identified on close examination of the static maps and careful comparison to the corresponding dynamic maps. To illustrate this comparison, static maps of the same rings chosen as examples of typical dynamic ring maps are shown in Figures 54 to 57. These diagrams include Figure 54, the inplane static map of the one ring in $NH_4B(C_6H_5)_4$ (with symmetry), and Figure 55, the inplane static map of ring 1 in $[N(C[NH_2]_2)_2][B(C_6H_5)_4]$ (with no symmetry), as the best experimental examples. Figure 56 illustrates the inplane static maps of ring 1 in [DabcoH] $[B(C_6H_5)_4]$ (with symmetry) and Figure 57 shows ring 3 in $[C(NH_2)_3][B(C_6H_5)_4]\cdot CH_3CN$ (with no symmetry) as somewhat less than ideal examples, to contrast features in each. Of course it must be remembered that the static maps in the planes of the phenyl rings have been plotted with a contour interval of 0.10 e/Å^3, twice that used in the corresponding dynamic maps.

In the best inplane static maps of the phenyl rings, the contours on the bonds of all types share a number of consistent features, also common to the dynamic maps. There will be an even distribution of density on the bonds of different types around the ring. In the less than ideal maps, the density on the different bonds of one type or another around the

ring may be very uneven. Also, maps with more overall density placed on the bonds will appear better than those with less density, at least up to a certain reasonable limit.

The contours on the C-C bonds in the static deformation density maps are rather different in appearance from those in the dynamic maps of the phenyl ring planes. In fact, this difference is often the most obvious change on going from the dynamic to the static maps. In the best experimental static maps, the C-C bond contours are not discrete but flow in a continuous circuit around the ring, covering each bond completely from one carbon atom to the next. The C-C bond contours tend to be less oval in appearance than those in the dynamic maps, being stretched out along the entire length of the bonds. Near the atoms, the contours are compressed and run parallel to the bond. As they move along the bond they elongate perpendicularly to the expected circular/oval shape. In the best maps the contours remain regular, symmetrical and relatively uniform in appearance around the ring. The C-C bond contours are well centered on the bond and are oriented perpendicular to the bond with the maximum located on or near the bond midpoint. In the worse looking static maps a variety of the features just described may be compromised. The C-C bond contours may no longer be so well centered on the bonds or they may be skewed somewhat on the bonds such that they are no longer oriented perpendicular to the bonds. The maxima may be shifted away from the midpoints of the bonds, closer to one carbon atom or another. All this can result in the contours no longer appearing uniform and symmetrical around the ring. Perhaps most importantly, in the poorer static maps of the phenyl ring planes, the bond contours do become discrete on some or all of the C-C bonds. Rather than

flowing continuously around the ring there is a break in the density, where a set of contours becomes isolated on a bond, no longer joining a pair of adjacent atomic centers. These maps (see the "worse" examples, Figures 56 and 57) tend to have less overall density on the C-C bonds which may contribute to the problem. The C-C bond contours become more similar in appearance to the contours in a typical dynamic map rather than to those in the better static maps.

The C-H bond contours in the static maps of the phenyl ring plane from the structure of $NH_4B(C_6H_5)_4$ are slightly different from those in all the other maps studied (Figure 54). In the ammonium tetraphenylborate map these contours begin at each carbon atom and extend along the entire length of the bond before terminating just beyond the hydrogen atom; only on the C(14)-H(14) bond are the contours discrete. The C-H bond contours are similar in appearance to the C-C bond contours in the same map, except that they end at each hydrogen atom. Except for their origin, the C-H bond contours in the $NH_4B(C_6H_5)_4$ static map share all of the better features observed for the C-H bonds in the static maps of the other structures.

In all of the other static maps of all of the other phenyl ring planes, the contours on the C-H bonds are discrete, lying on the bonds away from the adjacent atomic centers. The oval shaped contours are elongated perpendicular to the bond and compressed slightly toward the hydrogen atom. The contours are sometimes drawn down the bond toward carbon slightly, particularly when the bond density is high. In the best maps, the contours tend to be compact, regular and symmetrical in appearance. The contours in good maps are well centered on the bonds, are not skewed with respect to the bonds, and the maxima lie closer to hydrogen

than to the carbon atoms, approximately three quarters of the distance along the C-H bonds. The distribution of the C-H bond density and the appearance of the contours will be uniform around the ring. In the worse static maps, contours may no longer be so well centered on the bonds; they may be skewed or they may be not be symmetrical with respect to the bond. The individual bond contours may not be regularly shaped, the appearance of the bond contours may not be generally uniform around the ring, or the density in the C-H bonds may be very low or unevenly distributed around the ring. These features are all present, to a greater or lesser extent, in the "worse" static maps illustrated in Figures 56 and 57.

One other unusual feature was observed for certain C-H bonds in some of the static maps. In those cases where the phenyl ring possesses mirror symmetry ($NH_4B(C_6H_5)_4$ and rings 1 and 2 of [DabcoH][$B(C_6H_5)_4$]), the C(x4)-H(x4) bond actually lies on the mirror plane. These C(x4)-H(x4) bonds show no special features in the inplane dynamic maps but in the static maps these bonds consistently show more density/contours than the other C-H bonds in the same ring. This effect is particularly pronounced in the static maps of [DabcoH][$B(C_6H_5)_4$] (see Figure 56). The static model must put more density onto this bond, relative to the others in the ring, most likely because of the way the XD program deals with the symmetry involved. In the static map of the [DabcoH][$B(C_6H_5)_4$] ring 3 plane, in which there is no mirror symmetry, the C(34)-H(34) bond density is not significantly different from that on any other C-H bond in the ring, supporting this idea.

In almost every phenyl ring plane static map studied, the contours on the B-C bond begin from the carbon atom and end on the bond before

reaching the boron atom; the contours extend approximately two thirds of the distance along the bond. The contours are narrowly spaced where they begin at the carbon atom but they expand rapidly to become quite circular and diffuse along the bond. In the better maps, the contours are symmetrical and well centered on the bonds. The maximum lies somewhat closer to carbon than to boron, approximately one third of the distance along the B-C bond. In the worse looking maps, the contours are generally not as well centered on the bond. They may also be more diffuse and/or less symmetrical than the contours in the better maps.

Peaks of negative contours (holes) are visible centered around each carbon atom in the phenyl ring static maps. Generally three small holes are found at each atomic center, in a triangular arrangement between the bonds. However, the hole inside the ring is often weak or absent at some or all of the carbon atoms. The holes are normally from one to four negative contours in depth. Many maps show fewer contours on the holes at C(x1) than at the other C_{ring} atoms. In the better looking maps, the holes are well centered on the atoms and the distribution around each atom and around the ring is relatively uniform. In the less than ideal maps, the negative contours may not be well centered on the carbon atoms or the distribution of the negative density around the individual carbon atoms or around the ring may be more uneven.

In some static maps negative contours are also visible beyond the hydrogen atoms in the phenyl ring planes. However, the situations in which these contours are observed is quite interesting. Like the C-H bond contours, in the maps of rings possessing vertical mirror symmetry the H(x4) atom, which lies on the mirror plane, shows a considerable depletion

of charge compared to the other hydrogen atoms of that ring. This again likely arises from the way the XD program deals with the symmetry and it is likely not true that such a strong depletion of charge develops at H(x4) compared to the rest of the ring hydrogen atoms. This effect is visible in the static map of the $NH_4B(C_6H_5)_4$ anion ring (Figure 54), where a hole of one negative contour is developed only beyond H(14). It is also particularly evident in the static maps of rings 1 (Figure 56) and 2 of the $[DabcoH][B(C_6H_5)_4]$ structure where the H(x4) atom show holes of four negative contours, while all other ring hydrogen atoms have holes of only one contour. In ring 3 of the $DabcoH^+$ structure, which does not possess a vertical mirror plane, all of the hydrogen atoms including H(34) have only a small hole of one negative contour; H(34) is no different from the other ring hydrogen atoms.

If the symmetry related problems at those H(x4) atoms lying on a mirror plane are ignored for a moment, it is interesting to note the pattern of charge depletion observed at the hydrogen atoms in the phenyl ring planes of the static maps. The static maps of the anion phenyl rings from the structures of $NH_4B(C_6H_5)_4$ [except H(14)] and $[N(C[NH_2]_2)_2][B(C_6H_5)_4]$ do not show holes of negative contours beyond the hydrogen atoms. Accumulation or depletion of charge is not visible at these hydrogen atoms in the static maps, nor would it generally be expected. As discussed in the introduction, this is evidence that the multipoles on the hydrogen atoms have been correctly assigned. It is another indication that the models developed are correct and of the high quality of the phenyl ring plane static maps in these two structures. In the static maps of the anion ring planes in $[C(NH_2)_3][B(C_6H_5)_4]\cdot CH_3CN$ and $[DabcoH][B(C_6H_5)_4]$ almost all

the hydrogen show holes of negative contours centered beyond the atoms. (However, it is interesting to note that in the static map of ring 1 in $[C(NH_2)_3][B(C_6H_5)_4]\cdot CH_3CN$, the best in the structure, charge is not depleted on any of the hydrogen atoms.) These holes are generally small in area and of only one negative contour. They are yet another indication that the DabcoH$^+$ and $C(NH_2)_3^+$ maps are of slightly lower overall quality than those of the NH_4^+ and $N(C[NH_2]_2)_2^+$ structures.

Only a single inplane phenyl ring static map is needed to define the anion in the structure of $NH_4B(C_6H_5)_4$. This excellent map has been used to illustrate the best features of such static maps (Figure 54), although it should be noted that on some C-C bonds the contours are slightly skewed. The map shows a continuous flow of the electron density around the entire ring, with the contours on all the bonds meeting at the atomic centers. There is a relatively even distribution of the density in all the bonds of each type around the ring. However, unlike the corresponding dynamic map, the inplane static map from the phenyl ring in $NH_4B(C_6H_5)_4$ does not have the highest average density on all the bonds of different types of all the structures studied. In fact, the ammonium structure has the lowest average density on the C-H bonds of the phenyl ring plane static maps for some reason. Still, it does not affect the quality of the map because the distribution of the density is so even.

The inplane static maps from rings 1 (Figure 56) and 2 in the anion of $[DabcoH][B(C_6H_5)_4]$ have the unusual features already described, including increased density on the C(x4)-H(x4) bonds and excessive charge depletion at H(x4), arising from the vertical symmetry each ring possesses. For these reasons, rings 1 and 2 show a higher average density

on the C-H bonds than does ring 3, in which mirror symmetry is absent. It also contributes to the observation that the C-H bonds in the static maps of [DabcoH][$B(C_6H_5)_4$] show a higher average overall bond density than that found in any other of the three structures.

All of the inplane static maps in [DabcoH][$B(C_6H_5)_4$] show a continuous flow of electron density through the contours on the C-C bonds around the ring. However, the static map of ring 1 shows considerably less density on the C-C bonds than do the maps of the other two rings, rendering it less satisfactory in appearance. Rings 2 and 3 show equal C-C bond densities, on average, and are of similar quality. The static map of the ring 1 plane is illustrated in Figure 56. The contours tend not to be well centered on the C-C bonds and they tend to be skewed relative to the bond axes in the ring 1 map. However, aside from the C(14)-H(14) bond, the distribution of the electron density around the ring is quite even. In the static map of ring 2 many of the same undesirable features are also evident but since the average C-C bond density is higher than in ring 1 the map appears better overall. In the ring 2 map the C-C contours remain well centered on the bonds but the maxima are often shifted away from the bond midpoints. This effect is even more pronounced in the static map of phenyl ring 3, where the maximum on every C-C bond lies much closer to one C_{ring} atom than the other. This offset arrangement of bond maxima is symmetrical around the ring, the maximum on each individual bond lying closer to the lower numbered atom [except in the case of the C(31)-C(36) bond where the maximum is closer to C(36)]. This is yet another indication that the model electron density distribution developed for the structure of [DabcoH][$B(C_6H_5)_4$] is not perfect; it is perhaps an indication that the

multipoles on the aromatic carbon atoms may not have been assigned completely correctly.

Although the static maps of [DabcoH] $[B(C_6H_5)_4]$ all show a fairly even distribution of the density on the C-C bonds around the rings, in each ring one C-C bond or another always shows more or less density than the others. In the $DabcoH^+$ structure the bonds with less density stand out, C(12)-C(13) in the map of ring 1, C(21)-C(22) in the map of ring 2 and C(31)-C(36) in the ring 3 map. There is no obvious pattern or consistency in the distributions of the C-C bond densities in the different ring maps, in this structure or in any of the other structures studied. Similarly, the distribution of the density observed on the C-C ring bonds does not appear to be correlated in any way with the interactions in which the ring might be involved.

The static maps of the phenyl ring planes from the anion of $[C(NH_2)_3][B(C_6H_5)_4]\cdot CH_3CN$ are of lower overall quality than those from the other structures studied, as was also observed for the dynamic maps. The C-C bonds in the guanidinium static maps show considerably less density on average than observed in the maps of any of the other three structures. As well, the distribution of the electron density on the C-C bonds around the phenyl rings is more uneven in the guanidinium static maps, which adversely affects their quality. Unlike the previous two structures, in the static maps of $[C(NH_2)_3][B(C_6H_5)_4]\cdot CH_3CN$ the contours on the C-C bonds do not always form a continuous circuit around the ring. Contours tend to be discrete, no longer extending over the entire length of the bond, on those bonds with the lowest observed densities. Even in the static map of the ring 4 plane, the best in the structure, the contours on the opposing

C(41)-C(42) and C(44)-C(45) bonds are discrete, breaking the continuity around the ring. The ring 4 map does have a higher average density on the C-C bonds than any other of the guanidinium static maps but the distribution of that density is still somewhat uneven.

The ring 3 inplane static map from the same structure (Figure 57) shows significantly less density on all the bonds, on average, than any other of the rings. It does show the most even distribution of the bond densities of all the maps in the structure. Still, this is the worst looking static map from the anion in the guanidinium structure and quite possibly the worst in all the structures studied. The C-C bond contours are completely discrete, rather than continuous around the ring, more like a typical dynamic map in appearance. The static maps of rings 1 and 2 also show discrete contours on some of the phenyl C-C bonds. The density of the contours on the C-C bonds is somewhat greater in ring 1 than in ring 2 but the ring 1 bond contours are more diffuse for some reason. The distribution of the density around each ring is quite uneven and overall both maps are less than ideal.

The static maps generated for the ring planes in the structure of $[N(C[NH_2]_2)_2][B(C_6H_5)_4]$ are better overall than those of [DabcoH]$[B(C_6H_5)_4]$ or $[C(NH_2)_3][B(C_6H_5)_4]\cdot CH_3CN$. Maps of the former suffer from problems in accurately locating the C-C contours on the bonds and maps of the latter suffer from a lack of bonding electron density and from an uneven distribution of that density. The ring 1 static map from the biguanidinium structure is similar in quality and appearance to that of $NH_4B(C_6H_5)_4$; it is shown in Figure 55. In ring 1 there is an even distribution of the electron density in the contours of the C-C bonds that flow continuously

around the ring. The static map in the plane of ring 2 has the least density on the C-C bonds of any in the structure, yet the C-C bonds remain continuous around the entire ring. The static maps of rings 3 and 4 are intermediate, and equal, in average C-C bond density and are very similar in appearance. In these maps, discontinuities are observed in the flow of the C-C bond contours, on the C(x1)-C(x2) bond at C(x1) and on the C(x4)-C(x5) bond at C(x4), so that the contours fall into two groups of three bonds each that are continuous around one half of the ring.

It is possible to compare the densities observed on the C-C bonds in the static maps of the phenyl ring planes in all the structures studied. Overall, based on all the C-C bonds in all the rings of all the structures, an average of 5.3 contours/bond was calculated. The overall average in the dynamic map was similar in number, 5.0 contours/bond. However, the contour interval of the phenyl ring planes in the dynamic maps (0.05 e/Å^3) is half that used in the static maps (0.10 e/Å^3) so differences in the number of contours between the two maps cannot be directly compared. Instead, the actual electron densities on the bonds must be used but this comparison will be saved until after discussion of the static maps themselves.

In the four structures, the average number of contours per C-C bond differs somewhat from the overall average. The C-C bond densities in the [DabcoH][$B(C_6H_5)_4$] (5.9 contours/bond), $NH_4B(C_6H_5)_4$ (5.7 contours/bond) and [$N(C[NH_2]_2)_2$][$B(C_6H_5)_4$] (5.5 contours/bond) static maps are, on average, quite similar while in the [$C(NH_2)_3$][$B(C_6H_5)_4$]·CH_3CN maps the average is considerably lower, 4.3 contours/bond. The average C-C bond density in the dynamic maps of [$C(NH_2)_3$][$B(C_6H_5)_4$]·CH_3CN was also considerably lower than

that in the other three structures, however, in the dynamic maps more variation was observed between all the values. In fact, in the dynamic maps $NH_4B(C_6H_5)_4$ displayed the highest average density ($DabcoH^+$ second) while in the static maps $[DabcoH][B(C_6H_5)_4]$ has the higher average density (NH_4^+ second). This reversal in order is likely not significant since in the static maps the two averages are very similar. The difference in the average number of contours on the C-C bonds of the static maps in the structure of $[DabcoH][B(C_6H_5)_4]$, the maximum, and $[C(NH_2)_3][B(C_6H_5)_4]\cdot CH_3CN$, the minimum, is 1.6 contours/bond. In the dynamic maps the equivalent spread was 3.0 contours/bond but since the contour interval is twice as large in the static maps, the difference is approximately equal in both types of maps.

Within each structure differences were also observed in the average C-C bond density in the static maps of each individual ring (except for the structure of $NH_4B(C_6H_5)_4$ where there is only one unique ring). In the static maps of $[DabcoH][B(C_6H_5)_4]$ rings 2 and 3 were both found to average 6.3 contours per C-C bond, while ring 1 has an average density of 4.7 contours per C-C bond, for a difference of 1.7 contours/bond on average. In $[N(C[NH_2]_2)_2][B(C_6H_5)_4]$ the static maps of the ring were found to average 6.5 (ring 1), 5.3 (rings 3 and 4) and 4.7 (ring 2) contours per C-C bond. The difference in the distribution between the maps with the greatest and least densities on the C-C bonds is 1.8 contours/bond. Exactly the same difference was observed between the static maps with the greatest and least densities on the C-C bonds in $[C(NH_2)_3][B(C_6H_5)_4]\cdot CH_3CN$. In this structure the static map of ring 4 has the highest C-C bond density (5.2 contours/bond), the maps of ring 1 (4.8 contours/bond) and ring 2

(4.0 contours/bond) have somewhat less density and the map of ring 3 has the lowest average density (3.3 contours/bond). In the three applicable structures, the average difference in the number of C-C bond contours in the static ring map with the most versus that with the least density on the C-C bonds is 1.8 contours/bond. Each structure very consistently shows this same difference between the rings with the maximum and minimum C-C bond densities. The distribution of the C-C bond densities between the different rings in a given structure is visually more even in the static maps compared to the dynamic maps (based on the number of contours per bond rather than the actual bond densities). Within each individual structure the order of the rings with respect to the C-C bond density is very similar to that observed in the dynamic maps.

In each ring of each structure the static maps show that the distribution of the C-C bond density around the ring can also vary greatly, although again it appears somewhat more even in the static maps compared to the corresponding dynamic maps. Both the static and dynamic maps show the same basic patterns for the C-C bond density distribution on each ring. This distribution does not appear to be related in any obvious way to the interactions the rings are involved with.

The distribution of the density on the C-H bonds of the static maps in the planes of the phenyl rings can also be analyzed. Considering the C-H bonds in the maps of all the rings in all the structures studied, an average density of 5.6 contours/bond is observed. This is almost equal to the observed average C-C bond density in the static maps, 5.3 contours per bond, but it is slightly larger. This is in contrast to the dynamic maps, where the average overall density on the C-H bonds was 1.0 contour/bond

less than the C-C bond density.

If the individual structures are considered, discrepancies from the overall average are observed. The static maps from [DabcoH] $[B(C_6H_5)_4]$ show a considerably higher density on the C-H bonds, 7.6 contours/bond on average, than any of the other structures. Such an effect was not visible in the dynamic maps of the $DabcoH^+$ structure and a possible partial explanation for this has been discussed previously. The structures of $[N(C[NH_2]_2)_2][B(C_6H_5)_4]$, 5.5 contours/bond, and $[C(NH_2)_3][B(C_6H_5)_4]\cdot CH_3CN$, 5.1 contours/bond, show similar densities in their inplane static maps. For some unexplained reason, the density on the C-H bonds in the static map of the phenyl ring plane in $NH_4B(C_6H_5)_4$ is much lower, averaging only 4.4 contours/bond. The difference in the average number of contours on the C-H bonds in the structure with the highest density ($DabcoH^+$) compared to the structure with the lowest (NH_4^+) is large, 3.2 contours/bond. This difference is almost twice as large as the corresponding difference observed for the C-C bonds in the static maps (1.8 contours/bond). The density on the C-H bonds in the static maps of the phenyl rings is much less consistent among the four structures than the C-C bond density. It is also less consistent than was observed for the C-H bond density in the dynamic maps, where the difference between the highest and lowest average densities in the four structures was only 2.1 contours/bond (and in the dynamic maps the contour interval is smaller). The most obvious inconsistencies are that the average C-H bond density in [DabcoH] $[B(C_6H_5)_4]$ is very high, likely due at least partially to symmetry related problems, and that for some unknown reason the C-H bond density in $NH_4B(C_6H_5)_4$ is very low.

For whatever reasons, among the four structures the average density on the C-H bonds in the static maps is not consistent, unlike the C-C and B-C bonds that do behave quite consistently. Two of the compounds studied, [DabcoH] $[B(C_6H_5)_4]$ and $[C(NH_2)_3][B(C_6H_5)_4]\cdot CH_3CN$, show more density on the C-H bonds compared to the C-C bonds in the static maps, while the other two, $NH_4B(C_6H_5)_4$ and $[N(C[NH_2]_2)_2][B(C_6H_5)_4]$, actually show less density on the C-H bonds compared to the C-C bonds. In the dynamic maps, all four compounds were observed to have less density on the C-H bonds compared to the C-C bonds (1.0 contour per bond less on average). This fact, and the fact that the NH_4^+ and $N(C[NH_2]_2)_2^+$ structures have the overall better maps, suggest that the static maps should be expected to show less density on the C-H bonds compared to the C-C bonds. However, a second factor tends to work against this expectation. In the dynamic maps of the phenyl ring planes, the C-H bonds undergo more thermal motion on average than the C-C bonds. When the effects of thermal motion are removed, in the static maps, the C-H bonds show a greater change and increase in density relative to the C-C bonds. This must contribute to the fact that two of the four structures show more density on the C-H bonds of the static maps compared to the C-C bonds. In all the structures, the increase in density on going from the dynamic maps to the static maps should be consistent for all the bond types. This will be examined in more detail in the following section.

The average C-H bond density in the inplane static maps for each ring of each individual structure also shows some variation from that structure's overall average. However, this variation tends to be small and consistent from structure to structure. In [DabcoH] $[B(C_6H_5)_4]$ the static map of ring 2 (8.2 contours/bond) and ring 1 (7.8 contours/bond) show more

density on the C-H bonds than the map of ring 3 (7.2 contours/bond), for a maximum difference of 1.0 contour/bond between the rings. The increased density on the C-H bonds of those static maps possessing vertical mirror planes (rings 1 and 2 in the DabcoH$^+$ structure) has been noted previously. In $[C(NH_2)_3][B(C_6H_5)_4]\cdot CH_3CN$ the static maps of rings 1, 2 and 4 all have average C-H bond densities of 5.6 contours/bond, while the density on ring 3 is only slightly less, 5.2 contours/bond. The maximum difference between the ring with the highest C-H bond density and that with the lowest is only 0.4 contours/bond. In the static maps of the anion planes in the structure of $[N(C[NH_2]_2)_2][B(C_6H_5)_4]$ that difference is again small, only 1.0 contour/bond. The average C-H bond densities on the four rings are 5.6 contours/bond (ring 1), 5.2 contours/bond (ring 3), 5.0 contours/bond (ring 4) and 4.6 contours/bond (ring 2). The order of the rings in each structure is similar to that observed for the C-C bonds in the same static maps. In the structure of $NH_4B(C_6H_5)_4$ no variation exists because there is only one unique ring in the anion. For the three applicable structures, the average difference between the ring with the maximum C-H bond density in the static map and that with the least is 0.8 contours per bond. The distribution of the density on each C-H bond in the rings of each individual structure is quite even and consistent. However, the variation in the C-H bond density between structures is much higher. The variation of the C-H bond density (0.8 contours/bond) within the static maps of the individual structures is smaller than that observed for the C-C bond density (1.8 contours/bond). It is the same average difference observed for the C-H bond contours in the corresponding dynamic maps (0.8 contours/bond) but it must be remembered that the contour interval

has been doubled in the static maps.

Finally, within any given ring the distribution of the C-H bond density in the inplane static map may show some variation. However, this variation appears to be less than that observed for the C-H bonds of the dynamic maps or for the C-C bonds of the static maps. In fact, the distribution of the density on the C-H bonds of the static maps is normally very even. The observed distributions give no evidence as to the nature of the interactions the ring might be involved in.

In the four structures studied, the average B-C bond density in the static maps of the phenyl ring planes is overall 4.2 contours/bond. As with the other bond types, some discrepancies are observed between the averages of the individual structures and the overall average. However, like the C-C bonds and unlike the C-H bonds, the B-C bond averages are relatively consistent among the different structures. The average B-C bond density in the static maps of the phenyl ring planes is 5.0 contours/bond in $NH_4B(C_6H_5)_4$, 4.8 contours/bond in [DabcoH][$B(C_6H_5)_4$], and the somewhat smaller 3.8 contours/bond in $[N(C[NH_2]_2)_2][B(C_6H_5)_4]$ and 3.5 contours/bond in $[C(NH_2)_3][B(C_6H_5)_4]\cdot CH_3CN$. The difference between the minimum and maximum observed B-C bond densities in the four structures studied is 1.5 contours per bond, similar to the corresponding C-C bond density difference of 1.8 contours per bond. The order of the structures regarding B-C bond density is also similar to that observed for the C-C bond density, $NH_4B(C_6H_5)_4$ and [DabcoH][$B(C_6H_5)_4$] being greater than $[C(NH_2)_3][B(C_6H_5)_4]\cdot CH_3CN$ and $[N(C[NH_2]_2)_2][B(C_6H_5)_4]$. In fact, the only real discrepancies are seen in the C-H bond densities where specifically, the $DabcoH^+$ density is somewhat high and the NH_4^+ density is very low.

The B-C bonds in the static maps of the phenyl ring planes consistently show less density than the C-C bonds, the average being 1.1 fewer contours per bond. In the dynamic maps, the B-C and C-C bonds showed approximately equal numbers of contours on each bond on average. Again, this difference can be explained by considering thermal motion and its differing effect on the bond types in the tetraphenylborate anion. The B-C bonds undergo less thermal motion, on average, than the C-C bonds even though they show similar bond densities in the dynamic maps. When the thermal motion is removed in the static maps, the effect on the C-C bonds is relatively greater than on the B-C bonds. This results in the average density on the C-C bonds becoming greater than that on the B-C bonds in the static maps, a reasonable observation.

3.5.1.3. Comparison of the Dynamic and Static Maps of the Anion Rings

The appearance of the contours in the static and dynamic maps of the phenyl ring planes, particularly those on the C-C bonds, is quite different as already discussed. The distribution of the density on the bonds of different types appears to be somewhat more even in the static maps compared to the corresponding dynamic maps. However, the patterns of distribution on the bonds around the rings remain consistent between the static and dynamic maps of the same planes. The contour interval used in the dynamic maps (0.05 e/Å^3) is one half that used in the static maps of the phenyl ring planes (0.10 e/Å^3), so the number of contours on the bonds cannot be directly compared. Instead, the actual bond densities must be calculated before the two types of maps can be compared. A summation of the data collected for the inplane dynamic and static maps, as well as a

comparison between the two, is given below:

Compound and Bond Type	Dynamic Map (0.05 e/Å^3) contours	density (e/Å^3)	Static Map (0.10 e/Å^3) contours	density (e/Å^3)	Difference (e/Å^3)
$NH_4B(C_6H_5)_4$					
C-B	7.0	0.35	5.0	0.50	0.15
C-C	6.3	0.32	5.7	0.57	0.25
C-H	5.0	0.25	4.4	0.44	0.19
[DabcoH] $[B(C_6H_5)_4]$					
C-B	6.5	0.32	4.8	0.48	0.15
C-C	5.8	0.29	5.9	0.59	0.30
C-H	5.1	0.26	7.6	0.76	0.50
$[C(NH_2)_3][B(C_6H_5)_4]\cdot CH_3CN$					
C-B	4.2	0.21	3.8	0.38	0.16
C-C	4.6	0.23	5.5	0.55	0.32
C-H	3.2	0.16	5.1	0.51	0.35
$[N(C[NH_2]_2)_2][B(C_6H_5)_4]$					
C-B	3.0	0.15	3.5	0.35	0.20
C-C	3.4	0.17	4.3	0.43	0.26
C-H	3.0	0.15	5.5	0.55	0.40

Differences (averaged by bond type for the four structures)	Mean	σ
C-B	0.17 e/Å^3	0.02
C-C	0.28 e/Å^3	0.03
C-H	0.36 e/Å^3	0.13

where the standard deviation of the population, $\sigma = [(\Sigma x_i^2 - n(\Sigma x_i)^2) / n]^{1/2}$

All of the bonds in all of the anions show an increase in density on going from the dynamic maps to the static maps, even though the change in the number of contours may not directly reflect this. Removal of thermal motion concentrates more electron density in the bonding regions of the static maps, explaining the observed increase in density. The average increase in density on going from the dynamic maps to the static maps is not uniform, rather it is different for each of the different bond types studied. The increase in the density is smallest for the B-C bonds, 0.17 e/Å^3, intermediate for the C-C bonds, 0.28 e/Å^3, and largest for the C-H bonds, 0.36 e/Å^3. Those bonds most subject to thermal motion (included in the dynamic maps) show the greatest increase in density on going to the static maps where the effects of thermal motion have been removed.

The four structures can show quite different densities on the bonds of different types in both the static and dynamic maps. However, in most cases the difference in the densities on the bonds in the four structures is very consistent between the two types of maps. This is particularly true for the C-C and B-C bonds, where the overall average density changes on going from the dynamic to the static maps were calculated to be 0.17 e/Å^3 and 0.28 e/Å^3, with standard deviations of only 0.02 e/Å^3 and 0.03 e/Å^3, respectively. All of the structures show very similar increases in density on going from the dynamic to the static maps for the C-C and B-C bonds of the phenyl rings.

The situation is rather different for the C-H bonds, however, where the results are not consistent between the four different structures studied. The average increase in the density on the C-H bonds on going from the dynamic maps to the static maps is a reasonable 0.36 e/Å^3 but the

standard deviation is quite large, 0.13 e/Å^3. The four different structures show relatively different amounts of change in the density on the C-H bonds on going from the dynamic to the static maps. This observation is perhaps not so surprising since the C-H bonds may be subject to varying amounts of thermal motion in the dynamic maps. As well, the multipoles on the hydrogen atoms are often difficult to assign correctly during the refinement, making hydrogen atoms (and the bonds they participate in) particularly sensitive to the final model chosen. This may have helped to create the differences observed between the different structures studied experimentally.

However, if the differences calculated between the dynamic and static C-H bond densities for the individual structures are compared, only one value really stands out as being unusual. In $NH_4B(C_6H_5)_4$ this difference is very low, only 0.19 e/Å^3, while the other three structures average a difference of 0.42 e/Å^3 (standard deviation 0.08 e/Å^3), more than twice as large. The C-H bond density in the inplane static map of the phenyl ring in $NH_4B(C_6H_5)_4$ is very low for some reason and this is reflected by a smaller than average increase in the C-H bond density on going from the dynamic map to the static map.

3.5.1.4. Residual Electron Density Maps

The residual map drawn in the plane of the one unique phenyl ring in the structure of **ammonium tetraphenylborate** is very flat and featureless as would be expected for a refinement of high quality; it is shown in Figure 58. There are no holes of negative contours visible anywhere near the ring plane. The model has not placed extra density of

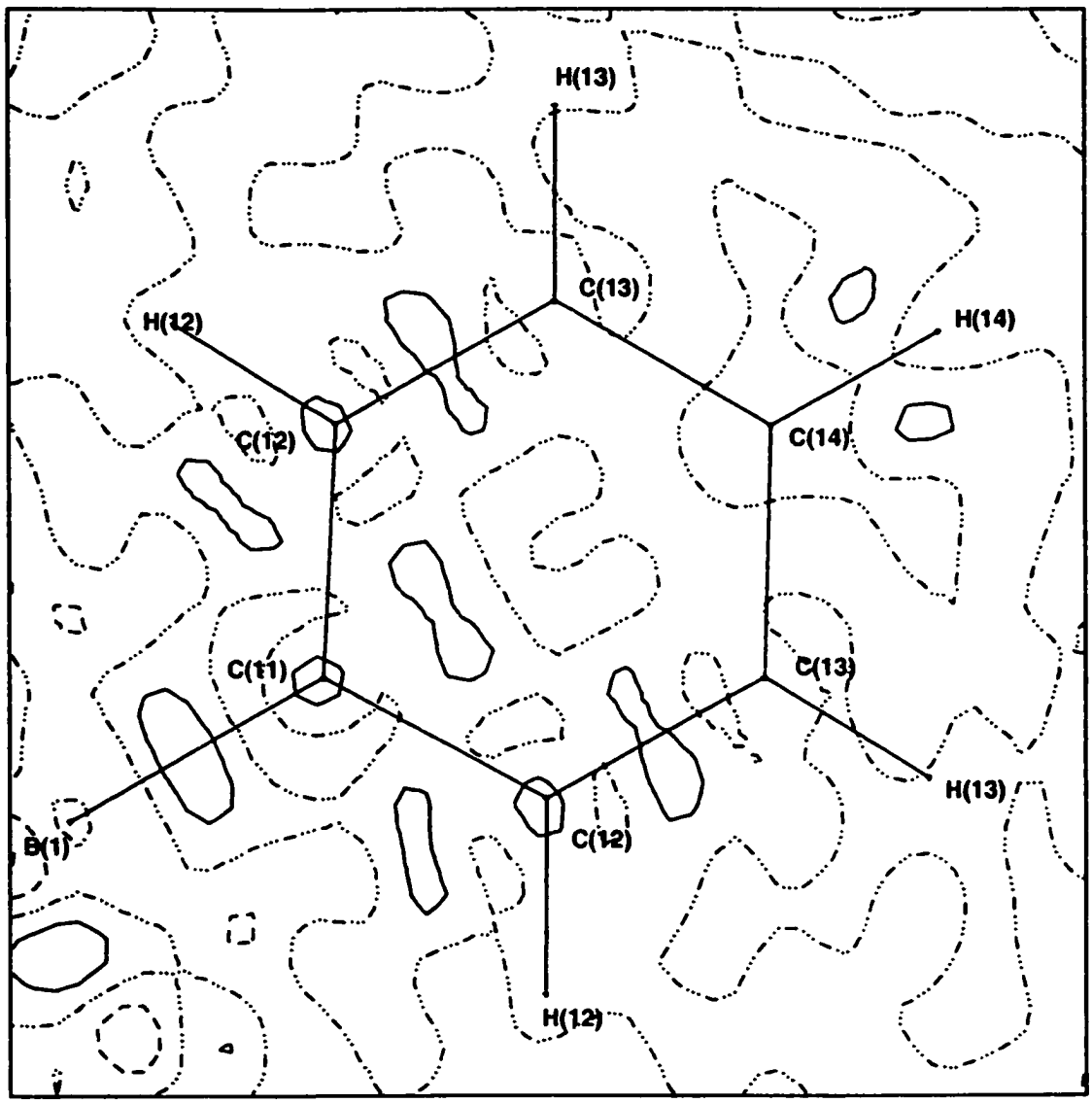

Figure 58. Residual electron density map drawn in the plane of phenyl ring #1 from the structure of ammonium tetraphenylborate. Positive contours are drawn with solid lines, negative contours with dashed lines and the zero level contour with a {dash dot dot dot} pattern. The contour interval is 0.05 $eÅ^{-3}$. This was chosen as one of the best examples of this type of map from the four structures studied.

any significance anywhere on the ring. The peaks of maximum strength are composed of only one contour, equivalent to 0.05 e/Å^3, a very reasonable residual density. Small positive peaks are visible at the ring atoms C(11) and C(12), and on the B(1)-C(11) and C(12)-C(13) ring bonds. The model must not have placed enough density in these areas, on some of the ring atoms in particular. It is interesting to note that the C(12)-C(13) bond has one fewer contour in the maps plotted than the other C-C bonds of ring 1. The decreased density that the multipole model has placed on this bond shows up as a peak in the residual map when the model is compared to the experimental data. There are no other significant features or patterns visible in the residual map of the anion in $NH_4B(C_6H_5)_4$.

The residual map for the ring 1 plane from the **biguanidinium tetraphenylborate** structure is shown in Figure 59. Like all of the anion phenyl ring residual maps from this structure it is relatively flat and featureless. They all show no real pattern or trends in the distribution of the peaks and holes in the regions of the phenyl ring planes. In all the $N(C[NH_2]_2)_2^+$ maps the strongest peaks are always only two contours, whether positive or negative, and thus represent a residual density of only ±0.10 e/Å^3. Although larger than the residual density observed in the map of $NH_4B(C_6H_5)_4$, this is a very reasonable value.

The residual map in the plane of ring 1 shows one peak of two positive contours close to C(12) on the C(12)-H(12) bond; the peak curves away from the bond to the outside of the ring. Small peaks of only one contour are also visible on or near the midpoints of the C(12)-C(13), C(13)-C(14) and C(11)-C(12) bonds. The largest hole, of only one negative contour, curves around the C(14) atom, cutting across both C-C bonds

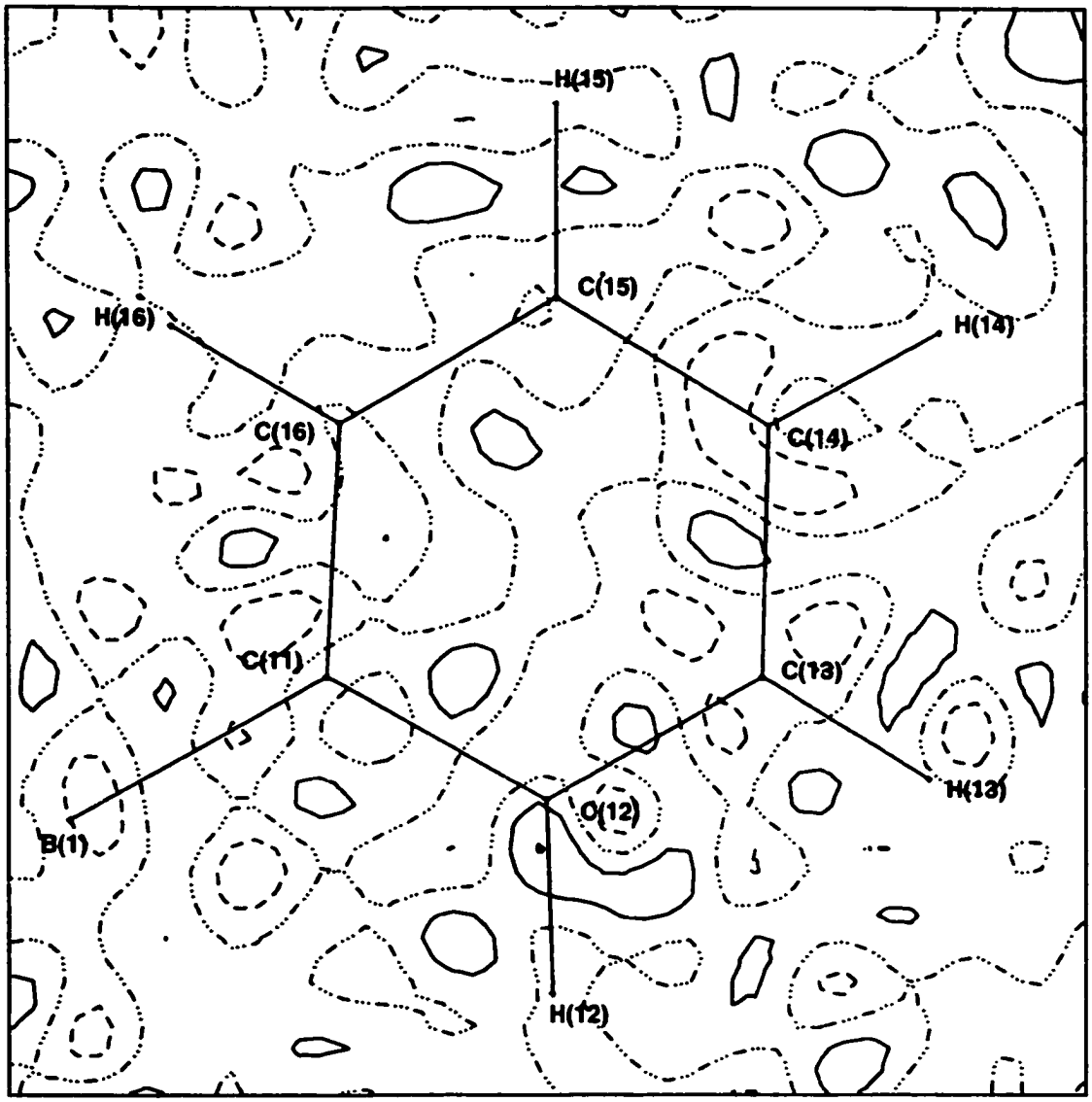

Figure 59. Residual electron density map drawn in the plane of phenyl ring #1 from the structure of biguanidinium tetraphenylborate. Positive contours are drawn with solid lines, negative contours with dashed lines and the zero level contour with a {dash dot dot dot} pattern. The contour interval is 0.05 $e\text{Å}^{-3}$. This was chosen as one of the best examples of this type of map from the four structures studied.

associated with that atom. A hole of one negative contour is also visible at B(1). Clearly, there is no real pattern evident in the distribution of the residual density in the ring 1 map. This is also true for the maps of rings 2, 3 and 4 as well. Overall, the residual maps of all the anion planes in $[N(C[NH_2]_2)_2][B(C_6H_5)_4]$ are flat, featureless and of high quality.

The residual electron density maps in the planes of the anion phenyl rings in the structure of **guanidinium tetraphenylborate acetonitrile solvate** are relatively flat and featureless as well. The strongest peaks and holes on any of the maps are of only two contours, either positive or negative. The minimum and maximum residual electron densities, ± 0.10 e/Å^3, are the same as those observed in the residual maps of the biguanidinium structure, and are very reasonable values. However, overall the residual maps of $[C(NH_2)_3][B(C_6H_5)_4]\cdot CH_3CN$ show a few more and larger (in area) peaks and holes than the maps of the previous two structures.

Ring 3 in $[C(NH_2)_3][B(C_6H_5)_4]\cdot CH_3CN$ was found to have the worst inplane static and dynamic maps of the four rings in the structure, mainly because of the lack of electron density visible on the bonds. The corresponding residual map in the plane of ring 3 is shown in Figure 60 and is fairly representative of the structure. Two peaks of two positive contours are observed in the map, one on the C(31)-C(36) bond and one inside the ring, above the midpoint of the C(31)-C(32) bond. Other peaks and holes of ± 1 contour are visible scattered around the map but in no obvious pattern.

The residual maps of rings 1 and 2 are very similar in appearance to the ring 3 map just described; the map of ring 4 is even flatter and more featureless. This to be expected since ring 4 also has the best

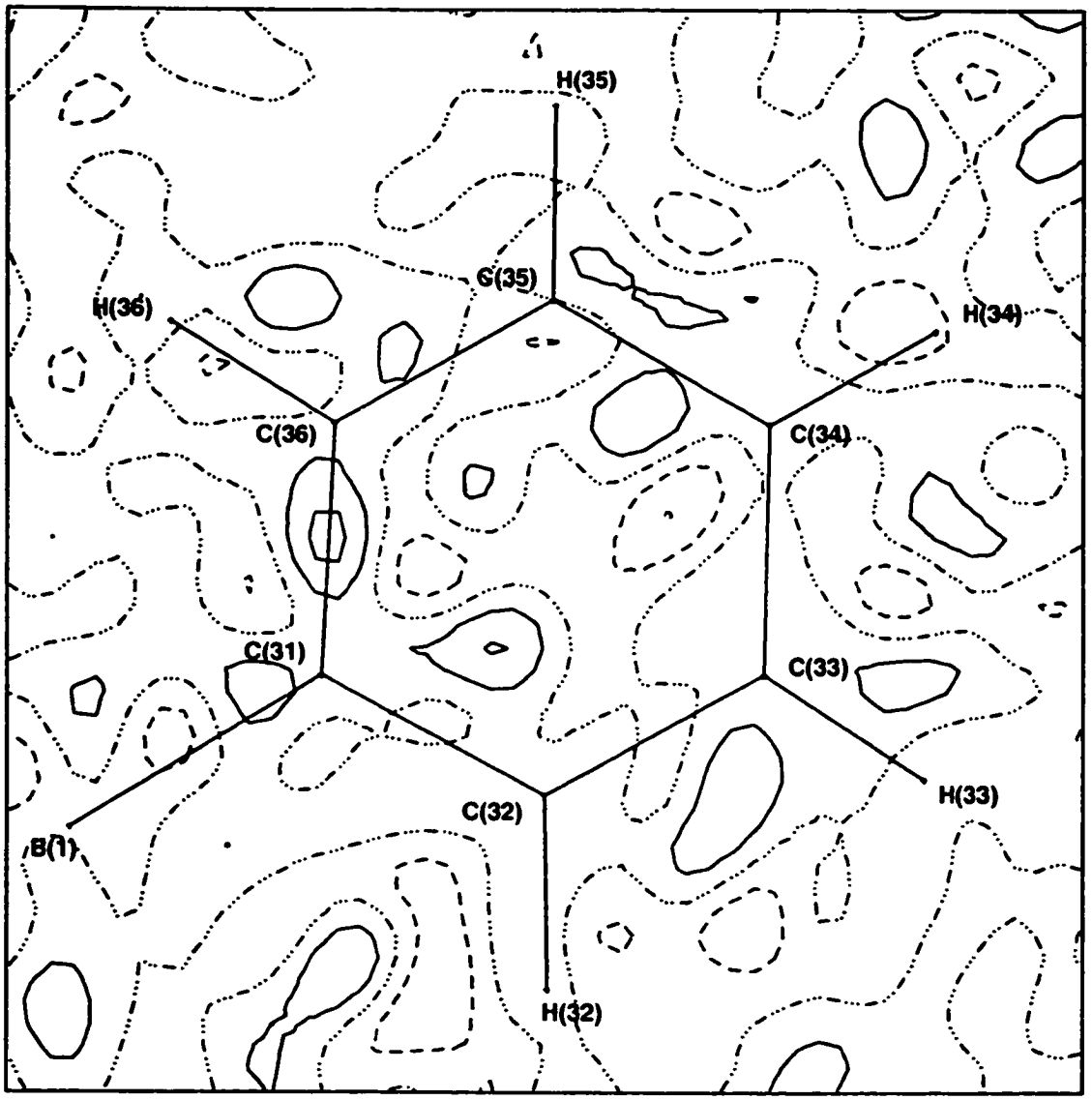

Figure 60. Residual electron density map drawn in the plane of phenyl ring #3 from the structure of guanidinium tetraphenylborate acetonitrile solvate. Positive contours are drawn with solid lines, negative contours with dashed lines and the zero level contour with a {dash dot dot dot} pattern. The contour interval is 0.05 $eÅ^{-3}$. This was chosen as one of the worst examples of this type of map from the four structures studied.

dynamic and static maps of the anion planes in the structure. Overall, the maps of $[C(NH_2)_3][B(C_6H_5)_4]\cdot CH_3CN$ are of good quality, similar in appearance to the maps of $NH_4B(C_6H_5)_4$ and $[N(C[NH_2]_2)_2][B(C_6H_5)_4]$. The multipole model developed must fit the experimental data quite well.

Unlike the residual maps of the other three structures, the inplane residual maps of the **[DabcoH][B(C$_6$H$_5$)$_4$]** anion show considerably greater numbers of peaks and holes, of considerably greater strengths, than observed previously. Peaks and holes are visible virtually everywhere in the maps and densities of up to four contours (both positive and negative) are reached. This corresponds to maximum/minimum residual densities of ± 0.20 e/Å^3; twice as large as those in any other structure, these are fairly high but still acceptable values.

Also in the [DabcoH][B(C$_6$H$_5$)$_4$] residual maps, unlike those of any other structure, certain patterns are apparent in the distribution of the residual electron density. The deepest holes observed in the maps always occur at the boron and/or the carbon atoms of the phenyl rings, and holes of some type are visible at almost every ring carbon atom in every map. Shallower holes are also found in the vicinity of the ring hydrogen atoms in all the maps. The multipole model of the [DabcoH][B(C$_6$H$_5$)$_4$] structure has placed too much density on the atomic centers of all types, resulting in the holes visible in the residual maps.

The deep holes at the ring carbon atoms are often surrounded by large, diffuse peaks of positive density in the residual maps. This is most visible in the ring 3 map (shown in Figure 61), where a single large continuous peak with numerous maxima virtually surrounds the C(31), C(32) and C(33) atoms. This peak often cuts across one or more of the bonds

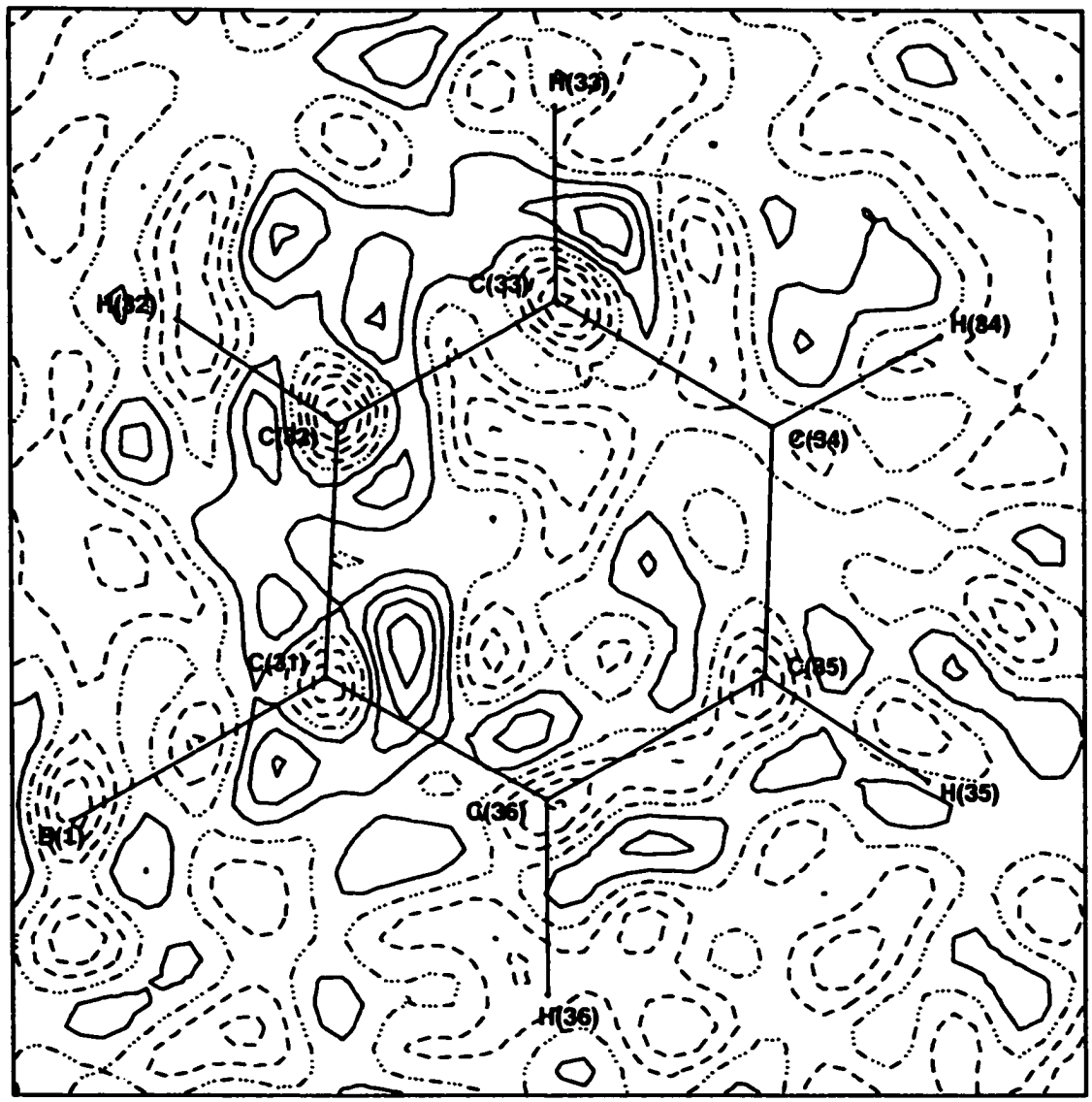

Figure 61. Residual electron density map drawn in the plane of phenyl ring #3 from the structure of [DabcoH][$B(C_6H_5)_4$]. Positive contours are drawn with solid lines, negative contours with dashed lines and the zero level contour with a {dash dot dot dot} pattern. The contour interval is 0.05 $eÅ^{-3}$. This was chosen as one of the worst examples of this type of map from the four structures studied.

surrounding each atom and the maxima tend to occur on or close to the bonds. In all three residual maps of the [DabcoH][$B(C_6H_5)_4$] anion, one of the strongest peaks is always found just inside the ring close to C(x1). All of the residual maps show these features to a greater or lesser extent. The same model that placed too much density directly on the atomic centers appears to have placed too little density in the regions just beyond the atoms, particularly on the bonds. The model has failed in several obvious respects, most likely related to incorrect assignment of some of the multipoles on the atoms.

In fact, this problem introduces another possible avenue of investigation that could have been undertaken with the data generated for this work. Careful comparison of the multipole parameters on the atoms in the four structures, particularly those on the four tetraphenylborate anions, might have revealed more specific problems in the refinement of [DabcoH][$B(C_6H_5)_4$]. Such an investigation could also have included an examination of the feasibility of transferring the multipole parameters between structures or of creating an optimal set of multipoles that could be used for all equivalent groups, such as the tetraphenylborate anion in this work. However, time did not permit such a study to be carried out.

Why are the maps of the [DabcoH][$B(C_6H_5)_4$] anion ring planes of lower overall quality than those of the other structures studied? The final R factors for the refinement (R = 4.68% and R_w = 3.79% based on 3σ data) and the goodness of fit (1.189) are similar to those of the other structures. However, the R factor calculated using the entire data set is 14.73%, higher than that of any of the other structures, as is the merging R value of 5.50%. These values suggest that the data set collected for the

[DabcoH][$B(C_6H_5)_4$] structure may be of slightly lower overall quality, which contributes to the problems observed in the multipole refinement and in the maps drawn.

3.5.1.5. Summary

Overall, the maps drawn in the planes of the anion phenyl rings in the four structures studied, whether static, dynamic or residual, are excellent. The maps of $NH_4B(C_6H_5)_4$ and [$N(C[NH_2]_2)_2$][$B(C_6H_5)_4$] are, in general, slightly better than those of the other two structures, although the static map of $NH_4B(C_6H_5)_4$ does show low electron density on the C-H bonds of the ring for some reason. The dynamic and static maps of [$C(NH_2)_3$][$B(C_6H_5)_4$]·CH_3CN exhibit a lack of electron density on all the bonds, and a more uneven distribution of the density that is present, detracting from their appearance. In contrast, the dynamic and static maps of [DabcoH][$B(C_6H_5)_4$] suffer from poor alignment of the contours on the bonds and the displacement of the bond maxima from their expected positions. This led to the suspicion that the multipole parameters might not have been assigned completely correctly on some of the atoms in this structure. The residual maps of the [DabcoH][$B(C_6H_5)_4$] anion were also poorer than those of any other structure, another sign of problems in the refinement, likely arising from a lower quality data set. However, the real value of this investigation comes not from the fact that four individual structures have been studied, but from the cumulative knowledge gained by combining the results from four related compounds. The total information generated by comparing and contrasting the individual results from the four structures is greater than the sum of the independent parts.

3.5.2. Cation - Inplane Maps

Dynamic and static deformation density maps plotted in the planes of the anion phenyl rings were found to have relatively consistent patterns of the electron density distribution. The static maps, however, tended to be cleaner with more density centered on the bonds because of their lack of thermal motion effects. For this reason, only the static maps in the planes of the cations will be discussed in detail; the dynamic maps will be mentioned only when they differ significantly from the static maps and/or in connection with the differences in bonding densities between the two types of maps. All of the maps in the planes of the cations were drawn with contour intervals of 0.05 e/Å^3, so the number of bond contours in the dynamic and static maps can be directly compared.

3.5.2.1. Ammonium Tetraphenylborate

Only the nitrogen atom and one hydrogen atom must be defined to generate the entire ammonium cation by symmetry in the structure of $NH_4B(C_6H_5)_4$. Thus, only one plane needs to be mapped in the cation, specified by H(1), N(1) and one other hydrogen atom, H(1)'. The static map of the NH_4^+ cation plane is shown in Figure 62. It is similar to, and consistent with, the dynamic map drawn in the same plane. The static map is, however, smoother and more symmetrical.

Holes of negative contours dominate the cation static map, being more visible than peaks of positive contours. The N(1) atom is surrounded by a hole of four negative contours that expands slightly into the regions between the bonds. The outermost contour cuts the N-H bonds that lie in the plane drawn at about their midpoints. At the two hydrogen atoms lying

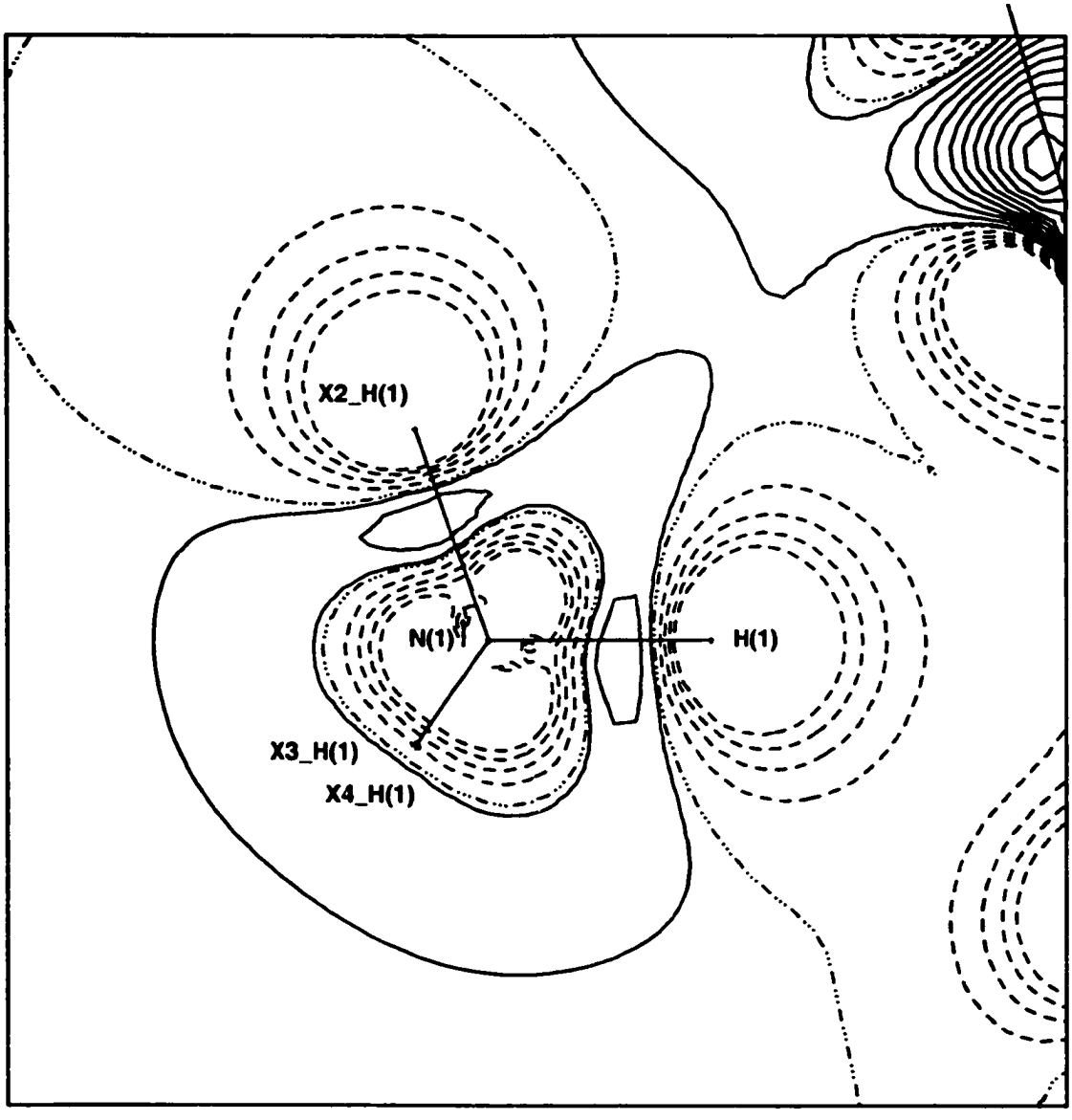

Figure 62. Static deformation density map drawn in the plane defined by H(1)-N(1)-H(1)' of the cation in ammonium tetraphenylborate. Positive contours are drawn with solid lines, negative contours with dashed lines and the zero level contour with a {dash dot dot dot} pattern. The contour interval is 0.05 $e\text{Å}^{-3}$.

in the plane drawn, large diffuse holes of four negative circularly shaped contours are also visible, centered just beyond each atom. Charge is depleted in these areas. Equivalent features are also observed in the corresponding dynamic map of the cation.

A pair of positive contours, each indicative of an electron density of 0.05 e/Å^3, completely encircle the cation, lying between the negative contours at N(1) and those beyond the hydrogen atoms. Again, the dynamic and static maps are similar in appearance but the outer positive contour in the static map is smoother and more regular around the cation. In the static map, the two positive contours are close together where they cut the inplane N-H bonds. In the areas between the bonds, the outer contour expands outward away from the inner contour; the two are farthest apart exactly between each pair of N-H bonds. Between the two "original" positive contours, and centered on the inplane N-H bonds lies another small circular contour, for a maximum density on the bonds of 0.10 e/Å^3. This is somewhat different from the dynamic map where the maxima are actually located between the N-H bonds rather than on them.

Both maps, with their two positive contours encircling the cation rather than having the density well centered on the bonds, suggest that there is some smearing of the electron density around the cation. This is not unexpected, since the cation has been shown to undergo relatively free rotation in the anion cavity in the crystalline state, as discussed in detail previously. The rotation could give rise to the observed pattern of electron density visible in the cation maps. However, it must be remembered that the original hydrogen atom position was taken from a Fourier difference map and that it could be stably refined. The chosen

position also gave a close to ideal N-H...π(Ph) hydrogen bond geometry for the interaction between the cation and the anion. These are all indications that the hydrogen atom has been placed correctly, in the best possible position. The static map also supports this idea, since maxima are observed on the N-H bonds, even if they are of only low density. This low density visible on the N-H bonds of the cation [2 contours, 0.10 e/Å^3] in the static map is likely primarily due to the rotation of the cation in the solid state. However, it should also be noted that the static map in the plane of the anion in $NH_4B(C_6H_5)_4$ also showed a surprisingly low density on the C-H ring bonds.

The static map of the cation H(1)-N(1)-H(1)' plane also suggests that the electron density of the cation may be perturbed by interaction with the bonding density of a neighbouring tetraphenylborate anion. The static map clearly shows that the density on the cation, lying between the two inplane N-H bonds, is drawn out away from the cation toward the anion, specifically toward the density on a pair of adjacent anion B-C bonds. This density on the anion is also visibly perturbed toward the cation. The interaction will be discussed in more detail in the section on N-H...π(Ph) hydrogen bonds and the evidence for them in the electron density maps. However, it must have at least some covalent character since the electron density is actually moved into the region between the participating groups. It is rare for the effects of an interaction to be so clearly visible in the inplane map(s) of the cation.

Like the residual map in the plane of the anion phenyl ring, the $NH_4B(C_6H_5)_4$ cation plane residual map is very featureless and relatively flat (Figure 63). The strongest peaks and holes are of two contours,

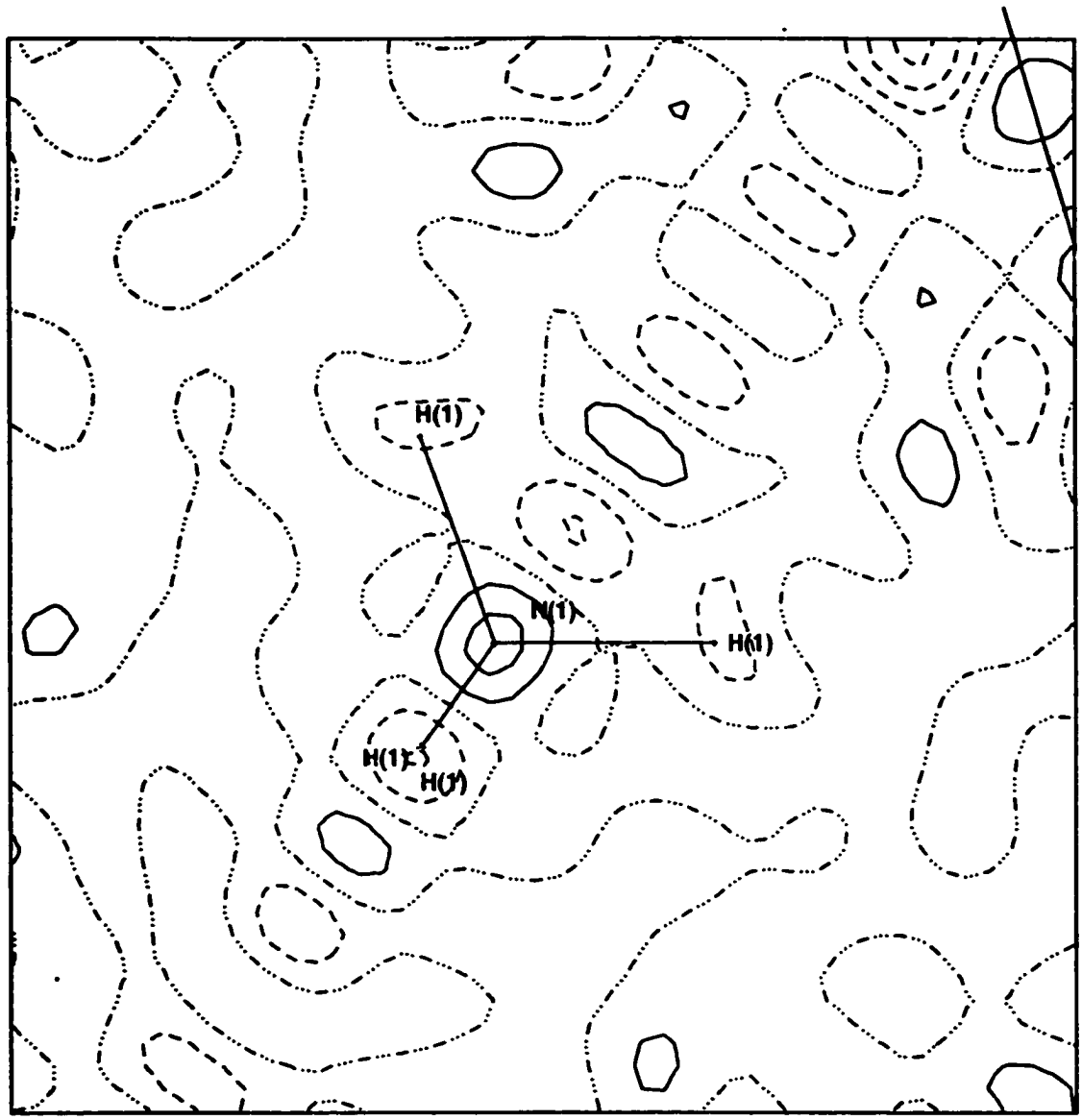

Figure 63. Residual electron density map drawn in the plane defined by H(1)-N(1)-H(1)' of the cation in ammonium tetraphenylborate. Positive contours are drawn with solid lines, negative contours with dashed lines and the zero level contour with a {dash dot dot dot} pattern. The contour interval is 0.05 $eÅ^{-3}$.

either positive or negative, for a residual density of ±0.10 e/Å^3 which is very reasonable. The map does appear to show a definite pattern in the arrangement of the residual electron density but this likely arises only because of the high symmetry of the cation and its related map.

The strongest peak in the map (2 contours) is centered on N(1), perhaps indicating that the model has not placed enough density on that atom. A single peak of one contour is also visible on a line bisecting the two inplane N-H bonds, lying just beyond the cation. The deepest hole, also of two contours, lies on the same line bisecting the two inplane N-H bonds, directly between the two hydrogen atoms. A symmetry equivalent peak is visible in the plane drawn, which also bisects the two out of plane N-H bonds. As would be predicted, it lies exactly on the projected positions of these two hydrogen atoms in the static map of the cation. In addition, a hole of only one contour in depth is visible at each hydrogen atom. The model must have placed too much density in these areas. The holes visible in the residual map might also be significant in the interpretation of the hydrogen bonding interaction in the structure of $NH_4B(C_6H_5)_4$.

3.5.2.2. [DabcoH] [$B(C_6H_5)_4$]

In the DabcoH$^+$ cation only half of the atoms are unique; the other half of the cation is generated by symmetry across the vertical mirror plane. The N(1), N(2), C(1), C(2) and H(1) atoms of the cation all lie directly on the mirror plane. The [DabcoH] [$B(C_6H_5)_4$] maps were drawn in two planes to completely characterize the cation (or at least its heavy atoms). The first plane was defined using the N(1), C(1), C(2) and N(2) atoms, while the second plane was defined using the N(1), C(3), C(4) and

N(2) atoms of the cation. None of the H(C) atoms of the cation actually lie in the planes drawn, a minor oversight that makes interpretation of their bond densities impossible.

The static and dynamic maps in the planes of the cation share similar features, so only the static maps will be discussed in detail. They are shown in Figure 64 (a) and (b). The N(1)-H(1) bond contours, equally visible in both planes, clearly begin from N(1) and cover the entire length of the bond before ending at H(1). The contours are well centered on the bond, with the maximum lying closer to the hydrogen atom than to nitrogen, approximately two thirds of the distance along the bond. The contours are elongated perpendicular to the bond and compressed on either end. The outermost contour is shared with the contours on the two adjacent N(1)-C(x) bonds [x = 1 or 3], so the density is not completely symmetrical about the N(1)-H(1) bond.

A set of contours, attributable to a lone pair of electrons, are visible in both static maps beyond N(2). The density on the lone pair (11 contours) is similar to, but slightly less than, that observed on the N(1)-H(1) bond (14 contours). The contours clearly begin from N(2) and expand outward away from the atom. They are regular and uniform in appearance, compressed somewhat toward N(2) and quite circular away from the cation. The contours are centered on the same line as the N(1)-H(1) bond. The three outer contours are shared with contours on the N(2)-C(x) bonds.

Holes of four negative contours are visible at both the N(1) and N(2) atoms of the cation. The holes cover a wide area around the nitrogen atoms, expanding into regions away from the bonding density. A hole of four negative contours is also visible in the static maps beyond H(1) of

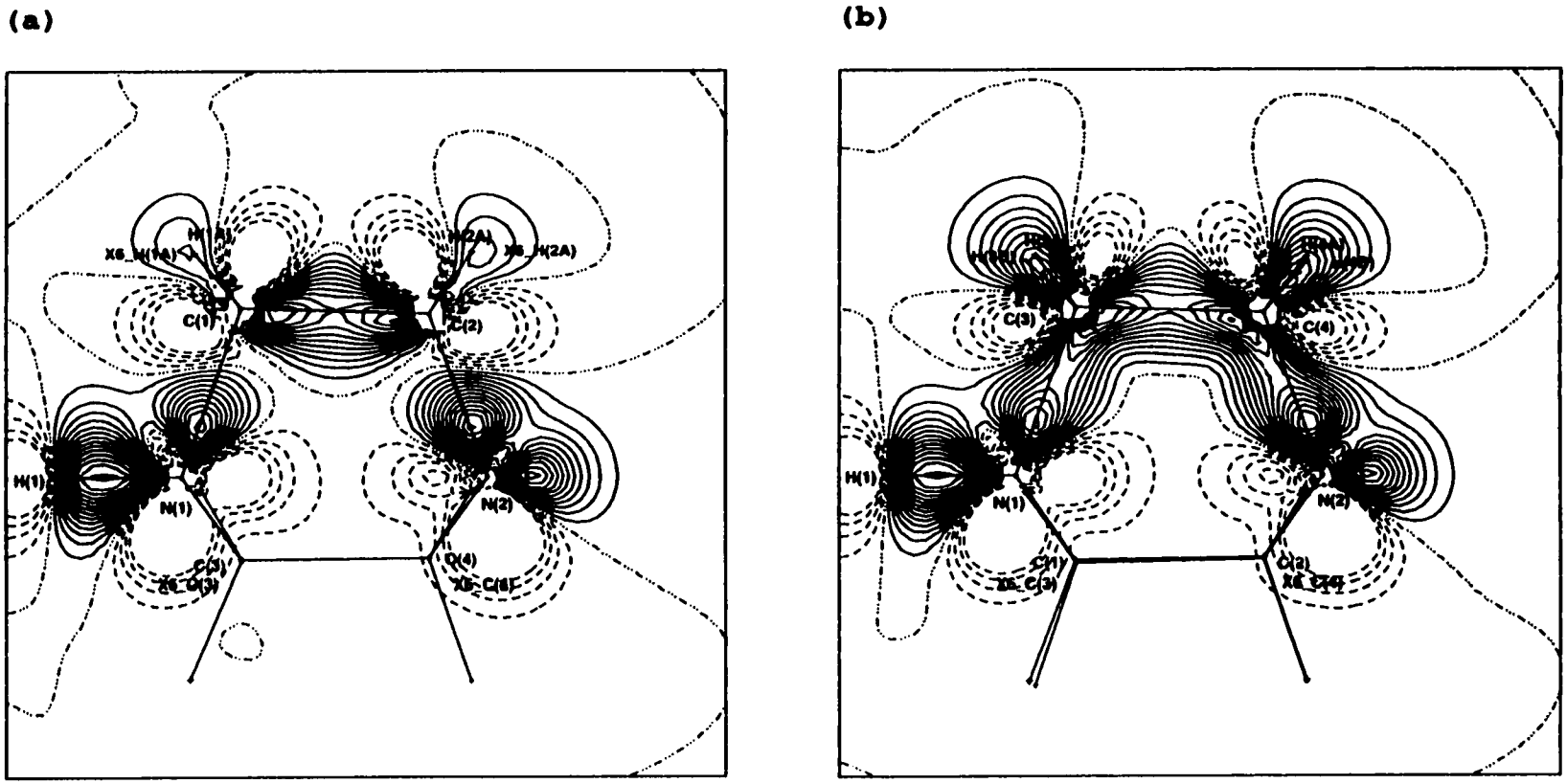

Figure 64. Static deformation density maps drawn in the planes defined by (a) N(1), C(1), C(2) and N(2) and (b) N(1), C(3), C(4) and N(2) of the cation from the structure of [DabcoH][$B(C_6H_5)_4$]. Positive contours are drawn with solid lines, negative contours with dashed lines and the zero level contour with a (dash dot dot dot) pattern. The contour interval is 0.05 $eÅ^{-3}$.

the cation. This observed depletion of charge may be accurate (a consequence of the cationic charge) but it must also be remembered that in the static maps of the phenyl ring planes of the [DabcoH][$B(C_6H_5)_4$] structure, bonds lying on the mirror plane showed excess electron density and the hydrogen atoms lying on the mirror plane showed an excessive depletion of charge.

The C-N bonds of the DabcoH$^+$ cation show a relatively even distribution of the electron density in the static maps, more even than that in the corresponding dynamic maps. The density observed on the C-N bonds [11.8 contours/bond, on average] is similar to that found on the N(1)-H(1) bond and on the lone pair at N(2). The contours on the N-C bonds clearly begin from the N(x) atoms (x = 1 or 2). They are all well centered on the bonds, with the maxima lying closer to the nitrogen than to the carbon atoms, approximately one third of the distance along each bond. The contours are generally uniform in appearance and regularly shaped, although they are shared with contours on the adjacent N(1)-H(1) bond [N(1)-C(x) bonds] or the lone pair at N(2) [N(2)-C(x) bonds]. There is a major difference in the two planes mapped, however. The contours on the N(1)-C(1) and N(2)-C(2) bonds do not interact with those on the C(1)-C(2) bond; they end on the bond before reaching C(x). In contrast, the contours on the N(1)-C(3) and N(2)-C(4) bonds are joined with those on the C(3)-C(4) bond, eight contours being common to all the bonds. A continuous flow of electron density, with various maxima, passes from N(1) through C(3)-C(4) to N(2). The N(1)-C(3) and N(2)-C(4) bonds each show a second maximum, located just inside the cation cage, very close to C(x). These appear to be related to problems in modelling the C-C bond, or more

specifically the multipoles on those carbon atoms, correctly rather than true features of the N-C bonds. Similar maxima are not observed on the N(1)-C(1) or the N(2)-C(2) bonds, where the contours do not interact in any way with those on the C(1)-C(2) bond.

As can be surmised from the above discussion, the contours on the C-C bonds in the static maps of the DabcoH$^+$ cation are not pretty, although the density on the bonds is similar to that on the other bonds already examined. Aside from the fact that the contours on the C(3)-C(4) bond are shared with those on the N(1)-C(3) and N(2)-C(4) bonds while the C(1)-C(2) bond contours are discrete, the two sets of C-C bond contours are quite similar in appearance. Both bonds show two distinct maxima, each one lying on the bond close to one of the carbon atoms, approximately one eighth of the distance along the bond from each carbon atom. The eight outer contours run the entire length of each bond while the remaining contours are centered on the bond at the maxima. The contours inside the cation cage are nearly flat and parallel while outside the cage they are more expanded, curving outward away from the bonds. Holes of four negative contours are visible, centered on each carbon atom of the cation, in the static maps drawn. The negative contours lie outside the cation cage in regions away from the bonding density at each carbon atom. The H(C) atoms of the cation do not lie in any of the planes drawn, so little can be inferred about them from the static maps.

The two most distinctive features of the inplane cation static maps in the structure of [DabcoH][$B(C_6H_5)_4$] were also observed in the static maps of the anion ring planes. The first is that extra density may be accumulated on the N(1)-H(1) bond lying on the vertical mirror plane in

the cation. This was also observed in the C(x4)-H(x4) bonds of the anion lying on the same vertical mirror plane. In the static maps of the cation, the N(1)-H(1) bond does show more density than any other type of cation bond on average. In the anion, this was attributed to an inability of the XD program to correctly handle the symmetry which must be applied to those hydrogen atoms and their multipoles. The same explanation appears to be reasonable in the case of the cation N(1)-H(1) bond.

The second feature obvious in the static maps drawn in the planes of the cation is the relatively poor appearance of the contours on the C-C bonds, attributed to poor modelling of the multipoles on those carbon atoms. A similar problem was observed in the C-C bonds of the anion phenyl rings, where the contours were often not well centered on the bonds and the maxima were moved away from the midpoints of the bonds. This was also attributed to poor assignment of the multipoles on the ring carbon atoms, likely arising ultimately from problems with the data set collected. Both the cation and anion inplane static maps are consistent in their features, both good and bad, in the [DabcoH][$B(C_6H_5)_4$] structure.

The change in bond densities on going from the dynamic maps to the static maps for the $DabcoH^+$ cation can be compared to the corresponding changes observed in the maps of the anion. The contour interval chosen for the cation maps, both static and dynamic, was the same (0.05 e/Å^3) so the number of contours or the densities on the bonds can be directly compared. The N(1)-H(1) bond increases from 6 contours in the dynamic maps to 14 contours in the static maps, for a difference of 8 contours/bond or 0.40 e/Å^3. Similarly, the lone pair at N(2) is characterized by 3 contours in the dynamic maps and 11 contours in the static maps for an equivalent

difference of 8 contours/bond (0.40 e/Å^3). The N-C bonds were observed to average 3.5 contours per bond in the dynamic maps, 8.3 contours per bond fewer (0.42 e/Å^3) on average, than the corresponding N-C bonds in the static maps (11.8 contours/bond on average). Finally, the C-C bonds were found to differ by 7.8 contours/bond (0.39 e/Å^3) between the dynamic maps (3.7 contours/bond on average) and the static maps (11.5 contours/bond on average). The C-H bonds could not be compared, not lying in the planes drawn for either type of map.

All of the bonds (lone pairs) of different types show an increase in density on going from the dynamic maps to the static maps, as expected. However, in the cation the increase observed in the density is nearly constant for each of the different bond types studied, approximately 0.40 e/Å^3. In the anion the increase seen on going from the dynamic to the static maps was found to be related to the amount of thermal motion that bond was subject to, the greater the thermal motion, the greater the increase observed in the static maps for bonds of that type. In the cation all the bonds, except perhaps N(1)-H(1), are held quite rigidly so it is perhaps not surprising that they might be subject to similar amounts of thermal motion. This, in turn, could explain the nearly equal increases in density observed on the bonds of different types in going from the dynamic to the static maps.

Like the inplane residual maps drawn for the phenyl rings of the anion in [DabcoH][B(C_6H_5)$_4$], the residual maps in the planes of the cation show many peaks and holes of all sizes, shapes and strengths. They are illustrated in Figure 65(a) and (b). Also like the maps of the anion planes, these are the poorest residual cation maps found for any of the

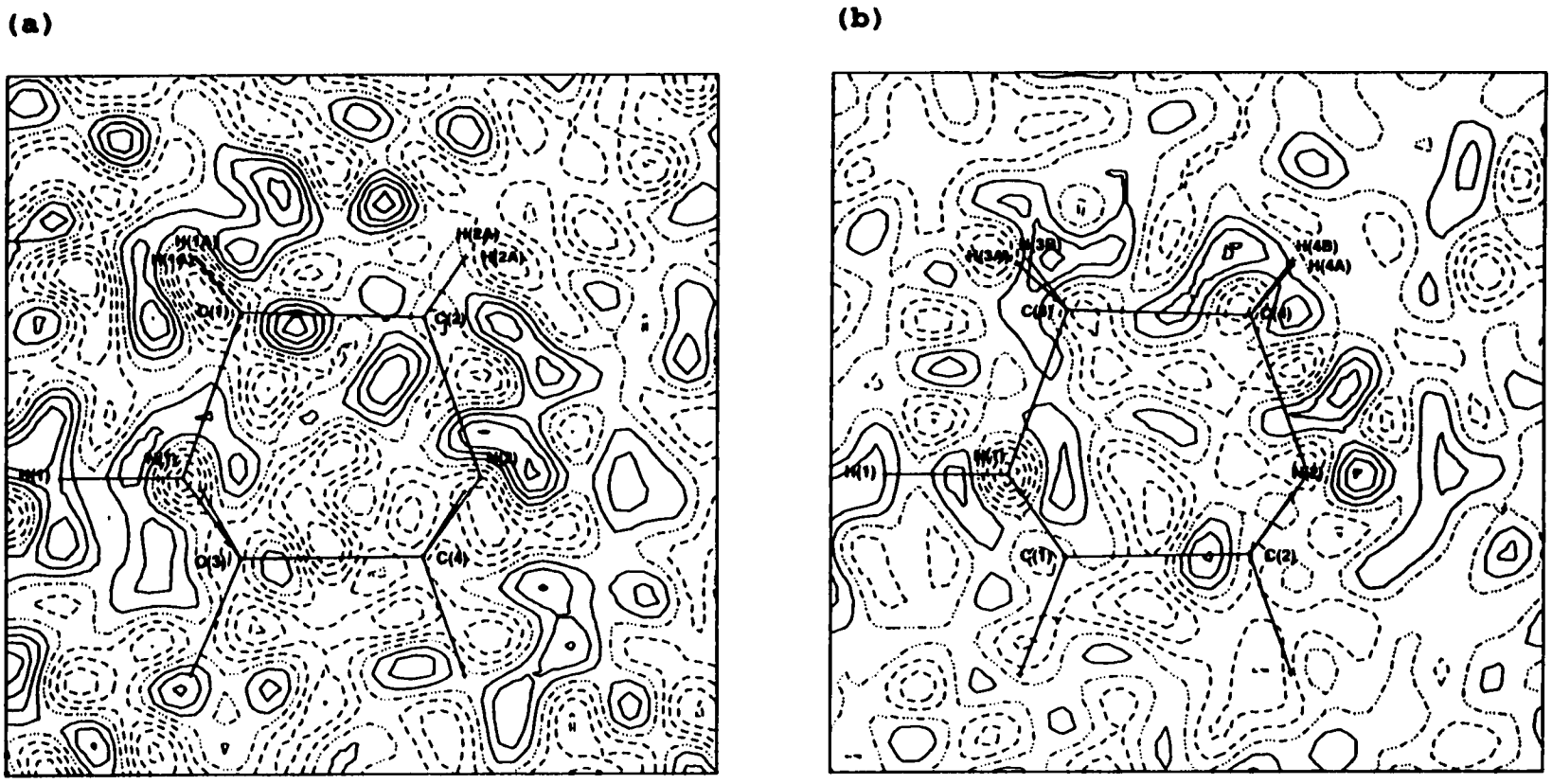

Figure 65. Residual electron density maps drawn in the planes defined by (a) N(1), C(1), C(2) and N(2) and (b) N(1), C(3), C(4) and N(2) of the cation from the structure of [DabcoH][$B(C_6H_5)_4$]. Positive contours are drawn with solid lines, negative contours with dashed lines and the zero level contour with a (dash dot dot dot) pattern. The contour interval is 0.05 $eÅ^{-3}$.

four structures studied. The strongest peaks and holes are of four contours, which corresponds to a residual density of ±0.20 e/Å^3. It is the same residual density observed in the maps of the anion ring planes but it is higher than that found in any other structure and although acceptable it is high for a multipole refinement.

The residual maps in the planes of the DabcoH$^+$ cation also show consistent patterns in the distribution of the residual electron density. Trends were not observed in the residual maps of any of the other structures but they were observed in the residual maps of the anion ring planes in [DabcoH][$B(C_6H_5)_4$]. In the residual maps, holes of differing depths are visible at every cation lying in the plane drawn, whether nitrogen or carbon, particularly N(1) where a hole of four contours in depth is centered. A similar hole is also visible just beyond H(1) and several large holes are located within the cation cage. It appears that the multipole model has placed too much density directly on the heavy atoms of the cation. The same conclusion was reached after examination of the [DabcoH][$B(C_6H_5)_4$] anion ring plane residual maps.

The peaks of positive contours are observed to encircle the holes found at each atomic center, including H(1). These peaks tend to have maxima located where they cut across the bonds of the atoms that they encircle. A strong peak of four contours is also evident at N(2), in the lone pair region. Again, it appears that the model has not placed enough density in these regions, on the multipoles that would be involved in the bonding type interactions. A similar observation was made after studying the residual maps of the [DabcoH][$B(C_6H_5)_4$] anion.

All of the inplane maps from the DabcoH$^+$ structure, whether cation

or anion, are consistent. The overwhelming conclusion that is reached after studying all the maps is that not all the multipoles have been assigned completely correctly. The problems likely arise primarily because of a less than ideal data set but they may also have been complicated by the XD program and its apparent inability to deal with symmetry properly in certain situations.

3.5.2.3. Guanidinium Tetraphenylborate Acetonitrile Solvate

The cation in the structure of guanidinium tetraphenylborate acetonitrile solvate is essentially planar with all atoms lying on general positions. Only a single map has to be drawn to cover the entire cation plane, defined by the three nitrogen atoms, N(1), N(2) and N(3). Before discussing the static map of the guanidinium cation in detail, it must be noted that the anion ring plane maps of this structure were the worst overall of the four compounds studied. The static maps of the anion were characterized by a lack of visible bonding electron density and by an uneven distribution of that density, trends continued in the cation map, which is illustrated in Figure 66.

The distribution of the density on the N-C bonds of the cation in the static map is not even, as was also observed in the corresponding dynamic map. The distribution of the density on these bonds in the two maps is similar, however. In both maps, all three sets of N-C bond contours are very different in appearance. The contours on the N(2)-C(1) bond [10] in the static map are discrete, symmetrical and oval shaped. They are elongated perpendicular to the bond and compacted slightly toward N(2). The contours are well centered on the bond with the maximum lying

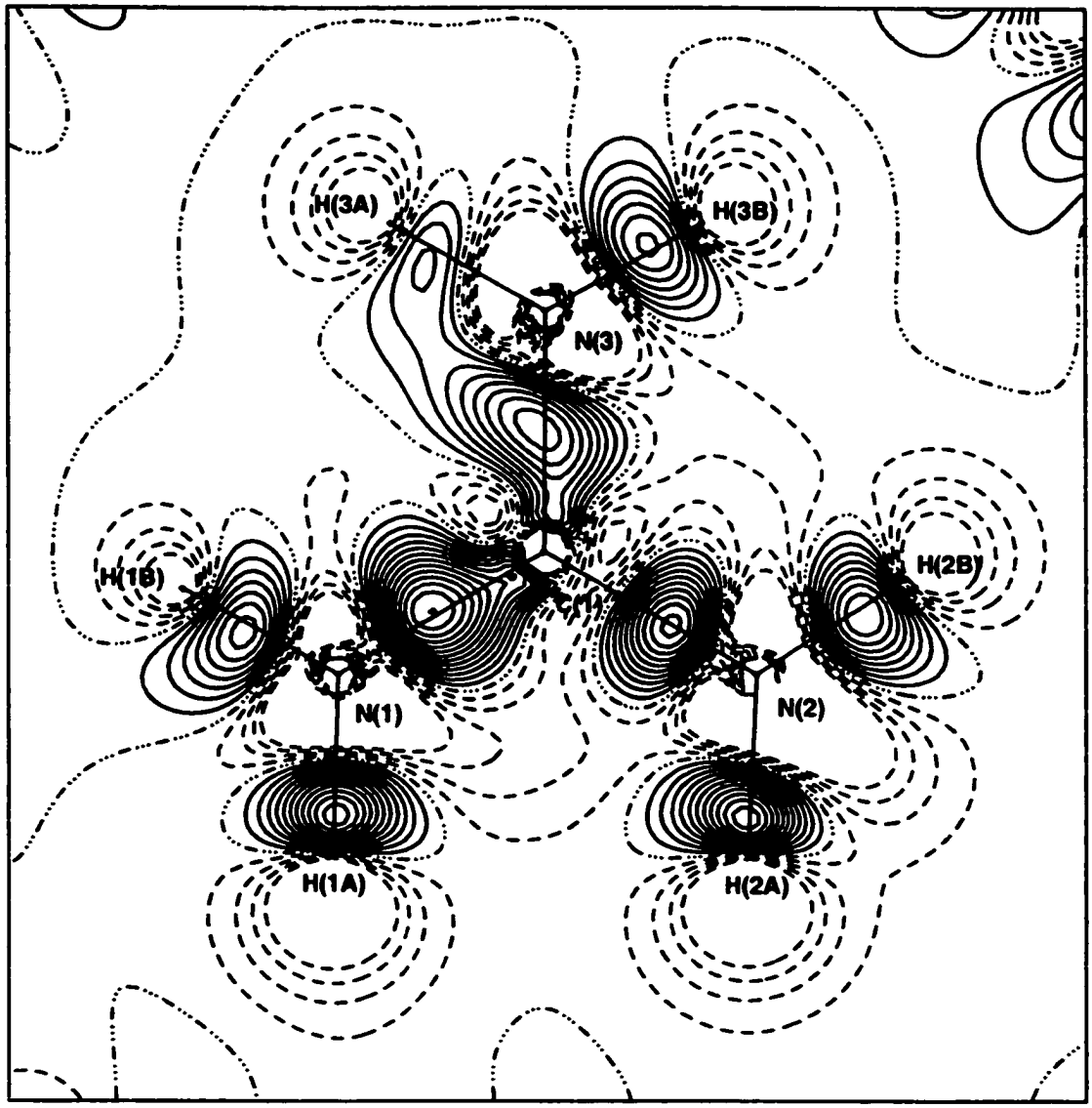

Figure 66. Static deformation density map drawn in the plane defined by N(1), N(2) and N(3) of the cation from the structure of guanidinium tetraphenylborate acetonitrile solvate. Positive contours are drawn with solid lines, negative contours with dashed lines and the zero level contour with a {dash dot dot dot} pattern. The contour interval is 0.05 $eÅ^{-3}$.

slightly closer to N(2) than to C(1). The contours on the N(1)-C(1) bond [13] clearly begin from the carbon atom and end on the bond before reaching N(1). They are elongated perpendicular to the bond but not equally on both sides of the bond, so they are not symmetrical in appearance. The contours are still quite well centered on the bond, with the maximum lying close to the bond midpoint. The contours are drawn out toward C(1) and contracted on the N(1) side. The contours on the N(3)-C(1) bond [8] also clearly originate from C(1) atom. However, they curve off the bond well before reaching N(3) and circle up onto the N(3)-H(3A) bond, sharing two contours with that bond. As a result, the contours on the N(3)-C(1) bond are skewed and are not symmetrical with respect to the bond axis. They still remain quite well centered on the bond, with the maximum close to the bond midpoint. There is no obvious reason that the N-C bond contours should be of such widely disparate appearance.

Small holes, of four negative contours each, are visible in a triangular arrangement around the C(1) atom in the static map of the cation plane. The holes lie in the areas between the N(x)-C(1) bonds. The negative contours at C(1) join with negative contours centered on the nitrogen atoms. Single holes, four contours each in depth, are visible at each nitrogen atom. These holes are broader and more diffuse than those at C(1). They are centered on the atoms and expand into areas between the bonds involving nitrogen. The outermost negative contours are shared between nitrogen atoms, either directly or via the contours at C(1). At N(2), the outermost negative contour is also shared with those on H(2A); the negative contours visible beyond all the other hydrogen atoms are discrete, uniform in shape and four contours in depth. Not unexpectedly,

significant charge depletion is visible over the entire cation.

The distribution of the electron density on the N-H bonds in the static map in the plane of the guanidinium cation is also not as uniform as normally observed, based on the other structures studied. There is less density visible on the N-H bonds (7.8 contours/bond on average) compared to the N-C bonds (10.3 contours/bond on average), a pattern different from that observed in the DabcoH$^+$ cation, where the N-H bond has the greater electron density. Of course the two situations are not completely analogous because of the difference in the N-C bond orders and because of the possible symmetry problems involving the DabcoH$^+$ N(1)-H(1) bond.

As already discussed above, the contours on the N(3)-H(3A) bond are shared with those on the N(3)-C(1) bond so they are irregularly shaped, drawn down off the bond toward the contours of the second bond. They are greatly elongated perpendicular to the bond in only one direction so that they are neither symmetrical or well centered on the bond. The contours on the remaining N-H bonds are relatively regular and uniform in shape. The contours on the bonds with less density appear to be more diffuse than those on the other bonds. The contours are basically oval in shape, elongated perpendicular to the bond and contracted slightly toward the hydrogen atoms. All of the maxima lie much closer to hydrogen than to the nitrogen atom, roughly two thirds of the distance along the bond. On most of the N-H bonds the contours are somewhat unsymmetrical and centered slightly off the bond. This turned out to be a consistent feature of the cation N-H bonds and will be discussed further in connection with the N-H...X [X = N or π(Ph)] hydrogen bonds the cation participates in.

It is possible to compare the densities observed on the bonds of the

guanidinium cation in the corresponding dynamic and static maps. As in all of the other maps examined, all of the cation bonds show an increase on going from the dynamic to the static map. The N(x)-C(1) bonds average 3.0 contours/bond in the dynamic map and 10.3 contours/bond in the static map, an increase of 7.3 contours/bond or 0.37 e/Å^3. The N-H bonds show a similar difference in the bond density between the dynamic and static maps, 0.34 e/Å^3, increasing from 1.0 contour/bond on average in the former to 7.8 contours/bond on average in the latter. These results are somewhat surprising considering the conclusions reached after studying the inplane maps of the anion phenyl rings in the four structures. The difference in density observed on the N-C bonds is slightly larger than that on the N-H bonds, even though the latter bonds would have been expected to be more affected by thermal motion. Thus, the N-H bonds would also have been expected to show a greater increase in density on going from the dynamic to the static map. Still, the two values are relatively equal which is not completely unreasonable, the cation being small and compact. The bonds of different types in the DabcoH$^+$ cation also showed relatively equal density increases on going from the dynamic to the static maps, although in the DabcoH$^+$ structure the average increase was slightly larger, approximately 0.40 e/Å^3. In the inplane phenyl ring maps, the increases observed for the different bonds of the [DabcoH][$B(C_6H_5)_4$] anion were also consistently larger than those observed for the equivalent bonds in the structure of [$C(NH_2)_3$][$B(C_6H_5)_4$]·CH_3CN.

The residual map in the plane of the cation in the structure of [$C(NH_2)_3$][$B(C_6H_5)_4$]·CH_3CN is very flat and featureless. Peaks and holes of a maximum of one single contour are visible, for a very small residual of

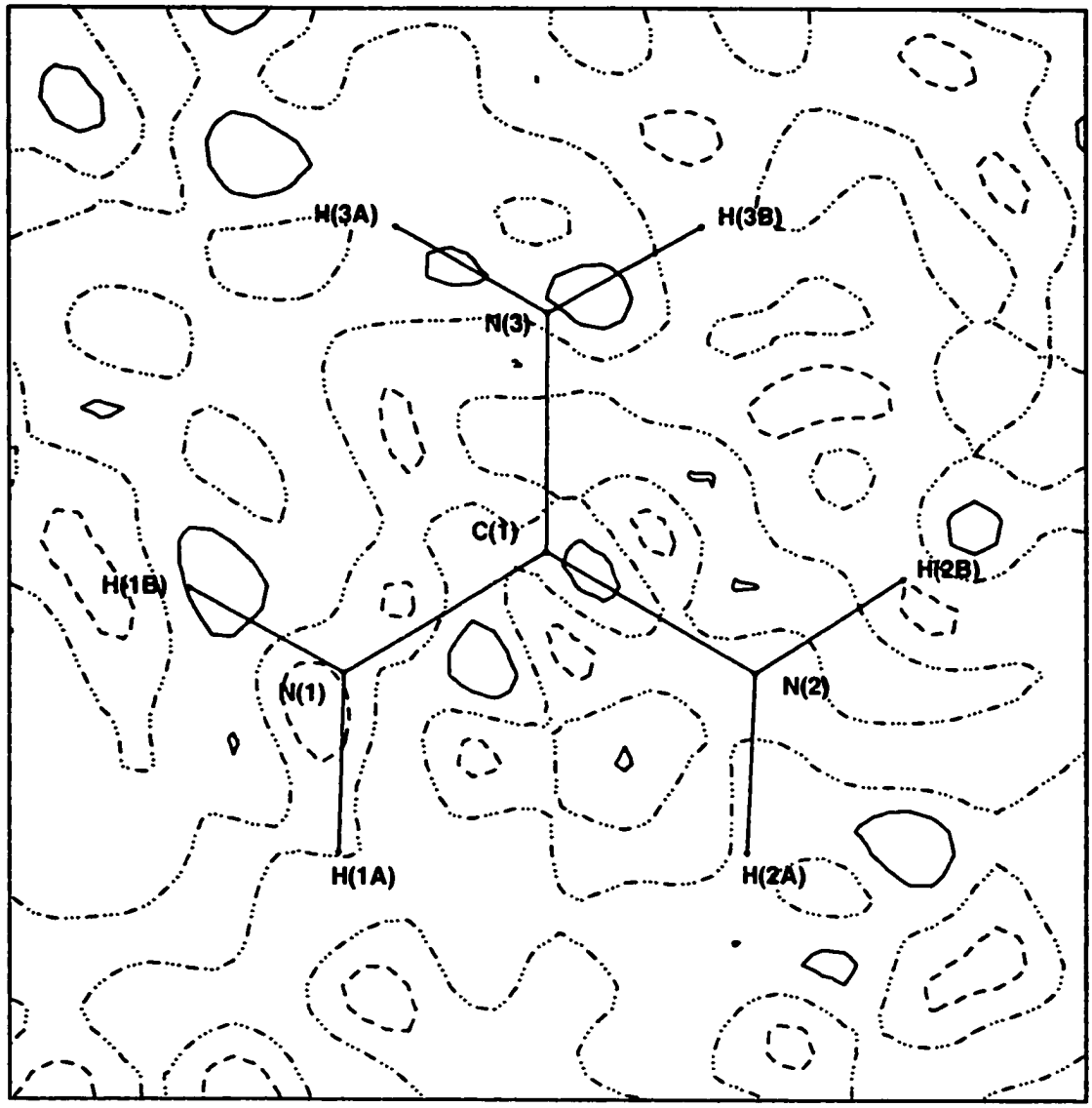

Figure 67. Residual electron density map drawn in the plane defined by N(1), N(2) and N(3) of the cation from the structure of guanidinium tetraphenylborate acetonitrile solvate. Positive contours are drawn with solid lines, negative contours with dashed lines and the zero level contour with a {dash dot dot dot} pattern. The contour interval is 0.05 $eÅ^{-3}$.

only ±0.05 e/Å^3, smaller even than that observed in the anion residual maps from the same structure. There is also no evident pattern in the distribution of the density in the residual map of the cation, which is shown in Figure 67. Peaks of a single contour are visible beyond H(2B) and well beyond H(3B). They are also located on the N(2)-C(1) bond close to C(1), near the midpoint of the N(3)-H(3A) bond, on the N(3)-H(3B) bond close to N(3), on the N(1)-H(1B) bond close to H(1B) and just below the midpoint of the N(1)-C(1) bond. Holes (again of only one negative contour) are even less evident in the residual map of the cation, being observed at N(1) on the N(1)-H(1A) bond and at H(2B). Clearly, no trends are apparent in the peak/hole distribution in the residual map of the cation.

In the structure of $[C(NH_2)_3][B(C_6H_5)_4]\cdot CH_3CN$ the maps of the acetonitrile solvent molecule must also be examined. All three possible static map planes were plotted, defined using the N(4), C(3) and the H(60), H(61) or H(62) methyl hydrogen atoms. One map, that which includes the C(3)-H(61) bond in the plane drawn, is shown in Figure 68. All three of the maps convey basically the same information about the static deformation density distribution in the acetonitrile molecule.

The lone pair of electrons gives rise to contours visible in the static maps of CH_3CN beyond the N(4) atom. The contours (6 or 7 depending on the plane drawn) are large, diffuse ovals which expand away from the molecule and are compressed towards N(4). The contours are centered roughly perpendicular to, and aligned on, the N(4)-C(2)-C(3) backbone of the solvent molecule. The density on the lone pair at N(4) in CH_3CN is less than that observed at N(2) in the static map of the DabcoH$^+$ cation (11 contours). However, this is not surprising since generally the maps

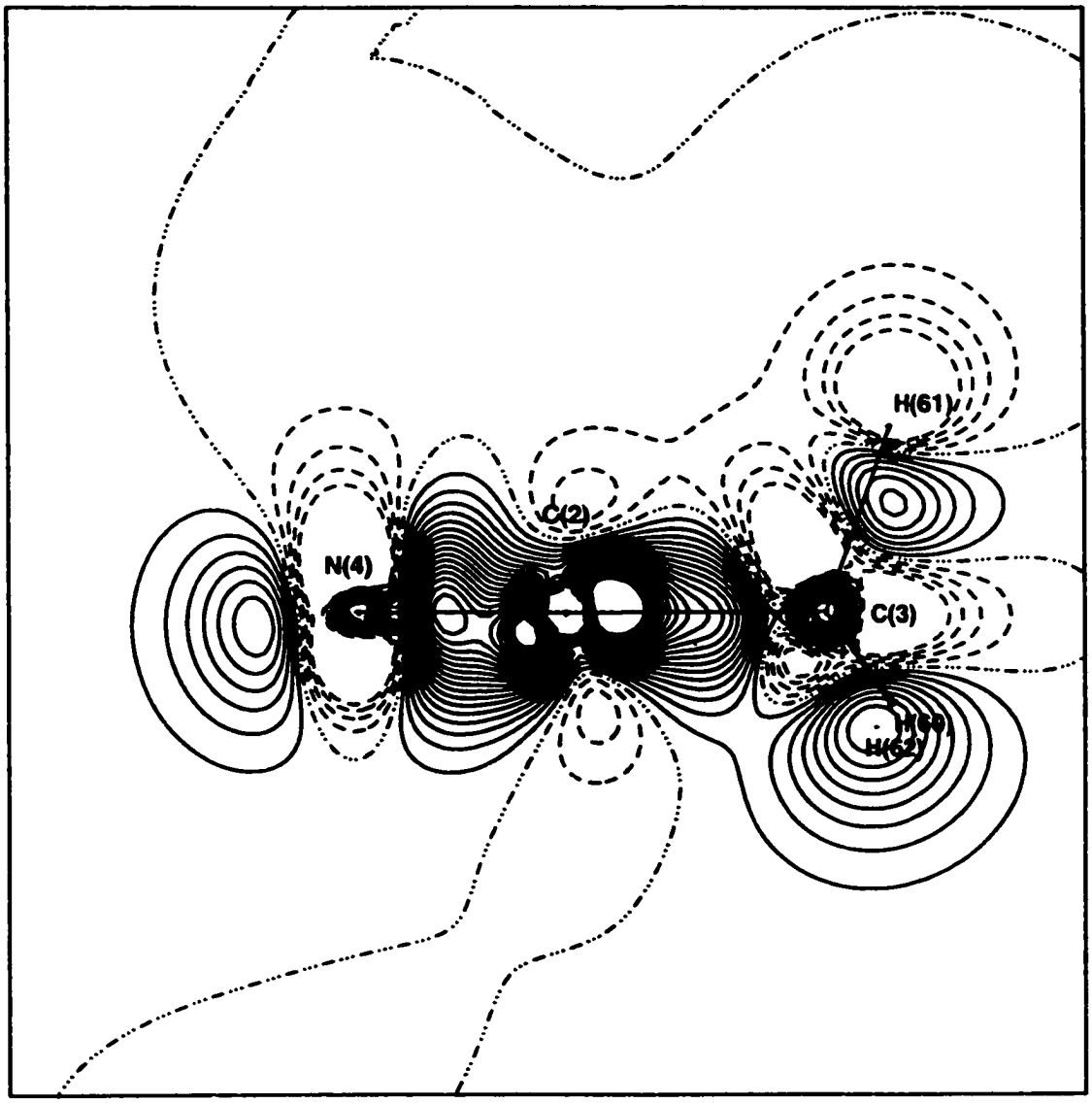

Figure 68. Static deformation density map drawn in the plane defined by N(4), C(3) and H(61) of the solvent from the structure of guanidinium tetraphenylborate acetonitrile solvate. Positive contours are drawn with solid lines, negative contours with dashed lines and the zero level contour with a {dash dot dot dot} pattern. The contour interval is 0.05 $eÅ^{-3}$.

of $[C(NH_2)_3][B(C_6H_5)_4]\cdot CH_3CN$ exhibit lower average densities on the bonds of all types.

The contours on the N(4)-C(2) bond of acetonitrile in the static maps of the solvent are somewhat unusual in appearance, exhibiting a pair of maxima, one close to N(4) [16 contours] and the other even closer to C(2) [20 contours]. The outer 15 contours extend the entire length of the N-C bond while the remainder form the two maxima. The contours are not symmetrical. The maximum at N(4) is well centered on the bond, roughly two fifths of the distance along the bond, while that at C(2) lies slightly off the bond, approximately four fifths of the distance along the N(4)-C(2) bond. In one of the planes drawn, the contours of the N(4)-C(2) bond flow continuously onto the C(2)-C(3) bond; in the other two planes the two sets of contours are discrete/separate. The density observed on the N(4)-C(2) bond in the plane of the acetonitrile molecule is high; even though the inplane maps detail the σ bonding electron density, there is likely still evidence of the triple bond nature of N(4)-C(2) visible in the maps drawn. The two maxima visible on the N(4)-C(2) bond likely arise from incorrect multipole populations assigned to those atoms, particularly C(2). A similar phenomenon was also observed on the C-C bonds of the DabcoH$^+$ cation in the static maps and was attributed to the same problem. In the acetonitrile molecule the multipoles are difficult to refine correctly because there is only a single atom of each type [N(4), C(2) and C(3) all have unique environments] present in the entire structure. This makes them difficult to model well, likely giving rise to the observed double maxima on the N(4)-C(2) bond.

The C(2)-C(3) bond in the static maps of the acetonitrile planes

shows a density of approximately 20 contours, roughly the same as that observed on the N(4)-C(2) bond. The model has placed significant density on the entire solvent molecule compared to the rest of the structure. It also appears that the model has transferred some of the N(4)-C(2) bond density onto the adjoining C(2)-C(3) bond, either legitimately or as a result of the problem in assigning the multipoles. The C(2)-C(3) bond contours clearly begin from C(2), or beyond, and travel along the bond, terminating just before reaching C(3). The contours are well centered on the bond with the maximum lying close to C(2), only approximately one fifth of the distance along the bond. They expand along the bond rather than perpendicular to it. The outermost contours, one or two depending on the plane drawn, extend down to join with density located on the plane in the area where the two out of plane C-H methyl bonds bisect. Again, the contours on the C(2)-C(3) bond suggest a problem with the modelling of the multipoles on these atoms, particularly at C(2).

The C-H bonds of the acetonitrile methyl group, each featured in one of the static maps drawn, all show very little bonding electron density, only 3.3 contours/bond on average. This is very low even for this structure. The small oval shaped contours are elongated somewhat perpendicular to the bonds. They are not well centered on the bonds; all lie to the outside of the bond away from the rest of the molecule. All have maxima that lie closer to hydrogen than to carbon, approximately two thirds of the distance along the bonds. The distribution of the density on the methyl C-H bonds in the static maps is very uneven, with far more density visible on the C(3)-H(61) bond [6 contours] than on the other two bonds [2 contours each]. In fact, in each of the three maps more density

is always observed in the plane defined by the bisector of the two out of plane C-H bonds (in the region between those bonds) than on the inplane C-H bond, 6.3 contours in each plane on average. These are visible as diffuse, circular contours centered just beyond the projection of the of the bisected C-H bonds onto the plane. The static maps agree with the dynamic maps drawn, all of which suggest that the methyl group of the acetonitrile molecule must undergo rotation about its C(3) axis, even in the solid state. This would explain finding significant electron density in the planes between, rather than on, the C-H bonds. The methyl hydrogen atom positions were located in a Fourier difference map and were refined before normalizing the geometry of the group. And, these positions gave sensible interaction geometries for all the CH_3CN hydrogen atoms. It would appear that the positions chosen are reasonable but it is also possible that they are not completely correct.

Holes of negative contours are visible at each atomic center in the static maps of the acetonitrile solvent molecule. All are of four contours in depth. Large circular negative contours are visible centered just beyond H(60), H(61) and H(62). These are sometimes joined with the negative contours centered on the C(2) and/or the C(3) atoms. The hole visible at C(3) is roughly triangularly shaped with the negative contours expanded into the regions between the bonds, away from the bond densities. At C(2) the oval shaped contours are contracted near the bonds and expanded above and below the bond plane. At N(4) a diffuse oval shaped hole is observed in the static maps, well centered on the atom and expanded perpendicular to the N(4)-C(2) bond but lying away from the lone pair density.

Overall, the static maps in the planes of the acetonitrile solvent suggest some problems exist in the modelling of the molecule, both in the assignment of the positions of the methyl hydrogen atoms and in the assignment of the of the multipoles, particularly on the carbon atoms. The second problem was also observed in the [DabcoH] $[B(C_6H_5)_4]$ structure, where the C-C bonds of the cation were of unusual appearance in the static maps. The results appear to substantiate the conclusions reached after studying the anion phenyl ring plane maps, that the maps generated for $NH_4B(C_6H_5)_4$ and $[N(C[NH_2]_2)_2][B(C_6H_5)_4]$ are of somewhat higher overall quality than those of the $[C(NH_2)_3][B(C_6H_5)_4]\cdot CH_3CN$ and [DabcoH] $[B(C_6H_5)_4]$ structures.

A residual map of the acetonitrile solvent molecule was plotted only in the plane defined by N(4), C(3) and H(60), as illustrated in Figure 69. Despite the minor problems visible in the corresponding static maps, the residual map drawn (and the other two planes by assumption) is virtually flat and featureless. There are no peaks or holes visible on any of the bonds, and only a single small peak lies close to H(60). The strongest peaks and holes, of the few observed in the map, are of only one contour, equivalent to ± 0.05 e/Å^3. This residual density is very reasonable, being equal to that observed in the cation residual map and smaller than that observed in the residual maps of the anion for the same structure. The model must fit the experimental data quite well overall. This suggests that the positions of the hydrogen atoms, if not completely correct must at least be reasonable, even considering the possible rotation of the CH_3CN methyl group in the crystal structure.

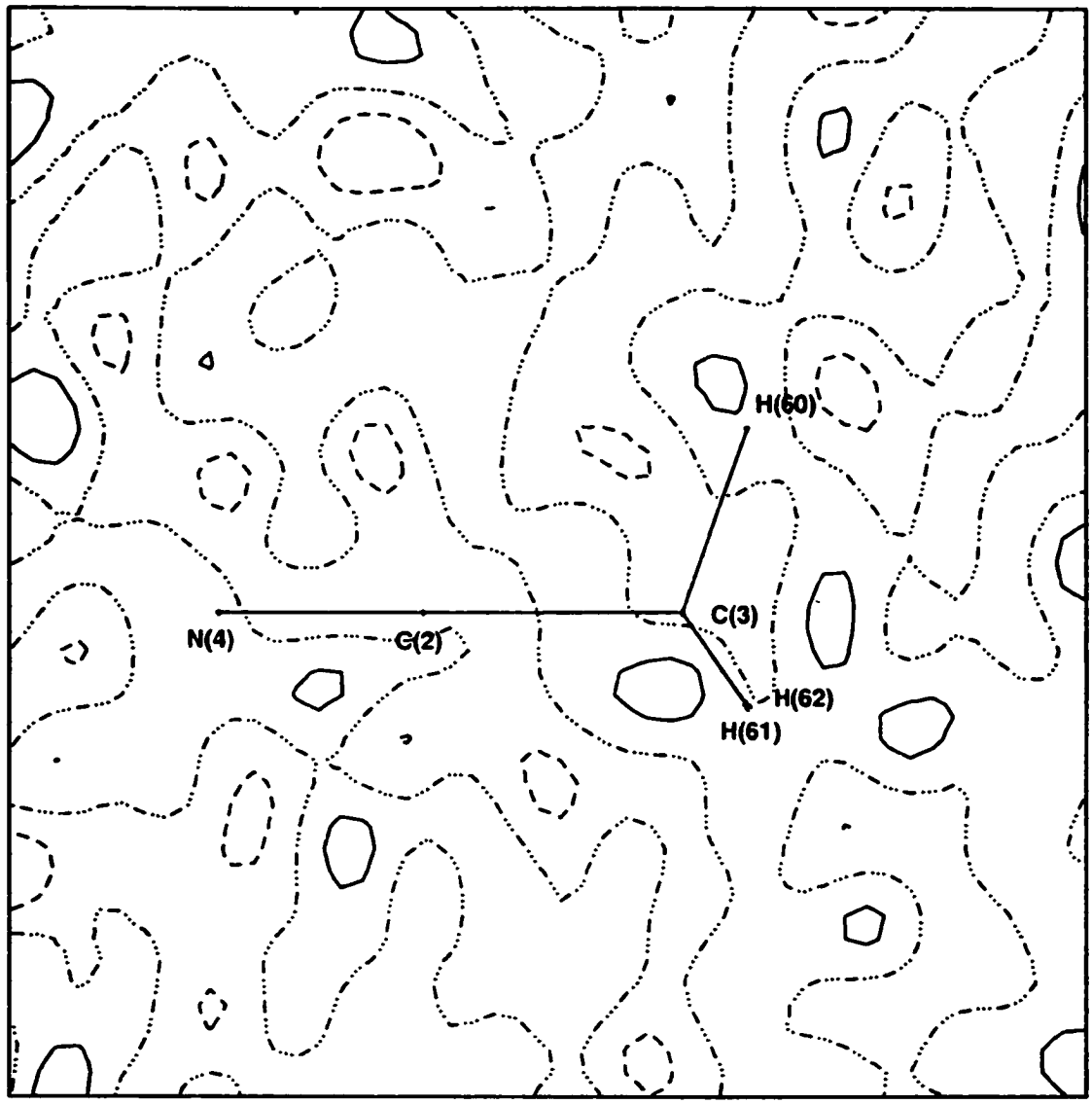

Figure 69. Residual electron density map drawn in the plane defined by N(4), C(3) and H(60) of the solvent from the structure of guanidinium tetraphenylborate acetonitrile solvate. Positive contours are drawn with solid lines, negative contours with dashed lines and the zero level contour with a {dash dot dot dot} pattern. The contour interval is 0.05 $eÅ^{-3}$.

3.5.2.4. Biguanidinium Tetraphenylborate

The cation in the structure of biguanidinium tetraphenylborate lies in completely general positions. It was mapped in three overlapping planes, defined by (a) [N(1), C(1) and N(2)], (b) [N(1), N(2) and N(3)] and (c) [N(1), N(4) and N(5)]; the static maps of these planes are shown in Figure 70 (a),(b),(c). There are two different types of N-C bonds in the biguanidinium cation, the two central bonds, N(1)-C(1) and N(1)-C(2), and four "terminal" bonds, N(2)-C(1), N(3)-C(1), N(4)-C(2) and N(5)-C(2). In the static maps, the distribution of the density on the two central type bonds, N(1)-C(1) [9 contours] and N(1)-C(2) [5 contours] is somewhat uneven, as was also observed in the corresponding dynamic maps. Both sets of contours clearly begin from the carbon atoms and end on the bond before reaching N(1). The contours on each bond are skewed toward each other, so they are not symmetrical. However, the maxima remain well centered on the bonds, lying slightly closer to the carbon than to the nitrogen atoms, near the midpoints of the bonds.

The distribution of the density on the "terminal" N-C bonds is also uneven in both the static and dynamic inplane maps of the cation, ranging from 6 to 11 contours/bond in the former. Only on the N(1)-C(3) bond do the contours extend the entire length of the bond. They are not quite symmetrical on either side of the bond but are well centered on the bond. On the remaining bonds, the contours clearly begin from the nitrogen atoms and end on the bonds before reaching the carbon atoms. The contours on the N(2)-C(1) bond are much fewer and smaller than those on any other of the "terminal" N-C bonds. The contours on all the bonds are somewhat unsymmetrical, being expanded more on one side of the bond than the other.

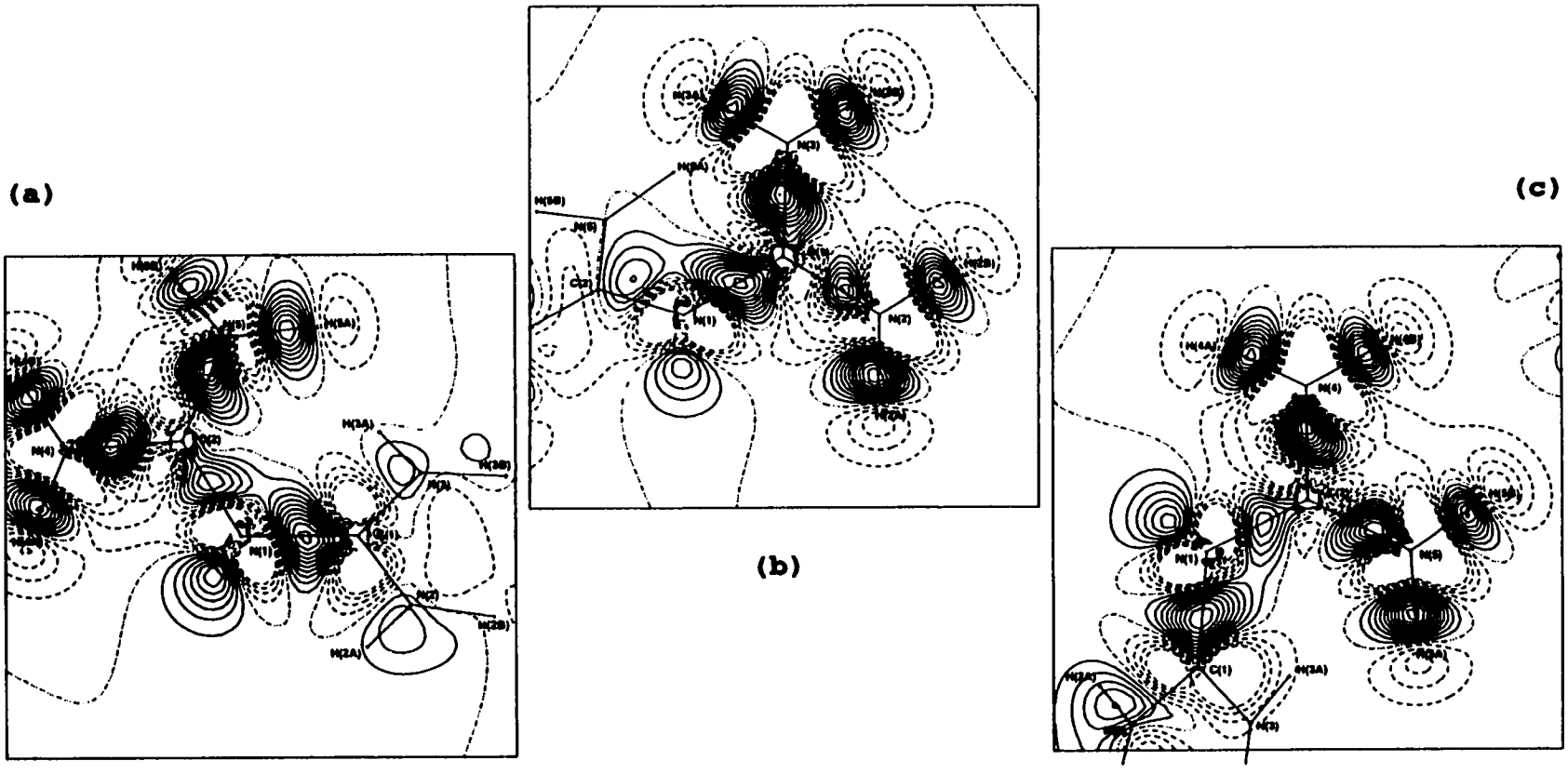

Figure 70. Static deformation density maps drawn in the planes defined by (a) N(1), C(1) and C(2), (b) N(1), N(2) and N(3), and (c) N(1), N(4) and N(5) of the cation in biguanidinium tetraphenylborate. Positive contours are drawn with solid lines, negative contours with dashed lines and the zero level contour with a (dash dot dot dot) pattern. The contour interval is 0.05 eÅ^{-3}.

However, they are all quite well centered on the bonds, with the maxima located closer to the nitrogen atoms than to carbon, approximately three eighths of the distance along the bonds. More contours are visible, on average, on the "terminal" N-C bonds [9.2 contours/bond] than on the central N-C bonds [7.0 contours/bond] of the static maps drawn in the planes of the cation. This is somewhat surprising considering that Lewis structures suggest a higher bond order for the central N-C bonds than for the "terminal" N-C bonds. Still, the inplane maps detail primarily the σ bond density which should be similar for the two types of bonds.

Contours of electron density are also visible in the static maps of the cation just beyond the N(1) atom, indicative of a lone pair of electrons centered on that atom. The contours are quite circular, expanding outward from their origin just beyond N(1). The contours lie on a line bisecting the N(1)-C(1) and N(1)-C(2) bonds on the external face of the cation, which allows formation of the N-H...N hydrogen bonds that hold the cation dimer together. The lone pair at N(1) serves as the acceptor in this interaction, N(4)-H(4A)...N(1). The peak at N(1) is 6 contours in height, a density very similar to that observed for the lone pair at N(4) of the acetonitrile solvent molecule in $[C(NH_2)_3][B(C_6H_5)_4]\cdot CH_3CN$. Density attributable to a lone pair of electrons is not observed at any other nitrogen atom in the $[N(C[NH_2]_2)_2][B(C_6H_5)_4]$ structure. Any potential lone pair density on the "terminal" nitrogen atoms must be accommodated in the π system of the cation.

Holes of four negative contours are observed at each carbon atom in the inplane static maps of the cation. Three holes are centered around each atom, in a triangular arrangement between the bonds. These contours

join with the negative contours visible at each nitrogen center. The larger holes centered on the nitrogen atoms are also four contours in depth and lie principally between the bonds away from the bonding electron density. Again, the negative contours on the nitrogen atoms are shared with those on the carbon atoms and often also with those on adjacent nitrogen atoms.

The static maps of the cation planes show a somewhat uneven distribution of the density on the N-H bonds [9.2 contours/bond on average]. Holes of from 2 to 4 negative contours are also visible beyond every H(N) atom of the cation [3.2 negative contours/atom on average]. Such strong charge depletion was not observed in the static maps of the phenyl ring planes of the anion in $[N(C[NH_2]_2)_2][B(C_6H_5)_4]$, where holes were not normally observed beyond the H(C) atoms. In this structure, the multipoles on the hydrogen atoms, whether H(N) or H(C), appear to have been assigned correctly, with the holes at H(N) arising primarily from the distribution of the cationic charge.

The average density on the N-H bonds of the cation in the static maps is equal to that on the "terminal" N-C bonds. This is again different from the static maps of the DabcoH$^+$ cation, where the N-H bond density was greater, and from the $C(NH_2)_3^+$ cation, where the N-C bond density was greater. It illustrates once more the greater variation observed between the different cations, compared to the similarity of the tetraphenylborate anions, in the four structures studied. The contours on the N-H bonds are all discrete ovals, quite regular and uniform in appearance around the cation, although some variation in the density of the contours is apparent as already mentioned. The bond maxima consistently lie much closer to

hydrogen than to nitrogen, approximately four fifths of the distance along the N-H bonds. The contours are elongated perpendicular to the bonds, often somewhat more on one of the bond than the other, moving the maxima slightly off of the bonds. There is only this minimal evidence visible in the inplane static maps of the cation that the N-H bond contours have been affected by participation in hydrogen bonding type interactions, N-H...X [X = N or π(Ph)]. Every N-H group of the cation is involved in such an interaction, so it might have been expected that the bonds would show differing effects depending on the nature and the strengths of the contacts. This will be discussed in more detail in the section on hydrogen bonding and its effects on the experimental electron density maps of the compounds studied but the visible effects of hydrogen bonding on the inplane static maps of the biguanidinium cation are only slight.

On going from the dynamic to the static maps, all of the bonds in the biguanidinium cation show an increase in the bonding density, as by now expected. The greatest increase is observed for the N-H bonds, 0.37 e/Å^3, which go from a density of 0.094 e/Å^3 in the dynamic maps to 0.46 e/Å^3 in the static maps. The "terminal" N-C bonds increase from 0.15 e/Å^3 (on average) in the dynamic maps to 0.46 e/Å^3 in the static maps, for an average increase in density of 0.31 e/Å^3. The central N-C bonds show a much smaller difference in the bond density between the two map types, 0.22 e/Å^3, 2.5 contours/bond (0.12 e/Å^3) being observed on average in the dynamic maps and 7.0 contours/bond (0.35 e/Å^3) in the static maps. The lone pair at N(1) of the cation also shows a very small increase in density on going from the dynamic maps (0.10 e/Å^3) to the static maps (0.30 e/Å^3), only 0.20 e/Å^3.

In the biguanidinium cation, the bonds subject to the greatest thermal motion show the largest increase in the bonding electron density on comparison of the dynamic and static maps. This same pattern was observed in the maps of all the tetraphenylborate anion ring planes, although not necessarily in the maps of the other cations studied. In the biguanidinium cation the different bond types would be expected to show decreased thermal motion moving inward from the N-H to the "terminal" N-C to the central N-C bonds, with the lone pair on the central N(1) atom being the least affected; the difference in the observed bonding densities between the dynamic and static maps is the exact opposite of this order, as predicted. The results of the $[N(C[NH_2]_2)_2][B(C_6H_5)_4]$ cation analysis, once again suggest that this refinement might be of higher quality than some of the others, for which the cations did not follow the anticipated trends.

It is quite reasonable to compare the results calculated for the biguanidinium cation with the corresponding results for the closely related guanidinium cation. In the $C(NH_2)_3^+$ cation, the N-C bonds, roughly equivalent to the "terminal" N-C bonds of the $N(C[NH_2]_2)_2^+$ cation, were found to increase in density by 0.37 e/Å^3 on going from the dynamic map to the static map, while the N-H bond density increased by 0.34 e/Å^3, on average. The results for the two cations are not dissimilar although the bond orders are reversed. It does appear that the increase in density observed on going from the dynamic to the static map for the N-C bonds of the guanidinium cation is somewhat large for some undetermined reason. The N-H bond density increase in the $C(NH_2)_3^+$ structure seems more reasonable, being close to that observed for the $N(C[NH_2]_2)_2^+$ cation.

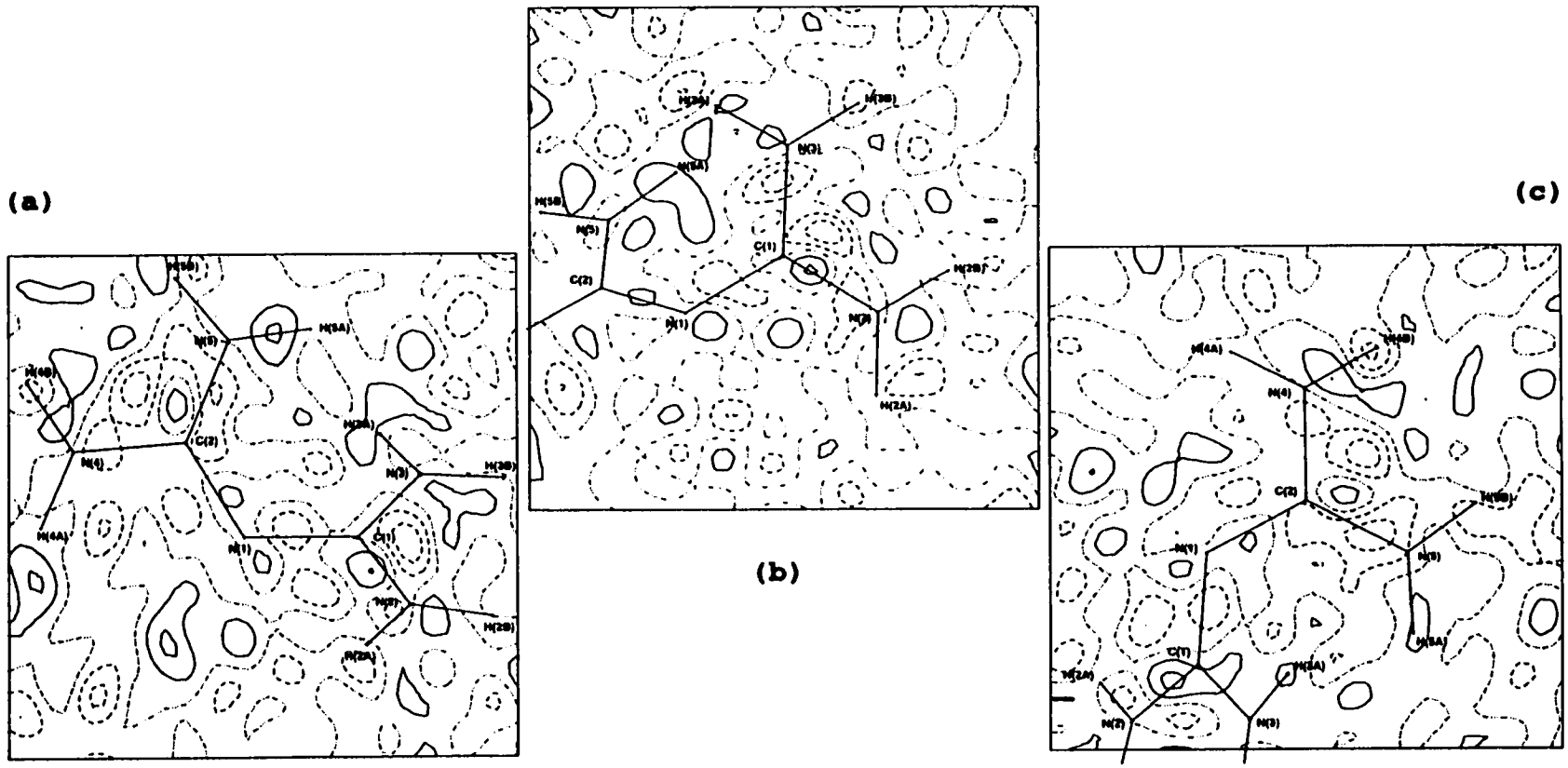

Figure 71. Residual electron density maps drawn in the planes defined by (a) N(1), C(1) and C(2), (b) N(1), N(2) and N(3), and (c) N(1), N(4) and N(5) of the cation in biguanidinium tetraphenylborate. Positive contours are drawn with solid lines, negative contours with dashed lines and the zero level contour with a (dash dot dot dot) pattern. The contour interval is 0.05 eÅ^{-3}.

The residual maps drawn in the cation planes for the structure of biguanidinium tetraphenylborate are very flat and featureless, as expected. They are similar to the residual maps drawn for the phenyl ring planes of the anion from the same structure. The residual maps in the cation planes are shown in Figure 71 (a),(b),(c). The strongest peaks and holes in the cation maps are of only two contours or ±0.10 e/Å^3, a reasonable residual value, the same as that observed in the anion maps. There are very few strong peaks or holes of any note in the residual maps of the cation planes. There is a single peak of two contours visible on the N(2)-C(1) bond close to C(1). There are several holes of two negative contours in depth also visible in the maps. These occur at H(3A) and H(4B), along the N(5)-C(2) bond with the maximum closer to N(5), on the N(3)-C(1) bond closer to N(3), and at one or two other places between the N-C bonds on the cation planes. There is no obvious trend or pattern present in the distribution of the peaks and holes in the residual maps of the biguanidinium cation.

3.5.2.5. Summary

The results obtained after analysis of the inplane maps for the cations of the four compounds investigated experimentally are not as consistent as the results obtained for the corresponding anions. This is not surprising considering that four different cations are involved, while each structure contains the same anion. Also, the cations studied are considerably smaller than the tetraphenylborate anion, making them more difficult to model and refine accurately. This could account for many of the inconsistencies observed.

Overall, the cation of the $[N(C[NH_2]_2)_2][B(C_6H_5)_4]$ structure was judged to have the best maps, being both self-consistent and consistent with the anion results from the same structure. Some unevenness was observed in the density distribution on the bonds of the cation but otherwise the maps were of reasonable quality with well defined features. The question remains as to whether the density differences observed on the bonds of all the cations are artifacts of the refinements or whether they arise as a consequence of the hydrogen bonds in which the cations participate. The likelihood that the latter is true appears to be minimal, except perhaps for the N-H bonds, based on the lack of evidence observed in the inplane static maps of the cations.

Considering the maps of the rings in the tetraphenylborate anions, those of the ammonium and biguanidinium structures were found to be of higher overall quality than those of the DabcoH$^+$ and guanidinium salts. The biguanidinium cation was also judged to have the best maps of the four cations studied. The inplane maps of the cation in $NH_4B(C_6H_5)_4$ suffer from smearing of the electron density around the cation, thought to arise from rotation of the cation in the crystal structure. The guanidinium and DabcoH$^+$ cation maps show problems on the contours of several of the bonds, with double maxima attributed to multipole populations being incorrectly assigned on some atoms. The $C(NH_2)_3^+$ and DabcoH$^+$ maps also did not show the consistent trends expected on going from the dynamic to the static maps. The results suggest that, like the anion maps, the cation maps of $[DabcoH]^+$ and $[C(NH_2)_3]^+$ are of slightly lower overall quality than those of $[N(C[NH_2]_2)_2]^+$, with the maps of the $NH_4B(C_6H_5)_4$ cation left out of the ranking because of the motion problems they exhibit.

3.5.3. Hydrogen Bonds in the Electron Density Maps

3.5.3.1. N-H...N Hydrogen Bonds

The investigation of the N-H...X [X = N or π(Ph)] hydrogen bonds in the four structures studied experimentally located two N-H...N type hydrogen bonds and 14 N-H...π(Ph) type hydrogen bonds. Of these, the N-H...N type interactions would be expected to be the stronger, since the lone pair at nitrogen is a better acceptor than the π electrons of the phenyl ring. The geometric investigation of the N-H...X hydrogen bonds also showed the N-H...N type contacts to have short H(N)...N distances, indicative of stronger interactions compared to the N-H...π(Ph) contacts. In the N-H...π(Ph) interactions the H(N)...π_c ring centroid distance was sometimes found to be shorter than the H(N)...N distances. However, the minimum H(N)...C_{ring} distance was always longer than the H(N)...N distances characterizing the N-H...N hydrogen bonds. Thus, by all criteria the N-H...N type interactions are the strongest studied and their static maps will be investigated first.

Of the two N-H...N hydrogen bonds studied in this work, that in the structure of $[C(NH_2)_3][B(C_6H_5)_4]\cdot CH_3CN$ would be expected to be the stronger based on the H(N)...N distances. The N(1)-H(1B)...N(4) hydrogen bond occurs between the guanidinium cation and the acetonitrile solvent molecule, in which the lone pair of electrons on N(4) acts as the hydrogen bond acceptor. The interaction is characterized by an N(1)...N(4) separation of 2.933(4)Å and an H(1B)...N(4) distance of 2.082Å, both short for this investigation. Somewhat surprisingly, this hydrogen bond is not linear and, in fact, is significantly bent, N(1)-H(1B)...N(4) = 143.4°.

To investigate the N(1)-H(1B)...N(4) hydrogen bond in the structure

of $[C(NH_2)_3][B(C_6H_5)_4]\cdot CH_3CN$ a static map was drawn in the plane defined by N(1) of the cation and N(4) and C(2) of the acetonitrile molecule. This map is shown in Figure 72. The contour interval chosen, 0.05 $eÅ^{-3}$, was the same as that used to plot the inplane static maps of the cations including $C(NH_2)_3^+$. In fact, the plane found to best emphasize the N(1)-H(1B)...N(4) hydrogen bond is not far different from the plane of the guanidinium cation itself. However, the one major difference in the hydrogen bond static map is that the first positive contour was drawn at the +0.015 $eÅ^{-3}$ level, to locate areas of low electron density (possibly related to the hydrogen bonding interaction). This is in contrast to the static map of the cation plane where the first positive contour was drawn at the normal +0.05 $eÅ^{-3}$ level.

The static map of the N(1)-H(1B)...N(4) hydrogen bond clearly shows that the contours of the N(1)-H(1B) bond of the cation are shared with the contours arising from the lone pair on N(4) of the solvent molecule. The outermost contour is common, spanning the area between the two groups. Electron density has been moved into the area between N(1)-H(1B), the hydrogen bond donor, and N(4), the hydrogen bond acceptor. This concentration of electron density in the area between the interacting groups shows that the hydrogen bond must have a significant covalent component. However, significant charge depletion is also observed at H(1B) in the static map, where a hole of four negative contours is visible. The hydrogen bond, therefore, likely has a sizable electrostatic component as well.

The hydrogen bond static map is different from the inplane static map of the guanidinium cation, shown previously in Figure 66, in the

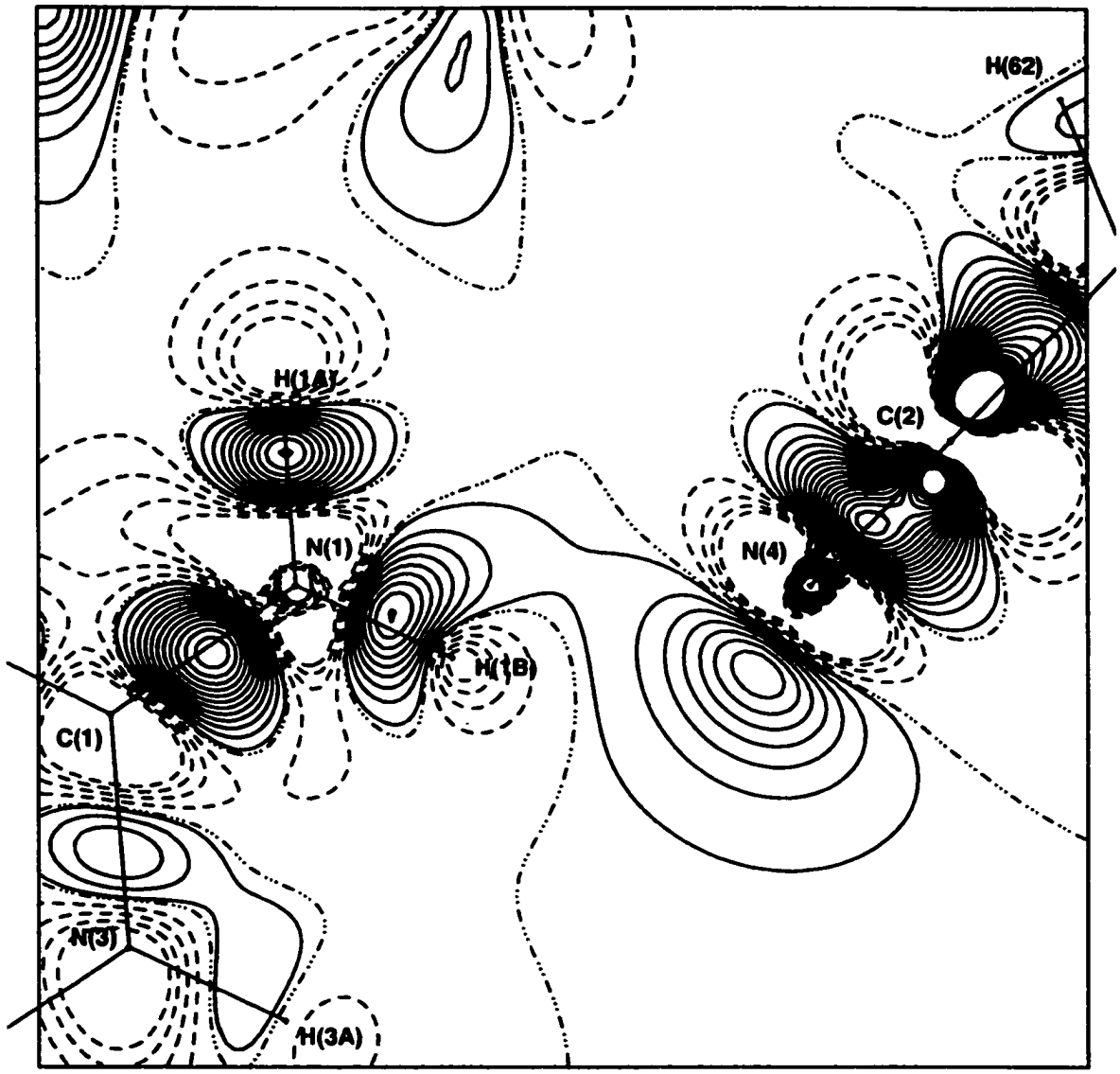

Figure 72. Static deformation density map drawn in the plane defined by N(1), N(4) and C(2) to illustrate the N-H...N (cation/solvent) hydrogen bond from the structure of guanidinium tetraphenylborate acetonitrile solvate. Positive contours are drawn with solid lines, negative contours with dashed lines and the zero level contour with a {dash dot dot dot} pattern. The contour interval is 0.05 $eÅ^{-3}$.

level of the first positive contour drawn (0.015 $e\text{Å}^{-3}$ versus 0.05 $e\text{Å}^{-3}$, respectively). The map in the cation plane shows a slight elongation of the N(1)-H(1B) contours perpendicular to the bond, somewhat more on one side of the bond than the other, toward N(4) of the CH_3CN molecule. However, the contours on the bond remain discrete and a similar slight asymmetry was observed for the contours on several other of the N-H bonds of the cation. When evaluating the maps of the cation plane, the N(1)-H(1B) bond contours did not appear significantly different from the others in the structure and did not give any real indication of participation in the N-H...N hydrogen bond.

However, when the static map is drawn to emphasize the N-H...N hydrogen bond, by adding an extra low level positive contour, the true nature of the interaction becomes apparent. The perturbation of the bonding electron density into the region between the interacting groups (indicative of a significant covalent component to the hydrogen bond) is seen only in the maps of strong hydrogen bonds, as discussed in the introduction. Maps of N-H...X type hydrogen bonds strong enough to contain a visible covalent component contribution are not common in the literature; unfortunately, Mallinson et al.[22] did not include a static deformation density map in their publication on the strong N-H...N type hydrogen bond in a "proton sponge" complex. The best literature examples tend to have been described for strong O-H...O hydrogen bonds, but these are undoubtedly stronger than the present example, even though the maps share many common features. The static map drawn in the plane of the N(1)-H(1B)...N(4) interaction from the $[C(NH_2)_3][B(C_6H_5)_4]\cdot CH_3CN$ structure is an excellent example of a relatively strong hydrogen bond which visibly

exhibits both covalent and electrostatic features. The fact that the hydrogen bond is not linear does not appear to significantly diminish its strength and actually aids in showing the concentration of electron density in the region between the interacting groups, a feature often not so clear in the maps of linear hydrogen bonds. The map of the N(1)-H(1B)...N(4) hydrogen bond is an important contribution to the current volume of static maps detailing hydrogen bonding interactions of different types.

The second N-H...N type hydrogen bond studied in this investigation was located in the structure of biguanidinium tetraphenylborate where it was found to hold the cation dimer together. The N(4)-H(4A) group of one cation serves as the hydrogen bond donor while the lone pair at N(1) of a symmetry related cation (inversion) serves as the hydrogen bond acceptor. The N(4)-H(4A)...N(1) hydrogen bond is characterized by an N(4)...N(1) distance of 3.111(2)Å and an H(4A)...N(1) distance of 2.127Å. Both distances are longer than the corresponding values for the $[N(1)\text{-}H(1B)]_{cation}\cdots[N(4)]_{solvent}$ hydrogen bond of $[C(NH_2)_3][B(C_6H_5)_4]\cdot CH_3CN$ leading to the conclusion that the biguanidinium interaction must be the weaker of the two. However, the hydrogen bond in $[N(C[NH_2]_2)_2][B(C_6H_5)_4]$ is a much more linear interaction, N(4)-H(4A)...N(1) = 175.1°.

The static map drawn to emphasize the N(4)-H(4A)...N(1) hydrogen bond is shown in Figure 73. It is a symmetric map illustrating the central region of the cation dimer. It was plotted in a plane defined by N(1) and N(4) of the original cation and C(2) of the symmetry related cation. As in the static map of the N-H..N hydrogen bond in the structure of $[C(NH_2)_3][B(C_6H_5)_4]\cdot CH_3CN$, the first positive contour was drawn at

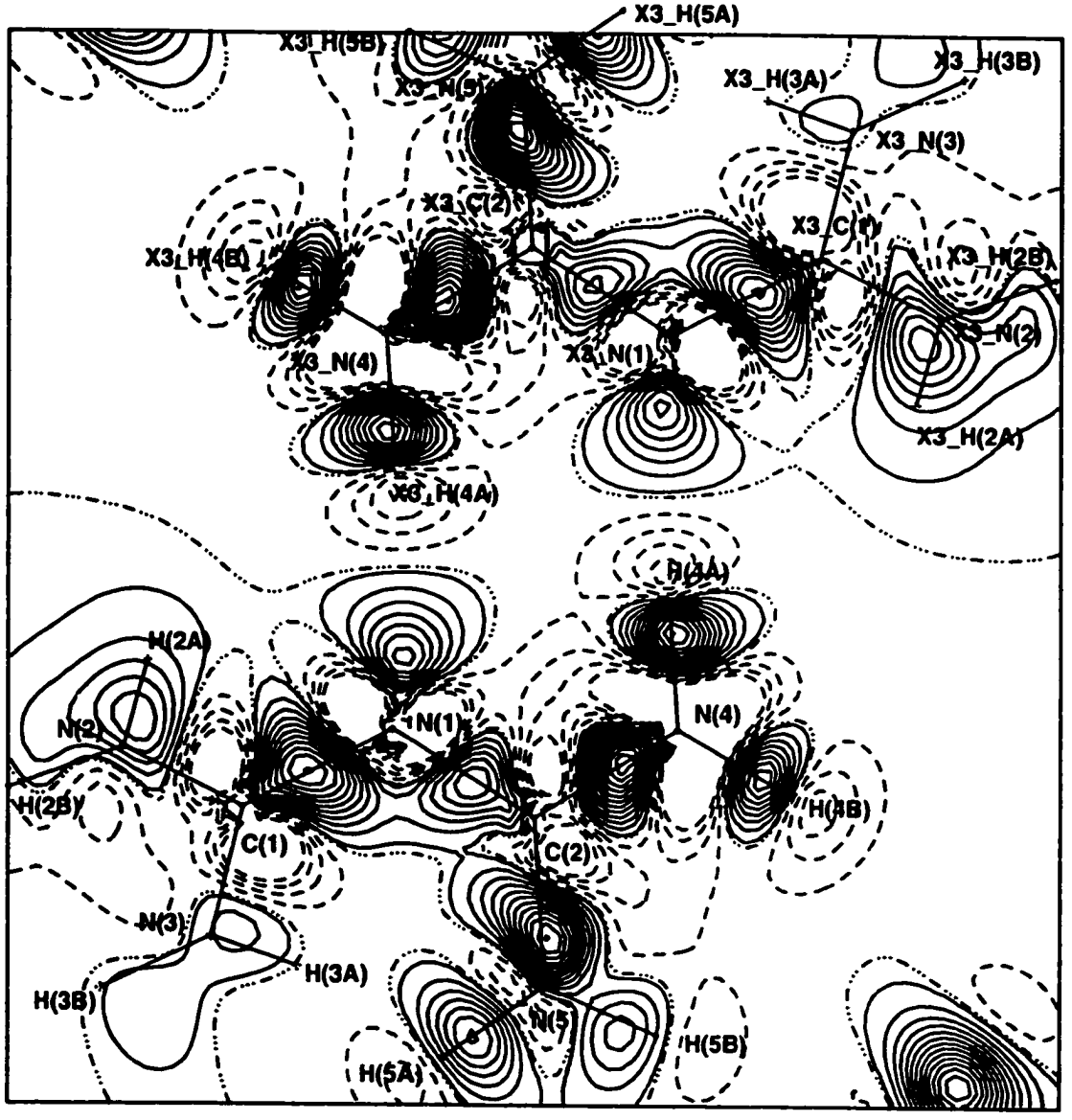

Figure 73. Static deformation density map drawn in the plane defined by N(1), N(4) and C(2)' to illustrate the symmetric pair of N-H...N hydrogen bonds in the cation dimer of biguanidinium tetraphenylborate. Positive contours are drawn with solid lines, negative contours with dashed lines and the zero level contour with a {dash dot dot dot} pattern. The contour interval is 0.05 $eÅ^{-3}$.

+0.015 eÅ^{-3} (the contour interval used was 0.05 eÅ^{-3}) to highlight any low levels of electron density that might have been accumulated in the region between the interacting groups of the hydrogen bond.

The map drawn clearly shows that the density on the N(4)-H(4A) bond is not visibly involved in the hydrogen bonding interaction, in contrast to the guanidinium case. The contours on the N(4)-H(4A) bond are somewhat unsymmetrical, being elongated perpendicular to the bond more in one direction than the other but they remain discrete. They do not curve down toward, or join with, the lone pair density on N(1) of the second cation in any way. Even with the change in the contour mapping, the N(4)-H(4A) bond contours are similar in appearance to those of the original inplane map of this region of the biguanidinium cation. There is no significant indication in the N(4)-H(4A) bond contours of their having been affected by participation in the N-H...N hydrogen bond.

A large diffuse hole, four contours in depth, is visible beyond H(4A) in the region between N(4)-H(4A) and the lone pair density on N(1) in the hydrogen bond static map. This indicates a significant electrostatic component in the N(4)-H(4A)...N(1) hydrogen bond of biguanidinium tetraphenylborate, which is typical of a normal to weaker strength hydrogen bond. It is more difficult, however, to discern whether there is a covalent component to this hydrogen bond which makes itself evident in the static map drawn. Because the hydrogen bond is essentially linear, the lone pair density at N(1) naturally lies on the interaction line. There is no need for it to be perturbed into a new area for it to lie between the two interacting groups (unlike the guanidinium case), if a covalent contribution is involved in this hydrogen bond. It does appear that the

contours arising from the lone pair at N(1), although regularly shaped, are somewhat diffuse, being expanded toward H(4A) of the second cation. This likely indicates that there is some covalent character in the N(4)-H(4A)...N(1) hydrogen bond, however, it also appears that it must be relatively slight. The biguanidinium tetraphenylborate maps were judged to be the best of the four compounds studied experimentally so the small effects visible in this map are likely to be true features and not artifacts of the refinement.

The N(4)-H(4A)...N(1) hydrogen bond static map in the structure of $[N(C[NH_2]_2)_2][B(C_6H_5)_4]$ is more like the maps expected for "normal" strength hydrogen bonds from the literature survey. Effects observed in the map and attributed to the covalency of the interaction are minor at best. The N(4)-H(4A)...N(1) hydrogen bond is likely predominantly electrostatic in nature with a small covalent component. This is in contrast to the N(1)-H(1B)...N(4) hydrogen bond in the $[C(NH_2)_3][B(C_6H_5)_4]\cdot CH_3CN$ structure which was found to have a more significant covalent component, with clearly visible features in the static map drawn.

3.5.3.2. X-H...π(Ph) Hydrogen Bonds [X = N or C]

Although significant features attributable to the N(1)-H(1B)...N(4) hydrogen bond were observed in the $[C(NH_2)_3][B(C_6H_5)_4]\cdot CH_3CN$ static maps, only small effects were observed in the static maps drawn to study the N(4)-H(4B)...N(1) hydrogen bond in the $[N(C[NH_2]_2)_2][B(C_6H_5)_4]$ structure. If the stronger N-H...N hydrogen bonds can have such minimal visible effects on the static maps, what influence would the normally weaker X-H...π(Ph) [X = N or C] hydrogen bonds be expected to show? If minor

changes do occur in the maps because of the formation of such contacts, would they be consistent and identifiable? Or, would they remain mixed with background noise and artifacts of the refinement process, such that they could not be singled out as characteristic features of the X-H...π(Ph) type interactions? In an attempt to answer these questions, it seemed most reasonable to begin with the structure found to have the best inplane maps for both the cation and the anion, biguanidinium tetraphenylborate. If characteristic features were identified in these maps, the maps of the other structures could then be compared to see if they showed the same effects. Overall, the same changes should be consistently observed in all the static maps where such contacts occur, if they truly represent characteristics of X-H...π(Ph) interactions.

Two types of maps were plotted to investigate the effect of the X-H...π(Ph) [X = N or C] interactions on the electron density distributions of the phenyl rings of the $B(C_6H_5)_4^-$ anions in the four experimental structures. In the first set of static maps, perpendicular cuts were made through opposing C-C bonds of the phenyl ring planes. Three cuts were made through each ring (if it occupied general positions) so that the contours of every C-C ring bond would be (approximately) bisected. In the second set of maps drawn, the cuts were made vertically through a pair of opposing ring carbon atoms. Again, three different cuts were required to completely define each phenyl ring occupying totally general positions. Every unique phenyl ring and its X-H...π(Ph) interactions, in every anion, in the four structures studied were analyzed from the complete set of static maps of both types plotted. The cuts made through the ring bonds will be discussed first (as a group) and then the cuts made through the

ring atoms will be discussed.

The **cuts made through the opposing C-C bonds of the phenyl rings** emphasize the contours on the C-C bonds themselves, exposed perpendicular to the plane of the ring. The C-C bond contours would be expected to show changes if the formation of X-H...π(Ph) interactions to that ring alters the electron density sufficiently to be observed. Every phenyl ring involved in this investigation forms at least one, and normally more, X-H...π(Ph) interaction [X = N or C] of some type. After carefully studying all the cuts made through all of the phenyl rings in the four structures, it became apparent that certain, small features were consistently observed in the static maps plotted.

Overall, the most commonly observed, and possibly characteristic, feature indicative of the presence of X-H...π(Ph) interaction(s) in the static maps made of cuts through the phenyl ring bonds is an expansion/ diffuseness of the outer contour(s) on the C-C ring bonds. In cases where one or more interaction(s) are made to one phenyl ring, whether N-H or C-H type, the contours on all the C-C bonds of that ring will show roughly the same effect. The diffuseness occurs because of the interaction between the donor X-H group and the acceptor, the π electron density of the phenyl ring, which is slightly perturbed toward the donor. In the maps, it is visible as an expansion/elongation of the outer C-C bond contours, perpendicular to the ring plane. As mentioned, the effect is normally relatively equal around the ring and not just centered on the those atoms or bonds of the ring closest to the donor group. The diffuseness is also observed both above and below the ring plane, regardless of the face(s) of the ring to which the interaction(s) is actually made. However, as will

be discussed subsequently, it is often difficult to even identify this feature in the maps of a pair of individual ring bonds. It is also difficult to judge the magnitude of the effect and whether it is correlated with the number and strengths of the interaction(s) occurring. It was only after careful analysis of all the experimental results that it became apparent that a slight expansion of the outer C-C bond contours was consistently observed in the cuts through the phenyl ring planes involved in X-H...π(Ph) type interactions.

The second feature characteristically visible in the static maps drawn to investigate N-H...π(Ph) hydrogen bonds, via cuts through the phenyl ring planes, is that the N-H bonds involved as the donor group in such contacts show distortions of their electron density in the direction of the interaction. The perturbation of the N-H bond contours is usually slight and is not always visible in all of the planes drawn to illustrate a particular interaction but it is observed for almost all of the N-H bonds studied. The contours are normally elongated somewhat perpendicular to the bond, more on one side of the bond than the other, and these contours are drawn very slightly towards the electron density of the phenyl ring acceptor. Slight distortions of the N-H bond contours were also sometimes observed in the inplane maps of the cations themselves, but this pattern was not consistent enough for this to be judged as a characteristic feature of the N-H...π(Ph) interaction. With the addition of an extra low level contour (+0.015 e$\AA^{-3}$) it becomes apparent that a slight perturbation of the N-H bond density is almost always visible in the static maps cut through the phenyl ring bonds to investigate the X-H...π(Ph) interactions. Again, since the observed distortion is only

very slight, the question arises as to whether this is a true feature of the N-H...π(Ph) interactions or if it only arises because of the imperfect nature of the experimental data and the refinement process. However, since the N-H bond contours show similar, if small, distortions in almost every case, in every structure studied, it appears to be a true, characteristic feature of the N-H...π(Ph) interaction.

Both of these features, if truly representative of N-H...π(Ph) interactions, indicate a covalent component (although still likely very small) to even these weak hydrogen bonds. There is visible evidence of the electron density on both the donor (N-H bonds) and the acceptor (phenyl ring π electron density) being slightly perturbed into the area between the interacting groups; an actual sharing of the electron density is characteristic of a covalent bond. This is in contrast to the much larger electrostatic contribution made to these interactions, evidence of which is also always observed in the static maps drawn. At every H(N) atom involved in an N-H...π(Ph) interaction, a significant depletion of charge is always visible in the static maps drawn. This takes the form of a hole of considerable depth, normally three or four negative contours, visible just beyond every H(N) atom toward the density of the interacting ring. It is observed in every N-H...π(Ph) interaction examined and is suggestive of a sizeable electrostatic component to these hydrogen bonds as expected.

It is also interesting to contrast the N-H and C-H type X-H...π(Ph) interactions evident in the different maps. While every N-H group in the four structures studied is involved in such an interaction, only a small number of the potential C-H donor groups (whether cation, anion or solvent in origin) participate in such contacts. In the static maps of the cuts

made through the phenyl C-C ring bonds, the C-H type interactions observed are almost invariably of the hydrogen bond type rather than H...H type or intermediate type contacts. The presence of either N-H or C-H type X-H...π(Ph) hydrogen bonds appears to give rise to some diffuseness of the C-C bond contours in the static maps of the interacting rings. However, only the N-H bonds consistently show evidence of the contours/electron density having been perturbed by the interaction. The contours on the interacting C-H bonds normally remain relatively uniform and symmetrical in appearance in spite of their participation in the C-H...π(Ph) hydrogen bonds. They show no evidence of having been changed by their interaction with the ring.

This observation is of interest for two reasons. First, it suggests that the C-H...π(Ph) type interactions do not have as large a covalent component contribution as their N-H counterparts. Rather, they are more completely electrostatic in nature, with possibly a very small covalent component. Charge depletion is again always visible in the static maps at every H(C) atom involved in such an interaction. It is normally less than that observed for the somewhat stronger H(N) interactions (charge is also important) but still it is always observed, usually as a hole of roughly two contours in depth just beyond each H(C) atom. In the second place, since distortions of the C-H bond contours are not normally observed in the static maps, even in the presence of C-H...π(Ph) interactions, it supports the idea that the observed perturbations of the N-H bond contours are legitimate features of the stronger and more covalent N-H...π(Ph) interactions.

Having summarized the overall conclusions reached after careful

analysis of all the C-H bond cuts made through the phenyl rings, it is instructive to show how they were actually reached by discussing some of the individual maps from the different structures. As mentioned earlier, the maps were considered in the order $[N(C[NH_2]_2)_2][B(C_6H_5)_4]$, $NH_4B(C_6H_5)_4$, $[DabcoH][B(C_6H_5)_4]$ and $[C(NH_2)_3][B(C_6H_5)_4]\cdot CH_3CN$, based on the perceived quality of their inplane static maps (both cation and anion).

In the structure of biguanidinium tetraphenylborate, the maps drawn of the anion phenyl ring planes were ranked in order from ring 1 (best) to ring 2 (worst) with rings 3 and 4 of intermediate quality. This ranking was based primarily on the observed C-C bond density in the plane of the anion rings (more density being favoured) and the evenness of the distribution of that density around the rings. The same relative patterns of electron density distribution are consistently observed in the static maps of cuts made through the C-C bonds of the anion phenyl rings as well. The four different structures show different average overall densities on the C-C bonds in the cuts made vertically through the rings, with the $[DabcoH][B(C_6H_5)_4]$ (12.0 contours/bond), $NH_4B(C_6H_5)_4$ (11.9 contours/bond) and $[N(C[NH_2]_2)_2][B(C_6H_5)_4]$ (11.7 contours/bond) structures showing relatively equal densities and the $[C(NH_2)_3][B(C_6H_5)_4]\cdot CH_3CN$ structure averaging significantly less (9.6 contours/bond) for some reason. These values match well with the average C-C bond densities observed in the corresponding inplane static maps of the anions in the four experimental structures, 5.9, 5.7, 5.5 and 4.3 contours/bond, respectively. The same general order is followed in both types of static maps, with the number of contours observed on the C-C bonds of the inplane maps consistently being roughly one half that observed on the C-C bonds of the perpendicular

cuts, as expected since the contour interval is twice as large for the inplane maps.

Within a given structure, the different rings also show different average C-C bond densities, in both the inplane and perpendicular cuts of the anion phenyl rings. For example, in $[N(C[NH_2]_2)_2][B(C_6H_5)_4]$ the following average numbers of C-C bond contours were observed for ring 1 (6.5/13.3), ring 4 (5.3/11.5), ring 3 (5.3/11.3) and ring 2 (4.7/10.7) for the inplane and perpendicular cuts, respectively. The same general order is followed in both types of static maps, and again, the perpendicular cuts through the phenyl ring bonds show roughly double the density evident in the inplane maps on the C-C bonds. The same pattern is observed in all four structures, with the inplane static maps of the phenyl rings showing the same order as the cuts made through the phenyl ring bonds, as far as the average density on the C-C ring bonds is concerned.

Within each individual ring of each structure there is also some variation in the density/number of contours observed on the C-C bonds. Generally, on the better quality rings of the better quality structures this variation tends to be slight. For example, it is small in all the rings of $[N(C[NH_2]_2)_2][B(C_6H_5)_4]$ but larger in the perpendicular cuts of the C-C bonds in the anion rings of $[C(NH_2)_3][B(C_6H_5)_4]\cdot CH_3CN$. Previously, after analysis of the inplane static maps of the anions, it had been found that there was no obvious correlation between the density visible on the individual C-C bonds of the ring and the X-H...π(Ph) [X = N or C] interactions made to that ring. This also appears to be true of the density observed on the C-C bonds in the perpendicular cuts; the individual bond densities do not appear to be directly influenced by the interactions made

to the ring. The variation in the density observed on the C-C bonds around the anion rings must arise for some other reason.

In the structure of biguanidinium tetraphenylborate, ring 1 of the anion was judged to have the best maps and thus will be discussed first. In the cuts made through the ring 1 bonds [the C(12)-C(13)/C(15)-C(16) cut is shown in Figure 74], two cations are visible, one above and one below the ring plane. Three interactions of importance are made to this ring, all of the N-H...π(Ph) type. The first cation, that lying above the ring plane as drawn, forms two N-H...π(Ph) interactions with the ring, in the previously described "pincer" type arrangement. By geometry, the N(5)-H(5B)...ring 1 interaction is classified as a centroid type hydrogen bond with the closest approach made to the C(15)-C(16) ring bond, while the N(4)-H(4B)...ring 1 contact is classified as an edge type hydrogen bond, interacting primarily with the C(15)-C(16) bond of the ring but also with possible involvement of the H(15) and H(16) ring atoms. Below the ring, the second cation engages in a single atom type hydrogen bond, N(2)-H(2B)...ring 1, to C(13) of the anion ring. However, all the N-H...π(Ph) hydrogen bonds involving ring 1 in $[N(C[NH_2]_2)_2][B(C_6H_5)_4]$ are fairly weak, judging from their relatively long H(N)...C_{ring} minimum distances.

In the cut illustrated in Figure 74, the N(5)-H(5B) bond of the first cation lies substantially in the plane drawn, centered above and approximately perpendicular to the ring plane. The N(5)-H(5B) bond contours are elongated somewhat more on one side of the bond than the other and are drawn very slightly down towards the C(12)-C(13) bond contours of the ring. This effect is very slight but it is noticeable. A

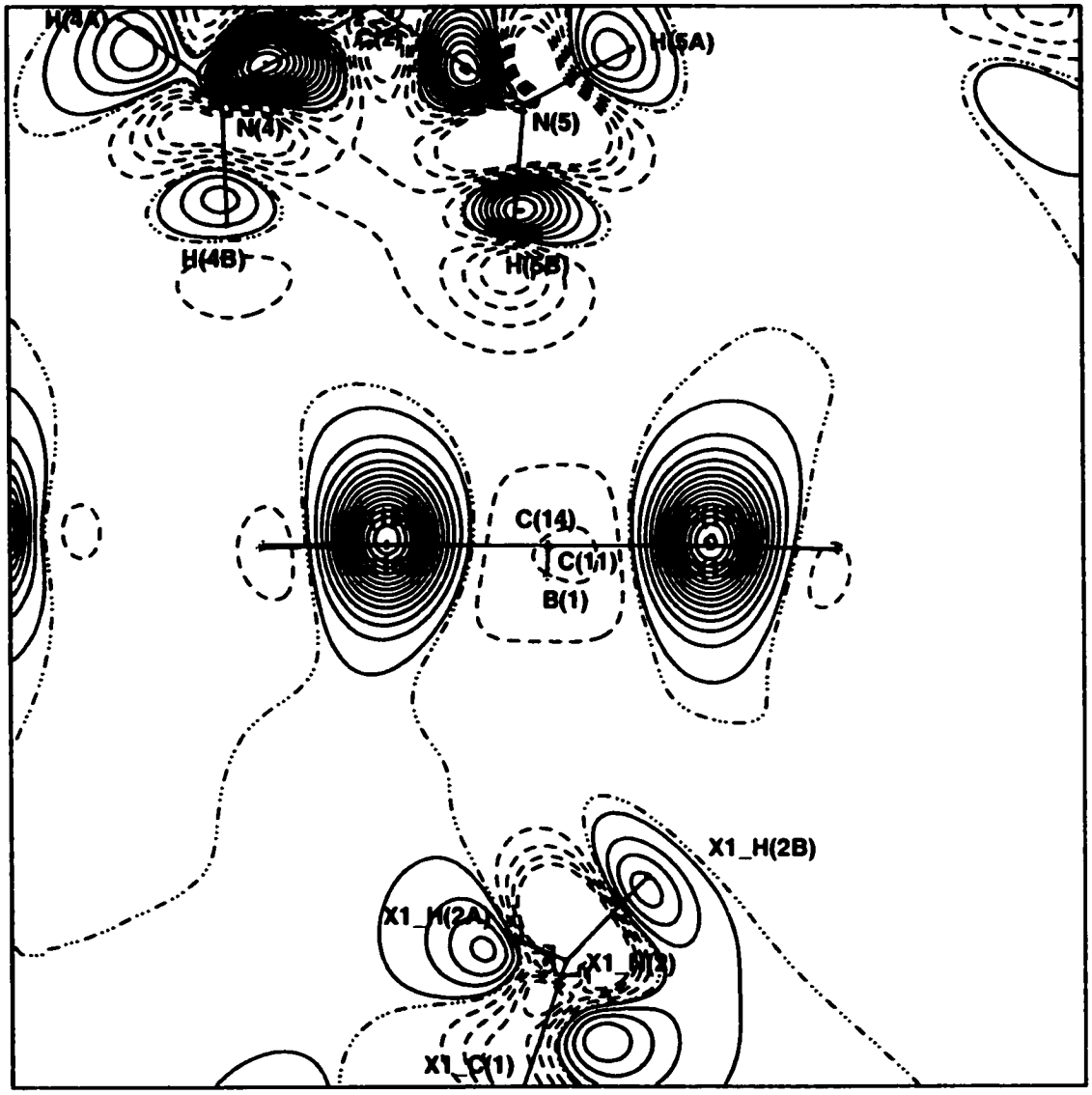

Figure 74. Static deformation density map drawn in the perpendicular plane bisecting the C(12)-C(13) and C(15)-C(16) bonds of the anion phenyl ring #1 in the structure of biguanidinium tetraphenylborate. Positive contours are drawn with solid lines, negative contours with dashed lines and the zero level contour with a {dash dot dot dot} pattern. The contour interval is 0.05 $eÅ^{-3}$. The outline of the remainder of the tetraphenylborate anion has been omitted for clarity.

considerable charge depletion is also observed at H(5B), where a hole of four negative contours is found between the hydrogen atom and the ring. This substantiates the overall conclusions reached previously quite well; the interaction is composed of a minor covalent component [slight perturbation of the N-H bond contours] and a major electrostatic component [significant charge depletion at H(5B)].

This static map also shows the best view of the N(4)-H(4B)...ring 1 hydrogen bond of any of the cuts drawn through the ring 1 bonds. The N(4)-H(4B) bond also lies perpendicular to the phenyl ring plane but outside the confines of the ring past the C(15)-C(16) bond. Although the map shows only three contours on the N(4)-H(4B) bond, meaning that it lies almost completely out of the plane drawn, there is no visible evidence of interaction with the ring in this cut (or any of the cuts plotted). Judging from the maps drawn, this interaction is likely weaker than the first and almost entirely electrostatic in nature. Charge depletion is observed at H(4B) in some maps, as expected for an electrostatic based interaction. The N(2)-H(2B)...ring 1 hydrogen bond, although visible in Figure 74, is best viewed in the static map cut through the C(11)-C(16) and C(13)-C(14) bonds of the ring. In that view, the N(2)-H(2B) bond contours are clearly drawn slightly upward off of the bond in the direction of ring 1, although they remain discrete. This is visible evidence that there is a covalent component to the N(2)-H(2B)...ring 1 interaction as well.

The C-C bond contours illustrated in the map shown in Figure 74 are typical of those on the ring 1 bonds in general. The contours are tight and compact on both bonds. The outer contour on each bond shows a very

slight diffuseness and an elongation perpendicular to the ring plane. It is relatively equal on both bonds and also approximately equal above and below the ring plane, although in this case contacts are actually made to each ring face so this observation is not unexpected. In fact, all of the C-C bonds of ring 1 show a similar, very slight diffuseness of the outer contours, attributed to the three N-H...π(Ph) hydrogen bonds in which the ring participates. The C-C bonds physically closest to the interacting N-H groups show no obvious differences in the appearance of their contours relative to the rest of the ring. The expansion observed on the outer C-C bond contours is very slight in this ring because of the high density on the bonds themselves. When the bond density is larger, it appears to be more difficult to expand the outer contours away from the bond. The visible effect arising from the interaction(s) is thus smaller in the static maps of cuts made through denser C-C bonds. The slight elongation observed on the C-C bond contours of this ring again suggests a small covalent component in at least some of the hydrogen bonds made to this ring.

If the ring 1 maps, the best from the $[N(C[NH_2]_2)_2][B(C_6H_5)_4]$ structure, show only such small features attributable to the X-H...π(Ph) interactions, what will be observed in the (lower quality) maps of the other rings, both in this structure and the other structures studied? In biguanidinium tetraphenylborate, ring 2 was judged to have the worst overall maps, so it is of interest to compare its cuts through the C-C ring bonds with those of ring 1. There is only a single N-H centroid type hydrogen bond made to this ring, N(2)-H(2A)...ring 2, but it should be one of the strongest in the structure based on the minimum H(N)...C_{ring}

distance [to C(26)]. There are also two C-H...π(Ph) hydrogen bonds made to this ring, both involving C-H groups on a single ring 1 from a second tetraphenylborate anion. The first interaction, C(13)-H(13)...ring 2, is an edge type hydrogen bond with the closest contact made to the C(25)-C(26) ring bond, while the second interaction, C(14)-H(14)...ring 2, is a centroid type hydrogen bond with the closest contact made to the C(22)-C(23) bond of the ring. All of these interactions are clearly visible in the cut shown in Figure 75, made through the C(22)-C(23) and C(25)-C(26) ring bonds.

Below the ring 2 plane, ring 1 of a second anion lies approximately perpendicular to the first ring. Both the C(13)-H(13) bond, below the C(25)-C(26) bond contours and the C(14)-H(14) bond, below the C(22)-C(23) contours, are oriented appropriately for interaction with ring 2. Both ring 1 bonds must lie almost exactly in the plane drawn since considerable density is visible on each bond. However, neither set of C-H bond contours shows any evidence of having been changed or perturbed by their interaction with the phenyl ring, leading to the conclusion that these C-H...π(Ph) hydrogen bonds are almost entirely electrostatic in nature. There is a slight charge depletion visible at both H(C) atoms.

Above the ring 2 plane, the N(2)-H(2A) bond of the cation is positioned for a possible interaction, pointing diagonally down towards the contours on the C(25)-C(26) bond of the ring. Judging from the contours visible on the N(2)-H(2A) bond [7] it does not lie completely in the plane drawn but somewhere close to it. The maximum is well centered on the bond but on one side the outer contour joins with those on the adjacent N(2)-C(1) bond. On the other side, the contours are slightly more

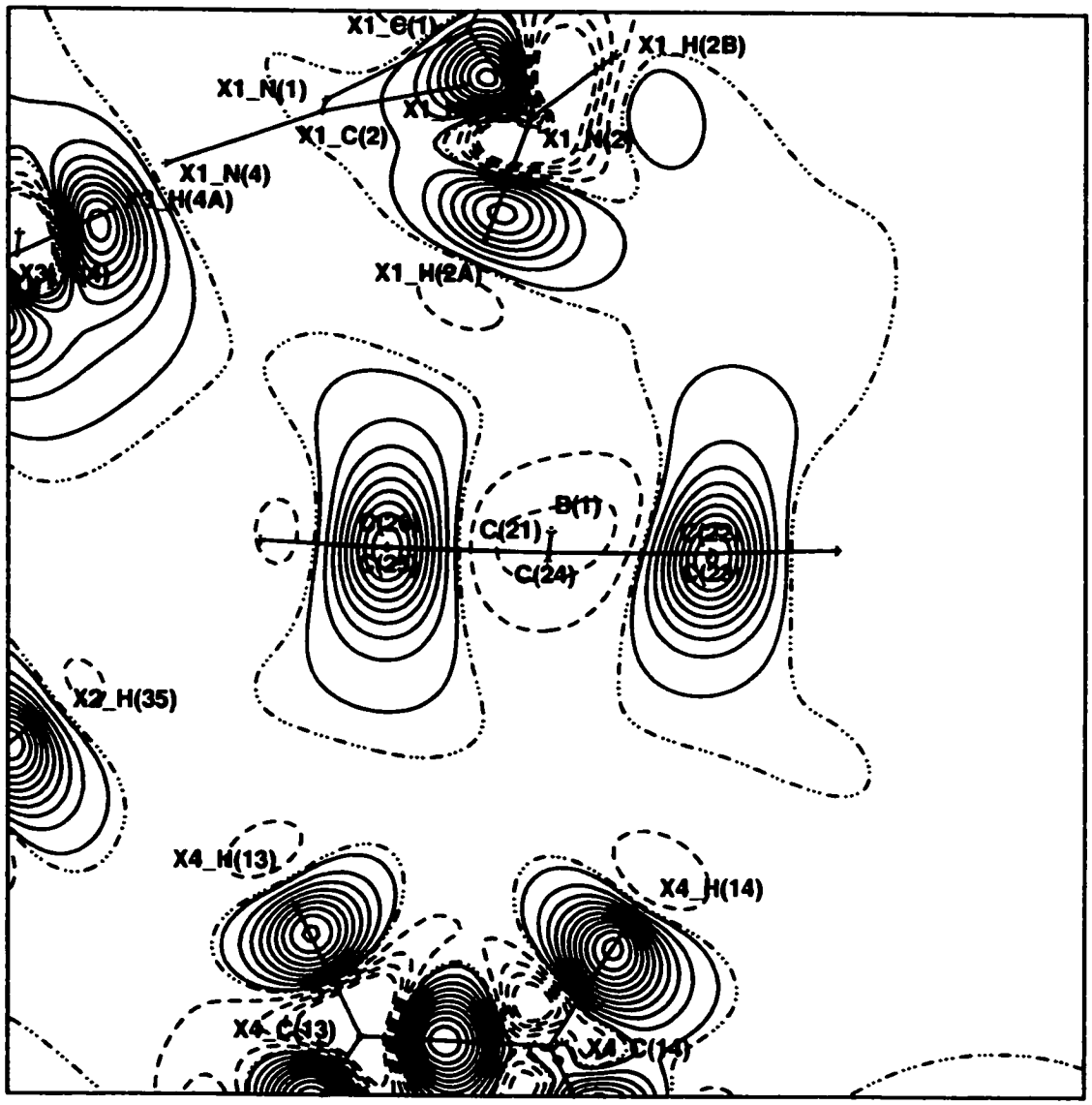

Figure 75. Static deformation density map drawn in the perpendicular plane bisecting the C(22)-C(23) and C(25)-C(26) bonds of the anion phenyl ring #2 in the structure of biguanidinium tetraphenylborate. Positive contours are drawn with solid lines, negative contours with dashed lines and the zero level contour with a {dash dot dot dot} pattern. The contour interval is 0.05 $eÅ^{-3}$. The outline of the remainder of the tetraphenylborate anion has been omitted for clarity.

expanded, appearing to be drawn somewhat towards the contours on the ring bonds, as described previously for other N-H type interactions. As well, charge depletion, in the form of a hole of one negative contour, is visible beyond H(2A) towards the ring. As in the previous cases discussed, this suggests a small covalent component, in addition to the large electrostatic contribution, in the N(2)-H(2A)...ring 2 hydrogen bond.

The contours on the two C-C bonds in the cut shown in Figure 75 are typical of those on all the bonds of this ring (#2). On each bond the outer contour is consistently expanded perpendicular to the ring plane, both above and below the ring. The diffuseness observed is relatively equal on the two C-C bonds shown and all around the ring. Again, all of the ring C-C bonds show an approximately equal effect from the interactions made to that ring; the effect is not limited to those bonds most directly involved (the closest) in the interactions. This is as expected, since the π electron density, delocalized over the entire ring, acts as the hydrogen bond acceptor. This density lies in planes above and below the ring, and the effect of the hydrogen bond(s) on this density causes the expansion/diffuseness observed on the outer contours of the C-C bonds.

The diffuseness observed on the C-C bond contours of the static maps cut through ring 2 of the anion in the structure of $[N(C[NH_2]_2)_2][B(C_6H_5)_4]$ appears to be greater than that observed on the corresponding ring 1 bonds. This is likely at least partially related to the strengths of the interactions made to the two rings. Ring 1 serves as the acceptor in three N-H. .π(Ph) hydrogen bonds, while ring 2 serves as the acceptor in only one N-H type interaction. However, it is the strongest such hydrogen bond in the structure (and of all of those studied in this work) and ring 2

also serves as the acceptor in two C-H...π(Ph) hydrogen bonds. This could explain why greater effects are observed in the maps of ring 2 compared to those of ring 1 in the $[N(C[NH_2]_2)_2][B(C_6H_5)_4]$ structure.

In addition, the greater diffuseness observed on the ring 2 C-C bond contours compared to those of ring 1 could also be related to the original C-C bond densities on the two rings. The average C-C bond density of ring 1 (13.3 contours/bond) is considerably greater than that of ring 2 (10.7 contours/bond). The density is more tightly concentrated on the bonds of ring 1 and the hydrogen bonding interactions have relatively less influence on these denser bonds. The expansion of the outer contours is thus less on the denser bonds and less diffuseness of the outer bond contours is observed. In contrast, on bonds that are originally less dense, such as those of ring 2, the hydrogen bonding interactions have an easier time distorting the outer bond contours. A greater visible effect is observed as the already less dense bonds become even more diffuse.

The results observed for the ring 1 (best) and ring 2 (worst) static maps drawn through opposing C-C bonds in phenyl rings of the anion in $[N(C[NH_2]_2)_2][B(C_6H_5)_4]$ are reasonable and consistent. The maps discussed show all the features found to be characteristic of X-H...π(Ph) interactions. The static maps drawn of perpendicular cuts made through the bonds of rings 3 and 4 of the same structure share the same characteristic features, supporting the conclusions reached. Only one final cut through the ring bonds of $[N(C[NH_2]_2)_2][B(C_6H_5)_4]$ will be shown here, for discussion of a rather different feature of the map.

Figure 76 shows a vertical cut made through the C(42)-C(43) and C(45)-C(46) bonds of ring 4 in the biguanidinium tetraphenylborate anion.

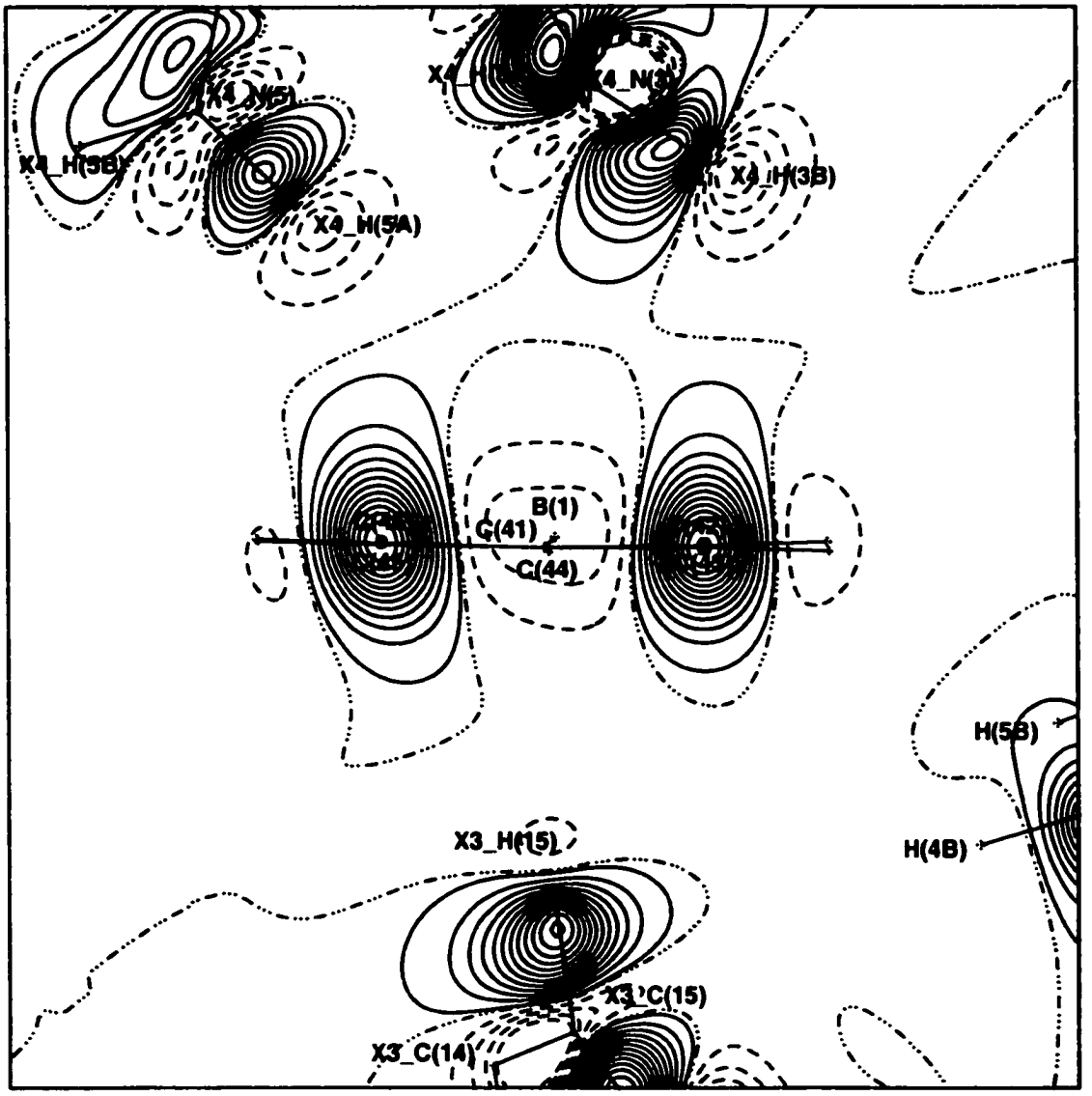

Figure 76. Static deformation density map drawn in the perpendicular plane bisecting the C(42)-C(43) and C(45)-C(46) bonds of the anion phenyl ring #4 in the structure of biguanidinium tetraphenylborate. Positive contours are drawn with solid lines, negative contours with dashed lines and the zero level contour with a {dash dot dot dot} pattern. The contour interval is 0.05 $e\text{Å}^{-3}$. The outline of the remainder of the tetraphenylborate anion has been omitted for clarity.

In this map, the C(15)-H(15) group of a second $B(C_6H_5)_4^-$ anion is visible, centered below and nearly perpendicular to the original ring 4 plane, in an orientation characteristic of a centroid type hydrogen bonding interaction. The C(15)-H(15) bond does appear to lie almost exactly in the plane drawn. The C(15)-H(15) bond contours, although not completely symmetrical, show no evidence of interaction with the ring. This is as expected, since the presence of C-H...π(Ph) hydrogen bonds have generally been found to have no visible effect on the contours of the C-H bonds in the static maps, their being primarily electrostatic. A small area of charge depletion is visible at H(15) in this and all the ring 4 maps drawn.

Above the ring 4 plane a single cation is visible, with two N-H groups in suitable positions to interact with the ring, although in the map drawn the two groups do not appear to be directly related. In fact, these two N-H groups, N(3)-H(3B) and N(5)-H(5A), come from different halves of the same cation, so the familiar "pincer" type arrangement is not formed in this case. The map shown in Figure 76 is the only cut made through the bonds of ring 4 in which the N(5)-H(5A) bond is at least close to being in the plane drawn. In this plane, the N(5)-H(5A) bond contours show no evidence of having been influenced by the hydrogen bonding interaction made with the ring. There is, however, a considerable depletion of charge observed at H(5A), leading to the conclusion that the N(5)-H(5A)...ring 4 hydrogen bond is primarily electrostatic in nature.

It is the N(3)-H(3B)...ring 4 hydrogen bond that is of the greatest interest in the map shown in Figure 76. Both the N(3)-H(3B) and the N(3)-C(1) bonds of the cation appear to lie substantially in the plane

drawn, directly above ring 4 of the anion. For some reason, the contours of the N(3)-H(3B) bond are significantly elongated down towards the ring plane, a much larger effect than normally observed for such interactions. The outermost N(3)-H(3B) bond contour is joined on one side with contours from the adjacent N(3)-C(1) bond. In addition, the contours on the N(3)-C(1) bond also appear to be perturbed, drawn down off the bond towards the ring. As a result, an almost complete circle of electron density surrounds the N(3) atom. It is not clear why such a strong effect is observed at N(3)-H(3B) since it is one of the weakest N-H...π(Ph) interactions in the structure. However, the map does illustrate why an unusual bond path was subsequently found for this interaction, beginning from N(3) rather than the expected H(3B). The electron density in this region of the cation encircles N(3) and it funnels the bond path in the direction of N(3) before proceeding to the ring, leading to the unusual bond path observed. The fact that such a large effect is observed on the cation bonds involved in this interaction appears to be an anomaly, nothing else of this nature is observed in the maps illustrating the other N-H...π(Ph) hydrogen bonds in biguanidinium tetraphenylborate. The C-C bond contours in this cut do show the slight diffuseness expected, more in keeping with the effects observed for the other X-H...π(Ph) interactions of this structure.

The characteristic features identified as resulting from the presence of X-H...π(Ph) [X = N or C] hydrogen bonds in the static maps cut through the phenyl ring bonds in the structure of $[N(C[NH_2]_2)_2][B(C_6H_5)_4]$ can be compared with the features identified in the maps of the other structures studied. Conversely, the maps of the other structures can be

compared to see if they consistently exhibit the same characteristic features identified in the $[N(C[NH_2]_2)_2][B(C_6H_5)_4]$ maps. The $NH_4B(C_6H_5)_4$ structure is interesting in this respect because only two static maps of cuts through the C-C ring bonds completely define the anion. The vertical cut made through the C(11)-C(12)' and C(13)-C(14) anion phenyl ring bonds is shown in Figure 77. This static map is the more interesting of the two cuts because it shows greater evidence of interaction between the cation and the anion. It also includes the two C-H...phenyl interactions which occur in the structure. Besides the N(1)-H(1)...ring 1 centroid type hydrogen bond, there is a C(14)-H(14)...ring 1 centroid type hydrogen bond, in which the closest contact is made to C(11), and an interaction, C(12)-H(12)... ring 1, which was found to have an edge type geometry involving the C(13)-C(14) ring bond with possible contributions from the H(13) and H(14) atoms as well.

Below the ring plane, the C(14)-H(14) bond from ring 1 of a second anion lies centered directly under and perpendicular to the original ring. The C(14)-H(14) bond appears to be almost entirely coincident with the plane drawn. The contours are discrete and well centered on the C(14)-H(14) bond, showing no evidence of having been perturbed by interaction with the ring. The C(12)-H(12) bond of a third anion is also visible in the map shown in Figure 77. The projected bond lies below and outside the original ring plane, beyond the C(13)-C(14) bond contours; it points diagonally up towards that side of the ring. The C(12)-H(12) bond, although it actually lies somewhat out of the plane drawn, still shows considerable density in this static map. The bond contours are discrete and symmetric; again, they show no sign of having been affected by

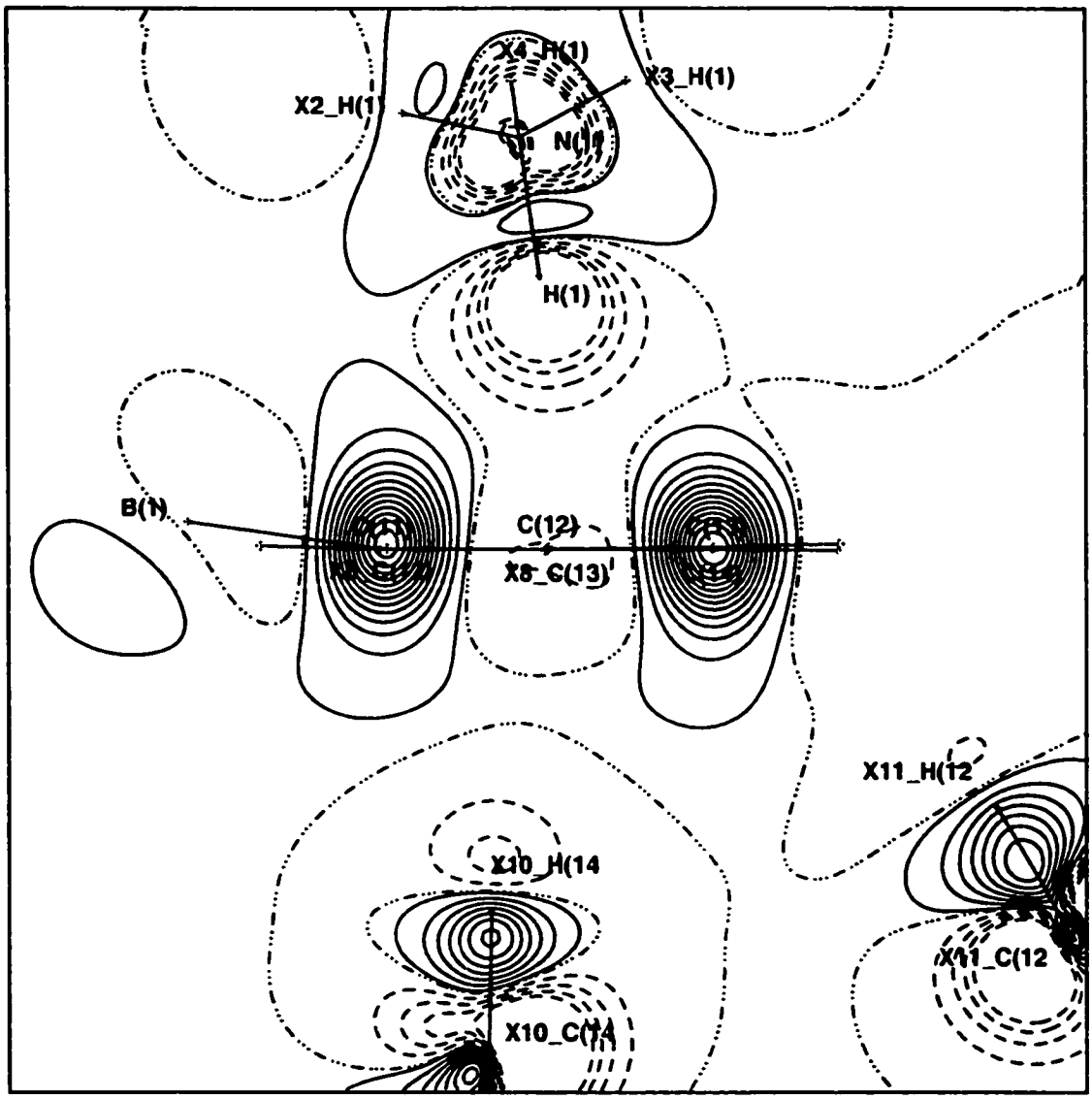

Figure 77. Static deformation density map drawn in the perpendicular plane bisecting the C(11)-C(12)' and C(13)-C(14) bonds of the anion phenyl ring #1 in the structure of ammonium tetraphenylborate. Positive contours are drawn with solid lines, negative contours with dashed lines and the zero level contour with a {dash dot dot dot} pattern. The contour interval is 0.05 $eÅ^{-3}$. The outline of the remainder of the tetraphenylborate anion has been omitted for clarity.

interaction with the original ring. Both of the C-H...phenyl type interactions in $NH_4B(C_6H_5)_4$, as observed in this cut through the phenyl ring bonds of the anion, must be primarily electrostatic. They do both show depletion of charge at the H(C) atoms involved.

Above the ring plane an ammonium cation is visible, with one N(1)-H(1) bond centered directly over, but not quite perpendicular to, ring 1. The cation N(1)-H(1) bond appears to lie in or very close to the plane drawn, likely due to symmetry requirements. Although only two contours are visible on the N(1)-H(1) bond in this cut, the cation density distribution appears very similar to that observed in the inplane static map of the cation itself, substantiating the fact that the N(1)-H(1) bond lies in the plane drawn. The density on the N(1)-H(1) bond shows no direct evidence of interacting with the ring. However, as already discussed, the distribution of the electron density around the NH_4^+ cation is rather unusual, an effect attributed to rotation of the cation, even at low temperatures, in the solid state structure. The bonding electron density, visible as a continuous ring smeared around the cation, does however show evidence of direct interaction with the anion phenyl ring. Midway between the two inplane N-H bonds the cation density is visibly perturbed, pulled down away from the cation towards the density on the C(11)-C(12)' bond of the anion. This visible movement of the cation electron density into the region between the two interacting groups suggests a significant covalent component to this contact. It also suggests a possible reason why in this case an unusual bond path was again subsequently observed for the interaction, beginning from N(1) and not the H(1) atom as expected. The path of maximum electron density appears to flow between the N(1)-H(1) bonds

of the cation (rather than along the bonds) then down towards the ring via the C(12)-C(11)-C(12)' region of the anion.

The contours on the C-C bonds of the phenyl ring in this cut are unusual for a variety of reasons. They do both show the diffuseness expected for a ring involved in a number of X-H...π(Ph) interactions. All of the C-C bonds of the ring show relatively equal effects, not just those most directly involved in the interactions, as expected. However, as the static map in Figure 77 shows, the expansion of the C-C bond contours is consistently more pronounced below the ring than above; it is normally observed to be approximately equal above and below the ring plane. A possible explanation is also visible in the map shown. A large, deep hole of depleted charge is visible just beyond H(1) of the cation. This hole, of four negative contours, is larger in area than usually observed in the static maps of the experimental structures, occupying much of the region between the cation and the anion. This, in turn, could prevent the normal slight expansion of the electron density of the phenyl ring into this area. The result would be the pattern observed on the C-C bonds in the static maps of $NH_4B(C_6H_5)_4$, with the density relatively compact above and more diffuse below the ring plane.

The C(11)-C(12)' bond contours (and those of the symmetry equivalent C(11)-C(12) bond) also show distinct evidence of further interaction with the cation in this map, an effect not normally observed for X-H...π(Ph) hydrogen bonds. Above the ring plane, the outermost contour on the C(11)-C(12)' bond is visibly perturbed, drawn up towards the density on the cation centered between the two inplane N-H bonds. Electron density has definitely been accumulated in the region between the two interacting

groups, evidence of a significant covalent contribution to this hydrogen bond. However, the electrostatic contribution must also be strong, judging from the major charge depletion visible at H(1). Such a large covalent effect is not normally observed for the X-H...π(Ph) hydrogen bonds, being characteristic of stronger hydrogen bonding interactions (with more traditional acceptors). In the structure of $NH_4B(C_6H_5)_4$, it is not completely clear what the true nature of the interaction actually is, since it does not obviously involve the N-H bond. The nature of the acceptor is somewhat uncertain also, as will be seen when the cuts through the phenyl ring atoms are discussed. However, this static map clearly illustrates why such an unusual bond path was subsequently determined for this interaction. Both the large charge developed on such a small cation and the rotation of the cation within the anion cavity clearly affect the interaction (and the maps plotted) in a variety of ways.

Ring 1 of the anion in [DabcoH][$B(C_6H_5)_4$] serves as the acceptor in the one N-H...π(Ph) hydrogen bond formed in this structure. The centroid type hydrogen bond, N(1)-H(1)...ring 1, makes the closest physical contact between H(1) and C(12). It also serves as the acceptor in a pair of equivalent C-H...phenyl interactions between the cation and the anion; C(2)-H(2A)...ring 1 forms a single atom type hydrogen bond, with C(13) making the closest contact to H(2A). Figure 78 shows the static maps of cuts made (a) through the equivalent C(12)-C(13) and C(12)'-C(13)' bonds of the anion ring 1 and (b) through the C(11)-C(12) and C(13)'-C(14) bonds of ring 1. The ring 1 plane is bisected by a vertical mirror plane through the C(11) and C(14) atoms, so only these two bond cuts are needed to completely characterize the ring.

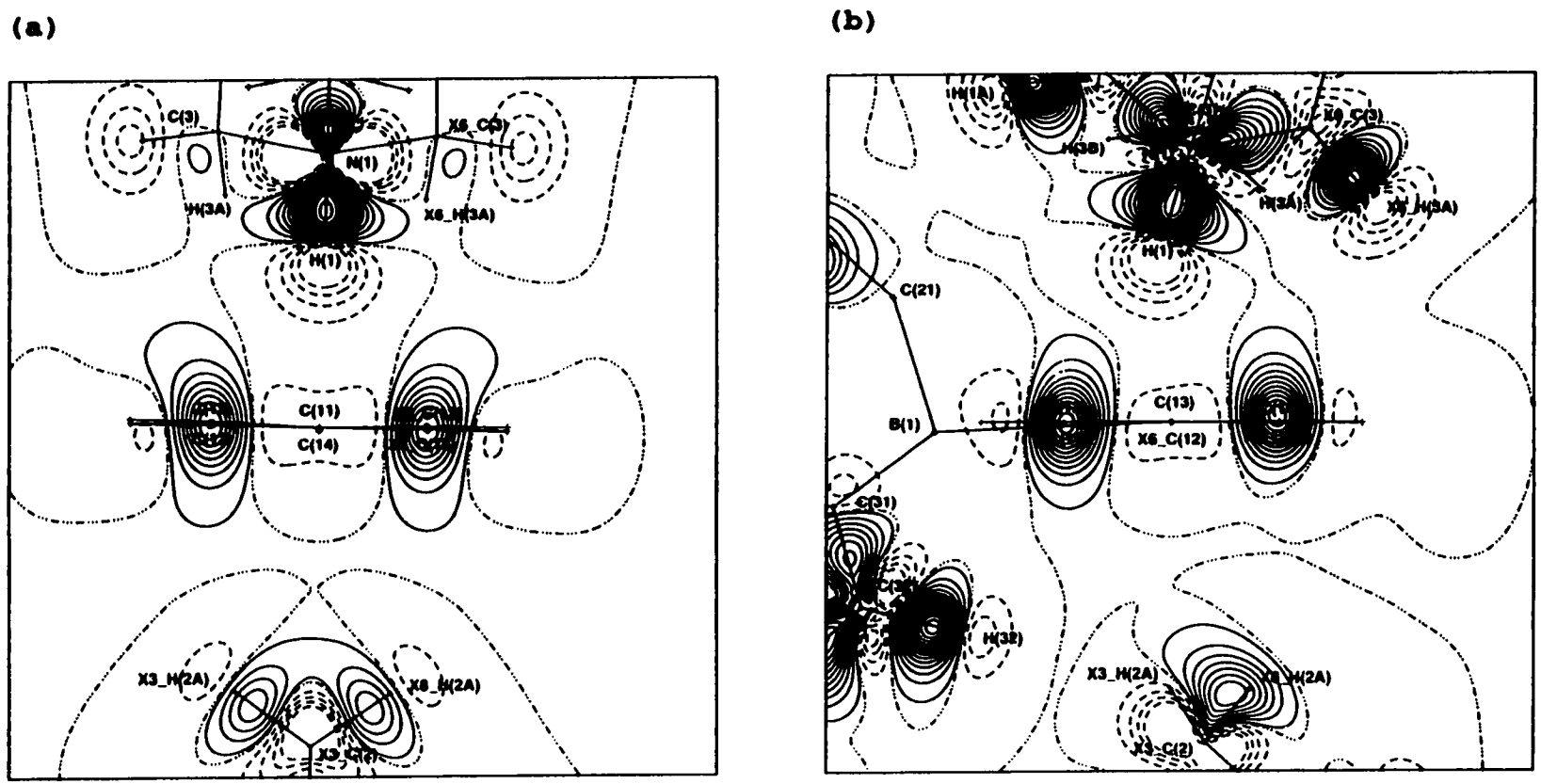

Figure 78. Static deformation density maps drawn in the perpendicular planes bisecting (a) the C(12)-C(13) and C(12)'-C(13)' bonds and (b) the C(11)-C(12) and C(13)'-C(14) bonds of the anion phenyl ring #1 in the structure of [DabcoH][$B(C_6H_5)_4$]. Positive contours are drawn with solid lines, negative contours with dashed lines and the zero level contour with a (dash dot dot dot) pattern. The contour interval is 0.05 $eÅ^{-3}$. The outline of the remainder of the tetraphenylborate anion has been omitted for clarity in both maps.

In the C(12)-C(13)/C(12)'-C(13)' bond cut, (a), the N(1)-H(1) bond of a cation lies well centered above, and almost perpendicular to, the ring 1 plane. The N(1)-H(1) group is oriented as expected for a relatively strong, centroid type hydrogen bonding interaction with the ring. The N(1)-H(1) bond lies exactly in the plane drawn (as defined by the symmetry) with considerable density visible on the bond and an area of strong charge depletion visible just beyond H(1). The contours on the N(1)-H(1) bond appear regular, discrete and symmetrical in the first map drawn (Figure 78a) and give no sign of having been affected by interaction with the ring. This is also true of the cut made through the C(11)-C(12) and C(13)'-C(14) ring bonds (Figure 78b), where the N(1)-H(1) bond contours remain discrete and uniform in appearance. However, in the second map, the N(1)-H(1) bond itself is angled toward the C(11)-C(12) side of the ring. As a result, the N(1)-H(1) bond contours naturally point down towards the contours on the C(13)'-C(14) bond, without having been visibly perturbed. Because of the symmetry involved there is an equivalent "contact" between the N(1)-H(1) bond and the C(13)-C(14) bond of phenyl ring 1. The N(1)-H(1) bond contours are thus equally inclined towards the C(13)-C(14)-C(13)' bond contours of the ring, explaining the bond path to C(14) subsequently observed. The N(1)-H(1) bond contours are oriented in a position to interact with the ring because of symmetry and the geometry of the contact without having to be greatly perturbed. It is slightly surprising that the N-H bond contours do not show a greater effect because of the N(1)-H(1) hydrogen bond but there are several possible explanations for this. The mirror symmetry of the N(1)-H(1) bond could mask the influence of the interaction on the bond contours. Or, perhaps since the

density on the N(1)-H(1) bond is so strong, with such tightly held contours, that the visible influence of the interaction on the outer bond contours is less than might normally be expected. The large area of charge depletion observed at H(1) does give evidence of a strong electrostatic component to the interaction.

The C(3)-H(3A) bond of the same cation was also found to make a close physical contact with C(13) of ring 1 in the geometry search carried out initially. However, a bond path could never be located for such an interaction. In the static map cut through the C(12)-C(13)/C(12)'-C(13)' ring bonds there is no density visible on the C(3)-H(3A) bonds meaning they do not lie in the plane drawn and so are in no position to interact with this portion of the ring. In the second map, that cut vertically through the C(11)-C(12) and C(13)'-C(14) bonds of ring 1, the C(3)-H(3A) bond does lie in the plane drawn but points directly away from the ring. It shows no evidence of interacting with the ring in any way. This could explain why no interaction line or bond path was found between C(3)-H(3A) and ring 1 in the [DabcoH][$B(C_6H_5)_4$] structure.

Below ring 1 in each of the cuts a second cation is visible, with two equivalent C(2)-H(2A) groups oriented for potential interaction with the ring. The two C(2)-H(2A) groups share a common C(2) atom and each points diagonally towards opposite C(12)-C(13) bonds of the ring. In Figure 78(a), the C(2)-H(2A) bonds appear to lie somewhat out of the plane drawn. The outermost contour on each of the equivalent bonds is visibly shared in this symmetric cut. However, the maxima remain well centered on the bonds and show no evidence of having been affected in any way due to the interaction with the ring. In the case of the C-H...phenyl contact,

this is as expected based on the overall observations made. Interactions of the C-H...phenyl type appear to be almost entirely electrostatic in nature (charge depletion is visible at each H(2A) atom) whether they arise from cation/anion contacts, as observed here, or anion/anion contacts, as observed previously.

The outer contours on the C(12)-C(13) and C(12)'-C(13)' bonds are diffuse and substantially elongated perpendicular to the ring 1 plane, but relatively equally above and below the ring. The diffuseness of the outer C-C bond contours is common to all the ring bonds but is more pronounced on the bonds of Figure 78(a). In fact, the elongation of these bond contours is somewhat larger than normally observed both in this structure and the other structures studied. However, it must also be noted that the density on the C-C bonds in this cut (a) is also less than usual. It appears that when the original bond density is less, the presence of X-H...π(Ph) interactions has a relatively larger effect on the C-C bond contours, resulting in a visibly greater expansion of the outer contours than normally observed.

There is one other unusual feature of the C(12)-C(13) and the equivalent C(12)'-C(13)' bond contours visible in the static map shown in Figure 78(a). Above the ring plane, the outer contour on each bond curves appreciably outward away from the ring. This effect was not observed on any other of the C-C bonds studied, whether on this ring, in this or in any other structure. It is not clear why this might have happened but it is possible that the C-C bond density has curved outward to avoid the large area of depleted charge visible at H(1) of the cation. This would be similar to the situation just described for $NH_4B(C_6H_5)_4$, where the C-C

bond contours all around the ring were observed to be more diffuse below the ring plane than above. This was attributed to the large region of depleted charge at H(1) of the ammonium cation which appeared to inhibit expansion of the bond contours into that area. In this case, the area of depleted charge at H(1) of the DabcoH$^+$ cation could cause the electron density on the C-C bonds to curve outward away from that region, giving the contours their unusual shape.

One final map from the [DabcoH] [$B(C_6H_5)_4$] structure will be discussed here; the static map of a perpendicular cut made through the C(22)-C(23) and C(22)'-C(23)' bonds of the anion phenyl ring is shown in Figure 79. This map was chosen as an example of a ring to which no N-H...π(Ph) interactions are made but which still forms four (two pairs of equivalent) $[C\text{-}H]_{cation}\cdots[phenyl]_{anion}$ type interactions. The C(1)-H(1A)...ring 2 contact was identified as an edge type hydrogen bond [to C(22)-C(23)] based on its geometry, while the C(4)-H(4B)...ring 2 contact was also classified as an edge type hydrogen bond involving the same C(22)-C(23) bond of the anion.

In the static map shown, the C(1) atom of the first cation is centered directly above the middle of the ring 2 plane. The two equivalent C(1)-H(1A) bonds (sharing a common C(1) atom) point diagonally towards opposite sides of the ring. Both bonds lie almost exactly in the plane drawn, judging from the density observed on those bonds. The three outer contours on the two C(1)-H(1A) bonds are shared. However, the maxima remain well centered on the bonds and the contours show no evidence of having been affected by interaction with the ring.

Below the ring 2 plane, two equivalent C(4)-H(4B) bonds from a

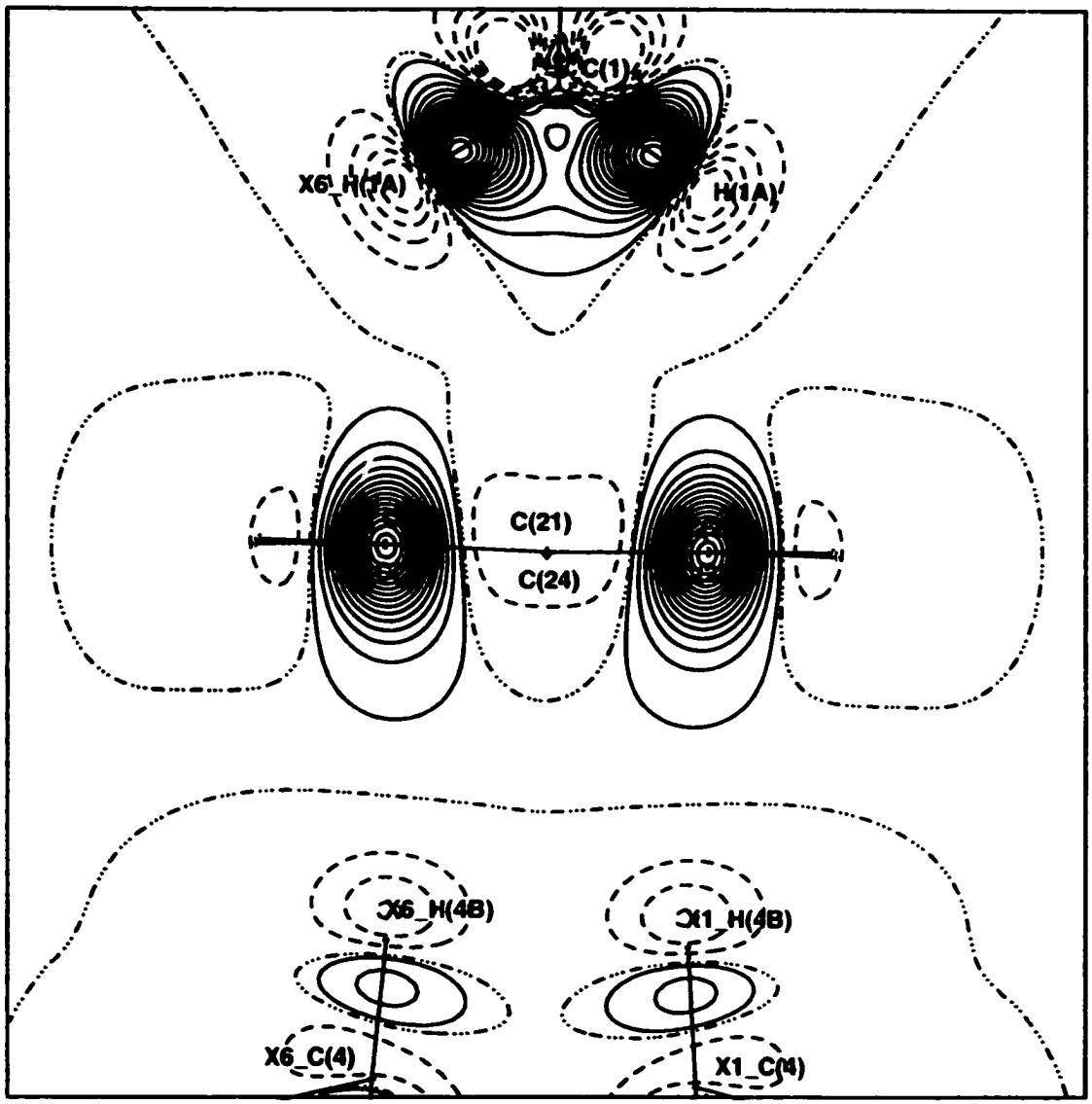

Figure 79. Static deformation density map drawn in the perpendicular plane bisecting the C(22)-C(23) and C(22)'-C(23)' bonds of the anion phenyl ring #2 in the structure of [DabcoH][$B(C_6H_5)_4$]. Positive contours are drawn with solid lines, negative contours with dashed lines and the zero level contour with a {dash dot dot dot} pattern. The contour interval is 0.05 $eÅ^{-3}$. The outline of the remainder of the tetraphenylborate anion has been omitted for clarity.

second cation are visible, each bond centered below and perpendicular to a C(22)-C(23) ring bond. The C(4)-H(4B) bonds only partially coincide with the plane drawn, only two contours being found on each bond. As with the first two bonds, the C(4)-H(4B) bond contours show no visible evidence of interaction with the ring, leading to the conclusion (reached previously) that C-H...phenyl contacts of this type are almost entirely electrostatic in nature. Significant charge depletion, in the form of holes of three or four negative contours, is visible at each H(C) atom in the plane shown.

The contours on the C-C bonds in this static map are similar in appearance to the majority of the bonds examined previously, even though this ring is not involved in any N-H...π(Ph) type interactions. The outermost contours on these C-C bonds are somewhat diffuse and expanded, slightly more below the ring than above (but this is likely not significant). All of the bonds of ring 2 show this diffuseness, not just those bonds most directly involved in the interactions. Again, the entire π system of the ring appears to act as the acceptor for the C-H...π(Ph) hydrogen bonds made to the ring. The C-H...phenyl type interactions appear to have a similar slight influence on the electron density of the ring as do the N-H...π(Ph) hydrogen bonds. Although the former contacts do not normally have a visible effect on the C-H bonds of the donor, there must still be a small covalent component to the largely electrostatic interactions since the C-C bond contours of the phenyl ring acceptor are perturbed.

Several of the static maps of the cuts made through opposing C-C bonds in the anion phenyl rings of the $[C(NH_2)_3][B(C_6H_5)_4]\cdot CH_3CN$ structure also show interesting features. Two cuts involving ring 2 of the anion are

illustrated, the first through the C(22)-C(23) and C(25)-C(26) ring bonds in Figure 80(a). It was included because it so nicely shows the "pincer" type arrangement between the cation [N(1)-H(1A) and N(2)-H(2A)] and the phenyl ring of the anion. In the top corner, this map also shows a portion of the strong $[N(1)\text{-}H(1B)]_{cation}\cdots[N(4)]_{solvent}$ hydrogen bond, while below the ring plane two other acetonitrile molecules are visible. The cation lies almost exactly in the plane drawn, with N(1)-H(1A) centered directly over, and almost perpendicular to, the ring, typical of a centroid type geometry. The N(2)-H(2A) group [of the edge type hydrogen bond] is also perpendicular to the ring plane but lies outside the ring beyond the physically closest C(25)-C(26) bond. Both H(N) atoms, H(1A) and H(2A), show considerable charge depletion in the area towards the anion ring, setting up a potential electrostatic interaction between the two groups. In the map plotted in Figure 80(a), the two N-H bonds show little evidence of interaction with the ring, although the N(2)-H(2A) bond contours are expanded slightly on the side toward the ring. However, the effects are more evident in other planes of this ring, as observed in the following diagram.

The C-C bonds in both the ring 2 maps shown have the expected diffuseness on the outer bond contours, believed to arise because of the interactions the ring participates in. The elongation of the outermost C-C bond contours is relatively equal on all the ring 2 bonds and equal both above and below the ring plane. It is interesting to note that in Figure 80(a) the contours on the C(22)-C(23) and the C(25)-C(26) bonds do not lie exactly perpendicular to the ring plane as normally observed. The two sets of contours appear to be slanted towards the two N-H groups of the

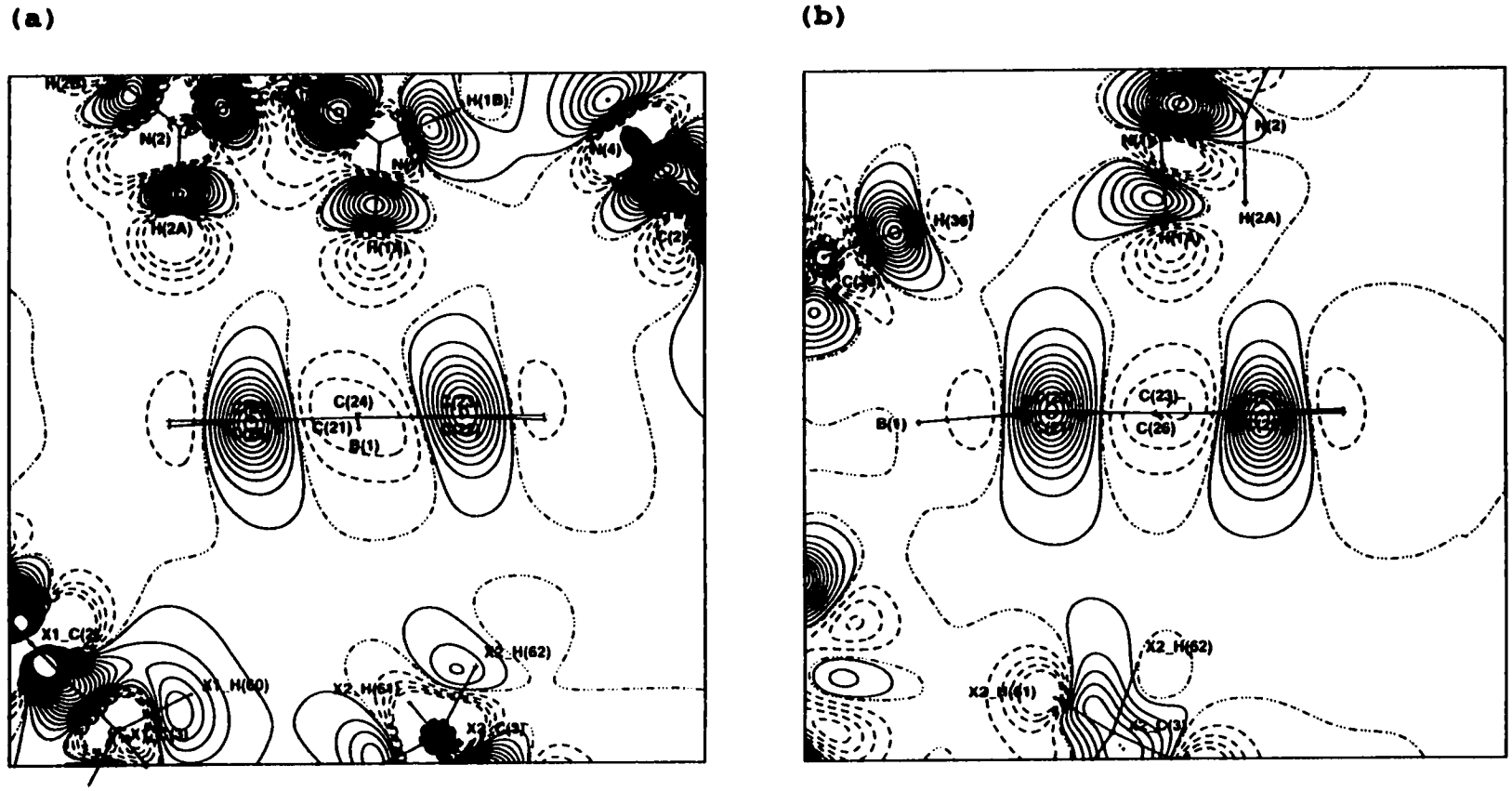

Figure 80. Static deformation density maps drawn in the perpendicular planes bisecting (a) the C(22)-C(23) and C(25)-C(26) bonds and (b) the C(21)-C(22) and C(24)-C(25) bonds of the anion phenyl ring #2 in guanidinium tetraphenylborate acetonitrile solvate. Positive contours are drawn with solid lines, negative contours with dashed lines and the zero level contour with a (dash dot dot dot) pattern. The contour interval is 0.05 $e\text{Å}^{-3}$. The outline of the remainder of the tetraphenylborate anion has been omitted for clarity in both maps.

cation with which the ring interacts. It is difficult to know if this is a genuine feature of these two interactions or if it is just an anomaly; it was not observed in any other of the maps plotted. In any case, a slight covalent component is expected for these interactions, judging from the observed minor perturbations of the contours on the N-H bonds (donor) and the C-C bonds (phenyl ring acceptor) of the interacting groups.

A second static map involving ring 2, cut through the opposing C(21)-C(22) and C(24)-C(25) phenyl ring bonds, is illustrated in Figure 80(b). Many of the features visible are common to those in the map just discussed but several interesting differences are also observed. In this plane, the cation above the ring is oriented such that the N(2)-H(2A) bond does not lie at all in the plane drawn, while the N(1)-H(1A) bond is still partially coincident with the map plane. In this view, it is clearly apparent that the N(1)-H(1A) bond contours are perturbed, being drawn off of the bond towards the C(21)-C(22) bond contours of the ring. However, an even more interesting feature is observed below the ring plane in this static map, where an acetonitrile solvent molecule is partially visible. The ring is involved in a geometrically close contact with the C(3)-H(62) group of this CH_3CN molecule. As known from the inplane static maps of acetonitrile, little density is ever visible on the C-H bonds of the methyl group and none at all is observed in this cut, even though the C(3)-H(62) bond is oriented towards the ring. There is a set of unusual looking contours that expand outward from the CH_3CN molecule, between the C(3)-H(61) and C(3)-H(62) bonds of the methyl group. This density is directed upwards towards the ring plane, specifically the contours on the C(21)-C(22) bond. It is not clear where exactly this density originates

from on the CH_3CN molecule (likely related to the problems previously described in modelling acetonitrile) but it definitely explains the unusual bond path subsequently located for this interaction. This map clearly shows that the path of maximum electron density passes from C(3) up between the two methyl C-H bonds towards the C(21)-C(22) bond of the phenyl ring, the bond path later calculated.

Two final static maps of perpendicular cuts made through opposing C-C phenyl ring bonds in the structure of $[C(NH_2)_3][B(C_6H_5)_4]\cdot CH_3CN$ will be discussed. Figure 81 (a) illustrates a cut made through the C(31)-C(32) and C(34)-C(35) bonds of ring 3, while Figure 81 (b) shows a corresponding cut made through the C(31)-C(36) and C(33)-C(34) ring bonds. In the first diagram (a) ring 1 of two different anions and an acetonitrile solvent molecule are visible below the original ring plane. Of these, only the C(16)-H(16) bond of one anion lies in the plane drawn. This bond is visible in the lower corner of the map, beyond the C(34)-C(35) contours of the ring. It makes a geometrically close approach to only H(35) of the ring, forming an H...H type contact. As expected, the C(16)-H(16) bond contours show no evidence of having been perturbed by the interaction with the ring.

Above the original ring plane a cation is again visible, oriented in such a way that a bidentate "pincer" type arrangement is formed with the ring, involving in this case the N(2)-H(2B) and N(3)-H(3B) groups of the cation. N(3)-H(3B) engages in a centroid type hydrogen bond, with the closest approach made to C(32), and N(2)-H(2B) forms an edge type hydrogen bond with the C(34)-C(35) bond of ring 3. The cation lies almost exactly in the plane drawn, judging from the density of the contours visible on

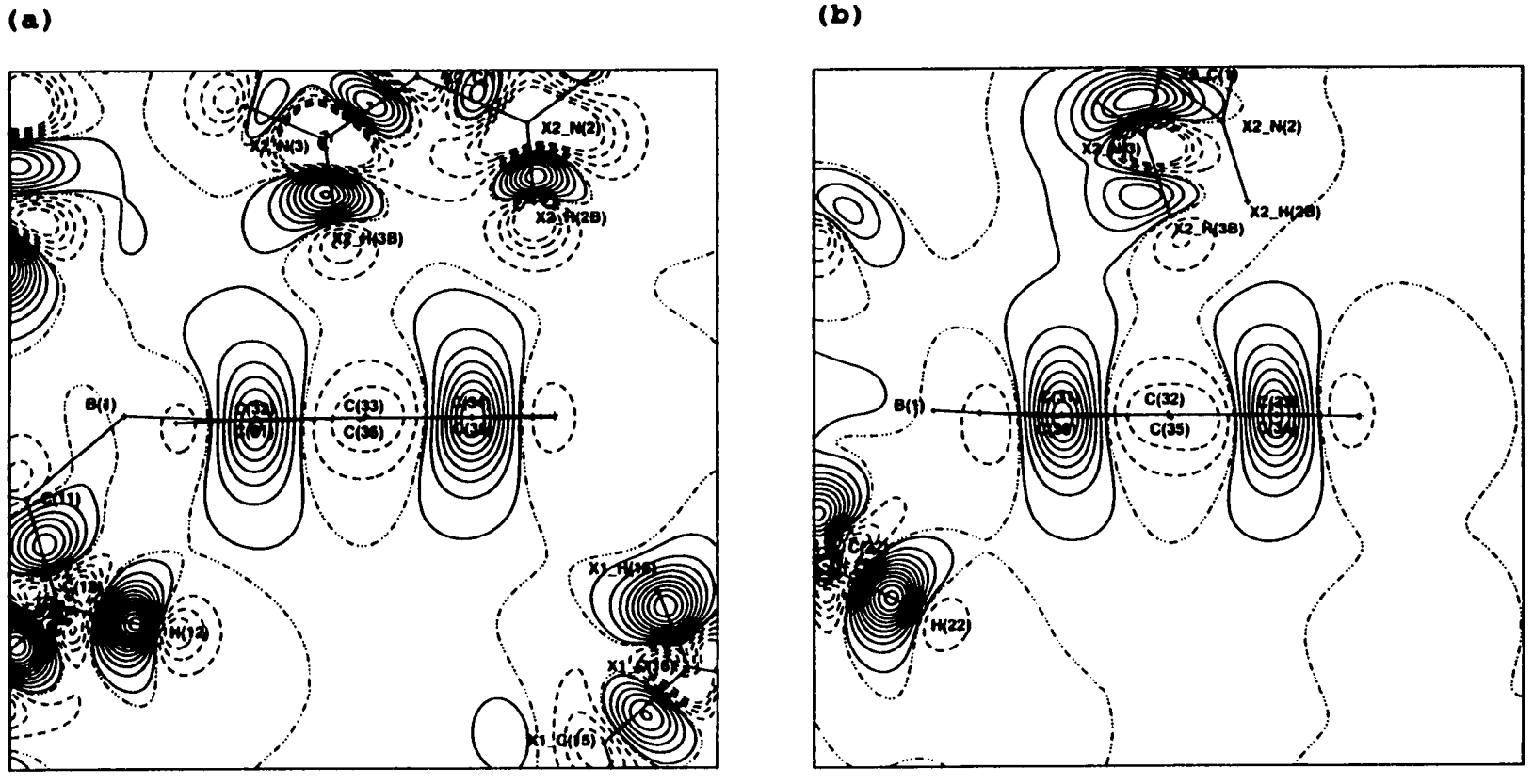

Figure 81. Static deformation density maps drawn in the perpendicular planes bisecting (a) the C(31)-C(32) and C(34)-C(35) bonds and (b) the C(31)-C(36) and C(33)-C(34) bonds of the anion phenyl ring #3 in guanidinium tetraphenylborate acetonitrile solvate. Positive contours are drawn with solid lines, negative contours with dashed lines and the zero level contour with a (dash dot dot dot) pattern. The contour interval is 0.05 eA^{-3}. The outline of the remainder of the tetraphenylborate anion has been omitted for clarity in both maps.

the bonds. The N(2)-H(2B) bond shows little visible evidence of interaction with the ring in this map. The contours on the N(3)-H(3B) bond are clearly perturbed, however, curving downward off the bond towards the contours on the C(31)-C(32) bond of the ring. The outer C(31)-C(32) bond contours appear to show a corresponding perturbation (in addition to the usual diffuseness) upwards towards the N(3)-H(3B) bond contours. This effect is much larger than normally observed for such N-H...π(Ph) interactions but it is minor compared to that observed in the following diagram.

In Figure 81(b), the static map cut through the C(31)-C(36) and C(33)-C(34) bonds of phenyl ring 3, only the N(3)-H(3B) bond of the cation lies even partially in the plane drawn. The outer two contours on the N(3)-H(3B) bond join upwards with those on adjacent cation bonds. Most surprisingly, the N(3)-H(3B) bond contours also actually join with those on the C(31)-C(36) anion ring bond. This was never observed for any other of the N-H...π(Ph) interactions studied experimentally. The contours on all the C-C bonds of ring 3 are very diffuse, both above and below the ring plane. However, much of this effect is reasonably explained by the low density visible on all the ring 3 bonds, the lowest average density of any ring in this structure (or any of the four experimental structures). This increases the effect the X-H...π(Ph) type interactions have on the C-C bond contours, making them more diffuse than might otherwise be expected. In addition, the outer contour on the C(31)-C(36) bond actually opens above the ring plane and is shared with the density on the N(3)-H(3B) bond of the cation, as just described an effect never previously observed.

The inplane static map of ring 3 in $[C(NH_2)_3][B(C_6H_5)_4]\cdot CH_3CN$ was found to be the worst, in the structure that was judged to give the maps of lowest overall quality, making the nature of this result somewhat questionable. However it is also true that N(3)-H(3B)...ring 3 is the strongest N-H...π(Ph) hydrogen bond in the structure and the second strongest studied in this investigation. It is not unreasonable that it might have a larger effect on the electron density distribution of the ring, and as a result on the static maps plotted, than normally observed. It is also possible that the second, relatively strong interaction made to the same face of ring 3 [N(2)-H(2B)...ring 3] contributes to the magnitude of the features observed in the static maps. One final possible explanation comes to mind. In this case, it could be that the model has placed too much density into the regions between the interacting groups rather than on the ions/molecules themselves. This could be at least a partial explanation as to why less density was consistently observed on the bonds of $[C(NH_2)_3][B(C_6H_5)_4]\cdot CH_3CN$ compared to the other structures. It appears that in this refinement the model may have moved bonding density further off the bonds into the intermolecular regions. However, it also appears that the model has not generated any new incongruous features in the static maps drawn. Rather, the model may only have magnified true features of the structure, including the effects of the X-H...π(Ph) interactions, to an extent greater than normally observed. Having said all this, however the features visible in the static maps of ring 3 in the $[C(NH_2)_3][B(C_6H_5)_4]\cdot CH_3CN$ structure arise, they are consistent with the previous observations made after investigation of the static maps from the other three structures.

Similar to the maps plotted through opposing ring C-C bonds, a second complete set of maps was generated for the phenyl rings in the tetraphenylborate anion of each structure. These **maps were drawn through opposing pairs of carbon atoms for each phenyl ring**. For a ring occupying completely general positions a total of three maps are required to define the ring, fewer if higher symmetry is present. The participation of the X-H groups in the interactions [X-H...π(Ph) X = N or C] shown in the maps has been discussed in detail in the previous section, on the cuts made through the phenyl ring bonds. The appearance of the X-H bond contours will not be discussed again in this section unless the bond is directly involved in an interaction in the map in question.

Analysis of the inplane maps showed that ring 1 in the structure of $[N(C[NH_2]_2)_2][B(C_6H_5)_4]$ had the best maps of all the rings in all of the structures studied experimentally. Thus, it is a logical place from which to begin the discussion on the maps drawn through the opposing carbon atoms of the phenyl rings in the anions. The maps of all three cuts through the atoms of ring 1 in the structure of $[N(C[NH_2]_2)_2][B(C_6H_5)_4]$ are remarkably consistent, showing virtually identical features (or lack thereof). The map plotted in a vertical plane cutting through the C(13) and C(16) atoms of ring 1 is shown in Figure 82 as a representative example.

In this static deformation density map, the three N-H...π(Ph) interactions made to ring 1 are all clearly visible. Above the ring plane, a cation is oriented in a bidentate "pincer" type arrangement, with N(4)-H(4B) projecting above the C(16)-H(16) ring bond and N(5)-H(5B) projecting above the middle of the ring. Based on the interaction

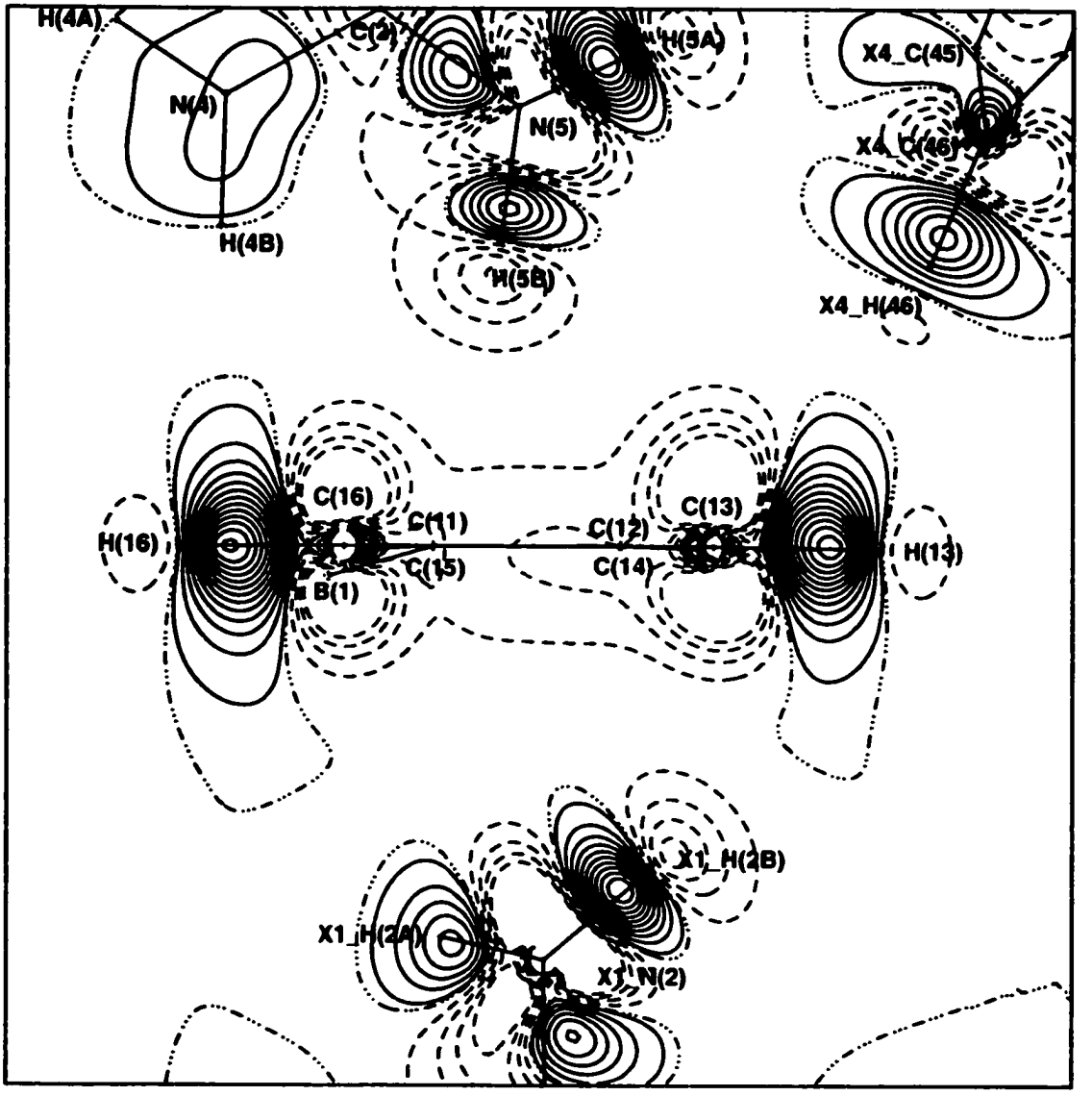

Figure 82. Static deformation density map drawn in the perpendicular plane cutting through the opposing C(13) and C(16) atoms of the anion phenyl ring #1 in the structure of biguanidinium tetraphenylborate. Positive contours are drawn with solid lines, negative contours with dashed lines and the zero level contour with a {dash dot dot dot} pattern. The contour interval is 0.05 $e\text{Å}^{-3}$. The outline of the remainder of the tetraphenylborate anion has been omitted for clarity.

geometries, the former was classified as an edge type hydrogen bond, to C(15)-C(16) with possible involvement of H(15) and H(16) as well, while the latter was classified as a centroid type hydrogen bond with the closest contact made to the same C(15)-C(16) ring bond. Below the ring plane a second cation is also visible, with N(2) centered under the middle of ring 1 in this projection. The N(2)-H(2B) bond points diagonally up towards the C(13)-H(13) bond of the ring, while the N(2)-H(2A) bond lies almost parallel to the ring plane, explaining why no interaction/bond path was subsequently located between N(2)-H(2A) and ring 1. The interaction N(2)-H(2B)...ring 1 was found to be a single atom type hydrogen bond [to C(13)], based on its geometry, explaining why the bond is observed to be almost completely coincident with the plane mapped in Figure 82.

One further interaction is evident in the map shown in Figure 82. The C(46)-H(46) bond of a second anion ring 4 is situated above and slightly outside the C(13)-H(13) bond of the original ring 1. The C(46)-H(46) bond projects diagonally down towards the C(13)-H(13) bond from outside the ring, indicative of an H...H type contact between the two rings. The C(46)-H(46) bond lies substantially in the plane drawn, as indicated by the large number of contours observed on the bond, but there is no visible evidence of it having been affected by the interaction made with ring 1.

Of the N-H...π(Ph) interactions made to ring 1, N(2)-H(2B) appears to lie almost completely in the plane shown in Figure 82, while N(5)-H(5B) of the other cation lies at least partially in this plane and N(4)-H(4B) lies almost entirely out of the plane, judging from the contours visible on the bonds. None of the N-H bonds show any evidence of having been

perturbed because of the interactions made with the ring. These are some of the weaker N-H...π(Ph) interactions studied experimentally so this is perhaps not surprising.

Of more interest is the ring 1 plane itself. The cuts made through the opposing carbon atoms of the phenyl ring highlight the bisected C-H bonds, as well as the bisected atoms used to define the plane. In Figure 82, and all of the cuts made through the atoms of ring 1, the features observed are regular and consistent. At the C(13) and C(16) atoms, holes of four negative contours are visible both above and below the ring plane. The holes are relatively equal in size and shape on each atom, and above and below the ring 1 plane. This same feature is observed on all the ring carbon atoms in all of the maps drawn. The holes vary little in appearance from one map to another and are always of the same depth (4 negative contours) at every ring carbon atom in every structure studied in this work, even when other features arising from X-H...π(Ph) interactions are also present in the maps.

The maps plotted through opposing carbon atoms of the phenyl rings also bisect (along the bond) the density on the inplane C-H bonds, cutting through the maximum bond density; normally 10 to 14 contours are observed on each bond. In Figure 82, and on all the C-H bonds of ring 1, the contours are uniform and symmetrical in appearance. They are roughly oval shaped, being elongated perpendicular to the bond. The outer contour tends to be slightly diffuse, by relatively equal amounts above and below the ring plane. The maximum always lies on the bond and considerably closer to the hydrogen atom than to the carbon atom. The C-H bond contours are of similar size, shape and density on all of the ring 1 bonds in the

structure of $[N(C[NH_2]_2)_2][B(C_6H_5)_4]$. None show any sign of having been perturbed in any way because of the N-H...π(Ph) interactions made to the ring. They all remain regular and symmetric around the ring despite the interactions formed.

There are no other peaks of any type visible in the map of Figure 82 or in any other of the ring 1 maps cut through opposing carbon atoms in the structure of $[N(C[NH_2]_2)_2][B(C_6H_5)_4]$. In particular, peaks are not observed in areas between the ring 1 plane and any of the interacting N-H groups on the cations. Such peaks (showing accumulation of electron density between the interacting groups), if they were observed, could be representative of a covalent component to the N-H...π(Ph) hydrogen bonds. If the interactions made to this ring are considered in abbreviated form, (i) N(4)-H(4B)...C(16)-H(16), (ii) N(5)-H(5B)...C(15)-C(16) and (iii) N(2)-H(2B)...C(13), it would appear that (i), (iii) and possibly (ii) should show visible effects in the map of Figure 82 if such effects were to occur. The three N-H...π(Ph) interactions, although not the strongest studied experimentally, do not give rise to any characteristic features in the maps plotted through the vertical planes defined by opposing carbon atoms in ring 1 of $[N(C[NH_2]_2)_2][B(C_6H_5)_4]$. Since these maps are the best examples obtained experimentally, the fact that they show no features attributable to the X-H...π(Ph) interactions is significant. It appears that weak N-H...π(Ph) hydrogen bonds should give rise to no visible effects in the maps plotted through opposing ring carbon atoms.

However, this is not what is commonly observed. Only a very few of the maps studied were found to be completely clean and featureless. In many of the maps drawn, peaks were observed to arise for reasons other

than the X-H...π(Ph) interactions made to the ring. These peaks do not normally occur in areas where they might reasonably represent an X-H...π(Ph) interaction, either close to or directly on the ring plane rather than between the X-H group and the phenyl ring. Such peaks might arise because of poor modelling of the multipoles on the ring atoms or they might simply be artifacts of the refinement process. In other cases, features were observed in the maps that could be directly attributed to the X-H...π(Ph) interactions made to the ring. These will be discussed as they arise, on an individual basis. The features observed include perturbation of the C-H or B-C contours of the ring towards electron density on the cation and/or peaks of positive density lying in regions between the ring and the interacting X-H group(s) of the cation. These features are not always consistently observed, even under similar conditions, and are often intermingled with peaks arising for other, unrelated reasons making them difficult to characterize accurately. Still, they are observed often enough to be worthy of discussion, particularly in the maps illustrating the stronger N-H...π(Ph) hydrogen bonds.

The maps from the structure of ammonium tetraphenylborate are of interest because only two cuts, through [C(11) and C(14)] and [C(12) and C(13)'] are sufficient to define the entire anion because of its high symmetry. The two maps are shown in Figure 83 (a) and (b) respectively. They share many common features with the maps just discussed from ring 1 in the structure of $[N(C[NH_2]_2)_2][B(C_6H_5)_4]$.

Above the ring 1 plane a cation is visible in both maps, the N(1)-H(1) bond projecting slightly diagonally toward the middle of the ring in each case, typical of a well centered, centroid type hydrogen

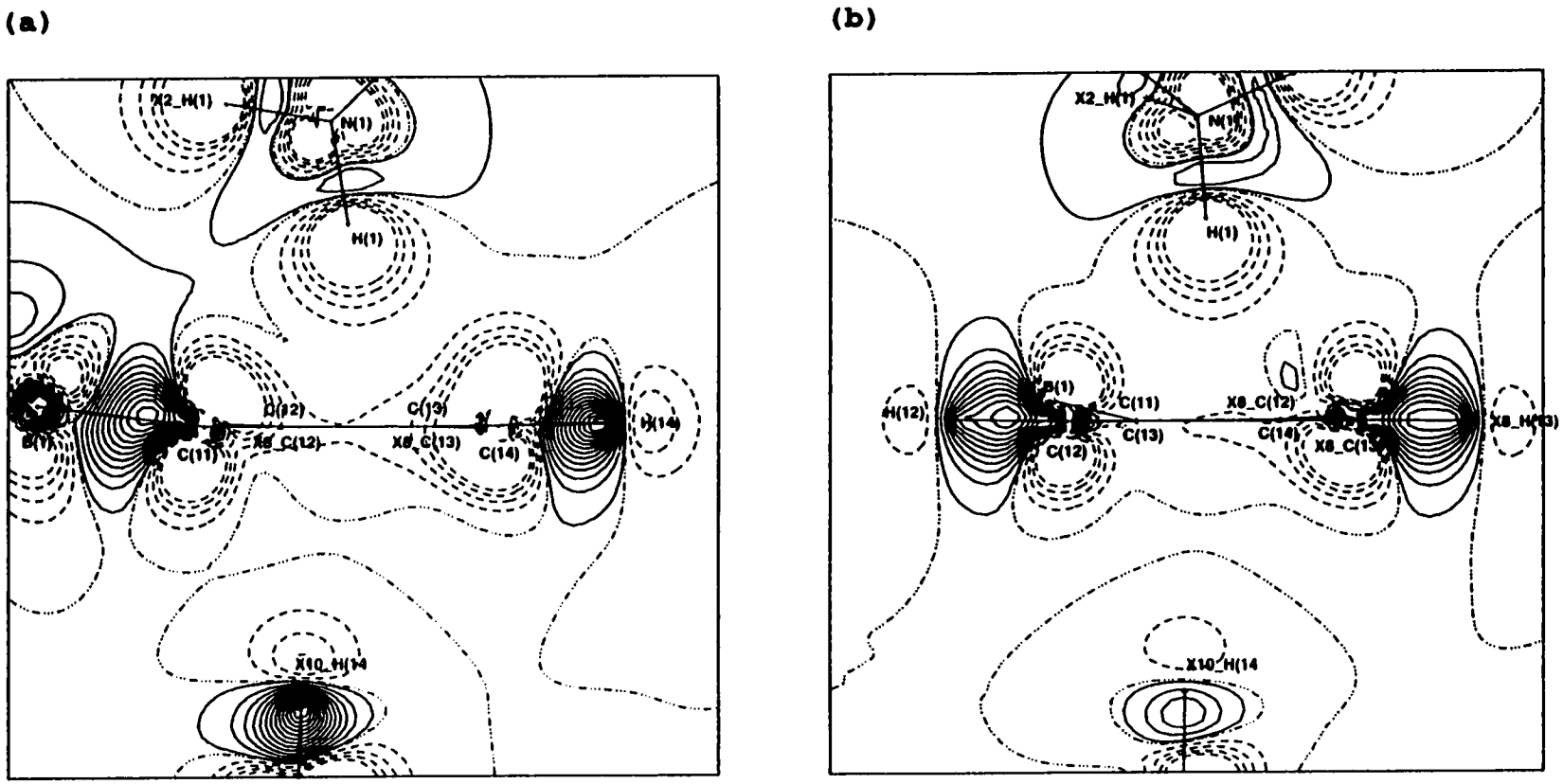

Figure 83. Static deformation density maps drawn in the perpendicular planes cutting through the opposing (a) C(11) and C(14) atoms and (b) C(12) and C(13)' atoms of the anion phenyl ring #1 in the structure of ammonium tetraphenylborate. Positive contours are drawn with solid lines, negative contours with dashed lines and the zero level contour with a {dash dot dot dot} pattern. The contour interval is 0.05 eÅ^{-3}. The outline of the remainder of the tetraphenylborate anion has been omitted for clarity in both maps.

bond. Below the ring 1 plane, the C(14)-H(14) bond of a second anion ring 1 is visible in each map. The bond projects perpendicular to, and centered below, the original ring plane, again indicative of a centroid type interaction. The second C-H...phenyl contact formed in the $NH_4B(C_6H_5)_4$ structure, C(12)-H(12)...ring 1, does not lie in either of the planes and was removed from the maps for their simplification. The N(1)-H(1) bond lies exactly in the plane of map (a), for symmetry reasons, and judging from the bond contours, it also lies substantially in the plane of map (b). The C(14)-H(14) bond of the second anion also lies exactly in the plane drawn in the cut made through the C(11) and C(14) ring atoms [a] but is only partially coincident with the plane in the map drawn through C(12) and C(13)' [b]; only three contours are visible on the bond in this plane. In neither map do the C(14)-H(14) bond contours show any evidence of interaction with the ring.

In the $NH_4B(C_6H_5)_4$ maps, the contours on the C-H bonds are regular and symmetrical all around ring 1 of the anion. They appear very similar to the C-H bond contours observed in the ring 1 maps of biguanidinium tetraphenylborate discussed previously. The C-H bond contours are elongated perpendicular to the bond, approximately equally above and below the ring plane. The outer contours are slightly diffuse but none show any evidence of having been perturbed by the X-H...π(Ph) interactions made to the ring. In $NH_4B(C_6H_5)_4$, the contours on the C-H bonds of the anion are not visibly involved in any of these interactions.

Similarly, the ring carbon atoms (when they lie in the plane of the map drawn) show no evidence of any features that could be attributed to the X-H...π(Ph) interactions accepted by the ring. Each atom, when

bisected in the map plane, shows a hole of four negative contours both above and below the ring plane, centered on the atom. The holes are relatively uniform in appearance but some variation is observed around the ring. These results are analogous with the observations made after examination of the ring 1 maps in $[N(C[NH_2]_2)_2][B(C_6H_5)_4]$.

In addition, however, a very small peak is observed in the map of Figure 83(b), just above the ring plane at C(13)'. No such peaks were found in the ring 1 maps of $[N(C[NH_2]_2)_2][B(C_6H_5)_4]$ and this is the only peak visible on any of the carbon atoms in the maps of $NH_4B(C_6H_5)_4$. It is very small and lies close to the ring plane, not in an area that would be considered representative of the X-H...π(Ph) interactions; that would require it to lie further from the ring plane, more in the area between the ring and the cation. This fact suggests that the small peak observed at C(13)' in the map of Figure 83(a) is not attributable to the X-H...π(Ph) interactions made to the ring. It must arise for some other reason, probably being a minor artifact of the refinement process.

One other feature of considerable interest is observed in the map of Figure 83(a). It is unlike anything observed in the ring 1 maps of $[N(C[NH_2]_2)_2][B(C_6H_5)_4]$ and appears to be truly characteristic of the N(1)-H(1)...ring 1 interaction made in $NH_4B(C_6H_5)_4$. The outer contour on the C(11)-B(1) bond [to the left in Figure 83(a)] is shared with the adjacent, and equivalent, C(11)'-B(1) bond of the same anion. This outer contour is visibly perturbed away from the anion towards the ammonium cation. The density on the C(11)-B(1) bond is visibly drawn upwards toward the cation, while in return, the cation density is drawn out, midway between the two inplane N-H bonds, towards the C(11)-B(1) bond of the

anion. The two regions of positive electron density nearly meet in the area halfway between the cation and the anion. Accumulation of electron density in the region between the two interacting groups is indicative of a covalent component to the N(1)-H(1)...ring 1 hydrogen bond.

The N(1)-H(1)...ring 1 interaction in the structure of $NH_4B(C_6H_5)_4$ is the third strongest N-H...π(Ph) hydrogen bond studied experimentally based on its geometry, particularly the minimum H...C_{ring} distance. This could explain why it gives rise to observable features in the maps cut through the phenyl ring atoms while the ring 1 atoms of $[N(C[NH_2]_2)_2][B(C_6H_5)_4]$ do not. Although three N-H...π(Ph) interactions are made to ring 1 in the latter structure, they are weaker than the single interaction made in the former. It also appears that the features actually observed in the $NH_4B(C_6H_5)_4$ maps arise only because of the N(1)-H(1)...ring 1 hydrogen bond; the C-H type contacts appear to have no visible effects on the maps drawn.

The perturbation of the density on the C(11)-B(1) bond in the static maps of $NH_4B(C_6H_5)_4$ suggests that σ electron density, and not only the π electron density, of the ring is involved in the N(1)-H(1)...ring 1 interaction. The C(11)-B(1) bond would be expected to be a σ type bond (sp^3 hybridization) yet it is still visibly involved in the interaction with the ammonium cation, NH_4^+. This is only the first of several examples in which the C-B and/or the C-H bonds of the anion [both σ type bonds] are perturbed by the N-H...π(Ph) interactions made to a specific phenyl ring. It appears to be a legitimate observation that the σ electron density of the anion, as well as the π electron density, can be affected by participation, as the acceptor, in N-H...π(Ph) type hydrogen bonds.

It is also interesting to consider the static maps of the cuts through the phenyl ring carbon atoms [Figure 83 (a) and (b)] in conjunction with the cuts made through the opposing C-C bonds [Figure 77 shows the C(11)-C(12)'/C(13)-C(14) map] of the one unique ring in the anion of $NH_4B(C_6H_5)_4$. The cuts through the ring atoms clearly show involvement of the C(11)-B(1) bond in the N(1)-H(1)...ring 1 interaction. The maps cut through the ring C-C bonds show perturbation of the C(11)-C(12), and the equivalent C(11)-C(12)', bond contours as well. This suggests that the entire region of the ring surrounding C(11), C(12)'-C(11)[B(1)]-C(12), serves as the "principal" acceptor for the interaction between the cation and the anion in the structure of $NH_4B(C_6H_5)_4$. This definitely explains why the bond path for this N-H...π(Ph) hydrogen bond was subsequently found to terminate at C(11) of the ring. It remains somewhat surprising that the cation density is perturbed between, rather than on the N-H bonds of the ammonium ion. As discussed previously, this could arise because of the rotation of the NH_4^+ cation in the solid state structure, making accurate modelling difficult. It does explain why an unusual bond path was observed, beginning from N(1) rather than the expected H(1) atom of the cation.

The static map plotted in vertical planes cut through the phenyl ring atoms of the anion in the structure of [DabcoH][$B(C_6H_5)_4$] are all very similar and uniform in appearance. The features observed are consistent with the results discussed thus far, for ring 1 of [$N(C[NH_2]_2)_2$][$B(C_6H_5)_4$] and for $NH_4B(C_6H_5)_4$. A map from each ring has been chosen as representative examples from the [DabcoH][$B(C_6H_5)_4$] structure.

Figure 84(a) illustrates the cut made through the C(12)' and C(13)

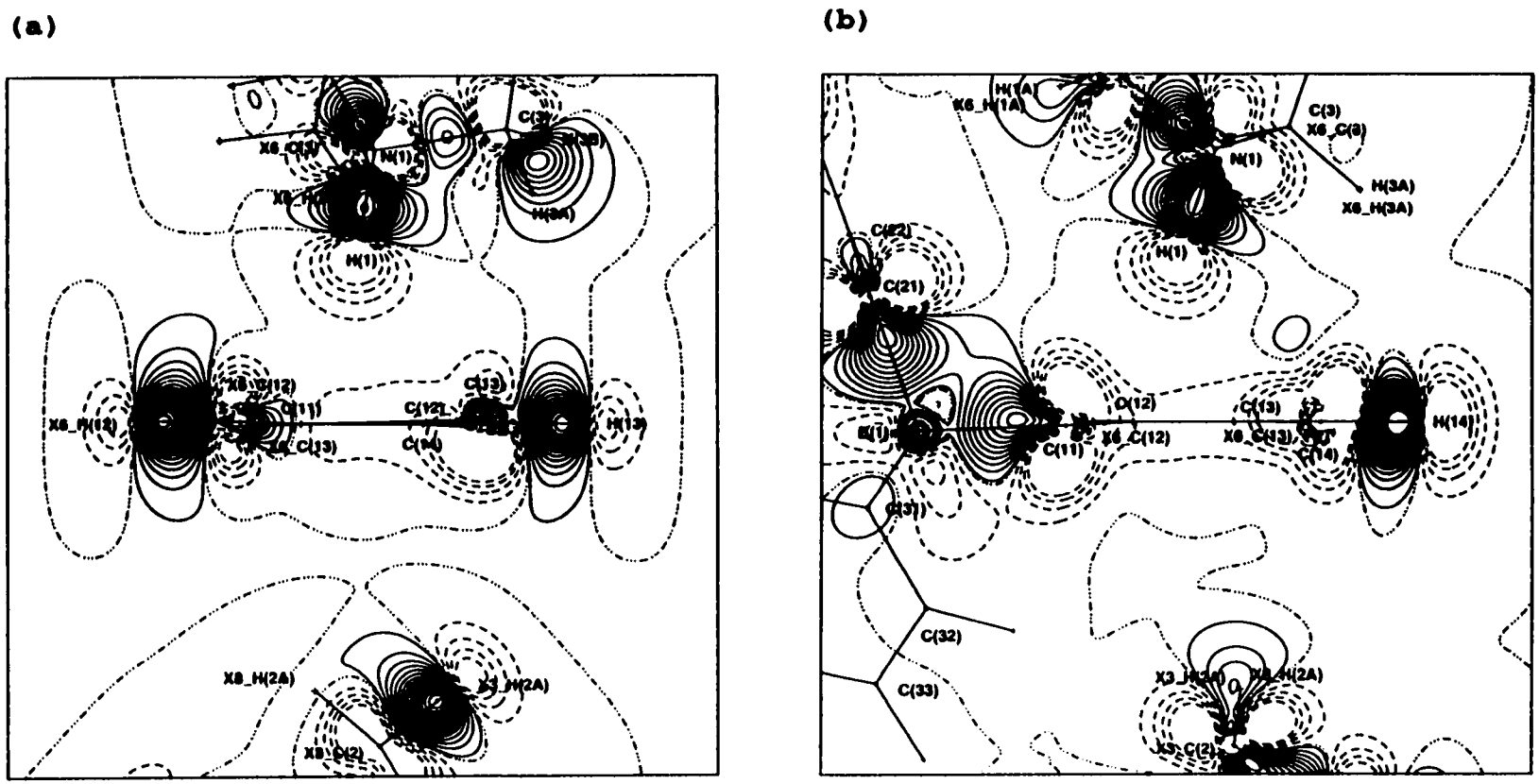

Figure 84. Static deformation density maps drawn in the perpendicular planes cutting through the opposing (a) C(12)' and C(13) atoms and (b) C(11) and C(14) atoms of the anion phenyl ring #1 in [DabcoH][B(C_6H_5)$_4$]. Positive contours are drawn with solid lines, negative contours with dashed lines and the zero level contour with a (dash dot dot dot) pattern. The contour interval is 0.05 eÅ^{-3}. The outline of the remainder of the tetraphenylborate anion has been omitted for clarity in both maps.

atoms of ring 1. Only two maps are needed to completely characterize ring 1 because of its mirror symmetry. Ring 1 is also the only ring of the anion involved in an N-H...π(Ph) hydrogen bond [N(1)-H(1)...ring 1], only a single such contact being formed in the structure of [DabcoH][$B(C_6H_5)_4$]. However, it also participates in a pair of equivalent C-H...π(Ph) interactions [C(2)-H(2A)...ring 1]. In the map shown in Figure 84(a), one cation is visible above and one cation below the ring 1 plane. Below the ring plane, C(2) of one cation lies directly on the plane drawn, centered under the middle of the ring. Only one of the two equivalent C(2)-H(2A) bonds, which share a common C(2) atom, is substantially coincident with the map plane. That bond projects diagonally toward the C(13)-H(13) bond of ring 1 but the bond contours show no evidence of having been affected by the interaction made with the ring. The other, equivalent C(2)-H(2A) bond, which projects diagonally in the opposite direction towards the C(12)'-H(12)' bond of ring 1, does not lie at all in the map plane drawn and thus can have no visible interaction with the ring in this view.

Above the ring plane, the principal interaction of ring 1 is formed to a second cation. The N(1)-H(1) bond of this cation is oriented directly above the middle of the ring 1 plane and projects very slightly diagonally towards the C(12)' side of the ring, an arrangement characteristic of a centroid type hydrogen bond. The N(1)-H(1) bond appears to lie almost exactly in the map plane drawn. Its outermost contour is shared with the N(1)-C(3) bond adjacent in the cation, curving upward onto that bond. In the map shown, the N(1)-H(1) bond contours give no evidence of having been perturbed because of the interaction with the ring. Although no evidence of the N-H...π(Ph) interaction is seen in the map shown in Figure 84(a),

it does not mean that no such evidence exists. The cut through the C(11) and C(14) atoms of ring 1 will be discussed subsequently in this context. Figure 84(a) is included to illustrate the general features of the ring 1 plane, common to all the [DabcoH][$B(C_6H_5)_4$] ring planes and their maps.

In the same cation, one of the two equivalent C(3)-H(3A) bonds lies above the C(13)-H(13) bond of ring 1 but projects diagonally down and outside the ring. The contours visible in the map in the region of the C(3)-H(3A) bond are somewhat unusual in appearance, being diffuse and centered well off the bond, but this likely occurs because the C(3)-H(3A) bond is only partially coincident with the plane drawn. In any case, the contours observed show no evidence of interaction with the ring 1 plane. In fact, no bond path was ever located for this relatively close physical contact because of its unfavourable geometry.

Figure 85 illustrates the map produced by cutting through the C(21) and C(24) atoms of ring 2. As with ring 1, only two maps are needed to completely describe the ring because it possesses a vertical mirror plane. Ring 2 accepts two unique C-H...π(Ph) type interactions, each formed twice (to equivalent bonds) in the symmetric ring, C(1)-H(1A)...ring 2 and C(4)-H(4B)...ring 2. Although one cation is visible above the ring 2 plane and another is visible below the ring plane in the map shown, neither is oriented for a strong interaction with the ring in this view. Below ring 2, a pair of equivalent C(4)-H(4B) bonds from one cation project on top of one another in the same position, beneath the C(21) side of ring 2. Neither bond lies at all in the plane drawn (no contours are visible on the bonds) so obviously no evidence of interaction with the ring can be observed in this map. Similarly, above the ring 2 plane a second cation

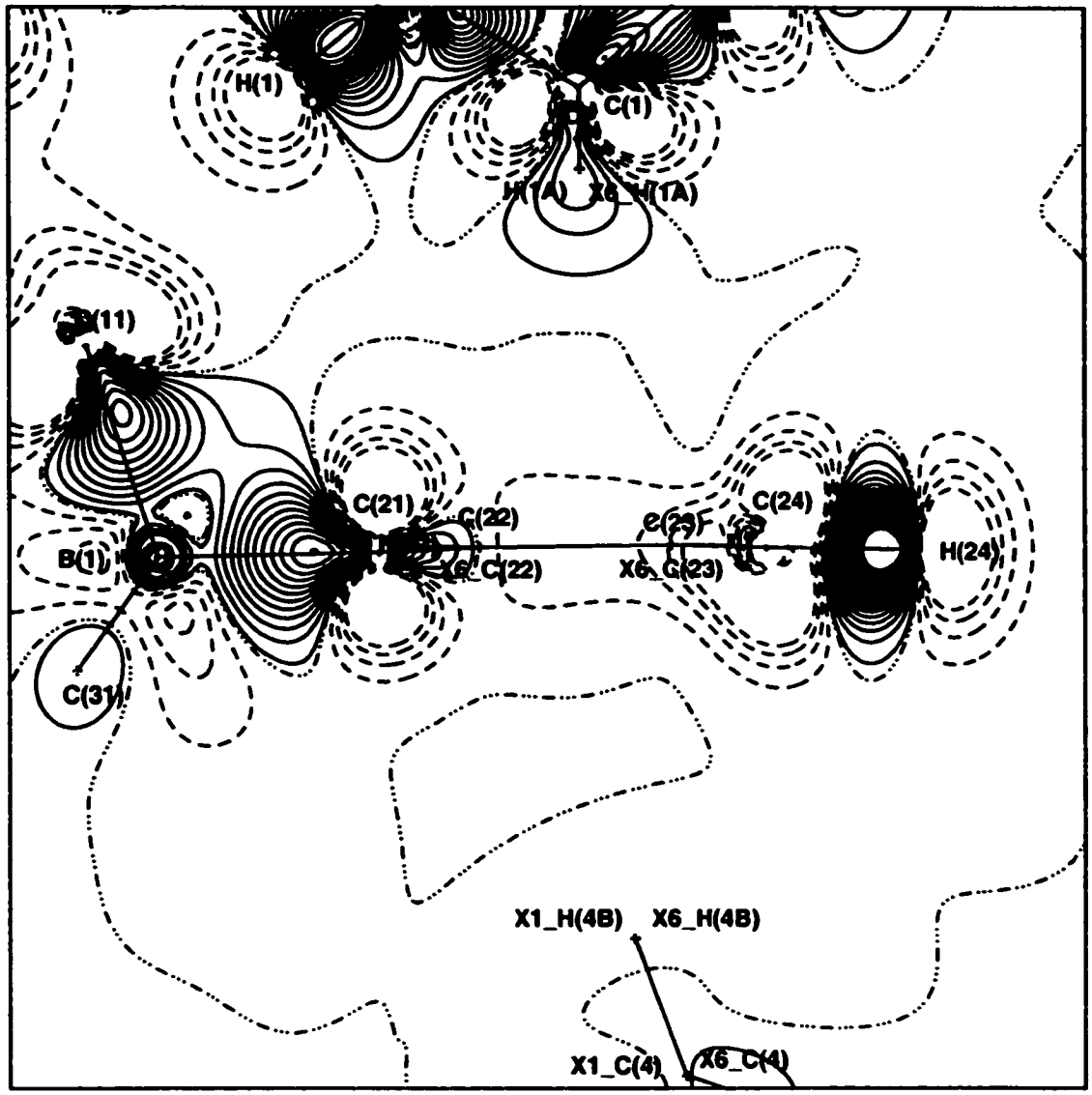

Figure 85. Static deformation density map drawn in the perpendicular plane cutting through the opposing C(21) and C(24) atoms of the anion phenyl ring #2 in the structure of [DabcoH][$B(C_6H_5)_4$]. Positive contours are drawn with solid lines, negative contours with dashed lines and the zero level contour with a {dash dot dot dot} pattern. The contour interval is 0.05 $eÅ^{-3}$. The outline of the remainder of the tetraphenylborate anion has been omitted for clarity.

is observed, with its C(1) atom well centered over the ring and lying directly in the plane of the map. The two equivalent C(1)-H(1A) bonds, sharing a common C(1) atom, must actually come equally into and out of the plane drawn and they also project on top of one another in the map. The few contours observed in this region of the map must lie in the plane bisecting the two C(1)-H(1A) bonds. Although relatively broad and diffuse, they show no evidence of having been affected by participation in the C-H...π(Ph) interactions made to the ring.

The map plotted in the plane cut vertically through the C(31) and C(34) atoms of ring 3 is shown in Figure 86. Ring 3 occupies entirely general positions and so is completely characterized by three maps of this type. The fourth anion is generated from ring 3 by reflection through the vertical mirror plane that bisects the anion. As with ring 2, ring 3 serves as the acceptor in only C-H...π(Ph) type interactions, being involved in a total of six such contacts, not all of which are observed in all of the maps. In the figure shown, ring 2 of a second $B(C_6H_5)_4^-$ anion is visible above the ring plane rather than a cation. The C(23)-H(23) bond of this anion lies above and projects slightly diagonally towards the outside of the C(34)-H(34) bond of the original ring. However, the C(23)-H(23) bond does not lie at all in the plane drawn (no contours are visible on the bond) and consequently can give no indication of any interaction with ring 2. Below the ring plane a cation is visible, oriented in a very symmetrical arrangement. The C(4)-H(4A) and the C(3)-H(3B) bonds project close to one another, lying under the ring 2 plane and pointing almost perpendicularly up towards the ring. The C(1)-H(1A) and C(2)-H(2A) bonds lie under the C(34)-H(34) bond of ring 2 and project nearly

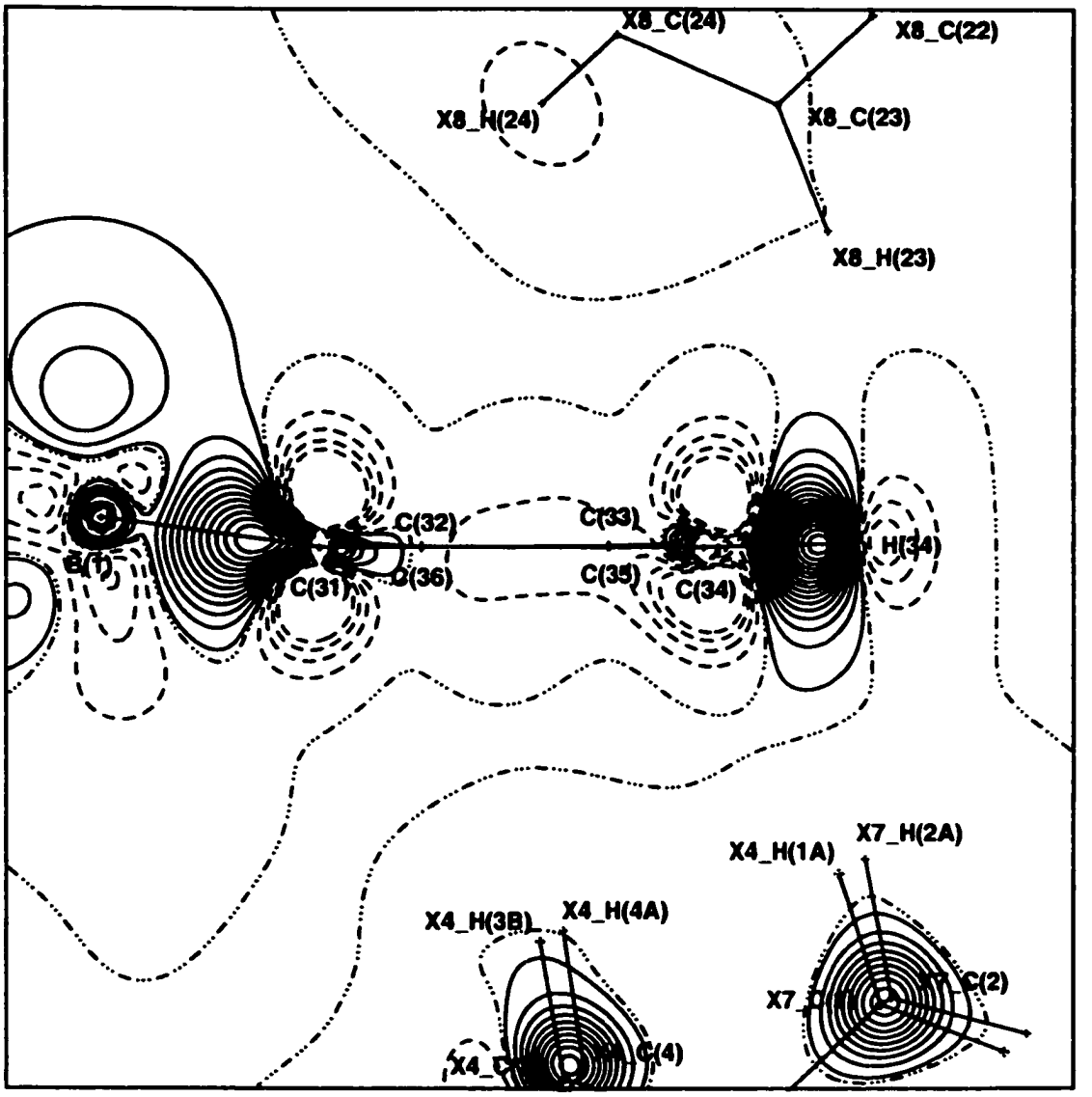

Figure 86. Static deformation density map drawn in the perpendicular plane cutting through the opposing C(31) and C(34) atoms of the anion phenyl ring #3 in the structure of [DabcoH][$B(C_6H_5)_4$]. Positive contours are drawn with solid lines, negative contours with dashed lines and the zero level contour with a {dash dot dot dot} pattern. The contour interval is 0.05 $e\text{Å}^{-3}$. The outline of the remainder of the tetraphenylborate anion has been omitted for clarity.

perpendicularly towards that same ring bond. However, none of these bonds actually lie in the plane drawn, no contours being visible on any of the bonds. In fact, only the C(1)-C(2) and C(3)-C(4) bonds of the cation, which are roughly bisected in the plane drawn, show any visible contours in the map. The C-H bonds of this cation can show no visible effects, as a result of the C-H...π(Ph) interactions made to ring 2, in this plane cut through the C(31) and C(34) phenyl ring atoms.

In the maps illustrated [Figures 84 to 86] and in all the related [DabcoH] [$B(C_6H_5)_4$] anion maps, the features observed at the phenyl ring plane are remarkably regular and consistent. The C-H bond contours of the phenyl rings, when bisected in the planes drawn, are always relatively uniform in appearance. They never show any indication of having been perturbed because of any X-H...π(Ph) interactions made to the rings. This is true for all three unique phenyl rings in the structure. The bond contours are roughly oval shaped and are elongated perpendicular to the ring plane. The outermost C-H bond contours may be somewhat diffuse but they tend to maintain the same oval shape. The bond contours are relatively equal in size and shape, both above and below the ring planes, and around the various rings. No C-H bond in the entire $B(C_6H_5)_4^-$ anion shows any evidence of having been perturbed because of interactions made with the $DabcoH^+$ cation.

The appearance of the ring carbon atoms, when bisected in the map plane, is however somewhat different than had been observed previously. At a number of the carbon atoms, small dense peaks of many contours are visible directly on the ring plane. Although such peaks had never been observed in any of the earlier maps, they are visible at [C(12)', C(13)],

[C(22)] and [C(31),C(34)], respectively, in the figures shown and at many of the other carbon atoms in the remaining [DabcoH][$B(C_6H_5)_4$] maps. They clearly do not arise because of any X-H...π(Ph) interactions made to the ring, being located away from the groups that would be involved. Rather, such peaks can reasonably be attributed to poor fitting of the multipole parameters on the ring carbon atoms and a resulting poor modelling of the C-C bonds in the phenyl rings of the anion, an effect also observed in the inplane maps of the [DabcoH][$B(C_6H_5)_4$] structure. In some of the maps plotted, the small peaks at the ring carbon atoms are slightly elongated, curving off and away from the ring plane [C(23) and C(36)] for some unknown reason. The usual holes of four negative contours are still observed at every ring carbon atom when it is bisected, both above and below the ring plane. However, their size and shape may be somewhat distorted because of the small dense peaks of positive density also present at some of the ring carbon atoms.

None of the maps shown in Figures 84 to 86 have peaks visible anywhere else near the ring plane or the ring carbon atoms. Several of the ring 2 and ring 3 maps, not shown here, do have peaks lying somewhat off the ring plane; specifically such peaks are observed at C(22), C(35) and C(36). However, these peaks are never observed to lie in an area that could be considered representative of one of the C-H...π(Ph) interactions made to that ring. Rather, these must again be minor artifacts of the refinement process.

The results observed for rings 2 and 3 of [DabcoH][$B(C_6H_5)_4$] suggest that the C-H...π(Ph) interactions give rise to no visible characteristic features in the static maps cut through opposing carbon atoms of the anion

phenyl rings. (Rings 2 and 3 do not participate in any N-H...π(Ph) type interactions.) The fact that no specific features can be identified as arising when C-H...π(Ph) interactions occur was also suggested after the analysis of the maps from the $NH_4B(C_6H_5)_4$ structure. These interactions must be too weak to give rise to observable effects in the maps. It would appear that the C-H...π(Ph) contacts must be almost completely electrostatic in nature, with only a very small covalent component at best. The covalent contribution must be too small to give rise to characteristic features in the maps drawn. This is consistent with the conclusions reached after studying the static maps cut through opposing phenyl ring C-C bonds in the anions of the four experimental structures.

The case of the N-H...π(Ph) interactions in general, and of the N(1)-H(1)...ring 1 hydrogen bond of [DabcoH][$B(C_6H_5)_4$] in particular, is rather different. The map drawn through the opposing C(11) and C(14) atoms of ring 1 in the [DabcoH][$B(C_6H_5)_4$] structure is shown in Figure 84(b). Overall, the general map features are consistent with those discussed for the previous [DabcoH][$B(C_6H_5)_4$] maps. The C(14)-H(14) bond of ring 1 shows no evidence of any interaction with the cation; the oval shaped contours are not perturbed in any way, if anything they are denser and more compact than normally observed. Similarly, the C(11)-B(1) bond contours, although the outer two are shared with the adjacent C(21)-B(1) bond, show no indication of having been altered or perturbed because of the interaction made with the cation (unlike the $NH_4B(C_6H_5)_4$ case). There are no peaks visible at either the C(11) or C(14) atoms on or near the ring plane. In fact, these two atoms do not even exhibit the small dense peaks, associated with poor assignment of the multipole populations, that were

observed at many other of the ring carbon atoms in the [DabcoH] [$B(C_6H_5)_4$] maps. The usual holes of four negative contours are observed above and below the ring plane at the carbon atoms bisected in the map.

Below ring 1, two equivalent C(2)-H(2A) bonds of a single cation project perpendicular to, and close to the center of, the original plane. Neither bond, which share a common C(2) atom, lies in the plane drawn (although C(2) does) and the few contours actually visible in the map plane show no evidence of interaction with the ring. In fact, no features characteristic of an X-H...π(Ph) interaction are observed below the ring plane, substantiating the observation that C-H...π(Ph) type contacts have no visible effects in the static maps of the phenyl ring planes cut through opposing carbon atoms.

Above the ring plane, the most important X-H...π(Ph) interaction made in the structure [N(1)-H(1)...ring 1] is clearly visible. No other C-H bonds of this cation are coincident with the map plane, nor do they form any important C-H...π(Ph) interactions to this face of ring 1. The N(1)-H(1) bond of this cation lies completely in the plane plotted, as defined by the symmetry of the system. The outer contours on the dense N(1)-H(1) bond join with those on the adjacent N(1)-C(1) bond of the cation, which also lies in the map plane. The N(1)-H(1) bond projects slightly diagonally toward the C(11) side of the ring but because of the angle made to the ring, the bond contours actually slant down toward the opposite C(14) side of the ring. The N(1)-H(1) bond contours themselves give no visible sign of having been perturbed by involvement in the hydrogen bond. However, there is a small single peak of one contour observed in the map, directly between the N(1)-H(1) bond contours and

C(14) of the anion ring 1. This peak definitely lies in an area that could be characteristic of the N-H...π(Ph) interaction. The N(1)-H(1)...ring 1 centroid type hydrogen bond in the [DabcoH][$B(C_6H_5)_4$] structure is relatively strong, judging from the minimum H(1)...C_{ring} distance. It appears to legitimately give rise to the peak observed in the static map of Figure 84(b), between N(1)-H(1) of the cation and C(14) of the anion phenyl ring, rather than it simply being an artifact of the refinement process. Like the N-H...π(Ph) hydrogen bond in $NH_4B(C_6H_5)_4$, there appears to be a significant covalent component to the N(1)-H(1)...ring 1 hydrogen bond in [DabcoH][$B(C_6H_5)_4$]. Electron density is visibly accumulated in the region between the two interacting groups.

After analysis of the static maps cut through the opposing C-C bonds of ring 1 in the [DabcoH][$B(C_6H_5)_4$] structure [Figure 84 (a) and (b)], a covalent component was postulated for the N(1)-H(1)...ring 1 hydrogen bond but little actual evidence was observed in the maps. The features visible in the static map cut through the C(11) and C(14) ring atoms support the idea that this N-H...π(Ph) hydrogen bond has an important covalent contribution, in addition to its electrostatic component. The bond path for this interaction was subsequently determined to travel from H(1) of the cation to C(14) of ring 1 in the anion, a result in keeping with the observations made after considering all of the static maps cut through the ring 1 plane in the structure of [DabcoH][$B(C_6H_5)_4$].

Ring 1 in the [$C(NH_2)_3$][$B(C_6H_5)_4$]·CH_3CN structure is similar to rings 2 and 3 of [DabcoH][$B(C_6H_5)_4$] in that it does not participate in any N-H...π(Ph) type contacts. Instead, it serves as the acceptor in a number of C-H..π(Ph) type interactions. Ring 1 occupies completely general

positions so it is characterized by three different vertical cuts through the opposing carbon atoms of the phenyl ring. The static map of the cut made through the C(12) and C(15) atoms, the best of ring 1, is shown in Figure 87.

Below the ring 1 plane, the C(24)-H(24) bond from ring 2 of a second anion is visible in all of the maps. It projects under the middle of the ring, almost perpendicular to the ring plane. The C(24)-H(24) bond lies almost exactly in the plane drawn in the C(11)/C(14) map but not in the other two cuts; in the map shown in Figure 87 only a single contour is visible on the bond. In any event, the C(24)-H(24) bond contours show no evidence of having been perturbed by interaction with ring 1 in any of the three maps drawn.

A pair of acetonitrile solvent molecules are situated above the ring 1 plane in the maps of $[C(NH_2)_3][B(C_6H_5)_4]\cdot CH_3CN$. However, in the map shown, and all of the ring 1 maps, only the C(3)-H(61) bond of one of the CH_3CN solvent molecules lies at all in the plane and so is oriented for a possible interaction with the ring. The second, uninvolved CH_3CN molecule was removed from the maps to simplify them. In the map cut through the C(12) and C(15) ring atoms, shown in Figure 87, the C(3)-H(61) bond of the remaining acetonitrile molecule lies centered directly over the middle of the ring and projects almost exactly perpendicular to it. The contours on the C(3)-H(61) bond are again somewhat unusual in appearance. In fact, the contours in the entire methyl region of CH_3CN lie more between the bonds than on them, at least in this view. This is presumably related to the problems encountered in accurately modelling the acetonitrile molecule, and its methyl group in particular, described previously. The

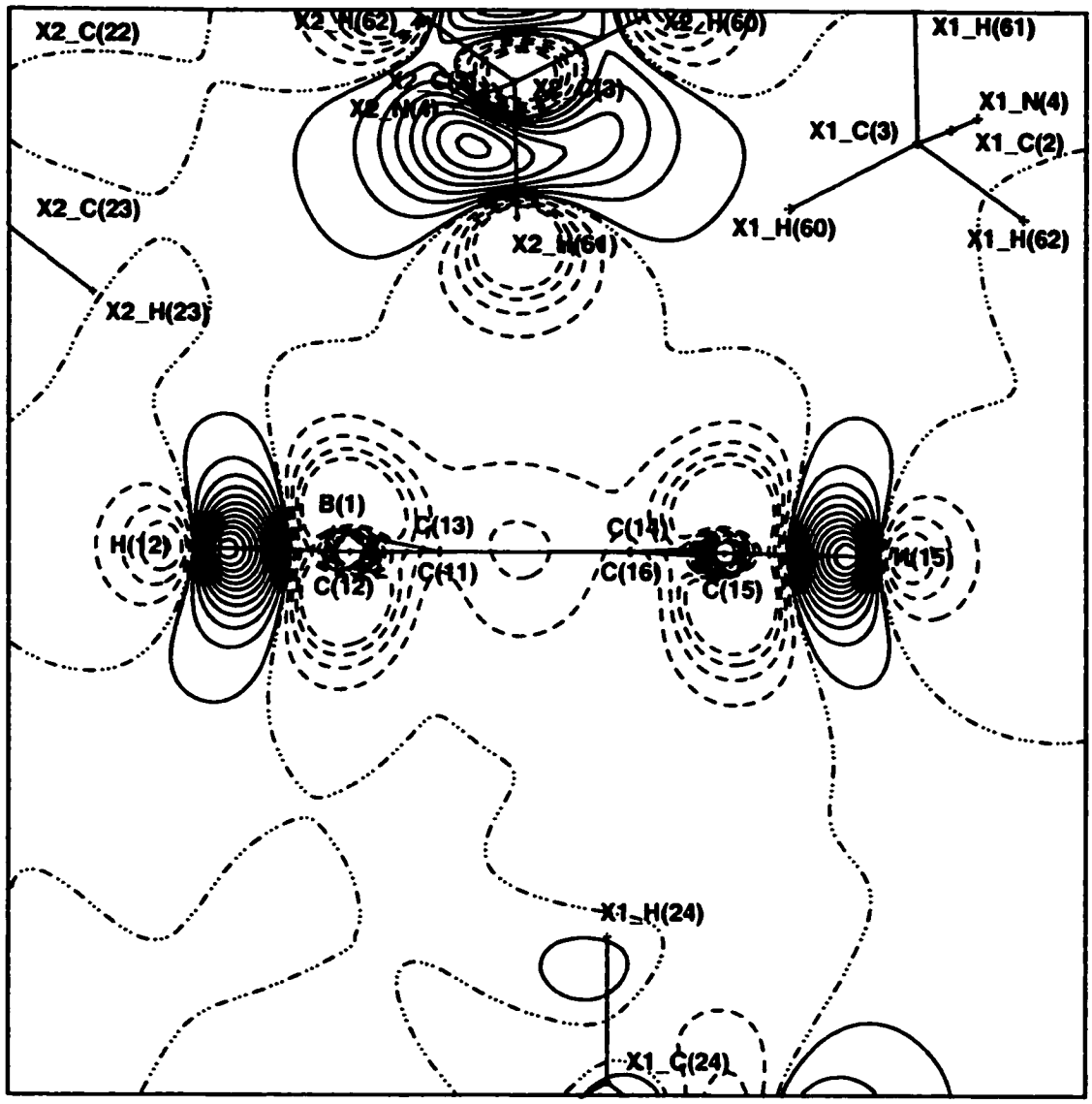

Figure 87. Static deformation density map drawn in the perpendicular plane cutting through the opposing C(12) and C(15) atoms of the anion phenyl ring #1 in guanidinium tetraphenylborate acetonitrile solvate. Positive contours are drawn with solid lines, negative contours with dashed lines and the zero level contour with a {dash dot dot dot} pattern. The contour interval is 0.05 $e\text{Å}^{-3}$. The outline of the remainder of the tetraphenylborate anion has been omitted for clarity.

contours near the C(3)-H(61) bond are broad and curve down toward the ring 1 plane on either side of the bond. However, they show no evidence of any interaction with the ring and CH_3CN does not have any visible effect on the electron density distribution of the ring either.

The C-H bond contours, visible when bisected by the map plane, are regular and uniform in appearance, both above and below the ring plane, and all around the ring. As shown in Figure 87, for the C(12)-H(12) and C(15)-H(15) bonds, the contours have a slightly distorted oval shape and are elongated perpendicular to the bond. They are slightly convex in appearance, curving outward away from the ring plane both above and below the ring, which is rather unusual. The outer contour on each C-H bond is somewhat diffuse, relatively equally above and below the bond. The C-H bond contours are otherwise quite normal in appearance; they are not visibly perturbed in any way because of the C-H...π(Ph) interactions made to the ring.

Similarly, holes of four negative contours are visible above and below the plane at each ring carbon atom, when that atom is bisected in the plane drawn. In this respect the ring carbon atoms all appear completely normal in the static maps drawn. The map shown in Figure 87 has no other visible peaks anywhere near the ring 1 plane, specifically near the C(12) and C(15) atoms. In the other two maps cut through opposing ring carbon toms (those not shown), small peaks are visible at C(11), just above the ring plane, and at C(16), just below the ring plane. In addition, a strange looking, long thin peak runs vertically across the ring plane at C(14). Such a peak was never observed under any other circumstances. None of these peaks is located in a position that could be

considered characteristic of an X-H...π(Ph) type interaction; they all lie very close to the ring 1 plane. The peaks must arise for other reasons which are not immediately apparent.

The maps plotted in vertical planes cut through opposing ring 1 carbon atoms in the structure of $[C(NH_2)_3][B(C_6H_5)_4]\cdot CH_3CN$ are consistent in their features and in agreement with the previous results. The maps show no special features that can be attributed as arising from the C-H...π(Ph) interactions made to the ring. It appears certain that the C-H...π(Ph) type contacts are almost exclusively electrostatic in nature. Any covalent contribution must be so small as to not give rise to any visible effects in the static maps plotted, both those cut through opposing ring carbon atoms and those cut through opposing C-C ring bonds of the $B(C_6H_5)_4^-$ anion.

The static maps drawn through opposing ring carbon atoms for rings 3 and 4 in the structure of $[N(C[NH_2]_2)_2][B(C_6H_5)_4]$ and rings 4 and 2 in the structure of $[C(NH_2)_3][B(C_6H_5)_4]\cdot CH_3CN$ show a number of features, a few of which possibly arise from the N-H...π(Ph) interactions made to the ring. (The features tend to be rather minor in the first ring mentioned for each structure and more pronounced in the second ring listed.) However, the effects observed can be somewhat ambiguous and difficult to interpret, possible true features being intermingled with artifacts from the refinement process. It is more instructive to consider ring 2 from the $[N(C[NH_2]_2)_2][B(C_6H_5)_4]$ and ring 3 from the $[C(NH_2)_3][B(C_6H_5)_4]\cdot CH_3CN$ structures. Although these two rings were found to have the worst inplane static maps in their respective structures (and ring 3 from the structure of $[C(NH_2)_3][B(C_6H_5)_4]\cdot CH_3CN$ was judged to have the worst overall maps of

those studied), they also serve as the acceptors in the two strongest N-H...π(Ph) contacts located in this work [(#1) N(2)-H(2A)...ring 2 in $[N(C[NH_2]_2)_2][B(C_6H_5)_4]$ and (#2) N(3)-H(3B)...ring 3 in the structure of $[C(NH_2)_3][B(C_6H_5)_4]\cdot CH_3CN$]. The static maps cut through opposing carbon atoms for ring 2 in the structure of $[N(C[NH_2]_2)_2][B(C_6H_5)_4]$ will be considered first, since the maps of this structure were found to be of higher overall quality than those of $[C(NH_2)_3][B(C_6H_5)_4]\cdot CH_3CN$ and it forms the strongest individual N-H...π(Ph) interaction studied. After discussion of all the remaining maps from the $[N(C[NH_2]_2)_2][B(C_6H_5)_4]$ structure, the $[C(NH_2)_3][B(C_6H_5)_4]\cdot CH_3CN$ maps will be discussed as a final group.

Ring 2 in the structure of biguanidinium tetraphenylborate occupies completely general positions and is characterized by three different static maps cut through opposing carbon atoms of the ring. The map plotted in the vertical plane passing through the C(23) and C(26) atoms of ring 2 is shown in Figure 88, since it illustrates the various interactions made to the ring most clearly. A cation is observed above ring 2 in all of the maps drawn, with its N(2)-H(2A) bond oriented towards the ring plane. Based on its geometry, the N(2)-H(2A)...ring 2 hydrogen bond was determined to have a centroid type geometry with a close single contact made to C(26) of the ring. As expected from this, the N(2)-H(2A) bond lies almost exactly in the plane of the map shown in Figure 88 [cut through C(23) and C(26)] but is only partially coincident with the planes of the other two maps. In the map shown, the outer contours on the N(2)-H(2A) bond are shared, on both sides of the bond, with density on adjacent bonds of the cation, curving upwards towards those bonds. The contours on the N(2)-H(2A) bond show no evidence of an interaction with the ring, in any

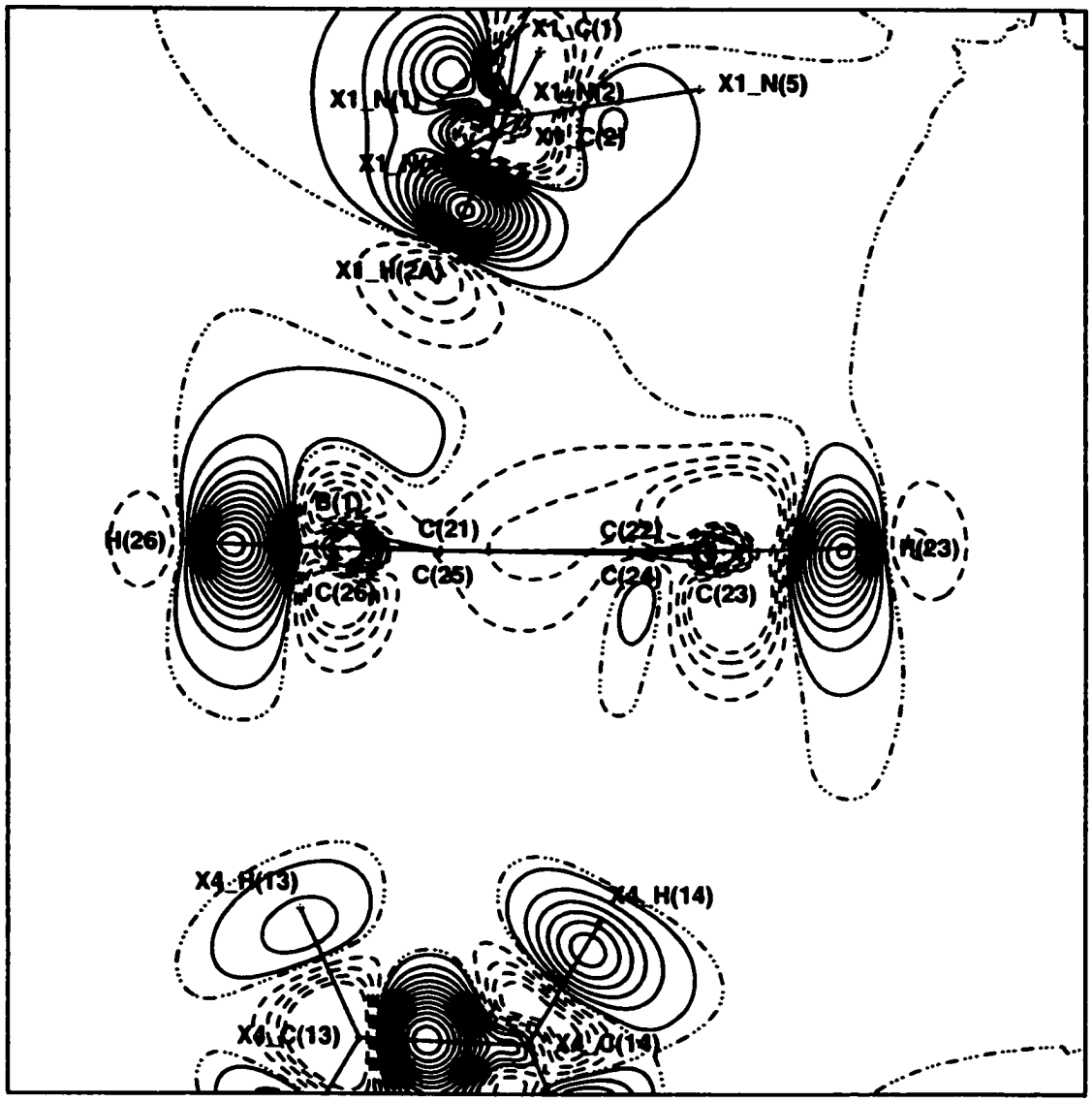

Figure 88. Static deformation density map drawn in the perpendicular plane cutting through the opposing C(23) and C(26) atoms of the anion phenyl ring #2 in biguanidinium tetraphenylborate. Positive contours are drawn with solid lines, negative contours with dashed lines and the zero level contour with a {dash dot dot dot} pattern. The contour interval is 0.05 $eÅ^{-3}$. The outline of the remainder of the tetraphenylborate anion has been omitted for clarity.

of the maps of this type drawn.

Below ring 2 of the original anion, ring 1 of a second anion is visible in all three maps. Both the C(13)-H(13) and the C(14)-H(14) groups of this ring 1 form C-H...π(Ph) type interactions with ring 2. The C(13)-H(13)...ring 2 interaction was classified as an edge type hydrogen bond, involving the C(25)-C(26) bond of ring 2, based on its geometry. The C(14)-H(14)...ring 2 interaction is a centroid type hydrogen bond which also makes its closest contact to one edge of ring 2, to C(22)-C(23). In the static maps drawn through opposing carbon atoms of ring 2, the C(13)-H(13) bond always lies predominantly out of the plane mapped; in the figure shown there are only two contours visible on the projected bond. In contrast, the C(14)-H(14) bond lies substantially in the plane drawn in both the C(22)/C(25) cut and the C(23)/C(26) cut (shown). Neither set of C-H bond contours is perturbed by the interactions made with the ring in any of the maps drawn.

At the ring 2 plane, peaks are observed on several of the carbon atoms, when they are bisected by the map plane. No peaks are observed at the C(21), C(22), C(24) or C(26) atoms when they lie on the plane. In the map shown in Figure 88, there is a small peak visible just below the ring plane at the C(23) atom, which is bisected by the vertical plane drawn. The peak does not occur in an area where it could be attributed to an X-H...π(Ph) type contact, lying close to the ring plane rather than between any two interacting groups. It must arise for some other reason; several such peaks had been observed in previous maps examined. The final carbon atom of ring 2, C(25), shows peaks above and below the ring plane, both lying well off the plane in areas that could be characteristic of

X-H...π(Ph) interactions. The peak at C(25) below the ring plane lies directly between the two anion phenyl rings but is very small. Also, it is not positioned in an area that would be expected for either of the specific C-H...π(Ph) hydrogen bonds formed to ring 2. The peak does not visibly lie between either of the interacting C-H groups of the anion rings in the static maps. It is more likely an artifact of the refinement process rather than a true feature arising from one of the C-H...π(Ph) interactions, especially considering the previously made observation that such C-H...π(Ph) contacts generally do not give rise to any characteristic features in the static maps drawn through opposing phenyl ring carbon atoms.

The final peak is observed well above the ring plane at C(25) when that atom is bisected in the static map drawn. The peak, of one single contour, lies directly between the N(2)-H(2A) group of the cation and C(25) of ring 2 in the anion. It appears that it could arise because of the formation of the N(2)-H(2A)...ring 2 hydrogen bond. It is somewhat surprising that a peak is observed between H(2A) and C(25), rather than at the closer C(26) atom, but a rather different (but complementary) effect is observed at C(26) which will be discussed next. Since the N(2)-H(2A)...ring 2 interaction is a strong, centroid type hydrogen bond it is not unreasonable that its effects might be observed at other ring carbon atoms in addition to C(26).

The contours on several of the ring 2 C-H bonds, when bisected in the plane of the map drawn, are very unusual in appearance. The outermost contours on the C(22)-H(22), C(24)-H(24) and C(26)-H(26) bonds are visibly and distinctly perturbed in a manner never previously observed. An example

of this type of perturbation is shown in Figure 88 where the outer contour on the C(26)-H(26) bond curves up and over the ring 2 plane, to lie in the region between C(26) and the cation. There is a significant area of accumulated density (1 contour in height) between C(26) and the N(2)-H(2A) group of the cation. This density appears to have been perturbed into an area characteristic of the N-H...π(Ph) interaction even though it lies on a σ type C-H bond. The visible accumulation of density in the region between the cation and the anion ring suggests a significant covalent component to this N-H...π(Ph) hydrogen bond.

It is not only the C(26)-H(26) bond of ring 2 that participates in the N(2)-H(2A)...ring 2 interaction. The C(22)-H(22) bond shows a similar perturbation of its outer contour into the region between the ring and the cation. This contour curves up and around to lie above the C(22) atom but covers a smaller area than the peak above C(26) arising from the perturbed C(26)-H(26) bond contour. Similarly, the outer contour on the C(24)-H(24) ring bond is affected, but surprisingly in this case, it curves around both above and below the ring 2 plane. Although above the ring plane this density lies in an area that suggests it could result from the N(2)-H(2A)...ring 2 interaction, below the ring plane no such X-H...π(Ph) interaction involving C(24) exists. The reason the C(24)-H(24) bond density curves off the bond below the ring plane is not certain.

Around the ring 2 plane the following features are clearly visible in the static maps drawn. The density on the C(26)-H(26), C(24)-H(24) and C(22)-H(22) bonds is perturbed into the region between the ring 2 plane and the N(2)-H(2A) bond of the cation. The outer contour on each bond curves up and around, off the bond toward the ring carbon atom involved.

The perturbation is greatest on the first bond mentioned and least on the C(22)-H(22) bond. In addition, a peak lying in an area suggestive of an N-H...π(Ph) interaction is observed at C(25) of the ring. For the N(2)-H(2A)...ring 2 interaction, the H(2A)...C_{ring} distances increase in the order C(26) < C(21) < C(25) < C(22) < C(24) < C(23). The magnitude of the features observed in the static maps also generally agree with this order, the largest effect being observed on the C(26)-H(26) bond and no visible effect being observed at C(23). The entire ring is affected by the interaction as might be expected for a strong centroid type hydrogen bond, the strongest investigated experimentally. The only significant exception occurs at C(21) where no peaks are observed and where the C(21)-B(1) bond contours are not perturbed (although such an effect had been observed previously on the C(11)-B(1) bond in the $NH_4B(C_6H_5)_4$ structure). Overall, the observations suggest that the strong N(2)-H(2A)...ring 2 hydrogen bond has a large effect on the complete set of static maps drawn through opposing carbon atoms of the anion ring 2 in $[N(C[NH_2]_2)_2][B(C_6H_5)_4]$. The strength of this interaction is enough to significantly perturb the σ electron density of three of the ring 2 C-H bonds into the region between the cation and the anion, an effect never previously observed. However, there is a parallel in the observed perturbation of the C(11)-B(1) σ bond density because of the N(1)-H(1)...ring 1 hydrogen bond in the structure of $NH_4B(C_6H_5)_4$. In addition, a peak of one contour is observed between C(25) of the anion and the cation, a more typical feature that has been observed previously in maps illustrating other N-H type interactions. Conversely, the large number of features visible in the static maps of ring 2 suggest that the N(2)-H(2A)...ring 2 centroid type

hydrogen bond is stronger than the other examples of N-H...π(Ph) interactions studied previously. It also appears that there is a significant covalent contribution to this interaction, perhaps even larger than that observed in the other experimental examples.

Having studied the ring 2 maps from the $[N(C[NH_2]_2)_2][B(C_6H_5)_4]$ structure and reached certain conclusions about the features arising from the X-H...π(Ph) hydrogen bonds made to that ring, it is possible to return to the maps from rings 3 and 4 of the same structure to see if they also show similar features in the presence of X-H...π(Ph) interactions. The maps of both rings show a variety of effects some of which actually appear to arise from the X-H...π(Ph) type contacts formed. The ring 3 maps have fewer visible features than those of ring 4 and will be discussed first. Each ring occupies general positions and thus requires a total of three maps to define the planes cut through opposing ring carbon atoms. The inplane maps of rings 3 and 4 were judged to be of intermediate quality in the structure of $[N(C[NH_2]_2)_2][B(C_6H_5)_4]$, worse than those of ring 1 but better than those of ring 2.

Above the ring 3 plane in all three of the static maps plotted, a cation lies in a position suitable for possible interaction with the ring. The N(3)-H(3A) bond of the cation remains quite well centered over the ring plane in all of the maps, typical of a centroid type hydrogen bond. The geometry of the N(3)-H(3A) interaction also suggested a centroid type hydrogen bond, with the closest contact made to C(35) and C(36) of the ring. As expected from this, the N(3)-H(3A) bond lies substantially in the plane drawn in the C(32)/C(35) and C(33)/C(36) cuts but not in the C(31)/C(34) map. In none of the maps do the N(3)-H(3A) bond contours show

any visible evidence of having been affected by the interaction made to the ring.

Below the ring 3 plane, rings 1 and 2 from a second anion are visible in all three of the maps. The geometry analysis had shown the C(12)-H(12) bond of this anion to be involved in a single atom type hydrogen bond [to C(34)] with ring 3 of the original anion. The C(12)-H(12) bond is at least partially coincident with the plane drawn only in the C(31)/C(34) cut, reasonable considering the geometry of the interaction. The C(12)-H(12) bond contours visible in the C(31)/C(34) map also show no evidence of having been perturbed by the interaction made to the ring.

The previous results suggest that the C(12)-H(12)...ring 3 hydrogen bond should not give rise to any features, either at the cation or at the anion plane, in any of the static maps plotted. The N(3)-H(3A)...ring 3 centroid geometry hydrogen bond is a different matter. It is the second strongest N-H...π(Ph) type interaction in the structure and one of the strongest (#4) of the 14 such interactions studied overall in the four experimental structures. Thus, it might reasonably be expected to give rise to certain characteristic features in the static maps plotted, including peaks between the cation and anion groups.

The ring 3 C-H bond contours are all very regular and uniform in appearance, as observed when they are bisected in one of the map planes drawn. The C-H bond contours are all oval shaped and elongated perpendicular to the bond, relatively equally around the ring. The outer bond contours are always somewhat diffuse, both above and below the ring plane. However, all of the ring 3 C-H bond contours show no evidence of having

been perturbed because of the interactions accepted by the ring. In no case do the C-H contours curve off the bond back over the ring plane, into the area between the ring and N(3)-H(3A) of the cation, as had been observed in the ring 2 maps from the same structure.

The N(3)-H(3A)...ring 3 hydrogen bond is relatively strong and yet in the ring 3 maps there is never any involvement of the C-H ring bonds in the interaction. This suggests that only under special circumstances, the strongest N-H...π(Ph) hydrogen bonds studied experimentally [the N-H...π(Ph) interaction made to ring 2 in $[N(C[NH_2]_2)_2][B(C_6H_5)_4]$ is the strongest of the examples studied], are the interactions strong enough to involve the C-H bonds of the ring. Under any other conditions, even the second strongest N-H...π(Ph) hydrogen bond in the $[N(C[NH_2]_2)_2][B(C_6H_5)_4]$ structure, the C-H bond contours show no evidence of interaction in the static maps drawn through opposing ring carbon atoms.

Holes of four negative contours are visible at every ring carbon atom, both above and below the ring plane, when the atom is bisected in the map plane. In this respect the static maps of ring 3 are completely normal in appearance. In addition, a number of other peaks are observed in the maps, close to certain of the ring carbon atoms. No peaks are observed at either the C(31) or C(35) atoms. At C(32), a strange looking peak, similar to several observed in the $[DabcoH][B(C_6H_5)_4]$ maps, is visible. It appears to arise from poor assignment of the multipole parameters on the C(32) atom. However, for some reason it then expands and curves upward away from the ring plane. Similar behaviour was again also observed at several of the atoms in the $[DabcoH][B(C_6H_5)_4]$ maps. The peak at C(32) does not lie in a region considered to be representative of an

X-H...π(Ph) interaction, being found too close to the ring plane. A peak of one contour is observed just above the ring plane at C(34) and a similar small peak is observed just below the ring plane at C(36). Both peaks again lie close to the ring 3 plane, not in areas characteristic of an X-H...π(Ph) interaction. None of these peaks appear to arise from the X-H...π(Ph) interactions made to the ring; they must occur for some other reason(s), likely as artifacts of the multipole refinement process.

This leaves only C(33), where a small peak is observed directly between the ring plane and N(3)-H(3A) of the cation. This peak does occur in an area where it might have arisen because of the N-H...π(Ph) interaction made to the ring. However, it is unlikely that this is so, since the N(3)-H(3A)...ring 3 hydrogen bond forms its closest contacts to C(35) and C(36). The peak at C(33) also appears to arise for some reason unrelated to the N(3)-H(3A)...ring 3 hydrogen bond.

The static maps drawn in vertical planes cut through opposing carbon atoms of the anion phenyl ring 3 in the structure of $[N(C[NH_2]_2)_2][B(C_6H_5)_4]$ do not show any features identifiable as characteristic of the X-H...π(Ph) interactions made to the ring. This was also observed for the ring 1 maps from the same structure. However, the ring 2 maps showed a number of features attributed to the N(2)-H(2A)...ring 2 hydrogen bond, the strongest studied in this work. It would appear that only for very strong N-H...π(Ph) hydrogen bonds do characteristic effects arise in the static maps drawn, because of the redistribution of the electron density caused by the interaction.

Similar to the maps of ring 3 from $[N(C[NH_2]_2)_2][B(C_6H_5)_4$, the ring 4 maps show a number of features that could arise from X-H...π(Ph) contacts

made to the ring. In fact, the ring 4 maps show an even greater array of effects requiring assignment than the ring 3 maps. The ring 3 maps were ultimately found to have no features that could be assigned unambiguously as arising from the X-H...π(Ph) interactions accepted by the ring. In contrast, features attributable to the X-H...π(Ph) interactions formed do appear to be observed in the ring 4 maps cut through opposing ring carbon atoms in the structure of $[N(C[NH_2]_2)_2][B(C_6H_5)_4]$. The X-H...π(Ph) interactions involving ring 4 as the hydrogen bond acceptor include two of the weaker N-H...π(Ph) type hydrogen bonds studied experimentally and one relatively average strength C-H...π(Ph) contact. The two N-H...π(Ph) interactions arise from different halves of the same cation, so do not form a "pincer" type arrangement to the ring. Because they are relatively weak, no effects are expected to be observed in the static maps attributable to any of the X-H...π(Ph) interactions formed by ring 4. Similar interactions made to rings 1 and 3 in this structure were found not to give rise to any visible effects in the corresponding static maps.

In all the static maps plotted for ring 4, ring 1 of a second tetraphenylborate anion is visible below the horizontal ring plane. The C(15)-H(15) bond of this ring forms a centroid geometry hydrogen bond to ring 4, making the closest physical contact to C(41) and C(42) of the ring. The C(15)-H(15) bond lies well centered under the ring and projects slightly diagonally towards the C(41) side of the ring. The bond lies almost exactly in the map plane in each of the three cuts plotted. However, in none of the maps do the C(15)-H(15) bond contours show any evidence of having been perturbed because of the C-H...π(Ph) interaction made with ring 4.

Above the ring 4 plane a single cation is visible in each of the maps. There are two N-H...π(Ph) interactions formed between this cation and ring 4. The first, N(5)-H(5A)...ring 4, was determined to be an edge type hydrogen bond [to C(45)-C(46)] based on its geometry. The second, N(3)-H(3B)...ring 4, was also predicted to have an edge type hydrogen bond geometry [to C(42)-C(43)] but was subsequently found to have an unusual bond path beginning from N(3) rather than from the expected H(3B). The latter is the weakest of the experimental N-H...π(Ph) hydrogen bonds studied, while the former is also relatively weak. In combination, they would at best be expected to give rise to only very minimal features in the static maps plotted. Neither bond lies completely in any of the planes mapped through opposing ring carbon atoms, as often observed for edge type interactions. Where contours are visible on the N-H bonds, they show no real evidence of having been affected because of the interactions made with the ring.

The ring 4 plane can be completely described by compiling the results from the three individual cuts made through opposing pairs of ring carbon atoms. Around the ring the C-H bond contours, visible when bisected in the plane of the map, are relatively normal in appearance except for those on the C(44)-H(44) bond. On the C(44)-H(44) bond the outer two contours curve up and around to lie over the ring plane above C(44). The C(44)-H(44) bond density is perturbed into the region between the anion ring and the cation, an effect that could signify formation of an interaction between the two groups. Such an effect was also observed in the ring 2 maps of the $[N(C[NH_2]_2)_2][B(C_6H_5)_4]$ structure. However, the question remains as to whether this is a legitimate feature of the N-H...π(Ph)

interactions made to ring 4.

The two N-H...π(Ph) edge type hydrogen bonds made to the top face of the ring 4 plane in $[N(C[NH_2]_2)_2][B(C_6H_5)_4]$ can be written in abbreviated form as N(3)-H(3B)...C(42)-C(43) and N(5)-H(5A)...C(45)-C(46). They are both weak interactions on the relative scale of the experimental examples studied. It is surprising, therefore, that the only C-H bond contours visibly affected in the maps drawn are those on the C(44)-H(44) bond for two main reasons. The two N-H...π(Ph) interactions made to ring 4 are both very weak. Somewhat similar but slightly stronger N-H...π(Ph) interactions were observed to have no effects on the C-H bond contours of rings 1 and 3 in $[N(C[NH_2]_2)_2][B(C_6H_5)_4]$ and in the structures of $NH_4B(C_6H_5)_4$ and [DabcoH]$[B(C_6H_5)_4]$. It would be unusual if the two weak interactions to ring 4 in $[N(C[NH_2]_2)_2][B(C_6H_5)_4]$ were sufficient, even in combination, to perturb the C-H bond contours. In addition, the two interactions made to ring 4 involve principally the two opposing C(42)-C(43) and C(45)-C(46) edges of the ring. It makes little sense that the only C-H bond contours affected by these interactions would be those least involved, on the C(44)-H(44) bond. This leads to the conclusion that the perturbation observed at the C(44)-H(44) bond contours cannot arise because of the two N-H...π(Ph) interactions made to ring 4. In this case, the perturbation must occur for some other reason.

In the maps cut through the opposing atoms of ring 4 in the anion of $[N(C[NH_2]_2)_2][B(C_6H_5)_4]$, features of interest are also visible at or near several of the ring carbon atoms themselves, when they are bisected in the map plane. No peaks of any type are observed at the C(43), C(44) or C(45) atoms. However, at C(42) and C(46) peaks are observed above the

ring, between the anion and the N-H groups of the cation. At C(42), the peak lies directly between the ring and the N(3)-H(3B) group and could reasonably be considered characteristic of the N(3)-H(3B)...C(42)-C(43) interaction. At C(46), a peak is also observed between ring 4 and the cation. Again, it could reasonably arise from the N(5)-H(5A)...C(45)-C(46) interaction, although in the appropriate map [C(43)/C(46)] it appears to lie more towards the N(3)-H(3B) bond than N(5)-H(5A) of the cation. Even more unusual, is the peak located at C(41) below the ring 4 plane. It appears to lie directly between C(41) and the C(15)-H(15) group of ring 1 from a second anion, in an area characteristic of X-H...π(Ph) type interactions. This is a most uncommon observation; all the other C-H...π(Ph) contacts examined were found not to give rise to any features attributable to the interaction in the static maps drawn. Yet, in this case, it appears that the peak observed at C(46) could legitimately arise because of the C(15)-H(15)...ring 4 interaction formed. The minimum H(15)...C_{ring} distance in this contact is not particularly short [H(15)...C(41) = 2.952Å]. It is surprising that the very average C(15)-H(15)...ring 4 interaction should give rise to a plausible, observed effect in the static maps when all the other C-H...π(Ph) interactions studied, even those with closer contacts, did not. There is no obvious reason that this should occur.

The two N-H...π(Ph) interactions made to ring 4 are relatively weak. Again, it is somewhat surprising that they both give rise to peaks [at C(42) and C(46)] in the appropriate static maps when stronger interactions made to rings 1 and 3 in the same structure did not give rise to any corresponding peaks. There are a number of possible explanations for this observation. The peaks observed in the ring 4 maps may be artifacts of the

refinement process that simply happen to occur in positions that coincide with those that would be predicted from the geometries of the N-H...π(Ph) interactions made to the ring. These then might be misinterpreted as arising because of the N-H...π(Ph) interactions, when in fact they do not. Or, the peaks observed may truly arise because of the N-H...π(Ph) interactions formed to the ring. Why they should be observed here and not in other similar cases is uncertain. It is possible that the two weak N-H...π(Ph) hydrogen bonds made to one face of ring 4 act in a concerted manner to have a larger than expected effect in the static maps plotted. However, if this was true, a similar effect should have been observed in the maps of ring 1 where a "pincer" type arrangement of two N-H...π(Ph) hydrogen bonds is formed. Or, in some instances it may have to do with the way the map planes are defined and the very low levels of electron density involved. The planes are defined by the ring carbon atoms rather than by the hydrogen bonds themselves. Thus, sometimes peaks may not be observed when they are expected, simply because the hydrogen bond does not lie exactly in the map plane drawn. The small accumulation of electron density expected for the stronger N-H...π(Ph) type interactions (the peak is usually only one contour and that contour is drawn at the $+0.015 e\text{Å}^{-3}$ level) may lie slightly out of the map plane plotted in some cases because of the way that plane has been defined. This could result in peaks not being observed in certain instances when "visible" interactions actually are formed. However, it is difficult to define the map planes in any other reasonable way. It is impossible to tell from the evidence available if or which of these alternate theories is correct in the case of the $[N(C[NH_2]_2)_2][B(C_6H_5)_4]$ structure.

It is possible to briefly summarize the conclusions reached after studying the $[N(C[NH_2]_2)_2][B(C_6H_5)_4]$ maps through opposing pairs of carbon atoms in the four anion phenyl rings. Neither the maps of ring 1 nor ring 3 were found to have any significant or characteristic features that could be assigned to the X-H...π(Ph) [X = N or C] interaction(s) made to the ring. Ring 1 forms three weak N-H...π(Ph) hydrogen bonds, two to a single face of the ring in a "pincer" type arrangement, while ring 3 participates in a single, stronger N-H...π(Ph) hydrogen bond. It would appear that often the N-H...π(Ph) interactions formed are not sufficient to visibly affect the electron density in the maps drawn. However, ring 4 in the same structure also accepts only a pair of very weak N-H...π(Ph) interactions to one face of the ring. And yet, in the ring 4 maps features that could be attributed to the hydrogen bonds were observed, in the form of single peaks lying directly between the interacting N-H groups of the cation and the anion phenyl ring. Under certain conditions, even weak N-H...π(Ph) interactions must be capable of giving rise to visible perturbations of the electron density in the static maps plotted. The exact reason(s) that this occurs in some cases and not on others is uncertain. Other peaks were sometimes observed in the static maps, particularly in those of rings 3 and 4. However, these peaks tend to lie on or close to the ring plane. They do not appear to arise because of the N-H...π(Ph) interactions but for other reason(s). In addition, the C-H...π(Ph) interactions do not appear to have any visible affect on the static maps drawn in the vast majority of the cases studied.

This leaves only ring 2 of the anion in the $[N(C[NH_2]_2)_2][B(C_6H_5)_4]$ structure to be discussed. The N-H...π(Ph) hydrogen bond formed to ring 2

is not only the strongest in the structure but the strongest studied overall in this work. Although the quality of the ring 2 maps was judged to be the worst in the structure (based on a comparison of the inplane static maps), the features observed provide ample evidence of the interaction occurring between the cation and the anion ring. Very strong N-H...π(Ph) hydrogen bonds appear to give rise to a variety of significant effects in the static maps plotted. As well as the characteristic peaks (located between the interacting N-H group and the appropriate C_{ring} atom), perturbation of the density on the C-H bonds is also observed all around the ring. The entire ring is involved as the acceptor when the strongest N-H...π(Ph) hydrogen bonds are formed. In addition to the π electron density of the ring, traditionally viewed as the acceptor in such a hydrogen bond, σ electron density is also perturbed when the interaction is formed to the ring.

The $[N(C[NH_2]_2)_2][B(C_6H_5)_4]$ results are consistent with the observations made previously for the $[DabcoH][B(C_6H_5)_4]$ and $NH_4B(C_6H_5)_4$ structures. In particular, the C(11)-B(1) bond of the anion in $NH_4B(C_6H_5)_4$ was also found to be perturbed in the maps drawn to investigate the N-H...π(Ph) hydrogen bond in that structure. Involvement of the σ electron density (in addition to the π electron density of the ring) in the interaction appears to be a characteristic feature of the strongest N-H...π(Ph) hydrogen bonds investigated experimentally. The electron density distribution of the entire ring is affected by its participation in such a strong interaction. The postulated involvement of the σ electron density of the ring C-H and C-B bonds in some N-H...π(Ph) interactions does not appear to have been suggested previously in the literature.

The static maps drawn through opposing carbon atoms of the anion rings 4 and 2 from the structure of $[C(NH_2)_3][B(C_6H_5)_4]\cdot CH_3CN$ show features similar to those observed in the maps of rings 3 and 4, respectively, from the structure of $[N(C[NH_2]_2)_2][B(C_6H_5)_4]$ (just described). The ring 4 maps were determined to be the best in the structure, based on a comparison of the inplane static maps. The ring 4 maps also show relatively fewer features than those visible in the ring 3 maps. For these reasons, the ring 4 maps will be discussed first, followed by those of ring 2.

Below the ring 4 plane, ring 3 of a second tetraphenylborate anion and a cation are visible in all three of the maps drawn. However, in none of the maps are any bonds coincident with the planes plotted; no contours are observed on any of the projected bonds. In the case of ring 3 from the second $B(C_6H_5)_4^-$ anion, the C(34)-H(34) bond is directed perpendicularly towards the ring 4 plane. The C(34)-H(34) bond was found (by geometry) to form a close contact to C(42) of ring 4 and subsequently this was determined to be an H...H type interaction [H(34)...H(42)]. No evidence of this interaction is observed in any of the maps at either bond on either ring. In the case of the cation lying below the ring plane, the N(2)-H(2B) bond is oriented roughly parallel to the ring 4 plane, while the N(2)-H(2A) bond projects diagonally up towards the ring plane. No geometrically close contact (less then 3Å) was located between the ring and either of these groups and no evidence of an interaction is observed in any of the maps. For these reasons, features would not be expected to arise in the ring 4 maps below the ring plane and, in fact, no significant features are observed. The contours on all the C-H bonds of ring 4 are quite regular overall and uniform in appearance below the ring 4 plane. Small peaks are

observed below the ring plane at the C(42) and C(44) atoms. However, these peaks originate at the ring plane and extend only slightly below the ring. They do not lie in an area considered to be characteristic of X-H...π(Ph) type interactions, nor are any such interactions formed to this face of ring 4. The peaks observed, similar to those seen in previous maps, must arise for other reasons. The results are entirely consistent with earlier observations made.

Above the ring 4 plane, a cation lies in an orientation suitable for interaction with the ring. Although both the N(3)-H(3A) and N(1)-H(1B) bonds of the cation project towards the ring plane in the static maps, N(1)-H(1B) actually is involved in the strong, traditional hydrogen bond, $[N(1)\text{-}H(1B)]_{cation}\cdots[N(4)]_{solvent}$, and makes no significant contact with ring 4. The N(3)-H(3A)...ring 4 interaction was determined to have a centroid type geometry, with the closest contact made between H(3A) and C(44). As expected for a centroid type hydrogen bond, the N(3)-H(3A) bond remains well centered over ring 4 in all of the maps, although it does not always project perpendicular to the ring plane. Rather, it projects toward the C(43)-C(44) side of the ring. Only two to four contours are observed on the N(3)-H(3A) bond in the three maps drawn through opposing carbon atoms of phenyl ring 4. Similarly few contours were observed on this bond in the inplane static maps of the guanidinium cation, meaning that the N(3)-H(3A) bond must actually be nearly coincident with each of the map planes drawn. The contours on the N(3)-H(3A) bond are somewhat unusual in appearance as well. They tend to be quite diffuse, curving upwards off the bond to join with density on adjacent cation bonds including C(1)-N(3). However, despite this they show no visible sign of having been perturbed

by interaction with ring 4. In fact, a much more obvious interaction is observed in the C(41)/C(44) cut, involving the N(3)-H(3B) bond of this same cation and ring 3 of the anion, an interaction that will be discussed in the final section on $[C(NH_2)_3][B(C_6H_5)_4]\cdot CH_3CN$.

As already mentioned, the contours on the C-H bonds of ring 4 are all quite regular and relatively uniform in appearance around the ring. The contours on all the C-H bonds are elongated perpendicular to the ring plane resulting in their having the usual oval shape. The outer bond contour tends to be somewhat diffuse, relatively equally on all the bonds, and above and below the ring plane. As with the other phenyl rings in the $[C(NH_2)_3][B(C_6H_5)_4]\cdot CH_3CN$ structure, the contours on the ring 4 C-H bonds are slightly convex in shape, curving outward away from the ring both above and below the plane. This was not observed for the C-H bonds in the anions of any other of the structures studied. The C(41)-B(1) bond contours are also quite regular in appearance. Although the outermost contour is shared above the ring 4 plane with density on the adjacent C(31)-B(1) bond, this density is not perturbed towards the cation. In addition, none of the C-H bond contours show any sign of having been significantly perturbed by the interactions made to the ring. This is true both below the ring 4 plane, where no close interactions were identified in the maps, and above it, where the single N(3)-H(3A)...ring 4 centroid type hydrogen bond is formed. This average strength N-H...π(Ph) interaction cannot be enough to cause any perturbation of the C-H bond densities. The σ density of the ring C-H and C-B bonds is not involved in the N(3)-H(3A)...ring 4 hydrogen bond, as expected from previous observations made; only the very strongest interactions studied experimentally

were found to perturb the σ electron density of the anion phenyl ring.

The usual holes of four negative contours are observed above and below the ring 4 plane at each carbon atom, when that atom lies on the plane being mapped. In addition, peaks are observed at C(41) and C(46) above the ring 4 plane. Both of these peaks are small and of only one contour. They originate very close to the ring plane and extend upwards only a very short distance. They do not lie between any two interacting groups of the cation and the anion ring. Since the peaks are not observed to lie in an area characteristic of such an interaction, they likely do not arise because of the N-H...π(Ph) hydrogen bond made to ring 4. Similar peaks have been observed in the maps of other structures. They must originate for other, undetermined reason(s).

One other peak of possible import is observed in the ring 4 maps of $[C(NH_2)_3][B(C_6H_5)_4]\cdot CH_3CN$, at the C(44) atom in the C(41)/C(44) cut. In this map, the N(3)-H(3A) bond of the cation projects directly towards C(44) of the anion phenyl ring. There is a small peak of one contour visible in the map, lying well centered between these two groups. It would appear to be present as a direct consequence of the N-H...π(Ph) hydrogen bond accepted by ring 4. The formation of the N(3)-H(3A)...ring 4 interaction should most reasonably give rise to a peak at C(44), the closest C_{ring} contact to H(3A), as observed. The accumulation of electron density in the area between the two interacting groups suggests a covalent component to the N(3)-H(3A)...ring 4 hydrogen bond. However, this cannot be as strong as some of the N-H...π(Ph) interactions studied since the σ density of the ring is not visibly perturbed in the static maps drawn. The peak observed between C(44) and H(3A) does appear to be a true feature of the

interaction and not just a random artifact of the refinement process.

In the three maps drawn in planes defined by pairs of opposing carbon atoms from ring 2 of the anion in $[C(NH_2)_3][B(C_6H_5)_4]\cdot CH_3CN$, two symmetry related acetonitrile solvent molecules are visible below the ring plane. In one of these two CH_3CN molecules the C(3)-H(60) bond consistently projects diagonally up towards the ring 2 plane. However, this C(3)-H(60) bond, and all the remaining bonds of this solvent molecule, never lie directly in the map planes drawn. No contours are ever observed on the bonds in the maps and thus visible evidence of interaction with the ring 2 plane is not observed. The second acetonitrile molecule is more well centered below the ring 2 plane in the maps drawn. In this second solvent molecule, both the C(3)-H(61) and the C(3)-H(62) bonds of the methyl group project diagonally upwards toward the ring 2 plane. Of these two bonds, C(3)-H(62) appears to consistently lie closer to the map plane, although neither bond ever appears to be completely coincident with the plane drawn. Of more interest than the density observed on the C-H bonds of this CH_3CN molecule, is the density observed in the maps between the C-H bonds, particularly between C(3)-H(61) and C(3)-H(62). In the cut made through the C(22) and C(25) atoms of ring 2, this density is considerable (9 contours), extending upward away from CH_3CN towards the ring plane. The distribution of the electron density on the acetonitrile molecule, as observed in the three ring 2 static maps drawn, substantiates the results reported earlier. The acetonitrile molecule appears to have been poorly modelled, with more density lying between the C-H bonds rather than on them, possibly because of the rotation of the CH_3CN methyl group even in the solid state. This has consequences visible not just in the inplane

static maps of the CH_3CN molecule but also in the maps of the anion phenyl rings that interact with the acetonitrile C-H groups.

Consider the contours on the C-H bonds of ring 2 in the $B(C_6H_5)_4^-$ anion and more specifically the appearance of those contours below the ring plane (towards CH_3CN) in the static maps drawn. All of the C-H bond contours are quite normal in appearance below the ring 2 plane, with the exception of those on the C(22)-H(22) bond, visible in the C(22)/C(25) map. On the C(22)-H(22) bond the outer contour curves down off the bond and around under the ring 2 plane ending below C(22). The C(22)-H(22) bond density is perturbed into an area very close to the broad contours arising from the methyl region of the CH_3CN molecule in the plane drawn. The involvement of the C(22)-H(22) bond in the interaction is reasonable in so far that C(3)-H(62) does make the closest contact with C(22) of the ring 2 plane. However, it is not normal for perturbation of the C-H bond contours in the anion phenyl ring to be observed because of the formation of a primarily electrostatic C-H...π(Ph) interaction. This particular C(3)-H(62)...ring 2 interaction is only average in its contact distance and would not be expected to be unusual in any respect. It appears more likely that the poor modelling of the CH_3CN molecule could contribute to the observed perturbation of the C(22)-H(22) bond. The large contours of electron density visible between the C(3)-H(61) and C(3)-H(62) bonds of CH_3CN in the C(22)/C(25) plane, suggest that this density serves as an attractor of the density on the C(22)-H(22) bond, drawing it down off the bond towards the acetonitrile molecule. Similarly, the density visible at the methyl region of the CH_3CN molecule is perturbed towards the anion ring. However, the very location of the electron density in this plane on

the CH_3CN molecule is suspect and so must be any interactions in which it is directly involved. The covalent nature of the C(3)-H(62)...ring 2 interaction suggested in the maps is likely incorrect and not a true representation of the C-H...π(Ph) contact actually formed.

In addition, peaks are observed at most of the carbon atoms below the ring 2 plane [C(21), C(24), C(25) and C(26)] when those particular atoms are bisected in the map plane drawn. Some of these peaks are found in areas considered characteristic of an X-H...π(Ph) interaction, between CH_3CN and the anion ring. However, because of the questionable modelling of the density on the CH_3CN molecule, the nature of the C(3)-H(62)...ring 2 interaction remains somewhat uncertain and it is not clear exactly what features (or lack thereof) should be observed in the static maps drawn. If the density on the acetonitrile molecule is incorrectly distributed this may, in turn, falsely influence the modelling of the ring 2 density when the C(3)-H(62)...ring 2 interaction is formed. The peaks observed in the static maps may not be true features of the C(3)-H(62)...ring 2 interaction. They do not necessarily occur at the atoms expected based on the geometry of the interaction (which in turn may or may not be correct), another indication that they do not arise directly from the C-H...π(Ph) contact. The C(3)-H(62)...ring 2 interaction is certainly almost entirely electrostatic in nature, as all other C-H...π(Ph) interactions have also been determined to be. It is unlikely to have a significant covalent component, as perhaps is suggested by the static maps drawn through opposing carbon atoms of ring 2 in $[C(NH_2)_3][B(C_6H_5)_4]\cdot CH_3CN$.

Above the ring 2 plane, a single cation forms a pair of N-H...π(Ph) hydrogen bonds in a "pincer" type arrangement to the top face of the ring.

Typical of a centroid type hydrogen bond, the N(1)-H(1A) bond of the cation projects almost perpendicular to, and well centered over the middle of, ring 2 of the anion. This bond lies substantially in each of the three planes drawn, being almost completely coincident with the C(23)/C(26) defined plane. This is as expected since the shortest H(1A)...C_{ring} contact is made to C(23) in this interaction. In the C(21)/C(24) cut, the contours on the N(1)-H(1A) bond are quite broad and diffuse. On either side of the bond, the outer contour curves upward and is shared with density on adjacent cation bonds. In the other two views the N(1)-H(1A) bond contours are discrete. In all three maps drawn through pairs of opposing ring 2 carbon atoms, the contours on the N(1)-H(1A) bond appear to be slightly perturbed because of the interaction made with the ring. In each view, the contours are expanded more on one side of the bond than the other, and often, they appear to be pulled down towards the ring 2 plane on that side of the bond. In the static maps the perturbation appears to occur towards the C(26)-C(21)-C(22) half of the ring, even though the physically closest contact is actually made to C(23).

The situation observed for the second hydrogen bond involving this cation, N(2)-H(2A)...ring 2, is quite different. The N(2)-H(2A) bond does not lie in, or even near, any of the map planes drawn. At most, one single contour is visible on the bond (in the C(23)/C(26) map). As a result, nothing can be discerned about the nature of the N(2)-H(2A)...ring 2 interaction from observing the static maps plotted through opposing ring 2 carbon atoms.

Above the ring 2 plane, the contours on all the C-H bonds are quite normal in appearance, except those on the C(26)-H(26) bond. In the map

defined in the plane of the C(23) and C(26) ring atoms, which bisects the C(26)-H(26) bond and illustrates those contours, the N(2)-H(2A) bond of the cation projects directly above and perpendicular to C(26)-H(26). The C(26)-H(26) bond contours are significantly more diffuse above the ring 2 plane than below. The outermost contour appears to be drawn up towards the N(2)-H(2A) bond of the cation (even though that bond does not actually lie in the map plane) rather than towards the greater density on the N(1)-H(1A) bond. The outer C(26)-H(26) bond contour does not curve around to lie over the ring plane (into the region between C(26) of ring 2 and N(1)-H(1A) of the cation) as sometimes had been observed in previous situations, when very strong N-H...π(Ph) type hydrogen bonds were formed. There is only a slight hook visible on the outermost C(26)-H(26) bond contour above the ring 2 plane.

In the map drawn through the C(21) and C(24) atoms of ring 2, it is also clearly evident that the density on the C(21)-B(1) bond of the anion has been significantly perturbed above the ring plane. The outer contour on this bond is greatly expanded; it curves upward and inward over the ring 2 plane, occupying a large area above the C(21) atom. In the C(21)/C(24) cut, which includes the C(21)-B(1) bond contours in the plane, the cation lies approximately perpendicular to both the map plane and the ring 2 plane. Still, there is density visible on the cation in the map plane, which lies between N(1)-H(1A) and N(2)-H(2A) [likely closer to the former bond than to the latter], and the C(21)-B(1) density is obviously perturbed towards this density on the cation. The density on the cation is also slightly perturbed, so that the two sets of contours nearly meet between the two interacting ions.

As just described, the density on the C(21)-B(1) bond is significantly perturbed and that on the neighbouring C(26)-H(26) bond is also somewhat distorted. However, it is not completely clear which of the two ring 2 N-H...π(Ph) hydrogen bonds gives rise to the map features observed. The N(1)-H(1A)...ring 2 interaction is the stronger of the two but both are relatively weak on the scale of interactions studied. As suggested in the C(21)/C(24) map, it maybe the combination of the two concerted interactions that is strong enough to give rise to the observed σ bond perturbations.

The N(1)-H(1A) centroid type hydrogen bond actually makes its closest physical contact to C(23) of ring 2. However, in the static maps drawn through pairs of opposing ring carbon atoms, the N(1)-H(1A) bond is observed to interact most strongly with the C(22)-C(21)-C(26) half of the ring, while N(2)-H(2A) appears to interact with C(25)-C(26), as expected based on the geometry of this edge type interaction. Combined, the overlap of the effects of the two interactions may be enough to cause the perturbations observed on C(21)-B(1) and C(26)-H(26) bonds in the static maps. The presence of the two N-H...π(Ph) hydrogen bonds in a "pincer" type arrangement may explain why features are visible in the static maps of ring 2, even though individually each interaction is rather weak. In previous cases such weak interactions often did not give rise to any map features, attributed to their acting in an isolated fashion (even when present in the same "pincer" type arrangement as seen here). Of course, it is also possible that the features observed in the static maps occur only because of the poor quality of the $[C(NH_2)_3][B(C_6H_5)_4]\cdot CH_3CN$ maps in general and ring 2 in particular. Problems arising from the poor modelling

of the acetonitrile solvent molecule may be transferred to ring 2 of the anion via the C-H...π(Ph) interaction formed and from there on to the other interactions involving ring 2 as the hydrogen bond acceptor.

To complete the discussion of ring 2 in the $[C(NH_2)_3][B(C_6H_5)_4]\cdot CH_3CN$ anion, no peaks are observed above the ring plane at C(21), C(24), C(25) or C(26) in the static maps drawn through opposing carbon atoms of the ring. A small peak is observed at C(23) but it lies close to the ring 2 plane in an area not considered to be representative of an X-H...π(Ph) interaction. No significant features are observed even though C(23) is the closest ring contact to the N(1)-H(1A) group of the cation, supporting the idea that the N(1)-H(1A) and N(2)-H(2A) bonds may be acting in concert rather than individually, as far as their effect on the electron density distribution of ring 2 is concerned. At C(22) a peak is observed well above the ring plane, in an area that could be characteristic of an X-H...π(Ph) interaction. It lies further away from the ring plane than the peak at C(23), in the area directly between C(22) and N(1)-H(1A). This feature appears to be related to the perturbations observed on the neighbouring C(26)-H(26) and C(21)-B(1) bonds. All three suggest a covalent component to at least one, or possibly both, N-H...π(Ph) hydrogen bonds accepted by ring 2 in the structure of $[C(NH_2)_3][B(C_6H_5)_4]\cdot CH_3CN$.

The most interesting static maps from the $[C(NH_2)_3][B(C_6H_5)_4]\cdot CH_3CN$ structure involve ring 3 of the anion. They are comparable to the ring 4 maps from the structure of $[N(C[NH_2]_2)_2][B(C_6H_5)_4]$ because of the strong N-H...π(Ph) hydrogen bonds formed to these rings and the resulting features observed in the static maps plotted. Comparison of the inplane static maps showed ring 3 in $[C(NH_2)_3][B(C_6H_5)_4]\cdot CH_3CN$ to have the worst

quality maps of the four phenyl rings in the structure and the worst maps of all the rings in all of the structures studied. However, in spite of this, the ring 3 maps are of considerable interest because of the two strong N-H...π(Ph) hydrogen bonds accepted by this ring. The two interactions, from a single cation donor, form a "pincer" type arrangement of hydrogen bonds to one face of the anion ring 3. They are the two strongest N-H...π(Ph) interactions in the $[C(NH_2)_3][B(C_6H_5)_4]\cdot CH_3CN$ structure and two of the stronger examples studied in this investigation, perhaps explaining the many features observed in the static maps plotted. All three of the maps drawn in planes cut through opposing carbon atoms of ring 3 in the structure of $[C(NH_2)_3][B(C_6H_5)_4]\cdot CH_3CN$ are included in Figure 89, (a) C(31)/C(34), (b) C(32)/C(35) and (c) C(33)/C(36).

Below the ring 3 plane in all three of the static maps drawn, an acetonitrile solvent molecule and ring 1 of two different $B(C_6H_5)_4^-$ anions (not including the original anion) are visible. Of all of these, in all of the maps plotted, only one bond ever lies even partially in the plane drawn. In the C(33)/C(36) cut, the C(13)-H(13) bond of one of the $B(C_6H_5)_4^-$ anions lies below, and projects diagonally up toward, the C(33)-H(33) bond of ring 3. The C(13)-H(13) bond appears to be only partially coincident with the map plane in this cut; only five contours are visible on the bond. It shows no evidence of having been perturbed because of an interaction made to the ring. In fact, the C(13)-H(13) bond was not found to make a geometrically close contact with ring 3 of the anion in the structure of $[C(NH_2)_3][B(C_6H_5)_4]\cdot CH_3CN$ and it was not investigated any further. The groups lying completely out of the first map planes drawn were removed from later maps to simplify their analysis. No interactions

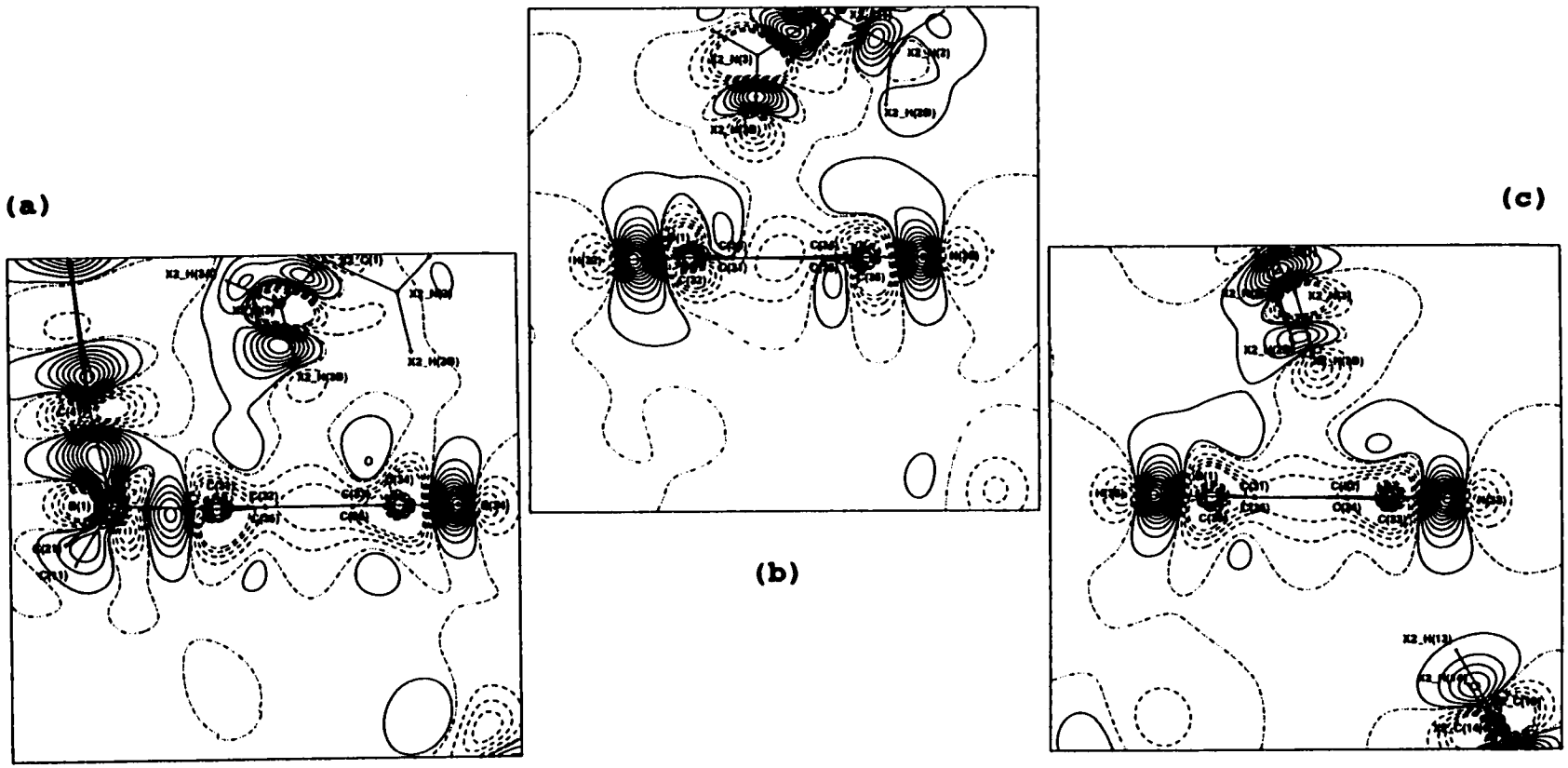

Figure 89. Static deformation density maps drawn in the perpendicular planes cutting through the opposing (a) C(31) and C(34) atoms, (b) C(32) and C(35) atoms and (c) C(33) and C(36) atoms of the anion phenyl ring #3 in guanidinium tetraphenylborate acetonitrile solvate. Positive contours are drawn with solid lines, negative contours with dashed lines and the zero level contour with a (dash dot dot dot) pattern. The contour interval is 0.05 $e\text{Å}^{-3}$. The outline of the remainder of the tetraphenylborate anion has been omitted for clarity in all of the maps.

of any significance are made below the ring 3 plane with any of the groups (ring 1 of two different anions and one CH_3CN molecule) observed in the original maps. As a result, no features characteristic of X-H...π(Ph) interactions would be expected to arise in the ring 3 static maps below the ring plane.

In the static maps drawn through pairs of opposing ring carbon atoms, the opposing ring C-H bonds are also bisected (along the bond) highlighting the bond densities. In the ring 3 maps from the structure of $[C(NH_2)_3][B(C_6H_5)_4]\cdot CH_3CN$, the C(31)-B(1) bond and the majority of the C-H bonds have contours that are quite normal in appearance below the ring plane. Only the contours on the C(32)-H(32) bond show evidence of being slightly perturbed below the ring 3 plane. The outer contour on this bond is very diffuse both above and below the ring plane. Below the ring plane there is a slight hook on the inside of this contour toward the ring. It shows a very slight tendency to curve around under the ring. However, the observed perturbation is small, particularly when compared to the large distortion visible on the same bond above the ring plane. It does not correspond to any X-H...π(Ph) interaction made to the ring, since none occur to this face of ring 3. The observed, minor perturbation must occur for some other reason.

Peaks are also observed at several of the ring 3 carbon atoms below the ring plane, in the static maps in which those specific atoms are bisected. At C(35), a peak of two contours is observed but it originates very close to the ring 3 plane before extending downward away from the ring. This peak does not lie in an area considered characteristic of an X-H..π(Ph) interaction. In contrast, small peaks are also observed below

the ring 3 plane at the C(31), C(34) and C(36) atoms. These peaks are located well below the ring plane in areas where they could be attributed to the presence of X-H...π(Ph) interactions (if such interactions existed). However, since no close contacts are made to this face of ring 3 the peaks must arise for other reasons. Like the remainder of the $[C(NH_2)_3][B(C_6H_5)_4]\cdot CH_3CN$ maps, the features observed are more uncertain in origin than those observed in the maps of the other structures studied. This make interpretation of the $[C(NH_2)_3][B(C_6H_5)_4]\cdot CH_3CN$ maps of all types more difficult.

The static maps shown in Figure 89, (a) through (c), illustrate how a single cation is oriented above the ring 3 plane in the structure of $[C(NH_2)_3][B(C_6H_5)_4]\cdot CH_3CN$, in the now familiar, bidentate, "pincer" type arrangement. The N(2)-H(2B) group of the cation forms an edge type hydrogen bond, to C(34)-C(35), while N(3)-H(3B) forms a centroid geometry hydrogen bond to ring 3, with the closest physical contact made to C(32) of the ring. The latter interaction is the strongest N-H...π(Ph) hydrogen bond in the structure and the second strongest studied overall in this work. The N(2)-H(2B)...ring 3 hydrogen bond is also relatively strong overall, being the second strongest in the structure. Together, the two N-H...π(Ph) hydrogen bonds would be expected to have a large influence on the ring 3 static maps, an effect greater than that found for any other of the anion rings investigated, particularly if they were found to act in a concerted fashion.

The N(3)-H(3B) bond of the cation projects down toward the middle of the ring 3 plane in all three of the static maps plotted through opposing ring carbon atoms [Figure 89 (a) to (c)], as expected for a

hydrogen bond with a centroid type geometry. In every map, the N(3)-H(3B) bond is at least partially coincident with the plane drawn; significant density is visible on the bond in each view. In addition, the contours on the N(3)-H(3B) bond show definite evidence of having been perturbed in all three maps because of the N-H...π(Ph) interaction made with ring 3. The C(32)/C(35) cut (b) gives an almost perpendicular view of the N(3)-H(3B) bond relative to the ring. The N(3)-H(3B) bond contours in this map are discrete and well centered on the bond. In the C(33)/C(36) cut (c), the guanidinium cation lies almost perpendicular to both the map plane and the ring 3 plane. The density visible on the cation in the plane of this map appears to arise primarily from the N(3)-H(3B) bond rather than from the N(2)-H(2B) bond, which also projects at approximately the same position but presumably lies further out of the ring plane. This density is shared with density on the adjacent C(1)-N(3) bond of the cation but is also visibly perturbed down away from the cation toward the ring 3 plane. It very nearly but does not quite meet contours of electron density perturbed upward off the C(36)-H(36) bond of ring 3, a definite accumulation of electron density in the region between the two interacting groups. In the final C(31)/C(34) cut (a), perturbation of the density on the N(3)-H(3B) bond is even greater and more evident than observed in the previous two maps. Again, the N(3)-H(3B) contours are not well centered on the bond, nor are they discrete. On one side of the bond, the outer N(3)-H(3B) contour is shared with the N(3)-H(3A) bond above it in the cation. The shared density on this side of the cation is even more dramatically perturbed than had been observed in the first two maps. It is drawn down off the cation well toward the ring 3 plane, where it actually meets and

is shared with density visible in the map as a peak above the C(31) atom of ring 3. The effects observed in the maps on the N(3)-H(3B) bond contours are definitely much larger than normally observed. Whether these arise from the strength of the interaction itself or whether they are a magnification of the true features of the interaction (or even if these are true features of the interaction) is difficult to determine from the evidence available.

The case of the second bond involved in the bidentate "pincer" type arrangement to ring 3, N(2)-H(2B), is quite different. It never lies in the plane of any of the three maps drawn. At most, one single contour is observed [in the C(32)/C(35) cut (b)] and it does not lie exactly on the bond as projected. Thus, it is impossible to discern the effect of the N(2)-H(2B)...ring 3 interaction on the cation bond from the maps drawn. However, considering the evidence visible in all the maps, both on the cation N-H bonds and on the ring 3 bonds and atoms, it appears that the situation may be similar to that just described for ring 2 of the same structure. Both rings have a bidentate, "pincer" type arrangement of N-H...π(Ph) hydrogen bonds and in both cases the two related interactions appear to exert a concerted effect on the electron density distribution of the ring involved. The combined effect is even larger for ring 3 than for ring 2, as is evident from the features observed in their respective static maps, because of the stronger hydrogen bonds formed to ring 3. It appears likely that the N(2)-H(2B)...ring 3 hydrogen bond does contribute to the effects visible at the ring 3 plane in the static maps of the $[C(NH_2)_3][B(C_6H_5)_4]\cdot CH_3CN$ structure.

Considering all three maps plotted through opposing carbon atoms of

ring 3 [Figure 89 (a) to (c)], it is evident that the C-H bond contours have been significantly perturbed, above the ring plane, all around the ring. Except for the C(31)-B(1) and C(34)-H(34) bonds, which are not visibly perturbed as shown in Figure 89(a), all of the remaining C-H bonds show distinct features, attributed to their involvement in the N-H...π(Ph) interaction(s). The outermost C(32)-H(32) bond contour curves upward and inward to lie over the ring 3 plane above C(32). It actually joins with a peak of two contours which lies close to the ring plane, also at C(32) [a peak not ascribed to the N-H...π(Ph) interactions], forming a semi-circle of electron density around C(32) above the ring plane. The outer C(33)-H(33) bond contour also curves up and over the ring 3 plane, forming a lobe of two contours between C(33) and H(3B) of the cation. Otherwise, the perturbed contours on the four affected C-H bonds are similar in appearance. Above the ring 3 plane, the outermost C-H contour on each bond curves upward and inward, moving into the region directly between the anion ring and the interacting cation. The peaks cover a relatively large area above the ring carbon atoms involved. There is a clear perturbation of the σ electron density on the C-H bonds into an area above the ring plane that suggests that ring 3 is involved in at least a partially covalent interaction with the guanidinium cation.

In addition, peaks are observed at the two ring carbon atoms, C(31) and C(34), whose bond contours are not visibly perturbed, C(31)-B(1) and C(34)-H(34) respectively. The peaks lie well above the ring 3 plane in areas that suggest that they too arise from the N-H...π(Ph) interactions made to the ring. At C(34) a peak of two contours is observed, while at C(31) the peak consists of only a single contour. Both peaks cover a

relatively large area and lie directly between the cation and the respective ring carbon atoms. In the C(31)/C(34) cut (a), the density from the N(3)-H(3B) bond of the cation is drawn down off the bond and actually joins with the density visible as a peak at C(31). There are no other peaks observed in the static maps at the remaining ring carbon atoms above the ring 3 plane.

The features observed in the ring 3 maps of $[C(NH_2)_3][B(C_6H_5)_4]\cdot CH_3CN$ are more pronounced (larger in number and magnitude) than those observed in the maps of any other ring in this, or any other of the structures, studied. The entire ring is affected by the two N-H...π(Ph) interactions made to one of its faces. Either the C-H bonds of ring 3 are perturbed, with density drawn off the bond into the interionic region [C(32)-H(32), C(33)-H(33), C(35)-H(35) and C(36)-H(36)] or peaks are formed at the ring carbon atoms, between the ring plane and the cation N-H groups [C(31) and C(34)]. All of the features suggest an accumulation of electron density occurs between the interacting groups, characteristic of a covalent component in these N-H...π(Ph) hydrogen bonds.

A similar situation [involvement of the entire ring, including the σ electron density on the C-H and/or C-B bonds, in the interaction] has been observed in only one other case, ring 2 of the anion in the structure of $[N(C[NH_2]_2)_2][B(C_6H_5)_4]$. It is interesting to note that ring 2 in $[N(C[NH_2]_2)_2][B(C_6H_5)_4]$ accepts the strongest N-H...π(Ph) hydrogen bond of the experimental examples studied, while ring 3 in $[C(NH_2)_3][B(C_6H_5)_4]\cdot CH_3CN$ accepts the second strongest such interaction (and another relatively strong interaction as well). Only the very strongest N-H...π(Ph) have been found to give rise to such pronounced features in the static maps, but

they do so consistently and in different structures. The features observed in the ring 3 static maps of $[C(NH_2)_3][B(C_6H_5)_4]\cdot CH_3CN$ are, if anything, even greater than those of the ring 2 $[N(C[NH_2]_2)_2][B(C_6H_5)_4]$ maps. This is somewhat surprising considering that the latter ring accepts the stronger interaction. The distinct features observed in the $[C(NH_2)_3][B(C_6H_5)_4]\cdot CH_3CN$ static maps may arise because the two related "pincer" type N-H...π(Ph) contacts formed to the ring act in a concerted fashion to significantly perturb the electron density distribution around the ring. Since both the hydrogen bonds involved are strong (on the relative scale of the interactions studied) the effects observed in the ring 3 static maps of $[C(NH_2)_3][B(C_6H_5)_4]\cdot CH_3CN$ are the greatest of any ring in the four structures investigated.

The fact that the two N-H...π(Ph) hydrogen bonds arranged in a "pincer" type fashion to ring 3 in the $[C(NH_2)_3][B(C_6H_5)_4]\cdot CH_3CN$ structure appear to have a concerted effect on the electron density of the ring is not unprecedented. The electron density of ring 2 in the same structure was also found to have been perturbed more than expected from the pair of weak N-H...π(Ph) hydrogen bonds formed in a "pincer" type arrangement to the ring. It appears that the combined effect of a pair of related N-H...π(Ph) hydrogen bonds may be larger than predicted on an individual basis, resulting in more pronounced map features than might otherwise have been observed.

Of course, it is also possible that the effects observed in the ring 3 maps of $[C(NH_2)_3][B(C_6H_5)_4]\cdot CH_3CN$ may have been magnified somewhat, as suggested after analysis of the static maps cut through opposing C-C bonds of the phenyl ring. They do appear to be true, representative

features of the N-H...π(Ph) hydrogen bonds actually formed to ring 3 but it is possible that the multipole model chosen has placed too much density in the internuclear regions, emphasizing the weaker interactions unduly. It is difficult to know whether one or the other or a combination of both explanations is correct, especially considering that the ring 3 static maps were judged to be of the lowest overall quality in the structure. Still, it appears reasonable that the two relatively strong N-H...π(Ph) hydrogen bonds acting in a concerted fashion could give rise to the many features observed in all the ring 3 maps of $[C(NH_2)_3][B(C_6H_5)_4]\cdot CH_3CN$.

The conclusions reached after analysis of the complete set of $[C(NH_2)_3][B(C_6H_5)_4]\cdot CH_3CN$ static maps do fit with those described previously for the other three structures. Besides the maps of rings 2 and 3, just discussed, the maps of ring 4 show minor features (peaks but no involvement of the σ density on the C-H and C-B bonds) attributable to the single, average strength N-H...π(Ph) hydrogen bond formed. In contrast, the maps of ring 1 show no features that can be assigned to X-H...π(Ph) interactions. This result coincides with earlier observations made. Ring 1 forms only C-H...π(Ph) type contacts, which under normal circumstances do not visibly affect the static maps plotted. The $[C(NH_2)_3][B(C_6H_5)_4]\cdot CH_3CN$ maps form a consistent set and also correspond with the maps of the other three structures studied in this investigation.

3.5.3.2.1. Summary

Interpretation of the static maps plotted to investigate the X-H...π(Ph) [X = N or C] interactions formed in the four experimental structures proved difficult for a variety of reasons. The maps were found

to contain many features, not all of which could be assigned to the hydrogen bonds formed, "true" features being intermingled with peaks arising for a variety of other reasons. In addition, different interactions were found to give rise to effects differing in origin, position and magnitude in the maps, depending on the nature and the strength of the hydrogen bond formed. All of this made analysis of the maps difficult. However, a variety of characteristic features were identified and these were shown to be consistently observed when similar strength X-H...π(Ph) hydrogen bonds are present in the static maps of the anion phenyl rings.

In the first maps studied, the inplane static maps of the cations and the anions, no correlation was found between the observed bond densities and the formation of X-H...π(Ph) hydrogen bonds. The density on the C-C bonds of the anion phenyl rings was often observed to be somewhat uneven around a given ring in a given structure, however, the variation could not be shown to be related to the X-H...π(Ph) hydrogen bond(s) formed to that ring. Similarly, the variation in the average C-C bond density, between rings in the anion of a given structure and the variation observed between the four experimental structures, could not be correlated with the various combinations of X-H...π(Ph) hydrogen bonds formed. The density observed on the N-H bonds of the cations and that on the C-H bonds of groups participating as donors in C-H...π(Ph) type hydrogen bonds, were again not obviously correlated with the X-H...π(Ph) hydrogen bonds nor with their strengths.

Two different types of static maps were plotted in planes perpendicular to the anion phenyl rings, to illustrate and study the X-H...π(Ph) hydrogen bonds formed in the four structures. In the first

group of maps, the plane bisects a pair of opposing C-C ring bonds, while in the second it passes through a pair of opposing ring carbon atoms. Analysis of the combination of the two complete sets of maps allowed the following conclusions to be reached.

The features arising from C-H...π(Ph) interactions in the static maps will be discussed first since they form a relatively consistent group. Generally only C-H...π(Ph) interactions with hydrogen bond type geometries are ever clearly visible in the maps drawn. Overall, the formation of C-H...π(Ph) interactions of any type appears to have little effect on the electron density of the interacting groups in all of the static maps plotted. The contours on the C-H bonds of the donor groups are not visibly perturbed in the static maps; they remain regular, symmetrical and well centered on the bonds. Charge depletion is observed, in the area towards the anion ring, at every H(C) atom that participates in a C-H...π(Ph) hydrogen bond, a feature characteristic of an electrostatic interaction.

It was possible to study the maps of several anion phenyl rings involved as the acceptor in only C-H...π(Ph) interactions from the four structures investigated (rings 2 and 3 in [DabcoH][$B(C_6H_5)_4$] and ring 1 in [$C(NH_2)_3$][$B(C_6H_5)_4$]·CH_3CN). These maps also showed only minimal effects (at best) that were consistently observed and could be attributed to the C-H...π(Ph) interactions made to the ring. The only regularly observed feature was a slight diffuseness/expansion of the outermost contour on all of the C-C bonds of the interacting ring. No characteristic features were identified in the maps drawn through opposing ring carbon atoms. All of the maps suggest that the C-H...π(Ph) interactions are almost completely

electrostatic in nature, with possibly a very small covalent component.

The N-H...π(Ph) interactions were found to give rise to quite different effects in the static maps drawn, illustrating the fact that they do differ in a substantial way from the C-H...π(Ph) interactions. The differences observed in the map features for the two type of interactions suggest that the effects observed are real and characteristic of each group. The maps drawn to study the N-H...π(Ph) hydrogen bonds also show varying effects depending on the strength of the interaction formed. The features observed range from very minor to large and extensive, involving the entire phenyl ring of the anion acceptor.

The N-H bond density, in both types of phenyl ring maps, is consistently perturbed when involved in an N-H...π(Ph) interaction. In the maps, the N-H contours tend to be elongated more on one side of the bond than the other, such that they no longer remain well centered on the bond. The contours are drawn down off the bond towards the ring plane, to an extent that appears to be related to the strength of the interaction formed. In the stronger interactions, the density on the cation N-H bond is usually more obviously perturbed. The outer N-H bond contour is often more distorted, pulled further off the bond towards the anion ring plane. In the most extreme case, ring 3 in the anion of $[C(NH_2)_3][B(C_6H_5)_4]\cdot CH_3CN$, the electron density of the cation N-H bond actually meets and is shared with density arising from the anion ring. Accumulation of electron density between the interacting groups, visible in the static maps, is indicative of a covalent contribution to the hydrogen bond being formed. The fact that the N-H...π(Ph) hydrogen bonds have an even larger electrostatic component is evident in the large areas of significantly depleted charge

observed in the static maps at every interacting cation H(N) atom and oriented toward the phenyl ring plane of the anion.

In the maps drawn, in planes cut perpendicular to the anion phenyl rings through opposing C-C bonds, a certain diffuseness/expansion was observed on the outer C-C bond contours when the ring was found to participate in N-H...π(Ph) hydrogen bond(s). This diffuseness is visible and relatively equal on all the C-C bonds around the interacting ring. It is also observed to be relatively equal both above and below the ring plane, regardless of the face to which the interaction(s) is made. A very similar effect was observed for all the X-H...π(Ph) interactions studied [X = N or C], making it difficult to correlate the magnitude of this feature with the strength of the interaction(s) made to the ring. This was further complicated by the fact that the diffuseness observed on the outer C-C bond contours appears also to be related to the original bond density. Still, diffuseness of the outer C-C bond contours around the phenyl ring is a feature consistently observed in the static maps plotted through pairs of opposing C-C bonds, in rings accepting X-H...π(Ph) hydrogen bonds.

It is the cuts made through pairs of opposing anion phenyl ring carbon atoms that most clearly show the effects of the N-H...π(Ph) interactions on the electron density distribution of the ring. The features observed in these maps vary quite consistently and characteristically with the strength of the interaction formed. The strength of an N-H...π(Ph) hydrogen bond was first estimated from its geometry, particularly the minimum H(N)...C_{ring} distance(s), and later was determined from the bond path and the properties of the electron density at the bond critical

point.

The weakest N-H...π(Ph) hydrogen bonds investigated, normally do not give rise to any visible features in the static maps drawn through pairs of opposing ring carbon atoms. This was found to be especially true of isolated interactions, single weak interactions made to one face of an anion ring. No peaks are observed in the maps, in the middle region between the ring plane and the interacting N-H group of the cation. No specific deformations of the density on any of the ring bonds (C-C, C-H or C-B) are observed either.

Other peaks are often observed in these maps but not in areas considered characteristic of the N-H...π(Ph) interactions. These peaks tend to lie right on, or very close to, the ring plane. There is never any obvious pattern in their number and distribution around the ring. They tend to complicate the maps and make the analysis more difficult but they can usually be differentiated from the "true" peaks arising from the N-H...π(Ph) interactions. The spurious peaks arise for a number of different reasons, from poor assignment of the multipoles on the ring carbon atoms to their being artifacts of the refinement process.

As the N-H...π(Ph) hydrogen bonds become somewhat stronger, new features, attributed to the interaction, become visible in the static maps. The first characteristic feature usually observed is a single small peak (1 contour) lying somewhat off of the ring plane at one of the ring carbon atoms. This peak is normally observed at that ring carbon atom making the closest contact with the H(N) atom of the interacting cation and will lie directly between those two groups. Only one peak arising from the weak interaction is usually observed for each ring, so a peak is

observed in only one of the three map planes drawn, that cut where the appropriate ring carbon atom is bisected.

There is some overlap between these first two groups of N-H...π(Ph) hydrogen bonds, those weak interactions which do not show features (peaks) in the static maps and those slightly stronger interactions that do (sometimes slightly stronger interactions show no features while other times slightly weaker interactions do). This most likely has to do with the way the map planes are defined and with the fact that the peaks involved are of only very low density, normally only one contour or +0.015 $e\text{Å}^{-3}$. The maps are not plotted exactly in the planes of the N-H...π(Ph) hydrogen bonds; this would be impossible since the nature of the acceptor is ill-defined. Rather, the maps are defined using the phenyl ring carbon atoms themselves. There will often be a slight discrepancy between the map plane and the plane of the N-H...π(Ph) hydrogen bond, that plane in which electron density is actually shared between the cation and the anion. Because of the very low levels of electron density involved, peaks lying even slightly out of the map plane have a good chance of not being observed. If a peak is observed, it represents a visible accumulation of electron density between the interacting anion phenyl ring and the N-H group of the cation, characteristic of a covalent component in the hydrogen bond. Again, only a very low level of electron density is actually shared between the two groups, usually a peak of one contour or +0.015 $e\text{Å}^{-3}$ is observed, meaning that the hydrogen bond remains predominantly electrostatic. However, N-H...π(Ph) hydrogen bonds do contain a covalent contribution which appears to increase somewhat with the strength of the interaction.

As the N-H...π(Ph) hydrogen bonds become even stronger, or if two weak interactions act in a concerted fashion to a single ring face (the "pincer" type arrangement of bonds in particular), even more prominent features are observed in the static maps drawn through opposing ring carbon atoms. In addition to peaks at the appropriate ring carbon atoms (which may or may not be observed depending on the geometry of the interaction), perturbation of the σ electron density on certain of the ring bonds becomes evident in the maps. For example, the C(11)-B(1) bond density is visibly distorted towards the cation in the static maps of $NH_4B(C_6H_5)_4$ because of the N(1)-H(1)...ring 1 hydrogen bond formed in the structure, the third strongest studied overall. A similar perturbation of the C(21)-B(1) bond density, and also of the adjacent C(26)-H(26) bond density, is observed in the static maps of ring 2 from the structure of $[C(NH_2)_3][B(C_6H_5)_4]\cdot CH_3CN$. In this case, two weaker N-H...π(Ph) interactions are formed to one face of the anion ring but they appear to act in a concerted fashion to give rise to the significant features observed in the maps. Electron density, at least partially from σ bonds of the anion phenyl ring, is visibly perturbed into the region between the two interacting groups, suggesting an even larger covalent contribution to these hydrogen bonds. In this group, only one or two specific atom(s) and/or bond(s), in one distinct region of the anion ring, are visibly involved in the interaction made with the cation, not the entire ring. These are normally the atom(s)/bond(s) lying closest to the cation, as predicted from the geometry of the interaction.

In the very strongest N-H...π(Ph) hydrogen bonds studied in this work, the electron density of the entire phenyl ring is visibly perturbed

because of the contact(s) it accepts. The strongest individual N-H...π(Ph) hydrogen bond is formed to ring 2 in the $[N(C[NH_2]_2)_2][B(C_6H_5)_4]$ structure and it gives rise to such significant features in the static maps plotted. The second strongest N-H...π(Ph) hydrogen bond investigated is made to ring 3 in the structure of $[C(NH_2)_3][B(C_6H_5)_4]\cdot CH_3CN$. However, the maps of ring 3 have the most prominent features observed in any of the static maps drawn for the anion phenyl rings in the four experimental structures. This presumably occurs because there are actually two hydrogen bonds formed to one face of ring 3 in a "pincer" type arrangement and these act in a concerted fashion on the electron density of the phenyl ring acceptor, causing the large effects observed in the maps. In fact, in the ring 3 maps of $[C(NH_2)_3][B(C_6H_5)_4]\cdot CH_3CN$, the electron density on the cation and anion is so greatly perturbed that it actually meets and is shared in the area between the two interacting ions.

In the strongest N-H...π(Ph) hydrogen bonds, the entire anion ring is visibly involved in the interaction. Peaks at ring carbon atoms and/or perturbation of the σ bond density (C-H or C-B) is observed all around the phenyl ring. Where C-H bonds are involved, the outer bond contour curves over/under the ring plane to form a lobe of electron density lying between the anion and the N-H group of the cation. The peaks observed also lie well off of the ring plane, between the ring carbon atom involved and the cation. Normally one feature or the other (not both) is observed at every carbon atom of the ring.

Participation of the σ electron density of the anion phenyl ring C-H and C-B bonds in the N-H...π(Ph) type hydrogen bonds has never before been demonstrated or even postulated. The features observed in the maps from

this investigation, for two different rings in two different structures, suggest that in the strongest such interactions the σ electron density of the ring does become involved. In addition to the π electron density of the aromatic ring, the "traditional" acceptor of the N-H...π(Ph) hydrogen bond, the σ electron density is perturbed all around the ring in the strongest interactions. The magnitude of the features observed also suggest that the covalent contribution to the N-H...π(Ph) hydrogen bond is larger in the stronger interactions.

There are no electron density maps illustrating X-H...π(Ph) hydrogen bonds [X = O, N or C] available in the literature with which the experimental results might be compared. However, the present results do fit reasonably well with the maps and features described for hydrogen bonds with traditional acceptors (summarized in the introduction) being only somewhat weaker in most instances. The fact that such consistent and similar results were observed for the 14 N-H...π(Ph) hydrogen bonds and 12 unique anion phenyl rings in the four different structures investigated in this work, supports the idea that the conclusions reached are valid.

A 1997 book by P. Coppens, "X-ray Charge Density and Chemical Bonding",[6a] includes a chapter on electron density structures of molecular crystals, in which electron density maps and the effect of hydrogen bonding on those maps are discussed. In it the author writes "the induced polarization of the [hydrogen bond] acceptor density towards the H atom is apparently still present for the longer distances, but very diffuse and below the lowest contour level on most maps." It is being suggested that a covalent contribution is still made in weak hydrogen bonds but that it may be too small to be observed in the maps normally plotted. The present

results support this observation. The static electron density maps drawn to investigate the weak X-H...π(Ph) hydrogen bonds were plotted with an extra, low level positive contour (+0.015 eÅ^{-3}) included. In many cases, this allowed perturbation of the electron density on the groups involved in the hydrogen bonds to be observed in the maps, perturbation that might otherwise not have been visible. Even though the X-H...π(Ph) hydrogen bonds investigated were weak, they often gave rise to visible effects in the static maps (as had been predicted by Coppens) when an extra, low level contour was drawn. This substantiates the idea that a covalent contribution, though it may be small, is still present in even very weak hydrogen bonds. The results from this study also suggest that for some X-H...π(Ph) hydrogen bonds the covalent contribution may be significant.

In most cases, the features observed in the static maps plotted can be directly correlated with the geometry of the N-H...π(Ph) interaction(s) made to the ring. Only the very strongest N-H...π(Ph) hydrogen bonds studied affect the electron density of the entire anion phenyl ring. The weaker hydrogen bonds tend to visibly affect only the geometrically closest ring carbon atoms. In the static maps, features are observed only at specific ring carbon atoms and/or bonds, rather than distributed around the entire ring. The "principal" acceptor of the hydrogen bond may be an isolated fragment of the ring, an atom or a bond, rather than the complete ring. As already has been shown, this can be predicted reasonably well from the geometry of the interaction. It will be shown subsequently that the map features observed (and the geometry of the interaction) are also directly related to the bond path of the hydrogen bond and its properties at the bond critical point.

Appendix 4

4. Collected Tables

Table 16. Positional parameters and isotropic temperature factors ($Å^2 \times 10^3$) for the nonhydrogen atoms of ammonium tetraphenylborate.

atom	x	y	z	U(eq)
B(1)	0	0	1/2	17
N(1)	0	0	1	23
C(11)	0.0817(1)	0.0817(1)	0.6264(1)	18
C(12)	0.1906(1)	0.0398(1)	0.6929(1)	22
C(13)	0.2532(1)	0.1015(1)	0.8160(1)	27
C(14)	0.2086(1)	0.2086(1)	0.8801(2)	29

Table 17. Atomic distances (Å) and angles (°) for ammonium tetraphenylborate.

Atoms	Distance	Atoms	Angle
B(1)-C(11)	1.6443(10)	C(11)-B(1)-C(11)#1	103.7(1)
C(11)-C(12)	1.4094(8)	C(11)-B(1)-C(11)#2	112.4(1)
C(12)-C(13)	1.3954(12)	B(1)-C(11)-C(12)	121.9(1)
C(13)-C(14)	1.3962(11)	C(12)-C(11)-C(12)#3	115.6(1)
N(1)-H(1)	1.032	C(11)-C(12)-C(13)	122.5(1)
C(12)-H(12)	1.076	C(12)-C(13)-C(14)	120.4(1)
C(13)-H(13)	1.076	C(13)-C(14)-C(13)#3	118.5(2)
C(14)-H(14)	1.076	H(1)-N(1)-H(1)#1	109.5
		C(11)-C(12)-H(12)	118.2
		C(13)-C(12)-H(12)	119.3
		C(12)-C(13)-H(13)	119.8
		C(14)-C(13)-H(13)	119.8
		C(13)-C(14)-H(14)	120.7

#1 -x, -y, z
#2 y, -x, -z+1
#3 y, x, z

Table 18. Anisotropic temperature factors ($Å^2$) for the nonhydrogen atoms of ammonium tetraphenylborate.

atom	U11	U22	U33	U12	U13	U23
B(1)	0.016(1)	0.016(1)	0.020(1)	0	0	0
N(1)	0.025(1)	0.025(1)	0.019(2)	0	0	0
C(11)	0.016(1)	0.016(1)	0.021(1)	-0.001(1)	-0.001(1)	-0.001(1)
C(12)	0.018(1)	0.022(1)	0.025(1)	-0.001(1)	-0.003(1)	0.000(1)
C(13)	0.021(1)	0.031(1)	0.029(1)	-0.000(1)	-0.007(1)	-0.005(1)
C(14)	0.030(1)	0.030(1)	0.027(1)	-0.005(1)	-0.005(1)	-0.010(1)

Table 19. Positional parameters and isotropic temperature factors ($Å^2 \times 10^3$) for the hydrogen atoms of ammonium tetraphenylborate.

atom	x	y	z	U(eq)
H(1)	0.0533	0.0533	0.9259	38
H(12)	0.2251	-0.0440	0.6479	37
H(13)	0.3365	0.0663	0.8619	42
H(14)	0.2554	0.2554	0.9773	44

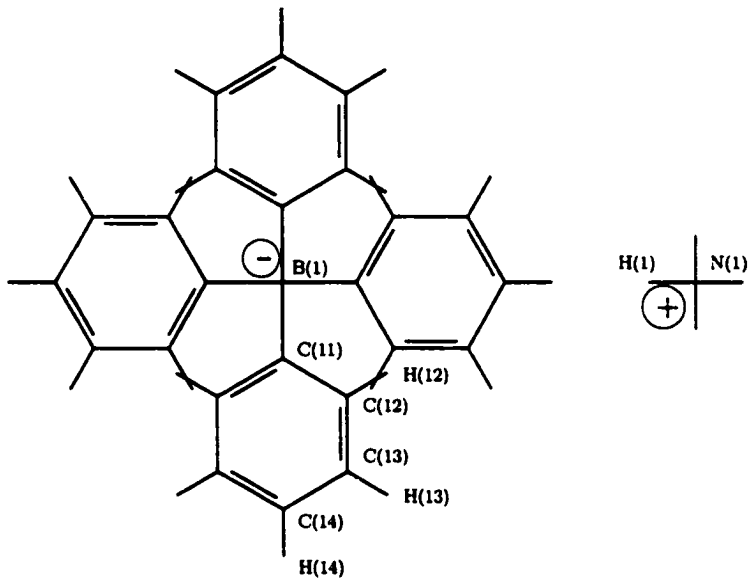

Table 20. Scale factor, extinction, kappa values, local coordinate system, and multipole population coefficients for ammonium tetraphenylborate (atom numbering as shown above).

	Scale Factor	Extinction
	4.286(21)	0.0
	κ'	κ''
1.	0.848(43)	0.96(20)
2.	0.972(36)	1.11(95)
3.	0.935(9)	1.01(3)
4.	0.827(51)	1.08(20)
5.	1.111(31)	1.30(20)

atom	atom0	axis1	atom1	atom2	axis2	right/left	kappa set
B(1)	N(1)	Z	B(1)	DUM0	X	R	1
N(1)	B(1)	Z	N(1)	DUM1	X	R	2
C(11)	B(1)	X	C(11)	H(1)	Y	R	3
C(12)	C(13)	X	C(12)	C(11)	Y	R	3
C(13)	C(12)	X	C(13)	C(14)	Y	L	3
C(14)	H(14)	X	C(14)	H(1)	Y	R	3
H(1)	N(1)	X	H(1)	B(1)	Y	R	4
H(12)	C(12)	Z	H(12)	C(11)	Y	R	5
H(13)	C(13)	Z	H(13)	C(14)	Y	R	5
H(14)	C(14)	X	H(14)	H(1)	Y	R	5

DUM0=1.0000 0.0000 0.5000
DUM1=1.0000 0.0000 1.0000

Table 20. Multipole populations

atom	P_v	P_{00}	P_{11}	P_{1-1}	P_{10}
B(1)	0.46(7)	0.00(0)	0.00(0)	0.00(0)	0.00(0)
N(1)	0.57(5)	0.00(0)	0.00(0)	0.00(0)	0.00(0)
C(11)	2.03(6)	0.00(0)	0.03(2)	−0.02(1)	0.00(0)
C(12)	4.26(8)	0.00(0)	0.01(2)	0.01(2)	−0.02(2)
C(13)	4.10(7)	0.00(0)	0.01(3)	0.00(2)	0.01(2)
C(14)	1.99(5)	0.00(0)	−0.02(2)	0.00(1)	0.00(0)
H(1)	0.43(5)	0.00(0)	0.11(4)	0.00(0)	0.00(0)
H(12)	0.82(6)	0.00(0)	0.00(0)	0.00(0)	0.05(3)
H(13)	0.87(5)	0.00(0)	0.00(0)	0.00(0)	0.07(2)
H(14)	0.48(4)	0.00(0)	0.07(2)	0.00(0)	0.00(0)

atom	P_{20}	P_{21}	P_{2-1}	P_{22}	P_{2-2}
B(1)	−0.02(1)	0.00(0)	0.00(0)	0.00(0)	0.00(0)
N(1)	0.00(1)	0.00(0)	0.00(0)	0.00(0)	0.00(0)
C(11)	0.07(1)	0.00(0)	0.00(0)	0.10(1)	0.06(1)
C(12)	−0.22(2)	−0.16(2)	0.04(2)	−0.09(2)	0.01(2)
C(13)	−0.19(2)	0.17(2)	−0.04(2)	−0.06(2)	0.01(2)
C(14)	0.13(2)	0.00(0)	0.00(0)	0.05(2)	−0.03(1)
H(1)	0.00(0)	0.00(0)	0.00(0)	0.00(0)	0.00(0)
H(12)	0.00(0)	0.00(0)	0.00(0)	0.00(0)	0.00(0)
H(13)	0.00(0)	0.00(0)	0.00(0)	0.00(0)	0.00(0)
H(14)	0.00(0)	0.00(0)	0.00(0)	0.00(0)	0.00(0)

atom	P_{30}	P_{31}	P_{3-1}	P_{32}	P_{3-2}	P_{33}	P_{3-3}
B(1)	0.00(0)	0.00(0)	0.00(0)	0.00(0)	0.04(2)	0.00(0)	0.00(0)
N(1)	0.00(0)	0.00(0)	0.00(0)	0.00(0)	−0.01(2)	0.00(0)	0.00(0)
C(11)	0.00(0)	−0.12(3)	−0.02(3)	0.00(0)	0.00(0)	0.05(3)	−0.01(2)
C(12)	−0.02(7)	−0.03(3)	0.01(2)	−0.09(3)	−0.03(1)	0.26(6)	0.01(2)
C(13)	−0.04(7)	0.03(4)	0.00(2)	0.02(3)	0.02(2)	0.24(6)	−0.02(2)
C(14)	0.00(0)	−0.11(3)	0.05(3)	0.00(0)	0.00(0)	0.04(2)	0.00(3)

Table 21. Results of the rigid body thermal motion analysis for the anion in ammonium tetraphenylborate.[a]

Rigid body variables fitted		8	
Translational tensor, **T** ($Å^2$)	0.0145(3)	0	0
		0.0145(3)	0
			0.0211(3)
Principal values ($Å^2$)	0.0145	0.0145	0.0211
Square root (Å)	0.12	0.12	0.15
Librational tensor, **L** (deg^2)	2.5(1)	0	0
		2.5(1)	0
			4.9(1)
Principal values (deg^2)	2.5	2.5	4.9
Square root (deg)	1.6	1.6	2.2
Cross tensor, **S** (Å-deg)	0.000(6)	0	0
	0	0.000(6)	0
	0	0	0
R_w[b]		0.0615	
Z[c]		0.00110	
Corrections to interatomic distances due to libration		0.0013 to 0.0016Å	
Esd's on the calculated interatomic distances		0.0008 to 0.0012Å	

[a] Tensor components are given with respect to the axes of the principal moments of inertia and with the origin at the center of mass.

[b] $R_w = (X^2 / \Sigma[U_{ij}/\sigma_{Uij}]^2)^{½}$ where $X^2 = \Sigma[\Delta U_{ij}/\sigma_{Uij}]^2)$

[c] $Z = (X^2 / NFREE)^{½}$ where NFREE = 142

Table 22. Short intermolecular anion...anion contacts for ammonium tetraphenylborate.

	C-H...phenyl		(anion/anion)
contact	C...C (Å)	H...C (Å)	C-H...C (°)
C(14)-H(14)...ring 1 symmetry (1/2-x, 1/2-y, 1/2+z) and (1/2-y, 1/2-x, 1/2+z)			
C(11)	3.862(1)	2.841	158.4
C(12)	3.938(1)	2.935	155.3
C(13)	4.119(2)	3.159	149.0
C(14)	4.2256(6)	3.286	146.5
mean	**4.033[3]**	**3.052**	**152.2**
centroid[a]	3.785	2.717	171.6
plane[b]	3.749	2.673	88.1
C(12)-H(12)...ring 1 symmetry a (1/2-y, -1/2+x, 3/2-z) and b (1/2-x, -1/2+y, 3/2-z)			
C(11)	5.902(1)	5.047	139.0
C(12a)	5.0192(9)	4.167	138.1
C(12b)	5.8207(4)	4.919	143.7
C(13a)	3.960(1)	2.998	149.1
C(13b)	4.942(1)	3.983	149.8
C(14)	3.916(1)	2.873	163.3
mean	**4.927[2]**	**3.998**	**147.2**
centroid[c]	4.789	3.838	148.5
plane[b]	2.837	1.917	58.7

[a] The position of the centroid of the symmetry generated ring 1 is (0.3541, 0.3541, 1.2541). The values listed are *d*(C...centroid), *d*(H...centroid) and the angle C-H...centroid.
[b] The values listed are *d*(C...plane), *d*(H...plane) and the angle the C-H vector makes with the plane of the symmetry generated ring.
[c] The position of the centroid of the symmetry generated ring 1 is (0.3541, -0.3541, 0.7459). The values listed are *d*(C...centroid), *d*(H...centroid) and the angle C-H...centroid.

Table 23. Bond critical points for the short intermolecular anion...anion contacts in ammonium tetraphenylborate.

				C-H...phenyl			(anion/anion)	
Contact	Hessian Eigenvalues			Charge Density	Laplacian	Ellipticity	Position	
Bond Path	λ_1	λ_2	λ_3	$\rho_b(\mathbf{r})$ ($eÅ^{-3}$)	$\nabla^2\rho_b(\mathbf{r})$ ($eÅ^{-5}$)	ε	x	y (fractional)	z
C(14)-H(14)...ring 1[a] symmetry (1/2-x, 1/2-y, 1/2+z) and (1/2-y, 1/2-x, 1/2+z) centroid type hydrogen bond									
H(14)...C(11)	-0.07,	-0.03,	0.61	0.044(8)	0.514(4)	1.51	0.3152,	0.3152,	1.0324

Bond Lengths and Angles at the Critical Point

Atoms	Distance (Å)	Atoms	Angle (°)
Cp...C(14)	2.083	C(14)...Cp...C(11)	168.9
Cp...H(14)	1.044	H(14)...Cp...C(11)	179.7
Cp...C(11)	1.797	C(14)-H(14)...Cp	158.6
Cp...plane	1.689		
Cp...centroid	1.884		

[a] Single atom type bond path from H(14) to C(11).

Table 23. Bond critical points for the short intermolecular anion...anion contacts in ammonium tetraphenylborate (continued).

	C-H...phenyl (anion/anion)								
Contact	Hessian Eigenvalues			Charge Density	Laplacian	Ellipticity	Position		
Bond Path	λ_1	λ_2	λ_3	$\rho_b(\mathbf{r})$ (eÅ^{-3})	$\nabla^2\rho_b(\mathbf{r})$ (eÅ^{-5})	ε	x	y (fractional)	z
C(12)-H(12)...ring 1[a] symmetry a (1/2-y, -1/2+x, 3/2-z) and b (1/2-x, -1/2+y, 3/2-z) intermediate type contact									
H(12)...C(14)-H(14)	-0.11	-0.06	0.66	0.046(9)	0.495(6)	0.75	0.2453	-0.1401	0.6261

Bond Lengths and Angles at the Critical Point

Atoms	Distance (Å)	Atoms	Angle (°)
Cp...C(12)	2.170	C(12)...Cp...C(14)	167.3
Cp...H(12)	1.112	H(12)...Cp...C(14)	171.0
Cp...C(14)	1.769	C(12)...Cp...H(14)	153.8
Cp...H(14)	1.434	H(12)...Cp...H(14)	151.4
		C(12)-H(12)...Cp	165.3
Cp...plane	1.140		
Cp...centroid	2.852		

[a] The bond path is from H(12) to the approximate midpoint of the C(14)-H(14) bond in the ring and terminates at C(14).

Table 24. Positional parameters and isotropic temperature factors ($Å^2 \times 10^3$) for the nonhydrogen atoms of [DabcoH][$B(C_6H_5)_4$].

atom	x	y	z	U(eq)
N(1)	0.7952(2)	-1/4	0.6707(2)	32
N(2)	0.9102(2)	-1/4	0.5276(2)	43
C(1)	0.8616(2)	-1/4	0.7605(2)	37
C(2)	0.9307(1)	-1/4	0.6692(3)	38
C(3)	0.7961(1)	-0.3433(2)	0.5848(2)	46
C(4)	0.8667(1)	-0.3402(2)	0.4987(2)	50
C(11)	0.6508(1)	-1/4	0.9181(2)	25
C(12)	0.6421(1)	-0.3403(2)	0.8443(2)	33
C(13)	0.6212(1)	-0.3397(3)	0.7083(2)	44
C(14)	0.6109(2)	-1/4	0.6397(3)	49
C(21)	0.7621(1)	-1/4	1.0909(2)	25
C(22)	0.8035(1)	-0.3398(2)	1.0942(2)	30
C(23)	0.8810(1)	-0.3407(2)	1.1055(2)	34
C(24)	0.9200(2)	-1/4	1.1141(3)	35
C(31)	0.6343(1)	-0.3465(1)	1.1582(2)	24
C(32)	0.5641(1)	-0.3839(2)	1.1240(2)	30
C(33)	0.5272(1)	-0.4568(2)	1.2017(2)	35
C(34)	0.5602(1)	-0.4949(2)	1.3182(2)	35
C(35)	0.6294(1)	-0.4589(2)	1.3547(2)	36
C(36)	0.6657(1)	-0.3868(2)	1.2763(2)	31
B(1)	0.6717(1)	-1/4	1.0790(1)	23

Table 25. Atomic distances (Å) and angles (°) for [DabcoH] $[B(C_6H_5)_4]$.

Atoms	Distance	Atoms	Angle
N(1)-C(1)	1.499(3)	C(1)-N(1)-C(3)	109.3(2)
N(1)-C(3)	1.501(2)	C(3)-N(1)-C(3)#1	110.6(3)
N(2)-C(2)	1.457(3)	C(2)-N(2)-C(4)	109.2(2)
N(2)-C(4)	1.458(3)	C(4)-N(2)-C(4)#1	109.7(3)
C(1)-C(2)	1.547(4)	N(1)-C(1)-C(2)	107.4(2)
C(3)-C(4)	1.540(4)	N(2)-C(2)-C(1)	111.2(2)
C(11)-B(1)	1.646(2)	N(1)-C(3)-C(4)	107.7(2)
C(11)-C(12)	1.411(2)	N(2)-C(4)-C(3)	111.2(2)
C(12)-C(13)	1.404(3)	C(12)-C(11)-B(1)	122.2(2)
C(13)-C(14)	1.382(4)	C(12)-C(11)-C(12)#1	115.6(3)
C(21)-B(1)	1.641(3)	C(11)-C(12)-C(13)	121.8(3)
C(21)-C(22)	1.405(2)	C(12)-C(13)-C(14)	121.2(3)
C(22)-C(23)	1.408(2)	C(13)-C(14)-C(13)#1	118.3(3)
C(23)-C(24)	1.394(3)	C(22)-C(21)-B(1)	122.3(2)
C(31)-B(1)	1.645(2)	C(22)-C(21)-C(22)#1	115.3(3)
C(31)-C(32)	1.408(2)	C(21)-C(22)-C(23)	122.8(2)
C(32)-C(33)	1.405(2)	C(22)-C(23)-C(24)	120.2(3)
C(33)-C(34)	1.398(3)	C(23)-C(24)-C(23)#1	118.6(3)
C(34)-C(35)	1.390(3)	C(32)-C(31)-B(1)	121.9(2)
C(35)-C(36)	1.398(3)	C(36)-C(31)-B(1)	121.7(2)
C(31)-C(36)	1.410(2)	C(32)-C(31)-C(36)	115.7(2)
N(1)-H(1)	1.032	C(31)-C(32)-C(33)	122.5(2)
C(1)-H(1A)	1.085	C(32)-C(33)-C(34)	120.1(2)
C(2)-H(2A)	1.085	C(33)-C(34)-C(35)	118.6(2)
C(3)-H(3A)	1.085	C(34)-C(35)-C(36)	120.9(2)
C(3)-H(3B)	1.085	C(31)-C(36)-C(35)	122.2(2)
C(4)-H(4A)	1.085	C(11)-B(1)-C(21)	107.5(2)
C(4)-H(4B)	1.085	C(11)-B(1)-C(31)	111.8(1)
C(12)-H(12)	1.076	C(21)-B(1)-C(31)	112.1(1)
C(13)-H(13)	1.076	C(31)-B(1)-C(31)#1	101.7(2)
C(14)-H(14)	1.076	C(1)-N(1)-H(1)	109.2
C(22)-H(22)	1.076	C(3)-N(1)-H(1)	109.2
C(23)-H(23)	1.076	N(1)-C(1)-H(1A)	107.1
C(24)-H(24)	1.076	C(2)-C(1)-H(1A)	111.3
C(32)-H(32)	1.076	H(1A)-C(1)-H(1A)#1	112.3
C(33)-H(33)	1.076	N(2)-C(2)-H(2A)	110.3
C(34)-H(34)	1.076	C(1)-C(2)-H(2A)	108.1
C(35)-H(35)	1.076	H(2A)-C(2)-H(2A)#1	108.7
C(36)-H(36)	1.076	N(1)-C(3)-H(3A)	102.5
		N(1)-C(3)-H(3B)	106.7
		C(4)-C(3)-H(3A)	113.4

Table 25. Atomic distances (Å) and angles (°) for [DabcoH][$B(C_6H_5)_4$] (continued).

Atoms	Distance	Atoms	Angle
		C(4)-C(3)-H(3B)	109.1
		H(3A)-C(3)-H(3B)	116.8
		N(2)-C(4)-H(4A)	107.5
		N(2)-C(4)-H(4B)	105.6
		C(3)-C(4)-H(4A)	107.9
		C(3)-C(4)-H(4B)	108.7
		H(4A)-C(4)-H(4B)	116.0
		C(11)-C(12)-H(12)	117.5
		C(13)-C(12)-H(12)	120.7
		C(12)-C(13)-H(13)	119.4
		C(14)-C(13)-H(13)	119.4
		C(13)-C(14)-H(14)	120.8
		C(21)-C(22)-H(22)	117.7
		C(23)-C(22)-H(22)	119.5
		C(22)-C(23)-H(23)	118.7
		C(24)-C(23)-H(23)	121.1
		C(23)-C(24)-H(24)	120.7
		C(31)-C(32)-H(32)	119.9
		C(33)-C(32)-H(32)	117.6
		C(32)-C(33)-H(33)	119.3
		C(34)-C(33)-H(33)	120.5
		C(33)-C(34)-H(34)	121.1
		C(35)-C(34)-H(34)	120.3
		C(34)-C(35)-H(35)	120.2
		C(36)-C(35)-H(35)	118.9
		C(31)-C(36)-H(36)	118.9
		C(35)-C(36)-H(36)	118.9

#1 x, -y-1/2, z

Table 26. Anisotropic temperature factors ($Å^2$) for the nonhydrogen atoms of [DabcoH] [$B(C_6H_5)_4$].

atom	U11	U22	U33	U12	U13	U23
N(1)	0.026(1)	0.042(1)	0.026(1)	0	0.006(1)	0
N(2)	0.029(1)	0.063(2)	0.035(1)	0	0.008(1)	0
C(1)	0.039(1)	0.049(1)	0.023(1)	0	-0.001(1)	0
C(2)	0.025(1)	0.046(1)	0.041(1)	0	-0.003(1)	0
C(3)	0.042(1)	0.052(1)	0.044(1)	-0.017(1)	0.006(1)	-0.016(1)
C(4)	0.039(1)	0.068(1)	0.043(1)	-0.026(1)	0.006(1)	0(1)
C(11)	0.023(1)	0.029(1)	0.022(1)	0	-0.002(1)	0
C(12)	0.035(1)	0.037(1)	0.029(1)	-0.005(1)	0.004(1)	-0.009(1)
C(13)	0.038(1)	0.065(1)	0.030(1)	-0.012(1)	0.003(1)	-0.017(1)
C(14)	0.030(1)	0.093(2)	0.024(1)	0	-0.002(1)	0
C(21)	0.023(1)	0.027(1)	0.024(1)	0	-0.001(1)	0
C(22)	0.026(1)	0.030(1)	0.033(1)	-0.005(1)	-0.001(1)	0.003(1)
C(23)	0.028(1)	0.038(1)	0.037(1)	-0.003(1)	-0.001(1)	0.008(1)
C(24)	0.024(1)	0.048(1)	0.032(1)	0	-0.003(1)	0
C(31)	0.024(1)	0.024(1)	0.024(1)	0.003(1)	0.000(1)	-0.001(1)
C(32)	0.025(1)	0.033(1)	0.032(1)	0.007(1)	0.000(1)	-0.003(1)
C(33)	0.029(1)	0.036(1)	0.039(1)	0.007(1)	0.001(1)	-0.006(1)
C(34)	0.038(1)	0.032(1)	0.035(1)	0.007(1)	0.007(1)	-0.005(1)
C(35)	0.045(1)	0.033(1)	0.030(1)	0.008(1)	-0.002(1)	-0.005(1)
C(36)	0.033(1)	0.034(1)	0.027(1)	0.005(1)	-0.005(1)	-0.005(1)
B(1)	0.024(1)	0.024(1)	0.021(1)	0	0.000(1)	0

Table 27. Positional parameters and isotropic temperature factors ($Å^2 \times 10^3$) for the hydrogen atoms of [DabcoH] [$B(C_6H_5)_4$].

atom	x	y	z	U(eq)
H(1)	0.7481	-1/4	0.7290	47
H(1A)	0.8589	-0.3182	0.8210	52
H(2A)	0.9632	-0.1833	0.6927	53
H(3A)	0.7458	-0.3354	0.5265	61
H(3B)	0.7990	-0.4073	0.6528	61
H(4A)	0.9001	-0.4053	0.5251	65
H(4B)	0.8510	-0.3339	0.3938	65
H(12)	0.6501	-0.4105	0.8969	48
H(13)	0.6132	-0.4104	0.6567	59
H(14)	0.5947	-1/4	0.5356	64
H(22)	0.7740	-0.4103	1.0880	45
H(23)	0.9089	-0.4123	1.1109	49
H(24)	0.9790	-1/4	1.1257	50
H(32)	0.5359	-0.3550	1.0369	45
H(33)	0.4729	-0.4812	1.1723	50
H(34)	0.5321	-0.5491	1.3807	50
H(35)	0.6556	-0.4859	1.4449	51
H(36)	0.7195	-0.3611	1.3070	46

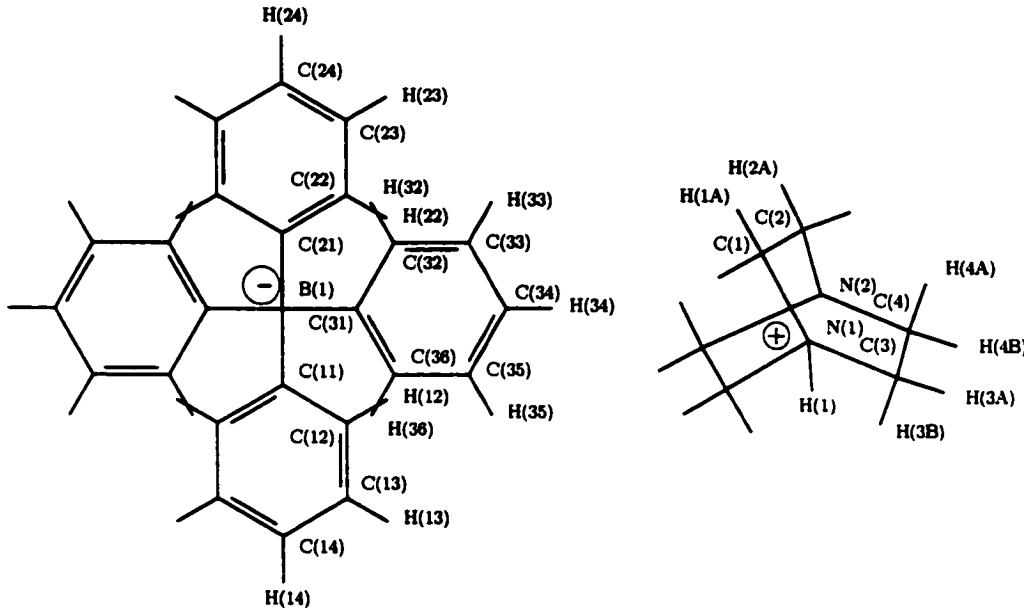

Table 28. Scale factor, extinction, kappa values, local coordinate system, and multipole population coefficients for [DabcoH][BPh4] (atom numbering as shown above).

Scale Factor	Extinction
2.278(14)	0.292(15)

	κ'	κ''
1.	0.913(26)	0.823(69)
2.	0.986(17)	1.106(97)
3.	0.962(8)	1.030(25)
4.	0.989(16)	1.141(67)
5.	0.952(16)	1.231(46)

atom	atom0	axis1	atom1	atom2	axis2	right/left	kappa set
N(1)	C(1)	Y	N(1)	N(2)	X	R	2
N(2)	C(2)	Y	N(2)	N(1)	X	L	2
C(1)	N(1)	Y	C(1)	C(2)	X	R	4
C(2)	N(2)	Y	C(2)	C(1)	X	L	4
C(3)	N(1)	Y	C(3)	C(4)	X	L	4
C(4)	N(2)	Y	C(4)	C(3)	X	R	4
C(11)	B(1)	X	C(11)	DUM0	Y	R	3
C(12)	C(13)	X	C(12)	C(11)	Y	R	3
C(13)	C(12)	X	C(13)	C(14)	Y	L	3
C(14)	H(14)	X	C(14)	DUM0	Y	R	3
C(21)	B(1)	X	C(21)	DUM0	Y	L	3
C(22)	C(23)	X	C(22)	C(21)	Y	L	3
C(23)	C(22)	X	C(23)	C(24)	Y	R	3
C(24)	H(24)	X	C(24)	DUM0	Y	L	3

Table 28. Local coordinate systems continued...

atom	atom0	axis1	atom1	atom2	axis2	right/left	kappa set
C(31)	B(1)	X	C(31)	DUM1	Y	R	3
C(32)	C(33)	X	C(32)	C(31)	Y	R	3
C(33)	C(32)	X	C(33)	C(34)	Y	L	3
C(34)	H(34)	X	C(34)	DUM1	Y	R	3
C(35)	C(36)	X	C(35)	C(34)	Y	R	3
C(36)	C(35)	X	C(36)	C(31)	Y	L	3
B(1)	DUM0	Z	B(1)	DUM2	X	R	1
H(1)	N(1)	Y	H(1)	C(1)	X	R	5
H(1A)	C(1)	Z	H(1A)	C(2)	Y	R	5
H(2A)	C(2)	Z	H(2A)	C(1)	Y	R	5
H(3A)	C(3)	Z	H(3A)	C(4)	Y	R	5
H(3B)	C(3)	Z	H(3B)	C(4)	Y	R	5
H(4A)	C(4)	Z	H(4A)	C(3)	Y	R	5
H(4B)	C(4)	Z	H(4B)	C(3)	Y	R	5
H(12)	C(12)	Z	H(12)	C(11)	Y	R	5
H(13)	C(13)	Z	H(13)	C(14)	Y	R	5
H(14)	C(14)	Z	H(14)	C(13)	Y	R	5
H(22)	C(22)	Z	H(22)	C(21)	Y	R	5
H(23)	C(23)	Z	H(23)	C(24)	Y	R	5
H(24)	C(24)	Z	H(24)	C(23)	Y	R	5
H(32)	C(32)	Z	H(32)	C(31)	Y	R	5
H(33)	C(33)	Z	H(33)	C(34)	Y	R	5
H(34)	C(34)	Z	H(34)	C(33)	Y	R	5
H(35)	C(35)	Z	H(35)	C(34)	Y	R	5
H(36)	C(36)	Z	H(36)	C(31)	Y	R	5

DUM0=0.706368 -0.250000 1.00456
DUM1=0.634295 -0.250000 1.15795
DUM2=0.642563 -0.298276 1.03803

Table 28. Multipole populations

atom	P_v	P_{00}	P_{11}	P_{1-1}	P_{10}
N(1)	2.37(8)	0.00(0)	0.00(0)	0.00(0)	0.02(2)
N(2)	2.49(8)	0.00(0)	0.00(0)	0.00(0)	0.00(2)
C(1)	1.58(7)	0.00(0)	0.04(1)	0.01(2)	0.00(0)
C(2)	1.58(0)	0.00(0)	0.04(0)	0.01(0)	0.00(0)
C(3)	3.19(14)	0.00(0)	0.09(3)	0.05(3)	0.02(2)
C(4)	3.19(0)	0.00(0)	0.09(0)	0.05(0)	0.02(0)
C(11)	1.85(5)	0.00(0)	0.01(2)	0.03(2)	0.00(0)
C(12)	3.76(8)	0.00(0)	0.11(4)	0.19(4)	−0.05(3)
C(13)	3.67(10)	0.00(0)	0.13(5)	0.05(5)	0.13(3)
C(14)	1.70(8)	0.00(0)	−0.12(3)	−0.04(3)	0.00(0)
C(21)	1.95(5)	0.00(0)	0.00(2)	0.00(2)	0.00(0)
C(22)	3.75(8)	0.00(0)	0.13(4)	0.13(4)	−0.02(3)
C(23)	3.72(9)	0.00(0)	0.09(4)	0.18(4)	−0.13(3)
C(24)	1.61(7)	0.00(0)	−0.10(3)	−0.01(2)	0.00(0)
C(31)	3.91(8)	0.00(0)	0.00(3)	0.00(2)	−0.05(4)
C(32)	3.76(8)	0.00(0)	0.12(4)	0.14(4)	−0.01(3)
C(33)	3.77(9)	0.00(0)	0.10(4)	0.18(4)	−0.03(3)
C(34)	3.89(9)	0.00(0)	−0.17(4)	0.03(3)	−0.04(6)
C(35)	3.75(9)	0.00(0)	0.14(5)	0.02(4)	−0.03(3)
C(36)	3.79(8)	0.00(0)	0.00(4)	0.21(4)	0.01(3)
B(1)	1.71(14)	0.00(0)	0.00(0)	0.00(0)	0.00(0)

Table 28. Multipole populations continued...

atom	P_v	P_{00}	P_{11}	P_{1-1}	P_{10}
H(1)	0.57(4)	0.00(0)	0.00(0)	0.13(2)	0.00(0)
H(1A)	1.34(6)	0.00(0)	0.00(0)	0.00(0)	0.29(3)
H(2A)	1.34(0)	0.00(0)	0.00(0)	0.00(0)	0.29(0)
H(3A)	1.34(0)	0.00(0)	0.00(0)	0.00(0)	0.29(0)
H(3B)	1.34(0)	0.00(0)	0.00(0)	0.00(0)	0.29(0)
H(4A)	1.34(0)	0.00(0)	0.00(0)	0.00(0)	0.29(0)
H(4B)	1.34(0)	0.00(0)	0.00(0)	0.00(0)	0.29(0)
H(12)	1.34(0)	0.00(0)	0.00(0)	0.00(0)	0.24(0)
H(13)	1.34(0)	0.00(0)	0.00(0)	0.00(0)	0.24(0)
H(14)	0.71(0)	0.00(0)	0.00(0)	0.00(0)	0.24(0)
H(22)	1.34(5)	0.00(0)	0.00(0)	0.00(0)	0.24(2)
H(23)	1.34(0)	0.00(0)	0.00(0)	0.00(0)	0.24(0)
H(24)	0.71(0)	0.00(0)	0.00(0)	0.00(0)	0.24(0)
H(32)	1.34(0)	0.00(0)	0.00(0)	0.00(0)	0.24(0)
H(33)	1.34(0)	0.00(0)	0.00(0)	0.00(0)	0.24(0)
H(34)	1.34(0)	0.00(0)	0.00(0)	0.00(0)	0.24(0)
H(35)	1.34(0)	0.00(0)	0.00(0)	0.00(0)	0.24(0)
H(36)	1.34(0)	0.00(0)	0.00(0)	0.00(0)	0.24(0)

atom	P_{20}	P_{21}	P_{2-1}	P_{22}	P_{2-2}
N(1)	0.02(3)	0.00(0)	0.00(0)	0.00(0)	0.00(0)
N(2)	0.03(3)	0.00(0)	0.00(0)	0.00(0)	0.00(0)
C(1)	−0.03(2)	0.00(0)	0.00(0)	0.06(1)	0.01(1)
C(2)	−0.03(0)	0.00(0)	0.00(0)	0.06(0)	0.01(0)
C(3)	−0.23(4)	0.02(2)	−0.03(2)	0.06(2)	0.08(2)
C(4)	−0.23(0)	0.02(0)	−0.03(0)	0.06(0)	0.08(0)
C(11)	0.06(2)	0.00(0)	0.00(0)	0.09(2)	0.04(2)
C(12)	−0.05(3)	−0.10(3)	0.04(3)	−0.08(4)	0.03(4)
C(13)	−0.13(4)	0.13(4)	−0.02(4)	−0.05(5)	−0.11(5)
C(14)	0.11(4)	0.00(0)	0.00(0)	−0.03(2)	−0.02(2)
C(21)	0.03(2)	0.00(0)	0.00(0)	0.12(2)	0.00(2)
C(22)	−0.15(3)	0.01(3)	−0.05(3)	0.05(4)	−0.04(4)
C(23)	−0.20(3)	−0.04(3)	0.01(3)	0.00(4)	−0.03(4)
C(24)	0.10(3)	0.00(0)	0.00(0)	0.01(2)	−0.03(2)
C(31)	0.04(4)	0.04(4)	−0.08(3)	0.23(3)	−0.01(2)
C(32)	−0.12(3)	−0.02(3)	−0.07(3)	0.07(4)	−0.04(4)
C(33)	−0.13(4)	0.08(3)	0.00(3)	0.00(5)	−0.06(4)
C(34)	0.16(5)	0.08(5)	0.00(4)	0.09(3)	−0.04(3)
C(35)	−0.09(4)	0.13(4)	−0.02(3)	0.08(5)	−0.07(4)
C(36)	−0.11(4)	−0.05(3)	0.06(3)	−0.02(4)	0.03(4)
B(1)	0.00(3)	0.00(0)	0.00(0)	0.00(0)	0.00(0)
H(1)	0.00(2)	0.00(0)	0.00(0)	0.00(0)	0.00(0)
H(1A)	0.11(2)	0.00(0)	0.00(0)	0.00(0)	0.00(0)
H(2A)	0.11(0)	0.00(0)	0.00(0)	0.00(0)	0.00(0)
H(3A)	0.11(0)	0.00(0)	0.00(0)	0.00(0)	0.00(0)
H(3B)	0.11(0)	0.00(0)	0.00(0)	0.00(0)	0.00(0)
H(4A)	0.11(0)	0.00(0)	0.00(0)	0.00(0)	0.00(0)
H(4B)	0.11(0)	0.00(0)	0.00(0)	0.00(0)	0.00(0)
H(12)	0.09(0)	0.00(0)	0.00(0)	0.00(0)	0.00(0)
H(13)	0.09(0)	0.00(0)	0.00(0)	0.00(0)	0.00(0)
H(14)	0.09(0)	0.00(0)	0.00(0)	0.00(0)	0.00(0)

Table 28. Multipole populations continued...

atom	P_{20}	P_{21}	P_{2-1}	P_{22}	P_{2-2}
H(22)	0.09(2)	0.00(0)	0.00(0)	0.00(0)	0.00(0)
H(23)	0.09(0)	0.00(0)	0.00(0)	0.00(0)	0.00(0)
H(24)	0.09(0)	0.00(0)	0.00(0)	0.00(0)	0.00(0)
H(32)	0.09(0)	0.00(0)	0.00(0)	0.00(0)	0.00(0)
H(33)	0.09(0)	0.00(0)	0.00(0)	0.00(0)	0.00(0)
H(34)	0.09(0)	0.00(0)	0.00(0)	0.00(0)	0.00(0)
H(35)	0.09(0)	0.00(0)	0.00(0)	0.00(0)	0.00(0)
H(36)	0.09(0)	0.00(0)	0.00(0)	0.00(0)	0.00(0)

atom	P_{30}	P_{31}	P_{3-1}	P_{32}	P_{3-2}	P_{33}	P_{3-3}
N(1)	−0.10(2)	0.00(0)	0.00(0)	0.00(0)	0.00(0)	0.12(2)	0.00(0)
N(2)	−0.07(2)	0.00(0)	0.00(0)	0.00(0)	0.00(0)	0.16(2)	0.00(0)
C(1)	0.00(0)	−0.07(1)	−0.01(1)	0.00(0)	0.00(0)	0.01(1)	−0.07(1)
C(2)	0.00(0)	−0.07(0)	−0.01(0)	0.00(0)	0.00(0)	0.01(0)	−0.07(0)
C(3)	0.11(2)	−0.04(2)	0.02(2)	−0.02(2)	0.06(2)	−0.01(2)	−0.18(2)
C(4)	0.11(0)	−0.04(0)	0.02(0)	−0.02(0)	0.06(0)	−0.01(0)	−0.18(0)
C(11)	0.00(0)	−0.10(2)	−0.01(2)	0.00(0)	0.00(0)	0.05(1)	0.01(1)
C(12)	0.03(3)	0.00(3)	−0.04(2)	−0.04(3)	0.03(3)	0.27(3)	0.00(3)
C(13)	−0.08(3)	0.02(3)	−0.03(3)	−0.03(4)	−0.12(3)	0.16(4)	−0.09(4)
C(14)	0.00(0)	−0.09(3)	−0.01(3)	0.00(0)	0.00(0)	0.04(2)	−0.03(2)
C(21)	0.00(0)	−0.10(2)	0.02(2)	0.00(0)	0.00(0)	0.02(1)	0.01(1)
C(22)	−0.02(2)	−0.03(2)	0.03(2)	0.01(3)	−0.02(3)	0.26(3)	0.09(3)
C(23)	0.01(3)	0.06(3)	−0.01(3)	0.02(3)	0.01(3)	0.28(4)	−0.10(4)
C(24)	0.00(0)	−0.09(3)	−0.02(2)	0.00(0)	0.00(0)	0.05(2)	−0.01(1)
C(31)	−0.03(3)	−0.21(3)	0.02(2)	−0.02(3)	0.07(3)	0.08(2)	0.00(2)
C(32)	0.00(3)	−0.05(3)	−0.01(2)	−0.02(3)	0.02(2)	0.24(3)	0.04(3)
C(33)	0.03(3)	0.03(3)	−0.04(2)	0.03(3)	−0.01(3)	0.22(3)	−0.08(4)
C(34)	0.01(4)	−0.26(3)	0.04(3)	0.01(3)	0.01(3)	0.07(2)	0.01(2)
C(35)	0.02(3)	−0.02(3)	0.07(3)	0.04(3)	0.02(3)	0.19(3)	−0.06(4)
C(36)	−0.07(3)	0.01(3)	0.02(2)	−0.02(3)	−0.01(2)	0.24(3)	0.05(3)
B(1)	0.00(0)	0.00(0)	0.00(0)	0.00(0)	0.29(6)	0.00(0)	0.00(0)

Table 29. Results of the rigid body thermal motion analysis for the tetraphenylborate anion in [DabcoH][$B(C_6H_5)_4$].[a]

Rigid body variables fitted		12	
Translational tensor, **T** (Å^2)	0.0248(11)	0	0
		0.0217(10)	0.0014(8)
			0.0254(11)
Principal values (Å^2)	0.0248	0.0212	0.0259
Square root (Å)	0.16	0.15	0.16
Librational tensor, **L** (deg^2)	1.3(4)	0	0
		3.5(5)	1.2(3)
			7.6(7)
Principal values (deg^2)	1.3	3.2	7.9
Square root (deg)	1.2	1.8	2.8
Cross tensor, **S** (Å-deg)	0	-0.049(13)	0.026(10)
	-0.005(14)	0	0
	0.068(12)	0	0
R_w[b]		0.153	
Z[c]		0.00394	
Corrections to interatomic distances due to libration		0.0013 to 0.0022Å	
Esd's on the calculated interatomic distances		0.002 to 0.004Å	

[a] Tensor components are given with respect to the axes of the principal moments of inertia and with the origin at the center of mass.

[b] $R_w = (X^2 / \Sigma[U_{ij}/\sigma_{Uij}]^2)^{1/2}$ where $X^2 = \Sigma[\Delta U_{ij}/\sigma_{Uij}]^2)$

[c] $Z = (X^2 / NFREE)^{1/2}$ where NFREE = 138

Table 29. Results of the rigid body thermal motion analysis for the cation in [DabcoH] [$B(C_6H_5)_4$].[a]

Rigid body variables fitted		12	
Translational tensor, **T** ($Å^2$)	0.0267(10)	0	-0.0018(7)
		0.0368(10)	0
			0.0213(9)
Principal values ($Å^2$)	0.0272	0.0368	0.0208
Square root (Å)	0.17	0.19	0.14
Librational tensor, **L** (deg^2)	33.3(22)	0	-6.3(12)
		15.4(22)	0
			44.9(18)
Principal values (deg^2)	30.6	15.4	47.7
Square root (deg)	5.5	3.9	6.9
Cross tensor, **S** (Å-deg)	0	0.215(18)	0
	-0.083(18)	0	-0.097(24)
	0	-0.462(19)	0
R_w[b]		0.0465	
Z[c]		0.00174	
Corrections to interatomic distances due to libration		0.0114 to 0.0167Å	
Esd's on the calculated interatomic distances		0.002 to 0.004Å	

[a] Tensor components are given with respect to the axes of the principal moments of inertia and with the origin at the center of mass.

[b] $R_w = (X^2 / \Sigma[U_{ij}/\sigma_{Uij}]^2)^{1/2}$ where $X^2 = \Sigma[\Delta U_{ij}/\sigma_{Uij}]^2)$

[c] $Z = (X^2 / NFREE)^{1/2}$ where NFREE = 36

Table 29. Results of the rigid body thermal motion analysis for the cation in [DabcoH] [$B(C_6H_5)_4$] (continued).

Interatomic distances corrected for libration

Atoms		Librational Correction	Corrected Bond Length
N(1)	C(1)	0.0127(6)	1.5118
N(1)	C(3)	0.0167(5)	1.5179
N(2)	C(2)	0.0140(6)	1.4710
N(2)	C(4)	0.0153(4)	1.4733
C(1)	C(2)	0.0115(7)	1.5584
C(3)	C(4)	0.0114(7)	1.5513

Table 30. Short intermolecular cation...anion contacts for [DabcoH] [$B(C_6H_5)_4$].

Part 1	C-H...phenyl		(cation/anion)
contact	C...C (Å)	H...C (Å)	C-H...C (°)
C(2)-H(2A)...ring 1 symmetry a (1/2+x, -1/2-y, 3/2-z) and b (1/2+x, y, 3/2-z)			
C(11)	4.080(3)	3.681	103.9
C(12a)	4.013(3)	3.277	126.1
C(12b)	4.013(3)	3.866	89.8
C(13a)	3.848(3)	3.044	131.4
C(13b)	3.848(3)	3.667	91.3
C(14)	3.778(3)	3.275	109.5
mean	**3.930[8]**	**3.468**	**108.7**
centroid[a]	3.674	3.187	108.3
plane[b]	3.650	3.022	35.4
C(3)-H(3A)...ring 1 symmetry a (x, y, z) and b (x, -1/2-y, z)			
C(11)	4.411(3)	4.408	83.1
C(12a)	3.803(3)	3.680	88.1
C(12b)	4.511(3)	4.351	91.5
C(13a)	3.399(4)	2.894	108.6
C(13b)	4.172(3)	3.706	108.1
C(14)	3.616(4)	2.918	122.3
mean	**3.985[8]**	**3.660**	**100.3**
centroid[a]	3.754	3.438	99.0
plane[b]	3.376	2.662	42.3

Table 30. Short intermolecular cation...anion contacts for [DabcoH] [B(C_6H_5)$_4$] (continued).

Part 1	C-H...phenyl		(cation/anion)
contact	C...C (Å)	H...C (Å)	C-H...C (°)
C(1)-H(1A)...ring 2 symmetry a (x, y, z) and b (x, -1/2-y, z)			
C(21)	3.751(3)	3.332	104.3
C(22a)	3.680(3)	2.911	128.0
C(22b)	3.680(3)	3.571	87.1
C(23a)	3.653(3)	2.874	128.8
C(23b)	3.653(3)	3.547	86.9
C(24)	3.674(3)	3.247	104.6
mean	**3.682[7]**	**3.247**	**106.6**
centroid[c]	3.404	2.942	106.0
plane[d]	3.403	2.799	33.8
C(4)-H(4B)...ring 2 symmetry a (x, y, -1+z) and b (x, -1/2-y, -1+z)			
C(21)	4.635(3)	3.593	161.4
C(22a)	4.186(2)	3.105	174.1
C(22b)	4.815(2)	3.861	147.9
C(23a)	3.922(2)	2.921	153.4
C(23b)	4.593(2)	3.722	138.7
C(24)	4.123(2)	3.246	138.6
mean	**4.379[5]**	**3.408**	**152.4**
centroid[c]	4.161	3.125	159.9
plane[d]	3.912	2.894	69.7

Table 30. Short intermolecular cation...anion contacts for [DabcoH] [B(C_6H_5)$_4$] (continued).

Part 1	C-H...phenyl		(cation/anion)
contact	C...C (Å)	H...C (Å)	C-H...C (°)
C(1)-H(1A)...ring 3 symmetry (3/2-x, -1-y, -1/2+z)			
C(31)	5.433(2)	4.723	126.0
C(32)	5.205(2)	4.617	117.3
C(33)	4.407(3)	3.811	116.8
C(34)	3.703(2)	2.874	133.2
C(35)	3.965(2)	2.975	151.9
C(36)	4.831(1)	3.953	139.7
mean	**4.591[5]**	**3.825**	**130.8**
centroid[e]	4.416	3.631	130.7
plane[f]	3.371	2.414	61.9
C(2)-H(2A)...ring 3 symmetry (3/2-x, 1/2+y, -1/2+z)			
C(31)	5.466(2)	4.804	122.6
C(32)	4.862(2)	4.048	133.8
C(33)	3.964(2)	3.002	148.1
C(34)	3.688(2)	2.819	137.1
C(35)	4.406(2)	3.771	119.4
C(36)	5.221(3)	4.639	116.9
mean	**4.601[5]**	**3.847**	**129.6**
centroid[e]	4.429	3.660	129.4
plane[f]	3.323	2.304	69.9

Table 30. Short intermolecular cation...anion contacts for [DabcoH] [$B(C_6H_5)_4$] (continued).

Part 1	C-H...phenyl		(cation/anion)
contact	C...C (Å)	H...C (Å)	C-H...C (°)
C(3)-H(3A)...ring 3 symmetry (x, y, -1+z)			
C(31)	5.159(4)	4.187	150.4
C(32)	6.245(3)	5.225	158.0
C(33)	6.365(3)	5.358	156.1
C(34)	5.415(3)	4.479	146.3
C(35)	4.087(3)	3.169	142.9
C(36)	3.916(3)	2.961	147.0
mean	**5.198[8]**	**4.230**	**150.1**
centroid[e]	5.094	4.095	154.2
plane[f]	1.050	1.205	8.2
C(3)-H(3B)...ring 3 symmetry (3/2-x, -1-y, -1/2+z)			
C(31)	4.353(3)	3.473	139.3
C(32)	4.425(3)	3.722	124.3
C(33)	4.311(3)	3.656	120.6
C(34)	4.093(3)	3.300	130.9
C(35)	3.985(3)	2.975	155.1
C(36)	4.105(2)	3.055	163.0
mean	**4.212[7]**	**3.363**	**138.9**
centroid[e]	3.975	3.071	141.2
plane[f]	3.917	2.916	67.4

Table 30. Short intermolecular cation...anion contacts for [DabcoH] [$B(C_6H_5)_4$] (continued).

Part 1	C-H...phenyl		(cation/anion)
contact	C...C (Å)	H...C (Å)	C-H...C (°)
C(4)-H(4A)...ring 3	symmetry (3/2-x, -1-y, -1/2+z)		
C(31)	4.437(3)	3.594	135.8
C(32)	4.054(2)	3.026	158.4
C(33)	3.870(3)	2.854	156.0
C(34)	4.077(3)	3.282	131.0
C(35)	4.429(2)	3.778	120.6
C(36)	4.584(2)	3.902	122.9
mean	**4.242[6]**	**3.406**	**137.4**
centroid[e]	4.012	3.128	139.1
plane[f]	3.859	2.832	71.1

Part 2	Other cation/anion contacts of less than 3Å[g]		
N(2)...H(32)	symmetry (1/2+x, -1/2-y, 3/2-z) or (1/2+x, y, 3/2-z)		2.743 Å

[a] The position of the centroid of ring 1 is (0.6314, -0.2500, 0.7772). The values listed are *d*(N/C...centroid), *d*(H...centroid) and the angle N/C-H...centroid.

[b] The mean deviation of the carbon atoms from the ring 1 plane is 0.0100Å. The values listed are *d*(N/C...plane), *d*(H...plane) and the angle the N/C-H vector makes with the plane of the ring.

[c] The position of the centroid of ring 2 is (0.8418, -0.2500, 1.1007). The values listed are *d*(C...centroid), *d*(H...centroid) and the angle C-H...centroid.

[d] The mean deviation of the carbon atoms from the ring 2 plane is 0.0127Å. The values listed are *d*(C...plane), *d*(H...plane) and the angle the C-H vector makes with the plane of the ring.

[e] The position of the centroid of ring 3 is (0.5968, -0.4213, 1.2389). The values listed are *d*(C...centroid), *d*(H...centroid) and the angle C-H...centroid.

[f] The mean deviation of the carbon atoms from the ring 3 plane is 0.0015Å. The values listed are *d*(C...plane), *d*(H...plane) and the angle the C-H vector makes with the plane of the ring.

[g] This is the only other contact to the cation from the anion of less than 3Å (C-H...N).

Table 31. Bond critical points for the short intermolecular cation...anion contacts in [DabcoH][$B(C_6H_5)_4$].

Contact	Hessian Eigenvalues			Charge Density	Laplacian	Ellipticity	Position		
Bond Path	λ_1	λ_2	λ_3	$\rho_b(\mathbf{r})$ (eA^{-3})	$\nabla^2\rho_b(\mathbf{r})$ (eA^{-5})	ε	x	y (fractional)	z
C-H...phenyl (cation/anion)									
ring 1...H(3A)-C(3) symmetry (x, y, z)									
no critical point located									
ring 1...H(2A)-C(2) symmetry (-1/2+x, -1/2-y, 3/2-z) single atom type hydrogen bond									
C(13)...H(2A)	-0.05,	-0.02,	0.40	0.035(1)	0.322(1)	1.21	0.5283,	-0.3188,	0.7729

Bond Lengths and Angles at the Critical Point

Atoms	Distance (Å)	Atoms	Angle (°)
Cp...C(2)	2.070	C(2)...Cp...C(13)	162.5
Cp...H(2A)	1.229	H(2A)...Cp...C(13)	171.2
Cp...C(13)	1.823	C(2)-H(2A)...Cp	126.8
Cp...plane	1.793		
Cp...centroid	2.077		

Table 31. Bond critical points for the short intermolecular cation...anion contacts in [DabcoH][$B(C_6H_5)_4$] (continued).

Contact	C-H...phenyl (cation/anion)								
	Hessian Eigenvalues			Charge Density	Laplacian	Ellipticity	Position		
Bond Path	λ_1	λ_2	λ_3	$\rho_b(\mathbf{r})$ ($e\text{Å}^{-3}$)	$\nabla^2\rho_b(\mathbf{r})$ ($e\text{Å}^{-5}$)	ε	x	y (fractional)	z
ring 2...H(1A)-C(1)*	symmetry (x, y, z)			edge type hydrogen bond					
C(22)-C(23)...H(1A)	-0.06,	-0.05,	0.57	0.049(4)	0.467(2)	0.33	0.8540,	-0.3179,	0.9357

Bond Lengths and Angles at the Critical Point

Atoms	Distance (Å)	Atoms	Angle (°)
Cp...C(1)	1.966	C(1)...Cp...C(23)	153.8
Cp...H(1A)	1.145	H(1A)...Cp...C(23)	157.3
Cp...C(23)	1.784	C(1)...Cp...C(22)	149.8
Cp...C(22)	1.846	H(1A)...Cp...C(22)	152.8
		C(1)-H(1A)...Cp	123.7
Cp...plane	1.654		
Cp...centroid	1.884		

* The bond path is from H(1A) to the approximate midpoint of the C(22)-C(23) bond in the ring and terminates at C(23).

Table 31. Bond critical points for the short intermolecular cation...anion contacts in [DabcoH][$B(C_6H_5)_4$] (continued).

Contact	C-H...phenyl (cation/anion)								
	Hessian Eigenvalues			Charge Density	Laplacian	Ellipticity	Position		
Bond Path	λ_1	λ_2	λ_3	$\rho_b(\mathbf{r})$ ($e\text{Å}^{-3}$)	$\nabla^2\rho_b(\mathbf{r})$ ($e\text{Å}^{-5}$)	ε	x	y (fractional)	z
ring 2...H(4B)-C(4)[a]	symmetry (x, y, 1+z)				edge type hydrogen bond				
C(22)-C(23)...H(4B)	-0.11,	-0.08,	0.43	0.047(1)	0.248(1)	0.45	0.8502,	-0.3326,	1.2763

Bond Lengths and Angles at the Critical Point

Atoms	Distance (Å)	Atoms	Angle (°)
Cp...C(4)	2.235	C(4)...Cp...C(23)	153.6
Cp...H(4B)	1.169	H(4B)...Cp...C(23)	160.8
Cp...C(23)	1.792	C(4)...Cp...C(22)	161.9
Cp...C(22)	2.003	H(4B)...Cp...C(22)	155.5
		C(4)-H(4B)...Cp	165.0
Cp...plane	1.730		
Cp...centroid	2.066		

[a] The bond path from H(4B) follows the C(22)-C(23) bond of the ring for approximately one quarter of its length before terminating at C(23).

Table 31. Bond critical points for the short intermolecular cation...anion contacts in [DabcoH][$B(C_6H_5)_4$] (continued).

Contact	C-H...phenyl (cation/anion)								
	Hessian Eigenvalues			Charge Density	Laplacian	Ellipticity	Position		
Bond Path	λ_1	λ_2	λ_3	$\rho_b(\mathbf{r})$ ($e\text{Å}^{-3}$)	$\nabla^2\rho_b(\mathbf{r})$ ($e\text{Å}^{-5}$)	ε	x	y (fractional)	z
ring 3...H(1A)-C(1)*	symmetry (3/2-x, -1-y, 1/2+z)					edge type hydrogen bond			
C(34)-C(35)...H(1A)	-0.10,	-0.03,	0.48	0.050(7)	0.346(2)	1.93	0.6201,	-0.6023,	1.3308

Bond Lengths and Angles at the Critical Point

Atoms	Distance (Å)	Atoms	Angle (°)
Cp...C(1)	2.111	C(1)...Cp...C(34)	142.7
Cp...H(1A)	1.126	H(1A)...Cp...C(34)	158.7
Cp...C(34)	1.796	C(1)...Cp...C(35)	160.9
Cp...C(35)	1.910	H(1A)...Cp...C(35)	156.1
		C(1)-H(1A)...Cp	145.3
Cp...plane	1.433		
Cp...centroid	2.597		

* The bond path from H(1A) follows the C(34)-C(35) bond of the ring for approximately one quarter of its length before terminating at C(34).

Table 31. Bond critical points for the short intermolecular cation...anion contacts in [DabcoH][$B(C_6H_5)_4$] (continued).

Contact	C-H...phenyl (cation/anion)								
	Hessian Eigenvalues			Charge Density	Laplacian	Ellipticity	Position		
Bond Path	λ_1	λ_2	λ_3	$\rho_b(\mathbf{r})$ ($eÅ^{-3}$)	$\nabla^2\rho_b(\mathbf{r})$ ($eÅ^{-5}$)	ε	x	y (fractional)	z
ring 3...H(2A)-C(2)*	symmetry (3/2-x, -1/2+y, 1/2+z)					intermediate type contact			
C(34)-H(34)...H(2A)	-0.10,	-0.07,	0.55	0.053(1)	0.379(1)	0.49	0.5408,	-0.6098,	1.2429

Bond Lengths and Angles at the Critical Point

Atoms	Distance (Å)	Atoms	Angle (°)
Cp...C(2)	2.060	C(2)...Cp...C(34)	153.4
Cp...H(2A)	1.096	H(2A)...Cp...C(34)	172.0
Cp...C(34)	1.730	C(2)...Cp...H(34)	141.6
Cp...H(34)	1.596	H(2A)...Cp...H(34)	146.3
		C(2)-H(2A)...Cp	141.6
Cp...plane	1.359		
Cp...centroid	2.691		

* The bond path follows the C(34)-H(34) bond of the ring for approximately one third of its length before terminating at C(34).

Table 31. Bond critical points for the short intermolecular cation...anion contacts in [DabcoH][$B(C_6H_5)_4$] (continued).

Contact	Hessian Eigenvalues			Charge Density	Laplacian	Ellipticity	Position		
Bond Path	λ_1	λ_2	λ_3	$\rho_b(\mathbf{r})$ ($eÅ^{-3}$)	$\nabla^2\rho_b(\mathbf{r})$ ($eÅ^{-5}$)	ε	x	y (fractional)	z
C-H...phenyl (cation/anion)									
ring 3...H(3A)-C(3)	symmetry (x, y, 1+z)				H...H type contact				
H(36)...H(3A)	-0.15,	-0.08,	0.64	0.056(0)	0.413(1)	0.86	0.7248,	-0.3492,	1.4282

Bond Lengths and Angles at the Critical Point

Atoms	Distance (Å)	Atoms	Angle (°)
Cp...C(3)	2.028	C(3)...Cp...H(36)	144.2
Cp...H(3A)	1.066	H(3A)...Cp...H(36)	162.7
Cp...H(36)	1.222	C(3)...Cp...C(36)	166.3
Cp...C(36)	1.916	H(3A)...Cp...C(36)	165.8
		C(3)-H(3A)...Cp	141.1
Cp...plane	0.711		
Cp...centroid	3.136		

Table 31. Bond critical points for the short intermolecular cation...anion contacts in [DabcoH][$B(C_6H_5)_4$] (continued).

Contact	C-H...phenyl (cation/anion)								
	Hessian Eigenvalues			Charge Density	Laplacian	Ellipticity	Position		
Bond Path	λ_1	λ_2	λ_3	$\rho_b(\mathbf{r})$ ($e\text{Å}^{-3}$)	$\nabla^2\rho_b(\mathbf{r})$ ($e\text{Å}^{-5}$)	ε	x	y (fractional)	z
ring 3...H(3B)-C(3)*	symmetry (3/2-x, -1-y, 1/2+z)					edge type hydrogen bond			
C(35)-C(36)...H(3B)	-0.10,	-0.05,	0.40	0.045(1)	0.240(1)	0.96	0.6794,	-0.5252,	1.2207

Bond Lengths and Angles at the Critical Point

Atoms	Distance (Å)	Atoms	Angle (°)
Cp...C(3)	2.247	C(3)...Cp...C(35)	155.0
Cp...H(3B)	1.186	H(3B)...Cp...C(35)	159.9
Cp...C(35)	1.833	C(3)...Cp...C(36)	158.5
Cp...C(36)	1.930	H(3B)...Cp...C(36)	156.6
		C(3)-H(3B)...Cp	163.4
Cp...plane	1.737		
Cp...centroid	2.039		

* The bond path is from H(3B) to the approximate midpoint of the C(35)-C(36) bond in the ring and terminates at C(35).

Table 31. Bond critical points for the short intermolecular cation...anion contacts in [DabcoH][$B(C_6H_5)_4$] (continued).

Contact	C-H...phenyl (cation/anion)								
	Hessian Eigenvalues			Charge Density	Laplacian	Ellipticity	Position		
Bond Path	λ_1	λ_2	λ_3	$\rho_b(\mathbf{r})$ (eÅ^{-3})	$\nabla^2\rho_b(\mathbf{r})$ (eÅ^{-5})	ε	x	y (fractional)	z
ring 3...H(4A)-C(4)*	symmetry (3/2-x, -1-y, 1/2+z)					edge type hydrogen bond			
C(32)-C(33)...H(4A)	-0.12,	-0.09,	0.46	0.051(1)	0.253(1)	0.36	0.5725,	-0.5312,	1.0838

Bond Lengths and Angles at the Critical Point

Atoms	Distance (Å)	Atoms	Angle (°)
Cp...C(4)	2.196	C(4)...Cp...C(33)	159.4
Cp...H(4A)	1.137	H(4A)...Cp...C(33)	166.3
Cp...C(33)	1.737	C(4)...Cp...C(32)	150.7
Cp...C(32)	1.994	H(4A)...Cp...C(32)	149.1
		C(4)-H(4A)...Cp	162.6
Cp...plane	1.696		
Cp...centroid	2.165		

* The bond path from H(4A) follows the C(32)-C(33) bond of the ring for approximately one quarter of its length before terminating at C(33).

Table 31. Bond critical points for the short intermolecular cation...anion contacts in [DabcoH][B(C_6H_5)$_4$] (continued).

Contact	Hessian Eigenvalues			Charge Density	Laplacian	Ellipticity	Position (anion/cation)		
Bond Path	λ_1	λ_2	λ_3	$\rho_b(\mathbf{r})$ (eÅ^{-3})	$\nabla^2\rho_b(\mathbf{r})$ (eÅ^{-5})	ε	x	y (fractional)	z
C(32)-H(32)...N(2)	symmetry (-1/2+x, -1/2-y, 3/2-z)								
H(32)...N(2)	-0.10,	-0.07,	0.62	0.051(0)	0.456(1)	0.37	0.4830,	-0.3146,	1.0013

Bond Lengths and Angles at the Critical Point

Atoms	Distance (Å)	Atoms	Angle (°)
Cp...N(2)	1.598	N(2)...Cp...C(32)	155.2
Cp...H(32)	1.152	N(2)...Cp...H(32)	171.7
Cp...C(32)	2.118	Cp...H(32)-C(32)	143.8
H(32)...N(2)	2.743	C(32)-H(32)...N(2)	139.7
C(32)...N(2)	3.631		

Table 32. Short intermolecular anion...anion contacts for [DabcoH] [$B(C_6H_5)_4$].

Ring 1					
no contacts					
Ring 2					
C(22)	-	H(35)	2.841	symmetry	(3/2-x, -1-y, -1/2+z)
C(23)	-	H(35)	2.874	symmetry	(3/2-x, -1-y, -1/2+z)
Ring 3					
C(33)	-	H(23)	2.901	symmetry	(-1/2+x, y, 5/2-z)

Table 33. Bond critical points for the short intermolecular anion...anion contacts in [DabcoH][$B(C_6H_5)_4$].

				C-H...phenyl		(anion/anion)			
Contact	Hessian Eigenvalues			Charge Density	Laplacian	Ellipticity	Position		
Bond Path	λ_1	λ_2	λ_3	$\rho_b(\mathbf{r})$ ($eÅ^{-3}$)	$\nabla^2\rho_b(\mathbf{r})$ ($eÅ^{-5}$)	ε	x	y (fractional)	z
C(35)-H(35)...ring 2*	symmetry (3/2-x, -1-y, 1/2+z) and (3/2-x, 1/2+y, 1/2+z)								
	H...H type contact								
H(35)...H(22)	-0.17,	-0.11,	0.72	0.065(0)	0.441(0)	0.53	0.6765,	-0.5452,	1.5109

Bond Lengths and Angles at the Critical Point

Atoms	Distance (Å)	Atoms	Angle (°)
H(35)...H(22)	2.354	C(35)-H(35)...H(22)	159.6
H(35)...C(22)	2.841	C(35)-H(35)...C(22)	145.1
Cp...H(35)	1.091	H(35)...Cp...H(22)	155.2
Cp...H(22)	1.318	C(35)-H(35)...Cp	153.3
Cp...C(35)	2.109		
Cp...C(22)	1.769		

* The bond path from H(35) follows the C(22)-H(22) bond of the ring for approximately one quarter of its length before terminating at H(22).

Table 33. Bond critical points for the short intermolecular anion...anion contacts in [DabcoH][$B(C_6H_5)_4$] (continued).

Contact	C-H...phenyl Hessian Eigenvalues			Charge Density	Laplacian	(anion/anion) Ellipticity	Position		
Bond Path	λ_1	λ_2	λ_3	$\rho_b(\mathbf{r})$ ($eÅ^{-3}$)	$\nabla^2\rho_b(\mathbf{r})$ ($eÅ^{-5}$)	ε	x	y (fractional)	z
C(23)-H(23)...ring 3* symmetry (1/2+x, y, 5/2-z) H...H type contact									
H(23)...C(33)-H(33)	-0.09,	-0.06,	0.62	0.052(0)	0.472(0)	0.49	0.9552,	-0.4300,	1.1925

Bond Lengths and Angles at the Critical Point

Atoms	Distance (Å)	Atoms	Angle (°)
H(23)...C(33)	2.901	C(23)-H(23)...C(33)	124.0
H(23)...H(33)	2.613	C(23)-H(23)...H(33)	123.9
Cp...H(23)	1.191	H(23)...Cp...C(33)	174.9
Cp...C(33)	1.713	H(23)...Cp...H(33)	145.9
Cp...H(33)	1.540	C(23)-H(23)...Cp	122.6
Cp...C(23)	1.989		

* The bond path is from H(23) to the approximate midpoint of the C(33)-H(33) bond in the ring and terminates at C(33).

Table 34. Positional parameters and isotropic temperature factors ($Å^2 \times 10^3$) for the nonhydrogen atoms of guanidinium tetraphenylborate acetonitrile solvate.

atom	x	y	z	U(eq)
N(1)	0.7502(3)	0.6627(2)	0.4515(4)	56
N(2)	0.7214(2)	0.5590(2)	0.2460(3)	50
N(3)	0.6686(2)	0.5042(2)	0.4661(3)	48
N(4)	0.8318(3)	0.7654(2)	0.7395(3)	56
C(1)	0.7156(2)	0.5747(2)	0.3899(3)	36
C(2)	0.8936(4)	0.8364(3)	0.7781(4)	41
C(3)	0.9710(3)	0.9264(2)	0.8271(3)	54
C(11)	1.2690(1)	0.8462(1)	0.2713(2)	27
C(12)	1.3281(2)	0.9267(1)	0.3620(2)	32
C(13)	1.3874(2)	1.0083(1)	0.3056(2)	38
C(14)	1.3890(2)	1.0121(1)	0.1543(3)	42
C(15)	1.3316(2)	0.9338(2)	0.0608(2)	40
C(16)	1.2722(2)	0.8529(1)	0.1192(2)	33
C(21)	1.0196(1)	0.7909(1)	0.3027(2)	29
C(22)	0.9689(2)	0.8560(1)	0.4010(2)	36
C(23)	0.8318(2)	0.8931(1)	0.3703(3)	45
C(24)	0.7398(2)	0.8672(2)	0.2380(3)	47
C(25)	0.7871(2)	0.8050(2)	0.1361(2)	43
C(26)	0.9244(2)	0.7678(1)	0.1686(2)	34
C(31)	1.2504(2)	0.7377(1)	0.5117(2)	28
C(32)	1.3981(2)	0.7414(1)	0.5654(2)	33
C(33)	1.4597(2)	0.7221(1)	0.7127(2)	38
C(34)	1.3753(2)	0.6975(1)	0.8143(2)	41
C(35)	1.2292(2)	0.6913(1)	0.7651(2)	40
C(36)	1.1689(2)	0.7102(1)	0.6167(2)	33
C(41)	1.2038(1)	0.6500(1)	0.2522(2)	28
C(42)	1.3275(2)	0.6253(1)	0.2008(2)	32
C(43)	1.3477(2)	0.5318(1)	0.1435(2)	39
C(44)	1.2440(2)	0.4587(1)	0.1345(2)	42
C(45)	1.1204(2)	0.4802(1)	0.1853(2)	44
C(46)	1.1028(2)	0.5737(1)	0.2435(2)	37
B(1)	1.1852(2)	0.7557(1)	0.3350(2)	27

Table 35. Atomic distances (Å) and angles (°) for guanidinium tetraphenylborate acetonitrile solvate.

Atoms	Distance	Atoms	Angle
N(1)-C(1)	1.329(3)	N(1)-C(1)-N(2)	119.5(3)
N(2)-C(1)	1.346(3)	N(1)-C(1)-N(3)	120.7(3)
N(3)-C(1)	1.320(3)	N(2)-C(1)-N(3)	119.7(3)
N(4)-C(2)	1.144(4)	N(4)-C(2)-C(3)	179.7(3)
C(2)-C(3)	1.446(5)	C(12)-C(11)-C(16)	116.1(2)
C(11)-C(12)	1.4107(19)	C(12)-C(11)-B(1)	122.2(2)
C(11)-C(16)	1.403(2)	C(16)-C(11)-B(1)	121.3(2)
C(11)-B(1)	1.6391(19)	C(11)-C(12)-C(13)	122.6(2)
C(12)-C(13)	1.393(2)	C(12)-C(13)-C(14)	119.6(2)
C(13)-C(14)	1.391(3)	C(13)-C(14)-C(15)	119.6(2)
C(14)-C(15)	1.398(3)	C(14)-C(15)-C(16)	119.9(2)
C(15)-C(16)	1.395(2)	C(11)-C(16)-C(15)	122.1(2)
C(21)-C(22)	1.4176(19)	C(22)-C(21)-C(26)	115.5(2)
C(21)-C(26)	1.413(2)	C(22)-C(21)-B(1)	121.6(2)
C(21)-B(1)	1.6537(19)	C(26)-C(21)-B(1)	122.5(2)
C(22)-C(23)	1.407(2)	C(21)-C(22)-C(23)	122.7(2)
C(23)-C(24)	1.394(3)	C(22)-C(23)-C(24)	120.2(2)
C(24)-C(25)	1.401(3)	C(23)-C(24)-C(25)	118.8(2)
C(25)-C(26)	1.410(2)	C(24)-C(25)-C(26)	120.4(2)
C(31)-C(32)	1.4178(18)	C(21)-C(26)-C(25)	122.3(2)
C(31)-C(36)	1.4080(18)	C(32)-C(31)-C(36)	115.3(2)
C(31)-B(1)	1.642(2)	C(32)-C(31)-B(1)	120.5(2)
C(32)-C(33)	1.396(2)	C(36)-C(31)-B(1)	124.0(2)
C(33)-C(34)	1.393(3)	C(31)-C(32)-C(33)	123.0(2)
C(34)-C(35)	1.399(3)	C(32)-C(33)-C(34)	120.0(2)
C(35)-C(36)	1.400(3)	C(33)-C(34)-C(35)	118.8(2)
C(41)-C(42)	1.4140(18)	C(34)-C(35)-C(36)	120.6(2)
C(41)-C(46)	1.4055(19)	C(31)-C(36)-C(35)	122.3(2)
C(41)-B(1)	1.6502(19)	C(42)-C(41)-C(46)	115.1(2)
C(42)-C(43)	1.405(2)	C(42)-C(41)-B(1)	123.1(2)
C(43)-C(44)	1.392(3)	C(46)-C(41)-B(1)	121.4(2)
C(44)-C(45)	1.400(3)	C(41)-C(42)-C(43)	122.6(2)
C(45)-C(46)	1.402(2)	C(42)-C(43)-C(44)	120.5(2)
N(1)-H(1A)	0.986	C(43)-C(44)-C(45)	118.5(2)
N(1)-H(1B)	0.986	C(44)-C(45)-C(46)	120.2(2)
N(2)-H(2A)	0.986	C(41)-C(46)-C(45)	123.1(2)
N(2)-H(2B)	0.986	C(11)-B(1)-C(21)	103.5(2)
N(3)-H(3A)	0.986	C(11)-B(1)-C(31)	110.8(2)
N(3)-H(3B)	0.986	C(11)-B(1)-C(41)	112.4(2)
C(3)-H(60)	1.085	C(21)-B(1)-C(31)	113.7(2)
C(3)-H(61)	1.085	C(21)-B(1)-C(41)	112.2(2)
C(3)-H(62)	1.085	C(31)-B(1)-C(41)	104.5(2)

Table 35. Atomic distances (Å) and angles (°) for guanidinium tetraphenylborate acetonitrile solvate (continued).

Atoms	Distance	Atoms	Angle
C(12)-H(12)	1.076	C(1)-N(1)-H(1A)	122.1
C(13)-H(13)	1.076	C(1)-N(1)-H(1B)	121.0
C(14)-H(14)	1.076	H(1A)-N(1)-H(1B)	116.8
C(15)-H(15)	1.076	C(1)-N(2)-H(2A)	117.2
C(16)-H(16)	1.076	C(1)-N(2)-H(2B)	117.6
C(22)-H(22)	1.076	H(2A)-N(2)-H(2B)	125.0
C(23)-H(23)	1.076	C(1)-N(3)-H(3A)	118.7
C(24)-H(24)	1.076	C(1)-N(3)-H(3B)	119.2
C(25)-H(25)	1.076	H(3A)-N(3)-H(3B)	121.5
C(26)-H(26)	1.076	C(2)-C(3)-H(60)	109.6
C(32)-H(32)	1.076	C(2)-C(3)-H(61)	109.5
C(33)-H(33)	1.076	C(2)-C(3)-H(62)	109.9
C(34)-H(34)	1.076	H(60)-C(3)-H(61)	109.5
C(35)-H(35)	1.076	H(60)-C(3)-H(62)	110.1
C(36)-H(36)	1.076	H(61)-C(3)-H(62)	108.2
C(42)-H(42)	1.076	C(11)-C(12)-H(12)	119.3
C(43)-H(43)	1.076	C(13)-C(12)-H(12)	118.1
C(44)-H(44)	1.076	C(12)-C(13)-H(13)	120.1
C(45)-H(45)	1.076	C(14)-C(13)-H(13)	120.3
C(46)-H(46)	1.076	C(13)-C(14)-H(14)	121.2
		C(15)-C(14)-H(14)	119.2
		C(14)-C(15)-H(15)	120.1
		C(16)-C(15)-H(15)	120.0
		C(11)-C(16)-H(16)	120.1
		C(15)-C(16)-H(16)	117.7
		C(21)-C(22)-H(22)	120.1
		C(23)-C(22)-H(22)	117.2
		C(22)-C(23)-H(23)	119.6
		C(24)-C(23)-H(23)	120.2
		C(23)-C(24)-H(24)	119.9
		C(25)-C(24)-H(24)	121.2
		C(24)-C(25)-H(25)	120.7
		C(26)-C(25)-H(25)	118.9
		C(21)-C(26)-H(26)	120.3
		C(25)-C(26)-H(26)	117.3
		C(31)-C(32)-H(32)	119.1
		C(33)-C(32)-H(32)	117.8
		C(32)-C(33)-H(33)	118.4
		C(34)-C(33)-H(33)	121.6
		C(33)-C(34)-H(34)	120.5
		C(35)-C(34)-H(34)	120.7
		C(34)-C(35)-H(35)	119.4

Table 35. Atomic distances (Å) and angles (°) for guanidinium tetraphenylborate acetonitrile solvate (continued).

Atoms	Distance	Atoms	Angle
		C(36)-C(35)-H(35)	120.0
		C(31)-C(36)-H(36)	118.9
		C(35)-C(36)-H(36)	118.8
		C(41)-C(42)-H(42)	119.2
		C(43)-C(42)-H(42)	118.2
		C(42)-C(43)-H(43)	119.8
		C(44)-C(43)-H(43)	119.7
		C(43)-C(44)-H(44)	122.4
		C(45)-C(44)-H(44)	119.0
		C(44)-C(45)-H(45)	120.0
		C(46)-C(45)-H(45)	119.8
		C(41)-C(46)-H(46)	117.1
		C(45)-C(46)-H(46)	119.7

Table 36. Anisotropic temperature factors ($Å^2$) for the nonhydrogen atoms of guanidinium tetraphenylborate acetonitrile solvate.

atom	U11	U22	U33	U12	U13	U23
N(1)	0.066(1)	0.039(1)	0.059(1)	-0.006(1)	0.013(1)	-0.015(1)
N(2)	0.044(1)	0.061(1)	0.043(1)	-0.001(1)	0.012(1)	-0.010(1)
N(3)	0.053(1)	0.035(1)	0.053(1)	0.009(1)	0.013(1)	-0.002(1)
N(4)	0.061(1)	0.039(1)	0.068(2)	-0.006(1)	0.024(1)	-0.008(1)
C(1)	0.031(1)	0.033(1)	0.042(1)	0.003(1)	0.005(1)	-0.002(1)
C(2)	0.040(1)	0.034(2)	0.047(2)	0.001(1)	0.013(1)	0.001(1)
C(3)	0.048(1)	0.044(1)	0.064(1)	-0.006(1)	-0.005(1)	-0.003(1)
C(11)	0.025(1)	0.024(1)	0.031(1)	0.002(1)	0.007(1)	0.000(1)
C(12)	0.031(1)	0.024(1)	0.038(1)	0.001(1)	0.005(1)	-0.001(1)
C(13)	0.032(1)	0.028(1)	0.052(1)	0.006(1)	0.003(1)	-0.003(1)
C(14)	0.030(1)	0.036(1)	0.058(1)	0.015(1)	0.011(1)	-0.001(1)
C(15)	0.036(1)	0.041(1)	0.043(1)	0.013(1)	0.014(1)	0.002(1)
C(16)	0.033(1)	0.032(1)	0.033(1)	0.004(1)	0.010(1)	0.000(1)
C(21)	0.025(1)	0.026(1)	0.036(1)	0.003(1)	0.010(1)	0.002(1)
C(22)	0.035(1)	0.031(1)	0.043(1)	-0.001(1)	0.013(1)	0.005(1)
C(23)	0.041(1)	0.036(1)	0.059(1)	0.005(1)	0.022(1)	0.014(1)
C(24)	0.034(1)	0.046(1)	0.060(1)	0.014(1)	0.014(1)	0.015(1)
C(25)	0.030(1)	0.048(1)	0.049(1)	0.010(1)	0.003(1)	0.009(1)
C(26)	0.029(1)	0.037(1)	0.036(1)	0.005(1)	0.005(1)	0.006(1)
C(31)	0.027(1)	0.026(1)	0.031(1)	0.002(1)	0.008(1)	0.000(1)
C(32)	0.028(1)	0.033(1)	0.037(1)	0.006(1)	0.007(1)	0.000(1)
C(33)	0.034(1)	0.039(1)	0.037(1)	0.005(1)	0.001(1)	-0.001(1)
C(34)	0.045(1)	0.044(1)	0.033(1)	0.002(1)	0.004(1)	-0.002(1)
C(35)	0.043(1)	0.043(1)	0.032(1)	0.002(1)	0.012(1)	-0.003(1)
C(36)	0.031(1)	0.035(1)	0.033(1)	0.002(1)	0.011(1)	-0.002(1)
C(41)	0.024(1)	0.024(1)	0.034(1)	-0.001(1)	0.006(1)	0.001(1)
C(42)	0.028(1)	0.030(1)	0.039(1)	-0.001(1)	0.011(1)	0.002(1)
C(43)	0.041(1)	0.034(1)	0.043(1)	-0.003(1)	0.014(1)	0.009(1)
C(44)	0.049(1)	0.027(1)	0.047(1)	-0.006(1)	0.004(1)	0.006(1)
C(45)	0.039(1)	0.026(1)	0.064(1)	-0.004(1)	0.002(1)	-0.004(1)
C(46)	0.027(1)	0.027(1)	0.057(1)	0.000(1)	0.008(1)	-0.001(1)
B(1)	0.026(1)	0.023(1)	0.032(1)	0.000(1)	0.009(1)	0.000(1)

Table 37. Positional parameters and isotropic temperature factors ($Å^2 \times 10^3$) for the hydrogen atoms of guanidinium tetraphenylborate acetonitrile solvate.

atom	x	y	z	U(eq)
H(1A)	0.7785	0.7179	0.3945	70
H(1B)	0.7474	0.6759	0.5570	70
H(2A)	0.7559	0.6138	0.1926	64
H(2B)	0.6977	0.4925	0.2043	64
H(3A)	0.6687	0.5159	0.5726	62
H(3B)	0.6476	0.4387	0.4195	62
H(12)	1.3256	0.9264	0.4789	46
H(13)	1.4317	1.0679	0.3789	53
H(14)	1.4365	1.0733	0.1082	56
H(15)	1.3350	0.9353	-0.0559	54
H(16)	1.2266	0.7950	0.0431	47
H(22)	1.0373	0.8809	0.5022	50
H(23)	0.7985	0.9419	0.4493	59
H(24)	0.6338	0.8935	0.2170	61
H(25)	0.7184	0.7831	0.0335	58
H(26)	0.9566	0.7225	0.0847	49
H(32)	1.4664	0.7634	0.4915	47
H(33)	1.5725	0.7291	0.7457	52
H(34)	1.4217	0.6835	0.9285	56
H(35)	1.1631	0.6711	0.8422	54
H(36)	1.0563	0.7036	0.5818	47
H(42)	1.4107	0.6796	0.2069	47
H(43)	1.4433	0.5170	0.1044	53
H(44)	1.2568	0.3859	0.0932	57
H(45)	1.0386	0.4251	0.1797	59
H(46)	1.0113	0.5880	0.2902	52
H(60)	1.0241	0.9200	0.9422	69
H(61)	0.8986	0.9868	0.8173	69
H(62)	1.0473	0.9414	0.7573	69

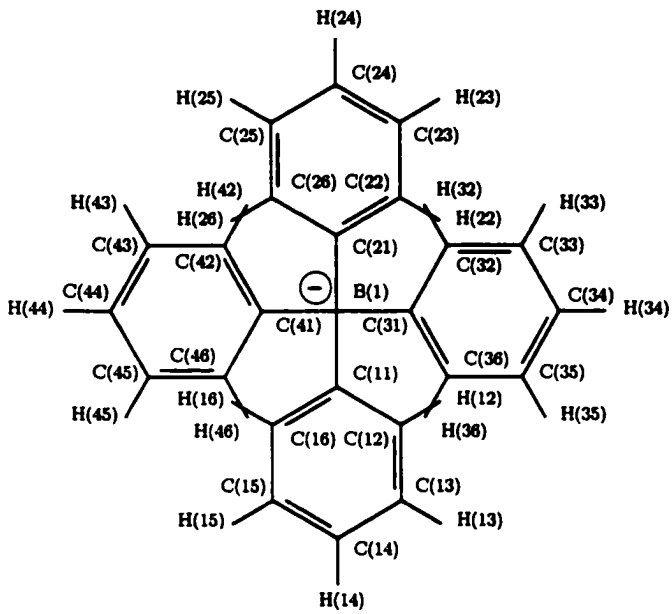

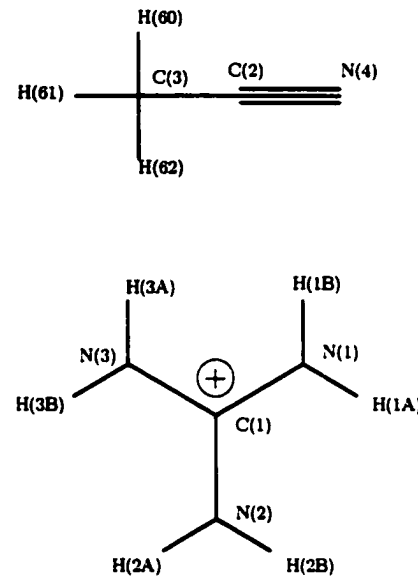

Table 38. Scale factor, extinction, kappa values, local coordinate system, and multipole population coefficients for guanidinium tetraphenylborate acetonitrile solvate (atom numbering as shown above).

	Scale Factor	Extinction
	5.237(22)	0.237(10)
	κ'	κ''
1.	0.939(21)	0.742(39)
2.	0.915(18)	0.733(86)
3.	0.972(68)	0.92(13)
4.	1.080(38)	1.44(34)
5.	0.860(30)	0.945(61)
6.	0.931(7)	0.837(15)
7.	0.870(29)	1.24(15)
8.	0.936(38)	1.32(16)
9.	1.003(17)	1.315(67)
10.	0.952(84)	1.31(25)

Table 38. Local coordinate systems

atom	atom0	axis1	atom1	atom2	axis2	right/left	kappa set
N(1)	C(1)	Z	N(1)	H(1B)	X	R	1
N(2)	C(1)	Z	N(2)	H(2B)	X	L	1
N(3)	C(1)	Z	N(3)	H(3B)	X	R	1
N(4)	C(2)	Z	N(4)	H(60)	X	R	2
C(1)	DUM3	Z	C(1)	DUM4	Y	R	3
C(2)	N(4)	Z	C(2)	H(60)	X	R	4
C(3)	C(2)	Z	C(3)	H(61)	X	R	5
C(11)	B(1)	X	C(11)	DUM0	Y	R	6
C(12)	C(13)	X	C(12)	C(11)	Y	R	6
C(13)	C(12)	X	C(13)	C(14)	Y	L	6
C(14)	H(14)	X	C(14)	DUM0	Y	R	6
C(15)	C(16)	X	C(15)	C(14)	Y	R	6
C(16)	C(15)	X	C(16)	C(11)	Y	L	6
C(21)	B(1)	X	C(21)	DUM0	Y	L	6
C(22)	C(23)	X	C(22)	C(21)	Y	L	6
C(23)	C(22)	X	C(23)	C(24)	Y	R	6
C(24)	H(24)	X	C(24)	DUM0	Y	L	6
C(25)	C(26)	X	C(25)	C(24)	Y	L	6
C(26)	C(25)	X	C(26)	C(21)	Y	R	6
C(31)	B(1)	X	C(31)	DUM2	Y	R	6
C(32)	C(33)	X	C(32)	C(31)	Y	R	6
C(33)	C(32)	X	C(33)	C(34)	Y	L	6
C(34)	H(34)	X	C(34)	DUM2	Y	R	6
C(35)	C(36)	X	C(35)	C(34)	Y	R	6
C(36)	C(35)	X	C(36)	C(31)	Y	L	6
C(36)	C(35)	X	C(36)	C(31)	Y	L	6
C(41)	B(1)	X	C(41)	DUM2	Y	L	6
C(42)	C(43)	X	C(42)	C(41)	Y	L	6
C(43)	C(42)	X	C(43)	C(44)	Y	R	6
C(44)	H(44)	X	C(44)	DUM2	Y	L	6
C(45)	C(46)	X	C(45)	C(44)	Y	L	6
C(46)	C(45)	X	C(46)	C(41)	Y	R	6
B(1)	DUM0	Z	B(1)	DUM1	X	R	7
H(1A)	N(1)	Z	H(1A)	H(1B)	X	R	8
H(1B)	N(1)	Z	H(1B)	H(1A)	X	L	8
H(2A)	N(2)	Z	H(2A)	H(2B)	X	R	8
H(2B)	N(2)	Z	H(2B)	H(2A)	X	L	8
H(3A)	N(3)	Z	H(3A)	H(3B)	X	R	8
H(3B)	N(3)	Z	H(3B)	H(3A)	X	L	8
H(12)	C(12)	Z	H(12)	C(11)	Y	R	9
H(13)	C(13)	Z	H(13)	C(14)	Y	R	9
H(14)	C(14)	Z	H(14)	C(13)	Y	R	9
H(15)	C(15)	Z	H(15)	C(14)	Y	R	9
H(16)	C(16)	Z	H(16)	C(11)	Y	R	9
H(22)	C(22)	Z	H(22)	C(21)	Y	R	9
H(23)	C(23)	Z	H(23)	C(24)	Y	R	9
H(24)	C(24)	Z	H(24)	C(23)	Y	R	9
H(25)	C(25)	Z	H(25)	C(24)	Y	R	9
H(26)	C(26)	Z	H(26)	C(21)	Y	R	9
H(32)	C(32)	Z	H(32)	C(31)	Y	R	9
H(33)	C(33)	Z	H(33)	C(34)	Y	R	9
H(34)	C(34)	Z	H(34)	C(33)	Y	R	9
H(35)	C(35)	Z	H(35)	C(34)	Y	R	9
H(36)	C(36)	Z	H(36)	C(31)	Y	R	9

Table 38. Local coordinate systems continued...

atom	atom0	axis1	atom1	atom2	axis2	right/left	kappa set
H(42)	C(42)	Z	H(42)	C(41)	Y	R	9
H(43)	C(43)	Z	H(43)	C(44)	Y	R	9
H(44)	C(44)	Z	H(44)	C(43)	Y	R	9
H(45)	C(45)	Z	H(45)	C(44)	Y	R	9
H(46)	C(46)	Z	H(46)	C(41)	Y	R	9
H(60)	C(3)	Z	H(60)	C(2)	X	R	10
H(61)	C(3)	Z	H(61)	C(2)	X	R	10
H(62)	C(3)	Z	H(61)	C(2)	X	R	10

DUM0=1.1441 0.8187 0.2867
DUM1=1.2596 0.7920 0.3913
DUM2=1.2270 0.6938 0.3818
DUM3=0.6157 0.5953 0.3600
DUM4=0.7360 0.5987 0.2937

Table 38. Multipole populations

atom	P_v	P_{00}	P_{11}	P_{1-1}	P_{10}
N(1)	5.04(37)	0.00(0)	0.19(12)	−0.11(5)	0.16(14)
N(2)	4.99(35)	0.00(0)	0.13(11)	−0.16(5)	0.31(14)
N(3)	5.06(37)	0.00(0)	−0.05(12)	−0.21(4)	0.12(13)
N(4)	5.84(25)	0.00(0)	0.03(5)	0.04(4)	0.33(14)
C(1)	3.03(76)	0.00(0)	0.08(9)	−0.08(9)	0.10(5)
C(2)	2.66(37)	0.00(0)	−0.02(4)	0.01(4)	−0.04(7)
C(3)	5.20(70)	0.00(0)	−0.02(3)	0.02(4)	0.07(7)
C(11)	3.99(11)	0.00(0)	0.04(6)	0.07(4)	0.03(7)
C(12)	3.86(12)	0.00(0)	−0.01(7)	0.14(5)	0.00(4)
C(13)	3.97(14)	0.00(0)	0.04(7)	0.13(7)	0.00(4)
C(14)	3.88(13)	0.00(0)	−0.08(6)	0.00(5)	−0.04(10)
C(15)	4.00(13)	0.00(0)	0.07(7)	0.14(7)	0.03(4)
C(16)	3.86(12)	0.00(0)	0.06(7)	0.06(6)	−0.04(4)
C(21)	4.03(11)	0.00(0)	0.08(5)	0.04(4)	0.05(7)
C(22)	4.14(12)	0.00(0)	−0.01(7)	0.17(6)	−0.05(4)
C(23)	3.85(13)	0.00(0)	0.10(8)	0.09(7)	0.01(5)
C(24)	3.84(14)	0.00(0)	−0.02(6)	0.01(5)	0.04(10)
C(25)	3.89(13)	0.00(0)	0.01(7)	0.04(7)	0.08(5)
C(26)	3.95(11)	0.00(0)	0.07(7)	0.17(6)	−0.01(4)
C(31)	4.04(11)	0.00(0)	0.07(6)	0.13(4)	0.03(6)
C(32)	3.95(12)	0.00(0)	0.01(7)	0.18(6)	0.00(4)
C(33)	3.91(13)	0.00(0)	0.03(8)	−0.01(7)	0.09(4)
C(34)	4.04(13)	0.00(0)	−0.10(6)	0.00(5)	−0.04(9)
C(35)	3.85(13)	0.00(0)	0.13(8)	0.16(7)	0.02(5)
C(36)	3.84(12)	0.00(0)	0.04(7)	0.09(5)	−0.03(4)
C(41)	4.02(11)	0.00(0)	0.04(6)	0.05(4)	0.03(6)
C(42)	3.96(11)	0.00(0)	0.04(6)	0.07(5)	−0.04(4)
C(43)	3.98(13)	0.00(0)	0.05(7)	0.16(7)	0.00(5)
C(44)	4.01(13)	0.00(0)	−0.04(6)	−0.03(5)	−0.04(9)
C(45)	3.89(13)	0.00(0)	0.06(8)	0.09(7)	0.00(5)
C(46)	3.78(12)	0.00(0)	0.04(7)	0.18(6)	−0.02(4)
B(1)	3.25(33)	0.00(0)	−0.04(3)	0.03(3)	0.02(3)
H(1A)	1.08(18)	0.00(0)	0.00(0)	0.00(0)	0.25(7)
H(1B)	0.78(19)	0.00(0)	0.00(0)	0.00(0)	0.02(6)
H(2A)	1.14(18)	0.00(0)	0.00(0)	0.00(0)	0.24(6)
H(2B)	0.95(18)	0.00(0)	0.00(0)	0.00(0)	0.13(6)
H(3A)	0.98(19)	0.00(0)	0.00(0)	0.00(0)	0.09(6)
H(3B)	0.96(16)	0.00(0)	0.00(0)	0.00(0)	0.12(6)

Table 38. Multipole populations continued...

atom	P_v	P_{00}	P_{11}	P_{1-1}	P_{10}
H(12)	1.11(0)	0.00(0)	0.00(0)	0.00(0)	0.15(0)
H(13)	1.11(0)	0.00(0)	0.00(0)	0.00(0)	0.15(0)
H(14)	1.11(0)	0.00(0)	0.00(0)	0.00(0)	0.15(0)
H(15)	1.11(0)	0.00(0)	0.00(0)	0.00(0)	0.15(0)
H(16)	1.11(0)	0.00(0)	0.00(0)	0.00(0)	0.15(0)
H(22)	1.11(0)	0.00(0)	0.00(0)	0.00(0)	0.15(0)
H(23)	1.11(0)	0.00(0)	0.00(0)	0.00(0)	0.15(0)
H(24)	1.11(0)	0.00(0)	0.00(0)	0.00(0)	0.15(0)
H(25)	1.11(0)	0.00(0)	0.00(0)	0.00(0)	0.15(0)
H(26)	1.11(0)	0.00(0)	0.00(0)	0.00(0)	0.15(0)
H(32)	1.11(0)	0.00(0)	0.00(0)	0.00(0)	0.15(0)
H(33)	1.11(0)	0.00(0)	0.00(0)	0.00(0)	0.15(0)
H(34)	1.11(0)	0.00(0)	0.00(0)	0.00(0)	0.15(0)
H(35)	1.11(0)	0.00(0)	0.00(0)	0.00(0)	0.15(0)
H(36)	1.11(0)	0.00(0)	0.00(0)	0.00(0)	0.15(0)
H(42)	1.11(0)	0.00(0)	0.00(0)	0.00(0)	0.15(0)
H(43)	1.11(0)	0.00(0)	0.00(0)	0.00(0)	0.15(0)
H(44)	1.11(0)	0.00(0)	0.00(0)	0.00(0)	0.15(0)
H(45)	1.11(4)	0.00(0)	0.00(0)	0.00(0)	0.15(2)
H(46)	1.11(0)	0.00(0)	0.00(0)	0.00(0)	0.15(0)
H(60)	0.77(21)	0.00(0)	0.00(0)	0.00(0)	0.12(5)
H(61)	0.77(0)	0.00(0)	0.00(0)	0.00(0)	0.12(0)
H(62)	0.77(0)	0.00(0)	0.00(0)	0.00(0)	0.12(0)

atom	P_{20}	P_{21}	P_{2-1}	P_{22}	P_{2-2}
N(1)	0.14(9)	−0.07(10)	0.07(6)	0.06(7)	0.01(4)
N(2)	0.10(10)	−0.12(10)	−0.01(5)	0.02(7)	0.00(4)
N(3)	0.05(9)	−0.17(10)	0.05(5)	0.06(6)	−0.01(4)
N(4)	0.50(11)	−0.10(5)	−0.01(4)	−0.03(4)	−0.03(4)
C(1)	−0.23(13)	−0.03(5)	0.04(5)	0.08(8)	0.13(8)
C(2)	0.15(8)	0.12(5)	0.01(5)	−0.05(4)	−0.08(4)
C(3)	0.06(6)	−0.05(3)	−0.01(4)	0.06(4)	0.03(3)
C(11)	0.12(5)	0.02(6)	0.06(4)	0.25(4)	−0.15(3)
C(12)	−0.25(4)	0.08(4)	−0.07(3)	0.04(6)	−0.10(5)
C(13)	−0.25(4)	−0.10(4)	−0.02(4)	0.11(7)	−0.04(6)
C(14)	0.11(6)	0.10(8)	0.01(6)	0.21(4)	0.03(4)
C(15)	−0.27(4)	−0.11(5)	0.02(4)	0.11(7)	−0.12(6)
C(16)	−0.19(4)	0.07(4)	−0.01(4)	0.00(6)	0.02(6)
C(21)	−0.02(5)	0.00(6)	−0.16(4)	0.11(4)	−0.04(3)
C(22)	−0.14(4)	0.02(4)	−0.12(4)	−0.04(6)	−0.08(5)
C(23)	−0.14(4)	−0.01(5)	−0.06(5)	−0.04(7)	0.05(6)
C(24)	0.21(7)	0.08(8)	0.18(7)	−0.01(4)	0.03(4)
C(25)	−0.14(4)	0.00(5)	0.09(5)	0.01(7)	−0.10(6)
C(26)	−0.07(4)	0.02(4)	0.08(4)	0.01(6)	0.03(5)
C(31)	0.13(5)	−0.05(6)	0.05(4)	0.09(4)	−0.06(3)
C(32)	−0.07(4)	0.06(4)	0.07(3)	−0.05(6)	0.09(5)
C(33)	−0.03(5)	−0.04(4)	0.05(4)	0.04(7)	−0.11(6)
C(34)	0.21(6)	0.04(8)	−0.05(5)	0.03(4)	−0.03(4)
C(35)	−0.06(5)	−0.02(5)	−0.11(4)	−0.03(7)	0.05(6)
C(36)	−0.06(4)	0.06(4)	−0.08(3)	−0.02(6)	−0.05(5)
C(41)	0.09(5)	−0.06(6)	−0.04(4)	0.24(4)	−0.12(3)
C(42)	−0.22(4)	0.06(4)	−0.05(3)	0.01(5)	0.01(5)

Table 38. Multipole populations continued...

atom	P_{20}	P_{21}	P_{2-1}	P_{22}	P_{2-2}
C(43)	−0.26(5)	−0.03(5)	0.02(4)	0.08(7)	−0.13(6)
C(44)	0.16(6)	−0.03(8)	0.08(6)	0.26(4)	0.08(4)
C(45)	−0.24(5)	−0.15(5)	0.05(5)	0.14(7)	0.03(6)
C(46)	−0.24(4)	0.11(5)	0.05(4)	0.03(6)	−0.05(6)
B(1)	0.03(3)	0.14(4)	−0.02(3)	0.01(3)	0.00(3)

atom	P_{30}	P_{31}	P_{3-1}	P_{32}	P_{3-2}	P_{33}	P_{3-3}
N(1)	0.21(7)	0.09(5)	−0.02(5)	−0.32(6)	0.05(4)	0.09(4)	−0.10(3)
N(2)	0.38(7)	0.09(5)	−0.11(5)	−0.14(6)	−0.03(4)	0.02(4)	−0.11(3)
N(3)	0.13(6)	0.01(4)	−0.04(4)	−0.14(6)	0.06(4)	0.02(4)	−0.03(3)
N(4)	0.07(8)	0.01(5)	−0.01(5)	−0.05(4)	0.01(4)	−0.07(3)	−0.03(3)
C(1)	−0.05(4)	−0.06(4)	0.08(4)	−0.01(5)	0.01(5)	0.17(14)	−0.05(8)
C(2)	−0.09(4)	0.00(3)	−0.02(3)	0.02(3)	0.01(3)	−0.05(2)	0.01(2)
C(3)	0.36(7)	0.01(4)	−0.02(4)	−0.13(3)	0.01(3)	−0.21(6)	0.14(3)
C(11)	0.08(5)	−0.26(5)	0.06(4)	0.03(5)	0.01(4)	0.11(3)	0.01(3)
C(12)	0.01(4)	−0.04(4)	0.00(3)	0.06(4)	0.00(4)	0.31(5)	0.07(5)
C(13)	0.00(4)	0.00(4)	0.00(4)	−0.04(4)	0.00(4)	0.35(5)	−0.01(6)
C(14)	−0.09(7)	−0.10(5)	−0.02(5)	−0.03(5)	−0.04(5)	0.10(3)	0.05(3)
C(15)	0.03(4)	−0.04(4)	0.01(4)	0.01(4)	−0.03(5)	0.30(5)	0.03(6)
C(16)	0.01(4)	−0.03(4)	0.07(3)	0.09(4)	0.04(4)	0.29(5)	−0.01(5)
C(21)	−0.02(5)	−0.20(5)	0.04(4)	0.07(5)	0.07(4)	0.09(3)	0.01(3)
C(22)	0.06(4)	0.02(4)	0.00(3)	0.02(4)	0.06(4)	0.39(5)	−0.05(5)
C(23)	−0.02(4)	−0.05(4)	0.01(4)	−0.09(5)	−0.09(5)	0.23(5)	−0.06(6)
C(24)	0.03(7)	−0.25(6)	0.02(6)	−0.04(6)	−0.02(5)	0.07(4)	−0.01(3)
C(25)	−0.07(4)	−0.02(4)	0.05(4)	0.00(5)	−0.07(4)	0.35(5)	−0.08(6)
C(26)	0.02(4)	−0.06(4)	0.01(3)	−0.01(4)	0.02(4)	0.31(4)	0.04(5)
C(31)	0.00(5)	−0.24(5)	0.10(4)	0.04(5)	−0.01(4)	0.08(4)	−0.06(3)
C(32)	0.01(4)	−0.07(4)	−0.01(3)	0.04(4)	0.10(4)	0.28(4)	0.04(5)
C(33)	0.04(4)	0.01(4)	0.01(4)	−0.01(4)	−0.08(4)	0.27(5)	−0.06(6)
C(34)	−0.08(6)	−0.28(5)	−0.07(5)	0.06(5)	0.02(5)	0.11(4)	0.07(3)
C(35)	0.06(4)	−0.03(4)	0.00(4)	0.07(4)	0.00(4)	0.25(5)	−0.05(6)
C(36)	0.04(4)	−0.01(4)	0.04(3)	0.00(4)	0.08(4)	0.30(5)	−0.07(5)
C(41)	0.05(5)	−0.30(5)	0.10(4)	0.00(5)	0.05(4)	0.11(3)	0.01(3)
C(42)	0.10(4)	−0.02(4)	0.01(3)	0.07(4)	0.01(4)	0.32(4)	−0.03(5)
C(43)	0.03(4)	−0.04(4)	0.04(4)	−0.02(4)	0.02(4)	0.34(5)	0.01(6)
C(44)	−0.03(6)	−0.27(5)	−0.12(5)	0.01(5)	−0.05(5)	0.08(3)	−0.03(3)
C(45)	−0.06(5)	−0.09(4)	0.01(4)	−0.10(5)	−0.10(5)	0.31(5)	−0.12(6)
C(46)	−0.03(4)	0.00(4)	0.03(3)	0.07(4)	0.04(4)	0.32(5)	0.02(5)
B(1)	0.06(3)	0.05(3)	0.02(3)	0.02(3)	0.25(6)	−0.02(3)	0.00(3)

Table 39. Results of the rigid body thermal motion analysis for the anion in guanidinium tetraphenylborate acetonitrile solvate.[a]

Rigid body variables fitted		20	
Translational tensor, **T** (Å^2)	0.0246(8)	-0.0027(6)	-0.0022(6)
		0.0292(8)	0.0026(6)
			0.0260(8)
Principal values (Å^2)	0.0229	0.0322	0.0247
Square root (Å)	0.15	0.18	0.16
Libirational tensor, **L** (deg^2)	3.2(3)	1.0(2)	-0.7(2)
		2.5(3)	0.9(2)
			6.9(5)
Principal values (deg^2)	3.9	1.6	7.1
Square root (deg)	2.0	1.3	2.7
Cross tensor, **S** (Å-deg)	0.040(16)	0.030(8)	0.007(7)
	-0.023(8)	-0.022(16)	0.018(8)
	0.010(8)	-0.025(8)	-0.018(0)
R_w[b]		0.0967	
Z[c]		0.00274	
Corrections to interatomic distances due to libration		0.0015 to 0.0025Å	
Esd's on the calculated interatomic distances		0.0018 to 0.0030Å	

[a] Tensor components are given with respect to the axes of the principal moments of inertia and with the origin at the center of mass.

[b] $R_w = (X^2 / \Sigma[U_{ij}/\sigma_{Uij}]^2)^{½}$ where $X^2 = \Sigma[\Delta U_{ij}/\sigma_{Uij}]^2)$

[c] $Z = (X^2 / NFREE)^{½}$ where NFREE = 130

Table 40. Short intermolecular cation/solvent...anion contacts for guanidinium tetraphenylborate acetonitrile solvate.

Part 1	C-H...phenyl		(solvent/anion)
contact	C...C (Å)	H...C (Å)	C-H...C (°)
Acetonitrile solvate			
C(3)-H(60)...ring 1	symmetry	(x, y, 1+z)	
C(11)	4.662(3)	3.619	161.7
C(12)	5.418(3)	4.361	165.3
C(13)	5.434(3)	4.481	148.4
C(14)	4.662(3)	3.864	132.2
C(15)	3.721(3)	2.965	127.1
C(16)	3.715(3)	2.799	142.1
mean	**4.602[7]**	**3.682**	**146.1**
centroid[a]	4.440	3.465	150.3
plane[b]	3.019	2.532	26.7
C(3)-H(61)...ring 1	symmetry	(2-x, 2-y, 1-z)	
C(11)	3.919(3)	2.855	166.6
C(12)	3.708(3)	2.765	145.1
C(13)	3.579(3)	2.781	130.2
C(14)	3.635(3)	2.847	129.6
C(15)	3.822(3)	2.901	142.8
C(16)	3.941(3)	2.886	164.0
mean	**3.767[7]**	**2.839**	**146.4**
centroid[a]	3.501	2.472	157.9
plane[b]	3.463	2.468	66.5

Table 40. Short intermolecular cation/solvent...anion contacts for guanidinium tetraphenylborate acetonitrile solvate (continued).

Part 1	C-H...phenyl		(solvent/anion)
contact	C...C (Å)	H...C (Å)	C-H...C (°)
C(3)-H(62)...ring 2	symmetry (2-x, 2-y, 1-z)		
C(21)	4.053(3)	3.749	98.5
C(22)	3.752(3)	3.130	117.2
C(23)	3.775(4)	2.886	139.2
C(24)	4.063(4)	3.290	129.2
C(25)	4.284(4)	3.819	108.2
C(26)	4.272(3)	4.012	96.5
mean	**4.033[9]**	**3.481**	**114.8**
centroid[c]	3.786	3.210	114.2
plane[d]	3.686	2.881	47.9

Part 2	Other cation/anion and solvent/anion contacts of less than 3Å[e]	
cation		
N(2)...H(43)	symmetry (-1+x, y, z)	2.797 Å
N(2)...H(46)	symmetry (x, y, z)	2.775 Å
solvent		
N(4)...H(33)	symmetry (-1+x, y, z)	2.561 Å
N(4)...H(36)	symmetry (x, y, z)	2.963 Å
N(4)...H(44)	symmetry (2-x, 1-y, 1-z)	2.805 Å
N(4)...H(45)	symmetry (2-x, 1-y, 1-z)	2.947 Å

[a] The position of the centroid of ring 1 is (1.3296, 0.9300, 0.2122). The values listed are *d*(C...centroid), *d*(H...centroid) and the angle C-H...centroid.

[b] The mean deviation of the carbon atoms from the ring 1 plane is 0.0017Å. The values listed are *d*(C...plane), *d*(H...plane) and the angle the C-H vector makes with the plane of the ring.

[c] The position of the centroid of ring 2 is (0.8786, 0.8300, 0.2694). The values listed are *d*(N/C...centroid), *d*(H...centroid) and the angle N/C-H...centroid.

[d] The mean deviation of the carbon atoms from the ring 2 plane is 0.0066Å. The values listed are *d*(N/C...plane), *d*(H...plane) and the angle the N/C-H vector makes with the plane of the ring.

[e] These are the only other contacts to the cation or the solvent from the anion of less than 3Å.

Table 41. Bond critical points for the short intermolecular cation/solvent...anion contacts in guanidinium tetraphenylborate acetonitrile solvate.

Contact	C-H...phenyl					(solvent/anion)			
	Hessian Eigenvalues			Charge Density	Laplacian	Ellipticity	Position		
Bond Path	λ_1	λ_2	λ_3	$\rho_b(\mathbf{r})$ ($e\text{Å}^{-1}$)	$\nabla^2\rho_b(\mathbf{r})$ ($e\text{Å}^{-5}$)	ε	x	y (fractional)	z
ring 1...H(60)-C(3)*	symmetry (x, y, -1+z)				Cpa1				
C(15)-C(16)...C(3)	-0.08,	0.00,	0.53	0.044(4)	0.449(3)	18.60	1.1643,	0.9258,	-0.0355

Bond Lengths and Angles at the Critical Point

Atoms	Distance (Å)	Atoms	Angle (°)
Cpa1...C(15)	1.687	C(3)...Cpa1...C(15)	172.5
Cpa1...C(16)	1.893	C(3)...Cpa1...C(16)	141.5
Cpa1...C(3)	2.042		

* The unusual bond path from C(3) does not follow the C(3)-H(60) bond but follows the C(15)-C(16) bond of the ring for approximately one quarter of its length before terminating at C(15).

Table 41. Bond critical points for the short intermolecular cation/solvent...anion contacts in guanidinium tetraphenylborate acetonitrile solvate (continued).

Contact	C-H...phenyl (solvent/anion)								
	Hessian Eigenvalues			Charge Density	Laplacian	Ellipticity	Position		
Bond Path	λ_1	λ_2	λ_3	$\rho_b(\mathbf{r})$ (eÅ^{-3})	$\nabla^2\rho_b(\mathbf{r})$ (eÅ^{-5})	ε	x	y (fractional)	z
ring 1...H(60)-C(3)*	symmetry (x, y, -1+z)				Cpa2 - intermediate type contact				
C(16)-H(16)...H(60)	-0.07,	-0.02,	0.53	0.043(7)	0.441(6)	2.49	1.1301,	0.8748,	-0.0151

Bond Lengths and Angles at the Critical Point

Atoms	Distance (Å)	Atoms	Angle (°)
Cpa2...C(16)	1.691	C(3)...Cpa2...C(16)	169.8
Cpa2...H(16)	1.482	C(3)...Cpa2...H(16)	150.1
Cpa2...C(3)	2.039	H(60)...Cpa2...C(16)	149.3
Cpa2...H(60)	1.209	H(60)...Cpa2...H(16)	161.7
		C(3)-H(60)...Cpa2	125.4

* The bond path is from H(60) to the approximate midpoint of the C(16)-H(16) bond in the ring and terminates at C(16).

Table 41. Bond critical points for the short intermolecular cation/solvent...anion contacts in guanidinium tetraphenylborate acetonitrile solvate (continued).

Contact	C-H...phenyl (solvent/anion)								
	Hessian Eigenvalues			Charge Density	Laplacian	Ellipticity	Position		
Bond Path	λ_1	λ_2	λ_3	$\rho_c(\mathbf{r})$ (eÅ^{-3})	$\nabla^2\rho_c(\mathbf{r})$ (eÅ^{-5})	ε	x	y (fractional)	z
ring 1...H(61)-C(3)*	symmetry (2-x, 2-y, 1-z)				Cpa3 - centroid type hydrogen bond				
C(13)-C(14)...H(61)	-0.13,	-0.04,	0.67	0.062(2)	0.498(1)	1.93	1.2127,	1.0223,	0.1994

Bond Lengths and Angles at the Critical Point

Atoms	Distance (Å)	Atoms	Angle (°)
Cpa3...C(13)	1.795	C(3)...Cpa3...C(13)	151.8
Cpa3...C(14)	1.840	C(3)...Cpa3...C(14)	153.5
Cpa3...C(3)	1.895	H(61)...Cpa3...C(13)	152.4
Cpa3...H(61)	1.063	H(61)...Cpa3...C(14)	156.5
		C(3)-H(61)...Cpa3	123.8

* The bond path is from H(61) to the approximate midpoint of the C(13)-C(14) bond in the ring and terminates at C(14).

Table 41. Bond critical points for the short intermolecular cation/solvent...anion contacts in guanidinium tetraphenylborate acetonitrile solvate (continued).

Contact	C-H...phenyl (solvent/anion)							
	Hessian Eigenvalues			Charge Density	Laplacian	Ellipticity	Position	
Bond Path	λ_1	λ_2	λ_3	$\rho_b(\mathbf{r})$ (eÅ^{-3})	$\nabla^2\rho_b(\mathbf{r})$ (eÅ^{-5})	ε	x	y z (fractional)
ring 2...C(3)* symmetry (2-x, 2-y, 1-z) Cpa4								
C(22)-C(23)...C(3)	-0.09,	-0.02,	0.51	0.047(1)	0.402(1)	3.72	0.9815,	0.9641, 0.2956

Bond Lengths and Angles at the Critical Point

Atoms	Distance (Å)	Atoms	Angle (°)
Cpa4...C(22)	1.789	C(3)...Cpa4...C(22)	169.3
Cpa4...C(23)	1.964	C(3)...Cpa4...C(23)	146.4
Cpa4...C(3)	1.980		

* The unusual bond path from C(3) does not follow the C(3)-H(62) bond but leaves directly from C(3) and proceeds to the C(22)-C(23) of the ring. It follows the bond for one quarter of its length before terminating at C(22).

Table 41. Bond critical points for the short intermolecular cation/solvent...anion contacts in guanidinium tetraphenylborate acetonitrile solvate (continued).

Contact	C-H...phenyl (solvent/anion)								
	Hessian Eigenvalues			Charge Density	Laplacian	Ellipticity	Position		
Bond Path	λ_1	λ_2	λ_3	$\rho_b(\mathbf{r})$ ($eÅ^{-3}$)	$\nabla^2\rho_b(\mathbf{r})$ ($eÅ^{-5}$)	ε	x	y (fractional)	z
ring 2...C(3)[a,b]	symmetry (x, y, -1+z)			Cpa5					
C(26)...C(3)	-0.03,	-0.02,	0.34	0.031(2)	0.284(2)	0.46	0.9564,	0.8430,	0.0118

Bond Lengths and Angles at the Critical Point

Atoms	Distance (Å)	Atoms	Angle (°)
Cpa5...C(26)	1.846	C(3)...Cpa5...C(26)	174.3
Cpa5...H(60)	1.447	H(60)...Cpa5...C(26)	155.2
Cpa5...C(3)	2.077	C(3)-H(60)...Cpa5	109.4
C(3)...C(26)	3.918	C(3)-H(60)...C(26)	123.2
H(60)...C(26)	3.218		

[a] The unusual bond path from C(3) does not exactly follow the C(3)-H(60) bond but is relatively close to it before proceeding to C(26).

[b] This interaction does not have a close contact of less than 3A.

Table 41. Bond critical points for the short intermolecular cation/solvent...anion contacts in guanidinium tetraphenylborate acetonitrile solvate (continued).

C-H...N (anion/cation)									
Contact	Hessian Eigenvalues			Charge Density	Laplacian	Ellipticity	Position		
Bond Path	λ_1	λ_2	λ_3	$\rho_b(\mathbf{r})$ (eÅ^{-3})	$\nabla^2\rho_b(\mathbf{r})$ (eÅ^{-5})	ε	x	y (fractional)	z
C(43)-H(43)...N(2) symmetry (1+x, y, z)									
H(43)...N(2)	-0.19,	-0.12,	0.83	0.061(1)	0.522(1)	0.62	1.5554,	0.5313,	0.1691

Bond Lengths and Angles at the Critical Point

Atoms	Distance (Å)	Atoms	Angle (°)
Cp...N(2)	1.659	N(2)...Cp...C(43)	157.4
Cp...H(43)	1.143	N(2)...Cp...H(43)	173.4
Cp...C(43)	1.978	C(43)-H(43)...Cp	126.1
H(43)...N(2)	2.797	C(43)-H(43)...N(2)	128.4
C(43)...N(2)	3.567		

Table 41. Bond critical points for the short intermolecular cation/solvent...anion contacts in guanidinium tetraphenylborate acetonitrile solvate (continued).

Contact	C-H...N (anion/cation)								
	Hessian Eigenvalues			Charge Density	Laplacian	Ellipticity	Position		
Bond Path	λ_1	λ_2	λ_3	$\rho_b(\mathbf{r})$ ($e\text{Å}^{-3}$)	$\nabla^2\rho_b(\mathbf{r})$ ($e\text{Å}^{-5}$)	ε	x	y (fractional)	z
C(46)-H(46)...N(2)	symmetry (x, y, z)								
H(46)...N(2)	-0.17,	-0.14,	0.83	0.062(1)	0.527(1)	0.21	0.8953,	0.5887,	0.2412

Bond Lengths and Angles at the Critical Point

Atoms	Distance (Å)	Atoms	Angle (°)
Cp...N(2)	1.732	N(2)...Cp...C(46)	160.5
Cp...H(46)	1.125	N(2)...Cp...H(46)	151.8
Cp...C(46)	2.018	C(46)-H(46)...Cp	133.0
H(46)...N(2)	2.775	C(46)-H(46)...N(2)	143.6
C(46)...N(2)	3.697		

Table 41. Bond critical points for the short intermolecular cation/solvent...anion contacts in guanidinium tetraphenylborate acetonitrile solvate (continued).

C-H...N (anion/solvent)									
Contact	Hessian Eigenvalues			Charge Density	Laplacian	Ellipticity	Position		
Bond Path	λ_1	λ_2	λ_3	$\rho_b(\mathbf{r})$ ($eÅ^{-3}$)	$\nabla^2\rho_b(\mathbf{r})$ ($eÅ^{-5}$)	ε	x	y (fractional)	z
C(33)-H(33)...N(4) symmetry (1+x, y, z)									
H(33)...N(4)	-0.14,	-0.11,	0.84	0.052(2)	0.588(1)	0.22	1.6761,	0.7346,	0.7366

Bond Lengths and Angles at the Critical Point

Atoms	Distance (Å)	Atoms	Angle (°)
Cp...N(4)	1.552	N(4)...Cp...C(33)	167.9
Cp...H(33)	1.024	N(4)...Cp...H(33)	167.3
Cp...C(33)	2.066	C(33)-H(33)...Cp	159.5
H(33)...N(4)	2.561	C(33)-H(33)...N(4)	161.8
C(33)...N(4)	3.598		

Table 41. Bond critical points for the short intermolecular cation/solvent...anion contacts in guanidinium tetraphenylborate acetonitrile solvate (continued).

Contact	C-H...N (anion/solvent)							
	Hessian Eigenvalues			Charge Density	Laplacian	Ellipticity	Position	
Bond Path	λ_1	λ_2	λ_3	$\rho_b(\mathbf{r})$ ($e\text{Å}^{-3}$)	$\nabla^2\rho_b(\mathbf{r})$ ($e\text{Å}^{-5}$)	ε	x	y z (fractional)
C(36)-H(36)...N(4)	symmetry (x, y, z)							
H(36)...N(4)	-0.08,	-0.05,	0.51	0.035(1)	0.384(1)	0.57	0.9831,	0.7472, 0.6708

Bond Lengths and Angles at the Critical Point

Atoms	Distance (Å)	Atoms	Angle (°)
Cp...N(4)	1.724	N(4)...Cp...C(36)	170.9
Cp...H(36)	1.322	N(4)...Cp...H(36)	152.9
Cp...C(36)	2.027	C(36)-H(36)...Cp	115.0
H(36)...N(4)	2.963	C(36)-H(36)...N(4)	129.3
C(36)...N(4)	3.739		

Table 41. Bond critical points for the short intermolecular cation/solvent...anion contacts in guanidinium tetraphenylborate acetonitrile solvate (continued).

Contact	C-H...N (anion/solvent)								
	Hessian Eigenvalues			Charge Density	Laplacian	Ellipticity	Position		
Bond Path	λ_1	λ_2	λ_3	$\rho_b(\mathbf{r})$ (eÅ^{-3})	$\nabla^2\rho_b(\mathbf{r})$ (eÅ^{-5})	ε	x	y (fractional)	z
C(44)-H(44)...N(4)	symmetry (2-x, 1-y, 1-z)								
H(44)...N(4)	-0.19,	-0.16,	0.98	0.066(3)	0.633(2)	0.20	1.2190,	0.3313,	0.1868

Bond Lengths and Angles at the Critical Point

Atoms	Distance (Å)	Atoms	Angle (°)
Cp...N(4)	1.602	N(4)...Cp...C(44)	163.5
Cp...H(44)	1.245	N(4)...Cp...H(44)	160.1
Cp...C(44)	1.833	C(44)-H(44)...Cp	104.1
H(44)...N(4)	2.805	C(44)-H(44)...N(4)	114.8
C(44)...N(4)	3.399		

Table 41. Bond critical points for the short intermolecular cation/solvent...anion contacts in guanidinium tetraphenylborate acetonitrile solvate (continued).

C-H...N (anion/solvent)									
Contact	Hessian Eigenvalues			Charge Density	Laplacian	Ellipticity	Position		
Bond Path	λ_1	λ_2	λ_3	$\rho_b(\mathbf{r})$ ($eÅ^{-3}$)	$\nabla^2\rho_b(\mathbf{r})$ ($eÅ^{-5}$)	ε	x	y (fractional)	z
C(45)-H(45)...N(4)	symmetry (2-x, 1-y, 1-z)								
H(45)...N(4)	-0.12,	-0.07,	0.73	0.050(2)	0.544(1)	0.74	1.1286,	0.3497,	0.2258

Bond Lengths and Angles at the Critical Point

Atoms	Distance (Å)	Atoms	Angle (°)
Cp...N(4)	1.644	N(4)...Cp...C(45)	168.9
Cp...H(45)	1.377	N(4)...Cp...H(45)	154.5
Cp...C(45)	1.824	C(45)-H(45)...Cp	95.3
H(45)...N(4)	2.947	C(45)-H(45)...N(4)	109.0
C(45)...N(4)	3.452		

Table 42. Short intermolecular anion...anion contacts for guanidinium tetraphenylborate acetonitrile solvate.

Ring 1					
C(12)	-	H(13)	2.981	symmetry	(3-x, 2-y, 1-z)
C(12)	-	H(23)	2.922	symmetry	(2-x, 2-y, 1-z)
C(14)	-	H(24)	2.863	symmetry	(1+x, y, z)
C(15)	-	H(14)	2.966	symmetry	(3-x, 2-y, -z)
Ring 2					
no contacts					
Ring 3					
C(35)	-	H(16)	2.903	symmetry	(x, y, 1+z)
Ring 4					
C(42)	-	H(34)	2.930	symmetry	(x, y, -1+z)

Table 43. Bond critical points for the short intermolecular anion...anion contacts in guanidinium tetraphenylborate acetonitrile solvate.

Contact	C-H...phenyl (anion/anion)								
	Hessian Eigenvalues			Charge Density	Laplacian	Ellipticity	Position		
Bond Path	λ_1	λ_2	λ_3	$\rho_b(\mathbf{r})$ ($e\text{Å}^{-3}$)	$\nabla^2\rho_b(\mathbf{r})$ ($e\text{Å}^{-5}$)	ε	x	y (fractional)	z
C(13)-H(13)...ring 1 symmetry (3-x, 2-y, 1-z) H...H type contact									
H(13)...H(12)	-0.15,	-0.14,	0.76	0.058(1)	0.467(1)	0.06	1.5447,	1.0647,	0.4553

Bond Lengths and Angles at the Critical Point

Atoms	Distance (Å)	Atoms	Angle (°)
H(13)...H(12)'	2.454	C(13)-H(13)...H(12)'	124.0
C(13)...H(12)'	3.183	C(13)-H(13)...C(12)'	130.6
H(13)...C(12)'	2.981		
Cp...H(13)	1.180	H(13)...Cp...H(12)'	168.9
Cp...H(12)'	1.286	C(13)-H(13)...Cp	122.3
Cp...C(13)	1.977		
Cp...C(12)'	1.876		

Table 43. Bond critical points for the short intermolecular anion...anion contacts in guanidinium tetraphenylborate acetonitrile solvate (continued).

	C-H...phenyl (anion/anion)								
Contact	Hessian Eigenvalues			Charge Density	Laplacian	Ellipticity	Position		
Bond Path	λ_1	λ_2	λ_3	$\rho_b(\mathbf{r})$ (eÅ^{-3})	$\nabla^2\rho_b(\mathbf{r})$ (eÅ^{-5})	ε	x	y (fractional)	z
C(23)-H(23)...ring 1 symmetry (2-x, 2-y, 1-z) H...H type contact									
H(23)...H(12)	-0.12,	-0.12,	0.68	0.051(1)	0.442(1)	0.07	0.7429,	1.0006,	0.4875

Bond Lengths and Angles at the Critical Point

Atoms	Distance (Å)	Atoms	Angle (°)
H(23)...H(12)	2.337	C(23)-H(23)...H(12)	154.8
C(23)...H(12)	3.342	C(23)-H(23)...C(12)	172.5
H(23)...C(12)	2.922		
Cp...H(23)	1.066	H(23)...Cp...H(12)	174.8
Cp...H(12)	1.274	C(23)-H(23)...Cp	157.5
Cp...C(23)	2.100		
Cp...C(12)	1.929		

Table 43. Bond critical points for the short intermolecular anion...anion contacts in guanidinium tetraphenylborate acetonitrile solvate (continued).

Contact	Hessian Eigenvalues			Charge Density	Laplacian	Ellipticity	Position		
Bond Path	λ_1	λ_2	λ_3	$\rho_b(\mathbf{r})$ ($eÅ^{-3}$)	$\nabla^2\rho_b(\mathbf{r})$ ($eÅ^{-5}$)	ε	x	y (fractional)	z
C-H...phenyl (anion/anion)									
C(24)-H(24)...ring 1 symmetry (-1+x, y, z) single atom type hydrogen bond									
H(24)...C(14)	-0.08,	-0.05,	0.50	0.042(1)	0.371(1)	0.84	0.5366,	0.9358,	0.2014

Bond Lengths and Angles at the Critical Point

Atoms	Distance (Å)	Atoms	Angle (°)
H(24)...C(14)	2.863	C(24)-H(24)...C(14)	164.8
C(24)...C(14)	3.912		
Cp...H(24)	1.099	H(24)...Cp...C(14)	171.6
Cp...C(24)	2.163	C(24)...Cp...C(14)	167.7
Cp...H(14)	1.771	C(24)-H(24)...Cp	167.8

Table 43. Bond critical points for the short intermolecular anion...anion contacts in guanidinium tetraphenylborate acetonitrile solvate (continued).

Contact	Hessian Eigenvalues			Charge Density	Laplacian	Ellipticity	Position		
Bond Path	λ_1	λ_2	λ_3	$\rho_c(\mathbf{r})$ (eÅ^{-3})	$\nabla^2\rho_c(\mathbf{r})$ (eÅ^{-5})	ε	x	y (fractional)	z
C-H...phenyl (anion/anion)									
C(14)-H(14)...ring 1 symmetry (3-x, 2-y, -z) H...H type contact									
H(14)...H(15)	-0.18,	-0.15,	0.83	0.061(2)	0.504(1)	0.15	1.5414,	1.0619,	0.0698

Bond Lengths and Angles at the Critical Point

Atoms	Distance (Å)	Atoms	Angle (°)
H(14)...H(15)'	2.357	C(14)-H(14)...H(15)'	121.3
C(14)...H(15)'	3.057	C(14)-H(14)...C(15)'	126.7
H(14)...C(15)'	2.966		
Cp...H(14)	1.150	H(14)...Cp...H(15)'	165.0
Cp...H(15)'	1.227	C(14)-H(14)...Cp	118.4
Cp...C(14)	1.912		
Cp...C(15)'	1.875		

Table 43. Bond critical points for the short intermolecular anion...anion contacts in guanidinium tetraphenylborate acetonitrile solvate (continued).

Contact	C-H...phenyl (anion/anion)							
	Hessian Eigenvalues			Charge Density	Laplacian	Ellipticity	Position	
Bond Path	λ_1	λ_2	λ_3	$\rho_b(\mathbf{r})$ (eÅ^{-3})	$\nabla^2\rho_b(\mathbf{r})$ (eÅ^{-5})	ε	x	y z (fractional)
C(16)-H(16)...ring 3	symmetry (x, y, -1+z)				H...H type contact			
H(16)...H(35)	-0.11,	-0.07,	0.62	0.049(1)	0.439(1)	0.54	1.2222,	0.7509, -0.0616

Bond Lengths and Angles at the Critical Point

Atoms	Distance (Å)	Atoms	Angle (°)
H(16)...H(35)	2.464	C(16)-H(16)...H(35)	167.9
C(16)...H(35)	3.523	C(16)-H(16)...C(35)	146.9
H(16)...C(35)	2.903		
Cp...H(16)	1.120	H(16)...Cp...H(35)	149.8
Cp...H(35)	1.431	C(16)-H(16)...Cp	151.1
Cp...C(16)	2.126		
Cp...C(35)	1.788		

Table 43. Bond critical points for the short intermolecular anion...anion contacts in guanidinium tetraphenylborate acetonitrile solvate (continued).

Contact	Hessian Eigenvalues			Charge Density	Laplacian	Ellipticity	Position		
Bond Path	λ_1	λ_2	λ_3	$\rho_b(\mathbf{r})$ ($eÅ^{-3}$)	$\nabla^2\rho_b(\mathbf{r})$ ($eÅ^{-5}$)	ε	x	y (fractional)	z
C(34)-H(34)...ring 4[a] symmetry (x, y, 1+z) H...H type contact									
H(34)...H(42)	-0.11,	-0.08,	0.60	0.046(1)	0.405(1)	0.53	1.3895,	0.6739,	1.0408

C-H...phenyl (anion/anion)

Bond Lengths and Angles at the Critical Point

Atoms	Distance (Å)	Atoms	Angle (°)
H(34)...H(42)	2.574	C(34)-H(34)...H(42)	151.6
H(34)...C(42)	2.930	C(34)-H(34)...C(42)	137.9
C(34)...H(42)	3.557		
Cp...H(34)	1.140	H(34)...Cp...H(42)	155.0
Cp...H(42)	1.496	H(34)...Cp...C(42)	164.6
Cp...C(34)	2.082	C(34)-H(34)...Cp	140.0
Cp...C(42)	1.816		

[a] The bond path from H(34) follows the C(42)-H(42) bond of the ring for approximately one third of its length before terminating at H(42).

Table 44. Positional parameters and isotropic temperature factors ($Å^2 \times 10^3$) for the nonhydrogen atoms of biguanidinium tetraphenylborate.

atom	x	y	z	U(eq)
N(1)	-0.5463(2)	0.3990(1)	-0.0795(1)	31
N(2)	-0.7281(2)	0.3004(2)	-0.0957(1)	44
N(3)	-0.6381(2)	0.3228(1)	-0.2103(1)	47
N(4)	-0.3355(2)	0.4625(1)	-0.0317(1)	38
N(5)	-0.3534(2)	0.3231(1)	-0.1061(1)	43
C(1)	-0.6360(1)	0.3400(1)	-0.1291(1)	30
C(2)	-0.4148(2)	0.3939(1)	-0.0752(1)	30
C(11)	0.0035(1)	0.2777(1)	-0.0079(1)	22
C(12)	-0.0219(1)	0.2137(1)	-0.0761(1)	26
C(13)	-0.0530(1)	0.2431(1)	-0.1608(1)	30
C(14)	-0.0609(1)	0.3388(1)	-0.1809(1)	32
C(15)	-0.0371(1)	0.4045(1)	-0.1152(1)	31
C(16)	-0.0058(1)	0.3736(1)	-0.0304(1)	27
C(21)	0.2261(1)	0.2353(1)	0.0989(1)	24
C(22)	0.2851(2)	0.1519(1)	0.0777(1)	31
C(23)	0.4213(2)	0.1461(1)	0.0761(1)	40
C(24)	0.5053(2)	0.2244(2)	0.0960(1)	43
C(25)	0.4504(2)	0.3090(1)	0.1158(1)	37
C(26)	0.3137(2)	0.3138(1)	0.1165(1)	28
C(31)	-0.0008(1)	0.1432(1)	0.1122(1)	25
C(32)	-0.1328(1)	0.1135(1)	0.0730(1)	32
C(33)	-0.1900(2)	0.0323(1)	0.0981(1)	41
C(34)	-0.1154(2)	-0.0225(1)	0.1645(1)	45
C(35)	0.0157(2)	0.0049(1)	0.2055(1)	41
C(36)	0.0714(1)	0.0862(1)	0.1794(1)	31
C(41)	0.0205(1)	0.3176(1)	0.1574(1)	23
C(42)	-0.1136(1)	0.3506(1)	0.1418(1)	29
C(43)	-0.1579(2)	0.4109(1)	0.1974(1)	37
C(44)	-0.0677(2)	0.4396(1)	0.2725(1)	44
C(45)	0.0652(2)	0.4065(1)	0.2915(1)	40
C(46)	0.1075(1)	0.3464(1)	0.2347(1)	30
B(1)	0.0624(1)	0.2434(1)	0.0908(1)	22

Table 45. Atomic distances (Å) and angles (°) for biguanidinium tetraphenylborate.

Atoms	Distance	Atoms	Angle
N(1)-C(1)	1.350(2)	C(1)-N(1)-C(2)	121.5(2)
N(1)-C(2)	1.325(2)	N(1)-C(1)-N(2)	117.6(2)
N(2)-C(1)	1.321(2)	N(1)-C(1)-N(3)	123.1(2)
N(3)-C(1)	1.336(2)	N(2)-C(1)-N(3)	119.2(2)
N(4)-C(2)	1.349(2)	N(1)-C(2)-N(4)	117.0(2)
N(5)-C(2)	1.347(2)	N(1)-C(2)-N(5)	125.3(2)
C(11)-C(12)	1.4086(14)	N(4)-C(2)-N(5)	117.6(2)
C(11)-C(16)	1.411(2)	C(12)-C(11)-C(16)	115.7(1)
C(11)-B(1)	1.6410(13)	C(12)-C(11)-B(1)	121.9(1)
C(12)-C(13)	1.398(2)	C(16)-C(11)-B(1)	121.7(1)
C(13)-C(14)	1.397(2)	C(11)-C(12)-C(13)	122.2(2)
C(14)-C(15)	1.395(2)	C(12)-C(13)-C(14)	120.5(2)
C(15)-C(16)	1.406(2)	C(13)-C(14)-C(15)	119.0(1)
C(21)-C(22)	1.411(2)	C(14)-C(15)-C(16)	119.7(2)
C(21)-C(26)	1.413(2)	C(11)-C(16)-C(15)	122.8(2)
C(21)-B(1)	1.6428(14)	C(22)-C(21)-C(26)	115.4(2)
C(22)-C(23)	1.395(2)	C(22)-C(21)-B(1)	121.6(2)
C(23)-C(24)	1.393(3)	C(26)-C(21)-B(1)	122.5(2)
C(24)-C(25)	1.397(3)	C(21)-C(22)-C(23)	122.7(2)
C(25)-C(26)	1.397(2)	C(22)-C(23)-C(24)	120.2(2)
C(31)-C(32)	1.403(2)	C(23)-C(24)-C(25)	119.0(2)
C(31)-C(36)	1.412(2)	C(24)-C(25)-C(26)	120.0(2)
C(31)-B(1)	1.6367(14)	C(21)-C(26)-C(25)	122.6(2)
C(32)-C(33)	1.400(2)	C(32)-C(31)-C(36)	115.8(2)
C(33)-C(34)	1.394(3)	C(32)-C(31)-B(1)	123.3(2)
C(34)-C(35)	1.392(3)	C(36)-C(31)-B(1)	120.6(2)
C(35)-C(36)	1.400(2)	C(31)-C(32)-C(33)	122.5(2)
C(41)-C(42)	1.406(2)	C(32)-C(33)-C(34)	120.1(2)
C(41)-C(46)	1.4060(14)	C(33)-C(34)-C(35)	119.2(2)
C(41)-B(1)	1.6425(14)	C(34)-C(35)-C(36)	119.9(2)
C(42)-C(43)	1.399(2)	C(31)-C(36)-C(35)	122.5(2)
C(43)-C(44)	1.395(2)	C(42)-C(41)-C(46)	115.6(1)
C(44)-C(45)	1.393(2)	C(42)-C(41)-B(1)	119.6(1)
C(45)-C(46)	1.402(2)	C(46)-C(41)-B(1)	124.6(2)
N(2)-H(2A)	0.986	C(41)-C(42)-C(43)	122.8(2)
N(2)-H(2B)	0.986	C(42)-C(43)-C(44)	119.8(2)
N(3)-H(3A)	0.986	C(43)-C(44)-C(45)	119.2(2)
N(3)-H(3B)	0.986	C(44)-C(45)-C(46)	120.0(2)
N(4)-H(4A)	0.986	C(41)-C(46)-C(45)	122.5(2)
N(4)-H(4B)	0.986	C(11)-B(1)-C(21)	102.5(1)
N(5)-H(5A)	0.986	C(11)-B(1)-C(31)	113.5(1)
N(5)-H(5B)	0.986	C(11)-B(1)-C(41)	111.2(1)

Table 45. Atomic distances (Å) and angles (°) for biguanidinium tetraphenylborate (continued).

Atoms	Distance	Atoms	Angle
C(12)-H(12)	1.076	C(21)-B(1)-C(31)	111.5(1)
C(13)-H(13)	1.076	C(21)-B(1)-C(41)	114.6(1)
C(14)-H(14)	1.076	C(31)-B(1)-C(41)	103.9(1)
C(15)-H(15)	1.076	C(1)-N(2)-H(2A)	120.1
C(16)-H(16)	1.076	C(1)-N(2)-H(2B)	116.8
C(22)-H(22)	1.076	H(2A)-N(2)-H(2B)	123.0
C(23)-H(23)	1.076	C(1)-N(3)-H(3A)	117.2
C(24)-H(24)	1.076	C(1)-N(3)-H(3B)	123.3
C(25)-H(25)	1.076	H(3A)-N(3)-H(3B)	118.5
C(26)-H(26)	1.076	C(2)-N(4)-H(4A)	117.0
C(32)-H(32)	1.076	C(2)-N(4)-H(4B)	118.4
C(33)-H(33)	1.076	H(4A)-N(4)-H(4B)	122.9
C(34)-H(34)	1.076	C(2)-N(5)-H(5A)	119.9
C(35)-H(35)	1.076	C(2)-N(5)-H(5B)	117.1
C(36)-H(36)	1.076	H(5A)-N(5)-H(5B)	122.4
C(42)-H(42)	1.076	C(11)-C(12)-H(12)	120.5
C(43)-H(43)	1.076	C(13)-C(12)-H(12)	117.2
C(44)-H(44)	1.076	C(12)-C(13)-H(13)	119.8
C(45)-H(45)	1.076	C(14)-C(13)-H(13)	119.7
C(46)-H(46)	1.076	C(13)-C(14)-H(14)	120.4
		C(15)-C(14)-H(14)	120.6
		C(14)-C(15)-H(15)	120.4
		C(16)-C(15)-H(15)	119.9
		C(11)-C(16)-H(16)	117.2
		C(15)-C(16)-H(16)	120.0
		C(21)-C(22)-H(22)	118.4
		C(23)-C(22)-H(22)	119.0
		C(22)-C(23)-H(23)	119.0
		C(24)-C(23)-H(23)	120.8
		C(23)-C(24)-H(24)	121.0
		C(25)-C(24)-H(24)	119.9
		C(24)-C(25)-H(25)	120.0
		C(26)-C(25)-H(25)	119.9
		C(21)-C(26)-H(26)	119.2
		C(25)-C(26)-H(26)	118.2
		C(31)-C(32)-H(32)	118.7
		C(33)-C(32)-H(32)	118.8
		C(32)-C(33)-H(33)	120.1
		C(34)-C(33)-H(33)	119.8
		C(33)-C(34)-H(34)	120.8
		C(35)-C(34)-H(34)	119.9
		C(34)-C(35)-H(35)	120.4

Table 45. Atomic distances (Å) and angles (°) for biguanidinium tetraphenylborate (continued).

Atoms	Distance	Atoms	Angle
		C(36)-C(35)-H(35)	119.7
		C(31)-C(36)-H(36)	118.8
		C(35)-C(36)-H(36)	118.7
		C(41)-C(42)-H(42)	117.8
		C(43)-C(42)-H(42)	119.4
		C(42)-C(43)-H(43)	120.3
		C(44)-C(43)-H(43)	119.9
		C(43)-C(44)-H(44)	118.8
		C(45)-C(44)-H(44)	121.9
		C(44)-C(45)-H(45)	118.9
		C(46)-C(45)-H(45)	121.2
		C(41)-C(46)-H(46)	119.5
		C(45)-C(46)-H(46)	118.0

Table 46. Anisotropic temperature factors ($Å^2$) for the nonhydrogen atoms of biguanidinium tetraphenylborate.

atom	U11	U22	U33	U12	U13	U23
N(1)	0.028(1)	0.034(1)	0.030(1)	-0.004(1)	0.010(1)	0.000(1)
N(2)	0.032(1)	0.070(1)	0.029(1)	-0.001(1)	0.010(1)	-0.015(1)
N(3)	0.056(1)	0.056(1)	0.027(1)	-0.008(1)	0.016(1)	-0.019(1)
N(4)	0.029(1)	0.037(1)	0.046(1)	-0.004(1)	0.005(1)	-0.002(1)
N(5)	0.032(1)	0.043(1)	0.051(1)	-0.009(1)	0.014(1)	0.004(1)
C(1)	0.028(1)	0.036(1)	0.024(1)	0.000(1)	0.009(1)	-0.002(1)
C(2)	0.026(1)	0.032(1)	0.029(1)	0.003(1)	0.008(1)	0.001(1)
C(11)	0.024(1)	0.023(1)	0.018(1)	0.000(1)	0.004(1)	-0.001(1)
C(12)	0.029(1)	0.027(1)	0.021(1)	-0.003(1)	0.004(1)	-0.001(1)
C(13)	0.031(1)	0.037(1)	0.019(1)	-0.004(1)	0.003(1)	-0.002(1)
C(14)	0.032(1)	0.042(1)	0.019(1)	0.004(1)	0.004(1)	0.002(1)
C(15)	0.039(1)	0.031(1)	0.022(1)	0.005(1)	0.006(1)	0.002(1)
C(16)	0.034(1)	0.024(1)	0.020(1)	0.001(1)	0.006(1)	0.000(1)
C(21)	0.025(1)	0.027(1)	0.019(1)	0.001(1)	0.005(1)	0.000(1)
C(22)	0.029(1)	0.032(1)	0.031(1)	0.001(1)	0.010(1)	0.005(1)
C(23)	0.031(1)	0.047(1)	0.042(1)	0.002(1)	0.014(1)	0.010(1)
C(24)	0.028(1)	0.065(1)	0.035(1)	0.006(1)	0.010(1)	0.005(1)
C(25)	0.024(1)	0.053(1)	0.030(1)	0.000(1)	0.007(1)	-0.007(1)
C(26)	0.026(1)	0.034(1)	0.023(1)	-0.002(1)	0.006(1)	-0.005(1)
C(31)	0.029(1)	0.022(1)	0.023(1)	0.001(1)	0.009(1)	-0.001(1)
C(32)	0.031(1)	0.032(1)	0.033(1)	-0.002(1)	0.010(1)	-0.006(1)
C(33)	0.040(1)	0.035(1)	0.048(1)	-0.007(1)	0.021(1)	-0.011(1)
C(34)	0.056(1)	0.025(1)	0.054(1)	-0.001(1)	0.033(1)	-0.005(1)
C(35)	0.053(1)	0.026(1)	0.042(1)	0.008(1)	0.022(1)	0.002(1)
C(36)	0.037(1)	0.026(1)	0.029(1)	0.005(1)	0.011(1)	0.002(1)
C(41)	0.027(1)	0.024(1)	0.018(1)	0.000(1)	0.006(1)	0.001(1)
C(42)	0.027(1)	0.032(1)	0.026(1)	-0.002(1)	0.007(1)	0.002(1)
C(43)	0.033(1)	0.041(1)	0.038(1)	-0.006(1)	0.015(1)	0.004(1)
C(44)	0.045(1)	0.049(1)	0.037(1)	-0.015(1)	0.019(1)	0.001(1)
C(45)	0.040(1)	0.050(1)	0.028(1)	-0.015(1)	0.009(1)	-0.001(1)
C(46)	0.029(1)	0.037(1)	0.022(1)	-0.005(1)	0.005(1)	0.000(1)
B(1)	0.026(1)	0.022(1)	0.018(1)	0.001(1)	0.006(1)	0.000(1)

Table 47. Positional parameters and isotropic temperature factors ($Å^2 \times 10^3$) for the hydrogen atoms of biguanidinium tetraphenylborate.

atom	x	y	z	U(eq)
H(2A)	-0.7219	0.3069	-0.0344	58
H(2B)	-0.8042	0.2687	-0.1353	58
H(3A)	-0.5778	0.3610	-0.2360	60
H(3B)	-0.7072	0.2832	-0.2478	60
H(4A)	-0.3781	0.5063	0.0010	53
H(4B)	-0.2365	0.4572	-0.0233	53
H(5A)	-0.4082	0.2759	-0.1440	56
H(5B)	-0.2539	0.3262	-0.0959	56
H(12)	-0.0143	0.1392	-0.0645	41
H(13)	-0.0695	0.1918	-0.2109	45
H(14)	-0.0837	0.3613	-0.2461	46
H(15)	-0.0403	0.4785	-0.1289	46
H(16)	0.0133	0.4240	0.0206	41
H(22)	0.2216	0.0910	0.0608	45
H(23)	0.4595	0.0808	0.0581	54
H(24)	0.6118	0.2198	0.0989	57
H(25)	0.5125	0.3711	0.1282	51
H(26)	0.2740	0.3803	0.1306	43
H(32)	-0.1912	0.1535	0.0203	47
H(33)	-0.2925	0.0129	0.0673	54
H(34)	-0.1590	-0.0841	0.1855	57
H(35)	0.0743	-0.0356	0.2578	54
H(36)	0.1729	0.1061	0.2120	45
H(42)	-0.1845	0.3271	0.0849	43
H(43)	-0.2606	0.4364	0.1817	51
H(44)	-0.1029	0.4872	0.3138	57
H(45)	0.1336	0.4276	0.3502	54
H(46)	0.2105	0.3215	0.2518	45

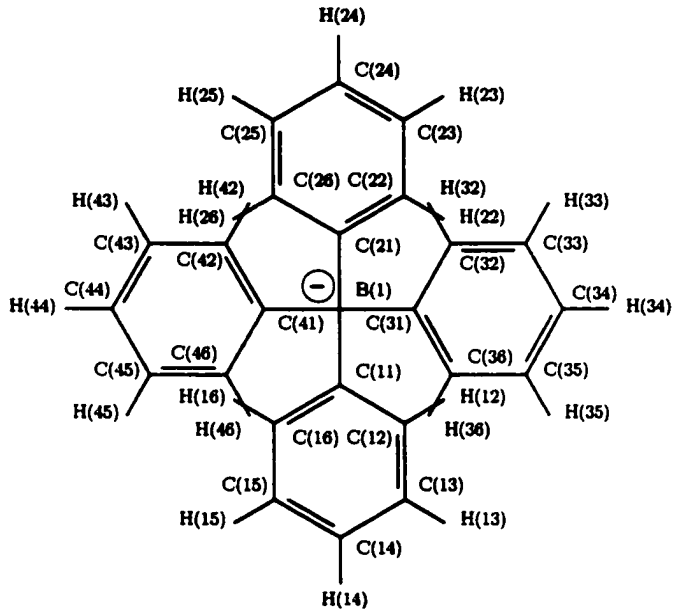

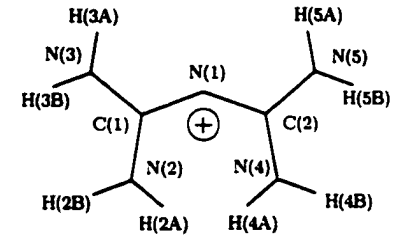

Table 48. Scale factor, extinction, kappa values, local coordinate system, and multipole population coefficients for biguanidinium tetraphenylborate (atom numbering as shown above).

Scale Factor	Extinction
4.348(15)	0.877(24)

	κ'	κ''
1.	0.944(16)	0.883(82)
2.	0.972(18)	0.850(31)
3.	0.964(25)	0.836(47)
4.	0.949(6)	0.912(15)
5.	0.849(21)	0.941(60)
6.	0.932(37)	1.074(67)
7.	0.950(21)	1.023(42)

atom	atom0	axis1	atom1	atom2	axis2	right/left	kappa set
N(1)	C(2)	Z	N(1)	C(1)	X	R	1
N(2)	C(1)	Z	N(2)	H(2B)	X	R	2
N(3)	C(1)	Z	N(3)	H(3A)	X	R	2
N(4)	C(2)	Z	N(4)	H(4A)	X	R	2
N(5)	C(2)	Z	N(5)	H(5B)	X	R	2
C(1)	N(1)	Z	C(1)	N(3)	X	R	3
C(2)	N(1)	Z	C(2)	N(4)	X	R	3
C(11)	B(1)	X	C(11)	DUM0	Y	R	4
C(12)	C(13)	X	C(12)	C(11)	Y	R	4
C(13)	C(12)	X	C(13)	C(14)	Y	L	4
C(14)	H(14)	X	C(14)	DUM0	Y	R	4

Table 48. Local coordinate systems continued...

atom	atom0	axis1	atom1	atom2	axis2	right/left	kappa set
C(15)	C(16)	X	C(15)	C(14)	Y	R	4
C(16)	C(15)	X	C(16)	C(11)	Y	L	4
C(21)	B(1)	X	C(21)	DUM0	Y	L	4
C(22)	C(23)	X	C(22)	C(21)	Y	L	4
C(23)	C(22)	X	C(23)	C(24)	Y	R	4
C(24)	H(22)	X	C(24)	DUM0	Y	L	4
C(25)	C(26)	X	C(25)	C(24)	Y	L	4
C(26)	C(25)	X	C(26)	C(21)	Y	R	4
C(31)	B(1)	X	C(31)	DUM1	Y	R	4
C(32)	C(33)	X	C(32)	C(31)	Y	R	4
C(33)	C(32)	X	C(33)	C(34)	Y	L	4
C(34)	H(34)	X	C(34)	DUM1	Y	R	4
C(35)	C(36)	X	C(35)	C(34)	Y	R	4
C(36)	C(35)	X	C(36)	C(31)	Y	L	4
C(41)	B(1)	X	C(41)	DUM1	Y	L	4
C(42)	C(43)	X	C(42)	C(41)	Y	L	4
C(43)	C(42)	X	C(43)	C(44)	Y	R	4
C(44)	H(44)	X	C(44)	DUM1	Y	L	4
C(45)	C(46)	X	C(45)	C(44)	Y	L	4
C(46)	C(45)	X	C(46)	C(41)	Y	R	4
B(1)	DUM0	Z	B(1)	DUM2	X	R	5
H(2A)	N(2)	Z	H(2A)	H(2B)	X	R	6
H(2B)	N(2)	Z	H(2B)	H(2A)	X	L	6
H(3A)	N(3)	Z	H(3A)	H(3B)	X	L	6
H(3B)	N(3)	Z	H(3B)	H(3A)	X	R	6
H(4A)	N(4)	Z	H(4A)	H(4B)	X	L	6
H(4B)	N(4)	Z	H(4B)	H(4A)	X	R	6
H(5A)	N(5)	Z	H(5A)	H(5B)	X	R	6
H(5B)	N(5)	Z	H(5B)	H(5A)	X	L	6
H(12)	C(12)	Z	H(12)	C(11)	Y	R	7
H(13)	C(13)	Z	H(13)	C(14)	Y	R	7
H(14)	C(14)	Z	H(14)	C(13)	Y	R	7
H(15)	C(15)	Z	H(15)	C(14)	Y	R	7
H(16)	C(16)	Z	H(16)	C(11)	Y	R	7
H(22)	C(22)	Z	H(22)	C(21)	Y	R	7
H(23)	C(23)	Z	H(23)	C(24)	Y	R	7
H(24)	C(24)	Z	H(24)	C(23)	Y	R	7
H(25)	C(25)	Z	H(25)	C(24)	Y	R	7
H(26)	C(26)	Z	H(26)	C(21)	Y	R	7
H(32)	C(32)	Z	H(32)	C(31)	Y	R	7
H(33)	C(33)	Z	H(33)	C(34)	Y	R	7
H(34)	C(34)	Z	H(34)	C(33)	Y	R	7
H(35)	C(35)	Z	H(35)	C(34)	Y	R	7
H(36)	C(36)	Z	H(36)	C(31)	Y	R	7
H(42)	C(42)	Z	H(42)	C(41)	Y	R	7
H(43)	C(43)	Z	H(43)	C(44)	Y	R	7
H(44)	C(44)	Z	H(44)	C(43)	Y	R	7
H(45)	C(45)	Z	H(45)	C(44)	Y	R	7
H(46)	C(46)	Z	H(46)	C(41)	Y	R	7

DUM0=0.1147 0.2565 0.0455
DUM1=0.0097 0.2304 0.1349
DUM2=0.0013 0.2104 0.0522

Table 48. Multipole populations

atom	P_v	P_{00}	P_{11}	P_{1-1}	P_{10}
N(1)	5.06(28)	0.00(0)	−0.01(5)	0.05(3)	0.02(6)
N(2)	4.47(30)	0.00(0)	−0.07(3)	0.08(4)	0.29(7)
N(3)	4.26(29)	0.00(0)	−0.03(3)	0.00(4)	0.23(6)
N(4)	4.43(29)	0.00(0)	0.07(3)	0.09(3)	0.28(6)
N(5)	4.49(29)	0.00(0)	0.00(4)	0.06(3)	0.27(6)
C(1)	3.52(31)	0.00(0)	0.11(6)	0.07(3)	0.09(7)
C(2)	3.46(30)	0.00(0)	−0.07(5)	−0.04(3)	0.20(9)
C(11)	3.78(9)	0.00(0)	0.01(4)	−0.06(2)	−0.01(4)
C(12)	3.79(10)	0.00(0)	0.03(4)	0.17(4)	−0.04(2)
C(13)	3.80(10)	0.00(0)	0.08(4)	0.15(4)	−0.01(3)
C(14)	3.53(11)	0.00(0)	−0.04(4)	0.03(3)	−0.06(5)
C(15)	3.91(10)	0.00(0)	0.04(4)	0.16(4)	−0.01(3)
C(16)	3.65(10)	0.00(0)	0.08(4)	0.15(4)	−0.02(2)
C(21)	3.92(9)	0.00(0)	0.00(4)	−0.01(2)	0.02(4)
C(22)	3.76(11)	0.00(0)	0.07(5)	0.16(4)	0.03(3)
C(23)	3.72(11)	0.00(0)	0.07(6)	0.18(5)	−0.01(3)
C(24)	3.60(12)	0.00(0)	0.05(6)	0.04(6)	−0.06(4)
C(25)	3.70(11)	0.00(0)	0.08(6)	0.15(5)	0.04(3)
C(26)	3.79(10)	0.00(0)	0.11(5)	0.15(4)	−0.01(3)
C(31)	3.80(9)	0.00(0)	0.03(4)	−0.05(3)	0.00(4)
C(32)	3.85(10)	0.00(0)	0.05(5)	0.20(4)	−0.01(3)
C(33)	3.80(11)	0.00(0)	0.08(5)	0.18(5)	0.01(3)
C(34)	3.52(12)	0.00(0)	−0.10(4)	0.03(3)	0.01(7)
C(35)	3.72(11)	0.00(0)	0.07(5)	0.17(5)	−0.03(3)
C(36)	3.82(10)	0.00(0)	0.07(4)	0.19(4)	−0.02(3)
C(41)	3.98(9)	0.00(0)	0.02(4)	0.01(3)	0.04(4)
C(42)	3.71(10)	0.00(0)	0.07(4)	0.19(4)	−0.01(3)
C(43)	3.74(11)	0.00(0)	0.05(5)	0.19(5)	0.04(3)
C(44)	3.40(11)	0.00(0)	−0.04(4)	0.01(4)	−0.06(6)
C(45)	3.82(11)	0.00(0)	0.10(5)	0.20(5)	0.08(4)
C(46)	3.64(10)	0.00(0)	0.10(4)	0.14(4)	0.01(3)
B(1)	3.58(26)	0.00(0)	0.03(3)	0.01(4)	0.02(3)
H(2A)	1.29(13)	0.00(0)	0.00(0)	0.00(0)	0.31(6)
H(2B)	1.29(0)	0.00(0)	0.00(0)	0.00(0)	0.31(0)
H(3A)	1.29(0)	0.00(0)	0.00(0)	0.00(0)	0.31(0)
H(3B)	1.29(0)	0.00(0)	0.00(0)	0.00(0)	0.31(0)
H(4A)	1.29(0)	0.00(0)	0.00(0)	0.00(0)	0.31(0)
H(4B)	1.29(0)	0.00(0)	0.00(0)	0.00(0)	0.31(0)
H(5A)	1.29(0)	0.00(0)	0.00(0)	0.00(0)	0.31(0)
H(5B)	1.29(0)	0.00(0)	0.00(0)	0.00(0)	0.31(0)
H(12)	1.33(7)	0.00(0)	0.00(0)	0.00(0)	0.27(3)
H(13)	1.33(0)	0.00(0)	0.00(0)	0.00(0)	0.27(0)
H(14)	1.33(0)	0.00(0)	0.00(0)	0.00(0)	0.27(0)
H(15)	1.33(0)	0.00(0)	0.00(0)	0.00(0)	0.27(0)
H(16)	1.33(0)	0.00(0)	0.00(0)	0.00(0)	0.27(0)
H(22)	1.33(0)	0.00(0)	0.00(0)	0.00(0)	0.27(0)
H(23)	1.33(0)	0.00(0)	0.00(0)	0.00(0)	0.27(0)
H(24)	1.33(0)	0.00(0)	0.00(0)	0.00(0)	0.27(0)
H(25)	1.33(0)	0.00(0)	0.00(0)	0.00(0)	0.27(0)
H(26)	1.33(0)	0.00(0)	0.00(0)	0.00(0)	0.27(0)
H(32)	1.33(0)	0.00(0)	0.00(0)	0.00(0)	0.27(0)
H(33)	1.33(0)	0.00(0)	0.00(0)	0.00(0)	0.27(0)

Table 48. Multipole populations continued...

atom	P_v	P_{00}	P_{11}	P_{1-1}	P_{10}
H(34)	1.33(0)	0.00(0)	0.00(0)	0.00(0)	0.27(0)
H(35)	1.33(0)	0.00(0)	0.00(0)	0.00(0)	0.27(0)
H(36)	1.33(0)	0.00(0)	0.00(0)	0.00(0)	0.27(0)
H(42)	1.33(0)	0.00(0)	0.00(0)	0.00(0)	0.27(0)
H(43)	1.33(0)	0.00(0)	0.00(0)	0.00(0)	0.27(0)
H(44)	1.33(0)	0.00(0)	0.00(0)	0.00(0)	0.27(0)
H(45)	1.33(0)	0.00(0)	0.00(0)	0.00(0)	0.27(0)
H(46)	1.33(0)	0.00(0)	0.00(0)	0.00(0)	0.27(0)

atom	P_{20}	P_{21}	P_{2-1}	P_{22}	P_{2-2}
N(1)	−0.12(6)	0.09(5)	−0.06(3)	0.04(3)	0.03(3)
N(2)	−0.01(5)	0.02(3)	0.08(4)	−0.10(4)	0.02(3)
N(3)	0.05(5)	0.01(3)	−0.05(4)	−0.11(4)	0.13(3)
N(4)	0.07(5)	−0.02(4)	0.04(4)	−0.18(4)	0.01(3)
N(5)	0.04(5)	0.09(4)	0.02(4)	−0.15(4)	0.03(3)
C(1)	0.32(7)	−0.17(5)	−0.06(4)	0.15(6)	0.09(4)
C(2)	0.16(7)	−0.06(5)	0.10(3)	0.12(6)	−0.06(4)
C(11)	0.16(3)	−0.05(4)	0.02(3)	0.27(3)	−0.02(2)
C(12)	−0.24(3)	−0.03(3)	0.05(2)	0.00(4)	−0.04(3)
C(13)	−0.31(3)	0.04(3)	0.00(3)	0.05(4)	−0.14(4)
C(14)	0.08(4)	−0.04(4)	0.01(3)	0.08(3)	−0.03(2)
C(15)	−0.26(3)	0.09(3)	−0.01(3)	0.03(4)	−0.13(4)
C(16)	−0.22(3)	−0.06(3)	0.03(2)	0.01(4)	−0.02(3)
C(21)	0.14(4)	−0.05(4)	0.01(3)	0.14(3)	0.02(2)
C(22)	−0.10(3)	−0.05(3)	0.01(3)	−0.02(5)	−0.03(4)
C(23)	−0.19(4)	0.04(3)	−0.05(3)	0.01(6)	−0.13(4)
C(24)	0.03(4)	−0.08(4)	0.03(4)	−0.09(6)	−0.14(5)
C(25)	−0.14(3)	0.07(3)	0.00(3)	0.04(6)	−0.09(4)
C(26)	−0.09(3)	−0.09(3)	0.04(3)	−0.06(4)	−0.03(4)
C(31)	0.06(4)	−0.09(4)	0.10(3)	0.22(3)	−0.01(3)
C(32)	−0.17(3)	−0.11(3)	0.10(3)	−0.01(4)	0.01(4)
C(33)	−0.18(3)	0.08(3)	0.03(4)	0.08(5)	−0.19(5)
C(34)	0.03(5)	−0.09(6)	−0.10(5)	0.05(3)	−0.07(3)
C(35)	−0.20(3)	0.12(3)	−0.11(4)	0.01(5)	−0.08(4)
C(36)	−0.13(3)	−0.08(3)	−0.04(3)	0.00(4)	−0.09(4)
C(41)	0.08(3)	−0.12(4)	0.04(3)	0.20(3)	0.03(3)
C(42)	−0.16(3)	−0.06(3)	0.07(3)	−0.01(4)	0.06(4)
C(43)	−0.17(4)	0.06(3)	0.03(3)	0.05(4)	−0.22(4)
C(44)	0.08(5)	−0.07(5)	0.01(5)	0.02(3)	−0.06(4)
C(45)	−0.15(4)	0.04(4)	−0.03(4)	0.02(4)	−0.03(4)
C(46)	−0.14(3)	−0.06(3)	−0.02(3)	0.01(4)	−0.09(4)
B(1)	−0.02(3)	0.09(4)	0.07(4)	−0.01(3)	−0.04(3)
H(2A)	0.10(4)	0.00(0)	0.00(0)	0.00(0)	0.00(0)
H(2B)	0.10(0)	0.00(0)	0.00(0)	0.00(0)	0.00(0)
H(3A)	0.10(0)	0.00(0)	0.00(0)	0.00(0)	0.00(0)
H(3B)	0.10(0)	0.00(0)	0.00(0)	0.00(0)	0.00(0)
H(4A)	0.10(0)	0.00(0)	0.00(0)	0.00(0)	0.00(0)
H(4B)	0.10(0)	0.00(0)	0.00(0)	0.00(0)	0.00(0)
H(5A)	0.10(0)	0.00(0)	0.00(0)	0.00(0)	0.00(0)
H(5B)	0.10(0)	0.00(0)	0.00(0)	0.00(0)	0.00(0)
H(12)	0.09(2)	0.00(0)	0.00(0)	0.00(0)	0.00(0)

Table 48. Multipole populations continued...

atom	P_{20}	P_{21}	P_{2-1}	P_{22}	P_{2-2}
H(13)	0.09(0)	0.00(0)	0.00(0)	0.00(0)	0.00(0)
H(14)	0.09(0)	0.00(0)	0.00(0)	0.00(0)	0.00(0)
H(15)	0.09(0)	0.00(0)	0.00(0)	0.00(0)	0.00(0)
H(16)	0.09(0)	0.00(0)	0.00(0)	0.00(0)	0.00(0)
H(22)	0.09(0)	0.00(0)	0.00(0)	0.00(0)	0.00(0)
H(23)	0.09(0)	0.00(0)	0.00(0)	0.00(0)	0.00(0)
H(24)	0.09(0)	0.00(0)	0.00(0)	0.00(0)	0.00(0)
H(25)	0.09(0)	0.00(0)	0.00(0)	0.00(0)	0.00(0)
H(26)	0.09(0)	0.00(0)	0.00(0)	0.00(0)	0.00(0)
H(32)	0.09(0)	0.00(0)	0.00(0)	0.00(0)	0.00(0)
H(33)	0.09(0)	0.00(0)	0.00(0)	0.00(0)	0.00(0)
H(34)	0.09(0)	0.00(0)	0.00(0)	0.00(0)	0.00(0)
H(35)	0.09(0)	0.00(0)	0.00(0)	0.00(0)	0.00(0)
H(36)	0.09(0)	0.00(0)	0.00(0)	0.00(0)	0.00(0)
H(42)	0.09(0)	0.00(0)	0.00(0)	0.00(0)	0.00(0)
H(43)	0.09(0)	0.00(0)	0.00(0)	0.00(0)	0.00(0)
H(44)	0.09(0)	0.00(0)	0.00(0)	0.00(0)	0.00(0)
H(45)	0.09(0)	0.00(0)	0.00(0)	0.00(0)	0.00(0)
H(46)	0.09(0)	0.00(0)	0.00(0)	0.00(0)	0.00(0)

atom	P_{30}	P_{31}	P_{3-1}	P_{32}	P_{3-2}	P_{33}	P_{3-3}
N(1)	0.09(4)	0.05(3)	0.01(3)	−0.13(3)	−0.05(2)	0.03(2)	0.01(2)
N(2)	0.16(4)	0.07(3)	−0.03(3)	−0.24(3)	−0.01(3)	−0.04(2)	0.02(2)
N(3)	0.20(4)	0.07(3)	−0.16(3)	−0.21(3)	−0.05(3)	−0.01(2)	−0.11(2)
N(4)	0.21(4)	0.06(3)	0.00(3)	−0.20(3)	−0.10(2)	0.04(2)	−0.01(2)
N(5)	0.19(4)	0.06(3)	0.07(3)	−0.17(3)	0.03(3)	−0.09(2)	0.04(2)
C(1)	0.21(7)	−0.06(6)	0.01(4)	−0.12(5)	−0.15(5)	0.02(4)	0.02(4)
C(2)	0.19(8)	0.20(7)	0.02(4)	−0.17(5)	−0.08(4)	−0.02(4)	0.02(3)
C(11)	0.00(4)	−0.24(3)	0.05(3)	0.02(3)	0.05(3)	0.07(2)	−0.04(2)
C(12)	0.01(3)	0.00(2)	0.00(2)	−0.01(3)	−0.02(3)	0.29(3)	0.02(3)
C(13)	0.08(3)	0.02(2)	−0.04(2)	0.02(3)	0.03(3)	0.35(3)	−0.03(4)
C(14)	0.00(4)	−0.17(4)	0.00(3)	0.00(3)	0.00(3)	0.07(2)	−0.02(2)
C(15)	0.05(3)	−0.03(3)	−0.05(2)	0.02(3)	−0.03(3)	0.29(3)	−0.04(4)
C(16)	0.03(3)	0.01(2)	−0.05(2)	−0.07(3)	0.02(3)	0.34(3)	0.05(3)
C(21)	0.06(4)	−0.25(3)	0.00(3)	−0.02(3)	−0.02(3)	0.04(2)	0.01(2)
C(22)	0.02(3)	0.01(3)	−0.02(3)	−0.03(3)	−0.01(3)	0.29(3)	0.09(4)
C(23)	0.09(3)	−0.01(3)	−0.02(3)	0.06(3)	−0.05(3)	0.20(4)	−0.12(4)
C(24)	0.00(4)	−0.01(3)	0.02(3)	−0.14(4)	−0.07(4)	0.07(5)	−0.22(4)
C(25)	−0.02(3)	0.06(3)	0.01(3)	0.10(3)	0.00(3)	0.21(4)	0.01(4)
C(26)	0.07(3)	0.00(3)	−0.01(3)	−0.04(3)	0.00(2)	0.29(3)	0.00(3)
C(31)	0.01(4)	−0.22(3)	−0.03(3)	0.03(3)	−0.03(3)	0.07(2)	0.00(2)
C(32)	0.00(3)	0.02(3)	0.04(3)	−0.04(3)	−0.04(3)	0.29(3)	0.07(3)
C(33)	0.04(3)	0.01(3)	0.01(3)	0.12(3)	0.01(4)	0.26(4)	−0.01(4)
C(34)	0.00(5)	−0.18(4)	0.01(4)	−0.01(4)	0.03(4)	0.08(2)	0.01(2)
C(35)	0.01(3)	0.05(3)	−0.08(3)	0.02(3)	−0.02(3)	0.28(4)	−0.06(4)
C(36)	0.00(3)	−0.02(3)	−0.01(2)	−0.04(3)	−0.03(3)	0.31(3)	0.06(3)
C(41)	−0.02(3)	−0.22(3)	0.06(3)	0.09(3)	0.07(3)	0.11(2)	−0.01(2)
C(42)	0.06(3)	−0.02(3)	0.02(2)	0.01(3)	0.01(3)	0.33(3)	0.05(3)
C(43)	0.00(3)	−0.01(3)	−0.05(3)	0.04(3)	−0.08(3)	0.30(3)	−0.07(4)
C(44)	0.08(4)	−0.18(4)	−0.03(4)	0.10(4)	−0.20(4)	0.12(3)	−0.04(3)
C(45)	−0.03(4)	−0.02(3)	−0.03(3)	0.06(3)	−0.06(3)	0.29(3)	−0.05(4)
C(46)	0.06(3)	−0.02(3)	0.03(2)	−0.01(3)	0.00(3)	0.29(3)	0.03(3)
B(1)	0.00(4)	0.00(4)	0.00(4)	0.04(4)	0.49(9)	−0.07(4)	−0.05(3)

Table 49. Results of the rigid body thermal motion analysis for the anion in biguanidinium tetraphenylborate.[a]

Rigid body variables fitted		20	
Translational tensor, **T** ($Å^2$)	0.0212(7)	-0.0006(5)	-0.0017(5)
		0.0230(7)	-0.0011(5)
			0.0211(6)
Principal values ($Å^2$)	0.0227	0.0235	0.0191
Square root (Å)	0.15	0.15	0.14
Librational tensor, **L** (deg^2)	3.5(3)	0.0(2)	0.4(2)
		2.9(3)	0.4(2)
			7.2(4)
Principal values (deg^2)	3.5	2.8	7.3
Square root (deg)	1.9	1.7	2.7
Cross tensor, **S** (Å-deg)	-0.009(14)	-0.026(6)	0.013(6)
	0.026(7)	0.006(14)	-0.003(7)
	0.072(7)	0.053(7)	0.004(0)
R_w[b]		0.0933	
Z[c]		0.00237	
Corrections to interatomic distances due to libration		0.0018 to 0.0024Å	
Esd's on the calculated interatomic distances		0.0013 to 0.0030Å	

[a] Tensor components are given with respect to the axes of the principal moments of inertia and with the origin at the center of mass.

[b] $R_w = (X^2 / \Sigma[U_{ij}/\sigma_{Uij}]^2)^{½}$ where $X^2 = \Sigma[\Delta U_{ij}/\sigma_{Uij}]^2)$

[c] $Z = (X^2 / NFREE)^{½}$ where NFREE = 130

Table 49. Results of the rigid body thermal motion analysis for the cation in biguanidinium tetraphenylborate.[a]

Rigid body variables fitted		20	
Translational tensor, **T** ($Å^2$)	0.0269(20)	0.0038(15)	-0.0012(11)
		0.0237(17)	0.0013(10)
			0.0295(11)
Principal values ($Å^2$)	0.0292	0.0208	0.0300
Square root (Å)	0.17	0.14	0.17
Librational tensor, **L** (deg^2)	9.4(19)	-1.6(15)	-3.7(23)
		8.7(21)	1.6(15)
			64.4(90)
Principal values (deg^2)	10.4	7.3	64.7
Square root (deg)	3.2	2.7	8.0
Cross tensor, **S** (Å-deg)	0.152(79)	-0.008(19)	-0.109(28)
	-0.070(20)	-0.003(92)	0.028(35)
	-0.040(57)	0.046(55)	-0.149(0)
R_w[b]		0.0723	
Z[c]		0.00274	
Corrections to interatomic distances due to libration		0.0059 to 0.0153Å	
Esd's on the calculated interatomic distances		0.0020 to 0.0030Å	

[a] Tensor components are given with respect to the axes of the principal moments of inertia and with the origin at the center of mass.

[b] $R_w = (X^2 / \Sigma[U_{ij}/\sigma_{Uij}]^2)^{½}$ where $X^2 = \Sigma[\Delta U_{ij}/\sigma_{Uij}]^2)$

[c] $Z = (X^2 / NFREE)^{½}$ where NFREE = 22

Table 49. Results of the rigid body thermal motion analysis for the cation in biguanidinium tetraphenylborate (continued).

Interatomic distances corrected for libration

Atoms		Librational Correction	Corrected Bond Length
N(1)	C(1)	0.0059(6)	1.3561
N(1)	C(2)	0.0069(7)	1.3323
N(2)	C(1)	0.0097(8)	1.3303
N(3)	C(1)	0.0140(15)	1.3503
N(4)	C(2)	0.0068(6)	1.3561
N(5)	C(2)	0.0153(15)	1.3625

Table 50. Short intermolecular cation...anion contacts for biguanidinium tetraphenylborate.

$C\text{-}H_{anion}\cdots N_{cation}$ contacts of less than 3Å			
N(4)...H(26)	symmetry	(-x, 1-y, -z)	2.912 Å
N(4)...H(42)	symmetry	(x, y, z)	2.867 Å

Table 51. Bond critical points for the short intermolecular cation...anion contacts in biguanidinium tetraphenylborate.

Contact	C-H...N (anion/cation)								
	Hessian Eigenvalues			Charge Density	Laplacian	Ellipticity	Position		
Bond Path	λ_1	λ_2	λ_3	$\rho_b(\mathbf{r})$ (eÅ^{-3})	$\nabla^2\rho_b(\mathbf{r})$ (eÅ^{-5})	ε	x	y (fractional)	z
C(26)-H(26)...N(4)	symmetry (-x, 1-y, -z)								
H(26)...N(4)	-0.10,	-0.05,	0.67	0.042(1)	0.520(1)	1.14	0.3182,	0.4361,	0.0774

Bond Lengths and Angles at the Critical Point

Atoms	Distance (Å)	Atoms	Angle (°)
Cp...N(4)	1.654	N(4)...Cp...C(26)	170.6
Cp...H(26)	1.331	N(4)...Cp...H(26)	154.6
Cp...C(26)	1.857	Cp...H(26)-C(26)	100.5
H(26)...N(4)	2.912	C(26)-H(26)...N(4)	114.6
C(26)...N(4)	3.499		

Table 51. Bond critical points for the short intermolecular cation...anion contacts in biguanidinium tetraphenylborate (continued).

Contact	C-H...N (anion/cation)								
	Hessian Eigenvalues			Charge Density	Laplacian	Ellipticity	Position		
Bond Path	λ_1	λ_2	λ_3	$\rho_b(\mathbf{r})$ (eÅ^{-3})	$\nabla^2\rho_b(\mathbf{r})$ (eÅ^{-5})	ε	x	y (fractional)	z
C(42)-H(42)...N(4) symmetry (x, y, z)									
H(42)...N(4)	-0.15,	-0.11,	0.94	0.055(1)	0.679(1)	0.28	-0.2277,	0.3962,	0.0419

Bond Lengths and Angles at the Critical Point

Atoms	Distance (Å)	Atoms	Angle (°)
Cp...N(4)	1.695	N(4)...Cp...C(42)	164.4
Cp...H(42)	1.223	N(4)...Cp...H(42)	158.2
Cp...C(42)	1.863	Cp...H(42)-C(42)	108.1
H(42)...N(4)	2.867	C(42)-H(42)...N(4)	119.6
C(42)...N(4)	3.525		

Table 52. Short intermolecular anion...anion contacts for biguanidinium tetraphenylborate.

Ring 1				
C(13)	- H(46)	2.640	symmetry	(-1/2+x, 1/2-y, -1/2+z)
C(14)	- H(36)	2.941	symmetry	(-1/2+x, 1/2-y, -1/2+z)
C(15)	- H(16)	2.863	symmetry	(-x, 1-y, -z)
C(16)	- H(16)	2.887	symmetry	(-x, 1-y, -z)
Ring 2				
C(22)	- H(14)	2.849	symmetry	(1/2+x, 1/2-y, 1/2+z)
C(23)	- H(14)	2.904	symmetry	(1/2+x, 1/2-y, 1/2+z)
C(25)	- H(13)	2.873	symmetry	(1/2+x, 1/2-y, 1/2+z)
C(26)	- H(13)	2.762	symmetry	(1/2+x, 1/2-y, 1/2+z)
C(26)	- H(35)	2.985	symmetry	(1/2-x, 1/2+y, 1/2-z)
Ring 3				
C(33)	- H(44)	2.899	symmetry	(-1/2-x, -1/2+y, 1/2-z)
C(34)	- H(44)	2.978	symmetry	(-1/2-x, -1/2+y, 1/2-z)
C(34)	- H(12)	2.866	symmetry	(-x, -y, -z)
C(35)	- H(13)	2.850	symmetry	(-x, -y, -z)
Ring 4				
C(41)	- H(15)	2.952	symmetry	(-x, 1-y, -z)
C(42)	- H(15)	2.927	symmetry	(-x, 1-y, -z)
C(43)	- H(15)	2.983	symmetry	(-x, 1-y, -z)
C(43)	- H(34)	2.977	symmetry	(-1/2-x, 1/2+y, 1/2-z)

Table 53. Bond critical points for the short intermolecular anion...anion contacts in biguanidinium tetraphenylborate.

	C-H...phenyl					(anion/anion)			
Contact	Hessian Eigenvalues			Charge Density	Laplacian	Ellipticity	Position		
Bond Path	λ_1	λ_2	λ_3	$\rho_b(\mathbf{r})$ (eÅ^{-3})	$\nabla^2\rho_b(\mathbf{r})$ (eÅ^{-5})	ε	x	y (fractional)	z
C(46)-H(46)...ring 1	symmetry (1/2+x, 1/2-y, 1/2+z)					H...H type contact			
H(46)...H(13)	-0.26,	-0.24,	1.20	0.078(1)	0.703(1)	0.10	0.3046,	0.3059,	0.2767

Bond Lengths and Angles at the Critical Point

Atoms	Distance (Å)	Atoms	Angle (°)
H(46)...H(13)	2.179	C(46)-H(46)...H(13)	165.8
C(46)...H(13)	3.233	C(46)-H(46)...C(13)	162.6
H(46)...C(13)	2.640		
Cp...H(46)	0.969	H(46)...Cp...H(13)	158.5
Cp...H(13)	1.248	C(46)-H(46)...Cp	169.3
Cp...C(46)	2.036		
Cp...C(13)	1.700		

Table 53. Bond critical points for the short intermolecular anion...anion contacts in biguanidinium tetraphenylborate (continued).

				C-H...phenyl		(anion/anion)			
Contact	Hessian Eigenvalues			Charge Density	Laplacian	Ellipticity	Position		
Bond Path	λ_1	λ_2	λ_3	$\rho_b(\mathbf{r})$ ($e\text{Å}^{-3}$)	$\nabla^2\rho_b(\mathbf{r})$ ($e\text{Å}^{-5}$)	ε	x	y (fractional)	z
C(36)-H(36)...ring 1 symmetry (1/2+x, 1/2-y, 1/2+z)						H...H type contact			
H(36)...H(14)	-0.13,	-0.11,	0.65	0.045(1)	0.406(1)	0.21	0.2794,	0.1254,	0.2442

Bond Lengths and Angles at the Critical Point

Atoms	Distance (Å)	Atoms	Angle (°)
H(36)...H(14)	2.446	C(36)-H(36)...H(14)	166.0
C(36)...H(14)	3.500	C(36)-H(36)...C(14)	173.4
H(36)...C(14)	2.941		
Cp...H(36)	1.116	H(36)...Cp...H(14)	157.9
Cp...H(14)	1.376	C(36)-H(36)...Cp	178.1
Cp...C(36)	2.191		
Cp...C(14)	1.844		

Table 53. Bond critical points for the short intermolecular anion...anion contacts in biguanidinium tetraphenylborate (continued).

Contact	Hessian Eigenvalues			Charge Density	Laplacian	Ellipticity	Position		
Bond Path	λ_1	λ_2	λ_3	$\rho_b(\mathbf{r})$ ($e\text{Å}^{-3}$)	$\nabla^2\rho_b(\mathbf{r})$ ($e\text{Å}^{-5}$)	ε	x	y (fractional)	z
C(16)-H(16)...ring 1	symmetry (-x, 1-y, -z)			H...H type contact					
H(16)...H(15)	-0.18,	-0.13,	0.89	0.056(1)	0.583(1)	0.37	0.0260,	0.4772,	0.0669

Bond Lengths and Angles at the Critical Point

Atoms	Distance (Å)	Atoms	Angle (°)
H(16)...H(15)'	2.205	C(16)-H(16)...H(15)'	175.5
C(16)...H(15)'	3.278	C(16)-H(16)...C(15)'	163.0
H(16)...C(15)'	2.863		
Cp...H(16)	1.053	H(16)...Cp...H(15)'	166.5
Cp...H(15)'	1.167	C(16)-H(16)...Cp	175.0
Cp...C(16)	2.127		
Cp...C(15)'	1.849		

Table 53. Bond critical points for the short intermolecular anion...anion contacts in biguanidinium tetraphenylborate (continued).

				C-H...phenyl			(anion/anion)		
Contact	Hessian Eigenvalues			Charge Density	Laplacian	Ellipticity	Position		
Bond Path	λ_1	λ_2	λ_3	$\rho_b(\mathbf{r})$ (eÅ^{-3})	$\nabla^2\rho_b(\mathbf{r})$ (eÅ^{-5})	ε	x	y (fractional)	z
C(16)-H(16)...ring 1 symmetry (-x, 1-y, -z) H...H type contact									
H(16)...H(16)	-0.17,	-0.11,	1.06	0.057(1)	0.782(1)	0.52	-0.0007,	0.5000,	-0.0001

Bond Lengths and Angles at the Critical Point

Atoms	Distance (Å)	Atoms	Angle (°)
H(16)...H(16)'	2.261	C(16)-H(16)...H(16)'	115.1
C(16)...H(16)'	2.887	C(16)-H(16)...C(16)'	134.8
Cp...H(16)	1.131	H(16)...Cp...H(16)'	179.3
Cp...H(16)'	1.131	C(16)-H(16)...Cp	115.0
Cp...C(16)	1.862		
Cp...C(16)'	1.862		

Table 53. Bond critical points for the short intermolecular anion...anion contacts in biguanidinium tetraphenylborate (continued).

Contact	C-H...phenyl (anion/anion)							
	Hessian Eigenvalues			Charge Density	Laplacian	Ellipticity	Position	
Bond Path	λ_1	λ_2	λ_3	$\rho_c(\mathbf{r})$ ($e\text{Å}^{-3}$)	$\nabla^2\rho_c(\mathbf{r})$ ($e\text{Å}^{-5}$)	ε	x	y z (fractional)
C(14)-H(14)...ring 2*	symmetry (-1/2+x, 1/2-y, -1/2+z)						centroid type hydrogen bond	
H(14)...C(22)-C(23)	-0.11,	-0.07,	0.63	0.049(1)	0.451(1)	0.52	-0.1192,	0.3540, -0.3163

Bond Lengths and Angles at the Critical Point

Atoms	Distance (Å)	Atoms	Angle (°)
H(14)...C(22)	2.849	C(14)-H(14)...C(22)	154.5
C(14)...C(22)	3.849	C(14)-H(14)...C(23)	156.4
H(14)...C(23)	2.904		
C(14)...C(23)	3.914		
Cp...H(14)	1.111	H(14)...Cp...C(22)	165.8
Cp...C(14)	2.142	H(14)...Cp...C(23)	149.0
Cp...C(22)	1.759	C(14)-H(14)...Cp	156.6
Cp...C(23)	1.894		

* The bond path from H(14) follows the C(22)-C(23) bond of the ring for approximately one quarter of its length before terminating at C(22).

Table 53. Bond critical points for the short intermolecular anion...anion contacts in biguanidinium tetraphenylborate (continued).

Contact	C-H...phenyl (anion/anion)								
	Hessian Eigenvalues			Charge Density	Laplacian	Ellipticity	Position		
Bond Path	λ_1	λ_2	λ_3	$\rho_b(\mathbf{r})$ (eÅ^{-3})	$\nabla^2\rho_b(\mathbf{r})$ (eÅ^{-5})	ε	x	y (fractional)	z
C(13)-H(13)...ring 2*	symmetry (-1/2+x, 1/2-y, -1/2+z)					edge type hydrogen bond			
H(13)...C(25)-C(26)	-0.12,	-0.08,	0.81	0.057(1)	0.608(1)	0.58	-0.0981,	0.1935,	-0.2809

Bond Lengths and Angles at the Critical Point

Atoms	Distance (Å)	Atoms	Angle (°)
H(13)...C(26)	2.762	C(13)-H(13)...C(26)	137.3
C(13)...C(26)	3.627	C(13)-H(13)...C(25)	135.2
H(13)...C(25)	2.873		
C(13)...C(25)	3.714		
Cp...H(13)	1.102	H(13)...Cp...C(26)	163.1
Cp...C(13)	2.019	H(13)...Cp...C(25)	150.2
Cp...C(26)	1.689	C(13)-H(13)...Cp	135.9
Cp...C(25)	1.864		

* The bond path from H(13) follows the C(25)-C(26) bond of the ring for approximately one quarter of its length before terminating at C(26).

Table 53. Bond critical points for the short intermolecular anion...anion contacts in biguanidinium tetraphenylborate (continued).

Contact	Hessian Eigenvalues			Charge Density	Laplacian	Ellipticity	Position		
Bond Path	λ_1	λ_2	λ_3	$\rho_b(\mathbf{r})$ ($eÅ^{-3}$)	$\nabla^2\rho_b(\mathbf{r})$ ($eÅ^{-5}$)	ε	x	y (fractional)	z
C(35)-H(35)...ring 2 symmetry (1/2-x, -1/2+y, 1/2-z) H...H type contact									
H(35)...H(26)	-0.13,	-0.09,	0.64	0.043(1)	0.423(1)	0.42	0.1280,	-0.0866,	0.3072

Bond Lengths and Angles at the Critical Point

Atoms	Distance (Å)	Atoms	Angle (°)
H(35)...H(26)	2.391	C(35)-H(35)...H(26)	173.7
C(35)...H(26)	3.463	C(35)-H(35)...C(26)	165.3
H(35)...C(26)	2.985		
Cp...H(35)	1.119	H(35)...Cp...H(26)	157.5
Cp...H(26)	1.319	C(35)-H(35)...Cp	171.9
Cp...C(35)	2.190		
Cp...C(26)	1.880		

Table 53. Bond critical points for the short intermolecular anion...anion contacts in biguanidinium tetraphenylborate (continued).

Contact	C-H...phenyl (anion/anion)								
	Hessian Eigenvalues			Charge Density	Laplacian	Ellipticity	Position		
Bond Path	λ_1	λ_2	λ_3	$\rho_b(\mathbf{r})$ (eÅ^{-3})	$\nabla^2\rho_b(\mathbf{r})$ (eÅ^{-5})	ε	x	y (fractional)	z
C(44)-H(44)...ring 3[a,b]	symmetry (-1/2-x, 1/2+y, 1/2-z)					H...H type contact			
H(44)...C(33)-H(33)	-0.12,	-0.07,	0.66	0.045(1)	0.479(1)	0.71	-0.1802,	0.5016,	0.3505

Bond Lengths and Angles at the Critical Point

Atoms	Distance (Å)	Atoms	Angle (°)
H(44)...H(33)	2.454	C(44)-H(44)...H(33)	149.5
C(44)...H(33)	3.425	C(44)-H(44)...C(33)	147.4
H(44)...C(33)	2.899		
C(44)...C(33)	3.849		
Cp...H(44)	1.118	H(44)...Cp...H(33)	147.0
Cp...C(33)	1.784	H(44)...Cp...C(33)	174.8
Cp...H(33)	1.439	C(44)-H(44)...Cp	146.7
Cp...C(44)	2.102		

[a] The bond path is from H(44) to the approximate midpoint of the C(33)-H(33) bond in the ring and terminates at H(33).

[b] This bond path joins the same two rings as the C(34)-H(34)...ring 4 bond path (below).

Table 53. Bond critical points for the short intermolecular anion...anion contacts in biguanidinium tetraphenylborate (continued).

	C-H...phenyl (anion/anion)								
Contact	Hessian Eigenvalues			Charge Density	Laplacian	Ellipticity	Position		
Bond Path	λ_1	λ_2	λ_3	$\rho_b(\mathbf{r})$ (eÅ^{-3})	$\nabla^2\rho_b(\mathbf{r})$ (eÅ^{-5})	ε	x	y (fractional)	z
C(12)-H(12)...ring 3 symmetry (-x, -y, -z) single atom type hydrogen bond									
H(12)...C(34)	-0.09,	-0.07,	0.71	0.048(4)	0.553(1)	0.35	0.0427,	0.0989,	-0.1118

Bond Lengths and Angles at the Critical Point

Atoms	Distance (Å)	Atoms	Angle (°)
H(12)...C(34)	2.865	C(12)-H(12)...C(34)	119.6
C(12)...C(34)	3.524		
Cp...H(12)	1.216	H(12)...Cp...C(34)	167.2
Cp...C(12)	1.904	C(12)...Cp...C(34)	161.3
Cp...C(34)	1.667	C(12)-H(12)...Cp	112.2

Table 53. Bond critical points for the short intermolecular anion...anion contacts in biguanidinium tetraphenylborate (continued).

Contact	Hessian Eigenvalues			Charge Density	Laplacian	Ellipticity	Position		
Bond Path	λ_1	λ_2	λ_3	$\rho_b(\mathbf{r})$ ($eÅ^{-3}$)	$\nabla^2\rho_b(\mathbf{r})$ ($eÅ^{-5}$)	ε	x	y (fractional)	z
C(13)-H(13)...ring 3 symmetry (-x, -y, -z) H...H type contact									
H(13)...H(35)	-0.15,	-0.11,	0.88	0.053(1)	0.626(1)	0.44	-0.0560,	0.1164,	-0.2150

C-H...phenyl (anion/anion)

Bond Lengths and Angles at the Critical Point

Atoms	Distance (Å)	Atoms	Angle (°)
H(13)...H(35)	2.347	C(13)-H(13)...H(35)	151.1
C(13)...H(35)	3.330	C(13)-H(13)...C(35)	130.6
H(13)...C(35)	2.850		
Cp...H(13)	1.086	H(13)...Cp...H(35)	151.7
Cp...H(35)	1.333	C(13)-H(13)...Cp	135.9
Cp...C(13)	2.005		
Cp...C(35)	1.772		

Table 53. Bond critical points for the short intermolecular anion...anion contacts in biguanidinium tetraphenylborate (continued).

Contact	C-H...phenyl					(anion/anion)			
	Hessian Eigenvalues			Charge Density	Laplacian	Ellipticity	Position		
Bond Path	λ_1	λ_2	λ_3	$\rho_c(\mathbf{r})$ (eÅ^{-3})	$\nabla^2\rho_c(\mathbf{r})$ (eÅ^{-5})	ε	x	y (fractional)	z
C(15)-H(15)...ring 4*	symmetry (-x, 1-y, -z)				centroid type hydrogen bond				
H(15)...C(41)-C(42)	-0.08,	-0.05,	0.55	0.050(1)	0.412(1)	0.54	-0.0251,	0.5542,	-0.1444

Bond Lengths and Angles at the Critical Point

Atoms	Distance (Å)	Atoms	Angle (°)
H(15)...C(41)	2.952	C(15)-H(15)...C(41)	174.3
C(15)...C(41)	4.024	C(15)-H(15)...C(42)	147.0
H(15)...C(42)	2.927		
C(15)...C(42)	3.874		
Cp...H(15)	1.126	H(15)...Cp...C(41)	169.8
Cp...C(15)	2.193	H(15)...Cp...C(42)	143.0
Cp...C(41)	1.838	C(15)-H(15)...Cp	170.0
Cp....C(42)	1.949		

* The bond path from H(15) follows the C(41)-C(42) bond of the ring for approximately one quarter of its length before terminating at C(41).

Table 53. Bond critical points for the short intermolecular anion...anion contacts in biguanidinium tetraphenylborate (continued).

Contact	Hessian Eigenvalues			C-H...phenyl (anion/anion) Charge Density	Laplacian	Ellipticity	Position		
Bond Path	λ_1	λ_2	λ_3	$\rho_b(\mathbf{r})$ (eÅ^{-3})	$\nabla^2\rho_b(\mathbf{r})$ (eÅ^{-5})	ε	x	y (fractional)	z
C(34)-H(34)...ring 4* symmetry (-1/2-x, -1/2+y, 1/2-z) H...H type contact									
H(34)...H(43)	-0.10,	-0.07,	0.70	0.040(1)	0.533(1)	0.46	-0.2152,	-0.0698,	0.2431

Bond Lengths and Angles at the Critical Point

Atoms	Distance (Å)	Atoms	Angle (°)
H(34)...H(43)	2.508	C(34)-H(34)...H(43)	115.1
C(34)...H(43)	3.121	C(34)-H(34)...C(43)	126.5
H(34)...C(43)	2.977		
Cp...H(34)	1.230	H(34)...Cp...H(43)	162.5
Cp...H(43)	1.307	C(34)-H(34)...Cp	114.3
Cp...C(34)	1.940		
Cp...C(43)	1.815		

* This bond path joins the same two rings as the C(44)-H(44)...ring 3 bond path (above).

Table 54a. Summary of the bond critical points located for N-H...X [X = N or π(Ph)] hydrogen bonds in the four tetraphenylborate compounds studied.

	Compound and Contact[a]	Type of Interaction[b]	Bond Path[c,d]	Contact Distance (Å)	Charge Density[e] $\rho_b(\mathbf{r})$ ($eÅ^{-3}$)	Laplacian $\nabla^2\rho_b(\mathbf{r})$ ($eÅ^{-5}$)
G	N(1)-H(1B)...N(4) N-H...N hydrogen bond	c/s	H(1B)...N(4)	2.082	0.200(54)	1.637(4)
B	N(4)-H(4A)...N(1) N-H...N hydrogen bond	c/c	H(4A)...N(1)	2.127	0.141(2)	1.519(3)
B	N(2)-H(2A)...ring 2 N-H...π(Ph) centroid type hydrogen bond	c/a	H(2A)...C(26)	2.392	0.104(14)	0.918(19)
G	N(3)-H(3B)...ring 3 N-H...π(Ph) centroid type hydrogen bond	c/a	H(3B)...C(32)	2.498	0.102(29)	0.885(11)
N	N(1)-H(1)...ring 1 N-H...π(Ph) centroid type hydrogen bond - unusual bond path	c/a	N(1)...C(11)	3.268	0.099(7)	0.872(1)
B	N(3)-H(3A)...ring 3 N-H...π(Ph) centroid type hydrogen bond	c/a	H(3A)...C(35)-C(36)	2.430	0.097(2)	0.857(1)
G	N(2)-H(2B)...ring 3 N-H...π(Ph) hydrogen bond - edge type by geometry and single atom type by bond path	c/a	H(2B)...C(35)	2.622	0.087(23)	0.677(12)
D	N(1)-H(1)...ring 1 N-H...π(Ph) centroid type hydrogen bond	c/a	H(1)...C(14)	2.640	0.086(5)	0.823(3)

Table 54a. Summary of the bond critical points located for N-H...X [X = N or π(Ph)] hydrogen bonds in the four tetraphenylborate compounds studied (continued).

	Compound and Contact[a]	Type of Interaction[b]	Bond Path[c,d]	Contact Distance (Å)	Charge Density[e] $\rho_b(\mathbf{r})$ ($eÅ^{-3}$)	Laplacian $\nabla^2\rho_b(\mathbf{r})$ ($eÅ^{-5}$)
G	N(3)-H(3A)...ring 4	c/a	H(3A)...C(43)-C(44)	2.668	0.081(28)	0.638(14)
	N-H...π(Ph) centroid type hydrogen bond					
B	N(2)-H(2B)...ring 1	c/a	H(2B)...C(13)	2.490	0.081(2)	0.883(1)
	N-H...π(Ph) single atom type hydrogen bond					
G	N(1)-H(1A)...ring 2	c/a	H(1A)...C(22)-C(23)	2.458	0.073(34)	0.706(11)
	N-H...π(Ph) centroid type hydrogen bond					
B	N(5)-H(5B)...ring 1	c/a	H(5B)...C(15)-C(16)	2.560	0.071(1)	0.654(1)
	N-H...π(Ph) centroid type hydrogen bond					
B	N(5)-H(5A)...ring 4	c/a	H(5A)...C(45)-C(46)	2.664	0.059(1)	0.614(1)
	N-H...π(Ph) edge type hydrogen bond					
B	N(4)-H(4B)...ring 1	c/a	H(4B)...C(16)-H(16)	2.661	0.055(1)	0.477(1)
	N-H...phenyl interaction - intermediate type contact					
G	N(2)-H(2A)...ring 2	c/a	H(2A)...C(25)-C(26)	2.672	0.055(20)	0.474(12)
	N-H...π(Ph) edge type hydrogen bond					
B	N(3)-H(3B)...ring 4	c/a	N(3)...C(42)	3.498	0.049(1)	0.544(1)
	N-H...π(Ph) edge type hydrogen bond - unusual bond path					

[a] N - ammonium tetraphenylborate B - biguanidinium tetraphenylborate
D - [DabcoH][$B(C_6H_5)_4$] G - guanidinium tetraphenylborate acetonitrile solvate

[b] a - anion c - cation s - solvent

[c] If the bond path is directed towards a bond it is shown; the underlined atom is where the bond path terminates.

[d] The distance quoted is the calculated direct separation between the two atoms joined by the bond path.

[e] The data are sorted in order of decreasing charge density at the bond critical point.

Table 54b(i). Summary of the bond critical points located for N-H...N hydrogen bonds in the four tetraphenylborate compounds studied.

	Compound and Contact[a]	Type of Interaction[b]	Bond Path[c,d]	Contact Distance (Å)	Charge Density[e] $\rho_b(\mathbf{r})$ ($eÅ^{-3}$)	Laplacian $\nabla^2\rho_b(\mathbf{r})$ ($eÅ^{-5}$)
G	N(1)-H(1B)...N(4)	c/s	H(1B)...N(4)	2.082	0.200(54)	1.637(4)
B	N(4)-H(4A)...N(1)	c/c	H(4A)...N(1)	2.127	0.141(2)	1.519(3)
Mean	(n = 2)			2.104	0.170	1.578
σ[f]				0.022	0.030	0.059

[a] B - biguanidinium tetraphenylborate
G - guanidinium tetraphenylborate acetonitrile solvate

[b] c - cation s - solvent

[c] If the bond path is directed towards a bond it is shown; the underlined atom is where the bond path terminates.

[d] The distance quoted is the calculated direct separation between the two atoms joined by the bond path.

[e] The data are sorted in order of decreasing charge density at the bond critical point.

[f] σ is the standard deviation of the population, $\sigma = [(\Sigma x_i^2 - n(\Sigma x_i)^2) / n]^{\frac{1}{2}}$.

Table 54b(ii). Summary of the bond critical points located for N-H...π(Ph) hydrogen bonds in the four tetraphenylborate compounds studied.

	Compound and Contact[a]	Type of Interaction[b]	Bond Path[c,d]	Contact Distance (Å)	Charge Density[e] $\rho_b(\mathbf{r})$ ($eÅ^{-3}$)	Laplacian $\nabla^2\rho_b(\mathbf{r})$ ($eÅ^{-5}$)
B	N(2)-H(2A)...ring 2	c/a	H(2A)...C(26)	2.392	0.104(14)	0.918(19)
	N-H...π(Ph) centroid type hydrogen bond					
G	N(3)-H(3B)...ring 3	c/a	H(3B)...C(32)	2.498	0.102(29)	0.885(11)
	N-H...π(Ph) centroid type hydrogen bond					
N	N(1)-H(1)...ring 1	c/a	N(1)...C(11)	3.268	0.099(7)	0.872(1)
	N-H...π(Ph) centroid type hydrogen bond - unusual bond path					
B	N(3)-H(3A)...ring 3	c/a	H(3A)...C(35)-C(36)	2.430	0.097(2)	0.857(1)
	N-H...π(Ph) centroid type hydrogen bond					
G	N(2)-H(2B)...ring 3	c/a	H(2B)...C(35)	2.622	0.087(23)	0.677(12)
	N-H...π(Ph) hydrogen bond - edge type by geometry and single atom type by bond path					
D	N(1)-H(1)...ring 1	c/a	H(1)...C(14)	2.640	0.086(5)	0.823(3)
	N-H...π(Ph) centroid type hydrogen bond					
G	N(3)-H(3A)...ring 4	c/a	H(3A)...C(43)-C(44)	2.668	0.081(28)	0.638(14)
	N-H...π(Ph) centroid type hydrogen bond					
B	N(2)-H(2B)...ring 1	c/a	H(2B)...C(13)	2.490	0.081(2)	0.883(1)
	N-H...π(Ph) single atom type hydrogen bond					

Table 54b(ii). Summary of the bond critical points located for N-H...π(Ph) hydrogen bonds in the four tetraphenylborate compounds studied (continued).

	Compound and Contact[a]	Type of Interaction[b]	Bond Path[c,d]	Contact Distance (Å)	Charge Density[e] $\rho_b(\mathbf{r})$ (eÅ^{-3})	Laplacian $\nabla^2\rho_b(\mathbf{r})$ (eÅ^{-5})
G	N(1)-H(1A)...ring 2	c/a	H(1A)...C(22)-C(23)	2.458	0.073(34)	0.706(11)
	N-H...π(Ph) centroid type hydrogen bond					
B	N(5)-H(5B)...ring 1	c/a	H(5B)...C(15)-C(16)	2.560	0.071(1)	0.654(1)
	N-H...π(Ph) centroid type hydrogen bond					
B	N(5)-H(5A)...ring 4	c/a	H(5A)...C(45)-C(46)	2.664	0.059(1)	0.614(1)
	N-H...π(Ph) edge type hydrogen bond					
B	N(4)-H(4B)...ring 1	c/a	H(4B)...C(16)-H(16)	2.661	0.055(1)	0.477(1)
	N-H...phenyl interaction - intermediate type contact					
G	N(2)-H(2A)...ring 2	c/a	H(2A)...C(25)-C(26)	2.672	0.055(20)	0.474(12)
	N-H...π(Ph) edge type hydrogen bond					
B	N(3)-H(3B)...ring 4	c/a	N(3)...C(42)	3.498	0.049(1)	0.544(1)
	N-H...π(Ph) edge type hydrogen bond - unusual bond path					
Mean	(n = 12)[f]			2.563	0.079	0.717
σ[g]				0.010	0.016	0.149

[a] N - ammonium tetraphenylborate
D - [DabcoH][$B(C_6H_5)_4$]
G - guanidinium tetraphenylborate acetonitrile solvate
B - biguanidinium tetraphenylborate

[b] a - anion
c - cation
s - solvent

[c] If the bond path is directed towards a bond it is shown; the underlined atom is where the bond path terminates.

[d] The distance quoted is the calculated direct separation between the two atoms joined by the bond path.

[e] The data are sorted in order of decreasing charge density at the bond critical point.

[f] Two interactions were deleted because of their unusual bond paths, beginning from the N atom and not the H atom.

[g] σ is the standard deviation of the population, $\sigma = [(\Sigma x_i^2 - n(\Sigma x_i)^2) / n]^{1/2}$.

Table 5.4c. Summary of the bond critical points located for C-H...X [X = N or phenyl] interactions in the four tetraphenylborate compounds studied.

	Compound and Contact[a]	Type of Interaction[b]	Bond Path[c,d]	Contact Distance (Å)	Charge Density[e] $\rho_b(\mathbf{r})$ ($eÅ^{-3}$)	Laplacian $\nabla^2\rho_b(\mathbf{r})$ ($eÅ^{-5}$)
B	C(46)-H(46)...ring 1 C-H...phenyl interaction - H...H type contact	a/a	H(46)...H(13)	2.179	0.078(1)	0.703(1)
G	C(44)-H(44)...N(4) C-H...N interaction	a/s	H(44)...N(4)	2.805	0.066(3)	0.633(2)
D	C(35)-H(35)...ring 2 C-H...phenyl interaction - H...H type contact	a/a	H(35)...C(22)-H(22)	2.354	0.065(0)	0.441(0)
G	C(46)-H(46)...N(2) C-H...N interaction	a/c	H(46)...N(2)	2.775	0.062(1)	0.527(1)
G	C(3)-H(61)...ring 1 C-H...π(Ph) centroid type hydrogen bond	s/a	H(61)...C(13)-C(14)	2.847	0.062(2)	0.498(1)
G	C(43)-H(43)...N(2) C-H...N interaction	a/c	H(43)...N(2)	2.797	0.061(1)	0.522(1)
G	C(14)-H(14)...ring 1 C-H...phenyl interaction - H...H type contact	a/a	H(14)...H(15)	2.357	0.061(2)	0.504(1)
G	C(13)-H(13)...ring 1 C-H...phenyl interaction - H...H type contact	a/a	H(13)...H(12)	2.454	0.058(1)	0.467(1)

Table 5c. Summary of the bond critical points located for C-H...X [X = N or phenyl] interactions in the four tetraphenylborate compounds studied (continued).

	Compound and Contact[a]	Type of Interaction[b]	Bond Path[c,d]	Contact Distance (Å)	Charge Density[e] $\rho_b(\mathbf{r})$ ($eÅ^{-3}$)	Laplacian $\nabla^2\rho_b(\mathbf{r})$ ($eÅ^{-5}$)
B	C(16)-H(16)...ring 1 C-H...phenyl interaction - H...H type contact	a/a	H(16)...H(16)	2.261	0.057(1)	0.782(1)
B	C(13)-H(13)...ring 2 C-H...π(Ph) edge type hydrogen bond	a/a	H(13)...C(25)-C(26)	2.762	0.057(1)	0.608(1)
B	C(16)-H(16)...ring 1 C-H...phenyl interaction - H...H type contact	a/a	H(16)...H(15)	2.205	0.056(1)	0.583(1)
D	C(3)-H(3A)...ring 3 C-H...phenyl interaction - H...H type contact	c/a	H(3A)...H(36)	2.262	0.056(0)	0.413(1)
B	C(42)-H(42)...N(4) C-H...N interaction	a/c	H(42)...N(4)	2.867	0.055(1)	0.679(1)
B	C(13)-H(13)...ring 3 C-H...phenyl interaction - H...H type contact	a/a	H(13)...H(35)	2.347	0.053(1)	0.626(1)
D	C(2)-H(2A)...ring 3 C-H...phenyl interaction - intermediate type contact	c/a	H(2A)...C(34)-H(34)	2.819	0.053(1)	0.379(1)
G	C(33)-H(33)...N(4) C-H...N interaction	a/s	H(33)...N(4)	2.561	0.052(2)	0.588(1)

Table 54c. Summary of the bond critical points located for C-H...X [X = N or phenyl] interactions in the four tetraphenylborate compounds studied (continued).

	Compound and Contact[a]	Type of Interaction[b]	Bond Path[c,d]	Contact Distance (Å)	Charge Density[e] $\rho_b(\mathbf{r})$ ($eÅ^{-3}$)	Laplacian $\nabla^2\rho_b(\mathbf{r})$ ($eÅ^{-5}$)
D	C(23)-H(23)...ring 3	a/a	H(23)...C(33)-H(33)	2.901	0.052(0)	0.472(0)
	C-H...phenyl interaction - intermediate type contact					
G	C(23)-H(23)...ring 1	a/a	H(23)...H(12)	2.337	0.051(1)	0.442(1)
	C-H...phenyl interaction - H...H type contact					
D	C(4)-H(4A)...ring 3	c/a	H(4A)...C(32)-C(33)	2.854	0.051(1)	0.253(1)
	C-H...π(Ph) edge type hydrogen bond					
D	C(32)-H(32)...N(2)	a/c	H(32)...N(2)	2.743	0.051(0)	0.456(1)
	C-H...N interaction					
G	C(45)-H(45)...N(4)	a/s	H(45)...N(4)	2.947	0.050(2)	0.544(1)
	C-H...N interaction					
B	C(15)-H(15)...ring 4	a/a	H(15)...C(41)-C(42)	2.952	0.050(1)	0.412(1)
	C-H...π(Ph) centroid type hydrogen bond					
D	C(1)-H(1A)...ring 3	c/a	H(1A)...C(34)-C(35)	2.874	0.050(7)	0.346(2)
	C-H...π(Ph) edge type hydrogen bond					
D	C(1)-H(1A)...ring 2	c/a	H(1A)...C(22)-C(23)	2.874	0.049(4)	0.467(2)
	C-H...π(Ph) edge type hydrogen bond					

Table 54c. Summary of the bond critical points located for C-H...X [X = N or phenyl] interactions in the four tetraphenylborate compounds studied (continued).

	Compound and Contact[a]	Type of Interaction[b]	Bond Path[c,d]	Contact Distance (Å)	Charge Density[e] $\rho_b(\mathbf{r})$ ($eÅ^{-3}$)	Laplacian $\nabla^2\rho_b(\mathbf{r})$ ($eÅ^{-5}$)
B	C(14)-H(14)...ring 2	a/a	H(14)...C(22)-C(23)	2.849	0.049(1)	0.451(1)
	C-H...π(Ph) centroid type hydrogen bond					
G	C(16)-H(16)...ring 3	a/a	H(16)...H(35)	2.464	0.049(1)	0.439(1)
	C-H...phenyl interaction - H...H type contact					
B	C(12)-H(12)...ring 3	a/a	H(12)...C(34)	2.865	0.048(4)	0.553(1)
	C-H...π(Ph) single atom type hydrogen bond					
G	C(3)...ring 2	s/a	C(3)...C(22)-C(23)	3.752	0.047(1)	0.402(1)
D	C(4)-H(4B)...ring 2	c/a	H(4B)...C(22)-C(23)	2.921	0.047(1)	0.248(1)
	C-H...π(Ph) edge type hydrogen bond					
G	C(34)-H(34)...ring 4	a/a	H(34)...C(42)-H(42)	2.574	0.046(1)	0.405(1)
	C-H...phenyl interaction - H...H type contact					
N	C(12)-H(12)...ring 1	a/a	H(12)...C(14)-H(14)	2.873	0.046(9)	0.495(6)
	C-H...phenyl interaction - intermediate type contact					
B	C(44)-H(44)...ring 3	a/a	H(44)...C(33)-H(33)	2.454	0.045(1)	0.479(1)
	C-H...phenyl interaction - H...H type contact					

Table 5c. Summary of the bond critical points located for C-H...X [X = N or phenyl] interactions in the four tetraphenylborate compounds studied (continued).

	Compound and Contact[a]	Type of Interaction[b]	Bond Path[c,d]	Contact Distance (Å)	Charge Density[e] $\rho_b(\mathbf{r})$ ($eÅ^{-3}$)	Laplacian $\nabla^2\rho_b(\mathbf{r})$ ($eÅ^{-5}$)
B	C(36)-H(36)...ring 1	a/a	H(36)...H(14)	2.446	0.045(1)	0.406(1)
	C-H...phenyl interaction - H...H type contact					
D	C(3)-H(3B)...ring 3	c/a	H(3B)...C(35)-C(36)	2.975	0.045(1)	0.240(1)
	C-H...π(Ph) edge type hydrogen bond					
N	C(14)-H(14)...ring 1	a/a	H(14)...C(11)	2.841	0.044(8)	0.514(4)
	C-H...π(Ph) centroid type hydrogen bond					
G	C(3)...ring 1	s/a	C(3)...C(15)-C(16)	3.721	0.044(4)	0.449(3)
G	C(3)-H(60)...ring 1	s/a	H(60)...C(16)-H(16)	2.799	0.043(7)	0.441(6)
	C-H...phenyl interaction - intermediate type contact					
B	C(35)-H(35)...ring 2	a/a	H(35)...H(26)	2.391	0.043(1)	0.423(1)
	C-H...phenyl interaction - H...H type contact					
B	C(26)-H(26)...N(4)	a/c	H(26)...N(4)	2.912	0.042(1)	0.520(1)
	C-H...N interaction					
G	C(24)-H(24)...ring 1	a/a	H(24)...C(14)	2.863	0.042(1)	0.371(1)
	C-H...π(Ph) single atom type hydrogen bond					

Table 54c. Summary of the bond critical points located for C-H...X [X = N or phenyl] interactions in the four tetraphenylborate compounds studied (continued).

	Compound and Contact[a]	Type of Interaction[b]	Bond Path[c,d]	Contact Distance (Å)	Charge Density[e] $\rho_b(\mathbf{r})$ ($eÅ^{-3}$)	Laplacian $\nabla^2\rho_b(\mathbf{r})$ ($eÅ^{-5}$)
B	C(34)-H(34)...ring 4	a/a	H(34)...H(43)	2.508	0.040(1)	0.533(1)
	C-H...phenyl interaction - H...H type contact					
G	C(36)-H(36)...N(4)	a/s	H(36)...N(4)	2.963	0.035(1)	0.384(1)
	C-H...N type interaction					
D	C(2)-H(2A)...ring 1	c/a	H(2A)...C(13)	3.044	0.035(1)	0.322(1)
	C-H...π(Ph) single atom type hydrogen bond					
G	C(3)...ring 2	s/a	C(3)...C(26)	3.918	0.031(2)	0.284(2)

[a] N - ammonium tetraphenylborate; B - biguanidinium tetraphenylborate; D - [DabcoH][$B(C_6H_5)_4$]; G - guanidinium tetraphenylborate acetonitrile solvate

[b] a - anion; c - cation; s - solvent

[c] If the bond path is directed towards a bond it is shown; the underlined atom is where the bond path terminates.

[d] The distance quoted is the calculated direct separation between the two atoms joined by the bond path.

[e] The data are sorted in order of decreasing charge density at the bond critical point.

Table 54d(i). Summary of the bond critical points located for C-H...N interactions in the four tetraphenylborate compounds studied.

	Compound and Contact[a]	Type of Interaction[b]	Bond Path[c,d]	Contact Distance (Å)	Charge Density[e] $\rho_b(\mathbf{r})$ (eÅ^{-3})	Laplacian $\nabla^2\rho_b(\mathbf{r})$ (eÅ^{-5})
G	C(44)-H(44)...N(4)	a/s	H(44)...N(4)	2.805	0.066(3)	0.633(2)
G	C(46)-H(46)...N(2)	a/c	H(46)...N(2)	2.775	0.062(1)	0.527(1)
G	C(43)-H(43)...N(2)	a/c	H(43)...N(2)	2.797	0.061(1)	0.522(1)
B	C(42)-H(42)...N(4)	a/c	H(42)...N(4)	2.867	0.055(1)	0.679(1)
G	C(33)-H(33)...N(4)	a/s	H(33)...N(4)	2.561	0.052(2)	0.588(1)
D	C(32)-H(32)...N(2)	a/c	H(32)...N(2)	2.743	0.051(0)	0.456(1)
G	C(45)-H(45)...N(4)	a/s	H(45)...N(4)	2.947	0.050(2)	0.544(1)
B	C(26)-H(26)...N(4)	a/c	H(26)...N(4)	2.912	0.042(1)	0.520(1)
G	C(36)-H(36)...N(4)	a/s	H(36)...N(4)	2.963	0.035(1)	0.384(1)
Mean (n = 9)				2.819	0.053	0.539
σ'				0.117	0.009	0.083

[a] B - biguanidinium tetraphenylborate D - [DabcoH][$B(C_6H_5)_4$]
G - guanidinium tetraphenylborate acetonitrile solvate

[b] a - anion c - cation s - solvent

[c] If the bond path is directed towards a bond it is shown; the underlined atom is where the bond path terminates.

[d] The distance quoted is the calculated direct separation between the two atoms joined by the bond path.

[e] The data are sorted in order of decreasing charge density at the bond critical point.

[f] σ is the standard deviation of the population, $\sigma = [(\Sigma x_i^2 - n(\Sigma x_i)^2) / n]^{1/2}$.

Table 54d(ii). Summary of the bond critical points located for C-H...phenyl interactions in the four tetraphenylborate compounds studied.

	Compound and Contact[a]	Type of Interaction[b]	Bond Path[c,d]	Contact Distance (Å)	Charge Density[e] $\rho_b(\mathbf{r})$ ($eÅ^{-3}$)	Laplacian $\nabla^2\rho_b(\mathbf{r})$ ($eÅ^{-5}$)
B	C(46)-H(46)...ring 1 C-H...phenyl interaction - H...H type contact	a/a	H(46)...H(13)	2.179	0.078(1)	0.703(1)
D	C(35)-H(35)...ring 2 C-H...phenyl interaction - H...H type contact	a/a	H(35)...C(22)-H(22)	2.354	0.065(0)	0.441(0)
G	C(3)-H(61)...ring 1 C-H...π(Ph) centroid type hydrogen bond	s/a	H(61)...C(13)-C(14)	2.847	0.062(2)	0.498(1)
G	C(14)-H(14)...ring 1 C-H...phenyl interaction - H...H type contact	a/a	H(14)...H(15)	2.357	0.061(2)	0.504(1)
G	C(13)-H(13)...ring 1 C-H...phenyl interaction - H...H type contact	a/a	H(13)...H(12)	2.454	0.058(1)	0.467(1)
B	C(16)-H(16)...ring 1 C-H...phenyl interaction - H...H type contact	a/a	H(16)...H(16)	2.261	0.057(1)	0.782(1)
B	C(13)-H(13)...ring 2 C-H...π(Ph) edge type hydrogen bond	a/a	H(13)...C(25)-C(26)	2.762	0.057(1)	0.608(1)
B	C(16)-H(16)...ring 1 C-H...phenyl interaction - H...H type contact	a/a	H(16)...H(15)	2.205	0.056(1)	0.583(1)

Table 54d(ii). Summary of the bond critical points located for C-H...phenyl interactions in the four tetraphenylborate compounds studied (continued).

	Compound and Contact[a]	Type of Interaction[b]	Bond Path[c,d]	Contact Distance (Å)	Charge Density[e] $\rho_b(\mathbf{r})$ ($eÅ^{-3}$)	Laplacian $\nabla^2\rho_b(\mathbf{r})$ ($eÅ^{-5}$)
D	C(3)-H(3A)...ring 3	c/a	H(3A)...H(36)	2.262	0.056(0)	0.413(1)
	C-H...phenyl interaction - H...H type contact					
B	C(13)-H(13)...ring 3	a/a	H(13)...H(35)	2.347	0.053(1)	0.626(1)
	C-H...phenyl interaction - H...H type contact					
D	C(2)-H(2A)...ring 3	c/a	H(2A)...C(34)-H(34)	2.819	0.053(1)	0.379(1)
	C-H...phenyl interaction - intermediate type contact					
D	C(23)-H(23)...ring 3	a/a	H(23)...C(33)-H(33)	2.901	0.052(0)	0.472(0)
	C-H...phenyl interaction - intermediate type contact					
G	C(23)-H(23)...ring 1	a/a	H(23)...H(12)	2.337	0.051(1)	0.442(1)
	C-H...phenyl interaction - H...H type contact					
D	C(4)-H(4A)...ring 3	c/a	H(4A)...C(32)-C(33)	2.854	0.051(1)	0.253(1)
	C-H...π(Ph) edge type hydrogen bond					
B	C(15)-H(15)...ring 4	a/a	H(15)...C(41)-C(42)	2.952	0.050(1)	0.412(1)
	C-H...π(Ph) centroid type hydrogen bond					
D	C(1)-H(1A)...ring 3	c/a	H(1A)...C(34)-C(35)	2.874	0.050(7)	0.346(2)
	C-H...π(Ph) edge type hydrogen bond					

Table 54d(ii). Summary of the bond critical points located for C-H...phenyl interactions in the four tetraphenylborate compounds studied (continued).

	Compound and Contact[a]	Type of Interaction[b]	Bond Path[c,d]	Contact Distance (Å)	Charge Density[e] $\rho_{b,i}(\mathbf{r})$ (eÅ^{-3})	Laplacian $\nabla^2\rho_{b,i}(\mathbf{r})$ (eÅ^{-5})
D	C(1)-H(1A)...ring 2	c/a	H(1A)...C(22)-C(23)	2.874	0.049(4)	0.467(2)
	C-H...π(Ph) edge type hydrogen bond					
B	C(14)-H(14)...ring 2	a/a	H(14)...C(22)-C(23)	2.849	0.049(1)	0.451(1)
	C-H...π(Ph) centroid type hydrogen bond					
G	C(16)-H(16)...ring 3	a/a	H(16)...H(35)	2.464	0.049(1)	0.439(1)
	C-H...phenyl interaction - H...H type contact					
B	C(12)-H(12)...ring 3	a/a	H(12)...C(34)	2.865	0.048(4)	0.553(1)
	C-H...π(Ph) single atom type hydrogen bond					
G	C(3)...ring 2	s/a	C(3)...C(22)-C(23)	3.752	0.047(1)	0.402(1)
D	C(4)-H(4B)...ring 2	c/a	H(4B)...C(22)-C(23)	2.921	0.047(1)	0.248(1)
	C-H...π(Ph) edge type hydrogen bond					
G	C(34)-H(34)...ring 4	a/a	H(34)...C(42)-H(42)	2.574	0.046(1)	0.405(1)
	C-H...phenyl interaction - H...H type contact					
N	C(12)-H(12)...ring 1	a/a	H(12)...C(14)-H(14)	2.873	0.046(9)	0.495(6)
	C-H...phenyl interaction - intermediate type contact					

Table 54d(ii). Summary of the bond critical points located for C-H...phenyl interactions in the four tetraphenylborate compounds studied (continued).

	Compound and Contact[a]	Type of Interaction[b]	Bond Path[c,d]	Contact Distance (Å)	Charge Density[e] $\rho_b(\mathbf{r})$ ($eÅ^{-3}$)	Laplacian $\nabla^2\rho_b(\mathbf{r})$ ($eÅ^{-5}$)
B	C(44)-H(44)...ring 3 C-H...phenyl interaction - H...H type contact	a/a	H(44)...C(33)-H(33)	2.454	0.045(1)	0.479(1)
B	C(36)-H(36)...ring 1 C-H...phenyl interaction - H...H type contact	a/a	H(36)...H(14)	2.446	0.045(1)	0.406(1)
D	C(3)-H(3B)...ring 3 C-H...π(Ph) edge type hydrogen bond	c/a	H(3B)...C(35)-C(36)	2.975	0.045(1)	0.240(1)
N	C(14)-H(14)...ring 1 C-H...π(Ph) centroid type hydrogen bond	a/a	H(14)...C(11)	2.841	0.044(8)	0.514(4)
G	C(3)...ring 1	s/a	C(3)...C(15)-C(16)	3.721	0.044(4)	0.449(3)
G	C(3)-H(60)...ring 1 C-H...phenyl interaction - intermediate type contact	s/a	H(60)...C(16)-H(16)	2.799	0.043(7)	0.441(6)
B	C(35)-H(35)...ring 2 C-H...phenyl interaction - H...H type contact	a/a	H(35)...H(26)	2.391	0.043(1)	0.423(1)
G	C(24)-H(24)...ring 1 C-H...π(Ph) single atom type hydrogen bond	a/a	H(24)...C(14)	2.863	0.042(1)	0.371(1)

Table 54d(ii). Summary of the bond critical points located for C-H...phenyl interactions in the four tetraphenylborate compounds studied (continued).

	Compound and Contact[a]	Type of Interaction[b]	Bond Path[c,d]	Contact Distance (Å)	Charge Density[e] $\rho_b(\mathbf{r})$ ($eÅ^{-3}$)	Laplacian $\nabla^2\rho_b(\mathbf{r})$ ($eÅ^{-5}$)
B	C(34)-H(34)...ring 4	a/a	H(34)...H(43)	2.508	0.040(1)	0.533(1)
	C-H...phenyl interaction - H...H type contact					
D	C(2)-H(2A)...ring 1	c/a	H(2A)...C(13)	3.044	0.035(1)	0.322(1)
	C-H...π(Ph) single atom type hydrogen bond					
G	C(3)...ring 2	s/a	C(3)...C(26)	3.918	0.031(2)	0.284(2)
Mean	(n = 32)[f]			2.641	0.051	0.460
σ[g]				0.267	0.008	0.118

[a] N - ammonium tetraphenylborate B - biguanidinium tetraphenylborate
D - [DabcoH][$B(C_6H_5)_4$] G - guanidinium tetraphenylborate acetonitrile solvate

[b] a - anion c - cation s - solvent

[c] If the bond path is directed towards a bond it is shown; the underlined atom is where the bond path terminates.

[d] The distance quoted is the calculated direct separation between the two atoms joined by the bond path.

[e] The data are sorted in order of decreasing charge density at the bond critical point.

[f] Three interactions were deleted because of their unusual bond paths, beginning from the C atom and not the H atom.

[g] σ is the standard deviation of the population, $\sigma = [(\Sigma x_i^2 - n(\Sigma x_i)^2) / n]^{1/2}$.

Table 54e(i). Summary of the bond critical points located for C-H...phenyl anion/anion interactions in the four tetraphenylborate compounds studied.

	Compound and Contact[a]	Type of Interaction[b]	Bond Path[c,d]	Contact Distance (Å)	Charge Density[e] $\rho_b(\mathbf{r})$ ($eÅ^{-3}$)	Laplacian $\nabla^2\rho_b(\mathbf{r})$ ($eÅ^{-5}$)
B	C(46)-H(46)...ring 1	a/a	H(46)...H(13)	2.179	0.078(1)	0.703(1)
D	C(35)-H(35)...ring 2	a/a	H(35)...H(22)	2.354	0.065(0)	0.441(0)
G	C(14)-H(14)...ring 1	a/a	H(14)...H(15)	2.357	0.061(2)	0.504(1)
G	C(13)-H(13)...ring 1	a/a	H(13)...H(12)	2.454	0.058(1)	0.467(1)
B	C(16)-H(16)...ring 1	a/a	H(16)...H(16)	2.261	0.057(1)	0.782(1)
B	C(13)-H(13)...ring 2	a/a	H(13)...C(26)	2.762	0.057(1)	0.608(1)
B	C(16)-H(16)...ring 1	a/a	H(16)...H(15)	2.205	0.056(1)	0.583(1)
B	C(13)-H(13)...ring 3	a/a	H(13)...H(35)	2.347	0.053(1)	0.626(1)
D	C(23)-H(23)...ring 3	a/a	H(23)...C(33)-H(33)	2.901	0.052(0)	0.472(0)
G	C(23)-H(23)...ring 1	a/a	H(23)...H(12)	2.337	0.051(1)	0.442(1)
B	C(15)-H(15)...ring 4	a/a	H(15)...C(41)	2.952	0.050(1)	0.412(1)
B	C(14)-H(14)...ring 2	a/a	H(14)...C(22)	2.849	0.049(1)	0.451(1)

Table 54e(i). Summary of the bond critical points located for C-H...phenyl anion/anion interactions in the four tetraphenylborate compounds studied (continued).

	Compound and Contact[a]	Type of Interaction[b]	Bond Path[c,d]	Contact Distance (Å)	Charge Density[e] $\rho_b(\mathbf{r})$ ($eÅ^{-3}$)	Laplacian $\nabla^2\rho_b(\mathbf{r})$ ($eÅ^{-5}$)
G	C(16)-H(16)...ring 3	a/a	H(16)...H(35)	2.464	0.049(1)	0.439(1)
B	C(12)-H(12)...ring 3	a/a	H(12)...C(34)	2.865	0.048(4)	0.553(1)
G	C(34)-H(34)...ring 4	a/a	H(34)...C(42)-H(42)	2.574	0.046(1)	0.405(1)
N	C(12)-H(12)...ring 1	a/a	H(12)...C(14)-H(14)	2.873	0.046(9)	0.495(6)
B	C(44)-H(44)...ring 3	a/a	H(44)...C(33)-H(33)	2.454	0.045(1)	0.479(1)
B	C(36)-H(36)...ring 1	a/a	H(36)...H(14)	2.446	0.045(1)	0.406(1)
N	C(14)-H(14)...ring 1	a/a	H(14)...C(11)	2.841	0.044(8)	0.514(4)
B	C(35)-H(35)...ring 2	a/a	H(35)...H(26)	2.391	0.043(1)	0.423(1)
G	C(24)-H(24)...ring 1	a/a	H(24)...C(14)	2.863	0.042(1)	0.371(1)
B	C(34)-H(34)...ring 4	a/a	H(34)...H(43)	2.508	0.040(1)	0.533(1)
Mean (n = 22)				2.556	0.052	0.505
σ'				0.250	0.009	0.101

[a] B - biguanidinium tetraphenylborate
D - [DabcoH][$B(C_6H_5)_4$]
G - guanidinium tetraphenylborate acetonitrile solvate
N - ammonium tetraphenylborate

[b] a - anion
c - cation
s - solvent

[c] If the bond path is directed towards a bond it is shown; the underlined atom is where the bond path terminates.

[d] The distance quoted is the calculated direct separation between the two atoms joined by the bond path.

[e] The data are sorted in order of decreasing charge density at the bond critical point.

[f] σ is the standard deviation of the population, $\sigma = [(\Sigma x_i^2 - n(\Sigma x_i)^2) / n]^{1/2}$.

Table 54e(ii). Summary of the bond critical points located for C-H...phenyl cation/anion interactions in the four tetraphenylborate compounds studied.

	Compound and Contact[a]	Type of Interaction[b]	Bond Path[c,d]	Contact Distance (Å)	Charge Density[e] $\rho_b(\mathbf{r})$ ($eÅ^{-3}$)	Laplacian $\nabla^2\rho_b(\mathbf{r})$ ($eÅ^{-5}$)
D	C(3)-H(3A)...ring 3	c/a	H(3A)...H(36)	2.262	0.056(0)	0.413(1)
D	C(2)-H(2A)...ring 3	c/a	H(2A)...C(34)-H(34)	2.819	0.053(1)	0.379(1)
D	C(4)-H(4A)...ring 3	c/a	H(4A)...C(33)	2.854	0.051(1)	0.253(1)
D	C(1)-H(1A)...ring 3	c/a	H(1A)...C(34)-C(35)	2.874	0.050(7)	0.346(2)
D	C(1)-H(1A)...ring 2	c/a	H(1A)...C(22)-C(23)	2.874	0.049(4)	0.467(2)
D	C(4)-H(4B)...ring 2	c/a	H(4B)...C(23)	2.921	0.047(1)	0.248(1)
D	C(3)-H(3B)...ring 3	c/a	H(3B)...C(35)-C(36)	2.975	0.045(1)	0.240(1)
D	C(2)-H(2A)...ring 1	c/a	H(2A)...C(13)	3.044	0.035(1)	0.322(1)
Mean (n = 8)				2.828	0.048	0.334
σ[f]				0.224	0.006	0.078

[a] D - [DabcoH][$B(C_6H_5)_4$]

[b] a - anion c - cation

[c] If the bond path is directed towards a bond it is shown; the underlined atom is where the bond path terminates.

[d] The distance quoted is the calculated direct separation between the two atoms joined by the bond path.

[e] The data are sorted in order of decreasing charge density at the bond critical point.

[f] σ is the standard deviation of the population, $\sigma = [(\Sigma x_i^2 - n(\Sigma x_i)^2) / n]^{\frac{1}{2}}$.

Table 54e(iii). Summary of the bond critical points located for C-H...phenyl solvent/anion interactions in the four tetraphenylborate compounds studied.

	Compound and Contact[a]	Type of Interaction[b]	Bond Path[c,d]	Contact Distance (Å)	Charge Density[e] $\rho_b(\mathbf{r})$ ($eÅ^{-3}$)	Laplacian $\nabla^2\rho_b(\mathbf{r})$ ($eÅ^{-5}$)
G	C(3)-H(61)...ring 1	s/a	H(61)...C(13)-C(14)	2.847	0.062(2)	0.498(1)
G	C(3)...ring 2	s/a	C(3)...C(22)	3.752	0.047(1)	0.402(1)
G	C(3)...ring 1	s/a	C(3)...C(15)	3.721	0.044(4)	0.449(3)
G	C(3)-H(60)...ring 1	s/a	H(60)...C(16)-H(16)	2.799	0.043(7)	0.441(6)
G	C(3)...ring 2	s/a	C(3)...C(26)	3.918	0.031(2)	0.284(2)
Mean (n = 2)[f]				2.823	0.052	0.470
σ[g]				0.024	0.010	0.028

[a] G - guanidinium tetraphenylborate acetonitrile solvate

[b] a - anion s - solvent

[c] If the bond path is directed towards a bond it is shown; the underlined atom is where the bond path terminates.

[d] The distance quoted is the calculated direct separation between the two atoms joined by the bond path.

[e] The data are sorted in order of decreasing charge density at the bond critical point.

[f] Three interactions were deleted because of their unusual bond paths, beginning from the C atom and not the H atom.

[g] σ is the standard deviation of the population, $\sigma = [(\Sigma x_i^2 - n(\Sigma x_i)^2) / n]^{\frac{1}{2}}$.

Table 54f(i). Summary of the bond critical points located for C-H...phenyl H...H type interactions in the four tetraphenylborate compounds studied.

	Compound and Contact[a]	Type of Interaction[b]	Bond Path[c,d]	Contact Distance (Å)	Charge Density[e] $\rho_b(\mathbf{r})$ ($eÅ^{-3}$)	Laplacian $\nabla^2\rho_b(\mathbf{r})$ ($eÅ^{-5}$)
B	C(46)-H(46)...ring 1	a/a	H(46)...H(13)	2.179	0.078(1)	0.703(1)
D	C(35)-H(35)...ring 2	a/a	H(35)...C(22)-H(22)	2.354	0.065(0)	0.441(0)
G	C(14)-H(14)...ring 1	a/a	H(14)...H(15)	2.357	0.061(2)	0.504(1)
G	C(13)-H(13)...ring 1	a/a	H(13)...H(12)	2.454	0.058(1)	0.467(1)
B	C(16)-H(16)...ring 1	a/a	H(16)...H(16)	2.261	0.057(1)	0.782(1)
B	C(16)-H(16)...ring 1	a/a	H(16)...H(15)	2.205	0.056(1)	0.583(1)
D	C(3)-H(3A)...ring 3	c/a	H(3A)...H(36)	2.262	0.056(0)	0.413(1)
B	C(13)-H(13)...ring 3	a/a	H(13)...H(35)	2.347	0.053(1)	0.626(1)
G	C(23)-H(23)...ring 1	a/a	H(23)...H(12)	2.337	0.051(1)	0.442(1)
G	C(16)-H(16)...ring 3	a/a	H(16)...H(35)	2.464	0.049(1)	0.439(1)
G	C(34)-H(34)...ring 4	a/a	H(34)...C(42)-H(42)	2.574	0.046(1)	0.405(1)

Table 54f(i). Summary of the bond critical points located for C-H...phenyl H...H type interactions in the four tetraphenylborate compounds studied (continued).

	Compound and Contact[a]	Type of Interaction[b]	Bond Path[c,d]	Contact Distance (Å)	Charge Density[e] $\rho_b(\mathbf{r})$ ($eÅ^{-3}$)	Laplacian $\nabla^2\rho_b(\mathbf{r})$ ($eÅ^{-5}$)
B	C(44)-H(44)...ring 3	a/a	H(44)...C(33)-H(33)	2.454	0.045(1)	0.479(1)
B	C(36)-H(36)...ring 1	a/a	H(36)...H(14)	2.446	0.045(1)	0.406(1)
B	C(35)-H(35)...ring 2	a/a	H(35)...H(26)	2.391	0.043(1)	0.423(1)
B	C(34)-H(34)...ring 4	a/a	H(34)...H(43)	2.508	0.040(1)	0.533(1)
Mean	(n = 15)			2.373	0.054	0.510
σ'				0.109	0.009	0.112

[a] B - biguanidinium tetraphenylborate
D - [DabcoH][$B(C_6H_5)_4$]
G - guanidinium tetraphenylborate acetonitrile solvate
N - ammonium tetraphenylborate

[b] a - anion c - cation s - solvent

[c] If the bond path is directed towards a bond it is shown; the underlined atom is where the bond path terminates.

[d] The distance quoted is the calculated direct separation between the two atoms joined by the bond path.

[e] The data are sorted in order of decreasing charge density at the bond critical point.

[f] σ is the standard deviation of the population, $\sigma = [(\Sigma x_i^2 - n(\Sigma x_i)^2) / n]^{\frac{1}{2}}$.

Table 54f(ii). Summary of the bond critical points located for C-H...phenyl intermediate type interactions in the four tetraphenylborate compounds studied (continued).

	Compound and Contact[a]	Type of Interaction[b]	Bond Path[c,d]	Contact Distance (Å)	Charge Density[e] $\rho_b(\mathbf{r})$ ($eÅ^{-3}$)	Laplacian $\nabla^2\rho_b(\mathbf{r})$ ($eÅ^{-5}$)
D	C(2)-H(2A)...ring 3	c/a	H(2A)...C(34)-H(34)	2.819	0.053(1)	0.379(1)
D	C(23)-H(23)...ring 3	a/a	H(23)...C(33)-H(33)	2.901	0.052(0)	0.472(0)
N	C(12)-H(12)...ring 1	a/a	H(12)...C(14)-H(14)	2.873	0.046(9)	0.495(6)
G	C(3)-H(60)...ring 1	s/a	H(60)...C(16)-H(16)	2.799	0.043(7)	0.441(6)
Mean	(n = 4)			2.848	0.048	0.447
σ'				0.041	0.004	0.044

[a] D - [DabcoH][$B(C_6H_5)_4$]
G - guanidinium tetraphenylborate acetonitrile solvate
N - ammonium tetraphenylborate

[b] a - anion c - cation s - solvent

[c] If the bond path is directed towards a bond it is shown; the underlined atom is where the bond path terminates.

[d] The distance quoted is the calculated direct separation between the two atoms joined by the bond path.

[e] The data are sorted in order of decreasing charge density at the bond critical point.

[f] σ is the standard deviation of the population, $\sigma = [(\Sigma x_i^2 - n(\Sigma x_i)^2) / n]^{\frac{1}{2}}$.

Table 54f(iii). Summary of the bond critical points located for C-H...π(Ph) hydrogen bonds in the four tetraphenylborate compounds studied.

	Compound and Contact[a]	Type of Interaction[b]	Bond Path[c,d]	Contact Distance (Å)	Charge Density[e] $\rho_b(\mathbf{r})$ ($eÅ^{-3}$)	Laplacian $\nabla^2\rho_b(\mathbf{r})$ ($eÅ^{-5}$)
G	C(3)-H(61)...ring 1 C-H...π(Ph) centroid type hydrogen bond	s/a	H(61)...C(13)-C(14)	2.847	0.062(2)	0.498(1)
B	C(13)-H(13)...ring 2 C-H...π(Ph) edge type hydrogen bond	a/a	H(13)...C(25)-C(26)	2.762	0.057(1)	0.608(1)
D	C(4)-H(4A)...ring 3 C-H...π(Ph) edge type hydrogen bond	c/a	H(4A)...C(32)-C(33)	2.854	0.051(1)	0.253(1)
B	C(15)-H(15)...ring 4 C-H...π(Ph) centroid type hydrogen bond	a/a	H(15)...C(41)-C(42)	2.952	0.050(1)	0.412(1)
D	C(1)-H(1A)...ring 3 C-H...π(Ph) edge type hydrogen bond	c/a	H(1A)...C(34)-C(35)	2.874	0.050(7)	0.346(2)
D	C(1)-H(1A)...ring 2 C-H...π(Ph) edge type hydrogen bond	c/a	H(1A)...C(22)-C(23)	2.874	0.049(4)	0.467(2)
B	C(14)-H(14)...ring 2 C-H...π(Ph) centroid type hydrogen bond	a/a	H(14)...C(22)-C(23)	2.849	0.049(1)	0.451(1)
B	C(12)-H(12)...ring 3 C-H...π(Ph) single atom type hydrogen bond	a/a	H(12)...C(34)	2.865	0.048(4)	0.553(1)

Table 54f(iii). Summary of the bond critical points located for C-H...π(Ph) hydrogen bonds in the four tetraphenylborate compounds studied (continued).

	Compound and Contact[a]	Type of Interaction[b]	Bond Path[c,d]	Contact Distance (Å)	Charge Density[e] $\rho_b(\mathbf{r})$ ($eÅ^{-3}$)	Laplacian $\nabla^2\rho_b(\mathbf{r})$ ($eÅ^{-5}$)
D	C(4)-H(4B)...ring 2 C-H...π(Ph) edge type hydrogen bond	c/a	H(4B)...C(22)-C(23)	2.921	0.047(1)	0.248(1)
D	C(3)-H(3B)...ring 3 C-H...π(Ph) edge type hydrogen bond	c/a	H(3B)...C(35)-C(36)	2.975	0.045(1)	0.240(1)
N	C(14)-H(14)...ring 1 C-H...π(Ph) centroid type hydrogen bond	a/a	H(14)...C(11)	2.841	0.044(8)	0.514(4)
G	C(24)-H(24)...ring 1 C-H...π(Ph) single atom type hydrogen bond	a/a	H(24)...C(14)	2.863	0.042(1)	0.371(1)
D	C(2)-H(2A)...ring 1 C-H...π(Ph) single atom type hydrogen bond	c/a	H(2A)...C(13)	3.044	0.035(1)	0.322(1)
Mean	(n = 13)			2.886	0.048	0.406
σ[f]				0.069	0.006	0.116

[a] N - ammonium tetraphenylborate; B - biguanidinium tetraphenylborate; D - [DabcoH][$B(C_6H_5)_4$]; G - guanidinium tetraphenylborate acetonitrile solvate

[b] a - anion c - cation s - solvent

[c] If the bond path is directed towards a bond it is shown; the underlined atom is where the bond path terminates.

[d] The distance quoted is the calculated direct separation between the two atoms joined by the bond path.

[e] The data are sorted in order of decreasing charge density at the bond critical point.

[f] σ is the standard deviation of the population, $\sigma = [(\Sigma x_i^2 - n(\Sigma x_i)^2) / n]^{\frac{1}{2}}$.

References

(1) "Fundamentals of Crystallography." C. Giacovazzo, H.L. Monaco, D. Viterbo, F. Scordari, G. Gilli, G. Zanotti and M. Catti (C. Giacovazzo editor), International Union of Crystallography, Oxford University Press, England (1992).

(2) "X-ray Structure Determination, A Practical Guide, Second Edition." G.H. Stout and L.H. Jensen, John Wiley and Sons, New York (1989).

(3) P. Becker, Physica Scripta, 15, 119 (1977).

(4) P. Coppens in "Neutron Diffraction." H. Dachs editor, Chapter 3, page 71 (1978).

(5) Israel Journal of Chemistry, Volume 16(2-3), F.L. Hirshfeld guest editor, all included papers.

(6) "X-ray Charge Densities and Chemical Bonding." P. Coppens, International Union of Crystallography, Oxford University Press, England (1997).

N.K. Hansen and P. Coppens, Acta Crystallogr., A34, 909 (1978);

P. Coppens, T.N. Guru Row, P. Leung, E.D. Stevens, P.J. Becker and

Y.W. Yang, Acta Crystallogr., A35, 63 (1979);

P. Coppens, J. Chem. Ed., 61, 761 (1984);

P. Coppens, J. Phys. Chem., 93, 7979 (1989).

(7) K. Kurki-Suonio, Israel J. Chem., 16, 115 (1977).

(8) N.K. Hansen, T. Koritsanszky and P.R. Mallinson, MOLLY: Program for Multipole Refinement (1991).

(9) T. Koritsanszky, S.T. Howard, T. Richter, P.R. Mallinson, Z. Su and N.K. Hansen, XD: A Computer Program Package for Multipole Refinement and Analysis of Charge Densities from X-ray Diffraction Data (1995).

(10) M. Souhassou, E. Espinosa, C. Lecomte and R.H. Blessing, Acta Crystallogr., B51, 661 (1995).

(11) E.D. Stevens and P. Coppens, Acta Crystallogr., A32, 915 (1976).

(12) P. Coppens and E.D. Stevens, Adv. Quantum Chem., 10, 1 (1977).

(13) C.L. Klein and E.D. Stevens in "Structure and Reactivity." J.F. Liebman and A. Greenberg editors, Chapter 2, 25 (1988).

(14) "Atoms in Molecules - A Quantum Theory." R.F.W. Bader, University of Oxford Press, England (1990).

(15) R.F.W. Bader, Chem. Rev., 91, 893 (1991).

(16) "Hydrogen Bonding in Biological Structures." G.A. Jeffrey and W. Saenger, Springer-Verlag, Berlin (1991).

(17) G.A. Jeffrey, Cryst. Rev., 4, 213 (1995).

(18) "The Nature of the Chemical Bond." Linus Pauling, Cornell University Press, Ithaca, New York (1939).

(19) E.D. Stevens, M.S. Lehmann and P. Coppens, J. Amer. Chem. Soc., 99, 2829 (1977).

(20) B. Hsu and E.O. Schlemper, Acta Crystallogr., B36, 3017 (1980).

(21) D. Madsen, C. Flensburg and S. Larsen, J. Phys. Chem., A102, 2177 (1998).

(22) P.R. Mallinson, K. Woźniak, G.T. Smith and K.L. MacCormack, J. Amer. Chem. Soc., 119, 11502 (1997).

(23) E.D. Stevens and P. Coppens, Acta Crystallogr., B36, 1864 (1980).

(24) J. Dam, S. Harkema and D. Feil, Acta Crystallogr., B39, 760 (1983).

(25) D. Zobel, P. Luger, W. Dreisig and T. Koritsànszky, Acta Crystallogr., B48, 837 (1992).

(26) E.D. Stevens, Acta Crystallogr., B36, 1876 (1980).

(27) M.P.C.M. Krijn, H. Graafsma and D. Feil, Acta Crystallogr., B44, 609 (1988).

(28) M.P.C.M. Krijn and D. Feil, J. Chem. Phys., 89, 4199 (1988).

(29) T. Kellersohn, R.G. Delaplane and I. Olovsson, Acta Crystallogr., B50, 316 (1994).

(30) H.S. Sheu, J.C. Wu, Y. Wang and R.B. English, Acta Crystallogr., B52, 458 (1996).

(31) F. Hamzaoui, F. Baert and G. Wojcik, Acta Crystallogr., B52, 159 (1996).

(32) T. Koritsànszky, J. Buschmann, L. Denner, P. Luger, A. Knöchel, M. Haarich and M. Patz, J. Amer. Chem. Soc., 113, 8388 (1991).

(33) M. Souhassou, C. Lecomte, R.H. Blessing, A. Aubry, M.-M. Rohmer, R. Weist, M. Bénard and M. Marraud, Acta Crystallogr., B47, 253 (1991).

(34) R. Destro, R.E. Marsh and R. Bianchi, J. Phys. Chem., 92, 966 (1988).

(35) R. Destro, R. Bianchi, C. Gatti and F. Merati, Chem. Phys. Lett., 186, 47 (1991).

(36) W.T. Klooster, S. Swaminathan, R. Nanni and B. M. Craven, Acta Crystallogr., B48, 217 (1992).

(37) S.T. Howard, M.B. Hursthouse, C.W. Lehmann and E.A. Poyner, Acta Crystallogr., B51, 328 (1995).

(38) C. Flensberg, S. Larsen and R.F. Stewart, J. Phys. Chem., 99, 10130 (1995).

(39) V.G. Tsirelson, Can. J. Chem., 74, 1171 (1996).

V. Zavodnik, A. Stash, V. Tsirelson, R. De Vries and D. Feil, Acta Crystallogr., B55, 45 (1999).

(40) E. Espinosa, C. Lecomte, E. Molins, S. Veintemillas, A. Cousson and W. Paulus, Acta Crystallogr., B52, 519 (1996).

(41) K.L. MacCormack, P.R. Mallinson, B.C. Webster, D.S. Yufit, L.A. Slater and D.J. Robins, Acta Crystallogr., B53, 181 (1997).

(42) R. Bianchi, G. Gervasio and G. Viscardi, Acta Crystallogr., B54, 66 (1998).

(43) R. Flaig, T. Koritsanszky, D. Zobel and P. Luger, J. Amer. Chem. Soc., 120, 2227 (1998).

(44) R. Destro and F. Merati, Acta Crystallogr., B51, 559 (1995).

(45) R. Bianchi, C. Gatti, V. Adovasio and M. Nardelli, Acta Crystallogr., B52, 471 (1996).

(46) P. Roversi, M. Barzaghi, F. Merati and R. Destro, Can. J. Chem., 74, 1145 (1996).

(47) C. Gatti, R. Bianchi, R. Destro and F. Merati, J. Mol. Struct. (Theochem), 255, 409 (1992).

(48) R.F.W. Bader, T.-H. Tang, Y. Tal and F.W. Biegler-König, J. Amer. Chem. Soc., 104, 946 (1982).

(49) R.J. Boyd and S.C. Choi, Chem. Phys. Lett., 120, 80 (1985).

(50) R.J. Boyd and S.C. Choi, Chem. Phys. Lett., 129, 62 (1986).

(51) M.T. Carroll and R.F.W. Bader, Mol. Phys., 65, 695 (1988).

(52) U. Koch and P.L.A. Popelier, J. Phys. Chem., 99, 9747 (1995).

(53) T.-H. Tang, W.-J. Hu, D.-Y. Yan and Y.-P. Cui, J. Mol. Struct. (Theochem), 207, 319 (1990).

(54) I. Rozas, I. Alkorta and J. Elguero, J. Phys. Chem., A101, 9457 (1997).

(55) M.C. Etter, Acc. Chem. Res., 23, 120 (1990).

(56) T. Steiner, Chem. Commun., 727 (1997).

(57) T. Steiner and G.R. Desiraju, Chem. Commun., 891 (1998).

(58) L.R. Hanton, C.A. Hunter and D.H. Purvis, J. Chem. Soc., Chem. Commun., 1134 (1992).

(59) T. Davies and L.A.K. Staveley, Trans. Faraday Soc., 53, 19 (1957).

(60) A.D.U. Hardy and D.D. MacNicol, J. Chem. Soc., Perkin Trans II, 1140 (1976).

(61) A. Aubry, J. Protas, E. Moreno-Gonzalez and M. Marraud, Acta Crystallogr., B33, 2572 (1977).

(62) K. Nakatsu, H. Yoshioka, K. Kunimoto, T. Kinugasa and S. Ueji, Acta Crystallogr., B34, 2357 (1978).

(63) S. Ueji, K. Nakatsu, H. Yoshioka and K. Kinoshita, Tetrahedron Letters, 23, 1173 (1982).

(64) T. Steiner, E.B. Starikov and M. Tamm, J. Chem. Soc., Perkin Trans 2, 67 (1996).

(65) T. Steiner, S.A. Mason and M. Tamm, Acta Crystallogr., B53, 843 (1997).

(66) J.L. Atwood, F. Hamata, K.D. Robinson, G.W. Orr and R.L. Vincent, Nature, 349, 683 (1991).

(67) H.S. Rzepa, M.L. Webb, A.M.Z. Slawin and D.J. Williams, J. Chem. Soc., Chem. Commun., 765 (1991).

(68) S. Suzuki, P.G. Green, R.E. Bumgarner, S. Dasgupta, W.A. Goddard III and G.A. Blake, Science, 257, 942 (1992).

(69) S.Y. Fredricks, K.D. Jordan and T.S. Zwier, J. Phys. Chem., 100, 7810 (1996).

(70) M. Nishio, Y. Umezawa, M. Hirota and T. Takeuchi, Tetrahedron, 51, 8665 (1995).

(71) T. Steiner, E.B. Starikov, A.M. Amado and J.J.C. Teixeira-Dias, J. Chem. Soc., Perkin Trans. 2, 1321 (1995).

(72) P. Hobza, V. Spirko, H.L. Selzle and E.W. Schlag, J. Phys. Chem., A102, 2501 (1998).

(73) M.F. Perutz, G. Fermi, D.J. Abraham, C. Poyart and E. Bursaux, J. Amer. Chem. Soc., 108, 1064 (1986).

(74) E. Tüchsen and C. Woodward, Biochemistry, 26, 1918 (1987).

(75) K.M. Armstrong, R. Fairman and R.L. Baldwin, J. Mol. Biol., 230, 284 (1993).

(76) G. Waksman, D. Kominos, S.C. Robertson, P. Nalin, D. Baltimore, R.B. Birge, D. Cowburn, H. Hanafusa, B.J. Mayer, M. Overduim, M.D. Resh, C.B. Rios, L. Silverman and J. Kuriyan, Nature (London), 358, 646 (1992).

(77) M.F. Perutz, Phil. Trans. R. Soc., A345, 105 (1993).

(78) S.K. Burley and G.A. Petsko, FEBS Letters, 203, 139 (1986).

(79) J.B.O. Mitchell, C.L. Nandi, I.K. McDonald, J.M. Thornton and S.L. Price, J. Mol. Biol., 239, 315 (1994).

(80) C.S.Page and H.S. Rzepa, Electron. Conf. Trends Org. Chem. [CD-ROM], paper 47 (1995).

(81) M.A. Viswamitra, R. Radhakrishnan, J. Bandekar and G.R. Desiraju, J. Amer. Chem. Soc., 115, 4868 (1993).

(82) F.H. Allen, V.J. Hoy, J.A.K. Howard, V.R. Thalladi, G.R. Desiraju, C.C. Wilson and G.J. McIntyre, J. Amer. Chem. Soc., 119, 3477 (1997).

(83) P.K. Bakshi, A. Linden, B.R. Vincent, S.P. Roe, D. Adhikesavalu, T.S. Cameron and O. Knop, Can. J. Chem., 72, 1273 (1994).

(84) M. Levitt and M.F. Perutz, J. Mol. Biol., 201, 751 (1988).

(85) D.A. Rodham, S. Suzuki, R.D. Suenram, F.J. Lovas, S. Dasgupta, W.A. Goddard III and G.A. Blake, Nature, 362, 735 (1993).

(86) Y. Inoue, S. Sugio, J. Andzelm and N. Nakamura, J. Phys. Chem., A102, 646 (1998).

(87) E.M. Duffy, P.J. Kowalczyk and W.L. Jorgensen, J. Amer. Chem. Soc., 115, 9271 (1993).

(88) E.B. Starikov and T. Steiner, Acta Crystallogr., B54, 94 (1998).

(89) J.P. Bouquiere, J.L. Finney, M.S. Lehmann, P.F. Lindley and H.F.J. Savage, Acta Crystallogr., B49, 79 (1993).

(90) T. Steiner, A.M.M. Schreurs, J.A. Kanters, J. Kroon, J. van der Maas and B. Lutz, J. Mol. Struct., 436-437, 181 (1997).

(91) P. Tarakeshwar, S.J. Lee, J.Y. Lee and K.S. Kim, J. Phys. Chem., 108, 7217 (1998).

(92) Inorganic Syntheses, Volume VII, J. Kleinberg (editor in chief), McGraw-Hill Book Company Inc, U.S.A. (1963).

(93) R.H. Blessing, Program SORTAV, Hauptman-Woodward Institute, Buffalo, New York, U.S.A. (1996).

(94) G.M. Sheldrick, SHELXS-86, in "Crystallographic Computing 3" (G.M. Sheldrick, C. Kruger and R. Goddard editors) Oxford University Press, pp. 175-189 (1985).

(95) G.M. Sheldrick, SHELXL-93: Crystal Structure Refinement Program, Institute of Inorganic Chemistry, University of Gottingen, Germany (1993).

(96) R.F. Stewart, Acta Crystallogr., A32, 565 (1976).

(97) E. Clementi and C. Roetti, Atomic Data and Nuclear Data Tables, 14, 177 (1974).

(98) P.J. Becker and P. Coppens, Acta Crystallogr., A30, 129 (1974).

P.J. Becker and P. Coppens, Acta Crystallogr., A30, 148 (1974).

P.J. Becker and P. Coppens, Acta Crystallogr., A31, 417 (1975).

(99) F.H. Allen, Acta Crystallogr., B42, 515 (1986).

(100) F.H. Allen and O. Kennard, " 3D Search and Research Using the Cambridge Structural Database." Chemical Design Automation News, 8(1), 1 and 31 (1993). Cambridge Structural Database Version of April 1997.

(101) K.M. Barkigia, L.M. Rajković-Blazer, M.T. Pope, E. Prince and C. Quicksall, Inorg. Chem., 19, 2531 (1980).

(102) V. Schomaker and K.N. Trueblood, Acta Crystallogr., B24, 63 (1968).

(103) X. He and B.M. Craven, EKRT program, Acta Crystallogr., A49, 10 (1993).

(104) M.A. James, O. Knop and T.S. Cameron, Can. J. Chem., 70, 1795 (1992).

(105) W.J. Westerhaus, O. Knop and M. Falk, Can. J. Chem., 58, 1355 (1980).

(106) M.P. Roberts, D. Clavell-Grunbaum and H.L. Strauss, J. Chem. Phys., 87, 6393 (1987).

(107) G. Lucazeau, A. Chahid, J.F. Bocquet, A.J. Dianoux and M.P. Roberts, Physica B, 164, 313 (1990).

(108) M.P. Roberts, G. Lucazeau, G.J. Kearly and A.J. Dianoux, J. Chem. Phys., 93, 8963 (1990).

(109) M.P. Roberts, R.M. Cavagnat, G. Lucazeau, J.-F. Bocquet and H.L. Strauss, J. Chem. Phys., 93, 7632 (1990).

(110) M.P. Roberts, J. Chem. Phys., 93, 8524 (1990).

(111) M.L.H. Gruwel and R.E. Wasylishen, Z. Naturforsch., 45A, 55 (1990).

(112) H. Bock, T. Vaupel and H. Schödel, J. prakt. Chem., 339, 26 (1997).

(113) P.K. Bakshi, PhD. Thesis, Dalhousie University, Halifax, Nova Scotia, Canada (1995).

(114) W. Frey, M. Vettel, K. Edelmann and W. Kantlehner, Z. Kristallogr. - New Cryst. Struct., 213, 77 (1998).

(115) A. Martin and A.A. Pinkerton, Acta Crystallogr., C52, 1048 (1996).

(116) A. Martin, A.A. Pinkerton and A. Schiemann, Acta Crystallogr., C52, 996 (1996).

(117) A. Martin, A.A. Pinkerton, R.D. Gilardi and J.C. Bottaro, Acta Crystallogr., B53, 504 (1997).

(118) T. Steiner, Acta Crystallogr., C54, 1121 (1998).

(119) Y. Umezawa, S. Tsuboyama, K. Honda, J. Uzawa and M. Nishio, Bull. Chem. Soc. Jpn., 71, 1207 (1998).

(120) Y. Umezawa, S. Tsuboyama, H. Takahashi, J. Uzawa and M. Nishio, Tetrahedron, 55, 10047 (1999).

(121) H.W. Yang and B.M. Craven, Acta Crystallogr., B54, 912 (1998).

(122) P.R. Mallinson, K. Woźniak, C.C. Wilson, K.L. MacCormack and D.S. Yufit, J. Amer. Chem. Soc., 121, 4640 (1999).

(123) E. Cubero, M. Orozco, P. Hobza and F.J. Luque, J. Phys. Chem., A103, 6394 (1999).

(124) E. Cubero, M. Orozco and F.J. Luque, J. Phys. Chem., A103, 315 (1999).

(125) E. Espinosa, M. Souhassou, H. Lachekar and C. Lecomte, Acta Crystallogr., B55, 563 (1999).

(126) I. Alkorta, I. Rozas and J. Elguero, Struct. Chem., 9, 243 (1998).

(127) I. Alkorta and J. Elguero, J. Phys. Chem., A103, 272 (1999).

(128) O. Knop, unpublished results.

(129) T. Steiner and S.A. Mason, Acta Crystallogr., B56, 254 (2000).

CONTESTED FUTURE(S):
THE SOCIAL OPPOSITION TO THE OECD-MAI

by

Catherine Schittecatte

Submitted in partial fulfillment of
the requirements for the degree of
Doctor of Philosophy

at

Dalhousie University
Halifax, Nova Scotia
July 2001

DALHOUSIE UNIVERSITY

FACULTY OF GRADUATE STUDIES

The undersigned hereby certify that they have read and recommend to the Faculty of Graduate Studies for acceptance a thesis entitled "Contested Future(s): The Social Opposition to the OCED-MAI" by Catherine Schittecatte in partial fulfillment of the requirements for the degree of Doctor of Philosophy.

Dated: August 9, 2001

External Examiner: L. Macdonald

Research Supervisor: David Black

Examining Committee: Gillian R. Wright

Timothy M Shaw.

Denis Stairs

DALHOUSIE UNIVERSITY

DATE: August 22, 2001

AUTHOR: Catherine Schittecatte

TITLE: Contested Future(s): The Social Opposition to the OECD-MAI

DEPARTMENT: Political Science

DEGREE: Doctor of Philosophy CONVOCATION: October YEAR: 2001

Permission is herewith granted to Dalhousie University to circulate and to have copied for non-commercial purposes, at its discretion, the above title upon the request of individuals or institutions.

Signature of Author

DEDICATION

To the memories of my mother Christiane (Schittecatte) Moreau née Van Gend and her mother Simone (Van Gend) née Levril whose spirits animated this endeavour

TABLE OF CONTENTS

SECTION THREE: THEORETICAL IMPLICATIONS

LIST OF ILLUSTRATIONS

ABSTRACT

This thesis concerns the social opposition to international negotiations for a Multilateral Agreement on Investment (MAI) that took place between 1995 and 1998 at the Organization for Economic Cooperation and Development. The results obtained from the collection of data and the application of three theoretical frameworks support the following arguments: (i) the MAI negotiations were initiated within historical and intellectual contexts that rendered the treaty controversial due to its meaning as a symbol of economic globalization; (ii) as such, these negotiations gave rise to transnational social movement networks that oppose (corporate) economic globalization; (iii) these MAI opponents in coalition with other non-state actors exercised direct influence on the MAI draft text and indirect political influence on the negotiations that contributed to their demise; and (iv) the growth of the movement and its activities since the end of the negotiations are likely to have an ideational impact on societies and the processes of economic liberalization that will affect international economic relations. In order to support these findings, the research relies upon insights from three existing theoretical frameworks and the process tracing methodology. Social movement theory provides tools of analysis with which to understand the evolution of this novel non-state actor and its likely societal influences regarding our understanding(s) of economic globalization. Social constructivist frameworks used in the study of international relations illuminate how such non-state actors influence international outcomes. Finally, critical analytical frameworks of international relations provide a historical explanation of the emergence of such opposition to economic globalization. The contested future(s) we have witnessed in the numerous protests against the World Trade Organization, the International Monetary Fund and the World Bank can thus be understood as a response to the increased liberalization of domestic markets which has been associated with the policies emanating from these organizations.

ABBREVIATIONS

AFL-CIO	American Federation of Labor — Congress of Industrial Organizations
BIAC	Business and Industry Advisory Committee (OECD)
CCAMI	Coordination Contre l'AMI
CCCA	Coordination Contre les Clônes de l'AMI
CCCOMC	Coordination pour le Contrôle Citoyen de l'OMC
CIME	Committee on International Investment and Multinational Enterprises (OECD)
CMIT	Committee on Capital Movements and Invisible Transactions (OECD)
CIEL	Centre for International Environmental Law
CSD	Commission on Sustainable Development
CUTS	Consumer Unity and Trust Society
DG	Drafting Group (of MAI text)
DAN	Direct Action Network
DFAIT	Department of Foreign Affairs and International Trade (Canada)
EC	European Commission
ECOSOC	Economic and Social Council (of the United Nations)
EG	Expert Group (of MAI negotiations)
EU	European Union
FDI	Foreign Direct Investment
FOE	Friends of the Earth
GATS	General Agreement on Trade in Services (Uruguay Round)
GATT	General Agreement on Tariffs and Trade
IACHR	Inter-American Commission on Human Rights
ICC	International Chamber of Commerce
IFG	International Forum on Globalization
IGO	Intergovernmental Organization
INGO	International Non-Governmental Organization
IO	International Organization
MAI	Multilateral Agreement on Investment
MEA	Multilateral Environment Agreement
MFN	Most Favoured Nation
MNC	Multinational Corporation
NAFTA	North American Free Trade Agreement
NG	Negotiating Group (of the MAI)
NGO	Non-Governmental Organization
NT	National Treatment
OAS	Organization of American States
OECD	Organization for Economic Cooperation and Development
PGA	Peoples' Global Action Network

RAN	Rainforest Action Network
REIO	Regional Economic Integration Organization
SMO	Social Movement Organization
TRIM	Trade Related Investment Measure (Uruguay Round)
TSMO	Transnational Social Movement Organization
TUAC	Trade Union Advisory Committee (OECD)
U.K.	United Kingdom
UN	United Nations
UNCED	United Nations Conference on Environment and Development
UNICE	Union of Industrial and Employers' Confederation of Europe
UNCTAD	United Nations Conference on Trade and Development
USCIB	United States Council for International Business
WTO	World Trade Organization

ACKNOWLEDGEMENTS

I would like to thank the Faculty of Graduate Studies and the Department of Political Science of Dalhousie University for their financial support without which I would not have been able to undertake Doctoral studies. I am indebted to Bob Finbow in the Department of Political Science for introducing me to social movement analysis, a framework that proved extremely useful to my initial understanding of the significance of the socio-political phenomenon that I witnessed.

I am grateful to the members of my committee for showing sustained interest in my work and for providing fruitful comments throughout. Tim Shaw's relentless support gave me the confidence to follow my intuition and pursue my research interests early on. Gil Winham's vigilance for clarity in policy analysis motivated me to search for excellence in that area of my work. Last but not least, I am most deeply grateful to my supervisor Dave Black who has been a true mentor and without whom this research would simply not have taken place. His strength, unwavering support and encouragements sustained me from beginning to end, particularly when I needed them most. These did not hinder valuable prodings, continued vigilance and scrutiny of my work which have been truly inspiring and enlightening throughout my research and writing.

Finally, I must thank my immediate family for accepting long periods of absenteeism, moods of anxiety and work-related soliloquies during our family reunions. Their reassurances, support and understanding have contributed to my emotional well being throughout. To my extended family in Belgium, our "cousins Van Gend," I am indebted for their hospitality during the course of my research in Europe. Their welcome enriched my stay and contributed to a fruitful research experience by rekindling old memories, reminding me of my trans-Atlantic ties. The last, most heartfelt and deserved gratitude of all is owed to Keir Armstrong, my partner, friend, mentor and most respected counterpart in numerous debates on a variety of topics related to my research. I am fortunate to continue to benefit from his inexorable optimism, belief in my abilities and vigorous intellectual exchanges.

SECTION I

CONCEPTUAL FRAMEWORK

CHAPTER I

THE MAI EVENTS: QUESTIONS UNANSWERED

Introduction

The events which spurred the following analysis reside in the unexpected and unanticipated outcome of what appeared to be a reasonably attainable objective among major states in the mid- to late-1990s. The Multilateral Agreement on Investment (MAI) was an international commercial agreement negotiated among the like-minded members of the Organization for Economic Co-operation and Development (OECD) between 1995 and 1998. The objective of the proposed agreement was to further foster the liberalization and protection of investment flows among OECD member countries and eventually worldwide. Not only did the OECD negotiations fail to produce such an agreement, but an unexpected transnational public opposition emerged midway through the process. The objective of the research undertaken herein is to provide an understanding of this social opposition, its role in the demise of the negotiations, and its meaning for world politics.

I begin this introductory chapter with a brief history of the events which took place over the three-year period of MAI negotiations. In closing that section I identify the questions addressed in the research. Next I describe the methodology of research. A third section explains the usage of various theoretical frameworks applied in the analysis. I close with a summary of findings and an outline of the remaining chapters.

A Brief History

In June of 1995 in Paris, the then 25 OECD ministers authorized the negotiations for a Multilateral Agreement on Investment (MAI).[1] Negotiations began in September of

---

[1] Since then four more members were added to the OECD: the Czech Republic (December 1995), Hungary (May, 1996), Poland (November 1996), and South Korea (December 1996).

that year. The choice of the forum for these negotiations—the OECD—albeit controversial, raised expectations of speedy success for a state-of-the-art investment agreement since its members were considered to be like-minded, and since they had already committed to several codes and instruments on investments.[2] Expectations were so high that the deadline for the agreement was set for May 1997. Yet, two subsequent extensions to the original mandate would be required in order to pursue the negotiations.

By the spring of 1997 it had become clear that the first deadline was unrealistic. Negotiators issued a report to the OECD ministers which, according to one official, contained "[t]he basic message that a lot of progress has been made [and that] the commitment to the process is definitely there" (*Inside U.S. Trade*, May 23, 1997: 11, 12). In spite of a number of outstanding issues, it was still believed that an agreement could be reached and the negotiations were pursued accordingly. It was agreed to extend the deadline to the May 1998 OECD ministerial meeting. Also, over these first two years of negotiations negotiators were contacted by environmental organizations that objected to some aspects of the draft treaty and they had agreed to modify the MAI draft text to reflect these concerns. Thus a third year of MAI negotiations was agreed-to and monthly negotiating sessions resumed with a meeting on June 30, 1997.

However in April 1997, as the first extension for the negotiations mandate was being agreed to, an unexpected development occurred with the emergence of a much more

---

[2] Several investment-related "codes" or "instruments" already existed at the OECD to which members were committed: the 1976 OECD Declaration and Decisions on International Investment and Multinational Enterprises which contains a National Treatment instrument, Guidelines for Multinational Enterprises, an instrument on Investment Incentives and Disincentives and an instrument on Conflicting Requirements; and, the Codes of Liberalization of Capital Movements and Current Invisible Operations adopted by OECD members in 1961 (Witherell, 1996: 18).

noticeable social opposition to the MAI that reached global dimensions. These actors made their appearance with the release of an early MAI draft text and its analysis on the Internet. Those MAI opponents included an array of groups representing diverse types of concerns. These included environmental organizations that coalesced with labour unions, development organizations and grassroots organizations, some of which were religious. From that point on, this opposition sustained an effective global public forum on the Internet that critiqued not only the agreement itself but also the alleged secretive process of these inter-state negotiations.

The pressure became such that in October of 1997, a group of international and domestic Non-Governmental Organizations (NGOs) were invited to meet with the OECD negotiators.[3] Negotiators were then confronted by an unprecedented transnational coalition of activists and NGOs who requested that the negotiations be suspended. Their joint statement to the OECD was subsequently posted on the Internet and from then on the MAI opponents from diverse stripes remained united with one objective: to suspend the negotiations. Over the following months not only did the Internet campaign intensify but campaigns spread to the streets and legislatures of various member countries.

By April 1998, when it became clear that the second deadline would not be met, the agreement and its opponents had gained considerable media attention in most OECD

---

[3] It has been observed that this meeting in itself represented a departure from OECD practice. Smythe (1998*b*: 247) reported that "[t]he OECD has historically provided for the views of capital and labor to be heard on economic issues, including investment, through the Trade Union Advisory Committee (TUAC), which was founded in 1948, and the Business and Industry Advisory Committee (BIAC), founded in 1963." Indeed, aside from its environmental section that engaged in consultation with some environmental NGOs, that organization was much more closed to such consultations than were, for example, various multilateral fora within the United Nations or even the World Bank.

countries. On 27 April, 1998, OECD members agreed to suspend the negotiations for a period of six months. Before that meeting took place, France declared it was withdrawing from the negotiations, a declaration which ended them (*Inside U.S. Trade*, October 23, 1998: 5).

The apparently sudden and unexpected opposition with its use of the Internet clearly took most officials by surprise. This was reflected in the media through interviews and reports that evoked a sense of widespread shock. Thus reporter Guy de Jonquières wrote in the British *Financial Times* of April 30, 1998:

> There is a memorable scene in the film Butch Cassidy and the Sundance Kid when the outlaw heroes are hounded for days by a bunch of armed men on horseback. After failing to shake off their mysterious pursuers, one of the hunted men asks despairingly: "Who are these guys?"

Questions Addressed in the Research

This research project began with that question. Such a visible, vociferous and geographically widespread yet united social opposition to the negotiations of such an arcane and obscure economic agreement was unusual. Furthermore, relative to the habitual protectionist claims made by specific domestic economic interests during multilateral economic negotiations, the claims made by this opposition were equally unusual. In addition, since the emergence and visibility of the transnational anti-MAI coalition coincided with the setback and eventual demise of the MAI, its impact on the negotiations has been the object of much speculation. That debate needed to be addressed empirically. The third object of curiosity was whether such an opposition was unique to the MAI or whether it would be sustained.

In the light of these, the purpose of this research was to examine the three and a half year-period of negotiations and the social opposition to the MAI in order to answer three questions. The first is, how are we to understand the social opposition to the MAI in terms of its politics, organization, motives, objectives and strategies? The second question asks, how effective was the social opposition to the MAI in achieving its objectives and how much of the failure of the negotiations can be attributed to it? Finally, a third question asks what this opposition represents for world politics? These three questions can be formulated in terms of testing three interrelated hypotheses: (i) the social opposition to the MAI influenced substantive outcomes in the treaty as well as the demise of the negotiations; (ii) the MAI opposition engendered transnational social movement networks against economic globalization; and, (iii) societal actors such as the social movement against economic globalization have, starting with the MAI events, affected inter-state relations and world politics and they will continue to do so.

Research Methodology

One of the approaches followed in the research can be broadly identified as a "descriptive-empirical approach" in that one objective of the research is to establish causal relationships (Marsh and Stoker, 1995: 17). That aspect of the analysis relies on thick description of events and is therefore inductive. In order to answer the two first questions of the research I relied upon four types of data sources. One was participant observation, the second was open-ended interviews and eyewitness testimony, and the third and fourth consisted of written documents from primary and secondary sources. Participant observation and open interviews of MAI opponents contributed to gaining an

understanding of their strategies, rationales and objectives as well as their perception of one another (See Appendix C for details on these). These were further explored in their publications, media documentation and reports.

Interviewees were selected through the "snowball sampling" method (Marsh and Stoker, 1995: 142). This method consists of asking interviewees "to nominate potential informants and the request is made at each subsequent interview" (ibid.). The objective is to obtain as great a diversity of informants as possible and heterogeneity of experience. A preliminary list of potential interviewees was drawn from secondary readings, participant observation and discussions with activists and officials. Initially, I strove for a balance between activists and officials in order to gain these participants' different perspectives. As interviews progressed it became apparent that these interviewees drew a distinction between activists that adopted a "reformist" approach and those that adopted a "radical" approach to their critiques of the MAI. This distinction was stressed by officials and radicals. I therefore also selected interviewees in order to obtain representative insights from these two categories of opponents.

Although the anti-MAI campaigns that took place in a significant number of OECD countries all contributed to undermine the MAI negotiations, the data focused on three countries: Canada, France and the United States. Several reasons motivated these choices. First, since the emphasis of the research was placed upon the transnational dimension of the opposition rather than on a comparative analysis between countries, these three countries provided ample data to research that aspect of the opposition.

Second, each of these countries' anti-MAI campaigns offered peculiarities pertinent to the MAI.

Canada and the United States were chosen because of these countries' previous experience with the North American Free Trade Agreement (NAFTA) and its social opposition. Not only were the investment provisions of the NAFTA similar to the MAI, but the opposition to that agreement proved significant to the subsequent MAI opposition. Also, the Internet campaign against the MAI, which gave the opposition its global impetus, emerged as a result of collaboration among activists from these two countries. As such, North American activists played a significant role in radicalizing a global opposition against the MAI and generating public information strategies that engendered grassroots opposition elsewhere. The U.S. was also included because of the relevance of that country's position for the success of any international agreement. France was chosen because of its eventual withdrawal from the negotiations that effectively terminated any hope of pursuing MAI negotiations at the OECD. In addition, with the OECD being located in Paris, bureaucrats and officials who were involved in the negotiations were located there and the transnational dimension of the opposition was most visible in that country. Nevertheless, in spite of the focus on these three countries, the broader dimension of the MAI opposition has been acknowledged and substantiated in the research.

Interviews in France provided a rich perspective on the diversity of actors among the more radical MAI opponents. In particular, although so-called "intellectuals-engagés" were present throughout the global networks, French opponents of the MAI stressed the

novelty and importance of these participants' contribution to the campaign. As my research in the field progressed it became apparent that activists who resided in countries other than the three main cases selected were also valuable informants as they were identified by others as having contributed to the transnational effort in a significant way. This diversity is reflected in the number of West European countries listed in Appendix C. For example, activists in the Netherlands had maintained the anti-MAI electronic listserv and they had participated in "teach-ins" in North America thereby encouraging similar collaboration and forms of activism in Europe. These roles provided them with a broader understanding of the various anti-MAI campaigns and groups' actions over time.

The official interviewees who were selected had played various roles during the MAI negotiations. As such, they also offered a rich diversity of perspectives on the events. Some had participated directly in the negotiations while others were involved indirectly through their role within a supranational organization such as the OECD, the European Parliament or the European Commission. This provided a useful balance of views between close observers of the negotiations and those who directly participated in them. Other officials, such as members of Parliaments, helped bring the MAI to their colleagues' attention through their contacts with MAI opponents. Since interviews of U.S. officials had been published as the negotiations progressed, and since these reflected the U.S. position, I relied on these for U.S. data.

Open interviews with individuals who had participated either in the MAI negotiations or in opposing them provided some data toward building the sequence of events that was required to answer the second question of the research regarding the

influence of MAI opponents. The data collected in this manner sought to establish causal evidence by retracing the chain of events that caused the demise of the negotiations. This data also proved useful to ascertain other types of objectives and influences that the MAI opponents may have sought and achieved. Evidence collected from interviews was supported with evidence collected from primary documents. These were OECD documents emanating from the negotiations, governmental archives and MAI opponents' records. Finally, secondary sources of evidence in the form of media reports that were published as events unfolded, and their subsequent analyses by analysts and participants further supported verbal accounts of these events. Thus the "process tracing" method relied upon to establish an answer to the second question of the research was corroborated by what historians refer to as "convergence of evidence."[4]

While the two first questions of the research are thus answered by adopting qualitative research methods, thick description and an interpretive understanding of the events surrounding the MAI negotiations, the third question of the research is answered by theory testing and the comparative method. In a first instance the third question is answered by undertaking what Van Evera (1997: 90) referred to as a "literature-assessing" endeavour. First, a summary and evaluation of existing theoretical and empirical literature of phenomena similar to the MAI opposition is undertaken. Then a comparison of the

---

[4] Van Evera (1997: 64) describes the process tracing method as follows: "the investigator explores the chain of events or the decision-making process by which initial case conditions are translated into case outcomes. The cause-effect link that connects independent variable and outcome is unwrapped and divided into smaller steps; then the investigator looks for observable evidence of each step." Given that one testimony or account would not be sufficient evidence of causality, historians rely upon what Shermer and Grobman (2000: 31-32) refer to as "convergence of evidence." This approach to history requires that "multiple inductions ... converge upon one another, independently but in conjunction."

MAI opposition to other similar cases is carried out in order to test certain hypotheses advanced by different theoretical frameworks.

Theoretical Frameworks

The first objective of the research—to provide an understanding of the MAI opponents—proved challenging and crucial to an accurate analysis of their influence and an understanding of their meaning for world politics. The challenge stemmed from the geographical spread of the MAI opposition and the united front presented by groups who, traditionally, espoused different causes and behaved differently. I needed a way to understand diverse self-references and mutual distinctions expressed by MAI opponents themselves.

Preliminary observations of MAI opponents in Canada seemed to indicate that a process of grassroots mobilization was under way. Also, early on in the research, some of the MAI opponents described themselves as participating in a broader and longer-term project, which, they hoped, would grow into a sustained opposition to economic globalization (defined in Chapter 2). However, secondary sources also revealed that less popular attempts at policy dialogue were also taking place. Yet, preliminary research seemed to indicate that in their struggle against the MAI these diverse groups displayed an unusual common front with common goals. In addition, MAI opponents campaigned at various levels. Some limited their actions to either the local, national, or transnational level whereas others were active at multiple levels. No single concept available in the literature on societal actors could accommodate this apparently simultaneous diversity and unity.

Given the self-description of some of these actors and my early observations, social movement theory provided a useful starting point and the conceptual tools with which to distinguish these actors from one another. The literature also draws distinctions between social movements and other societal actors. In addition analysts explore the domestic as well as the transnational aspects of social movements.

Furthermore, those MAI opponents who described themselves as participating in a broader project against economic globalization gained momentum with the anti-MAI campaign, and we have witnessed since then numerous protests that espouse such a theme. Indeed, starting with the Seattle protests against the World Trade Organization (WTO) in November-December, 1999, similar expressions of opposition against international economic policy-making processes and their policies have been manifest on a regular basis in various countries. The roots of these subsequent protests can be traced back to the anti-MAI campaigns of the MAI opponents who also opposed economic globalization. As such, social movement analysis was also useful in understanding the evolution of the latter opponents to the MAI, and what began as a heuristic tool based upon social actors' description of themselves became a theory confirming analysis.

As such, the distinction between this type of social opponent to the MAI and others is also relevant to our understanding of their meaning for world politics. The objectives sought by those opponents, when opposing the MAI, have persisted and they bring a new type of challenge to international economic relations worthy of further investigation. For that reason, the theoretical implications of the MAI opponents'

meaning for world politics that is undertaken in Section III focuses on those MAI opponents in particular.

In order to assess the significance of these societal actors for world politics—the third question raised in this research—I rely upon three theoretical frameworks. One concerns social movement theory's understanding of movements' influence on larger collectivities. The other two theoretical frameworks have been used to explain outcomes in world politics. Each of these helps to explain the meaning of these emergent anti-globalization movement networks for world politics. That undertaking enables me not only to evaluate the usefulness of these frameworks in providing an understanding of this phenomenon, but also to compare those MAI opponents to existing studies and thereby draw inferences on their future meaning for world politics.

First, I question whether the sustained opposition to economic globalization can be explained by Robert Cox's (1996: 514-519) historical dialectic framework. This aspect of the movement networks relates to these actors' evident opposition to international economic institutions and their policies and Cox's understanding of world orders. Historical dialectic "enquires into the social processes that create and transform forms of state and the state system itself" (ibid.) This approach is premised upon the idea that "society produces in its structure the antagonisms that lead to its modification" (Dahrendorf in Cox, 1996: 514). Such social processes were observed and conceptualized by Karl Polanyi and Antonio Gramsci earlier in this century, and Cox adopts these concepts in his framework.

Polanyi's (1957) dialectical interpretation of European economic and social history from the 19th century to the 1930s identified two "phases of movement" in that history. The first phase of movement consisted of the "introduction of the self-regulating market: what Polanyi saw as a utopian vision backed by the state. The second phase of movement was society's unplanned and unpredicted response of self-preservation against the disintegrating and alienating consequences of market-oriented behavior" Cox (1996: 515). Cox also applies Gramsci's concept of hegemony to contemporary international relations.[5] Gramsci developed the concept of "war of position" which consisted of "actively building a counter-hegemony within an established hegemony" through civil society. In Chapter 7, I apply this framework to the selected MAI opponents and question whether it enables us to explain the emergence of these societal actors. More specifically, are these movement networks counter-hegemonic and have they emerged for reasons similar to that of Polanyi's "second movement"?

While Cox's critical IR framework might enable us to understand the opposition to globalization as a response to a changing world order at the end of the 20th century, it does not enable us to empirically assess how these actors might be undertaking a war of position. This type of analysis has been undertaken by social movement analysts. These analysts have demonstrated the ideational and cultural influences of such collective action

---

[5] Hegemony here is used by applying "the Gramscian concept of hegemony to explain varying degrees of global, as well as domestic stability" (Gill and Law, 1988: 76). In that sense, "hegemony at the international level is thus not merely an order among states. It is an order with a world economy with a dominant mode of production which penetrates into all countries and links into other subordinate modes of production....World hegemony can be described as a social structure, an economic structure, and a political structure; and it cannot be simply one of these things but must be all three....[I]t is expressed in universal forms, institutions, and mechanisms which lay down general rules of behavior for states" (Cox, 1996: 137).

on societies at large. Indeed, one analyst has termed challenges posed by social movements as "excluded realities" to reflect the fact that these are typically "marginal to or excluded from mainstream society" (Lofland, 1996: 3). As such, that theoretical framework illuminates a dimension of the opponents to economic globalization that enables me to document counter hegemonic cultural and ideational challenges expressed by actors from the anti-globalization movement networks. In that sense, the framework provides analytical tools with which to analyse and empirically document the ways in which these societal actors may be conducting a war of position. We can therefore use social movement theory to complement Cox's framework.

If social movement analysis enables us to document the influence of the opponents of globalization on society, we must turn to another international relations framework to understand how such influences could affect world politics. That framework is referred to as social constructivist approaches to international relations or IR social constructivism. IR social constructivists seek to show how international reality is socially constructed. They argue that normative factors "shape [states'] interests, or their behaviour directly" (Ruggie, 1998*a*: 15). This type of influence takes place through a process of socialization. Socialization is a process through which actors internalize norms and the related behaviour that emanate from shared ideas in a particular society.[6] In doing so, actors become part of

---

[6] This perspective finds its roots in the so-called English school and Hedley Bull's (1977) understanding of the state system as a "society of states" (Ruggie, 1998*a*: 11; Risse et al., 1999: 11). This understanding of the state system is made with the caveat that not all states are considered part of this society and that it is the process of socialization that makes them so. As Risse et al. (1999: 11) worded it: "[c]ontrary to some conceptions of international society...this definition suggests that international society is a smaller groups than the total number of states in the international system, and that socialization is for actors to internalize norms, so that external pressure is no longer needed to ensure compliance."

a society that shares "collective understandings about appropriate behaviour" (Risse et al., 1999: 11). Processes of socialization may include the way in which "principled ideas ('beliefs about right and wrong held by individuals') become norms ('collective expectations about proper behaviour for a given identity')"(Jepperson, Wendt and Katzenstein 1996:54, in Risse et al., 1999: 11). A third societal influence in world politics takes place through "causal beliefs." Causal beliefs consist of agreements on cause-and-effect relationships of complex problems shared by epistemic communities— "a network of professionals with recognized expertise" (Haas, 1992: 3).

Empirical analyses undertaken within that framework have already demonstrated the relevance of such societal influences in world politics.[7] In chapter 7, I question whether the emergent transnational social movement networks against economic globalization can be understood as a phenomenon similar to those examined in IR social constructivist frameworks. I compare similar case studies to the selected MAI opponents and their genealogy. This enables me to assess how my case study relates to these other cases and thereby hypothesize their future relevance for world politics. Thus I apply these conceptual tools to ask whether opponents to economic globalization have already

---

[7] Thus Richard Price (1998: 613, 639) documented processes through which societal actors, motivated by principled beliefs, *taught* governments "what is appropriate to pursue in politics" by generating "an international norm prohibiting Anti Personnel (AP) land mines." Keck and Sikkink (1998) and Risse et al. (1999: 5) found societal actors active at the domestic and international levels within "transnational advocacy networks." These networks, they argued, were motivated by shared principled beliefs and succeeded in engendering domestic policy changes towards the protection of human rights in states where such abuses had taken place. By tracing how an epistemic community succeeded in placing services on the international trade agenda, Drake and Nicolaïdis (1992: 37) argued that communities of experts, motivated by principled and causal beliefs, caused states to redefine their interests.

affected or in what ways they are likely to affect world politics that pertain to the economy.

Summary of Findings and Chapter Outlines

Robert Cox's (1996) analytical focus on world orders reminds us that the historical context within which the MAI took place should be taken into consideration. Indeed, the term "globalization" has been widely used by officials and some MAI opponents when referring to these events. All these usages of the term refer to a particular juncture the world finds itself at, albeit with different interpretations of its consequences. For this reason my study of the MAI events begins by providing, in Chapter 2, a discussion of the intellectual and historical meanings of globalization. I argue that the intellectual and historical contexts within which the MAI negotiations were launched influenced these events.

Chapter 3 establishes the conceptual identification of various societal actors that influence policy making processes at the domestic and international levels. Given the detailed descriptions of actors' characteristics, a parsimonious model is suggested to facilitate the application of these conceptual distinctions to the case study. In Chapter 4, I apply the model to the case study to answer the first question of the research. I thereby draw a distinction between three main types of MAI opponents. The first type of MAI opponents, commonly called reformists, sought specific changes in the MAI text that reflected their membership's particular policy concerns. They pursued these objectives through lobbying and policy dialogue. A second type of actor, commonly called radicals, placed the MAI opposition within a longer-term project of resistance to what they believe

were perverse processes of economic globalization. Finally, the eventual merging of these MAI opponents resulted in a third type of actor in the form of a coalition that espoused one clear objective: to stop the OECD MAI.

Given these conceptual characteristics, MAI opponents conducted different types of campaigns that emerged at different moments during the MAI negotiations. For these reasons, Chapters 5 and 6 juxtapose these actors' respective campaigns with the progress of the negotiations in order to answer the second question of the research and trace their joint and respective influences (a summary of these chronologies is provided in Annex D). Direct influence—substantive changes in the MAI draft text—was obtained through direct contacts with the negotiators and/or as a result of domestic lobbying. However, indirect influence—gained through political pressure—was more significant relative to MAI opponents' objectives in that it contributed to the failure of the negotiations. The objectives and strategies associated with the latter result are typical of the anti-systemic stance adopted by social movements. Likewise, the spread of the opposition to the MAI into the streets of OECD capitals, which enhanced these actors' indirect influence, is also an outcome typical of movement networks' actions.

The answers to the first and third questions took a life of their own early on in the project since, shortly after I began the research and writing, more visible signs of opposition against international economic agreements manifested themselves. While the coalition struck between reformist and radical opponents of the MAI did not last, the networks developed among radicals during their anti-MAI campaign sustained their common objective of opposition and transnational links. Indeed in the fall of 1999, as I

was interviewing those MAI opponents, they were preparing for another campaign. Thus in November-December 1999, nine months after I began writing the introductory chapters of this study, protests took place in Seattle against the World Trade Organization. Since then, several similar occurrences have been reported around the world. For reasons elaborated upon in the subsequent chapters, we can now assert that that MAI opposition was not a unique and isolated case but the beginning of a socio-political phenomenon—now broadly referred to as "the anti-(corporate) globalization movement"—of interest to several areas of inquiry in political science.

For these reasons, I query, in Chapter 7, whether the sustained opposition to economic globalization is explained by Cox's framework and whether empirical studies conducted within IR social constructivist frameworks shed light on these MAI opponents. I argue that the contest over future(s) engendered by these societal actors is explained by Cox's historical dialectic approach as a resistance to a changing world order that displays growing tendencies toward unfettered *laissez faire* policies. However, to understand how these actors may achieve changes of a counter-hegemonic nature we must rely upon social movement analysis and IR constructivist conceptual tools.

CHAPTER II
THE MAI NEGOTIATIONS:
A THRESHOLD IN INTERNATIONAL ECONOMIC RELATIONS

Introduction

A report on the MAI and its social opposition, which was produced by the French Government in the fall of 1998, observed that the agreement had become a symbol of globalization that had crystallized the claims and frustrations surrounding that concept.[1] In order to understand the meaning of that observation, this chapter provides an explanation of two divergent understandings of *globalization*, the relationship between globalization and the MAI and the attendant frustrations and claims raised against that treaty. In the first section of this chapter, I provide an explanation of two divergent interpretations of globalization and their relevance to the MAI. In the second section, I argue that the historical context within which the MAI negotiations took place sheds light on the opposition to globalization and the MAI.

At its most controversial, globalization is synonymous with the progression toward a greater liberalisation of markets worldwide. This ideological aspect of globalization is associated "with the displacement of embedded liberalism by market liberalism, deregulation and privatization" (Skogstad, 2000: 808). It has therefore entered the academic and intellectual debates along a familiar divide between those in favour of increasingly freer global markets and those against them. The debate is particularly animated around the degree to which the state should be involved in the economy. These divergent understandings of globalization also reflect disagreements regarding the benefits and costs that may ensue from the current trend toward increased economic globalization.

---

[1] See "Rapport sur l'Accord multilatéral sur l'investissement (AMI)," by Catherine Lalumière and Jean-Pierre Landau on the French Government's web site www.finances.gouv.fr, p.3.

Thus in a first instance the "contest over future(s)" takes place within an intellectual context as debates that oppose what I refer to as globophiles and globophobes.

Nevertheless, this intellectual context is only part of the story. How and why the MAI as a policy symbolised globalization in a manner that generated growing social opposition represents the other pertinent aspect of the MAI events. I argue, in the second section of this chapter, that when understood as an economic phenomenon, globalization is associated with a series of international agreements deemed to foster its progress. In that sense, the MAI was the latest in a series of such agreements, and the concerns, claims and frustrations expressed by MAI opponents must be understood as a reaction to concrete and negative experiences with these agreements.

I. Contested World Views: The Intellectual Context of the MAI

While many take the integration of the world economy as their point of reference to define globalization, they differ in their assessments regarding the reasons for its occurrence and its potential benefits. *Globophiles'* view these developments as a natural and beneficial progression of market forces and technological progress. *Globophobes* view economic globalization as the result of powerful and influential commercial interests that yields numerous social, political and economic hardships. I will begin with a dominant version of the positive view and follow with a critical view of globalization.

Globophiles' Understanding of Globalization

The economic aspect of globalization is defined as: "the deepening integration of markets as a result of heightened trade and investment, and enhanced capital mobility" (Skogstad, 2000: 808). Globophiles usually point to the evidence in support of

globalization by referring to statistical indicators that reflect what they refer to as growing global economic integration. These statistical indicators show the increasing flows of goods, services and most importantly capital between countries.[2] Most significant to these observers has been the increase in investment flows relative to trade since the 1980s. Globophiles' interpretation of globalization is an optimistic one. As Hart (1997: 81) wrote : "[t]here is every reason to be optimistic about the benefits that will flow from globalization."

Increased integration of economies and greater investment flows are two related processes in that different inputs which are used to produce one good may originate in several countries. Thus Winham (1996: 640) provides the example of "the manufacture of a product in which components come from factories in various countries for final assembly in yet another country, while financing for various stages of the production process is raised in the capital markets of different countries." In that sense, one of the main type of agent of globalization is the Multinational Corporation (MNC). Thus Ostry (1997: 238) observes that the MNC is "the main agent of globalization and the agenda for deeper integration." That is, the MNC is considered to be the main agent linking countries' production apparatuses and key ingredients of their future economic growth

---

[2] See Julius (1994: 269); Winham and Grant (1998: 249); Winham (1996: 640, 641); Hart (1997: 79); Schwanen (1996); Ostry (1997: 239); Smythe (1998*b*: 255). As Winham (1996: 641) reported, a significant transformation in the globalized economy is reflected in "[foreign investment flows [which] increased by 30 per cent annually throughout the 1980s, about three times faster than the growth of world exports and four times faster than world gross national product." These statistics are found in yearly reports published by various international bodies such as the Frascati Manual from the Organization for Economic Cooperation and Development (OECD), the series of World Investment Report from the United Nations conference on Trade and Development (UNCTAD), and the International Trade Trends and Statistics from the World Trade Organization (WTO).

geared to the outside world (Schwanen, 1996: 3). This linkage takes place through MNCs' foreign direct investment (FDI) in host countries. As Hart (1996: 40) explains: "[m]ost FDI today originates with [MNCs], involves large sums of money and the exercise of control, and is often part of a larger multinational global strategy."

For these reasons, globophiles interpret the increasing global economic integration not only as an evolutionary process which can be attributed to the success of international policy efforts to keep markets open, but also as the natural evolution of commercial activities due to the technological changes which have transformed communications, transportation and information (Hart, 1997: 80; Ostry, 1997; Winham, 1999: 11; Schwanen, 1996: 3). As Witherell (1996: 19) has explained, "[m]odern communications and financial integration have strengthened the tendency for international companies to operate on a regional or even global basis."

The concern is that this increased *de facto* integration via investments, albeit welcome, has not been addressed in multilateral fora in a comprehensive enough manner. Although the past Uruguay Round of trade negotiations reflected these global economic changes in that it deepened the rules-based international trade policy regime (Winham, 1999: 13), these were widely deemed insufficient to further investment flows globally.[3]

---

[3] According to trade policy analysts, the codes and instruments at the OECD that were mentioned in the previous chapter (see note number 2) are too weak. The Code on Liberalization of Capital Movements and the Code on Liberalization of Current Invisible Operations contain obligations that are binding in principle but weak in reality, while the National treatment Instrument is not binding even in principle (Graham and Sauvé, 1996: 102, 103). The OECD Declaration on International Investment and Multinational Enterprise "has the force of moral suasion and little more" (Hart, 1996: 60). Agreements at the international level are also considered unsatisfactory. These are the agreements which came into effect with the formal establishment of the World Trade Organization (WTO) January 1, 1995. The General Agreement on Trade in Services (GATS), the Trade-Related Investment Measures (TRIMS), are considered limited in terms of their coverage of investments (Hart, 1996: 70; Graham and Sauvé, 1996: 103; Whitherell, 1996: 20). In addition, it is estimated that over 600 bilateral investment treaties (BITs) are in effect. The number of agreements alone is

Globophiles find that, not only is there a confusing quilt of instruments, but they argue that there still exist investment barriers, and that foreign investors encounter discriminatory treatment and uncertainties. As a result, it is argued that the current situation helps "to distort the pattern of FDI flow and complicate[s] corporate activity which is increasingly global in strategy" (Witherell, 1996: 20, 21).

Therefore, globophiles share the view that the next logical step to the *de facto* economic globalization is the complementing of the trade regime with a multilateral investment regime (OECD, 1996*a*: 9; Smith, 1995: 103; Hart, 1996: 94). Underpinning this view is the belief that in the same way that the existing trade regime has fostered economic growth and development and has brought benefits to societies who have engaged in it, so too an investment regime such as that fostered by a MAI would have similar benefits. Such a course of action is perceived to be the most beneficial direction to follow in that "[j]ust as a country's standard of living improves as a result of both exports and imports in an open trade regime" there are "net advantages for both capital-exporting and capital-importing countries" (Schwanen, 1996: 3). These were the arguments espoused by the OECD which justified the negotiations for a MAI (Smythe, 1998*b*: 255; OECD, 1995*a*; OECD, 1996*a*).[4]

---

considered to be an undesirable patchwork of multiple and overlapping instruments. It is at the regional level that agreements containing comprehensive and binding rules are found. These are the European Union which has become a "full-fledged economic union" (Hart, 1996: 67), and Chapter 11 of the North American Free Trade Agreement (NAFTA). The investment chapter of the NAFTA was often referred to as a model upon which the MAI should be designed.

[4] Evidently, more arcane and complex arguments regarding various aspects of investments are involved in the conception of such a complex agreement. The gist of the rationale for a MAI however consisted of these main points. The most serious disagreement among those who called for a MAI was whether to negotiate it at the OECD or the WTO level. The disagreement revolved around the expediency and certainty of the OECD versus the inclusiveness of the South in particular that is inherent in the WTO (see

Globophobes' Critiques of Globalization[5]

Globophobes also take as their point of reference for globalization the transformation of the global economy. However, this critical view of globalization does not see its progression as a benign outcome attributed to the success of international commercial relations or technological changes. In general, globophobes present globalization as a phenomenon run amok, or at best one driven by particular interests, political manoeuvring and ideology.[6] The role of MNCs is understood as one of powerful global actors pushing a neo-liberal ideology because it serves their interests at the expense of those of ordinary citizens, and in which the governments of nation-states have become complicit. Critical theorists in international relations refer to the process of globalization as a structural change reflecting a move toward a posthegemonic world order and a

---

Graham and Sauvé, 1996: 105-108; Smythe, 1998*a*; Winham and Grant, 1997: 256; Hart, 1995: 9).

[5] This category is similar to that identified by David Held and Anthony McGrew (2001) as "hyperglobalists." It is not my intention to imply by this label that these critics of globalization suffer from some form of phobia. In fact, they are not opposed to all forms of globalization but rather, as will be explained in this section, they object to some of the negative impacts they observe as being linked to economic globalization.

[6] For such explanations of globalization and its consequences see Strange's (1986) argument on "casino capitalism"; Helleiner's (1994: 172, 173) analysis of the demise of Bretton Woods; Cerny's (1995) assessment of the impact of globalization on states' ability to provide public goods and the ensuing changes on democracy and collective action patterns; Barber's (1995) argument regarding the negative and mutually reinforcing impacts of globalization in terms of *Jihad vs. McWorlds*; McQuaig's (1998) understanding of the push to further economic globalization as a "cult of impotence"; Reich's (1991) critique of the growing inability or willingness of societies to provide for their weakest members as a result of globalization; Sjolander's (1996) explanation of the term globalization as an ideologically loaded agenda with negative and polarizing social consequences; Held's (1995) assessment of the impact of globalization on democracy. In addition to these, critical theorists in International Relations have produced a number of studies on globalization that examine its causes and consequences (see for example Mittelman *et al.*, 1997; Cox, 1996, 1999; Gill, 1997, 2000). This list is by no means exhaustive since studies on globalization have been published at an increasing rate over the past decade. Thus in his "feature review" article titled "Globalization: from domination to resistance" Kiely (2000: 1059-1070) reviews no less than ten books on globalization that were published between 1997 and 2000.

"system lacking the staying power of effective means of regulation" (Mittelman, 1997: 231).

Rather than seeing globalization as a *de facto* outcome, the benefits of which need to be harnessed (Schwanen, 1996: 2-6), globophobes "draw conclusions about globalization as a political and social phenomenon" (Sjolander, 1996: 603) and thereby interpret globalization in a more comprehensive manner. Rather than seeing globalization in terms of a natural progression which necessitates a response such as a MAI, globophobes perceive that governments are losing control over a globalizing economy which they now are facilitating to their own detriment.[7] Various aspects of this theme have been developed in academic literature.

Two main areas of concern regarding the *political repercussions of globalization* are the issue of the erosion of nation-states' policy autonomy in the globalized world and the resulting erosion of citizenship rights. At the centre of this erosion of autonomy argument is the understanding that the role that nation-states had assumed vis-à-vis the economy since World War II has been drastically eroded by globalization. The erosion of the powers of the welfare state, which were based upon Keynesian economic management, is attributed in part to globalization (Held, 1995: 131; Giddens, 1998: 31).[8] Among the culprits constraining the ability of nation states to follow such policies in an era of

---

[7] For example Mittelman (1997: 7) writes: "[t]he scope for state autonomy...is reduced in the context of economic globalization....the state no longer primarily initiates action in, but rather reacts to, worldwide economic forces. To realize material gain from globalization, the state increasingly facilitates this process, acting as its agent."

[8] Keynesian economic management was based upon John Maynard Keynes' *General Theory of Employment, Interest and Money*, that provided for government spending and taxing powers to restore the economy to full employment (James, 1991: 49). Keynes developed his *General Theory* in response to the severe and prolonged unemployment during the Great Depression of the late 1920s and 1930s. Note that for Keynes the interventionist welfare state needed to be protected from capital flows in order to maintain such policies.

globalization is the absence of capital controls and the operations of the world financial markets. The consequences of such capital mobility, Rodrik (1997: 6) explains, is that it diminishes the tax base of governments forcing them to increase "the tax rate disproportionately on labour income." These outcomes have also undermined the ability of the state to shield its domestic economy, and its citizens, from the external pressure of the market (Cox, 1996: 27). As Held (1995: 135) summarizes:

> [T]he operation of the states in an ever more complex international system both limits their autonomy (in some spheres radically) and impinges increasingly upon their sovereignty.

The effect of globalization on democracy is linked in part to the above-noted erosion of macroeconomic autonomy of states. The multiplication of regimes and international organizations that now manage whole areas of transnational activity such as economic relations is questioned. The most glaring example of such devolution of sovereignty cited is the European Union where the idea of "democratic deficit" emerged.[9] Criticizing various international economic arrangements such as the North American Free Trade Agreement (NAFTA), the Maastricht Treaty and the GATT, in particular, Gill (1997: 216) writes: "[t]hese arrangements are designed to supplement market discipline with binding constraints or 'rules' in ways that might prevent elected politicians from using a wide range of policies to defend national or local interests." Examples given are the GATT under which states are not permitted to block the entry of products which are

---

[9] See for example, *The Crisis of Representation in Europe*, edited by Jack Hayward (1995). Several articles in the book explain the issues surrounding this concept and the reasons for its emergence. The main critique of European Integration is that an increasing number of government functions are being undertaken exclusively or concurrently by the European Commission and the European Union. The fear is that if too many areas such as trade and the environment, for example, come under these jurisdictions, decision-making no longer resides in states and their elected parliaments (Weiler et al., ibid. pp. 4-9).

produced in ways that are contrary to domestic norms in areas such as workplace practices, legal rules and social safety nets (Rodrik, 1997: 5). However, and as Rodrik (ibid.) also observes, "people attach values to [production] processes." This is the way in which the loss of democracy is mostly criticized.

Flowing from these consequences of globalization is the view that the ability of citizens to collectively make choices on how they live together is eroding. That is, the demise of the welfare state, and the perceived inability of governments to protect their citizens from the external pressures of the market are identified as an erosion of responsible citizenship. This state of affairs, as observed in the United States, leads Reich (1991: 303) to ask the question: "[w]hat do we owe one another as members of the same society who no longer inhabit the same economy?" This question reveals concerns over the social consequences of globalization.

The *social consequences of globalization* consist of several issues in the area encapsulated in the term "social cohesion." Social cohesion "implies the capacity to live together in some harmony and a sense of mutual commitment among citizens of different social or economic circumstances" (Canada, Senate Committee on Social Affairs: 1999:5).[10] As the Canadian Senate report from which this quote is taken observed, globophiles do not refer to the idea of social cohesion. In contrast, globophobes point out that over the past two decades economic priorities have dominated governments' agendas at the expense of social considerations and that the result has been "social corrosion and

---

[10] That Senate report (1999: 6) provides definitions of social cohesion from other countries which are different wordings of the same idea.

fragmentation" (ibid.). For Rodrik (1997: 7), social disintegration is attributed to "the tension between the global market and social stability." These tensions are attributed to the economic challenges confronting the nation state that were described in the preceding paragraphs.

The consequences of these tensions vary. Most identify a decrease in public investments, an increasing polarization of income and wealth resulting in the erosion of the middle class, a reduction of the average real annual earning, a "casualisation" of the labour market and the attendant increase in the rate of involuntary part-time employment, and an increase in the incidence of poverty. Sjolander (1996: 609-616) sums up the predominant view from this literature that globalization creates not only polarization internationally but, increasingly, domestically as well. Among the domestic processes of polarization she mentions not only "the squeezing (out) of the middle class," but also "[t]he construction of 'the other' who can be compromised by the exigencies of globalization."

MNCs are clearly situated at the centre of these processes in that they have become a key determinant in terms of levels of domestic employment through their decisions regarding their investments and the location of their facilities. As a result, unskilled and semiskilled workers are vulnerable to out sourcing, a practice facilitated by reduced barriers to trade and investment (Rodrik, 1997: 4).[11] At the international level there also exists a construction of the foreign national worker as the "other" who is

[11] Rodrik (1997: 4, note) defines the practice of out sourcing as "companies' practice of subcontracting part of the production process—typically the most labor-intensive and least skill-intensive parts—to firms in other countries with lower costs."

assumed to be able to sustain the harsh economic conditions imposed by the exigencies of globalization (ibid.).

Symptoms of this social fragmentation which appear in this literature range from the resurgence of nationalism or ethnic identity (Giddens, 1998: 31, 32; Barber, 1995; Cox, 1997: 27) to the collapse of democratic society (Soros, 1997).[12] In a similar vein, Barber (1995) argues that subnational factions emerge as a reaction against processes of uniformization and integration inherent in globalization. He warns that both globalization (McWorlds) and ethnic affirmations (Jihads) are undemocratic processes.[13]

Nevertheless, critical IR theorists also contemplate the possibility that globalization may provoke the emergence of social forces at the domestic and international levels that will come to challenge the neoliberal global order. The possibility of social forces repeating Polanyi's "double movement" has been suggested. As Mittelman (1997: 3) has expressed it:

> Perhaps similar to the global economy of the 1930s, the contemporary globalization process appears to be approaching a conjuncture in which renewed liberal-economic structures will generate large-scale disruptions as well as sustained pressure of self-protection.

---

[12] George Soros (1997: 45), a major global financier who has benefitted from the lack of controls on capital flows wrote: "Although I have made a fortune in the financial markets, I now fear that the untrammeled intensification of laissez-faire capitalism and the spread of market values into all areas of life is endangering our open and democratic society." Soros has since published a book which expands on this article published in the *Atlantic Monthly*. The book is titled *The Crisis of Capitalism: Open Global Society Endangered.*

[13] "Our new tribes are murderous and fanatical but small-minded and defensive: trying to secure islands of parochial brotherhood in a sea that relentlessly leaches away essence and washes away fraternal bonds" (Barber, 1995: 165).

As mentioned in the previous chapter a related hypothesis of this theoretical framework concerns the emergence of counter-hegemonic forces. These hypotheses will be assessed in terms of the movement networks opposing globalization.

Globophiles and globophobes understand economic globalization as a phenomenon linked to the increased flow of investments globally and agree on the importance of MNCs in that process. They also link international economic agreements to this process. Thus the MAI, an international economic agreement aiming to further free the flow of investments globally is clearly considered to be a component of globalization albeit with divergent assessments of its potential benefits. However, while these debates have been the object of heated exchanges among the initiated for some time, why did the MAI—an arcane investment treaty—generate public opposition that was also linked to globalization?

II. From Contested World Views to Contested Future(s)

Historical Perspective

Some of the debates between globophiles' and globophobes' understandings of globalization are not new. As the following brief history of debates regarding investment liberalization over the past fifty years will illustrate, the desirability of allowing investments to flow freely between countries has long been disputed. What is new is that some of these debates have now entered into broad public discourse. Nowhere is this more apparent than in the events surrounding the MAI. How this occurred and what the repercussions will mean for world politics are the subjects of the subsequent chapters. This section suggests why the MAI's historical context triggered that reaction. I argue

that the MAI represented a concrete instance of globalization, and much of the controversies that it generated had to do with the perception of the impact that globalization and the agreement would have on the autonomy of nation-states in policy-making, and consequently, its negative impact on the democratic expression of their citizens' collective will.

By the time the MAI negotiations took place, there had been a growing awareness within civil society that an increasing number of recently ratified international economic agreements entrenched international economic commitments which have irreversible impacts on a wide range of domestic policies. The MAI draft was understood to have similar if not wider implications for domestic policy-making. As the following brief history illustrates, this threat to governments' autonomy over domestic policies is at the core of the disagreements surrounding the MAI and globalization.

Calls for freer and safer flows of investments can be traced as far back as the 1940s. Since then, the issue of capital flows has been the subject of much debate. As Goodman and Pauly (1993: 50) have observed: "[t]he movement of capital across borders has long raised sensitive political questions. Whatever the benefits, international investment complicates national economic management." These issues are reflected in the Bretton Woods negotiations which took place at the end of World War II and also in Northern industrialized states' relations with the newly independent states in the South. The concerns have been normative and political. The early Northern normative debates revolved around the role of the state in the economy and in particular its role as an interventionist welfare state. Thus the intellectual fathers of the Bretton Woods

institutions and the GATT, British negotiator John Maynard Keynes and his American counterpart Harry Dexter White, "argued that international movements of capital could not be allowed to disrupt the policy autonomy of the new interventionist welfare state" (Helleiner, 1994: 33). For Keynes, the interventionist welfare state needed to be protected from capital flows in order to maintain policies that would stimulate economic activity and employment through government spending.[14]

The events of the interwar period influenced the postwar economic arrangements. The almost universal demands for social protection on the one hand, and the recognition of the benefits of international economic multilateralism on the other, meant that there was a need to strike a "balance between 'market' and 'authority,' with governments assuming much more direct responsibility for domestic social security and economic stability" (Ruggie, 1998*a*: 69). The latter became a legitimate normative objective among industrialized countries where the difference concerned only the form and depth of state intervention. Ruggie (1982) referred to this instance of collective intentionality as "embedded liberalism." In such an arrangement it was expected that greater international openness would be "coupled with measures designed to cushion the domestic economy from external disruptions" (Ruggie, 1998*a*: 78). This interpretation of the post-World War II economic arrangements reflects a social constructivist understanding of the relevance of norms shared among a society of states and the ways in which such norms influence their behaviour.

---

[14] As already mentioned, Keynes' reasoning for the necessity of an interventionist welfare state was grounded in his understanding of the severe and prolonged unemployment during the Great Depression of the late 1920s and early 1930s (James, 1991: 498).

The efforts of Southern states to limit foreign inflows of capital reflected beliefs that an interventionist state was beneficial to economic development and fears for their newly acquired sovereignty. Development theory and practice in the South have been pulled between two views. One encouraged less government and more market-led economic development, while the other saw a greater role for governments to protect developing economies from global markets. The concerns of Southern states also reflected their keen interest in retaining their only newly won self-determination. Up until the 1980s, foreign direct investment (FDI) brought by MNCs was regarded suspiciously in that these wealthy corporations, backed at times by powerful Northern states, were perceived to be too powerful economically and politically.[15] Although the Southern debt crisis of the 1970s and its 1980s "solutions" of structural adjustment programs[16] compelled Southern economies to open up to foreign investors, and change some of these positions, a core group of Southern states still retains reservations regarding full liberalization of capital flows.[17]

---

[15] For a summary of the arguments and the literature see Spero and Hart (1997: 249-275).

[16] Structural adjustment policies consisted of "domestic austerity programs," in the form of "market-oriented structural changes" that were expected to lead to a "growth in output and exports." Policies aimed at encouraging "trade liberalization...[and] financial liberalization such as improved access to foreign direct investment; deregulation...; privatization of state-owned industries" (Spero and Hart, 1997: 189, 192).

[17] See Smythe (1998*a*) regarding Southern resistance to the inclusion of investment rules in the Uruguay Round. The comments made by India's Minister of State for Commerce as late as 1997 are illustrative of that opposition: "The fundamental issue which one needs to face squarely in addressing this subject [of foreign direct investment] is whether the present system of nation States, under which each country is free to pursue its own national development strategy and to decide about the role to be played by FDI in achieving various development goals, is compatible at all with a multilateral investment framework" (Ramaiah, 1997: 118).

Several key events combined to change these views. Space prevents an in-depth review of these events and their numerous interpretations.[18] Suffice it to say that by the 1990s domestic policy changes had contributed to a much more positive political and economic global disposition toward the liberalisation of domestic markets. Furthermore, the immediate post-Cold War period was marked by the ratifications of several international economic agreements of significance. In Europe the Maastricht Treaty, which provided for the establishment of a full Economic and Monetary Union, was signed in February 1992. In North America, the North American Free Trade Agreement (NAFTA) between Canada, the United States and Mexico, which entered into force on January 1, 1994, would also foster increasingly freer markets between the three countries. That agreement contained an unprecedented investment agreement with dispute resolution mechanisms. Finally, in January 1995, the World Trade Organization replaced the GATT with an organizational presence, the resources to further develop the multilateral trading system and the legal status for the resolution of trade disputes. While these three agreements do not represent an exhaustive list, in terms of the ongoing efforts at liberalizing the flows of goods, services and investments undertaken since the end of World War II, they represented giant forward steps.

---

[18] Different interpretations of the reasons for these transformations reflect the dichotomous intellectual positions described in the previous section. Note also that as Cohen (1996: 273) observed: "[t]he discord...is significant insofar as the past may be assumed to have some impact on the course of events in the future." The changes included: the restoration of currencies convertibility in industrial countries; the emergence of Eurocurrencies beginning in the 1950s; "[t]he disintegration in the early 1970s of the Bretton Woods system of pegged exchange rates" (Goodman and Pauly, 1993); the dramatic erosion of capital controls in advanced industrialized states beginning with Britain in 1979; and, as just mentioned the 1970s' debt crisis in the South and its solutions implemented in the 1990s. For a good discussion of the different interpretations see Benjamin J. Cohen, "Phoenix Risen: The Resurrection of Global Finance."

Nevertheless, the investment provisions which emanated from the Uruguay Round were not deemed satisfactory to some. Issues related to investments were to be addressed, albeit in a limited manner, through the General Agreement on Trade in Services (GATs) and the Trade-Related Investment Measures (TRIMs). Early on, however, Brazil and India led the opposition to the inclusion of investments in the Uruguary Round of negotiations. In the midst of the difficulties encountered in these negotiations and given the limited coverage that these two agreements were to provide, the United States began to pressure the OECD for "a comprehensive, binding investment treaty with high standards of liberalization, protection of investors, and a dispute resolution process" (Smythe, 1998*b*: 242). Starting in 1991, technical and analytical work was undertaken by "independent governmental experts" at the OECD in order "to explore the major issues" of such an agreement (OECD, 1996*a*: 13). Between that time and the beginning of the MAI negotiations four years later the three agreements just mentioned were ratified.

Contesting Globalization

These international economic arrangements were met with various degrees of enthusiasm by civil society in these countries, and the MAI negotiations were initiated in that context. Between the late 1980s and 1995 when the MAI was launched, awareness of these liberalizing instruments, from the impact of the structural adjustment policies implemented in the South under the guidance of the World Bank and the IMF, to the controversial outcomes of a growing number of disputes settled under the WTO, and the

budget cutbacks implemented in most Western democracies[19], an increasing level of discomfort was slowly mounting among various segments of civil society.

Development organizations became increasingly critical of the impact that structural adjustment programs were having on Southern States and in particular on the most vulnerable segments of their populations.[20] In addition, the debt load of these countries did not seem to diminish. With regard to the WTO, NGOs had already exercised pressure in order to be included in that international economic forum, claiming that "the rights of citizens and civil society have been infringed by GATT/WTO rules, and that certain interest groups have been able to exercise a disproportionate influence" (Marceau and Pedersen, 1999: 6). Furthermore, as the newly instituted dispute settlement process was resorted to, North American environmentalists became increasingly disillusioned with the ways in which this process dealt with their domestic environmental laws. In Europe, the Maastricht Treaty was also received with skepticism, at times by entire countries, at others by particular groups who felt that integration had gone too far. The NAFTA had caused enough opposition that two side agreements had been added to the commercial agreement in order to appease the opposition from labour and environmental groups. As a result of these campaigns, several groups in various countries had begun to unite and direct their efforts against the WTO. These efforts were mostly divided along thematic lines of advocacy such as environment, labour and development,

---

[19] In France, for example, these cutbacks were undertaken to bring the country into the Economic Monetary Union.

[20] For a critique of structural adjustment programs see Veltmeyer, Petras and Vieux *Neoliberalism and Class Conflict in Latin America*, chapter 4.

although in North America the NAFTA opposition had already seen cross-border and cross-thematic coalitions.

The MAI only added fuel to these incipient and disparate objections regarding the neo-liberal direction taken in international economic policy-making. The MAI transformed these regionalised oppositions by uniting all under one objective: to stop the negotiations. Furthermore, an increasingly unified opposition against globalization evolved into global networks. Although the MAI was only at the draft stage, civil society groups that secured an early copy of the document viewed it as a policy initiative with much more far reaching implications for domestic policy than any of the existing multilateral agreements they had challenged to date. Many of the concerns they expressed regarding the MAI echoed the historical and intellectual debates regarding the liberalisation of capital flows. The MAI also became a platform from which to criticize the ongoing process of globalization in terms of democratic deficits, and a process that served the interests of large and powerful MNCs. Eventually, these concerns had an impact not only on OECD members' publics but also on politicians.

Having been excluded from any consultation with the OECD when the research on the MAI began at the OECD in the early 1990s, while representatives of business groups had had such an opportunity, lent credibility to the latter NGO argument. A provision in the MAI draft for settling disputes by which MNCs were allowed to sue governments further supported the argument and also raised concerns over sovereignty and legislative

autonomy of states.[21] Among these, it was argued that the MAI would have a "chilling effect" on governments when considering new domestic policies, be they concerning the environment, health, education, social programs or culture.

The approach that was followed to negotiate the agreement, widely known as "top down" approach, also raised concerns regarding the future legislative capabilities of states. The approach was different from that adopted under the GATT or the WTO in that rather than offering lists of economic activities to be negotiated, "all aspects of [a country's] economy [would be] considered unless specifically excepted" from the treaty at the time of signature (Government of British Columbia, 1998: 44). The MAI opponents' argument was that the top-down approach made it much more likely that governments would unintentionally omit present and future measures they might wish to record as reservations to the obligations of the treaty, thereby further curtailing their legislative prerogatives.[22]

By all accounts, the MAI was a complex, technical and arcane agreement which went further than any existing international commercial agreement and covered as many

---

[21] Under this procedure, called investor-state dispute mechanism and which is the same as that of the NAFTA, a foreign investor can challenge a government measure or regulation that is alleged to breach the treaty. As such, governments consent, by signing the treaty, to submit to an international arbitration panel. The hearings of these panels are confidential and closed to the public, and the panels have binding authority to award monetary compensation. It was argued in various domestic venues that this provision would effectively give MNCs and international legal status equal to that of states (see Government of British Columbia, 1998: Lalumière and Landau, 1998).

[22] In a letter addressed to the Council of Canadians in November of 1997, a Canadian international trade lawyer, Barry Appleton, revealed the potential sources of error such as the fact that as at the time at which his letter was written, Canada had not listed such reservations (this was explained by the fact that that process had not yet begun). Thus he argued in his letter:

> Canada's proposed reservation to protect social services such as health and public education is inadequate to permit provincial governments to continue to provide these services without compensating affected foreign investors and governments....Canada has not proposed any reservations to the MAI to permit it to take measures to protect or conserve the Canadian environment. Thus, the MAI could reduce the financial capacity of governments to freely engage in these activities (Appleton, 1997: 1, 2).

countries as represented by the OECD membership (Lalumière and Landau, 1998: 3, 4). The few issues mentioned here involved complex legal arguments of international law, the implications of which, in terms of domestic law, are beyond the grasp of any superficial perusal by an expert, let alone a layperson. The fact that these issues came to public light thanks to NGOs rendered them all the more explosive and the negotiation process all the more suspect.

The Lalumière and Landau (1998: 4) report observes that none of the technicalities outlined above, nor their implications for the domestic policy-making process were brought to the attention of the national Ministers concerned.[23] The report points out that all the communiqués submitted for executive approval had done was to "repeat the same broad statements yearly" (p. 4, translation mine).[24] The report concludes on this matter that "it was a grave error to have treated the negotiations as a purely technical matter" (p. 4, translation mine) in that it spread the notion that the negotiations were secretive, even illicit. In the end this approach back-fired. Not only were politicians shown as either irresponsible or incapable of understanding an agreement that would undermine their legitimate right to legislate, but it was also observed that neither the Ministers responsible for specific portfolios nor their departments had been informed of an agreement that would affect their responsibilities.

---

[23] It is important to note that the authors of this report interviewed several ministers from the French government as well as officials at the European Parliament and the European Commission (see pp. 12 and 16 of the report).

[24] The progress of negotiations was communicated and submitted for political approval at the annual OECD ministers' meetings.

For these reasons, and as was observed in the Lalumière and Landau report (1998: 2, 3), civil society saw the MAI as a symbol of globalization with all its feared ill-effects. The Pandora's box of globalization was opened by the MAI as its main agents—the MNCs—and its main economic channel—the liberalization of investments—were perceived to be given increasingly free reign by this novel agreement, at the expense of citizen's rights.

Many agree with the assessment made in the French report that the breadth, speed and vociferousness of the opposition was unexpected. This public opposition was novel in several other ways: (i) it appeared simultaneously in several countries, (ii) the claims expressed by the opponents went beyond those traditionally made by various sectors of the domestic economy during multilateral trade negotiations, (iii) the MAI opposition was made up of new actors represented by the NGOs, (iv) for the first time the process of multilateral economic negotiations was being widely questioned and opposed, and finally (v) the effective use of the Internet. For these reasons, the Lalumière and Landau report (1998: 3) concludes that the MAI represented a threshold in economic relations in that the intervention from this "global civil society" was probably "irreversible." Likewise, at the conclusion of the October 21, 1998 OECD meeting on the MAI, OECD deputy director general Joanna Shelton observed that "[t]oday's meeting also made it clear that we are not engaged in business as usual, and the we must address the concerns that have been raised about the scope and direction of the efforts to date" (*Inside U.S. Trade*, October 23, 1998: 7).

Conclusion

The MAI must be understood as a symbol of economic globalization and its concomitant policies which raise controversial issues of sovereignty and democracy. In as much as the MAI represented yet another international policy aimed at fostering global liberalization of markets it symbolized globalization. The nature of the agreement touched upon core issues raised by the liberalization of investments. These have been issues of considerable debate since the end of World War II. The content and nature of the MAI re-opened debates about sovereignty, regulatory autonomy of states and the power of MNCs. That is, the MAI challenged existing norms understood to be just and appropriate concerning behaviour among a society of states and between these states and their societies.

A constructivist understanding of international economic relations over the past fifty years highlights the ways in which world economic relations have been "socially constructed." The debates and protests against globalization can be better understood when seen in this light. What has become evident since the MAI is that, in the post-Cold War era, two broad, competing perspectives have come to the fore. Whereas these two world views have been at loggerhead in various fora over the past fifty years, the international political tensions between East and West helped to overshadow them. That is, the Cold War shifted collective attention to two more clearly defined alternatives of social, political and economic organizations: the communist and the the liberal democratic systems respectively. While the communist world view was being implemented with a completely planned economy and society, the "embedded" liberal democratic world

displayed various version of capitalism, some of which allowed a greater role for governments than others.

What has emerged since the end of the Cold War is a debate around these versions of capitalism. Since the end of the Cold War, the struggles over ideas about the ideal social, political and economic organization have moved to a debate between a view that condones an extreme implementation of laissez-faire policies with the least possible government interference with markets, and another which reflects a desire to pursue the various versions of capitalisms implemented during the Cold War. These have now come out in the open because the former has come to supersede that latter. The way in which this ascendance has been most visible since the early 1990s has been through the proliferation of international economic arrangements that increasingly encroach on governments' legislative autonomy. These have become symbols of globalization and the MAI was the latest in a series of such agreements.

The difference between the former negotiations and the attempts to negotiate the MAI is that the latter opened a public debate on the desirability of furthering the ongoing processes of economic globalization. The chapters in Sections II and III explain how this came about and what the implications of such an outcome represent for world politics. The next and last chapter of this section provides an conceptual framework with which to understand the various civil society actors involved in the opposition to the MAI and globalization.

CHAPTER III
MAPPING SOCIAL ACTORS:
A HEURISTIC TOOL FOR CAMPAIGN ANALYSIS

Introduction

The purpose of this chapter is to provide a comprehensive conceptual model of societal actors and their relationship to domestic and international policy making processes. The model developed herein will be applied subsequently to the MAI opponents and their campaigns. Several considerations motivate this undertaking. One is the multiplicity of concepts available in various literatures on collective action and civil society. A clear taxonomy at the outset will avoid the confusion which ensues from using different terms interchangeably. This becomes an even more compelling necessity when faced with the task of analyzing a complex coalition such as the transnational social opposition to the MAI. The model becomes a useful tool of analysis in that it offers a parsimonious map upon which MAI opponents can be placed, thereby providing a tool with which to decipher actors from one another along with their respective roles, campaigns, effectiveness and meanings for world politics.

The complexity of the apparently unified opposition to the MAI also stemmed from the various levels of political and social organization within which MAI opponents were active. As has been widely observed, societal actors no longer limit their efforts to influencing domestic policy and/or society. Increasingly over the past decades, we have witnessed the involvement of all types of non-state actors at the transnational level. Thus some MAI opponents interacted with the domestic policy-making process as well as supranational institutions such as the European Parliament, the European Commission and the Organization for Economic Cooperation and Development (OECD). Other opponents' efforts were directed at raising broader public awareness at the domestic level

as well as abroad. Since actors active at the transnational level displayed characteristics similar to those at the domestic levels, I extend the domestic typology of societal actors to the transnational level.

In particular, the model draws a distinction between two main types of societal actors which are encapsulated by the concepts of "interest group system of action" and "social movement system of action." The conceptual distinctions drawn in this chapter are verified by the case study. They hold significance for the susbsequent analysis of the anti-MAI campaigns and the growth of social movement networks that oppose economic globalization.

I begin the description of the model with a discussion of a most contested concept: civil society. That discussion introduces the basic structure of the model. I then discuss the distinctions drawn in the model between different types of actors within domestic civil society. The model intends to accommodate several conceptualizations of associational life. This is illustrated by three categories of action systems. The three categories are compared according to four main criteria. I then extend these typologies to the transnational level and highlight where they apply to the MAI opponents. Section II builds upon this chapter by applying the model to the MAI opponents and their respective campaigns.

I. A Model of Domestic Civil Society as a Heuristic Tool of Analysis

Civil Society: a contested concept

Civil society has emerged as a contested concept that reflects various biases on the part of analysts. Thus Cox (1999: 10) observed that at the end of the 20th century "[t]he

concept has been appropriated by those who foresee an emancipatory role for civil society." My objective in devising a model of societal actors is neither to engage in a protracted debate over the term civil society, nor to insist that my usage implies particular intentions on the part of societal actors. Rather, the model devised herein is intended to distinguish between various types of civil society actors and their interactions with domestic and international policy making processes. This means that no single conceptualization of collective action is collapsed with or substituted for the concept of civil society.

This means that various *types of collective action* are considered to be taking place within civil society simultaneously, and these can be differentiated from one another. As such, this model finds agreement with Wapner's (1995: 313) definition of civil society as a "complex network of economic, social, and cultural practices based on friendship, family, the market, and voluntary affiliation." This usage of the concept also agrees with the consensus, regardless of the analyst's understanding of civil society, that civil society is made up of uncoerced, voluntary associations that enjoy some degree of autonomy from the state (Wapner, 1996: 5,6; Cohen and Arato, 1992: 425; Walzer, 1991: 293; Held, 1995: 181; Lipschutz, 1996: 53).[1] Indeed, a variety of forms of associational life

---

[1] Note that this conceptualization of civil society serves the analytical purpose of "circumscribing different types of activity" while not negating some understandings of civil society such as the Gramscian perspective. The latter understanding of civil society perceives that "state rule often permeates throughout civil society to consolidate power" (Wapner, 1996: 6). The Gramscian concept of hegemonic society conceives of civil society as reproducing that hegemony through associational life such as the church, family, educational institutions and others. This still means that civil society can independently reproduce the existing state and economy (Cohen and Arato, 1992: 425). However, Gramsci also regarded civil society as "the realm in which cultural change takes place, in which the counter-hegemony of emancipatory forces can be constituted" (Cox, 1999: 10). One difference between my conception of civil society and that of Cohen and Arato (1992) and critical theorists in general is the inclusion of economic organizations within civil society.

within domestic civil society interact in one way or another with governmental institutions. As such, the model identifies civil society in contrast to governmental institutions.

The model (See Fig. 3.1) is divided horizontally in three layers: the top layer includes policy making processes and civil society at the transnational level. The middle layer represents domestic policy making processes and domestic civil society. The bottom layer lists the main characteristics of the action systems actors belong to. The following section provides a discussion of various concepts upon which the distinctions among systems of action are understood at the domestic level. The subsequent section provides an explanation of these same distinctions at the transnational level.

Three Systems of Action

(A) Proximity to the Policy Making Process

The bottom layer of the model divides domestic civil society vertically into three "systems of action."[2] The systems of action are labelled in the bottom section of the model from the left hand side of the model to the right hand side as: the party system of action, the interest group system of action and the social movement system of action. Their relative horizontal position corresponds to a continuum in terms of their proximity to the policy-making process, which is located in the left hand side of the model.

Proximity to the policy making process refers to actors' ability to access

---

[2] I borrow the term "system of action" from della Porta and Diani (1999) although these authors have not placed the systems on a continuum. The idea of a continuum is inspired by Scott's (1990: 132) suggestion that: "social movements are best understood in terms of a continuum stretching from informal network-like associations to formal party-like organizations. We can realistically assess the effects of social movements upon their [political] environment only, by viewing them as a political phenomenon related to other more ' institutional' expressions of political interests." While this is a useful observation in terms of the analysis of social movements' impact on the political environment, an important distinction, as will be discussed below, is that social movements also influence society.

FIGURE 3.1 POLICY INFLUENCE FROM CIVIL SOCIETY

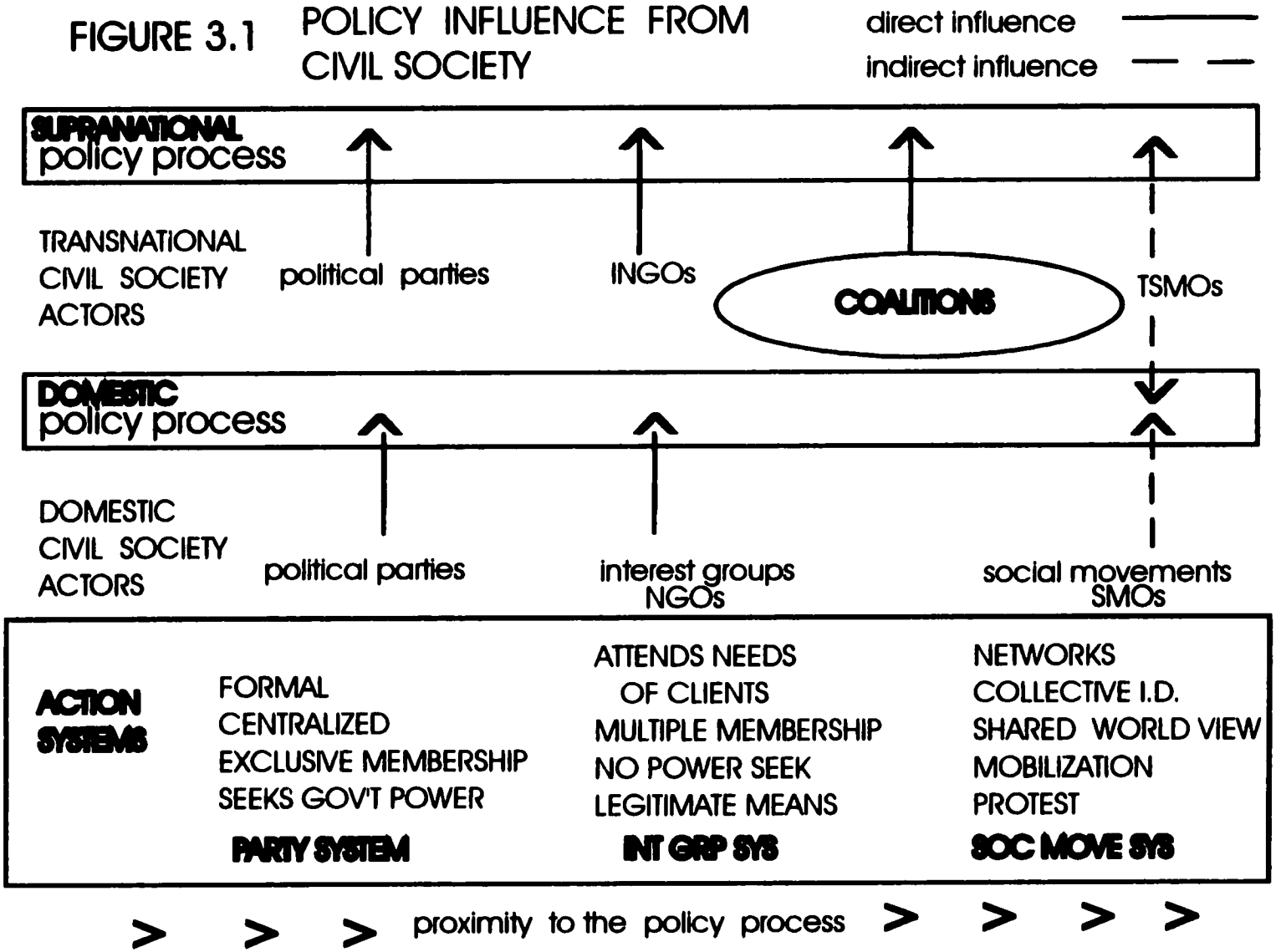

information, to dialogue with and thereby potentially influence the policy process. Thus actors that belong to the "party system of action" are closer to these processes than are actors that belong to the "interest group system of action" and they in turn are closer than would be actors that belong to the "social movement system of action." The other basis for the distinctions between these three ideal types of systems resides in actors' organizational structures, their motivations and objectives, and their behaviour. I elaborate upon these in turn.

(B) Organizational Structures

The interest group and the party systems of action display similar organizational structures. Actors in these systems consist of hierarchical organizations with formal, centralized structures. Both are based upon membership support. Party systems are somewhat more formalized than interest group systems in that leadership includes elections, and these organizations are legally constituted with set methods of fundraising (della Porta and Diani, 1999: 144, 145).

The organizational structure of interest groups is deemed crucial for their survival and ongoing influence on the policy making process (Pross, 1990: 286, 290):

> Their members have to be organized; brought together in structured relationships with one another and dragooned into identifying and expressing their common interests. Pressure groups are consequently distinct, clearly identifiable elements in the body politic.

By contrast, actors within the social movement system of action do not consist of one organization. "Social movements are not organizations, not even of a peculiar kind"

(Tilly, 1988 and Oliver, 1989 in della Porta and Diani, 1999: 16).[3] This does not mean that no organizational entities may be considered as part of the social movement system of action. Rather, no social movement organization (SMO) can be identified as the social movement, let alone be the sole representative of a movement's views or actions (della

---

[3] While social movement analysts rely at times upon the more concrete structures represented by social movement organizations (SMOs) they still recognize that "a social movement is certainly broader than its underlying structure" (Rucht, 1999: 207). However, the isolation of SMOs for analytical purposes and the exclusionary focus, at times, on these organizations' influence on government has caused some conceptual overlaps and theoretical confusion. These analytical foci lead some analysts to forget SMOs' ties with a broader movement, along with the peculiarities attached to this system of action. This has engendered a debate with those who see all NGOs as similar to "domestic interest groups of the traditional kind" (Stairs, 1998: 42; Pross, 1990: 293). The relevance of the distinction between the two types of organizations has been highlighted by social movement analysts in that societal actors that belong to the social movement system of action seek to influence not only policy outcomes but that they are also mostly associated with societal changes. Thus Rochon (1988: 205) points out that "[t]o look solely at its impact on policy is to reduce the peace movement to a lobbying organization. It is incorrect to do so, for not only are the organizational forms and political activities of the peace movement different from those of a typical interest group, its goals are different as well." Thiele (1993: 281) argues for a similar distinction on the basis that social movements and the organizations, such as Greenpeace, which consider themselves part of that movement "inject themselves directly into the processes of *socialization* and *politicization*" (italics added). In addition, Thiele (1993: 281) names peace and environmental movement organizations as "oriented to changing the world views and life-styles of the general public as much as influencing policy makers." Thus analysing the actions of SMOs such as Greenpeace solely as they interface with states or the state system, and forgetting to link them to their social movement roots derogates from the broader picture and therefore the understanding of the phenomenon we are encountering. While we can distinguish organizations within social movements, it is their ties to the movement that are significant in terms of their behaviour, motives and types of issues. In addition, it is their actions together with those of the broader movement with which they identify that represent "collective challenges to mainstream conceptions of how society ought to be organized and how people ought to live" (Lofland, 1996: 1). For example, Kuechler and Dalton (1990:279) draw a distinction among organizations concerned with environmental issues that illustrates the difference between those organizations that belong to the social movement system of action and those that do not. They point out that environmental organizations that have existed in Europe since the nineteenth century such as the French Society for the Protection of Nature or the British Fauna and Flora Preservation Society founded in 1903 "do not represent the particular ideological beliefs of the contemporary environmental movement." By comparison, organizations such as Friends of the Earth and Greenpeace "are closer to the core members of today's environmental movement" in that they share beliefs with movement participants at large. The debates also lead analysts toward arguments regarding the desirability of developing SMOs that express movement's claims (based on Rochon, 1988: 78-79). Thus, some argue that organizations lead to elitist tendencies and oligarchic consenquences, or that organizations have a tendency to become reformist thereby undermining "the ability to frighten authorities into concessions" or to be vulnerable to co-optation. Others claim that, on the contrary, organizations are crucial to movements' success because they are able to generate political resources or because they are "innovators in democratic forms of organization." For these reasons all the characteristics devised in this model, and not just organizational features, must be considered necessary to distinguish societal actors from one another.

Porta and Diani, 1999: 16, 141).[4] SMOs cannot, nor would they pretend to, represent the views of *participants* in the environmental movement as a whole.[5] This reality has led one observer of the peace and antinuclear movements in Western Europe to observe: "[i]t is the spread of protest against nuclear weapons, not the rental of an office and a duplicating machine, that determines the existence of a movement" (Rochon, 1988: 77).

Thus the distinctive organizational feature of social movements is that they are made up of networks. In terms of structure, social movements are : "(1) *segmented*, with numerous different groups or cells in continual rise and decline; (2) *policephalous*, having many leaders each commanding a limited following only; and (3) *reticular*, with multiple links between autonomous cells forming an indistinctly-bounded network" (from Gerlach, 1976 in della Porta and Diani, 1999: 140). Social movement analysis conceives of the least organized of these forms of collective action as "networks of everyday life" (Melucci, 1988: 338).

Unlike actors in the interest group system of action who rely on their members being "structured and dragooned" for a sustained effectiveness, the fluid networks that characterize the social movement system of action play a key role at different stages of

---

[4] This point is relevant to the extent that many scholars have used the term social movement interchangeably with specific NGOs. Thus SMOs such as the environmental NGO Greenpeace are erroneously referred to as "the environmental movement."

[5] Note that della Porta and Diani (1999: 17, 18) stress the importance of individuals in movements as participants and not members of particular organizations. This they argue is a significant distinctive feature of social movements relative to interest groups. Being involved in a movement "can never be reduced to a single act of adhesion. It consists, rather, of a series of differentiated acts, which, taken together, reinforce the feeling of belonging and of identity [with the movement]" (ibid.). Examples of such acts relevant to the movement are not limited to protests but may also include simply promoting the ideas of a movement among institutions or the media, or participating in public meetings, committees or work groups.

movement formation and development.[6] Therefore, implicit in the organizational characteristic of social movements are the achievement of a significant scale in terms of numbers of supporters and spread. Thus Lofland (1996: 11) explains that the "continuity and organization that are the marks of a social movement are signaled by the presence of several and perhaps hundreds or thousands of *named associations* that view themselves as part of 'the movement' and that are carrying on *campaigns* in the name of the movement." Rochon's (1988: 79-80) analysis of the peace and anti-nuclear movements in Western Europe illustrates the point well:

> The Dutch Committee Against Cruise Missiles ... brought together the IKV, Pax Christi, Church and Peace, the Humanist Peace Council, Stop the Neutron Bomb, the Union of Dutch Conscripts, Women for Peace, Women Against Nuclear Weapons, pacifist organizations united in the Platform of Radical Peace Groups, as well as the largest trade union federation and the leading leftist parties. In France, twenty-four peace organizations dedicated to pacifist, ecological, feminist, nonviolent, civil liberties, conscientious objection, student, Christian, and third world causes federated in November 1981 to form the Committee for Nuclear Disarmament (CODENE). In Germany.... In each of these countries, both the individual organizations and the federations put down roots in hundreds of communities. These groups contributed to national actions as well as to planning local activities.[7]

Although actors from the social movement system of action may thus be described

---

[6] For example, McAdam, McCarthy and Zald (1996: 4) report on the work undertaken by Charles Tilly in the 1970s that documented the role played by grassroots networks in facilitating collective action; in the 1980s Aldon Morris and Doug McAdam found that the black churches and colleges had played a critical role in the American civil rights movement. Summarizing the work of Melucci (1984), Rupp and Taylor (1987), Johnston (1991) and Mueller (1994), della Porta and Diani (1999: 89) explain that it is through informal networks that renewed mobilization takes place after periods of less visible movement activity. As Melucci (1995: 14) observed: "submerged networks nourish and give meanings to public mobilization."

[7] Of relevance to the model and as discussed in the second section of this chapter is the fact that early manifestations of such movements (from the 1960s onward) were largely confined within domestic borders. As such, early analyses of social movements were mostly concerned with comparisons of domestic manifestations of particular movements. However, over the past decade analysts have observed that "contentious politics is undergoing a process of change" (Passy, 1999: 148) in terms of a "gradual shift from national to transnational movement activity" (Rucht, 1999: 206).

as coalescing, the term coalition is reserved in this study for instrumental motives. The distinction between such coalitions and social movements is that, given their instrumental motives, coalitions, unlike social movements, rarely hold together once specific goals have been reached. As will be seen in the following chapter, the coalition against the MAI which brought together actors from both the interest group and social movement systems of action was instrumental and did not survive beyond the anti-MAI campaigns. However, some actors from that coalition remained united and pursued a common opposition against the World Trade Organization (WTO). The reason for this bifurcation can only be explained by the distinctions between the interest group system of action and the social movement system of action drawn herein.

(C) Motives and Objectives

A most significant distinction among the three types of action systems are actors' motives and objectives. A straightforward distinction has been drawn between actors in the interest group and the party systems of action in that the former are rarely motivated by the goal of obtaining governing powers.[8]

A further distinction has been drawn between interest groups and social movements. While interest groups are "interested in exerting influence and in persuading governments to accommodate the special interests of their members" (Pross, 1990: 285), SMOs and other actors considered part of the social movement system of action "do not

---

[8] I borrow this characterization from Pross (1990: 285) who distinguished political parties from interest groups in that manner. This distinction accords with the definition of political parties as "any group, however loosely organized, seeking to elect governmental office holders under a given label" (Epstein, 1967: 9, 10).

necessarily address themselves to those whose interests they wish to promote" (della Porta and Diani, 1999: 145). That is, societal actors who belong to the social movement system of action do not act in order to ensure a better future for themselves but "[t]hey envision a better society for all" (Kuechler and Dalton, 1990: 280).

More significantly, what actors from the social movement system of action envision typically challenges mainstream understandings of reality. So much so, that Lofland (1996) labelled these as "excluded realities." Thus actors from the social movement system of action are engaged in "political and/or cultural conflicts meant to promote or oppose social change at either the systemic or non systemic level" (della Porta and Diani, 1999: 15). This brings Lofland (1996: 3) to characterize the changes sought by these actors as residing in "idealistic and moralistic claims about how human personal or group life ought to be organized that, *at the time of their claims-making*, are marginal to or excluded from mainstream society—the then dominant constructions of what is realistic, reasonable and moral."[9] Kuechler and Dalton (1990: 280) describe such shared world views as "a humanistic critique of the prevailing system and the dominant culture, in particular a deep concern about the threats to the future of the human race, and a resolve to fight for a better world here and now." For these reasons actors who belong to the

---

[9] Lofland (1996: 3) stresses this feature by explaining that social movement actors espouse "a *claim about reality* that is, *at the time of its assertion*, ...not respectable or otherwise meriting serious consideration. Instead, the asserters and the realities they assert are, in mainstream views, best ignored, repressed, treated therapeutically as a sickness, or in some other manner kept excluded, marginal, or encysted." A good example of asserters of excluded realities that have been experiencing such symptoms are actors from the gay and lesbian movement. Lofland's insistence on the relevance of the timing of claims suggests that as movements' claims become accepted in mainstream reality they cease to belong to the definition of social movement. In my view, this is an important aspect of the definition of social movement and it lends a dynamic to the model that could be further explored.

social movement system of action are often referred to as anti-systemic.

Another distinctive motivational factor that differentiates actors from the social movement system of action from the interest group system of action resides in the notion of collective identity. A collective identity is born from actors' sense of being bearers of particular values and interests and defining adversaries in relation to these.[10] Thus the relationship between collective action and collective identity is explained as follows: "[c]ollective action cannot occur in the absence of a 'we' characterized by common traits and a specific solidarity. Equally indispensable is the identification of the 'other' to which can be attributed the responsibility for the actor's condition and against which the mobilization is called" (Gamson, 1992 in della Porta and Diani, 1999: 87). The processes through which this construction of action takes place has been referred to as "framing processes."[11]

(D) Behaviour: "Proper Channels" vs. "Disruptive Tactics"

Unlike social movements, interest groups seek to influence policy-making "through legitimate channels and by legitimate means" to a point where these actors are considered to "buttress the political system ... and ... provide, at least implicitly, support for that system" (Van Loon and Whittington, 1981, 407). Useem and Zald (1987: 273) also distinguish pressure groups from social movements in that the former "employ a political system's conventional form of collective action," while the latter "tend to use

---

[10] For a good understanding of the concept of collective identity in the analysis of social movements see della Porta and Diani (1999: 83-109).

[11] David Snow coined the concept and defined it as the "conscious strategic efforts by groups of people to fashion a shared understanding of the world and of themselves that legitimate and motivate collective action" (in McAdam, McCarthy and Zald, 1996: 6).

noninstitutionalized tactics, channels of influence, and organizational forms." Similarly, Paul Thiele (1993: 281) explains that social movements "are not limited to the traditional avenues of politics as defined by state structures and established governmental procedures." Thus a defining characteristic of social movements is their methods of persuasion which are "novel, unorthodox, dramatic and of questionable legitimacy" (Wilson 1973: 227 in della Porta and Diani, 1999: 168). Examples of such unorthodox practices range from street theatre to rubber boats confronting nuclear submarines, or tying oneself to a tree to prevent foresters from cutting it down. While analysts recognize that political parties and interest groups may at times resort to various forms of protest, "protest (particularly at its most innovative and radical) has been considered as a form of action typical of social movements" (della Porta and Diani, 1999: 170).

Thus one of the main behavioural characteristics of social movements is "mass mobilization, or threat of mobilization, as their prime source of social sanction, and hence power" (Scott, 1990: 6). These mass mobilizations and protests serve several purposes. Among them is the objective of attracting public attention through media coverage thereby gaining broader support for a cause. Another objective of these protests is referred to as "the logic of numbers" (DeNardo, 1985). As seen above, a defining characteristic of social movements resides in the scale of the support they achieve. Thus the logic of numbers refers to the idea that a movement's destiny depend largely on the number of its supporters since "there always seems to be power in numbers" (DeNardo, 1985: 35). The power derived from numbers in protests lies in the greater disruption caused by a larger number of protesters. Larger numbers of protesters also serve to demonstrate to elected

representatives the degree of support for a movement's claims and the potential electoral consequences of governmental response to those claims (della Porta and Diani, 1999: 175).

The distinction between these two types of behaviour also yields different types of influences on the policy process. Because of their closer interaction with the policy-making process, actors who belong to the interest group system of action may be described as seeking *direct influence*. Direct influence can be defined as specific and substantive influence on policies targetted by groups that get involved in lobbying activities or policy-making processes on a consultative basis. The additional objective and strategies behind actors from the social movement system of action such as changing mainstream reality and mobilizing for broader support for their claims qualify these actors' influence as *indirect influence* on the policy-making process. Indirect influence refers to the influence on the policy-making process through increased pressure on officials by various means. These distinctions are illustrated in the model with two different types of arrows.

The combination of the characteristics described in sections *A* to *D* yields the following definition of social movement:

> A *social movement* can be defined as an action system comprised of mobilized networks of individuals, groups and organizations which, based on a shared collective identity, attempt to achieve or prevent social change, predominantly by means of collective protest (Rucht, 1999:207).

II. Civil Society Actors at the Transnational Level: Parallels with Domestic Levels

Multiple Levels of Interaction

The changing political and institutional reality within which societal actors operate means that many are active transnationally as well as nationally. The inclusion of a supranational policy-making process in the model intends to reflect that reality. The leading example of a supranational arrangement that parallels governmental institutions at the domestic level is the European Union with its Parliament, its political parties and the European Commission. We would therefore place the European Parliament and the European Commission as supranational policy-making processes and the political parties who represent various domestic European constituencies in the political party system of action. However, there are other supranational institutional arrangements where policies are agreed-to, albeit with diverse and generally less authoritative legal status. While various governmental institutions are responsible for policy-making at the domestic level, we find at the supranational level, multilateral fora within which states agree to legally binding international policies that also affect their domestic policies.

Not only do societal actors increasingly interact with these supranational bodies but their relationships to one another are also no longer confined within nation-state borders. As Rucht (1999: 207) observes, "a single group can be at the same time part of a local, national and international movement" meaning that such societal actors can be active locally, nationally and transnationally autonomously, as part of larger coalitions or as member of umbrella organizations. Similarly, Non Governmental Organizations

(NGOs) that do not belong to the social movement system of action have been increasingly present at transnational events. Not only have their numbers mushroomed over the past decades, but the frequency of their interactions within official fora has also increased.

Domestic and international NGOs can be found within international governmental fora such as the United Nations' Economic and Social Council (ECOSOC) where they enjoy a consultative status autonomously, as federations or as coalitions. In addition, ECOSOC and its international secretariats have organized international conferences on specific issues that are attended by senior government officials as well as NGO representatives. For example, the UN Conference on the Environment and Development in Rio de Janeiro in 1992 registered 1,400 NGO representatives (Gordenker and Weiss, 1995). Such increasingly frequent encounters contribute to the establishment of direct links between officials and NGOs.

Other international governmental fora have developed ways to interact with NGOs. Thus the Trade and Environment Division of the WTO "pioneered the concept of issue-specific NGO symposia as early as June 1994 (under the then General Agreement on Tariffs and Trade, GATT) (Marceau and Pedersen, 1999: 16). According to that source two such symposia took place. In 1997 a joint WTO-United Nations Conference on Trade and Development (UNCTAD) Symposium on Trade-Related Issues Affecting Least-Developed Countries was held in Geneva, and was attended by 34 NGOs mostly from least developed countries. In 1998 the WTO held a Trade and Environment Symposium which included 150 individuals from environment and development NGOs,

private corporations and academia (ibid.).[12] Such arrangements have been referred to as "formal relations between 'interest groups' and an intergovernmental body" (Gordenker and Weiss, 1995: 365).

However, NGOs' activities and collaboration also take place outside formal institutional settings and, at times, quite independently of institutional prompting. Such interactions and the targets of their claims can be both domestic and transnational. Thus for example, a variety of local, national and international groups have emerged since the 1970s to address issues affecting indigenous peoples locally as well as globally (Brysk, 1996: 40). At the local level indigenous groups formed grassroots associations and were eventually supported by newly founded international NGOs such as the World Council of Indigenous Peoples and Cultural Survival. Local indigenous organizations received material support from international NGOs such as OXFAM, Cultural Survival and the Inter-American Foundation as well as support in terms of sympathetic foreign actors' presence during local conflicts. These coalitions also exercise political pressure, often through northern allies, on international organizations such as the World Bank in order to prevent the funding of development projects detrimental to indigenous groups.

. Given the motivation and behaviour of such actors, Rucht (1999: 207-209) refers to these coalitions as transnational social movements. He provides some examples of the ways in which such cross border and cross sectoral collaborations take place: "horizontal coordination between groups from different countries" such as the "worldwide

---

[12] See O'Brien et al. (2000) for a comprehensive study of NGOs' interactions with the World Bank, the IMF and the World Trade Organization.

coalition of some 700 groups that oppose the construction of the large Narmada dam system in India"; vertical and horizontal structures where "national groups not only coordinate directly, but do so through an international body which has some say" such as the worldwide environmental umbrella organization Friends of the Earth International that allows one group per country to become a member; the more structured and centralized type of organization such as Amnesty International and Greenpeace where "ideational and structural similarities between national groups" are induced. Each of these are part of broader movement networks such as the environment in the case of Friends of the Earth. Rucht (ibid.) refers to these structures as Transnational Social Movement Organizations (TSMOs) and considers them to be a distinct subset of International NGOs (INGOs). As just mentioned, these actors can join local groups in local campaigns spontaneously and quite quickly. Such was the case for the transnational mobilization protesting against the Nigerian government on the occasion of Ogoni writer and critic Ken Saro-Wiwa's death sentence (see Rucht, 1999: 213).

Thus not only are NGOs found to be active at several levels, but characteristics similar to those identified at the domestic level can be found at the transnational level. As such, the model reflects the fact that societal actors active at the transnational level display characteristics similar to those identified in our three systems of action at the domestic level. Therefore, the vertical division of civil society into three systems of action described in the bottom horizontal layer of the model applies to the transnational level of civil society. These parallels are made with the obvious reservation that there is no international central authority or global state, let alone political mechanisms for state-

society relations akin to those found at the domestic level.[13] The model intends to reflect the continued relevance of distinctions between the three systems of action in terms of civil society actors at the transnational level and in terms of the way these civil society actors interact with such supranational institutions.

Transnational Societal Actors' Proximity to the Policy Making Processes

In the same way that some societal actors at the domestic level are closer to the policy-making process so too at the international level some societal actors enjoy, and seek, more consultative privileges than others. Thus political parties in the European Parliament are considered closer to the policy making process than NGOs that lobby the European Commission. Although NGOs' access to these multilateral institutions varies from one institution to the other, we can still find NGOs that enjoy a closer relationship with some international policy-making processes than others.[14] As will be illustrated in the case of the MAI in Section II, some NGOs enjoyed more credibility, respect and access with OECD and WTO officials than did others. Also, such NGOs describe their activities and objectives in terms akin to the domestic actors within the interest group system of action.

Social Movement Actors at the Transnational Level

In addition to being more distant from the supranational policy-making processes,

---

[13] Many do in fact see transnational nonstate actors as substantively little different from domestic interest groups. In addition, others conceive of "pluralising global governance" (Gordenker and Weiss, 1995) or they refer to the relationship between nation-states and NGOs during international conferences as "a microcosm of global state-society relations" (Clark, Friedman and Hochstetler, 1998: 6). However, such oversimplifications hide the significant differences between the international and domestic systems.

[14] Thus Gordenker and Weiss (1995: 364) describe the procedures through which NGOs obtain various levels of consultative status within the United Nations system.

some International NGOs (INGOs) are also linked with domestic and transnational social movement networks and their behaviour and motives correspond to that system of action. These organizations are referred to as transnational social movement organizations (TSMOs).[15] In the same way that SMOs reflect the underlying organizational structure of domestic social movements, TSMOs reflect the organizational structure and evidence of transnational social movement networks. Examples of such TSMOs already referred to are Friends of the Earth, Amnesty International and Greenpeace International.[16] As do actors from the social movement system of action at the domestic level, actors from transnational movement networks exhibit "different layers of collective identities which are not mutually exclusive" and when they do join across borders they place their actions within a common and wider perspective.

Also, the TSMOs' means of pressuring for change are, as at the domestic level, less conventional than those of INGOs that belong to the interest group system of action. For example, Greenpeace is renowned for its "vicarious activism" and unconventional methods of protest (della Porta and Kriesi, 1999: 20). Thus Wapner (1996: 56) reports one instance among others where three Greenpeace activists "scaled half-way up the forty-seven-story Time-Life tower in New York to protest chlorine-bleached paper used in *Time*

---

[15] This paragraph is based on Rucht (1999: 206-222). The term TSMO was coined by Pagnucco and McCarthy (1992) "and it refers to social movement organizations which have members in two or more nation-states and which have an international office or secretariat charged with coordinating and/or facilitating transnational activities, communication and/or strategies" (Rucht, 1999: 221, note 3).

[16] Little systematic scholarly work has yet been undertaken to sort out NGOs in general (Chayes and Chayes, 1995: 252). The criteria based upon social movement framework would be one to start from. Another factor affecting the role of NGOs in general has been pointed out by Gordenken and Weiss (1995) and is based upon the degree of funding they receive from governments.

magazine." Not only did the activists attract media attention by climbing the building but they also pointed a conspicuous accusatory finger at the organization by unfurling a banner which read "'Chlorine Kills' and 'Take the poison out of paper' against a backdrop of a mock *Time* magazine cover."

Conclusion

The heuristic model devised herein distinguishes societal actors at the domestic and transnational levels in terms of four main distinctive features. These characteristics taken together define and distinguish various civil society actors from one another. Although three systems of action are identified, I have specifically drawn a distinction between actors that belong to the interest group system of action and the social movement system of action. The distinctions are based upon social movement theoretical frameworks. Given the thick descriptive nature of these dinstinctions a model was devised. This model is suggested as a parsimonious tool of reference and as a template to be applied to case studies as I do, in Section II, to analyze the MAI opposition.

The first feature distinguishes actors on the basis of their proximity to domestic and supranational policy-making processes. The three remaining characteristics distinguish actors on the basis of their organizational structures, motives and objectives of action, and behaviour. Firstly, actors in the social movement system of action enjoy less proximity to the policy-making processes than do those from the interest group system of action. This is partly due to the fact that their claims, which are based upon shared values and world views, typically reflect idealistic and moralistic challenges to mainstream reality.

As such, the analytical framework also highlights the respective differences

regarding the motives of actors that belong to these two action systems. Actors within the social movement system of action envision a better society for all, and, unlike actors in the interest group system of action, they do not pursue policy changes for themselves, their group or a specific membership but for society at large. In that sense, these actors not only seek to influence the policy-making process, as do actors in the interest group system, but they also seek to influence larger collectivities. One distinctive way in which these actors pursue that objective is through mobilization, protests or vicarious activism.

In contrast, actors from the interest group system of action pursue policy objectives through more legitimate or accepted means such as lobbying and taking part in the policy-making process. These actions seek specific policy changes that address their membership's interests. Policy orientation is determined through the membership and hierarchical structure of the organization in a manner that renders the NGO accountable to its membership. The main organizational distinction of actors that belong to the social movement system of action is that they are part of networks. These networks contribute to the formation, sustenance and expansion of social movements. As such, no single organization represents a movement. For these reasons, the term Social Movement Organization (SMO) has been devised as a sub-category to the more generic term Non Governmental Organizaiton (NGO). Likewise at the transnational level we find the generic term International NGO (INGO) and Transnational SMO (TSMO) to draw a difference between the two.

By all accounts the opposition to the MAI was made up of a complex, heterogeneous representation of organizations and individuals that presented an unusual

common front to OECD negotiators. This common front was misleading in terms of the hidden diversities among MAI opponents' campaigns and the chronology of these campaigns, their short- and long-term objectives, their motives for opposing the MAI and their preferred modes of action. As such the sequence of events, the respective roles of opponents and their effectiveness was not immediately apparent. However, collecting such empirical evidence was necessary in order to answer the question regarding MAI opponents' impact on the outcome of the negotiations. The model proved useful to achieve that objective.

In this chapter I have devised and explained a heuristic model that should enable us to decipher these societal actors from one another and to further understand their respective roles in the outcome of the MAI negotiations and their meaning for world politics. As will be demonstrated in Section II, the chronology of various campaigns led against the MAI became evident and understandable once the model was applied to the MAI opponents. Specific strategies and goals on the part of diverse opponents also came to light and their effectiveness was thus demonstrable.

Although the model was initiated on the basis of actors' self-description, it soon became clear that these differences held significance not only for the anti-MAI campaigns but for the longer-term meaning of some groups for world politics. The model and its underlying theoretical framework also enables me to trace the emergence of a new actor with significance for world politics in the movement against economic globalization. I trace this actor in pre-MAI campaigns and demonstrate its evolution during the MAI campaign and its continuation in the post-MAI opposition to the WTO that took place in

Seattle a little over a year after the MAI negotiations ended. The thick descriptions of characteristics gained from the conceptual identification of various MAI opponents further enables me to compare, in Section III, these opponents' significance for world politics to other case studies that use diverse taxonomy.

The following chapter relies upon the model to provide an understanding of the various MAI opponents' campaigns in terms of their politics, their objectives and strategies. Chapters 5 and 6 then incorporate that chronology with the progress inside the negotiations in order to demonstrate the influence of these societal actors.

SECTION II

CASE ANALYSIS

CHAPTER IV

"WHO ARE THESE GUYS?": THE SOCIAL OPPOSITION TO THE MAI—A CHRONOLOGY AND ANALYSIS

Introduction

Referring to the MAI opponents in his April 30, 1998 *Financial Times* article, journalist Guy de Jonquières asked: "Who are these guys?" In doing so, de Jonquières was using a scene from the movie *Butch Cassidy and the Sundance Kid* as a metaphor to portray officials' reaction to the MAI opposition. Thus, in the same way that the two outlaw heroes of the movie failed, for the first time in their career and to their growing dismay, "to shake off their mysterious pursuers" so too Governments of industrialised countries were described as expressing "fear and bewilderment" at a "horde of vigilantes whose motives and methods [were] only dimly understood in most national capitals." Indeed, by then the opposition to the MAI had become vociferous and noticeable in a majority of OECD member countries.

Most puzzling was the evolution and unprecedented nature of this opposition. The opposition to the MAI moved from sparse and tamed encounters between officials and NGOs that attempted to modify the treaty, to street protests and a common resolve to stop the negotiations altogether. Not only was such an objective on the part of societal actors bold, but several other aspects of this opposition justified officials' bewilderment. First, the sustained common front among a diverse array of groups from all corners of the globe was by all accounts an unprecedented event. Officials' encounter with a diverse group of MAI opponents that presented a common front and expressed their unified objective also caused some surprise. Activists' usage of the Internet was not only unexpected but officials could thereby witness the growth of the opposition and its vilification of their work. This apparently sudden and relentless resolve on the part of

activists, and the rapidity with which their critiques spread was all the more surprising given its delayed emergence in the MAI process. The puzzlement was exacerbated by the fact that the decision to delay and then abandon the negotiations coincided with the growing visibility of the MAI opposition.

Given MAI opponents' stated objective, the immediate question facing observers as well as participants in these events was whether the opponents had caused the demise of the negotiations. In order to answer that question, it is necessary to understand the campaigns led by various MAI opponents. This chapter undertakes this task by providing an analysis of the social opposition to the MAI and a chronology of the anti-MAI campaigns which took place between 1995 and 1998. The chronology of the campaigns thus related will provide the historical perspective necessary to evaluate, in Chapters 5 and 6, their impact on the negotiations.

The conceptual model devised in the previous chapter proved useful in deciphering the heterogenous composition of this opposition. MAI opponents' self-description and the distinction they drew among themselves could be accommodated by the model. Three main types of MAI opponents that are focused upon in the analysis can thus be placed in the interest group system of action and the social movement system of action. Rather than relying upon these conceptually useful but cumbersome phrases, I adopt simpler terms inspired by MAI opponents' self-reference and mutual distinctions. This practice will hopefully provide both a more eloquent narrative and a more illustrative picture of the MAI opponents.

Thus I borrow the broadly used terms "reformists" or "insiders" when referring to

MAI opponents whose characteristics correspond to the interest group system of action. Indeed, these actors preferred engaging in lobbying efforts and direct policy dialogue with officials at every level of governance. Furthermore, and as will be documented, these MAI opponents' self-description corresponds to characteristics of that system of action in terms of organizational features, objectives and preferred modes of action.

Similarly, the characteristics of those I refer to as "intellectuals-engagés"and their "militant-mobilizers" collaborators, also broadly referred to as "radicals," correspond to those of actors in the social movement system of action.[1] These actors were intent on generating broader public awareness of the MAI and its critiques in order to generate widespread mobilization and public support thereby generating indirect pressure on the process. Their objectives and motives reflected a concern regarding the impact of the MAI on societies at large. These concerns were grounded in common values and beliefs. Most significantly, intellectuals-engagés expressed the longer-term objective of building widespread awareness and resistance to a process of economic globalization that they judged detrimental to the future of societies at large.

The analysis of the MAI opposition reveals that the coalition struck among these diverse NGOs and activists did not last beyond the MAI negotiations. The radical stance of the coalition was the result of common instrumental purposes. As such the coalition itself was *sui generis*. Nevertheless its role in the MAI opposition deserves attention as

---

[1] The word *engagés* is borrowed from the French. The French word means someone who is politically committed and its usage here reflects what French activists referred to as intellectuals' collaboration with militant mobilizers. Although the term intellectuals-engagés was coined by French activists the patterned relationship was found in all countries.

do the reasons for its occurrence. However, that coalition must be distinguished from networks that evolved among other actors before, during and after the MAI opposition. Thus more significant to the meaning of the MAI opponents for world politics is the evidence of transnational linkages that point to the emergence of global transnational movement networks with growth potential. Yet, these actors were last to manifest their opposition to the MAI.

As might be expected, the earliest signs of opposition to the MAI were given by the so-called reformists who belong to the interest group system of action. This was due to their relatively earlier awareness of the MAI negotiations. As explained by the civil society model, these actors' earlier knowledge of the MAI is consistent with their proximity to the policy making process relative to that of actors from the social movement system of action. Thus, while these actors signalled their critiques of the MAI as early as the fall of 1996, it was not until April 1997 that actors from the social movement system of action also were manifest.

For that reason, I will begin this chronological analysis of the anti-MAI campaigns with that of the interest group system of action. Although the creation of the transnational coalition opposing the MAI took shape in October 1997, after the campaign of the social movement system had begun, I will include this event in the first section of the chapter since its occurrence was largely due to the groups that belong to the interest group system of action. The second and third sections of the chapter provide an analysis of the evolution of the anti-MAI campaign conducted by intellectuals-engagés and militant-mobilizers, and the development of the movement networks against economic

globalization that grew out of that campaign.

I. Confronting the Policy-Making Process

The Interest Group System of Action

The earliest signs of opposition to the MAI were given by NGOs commonly referred to in activists' circles as reformists or insiders. As illustrated in the following paragraphs, these groups' characteristics correspond to those of actors that belong to the interest group system of action. They are close to various policy-making processes, and directly engage officials on policy issues. This is due to the fact that their expert staff enjoy respect from the policy community and work closely with that community at the domestic and international levels. Policy experts from these organizations are close to the international trade policy-making circles in Geneva, and they also have access to OECD officials in Paris. Their organizational structure is hierarchical and accountable to a particular membership. Their staff seek policy reforms that satisfy specific organizational objectives.

Their early awareness of the MAI and their ability to formally engage officials in a debate on the MAI attest to these organizations' proximity to the policy-making process. The South Centre and the Indian NGO Consumer Unity and Trust Society (CUTS), a member of the INGO Consumers International, were among the first to draw their Northern counterparts' attention to the MAI negotiations. These organizations had followed the investment negotiations at the WTO and were aware, as early as 1995, that similar negotiations had moved to the OECD.

After obtaining a ten-page confidential draft of the MAI in June 1996, CUTS and

Consumers International organized an international seminar which took place on October 18-19, 1996 in Geneva, to discuss the ongoing MAI negotiations. Attending the seminar were several officials from the OECD who were involved in the MAI negotiations, officials from the European Commission, the WTO and the United Nations Conference on Trade and Development (UNCTAD) and several representatives of mission to the United Nations. Also attending was the representative of the Trade Union Advisory Committee to the OECD (TUAC), an organization which, along with its counterpart for the international business—the Business and Industry Advisory Committee (BIAC)—had been involved in the preliminary work leading up to the negotiations.[2] Also present were a number of Northern INGOs who played an important role in establishing contact between the OECD MAI negotiators and the broader community of MAI opponents. The World Wildlife Fund for Nature (WWF) and the Centre for International Environmental Law (CIEL) are NGOs whose expert staff enjoy the respect of the various policy communities and who at times work closely with these communities at the domestic and international levels.[3]

The WWF is widely acknowledged among activists as a typical "reformist" organization. The organizational structure and self-description of the WWF further confirm that INGO's position in the interest group system of action. According to its web

---

[2] TUAC, which was founded in 1948, and BIAC, which was founded in 1963, are umbrella organizations that include members from all OECD countries. These two organizations have enjoyed a consultation status with the OECD from its early days in the 1960s.

[3] These organizations engage in policy dialogues with the WTO on issues of trade, environment and sustainable development. See O'Brien et al. (2000) for a description of these organizations which they refer to as "reformists." Among their activities, the authors mention redirecting trade policies and conducting analysis and research aimed at making policy recommendations.

site: "[t]he organisation works with governments in two ways: as a collaborator and lobbyist" (www.panda.org). WWF staff is accountable to its 4.7 million members through an organizational hierarchy that ultimately reports to a Board of Directors. The specific focus of the organization's activities aims to: "conserve nature and ecological processes" by "combining science-based, solution-oriented conservation projects and policy work" (www.panda.org). Likewise, Consumers International is a federation of over 230 consumers' organizations that focus on consumers' interests and protection world wide "through institution building...research and lobbying at international decision-making bodies" (CUTS, 1997). The organization has a consultative status at the Economic and Social Council of the UN and "other international bodies."

Likewise, CUTS is an organization that engages in policy consultation with various policy-making process. Internationally, as was just explained, the organization invites officials to policy seminars that promote its membership's interests, domestically it also works with the government of India on policy issues. Thus it describes itself as follows: a "leading social action group in India" which founded the "International Center for Trade ans Sustainable Development" in Geneva and serves on several Government of India policy committees" (CUTS, 1997). The October 1996 meeting report reflects the policy orientation typical of interactions between actors from the interest group system of action with the policy-making process. The seminar itself was the third in a series that was organized by the consumers' organizations "to address issues of trade and economic liberalisation and their impact on consumers" (CUTS, 1997: ii).

Of significance was the fact that that first encounter contributed to future

encounters between NGOs and the OECD regarding the MAI. Thus an informal dinner meeting took place in December 1996 between WWF, CIEL and the Chairs of the Negotiating Group.[4] The latter invitation took place thanks these officials' respect for these NGO experts, earned through previous consultation work with the OECD Trade and Environment Committees and the WTO. The objectives of these NGOs were to reform the existing MAI draft document. The exclusion of developing countries from the MAI negotiations was also criticised.[5]

The reforms that these groups sought reflected their particular policy foci. International environmental NGOs argued that the draft MAI was incompatible with the Multilateral Environmental Agreements (MEAs).[6] The policy reforms that they suggested consisted of including binding environmental commitments in the MAI and a general exemption from the MAI conditions on the grounds of environmental protection or compliance with MEAs; amending the dispute settlement process to avoid its abuse by

---

[4] Attending this meeting were the Dutch Chair of the negotiations, Franz Engering, and his permanent representative in Paris, Jan Huner, the two deputy chairs, Alan Larson from the U.S. and Kenichi Suganuma from Japan, two representatives from the WWF, Nick Mabey (WWF-UK) and Charles Arden Clarke (WWF-International), the Geneva representative of the American NGO CIEL, Brennan van Dyke, and John Hontelez from Friends of the Earth International (WWF notes from the dinner meeting).

[5] The *de facto* exclusion of developing countries from the OECD negotiations (with the exception of South Korea and Mexico) , had raised concerns in many official circles. For NGOs, the move of investment negotiations to the OECD were seen as a strategic move aimed at undermining Southern opposition to such a multilateral agreement.

[6] In order to demonstrate the validity of their argument, they undertook analyses of the impact that the MAI obligations would have on trade related policies used to implement existing MEAs. For example, one critique focused on the Rio Principles and Agenda 21 through which countries had committed to manage their economies in a way that would prevent environmental risks with what was called the "precautionary principle." NGOs argued that it was important to ensure that the dispute settlement mechanism in the MAI not interpret such policies as covert protectionism (WWF, Consolidation Paper on the MAI, by Nick Mabey, 17 February 1997). In addition, the use of the OECD as a forum of negotiations excluded developing countries which was also an issue of concern. Developing countries had agreed to signing MEAs in exchange for compensation such as technology transfers which could be found in violation of MAI obligations.

corporations; including environmental expertise inside the dispute process; and, updating the 1976 OECD guidelines on Multinational Enterprises to reflect Agenda 21 (based on WWF draft letter to OECD Ministers).

As will be further elaborated upon in the following chapters, NGOs felt that these first attempts at consultation with the OECD were not yielding conclusive enough results to warrant abandoning their domestic lobbying strategies. Few satisfactory changes seemed to transpire in the MAI draft. In a letter dated February 13, 1997 addressed to U.S. Trade Representative, Charlene Barshefsky, they characterised the few meetings that the OECD held with NGOs as "token gestures."[7] Of significance, and evident by the signatories to the letter, was the fact that not only was the opposition spreading but that more radically oriented groups such as Friends of the Earth, Greenpeace and the Sierra Club were supporting those in the interest group system of action—groups known for their vicarious activism and grassroots mobilisation. In any event, organizations that belonged to the interest groups system of action pursued what they called their "inside work," which consisted in intensifying political pressure from within by getting Parliaments engaged, alerting opposition parties and lobbying domestic environmental ministries.

Another objective and subject of these NGOs' frustration concerned the request

---

[7] See *Inside U.S. Trade* (February 21, 1997: 12) for a reproduction of the letter dated February 13, 1977 to Charlene Barshefsky and endorsed by the Community Nutrition Institute, CIEL, Defenders of Wildlife, Friends of the Earth (U.S.), Greenpeace, Institute for Agriculture and Trade Policy, National Wildlife Federation, Sierra Club, and WWF. NGOs' frustration was also confirmed in interviews with representatives of WWF, U.K. and FOE International who participated in these efforts during the MAI negotiations. Not only had there been a lack of consultation but a difficulty of access to the officials involved in the process and when contacted officials demonstrated a lack of respect regarding the validity of the critiques raised by these NGOs.

made at the initial dinner meeting to conduct a broader consultation that would include other NGOs so that they could have input into the process. In terms of process, international environmental NGOs had requested, in vain, through several domestic environment ministries and through the OECD's own Trade and Environment Committees that the MAI Negotiating Group consult with them on such matters.[8] International environmental NGOs were accustomed to the consultative status they enjoyed at the United Nations Commission for Sustainable Development, the body responsible for monitoring Agenda 21 of the 1992 Rio Conference on Environment and Development.[9] However, the Negotiating Group was made up of Chief Negotiators from OECD member countries some of whom had consistently refused such consultations, which is why the informal dinner meeting of December was eventually organized.[10] Nevertheless, the

---

[8] Based on Jan Huner's presentation at Chatham House, October 29-30, 1998. Confirmed in interviews with environmental NGOs during the fall of 1999. The UN system, as seen in the preceding chapter, is more open to NGOs' participation in certain areas. See Kendall W. Stiles (1998)) for NGOs' relationship with multilateral donors; Peter Willets (2000) for their changing status in the UN; Charnovitz and Wickham (1995) for their history with the original trade regime; Marceau and Pedersen (1998) for relations with the WTO; and, O'Brien et al. (2000) for an empirical study of their relationship with the World Bank, the International Monetary Fund and the World Trade Organization.

[9] Per interview with FOE and WWF staff in London, fall 1999. Agenda 21 is an official agreement issued from the United Nations 1992 Conference on Environment and Development (UNCED) which took place in Rio de Janeiro. The Commission on Sustainable Development (CSD) was established to monitor the progress of Agenda 21. Its functions include receiving and analyzing input from NGOs as well as enhancing the dialogue with NGOs (based on Caldwell, 1996).

[10] As E. Smythe (1998*b*: 251, 252) has observed, the OECD was accustomed to consult with two OECD members' organizations—BIAC (the Business and Industry Advisory Committee) and TUAC (the Trade Union Advisory Committee). While the OECD Environment Directorate had experience consulting with environmental NGOs since 1991, this practice was not shared by other directorates in the organization. As such, the lack of consultation with NGOs was also due to the lack of communication across Directorates within the OECD. The MAI also presented a special situation in that it was a treaty negotiation. The fear was that such consultations would reveal parties' negotiating position. Note that TUAC and BIAC are also part of the interest group system of action. While BIAC and other international and domestic umbrella business organizations were active in promoting the MAI, TUAC played a marginal and ineffective role in raising critiques that reflected the concerns of the labor movement (see Wallach, *Le Monde Diplomatique*, February, 1998, p. 22).

December dinner meeting concluded with these officials promising to put a proposal before the Negotiating Group for a broader consultation process with NGOs.[11] However, that promise was not fulfilled until October 1997, almost a year later. By then, opposition to the MAI had spread considerably. As such, the outcome of the call was a radicalised opposition to the MAI.

The Birth of a Transnational Coalition

A larger and radicalised opposition to the MAI was well under way by September 1997 when the OECD called upon WWF to organize a consultation meeting between negotiators and NGOs.[12] As such, the timing of this meeting influenced the direction of all the anti-MAI campaigns. By then, a majority were determined not to request reforms to the agreement, as the initial OECD interlocutors had lobbied for, but to stop its progress altogether. Even though some groups had interests akin to those of the original OECD interlocutors, their concerns were no longer limited to reforming the draft text to include an environmental clause in the MAI. As one environmentalist explained: "our position wasn't we can't support the MAI till there is a clause respecting environment in it. It was we can't support the MAI at all."

For many activists, it was the meeting that took place among NGOs, prior to their

---

[11] Based on interviews with participants in the dinner meeting and WWF notes from the meeting. During the meeting officials expressed concerns regarding the critiques that had begun to appear on the Internet. NGOs responded that the best way to quieten these down was to hold broad consultations as soon as possible. They also attempted to reassure these officials on the ability of most NGOs to act professionally in light of officials concerns to the contrary.

[12] This organization was specifically called upon due to the respect on of its experts had gained with officials in his capacity as WWF representative in Geneva. Officials who were somewhat apprehensive of this encounter relied upon his ability not only to reunite a representative number of NGOs but also to keep a professional and orderly tone to the encounter.

October 27 encounter with the OECD negotiators, that was most significant for the anti-MAI campaign. The meeting led to an unprecedented transnational coalition opposing the MAI. As co-ordinators of the OECD/NGO meeting, the organizers from WWF International in Geneva and FOE International in Amsterdam were determined to use the occasion to call upon as great a diversity of groups from around the world as they could.[13] Eventually, over 70 NGO representatives from 30 countries came to Paris. Organizers also intended to present a united front to officials. However, their objectives were not shared by all.

The NGO meeting quickly revealed deep divisions between three main groups of MAI opponents. One group included the so-called reformists who sought to amend the existing draft treaty through a consultative process with the OECD. Another consisted of the more radical groups of mobilizers who critiqued any meeting with officials as co-optation and who favoured protests. In between was a majority that agreed to meet with the OECD this once, but who nevertheless espoused a firm stance against the treaty. In the end, the week-end meeting resulted in a compromise expressed in the "Joint NGO Statement on the MAI" which was submitted to the OECD. The newly formed coalition asked for a suspension of the negotiations, a public assessment of the draft and changes to the existing draft that reflected the diverse concerns of coalition members.[14]

---

[13] The OECD proposal restricted the time allocated for a meeting as well as the number of participants. Organizers pressed the OECD for more time and participants (based on a joint letter to the OECD from FOE International and the WWF International dated 17 September 1997, confirmed in an interview with the FOE International organizer, November 1999, London, England).

[14] The joint statement submitted to the OECD begins with the self-identification: "[a]s a coalition of development, environment and consumer groups from around the world..." This document appeared on numerous anti-MAI groups' web site as well as on the OECD web site. Copies are also found in publications

The result of that meeting illustrates the difference between a coalition brought together for instrumental purposes and one formed as a result of social movement formation. The eventual agreement reached was based upon the realisation that a common position needed to be struck. Organizers and meeting participants acknowledged that the consensus expressed through the "Joint NGO Statement" was the most politically difficult position to establish among NGOs. The coalition brought together such an array of groups from different backgrounds, philosophies of action and objectives that their coming together and reaching a consensus was an unprecedented achievement in itself. However, the coalition was of a different nature than the emergent social movement networks against globalization. As illustrated below, this coalition was motivated by instrumental calculations. Members did not share a common world-view, nor a sense of collective identity and solidarity based on trust as is typical of social movement participants.

Divergencies regarding the relationship vis-à-vis the OECD revealed a lack of trust among coalition members. Some perceived a tension within the coalition due to some NGOs wanting to pursue contacts with the OECD in spite of a general commitment not to do so. Peer pressure seems to have been exercised on would-be dissenters. Also, participants commented that they knew they needed one another to achieve their respective goals. As some mobilizers who attended that meeting commented: "[the NGOs] all saw that the only way to win was through unity and that, for example, resulted

---

such as the Canadian Center for Policy Alternatives' *Dismantling Democracy* edited by Graham and Sanger (pp. 319-324) and trade journals such as *Inside U.S. Trade* (November 7, 1997, pp. 16-17).

in everybody sharing all their information." Likewise, "insiders" realized that they needed the support of actors from the social movement system of action if they were going to have any impact. As one "insider" commented: "we couldn't have carried that [campaign] solely by our own individual pressure, because you have to absolutely have public pressure which is building in a variety of constituencies"—an activity these reformist groups typically do not engage in. Another indication of their instrumental motive lay in the shared intention to show OECD officials that NGOs were not divided.[15] Finally, the arguments made in support of the claims included in the "Joint NGO Statement" raised issues regarding the incompatibility of the MAI with various existing international regimes such as those of the environment. This thinking reflected the interest group approach rather than the more critical view of an emerging social movement against globalization.

Although the coalition represented a significant turning point for all anti-MAI campaigners, it must be distinguished from the movement that was taking shape among other groups. One month prior to the December 1999 WTO meetings in Seattle, coalition members observed that this coalition had dissolved in spite of some attempts to keep it together for a WTO campaign. The key outcome of the October 1997 event was a commitment among NGOs to respect diversities among activists' styles of action, as long as the general aims of suspending the negotiations and publicly assessing the treaty were maintained. By 1998, 565 organizations in 68 countries had endorsed the "NGO

---

[15] As one insider commented: "we knew the officials were saying the NGOs will never stick together...particularly the Canadians were saying they're fractured...don't worry they'll never hold together, they'll be bickering."

Statement on the MAI."[16] As such, the "Joint NGO Statement on the MAI" provided a common direction for the remainder of the campaign—one which was more radical than originally sought by reformists.

The meeting between the coalition and negotiators convinced mobilizers and grassroots NGOs that their campaigns should be intensified. The Negotiating Group advised the coalition that instructions to suspend the negotiations had to come from Parliaments. While it can therefore be argued that the OECD as a forum represented a political constraint in terms of its response to opponents, the predominance of democratic regimes among OECD members represented a political opportunity for actors in the social movement system of action. Many mobilizers observed that their mutual strength and success was rooted in the fact that there was campaigning happening in numerous OECD countries simultaneously.[17] These campaigns will be elaborated upon in the following

---

[16] See *Dismantling Democracy* pp. 324-337 for a list of these organizations. Space prevents reproducing the list here. See Appendix B for a list of countries represented and the number of organizations.

[17] In terms of OECD members and not considering Internet campaigns, anti-MAI activities of significance took place in the following European countries: Austria, Belgium, Finland, France, Germany, Italy, the Netherlands, Sweden, Switzerland, and the United Kingdom. Outside of Europe opposition was particularly strong in Canada, the U.S., Australia and New Zealand. These reports are based upon interviews with MAI opponents, as well as the following studies: Henderson (1999: 27) quotes a report by Oxfam (U.K.) which recorded that by the end of the MAI negotiations active anti-MAI campaigns were taking place in more than half of the OECD; Kobrin, 1998; and articles by Khor and others in *Resurgence* (1997). In spite of the fact that Mexico is conspicuously absent from this list, there is reason to believe that opposition was also strong in that country. The Internet support for the NGO statement from Mexico was one of the most impressive: seventy-four Mexican NGOs signed on (see *Dismantling Democracy*, pp. 330-333). In addition, as will be seen below, several Mexican groups are found in the social movements networks that also participated in anti-MAI, anti-WTO campaigns. Most notorious were the links of the People Global Action network (PGA) to the Mexican Zapatista movement. Therefore, the absence of Mexico from the list of OECD countries where MAI opposition was recorded can be attributed to the lack of information on activities in that country and the fact that the research was conducted in Europe, Canada and the U.S. Although some activists commented on the weakness of opposition in countries such as Greece, Iceland and Turkey, little information or research has been undertaken to find out why this was so. Although Japanese NGOs figured on the Internet campaign, little anti-MAI activity was recorded in that country. Only one South Korean NGO figures on the Internet list and no activity was recorded in that country.

section. Suffice it to say for now that these occurred at several levels be they local, national, regional and international.

However, up until the October 1997 meeting, in spite of a growing awareness and opposition to the MAI among NGOs world-wide, little media attention or public interest had been manifested particularly in Europe. In addition to the insiders' work in Europe, some successful grassroots campaigns were under way in Canada and Australia and lobbying campaigns were taking place in the U.S. After the October meeting, mobilizers and intellectuals-engagés combined their efforts to stimulate grassroots campaigns in Western Europe. I now turn to these anti-MAI campaigns and to the explanation of an emergent social movement. The subsequent chapters will document these actors' influence in more detail.

II. Building a Social Movement

As will be illustrated in this section, intellectuals-engagés clearly placed their work within the social movement system of action. This group of actors built upon networks and solidarities that had developed during and after campaigns opposing free trade agreements. Their campaign objectives consisted of engendering public awareness through educational means and thereby stimulating mobilization against the MAI. Their critique of the MAI was placed within a broader world-view that eventually brought together diverse movements domestically and across borders. In that sense, this group succeeded in creating a social movement with a new world-view that spoke to and challenged the changing structures of a top-down world governance. The movement opposed the current process of economic globalization and its institutional foundations.

This section traces the evolution of this new actor by relying upon social movement theory. In doing so, the analysis documents how these MAI opponents built their campaign and how that campaign in turn reinforced the growth of the movement networks opposing globalization.

From Networks to TSMO

Subsequent to the North American Free Trade Agreement (NAFTA) and the Uruguay Round of trade negotiations, some leading activists and intellectuals regrouped under an organization that would play a key role in the anti-MAI campaign.[18] The International Forum on Globalization (IFG) first convened in San Francisco in January 1994.[19] This meeting aimed at developing conceptual and strategic innovations. As stated on the IFG web site, the result was the realization that the struggle against economic liberalization had to be re-articulated and that the consensus "that a globalized economy would lift all boats" needed to be questioned: "[t]he problem needed to be understood systematically, as a global process...the participants agreed to begin speaking out against economic globalization" (www.ifg.org, 1999:1). Also, it was determined that the critiques needed to expose the role that transnational corporations were believed to be playing to influence the global economic and political reorganization that was under way. The main

---

[18] In spite of the emphasis placed on this organization, it is important to point out that all activists without exception insisted on the fact that no centralized organization took responsibility for organizing an anti-MAI campaign.

[19] IFG describes itself as "an alliance of sixty leading activists, scholars, economists, researchers, and writers formed to stimulate new thinking, joint activity, and public education in response to the rapidly emerging economic and political arrangement called the global economy....Representing 40 organizations in 20 countries, the Forum's participants have come together out of a shared concern that the world's corporate and political leadership is undertaking a restructuring of global politics and economics that may prove as historically significant as any event since the Industrial Revolution" (www.ifg.org). Evidence from interviews revealed that this organization was built upon existing informal networks.

objective of these new strategies would be to build a "globalization from below." This mobilization would take place through public education and regrouping of cross sectoral interests domestically and transnationally.

Such cross-sectoral collaboration had already taken place in North America during the campaigns opposing the Canada/U.S. Free Trade Agreement (FTA) and the North American Free Trade Agreement (NAFTA). After these campaigns, existing networks with common experiences in this area of activism were revived and joined by new groups. A good example of this process is the formation in the fall of 1996 of the Common Front on the WTO in Canada. The Common Front regrouped the following organizations: the Sierra Club (Canada), the Polaris Institute, the Council of Canadians, the Canadian Environmental Law Association, the Canadian Labour Congress and the West Coast Environmental Law Association.[20] Some of these groups, such as the Polaris Institute, the Council of Canadians and the Canadian Labour Congress had collaborated in previous campaigns against the FTA and the NAFTA. In addition to cross- sectoral collaboration, the NAFTA campaign witnessed the development of cross-border networks. The U.S. groups Alliance for Responsible Trade (ART) and the Citizens' Trade Watch Campaign (CTC), the Mexican national network Red de Acción Frente de Libre Comercio (RAMLC) which included the NGO Equipo Pueblo, and the Canadian coalition at the time—Action Canada Network, Réseau Canadien d'Action—developed working relationships in their trinational campaign against free trade (Healy and Macdonald, 1997). This entailed a different type of rationale that moved away from nationalist and

---

[20] Based on May (1998: 33) and an interview with same in September 1999.

protectionist arguments.[21]

When IFG was formed, these domestic networks were further linked through the new organization as these leading activists and intellectuals found themselves around the IFG table. The transcontinental linkages that were created with IFG expanded the networks to a much broader geographical area. French activists that had contributed to the anti-GATT campaigns were also found on the IFG membership list, along with intellectuals from developing countries.

The cross-sectoral and cross-border representation is well illustrated in the IFG membership. The list represented old and new partnerships such as, among others: the Canadian Polaris Institute, an organization that focuses on corporate power, the Council of Canadians, a citizens' NGO involved in a diversity of issues, and the environmental NGO called West Coast Environmental Law; the American consumers NGO Public Citizens and the environmental NGOs Sierra Club (U.S.), Friends of the Earth and Rainforest Action Network; the Mexican Equipo Pueblo, a grassroots NGO that promotes peace and human rights (Healy and Macdonald, 1997: 14), and the Mexican Action Network for Free Trade; the Third World Network based in Malaysia which brings together southern intellectuals working on issues specific to those countries; the French anti-GATT activist Agnes Bertrand involved with the Observatoire de la Globalisation

---

[21] For example in Canada, the anti-FTA group named "Pro-Canada Network" changes its name to "Action Canada Network" and "Réseau Canadien d'Action" for their campaign opposing NAFTA. There were two reasons for this new name. One was that the name Pro-Canada was also used by federalist groups involved in the campaigns against Quebec separation. The other was linked to the intention to transform a domestic coalition of labor unions, environmental groups, anti-poverty groups and others which was based on economic nationalism to one which regrouped a similar mix of groups from the U.S., Mexico and Canada and which moved beyond economic nationalism (interview with Tony Clarke, the Polaris Institute, Ottawa, September 1999).

Economique, the Observatoire de la Mondialisation and Ecoropa, a small NGO working on Third World issues, as well as the powerful French labour union Confédération Générale du Travail (www.ifg.org.).

A number of new additions to the network from North and South also appear on the IFG list. Southern members appear on the web site list such as: Walden Bello from the organization "Focus on the Global South," based in Thailand; representatives from the NGO RENACE based in Chile; the Foundation for Science, Technology and Ecology from India; South Africa's Development Research Institute; the Philippine's Center for Alternative Development Initiatives and the Indigenous People's Network; and Brasil's IBASE. Significantly, organizations such as Ralph Nader's Public Citizen, an American consumers' NGO which had collaborated with nationalist groups during the campaign against NAFTA (Healy and Macdonald, 1997: 4, 55), now appeared on the IFG membership list. In addition, IFG developed working relations with new groups on an ongoing basis through public workshops and "teach-ins" that helped to expand these networks.[22]

Framing the Issues

The anti-MAI campaign benefited from these developments and in turn fuelled

---

[22] For example, a series of "teach-ins" and public meetings were organized in Canada in collaboration with IFG in November 1997. A meeting was organized for activists from around the world at the Canadian Auto Workers Center in Port Elgin (Ontario). The conference, titled "International Symposium on Corporate Rule," was attended by 90 activists from every continent. This conference was followed by what activists refer to as a "teach-in" which consisted of educational and debates seminars that took place at the University of Toronto. The latter was attended by 2,000 people. Although not intended to focus on the MAI, the issue became a flashpoint in these two meetings. Two Dutch activists who had attended these events were so impressed at the degree of grassroots mobilization in Canada that they were convinced that this type of mobilization should be replicated in Europe. They found that in Europe, campaigning on trade issues had always been more in the style of NGO experts lobbying and that no significant grassroots campaigning had yet taken place (interviews with Corporate Europe Observatory, Amsterdam, October 22, 1999).

their progress. As such the MAI, as an issue, and its negotiations among the mostly-democratic OECD members represented a political opportunity. Reflecting upon the arrival of the MAI in the midst of this evolutionary process, one IFG member observed: "all of that was part of a building process so the MAI became a bits of a focal point and a bit of a gift in that sense because it was such a classic example of what was really going on." Indeed, with its sole focus on protecting and liberalizing FDI, which is mostly undertaken by MNCs, the MAI was a perfect symbol of the type of globalization criticized by these groups.[23]

Intellectuals-engagés achieved that objective by making their analyses of the MAI available to as wide a public as possible, both materially and intellectually. Once they had secured a draft copy of the MAI three key steps were taken: first, develop an analysis of the draft treaty; then release the draft MAI text as well as the analysis on the Internet in order to make these permanently available to as many individuals as possible, and finally to release these in the media.[24]

As mentioned in the introduction to this section, this anti-MAI campaign only became visible in April 1997 due to the group's distance from the policy community, and

---

[23] The MAI as an issue also lent itself to building a social movement. As one MAI opponent explained "there are some issues that lend themselves to very small identity kinds of politics, and there are other issues that are multifaceted, that bring in a variety of different sectors, and it is those issues that allow for serious coalition building of social movement." In that sense the issue becomes an "organizing tool to bringing people together." The MAI lent itself to this type of mobilization strategy in that a number of issues of concern to various advocacy groups and diverse domestic concerns could be raised as critiques of the treaty. From safeguarding the "break [the MAI] apart" in order to show its impact on these diverse concerns.

[24] Interview with the Polaris Institute, September 1999.

the fact that the draft MAI was confidential.[25] The first analysis to be publicized in the manner described above was titled "MAI-Day: A Corporate Rule Treaty." It argued that the MAI was a "Charter of Rights and Freedoms" for transnational corporations which threatened social and democratic rights "granted to the peoples' of the planet by the [United Nations Universal Declaration of Human Rights]" and "the commitments to ecological stewardship made by the world's nations at the 1992 Rio Earth Summit" of the planet (Tony Clarke, 1997*b*: 12; Clarke and Barlow, 1997: 8). The release of these texts on the Internet launched a virtual public campaign that crossed borders and networks of networks linked their sites domestically and internationally.[26] The recorded increase in visits to the original site was an indication of the popularity of the document and its potential exposure.[27]

Analyses of the draft treaty were undertaken in other OECD countries, and were

---

[25] As in the case of the insiders' campaign, it was an IFG member from a Southern NGO who warned his Northern colleagues of the MAI. IFG members knew of the MAI negotiations as early as 1996 and some had informed their domestic networks. However, it was not until March of 1997 that the Canadian contingent of IFG managed to secure a copy of the draft document. For the details of this stage of the campaign see Clarke and Barlow, *MAI, The Multilateral Agreement on Investment and the Threat to Canadian Sovereignty*, Toronto: Stoddart Publishing Co. Limited, 1997.

[26] For example, Friends of the Earth-U.S. distributed these through their own e-mail network which consisted of about 400 organizations around the world. These groups had already established patterns of co-ordinated activities such as calling-days (to politicians), demonstrations, designing joint pamphlets and distributing them to memberships (interview with FOE-U.S., September 1999).

[27] Interview with the Canadian Center for Policy Alternatives September 1999. As Ron Deibert (1999) confirmed in his article on the Internet aspect of the anti-MAI campaign, the Corporate Rule Treaty text was linked to over a dozen different sites around the world. Also, research in Europe revealed that that first analysis was circulated in Europe, translated in several languages and helped to ignite several campaigns at different levels, including the European Parliament.

also made available to the public electronically and in print as didactic materials.[28] The strategy of public education proved crucial to mobilizing publics. Grassroots organizations and "mobilizers" used the material in public campaigns. Publics previously unaware of and/or uninterested in trade agreements were made aware of the potential impact that such international treaties could have on their everyday life. Typically, the material included glossaries of the technical and arcane language contained in trade agreements. They also often referred to the United Nations Universal Declaration of Human Rights and its Covenant on Economic, Social and Cultural Rights and the International Covenant on Civil and Political Rights. As was done in the "Corporate Rule Treaty," these analyses exposed the potential impact of the MAI on domestic policies, and were based on two main arguments. One was that the MAI expanded corporate power, the other that it violated democratic rights. This critical focus provided the flexibility to adapt arguments to various interests and political contexts. Comprehensive critiques could be developed so that a common opposition to the MAI could be achieved. The critiques of the MAI reflected intellectuals-engagés' world-view and would popularize their interpretation of economic globalization. The fact that these arguments resurfaced in the streets of Seattle against the WTO pointed to a growing acceptance of that world-view.

The critiques of the MAI dispute settlement process and the definition of

---

[28] See for example the Australian STOP MAI Coalition web site (www.avid.net.au/stopmai); the French NGO l'Observatoire de la Mondialisation "Manifeste du 28 avril 1998: (28 of April 1998 Manifesto) and the accompanying brochure titled *L'AMI non merci*; Friends of the Earth-US document titled *License to loot*; and Public Citizen's Global Trade Watch web site (www.citizen.org).

"expropriation" best reflect the broad application of this focus.[29] Whether they referred to the legislative protection of the environment, education, social services, culture, rights to secondary boycotts or to strike, MAI opponents pointed to these MAI provisions to show that the treaty gave rights to corporations at the expense of democratically elected governments and their citizens.[30] Not only would democratically elected governments be vulnerable to expensive lawsuits and settlements for legislation intended to protect their constituents' wishes, but the MAI would create a "chilling effect" on the willingness of governments to introduce new laws. This critique was fortuitously illustrated when, in the midst of the MAI negotiations, a U.S. company sued the Canadian government under the NAFTA.[31]

---

[29] As in the NAFTA, the dispute settlement mechanism provided for in the MAI allowed foreign investors to sue domestic (host) governments in cases of expropriation and violation of national treatment. The ability of investors to sue governments was objected-to in itself, and in particular in combination with Article IV, which dealt with investment protection. The concerns raised by the latter resided in the wording of what an expropriation consisted of. Article IV. 2.1 included "measures having equivalent effect" of expropriation and Article IV 3.1 titled "Protection from Strife" rendered governments liable for losses suffered from "civil disturbance, or any other similar event" (OECD draft MAI, April 24, 1998: 57-60). The fear was that any legislation could be interpreted as expropriation and that these and citizens' collective action, such as strikes or boycotts could render governments liable for compensation.

[30] See for example, the French booklet published by the Observatoire de la Mondialisation and titled *Lumière sur l'A.M.I. Le Test de Dracula* that was distributed to the members of the legislative assembly (1998: 44-48); FOE brochure *License to Loot* (1998:88); Australia's STOPMAI website (p.5); the American brochure titled *A citizen's guide to the WTO* (1999:17) published by the Working Group on the WTO/MAI that includes among others Public Citizen, International Brotherhood Teamsters, District 11 of the United Steelworkers of America, Alliance for Democracy; the Government of Canada Report of the Standing Committee on Foreign Affairs and International Trade (1997: 25-28).

[31] Briefly, the American Ethyl Corporation sought compensation from the Canadian government under the NAFTA dispute resolution process which was similar to that provided for in the draft MAI text. The company claimed CD$350 million which, it argued, was equivalent to the amount it estimated to have lost due to a piece of environmental legislation enacted by the Canadian government. The law prevented the importation of Ethyl's gasoline additive MMT (a manganese based material) on the grounds that it was harmful to human health. The case was settled out of court for an amount estimated at CD$20 million and after Canada dropped its ban on MMT and retracted its critique of the product (*The Globe and Mail*, August 21, 1998; *The Magazine*, Canadian Broadcasting Corporation, November 19, 1998).

Thus the MAI provided a crucial opportunity to revive the opposition to free trade and build upon existing networks to expand a growing movement opposing economic globalization. The international networks developed during the NAFTA campaign between Canadian and American activists solidified during the anti-MAI campaign, and expanded to Europe. With this campaign, the arguments had clearly moved beyond protectionist or nationalist concerns. Awareness of a globalization process inimical to ordinary citizens and undertaken in a secretive manner validated the critique of corporate power and democratic deficits. They created a sense of moral outrage and a collective identity of "we" as citizens versus the "other" as corporations along with an alternative view of globalization based on a shared sense of values.[32]

As Melucci has observed, social movements experience moments of public activity where they are visible, followed by latent periods.[33] During active periods of public protest, networks expand and ties of solidarity and the collective sense of belonging to a cause develop. When these public moments recede, informal networks nurture the movement through activities of inner reflection and intellectual development. New waves of mass mobilization depend upon the ability of a small group to rekindle the sense of solidarity and collective identity over time. The process of network building around the

---

[32] Note for example the text of the Council of Canadians' *The MAI Inquiry, Confronting Globalization and Reclaiming Democracy*. "Citizens in Canada...weren't satisfied....Why did we never seem to see our values and principles in these international trade and investment deals? Why did they always seem to reflect only the interests of big business?" In her article relating the anti-MAI campaign, Elizabeth May (1998: 42) makes observations that reveal a similar perspective; "*We* had been FTA'd and NAFTA'd...to death" (italics mine).

[33] The following interpretation of the literature is based upon della Porta and Diani's comprehensive review in *Social Movements and Introduction* (1999).

MAI bears these observations out. The following section illustrates the processes through which mobilization occurred and led to the expansion of a transnational social movement network against globalization.

Mobilization in Europe — the French Movement

Subsequent to the OECD/NGO meeting, North American groups collaborated with European mobilizers and intellectuals to help stimulate the building of national and cross-sectoral anti-MAI campaigns in Europe and to encourage links between European and North American activists.[34] Drawing upon relations they had developed through IFG meetings, a group of North American activists began, in January 1998, a series of strategy meetings in England, France and the Netherlands that brought together grassroots activists from neighbouring countries.[35]

Mobilizers in the Netherlands, Belgium and France utilized the didactic material described above and conducted intensive public education campaigns throughout their respective countries. A manual Internet listserv was developed and monitored from Amsterdam. Activists co-ordinated cross-country activities such as the February 7-17, 1998 "International Week of Action" and logjamming strategies such as "operation monkey wrench." The latter aimed at creating stumbling blocks inside the negotiations by

---

[34] Based on interviews with activists in North America and Western Europe in the fall of 1999. As already mentioned, with the noticeable exception Japan and South Korea and some smaller OECD members, campaigns had spread across the pacific to Australia and New Zealand. We also noted that Mexican groups contributed to the Internet campaigns. It is safe to assume that the transatlantic bridge was partly due to the fact that a critical mass of OECD members are located on the European continent and that the OECD headquarters are located in Paris.

[35] Aside from conducting intensive grassroots information campaigns, some also conducted campaigns at various political levels, including municipalities, Green political parties at the national and the European Parliamentary levels, and with diverse ministries.

informing countries of others' reservations. Most of these campaigns were typical of social movements: street theatre in the Finish capital Helsinki, flyers handed out in Sweden denouncing a multinational's environmental practices, demonstrations in the streets of London in front of the ministry responsible for the negotiations, illegal occupation of the office of the Chief negotiator in the Netherlands (Khor, 1997*b*: 25, 26).

Unlike Canada where successful mobilization had begun in the Spring of 1997, mobilization only became visible in most OECD countries in early 1998.[36] Opposition campaigns intensified between January and October, 1998. Limited space prevents a more detailed account of these multiple campaigns and the following chapters will provide further details on the question of impact. Suffice it to say that the lack of political will to pursue the negotiations in October 1998 must be attributed, in part, to the intense campaigning at several political levels by insiders as well as by actors from the social movement system of action. As has been observed elsewhere, "most governments seized the opportunity to abandon the negotiations offered by the French reluctance to resume the project" (Dymond, 1999: 26; see also Henderson, 1999: 29).[37] The remainder of this section will focus on the anti-MAI campaigns which took place in France for several reasons.

First, mobilization in France was significant because it was decisive for the

---

[36] See May, 1998, pp. 32-47, for an account of the Canadian campaign.

[37] This view was shared by a senior European Commission official who had been involved in the negotiations. The perception within the negotiations, according to that official, was that there was a general sense of relief when France declared it would no longer participate in the negotiations. A good indication of this view was that non of the European Union members complained about France's unilateral announcement of its withdrawal prior to consulting with its fellow European Union members.

negotiations and also, since OECD headquarters were located in that country international protests and linkages were most visible there. As such, that campaign provides ample documentation for the study. Second, the anti-MAI campaign in France more than anywhere else showed signs of a social movement emerging against the kind of economic globalization critiqued by intellectuals-engagés. The evolution of the French anti-MAI campaign also generated the most media coverage. This media attention was directly linked to the successful cross-sectoral regrouping of diverse interests. The campaign began in earnest in January 1998 when intellectuals-engagés from the Observatoire de la Mondialisation and cultural groups, referred to in France as "les cultureux" (the culturals), joined forces and called in front line activists.

Not only did a coalition with the cultureux provide publicity to the MAI, but the union also meant a significant change in that group's opposition to multilateral economic agreements. During the Uruguay Round of negotiations, cultural groups and farmers' groups actively sought and succeeded in gaining protection for their sectoral interests. The anti-MAI campaign transformed this interest group approach as it united these diverse interests under one argument. As described in the remainder of this section and the next, the campaign ultimately transformed itself into a sustained movement which emerged in the anti-MAI demonstrations and continued with protests against the WTO in France and Seattle.[38]

---

[38] So many protests have taken place since that activists have devised codes to name them: *A16* for the April 16, 2000 World Bank and IMF annual meeting in Washington D.C.; *M8* for the protests against the annual Asia Development Bank meeting in May 2000; *J5* protests on the occasion of the June 2000 of the Organization of American States in Windsor, Ontario; *J12* on the occasion of the June 2000 meeting of the World Petroleum Congress in Calgary, Alberta; *J15* for an anti globlization protest in Bologna, Italy; *S11* at the September 2000 meeting of the World Economic Forum in Melbourne, Australia; *S26* again against the

According to French intellectuals-engagés, it was a February 10, 1998 article published in the main French daily newspaper *Le Monde* that kicked off the media campaign and gave their anti-MAI campaign its impetus.[39] The author of this article, Jack Lang, was a well-known and respected politician among the cultureux. He had been the French Minister of Culture under President François Mitterrand, and was considered the father of the idea of "cultural exception" in multilateral economic agreements. At the time of the MAI negotiations he was also the President of the External Affairs Committee of the French General Assembly. Rather than focusing specifically on the cultural exception the article reflects the broader critique against economic globalization espoused by intellectuals-engagés. In that sense, the article represents a significant departure.

Organizations from that sector of the French economy had held several public conferences on the MAI, mainly focusing on securing a cultural exception. As time progressed, and beginning with a February 16, 1998 meeting at the Théâtre de l'Odéon, the cultureux moved from the language of cultural exception to that of democratic rights to be safeguarded against multinational corporations and an ideology of free markets. On the occasion of the latter and most publicized meeting, high profile figures from the French cultural milieux denounced the MAI stressing that it was not their own particular

---

IFM/ World Bank semi-annual meeting of September 2000;*A17* was the name of the protests against the Summit of the Free Trade Are of the Americas (FTAA) in Quebec city (Barlow and Clarke, 2001: 32).

[39] See *Le Monde*, February 10, 1998, "L'AMI c'est l'ennemi," ("The Friend is the Enemy) by Jack Lang. The title is a play on words since in French the acronym of the MAI (AMI) means friend. Intellectuals-engagés approached Lang as early as October 1997. This was confirmed in Lang's speech to the symposium of April 22, 1998 which took place at the Assemblée Nationale. In that speech he stated that not only had the Observatoire de la Mondialisation warned him of the MAI in October of 1997, but that at the time neither politicians nor journalists were aware of the MAI (Actes du Colloque du 22 avril, 1998 à l'Assemblée Nationale, p. 71).

interests that they were defending but a much higher collective ideal named "democracy and freedom."[40] In his speech to the April 22, 1998 symposium organized at the General Assembly, the co-chair of the film producers' association (Société des réalisateurs de films) warned that securing a "cultural exception" in the MAI was less important than questioning the broader implications of the agreement. He argued that what was at stake in the MAI was not just creative rights but citizens' rights and the freedom to create within an environment chosen democratically.[41]

The third significant group to join the coalition was an organization called "Droits Devant!!." These activists brought to the campaign their successful experience in mobilization and their ties with a network of social movements. The group had successfully engendered a social movement in 1994 referred to as the "sans logis" (the homeless) which had won over public opinion.[42] These mobilizers were committed to grassroots mobilization and sought to reunite as many different "citizens' movements" as possible. Within six months this anti-MAI campaign had succeeded in rallying a diversity of French groups to its cause, and generated media attention and public interest to the

---

[40] See *Le Monde*, February 18, 1998. "A l'Odéon: ce n'est qu'un début, continuons le combat...." (At the Odeon: This is only the beginning, let us continue the struggle), by Jean Michel Frodon.

[41] Actes du Colloque du 22 avril 1998 à l'Assemblée Nationale, pp. 28-29.

[42] See Alain Touraine (1999) *Comment Sortir du Libéralisme*, for an analysis of the emergence and evolution of several social movements which emerged in France between 1994 and the legislative elections of 1997. Among those were groups who made claims with and on behalf of aliens "sans papiers" (immigrants and their children living in France without citizenship papers), those who made claims for the "sans logis" (the homeless) and those who made claims on behalf of the unemployed.

issues it raised.[43] These activists and members of their organizations planned to go to Seattle.[44]

One such group was the French farmers' organization called Confédération Paysanne. This organization and its well-known leader José Bové oppose large-scale, intensive industrial agriculture and make claims on behalf of small and medium producers. It denounces programs such as food aid and export subsidies that serve to support large grain producers, be they French or American, at the expense of small Third World farmers. As such, Confédération Paysanne calls for sustainable agriculture and food security through national self-sufficiency and "against a model of agriculture and food production that only serves multinational corporations' interests."[45] Bové also criticizes what he refers to as *Frankenfoods*, and he fosters a concept of agriculture called "multifonctionalité" (multi functionality). Multifunctionality of agriculture includes claims for a better quality food, safeguarding the environment through sustainable farming, and

---

[43] A testimony to this rapid evolution is captured in the name given to the emerging movement. The CCAMI, or "Coordination Contre l'AMI" (Co-ordination against the MAI), was formed in early 1998, two and a half years after the MAI negotiations were launched and six months before they collapsed. By the fall of 1998, the CCAMI had become the CCCA - "Coordination contre les clônes de l'AMI" (Coordination against MAI clones) as a reaction against other attempts at plurilateral economic agreements. Two months before the launch of the WTO Millenium Round in Seattle the movement was renamed the CCCOMC or "Coordination pour le contrôle citoyen de l'OMC" (Co-ordination for a citizens' control of the WTO). To the list of organizations which signed onto the 28 April 1998 Manifesto that marked the creation of the CCAMI were added newcomers such as the French NGO Attac. The latter organization grew spontaneously from an article in *Le Monde Diplomatique* which criticized capital movements. Within a year it grew to 14,000 members (*Le Point*, 26 November, 1999: 98).

[44] Their networks extended to the U.S. where a hospitality network was set up so that French demonstrators could find lodging in Seattle.

[45] See José Bové, *Le Monde Diplomatique*, October, 1999, p. 32 and *Campagnes Solidaires*, No. 134, October 1999, p. XII.

preserving farm employment, communities and cultures through traditional agriculture.[46]

The French organization extended its activities through a transnational network that includes the European farmers' organization CPE (Coordination paysanne européenne) and an international organization called Via Campesina that links 69 organizations in 37 countries from Europe, Asia, the U.S., Latin America and the Caribbean. Another way in which Bové's organization fosters its views is through work it conducts in collaboration with ecologists, producers and consumers.

Since the OECD headquarters are located in Paris, it was decided to organize transnational anti-MAI protests in the public parks that surrounded the OECD. French mobilizers organized a first small demonstration in February 1998. A much larger international protest took place on April 28, 1998 on the occasion of the OECD Ministerial meeting that was to decide the fate of the negotiations. For the occasion, French activists published the "Manifeste du 28 avril 1998) which was endorsed by 70 organizations. Among a cross-sectoral representation of French groups, organizations from other European countries and North America were also listed. Leading activists from other parts of the OECD contributed to the events planned for the occasion. Another "international Citizens' Summit" against the MAI took place from October 17-20, 1998 along a similar format and with the same international coalition.[47]

---

[46] This concept is gaining increasing popularity in Europe particularly since the multiple episodes of food contamination, such as the Mad Cow Disease and the dioxin contamination of chicken farms in Belgium (interview with OECD Environment Directorate, October 1999).

[47] Also, in January 1999, the newly formed French organization Attac and CCAMI organized the first in a series of demonstrations against the international business forum in Davos, Switzerland.

III. From anti-MAI to anti-Corporate Globalization

As with the Paris street demonstrations against the OECD MAI, since the WTO ministerial meeting was taking place in Seattle local groups from the U.S. West Coast organized the international anti-WTO protests. Mobilizers' organizations from the West Coast formed the Direct Action Network (DAN) to co-ordinate peaceful protests and other events. DAN was sponsored by, among others, the Rainforest Action Network (RAN), a member of IFG, and the People's Global Action (PGA), an organization that originated in the Mexican Zapatista movement (Moynihan, 1999: 5; Hahnel, 1999: 7). IFG also organized a successful teach-in on November 27 which was attended by over two thousand individuals.[48] As with many others who found themselves protesting in Seattle, the Confédération Paysanne was part of a growing transnational network. Its links and solidarity with international farmers' organizations and with the French movement, which was itself linked to networks on several continents, was a microcosmic example of a larger transnational pattern. Figure 4.1 illustrates some of these interconnected networks.[49] Thus, not only were anti-MAI mobilizers and intellectuals in Seattle but new groups had now joined and replicated their action patterns.

This chapter has located the roots of the Seattle protests in the anti-MAI campaign led by intellectuals-engagés and mobilizers. While a movement at the global level had not

---

[48] Canadian Broadcasting Corporation, interview with Maude Barlow, *The Magazine*, November 29, 1999, see also Barlow and Clarke (2001: 11).

[49] The model does not begin to represent all groups present in Seattle. For example, groups from the South were present: Kenya's Consumers' Information Network, Ecuador's Acción Ecológica and Trinidad and Tobago's Caribbean Association for Feminist Research (*Time*, November 29, 1999: 30), as well as individuals such as Guido Espana, a free-lance chemical engineer from Bolivia critical of the Southern diplomats' representation of their citizens at the WTO (*The Wall Street Journal*, December 2, 1999).

FIG. 4.1 - THE MOVEMENT AGAINST ECONOMIC GLOBALIZATION

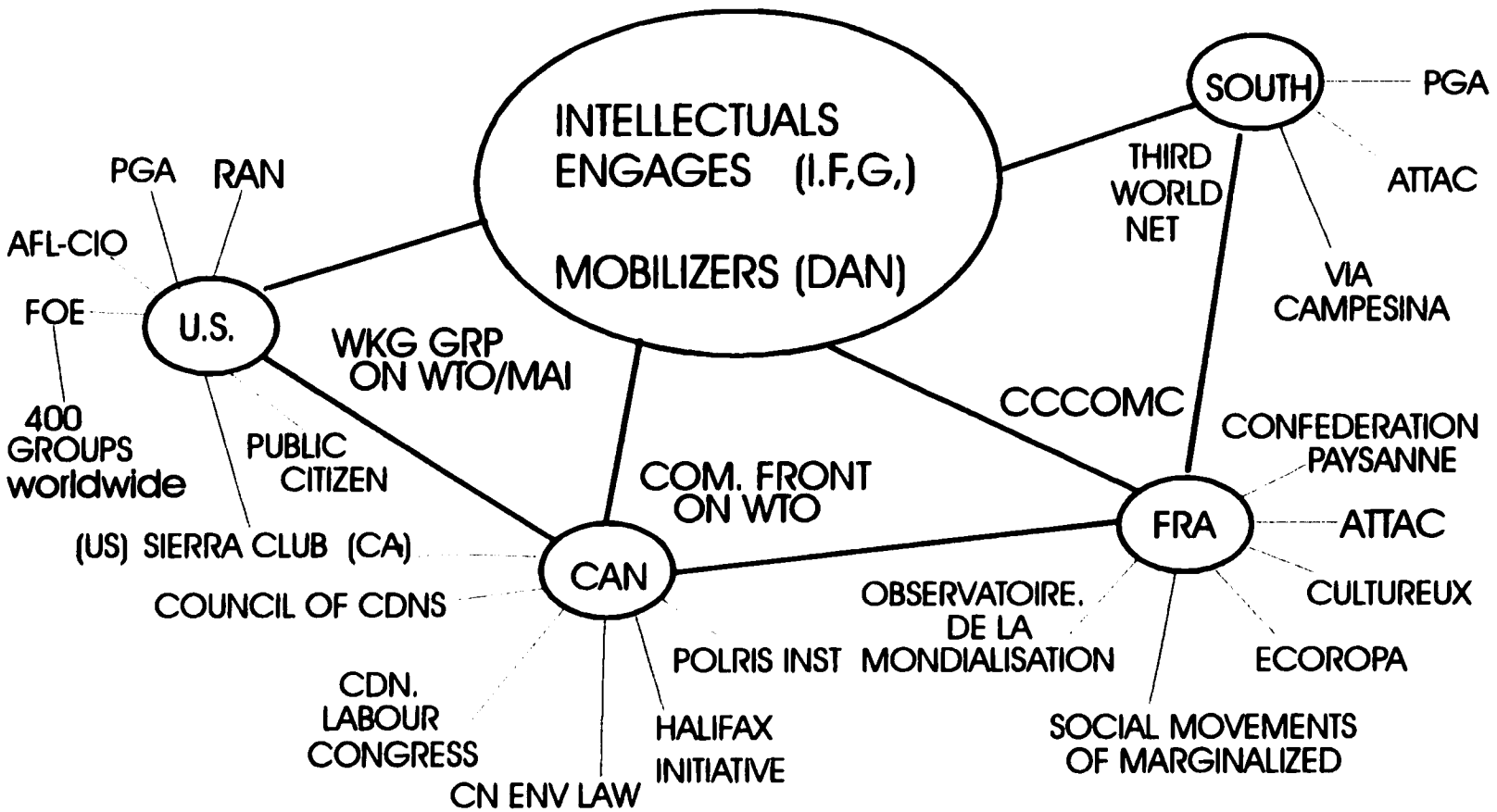

yet emerged in the anti-MAI campaign, the Seattle events strongly point in that direction. A good sign that the existence of a transnational movement resides in these networks is the adoption of a common world view and the sense of collective identity thus shared by protesters in many countries. The evolution of diverse oppositions against economic liberalization into a movement was in large part due to the formulation of arguments against a particular kind of economic globalization during the anti-MAI campaign. As was illustrated above, the increasing numbers of protesters from the post-NAFTA and Uruguay Round campaigns who shared the intellectuals' world-view confirms the successful evolution of processes described in social movement literature.

Indeed, arguments similar to those raised against the MAI resurfaced in the anti-WTO protests. They were well illustrated in slogans such as "No Globalization without representation," and the banner hung from a crane by the Rainforest Action Network which displayed two arrows pointing in opposite directions—one labelled "WTO" and the other "DEMOCRACY." Similarly, the WTO dispute settlement process was not only criticized for its "secretive" nature, but also for its consistent rulings against domestic legislation arrived at through a democratic process. The latter critique was highlighted by protesters in turtle costumes—symbol of a trade dispute lost at the cost of environmental legislation. The opposition to large multinationals was also expressed in diverse forms such as one bare-chested protester who had written on her back "RATHER NAKED THAN NIKE" (*The Globe and Mail*, December 4,1999: A7), and the banner used in a French anti-WTO demonstration claiming "LES MULTINATIONALES NE FERONT PAS LA LOI" (Multinationals will not rule) (*Le Point*, November 26, 1999: 101).

As such, the Seattle protests were the outcome of processes described in the social movement literature and reflected the outcomes explained in della Porta and Diani's (1999: 253) conclusion to the effect that:

> Most social movements survive the decline of mobilization, oscillating between visibility and latency (Melucci, 1989: 70-3), within a larger family of movements, the organizational infrastructure and mobilization potential of which they help to increase.

In light of such observations, the growth potential of this social opposition should not be dismissed. Together with the anti-MAI protests, the recurrence of protests and their growth in size at international economic ministerial meetings indicates that the processes described in social movement literature are at play. As one observer of trade meetings commented: "[t]en years ago, trade ministers' meetings attracted only a handful of protesters who were largely seen as cranks" (Greenhouse, 1999: A12). As the Seattle protests were winding down along with the WTO meeting, leading activists were already expressing their determination to pursue their common opposition to the present processes of economic globalization.[50]

In hindsight, the anti-MAI campaigns proved to be a threshold. Not only did they engender the Seattle protests but since Seattle, these societal actors have seized upon several opportunities to sustain mobilization and media attention. By 2001, two years after the MAI events ended, several protests took place in various countries against international economic institutions with a similar message. The semi-annual meeting of

---

[50] See Ralph Nader's interview in *Le Monde*, December 3rd, 1999*b*, p. 2: "I do not think that technocrats will take into account [the Seattle warnings]. This is why we will remain mobilized." See also John Sweeney's, head of the AFL-CIO, statement in the *New York Times*, December 6, 1999: "We're really in it for the long haul on the trade issue...We've been working on building this coalition for a few years now, and we'll now put our heads together to see how we build on this."

the two Bretton Woods institutions, the World Bank and the IMF, which take place in April in Washington D.C., also witnessed "anti-globalization" protests in April 2000. Demonstrations took place later that year against the same gathering in Prague. In Canada, a series of protests were planned around the Ministerial Meeting of the Organization of American States in the Spring of 2000 with another much larger international protest that took place against the Summit of the Americas in Quebec City in the Spring of 2001. In Europe, the annual January meetings of global corporate elites and high government officials which take place in the small Swiss resort of Davos have likewise been under assault. In January 2001, while the annual Davos meeting had become an "armed camp" a peaceful World Social Forum was organized in Porto Allegre, Brazil, as a counter statement to Davos. In France, the trial of José Bové, the leader of the Confédération Paysanne who dismantled a McDonald's, attracted thousands of protesters/supporters from around the world. The movement has now been more clearly identified as a movement against corporate globalization in order to clearly state that the critique is not against trade *per se* but against skewed rules that enable corporations "to usurp local control over the environment, labour, health, education and agriculture" (Johnson, March 12, 2001: 26).

Conclusion

The purpose of this chapter was to provide an understanding of the heterogeneous opposition to the MAI so that I could further analyse their influence on the negotiations and their meaning for world politics. In order to do so, I applied the conceptual framework of civil society devised in the form of a model in Chapter 3. The reasons for

devising a model were multiple. While most terms utilized in various case studies that look at societal actors' influence on the policy making process partially encapsulated the MAI opposition, none did so completely. This was due to the unprecedented coalition among societal opponents of the MAI and the association of particular concepts with distinct approaches in political science such as "liberal pluralism" and "critical theory" (Macdonald, 1994).

For example, the terms "transnational civil society" or "global civil society" (see for example, Lipschutz, 1996; Wapner, 1996; Price, 1998) are as much criticized as they are widely used to refer to a broad range of societal actors. Even when applied at the global level the evaluation of the political significance of such an entity reflects various perspectives. When the term is adopted to suggest the presence of a civil society beyond the nation-state, there are differences between liberal-pluralist and critical theorists' interpretations of such a society. Whereas the liberal-pluralist analysts see non-state actors as being akin to domestic pressure groups, critical theorists focus on "progressive NGOs" with counter-hegemonic potential (Macdonald, 1994: 284).

My contention is that both types of societal actors were present in the anti-MAI campaigns. The empirical evidence reflected such a dichotomy in the anti-MAI opposition. That observation was made possible with the use of the model of civil society devised in Chapter 3. The anti-MAI campaigns eventually presented an unprecedented common front in terms of one objective: to suspend the negotiations. Beyond that immediate objective, however, the strategies of influence and the concomitant changes sought out by these groups were distinct. As Macdonald (1994: 283, 284) observed in the case of

NGOs in Latin America, progressive NGOs hold a "transformational ideology" and "attempt to strengthen social movements linked to the popular sector," while others seek changes that "avoid modifications in the structure of power."

The analysis of the anti-MAI campaigns revealed that the groups identified with the social movement system of action belonged to the former category in that they pointed to the process of globalization as inimical to ordinary citizens and benefitting large corporations, and they seek to fundamentally alter that process. The groups and NGOs that we identified with the interest group system of action belonged to the second type described by Macdonald in that they did not criticize the objectives of the international economic regimes but only sought to have policy changes that reflected their concerns included within various international arrangements. As one such reformist MAI opponent confirmed: "you've got to take the views of the Board of Directors...you can't go in there with a 'trash capitalism' because half the people, well more than half of the people probably are heads of MNCs....My organization has no mandate to have an opinion about global democracy really."

Not all case studies described in the literature exhibit such dichotomies. The anti-MAI campaigns did so explicitly, as have other case studies that focused on the interactions of societal actors with various international economic fora. In such analyses the narrowness of one's question and the concomitant selection bias of the societal actors can affect the analyst's understanding of these actors. As such, the selection of one's topic and related non-state actors can provide a picture of societal actors involved in transnational relations that reflects either the liberal pluralist or the critical view of these

actors.

A good example of this problem is found in the study by O'Brien et al. (2000: 134-153). That case study examines the interactions between the global "Environmental Social Movement" (ESM) and the World Trade Organization (WTO). While providing a valuable empirical contribution to the literature, the study offers an incomplete picture of the societal actors that challenge the policies emanating from this regime. Focused as that research was on the interactions between societal actors and such supranational organizations as the WTO, the IMF and the World Bank, an inherent selection bias occurred in terms of the societal actors examined. By their own acknowledgement, the authors' study regarding these societal actors' interaction with the WTO was focused on "reformists" who "engaged in lobbying for reform of the rules of the trading systems" and who work "from a liberal belief in the efficacy of pluralism" (O'Brien et al., 2000: 141, 152). That meant that the analysis of another category of activists whom the authors called "radicals" was neglected. As a result, the meaning of the latter actors for world politics and the difference between the influence they sought to exercise and that sought by the "reformists" was excluded from the analysis.

There are several difficulties involved in referring to societal actors with overarching concepts such as "global social movement" or "global civil society." As was pointed out by Macdonald (1994), civil society at the domestic level includes all types of actors, some of whom are of the kind described by liberal-pluralists while others seek to advance what critical theorists refer to as more profound transformative projects. Furthermore, as Cox (1999: 5) has put it:

> Any fixed definition of the content of the concept "civil society" would just freeze a particular moment in history .... Rather than look for clearer definitions, we should try to understand the historical variations that have altered the meanings of the concept in the ongoing dialectic of concept and reality.

This observation applies to social movements that have experienced transformations over time. Social movements which emerged in the 1960s have changed and evolved over the past thirty years, as did the political and social environments within which they have evolved. Some movements' issues, such as those espoused by environmentalists, have become part of the political agenda at the domestic and transnational levels. In Europe, Green political parties have emerged from segments of those movements. In several countries these parties have attained shares of political power. Also, movements have grown since the 1960s from sporadic protests by scattered individuals to large TSMOs such as Greenpeace.[51] Many organizations have sprung up since then, some of which, although sharing similar concerns regarding the environment, seek to fulfil their objectives within existing regimes and interstate arrangements while others seek more profound societal and political transformations that challenge such arrangements. These differences can only come to light through the use of flexible tools of analysis that account for such fluctuations. This is what has been attempted with the model formulated in Chapter 3.

As a result of its application on the case study, I am now able to place various societal actors involved in the opposition to the MAI within the model (See fig. 4.2). Their relative position on the template indicate that those MAI opponents' display the same characteristics as those of the systems of actions identified in Chapter 3 in terms of:

---

[51] See Wapner (1996) for a good history of Greenpeace, the World Wildlife Fund and Friends of the Earth.

FIGURE 4.2 CIVIL SOCIETY INFLUENCE ON THE MAI

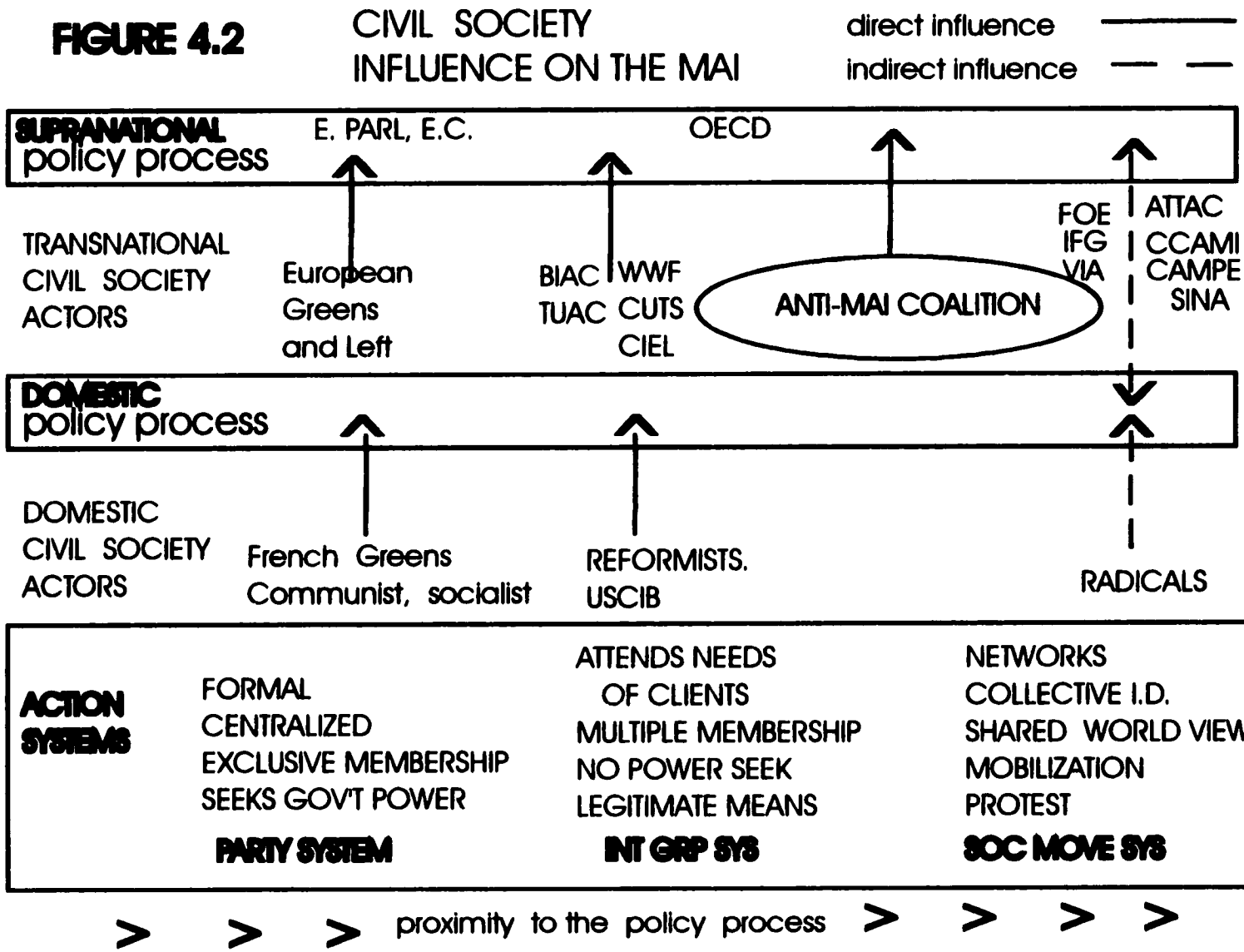

their proximity to the policy-making process, their motives and objectives and their behaviour. Differences among MAI opponents also correspond to those drawn between systems of action in the model. As such the model enables us to summarize the results of the analysis.

A number of organizations such as the World Wildlife Fund, CIEL, CUTS, TUAC and BIAC appear in the interest group system of action. These are organizations that have been included on a consultative basis in various economic multilateral fora for some time. As such they describe their activities in terms of collaborating with governments and lobbying. The issues that concern them vary from environmental conservation, labour, consumers' rights and business interests. Their opposition to the MAI reflected their specific issue of concern and their attempts to have changes included in the treaty focused on policies relating to these issues specifically. Their relative proximity to the policy-making process explained the earlier campaign led by reformists such as WWF, CUTS and CIEL, and the inclusion of TUAC and BIAC in consultations with the OECD regarding the MAI since the early 1990s.

A significant result of the analysis concerns the emergence of social movement networks. I relied upon social movement theory to demonstrate the emergence of transnational social movement networks. Although MAI opponents referred to as "intellectuals-engagés" expressed the desire to see a broader global opposition to the processes of economic globalization, of which they considered the MAI to be a crucial component, and although the mobilization against the MAI reached visible and widespread proportions, the long-term success of those actors' objectives were not immediately

apparent. However, and as demonstrated in this chapter, the anti-MAI campaigns undertaken by these opponents eventually led to the significant mobilization against the World Trade Organization (WTO) that took place in the streets of Seattle one year after the demise of the MAI at the OECD. Since then, numerous similar demonstrations have been visible in most parts of the world. This is a new societal actor that seeks to transform international economic relations. As such, the MAI events represent a threshold in world politics and in international economic relations.

Within the social movement system of action we find a new TSMO in the International Forum on Globalization (IFG) that regroups intellectuals-engagés active at the domestic and transnational levels. In addition, and as shown in Figure 4.1, several groups that include domestic SMOs and militant-mobilizers make up the transnational social movement networks. In between the interest group and social movement systems of action we find the coalition that was struck among these various MAI opponents in order to maximize their main objective: to stop the OECD MAI.

The anti-systemic nature of the claims espoused by intellectual-engagés and militant-mobilizers and their preferred mode of action explain these actors' distance from the policy making process. That is, the critique directed against the MAI by intellectuals-engagés and militant-mobilizers was linked to a broader critique against a process of economic globalization perceived to be detrimental to citizens and societies at large. The anti-systemic and normative challenges espoused by these MAI opponents differ from the policy focus of the so-called reformist NGOs such as WWF, CIEL and CUTS. The latter do not challenge processes of economic globalization nor do they argue that MNCs play a

negative role in that process. Rather, they work within existing policy regimes in order to have their particular policy concerns included within those regimes. In that sense they cannot be identified, as are social movement actors, as "anti-systemic." On the contrary, they describe themselves as collaborating and lobbying with various entities involved in the policy-making process at the domestic and international levels.

As such, the distinction between various MAI opponents was also highlighted by the way in which they led their respective campaigns. While INGOs such as WWF and CIEL attempted to engage a broader formal process of consultation between OECD officials and NGOs, intellectuals-engagés and militant-mobilizers pursued strategies of public information and mobilization. Their campaigns aimed to sensitize a broader public of their critiques, to gain broader support for their cause and thereby demonstrate to politicians through mobilization and the logic of numbers the strength of their opposition. As will be seen in the next two chapters, these respective strategies in the opposition to the MAI brought different results.

The research and analysis undertaken herein have also highlighted the fact that the initial warning about the MAI in both systems of action came from Southern NGOs. Both among insiders and intellectuals-engagés, these NGOs were acknowledged as having alerted their Northern colleagues to the MAI negotiations. The MAI involved two significant difficulties for Southern countries. One was the fact that they were excluded from the negotiations, the other was the reluctance on the part of some Southern states to forego their control on development policies concerning investments. Therefore the role of these Southern NGOs, and their location in the model also needs to be taken into

consideration and assessed within a broader context of international relations.

The coalition that was struck among these diverse MAI opponents did not survive the anti-MAI campaigns since it was motivated by instrumental goals on the part of all MAI opponents. In that sense, the coalition can best be understood as a radicalization of the opposition to the MAI in that the more moderate reformist groups that belong to the interest group system of action adopted an unusual radical stance. They agreed to cease all dialogue with OECD officials and to stop the negotiations of the agreement rather than reforming its content through continued dialogue. The only meeting between the coalition and the OECD negotiators, as will be explained in Chapter 6, did have some direct impact on the negotiations.

While the coalition had a direct impact inside the negotiations, the diverse strategies espoused by reformists and radicals also had distinct effects. These differences are highlighted in Chapters 5 and 6 where the differences among MAI opponents drawn in this chapter and their concomitant chronology of campaigns will be juxtaposed to the progress of the negotiations in order to assess their impact on the negotiations.

CHAPTER V

FIRST NEGOTIATIONS' MANDATE: CIVIL SOCIETY IN TRANSITION

Introduction

The analysis undertaken in this chapter and the next is based on a juxtaposition of the various anti-MAI campaigns documented in the previous chapter with the progress of the negotiations. The latter are broken down into three periods, each characterized by its temporal coincidence with the respective campaigns waged against the MAI. This chapter traces the developments which took place within the negotiations during a *transitional* period dominated by groups within civil society commonly referred to as insiders or reformists. This first period coincides with the first negotiating mandate and the first two years of negotiations from May 1995 to April 1997, the date set as the initial deadline in the mandate. The transitional characteristic of this period is attributed to the transformations which occurred in terms of civil society awareness of the MAI as the so-called insiders from the interest group system of action became aware of the MAI and pressed for substantive changes in the treaty that reflected their particular concerns. Transition also illustrates the beginning of a broader-based opposition towards the end of this period.

A second period characterized as one of *convergence* covers the months from April 1997 to the second deadline of April 1998. That period is taken up in the next chapter. As illustrated in Chapter 4 convergence during this period occurred in several ways. Most significant was the emergence of the so-called intellectuals-engagés' campaigns where groups from diverse backgrounds and nationalities conducted simultaneous campaigns at the domestic and transnational levels. Finally, a third period of *conjuncture*, also covered in Chapter 6, characterized the circumstances which resulted in

the demise of the MAI negotiations. The final period consisted of the six-month designated pause prior to the resumption of the negotiations in October 1998.

The following analysis begins by looking at the progress of the negotiations over the first 19 months and then turns to the influence of the insiders' campaign during that period. The chronology of the anti-MAI campaigns outlined in the previous chapter indicated that, during this first period of the negotiations, the opposition to the MAI had been mainly expressed by the so-called "insider" groups in Europe. Although by the end of the first period of negotiations a broader opposition was engendered by "intellectuals-engagés", that campaign was still embryonic and not yet publicly visible.

Two types of MAI opponents' influence are distinguished. *Direct influence* refers to influence on the substantive issues within the negotiations while *indirect influence* refers to the influence gained through increased pressure on elected officials by various means.[1] Since the analysis spreads over two chapters, the discussion regarding the assessment of those influences is undertaken in Chapter 6. Suffice it to say that the first period of negotiations was relatively uneventful as far as societal opposition was concerned. Although officials and negotiators became aware of reformists' concerns, the changes they proposed to address these NGOs' substantive concerns fell far short of their expectations. While insiders' critiques had some effect on the negotiations the failure to reach the first deadline can be clearly attributed to other difficulties inside the negotiations where unexpected and challenging stumbling blocks emerged that would delay OECD

---

[1] This distinction corresponds to Henderson's reference to direct and indirect impacts in *The MAI Affair* (1999: 28).

members' agreement on a high-standard MAI.

I. Negotiations Period I: May 1995 to April 1997

Completing the MAI Framework

The MAI negotiations were launched in a climate of extreme optimism. Not only were like-minded countries expected to reach an agreement in a short time frame but it was also expected that they would succeed in agreeing upon a high-standard treaty.[2] Although the mandate to negotiate a MAI at the OECD was adopted in May 1995, the Negotiating Group (NG) only began meeting on a regular basis in late September 1995, thereby leaving only 19 months to complete negotiations by the initial deadline. Since the NG had agreed early on that it would meet approximately every six weeks, the negotiators initially expected to reach an agreement after having met an average of twelve times.

The procedural arrangements under which the negotiations were to be undertaken reflected a desire for efficiency which was made necessary by the short time frame allocated to complete the agreement. Thus the decision was taken by a majority of delegates in the NG to by-pass the OECD committee structure. This was deemed necessary for a speedy conclusion of the negotiations in order to avoid "turf battles" and to eliminate "the need for co-ordination" which the involvement of these committees would have required (Huner, 1998: 4). The independence of the NG from standing OECD committees also reflected the fact that the MAI was to be an independent treaty so that non-OECD countries would later on be able to accede to the treaty. Also intended to

---

[2] The OECD ministerial mandate reflected such ambitious goals in that it called for "a broad multilateral framework for international investment with *high standards* for the liberalization of investment regimes and investment protection and with effective dispute settlement procedures" (OECD, 1995*a*:2).

save time was the idea of relying on ad hoc committees which would work under the authority of the NG. The NG would rely on two types of working groups made up of technical experts from member countries. The NG would be free to form "drafting groups" (DGs) and "expert groups" (EGs) for short periods and specific tasks according to its needs (OECD, 1995*b*). The latter arrangement would avoid groups "taking a life of their own" and spending time "studying theoretical issues behind the investment talks instead of focusing on getting an agreement" (*Inside U.S. Trade*, September 15, 1995: 28).

The program of work which was adopted for the so-called "first phase of negotiations" was to complete what the NG Chairman's metaphor referred to as "the building framework." The MAI framework consisted of a "foundation, two pillars and a roof."[3] The foundation corresponded to the definition of investments; the first pillar would include disciplines which applied to investments once established in the host country (post-establishment disciplines); the second pillar would represent disciplines which applied to investment prior to entry in the host-country (pre-establishment or market access); and finally, the roof consisted of dispute settlement mechanisms. These framework items appear in the final MAI draft of April 1998 (see Appendix A) under the following sections: (II) Scope and Application (definition); (III) Treatment of Investors and Investments (pre and post-establishment disciplines); (IV) Investment Protection (post-establishment); (V) Dispute Settlement (intended for pre- and post-establishment);

---

[3] Based on "Report to the Council by Negotiating Group (NG) Chairman Frans Engering - 30 April 1996 (OECD, 1996*e*).

and (IX) Country Specific Exceptions (the mechanisms which would apply to the listing and further liberalization of non conforming measures in the pre- or post-establishment phases).[4]

Once the first phase was completed, the "second phase" of the negotiations would consist of listing country-specific exceptions. This schedule was based upon the understanding that it would be desirable to reach a negotiated agreement on the MAI text prior to having countries engage in commitments on liberalizing particular measures or sectors of their economy. This preferred way to proceed is explained by the fact that in investment treaties all the framework items are subject to negotiations since each has an

---

[4] Several types of exceptions and derogations from investment treaty obligations appeared in the draft treaty and are discussed later in this chapter. Three broad categories of exceptions to the non-discrimination principles have been identified by UNCTAD (1999*a*, *b*). These are General exceptions, Subject-specific exceptions, and Country-specific exceptions. General exceptions enable contracting parties to derogate from the non-discrimination standards (national treatment - NT, and most favoured nation - MFN) as well as other obligations if necessary for the maintenance of public health, order and morals, and national security. Subject-specific exceptions exempt specific issues such as intellectual property or taxation from NT and MFN. Country-specific exceptions enable a contracting party to reserve the "right to differentiate between domestic and foreign investors under its laws and regulations -- in particular, those related to specific industries or activities" (1999*a*: 12). An example of such a non-conforming measure would be an investment legislation specific to a country's economic policies where some maximum percentage of foreign ownership is allowed in a particular sector. Note also that the NG agreed that the term *treatment* "covered all policies which affect investment (economic policy, financial policy, tax policy, policy on public sector subsidies, company law, etc.)" (Charolles, 1997: 19). Such measures would have to be listed as exceptions in order to ensure that that country would not be in violation of the non discrimination standards. Liberalization mechanisms referred to the way in which countries would list their exceptions, whether these exceptions would be negotiated and how future negotiations would take place. A standstill clause would prevent signatories from adding, later on, sectors they had omitted originally. A rollback liberalization mechanism would be: "the liberalization process by which the reduction and eventual elimination of non-conforming measures ... would take place....The most commonly known [way to achieve rollback] in the trade field is that of successive rounds of negotiations where rollback results from the trade-offs or exchange of trade concessions. Peer pressure through periodic examinations of Member countries' restrictions has been the approach of the OECD liberalization instruments" (Sickel, 1997: 24). Note that country-specific exceptions can at times be referred to as "reservations." The distinction is attributed to treaty law where the term reservations is used when these have reciprocal effect (see MAI draft text, April 1998: 90, OECD 1998). The draft OECD MAI specifically relied on the term "exception" while specifying that the usage of the term "would not prevent the listing of a measure with a reciprocity requirement." This specification was due to the fact that no agreement was reached on liberalization mechanisms.

impact on the final scope of the agreement and therefore on the degree of discretion retained by signatories. Thus for example, the scope of the definition of investment and investor affect "the extent of the treaty coverage granted to foreign investors and...the degree of host State discretion in directing and implementing its foreign investment policy" (UNCTAD *c*, 1999: 3).[5]

In addition, it had been agreed that the MAI negotiations would follow what is referred to as a "top-down approach." This meant that "only those sectors which [were] explicitly excluded by a party [would not be] entitled to national treatment" (Sikkel, 1997: 21.) In the light of these provisions, it would evidently be preferable that negotiators knew the scope of the agreement prior to listing their country-specific exceptions.

Negotiations on the "building framework" began immediately. The first drafting groups that were set up in the fall of 1995 were to focus on pillars one and two, disciplines that applied to pre- and post-establishment, while the NG immediately began work on the definitions.[6] The list of meetings planned in 1995 and 1996 showed a consistent focus on

---

[5] As Schekulin (1997: 10), the Chief MAI Negotiator for Austria pointed out, definitions of who is to be considered and what is to be considered an investment hold far reaching consequences for the scope of the MAI disciplines and the applicability of the dispute settlement process. As such, definitions in international investment agreements "raise difficult policy issues and are often the subject of hard bargaining between the negotiating parties. Accordingly, they should be seen not as objective formulations of the meaning of terms, but as part of an agreement's normative content, since they determine the extent and the manner in which the other provisions are to be applied" UNCTAD (1999 *c*).

[6] The list presented here is not exhaustive but intends to demonstrate how the plan of work was expected to progress over 1996, leading to the negotiation of the most relevant issue of liberalization. The first two NG meetings created a drafting group on Investment Protection (DG 1)a post-establishment treatment, and another on pre- and post-establishment treatment of investment and investors (DG 2). DG 1 received the mandate to draft specific provisions on investment protection such as expropriation, compensation, and transfer of funds, and was directed to submit a proposal to the NG by December 1995. DG 2 would draft provisions on selected topics regarding the treatment of investors and investment such as national treatment and most favoured nation, and was scheduled to submit proposals to the NG by March 1996. The latter group's mandate was expanded at the NG December 1995 meeting to include mechanisms for standstill, rollback and the listing of country-specific exceptions, as well as provisions on general exceptions. The group

these issues and the completion of the MAI text. Initially, it was believed that the NG would be able to enter the second phase of the negotiations after the June 1996 OECD ministerial meeting (*Inside U.S. Trade*, December 1995: 15). However, by April 30, 1996 the NG Chair's report to the OECD Council indicated that the initial plan to complete the framework by June 1996 had to be postponed to December.[7] By December 1996, disagreements on the text still remained and by February 1997, only three months prior to the deadline, negotiations moved "into a new phase, with parallel efforts to complete text ... and to negotiate exceptions" (Dymond, 1997: 7), in spite of the fact that there was still no final agreement on several significant items of the MAI text.

Although a majority supported a definition with a "non-exhaustive" list of assets to be considered investments, there was no final agreement on the definition (Dymond, 1997: 7; Schekulin, 1997: 10). As Canada's Chief Negotiator (Dymond, 1999: 40) reported later: "[a]n attempt by the chairman to declare the definition agreed upon was sharply rebuffed by Canada and other countries." Considering the relevance of the definition to the coverage of the agreement and to contracting parties' future discretion over their

---

was expected to be terminated once it completed its work and reported to the NG at its March 1996 meeting (OECD, 1996*b*). By January 1996 the NG began to experience difficulties with the definition of investor and investment and charged DG 2 with the additional task of analyzing the issue and reporting back to the NG by April 1996. Questions regarding the dispute settlement process would be handled by an Expert Group 1 (EG1) so that they could examine questions prior to commencing drafting. In March 1996 an Expert Group on Special Topics (EG3) was mandated to look into issues of key personnel, performance requirements, incentives, privatization, monopolies/state enterprises and corporate practices (all these fall under Section III of the MAI draft text "Treatment of Investors and Investments") (OECD, 1996*c*). These latter topics were added after the NG concluded that "observance of national treatment and most favoured nation treatment would not -- in itself -- be enough to guarantee the open investment regime" (Ahnlid, 1997: 27). Other topics which appear in Annex A were added on as negotiations progressed and the need to include them was agreed upon (for example taxation and financial services).

[7] Based on The Report to the Council by Negotiating Group (NG) Chairman Frans Engering - 30 April 1996. OECD document (OECD, 1996*e*).

foreign investment policy, disagreements regarding the definition were significant and held considerable implications for the overall negotiations on the substantive obligations of the MAI (Dymond, 1999: 40).

By comparison, the non-discrimination clause (national treatment and most favoured nation) fared much better. It was agreed early on that non-discrimination would apply to both the pre- and post-establishment phases of investments.[8] Nevertheless, the strength of the non-discriminatory obligations would be determined by the extent to which countries would be allowed to deviate from them through exceptions and derogations, and here, considerable disagreements remained. The latter issue will be covered in the next section.

As far as the dispute settlement mechanism was concerned, the most important stumbling block was whether investor-to-state arbitration should be covered.[9] One source reported that at the January 1997 NG meeting, seven delegations (Australia, Denmark, Finland, Hungary, Japan, Mexico and Austria) withheld their formal support for such a

---

[8] This was a considerable achievement since few existing international investment agreements included the pre-establishment phase. The practice of extending NT to the pre-establishment phase of investments has not been considered pertinent in the past due to the sovereign right of countries to control the entry of aliens and because an "outside" investor was not deemed to be in a similar or comparable position as a domestic investor (UNCTAD, 1999*a*).

[9] There are two types of dispute settlement mechanisms. State-to-state mechanisms provide rules to settle disputes between governments. Investor-to-state mechanisms regulate disputes between firms and governments. The latter is not included in the WTO but covers some of the NAFTA. In the NAFTA the mechanism provides "that investor's claims against governments can be submitted to a tribunal of three members....The tribunals have the authority to award damages based on their decisions" (Brewer, 1996: 88). By all accounts the investor-state dispute mechanism represents a major change in international law. Not only does this mechanism imply that investors have a status equal to states, but under "customary international law, there is no compulsory binding arbitration....[whereby] "an offending government can thus avoid or delay resolution of a dispute....The MAI [would] provide for automatic procedures which [would be] compulsory and binding" (Padt, 1997: 32). Should the MAI have included an investor-to-state mechanism, investors would have had "at their disposal a dispute settlement mechanism that they [could] activate" (Baldi, 1997: 33).

provision, and one delegation (Norway) proposed an exemption from an investor-state dispute mechanism altogether (*Inside U.S. Trade*, February 7, 1997: 15). In addition to these a number of "special topics" which had been added to the non-discrimination provisions were not completely agreed upon.[10]

The section of the framework which had progressed with most ease was investment protection. By February 1997, the draft provisions on Investment Protection enjoyed broad agreement on core principles (Dymond, 1997: 7). In particular, agreement on the core provisions of the article on expropriation and compensation was easily attained (Karl, 1997: 15).

Liberalization as a Stumbling Block

In addition to these unsettled issues, there was no agreement on several issues concerning exceptions from the MAI obligations. The two most difficult questions concerned country-specific exceptions and general exceptions. Neither the way in which country-specific exceptions would be listed nor the process through which liberalization would take place were agreed upon when delegations were invited to list their exceptions at the December 1996 NG meeting. Furthermore, the outstanding issue between the major

---

[10] Special topics referred to the inclusion of additional disciplines that would cover activities not necessarily covered by the observance of national treatment and most favoured nation treatment. These topics consisted of: "key personnel" whereby investors would be able to "transfer personnel to perform important key functions for an investment made abroad"; "performance requirements" which refer to "requirements governments impose on investors in order to secure perceived benefits for society as a whole" such as "domestic content requirements"; "investment incentives" that would aim at putting an end to "costly competition between countries" to attract investments"; applying the principles of non-discrimination to "privatisation" which would ensure that foreign investors would not be put in a disadvantaged position in relation to such occurrences; and "monopolies and state enterprises" whereby "government-designated monopolies should be covered by the MAI with the objective of ensuring that these entities do no treat foreign investors less favourably than national enterprises" when, for example, monopolies purchase or sell goods and services (Ahnlid, 1997)

players—the EU and the U.S.—concerning exceptions for Regional Economic Integration Organizations (REIOs) and binding sub-federal entities had not been resolved. In addition, several proposals for general exceptions had been tabled since the beginning of the negotiations, creating further divisions within the NG. These are discussed in the following three sub-sections.

(A) Country-Specific Exceptions

Two difficulties were encountered regarding the mechanism covered under Section IX— "Lodging Country Specific Exceptions." By the time countries submitted their exceptions in February 1997, all that was agreed to was that these exceptions would be subject to a standstill obligation.[11] Disagreement remained on the types of lists to be included and the liberalization process through which countries would remove exceptions.

With objections from Canada and the United States, each Contracting Party would list all its non-conforming measures to NT and MFN as an Annex of the Agreement called

---

[11] This meant that countries needed to exercise extreme care in listing their country-specific exceptions since, as one official characterized it, the standstill obligation in a top-down approach meant "list it or lose it." In addition, as described above in footnote 3, the article on transparency attached to the non-discrimination articles provided for the disclosure of not only "discriminatory measures but also of all policies which affect investment" (Charolles, 1997: 19). Of all OECD members, only the U.S., Canada and Mexico had undertaken such a time consuming exercise under the NAFTA. Considering the time left to the deadline this requirement alone represented a practical impossibility to complete in time for the signature. Exceptions in the NAFTA are listed in the section titled "Annexes I Through VII: Reservations and Exceptions to Investment, Cross-Border Trade in Services and Financial Services Chapters" where each country lists sectors of its economy it does not wish to be subject to certain disciplines. Each entry mentions the type of sector concerned by the reservation, the discipline to which the reservation applies, the level of government responsible for applying the relevant domestic law and a description of the commercial activity affected. Thus, for example, Canada's first entry stipulates that the National Treatment discipline for investments does not apply to credit granted the agricultural sector. Regulations or measures covering these activities are the Federal *Farm Credit Act* and the *Farm Credit Regulation*. The entry then describes how the reservation applies: "Loans by the Farm Credit Corporation may be made only to: (a) individuals who are Canadian citizens or permanent residents; (b) farming corporations controlled by Canadian citizens or permanent residends; or "cooperative farm associations, all members of which are Canadian citizens or permanent residents." There is no time limit on the reservation. (NAFTA, Annex I - Canada, I-C-I).

List A (titled *Annex A* in the NAFTA). Canada and the U.S. wanted to follow the NAFTA model and include two types of lists. List A would consist of "exceptions generally fixed in legislation and practice" which could be negotiated, whereas List B (titled *Annex B* in the NAFTA) would be non-negotiable in that they covered sectors where these countries "required flexibility to discriminate against foreign investors in respect not only to current measures but any measures in the future" (Dymond, 1999: 35). While future rounds of negotiations to liberalize investment policies were envisaged, no rollback process had been agreed to (UNCTAD, 1999*d*: 131). Underlying the controversy surrounding negotiations on the rollback mechanism was the understanding that the process would be guided by peer pressure, as was the OECD custom, rather than reciprocity as typically practiced in trade negotiations (Dymond, 1999: 35).

At its December 1996 meeting, the NG agreed to the chairman's proposal to table their list of country-specific exceptions by the end of February 1997 even as these issues had not been resolved. UNCTAD (1999*d*:131) reported that the move to undertake liberalization while still negotiating the MAI text resulted in numerous country-specific exceptions, varying greatly in quantity and character between countries. Without final agreement on the text, "most delegations were sceptical about negotiating away proposed exceptions." Some of the exceptions listed were believed to have been motivated by tactical considerations, to be used in case reciprocal negotiations would take place, while others were listed as a precautionary measure due to the uncertainty of the effect of some provisions. According to UNCTAD (1999*d*: 131), the outcome had the effect of raising the question of "balanced commitments" and legal certainty.

In fact, when the chairman proposed that delegations table their exceptions at the December 1996 NG meeting, he was already under pressure from the United States to negotiate "up-front liberalization." Reaching a satisfactory balance of commitments had been a U.S. objective all along. As officials observed at the time, "the U.S. effectively forced the issue by announcing it would table a complete list of federal and state measures that would not conform to MAI obligations" and it expressed its wish to undertake a "request-offer" process in which countries would negotiate away their listed exceptions (*Inside U.S. Trade*, January 10, 1997: 5). As explained in the following paragraphs, the premature listing of exceptions only exposed a more profound disagreement between most European delegations and the U.S.

The issue of liberalization—listing exceptions—revealed serious divergencies between European and American interpretations of the ministerial mandate (Dymond, 1999: 34). At issue was whether the MAI would reflect the degree of liberalization existing within the OECD and provide a framework that would eventually facilitate future progressive liberalization of investments, or whether the current MAI negotiations would also yield improved market access. While some, mostly European, countries were "convinced that the MAI as an agreement represente[d] a convincing liberalising effort," others insisted upon "a mechanism that ensure[d] that this level of liberalization [was] satisfactory to all" (Engering, 1996: 152).

For the former, the level of liberalization under the OECD Codes was sufficient and the objective with the MAI was to "establish a framework within which further liberalization could be achieved progressively" (UNCTAD, 1999*d*: 132). For the latter,

however, the simultaneous negotiation of improved market access through the MAI and between OECD members had been an objective all along. For those delegations, most notably the U.S., that had entered the MAI negotiations with the intention of improving market access, the outcome was a discouraging setback and one which became a pivotal issue for the remainder of the negotiations.[12]

(B) Other Derogations and General Exceptions

The area of general exceptions suffered from setbacks as well. The issues of Regional Economic Integration Organization (REIO) and binding sub-federal entities between Europe and North America that existed prior to launching the negotiations, had not yet been resolved.[13] In December 1996, the EU Commission tabled its proposal for a broad exception for REIOs. As Karl (1996:21) explained it, the question was whether the European Union should be allowed "to deviate from the MFN principle in order to preserve its capability to move ahead with its internal investment liberalization at a faster pace than other States [were] ready to go." The U.S. repeatedly argued throughout 1996 and into 1997 that the EU member states had either "not put forward a detailed explanation of why they should be allowed to violate" this principle (*Inside U.S. Trade*, May 3, 1996: 11) or that their explanation had "not been convincing" (*Inside U.S. Trade*,

---

[12] Since the respective negotiating position of various countries is the most confidential aspect of these documents, unless countries give information as to what their position was it is very difficult to determine which ones were in agreement with the U.S. The American position was expressed through various media.

[13] The inclusion of these issues in the OECD working paper that accompanied the ministerial mandate for the MAI had been a deciding factor in U.S. acceptance of the mandate. While an initial report indicated that the MAI would be binding on subfederal governments and identified the issue as "a key demand of the EU" there was no similar mention of U.S. demands regarding the issues of REIO and privatization (*Inside U.S. Trade*, May 5, 1995: 2). As a result, U.S. acceptance of the mandate had been conditional upon statements indicating the satisfactory inclusion of these two American demands in the report.

January 10, 1997: 4). The NG only began work on binding subfederal entities at its February 26-28, 1997 meeting when countries submitted their exceptions. As seen earlier, this exception was included in the U.S. list of exceptions to be negotiated as part of the balanced commitments (*Inside U.S. Trade*, February 7, 1997: 16).[14] Neither issue was resolved by the first deadline of May 1997.

Posturing - "Deal Breaking Issues"

As if the above hurdles were not enough, two issues surfaced during that first period which drew strong language from both the Europeans and the Americans. In March 1996 the Helms-Burton Act and Iran-Libya Oil Sanction Act became law in the U.S. In June 1996 the French delegation introduced France's proposal for a general exception for culture.[15] By the fall, some parties resorted to strong language to signal their intransigence with respect to these matters.

The U.S. laws attracted strong opposition inside the MAI negotiations from Canada and the European Union. At the March 14-15, 1996 NG meeting Canada

---

[14]The U.S. and Canada followed the approach they had adopted for the NAFTA which was to list states' measures and provincial jurisdiction as exceptions (Dymond, 1999: 36; *Inside U.S. Trade*, March 1997: 14).

[15] Title III of the Helms-Burton Act allowed "U.S. citizens and corporations whose property was confiscated by the Cuban government any time after January 1, 1959, to bring suits for damages in U.S. courts against anyone who [was deemed to] "traffic" in their former property after November 1, 1996. Title IV prohibit[ed] the entry into the United States by persons who traffic[ked] in confiscated property, as well as their families, after March 12, 1996" (Canner, 1998: 13). The Iran-Libya Act targeted companies which undertook investments in the petroleum industry in either of these countries (Dymond, 1999: 37). The French proposal on culture was that:"Nothing in this agreement shall be construed to prevent any Contracting Party to take any measure to regulate investment of foreign companies and the conditions of activities of these countries in the framework of policies designed to preserve and promote cultural and linguistic diversity" (reproduced in Dymond, 1999: 52). France was supported in this proposal by Canada, Italy, Belgium, Portugal, Greece and Australia. Opposing this proposal were the U.S., UK, Japan, Germany, the Netherlands, New Zealand and the Nordic countries (Dymond, 1999: 35).

announced that it would table suggestions to be included in the MAI that aimed at preventing the type of extraterritorial provisions contained in the U.S. laws (*Inside U.S. Trade*, March 15, 1996: 8). Although Canada tabled two proposals as early as June 1996 that were supported by virtually all OECD members except the U.S., the issue became the object of negotiations outside of the MAI between the EU and the U.S. As one official commented at the time, "Helms-Burton now seems to have become the political football in this negotiation, it will come back to haunt us" (*Inside U.S. Trade*, July 5, 1996: 8). In any event, Canada and the EU eventually indicated that the conclusion of the MAI negotiations depended upon a resolution of these issues of extraterritoriality and since an initial deadline for those negotiations was set for October 1997 (Canner, 1998: 15) it is difficult to see how these parties could have concluded an MAI by the first deadline date. For its part, the U.S. announced, at the NG meeting of October 23-24, 1996, that it would regard a broad cultural carve-out as deal-breaker (*Inside U.S. Trade*, November 1, 1996).

Thus, by the end of the first period, a number of unexpected challenges and delays confronted the NG. The substantive issues which arose during the first period of negotiations were due to unexpected differences concerning the draft text and misunderstandings regarding the degree of additional liberalization mandated in the MAI ministerial statement. That these were unexpected was evidenced by the optimistic time-frame initially envisaged for concluding the "building framework." Some observers have attributed these unanticipated difficulties to the fact that the MAI was an ambitious "big step forward" (Henderson, 1999: 23, 25). The MAI was not only meant to simplify and

render more transparent a complex patchwork of treaties but also to add value to the existing investment regime. Many of the issues identified during the first period of negotiations concerned these novel rules which, taken together, provided an ambitious package.[16]

While various parts of the agreement taken in isolation seemed innocuous, the package as a whole proved, in the end, "too much for governments to swallow" (Henderson, 1999: 25; Lalumière, 1998: 3; Picciotto, 1999: 84). Also, divergent understandings regarding the purpose of the MAI became most obvious when country-specific exceptions were listed. American calls for "up-front liberalization" and negotiated reciprocal commitments revealed a search for greater market access at the outset. What was becoming evident over this first period was that "there were much more diverse views on the scope and applicability of the agreement" (Smythe, 1998*b*: 250).

II. Civil Society: Response and Impact

As seen in Chapter 4, the only opposition campaign to the MAI that was well under way during this first period of the negotiations was voiced by "insider" groups that belonged to what has been described as the "interest group system of action." In particular, international environmental NGOs which were close to international policy circles in Europe had been the most active in their attempts to lobby for their objections at

---

[16] See Henderson (1999: 23-25), Picciotto (1999), Smythe (1998*b*) and Lalumière (1998) for further details on this aspect. For example, among Henderson's list of fifteen items that were new elements is included the "open-ended" definition of investments, including portfolio investments and intellectual property rights, as well as the listings of "all official actions;" the top-down approach, the inclusion of all phases of investments (pre-and post establishment); the dispute settlement processes; and the standstill and rollback applied to country specific exceptions. As Picciotto (1999: 83) summed, obligations were "at as high a level as possible, taking the strongest precedents from existing investment treaties."

the domestic and at the OECD levels.

Two other groups that belonged to this "system of action" had been included early on in the OECD discussions on the MAI, as part of the traditional corporatist arrangement which had been in place at the OECD for several decades.[17] The Business and Industry Advisory Committee (BIAC) representing business organizations from member states and the Trade Union Advisory Committee (TUAC) playing the same role for trade unions, shared their members' views on the MAI through exchanges with the OECD committees on a regular basis. While these two groups had had an opportunity to express how their specific interests would best be reflected in an investment treaty, the environmental NGOs had been virtually shut out from any consultation process. As a result, not only did the MAI draft text reflect lacunas in that area, but these NGOs were highly critical of the negotiation process which they labelled as secretive.[18]

BIAC demonstrated a strong interest in an investment treaty from the first stages of the MAI project in the early 1990s. The objective of a "high standard agreement" expressed in subsequent OECD papers, such as those appended to the negotiations mandate, met with BIAC's full support and enthusiasm.[19] To BIAC's satisfaction the

---

[17] The term corporatism is used as defined in comparative politics which "usually implies limits on the number of groups that can participate in the political process" (Wiarda, 1993: 154).

[18] These organizations were listed on the model in the conclusion to Chapter 4 as the WWF, CIEL, CUTS, Consumers International and the European Environmental Bureau.

[19] BIAC's support and approval was expressed at a March 1996 workshop meeting by a member of BIAC's Committee on International Investment and Multinational Enterprises. In his presentation the committee member recollected how BIAC was "first in" to produce, in the second half of 1992, a "Statement on a Potential Broader Investment Instrument" which contained the key elements for an eventual agreement along with the "business wish list" (OECD, 1996*d*: 20).

OECD reports "had taken up most of [its] suggestions" for a high standard agreement (OECD, 1996*d*: 20). In order to better follow the negotiations, BIAC nominated a special group of experts to liaise with the OECD Negotiating Group. TUAC had also contributed to the early discussions on a "Wider Investment Instrument," as the MAI was initially referred to. TUAC's request was that the "spirit and principles" contained in the 1976 OECD guidelines for Multinational Enterprises be reflected in the MAI (OECD, 1996*d*: 23).[20] Its initial proposal was that the Guidelines be annexed to the MAI without altering their voluntary nature. Another request was that contracting parties "continue to treat the provision of the Guidelines in parallel to those contained in the ILO [International Labour Organization] Tripartite Declaration on Multinational Enterprises and Social Policy."

In spite of these pre-MAI contributions and six consultation meetings during 1996, both these organizations were frustrated by the limited amount of information available to them and the lack of access to negotiators (Smythe, 1998*b*: 247). However, relative to

---

[20] The *Guidelines for Multinational Corporations* which are a core element of the 1976 OECD Declaration on International Investment and Multinational Enterprises consist of "voluntary standards of conduct representing the collective expectations of OECD Governments as to the behaviour of such enterprises" (Witherell, 1996: 18). The guidelines include several International Labour Organization core Conventions on workers' rights, and other standards such as environmental protection, competition policy, science and technology and taxation. TUAC had a clearly defined position: (i) "the OECD Guidelines must be incorporated in the Multilateral Agreement on Investment being negotiated in OECD; (ii) there should be an extensive reference to the Guidelines in the Preamble to the MAI; (iii) the full text of the Guidelines should be annexed to the Agreement; (iv) the text of the Agreement should include the OECD's decision in 1991 to establish National Contact Points in Member countries to implement and promote the Guidelines; and (iv) the OECD must conclude rapidly its review of National Contact Points and once the MAI is concluded in 1997 embark on a major initiative to improve the implementation and promotion of the National Contact Points" (TUAC, 1996).The rationale for TUAC's position was that when OECD members adopted the Guidelines in 1976 these had been considered as an essential part of a balanced package of measures to facilitate direct investment among OECD Members and that, as such, the MAI should respect these earlier objectives. Eventually, TUAC's position followed those of other NGOs in requesting much more stringent environmental and labour provisions.

these two organizations, environmentalists had obtained considerably less opportunity to express their views on the MAI. Aside from the October 18-19, 1996 meeting with OECD officials in Geneva and the informal dinner meeting of December 1996 with the NG in Paris (see Chapter 4), environmental NGOs had been completely shut out of any consultation process.[21] In addition, the procedural arrangement under which the negotiations were taking place meant that the OECD Environmental Policy Committee was excluded from the MAI negotiations (Huner, 1998), and also prevented the NG from consulting with NGOs due to the reluctance of some delegations to do so.[22]

As a result, environmental considerations were conspicuously absent from any working papers produced prior to the launching of the negotiations and the environment only came on the NG agenda in October 1996, a year after the negotiations had begun (Huner, 1998: 4). Over those remaining months of the first MAI negotiations' mandate, the approach adopted for the MAI discipline on environment was similar to that on labour.[23] Discussions regarding the environment focused on three "basic themes" referred to as the "three-anchor approach" (Huner, 1998: 4).The first consisted of reaffirming

---

[21] The October meeting included only two officials from the OECD: Anders Ahnlid, Chair, MAI EG3, from the Swedish Delegation to the OECD, and Robert Ley, the OECD Head of the International Investment and Services Division (CUTS, 1997). The December meeting, as seen in the previous chapter, included the NG Chair and his American and Japanese co-Chairs.

[22] As seen in the previous chapter, this outcome concerned and irritated "insider" environmental NGOs that were accustomed to a much broader consultative role provided NGOs within the United Nations and the environmental committees of the OECD, which prompted them to characterize the negotiations as excessively secretive.

[23] The "task of investigating options or precise formulations" of various alternatives regarding the environment was mandated to existing expert groups and drafting groups at the October meeting (*Inside U.S. Trade*, November 1, 1996: 5). Their proposals were to be discussed at the February 26-28 NG meeting along with the controversial issue of binding subfederal governments and the exceptions (*Inside U.S. Trade*, February 7, 1997).

parties' commitment to the relevant principles of the Rio Declaration in the preambular text. The second included language similar to Article 1114 of the NAFTA that aimed at not lowering standards in order to attract investments. Finally the third anchor consisted of annexing the OECD Guidelines for Multinational Corporations (*Inside U.S. Trade*, November 1, 1996: 5; WWF notes from December 1996 meeting).

None of these provisions would be binding—an omission of great concern to environmental NGOs as expressed during the December 1996 informal dinner meeting.[24] They argued that the "social and environmental guidelines for MNCs should be binding, and that [MNCs'] access to the dispute resolution mechanism should be conditional on adhering to such guidelines" in order to balance investors' rights with responsibilities. The two other main NGO critiques concerned the exclusion of developing countries from the negotiation and the lack of a broader NGO consultation process.[25]

In spite of the hurdles experienced inside the negotiations, a timely conclusion of the negotiations appeared much closer from the outside, and the imminent signature of the agreement deeply concerned environmental NGOs. In response, insider groups in the U.K. were now engaging the support of their American counterparts in a stern letter writing campaign. Evidently, some more radical organizations endorsed at least one letter, an indication that insiders' concerns were gaining broader support. Two main objectives were

---

[24] The following is based on WWF notes on the December 1996 meeting.

[25] Albeit modest at the time, the usage of the Internet to critique the MAI and denouncing the "secretive" process of negotiations had already raised concerns among the negotiators who expressed their fear that these criticisms could undermine the passage of the MAI through national parliaments. The worry was well founded as far as NGOs were concerned and one, they pointed out, which could be alleviated should a more transparent process take place. The idea of a meeting with the NGO community was discussed as a possible way to remedy the situation.

reflected in these letters. One was to postpone the deadline; the other was to change the non-binding aspect of the provisions to binding ones.[26]

These mounting critiques were not the only signs of future difficulties with civil society. Indeed, the combined pressures of increasing opposition and decreasing support for the MAI began to emerge at that point. These developments were the beginnings of a trend that would only intensify over time, and few delegations were prepared for the increased intensity of opposition to which the delay in the negotiations offered a window of opportunity.

As in any other multilateral economic negotiations, support from domestic groups was of concern to the negotiators. However, domestic business interest had been lukewarm in several OECD countries.[27] Of all OECD members, the American business

---

[26] A letter sent to U.S. officials and dated February 13, 1997 was signed by the American branches of WWF, Friends of the Earth, Greenpeace, the U.S. Center for International Environmental Law, the Sierra Club (U.S.) and other environmental organizations based in the U.S. (see *Inside U.S. Trade*, February 21, 1997: 12). Regarding the first point, NGOs requested that in order for their concerns to be addressed appropriately "the timetable for concluding the MAI must be substantially extended .... *We thus join a number of our NGO colleagues abroad* in calling for an extension of the MAI negotiating deadline by at least a year, *i.e.*, until May 1998" (emphasis added). Regarding the second point, the letter stated: "*[n]on-binding hortatory language* - such as 'green' preambular remarks, exhortations against competitive deregulation, or references to toothless guidelines on corporate behavior - *simply are not enough*. These provisions do not even offer the minimal environmental requirements found in the NAFTA - which, we are all agreed, must be substantially improved in the global context of the MAI" (emphasis added).

[27] This was due in part to the choice of forum which *de facto* excluded from the negotiation process geographical areas of greater interest to investors. Since most investment flows took place within the OECD and enjoyed an adequate level of protection, the area of interest to the business community lay in developing countries which were effectively outside the negotiations. This was the case for Canada as explained by Dymond (1999: 45) and France as referred to in the report undertaken by Catherine Lalumière (1998: 5). Japan's business community had expressed its opposition to the OECD negotiations favouring the "broader multilateral forum" of the WTO (*Inside U.S. Trade*, March 17, 1995: 10). The International Chamber of Commerce (ICC) was not perceived to be a strong supporter of the OECD MAI (Huner, 1998: 5). Another influential international business organization that supported the MAI was the Union of Industrial and Employers' Confederation of Europe (UNICE), an umbrella organization that represents European business organizations with European Union institutions such as the European Parliament and the European Commission. However, UNICE's support included the added reservation of the desirability of a double approach with the WTO, that would be consistent with the OECD treaty (UNICE, 8 March 1995: 2). This

community demonstrated the greatest interest in the MAI and it is fair to assume that BIAC's interest in the MAI was a reflection of the influence that the U.S. business community enjoyed in that committee.[28] Not only was the United States Council for International Business (USCIB) one of the most influential groups in the organization (Smythe, 1998*b*: 247) but it held the chair of BIAC's expert group on the MAI.[29] However, by March 1997, those in the business community that had demonstrated strong support for the MAI became increasingly critical of the developments which were taking place in the negotiations. As illustrated by a quote from the letter reproduced below, their criticisms betrayed their intent to withdraw support for the MAI. USCIB's March 21, 1997 letter to the U.S. Administration can be considered as indicative of the MAI supporters' reaction to the developments that were taking place.[30]

One of the negotiating issues which most affected business support of the MAI was the almost-certain carve-out for taxation. Indeed, throughout 1996 fiscal experts from finance ministries had insisted that applying non-discrimination to fiscal treatment, "could

---

business response explains why accession by non-members was considered an essential objective of the MAI. As the NG chair pointed out to the OECD Council in his April 1996 report: "Failure to secure non-member adherence to the MAI would be tantamount to failure of the project as a whole" (OECD, 1996*e*). An aggressive outreach campaign with the so-called NMEs (non-member economies) had been launched from the outset through a series of "workshops" which took place in various locations around the world.

[28] On the occasion of a business group meeting which took place in Brussels on March 9, 1995, a U.S. delegation made up of the National Association of Manufacturers, the U.S. Council for International Business (USCIB), the Pro-Trade Group and the American Electronics Association, declared itself "strongly in favor" of beginning negotiations for an investment treaty at the OECD (*Inside U.S. Trade*, March 17, 1995).

[29] See USCIB letter dated July 11, 1997 to U.S. officials reproduced in *Inside U.S. Trade* (July 18, 1997): "through our chairmanship of the experts group on the OECD's Business and Industry Advisory Committee, we provide participants in the negotiations our views on important issues."

[30] The letter was reproduced in the issue of *Inside U.S. Trade* dated March 28, 1997, pp. 4, 5.

conflict with obligations contained in the many bilateral agreements on the avoidance of double taxation" and that certain applications of the dispute settlement mechanism could also be used to "pre-empt the application of taxation treaties" (Engering, 1996: 158). By February 1997, it had been decided that taxation would not be covered by the MAI and that a so-called carve-out/carve-in approach would be followed (Sikkel, 1997: 21). This development contributed to a considerable decline in business support early on in the negotiations, a reaction which did not go unnoticed inside the negotiations (Huner, 1998: 5). As USCIB's letter confirms: "[w]e reiterate our view that tax measures must be included in the MAI." The second issue which would become increasingly worrisome for that group were the requests made by environmental NGOs. USCIB's strongest wording was reserved for the potential outcome of the environmental lobby: "*[w]e will oppose* any and all measures to create or even imply *binding obligations* for governments or business related to the environment or labour" (emphasis added) (*Inside U.S. Trade* dated March 28, 1997, pp. 4, 5).

What began to emerge as well was the effect of lobbying efforts on opposition parties as Europe was entering a period of electoral change. The first example of such developments were evidenced inside the negotiations by the change of attitude in the British delegation. Indeed, WWF had been lobbying the government in London as well as their shadow counterparts, a strategy which promised to bear fruit in the not-too-distant future as this letter from an opposition member to WWF promised:

> Thank you for your letter about the MAI. I have carefully noted the points you make and hope you have been in touch with ... Labour's Trade and Industry Spokesperson, as well. I have received representations on this subject from the

> trade union movement as well, and it is my intention - assuming we win the election and I am in this post in government - to talk to ... the Trade team about getting a development perspective into this issue.[31]

As the British election date of May 1997 approached, and a Labour victory appeared a near certainty, the British delegation which had demonstrated "a very sceptical line towards all of [the MAI discipline on environment and labour] ... became more silent on the issue" (Huner, 1998: 5).

Conclusion

Considering the fast approaching deadline of May 1997, difficulties regarding the inclusion of environmental and social clauses paled by comparison to the number of outstanding issues to be negotiated. Furthermore, at that point in time a majority of delegations supported "the three anchor" approach which provided for the inclusion of non binding environmental and labour rules.[32]

The draft text of the May 1997 MAI (OECD, 1997*c*) reflected the general consensus on the three anchor approach as it included: the preambular language reaffirming the negotiating parties' commitment to the Rio Declaration on Environment and Development and Agenda 21 along with similar references for labour standards and the ILO; a provision under Section IV which stated that Parties recognized that "it is inappropriate to encourage investment by lowering [domestic] health, safety or

---

[31] Letter from Labour's Spokesperson for Overseas Development to WWF, dated 11 April 1997.

[32] As mentioned earlier, the British delegation which had been "skeptical" began changing attitude as the elections approached. The "other opponents of labour and environment clauses in the MAI were Australia, New Zealand, Korea and Mexico" (Huner, 1998: 5). Thus the two major parties, Europe and the U.S., supported such inclusions.

environmental [standards] [measures] or relaxing [domestic] [core] labour standards, and; and the annexation of the OECD MNC Guidelines." Of these, only the preambular text was mostly in brackets at the request of the delegations which were against it. For these reasons, it is far from certain that insiders' concerns would have held back the conclusion of the negotiations had the NG been closer to an agreement on other outstanding issues.

Rather, the NG Chairman's first public statements regarding a possible extension of the mandate attributed the delay to the difficulties on the cultural exception, REIO, binding subfederal governments, non-member accession and the incomplete negotiations of country-specific exceptions (*Inside U.S. Trade*, March 28, 1997: 3). In fact, the U.S. had asked the Chairman earlier that year to submit a proposal for an extension. The reason given was that the U.S. Congress had not been informed of the MAI negotiations and that there was not enough time left to submit the MAI for approval. Thus, while relating the causes of the delay in the interview, the Chairman expressed his concern that the U.S. Administration include the MAI in its upcoming request for fast-track authority (*Inside U.S. Trade*, March 28, 1997: 3).[33] Furthermore, the U.S. was dissatisfied with the degree of liberalization achieved so far. On March 11, 1997 Alan Larson, the American Assistant Secretary of State for Economic and Business Affairs publicly stated the American position regarding the MAI. While emphasizing the "considerable success in drafting the text of MAI obligations" Larson was also quoted as saying "[w]e need to

---

[33] "Fast-track authority" refers to powers given by Congress to the President of the Unites States to negotiate international economic agreements. These are granted for a limited time and had run out by the time the United States engaged in the MAI negotiations. For a good understanding of this policy issue between 1994 and 1999, see Kerremans, 1999: 49-85.

make sure this progress is not undone by unreasonable exceptions in such critical areas as privatization, cultural industries and the right of establishment" and further stressed U.S. concerns "about a broad exception for Regional Economic Integration" (*Inside U.S. Trade*, March 14, 1997: 12). Also, considering its opposition to the listing of country-specific exceptions the U.S. would not have signed the treaty. As Larson further commented in an April 1997 interview:

> Frankly at this stage of the negotiation, we are not satisfied with the offers that have been made by other countries. We think they have not offered a degree of openness and a commitment to access that would result in a balanced agreement (U.S.Information Agency, April 1997: 3).

Furthermore, as suggested earlier, the negotiations regarding the Helms-Burton Act, an issue which was considered to be a "deal-breaker" for Europe and Canada, had not been completed. By March 1997, the NG had little difficulty recognizing that they were far from concluding a treaty. Thus the chairman proposed at the March 1997 meeting to postpone the deadline "with little consultation but no disagreement from the Negotiating Group" (Dymond, 1999: 30). At that point, therefore, even though the necessity to include environmental rules had been acknowledged, opposition from civil society was not a deciding factor in extending the negotiations.

However, there was a growing awareness that a timely resolution of the outstanding issues was of the essence for the success of the negotiations, and the NG debates regarding the length of the extension revealed concerns to that effect in Europe.[34] In general, European members feared that too long a delay would result in a loss of

---

[34] This paragraph is based on the issues of *Inside U.S. Trade*, dated March 28, 1997: 3; April 4, 1997: 7; and May 23, 1997: 11.

momentum and, as the Chair expressed it, "a loss of commitment [or] new problems in the economy or political setting". Nevertheless, for the U.S the quality of the treaty was not to be jeopardized by too short an extension, and it wanted to "keep things as open as possible". Eventually, a compromise was reached and expressed in the NG final report to ministers by emphasizing "the importance of concluding the agreement by the [May or June] 1998 ministerial". Although the political will and confidence in the NG's ability to solve the outstanding issues was still strong, in hindsight European fears were justified.

Indeed, had a treaty been signed at that point, little public awareness would have been awakened as intellectuals-engagés and mobilizers had had little time to obtain the necessary information and develop their campaigns. This however would all change very soon, and the seeds of the upcoming events were being planted just as the negotiators were debating the extension of the negotiations. In fact, the second period of the negotiations can be best characterized as one where the scales tipped in favour of the MAI opponents. For these reasons this first period of negotiations has been referred to as a period of transition whereas the second period to which we turn in the next chapter is better described as one of convergence.

CHAPTER VI

FROM CONVERGENCE TO CONJUNCTURE: SECOND AND THIRD NEGOTIATIONS' MANDATES

Introduction

The previous chapter provided an analysis of the progress of the MAI negotiations and the response on the part of civil society during the first mandate of the negotiations which took place from May 1995 to April 1997. We saw that during that first period the NG experienced unforeseen stumbling blocks as well as difficulties of a technical nature that required an extension of the negotiations' mandate. During that period only one type of societal actor, that of the interest group system of action, had had the opportunity to express its critiques of the MAI. I also argued that, in the light of the difficulties experienced within the negotiations, civil society had had no significant influence on the outcome of those two years of negotiations. Rather, it was the numerous stumbling blocks that caused the extension of the mandate for another year.

However, in the concluding paragraphs I suggested that apprehensions concerning the delayed ratification of the agreement were insightful. Indeed, as the NG was debating the extension of the mandate, actors belonging to the social movement system of action—also referred to as intellectuals-engagés and militant-mobilizers or radicals—were engaging their anti-MAI campaign. For that reason the first period of negotiations was characterized as a period of transition. Indeed, as will be seen in this chapter, by December 1997 a broad-based opposition had emerged and intensified considerably. Furthermore, a series of fortuitous concurrent circumstances, as far as MAI opponents were concerned, combined to worsen the prospects for the MAI.

The present chapter begins with the second period of negotiations which is best characterized as a period of *convergence* in terms of the developments which took place

within civil society. That section is followed by a third period characterized as one of *conjuncture* in that it resulted in a heightened social opposition to the MAI and the demise of those negotiations.

The chapter concludes with an assessment of the influences that the social opposition to the MAI had on the outcome of the negotiations. In terms of *direct influence*, which was defined in the previous chapter as influence on substantive issues within the negotiations, NGOs succeeded in bringing greater attention to the inclusion of labour and environmental standards in the text of the document. This, however, was deemed insufficient in terms of enforceability. Another substantive impact concerned the dispute settlement mechanism and the provisions on expropriation. In those cases, the influence was of significance not only because the latter part of the MAI text had already been agreed upon but also because they reflected novel concerns regarding such agreements and the process of globalization expressed by actors that belonged to the social movement system of action.

The analysis also reveals that it was societal actors' *indirect influence* exercised through pressure on elected officials that was most effective. Since this type of influence is also typically sought by actors from the social movement system of action, the meaning of this type of societal actor for world politics becomes a question of interest to this research. This is all the more so since we concluded in Chapter 4 that these actors' opposition to globalization was spreading through a growth in social movements networks.

I. Negotiations Period II: April 1997 to April 1998

As seen in Chapter 4, the intellectuals-engagés' campaign began in earnest in April 1997. These provided a new dimension to the ongoing insiders' campaign. Having obtained a copy of the draft MAI, North American activists collaborated to place the draft text on the Internet and simultaneously released a comprehensive critique of the MAI titled "MAI-Day: A Corporate Rule Treaty" (Clarke and Barlow, 1997: 3). At the same time, they organized the first world media release of an article on the MAI in the Canadian daily newspaper *The Globe and Mail* titled "Treaty to trim Ottawa's power."[1] These actions launched a virtual public campaign which quickly spread around the globe.

In North America, they revived anti-NAFTA sentiments. The fortuitous April 1997 announcement of a federal election in Canada enabled anti-MAI groups to draw public attention to the MAI as a threat to democracy. Canadian activists were as astonished as officials to witness the rapid spread of a grassroots MAI opposition. While no grassroots campaigns against the MAI took place in the U.S., more radical groups began to join insiders in their lobbying efforts, an outcome which U.S. officials must have viewed with growing concern.[2] Although similar campaigns were slower to start in Europe they were no less effective. By December 1997, several groups were collaborating across European borders and with North American activists in contacting politicians and raising public awareness through aggressive campaigns. Political responses

---

[1] See *The Globe and Mail*, April 3, 1997 p. A1.

[2] For example a letter dated June 30, 1997 addressed to the Assistant United States Trade Representative for Environment and Natural Resources was co-signed by, among others, Public Citizen and the Preamble Collaborative (see *Inside U.S. Trade*, July 4, 1997: 10).

in Europe were, in some cases, decisive for the MAI.

In addition, MAI opponents were assisted by a series of fortuitous events. The May 1997 elections in Britain brought down the Conservative government, a major supporter of a high standard agreement. In June, the French elections resulted in a coalition government made up of the Socialist, Greens and Communist parties. Considering the importance of these European members within the Union, these electoral changes were significant. Furthermore, an investor-state dispute launched under NAFTA in April 1997 would prove to be a powerful weapon in the hands of MAI critics. Finally, the Asian financial crisis which emerged full blown in early 1998 cast another shadow over a high standard investment agreement.

As a result, during the second period, the MAI drew increased political attention commensurate with the public opposition that was growing in several OECD countries.[3] From January to April 1998, multiple anti-MAI campaigns grew gradually, gaining considerable visibility as the need for another extension became evident.

These developments are addressed in the following sub-sections under separate headings. The first sub-section will provide an analysis of the indirect influence that MAI opponents exercised through politicians and the impact of public pressure. The second sub-section will analyse the progress of the negotiations and the direct influence of civil society groups inside the negotiations.

---

[3] One activist reported that campaigns took place in 11 of the 29 OECD countries (Clarke. 1998*b*: 20).

Indirect influence: Alerting Politicians

Perhaps the greatest vulnerability of the MAI stemmed from the lack of political sensitivity and the lack of domestic interdepartmental consultation which became evident in most countries as the negotiations proceeded.[4] As has been observed in hindsight, not only did the technical language and complexity of the agreement escape most lay persons, but the periodic communiqués submitted to the OECD Council for approval were worded in general terms giving little opportunity for political oversight of some potential problems (Huner, 1998: 7; Lalumière, 1998: 4). As anti-MAI campaigns progressed, activists increasingly capitalized on that weakness. Not only did they inform politicians and officials of the existence of the MAI, but as they did so, only their interpretation of the agreement was thus conveyed to members of Parliaments. As already explained, the insiders' characterization of the negotiation process as secretive became more widespread as the anti-MAI campaigns radicalized. This characterization seemed to be confirmed when elected Parliamentarians' ignorance of the MAI negotiations was exposed not only to them but also to their constituents.

(A) North American Campaigns

This tactic was very effective in Canada where the fortuitous call for a June 1997 election provided MAI opponents with an opportunity to publicly expose it as a threat to democracy. That message spread throughout the country when the national news

---

[4] It has been observed subsequently that indeed some delegations seemed to enjoy much autonomy and that little cross-departmental consultation seemed to have been taking place. Civil society groups from several countries commented on the difficulty they experienced in finding the government bureaucrats responsible for the negotiations.

broadcast a press conference called by the Common Front on the WTO.[5] Then, on May 29, 1997 the Council of Canadians, with the support of groups such as the Sierra Club, placed a full-page ad in *The Globe and Mail* which stated: "Next Election, your vote may be irrelevant...The New Multilateral Agreement on Investment gives the corporations so much power Parliament won't matter" (May, 1998: 33, 34). The concerns which had been generated at the grassroots level were exacerbated by the exposure of candidates' ignorance of the MAI in public election debates, especially when these were sitting members of the incumbent political party. Activists also sent letters to uninformed cabinet ministers in order to alert them about the implications of the MAI for their respective portfolios (Clarke and Barlow, 1997: 3, 4). As a result, political pressure for a public debate on the MAI came not only from a rapidly mounting public opposition, but also from the incumbent Parliamentarians of the governing Liberal Party whose ignorance of the matter had been exposed to their constituents.

By November 1997, the Canadian Government had organized a country-wide public inquiry on the MAI which tabled its report in December 1997. Among the recommendations made by the Committee responsible for the inquiry was one which called for "an open and transparent process so that public disclosure and consultations can be carried out in a timely manner" when undertaking negotiations "regarding matters of as

---

[5] As May (1998: 33), the President of Sierra Club (Canada) and a participant in the conference, remembered it: "[t]he Common Front held a press conference during the election focusing on the threat to democracy represented by globalization in general, and by the MAI in particular. The national radio news carried the news conference, and the Sierra Club and the Council of Canadians immediately felt the impact. People were calling in from all over the country, from the Maritimes to the Yukon, asking about the MAI."

widespread importance as the MAI."[6]

In the U.S., a similar opportunity presented itself on the occasion of the fast-track application process which took place in the fall of 1997. Activists used the fast-track application process undertaken in the fall of 1997 to bring the MAI to the attention of members of Congress. Anti-MAI NGOs alerted members of the American Congress not only to the existence of the MAI negotiations but of their own interpretation of the treaty's potential impact on a variety of policies. They did so by organizing membership "calling day" campaigns to members of Congress and officials in the Administration and by distributing the so-called "hill drops," or briefing sheets on the MAI, to members of Congress.[7] The strategy had some effect since in November 1997 a bipartisan group of 25 Members of Congress strongly criticized the Administration for having been engaged in the MAI negotiations without notifying Congress. As the letter questioned: "how has this agreement been under negotiation since May 1995, without any Congressional consultation or oversight, especially given Congress' exclusive constitutional authority to regulate international commerce?" (*Inside U.S. Trade*, November 14, 1997: 11). Of

---

[6] See "Canada and the Multilateral Agreement on Investment," Third Report of the Standing Committee on Foreign Affairs and International Trade, December 1997, p. 7. A Canadian Government information document titled "Multilateral Agreement on Investment (MAI): Consultations by the Federal Government (as of July 13, 1998)" revealed that up until the fall of 1997, the main parties consulted within civil society were those that belonged to particular sectors of the economy the so-called SAGITs (Sectoral Advisory Groups on International Trade), labour, and the provinces.

[7] Calling campaigns are a strategy used by NGOs where they invite their membership to phone particular individuals on specific dates. Since some of the NGOs have a particularly large membership base (for example the Sierra Club - U.S. counts some 600,000 members) the number of calls received by one individual can be overwhelming. NGOs target officials in the Administration as well as Members of Congress who are deemed to be likely to take political action on the issue rather than officials in USTR for example. In the case of the MAI, telephone calls to the White House Chief of Staff became so intense on one occasion that the responsible NGO, Public Citizen, was asked for a reprieve.

significance for the MAI negotiations was the subsequent withdrawal of the MAI from the second fast-track application (Dymond, 1999: 31). This represented a set-back for the MAI since the credibility of that United State's commitment to the MAI was then considerably diminished inside the NG, undermining other delegations' confidence in the process.[8]

(B) European Campaigns

Given the impact that the lack of Parliamentary oversight of the MAI had had in North America, bringing the treaty to the attention of politicians also became a key strategy in Europe. In addition to fostering the types of grassroots campaigns described in the previous chapter, intellectuals-engagés from Europe and North America collaborated to alert politicians.[9] Subsequent to the NG/NGO meeting of October 1997, MAI opponents intensified their work with political parties at every level. Parliamentarians within individual countries and at the European Parliament level were alerted to the

---

[8] Once the MAI was excluded from fast track authority the only way it could be submitted to the Congrss for approval was as a treaty. The latter solution meant that only the Senate would be required to pass the MAI by a two-thirds majority. However, in that case the difficulties would stem from the outstanding disagreements regarding the Helms-Burton and the Iran-Libya Acts. That is, should the Senate be asked to approve the MAI, the ongoing US-EU negotiations concerning these Acts would have to be resolved in a manner satisfactory to the Senate Foreign Relations Chairman and initiator of the Helms-Burton Act, Jesse Helms— a difficult feat in itself. Furthermore, since those negotiations failed to meet the October 15, 1997 deadline, and no solution was envisaged prior to April 1998, the issue was becoming a serious impediment to successful MAI negotiations (*Inside U.S. Trade*, November, 21, 1997 and January 16, 1998).

[9] As one North American activist worded it: "what we did when we met with [European] groups in January and afterwards was to say if you're going to mount a campaign in your country, one of the most important things that you need to do is to educate people in the government as well as the public at large about what this is about and to understand that there are different parts of your government that are going to be directly affected by it. So that the Minister of Health, the Minister of Education or the Minister of Culture, or the Minister of social programs or whatever, all of these and many more are going to be affected by the MAI. The question is are these departments even aware of what's going on" (interview with the Polaris Institute, September 1999).

existence of the MAI indirectly through the Internet and directly through contacts with European and North-American activists.[10] This section describes some successful examples of such collaboration between groups that belonged to the "social movement system of action" and the "political party system of action." These were successful in that they resulted in decisive political action which eventually had an impact on the fate of the negotiations.

The first critical analysis of the MAI titled "MAI-Day: the Corporate Rule Treaty" eventually made its way to elected officials in the European Parliament.[11] As a result, by the fall of 1997 the Greens along with other minority parties from the left focused their attention on the MAI. By December 1997 they had succeeded, with the help of the newly elected Austrian Presidency, in initiating the Parliamentary process necessary to produce an "initiative report" on the MAI.[12] The report, albeit modified, led to a Recommendation on the MAI negotiations from Parliament to the European Commission which was approved by a majority vote on March 11, 1998. Throughout the process staff and officials from these political parties were in direct contact with activists from the

---

[10] Unless otherwise indicated, the evidence collected to illustrate the remainder of this section was obtained though interviews with activists in Europe and North America and European officials in the fall of 1999.

[11] Note that this analysis of the MAI was translated into several languages.

[12] The Presidency of the European Parliament changes every six months. According to interviewees from the European Parliament, Austria was aware of and concerned by its own growing domestic opposition movement to the MAI. That movement was started by a feminist academic who had obtained the Internet copy of "MAI-day: The Corporate Rule Treaty." Although these reports do not represent executive decisions, they do hold some degree of political authority in that they may yield Parliamentary Recommendations.

social movement system of action.[13]

Consequently, the recommendations which transpired in the final text adopted by the European Parliament espoused many of the MAI opponents' critiques.[14] Among these were Parliament's concerns "that the draft multilateral agreement on investments (MAI) reflect[ed] an imbalance between the rights and obligations of investors," and that the compatibility of the MAI with EU environmental, social and cultural legislation and its relationship with MEAs had not yet been clarified. Parliament's explicit recommendations to the Commission called for: "a broader public debate and ongoing parliamentary monitoring of the negotiations," and an "independent and thorough impact assessment in the social environmental and development fields investigating to what extent the draft MAI [was] in conflict with relevant international agreements such as the Rio Declaration, Agenda 21" and the OECD MNC Code of Conduct of 1992. The Resolution further called upon "parliaments and governments of the Member States not to accept the MAI as it stands" and further instructed the President of the European Council "to forward this resolution to the Council, the Commission, the governments and parliaments of the Member States and the Secretariat of the OECD." The overwhelming majority of votes in

---

[13] Beginning with an informal meeting in December 1997, regular strategy meetings were scheduled and lasted throughout the anti-MAI campaign into the fall of 1998. As mentioned in Chapter three, subsequent to the NG/NGO meeting North American activists decided to engage in such meetings starting in January 1998. The latter reunited politicians with members of the French movement and in particular l'Observatoire de la Mondialisation and that organization's collaborators from France, Belgium and North America as well as activists from other Northern European countries. Even activists who considered themselves mobilizers contributed to a "fax sending" campaign in order to convince Parliamentarians to vote in favor of the Recommendation.

[14] The excerpts which follow in this paragraph were taken from the European Parliament document PE 267.866, pages 50-55 which were the "Minutes of the sitting of Wednesday 11 March 1998, Part II, Texts adopted by Parliament."

support of this document provided activists' with a formidable tool to question their respective governments' involvement in the MAI.[15]

Throughout their contacts with European activists, intellectuals-engagés from the U.S.-based NGO Public Citizens, Friends of the Earth-U.S. and the Canadian Polaris Institute not only stressed to their European colleagues the importance of alerting European politicians but participated in the process. Beginning in January, these activists briefed French politicians from the Communist and the Green parties that had formed a coalition government with Lionel Jospin's Socialist party.[16] In addition to holding private meetings with Parliamentarians, these North American activists joined their French counterparts and politicians in several colloquia which took place at the French Parliament.[17] The contribution made by North Americans through their knowledge of the NAFTA and examples of investor-state disputes provided European activists with concrete examples to illustrate what were at times abstract critiques of a treaty, the language of which few understood.

Contacts with politicians and high level officials from different ministries also enabled intellectuals-engagés to engage in a strategy they referred to as operation

---

[15] The final vote count was 437 in favor, 8 against and 62 abstentions (based on a Press Release dated 11 March 1998 from the Greens in the European Parliament and transmitted by electronic mail from the European Parliament to Friends of the Earth International).

[16] These activists also worked in close collaboration with the Greens from the franco phone region in Belgium called the Ecolos. The Ecolos party, which was in opposition at the time, undertook public information campaigns as well as political challenges in Parliament and with politicians. This political party was also involved in the campaign to pass the report at the European Parliament. There is also evidence of North American activists meeting with politicians as far North as Sweden (based on interviews with activists and archival documents from the Observatoire de la Mondialisation).

[17] At least two such meetings took place: one on December 4, 1997 and the other and more visible meeting on April 22, 1998.

"monkey wrench." This strategy consisted of drawing the attention of officials of one country to the exceptions of another country and pointing out discrepancies with the exceptions filed by those officials' own delegation. The objective was to create reactions that would help to increase the number of country-specific exceptions tabled. Although it is difficult to document whether such a strategy contributed to the growing number of exceptions which had been tabled by April 1998, there is little doubt that activists' interpretation of the MAI and its impact on various portfolios created concerns in several administrations.

The "absence of politics" from the MAI process, as it was referred to in Europe, resulted in a significant political backlash against the MAI. The difficulties activists experienced when attempting to obtain information on the MAI from their domestic bureaucracies only exacerbated the secrecy label that was becoming widespread. The apparent lack of transparency and interdepartmental communication increased politicians' concerns. Furthermore, the lack of consultation with or even information given to politicians left a vacuum which was filled by MAI opponents' views at the expense of the MAI proponents. Some have argued that the most "decisive impact" of NGOs was to make the MAI a "prominent and sensitive political issue" (Henderson, 1999: 28). While the grassroots campaigns and the media attention described in the previous chapter contributed to that influence in many OECD countries, NGOs' indirect influence on the MAI caused by "parliamentarians who felt that they had been insufficiently informed and consulted" (Henderson, 1999: 28) was as significant. As was observed in UNCTAD (1999*d*: 136): "NGO influence -- often through direct links to parliamentarians -- brought

about unexpected developments ... which appeared to have caught negotiators by surprise."

Direct Influence on the Negotiations: Raising Substantive Issues

The second period of negotiations began with a meeting at the end of June 1997 followed by a summer pause and the resumption of the usual schedule of meetings in September. The five meetings which took place in the latter half of 1997 failed to bring negotiators any closer on the most pressing issues which divided the largest negotiating parties involved, the United States and the EU. In particular, the European Commission and its members continued to defend the requests for REIO and cultural exceptions, a position strongly opposed by the U.S. Conversely, the outstanding issue of extra-territoriality continued to represent a threat to a successful conclusion of the negotiations. As the October 15, 1997 deadline initially set to conclude the negotiations on the Helms Burton and the Iran-Libya Sanction Acts came and went without an agreement, the likelihood of reaching a conclusion on the MAI negotiations by April 1998 became increasingly remote (*Inside U.S. Trade*, November 21, 1997: 13). Neither was any progress made on the issue of binding subnational levels of government which led Europeans to oppose North Americans. Continued disagreements on the process of liberalization and the listing of country-specific exceptions further stalled progress.

In the meantime, the issues of labour and environment were given increasing attention, an indication of the growing level of anxiety raised by MAI opponents in several OECD countries. As Canada's Chief Negotiator observed later: "by the latter half of 1997 [labour and environment] had attained status as major negotiating issues" (Dymond,

1999: 38). These were not only time-consuming; they also provided yet further grounds for division within the NG.

The growing opposition in North America began to affect the U.S. position inside the negotiations. At the first NG session of June 30-July 3, the American delegation engaged in informal discussions with other delegations on new proposals which went beyond existing ones.[18] The U.S. proposal included adding language similar to NAFTA Article 1114.1 (rather than the previous proposal of including NAFTA 1114.2) which was perceived to be tantamount to creating an exception from MAI rules for environmental measures. In addition, the U.S. proposed that language be included that would be similar to articles 3 and 5.1 of the NAFTA side agreements and "language on allowing countries to conduct environmental impact statements (EISs) for proposed investments which could have environmental effect" (*Inside U.S. Trade*, January 23, 1998: 5). Responses to the American proposals reportedly ranged from the "cool reaction" of European countries to "strong reservations" from other OECD members (*Inside U.S. Trade*, January 23, 1998: 5).

Similarly, insiders' lobbying efforts were felt inside the negotiations subsequent to the May 1997 British elections. As one negotiator commented, referring to the recent

---

[18] This sudden interest in improving upon the environment and labor provisions was indicative of the pressure exercised by European insiders' counterparts in the U.S. Indeed, as the NG Chair's representative observed, during the three years of preparatory work on the MAI, no discussions had taken place on how the MAI would relate to Multilateral Environmental Agreements (MEAs) although work on the relationship of the MAI to other agreements had taken place. Such inattention on the part of European experts might have been understood since outside of the NAFTA no other international economic agreement contained environmental provisions. Thus the question was raised as to why the U.S. had not raised the issue in light of that country's experience with the opposition to the NAFTA and the compromises on environment and labor that had enabled that Administration to obtain ratification of the agreement (Huner, 1998: 3).

British and French elections: "[labour and environment] will have to be addressed very carefully in the MAI. There has been a remarkable shift" (*Inside U.S. Trade*, July 11, 1997: 1). As early as September 1997, the British delegation began to pressure the NG for an environmental review of the MAI.[19] Considering the fact that the British delegation had been, until then, a strong proponent of a "high standard agreement" and highly sceptical of environmental provisions, the shift in that new central government's position was significant.

The intensification of the anti-MAI campaigns and that on the Internet in particular also had an impact on the NG. As the MAI draft text was made public, its labelling as a "Confidential" OECD document seemed to confirm the criticism of the process as secretive. In order to placate that critique, the Chair requested that MAI documents be declassified, an idea which never materialized since it was resisted by a small group of countries (Huner, 1998: 55). The second and more significant NG response to the virulent anti-MAI Internet campaign was that all delegations agreed to hold a consultation process with NGOs. As the Chair's representative worded it: "[b]y the early autumn of 1997 it became clear that some form of direct dialogue between NGOs and the negotiators

---

[19] This request had been the first item on a list of requests made in a letter from the WWF and endorsed by a group of NGOs (Correspondence from Dr. Claude Martin, Director General, WWF International, dated 19 May, 1997). The WWF had first requested this in vain from the previous British government as early as December 1996 (WWF, 1998). The initial British proposal was submitted in DAFFE/MAI/RD(97) 43 in September 1997 and the delegation followed up with another request submitted in DAFFE/MAI/RD(97)50 at the NG meeting of October 29-30, 1997. In a letter dated November 4, 1997, the Department of Trade and Industry wrote to WWF providing feedback on that meeting and stating that "[a]n important UK objective was to speed up work on an environmental review of the MAI....The review will be discussed in December and January and I expect a report will be published early in 1998 with a view to getting further NGO reactions/suggestions and taking necessary action before negotiations conclude."

was inevitable" (Huner, 1998: 5).[20] Thus, in September 1997, WWF and FOE International finally received the request from the OECD to organize a meeting with NGOs on October 27, 1997 prior to the scheduled NG meeting.

Although the impact of the encounter between negotiators and NGOs was not immediately evident to activists, the meeting had a direct influence on the negotiations. As explained in the previous chapter, by the time this meeting occurred, the opposition to the MAI had radicalized to a point where all NGOs' objective was to stop the agreement altogether. Since the NG rejected that request, the perception was that the meeting had served little purpose. However, several points which were raised provided constructive criticism which negotiators attempted to address subsequently. In particular, Canadian NGOs' description of a lawsuit filed under the NAFTA investor-state dispute settlement mechanism reverberated on several provisions.[21]

The "Ethyl case" convinced negotiators that the MAI provision on expropriation needed to be reconsidered. The prospect of corporations suing governments for "regulatory takings" had not been considered when the provisions on expropriation had been drafted. In response, the article on investment protection which dealt with

---

[20] Interviews also confirmed that officials agreed to meet NGOs in light of the growing opposition and in the hope of calming the antagonism which had been generated towards the MAI.

[21] On April 14, 1997, the United States-based Ethyl Corporation "launched a NAFTA claim against the Government of Canada for damages done to its Canadian subsidiary by legislation which prohibi[ted] the importation and interprovincial trade of MMT, a manganese-based gasoline additive produced by Ethyl" (letter from Ethyl Corporation to World Development Movement, Friends of the Earth UK and WWF-UK dated April 1998). Since the "damage" was deemed to have been done as a result of a Canadian Government legislation, MAI critics used this and other NAFTA cases as examples of potential misuse of several MAI provisions which were similar to the NAFTA investment provisions. See Steve Shrybman and Michelle Swenarchuk's respective articles in *Dismantling Democracy* for the legal critique adopted by NGOs.

expropriation, and which had been one of the first to be agreed upon, was re-examined.[22] Early in 1998, negotiators expressed their common view that the MAI would not interfere with the "normal regulatory powers of government and that the exercise of such powers [would] not amount to expropriation" (*Inside U.S. Trade*, February 20, 1998: 17). In March of 1998 the NG chairman proposed changes to the draft text to that effect (Graham, 1998: 611).

Linked to this issue was NGOs' opposition to the investor-state dispute settlement mechanism. Here also, MAI opponents found receptive ears in Europe. The Ethyl case seemed to confirm perceptions of cultural differences between Europeans and Americans with regard to legal conduct. For some Europeans, the Ethyl case was an example of the Americans' readiness to sue by taking provisions out of the broader context of an agreement —a prospect which frightened some delegations. As one European observer worded it: '[t]here is a tradition in the United States in particular of lawyers trying to pursue perverse interpretations of texts. There is a clash between North American and European culture, the European way of approaching things is that everything should be seen in its context."[23]

Europeans' understanding of the investor-state dispute processes was based upon their experience with bilateral investment treaties (BITs). Under BITs, which European countries have signed mostly with developing countries, the investor-state dispute

---

[22] Graham (1998: 604) defines the understanding of "regulatory takings" in the U.S. as "laws or regulations that reduce the value of a private asset or property."

[23] Based on interviews conducted with officials in Europe in the fall of 1999.

settlement mechanisms have been intended to provide corporations with legal recourse in cases where the judicial system in the host country was deemed inadequate.[24] The implicit situation was that of a Northern corporation investing in a developing country. The idea, exemplified by the Ethyl case, of a Northern corporation suing a (Northern) government that enjoyed a fully developed judicial system, was foreign and shocking.

The Ethyl case lent credibility to the MAI opponents' critique that the agreement would "subject state sovereignty to multinational corporations" (Dymond, 1999: 40). NGOs claimed that such law suits would result in a "chilling effect" on legislators.[25] As a result, the already embattled proposal for an investor-state dispute settlement mechanism was further set back by the exposure of the Ethyl case. As pointed out by UNCTAD (1999*d*: 135): "[f]ailure to resolve this matter would have thrown into question one of the main pillars of the MAI."

Several documents illustrate the way in which negotiators addressed NGOs' concerns. By the end of January 1998, negotiating parties were asked to carry out their respective environmental reviews (OECD, 1997*b*). As well, the OECD secretariat undertook studies on the relationship of the MAI to MEAs (DAFFE/MAI(98)1) and the relationship between FDI and the environment (DAFFE/MAI(97)3). Furthermore, the

---

[24] See Graham (1998) for an informed discussion on this topic.

[25] This argument appeared on many NGO web sites. Following is an example taken from the submission of the Sierra Club of Canada to the Canadian Government hearings on the MAI on November 18, 1997: "[t]he MAI would restrict Members of Parliament's freedom to legislate, without fear or threat of financial penalty to Canada, to protect the environment, public health and other non-monetary interests deeply valued by Canadians....While the proposed MAI wouldn't stop governments from enforcing environmental laws or enacting new ones, the MAI would allow those foreign investors to turn around and sue taxpayers, to recover their lost profits. And that's the chilling effect of the MAI and our primary concern. Governments aren't going to think once, they're going to think 50 times before enacting future environmental legislation."

NG Chair's proposal on labour and environment dealt with the issue of regulatory takings (DAFFE/MAI(98)10).[26] Concerns regarding regulatory takings were addressed by including language to the effect that contracting parties would be able to adopt measures "to ensure that investment activity is undertaken in a manner sensitive to health, safety or environmental concerns, provided such measures are consistent with this agreement." [27] Another article concerned the issue of "Not Lowering Measures" and read as follows: "A Contracting Party shall not waive or otherwise derogate from ... its domestic health, safety, environmental or labour measures as an encouragement [to investments]." While still under negotiation in April 1998, the Chair's proposal reportedly found majority support. The April 1998 MAI draft reflects the debates and number of alternatives submitted to that effect. Not only does the draft include the preambular language, the section on "Not Lowering Standards," and the annexation of the OECD Guidelines for Multinational Enterprises included in the 1997 draft, but a new section on "Additional Clauses on Labour and Environment" was added in Section III.

Whether these efforts provided the hoped-for results was a matter of some disagreement. As far as negotiators were concerned, significant attention and a genuine attempt to address NGOs' concerns were made, albeit in a way that would be balanced with the interests of business groups.[28] However, environmental NGOs felt that these

---

[26] See Mabey (1999: 77) regarding the three last OECD documents listed.

[27] The excerpts quoted are taken from the Annex to Engering's Paper on Labor and Environment as reproduced in *Inside U.S. Trade*, March 27, 1998: 17-19.

[28] As such, some negotiators were puzzled by the continued NGO opposition. It was felt that NGOs had missed an opportunity to see such provisions included in a multilateral economic agreement.

attempts fell far short of their demands and viewed them as "too little, too late" (Mabey, 1999: 77). This opinion applied to insiders as well as the more radical groups. Their reservations were informed by their experience of diverse rulings under the NAFTA and the WTO and the growing distrust which ensued in the environmental community regarding such provisions.[29]

While the NG attempts at dealing with the labour and environment issues did not ameliorate the MAI opposition they contributed to an erosion of support from the business community. Throughout the second period, as focus increased on the labour and environmental provisions, business groups' interest in the MAI moved from concerns to critiques to indifference, thereby undermining the only source of civil society support for the negotiations

At first, the early American proposals prompted an immediate and stern response not only from USCIB but also from other business groups that had been relatively quiet observers up until then. The American business lobby group objected to any provisions that "would turn the MAI into a vehicle to promote environmental and labour objectives unrelated to (and possibly inconsistent with) the goals originally outlined by the

---

[29] For an informed discussion of Environmental NGOs' concerns see Nick Mabey, "Defending the Legacy of Rio" in *Regulating International Business*, pp. 60-81. Regarding the Chair's proposal Mabey wrote: "the proposed amendments would still open up environmental laws to challenge under the MAI for discrimination, and the burden of proof they would have to surmount remained unclear. Experience with similar clauses under the GATT system shows that an environmental regulation has never survived a challenge from an international economic agreement .... As yet, the negotiators had not adequately dealt with the expropriation or MEA conflicts, and the issue of binding environmental standards on companies was yet to be addressed."

Agreement."[30] At a January 12, 1998 consultation meeting with the NG, 40 business representatives from 7 international and regional business groups supported BIAC in expressing their concerns over the new proposals on labour and environment.[31] In sum, the business community questioned whether the final package would "really add value to the current investment environment." Added to this growing concern were the developments on country-specific exceptions and other unresolved debates on liberalization provisions as well as the investor-state dispute settlement mechanisms. Thus, as Henderson (1999: 29) observed: "[f]or all these reasons, the feeling spread that whatever was eventually signed would not be worth a great deal."

Thus, by April 1998, negotiators and their governments were beginning to experience what Dymond (1999: 26) referred to as a "negative gain/pain ratio."[32] That is, as the "value added" of the MAI appeared to be waning governments were losing the fragile domestic support of those constituencies that stood to gain from such a treaty while still being criticized by other constituencies. That situation would prevent

---

[30] Letter from USCIB to Jeffrey Lang, Deputy Trade Representative dated July 11, 1997 as reproduced in *Inside U.S. Trade*, July 18, 1997, pp. 13, 14.

[31] See "BIAC Statement on MAI" reproduced in *Inside U.S. Trade*, January 23, 1998, pp. 6, 7 and signed by the European-American Business Council, Fédération Bancaire de l'Union Européenne, the International Chamber of Commerce (ICC), the International Organisation of Employers (IOE), UNICE, and World Business Council for Sustainable Development.

[32] Note, however, that Dymond (1999: 26) attributed the "negative political gain/pain ratio" solely to the fact that, as explained earlier, investors within the OECD had little to gain from a treaty being negotiated "among countries with well-established, liberal, and transparent foreign investment policies." Evidently, when that situation was combined with one where environmental and labor provisions threatened business interests, the situation was further exacerbated. Note also that Dymond's view reflects Canada's position that investment negotiations would have been preferable at the WTO. As explained earlier, although many negotiating parties found the investment regime within the OECD satisfactory, others, and among them powerful OECD members such as the U.S. were seeking greater liberalization within the OECD and through the MAI (see previous section on country-specific exceptions).

governments from balancing divergent interests in order to sway public support for the treaty and thereby justify the negotiations to their respective constituencies.

These challenges are best captured by Putnam's (1988) concept of the "two level game." The concept reflects the dual role that negotiators are called upon to play. This dual role was also observed in Winham's (1986) analysis of the Tokyo Round of trade negotiations where: "[t]he internal negotiation was characterized by discussions between government bureaucracies, legislators, and interest groups, and it was the arena where decisions were reached about how much the nation could accommodate the interests of other nations."[33] Thus the response of civil society was not only one where opposition became intolerable but also where the support that is normally relied upon to justify negotiations was eroding. Delegations also appeared to be experiencing difficulties in accommodating one another's divergent interests. Tensions between two alternatives seemed to have been at play: either they obtained domestic support by seeking greater openness in the existing OECD investment regime, or they sought the status quo and gained little domestic support. Either way, opposition created an increasingly untenable compromise. In the end, negotiators were faced with a sharply "negative political gain/pain ratio" (Dymond, 1999: 26).

April 1998: A Second Extension?

By December 1997, the NG had reached such an impasse with some of the outstanding substantive issues that the Chair felt it was necessary to resort to retreats.

---

[33] Note that as observed earlier the internal process between bureaucracies seemed to not have been undertaken in a majority of countries involved in the negotiations, a situation that MAI opponents benefitted from.

These were meant to bring key negotiators together in an attempt to break the deadlocks and restore some level of confidence in the negotiations. In addition, a "high level meeting" was called for February 1998 in order to make progress on the more political issues and in particular those of labour and environment, and exceptions/reservations (*Inside U.S. Trade*, January 23, 1998).

The U.S. delegation's announcement at that meeting to the effect that the MAI could not be completed in time for the April 28, 1998 OECD ministerial meeting shocked most delegations. That conclusion had been reached at a U.S. interagency meeting earlier in the month when deputy-level officials concluded that "finalizing the agreement at that time would not bring a significant reduction of barriers to U.S. investment, that there [was] at best lukewarm support for the MAI among private groups and in Congress" (*Inside U.S. Trade*, February 13, 1998: 1). While this announcement had negative repercussions on the morale of the NG, solutions to several outstanding substantive issues were proposed, reflecting a willingness to move to narrow the gaps which had resulted in the earlier impasse.[34]

Thus, in January, the European Commission had signalled its willingness to narrow its proposed exception for REIO and by February EU member states and the U.S. were discussing a compromise over this issue. The U.S. and European countries also reached a tentative agreement on cultural industries that aimed at adopting an approach for

---

[34] The following summary of the state of negotiations towards the end of the second period was taken from *Inside U.S. Trade* publications between January and May, 1998.

reservations in that economic sector similar to those of the Uruguay Round.[35] The most problematic and as yet unresolved issue concerned the Helms Burton and Iran-Libya sanctions, the investor-state dispute settlement mechanism and liberalization. However, work was progressing in the U.S./EU negotiations on extraterritoriality and by May parties declared they were closer to a resolution. Also, as seen in the previous section, labour and environment provisions were gaining increased support, such that only two delegations opposed the proposal.[36]

Nevertheless, between February 1998 and April 1998 the NG once again became embroiled in debates regarding the extension of the negotiations. As experienced the previous year, disagreements concerned the length of the extension. That issue was linked to the debates on the degree of liberalization to be achieved in this first round of negotiations. At issue was whether a more modest agreement with future liberalization would not be preferable to simultaneous negotiations of the framework and country-specific exceptions.[37] While the U.S. adopted its usual position of openness toward an indefinite period and a negotiated balanced commitment, delegations from countries such as Canada which had initially pushed for investment negotiations at the WTO attempted once again to move the negotiations to that forum.[38] The French government, under

---

[35] However, France reiterated its position in support of a general exception on culture.

[36] Indeed, by April 1998, only Australia, Mexico and New Zealand "expressed opposition to points in the statement on labor and environment, although they did agree tentatively to the draft" (*Inside U.S. Trade*, April 24, 1998: 23).

[37] Based on interviews with officials in Europe conducted during the fall of 1999.

[38] See *Inside U.S. Trade*, February 20, 1998, p. 16 where the statement made by U.S. Deputy Trade Representative Jeff Lang and the Under secretary of State, Stuart Eizenstat is quoted as follows: "[w]e are ready to continue at a steady, serious and meaningful pace and to conclude agreement at the earliest feasible

considerable public pressure, suggested a pause in order for negotiating parties to undertake domestic consultations and an assessment of the MAI. In the end, the French proposal was adopted with the mandate to resume negotiations in October 1998 without any specific deadline and with an acknowledgment of the work on investment at the WTO.[39]

II. May 1998 to October 1998: The "Coup de Grâce"

The crucial question raised by the debates concerning the extension of the negotiations and the ensuing six-months pause, is whether the negotiations could have resumed beginning October 1998. Such an understanding would shed light on the much-debated role that civil society played in the demise of the MAI.[40] Indeed, it was in the

---

date."

[39] Paragraph three of the OECD "Ministerial Statement on the Multilateral Agreement on Investment (MAI)" read as follows: "[t]aking into account the positive results produced by the Negotiating Group, as well as the remaining difficulties and the concerns that have been expressed. Ministers decide on a period of assessment and further consultation between the negotiating parties and with interested parts of their societies, and invite the Secretary-General to assist this process. Ministers note that the next meeting of the Negotiating Group will be held in October 1998. Ministers direct the negotiators to continue their work with the aim of reaching a successful and timely conclusion of the MAI and seeking broad participation in it. In the same spirit, they support the current work programme on investment in the WTO and once the work programme has been completed will seek the support of all their partners for next steps towards the creation of investment rules in the WTO" (OECD, 1998*b*).

[40] Examples of such debates appeared in the Canadian media as early as April 1998 when the six months pause was called. While some fully credited the MAI opponents for derailing the negotiations others denied their impact or simply ignored their relevance. Diverse opinions were not limited to officials and activists. They also embroiled think tanks, academics and the media. Thus the following quote attributed the failure of the negotiations to the MAI opponents' effective reliance on the Internet: "High-powered politicians had reams of statistics and analysis on why a set of international investing rules would make the world a better place. They were no match, however, for a global band of grassroots organizations, which with little more than computers and access to the Internet, helped derail a deal" (*The Globe and Mail*, 1998). In contrast, *The Economist*'s (1998: 18) assessment of the MAI troubles at the end of the second period makes no mention of the social opposition, and blames the difficulties on the venue chosen for the negotiations, countries' lack of enthusiasm for the MAI and the numerous reservations filed. Canadian researchers and academics also disagreed on the influence of the MAI opponents. Thus Robert Wolfe (1998), from the School of Policy Studies at Queen's University wrote in a short letter published in *The Globe and Mail* which he titled "MAI imploded all by itself": "[i]t may suit OECD Secretary-General Don Johnston to blame the fiasco on public

third period that anti-MAI campaigns achieved their greatest force and it was also during that period that hopes of reaching an agreement were brought to an end. In order to dispel misunderstandings surrounding the last six months of the MAI process, I begin with a more precise account of the negotiating parties' willingness to pursue the negotiations. That discussion will be followed by one regarding the reasons why the negotiations did not resume.

There is no doubt that this third period represented a turning point for the future of the MAI. However, the alternatives envisaged by the NG did not consist of a choice between abandoning negotiations or pursuing them. As the April 1998 deadline approached, the alternatives revolved around one question. The choices were to either reach a diluted agreement, consisting of a less ambitious text with a provision for future liberalization, or to pursue negotiations for an indefinite period of time until all parties agreed on balanced commitments.[41] Although the European delegations expressed their reluctance to consider another possible extension, when the U.S. declared its opposition to a speedy April conclusion, European countries obliged as they recognized that without the U.S. there would be no MAI.

---

opinion, but the reality is that the agreement was stillborn." His colleague at the University of Toronto, Alan Rugman (1998: 1), could not disagree more when he wrote: "the real reason for the defeat of the MAI...is due to the negative role of Non Governmental Organizations (NGOs) as critics of international trade agreements." For his part, Owen Lippert (1998) the director of the Law and Markets Project at the Fraser Institute, an economic think-tank based in Vancouver, publicly rejected the claims of victory made by Canadian MAI opponent Maude Barlow: "[t]he Multilateral Agreement on investment (MAI) has been indefinitely delayed, and Maude Barlow, keyboard in hand, is claiming at least partial credit. That's nonsense. The MAI process collapsed because countries such as Canada and France refused to question their rat's-nests of subsidies."

[41] In fact an alternative and more modest MAI draft was produced during the summer of 1998 at the OECD.

Such a power play applied only to the other main trading partner, the European Union. Any other negotiating party of lesser relevance could choose to withdraw from the OECD negotiations without preventing progress towards an agreement. Indeed, some commented that Mexico might have chosen that option due to that country's disagreement with the proposed labour provisions. Therefore the willingness of the U.S. to pursue the negotiations and the Europeans' acceptance of renewed negotiations in October were definite signals of the political willingness on the part of crucial players to pursue the negotiations to a satisfactory conclusion. The fact that delegations pursued negotiations in spite of growing differences which brought talks to a standstill during the second period, and that they accepted, albeit reluctantly, two extensions, are indications that the willingness to resume negotiations in October 1998 was never at issue in the minds of the negotiating parties.

Rather, the ultimate *coup de grâce* to the MAI came from France. As seen in Chapter 4, by February 1998 just prior to the high level meeting at the OECD French MAI opponents from the social movement system of action had succeeded in generating considerable media interest in the MAI and the public opposition to the negotiations was mounting rapidly thanks to the networks that were established among diverse groups. The arguments that mobilized such an opposition were those of the intellectuals-engagés; militant-mobilizers from other movements had contributed to generate this mobilization and visible protests. Similarly, the Greens and the Communists began questioning their

partners in Government on the MAI during Parliamentary sessions.[42]

These events prompted the French government to request the six-months pause. In May 1998, having argued with its OECD counterparts in favour of a pause to undertake public consultations and an assessment of the MAI, French President Lionel Jospin mandated a French member of the European Parliament, Catherine Lalumière, to undertake such a study. Lalumière began her work in June 1998 in collaboration with the French senior negotiator, Jean Pierre Landau, and produced a report for the government by mid-October, just before the MAI negotiations were to resume.[43] Consultations were undertaken with the public and private sectors including major business organizations and the SMOs Observatoire de la Mondialisation, Greenpeace France, and FOE France. Of significance to France's decision regarding its future course of action on the MAI were the alternative recommendations proposed to the government. In sum, one recommendation was that, should the government choose to resume negotiations, the current foundations of the MAI should be fundamentally altered. However, the report warned that, in such a case, France still ran the risk of not seeing all of its requests satisfied. Another alternative was to move investment negotiations to the WTO. Such arguments left little choice for the Government's decision.

The other events which moved the French government to its decision to withdraw came from the political parties sympathetic to actors from the social movement system of

---

[42] See, for example, *Le Monde*, February 13, 1998c where it is reported that the Green Representative Yves Cochet confronted Dominique Strauss-Kahn, the then French Minister of the Economy and Finance, on the MAI.

[43] See *Rapport sur l'Accord multilatéral sur l'investissement (AMI)* on the French Government's website at www.finances.gouv.fr.

action. These parties had formed a coalition government with Jospin's Socialist party. At their national meeting of October 10-11, 1998 the French Greens agreed, through a majority vote, on two significant decisions. One was to object to the continuation of the MAI negotiations and to call on the government to withdraw from the negotiations; the other was to withdraw from the Jospin coalition should the government ever sign the MAI.[44] As these decisions were reproduced in the media they were perceived by the Government to be tantamount to a public display of dissent within the coalition, a move which it found highly distasteful.[45] As a result, it was agreed that a Communist member of Parliament, Robert Hue, would speak on behalf of the "gauche plurielle" (the united left) during the next session of Parliament in expressing these parties' opposition to the MAI and require that Jospin explain France's intentions for the upcoming MAI NG meeting. It was in response to that question and in reference to the Lalumière report and the public opposition that Jospin announced publicly France's decision to withdraw from the negotiations.[46] These events took place during the October 14, 1998 session of Parliament, a week prior to the planned resumption of the MAI negotiations.

France's decision took the other members of the European Union and the European Commission by surprise. Technically, such a unilateral action was in breach of Community discipline. Indeed, the Council of the European Parliament had endorsed a mandate for the European Commission to negotiate the MAI alongside member states.

---

[44] These motions were found on the minutes from the meeting and numbered decisions Cnir-98-216 and Cnir-98-219.

[45] See the French daily newspapers such as *Le Figaro* and *L'Humanité* (1998*a*)from these dates.

[46] For a complete reproduction of these speeches see *L'Humanité*, October 15, 1998*b*, p. 4

This meant that unlike the case at the WTO negotiations where the European Commission was the spokesperson for the European Union, in the case of the MAI each country had a seat at the table with the European Union also playing a negotiating role. This meant that the European Union as a whole was considered to be part of the negotiations and, as such, France's decision to withdraw had an impact on all other members. However, none questioned the French government's decision. At the October 20, 1998 NG meeting, the European Commission announced that no European member would pursue the negotiations without France, thereby giving a decisive and final blow to the MAI negotiations. As the European Commission's attempts at pulling France back into the negotiations failed so did all subsequent attempts at reviving the negotiations (*Inside U.S. Trade*, October 23, 1998; Dymond, 1999: 32, 33). A December 1998 meeting only confirmed the inevitable. These meetings and the attempts to salvage the negotiations further testify to the determination of major parties to resume the process.

Given the intense domestic and international anti-MAI campaigns which took place in France, and given the close working relationships that had developed between activists, the Greens and the Communists of Jospin's coalition, as well as officials from the European Parliament, it is difficult to deny the impact that these groups exercised on the ultimate fate of the MAI. However, France encountered little protest and resistance from its fellow members of the European Union, an indication of the impact of anti-MAI sentiments in terms of these governments' loss of ardour for the negotiations. The significance of the election of left-leaning governments in key European states, including France, Britain and Germany (the latter in September 1998), should not be

underestimated. These political changes no doubt influenced France's response to the concerns of civil society groups and its fellow European Union members' reaction to it.

III. Assessing MAI Opponents' Influence

Respective Impacts

At the outset of this analysis I drew a distinction between *direct influence*, which concerned societal actors' influence on substantive issues, and *indirect influence*, which referred to increased political pressure on elected officials. I also pointed out in Chapter 3, that direct influence on substantive issues is an objective typically sought by actors who belong to *the interest group system of action* in that these are achieved through dialogue with officials, policy analysis and lobbying that aim to reform particular policies. While actors that belong to the *social movement system of action* may also seek to influence states and policies they primarily seek to promote changes through influence on society. As such the behaviour of actors from the social movement system of action typically consists of gaining media attention, alerting and educating publics and generating mobilization through protests. In doing so they seek not only societal change but also indirect influence on officials.

The empirical evidence indicates that direct influence strategies were less successful in meeting MAI opponents' objectives than were indirect influence strategies. The coalition saw its objective of interrupting the MAI negotiations realized. Since the coalition as a whole applied every means of pressure available it is difficult to decipher which specific actor was more effective. Nevertheless, as the following discussion highlights the radicalization of the campaign reflected a stance typical of actors from the

social movement system of action. Likewise the grassroots campaigns, critiques of the MAI and mobilization efforts typical of those actors' behaviour and motives gained media attention and, eventually, politicians' support. The following discussion provides an assessment of these respective types of influence as they affected various outcomes in the MAI negotiations.

(A) Direct Influence

I have shown in Chapters 4 and 5 that during the first period of negotiations, from May 1995 to April 1997, it was only the MAI opponents whom I referred to as "reformists" or "insiders" that had an opportunity to signal their objections regarding the MAI to OECD officials. During that period, these societal actors only enjoyed a minimal impact since the extension of the negotiations' mandate had more to do with the lack of progress on major stumbling issues.

However, the analysis of the two subsequent periods of negotiations revealed that these MAI opponents exercised some direct influence on the negotiations regarding the inclusion of labour and environmental provisions in the draft treaty. NGOs succeeded in raising the profile of these issues within the NG during the second period of negotiations, to a point were these figured among the main negotiating issues. This took place mainly through domestic lobbying pressure and some delegations' insistence inside the negotiations. In that sense, insiders' sustained lobbying efforts at the domestic level bore fruit. Nevertheless, the results of this direct influence did not meet insiders'

expectations.[47] The proposed changes to the MAI fell far short of reformist NGOs' objectives. Had the NG reached an agreement on all other outstanding issues it is very likely that the provisions on labour and environment to be included in the MAI would have remained similar to these unsatisfactory proposals. I also intimated that officials' response was most likely motivated by the threat of a growing opposition to the MAI—an outcome clearly resulting from the mobilizing efforts of actors from the social movement system of action in various countries and the eventual radical common front adopted by all MAI opponents when they formed a coalition.

Reformists' continued dissatisfaction with the way the NG addressed their concerns, the prolonged exclusion of NGOs from consultations with the NG and the apparently imminent ratification of an agreement resulted in the formation of a coalition with more radical objectives. Thus reformists coalesced with the more radical MAI opponents in October 1997 on the occasion of the first and only encounter between MAI opponents and the NG. Radicalization of the MAI opposition was illustrated by the common objective of the coalition to stop the OECD MAI and to cut further dialogue with OECD officials and the NG. Although the coalition requested that the NG suspend

---

[47] That dissatisfaction has been observed in another more comprehensive study of NGOs' relations with the main international economic organizations responsible for such multilateral policy making. Thus O'Brien et al. (2000: 141) ask whether the relationship between environmental NGOs and the WTO would not be best characterized as a "dialogue of the deaf." While these authors fall short of explicitly answering that question, their analysis of that relationship clearly indicates that an intellectual impasse between reformists and officials has been reached. In sum, the goal espoused by the WTO to combat protectionism conflicts with these societal actors' attempts to use that venue to defend and promote stronger environmental policies. One of the problems is that such enforcement could be used as a disguise for protectionist aims. In that sense, insiders' lobbying efforts confront states' commitment "to liberal international trade espoused by the leadership of the key advanced industrialized countries" (O'Brien et al., 2000: 141). The debate has been fuelled by all environmentalists' negative experience with the settlement of disputes that concerned environmental policies both within the WTO and the NAFTA.

the negotiations during that meeting, the decision to stop the OECD MAI did not result from such direct influence.

The coalition exercised other direct influence on the MAI on the occasion of its only meeting with the NG. As demonstrated earlier, the encounter of October 1997 resulted in the reexamination of the provisions on expropriation and a heightened debate concerning investor-state dispute settlement mechanisms. These issues were more broadly linked with actors that belonged to the social movement system of action as they were directly linked to their critique of globalization, the relationship of the MAI to that process and the role and interests of MNCs in that process.

For actors who belonged to the emergent social movement networks opposing economic globalization, the MAI was taken as a symbol of that phenomenon. They argued that current processes of economic globalization were influenced by powerful MNCs in order to promote their interests at the expense of ordinary citizens' democratic rights. The provisions on expropriation and investor-state dispute settlement were used as examples of the role that international economic treaties such as the MAI played in shaping such globalization. They were used to demonstrate the effect such policies would have on states' sovereignty, their future regulatory autonomy and democracy. Of interest is the fact that these concerns resonated not only with various domestic publics but also with politicians and European delegations.

(B) Indirect Influence

It was through their indirect influence that MAI opponents fostered their most urgent objective: to stop the MAI negotiations. With regard to that outcome, it was MAI

opponents' indirect influence that was most effective. Such influence was also associated with actors that belonged to the social movement system of action. Indirect political influence through successful mobilization at various domestic and transnational levels affected the future of the negotiations. The collaboration among actors from the social movement system of action that resulted in simultaneous campaigns in a majority of OECD countries enabled the interruption of the negotiation process.

More specifically, the analysis of events during the six months pause prior to resuming negotiations demonstrated that it was France's unilateral decision to withdraw from the negotiations that dealt the MAI its final blow. The grassroots campaigns, street protests, media attention and growing public opposition point to a strong influence from actors from the social movement system of action on that decision. Intellectuals-engagés' critiques were used to educate the public and engender broad mobilization. Those critiques were also used to inform politicians and convince them of the validity of these MAI opponents' arguments. In addition, direct relations between activists from the social movement system of action and politicians from that country also establish a direct link between those MAI opponents and the negative outcome of the negotiations.

The concerns which had thus been raised within many OECD members' Parliaments, including the European Parliament, and the aggressive anti-MAI campaigns that had developed throughout Europe provided little incentive, on the part of other EU members, to counter France's decision. Therefore, the failure of the MAI as it related to these anti-MAI campaigns must take into consideration the multiple and simultaneous domestic campaigns which occurred through an unprecedented collaboration among

actors from the social movement system of action across borders. As such, that MAI opposition effectively turned into transnational social movement networks that would grow beyond their opposition to the MAI to mobilize against the WTO. For these reasons, the impact of this new social actor merits further explanation.

Explaining Indirect Influence

(A) Transnational Social Movement Networks and International Fora

The outcome of the indirect influence applied by actors from the social movement system of action on the MAI negotiations can be explained by using existing understandings of similar events. Thus Rucht (1999: 208-209) observed that "when international bodies remain immobile because of internal disagreements, this may encourage social movements to put pressure on them." As we saw, the difficulties encountered early on in the negotiations and the resulting extensions of the mandate provided room for MAI opponents to challenge the treaty. Another aspect of supranational governmental bodies that Rucht (ibid.) identified as presenting a condition favourable to social movements was the fact that these bodies "lack direct democratic legitimation by voters." As seen in the anti-MAI campaigns this critique was useful and it was further enhanced by the fact that NGOs had been excluded from consultation while business organizations had not.

On the other hand, Rucht (ibid.) has observed that the "inflexibility and limited power of international institutions" to respond to movements' claims has meant that these societal actors continue to focus on national governments as their primary target. However, should such pressure not succeed, movements will seek to exert indirect

pressure by (i) increasing domestic pressure through strengthening oppositional forces, (ii) mobilising attentive publics and gaining supportive press coverage, and (iii), influencing particular governments and movements in other countries. Clearly these processes were at play in the case of the MAI opposition.

(B) Novel Dynamics

The latter point represents a novel element in terms of our understanding of state-society relations when analysing international economic negotiations. While the domestic support of business groups for a MAI can easily be explained with traditional models of analysis, the transnational interactions of social movement actors just described do not follow such patterns. For example, we saw that business support for the MAI in the United States was linked to that country's position in the negotiations—gaining increased access to other countries' markets. However, we also saw that disagreements among negotiating parties on the extent to which the MAI should simultaneously improve upon existing openness of OECD markets revealed that not all negotiating parties shared that objective. Few were willing to move immediately beyond the existing degree of liberalization already enjoyed within the OECD. The delegations of those countries enjoyed only lukewarm support from their business community. When it became evident to business organizations interested in the MAI that the treaty would not only fail to provide these benefits but that provisions on labour and environment would further undermine their interests, support vanished into criticism and then indifference. In the meantime, opposition did not wane. To explain these domestic societal factors, we referred to Dymond's (1999) explanation of the domestic political negative gain/pain

calculus that the MAI then represented for many delegations.

These challenges are explained by Putnam's (1988) two level game analysis whereby domestic policy makers and negotiators seek to strike a balance among various domestic pressures while at the same time accommodating the interests of their negotiating partners. These dynamics are represented in Figure 6.1 diagram (A). In the case of the MAI, negotiators and policy-makers found themselves in a position where a combination of conditions placed the MAI on precarious ground domestically and internationally.

Nevertheless, some MAI opponents also undertook novel interactions and expressions of advocacy against multilateral economic negotiations. The nature of the radicals' concerns, their convergence across borders and their interactions with foreign governments represented several departures from Putnam's model. As such, the generic label of "interest group" hides a considerable difference between the nature of those MAI opponents and the traditional interests considered in trade negotiations. In the case of the movement networks opposing globalization, the model no longer applies. That is, traditionally, domestic interest groups involved in trade negotiations have represented different economic sectors. This is not the case of the MAI opponents that belong to the social movement system of action. Not only are their concerns different from those of actors from specific economic sectors, but they do not limit their actions to the domestic level.

Although negotiators focus, as Putnam's model describes, on domestic interest groups, MAI opponents worked across borders and their claims were not limited to

FIG 6.1 Putnam's Two Level Game Compared with New Forms of International Interactions

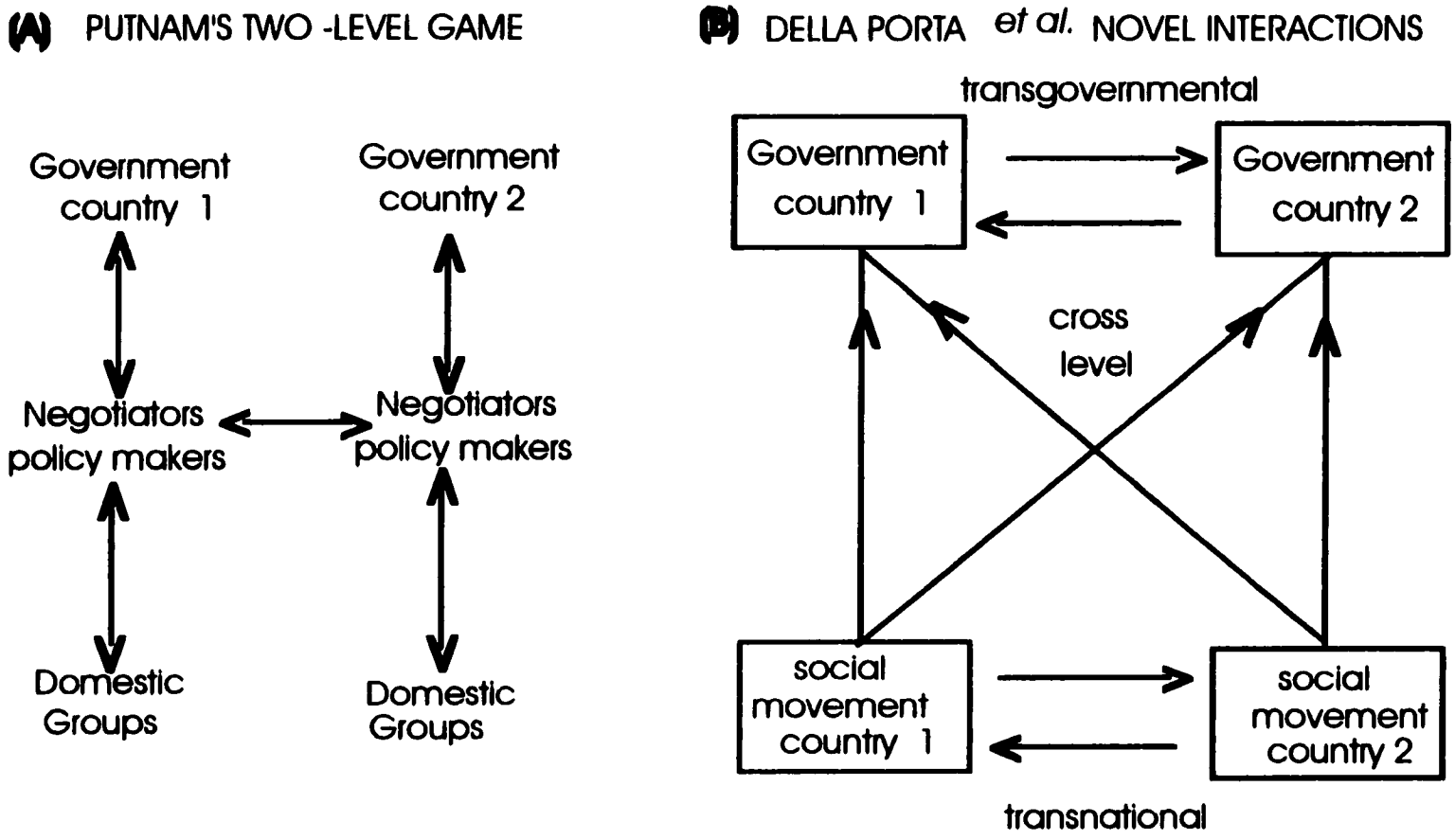

domestic sectoral economic interests. For example, from the standpoint of the Canadian MAI negotiators "public consciousness [in Canada] paled compared to the free trade debate in the 1980s" (Dymond, 1999: 26). However, Canadian MAI opponents, who belong to the emergent movement networks against globalization, found support for their objectives in other OECD member countries. Not only did they appear to find support but their objective of stopping the MAI was fulfilled, whereas their similar quest to stop the NAFTA was not. Diagram (B) in Figure 6.1 illustrates such new dynamics with a model suggested by della Porta *et al.* (1999: 3-5). The model, these authors argue, aims to reflect the novel forms of interactions attributed to "the changing international context on national social systems and national polities."

Contributing Factors

Nevertheless, the assessment of these MAI opponents' influence must take into consideration additional factors that represent conditions conducive to their success. Contributing to these campaigns was the political sea change that had taken place in Europe by October 1998. In addition, existing structures of influence within the OECD helped to push the MAI negotiations over the precipice. France alone would not have caused the demise of the MAI. Only the EU and the U.S., two major negotiating parties, could bring about such an outcome unilaterally. As such, France's decision was decisive only to the extent that its fellow members in the European Union remained united, and due to its relative importance in that forum.

In addition, the analysis revealed that the MAI negotiations suffered setbacks from other directions. The first consisted of stumbling blocks within the negotiations which

manifested themselves early on. A good number of difficult substantive issues had emerged within the negotiations well before those brought forward by NGOs. Most of the lasting substantive difficulties had been encountered by May 1997 during what we referred to as the first period of negotiations. Although it would be pure speculation to judge whether these outstanding issues would have been resolved had the negotiations resumed beyond October 1998, there is no doubt that progress had been considerably jeopardized by February 1998. In that sense, the MAI was "a leaky boat."

Finally, the role played by another group from civil society must also be considered when assessing the influence of MAI opponents. Most domestic business groups' lukewarm support for the MAI was due to the fact that it was being negotiated at the OECD. In addition, the partial accommodation of NGOs' demands in the MAI together with the substantive challenges on other issues were responsible for the negative reaction of business organizations and the erosion of interest and support from these groups.

These contributing factors raise questions for further research. One concerns the domestic and international political environments within which societal actors evolve. Given the enabling role of the OECD as a forum of negotiations, how does that international forum compare to others in terms of civil society's ability to influence world politics? For example, what is the difference between the OECD, the WTO or the United Nations in terms of leverage and impact of civil society? At the domestic level, the electoral system in France could be compared with those of Canada and the United States in terms of the alternative responses MAI opponents received from their mutual governments. Another question raised by the case of the MAI concerns the actors

themselves. I have drawn a distinction between reformist and radical societal actors and shown to the extent possible their relative influence on the MAI negotiations. Other distinctions were also drawn regarding the proximity of NGOs to their governments, their funding sources and relevance in terms of geographical location. One related question that deserves research was the role of Southern NGOs in the anti-MAI campaigns, given their governments' reluctance to an investment agreement such as the MAI.

Conclusion

The MAI was an investment agreement negotiated among the like-minded countries of the OECD where various instruments and codes had already fostered a high degree of investment liberalization and protection among these countries. Nevertheless, high expectations were shattered after difficult negotiations were abandoned without an agreement. The unexpected failure of these negotiations was all the more surprising in that the outcome was linked to a visible social opposition to the treaty in a majority of OECD countries. The preceding chapters have provided empirical evidence that verify these impressions.

While the influence of these societal actors on the MAI represents a noteworthy event, the research yielded other results of further interest. As I argued, the MAI events represented a threshold in international economic relations not only because of the influence the social opposition exercised but also because of the emergence of a novel societal actor in this domain of world politics. The discreet policy dialogues and lobbying efforts conducted by reformist groups would not have attracted broad public interest in an obscure and arcane agreement such as the MAI. It was the strategies of the radical

elements of the anti-MAI coalition that opened a public debate not solely on the MAI but on broader issues they find with current processes of economic globalization. As such, these MAI opponents succeeded not only in generating concerns over the MAI but by linking these concerns to their perception of the nefarious future all societies would face should such processes not be interrupted, they engendered a broader and longer lasting debate on the future(s) we might face under ongoing processes of economic globalization.

As Lalumière and Landau (1998) observed, the opposition to the MAI was not unique to France, nor was it restricted to the traditional claims from economic sectors. The authors observed other novelties in that MAI opposition. Among these they pointed out that: "it appeared simultaneously in several countries, it included new actors and the negotiation process itself was contested." The report went so far as to note that "for the first time we assist in the emergence of a global civil society" (Lalumière, 1998: 2,3). I have called this phenomenon emergent transnational social movement networks against economic globalization and demonstrated, in Chapter 4, its growth potential.

Many officials acknowledged the novelty of this MAI opposition. Such official understanding was expressed during one of the last public announcements concerning the MAI. On that occasion, the OECD Deputy Director General, Joanna Shelton, "hinted that countries realize they must find a new way to address criticisms of the MAI and issues that have been raised as a result of globalization" (*Inside U.S. Trade*, October 23, 1998: 7). Shelton was specifically quoted as saying: "[t]oday's meeting also made it clear that we are not engaged in business as usual, and that we must address the concerns that have been raised about the scope and direction of the efforts to date." As such, the MAI

represented a threshold moment in international economic negotiations, and the theoretical relevance of transnational social movement networks for world politics merits more study.

I have already demonstrated conceptually and empirically that this phenomenon had growth potential. Anti-globalization protests have been sustained since the interruption of the MAI negotiations. Questions of interest concern the reasons for which such widespread support for the arguments against economic globalization have taken hold, and given this support and the sustained activities of these networks, how we explain their meaning for world politics. Section III begins to address these questions by relying upon existing frameworks. Should the popularity of anti-globalization rationales be understood as a societal reaction to the recent progress toward a globalized economy, and if so, can we understand this new actor to represent a double movement or a counter-hegemonic social force as critical IR theorists suggest? Is it likely to have an impact on world politics beyond that of contributing to the failure of the MAI negotiations? If so, how do we explain such influence? Is that influence similar to existing cases of civil society influence on world politics?

SECTION III

THEORETICAL IMPLICATIONS

CHAPTER VII

CONTESTED FUTURE(S) AND NORM PATHS
A CONSTRUCTIVIST VIEW OF GLOBALIZATION'S OPPONENTS

Introduction

The protests we have witnessed over the three years since the suspension of the OECD MAI negotiations are now widely acknowledged as manifestations of worldwide anti-globalization sentiments. It would be fair to say that few intellectuals-engagés and militant-mobilizers, who participated in the anti-MAI campaign early on, dared hope such subsequent growth of anti-globalization sentiment would occur. Even though in the fall of 1999 just prior to the Seattle protests against the WTO they provided an accurate estimate of the number of protesters expected in Seattle, few of these activists hoped to say with certainty that movement networks had truly emerged.[1] By April 2001, on the occasion of the protests against the FTAA in Quebec city, activists were confident that they participated in worldwide movement networks that opposed economic globalization and that they shared views with other participants in distant places.

Their arguments have now become the subject of heated debates among citizens in televised talk shows and in the printed media. Likewise, anti-globalization activists and officials engage in debates through the media on the occasion of protests. As such, the awareness of the issues that initially concerned these particular MAI opponents has gained attention among a broader segment of the population in Northern as well as Southern countries. Given these outcomes, several questions are worthy of consideration.

I have already hypothesized, in Chapter 4, that there is little doubt that transnational social movement networks against economic globalization are now well

---

[1] In the course of interviews with French militant-mobilizers in early November of that year, they estimated their numbers in Seattle at around 30,000.

established and will continue to be active. Other questions of interest concern the meaning of this novel actor for world politics. The first question of interest is what is this an instance of? Does it represent a Polanyian double movement and the emergence of counter-hegemonic social forces of significance to world orders, as hypothesized in critical IR theory? What impact, if any, has this societal actor had so far other than its influence on the MAI negotiations? What is the meaning of the debates globalization opponents have engendered for world politics? In order to answer these questions I turn to three perspective that, I argue, provide us with the necessary complementary framework to explain the potential of this novel actor for world politics.

One is Robert Cox's (1996: 514-519) historical dialectic framework, which hypothesizes the potential emergence of counter-hegemonic social forces. The second builds upon social movement theory hypotheses that I have already alluded to in the previous chapters. These concern the meaning of social movements in terms of their influence on larger collectivities. Analyses of existing movements have already observerved the cultural and ideational influences that existing movements have exercised on society. I suggest that opponents to economic globalization display similar ideational and cultural challenges that are likely to influence larger collectivities. Finally, the IR social constructivist framework will be relied upon to explain how such ideas might influence world politics. Empirical case studies undertaken with the latter framework have demonstrated ways in which non-state actors have influenced international outcomes. I rely upon such examples to infer ways in which anti-globalization ideas have already engaged such a process and how they may further influence international economic

relations.

IR social constructivists refer to the processes through which the post-war arrangements were reached as the social construction of reality among a society of states whereby principled ideas (beliefs about right and wrong), and causal beliefs (beliefs about cause-and-effect relationships) become norms—collective expectations about proper behaviour. However, for critical IR theorists, these post-war developments are understood to be the result of a more perverse consequence of hegemony. These divergencies lead these two approaches towards different explanatory frameworks in terms of understanding societal actors' meaning for world politics.

Cox's (1996: 514-519) historical dialectic framework looks at societal actors through a structural materialist lens. It is based upon the hypothesis that society "produces in its structure the antagonisms that lead to its modification" (Cox, 1996: 514). As such, the objective of that framework is to determine whether societal actors such as the opponents to globalization represent counter-hegemonic social forces that will transform the current world order. In that sense, significant transformations must be observed to understand the role of social forces as counter-hegemonic. IR social constructivists argue that agency and ideas are theoretically relevant in and of themselves as sources of norm change that affect world politics. Thus, the two frameworks offer complementary tools of analysis. One places societal actors in a broader historical context, the other examines more closely how these actors may engender transformations.

Both approaches have strengths and weaknesses in understanding the significance of movement networks that oppose economic globalization. I begin with a discussion of

critical IR theory, showing that while that framework provides a good understanding of hegemony as the focus of opposition for these actors it lacks the necessary tools to understand the ways in which their influence could bring about changes at the societal and institutional levels. That is, critical IR theory refers to ways in which a change in world orders might occur but not how social forces might undertake such a "war of position."

I argue that a complementary framework that combines social movement analysis and IR constructivist conceptual tools fills that analytical gap. I first discuss ways in which social movement analysis conceives of such a role at the societal level. I follow with a discussion of the contribution that IR social constructivism brings to explaining influence at the institutional level. I discuss some of the conceptual tools provided by that framework which explain how world orders are socially constructed. That discussion includes comparisons between the opponents to economic globalization and existing case studies which suggest avenues to evaluate the transformative potential of the former.

I. Meaning of Radicals in Critical IR Theory

We saw in the previous chapter that this study of the MAI opposition shared with O'Brien et al. (2000) the understanding that there is a distinction between "reformers" and "radicals" among societal actors interacting with international economic regimes. These identities coincided with the NGOs that I located respectively in the interest group system of action and the social movement system of action. Among the reformers O'Brien et al. (2000: 142) mentioned those found in the anti-MAI campaign such as the World Wildlife Fund and the Centre for International Environmental Law (CIEL)—those identified in Chapter 4 as belonging to the interest group system of action. Among the

radicals they identified "the loose coalition called the Peoples' Global Action" (PGA) which I identified as being part of the emergent social movement networks against globalization. However, the narrower focus of that study on the interaction between environmental NGOs and the WTO prevented a more in-depth understanding of the meaning that radicals bring to these non-state actors' interactions with international economic regimes.

The distinctions drawn in the analysis of the anti-MAI campaigns, which were achieved with the help of a model of civil society and an analytical framework based upon social movement theory further elaborated upon the differences between radicals and reformists. They enabled us to trace the evolution of movement networks that were made up of societal actors opposing globalization, and which held transformative objectives. We traced the growth of networks and their re-emergence in the Seattle protests and subsequent gatherings that aimed at challenging various global economic fora. Thus I identified an emergent movement with growth potential that, unlike the reformists, contested the current trends toward economic globalization.

Such anti-globalization expressions were found not only among groups such as the PGA but also in broader coalitions of groups under the US "Working Group on WTO/MAI," the Canadian Common Front on the WTO and the French "Coordination pour le contrôle citoyen de l'OMC" (CCCOMC) along with their linkages to Southern individuals and organizations. We also identified a TSMO linked to the movement in the International Forum on Globalization (IFG). While here too there may have been a diversity of groups and individuals from different advocacy themes, they all shared a

similar criticism of economic globalization and likewise espoused transformative objectives.

The question raised by those MAI opponents and the subsequent events such as the Seattle protests against the WTO was whether these actors could be understood as what critical theorists refer to as "counter-hegemonic" social forces or a Polanyian double movement.[2] Three related questions are raised in this section. One concerns a definitional identification of globalization opponents with these concepts: do their struggles against globalization mean they struggle against a perceived hegemonic order or that they respond to a fear of the free market? A second question concerns empirical and/or quantitative assessment of their significance as a counter-hegemonic social force: are they numerous enough or is their composition such that they can eventually fulfill a counter-hegemonic role as foreseen in theory? Do their objectives represent such a goal? Thus a third question concerns the claims made by these societal actors in terms of what they would like to achieve and whether these goals coincide with critical theorists' vision of a counter-hegemonic order. I address these three questions in turn in this section.

Radicals as Opponents of the Hegemonic Order: A Definitional Match

According to Cox (1996: 137), the Gramscian concept of hegemony at the international level "is expressed in universal norms, institutions and mechanisms which lay down general rules of behaviour for states." That view of hegemony includes in particular "the rules governing world monetary and trade relations" and international organizations, such as the OECD and the Bretton Woods institutions, that foster such rules (ibid.).

---

[2] For debates on how to understand the Seattle protests see *Millennium*, Vol. 29, No. 1, pp. 103-140.

Based upon this definition of hegemony, the MAI opponents who belonged to the social movement system of action perceived themselves as being involved in a counter-hegemonic project. Their critiques of, and continued opposition to, processes of increased economic liberalization—be it through an MAI negotiated within the OECD or the World Trade Organization—and their understanding of this process as one reflecting particular power structures (see Chapter 4), clearly situated those MAI opponents as challengers of what critical IR analysts define as the current hegemonic order. Furthermore, as seen in the previous chapters, their strategies of public education, generating media attention and building domestic and transborder networks in order to build such a social force revealed that such a project was self-consciously under way.[3]

Likewise, based upon the concerns they have expressed, the opponents of economic globalization may also be identified with Polanyi's second movement which Cox (1996: 514-519) included in his "historical dialectic" approach. The approach relies upon the idea that society "produces in its structure the antagonisms that lead to its modification" (Dahrendorf in Cox, 1996: 514). Polanyi's analysis of nineteenth century European economic and social history provided such a dialectical understanding. The second movement was "society's unplanned and unpredicted response of self-preservation" from the first movement which was "the introduction of the self-regulating market ... a utopian vision backed by the state." Here again we can find confirmation of

---

[3] However, based on interviews with anti-globalization activists in the fall of 1999, it is important to point out that no activist will argue that the objective of building such a social force is even near completion. One French activist commented that so long as the majority of the public would not come on board and so long as the major media were controlled by commercial interests they saw little chance of any significant change occurring.

such fears in MAI opponents' requests to re-assert the regulatory power of the state to implement protective policies. It may therefore be argued that, from the standpoint of the opponents of economic globalization, their reaction can be understood as part of a Polanyian second movement.

These definitional "matches" between economic globalization opponents' perceptions of what they understand the processes of economic globalization to be and what Gramscian IR theorists define as hegemony provide some conceptual identification of these societal actors as counter-hegemonic social forces. However, there still remains the question of whether these radicals empirically represent such a meaning for world politics.

Empirical Assessments of Radicals as a Counter-Hegemonic Social Force

A counter-hegemonic social force would be one with the potential to transform an existing hegemonic order. Thus for Gramsci, a counter-hegemonic force (at the domestic level) was "one which could compete with, and eventually supplant, the bourgeois hegemony which prevailed in his time" (Gill and Law, 1988: 64). Likewise, a contemporary version of such a counter-hegemonic force would be one that would espouse an alternative vision for and seek to supplant what critical IR theorists have identified as the current hegemonic world order. This order, as just explained, includes international economic institutions and the policies that emanate from them.

Therefore, one way to assess empirically whether the opponents of economic globalization represent such a social force would consist of assessing their potential strength relative to the criteria that would identify such a force in theory. The existence of

a counter-hegemonic social force could also be empirically assessed in terms of social actors' objectives, their own perception of their goals/roles, and the way in which these would fulfill a counter-hegemonic role such as that envisioned by the theory. I will discuss each of these indicators in turn as they relate to the opponents of economic globalization.

(A) An Empirical Assessment of Globalization Opponents' Potential

So far, much caution has been exercised, even on the part of sympathetic observers, to avoid over-celebrating the opposition to economic globalization. Pointing to eruptions of domestic protests around the world in the 1990s, Cox (1999: 13) maintained that although "these various instances are indicative of something moving in different societies across the globe toward a new vitality of 'bottom-up' movement in civil society....This movement is, however, still relatively weak and uncoordinated." Diversity rather than unity among those who protested against globalization has been highlighted.[4] Likewise Kiely (2000: 1066) recently concurred with the literature in that: "while protest against a global neoliberal agenda is welcome, there is a danger of uncritically celebrating resistance. There was a wide variety of organizations and interests at Seattle." His argument highlights the tensions among environmentalists, between the claims of labour and deep ecology, local action versus global action and direct action versus the more diplomatic way of dialogue.[5]

There are several reasons for such a cautious assessment on the part of critical IR

---

[4] For an overview of that literature and such arguments see Ray Kiely (2000) "Globalization: from domination to resistance" in *Third World Quarterly*, Vol. 21, No. 6, pp. 1059-1070.

[5] These observations do not mean that other less sympathetic observers are not equally sceptical regarding the potential of this actor.

analysts. One of the difficulties resides in the fact that critical IR theory offers few if any tools to empirically assess such social actors. Over a decade ago, Gill and Law (1988:375, 376) speculated that for a counter-hegemonic movement to be successful "it would require the support of *more* material and institutional power" (such as that found in religious institutions for example) and that counter-hegemonic groups would need to "create a *grand*, transnational coalition in order to synergise their potential" (italics added). These suggestions offer little in terms of testing empirically whether we are witnessing such quantifiably significant support, or whether those opposing globalization are likely to reach such a stage. Neither are criteria provided that would enable analysts to identify when such a coalition would be deemed to have occurred or what critical amount of material and institutional power is required for achieving counter-hegemonic potential.

Although critical IR theorists such as Cox (1996: 30-35) have suggested the possibility of a Polanyian double movement at the end of the twentieth century, and although opponents of globalization espouse arguments that match that theoretical concept, the framework provides few criteria in terms of the critical mass required for such an occurrence. As Cox (1996: 515) acknowledged in 1992 regarding the possible emergence of a double movement: "[t]he question remains open as to what form these may take, as to whether and how they may become more coherent and more powerful, so that historical thesis and antithesis may lead to a new synthesis." Thus the theoretical framework lacks guidance in terms of empirically assessing the significance of societal actors such as those opposing economic globalization.

(B) An Empirical Assessment of the Objectives and the Role of Transformatory Social Forces

Another way of assessing empirically whether the opposition to economic globalization can be identified as what critical IR theorists identify as a counter-hegemonic social force would be to show that the role espoused by these actors is akin to that assigned such actors by the theory. A related empirical question would be whether the substantive alternatives to the current processes of economic globalization that have been expressed by its opponents represent an elaborated vision of an alternative hegemonic order as is conceived by the theory. I will begin with the substantive alternative envisioned by opponents to economic globalization and conclude this section with the role envisioned by critical IR theory for such social actors.

Based upon the critical description of the latest hegemonic order and the stated objectives expressed by the opponents of economic globalization, radicals' aspirations reflect a desire to reassert a world order based upon an interventionist state which would enjoy more regulatory autonomy than that permitted under the international economic rules recently ratified.[6] Likewise, their opposition to the MAI targeted rules which appear in the NAFTA, rules that, had the MAI been ratified, would have been extended to a broader region and could eventually have been adopted world wide. In that sense, their struggle reflects a desire to safeguard a type of democratic interventionist state that,

---

[6] It is clear that the objective is to undo the more recent international economic policies reached under the Uruguay Round with the creation of the WTO as well as other more recent regional economic agreements such as the NAFTA. Thus Lori Wallach a prominent contributor in the campaigns against the MAI and the WTO explains that one of the main goals of opponents to economic globalization "is to prune back the WTO....It's not just taking the rules out, it's either depowering the WTO relative to other institutions, international ones, or empowering institutions such as the International Labour Organization (ILO)" (Naim, 2000: 37, 39).

according to the critical IR framework, characterized the hegemonic order which emerged at the end of World War II.

This is clearly reflected in a document produced by MAI opponents as a proposed alternative MAI.[7] The desired principles underlying the alternative treaty include the rights of states to:

> Maintain control over their fiscal and monetary policies as well as to enact laws, policies and programs designed to regulate the economy in the public interest. In particular, states have the right and responsibility to protect (a) strategic areas of their economies [eg. finance, energy, communications] by establishing public enterprises and (b) sensitive areas known as the 'commons' [eg. environment, culture, health care] through government-run public services (p.5).

Likewise, the desired components of such an agreement would include a provision for "Public Enterprises" which stress governmental responsibilities as follows:

> Governments also have a responsibility to use tax revenues for protecting the commons by making public investments such as: (i) exercising public ownership of key sectors of the economy that affect all citizens [eg. electricity, communications, transport etc.]; (ii) establishing social programs and public services to ensure delivery of adequate education, health care, and social services (p. 8).

Critical IR theorists consider the type of state described in these quotes as an obsolete component of the latest hegemonic order known as *pax americana*. That order, which emerged in 1945 and began its decline by the late 1960s, was characterized in advanced industrialized countries by what Cox (1996: 198) referred to as a "neoliberal

---

[7] The excerpts quoted in the text were taken from a document prepared by Tony Clarke (1998*a*) of the Polaris Institute in collaboration with other MAI opponents working on investment and related issues from different countries. Also acknowledged is the work undertaken for the Popular Summit of the Americas in Santiago (1998) by the Ecumenical Coalition for Economic Justice of Canada and the Red Mexicana de Accion frente al Libre Commercio from Mexico along with other individuals from IFG, the Third World Network, Law and Democracy USA, and the Research Foundation for Science, Technology and Natural Resource Policy in India. The document was found on the web site of the Council of Canadians (www.canadians.org).

form of the state" which legitimated capitalism. Cox refers to the Keynesian interventionist welfare state as "neo" liberal in that unlike the liberal state of the *pax britannica*—the hegemonic order that preceded *pax americana*—the neoliberal state aimed to moderate the effects of classical liberalism (ibid.). The purpose of that state was not counter-hegemonic. On the contrary, its purpose was to legitimate that order. As Cox (1996: 200) explained: "[t]he neoliberal state played a hegemonic role by making capital accumulation on a world scale appear to be compatible with a wide range of interests of subordinate groups." That hegemonic order and its domestic arrangements were challenged by a world crisis from late 1968 to 1975. As that hegemonic order began its decline with the economic crises of the 1970s the form of state that enabled its stability also eroded.[8] For some, the internationalization of the state not only meant the demise of the interventionist welfare state but its desired return was also characterized as "mired in [the left] Keynesian positions of the 1960s" (Cox, 1996: 191).

While the latest hegemonic order was in decline, Cox (1996: 34) refrained from confirming that a new hegemonic order had emerged. Nevertheless, the continued decay of that post-war order led him to hypothesize the possible emergence of a new one. Of two alternative new world orders contemplated in the late 1970s early 1980s, one would be founded on a hyper-liberal state, and could emerge as a result of the Thatcher-Reagan hyper liberal tendencies which were espoused beginning in the 1980s.[9]

---

[8] For a discussion of various understandings of this process see Panitch (1997: 83-113).

[9] Hyper liberalism is defined as an ideology which "[r]ejects state intervention to influence the results of market behavior and views the state only as the enforcer of market rules....The key words...are competitiveness, deregulation, privatization, and restructuring....Competitiveness is the justification for dismantling the welfare states built up in the post-World War II period—negating the effort in the more

Opponents of globalization can be identified as struggling against what Cox perceived to be such a process of hyper-liberalism which began in the 1980s. From a critical theory perspective, their stated objectives indicate that, rather than attempting to create a new hegemonic order, opponents to globalization are attempting to reverse or prevent policies that foster tendencies toward the creation of a hyper-liberal state and the possibility of its concomitant world order. At the very least then, their objectives can be understood as ones which attempt to prevent the emergence of a new hegemonic order built upon the hyper-liberal state—the possible emergence of which Cox (1987) suggested.

There are, however, indications that some radicals' objectives seek transformations that go beyond a simple return to the post World War II nation-state and that world order. For example, their critiques of the power structures and their preferred international arrangements would affect the interests of MNCs who are deemed to benefit from the processes of economic globalization. The first critique is evident in the sympathy expressed for the plight of Southern populations faced with insurmountable debts, and the related critiques of the IMF and the World Bank.[10] The opposition to MNCs represents both a critique of hegemonic power and an attempt to alter the benefits these

---

industrialized countries to legitimate capitalism by avoiding a recurrence of the immiseration that occurred during the Great Depression of the 1930s" (Cox, 1996: 31).

[10] An expression of this challenge was voiced by a protester against the IMF and the World Bank: "most of us believe that decisions should be made in local communities and not by economists and trade bureaucrats in Washington and Geneva" (Cienski, 2000). See also Barlow and Clarke (2001: 137) regarding the links between the Jubilee 2000 campaign which manifested itself in Seattle as a human chain "demanding action to lift the debt burden."

organizations are deemed to be gaining from the current order.[11] These targeted criticisms and their attendant solutions correspond to counter hegemonic objectives in that they seek to affect "the ideas, practices and agents of governance fora so that interests of the status-quo are compromised in deference to the interests of alternative understandings and practices of authority" (Beir and Crosby, 1998: 88, 89).

However, for critical IR theorists, whether such anti-globalization forces succeed in their objectives is what will render them counter-hegemonic. That is, to qualify as counter-hegemonic social forces the transformative role envisaged by critical IR theory requires that profound transformations of the hegemonic order take place, not just that attempts to achieve such changes are made. For critical IR theorists social forces will have fulfilled their transformative role if these "forces of transition *succeed* in altering the ideas, practices and agents of governance fora so that interests of the status-quo are compromised in deference to the interests of alternative understandings and practices of authority..." (Beir and Crosby, 1998: 88, 89). Cox's (1996: 105-108) attribution of one such hegemonic change — from the nineteenth century *pax britannica* to twentieth century *pax americana* — to the emergence of industrial workers in the nineteenth century provides an illustrative example of the role expected from counter-hegemonic social forces by critical IR theory.[12] It is one where social forces could "ultimately bring

---

[11] As one activist worded it: "I would take intellectual property rules and revert them to the World Intellectual Property Organization, for instance....there is a need ... to have rules on how to balance the need of people to have access to medicine with the interests of the pharmaceutical industry.....I wouldn't impose a worldwide 20-year monopoly on patents on every single country" (interview of Lori Wallach from Public Citizen by Moisés Naím in *Foreign Policy*, Number 148, Spring 2000, pp. 29-55)

[12] Cox (ibid.) directly attributes the change from one hegemonic order to the other to the emergence of industrialised workers in that the emergence of this new social force "had an impact on the

about a transformation of the structure" of the international hegemonic order (Cox, 1996: 107). This understanding of social forces is perhaps the one that most strongly justifies critical theorists' cautious assessment of the opponents to economic globalization.

That is, the understanding of the role played by social forces envisaged in the critical IR framework, and therefore their meaning for world politics, can only be assessed *ipso facto*. Furthermore, short of a complete transformation of the existing order, the role played by social forces and their meaning for world politics are rendered insignificant in the sense that the lack of complete systemic transformation will mean that social actors have been effectively co-opted.

Thus Cox (1999: 11) expressed scepticism when considering social movements as potentially constituting "a basis for an alternative world order," observing that states and corporate interests will co-opt "elements of popular movements" in order to make civil society "an agency for stabilizing the social and political *status quo*." The Gramscian concepts of "war of movement" and "war of position" are relied upon to refer to two strategies available to oppose hegemonic state-societies. The war of movement, as occurred in Russia at the beginning of the twentieth century, is one through which "[t]he vanguard party could set about founding a new state." The war of position describes a strategy by which civil society would slowly build up "the strength of the social foundations of a new state."

---

structure of state" domestically whereby "the liberal form of state was slowly replaced by the welfare-nationalist form of the state." Thus "[t]he incorporation of the industrial worker, the new social force called into existence by manufacturing capitalism, into the nation involved an extension in the range of state action in the form of economic intervention and social policy. This in turn brought the factor of domestic welfare (i.e., the social minimum required to maintain the allegiance of the workers) into the realm of foreign policy." This also altered the international configuration of states power.

Since Cox (1996: 139) ruled out a war of movement of global proportions as a likely occurrence at the end of the twentieth century, it would appear that the theoretical framework leaves only one way of conceiving of a true counter-hegemony—a war of position. However here, an empirical assessment of such social forces is limited by the idea of *trasformismo* as one of co-optation due to the "pressures and temptations to relapse into pursuit of incremental gains for subaltern groups within the framework of bourgeois hegemony" (Cox, 1996, 28-139).[13] For example, critical analysts see co-optation of the concept of sustainable development (Gill, 2000: 139) and the emancipatory notion of self-reliance in development, in that these ideas were transformed and applied in a manner that became "complementary to and supportive of hegemonic goals for the world economy" (Cox, 1996: 139).[14] Examples of institutions deemed responsible for such outcomes are the UN Conference on Environment and Development (UNCED) at Rio in 1992, and the World Bank. Thus, the alternative outcomes caused by social forces which are contemplated in the theory render social actors either participants in hegemony or not.

(C) On Structure and Agency

Critical IR theory constitutes a historicist approach concerned with cyclical

---

[13] It is interesting to point out that one of the reasons opponents to globalization are referred to as radicals is that they refuse to dialogue with officials and corporate leaders. Their reason for such behavior was explained as a fear of being co-opted, and that dialogue was a tool of legitimation used by officials.

[14] Thus the notion of self-reliance went from meaning "endogenously determined autonomous development" to "do-it-yourself welfare programs" aimed at preventing mass migration to the cities of populations that the world economy cannot integrate (Cox, 1996: 139). Gill (2000: 139) finds such co-optation in the definition of "sustainable development" in "public policy as compatible with market forces and freedom of enterprises."

historical changes in "persistent patterns of human activity and thought that endure for relatively long periods of time" (Cox, 1996: 514). These patterns concern economic and political practices and the relations of social groups (ibid., p. 55). They are referred to as historical structures. The research program of historicism is to "reveal the historical structures characteristic of particular eras" and, more importantly, to "explain the transformations from one structure to another" (Cox, 1996: 53). As such, the framework provides useful tools with which to understand the broad contours of systemic changes and the forces involved in such processes.

Many of the difficulties in empirically accounting for the opponents of globalization are due to this theoretical focus and the ontologically primitive position of the structure that results from it. Such an approach yields an epistemological position whereby structures generate or explain agents themselves (Wendt, 1987: 340). As such, the meaning of social forces for world politics is determined by the role they play in structural transformations. The outcome of the structure defines the agent.

As a result, collective action is considered as a "means to an end" and assessed in terms of "instrumental rationality" (Melucci, 1989: 74). There are two difficulties with this limitation. One is that it prevents a more in-depth understanding of such social actors; the other is that there is a tendency to discount their actions and their influence should they not obtain the anticipated end. As such, what Cox's framework does less well is to provide an understanding of the counter hegemonic role of social forces in processes of transformation. More specifically, how do such forces engender changes and how can we see this process taking place?

Also implicit is the understanding that ideas and culture are produced by the structure, not by agency. Under a hegemonic order, the agent is restricted or constrained by the structure to behave in a certain way. Thus Gill and Law (1988: 77) explain: "Gramscian analysis highlights the role of ideas and culture, in that they serve to shape preferences and constrain perceptions of what is possible....such constraints are so internalised that they appear both natural and inevitable." How do we explain self-conscious counter hegemonic agency such as the opposition to economic globalization if "[h]egemony frames thought and circumscribes action" (Cox, 1996: 518)?

In spite of Cox's intentions to the contrary, the framework suffers from what social movement analysts have observed to be the weakness of traditional Marxist theories. That is, it conceives of an actor without an action (Melucci, 1995: 107; Touraine, 1999: 8). This lacuna leaves many questions regarding the role and meaning of societal actors for world politics unexamined. For example, what role does agency play in changing the ideas and culture which are critical components of the Gramscian concept of hegemony? How do counter hegemonic ideas and culture evolve and how do they spread to other collectivities and entities that sustain hegemony? That is, how do social forces engage in and build a war of position?

These analytical lacuna raise several difficulties for the analysis of collective action such as the opposition to economic globalization. The framework offers no tools to understand this societal actor in terms of its actions, potential for influence or interactions with its political and social environments. Until we can assess their role as having been counter hegemonic after-the-fact, what is the meaning of these societal actors for world

politics? And until such time how do we explain their transnational interactions, objectives and evolution?

II. Explaining Counter hegemony with Social Constructivist Frameworks

In order to address these lacuna, I propose a complementary framework which, I believe, fills the analytical vacuum left by the structural and materialist approach of critical IR theory. Social movement analysis in combination with the IR constructivist framework provide a framework that explains how social actors, and the ideas and norms they espouse can have influence at the societal and systemic levels. In that sense, these approaches can be seen as tools that enable the analyst to go inside a war of position and explain the diverse influences of counter-hegemonic social forces. Even if at the end of the research a complete transformation of the hegemonic order cannot be anticipated, such an analysis provides an understanding of the ways in which counter hegemonic ideas penetrate various levels of activity that are considered in the critical IR framework.

Social movement analysis provides an understanding of the influence and development of new ideas and culture at the societal level while the IR constructivist framework provides the tools with which to understand how such ideas may influence states and international institutions. Both approaches belong to what has broadly been identified as social constructivism. As the following description indicates, constructivism aims to provide an understanding of agency that is missing in the structural approach of critical IR theory. As Risse (2000: 55) explained:

> Constructivists claim...that agents do not exist independently from their social environment and its collectively shared systems of meanings ('culture' in a broad sense). At the same time, social constructivists maintain that human agency

> creates, reproduces, and changes culture by way of daily practice. In sum, social constructivism occupies a—sometimes uneasy—ontological middle ground between individualism and structuralism by claiming that there are properties of structures and of agents that cannot be reduced to or collapsed into each other.

Accordingly, to expect from a framework such as Cox's to provide both types of understandings may be too ambitious. For that reason, I suggest that the following choices of analytical tools enable the researcher to investigate empirically the processes through which counter hegemonic influences manifest themselves and penetrate sites of hegemonic power.

Social Movements as Social Forces of Transformation

The study of social movements emphasizes the analysis of processes by which societal actors construct reality for themselves and society at large. Like the constructivists in IR, social movement analysts in comparative politics rely upon sociological traditions that focus on the way in which identities and interests are shaped by actors through the social construction of reality (Keck and Sikkink, 1998: 4). As McAdam, Tarrow and Tilly (1997: 149) have expressed it: "[f]or a growing school of constructionists, social movements were *both* carriers of meanings and makers of meanings, that, by *naming* grievances and expressing new identities, [they] constructed new realities and made these identities collective."

As such, these analysts have rejected case studies that focus solely on these actors' impact on states or policies, arguing that the objectives and influences of such societal actors are much broader than such state- or policy-focused analyses suggest (Thiele, 1993; Rochon, 1988; Melucci, 1989; Wapner, 1996). Thus for example, Rochon (1988: 205)

argued that "[t]o look solely at its impact on policy is to reduce the peace movement to a lobbying organization." For Wapner (1996: 13), "NGOs are significant in world affairs not only because they influence states but also because they affect the behaviour of larger collectivities throughout the world." Thus an integral part of movement analysis concerns the role of such phenomena as agents of social change.

The emergence of social movements in the 1960s initiated a debate concerning the differences between these movements and the more familiar and "older" labour movements.[15] Among others, the observation was made that contemporary movements represent a departure from past movements in that the actors in the so-called "new" social movements challenge and overturn "the dominant codes upon which social relationships are founded" (Melucci, 1989: 75). For Melucci (ibid.), these cultural innovations affect "everyday life activities and the market" through modifications in areas such as language, sexual customs, affective relationships, dress and eating habits.[16] As such, these actors help to challenge existing social orders by challenging "dominant cultural codes" and rendering "visible the power that hides behind the rationality of administrative or organizational procedures" (Melucci, 1989: 75, 76).

We have already seen in the previous chapters how the MAI opponents that

---

[15] See Plotke, 1990; Epstein, 1990; Slater, 1994; Carrol and Ratner, 1994; Kearney, 1996; Steinmetz, 1994 and Melucci (1995) for examples of the debate.

[16] Thus to name a few examples, over the past three decades the women's movements have altered our understanding of the relationships between men and women, gay and lesbian movements have introduced the notion of diverse sexual identities, the environmental movement has raised awareness regarding the relationship of people to nature, their health and what they eat. We should, however, remain aware that many difficulties present themselves when attempting to attribute particular influences to social movements. For discussions and suggestions regarding these difficulties see della Porta and Diani (1999: 226-254); Lofland (1996: 345-354); Tilly (1999: 253-270).

belonged to the social movement system of action sought to render visible the power structures that they perceive to be inherent in international economic relations. In addition, the various networks that are part of the opposition to economic globalization also exhibit a variety of challenges to existing cultural codes. As reflected in a book titled *No Logo: Taking Aim at the Brand Bullies* (Klein, 2000), younger networks of the movement against economic globalization express resistance to what they perceive to be the homogenization of culture fostered by MNCs and their hijacking of identity politics (Johnson, 2001: 28). Much of this co-optation is perceived to be taking place through invasive advertising and several groups have accordingly given a response in kind. Thus Klein describes groups that undertake activities such as "cultural jamming" and "reclaim the streets" as cultural forms of protest against the invasion of public spaces by private interests. Cultural jammers fill advertising spaces with advertising parodies while street reclaimers attempt "to fill [space] with an alternative vision of what society might look like in the absence of commercial control" (Klein, 2000: 313). These types of activities are directed at what has been called a global commercial culture.

Likewise, the objections expressed against genetically modified organisms and "frankenfoods" (see Chapter 4) reflect not only concerns for the environment and agricultural communities, but also health and dietary practices. They also target large biotech companies and expose future risks caused by a lack of intellectual and regulatory oversight. Thus the head of Public Citizen, Ralph Nader, warned that

> Bio-engineered products are being sold under the process that we call autocratic corporate science. It's not open science like academic science. It's not peer-reviewed by scientists that don't have a vested interest in the outcome, the way

> (academic) science does....You've gotta know what you're doing. If you're doing it just to maximize next quarter's sales and profits, you're not as likely to be as careful—especially when your information is secret and subject to trade secret requirements (McGregor, 2001: 7).

These concerns translate into consumer activism such as that promoted by the Sierra Club of Canada, the Canadian Health Food Association and the Canadian Organic Growers.[17]

Thus we find among members of the antiglobalization movement networks new and old expressions of counter-hegemony. As such, the opposition to economic globalization represents radicalized networks of the new social movements that emerged in the 1960s as well as novel counter hegemonic cultural manifestations. The younger cultural networks just mentioned are joined by environmentalists, social justice groups, feminists, labour activists and consumer groups that have evolved over the past thirty years. In addition, a bridge has been built between North and South as evidenced through the various movement networks documented in Chapter 4. This represents a growth not only in numbers but in geographical and generational breadth. As such, the cross-border and cross-interests represent a strength rather than a weakness, and the diversity which troubles critical IR theorists should, on the contrary, encourage these sympathetic observers. While there may have been aspects of these movements that were co-opted over the past thirty years, the evidence indicates that co-optation has not been complete and that actors from the social movement system of action have re-ignited these counter

---

[17] A pamphlet produced by these three organizations encourages individuals to use their consumer buying power to undermine the production and sale of such products by encouraging readers to consume instead organic products. During a recent visit to Canada , Ralph Nader suggested requesting mandatory labeling so that consumers could choose (McGregor, 2001: 7).

hegemonic tendencies.[18]

As social movement analyst Alberto Melucci (1995: 112) observed:

> Contemporary movements are multi-dimensional realities that affect different levels of the social system, pursue diverse goals, and belong to different phases of development of a system or even to different historical systems....The analysis of a social movement should explain how these diverse elements are combined in a unified empirical actor.

We have throughout the analysis of the anti-MAI campaigns explained how and why this opposition brought together diverse groups and advocacies across borders into one empirical actor. As such, a more optimistic hypothesis regarding the significance of this social phenomenon would consist of explaining it as part of an ongoing war of position the beginning of which coincided with the decline of the hegemonic order known as *pax americana*.

In addition to these cultural influences of large collectivities, Paul Thiele (1993: 282) has observed that "[t]he importance of social movements is often most clearly observable in their creation of a background of social and political understandings and orientations that are participated in (for various reasons) by state officials, business leaders, and the general public. The political significance of this social osmosis should not be ignored."

In terms of political culture, the politicization of international economic negotiations as they relate to a renewed awareness of citizenship cannot be ignored. The awareness campaigns conducted during the anti-MAI campaigns and subsequently on the

---

[18] This renewed movement activity which brings together (old) new social movements and (new) new social movements deserves further comparative study and understanding of these developments.

occasion of other international meetings have contributed to a broader public debate on the implication of such agreements for democracy. Citizens' concerns over the implications that such agreements have on domestic policies and their claims for transparency have by now been amply documented in North America with the NAFTA and the negotiation for the Free Trade Area of the Americas (FTAA) as the most recent evidence.

In terms of radicals' concern regarding the unequal distributional effect of economic globalization (see Chapter 4), Thiele's process of osmosis quoted above appears to have been engendered. An example of such osmosis was the theme "how to sustain globalization" of the Davos annual World Economic Forum of January 2001, which brought together roughly 2,000 of the world's top business and political leaders (Drohan, 2001). The topic of the forum reflected the concern that in order to make globalization sustainable it had to work for every one (ibid.). Thus the new Mexican President, Vincente Fox, addressed the World Economic Forum by calling for an end to a "world in which 1.2 billion people live on less than a $1 a day, and where the gap between rich and poor continues to grow" (Carnegy and Barber, 2001: D3). In the same vein, billionaire financier George Soros, a regular forum attendant, argued that: "[m]arket fundamentalism seeks to abolish collective decision-making and to impose the supremacy of market values over all political and social values" (Francis, 2000: D3). Similarly, statements taken from the media quote the new director of the International Monetary Fund, Horst Kohler as saying that his organization is "willing to change" to meet some of the protesters expectations (Wallace, 2000: B4). Evidently, these comments may be understood as

necessary political appeasement tactics. They say little about the ways in which the critiques of opponents to globalization might translate into more profound transformations at the ideational level of world politics.

Nevertheless, a debate that reflects a contest over the future(s) we may face as a result of economic globalization is now taking place in several fora as well as the media. Thus a dialogue has taken place between the "Davos Men" and their opponents the "Porto Allegre Persons."[19] Indeed, on the occasion of their respective meetings, "Davos Man recognized Porto Alegre Person immediately, and proposed a debate through a TV link. On a Sunday night...the two sides entered the lists, and clashed" (Lloyd, 2001: A13). Not only is a direct dialogue taking place but the number of debates reproduced in diverse media that address issues of concern to the opponents of globalization have multiplied considerably since the MAI. In that manner, the arguments of this new societal actor in world politics have reached a broader segment of societies.

The extensive analyses of social movements which have been undertaken since their emergence in the 1960s provide an array of tools and observations that enable me to conclude that the numerous movement networks opposing globalization will in all likelihood be sustained and that they will continue to grow. In this section I have also relied on that literature to indicate that these actors will likely sensitize larger collectivities

---

[19] The expression "Davos Man" was coined by the American political scientist Samuel Huntington (Ash, 2001: A13). The term "Porto Alegre Person" appeared in a column written by John Lloyd (2001: A13) a few weeks later and, since not attributed to anyone, seems to have been his own. The term refers to the first World Social Forum in Porto Alegre, Brazil which was organized and attended by participants of the transnational anti-globalization movement networks in response to and coinciding with the latest Davos meeting of January 2001.

about the cultural, social, political and economic issues they find to be associated with economic globalization. This is not a negligible aspect of movements' influence since decision makers and officials who engage in interstate relations are not only part of these larger collectivities but they are also politically sensitive to shifts in public opinion. However, to understand how the ideas espoused by societal actors may influence world politics we must turn to IR social constructivist frameworks.

Contested Future(s): Causal Beliefs, Principled Beliefs and Norm Paths

As explained in the introductory chapter, the preoccupation of IR social constructivists with the normative sources of states' behaviour is rooted in their understanding that states can form a society and that their behaviour can be influenced by processes of socialization. That is, there exists the presupposition of a "community able to pass judgements on appropriateness" (Risse et. al., 1999: 7). Through processes of socialization, "principled ideas ('beliefs about right and wrong held by individuals') become norms ('collective expectations about proper behaviour for a given identity')"(Jepperson, Wendt and Katzenstein 1996: 54, in Risse et al., 1999: 11). The behaviour of states can thereby be understood as a result of "collective intentionality," which means that individual actors behave the way they do because of "intersubjective beliefs" (Ruggie, 1998*a*: 20).

While some analysts focus on the role of non-state actors in ensuring that existing international norms are respected domestically (Risse et al.,1999), others seek to understand the role of non-state actors in transforming such norms (Finnemore, 1996; Price, 1998; Drake and Nicolaïdis: 1992). The main focus of research then is on the

generation of ideas and processes of socialization through which norms that influence what states want or how they behave come to be shared. Several assumptions underlie these approaches. They are: (i) that "state interests are defined in the context of internationally held norms and understandings about what is good and appropriate," (ii) that "that normative context influences the behaviour of decision makers and of mass publics who may choose and constrain those decision makers," and that (iii) "the normative context also changes over time, and as internationally held norms and values change, they create coordinated shifts in state interests and behaviour across the system" (Finnemore, 1996: 2). As such, analyses have confirmed that norms compliance has, at times, been fostered by societal actors and that at other times norms have been transformed by societal actors.

Therefore, these approaches bridge the analytical gaps that leave out ways in which ideational influences of social forces can affect states' behaviour and developments in world politics. As such, IR social constructivism may provide an understanding of existing norms that may foster globalization opponents' objectives, should some of their ideas coincide with existing norms or, alternatively, indicate ways in which they could alter existing norms through principled or causal beliefs. Although no such analyses have been attempted as these concepts may apply to counter-hegemonic social forces or ideas, the conceptual framework offered by this approach and the existing empirical evidence of societal actors' influence provide useful means to understand how and why such ideas may influence international outcomes. Comparative analyses of existing cases with opponents of economic globalization would seek to reveal which types of norms are more likely to

sway the current tendencies toward a hyper-liberal world order in the direction of one that espouses its opponents' norms.

(A) The Power of Causal and Principled Beliefs

Gill and Law (1988: 64) made the interesting observation that Gramsci "went as far as to suggest that certain types of ideas can become akin to material forces, in that they can incorporate themselves into the way reality is perceived and understood by the mass of society and/or its leaders." IR constructivists suggest that principled and causal beliefs can be that powerful and play such roles. While Gill and Law refer to the power that hegemonic ideas play in maintaining hegemony, I suggest that we need to explore whether the process can be reversed. One way the opponents of economic globalization are attempting such a feat is through their challenge of the principled and causal beliefs invoked in support of the design of international economic agreements currently underway.

The IR constructivist framework enables us to better understand the challenges that opponents to economic globalization are undertaking at the ideational level. The following focuses in particular on three related concepts that concern the ideational source of international policy making. These concepts provide an improved understanding of the challenges that opponents to economic globalization have engaged in as they question the principled and causal beliefs and the resulting norms upon which international economic policies are founded. That is, by challenging these beliefs, opponents to economic globalization challenge the morality and credibility of the ways in which reality is understood and upon which the future of the global economy is being constructed.

These conceptual tools suggest that the targeting of domestic and international economic institutions by the opponents of economic globalization can be understood as an ideational contest over world views. As such, the "communicative action" (Risse, 2000) between the opponents of economic globalization, epistemic communities, the international bureaucracies and elected officials merit further enquiry. The following aims only to illustrate how the contest over future(s) takes place at the ideational level and suggest some avenues through which opponents could influence the outcome of international economic relations.

Drake and Nicolaïdis (1992) traced the influence of societal actors on states' understanding of their economic interests that resulted in a systemic shift in behaviour. In that case, it was an epistemic community consisting of "a group of experts with shared causal and principled beliefs, shared validity tests, and a common policy project (ibid., p. 38)" that succeeded in revolutionizing the way governments thought about services.[20] Up until the launching of the Uruguay Round of trade negotiations in 1986, the idea that services could be conceived of as tradeable goods was not only foreign but actively resisted. The reason for this, as the authors explain, was that not only had services never been conceived of as such but that they had been heavily regulated domestically for centuries.

The change in the meaning of services took place through a new understanding of these activities that illustrates what IR constructivists refer to as the social construction of

---

[20] Services make up a broad range of activities such as "transportation, shipping, banking and finance, management consulting, advertising, education, telecommunications, construction, entertainment, massages and hair cuts" (Drake and Nicolaïdis, 1992: 43).

reality. First, the redefinition of services as tradeable goods changed states' collective understanding of such domestic activities. Once this transformation had taken place it was possible to apply the language and norms of trade relations to services and their attendant domestic regulation. As the authors pointed out, "[t]he very act of defining services transactions as 'trade' established normative presumptions that 'free' trade was the yardstick for good policy against which domestic services regulations, redefined as non tariff barriers (NTBs), should be measured and justified only exceptionally" (Drake and Nicolaïdis, 1992: 40).

There are interesting parallels and contrasts between the above case study and the MAI opposition. The first parallel is that both concern the institutional settings of international economic relations and the global economy. Second, as was ascertained in Chapter 5, a similar epistemic community with similar causal and principled beliefs convinced decision makers of the desirability of liberalizing their investment policies. The contrasts concern the new societal actors involved in the MAI opposition and the nature of the ideas they advanced.

By definition, decision makers turn to epistemic communities in times of uncertainty when faced with changes (Haas, 1992). Thus the epistemic communities who conceived of services as tradeable goods were gathered as early as 1972 to provide analyses and solutions to what were generally perceived to be significant transformations in the structure of the world economy. Furthermore, the principled and causal beliefs and the concomitant norms regarding services that the epistemic community proposed were congruent with those of the trade regime. They resulted in the General Agreement on

Trade in Services (GATS) by which states adopted new norms in terms of services. These norms were, nevertheless, similar to those already applied for trade in goods. Unlike the epistemic communities promoting liberalized 'trade in services' or investments, MAI opponents were not invited to produce experts' reports. More importantly, the principled and causal beliefs they espoused diverge from those that justify such norms, and the new norms that flow from such beliefs conflict with those of the trade regime.

The principled and causal beliefs that inform the world view that increased liberalization of all domestic markets is good is that it will, in the long run, be better for all of humanity. The principled beliefs which inform the opponents of economic globalization concern the appropriateness of the post World War II collective intentionality regarding the regulatory role of the state. This is reflected in their concerns regarding the increased encroachment of such "trade" on domestic policies and democracy. The other ideational contest takes place at the level of causal beliefs. As seen in Chapter 4, the opponents to economic globalization argue that not all will benefit from this type of continuous liberalization. Not only, they argue, does globalization skew wealth distribution but large segments of population are excluded from this economy. They also question whether some of the rules included in these globalization instruments are necessary.

From a social constructivist perspective, the arguments and ensuing public policy debates that have begun to emerge contribute to what Risse (2000: 6, 7) identified as "the logic of truth seeking." According to that perspective, when actors engage in such activities they either attempt to demonstrate that they are correct or they attempt to justify the norms that guide their behaviour. Risse and Sikkink's (1999: 13) framework

conceives of four types of "socialization processes through which such communication can have an impact. Among these we find moral discourse which "challenge and seek justifications of norms." While principled beliefs exercise influence through "shaming and denunciations" and "changing minds by embarrassing" (Risse and Sikkink, 1999: 14), causal beliefs are powerful in several other ways.

The power of causal beliefs is directly linked to the power of epistemic communities. Such communities are powerful at the domestic and transnational levels because "decision makers solicit their information and delegate responsibility to them" Haas (1992: 4). Furthermore, to the extent that these consolidate bureaucratic power at these levels, they stand to institutionalize their influence and insinuate their views in broader international politics. These processes, I argue, are currently at play and they open avenues for social influence on norms. I refer to such avenues as norm paths.

(B) Norm Paths as Windows of Opportunity for Change

Risse-Kappen (1995: 31) observed that regimes affect the policy impact of non-state actors whereby "[r]egime norms tend to strengthen those domestic coalitions advocating compliance." The correlation between regimes and effectiveness of societal actors' success was further confirmed by Risse and his collaborators in a subsequent series of case studies on human rights campaigns. One of the conclusions reached in assessing the conditions under which human rights norms were most likely to lead to the domestic policy changes called for by advocacy networks was the "increasing strength and robustness of both the international human rights regime and the transnational advocacy networks" (Risse et al., 1999: 21) If, as these cases suggest, non-state actors' objectives

are better attained when they coincide with prevailing norms, it would appear unlikely that the anti-MAI forces who oppose current processes of economic globalization are likely to have any significant normative impact.

However, non-state actors' effectiveness at influencing norm changes at systemic levels have been documented. They provide some opening for conceiving of the potential influence that the opponents of globalization could have. At times, the norms these societal actors advocated were quite the opposite of those of the established regime. Thus Price (1998) has documented how states were taught (socialized) by societal actors to accept and adopt "more appropriate" norms in their security policies—removing land mines from their military arsenals. In this case, then, states were "taught" what was appropriate and good behaviour not by epistemic communities who espoused ideas congruent with the regime but by societal actors who espoused ideas challenging existing norms of the security regime.[21]

One of the conditions Price (1998: 639) identified for the success of the anti-personal (AP) land mines campaign resided in how the issue was defined. Rather than defining the issue as a war issue, where states would be reticent to change, the campaigns defined the issue as a "humanitarian or health crisis for which norms have developed that legitimize rapid multilateral action." Thus Price (1998: 628) explains that the norms invoked related to the international humanitarian law of civilian discrimination and

---

[21] Note however, that the changes sought out by these advocacy networks were modest by comparison to those who critique economic globalization in that they aimed solely at preventing the use of AP landmine and removing mines left after conflicts were over. In that sense, their objectives did not specifically reflect counter-hegemonic challenges to the existing world order.

unnecessary suffering. As the author explains "discrimination (or noncombatant immunity) is one of the oldest notions of the just war doctrine" and unnecessary suffering "refers to the principle that means of warfare that cause superfluous injury are prohibited."

Such a condition could be redefined as a "*norm path*." Thus, I define norm paths as the inconsistencies that exist among internationally shared principled and causal beliefs and the norms that flow from them. Such inconsistencies provide opportunities for social forces that seek to influence world politics to challenge existing norms. For example, Jones (1992: 54) observed that there exists a tension "between the principle of nonintervention and the principle of respect for human rights and fundamental freedoms." These tensions provide windows of opportunity in terms of justifying interfering in a state's domestic affairs, as has happened in the case of human rights violations. The redefinition of issues can create such an effect provided the redefinition places the issue in a category of activities for which different norms apply. In the cases of AP Landmines and trade in services the redefinition of these issues enabled the application of norms that did not previously apply to them. As a result the newly defined issues could be made to comply with norms that were based upon different principled and causal beliefs. Norm paths differ from Risse and Sikkink's (1999) understanding of regimes as facilitating influence in that the norms invoked may not necessarily be those of that particular regime.

We can find such tensions between the *principled beliefs* and norms that inform trade proponents and globalization opponents. IR constructivists have explained that the post-World War II economic order was built upon the principled beliefs that governments had the responsibility to protect their population from the ills of international economic

adjustments.[22] The increasing impact of trade norms on domestic policies challenge that prior collective intentionality. Opponents of economic globalization have pointed out that economic agreements that foster economic globalization undermine governments' regulatory autonomy. This autonomy, they claim, is necessary to protect societies from negative effects such as ecological damage, unemployment and deteriorating work conditions, growing socio-economic inequalities and the deterioration of public goods such as health and education.[23]

If IR constructivists are correct in their understanding of the post-World War II collective intentionality regarding the domestic regulatory role of states, the critics of economic globalization may successfully remind states that the international agreements they are now signing are undermining the norms informed by those collective intentions. The debate changes from one which questions the goodness of trade to one which questions the relative appropriateness of the principled beliefs and causal beliefs that informed states' understanding of their domestic responsibilities and the trade policies that undermine them. As such, the argument for the re-assertion of the regulatory state as expressed by the opponents of economic globalization may be an effective norm path.

---

[22] We referred earlier to Ruggie's explanation of "embedded liberalism." Ikenberry (1992: 296, 303) confirms this understanding of the post World War II rationales: "After World War I, the main purpose of postwar economic policy was to 'reconstitute as rapidly as possible the automatic forces in economic life. The drive all around was a return, in the broad essentials, to laissez-faire.' By the late-1930s...all of this had changed. A new social purpose infused postwar planning the second time around....The overriding view...was that social welfare and economic management must dictate postwar international economic plans, rather than the other way around."

[23] This view is exemplified in the chapters of a book by Canadian opponents of the MAI: "The Assault on Economic Rights, The Threat to Environmental Rights, The Demise of Social Rights, The War on Cultural Rights" (Clarke and Barlow, 1997).

Indeed, these MAI opponents' success in highlighting the infringement of the new norms inherent in the MAI, such as the investor-state dispute mechanism, on states' regulatory autonomy was one of their most effective direct influences.[24] By comparison, activists' insistence on applying "the precautionary principle" for products such as genetically modified organisms has been less successful.[25] The latter norm change directly challenges those that seek to eliminate protectionism and has been strongly resisted. A more useful path consists of redefining the issue as one of customers' right to know what they are consuming through compulsory labelling.

Another norm path would relate to the challenge of the *causal beliefs* expressed by opponents to economic globalization. As seen throughout the foregoing analyses, radicals challenge the causal beliefs which are embedded in the domestic and international bureaucracies that are responsible for the design, negotiation and implementation of international economic treaties. While social movement analyses have demonstrated that "the logic of numbers" sought through protests is a source of movements' influence on policy makers they also point to the power of allies at other levels of the policy making process. Thus in terms of their challenge to the causal beliefs that inform the international economic agreements the opponents to globalization may find avenues of influence

---

[24] The reader may recall that MAI opponents drew the attention of negotiators to the dispute settlement process whereby investors would be allowed to sue governments. This resulted in reconsidering several provisions already agreed to in the draft treaty so that the "regulatory autonomy" of different levels of governments would not be considered as "regulatory takings."

[25] For example, the Rio Principles and Agenda 21 "commit countries to managing their economies in a way that prevents environmental risks — operationalising the 'precautionary principle.' This may involve placing restrictions on new and novel processes (e.g. biotechnology and new chemicals) which an investor wishes to use inside a country" (WWF, 1997). A country could thereby restrict the importation of such products unless the importer demonstrates that the product to be imported is safe.

through what social movement analysts have called "influential allies" (Klandermans and Tarrow, 1988). Experts whose understandings influence epistemic communities should not be discounted as such influential allies. The degree to which experts such as economists and trade lawyers, for example, agree with the arguments presented by opponents to economic globalization will foster their challenges.

To the extent that epistemic communities will agree with some of the critiques of the causal beliefs relied upon to justify international economic agreements, the opponents to globalization may enhance their influence. It is therefore noteworthy to point out that the renowned trade economist Jagdish Bhagwati criticized the inclusion of intellectual property rights in the WTO and questioned the validity of the MAI.[26] Similarly, the critiques of the Washington consensus expressed by an economist from the World Bank lend support to some of the concerns formulated by the opponents of economic globalization.[27] Thus Augusto de la Torre, a World Bank economist and co-chair of a research group established by the Carnegie Endowment for International Peace, was quoted as saying that such prescriptions failed to address "the root causes of poverty in [Latin America]—lack of education [and] absence of workers rights" among others (McCarthy, 2001: B8).

Space prevents further elaboration of "norm paths" as conditions facilitating non-state actors' influence on international outcomes. These observations suggest, however,

---

[26] Based on a public presentation made at Carleton University during the fall of 2000.

[27] The policies prescribed by the Washington consensus relate to the type economic liberalization fostered by the treaties under scrutiny in that they include privatizing the state-owned sector, reducing tariffs, and liberalizing trade and investment rules.

that among existing international norms and principles shared by an international society of states, some are held in greater esteem than others and tensions exist between them at various times. The ongoing debates on causal beliefs that relate to international economic relations should also be understood as indicators of possible shifts in policy direction. Further research is required on these conditions of influence in order to understand "norm paths" as conditions of success.

Conclusion

Critical IR theorists and IR constructivists disagree on the motivations that lie behind the adoption of the interventionist welfare state in the post World War II industrialized countries. However, they agree that such an outcome was rendered necessary as a response to the effects of unfettered *laissez-faire* policies on domestic societies. As such, each of these frameworks can contribute to a more comprehensive understanding of the contested future(s) we are witnessing at the dawn of the twenty-first century. Cox's (1987) framework enables him to foresee and interpret broad transformations in the post-World War II order. IR constructivism provides tools with which to understand the role of agency in these transformations.

The strength of critical IR theory lies in its historicist approach and its structural framework. That framework has enabled Cox (1987) to hypothesize that a transformation of the world order based upon the interventionist welfare state—what Ruggie (1982) referred to as "embedded liberalism"— was coming to an end. Cox hypothesized that, as the twentieth century was ending, a struggle between two types of capitalisms would be taking place. One of these capitalisms would be founded upon the hyper-liberal state.

The other, which he called "state capitalism" included corporatism and social democracy (Cox, 1996: 31). The outcome of this rivalry and the pressures of globalization could "lead towards a more democratically participant kind of economic management and planning inspired by the egalitarian idea innate in socialism" (Cox, 1996: 206). Such an outcome would depend upon civil society and its role in "the emergence of an alternative political culture that would give greater scope to collective action and place greater value on collective goods." The latter would only come about through a long war of position.

As seen throughout the foregoing, the opponents of economic globalization espouse aspirations such as those described by Cox and there is no doubt that their claims are made against the building of a world order based on a hyper-liberal state. In that sense, Cox's framework is insightful. Nevertheless, Cox's framework prevents a more in-depth understanding of the various levels at which these claims and aspirations take place or how they may translate into transformations at these levels. In order to provide such explanations, I suggested relying upon two other constructivist frameworks.

The strength of these social constructivist frameworks lies in their understanding of agency and collective intentionality. As such, they conceive of transformations as being the result of cognitive frames and intersubjective meanings. These are analyzed in order to understand interactions at the transnational level and the conditions that foster societal influence on the behaviour of states and larger collectivities. I have suggested that the conceptual frameworks provided by these approaches would enable analysts to understand the evolution of a war of position. I offered two such approaches: a social movement approach that explains the influence of economic globalization opponents at the societal

level, and an IR constructivist approach that explains social forces' ideational challenges at the institutional level.

Social movement frameworks have enabled us to see that the anti-MAI campaign spurred nascent transnational movement networks against globalization. Actors from the social movement system of action who opposed the MAI and expressed that world view subsequently sustained and expanded their struggle against all processes that fostered such outcomes in international economic relations. As seen in the foregoing chapters, movement networks spanned borders, advocacies and generations. They linked North and South in the issues they raised, and various previously divergent advocacies such as labour and the environment. They also generated new cultural codes.

As these words are being written, it is fair to say that this sustained growth and opposition has not yet abated. Not only do the repeated occurrences of protest indicate a virtual and tangible global vigilance, but the impact of economic globalization opponents' arguments on public discourse has been clearly established. Previous studies of earlier and similar movements have demonstrated the effect of such phenomena on broader collectivities. The cultural expressions and concomitant values of these movement networks challenge a social construction of the future where commercial rights would supercede other values such as a broader definition of collective goods and a more inclusive implementation of democracy. As such, globalization opponents' influence at the societal level may succeed in affecting outcomes in ways hypothesized by Cox.

IR constructivists focus on the influence of societal actors on international outcomes. They draw attention to the ways in which societal actors' influence on states'

behaviour takes place through ideas. The mobilization against the MAI, and its subsequent evolution against the WTO and other economic fora that espouse neoliberal policies is a reflection of an ongoing struggle over contested conceptions of the future. These contests take place at the ideational level in terms of what IR constructivists refer to as causal beliefs and principled beliefs. As such, the constructivist conceptual framework provides the tools with which to understand this struggle as one that may come to affect norms in the domain of international economic relations.

The debates generated by the social movement networks against economic globalization through their dramatic protests are different from attempts at direct policy influence. They seek more profound transformations both at the transnational and various domestic societal levels. As such, the social movement networks that oppose (corporate) economic globalization are not liberal pluralist groups whose ideas are vulnerable to co-optation. Neither should they be understood as representing the long awaited social forces of socialist transformation. Rather, they should be understood as societal actors involved in a construction of reality that espouse ideas, values and cultural expressions that seek to prevent the creation of a world order based upon a hyper-liberal state. To the extent that the ongoing process of economic globalization is understood as one that reflects particular power structures and ideas that foster a hegemonic order based upon the power of MNCs and some states, the social movement networks that oppose that process are counter-hegemonic. While it is difficult to predict what type of state or world order will result from the ongoing contest over the future(s), the various challenges that the opponents to economic globalization present to the current treaty-making processes

should not be underestimated.

Analyses of movements that have emerged in the 1960s have revealed that, over time, movements reflect radical and moderate elements. This outcome has been referred to as the "radical flank effect[s]" in order to illustrate the consequences of this duality (McAdam, McCarthy and Zald, 1996: 14). While extremist groups may strengthen the bargaining hand of moderate NGOs, they also can sway the moderates to adopt more radical positions themselves. The latter dynamic was clearly illustrated in the case of the anti-MAI campaign when reformist NGOs joined the more radical antiglobalization opponents of the MAI. In any event, these authors point out that most often the duality results in "policy changes once deemed far too radical by both moderates and the state alike." As we saw in the case of the MAI, negotiations were abandoned while officials acknowledged that such negotiations would never again take place as "business as usual." In hindsight, this prediction was insightful. The MAI negotiations did represent a threshold event in international economic relations.

If the MAI experience led to insightful predictions, officials' responses to the growing opposition expressed on the occasion of similar campaigns have as yet been less so. The strongest incentive for continued militancy against economic globalization resides in deeply entrenched and polarized world views. The world view espoused by the opponents to economic globalization contests an equally strongly held vision of the future where all will benefit from the ongoing trend in international economic treaty-making. In that sense, the developments that we have witnessed in the media on the occasion of various protests against international economic fora indicate that we are facing an impasse.

Little has been undertaken to accommodate reformists' claims while radicals have been repressed—at times violently. We are at a crossroads. Moreover, the future(s) envisaged by globophiles and globophobes are not just about economics. They are also and more importantly about democracy. The way chosen out of the impasse will be decisive for democracy. As Cox (1996: 533) wisely pointed out "[p]eople, collectively, may be confronted with opportunity, but whether or not they take it is up to them." The evolution of the dynamics between opponents and proponents of economic globalization will be a good indicator of the way in which we collectively choose our future(s).

ANNEX A

THE MAI STRUCTURE[1]

I. GENERAL PROVISIONS
Preamble

II. SCOPE AND APPLICATION
Definition
Geographical Scope of Application
Application to Overseas Territories

III. TREATMENT OF INVESTORS AND INVESTMENTS
National Treatment and Most Favoured Nation Treatment
Transparency
Temporary entry, stay and work of Investors and Key Personnel
Nationality Requirements for Executives, Managers and Members of Boards of Directors
Employment Requirements
Performance Requirements
Privatisation
Monopolies/State Enterprises/Concessions
Entities with Delegated Governmental Authority
Investment Incentives
Recognition Arrangements
Authorisation Procedures
Membership of Self-Regulatory Bodies
Intellectual Property
Public Debt
Corporate Practices
Technology R&D
Not Lowering Standards
Additional Clause on Labour and Environment

IV. INVESTMENT PROTECTION
General Treatment
Expropriation and Compensation
Protection from Strife
Transfers
Information Transfer and Data Processing
Subrogation
Protecting Existing Investments

---

[1] Based on MAI draft text of April 24, 1998 as posted on the OECD website.

ANNEX B

NUMBER OF ORGANIZATIONS SUPPORTING THE OCTOBER 1997 NGO STATEMENT[2]

Argentina (1), Australia (17), Austria (15), Bangladesh (2), Belarussia (1), Belgium (3), Bosnia Herzegovina (1), Brazil (11), Bulgaria (3), Canada (90), Chile (2), Costa Rica (1), Croatia (2), Czech Republic (2), Curacao (1), Denmark (1), El Salvador (1), Egypt (1), Estonia (1), Europe (5), Finland (2), France (3), Germany (10), Greece (1), Grenada (1), Haiti (1), Hungary (4), India (8), Indonesia (1), International (17), Ireland (2), Israel (2), Italy (15), Japan (12), Jordan (1), Kenya (4), Latvia (2), Lithuania (2), Luxembourg (1), Macedonia (2), Malaysia (1), Mauratinia (2), Mexico (74), Moldovia (1), Nepal (3), Netherlands (18), New Zealand (3), Nicaragua (4), Nigeria (1), Norway (2), Palestine (1), Pakistan (1), Philippines (6), Poland (2), Romania (2), Russia (9), Slovakia (2), Slovenia (4), South Africa (1), South Korea (1), Sri Lanka (1), Sweden (4), Switerland (4), Thailand (1), United Kingdom (14), United States (150), Ukraine (4), Uruguay (1), Yugoslavia (1).

---

[2] This tabulation of organizations per country is based upon the list published in the book *Dismantling Democracy* co-published by the The Canadian Centre for Policy Alternatives, and James & Lorimer & Company Ltd., 1998, pp. 324-337.

ANNEX C

LIST OF INTERVIEWEES[3]

Country/organization	Officials	Civil Society
Belgium	1	1
Britain		2
Canada	10	3
European Commission	1	
European Parliament	1	
France	1	5
The Netherlands	1	2
OECD	6	
United States		1

PARTICIPANT OBSERVATION ACTIVITIES

Council of Canadians, Citizens' MAI Inquiry, Halifax, Fall, 1998

Government of Canada Hearings on WTO, Halifax, Spring 1999

Council of Canadians, Citizens' Water Summit, Ottawa, Fall 1999

CCOMC, Anti-WTO/Corporate demonstrations, Paris, Fall 1999

FTAA opposition, Meetings held on Parliament Hill, Ottawa, Canada, April 2001

FTAA opposition, Demonstration at DFAIT, Ottawa, Canada, April 2001

---

[3] Open interview technique was adopted to interview the following individuals. Since confidentiality forms were signed no individual can be directly identified. The following represents the countries, organizations and status (officials such as negotiators or Member of Parliament and MAI opponents) of interviewees.

ANNEX D

CHRONOLOGY OF NEGOTIATIONS AND ANTI-MAI CAMPAIGNS

MAIN DATES	NEGOTIATIONS	CAMPAIGNS
PERIOD ONE		
May '95-April '97	First Period of Negotiations	
June '96		Reformists Obtain Draft MAI and begin their campaign
October '96		Reformists Meet Officials - Geneva
December '96		Reformists Meet NG Chairs
March '97		Radicals Obtain Draft MAI
PERIOD TWO		
April '97-April '98	Second Period of Negotiations	
April '97		Radicals Release MAI Draft Text and Critique on Internet - Begin Campaign
October '97		Transnational Coalition Meets NG
February '98		Media Campaign Kicks Off in France CCAMI Formed
April 28,'98	OECD Ministerial Announces Six-Month Pause	Transnation Protest Against MAI in Paris Outside OECD Offices
PERIOD THREE		
April 98-Oct. '98		
Oct.14 '98	French Withdrawal from MAI Negotiations	
Oct. 22 '98	MAI NG Meets in Paris EC Announces Europe's Withdrawal	
Dec. '98	Last MAI Meeting - Negotiations Abandoned	

BIBLIOGRAPHY

Appleton, Barry (1997) Letter to the Council of Canadians submitted to the House of Commons Sub-Committee on International Trade, Trade Disputes and Investment. Hearings on the Multilateral Agreement of Investment.

Ahnlid, Anders (1997) "Special Topics," in *The Multilateral Agreement on Investment State of Play as of February 1997.* OECD Working Papers Vol.V, No. 18. Paris: OECD.

Ash, Timothy (2001) "Money see, Money do," in *The Globe and Mail*, 2 February, 2001, p. A13.

Assemblée Nationale (1998) "Actes du Colloque du 22 avril, 1998." Paris.

Baldi, Marino (1997) "Dipute Settlement," in in *The Multilateral Agreement on Investment State of Play as of February 1997.* OECD Working Papers Vol.V, No. 18. Paris: OECD.

Barber, Benjamin (1995) *Jihad vs. McWorlds.* New York: Times Books.

_____ (1992) "Jihad vs. McWorlds," in *The Atlantic Monthly*. March, pp. 53-6.

Barlow, Maude and Tony Clarke (2001) *Global Showdown.* Toronto: Stoddart.

Beir, Marshall J., and Ann Denholm Crosby (1998) "Harnessing Change for Continuity: The Play of Political and Economic Forces Behind the Ottawa Process," in *Canadian Foreign Policy.* Vol. 5, No. 3, Spring, pp. 85-103.

Bové, José (1999*a*) "Pour une agriculture paysanne," in *Le Monde Diplomatique*, October, p.32.

_____ (1999*b*) "La Mafia Globale," in *Campagnes Solidaires*, Bagnolet, No.134, October.

Brewer, Thomas (1996) "International investment dispute settlement mechanisms: agreements, institutions ans issues," in *Towards Multilateral Investment Rules.* Paris: OECD, pp. 85-93.

Brysk, Allison (1996) "Turning Weakness Into Strength: The Internationalization of Indian Rights," in *Latin American Perspectives*, issue 89, Vol. 23 No.2, Spring, pp. 38-57.

Bull, Hedley (1977) *The Anarchical Society: A Study of Order in World Politics*. London: Macmillan.

Caldwell, L.K. (1996) *International Environmental Policy* (3rd. ed.). Durham and London: Duke University Press.

Canadian Broadcasting Corporation (1999) *The Magazine*. Toronto, November 29.

_____ (1998) *The Magazine*. Toronto, November 19.

Canner, Stephen J. (1998) "The MAI," in *Cornell International Law Journal*, 31, 3, pp. 657-681.

Carnegy, Hugh, and Lionel Barber (2001) "Fox assails gap between rich and poor," in *Financial Post*, 27 January, p. D3.

Carrol, William K. And R.S. Ratner (1994) "Between Leninism and Radical Pluralism: Gramscian Reflections on Counter-Hegemoniy and the New Social Movements," in *Critical Sociology*, Vol. 20, No. 22, pp. 3-26.

Cerny, Philip G. (1995) "Globalization and the changing logic of collective action," in *International Organization*, Vol. 49, 4, pp. 595-625.

Charnovitz , Steve and John Wickham (1995) "Non-Governmental Organizations and the Original International Trade Regime," in *Journal of World Trade*. October, pp. 111-122.

Charolles, Valérie (1997) "Treatment of Investors and their Investments: National Treatment, Most Favoured Nation Treatment and Transparency," in *The Multilateral Agreemnt on Investment: State of Play as of February 1997*. OECD Working Papers Vol. V, No.18. Paris: OECD.

Chayes, Abram and Antonia Handler Chayes (1995) *The New Sovereignty*. Cambridge, Mass. and London, England: Harvard University Press.

Cienski, Jan (2000) "Washington police bracing for dust-up on the Potomac," in *National Post*, 6 April, p. A14.

Clark, Anne Marie, Elisabeth J. Friedman, and Kathryn Hochstetler (1998) "The Sovereign Limits of Global Civil Society," in *World Politics*, 51, October, pp. 1-35.

Clarke, Tony and Barlow Maude (1997) *M A I: The Multilateral Agreement on Investment and the Threat to Canadian Sovereignty*. Toronto: Stoddart.

Clarke, Tony (1998*a*) "Towards a Citizens' MAI: An Alternative Approach to Developing a Global Investment Treaty Based on Citizens' Rights and Democratic Control." Ottawa: Polaris Institute (at www.canadians.org).

Clarke, Tony (1998*b*) "M.A.I. Machinations: An Update," in *Canadian Forum*, July/August, pp. 2-4.

_____ (1997*a*) Submission to the Standing Committee on Foreign Affairs and International Trade Re. the Multilateral Agreement on Investment. Ottawa: Polaris Institute, November 17, 1997.

_____ (1997*b*) "MAI-Day: A Corporate Rule Treaty." Ottawa: The Canadian Centre for Policy Alternatives, www.policyalternatives.ca.

_____ (1996) "Phoenix Risen: The Resurrection of Global Finance," in *World Politics*, Vol. 48, No. 2, pp. 268-296.

Cohen, Jean and Andrew Arato (1992) *Civil Society and Political Theory*. Cambridge: MIT Press.

Consumer Unity and Trust Society (1997) *Investments: Consumers, Development and the Environment*. Jaipur, India: CUTS & Consumers International.

Committee on International Investment and Multinational Enterprises (CIME), and Committee on Capital Movement and Invisible Transactions (CMIT) (1996) "A Multilateral Agreement on Investment," in *Towards Multilateral Investment Rules*. Paris: OECD.

Common Front on the World Trade Organization (1999) "Submission to the House of Commons Standing Committe on Foreign Affairs and International Trade on the Environmental Impacts of International Trade." Vancouver: West Coast Environmentat Law.

Conseil national interrégional des Verts (1998) *Compte rendu des décisions: cnir-98-216, cnir-98-219*, 10 and 11 October 1998, Paris.

Coordination contre les clones de l'AMI (CCAMI) (1999) *l'AMI cloné à l'Organisation Mondiale du Commerce*. Paris.

Cox, Robert (1999) "Civil Society at the turn of the Millenium: prospects for an alternative world order," in *Review of International Studies*, 25: 3-28.

_____ (1997) "A Perspective on Globalization," in James H. Mittelman (ed.) *Globalization: Critical Reflections*. Boulder, London: Lynne Rienner Publishers.

_____ (1996) with Timothy J. Sinclair *Approaches to World Order*. Cambridge: Cambridge University Press.

_____ (1987) *Production Power and World Order: Social Forces in the Making of History*. New York: Columbia University Press.

Council of Canadians (1998) *The MAI Inquiry: Confronting Globalization & Reclaiming Democracy*. Ottawa: The Council of Canadians.

CUTS (1997) *Investments: Consumers, Development and the Environment*. Jaipur, India: CUTS Centre for International Trade, Economic & Environment.

Dahrendorf, Ralf (1959) *Class and Class Conflict in Industrial Society*. Stanford, Calif.: Stanford University Press.

Deibert, R.J. (1999) "Civil Society Activism on the World-Wide Web: The case of an anti-MAI Lobby." Global Trends Project, August, 30.

De Jonquières, Guy (1998) "Network Guerrillas," *Financial Times*, 30 April, 1998.

Della Porta, Donatella, and Mario Diani (1999) *Social Movements: an introduction*. Oxford: Blackwell Publishers.

Della Porta, Donatella, Hanspeter Kriesi, and Dieter Rucht (eds.) (1999) *Social Movements in a Globalizing World*. London: Macmillan Press Ltd, and New York: St.Martin's Press, Inc.

Della Porta, Donatella and Hanspeter Kriesi (1999) "Social Movements in a Globalizing World: an Introduction," in Donatella della Porta, H. Kriesi and D. Rucht (eds.) *Social Movements in a Globalizing World*. London: Macmillan Press Ltd., and New York: St.Martin's Press, Inc., pp. 3-22.

DeNardo, James (1985) *Power in Numbers: The Political Strategy of Protest and Rebellion*. Princeton, NJ: Princeton University Press.

Drake, William J., and Kalypso Nicolaïdis (1992) "Ideas, interests, and institutionalization: 'trade in services' and the Uruguay Round," in *International Organization*, 46, 1, Winter, pp. 37-100.

Drohan, Madelaine (2001) "Spoils of globalization must go to all," in *The Globe and Mail*, 27 January, p. B9.

Dymond, William A. (1999) "The MAI: A Sad and Melancholy Tale," in O. Hampson, M. Hart and M. Rudnet (eds.) *Canada Among Nations, A Big League Player?* Toronto: Oxford University Press.

_____ (1997) "State of Play of the MAI Negotiations," in *The Multilateral Agreement on Investment State of Play as of February 1997.* OECD Working Papers Vol.V, No. 18. Paris: OECD.

Engering, Frans (1996) "The Multilateral Investment Agreement," in *Transnational Corporations.* Vol.5, no.3, December, pp 147-161.

Epstein, Barbara (1990) "Rethinking Social Movement Theory," in *Socialist Review.* Vol. 20, No. 1, January-March, 1990, pp. 35-65.

Epstein, Leon D. (1967) *Political Parties in Western Democracies.* New York: Praeger.

Ethyl Corporation (1998) Letter to World Development Movement, Friends of the Earth-UK, and the World Wildlife Fund dated 3 April, 1998.

European Parliament (1998) "Minutes of the sitting of Wednesday 11 March 1998." Part II, Texts adopted by Parliament. (PE 267.866).

Eyerman, Ron and Jamison, Andrew (1991) *Social Movements: A Cognitive Approach.* University Park, Pennsylvania: The Pennsylvania State University Press.

Finnemore, Martha (1996) *National Interests in International Society.* Ithaca and London: Cornell University Press.

Francis, Diane (2000) "Soros delivers an ironic new message," in *Financial Post,* 16 September, p. D3.

Friends of the Earth (1998) *License to Loot. The MAI and How to Stop It.* Washington, D.C.: Friends of the Earth.

Friends of the Earth and the World Wildlife Fund for Nature (1997) "Letter to the OECD" dated September 17, 1997.

Frodon, Jean-Michel (1998) "A l'Odéon: ce n'est qu'un début, continuons le combat....," in *Le Monde*, February, 8.

Gamson, William (1992) *Talking Politics*. CambridgeNew York: Cambridge University Press.

Gerlach, Luther (1976) "La Struttura dei Nuovi Movimenti di Rivolta," in Alberto Melucci (ed.) *Movimenti di Rivolta*. Milan: Etas, pp. 218-232.

Gervais, Daniel and Vera Nicholas-Gervais (1999) "Intellectual Property in the Multilateral Agreement on Investment," in *Journal of World Intellectual Property*. Vol.2, No.2, 1999, pp. 257-274.

Giddens, Anthony (1998) *The Third Way*. Cambridge: Polity Press.

Gill, Stephen (2000) "Toward a Postmodern Prince? The Battle in Seattle as a Moment in the New Politics of Globalisation," in *Millennium: Journal of International Studies*, Vol. 29, No.1, pp. 131-140.

_____ (1997) "Globalization, Democratization, and the Politics of Indifference," in James H. Mittelman (ed.) *Globalization: Critical Reflections*. Boulder, London: Lynne Rienner Publishers, pp. 205-228.

Gill, Stephen and David Law (1988) *The Global Political Economy*. Hertfordshire: Harverster, Wheatsheaf.

Giugni, Marco, Dough McAdam and Charles Tilly (eds.) (1999) *How Social Movements Matter*. Minneapolis and London: University of Minnesota Press.

Goldstein, J. and Keohane, R. O. (eds) (1993) *Ideas and Foreign Policy*, Ithaca, NY: Cornell University Press.

Goodman, John B., and Louis W. Pauly (1993) "The Obsolescence of Capital Controls?" in *World Politics*, Vol. 46, October, pp. 50-82.

Gordenker, Leon and Weiss, Thomas G. (1995) "Pluralising global governance: analytical approaches and dimensions," in *Third World Quarterly*, Vol. 16, No.3, pp. 357-393.

Government of British Columbia (1998) *First Report of The Special Committee on The Multilateral Agreement on Investment*. Victoria, British Columbia, December 29, 1998.

Government of Canada (1999) *Final Report on Social Cohesion*. Report of the Standing Senate Committee on Social Affairs, Science and Technology. Ottawa: Government of Canada.

_____ (1998) "Multilateral Agreement on Investment (MAI): Consultations by the Federal Government (as of July 13, 1998)." Ottawa: Department of Foreign Affairs and International Trade.

Government of Canada (1997) "Canada and the Multilateral Agreement on Investment." Report of the Standing Committee on Foreign Affairs and International Trade, Sub-Committee on International Trade, Trade Disputes and Investment. Ottawa, Government of Canada.

_____ (1993) *North American Free Trade Agreement*. Ottawa, Canada.

Government of the United Kingdom (1998) Letter to Dr. Claude Martin, Director General, WWF International from the Secretary of State, Department of Trade and Industry, dated 16 June, 1997.

Graham, Edward M. (1998) "Regulatory Takings, Supernational Treatment and the Multilateral Agreement on Investment: Issues Raised by Nongovernmental Organizations," in *Cornell International Law Journal*. Vol. 31, 3, pp. 599-614.

Graham, Edward M. and Pierre Sauvé (1996) "Toward a Rules-Based Regime for Investment: Issues and Challenges," in Daniel Schwanen and Pierre Sauvé (eds.) *Investment Rules for the Global Economy*. Toronto: C.D. Howe Institute.

Greenhouse, S. (1999) "A Carnival of Derision to Greet the Princes of Global Trade," in *The New York Times*, November 29, p. A12.

Greens of the European Parliament (1998) Press Release "EP supports with overwhelming majority Kreissl-Dorfler Report," dated 11 March 1998, Strasbourg, Austria.

Haas, Peter M. (1992) "Introduction: epistemic communities and international policy coordination," in *International Organization*. Vol. 46, 1, Winter, pp. 1-35.

Hahnel, R. (1999) "Going to Greet the WTO in Seattle," in *Z Magazine*, November, pp. 7-13.

Hart, Michael (1997) "The WTO and the Political Economy of Globalization," in *Journal of World Trade*, October, Vol. 31, No.5, pp. 75-93.

Hart, Michael (1996) "A Multilateral Agreement on Foreign Direct Investment: Why Now," in Daniel Schwanen and Pierre Sauvé (eds.) *Investment Rules for the Global Economy*. Toronto: C.D. Howe Institute.

Hayward, Jack (1995) *The crisis of Representation in Europe*. London: Frank Cass.

Healy, Teresa, and Laura Macdonald (1997) "Continental Divide? Competing Approaches to Understanding Social Movement Organizing Across North America." Paper presented at the 38th Annual International Studies Association meeting, Toronto, Ontario, 18-22 March, 1997.

Held, David (1995) *Democracy and the Global Order*. Stanford: Stanford University Press.

Held, David and Anthony McGrew (2001) *Globalization* at web site "Global Transformations," www.polity.co.uk.

Helleiner, Eric (1994) "From Bretton Woods to Global Finance: A World Turned Upside Down," in Richard Stubbs and Geoffrey R.D. Underhill (eds.) *Political Economy and the Changing Global Order*. New York: St.Martin's Press.

Henderson, David (1999) *The MAI Affair: A Story and its Lessons*. London: The Royal Institute of International Affairs.

Huner, Jan (1998) "Environmental regulation and international agreements: lessons from the MAI." Presentation to the Chatham House Meeting on Trade, Investment and the Environment, October 29-30, 1998.

Ikenberry, John (1992) "A world economy restored: expert consensus and the Anglo-American postwar settlement," in *International Organization*. Vol 46, 1, pp. 289-321.

Inside U.S. Trade (January 1995-December 1998) Washington D.C.: Inside Washington Publishers.

International Forum on Globalization (IFG) (1999) website at www.ifg.org.

Jackson, A. And M. Sanger (eds) (1998) *Dismantling Democracy*. Ottawa: The Canadian Centre for Policy Alternatives and Toronto: James Lorimer & Company Ltd.

James, Elijah M. (1991) *Macro Economics: A Problem Solving Approach* (2nd ed.). Scarborough, Ontario: Prentice Hall Canada Inc.

Jepperson, Ronald, Alexander Wendt, and Peter J. Katzenstein (1996) "Norms, Identity, and Culture in National Security," in P.J. Katzenstein (ed.) *The Culture of National Security: Norms and Identity in World Politics*, New York: Columbia University Press, pp. 33-75.

Johnson, Brian D. (2001) "Naomi and the Brand-New Left," in *McLean's*, 12 March 2001, pp. 26-30.

Johnston, H. (1991) *Tales of Nationalism: Catalonia, 1939-1979*. New Brunswick, NJ.: Rutgers University Press.

Jones, Dorothy V. (1992) "The Declaratory Tradition in Modern International Law," in Terry Nardin and David R. Mapel (eds.) *Traditions of International Ethics*. Cambridge: Cambridge University Press, pp. 42-61.

Julius, DeAnn (1994). "International Direct Investment: Strengthening the Policy Regime," in Peter B. Kenen (ed.) *Managing the World Economy Fifty Years After Bretton Woods*. Washington, D.C.: Institute for International Economics.

Karl, Joachim (1996) "Multilateral investment agreements and regional economic integration," in *Transnational Corporations*. Vol.5, no.2, August, pp. 19-50.

_____ (1997) "Investment Protection,"in *The Multilateral Agreement on Investment State of Play as of February 1997*. OECD Working Papers, Vol.V, No. 18, 1997. Paris.

Kearney, Michael (1996) "Introduction," in *Latin American Perspectives*,Vol. 23, No.2, pp. 5-16.

Keck, Margaret E., and Sikkink Kathryn (1998) *Activists beyond Borders: advocacy networks in international politics*, Ithaca and London: Cornell University Press.

Kerremans, Bart (1999) "The US Debate on Trade Negotiating Authority between 1994 and 1999," in *Journal of World Trade*, 33(5): 49-85.

Khor, Martin (1997*a*) "L'OMC, fer de lance des transnationales," in *Le Monde Diplomatique*, May, p. 10.

_____ (1997*b*) "NGOs in OECD countries protest against MAI, " in *Resurgence*, pp. 25, 26.

Kiely, Ray (2000) "Globalization: from domination to resistance," in *Third World Quarterly*, Vol. 21, No.6, pp. 1059-1070.

Klandermans, B. And S. Tarrow (1988) "Mobilization Into Social Movements: Synthesizing European and American Approaches," in Klandermans, Kriesi, and Tarrow (eds.) *International Social Movement Research*. Connecticut: Jai Press Inc., Vol. 1, pp. 1-38. .

Klein, Naomi (2000) *No Logo: taking aim at the brand bullies*. Toronto: Vintage Canada.

Kobrin, Stephen J. (1998) "The MAI and the Clash of Globalizations," in *Foreign Policy*, Fall No. 112, pp. 97-105.

Krasner, Stephen D. (1983) *International Regimes*. Ithaca, NY: Cornell University Press.

Kuechler, Manfred and Russel J. Dalton. (1990) "New Social Movements and the Political Order," in Manfred Kuechler and Russell J. Dalton (eds.) *Challenging the Political Order*. New York: Oxford University Press.

Labour Party (of Britain) (1997) Letter to WWF-UK from Labour's Spokesperson for Overseas Development, dated 11 April, 1997. Obtained from WWF-UK archives in Goldaming, Surrey, U.K.

Lalumière, Catherine and Jean Pierre Landau (1998) *Rapport sur l'Accord multilatéral sur l'investissement (AMI)*. Published by the Ministry of the Economy, Finance and Industry, Republic of France, Paris, September, 1998. http://www.finances.gouv.fr

_____ (1999) *Rapport: Les négociations commerciales multilatérales*. Report submitted to the French Government in July 1999.

Lang, Jack (1998) "L'AMI c'est l'ennemi," in *Le Monde*, 10 February, 1998.

Le Figaro (1998) "L'avertissement des Verts," October 12, 1998.

Le Monde (1998) "La France ne reprendra pas les négociations sur la libéralisation des investissements," October 16, p. 4.

_____ (1998*b*) "Les réserves de Dominique Strauss-Kahn," 13 February 1998.

_____ (1999*a*) "José Bové contre les grands discours," 30 November, 1999, p. 2.

_____ (1999*b*) "Trois Questions à Ralph Nader," 3 December, 1999, p. 2.

Le Point (1999) "Les ONG à l'attaque," 26 November, 1999, p. 98.

L'Humanité (1998*a*) "Les Verts refusent l'AMI," 12 October 1998.

_____ (1998*b*) "Lionel Jospin: pas d'abandons de souveraineté à des intérêts privés," 15 October, 1998, p. 4.

Lippert, Owen (1998) "Where were the MAI's defenders?" in *The Globe and Mail*, May 5, 1998

Lipschutz, Ronnie D.with Judith Mayer (1996) *Global Civil Society & Global Environmental Governance*. New York: State University of New York.

Lloyd, John (2001) "From Porto Alegre to Quebec," in *The Globe and Mail*, 14 February, p. A13.

Lofland, John (1996) *Social Movement Organization: Guide to Research on Insurgent Realities*. New York: Aldine de Gruyter.

Mabey, Nick (1999) "Defending the Legacy of Rio: the Civil Society Campaign against the MAI," in S. Picciotto and R. Mayne (eds.) *Regulating International Business*. London: MacMillan Press Ltd. and New York, St.Martin's Press, Inc..

Macdonald, Laura (1994) "Globalising Civil Society: Interpreting International NGOs in Central America," in *Millennium: Journal of International Studies*. Vol. 23, 2, pp. 267-285.

Marceau, Gabrielle and Peter N. Pedersen (1999) "Is the WTO Open and Transparent?" in *Journal of World Trade*, Vol. 33, No. 1, pp. 6-49.

Marsh, David and Gerry Stoker (eds.) (1995). *Theory and Methods in Political Science*. New York: St. Martin's Press.

Martin, Claude, Director General, WWF International (1997) Letter to OECD Ministers of Foreign and Economic Affairs, endorsed by International Coalition for Development Action, World Development Movement, Consumers International, Save the Children Fund, Friends of the Earth-UK, OXFAM-UK, dated 19 May, 1997.

May, Elizabeth (1998) "Fighting the MAI," in A. Jackson and M. Sanger (eds.) *Dismantling Democracy*. Otttawa: The Canadian Centre for Policy Alternatives and Toronto: James Lorimer & Company Ltd.

McAdam, Doug (1982) *Political Process and the Development of Black Insurgency, 1930-1970*. Chicago: University of Chicago Press.

McAdam, Doug, D. McCarthy and M.N. Zald (1996) "Introduction: Opportunities, Mobilizing Structures, and Framing Processes – Toward a Synthetic, Comparative Perspective on Social Movements," in McAdam, D., D. McCarthy and M.N. Zald (eds.) *Comparative Perspectives on Social Movements: Political Opportunities, Mobilizing Structures, and Cultural Framings.* Cambridge: Cambridge University Press.

McAdam, Doug, Sidney Tarrow and Charles Tilly (1997) "Toward an Integrated Perspective on Social Movements and Revolution," in Mark Irving Lichbach and Alan S. Zuckerman (eds.) *Comparative politics: rationality, culture, and structure*. Cambridge: Cambridge University Pressl.

McCarthy, Shawn (2001) "Attacking poverty key to fixing economic woes of Latin America," *The Globe and Mail*, 20 April, 2001, p. B8.

McGregor, Sarah (2001) "GE whiz, Ralph Nader brings consumer advocacy to Canada," in *Ottawa X Press*, February 15, 2001, p. 7.

McQuaig, Linda (1994) *The Cult of Impotence*. Toronto: The Penguin Group.

Melucci, Alberto (1989) *Nomads of the Present*. London: Hutchison Radius.

_____ (1995) "The New Social Movemetns Revisited: Reflections on a Sociological Misunderstanding," in Louis Maheu (ed.) *Social Movements and Social Classes: The Future of Collective Action*. London: Thousand Oak and California: SAGE.

_____ (1988) "Getting Involved: Identity and Mobilization in Social Movements," in Klandermans, B., H. Kriesi and S. Tarrow (eds.) *International Social Movement Research*. Vol. 1., pp. 329-348. Greenwich, Conn.: JAI Press Inc.

_____ (ed.) (1984) *Altri Codici. Aree di Movimento nella Metropoli*. Bologna: il Mulino.

Millenium: Journal of International Studies (2000) "Seattle: December 1999?", Vol. 29, Nov. 1, pp. 103-140.

Mittelman, James H. (1997) "The Dynamics of Globalization," and "How does Globalization Work," in James H. Mittelman (ed.) *Globalization: Critical Reflections*. Boulder, London: Lynne Rienner Publishers, Inc., pp. 1-19 and 229-241.

Moynihan, D. (1999) "Anti-WTO Activist Camporee," in *Z Magazine*, November, pp. 5, 6.

Mueller, C. (1994) "Conflict Networks and the Origins of Women's Liberation," in E. Larana, H. Johnston, and J. Gusfield (eds.) *New Social Movements*. Philadelphia: Temple University Press, pp. 234-263.

Naim, Moisés (2000) "Lori's War," in *Foreign Affairs*, Spring 2000, Number 118, pp. 29-55.

Observatoire de la Mondialisation (1998*a*) *Lumière sur l'A.M.I. Le Test de Dracula*. Paris: L'Esprit Frappeur.

_____ (1998*b*) *L'AMI, Non merci!* Paris. April, 1998.

_____ (1998*c*) *Manifeste du 28 avril 1998*. Paris. April, 1998.

O'Brien, Robert, Anne Marie Goetz, Jan Aart Scholte, and Marc Williams (2000) *Contesting Global Governance: Multilateral Economic Institutions and Global Social Movements*, Cambridge: Cambridge University Press.

OECD (1995*a*). *Meeting of the OECD Council at Ministerial Level, 24 May, 1995*. Paris.OECD.

_____ (1995*b*) *AIDE MEMOIRE: Results of the First Two Meetings of the Negotiating Groups on the MAI on 26-27 September and 24-26 October 1995*. DAFFE/INV/IME (95) 47. Paris: OECD.

_____ (1996*a*) *Towards Multilateral Investment Rules*. Paris: OECD.

_____ (1996*b*) *AIDE MEMOIRE: Of the Meeting of the Negotiating Group on the MAI on 6-8 December 1995*. DAFFE/INV/IME (96)8. Paris.

_____ (1996*c*) *AIDE MEMOIRE: Of the Meeting of the Negotiating Group on the MAI on 14-15 March 1996*, DAFFE/INV/IME(96)20. Paris.

_____ (1996*d*) Speeches Made at OECD/DNME Workshop on Foreign Investment held in Hong Kong on the 26 and 27 March 1996, DAFFE/MAI/RD(96)25. Paris.

_____ (1996*e*) *OECD Multilateral Agreement on Investment (MAI)*. Report to the Council by Negotiating Group (NG) Chairman Frans Engering, 30 April, 1996, mai\coun2:102/7.

OECD (1997*a*) *Follow-up to the UK Proposal for Environmental Review of the MAI*, DAFFE/MAI/RD(97)50.

_____ (1997*b*) *Conclusion on Labour and Environment*, DAFFE/MAI/RD(97)51, November 1997.

_____ (1997*c*) *The MAI Negotiating* Text, DAFFE/MAI(97)1/REV2, May 1997. Paris.

_____ (1997*d*) *UK Proposal for Environmental Review of the MAI*, DAFFE/MAI/RD(97)43, September 1997. Paris.

_____ (1998) *The MAI Negotiating Text (as of 24 April 1998)*. www.oecd.org.

_____ (1998*b*) *Ministerial Statement on the MAI*, 28 April, 1998 at www.oecd.org

Oliver, Pamela (1989) "Bringing the Crowd Back In: The Nonorganizational Elements of Social Movements," in L.Kriesberg (ed.) *Research in Social Movement, Conflict and Change*, Vol. II, pp. 1-30.. Greenwich, Conn.: JAI Press Inc.

Ostry, Sylvia (1997). "Technological Change and International Economic Institutions," in Satya Dev Gupta (ed.) *The Political Economy of Globalization*. Boston: Kluwer Academic Publishers.

Padt, Diana (1997) "Dispute Settlement," in *Proceedings of the Special Session on the Multilateral Agreement on Investment Held in Paris on 17 September, 1997*. OECD Working Papers, Vol. 5, no. 96. Paris: OCED.

Pagnucco, Ron and John D. McCarthy (1992) "Advocating Nonviolent Direct Actionin Latin America: The Antecedents and Emergence of Serpaj," in Misztal Bronislaw and Anson Shupe (eds.) *Religion and Politics in Comparative Perspective*. New York: Praeger.

Panitch, Leo (1997) "The Role of the State," in James H. Mittelman (ed.) *Globalization: Critical Reflections*. Boulder, London: Lynne Rienner Publishers, Inc., pp. 83-113.

Passy, Florence (1999) "Supranational Political Opportunities as a Channel of Globalization of Political Conflicts," in Donatella della Porta, H. Kriesi and D. Rucht (eds.) *Social Movements in a Globalizing World*. London: MacMillan Press Ltd., and New York: St.Martin's Press, Inc., pp. 148-169.

Picciotto, Sol (1999) "A Critical Assessment of the MAI," in S. Picciotto and R. Mayne (eds.) *Regulating International Business.* London, MacMillan Press Ltd., New York, St.Martin's Press, Inc.

Plotke, David (1990) "What's So New About New Social Movements?" in *Socialist Review*. Vol. 20, No. 1, Jan-March 1990, pp. 81-102.

Polanyi, Karl (1957) *The Great Transformation: The Political and Economic Origins of our Time*. Boston: Beacon.

Price, Richard (1998) "Reversing the Gun Sights: Transnational Civil Society Targets Land Mines," in *International Organization*, Vol. 52, 3, Summer, pp. 613-644.

Pross, Paul (1990) "Pressure Groups: Talking Chameleons," in Michael S. Wittington and Glen Williams (eds.) *Canadian Politics in the 1990s*. Scarborough: Nelson Canada.

Putnam, R.D. (1988) "Diplomacy and Domestic Politics: the logic of two-level games," in *International Organization*,Vol. 42, 3, pp. 427-60.

Ramaiah, B.B. (1997) "Towards a multilateral framework on investment?" in *Transnational Corporations*, Vol. 6, no.1, April, pp. 117-121.

Reich, Robert B. (1991) *The Work of Nations*. New York: Vintage Books.

Risse-Kappen, Thomas (ed.) (1995) *Bringing transnational relations back in*. Cambridge: Cambridge University Press.

Risse, Thomas (2000) "'Let's Argue!':Communicative Action in World Politics," in *International Organization*, Vol. 54, 1, Winter, pp. 1-39.

Risse, Thomas, Stephen C. Ropp and Kathryn Sikkink (eds.) (1999) *The Power of Human Rights*. Cambridge: Cambridge University Press, 1999.

Rochon, Thomas R. (1988) *Mobilizing for Peace: The Antinuclear Movements in Western Europe*. Princeton, N.J.: Princeton University Press.

Rodrik, Dani (1997) *Has Globalization Gone Too Far?* Washington, D.C.: Institute for International Economics.

Rucht, Dieter (1999) "The Transnationalization of Social Movements: Trends, Causes, Problems," in della Porta, Kriesi, and Rucht (eds), *Social Movements in a Globalizing World*. New York: St.Martin' Press, Inc.

Ruggie, John Gerard (1998*a*) *Constructing the World Polity*. London and New York: Routledge.

_____ (1998*b*) "What Makes to World Hang Together? Neo-utilitarianism and the Social Constructivist Challenge," in *International Organization*. Vol. 52, 4, Autumn, pp. 855-885.

_____ (1982) "International Regimes, transactions, and change: embedded liberalism in the postwar economic order," in *International Organization*, 36 (2): 195-231.

Rugman, Alan M. (1998) "The Power of NGOs," at web site *The Political Economy of the Multilateral Agreement on Investment* @ library.utoronto.cs/www/g7/annual/rugman3.

Rupp, L. and V. Taylor (1987) *Survival in the Doldrums: The American Women's Rights Movement, 1945 to the 1960s.* Columbus: Ohio State University Press, 1987.

Schekulin, Manfred M. (1997) "Scope of the MAI: Definition of Investor and Investment," in *The Multilateral Agreement on Investment State of Play as of February 1997.* OECD Working Papers Vol.V, No. 18. Paris: OECD.

Schwanen, Daniel (1996) "Investment and the Global Economy: Key Issues in Rulemaking," in Pierre Sauvé and Daniel Schwanen (eds.) *Investment Rules for the Global Economy*. Toronto: C.D. Howe Institute.

Scoffield, Heather (1998) "NAFTA lawsuits cloud MAI discussions." *The Globe and Mail*, 21 August, 1998.

Scott, Alan (1990) *Ideology and The New Social Movements*. London: Unwin Hyman.

Shermer, Michael and Alex Grobman (2000) *Denying History*. Berkeley: University of California Press.

Shrybman, Steven (1998) "The MAI and Dispute Settlement," in A. Jackson and M. Sanger (eds.) *Dismantling Democracy*. Otttawa: The Canadian Centre for Policy Alternatives and Toronto, James Lorimer & Company Ltd..

Sierra Club of Canada (1997) Presentation to The Standing Committee on Foreign Affairs and International Trade Sub-Committee on Trade, Trade Disputes and Investment, November 18, 1997. Ottawa: Sierra Club of Canada.

Sikkel, Marinus W. (1997) "Treatment of Investors and their Investments: Exceptions, Derogations and National Reservations," in *The Multilateral Agreement on Investment State of Play as of February 1997.* OECD Working Papers Vol.V, No. 18. Paris: OECD.

Sjolander, Claire Turenne (1996) "The rhetoric of globalization: what's in a wor(l)d?" in *International Journal*, LI, Autumn, pp. 603-615.

Skogstad, Grace (2000) "Globalization and Public Policy: Situating Canadian Analyses," in *Canadian Journal of Political Science*, XXXIII:4, pp. 803-828.

Slater, David (1994) "Power and Social Movements in Other Occidents," in *Latin American Perspectives*, Vol. 21, No. 2, pp. 11-37.

Smith, Alister (1995) "The Development of a Multilateral Agreement on Investment at the OECD: A Preview," in Carl J. Green and Thomas L. Brewer *Investment Issues in Asia and the Pacific Rim*. New York: Oceana Publications Inc.

Smith, Jackie (2000) "Globalizing Resistance: The Battle of Seattle and the Future of Social Movements." Paper prepared for the Workshop on Contentious Politics, Lazarsfeld Center for the Social Sciences, Columbia University, February 2000.

_____ (1999) "Global Politics and Transnational Social Movements Strategies: The Transnational Campaign against International Trade in Toxic Wastes," in Donatella della Porta, H. Kriesi and D. Rucht (eds.) *Social Movements in a Globalizing World.* London: MacMillan Press Ltd. and New York: St.Martin's Press, Inc., pp. 170-188.

Smythe, Elizabeth (1998*a)* "Your place or mine? States, international organizations and the negotiations of investment rules," in *Transnational Corporations*, vol. 7, no. 3, December 1998, pp. 85-120.

Smythe, Elizabeth (1998*b*) "The Multilateral Agreement on Investment: A Charter of Rights for Global Investors or Just Another Agreement?" in Fen Osler Hampson and Maureen Appel Molot (eds.) *Canada Among Nations, 1998: Leadership and Dialogue*. Toronto: Oxford University Press, p. 239-266.

Soros, George (1997) "The Capitalist Threat," in *The Atlantic Monthly*, February, pp. 45-58.

_____ (1998) *The Crisis of Global Capitalism: Open Society Endangered.* New York: Public Affairs.

Spero Joan E., and Jeffrey A. Hart (1997) *The Politics of International Economic Relations*. New York: St. Martin's Press.

Stairs, Denis (1998) "The Policy Process and Dialogues with Demos: Liberal Pluralism with a Transnational Twist," in Fen Olser Hampson and Maureen Appel Molot (eds.) *Leadership and Dialogue*. Toronto, Oxford, New York: Oxford University Press.

Steinmetz, George (1994) "Regulation Theory, Post-Marxism, and the New Social Movements," in *Comparative Studies in Society and History*. Vol. 36, No. 1, January, pp. 176-212.

Stiles, Kendall W. (1998) "Civil Society Empowerment and Multilateral Donors: International Institutions and New International Norms," in *Global Governance*, 4: 199-216.

Strange, Susan (1986) *Casino Capitalism*. Oxford: Blackwell.

Swenarchuk, Michelle (1998) "The MAI and the Environment," in A. Jackson and M. Sanger (eds.) *Dismantling Democracy*. Otttawa: The Canadian Centre for Policy Alternatives and Toronto: James Lorimer & Company Ltd.

Tarrow, S. (1983) *Struggling to Reform: Social Movements and Policy Change During Cycles of Protest*. Western Societies Program Occasional Paper No.155, New York Center for International Studies. Ithaca: Cornell University Press.

The Council of Canadians (1998) *The MAI Inquiry, Confronting Globalization & Reclaiming Democracy*. Ottawa.

The Economist (1998) "The talking FDI blues," March 14, p. 18, 20.

The Globe and Mail (1999) "The WTO conflict moves inside," 4 December, 1999, p. A7.

_____ (1998*a*) "How the Net Killed the MAI," Wednesday, April 29, 1998.

_____ (1998*b*) "NAFTA lawsuits cloud MAI discussions," 21 August, 1998.

_____ (1997) "Treaty to trim Ottawa's power," 3 April, 1997, p. A1.

The New York Times (1999) "After Seattle, Unions Point to Sustained Fight on Trade," 6 December 1999.

The Wall Street Journal (1999) "Poorer Countries are Demonstrators' Strongest Critics," 2 December, 1999, p. A2.

Thiele, Leslie Paul (1993) "Making Democracy Safe for the World: Social Movements and Global Politics," in *Alternatives*, 18: 273-305.

Tilly, Charles (1978) *From Mobilization to Revolution*. Reading, MA: Addison-Wesley

_____ (1986) *The Contentious French*. Cambridge, MA: Harvard University Press.

_____ (1988) "Social Movements, Old and New," in L.Kriesberg (ed.) *Research in Social Movements, Conflict and Change*, Vol. 10. Greenwich, Ct.: JAI Press , 1-18.

_____ (1999) "From Interactions to Outcomes in Social Movements," in Giugni, Marco, Dough McAdam and Charles Tilly (eds.) *How Social Movements Matter*. Minneapolis and London: University of Minnesota Press, pp. 253-270.

TIME (1999) "The Battle in Seattle," 29 November, 1999, pp. 28-33.

Touraine, Alain (1999) *Comment sortir du libéralisme?"* Paris: Fayard.

Trade Union Advisory Committee (TUAC) (1996) "The Multilateral Agreement on Investment and the OECD Guidelines for Multinational Enterprises," briefing note (tuacmeet/mai-gdln.96e). Obtained from WWF archives on MAI.

Union des Confédérations de l'Industrie et des Employeurs d'Europe (UNICE) (1995) "UNICE Preliminary Comments on Trade and Investment." Brussels, 8 March 1995.

United Nations Conference on Trade and Development (UNCTAD) (1999*a*) "National Treatment," in *UNCTAD Series on issues in international investment agreements.* New York and Geneva: United Nations.

_____ (1999*b*) "Most Favoured Nation Treatment,"in *UNCTAD Series on issues in international investment agreements.* New York and Geneva: United Nations.

_____ (1999*c*) "Scope and Definition," in *UNCTAD Series on issues in international investment agreements.* New York and Geneva: United Nations.

_____ (1999*d*) *World Investment Report 1999*. New York and Geneva: United Nations.

United States Information Agency (USIA Electronic Journal) (1997) *Economic Perspectives.* Vol.2, No.2, April 1997.

Useem, Bert and Mayer N. Zald (1987) "From Pressure Group to Social Movement: Efforts to Promote Use of Nuclear Power," in Mayer N. Zald and John D. McCarthy (eds.) *Social Movements in an Organizational Society.* New Brunswick (U.S.A.) and Oxford (U.K.): Transaction Books.

Van Evera, Stephen (1997) *Guide to Methods for Students of Political Science.* Ithaca and London: Cornell University Press.

Van Loon, Richard J. And Michael S. Whittington (1981) *The Canadian Political System: Environment, Structure, and Process* (3rd ed.). Toronto: McGraw-Hill Ryerson Limited.

Veltmeyer, Henry, James Petras and Steve Vieux (1997) *Neoliberalism and Class Conflict in Latin America.* London: MacMilland Press Ltd, and New York: St.Martin's Press, Inc.

Wallace, Bruce (2000) "IMF 'willing to change' for protesters," in *The Ottawa Citizen,* 23 September, p. B4.

Wallach, Lori (1998) "Le nouveau manifeste du capitalisme mondial," in *Le Monde Diplomatique.* February, 1998.

Walzer, Michael (1991) "A Better Vision: The Idea of Civil Society," in *Dissent.* Spring, 1991, pp.293-303.

Wapner, Paul (1995) "Politics Beyond The State," in *World Politics,* Vol. 47:3, April, pp. 311-340.

_____ (1996) *Environmental Activism and World Civic Politics.* New York: State University of New York Press.

Wendt, Alexander (1992) "Anarchy is what states make of it: the social construction of power politics," in *International Organization,* 46, 2, Spring 1992, pp. 391-425.

_____ (1987) "The agent-structure problem in international relations theory," in *International Organization,* Summer, 41, 3, pp. 3355-370.

Wiarda, Howard J. (1993) *Introduction to Comparative Politics.* Belmont, Ca.: Wadsworth Publishing Company.

Willetts, Peter (2000) "From 'Consultative Arrangements' to 'Partnership': The Changing Status of NGOs in Diplomacy at the UN," in *Global Governance*, Vol. 6: 191-212.

Wilson, John (1973) *Introduction to Social Movements*. New York: Basic Books.

Winham, Gilbert (1999) "The Impact of Globalization on the International Trade Regime: The Genesis of the Uruguay Round." Paper presented at the Annual Meeting of the International Studies Association, Washington, D.C., February 16-20, 1999.

_____ (1996) "International trade policy in a globalizing economy," in *International Journal*, LI Autumn 1996, pp. 638-650

_____ (1986) *International Trade and the Tokyo Round Negotiation.* Princeton: Princeton University Press.

Winham, Gilbert and Grant, Heather A. (1997) "Designing institutions for global economic cooperation: investment and the WTO," in Gavin, Boyd and Rugman (eds.) *Euro-Pacific Investment and Trade*. Cheltenham, U.K.: Edward Elgar.

Witherell, William H. (1996) "Towards an international set of rules for investment," in *Towards Multilateral Investment Rules*. Paris: OECD.

Wolfe, Robert (1998) "MAI imploded all by itself," in *The Globe and Mail*, May 2, p. D7.

World Wildlife Fund for Nature (1998) "Memorandum of WWF-UK to the Environmental Audit Committee 15 September 1998." Goldaming, Surrey, UK, September 1998.

_____ (1997) Consolidated Paper on the MAI by Nick Mabey, 17 February. Goldaming: Panda House.

_____ (1996) "Note on Informal Meeting Between NGOs, and the MAI Negotiating Bureau," December 1996 from WWF archives in Goldaming, Surrey, U.K.

Working Group on the WTO/MAI (1999) *A citizen's Guide to the World Trade Organization*. New York: The Apex Press.

Computational Studies on the Properties and Reactions of Biological Radicals

by

Fuqiang Ban

Submitted in partial fulfillment of the requirements
for the degree of Doctor of Philosophy

at

Dalhousie University
Halifax, Nova Scotia
July, 2001

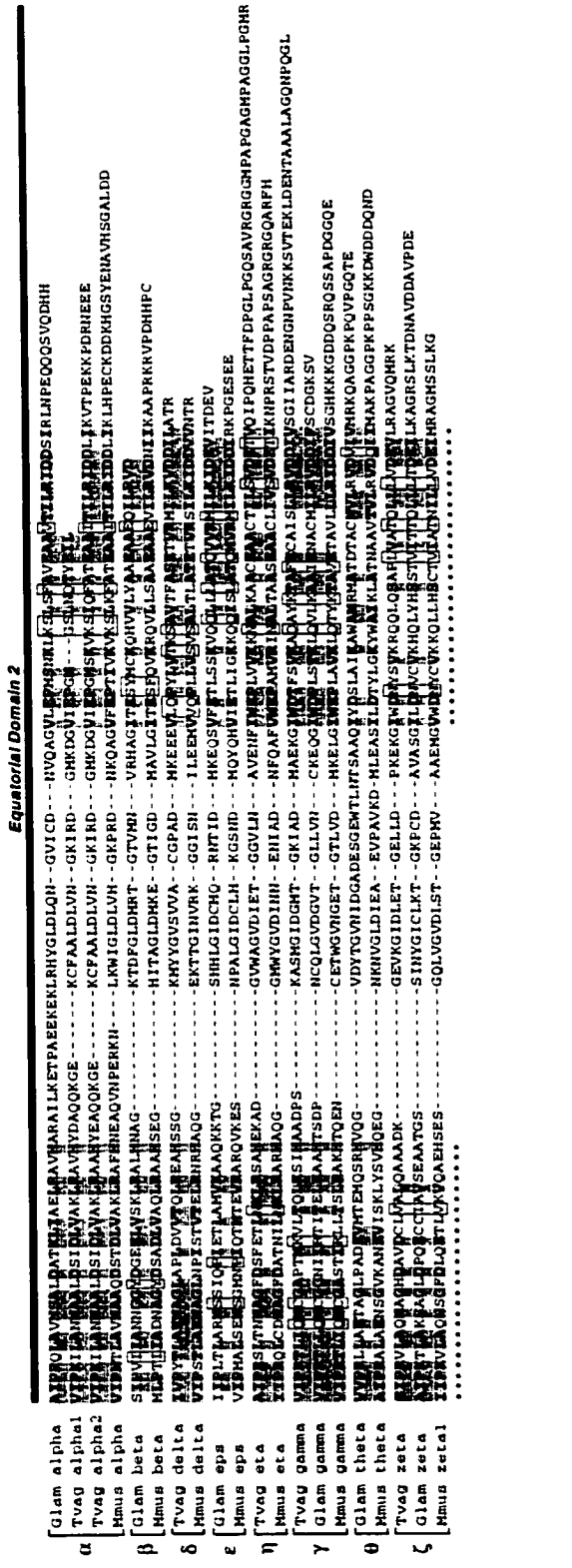

Figure 2.9 Site rate analysis of CCT subunits

the putative ATP-binding domains in the different subunits, as well as the presence of highly conserved 'paralog-specific' motifs present in the equatorial and intermediate domains (Figure 2.9). For example, the CCTθ subunit has the sequence GDGTN in the amino-terminal equatorial domain, a slight variation on the near-universally conserved motif GDGTT, which forms one of the loops of the ATP-binding pocket. In CCTγ, the highly conserved motif NDGAT (found in the amino-terminal equatorial domain of almost all the CCT subunits) has changed to NDGNA. Interestingly, multiple alanine replacements of highly conserved residues within the ATP-binding pocket of CCTζ (e.g., GDGTT to AAAAA) had relatively mild effects on cell growth in yeast (Lin *et al.* 1997), unlike the severe phenotypes observed with mutations in the same region of CCTα (Miklos *et al.* 1994; Ursic *et al.* 1994). When the sequences from a wide diversity of eukaryotes are considered, some parts of the ATP-binding domains of the different subunits appear to be less conserved than others, suggesting that their ATPase functions may in fact be redundant.

As was done for the variable regions of the molecule, the positions of the slowly evolving subunit-specific 'signatures' were mapped onto the structure of the α subunit of the *T. acidophilum* chaperonin (Figures 2.10 and 2.11). Within the conserved 'core' region of the apical domain, many of the CCT subunits possess a cluster of highly conserved, subunit-specific residues on the inside face of the apical domain, just below the helical protrusion (Figure 2.10). Significantly, this is precisely the region of the apical domain that appears to be in direct contact with actin and tubulin in CCT-substrate complexes (Llorca *et al.* 2000; Llorca *et al.* 1999a). CCTβ and ε, two of the three subunits implicated in the binding of actin (Llorca *et al.* 1999a), have more subunit-specific signatures in this region than the other subunits, while CCTθ has almost none (Figure 2.10). As well, CCTα and CCTζ have unique insertions in this area, very near helix H11 (data not shown).

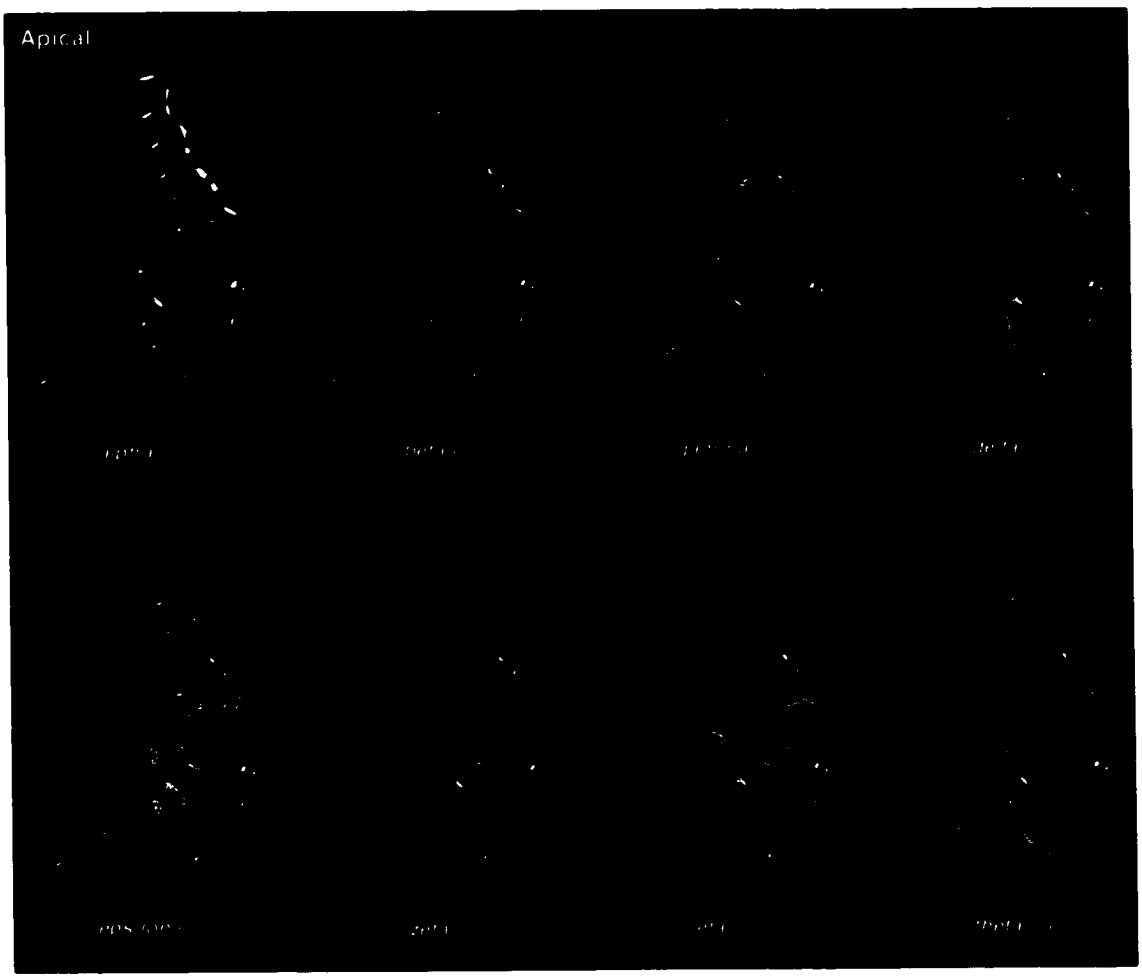

Figure 2.10 Subunit-specific 'signatures' in individual CCT apical domains. Isolated apical domains are shown, one for each of the eight CCT subunits (α, β, γ, δ, ε, ζ, η and θ). Amino acid residues unique to a particular CCT subunit apical domain ('signatures'; see text) are highlighted yellow. As in Figure 2.8, regions of the sequence found to be variable between the different CCT subunits are shaded gray. The domain orientation and color coding matches that in Figure 2.8B. Secondary structural elements are labeled according to Ditzel *et al.* (1998) (H=helix).